Calendar of forthcoming meetings

30 March – 2 April 2008
Dublin, Ireland
Europtrode IX: Ninth International Conference on Optical Chemical Sensors and Biosensors.
URL: www.europtrodeIX.eu

14–16 May 2008
Shanghai, China
Biosensors 2008: The Tenth World Congress on Biosensors. URL: www.biosensors-congress.elsevier.com

19–21 May 2008
Egmond aan Zee, The Netherlands
EuroResidue VI Conference on Residues of Veterinary Drugs in Food.
Contact: EuroResidue, PO Box 18, 5298 ZG Liempde, The Netherlands.
Tel. (+31-411) 611-199;
E-mail: euroresidue@congresservice.nl;
URL: www.euroresidue.nl

25–29 May 2008
Neuherberg, Germany
4th International Conference on Trace Element Speciation in Biomedical, Nutritional and Environmental Sciences.
URL: http://www.gsf.de/spec

30 June – 4 July 2008
Montpellier, France
CAC 2008: 11th Conference on Chemometrics in Analytical Chemistry.
Contact: Dr Jean-Michel Roger, Cemagraf, 361 rue J.F. Breton, BP 5095, F-34196 Montpellier, France.
Tel. (+33-4) 6704-6383;
Fax: (+33-4) 6704-6306;
E-mail: contact@cac2008.org;
URL: http://cac2008.teledetection.fr

7–11 September 2008
Bologna, Italy
ISLS 2008: XIIIth International Symposium on Luminescence Spectrometry.
Contact: Professor Aldo Roda, Department of Pharmaceutical Sciences, Faculty of Pharmacy, Unviersity of Bologna, Italy.
Tel. (+39-051) 343-398;
Fax: (+39-051) 343-398;
E-mail: isls2008@unibo.it;
URL: http://www.isls2008.unibo.it

14–16 September 2008
Muenster, Germany
SIMS Europe 2008: 6th European Workshop on Secondary Ion Mass Spectrometry. URL: http://www.sims-europe.uni-muenster.de

2–5 November 2008
Kaohsiung, Taiwan
APCE 2008: 8th Asia-Pacific International Symposium on Microscale Separations and Analysis.
URL: http://www.tl.ntu.edu.tw/apce2008

6–10 September 2009
Innsbruck, Austria
Euroanalysis 2009.
Contact: Euroanalysis 2009 Symposium Office, PCO Tyrol Congress, c/o Ina Kaehler, Rennweg 3, 6020 Innsbruck, Austria.
Tel. (+43-512) 575-600; Fax: (+43-512) 575-607;
E-mail: euroanalysis09@come-innsbruck.at;
URL: www.euroanalysis2009.at

doi:10.1016/S0039-9140(08)00039-8

Talanta

The International Journal of Pure and Applied Analytical Chemistry

Editors-in-Chief

Professor G.D. Christian, University of Washington, Department of Chemistry, 36 Bagely Hall, P.O. Box 351700, Seattle,WA 98195-1700, U.S.A.

Professor J.-M. Kauffmann, Université Libre de Bruxelles, Institut de Pharmacie, Campus de la Plaine, C.P. 205/6, Boulevard du Triomphe, B-1050 Bruxelles, Belgium

Associate Editors

Professor J.-H. Wang, Research Center for Analytical Sciences, Northeastern University, Box 332, Shenyang 110004, China

Professor J.L. Burguera, Los Andes University, IVAIQUIM, Faculty of Sciences, P.O. Box 542, 5101-A Mérida, Venezuela.

Assistant Editors

Dr R.E. Synovec, Department of Chemistry, University of Washington, Box 351700, Seattle, WA 98195-1700, U.S.A.

Professor J.-C. Vire, Université Libre de Bruxelles, Institut de Pharmacie, Campus de la Plaine, C.P. 205/6, Boulevard du Triomphe, B-1050 Bruxelles, Belgium

Talanta

R. Apak (Istanbul, Turkey)
E. Bakker (Auburn, AL, U.S.A.)
D. Barceló (Barcelona, Spain)
B. Birch (Luton, UK)
K. S. Booksh (Tempe, AZ, U.S.A.)
J.-L. Capelo-Martinez (Caparica, Portugal)
Z. Cai (Kowloon, Hong Kong)
S. Cosnier (Grenoble, France)
D. Diamond (Dublin, Ireland)
W. Frenzel (Berlin, Germany)
A.G. Gonzales (Seville, Spain)
E.H. Hansen (Lyngby, Denmark)
P. de B. Harrington (OH, U.S.A.)
A. Ho (Hsin-chu, Taiwan)
J. Kalivas (Pocatella, ID, U.S.A.)
B. Karlberg (Stockholm, Sweden)
J.-M. Lin (Beijing, China)
Y. Lin (Richland, WA, U.S.A.)
M.D. Luque de Caastro (Cordoba, Spain)
I.D. McKelvie (Victoria, Australia)
S. Motomizu (Okayama, Japan)
D. Nacapricha (Bangkwok, Thailand)
J.-M. Pingarron (Madrid, Spain)
E. Pretsch (Zürich, Switzerland)
W. Schuhmann (Bochum, Germany)
M. Shamsipur (Kermanshah, Iran)
M. Silva (Porto Alegre, Brazil)
P. Solich (Hradec Králové, Czech Republic)
K. Suzuki (Yokohama, Japan)
D.G. Themelis (Thessaloniki, Greece)
D.L. Tsalev (Sofia, Bulgaria)
Y. van der Heyden (Belgium)
B. Walzcak (Katowice, Poland)
J. Wang (Tempe, AZ, U.S.A.)
J.D. Winefordner (Gainesville, U.S.A)
Xiu-Ping Yan (Tianjin, China)
E.A.G. Zagatto (Piracicaba, SP, Brazil)

Copyright © 2008 Elsevier B.V. All rights reserved

Publication information: *Talanta* (ISSN 0039-9140). For 2008, volumes 74–76 are scheduled for publication. Subscription prices are available upon request from the Publisher or from the Regional Sales Office nearest you or from this journal's website (http://www.elsevier.com/locate/talanta). Further information is available on this journal and other Elsevier products through Elsevier's website: (http://www.elsevier.com). Subscriptions are accepted on a prepaid basis only and are entered on a calendar year basis. Issues are sent by standard mail (surface within Europe, air delivery outside Europe). Priority rates are available upon request. Claims for missing issues should be made within six months of the date of dispatch.

Orders, claims, and journal enquiries: please contact the Customer Service Department at the Regional Sales Office nearest you:
Orlando: Elsevier, Customer Service Department, 6277 Sea Harbor Drive, Orlando, FL 32887-480 USA; phone: (+1) (877) 8397126 [toll free number for US customers], or (+1) (407) 3454020 [customers outside US]; fax: (+1) (407) 3631354; e-mail: usjcs@elsevier.com
Amsterdam: Elsevier, Customer Service Department, PO Box 211, 1000 AE Amsterdam, The Netherlands; phone: (+31) (20) 4853757; fax: (+31) (20) 4853432; e-mail: nlinfo-f@elsevier.com
Tokyo: Elsevier, Customer Service Department, 4F Higashi-Azabu, 1-Chome Bldg, 1-9-15 Higashi-Azabu, Minato-ku, Tokyo 106-0044, Japan; phone: (+81) (3) 5561 5037; fax: (+81) (3) 5561 5047; e-mail: jp.info@elsevier.com
Singapore: Elsevier, Customer Service Department, 3 Killiney Road, #08-01 Winsland House I, Singapore 239519; phone: (+65) 63490222; fax: (+65) 67331510; e-mail: asiainfo@elsevier.com

USA mailing notice: *Talanta* (ISSN 0039-9140) is published monthly by Elsevier B.V. (P.O. Box 211, 1000 AE Amsterdam, The Netherlands). Annual subscription price in the USA US$ 4,085 (valid in North, Central and South America), including air speed delivery. Application to mail at periodical postage rate is paid at Rathway, NJ and additional mailing offices.
USA POSTMASTER: Send address changes to *Talanta*, Publications Expediting Inc., 200 Meacham Avenue, Elmont, NY 11003.
AIRFREIGHT AND MAILING in the USA by Publications Expediting Inc., 200 Meacham Avenue, Elmont, NY 11003.

Available online at www.sciencedirect.com
ScienceDirect
Talanta 74 (2008) 1113–1121
Talanta
www.elsevier.com/locate/talanta

Novel lipoate-selective membrane sensor for the flow injection determination of α-lipoic acid in pharmaceutical preparations and urine

M.N. Abbas *, A.A. Radwan

Microanalysis Laboratory, Applied Organic Chemistry Department, National Research Centre, Dokki, Cairo, Egypt

Received 15 May 2007; received in revised form 30 July 2007; accepted 12 August 2007
Available online 17 August 2007

Abstract

A potentiometric lipoate-selective sensor based on mercuric lipoate ion-pair as a membrane carrier is reported. The electrode was prepared by coating the membrane solution containing PVC, plasticizer, and carrier on the surface of graphite electrode. Influences of the membrane composition, pH, and possible interfering anions were investigated on the response properties of the electrode. The sensor exhibits significantly enhanced response toward lipoate ions over the concentration range 1×10^{-7} mol L^{-1} to 1×10^{-2} mol L^{-1} with a lower detection limit of (LDL) of 9×10^{-8} mol L^{-1} and a slope of −29.4 mV $decade^{-1}$, with S.D. of the slope is 0.214 mV. Fast and stable response, good reproducibility, long-term stability, applicability over a pH range of 8.0–9.5 is demonstrated. The sensor has a response time of ≤12 s and can be used for at least 6 weeks without any considerable divergence in its potential response. The proposed electrode shows good discrimination of lipoate from several inorganic and organic anions. The CGE was used in flow injection potentiometry (FIP) and resulted in well defined peaks for lipoate ions with stable baseline, excellent reproducibility and reasonable sampling rate of 30 injections per hour. The proposed sensor has been applied for the direct and FI potentiometric determination of LA in pharmaceutical preparations and urine; and has been also utilized as an indicator electrode for the potentiometric titration of LA.
© 2007 Elsevier B.V. All rights reserved.

Keywords: Lipoic acid; Potentiometric; Selective-sensor; Flow-injection; Pharmaceutical preparations; Urine

1. Introduction

α-Lipoic acid (ALA) or thioctic acid is also known as 1,2-dithiolane-3-pentanoic acid; its structure is shown in Fig. 1. It was discovered in 1937 by Snell et al. [1] who found that certain bacteria needed a compound from potato extract for growth. However, it was not before 1951 that the so-called potato growth factor was isolated and characterized by Reed et al. [2,3]. It has only recently become one of the most recognized and in-demand health supplements. It contains sulfur and is a vitamin like phytonutrient. ALA was found to be synthesized by both plants and animals [3,4] and functions as acetate replacing factor and pyruvate oxidation factor. α-Lipoic acid plays an essential role in mitochondrial dehydrogenase reactions [5] and has found considerable attention as a very potent antioxidant [6] that fights free radicals and improves recovery. Due to it's readily absorption throughout the body, being both fat and water soluble, it may protect the integrity of cells ranging from the brain to the liver. Its pharmaceutical preparation is readily absorbed from an oral dose and converts easily to its reduced form dihydrolipoic acid (DHLA) in many tissues of the body. Its antioxidant activity extends to both its oxidized and reduced form. Both LA and DHLA can chelate many transition metals like: Cu^{2+}, Zn^{2+}, Mn^{2+}, Pb^{2+}, Hg^{2+} and Fe^{3+}, where in animal studies, it has been found to protect from arsenic, mercury and cadmium poisoning [7,8]. Its chelation of iron and copper in the brain may reduce free-radical damage contributing to Alzheimer's diseases [9], and it has been recently suggested as a novel treatment for Alzheimer's disease and related dementias [10]. It is used for the therapy of diabetic polyneuropathy [11], and recently, was found to show positive effects in age-associated neurodegenerative diseases [12] and HIV infections [13]. The medical importance of LA, which is thought to be the drug of the future

* Corresponding author. Tel.: +20 2 2624 7002; fax: +20 2 2267 2867.
E-mail addresses: mnabbas@menanet.net, dr.nooreldin@yahoo.com (M.N. Abbas).

0039-9140/$ – see front matter © 2007 Elsevier B.V. All rights reserved.
doi:10.1016/j.talanta.2007.08.008

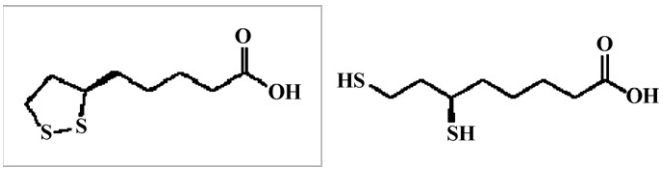

Fig. 1. Structure of lipoic acid (LA); and its reduced form dihydrogen lipoic acid (DHLA).

[14] has stimulated the research for developing accurate methods for its quantitative determination. Microbiological assays [15], enzyme immunoassays [16] and spectrophotometric methods [17] have been reported for the quantification of LA. A comprehensive overview of chromatographic methods for the determination of lipoic acid has been given by Kataoka [18]. One capillary electrophoretic method for the determination of lipoic acid based on electrokinetic chromatography has been reported [19]. To our knowledge no potentiometric electrochemical sensors has been yet described for the determination of LA. Recently, electrochemical sensors [20–22] have gained an increasing attention, as they are known to offer an excellent low cost tool for the selective, sensitive and rapid determination of a vast variety of analytes in different fields of application. The present work describes the construction and evaluation of a novel solid-state electrochemical sensor for the sensitive and selective flow-injection determination of LA in its pharmaceutical preparations and in urine.

2. Experimental

2.1. Reagents and materials

All chemicals used were of analytical reagent grade unless otherwise stated and doubly distilled water was used throughout. Dioctyl phthalate (DOP), dibutyl phthalate (DBP), dibutyl sebacate (DBS), and tetrahydrofuran (THF) were purchased from Aldrich. Sodium tetraphenyl borate was purchased from Reidel de Haen. Poly(vinyl chloride) (PVC) (high molecular weight) fine powder, sodium and potassium salts of all anions used (Merck) were of the highest purity available and used without any further purification. Tridodecyl methyl ammonium chloride (TDMAC) and tris(hydroxymethyl) aminomethane were purchased from Fluka, Switzerland. Cetylprydinium chloride (CPC) was purchased from ACROS and cetyltrimethyl ammonium bromide (CTAB) from BDH. Lipoic acid was obtained from Eva Pharma, Egypt. The pharmaceutical preparations, Thiotacid® tablets 600 mg, of Eva Pharma-Egypt, and Thiotex® capsules 300 mg of Marcyrl Pharmaceutical Industries, Egypt, were obtained from local market.

A standard stock solution of 0.1 mol L^{-1} was prepared by dissolving 2.06 g of lipoic acid in 5 mL of 0.1 mol L^{-1} NaOH solution and made to volume into 100 mL measuring flask with HCl–Tris buffer of pH 8.5. The working standards of 10^{-2} mol L^{-1}, 10^{-3} mol L^{-1}, 10^{-4} mol L^{-1}, 10^{-5} mol L^{-1}, 10^{-6} mol L^{-1} and 10^{-7} mol L^{-1} concentration were prepared by proper dilution of the stock solution.

2.2. Apparatus

All potentiometric measurements were made at 25 ± 1 °C unless otherwise stated using a Metrohm pH/Ion meter Model 692. A combined glass pH electrode Model Metrohm 6.0202.100 was used for all pH measurements and a Metrohm double junction Ag/AgCl reference electrode Model 6.0726.100 containing 3 mol L^{-1} potassium chloride in outer and inner tubes was used.

2.2.1. HPLC system

A Perkin-Elmer Series 200 HPLC UV/vis system, equipped with Series 200 Auto-sampler and Series 200 Pump was used.

2.3. Membrane preparation and sensor construction

The electrode was prepared from a spectroscopic-grade graphite rod (3 mm diameter and 10 mm long). An insulated copper wire was glued to one end of the graphite rod with silver loaded epoxy resin and the rod was inserted into the end of a PVC tube. The working surface of the electrode was polished with a polishing cloth; and was rinsed with water and methanol and allowed to dry. The specified weights of LA, 190 mg of PVC and 350 μL of a plasticizer were delivered into a 5 mL vial and dissolved in 5 mL THF with magnetic stirring until the solution became clear. The polished graphite electrode was repeatedly dipped (several times with few minutes between dips) to 5 mm depth in the membrane cocktail for 2 s each time. A membrane was formed on graphite surface and left overnight. The coating solutions were stable for several weeks and could be used for the construction of new membranes

2.4. In situ-preparation of the ion-pair LA–Hg and LA–Cu

After coating the graphite electrode with the membrane which contains LA, it was allowed to stay for 48 h in a solution of 10^{-2} mol L^{-1} of $Hg(NO_3)_2$ or $Cu(NO_3)_2$ (in dark place). The mercuric or copper lipoate ion-pair was formed *in situ* inside the membrane matrix. The developed membrane electrode was conditioned for the first time by immersing the electrode in 1×10^{-3} mol L^{-1} of sodium lipoate solution at pH 8.5 for 2 days; and it was always stored in the same solution when not in use with avoiding exposure to the light.

2.5. Calibration of the new ISE electrodes

The new ISE was calibrated by immersion in conjunction with a reference electrode in a 50-mL beaker containing 9.0 mL of a Tris buffer solution of pH 8.5 ± 0.2. Then a 1.0 mL aliquot of LA solution was added with continuous stirring, to give final lipoate concentration ranging from 1×10^{-2} mol L^{-1} to 1×10^{-7} mol L^{-1}; and the potential was recorded after stabilization to ±0.5 mV. A calibration graph was then constructed by plotting the recorded potentials as a function of log[LA^{2-}]. The resulting graph was used for subsequent determination of unknown lipoate ion concentration using the same procedure.

Alternatively, the lipoate concentration can be calculated by applying the following electrode equation:

$$E = E_0 + \left(\frac{RT}{ZF}\right) \times \log[\text{lipoate}].$$

where R is the general gas constant, T temperature, Z charge of lipoate ion and F is the Faraday constant.

2.6. Sensor selectivity

Potentiometric selectivity coefficients $K^{pot}_{LA,B}$ were evaluated according to IUPAC guidelines using the separate solutions method (SSM) [23,24], in which the potential of a cell comprising the membrane electrode and a reference electrode is measured with two separate solutions, one containing the lipoate ion (LA^{2-}) of the activity a_A (but no B) and the other containing the interfering ion B of the same activity $a_A = a_B$ (but no A). Here the measured potential values are expressed by E_{LA} and E_B, respectively. Different interfering anions of a concentration of 1×10^{-3} mol L^{-1} at pH 8.0 are utilized and the results are obtained using Eq. (1).

$$\log K^{pot}_{LA,B} = \frac{E_B - E_{LA}}{S} - \left[\frac{1 - z_{LA}}{z_B}\right] \log[LA] \quad (1)$$

where $K^{pot}_{LA,B}$ is the potentiometric selectivity coefficient, S the slope of the calibration plot, a_A the activity of lipoate, and Z_{LA} and Z_B are the charges on LA^{2-} and the interfering anion, respectively. For comparison; the selectivity factors for the same ions were measured using the matched potential method MPM. In this method, the potentiometric selectivity coefficient is defined as the activity ratio of primary and interfering ions that give the same potential change under identical conditions as given in Eq. (2).

$$k^{MPM}_{A,B} = \frac{a_A{}' - a_A}{a_B} \quad (2)$$

At first, a known activity (a_A') of the primary ion solution is added into a reference solution that contains a fixed activity (a_A) of primary ions, and the corresponding potential change (ΔE) is recorded. Next, a solution of an interfering ion is added to the reference solution until the same potential change (ΔE) is recorded. The change in potential produced at the constant background of the primary ion must be the same in both cases. The MPM recommended by IUPAC in 1995 [25] is considered to be closer to practical conditions.

2.7. Flow injection analysis

Test solutions were injected using Rheodyne injection valve, Model 5060. The carrier buffer solution was propelled by means of a four channels peristaltic pump model Ismatec MCP through Tygon tubing R-3603 of 0.25 mm i.d. The proposed LA-selective electrode was used as a detecting sensor against Ag/AgCl double junction reference electrode in a home-made micro-flow cell of 250 μL volume. PC-based EMF-16 high-resolution data logger (LAWSON) was used to record and manipulate the out put signals. The waste was withdrawn using another channel of the pump. A schematic diagram for the flow injection set-up and the different flow cells are shown in Fig. 2a and b .

2.8. Determination of lipoic acid in Thiotacid tablets (600 mg), Thiotex capsules (300 mg) and urine samples

Ten tablets or the contents of 10 capsules were grinded in porcelain mortar, and an accurately weighed portion which is equivalent to the weight of one tablet or one capsule was dissolved using 0.1 mol L^{-1} NaOH solutions. After filtration, the filtrate was acidified with 0.1 mol L^{-1} H_2SO_4 drop wisely and the lipoic acid was precipitated as fine yellow crystals. The dry precipitate was dissolved in few milliliters of 0.1 mol L^{-1} NaOH and made to 100 mL volume in a volumetric flask with Tris–HCl buffer of pH 8.5. The proper volume was then used for direct or FI analysis. For urine analysis, the pH of 25 mL urine samples were adjusted to pH 8.5 using equal volume of Tris–HCl buffer solution, and spiked with different concentrations of LA. The appropriate volumes were then used for direct or FI analysis.

2.9. HPLC determination of lipoic acid

A validated method for the determination of α-lipoic acid in pharmaceutical dosage forms was used [26]. The analysis was performed using a reversed phase C18 (150 mm × 4 mm, 3 μm) column. The mobile phase consisted of acetonitrile: water (65:35, v/v) at a flow rate of 1.0 mL/min. The UV detector was set at 332 nm. A calibration graph was constructed using standard lipoate solution before analyzing the pharmaceutical and urine samples. The data obtained with this method was utilized to compare the data obtained using the direct and FI potentiometric analysis using proposed Hg–LA sensor.

3. Results and discussion

3.1. Effect of membrane composition

Lipoic acid forms highly insoluble precipitates of mercury and copper chalets when its solution is treated with mercuric nitrate or copper sulphate solutions, respectively. Brown and Edwards [27,28] have investigated the reaction of LA with some metal ions including mercury(II) and copper(II), and concluded that the analytical data (elemental and spectral analysis) indicate that the combining ratio is close to one ligand per metal ion, and no evidence was found for substance with combining ratio of 2:1. At the same time, LA offers metal ions two different binding sites, the carboxylate group and the disulphide linkage. From IR spectra in 1400–1800 cm^{-1} region, they found that in the sample of the solid adduct of Hg^{2+} and LA has a very strong band at 1704 cm^{-1}, but no absorption band at 1500 and 1600 cm^{-1}. They concluded that, in each LA residue in Hg–LA the carboxyl group has a proton and that the mercaptan group is in mercaptide ion form (but complexed, of course). At the same time, the disulphide group and the carboxylate group are too far apart in this ligand to expect a stable

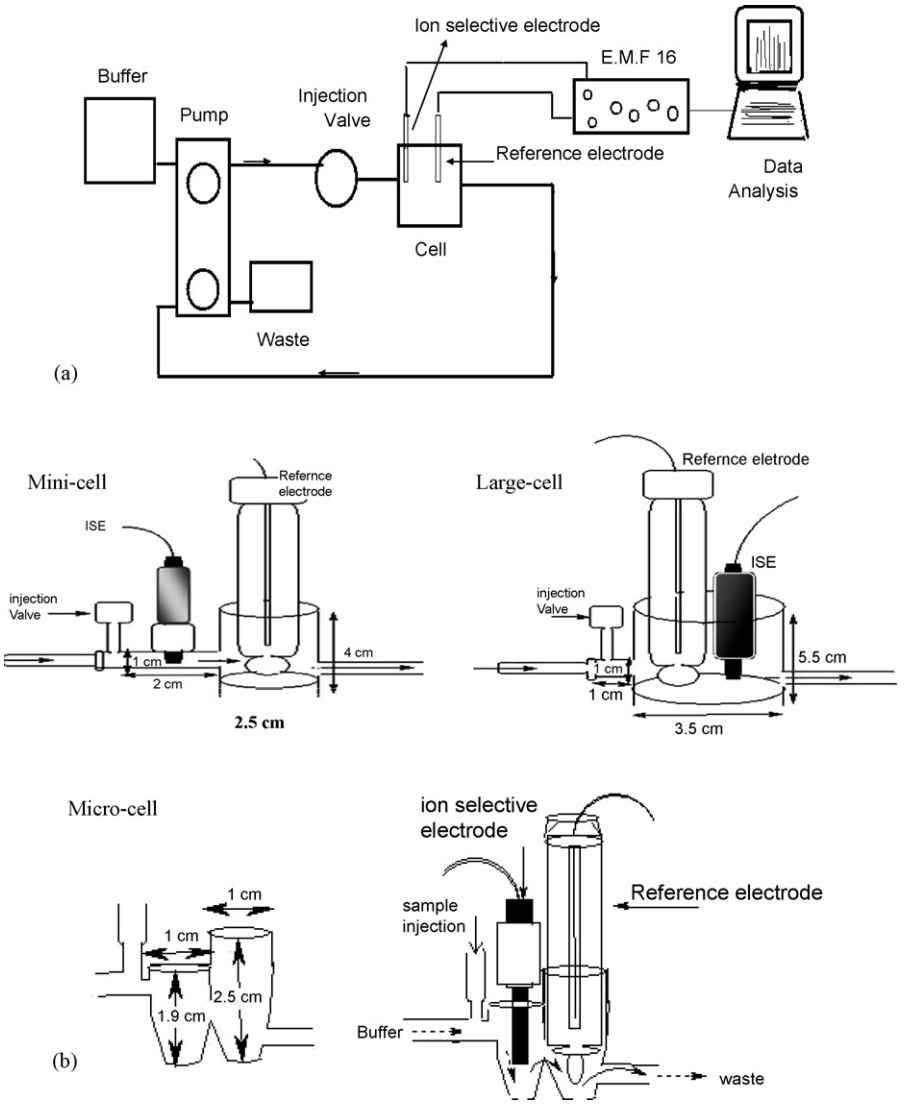

Fig. 2. (a) Schematic diagram of flow injection manifold. (b) Schematic diagram indicating shape and size of the large-, mini- and micro-flow cells.

chelation. Thus, it can be concluded that lipoate ion acts as a divalent ion in mercuric and cupric lipoate complexes, and it forms metal/lipoate charged ion complex between the metal and the sulphur atoms. Worth mentioning, that our elemental analysis and IR data of the prepared complexes are in complete agreement with that reported by Brown and Edwards. Both of the two ion-association compounds of mercury and copper were investigated as active membrane materials for constructing lipoate-selective ion-sensors. Calibration curves using PVC membranes without ion-pair (blank membrane), or containing lipoic acid, showed no potentiometric response toward the lipoate ions in solution. However, membranes contain Hg–LA or Cu–LA ion-pairs as the electroactive material, showed good linear response toward the lipoate concentration in solution as shown in Fig. 3 . It is already established that the potentiometric sensitivity and selectivity for a given ion-pair is known to depend significantly on the membrane composition [29,30]. Therefore, the variation of the type and percentage of the ion-pair and the plasticizer, and the presence of different lipophilic additives in

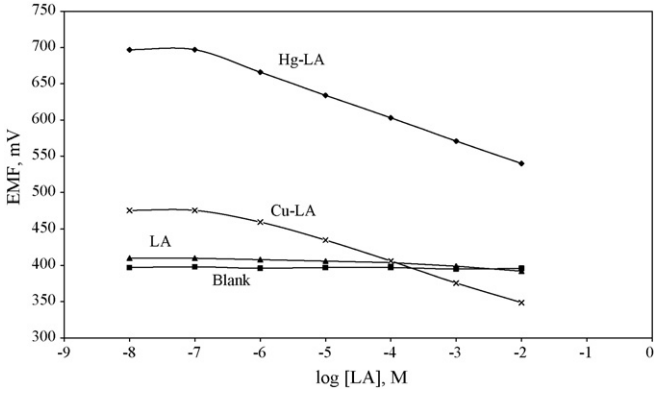

Fig. 3. Calibration graphs of different lipoate-sensors with membranes containing 7.3% of LA, Hg–LA, Cu–LA and blank membrane without any carrier, all plasticized with DOP.

Table 1
Effect of the membrane composition on the potentiometric performance of the sensor

No.	PVC (%)	DOP (%)	IP (%)	CPC (%)	TDMAC (%)	*S*	LDL	Linear range
1	35.0	65.0	0	0	0	0.5	–	–
2	30.9	61.8	7.3[a]	0	0	4.7	–	–
3	34.5	61.8	I, 3.7	–	–	25.0	3×10^{-5}	1×10^{-4} to 1×10^{-2}
4	33.0	61.8	I, 5.2	–	–	28.0	2×10^{-5}	7×10^{-5} to 1×10^{-2}
5	30.2	61.5	I, 7.3	–	–	33.2	1×10^{-5}	6×10^{-5} to 1×10^{-2}
6	33.1	61.8	II, 5.2	–	–	27.9	9×10^{-8}	2×10^{-7} to 1×10^{-2}
7	30.9	61.8	II, 7.3	0	0	29.4	9×10^{-8}	2×10^{-7} to 1×10^{-2}
8	30.5	60.0	II, 9.5	0	0	41.0	5×10^{-7}	5×10^{-5} to 1×10^{-2}
9	30.2	61.5	II, 7.3	1.0	0	27.5	3×10^{-6}	1×10^{-5} to 1×10^{-2}
10	30.0	60.1	II, 7.3	2.6	0	28.5	1×10^{-6}	1×10^{-7} to 1×10^{-2}
11	29.1	59.6	II, 7.3	4.0	0	35.5	1×10^{-5}	1×10^{-4} to 1×10^{-2}
12	30.6	61.2	II, 7.3	0	0.9	42.5	7×10^{-7}	1×10^{-6} to 1×10^{-2}
13	30.1	60.3	II, 7.3	0	2.3	29.5	8×10^{-8}	1×10^{-7} to 1×10^{-2}
14	28.8	60.0	II, 7.3	0	3.9	36.1	2×10^{-6}	1×10^{-6} to 1×10^{-2}
15	28.0	59.5	II, 7.3	0	5.2	42.0	8×10^{-6}	–

(I) for membranes containing Cu–LA and (II) for Hg–LA. *S*, slope in mV/conc. decade, LDL means lower detection limit. IP = ion-pair.
[a] Membrane contains lipoic acid.

the membrane and its effect on the potentiometric performance of membrane sensor has been carefully investigated. Table 1 , shows the effect of variation of the membrane composition on the potentiometric performance of the constructed sensor. The amount of ion-pair was found to affect the response of membrane electrode. The electrode response improved with increasing the ion-pair content in the membrane from 3.7% till the value of 7.3%. Further, addition of ion-pair resulted in diminishing the response of the electrode, which may be due to some inhomogenities and possible saturation of the membrane [31], as can be seen from Table 1. At the same time, the membranes that contain Hg–LA ion-pair expressed better performance compared to those containing Cu–LA, which may be attributed to the high stability of the mercuric–lipoate association complex and its lower water solubility. Hence, the Hg–LA ion-pair was used for further investigation. Also, it is known that the nature of the plasticizers influence both the dielectric constant of the membrane as well as the mobility of ions. Among the membranes examined using different plasticizers (NPOE, DBP, DOP, DBS) as solvent mediator, those membranes containing DOP generally, showed better potentiometric responses, i.e. better sensitivity and linearity of the calibration plots. It seems that DOP, as a low polarity compound among the plasticizers investigated, provides more appropriate conditions for incorporation of the lipophilic lipoate ion into the membrane. Therefore, we used DOP as a suitable plasticizer for further studies. At the same time, data in Table 2 reveals that by changing the plasticizer content in the membrane from 59.2% to 62.5%; the membrane containing 61.8% with a plasticizer/PVC ratio of about 2 has resulted in optimum membrane performance. As shown in Fig. 4, the potential response of the electrode was not improved in the presence of cationic additives like CTMAB, CPC and TDMAC, which confirms that the mercuric lipoate acts as a charged carrier. It is even worsened in the presence of anionic additives like STPB and Potassium tetrakis-*p*-Cl PB; and thus no additive was used in the membrane preparation.

3.2. Effect of pH value

The effect of the pH of the test solution on the response of the membrane electrode was examined at three lipoate^{2-} concentrations (1.0×10^{-3} mol L^{-1} to 1.0×10^{-5} mol L^{-1}). As illustrated in Fig. 5 the potentiometric response of the lipoiate-selective electrode was found to be independent on pH of solution in the range of 8.0–9.5. Variation of the potential at pH < 8.0 could be related to protonation of lipoate^{2-} in the aqueous phase, which results in a loss of its ability to interact with the ion-pair. At higher pH (>9.5), the potential drop (negative slope) may be due to interference of hydroxide ions.

3.3. Response time of the sensor

The response time of the electrode was measured after successive immersion of the electrode in a series of LA^{2-} solutions, where the LA^{2-} concentration was increased from 1.0×10^{-6} mol L^{-1} to 1×10^{-1} mol L^{-1}, by one order of magnitude in each time. The static response time thus obtained was 12 s for 1×10^{-2} mol L^{-1} LA^{2-}concentration. At lower concentrations, however, the response time was longer and reached 24 s for a LA^{2-} concentration of 1.0×10^{-6} mol L^{-1}. The sen-

Table 2
Effect of the ratio of different plasticizers in the Hg–LA (7.3%) membrane on the sensor performance

No.	PVC (%)	DOP	NPOE	DBS	DBP	Slope	R^2
1	30.95	0	61.8	0	0	14.8	0.9894
2	30.95	0	0	61.8	0	22.4	0.9983
3	30.95	0	0	0	61.8	21.8	0.9791
4	33.5	59.2	0	0	0	46.5	0.9997
5	32.77	59.93	0	0	0	38.0	0.9998
6	32.69	60.06	0	0	0	35.0	1.0
7	31.55	61.2	0	0	0	32.5	0.9996
8	30.95	61.8	0	0	0	31.5	0.9996
9	30.25	62.5	0	0	0	27.5	0.9999

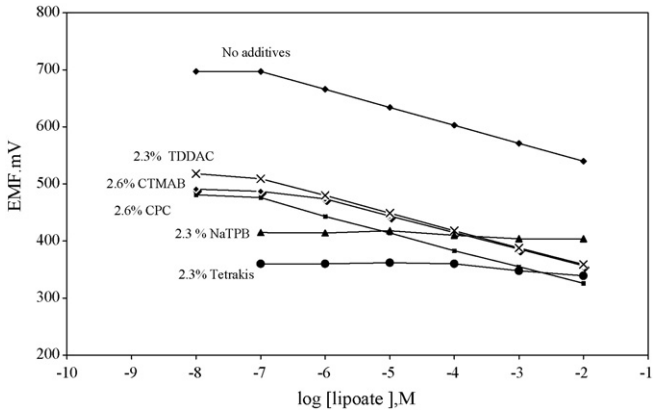

Fig. 4. Effect of both cationic and anionic lipophilic additives on the potentiometric performance of the Hg–LA membrane sensor.

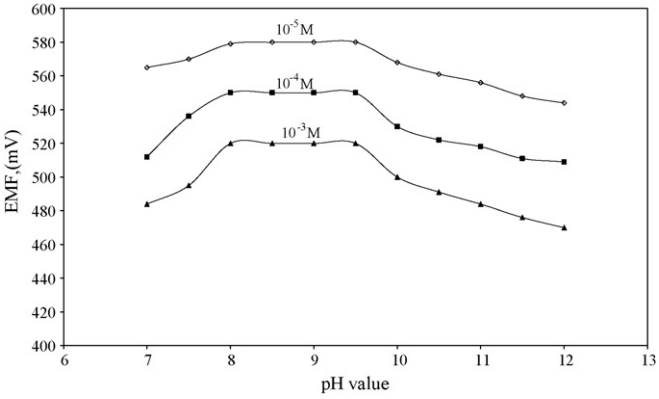

Fig. 5. Effect of pH on potential response of LA ion-selective electrode using 1.0×10^{-3} M, 1.0×10^{-4} M and 1.0×10^{-5} M of sodium lipoate solution.

sor response remained constant for approximately 5 min, after which very slow changes within the resolution of the meter were recorded. The sensing behavior of the membrane electrode did not depend on whether the potentials were recorded from low to high concentrations or vice versa.

3.4. Reproducibility and stability of the Hg–LA electrode

The reproducibility and stability of the coated graphite electrode was evaluated by repeated calibration of the electrode in sodium lipoate solutions. The repeated monitoring of potentials and calibration, using the same electrode, over several days gave good slope reproducibility; almost over a period of six weeks, with standard deviation (S.D.) of slope $\leq$0.5 mV decade^{-1}. For 10 successive replicate measurements at 1.0×10^{-3} mol L^{-1} lipoate concentrations the S.D. was 1.38 mV. The specifications and general characteristic performance of the proposed lipoate sensor is given in Table 3 .

Table 3
Specifications and characteristic performance of the lipoate ion-selective electrode based on the Hg–LA carrier

Properties	Values/range
Optimized membrane composition	IP (7.3%), PVC (30.9), DOP (61.8%)
DOP/PVC weight ratio	1.996
Electrode type	Coated-graphite electrode
pH range	8.0–9.5
Conditioning time	At least 24 h in 0.01 M LA solution
Linear range (LA^-, M)	1×10^{-7} to 1×10^{-2}
Slope (mV decade^{-1})	−29.4
Detection limit (M)	$<9 \times 10^{-8}$
S.D. of slope (mV decade^{-1})	0.22
S.D. of measurement, log conc.	0.2 at 1×10^{-2} M, 0.4 at 1×10^{-4} M
Response time (s)	12–24
Life time of the electrode	At least 6 weeks

3.5. Selectivity of the sensor

The most important characteristics of any ion-sensitive sensor are its response to the primary ion in the presence of other ions in solution, which is expressed in terms of the potentiometric selectivity coefficient. Potentiometric selectivity coefficients $K^{pot}_{LA,B}$ describing the preference of the membrane for an interfering ion B^- relative to LA^{2-} were determined by the separate solutions method (SSM), and matched potential method (MPM). Table 4 lists the potentiometric selectivity coefficient data of the sensor for several anions relative to LA^{2-}. From the table it is clear that all studied ions do not interfere with the determination of lipoate ion. Mercuric ions forms with sulfur a very insoluble complexes where for instance the solubility product of mercuric(II)sulfide being in the order of 2×10^{-54}, for the red form and 2×10^{-53} for the black form. Lipoic acid forms with mercuric ions spontaneous white precipitate of expected very low solubility product which is may be comparable to that of mercuric sulfide. Such high affinity of lipoate to mercuric ions

Table 4
Selectivity coefficients of diverse ions determined by SSM and MPM

Interfering ion	$K^{pot}_{LA,B}$	$k^{MPM}_{LA,B}$	Interfering ion	$K^{pot}_{LA,B}$	$k^{MPM}_{LA,B}$
SCN^-	1.12×10^{-3}	1.13×10^{-3}	S^{2-}	2.75×10^{-4}	2.78×10^{-3}
ClO_4^-	4.4×10^{-4}	4.01×10^{-4}	CO_3^{2-}	3.91×10^{-4}	3.21×10^{-4}
F^-	2.55×10^{-4}	1.77×10^{-4}	Sulfosalicylate^{2-}	1.72×10^{-4}	1.71×10^{-3}
Cl^-	1.26×10^{-4}	4.12×10^{-5}	Thiosalicylate^{2-}	2.45×10^{-3}	2.67×10^{-3}
Br^-	1.86×10^{-4}	9.9×10^{-5}	PO_4^{3-}	9.37×10^{-4}	2.08×10^{-3}
I^-	6.02×10^{-4}	5.76×10^{-4}	Citrate^{3-}	1.43×10^{-4}	2.38×10^{-4}
NO_3^-	1.47×10^{-4}	6.98×10^{-5}	Methionine$^-$	1.20×10^{-2}	5.29×10^{-3}
NO_2^-	1.16×10^{-4}	3.8×10^{-5}	Cystine^{2-}	2.10×10^{-2}	1.30×10^{-2}
CH_3COO^-	1.72×10^{-4}	9.49×10^{-5}	DHLA	7.40×10^{-2}	7.90×10^{-2}

may explain the enhanced selectivity of the mercuric lipoate carrier toward the lipoate ion.

3.6. Flow injection analysis

The proposed lipoate-selective CGE was successfully used as a suitable indicator electrode in flow injection potentiometry (FIP). In order to achieve the best FIP response, several flow injection parameters including the volume of the flow-cell, tubing length, flow-rate and sample volume were thoroughly investigated. The volume and shape of the home-made flow-cell was found to influence the potentiometric peaks of lipoate. It has been found that as the cell volume decreases the peak shape become more symmetrical with increase in the amplitude. The micro-flow cell (Fig. 2b) with a volume of about 1.5 mL for the sensor compartment and an actual volume of 250 μL with having the electrode inserted inside it, has allowed for optimum peaks .The length of tubing from injection valve port to cell was made as small as practical to minimize dispersion and dilution. Thus, for the proposed electrode, 1 cm was selected for tubing length with respect to peak heights. The home-made flow cell used in this study made it possible to work at flow rates higher than those previously reported in the literature [32]. The dependency of the peak heights and peak width (and time to recover the base line) with flow rate was studied using the electrode response to a 1.0×10^{-3} mol L^{-1} solution of lipoate ion. It has been found that when the flow rate increased, the peaks became narrower and increased in height, however, the peak width increased again at flow rates higher than 35 mL/min. At a flow rate of 30 mL/min. for sample concentration of 1.0×10^{-6} mol L^{-1} and 1.0×10^{-2} mol L^{-1} the peak reaches its maximum height in 10–15 s and the base line is recovered after 45–60 s, respectively. Thus, flow rate of 30 mL/min was selected as an optimum value for further studies, which allows for reasonable sampling rate and decreases the total time of analysis. In general, the peak heights increased with the increasing sample volume, although the effect was less marked at higher concentrations [33,34]. For the proposed sensor, different sample volumes of 100 μL, 250 μL and 500 μL were studied; the peak height reached nearly 100% of steady-state at 500 μL injected, and was selected as an optimum volume. It is well-known that, in FIP, the composition of the carrier solution also affects the response behavior of ion-selective electrode in terms of the base line stability [32]. In the proposed flow method, HCl –Tris buffer solution of pH 8.5 was used as carrier, which resulted in quite stable base lines. The proposed potentiometric FIA system revealed sampling rates higher than 30 injections per hour. In Fig. 6 are shown the triplicate peaks from the proposed FIP method obtained under optimal experimental conditions for varying concentrations of [LA^{2-}] solutions in the range of 1.0×10^{-6} to 1.0×10^{-2} mol L^{-1}. The repeatability of the electrode response, as evaluated from the peak height relative standard deviation (%R.S.D.) for more than 15 replicate injections of 1.0×10^{-3} mol L^{-1} solutions of lipoate ion was ±1.15%. A comparison of the characteristic performance of the lipoate sensor under direct and flow measuring conditions, including linear range and LDL, as recommended by IUPAC [35] is shown in Table 5, where the data reveals satisfactory agreement.

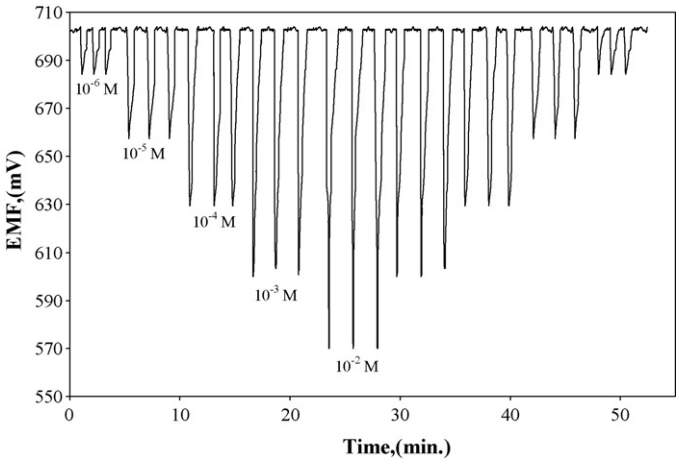

Fig. 6. Potentiometric peaks for triplicate measurements of different LA^{2-} ion concentrations at a flow rate of 30 mL/min. The lipoate ion concentrations (in sample volumes of 500 μL): 1.0×10^{-6} M, 1.0×10^{-5} M, 1.0×10^{-4} M, 1.0×10^{-3} M and 1.0×10^{-2} M. Stability of lipoate-sensor response over more than 15 replicate injections of 250 μL of 10^{-3}M lipoate solution at flow rate of 20 mL/min.

3.7. Analytical applications

3.7.1. Determination of LA in pure solution, pharmaceutical preparations and urine by direct potentiometry and FI methods

The proposed sensor in a FIP analysis was proved to work well under laboratory conditions. A quantitative recovery of LA in pure lipoic acid solution, tablet and capsule formulation, and spiked urine samples has been achieved using the direct and FI potentiometric methods. The results were compared to those provided by HPLC validated method [26]. The statistical Student's *t*-test and the *F*-tests were selected for this purpose. Considering as null hypothesis that the two methods agree, a paired two-tail test for 5% level of significance gave a calculated *t* values below the tabulated one ($t_{0.05(4)} = 2.77$), therefore accepting the null hypothesis. The comparison of variances attained for each sample was made by the *F*-test using the same assump-

Table 5
Comparison of the performance of the sensor in batch and dynamic methods

Potentiometric method	Slope ± S.D. (mV/decade)	Intercept (mV)	LDL[a] (M)	Linear range (M)	r^2	Response time (s)
Direct	29.4 ± 0.22	489.9	9×10^{-8}	1.5×10^{-7} to 1×10^{-2}	0.99998	12–24
Flow injection	29.1 ± 0.26	520.9	4×10^{-7}	2.5×10^{-6} to 1×10^{-2}	0.99923	10–25

[a] Lower detection limit

Table 6
Determination of LA in Thiotacid® tablets 600 mg and Thiotex® capsules 300 mg and urine by direct and FI potentiometric methods using the proposed sensor with comparison to HPLC recommended method

Sample	Taken (mg/mL)	Direct		FIA		HPLC
		Found (mg/mL)	Recovery (%)	Found (mg/mL)	Recovery (%)	Recovery (%)
Pure solution	2.00	1.98	99.14 ± 0.53, *t*-test = 1.3, *F*-test = 1.2	1.97	98.83 ± 0.72, *t*-test = 1.7, *F*-test = 1.5	99.59 ± 0.55
Thiotacid® tablet	6.00	5.93	98.88 ± 0.39, *t*-test = 1.5, *F*-test = 3.5	5.93	98.84 ± 0.31, *t*-test = 1.9, *F*-test = 5.4	99.33 ± 0.33
Thiotex® capsule	3.00	2.97	99.03 ± 0.61, *t*-test = 1.6, *F*-test = 1.98	2.98	99.2 ± 0.58, *t*-test = 1.3, *F*-test = 1.7	99.73 ± 0.44
Urine	3.00	2.98	99.57 ± 0.24, *t*-test = 2.1, *F*-test = 1.5	2.98	99.37 ± 0.34, *t*-test = 2.5, *F*-test = 1.3	100.03 ± 0.29

Theoretical values of $t = 2.77$ and $F^{2,2} = 19.0$, at 95% confidence level.

tions as for the Student's *t*-test, and the calculated values were always below the critical *F*-value ($F_{0.05(2,2)} = 19.0$), thus confirming the null hypothesis. The data summarized in Table 6, reveal that the results of both direct and FI methods are of comparable precision to those of the recommended method and there is no significant difference between the mean values obtained by both methods. The recovery of LA from spiked urine samples over concentration range of 0.2–2.0 mg/mL was found to be quantitative.

3.7.2. Potentiometric titration of lipoic acid with the proposed sensor

The proposed Hg–LA sensor in conjunction with a silver/silver chloride reference electrode has been applied as an indicator electrode for the potentiometric titration of lipoic acid with mercuric nitrate solution. The result for titration of 10 mL of 1×10^{-3} mol L^{-1} lipoate solution titrated with a 1×10^{-3} mol L^{-1} $Hg(NO_3)_2$ solution indicate that the concentration of lipoate could be accurately determined with the proposed electrode. The titration graph shows a very good inflection point, indicating perfect 1:1 stoichiometry.

4. Conclusions

CGE electrode that allows a highly selective FIP analysis of lipoate acid was successfully prepared. The use of home-made micro-flow cell enhanced the method sensitivity. The sensitivity, linear range and slope are independent on the pH of the between 8.0 and 9.5. The application of the proposed electrode to the determination of lipoic acid in its pure solutions and pharmaceutical preparations is characterized by a high degree of precision and accuracy when compared to the validated HPLC method. The FIA conditions shortened the time needed for the determination when compared with the previous published methods of determination of LA, besides being of less expenses and easy to construct and use.

References

[1] E.E. Snell, F.M. Strong, W.H. Peterson, Biochem. J. 31 (1937) 1789.
[2] L.J. Reed, B.G. DeBusk, I.C. Gunsalus, C.S. Hornberger, Science 114 (1951) 93.
[3] L.J. Reed, Adv. Enzymol. 18 (1957) 319.
[4] H.R. Rosenberg, R. Culik, Arch. Biochem. Biophys. 80 (1959) 86.
[5] L. Packer, H.J. Tritschler, K. Wessel, Free Radic. Biol. Med. 22 (1997) 359.
[6] H. Moini, L. Packer, N.L. Saris, Toxicol. Appl. Pharmacol. 182 (2002) 84.
[7] R.L. Keith, I. Setiarahardjo, Q. Fernando, H.V. Aposhian, A.J. Gandolfi, Toxicology 116 (1997) 67.
[8] P. Ou, Biochem. Pharm. 50 (1995) 123.
[9] A.I. Bush, Neurobiol. Aging 23 (2002) 1031.
[10] L. Holmquist, G. Stuchbury, K. Berbaum, S. Muscat, S. Young, K. Hager, J. Engel, G. Münch, Pharmacol. Ther. 113 (2007) 154.
[11] D.R. Tomlinson, Diab. Metab. 24 (1998) 79.
[12] S.A. Farr, H.F. Poon, A.K.D. Dogrukol, J. Drake, W.A. Banks, E. Eyerman, D.A. Butterfield, J.E. Morley, J. Neurochem. 84 (2003) 1173.
[13] L. Patrick, Altern. Med. Rev. 5 (2000) 290.
[14] A. Bilska, L. Wlodek, Pharmacol. Rep. 57 (2005) 570.
[15] A.A. Herbert, J.R. Guest, Methods Enzymol. 18A (1970) 269.
[16] A.I. MacLean, L.G. Bachas, Anal. Biochem. 195 (1991) 303.
[17] Y.J. Suzuki, M. Tsuchiya, L. Packer, Methods Enzymol. 234 (1994) 454.

[18] H. Kataoka, J. Chromatogr. B 717 (1998) 247.
[19] K.C. Panak, O.A. Ruiz, S.A. Giorgieri, L.E. Diaz, Electrophoresis 17 (1996) 1613.
[20] E. Bakker, E. Pretsch, Anal. Chem. 74 (2002) 420 A.
[21] E. Bakker, Y. Qin, Anal. Chem. 78 (2006) 3965.
[22] Z. Szigeti, T. Vigassy, E. Bakker, E. Pretsch, Electroanalysis 18 (2006) 1254.
[23] G.G. Guibault, R.A. Durst, M.S. Frant, H. Freiser, E.H. Hansen, T.S. Light, E. Pungor, G. Rechnitz, N.M. Rice, T.J. Rohm, W. Simon, J.D.R. Thomas, Pure Appl. Chem. 48 (1976) 127.
[24] K. Umezawa, Y. Umezawa, CRC Handbook of Ion-Selective Electrodes: Selectivity Coefficients, CRC Press, Boca Raton, 1990.
[25] Y. Umezawa, K. Umezawa, H. Sato, Pure Appl. Chem. 67 (1995) 507.
[26] H.Y. Aboul-Enein, H. Hoenen, J. Liq. Chromatogr. Relat. Technol. 27 (2004) 3029.
[27] P.R. Brown, J.O. Edwards, Biochemistry 8 (1969) 1200.
[28] P.R. Brown, J.O. Edwards, J. Inorg. Nucl. Chem. 32 (1970) 2671.
[29] G. Horvai, E. Graf, K. Toth, E. Pungor, R.P. Buck, Anal. Chem. 58 (1986) 2735.
[30] K.C. Gupta, M. Jeanne D' Arc, Talanta 52 (2000) 1087.
[31] X. Yang, N. Kumar, H. Chi, D.B. Hibbert, P.W. Alexander, Electroanalysis 9 (1997) 549.
[32] P.W. Alexander, T. Dimitrakopoulos, D.B. Hibbert, Electroanalysis 10 (1998) 707.
[33] X. Yang, D.B. Hibbert, P.W. Alexander, Anal. Chim. Acta 372 (1998) 378.
[34] C.M. Couto, J.L.F.C. Lima, M. Conceicao, B.S.M. Montenegro, S. Reis, J. Pharm. Biomed. Anal. 18 (1998) 527.
[35] R.P. Buck, E. Lindner, Pure Appl. Chem. 66 (1994) 2527.

Available online at www.sciencedirect.com
ScienceDirect
Talanta 74 (2008) 1450–1454
Talanta
www.elsevier.com/locate/talanta

A microcalorimetric sensor for food and cosmetic analyses: L-Malic acid determination

Marta Letizia Antonelli *, Claudio Spadaro, Rosalia Fortunata Tornelli

Dipartimento di Chimica, Università degli Studi di Roma "La Sapienza", Piazzale Aldo Moro, 5, 00185 Rome, Italy

Received 29 January 2007; received in revised form 5 September 2007; accepted 28 September 2007
Available online 2 October 2007

Abstract

Enzymatic microcalorimetry has been successfully employed in the reliable determination of the L-malic acid concentration in some foods and cosmetic products. The L-malic acid concentration during the wine-making process is particularly useful in order to control the progress of the malo-lactic fermentation. Total acidity, taste and flavour characteristics of wine depend on the L-malic acid quantity still present.

To point out the analytical methodology the dehydration process of L-malic acid, in the presence of *Fumarase* enzyme, has been used. The new method has been compared with a common spectrophotometric one.

By the proposed calorimetric method the L-malic acid concentration in different types of food (white and red wines, fruits and soft beverages) has been determined. In some cosmetic products too the L-malic acid was quantified.

The method outlined resulted simple, direct and reliable (good accuracy and precision), in particular it does not require any pre-treatment or clean up of the samples, save the dilution in buffer.
© 2007 Elsevier B.V. All rights reserved.

Keywords: L-Malic acid; *Fumarase* enzyme; Food; Cosmetics; Calorimetric sensor

1. Introduction

The L-isomer of malic acid is the natural form of this acid, therefore, it is present in many foods, for example, fruits and wine; only if the synthetic racemate is used as an additive in food industry, the D-malic acid could be found [1].

In the food industry, in particular in soft drinks, fruit juices and wine production, the L-malic acid determination is widely employed [2]. The L-malic acid being a component of those products gives the particularly acidic flavour and taste if present in the proper quantity, otherwise the good characteristics of those foods are altered.

Together with the tartaric acid the L-malic acid is a fundamental component of wine, they represent about the 90% of the wine total acidity [3]; L-malic acid is the substrate of a bio-transformation process named the malo-lactic fermentation (MLF) [4]. This is an important process in wine production, not only due to the partial de-acidification determined by the transformation of L-malic in L-lactic acid, but also because it contributes in the *bouquet* of fragrances and in the microbiological stability of wine [5]. The MLF fermentation, due to some bacteria naturally present in wine, is a spontaneous phenomenon really unpredictable, especially when the initial L-malic concentration in must is high: in these cases the final product could present a disagreeable taste and flavour [6].

In the literature many different methods for L-malic acid determination are reported: the chromatographic ones [7,8] present high sensitivity and precision, but need long and tedious clean up and generally are not so recommended if only one analyte must be quantified. Many other methods based on enzymatic reactions (i.e., photometric and electrochemical ones) make use of the enzymatic transformation of L-malic acid to oxaloacetic acid in the presence of NAD^+/NADH. Being this reaction unfavourable from a thermodynamic point of view, it is always necessary to force it by means of secondary reactions and particular pH conditions [9]. The electrochemical methods too necessitate of an enzymatic reactions chain in order to obtain a final product easily measurable by ISE electrodes [10,11].

The new method here outlined is direct and easy, is based on the microcalorimetric technique and uses the enzymatic dehy-

* Corresponding author. Tel.: +39 0649913618; fax: +39 06490631.
E-mail address: marta.antonelli@uniroma1.it (M.L. Antonelli).

0039-9140/$ – see front matter © 2007 Elsevier B.V. All rights reserved.
doi:10.1016/j.talanta.2007.09.035

dration of L-malic acid catalysed by the *Fumarase* enzyme [12,13].

By this methodology [14] the L-malic acid concentration is directly correlated with the heat quantity associated with the enzymatic reaction, a main parameter of the reaction employed (ΔH_{react}), without chain reactions. Moreover, by this technique samples as emulsions and suspensions can be immediately analysed [15], therefore, the proposed method can be usefully adopted to control food products and also the wine-making process.

Owing to the fact that in the last years the acids named AHA (α-hydroxy acids) such as the L-malic acid, have been widely used in the cosmetic field, especially for their anti-aging effect on skin, but at the same time they showed some sensitisation effects of the skin to the UV radiations, the accurate determination of their concentration in the cosmetic products has become of interest [16]. The method has been, therefore, applied to the analysis of some cosmetic creams containing AHA in hydrophobic matrices.

2. Experimental

2.1. Materials

All common chemicals were commercial products of analytical grade (purity ≥ 99%). L-Malic acid was a Sigma–Aldrich Co. product; Fumaric acid 99% of purity was from Sigma. *Fumarase* enzyme (EC 4.2.1.2) (1 IU-International Unit- will convert a 1.0 μmol of L-malate to fumarate per minute at pH 7.4 at 25 °C) suspension from porcine heart was from Sigma–Aldrich Co.

L-Tartaric acid and L-ascorbic acid were from Carlo Erba. The enzymatic kit (L-malic UV test) used for the spectrophotometric assay was from Boehringer-Mannheim.

Industrial wine samples were kindly provided from "Cantina Sivestri" and those of artisan production from "Teatini" and "Ambrosini" families. All other food and cosmetic samples were common shelf products. Buffer solution at pH 7.4 was obtained with KH_2PO_4 and Na_2HPO_4 (5×10^{-3} mol L^{-1}) salts. All solutions were prepared in doubly distilled water and maintained at 4 °C until used, if necessary.

2.2. Apparatus

The microcalorimeter used is an isothermal batch instrument [17] of the heat conduction type (LKB Model 2107), equipped with two gold vessels of about 7 mL total volume, a multi-temperature cooling circulator (LKB Model 2209), a control unit (LKB Model 2107-350) and a potentiometric recorder (LKB Model 2210). Each vessel consists of a chamber partially divided in two compartments (2.5 and 4.5 mL) by an interior wall. The reactants are inserted into the two compartments separately. When the experiment begins the calorimetric drum rotates, thereby the reactants are mixed and the reaction takes place.

All the equipment was housed in a thermostatic room at 25 ± 1 °C and all measurements were made at 25.00 ± 0.01 °C. The calorimetric accuracy was checked by measuring the sucrose dilution heat. The results were consistent with the literature values within 0.5% [18].

In order to check the purity of the L-malic acid standard a thermo-gravimetric measurement, by using a Perkin-Elmer TGS-2 thermo-balance, has been performed. Water content resulted less than 1% at low temperatures and after that the total decomposition of L-malic molecule was observed.

Spectrophotometric measurements were performed by means of the UV/vis Philips Pye-Unicam PU 8800 spectrophotometer.

The pH of the solutions has been measured with a pH-meter Gibertini with an Ingold glass-combined electrode.

A homogeniser Ika Ultra turrax T 18 Basic was used.

To sonicate some cosmetic and food samples the ultrasound apparatus AGE Elettronica mod. Acivar was employed.

2.3. Methods

2.3.1. Calorimetric method

The enzymatic reaction used in this analytical method is the dehydration of the L-malic acid to fumaric acid in the presence of the *Fumarase* enzyme. This reaction in fact is of the equilibrium type, but it is stereo-specific for the L-malic substrate, while it is not in the case of the fumaric acid [19]. The concentration and pH conditions strongly influence the reaction, and moreover, the low solubility of fumaric acid [13] allows the L-malic acid to be transformed in fumaric easier than the inverse.

The reaction is rapid and it is overseen by microcalorimetry [20,14], by using the linear relationship between the involved heat ($Q_{reaction}$) and the L-malic acid concentration:

$$Q_{reaction} \propto C_{substrate}.$$

This relationship is linear if the appropriate kinetic conditions are realised: that is in excess of enzyme, first order kinetics with respect to the substrate. The heat quantity involved in each run is obtained by the equation:

$$Q_{reaction} = \varepsilon A_{reaction}$$

where ε is an instrumental constant (expressed in mcal cm^{-2}), determined by a series of electrical calibrations, which depends on the physical features of the calorimeter in different experimental conditions of temperature, sensitivity and record scale. $A_{reaction}$ is the area (expressed in cm^2) subtended by the curve (voltage function of time), which is the instrumental output in each run and $Q_{reaction}{:}A_{reaction} = Q_{calib}{:}A_{calib}$. By means of a calibration curve ($Q_{reaction}$ in function of L-malic acid concentration) obtained with standards, it is possible to calculate the analyte content in samples.

The instrument was filled as follows: the two compartments of the sample vessel were filled with 2 mL of the enzyme solution and 2 mL of the substrate solution, respectively, while the reference vessel was filled with 2 mL of the buffer solution and 2 mL of the substrate solution, respectively, in order to subtract the dilution heat of the L-malic solution from the total heat of reaction. The dilution heat of the enzyme has been checked by preliminary experiments, and it was subtracted from the total heat measured in each measure.

The reported concentrations refer to the solutions inside the calorimeter before mixing.

To obtain the calibration curve and also to analyse real samples, preliminary experiments were run to find out the best operative conditions.

The optimum enzyme activity was determined by checking the calorimetric responses fixing the substrate concentration and changing the enzyme activity. The overall heat quantities recorded showed a maximum at about 18 IU mL^{-1} of enzyme activity. Therefore, all the analyses were performed in enzyme excess, i.e., first-order kinetics with respect to the substrate, with an enzymatic activity [E] equal to 18 IU mL^{-1}. To maintain the optimum pH value, as reported in the literature for this enzyme [21], two different buffers (Tris/HCl and phosphate) were checked and the phosphate one was chosen, giving the best calorimetric output.

The operative conditions used were: $T = 25\,^{\circ}$C; pH 7.4 (phosphate buffer, 5×10^{-3} mol L^{-1}); [E] = 18 IU mL^{-1}, which resulted the best for samples and enzyme solutions. Each calorimetric run took about 20 min.

The stability of the enzyme solution has been controlled during the period it was used (2 days at the most).

2.3.2. Spectrophotometric method

In order to test the calorimetric method here proposed a spectrophotometric method [22], which forecasts a commercial kit of analysis [23] based on the following enzymatic reaction sequence, has been used:

$$\text{L-malate} + \text{NAD}^{+} \overset{\text{L-MDH}}{\longleftrightarrow} \text{oxaloacetate} + \text{NADH} + \text{H}^{+}$$

$$\text{oxaloacetate} + \text{L-glutamate} \overset{\text{AST}}{\longleftrightarrow} \text{L-aspartate} + \alpha\text{-chetoglutarate}$$

where MDH is the *Malic dehydrogenase* enzyme and AST is the *Aspartate amino transferase* enzyme. By monitoring the formation of the maximum of absorbance of the NADH at 340 nm, the L-malic concentration is determined. The second enzymatic reaction is necessary in order to force the first reaction toward the oxaloacetate formation, as above reported.

3. Results

3.1. Calibration curve

By using the best operative conditions for L-malic acid analysis, the calibration curve has been obtained in a first-order kinetics with respect to the substrate (excess of enzyme). The calibration curve has been pointed out by using standards of pure L-malic acid at increasing concentrations; the values represent the average of three replicates of each standard solution. The investigated range of concentrations was between 5×10^{-4} and 2×10^{-2} mol L^{-1} (0.07–2.68 g L^{-1}). The equation describing the calibration plot is:

$$Q_i = 10.52 C_i$$

Q_i is the reaction heat associated with each concentration value examined and it is expressed in mcal, C_i is the L-malic acid concentration expressed in g L^{-1}, the r^2 is equal to 0.9991. The trend is linear in the examined interval; over 2.68 g L^{-1} a negative deviation from the linearity has been observed, probably due to the partial incoming of the inverse reaction catalysed by the same *Fumarase* enzyme.

To obtain the calibration curve useful for the L-malic acid analysis, the microcalorimeter was filled as follows, giving the overall heat quantity (Q_{tot}):

sample vessel	**reference vessel**
Fumarase solution (18 IU ml^{-1})	buffer solution
2 ml	2 ml
L-malic acid solution (C_i)	L-malic acid solution (C_i)
2 ml	2 ml

To calculate the correct heat quantity (Q_i) associated with each different concentration of standard L-malic acid (C_i), the calorimetric area submitted by the curve voltage versus time has been multiplied for the appropriate ε value to obtain the overall heat quantity and then the heat of dilution related with the enzyme solution (Q_E) has been subtracted as follows.

$$Q_i = Q_{tot} - Q_E$$

Being the excess of enzyme constant, the Q_E value is always the same in all runs.

Also, the standard addition method has been performed in order to validate the calorimetric method. By using a sample of wine, three different solutions with increasing additions of standard L-malic acid have been prepared. The concentration value of L-malic acid in the wine sample has been extrapolated by plotting the L-malic acid concentrations (g L^{-1}) versus volumes (mL) of standards added and it was in good agreement

Table 1
L-malic acid concentrations found in different food samples by the calorimetric method

Liquid food products	[L-Malic acid] (g L^{-1})	S.D.
New red wine (North-East Italy)	4.76	0.06
Red wine 2003 (North-West Italy)	2.84	0.02
White wine 2005 (Central Italy)	2.64	0.04
White wine 2004 (Central Italy)	2.99	0.03
Soft drink	0.40	0.02
Apple juice (50% of fruit)	1.70	0.03
Solid food products	**[L-Malic acid](g per 100 g)**	**S.D.**
"Fuji" apple (ripe)	0.59	0.02
Mandarin (unripe)	0.24	0.03
Mandarin (ripe)	0.14	0.02
Powder for making carbonated water	5.17	0.04

Operative conditions: $T = 25\,^{\circ}$C, pH 7.4 (phosphate buffer, 5×10^{-3} mol L^{-1}); [*Fumarase* enzyme] = 18 IU mL^{-1}.

Table 3
L-Malic acid determination in white wine samples, during the wine-making process by the calorimetric method

Samples	[L-Malic acid] ($g\,L^{-1}$)	S.D.
Must	6.42	0.06
Must-wine	3.94	0.04
Wine	2.57	0.04
Wine (just bottled)	1.76	0.03
Wine bottled (1 year later)	1.74	0.02

Operative conditions: $T = 25\,^{\circ}C$, pH 7.4 (phosphate buffer, 5×10^{-3} mol L^{-1}); [*Fumarase* enzyme] = 18 IU mL^{-1}.

Table 2
L-Malic acid concentrations found in cosmetic creams by the calorimetric method

Products	[L-Malic acid](g per 100 g)	S.D.
Night face-cream	0.86	0.07
Hand-cream	Not found	
Foot-cream	1.56	0.04
Scrub body-cream	1.95	0.05

Operative conditions: $T = 25\,^{\circ}C$, pH 7.4 (phosphate buffer, 5×10^{-3} mol L^{-1}); [*Fumarase* enzyme] = 18 IU mL^{-1}.

(within 1%) with the experimental value obtained by the direct calorimetric measure on the same sample of wine. The calorimetric method turned out good and reliable due to accuracy (0.05% < error < 0.4%) and precision (C.V. < 1%).

3.2. Application to real samples

3.2.1. Analysis of L-malic acid in foods and cosmetics

By means of the microcalorimetric methodology here described several food products: fruits, fruit juices, soft drinks, red and white wines and also some cosmetic creams for dermatological applications have been analysed.

The wine samples, owing to the high concentration of malic acid, have been diluted in buffer. The cosmetic samples have been homogenised and dissolved in buffer.

The analyses of real samples were repeated thee times for each sample and in Table 1 the relative average values and standard deviations (S.D.) are reported.

The high concentration of L-malic acid found in the new wine with respect to others seems not strange owing to the fact that the wine-making process is quite fast with respect to the MLF transformation and sometimes in red wine must the initial L-malic acid quantity can be high.

As it can be seen the L-malic acid concentration decreases in fruits during ripening.

For the cosmetic products the ultrasound treatment was needed to obtain a more dispersed emulsion. The obtained values for the L-malic acid concentration in Table 2 are listed.

3.2.2. L-Malic acid analysis in wine-making process

The MLF (Fig. 1) starts after the alcoholic fermentation (AF) because the yeast used for this fermentation (*Saccharomyces cerevisiae*) cannot transform the L-malic acid [24]. The MLF process is slow and difficult to control because if the L-malic concentration is high in the grapes, especially when they are unripe or coming from cold regions, the fermentation does not sufficiently go on. In some cases it could be necessary to introduce specific bacteria (for example, *Oenococcus oeni*) during the wine-making process, in order to decrease this concentration [25].

During last years several yeast families have been developed (for example, *Schizosaccharomices pombe*), they convert the L-malic acid into ethanol during the AF [26], especially if grapes with high L-malic levels are employed in wine making.

The wine-making process of a non-commercial white wine has been followed to monitor the L-malic acid concentration along to the production steps (conversion time), sampling has been made as follows: (a) must, after the wine-pressing and dripping; (b) must-wine, after the AF; (c) wine, after the MLF and (d) wine just bottled, that is the final product.

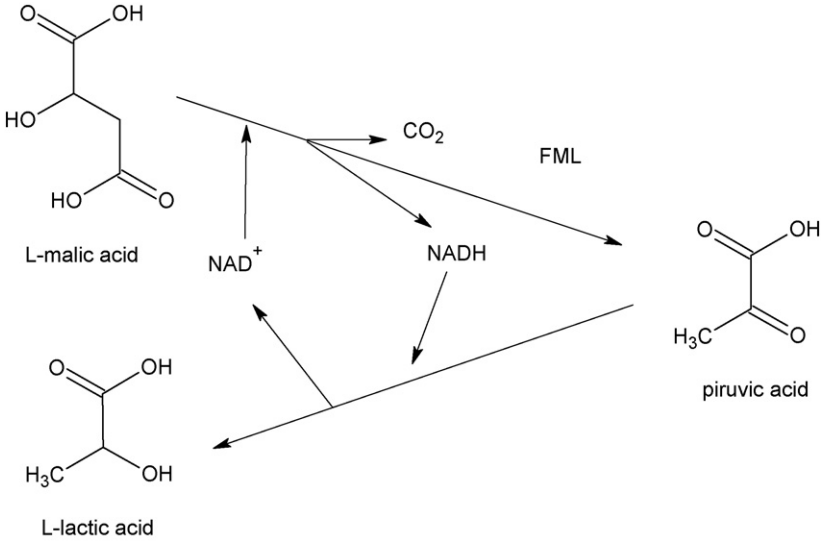

Fig. 1. Chemical reactions involved in the malo-lactic fermentation (MLF) of wine.

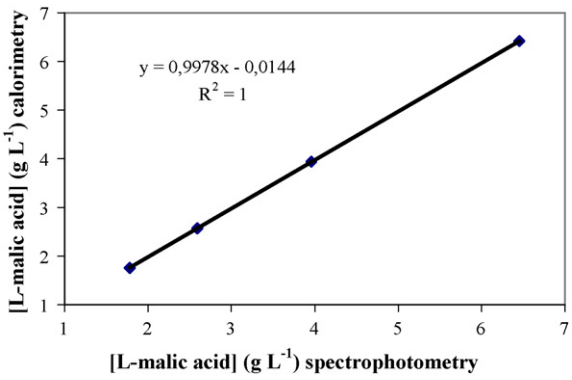

Fig. 2. Comparison between the results obtained with the new calorimetric method and a common spectrophotometric one for L-malic acid analysis.

All real samples have been diluted and the analyses were repeated three times for each sample, in Table 3 the relative average values and standard deviations (S.D.) are reported.

3.2.3. Comparison between calorimetric and spectrophotometric methods

A recommended official spectrophotometric method [22] has been used to show the validity of the new calorimetric method developed and here outlined.

Every sample listed in Table 3 has been also investigated by means of the spectrophotometric method and the correlation results are reported in Fig. 2.

As it can be observed there is a very good agreement between the two methods results.

The detection limit of the proposed calorimetric method is $0.05\,g\,L^{-1}$, the LOD is $0.07\,g\,L^{-1}$ and sensitivity is very good being the angular coefficient equal to 10,52.

Detection limit is better than that of the spectrophotometric method but a little bit worst than a sensor method proposed by Palleschi and co-workers which employs a bioreactor [11].

4. Conclusions

The new methodology here described is a good alternative for the spectrophotometric and electrochemical analysis of real complex samples such as must and wine, other beverages, solid foods and cosmetic creams.

In fact, it is a direct method, based on the measurement of an intrinsic characteristic of the reaction (the heat quantity involved in the enzymatic transformation) that can be easily and linearly related with the L-malic acid concentration. No other ancillary reactions are needed, no particular pre-treatment of the samples must be done.

The enzymatic transformation of L-malic acid into Fumaric acid, an enthalpy favoured reaction, assures the specificity of the analysis. The optimum agreement with spectrophotometric method demonstrates the validity and reliability of calorimetric method.

The calorimetric technique, in such a way used, becomes a useful biosensor for food analysis. The detection system used is available for direct routine wine analysis during wine-making process.

Moreover, the L-malic acid concentration can be assumed as a useful marker in food quality control.

References

[1] H.U. Bergmeyer, Methods of Enzymatic Analysis. Metabolites 2, vol. VII, VCH, Germany, 1985, pp. 2–12, 39–58.
[2] A.M. Almuiabed, A. Townshend, Anal. Chim. Acta 221 (1989) 337–340.
[3] V.I. Esteves, S.S.F. Lima, D.L.D. Lima, A.C. Durante, Anal. Chim. Acta 513 (2004) 163–167.
[4] D. Wibowo, R. Eschenbruch, C.R. Davis, T.H. Lee, Am. J. Enol. Vitic. 36 (1985) 302–307.
[5] F. Mizutani, S. Yabuki, M. Asai, Anal. Chim. Acta 245 (1991) 145–150.
[6] T. Henick-Kling, T.E. Acree, in: S.A. Lallemand (Ed.), Proceedings of International Symposium on the Management of the Malo-Lactic Fermentation and Quality of Wine, VINITALY, Verona, Italy, 16/04/1998, France, 1998, p. 17.
[7] S. Suarez-Luque, I. Mato, J.F. Huidobro, J. Simal-Lozano, M.T. Sancho, J. Chromatogr. A 955 (2002) 207–214.
[8] L. Alcazar, P.L. Fernandez-Caceres, M.J. Martin, F. Pablos, A.G. Gonzalez, Talanta 61 (2003) 95–101.
[9] G.C. Chemnitius, R.D. Schmid, Anal. Lett. 22 (15) (1989) 2897–2913.
[10] M.C. Messia, D. Compagnone, M. Esti, G. Palleschi, Anal. Chem. 68 (1996) 360–365.
[11] M. Esti, G. Volpe, L. Micheli, E. Delibato, D. Compagnone, D. Moscone, G. Palleschi, Anal. Chim. Acta 513 (2004) 357–364.
[12] D.A. Brant, L.B. Barnett, R.A. Alberty, J. Am. Chem. Soc. 85 (1963) 2204–2209.
[13] K. Belafi-Bako, N. Nemestothy, L. Gubicza, Desalination 162 (2004) 301–306.
[14] R.J. Wilson, A.E. Beezer, J.C. Mitchell, Thermochim. Acta 264 (1995) 27–40.
[15] M.L. Antonelli, G. D'Ascenzo, A. Laganà, P. Pusceddu, Talanta 58 (2002) 961–967.
[16] A. Al Bawab, S.E. Friberg, C. Fusco, Int. J. Cosmetic Sci. 26 (2004) 273–279.
[17] I. Wadsö, Acta Chem. Scand. 22 (1968) 927–937.
[18] P. Monk, I. Wadsö, Acta Chem. Scand. 22 (1968) 1842–1852.
[19] W. Marconi, F. Faiola, A. Piozzi, J. Mol. Catal. B: Enzymatic 15 (2001) 93–99.
[20] K.J. Grime, in: K.J. Grime (Ed.), Analytical Solution Calorimetry, vol. 79, Wiley Interscience, New York, 1985, p. 299, Chapter 7.
[21] V. Massey, Biochem. J. 53 (1953) 72–79.
[22] I. Mato, J.F. Huidobro, et al., Food Chem. 62 (1998) 503–508.
[23] H. Möllering, in: Bergmeyer (Ed.), Methods in Enzymatic Analysis, vol. VII, Verlag Chemie, Basel, 1985, pp. 39–47.
[24] G. De Revel, A. Bloem, M. Augustin, A. Lonvaud-Funel, A. Bertrand, Food Microb. 22 (2005) 569–575.
[25] J.F. Gallander, Am. J. Enol. Vitic. 28 (1997) 65–68.
[26] S. Redzepovic, S. Orlic, et al., Int. J. Food Microb. 83 (2003) 49–61.

Available online at www.sciencedirect.com
ScienceDirect
Talanta 74 (2008) 1218–1223
Talanta
www.elsevier.com/locate/talanta

Pressurized solvent extraction and monolithic column-HPLC/DAD analysis of anthocyanins in red cabbage

Panagiotis Arapitsas [a,b,*], Charlotta Turner [a]

[a] *Uppsala University, Department of Physical and Analytical Chemistry, Analytical Chemistry, P.O. Box 599, 751 24 Uppsala, Sweden*
[b] *University of Florence, Department of Pharmaceutical Sciences, Via Ugo Schiff 6, 50019 Sesto F.no, Florence, Italy*

Received 20 May 2007; received in revised form 10 August 2007; accepted 24 August 2007
Available online 1 September 2007

Abstract

The aim of this work was to develop a fast method for extraction and analysis of anthocyanins in red cabbage. Pressurized hot water containing 5% of ethanol was used as an extremely efficient extraction solvent. HPLC/DAD with a monolithic column was used to accomplish a fast analysis—24 anthocyanin peaks within 18 min. Statistical design was used to optimize the studied extraction parameters: temperature (80–120 °C); sample amount (1–3 g); extraction time (6–11 min); concentration of formic acid in the extraction solvent (0–5 vol.%). The best extraction conditions for a majority of the anthocyanin peaks were 2.5 g of sample, 99 °C (at 50 bar), 7 min of extraction and a solvent composition of water/ethanol/formic acid (94/5/1, v/v/v).
© 2007 Elsevier B.V. All rights reserved.

Keywords: Anthocyanins; Red cabbage; Monolithic column; Accelerated solvent extraction; Polyphenols

1. Introduction

Red cabbage (*Brassica oleracea* L. var. *capitata f. rubra*) belongs to the family of Brassicaceae, and is a native vegetable of the Mediterranean region and south-western Europe that now grows in regions all over the world. Studies concerning the influence of *Brassica* species in human health have verified their capacity to prevent cardiovascular diseases as well as their activity against some types of cancer [1–5]. Among the substances that seem to be responsible for those properties are polyphenols [2,3,5], and red cabbage is a rich source of phenolic compounds, with the anthocyanins being the most abundant class [5–8]. Anthocyanins are a group of plant pigments that are widely distributed in nature, among flowers, fruits and vegetables, and are responsible for their bright colors such as orange, red and blue [6,9,10]. They play an important role in the plant physiology and are valuable for food industry as well as in human health [2,5–7,9,10]. Red cabbage is a promising source of anthocyanins for the coloration of food since they are unique in being colored over a very broad pH-range, from red to blue and green, compared to other red vegetables [6,9]. Therefore, anthocyanins are not limited to acidic foodstuffs but can be extended to neutral-pH products, for which they may provide a natural alternative to synthetic blue colorants [9]. Regarding the chemical structure of red cabbage anthocyanins, only cyanidin has been identified as aglycon, glycosylated and acylated with various aromatic and aliphatic groups at positions 3 and 5 [5,6,8,9] (Fig. 1).

The analysis of anthocyanins is a difficult task, due to their low stability in high temperature, light and pH above 3.5 [6,7,9,11–17]. Hence, food and pharmaceutical industries request the development of fast and efficient analysis methods for these unstable compounds. Traditionally, the techniques employed in the extraction of anthocyanins from semi-solid or viscous samples involve the use of solvent extraction followed by liquid–liquid extraction or solid-phase extraction [5–9,11–15]. These methods are time consuming and use large amounts of organic solvent with negative consequences in the environment. Pressurized fluid extraction (PFE) is an alternative and innovative technique that combines elevated temperature and pressures with liquid solvents to achieve fast and efficient extraction [18–25], that has already been reported in the delicate extraction of anthocyanins from fruits and vegetables [15,17], and has

* Corresponding author at: University of Florence, Department of Pharmaceutical Sciences, Via Ugo Schiff 6, 50019 Sesto Fiorentino, Florence, Italy. Tel.: +39 055 4573677; fax: +39 055 4573667.
E-mail address: panagiotis.arapitsas@unifi.it (P. Arapitsas).

0039-9140/$ – see front matter © 2007 Elsevier B.V. All rights reserved.
doi:10.1016/j.talanta.2007.08.029

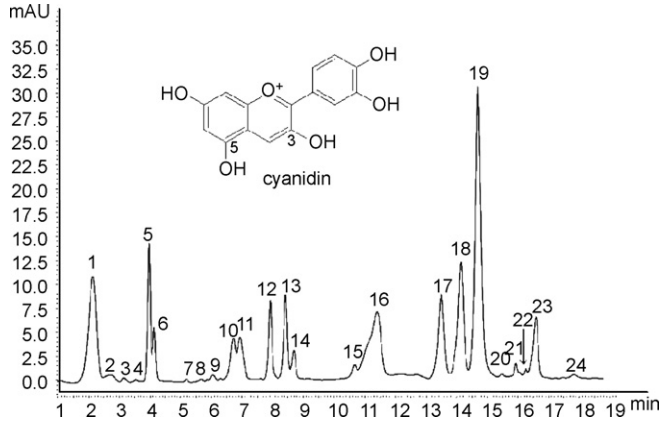

Fig. 1. Representative chromatogram of red cabbage extract reported at 520 nm.

lately been object of a patent [26]. Furthermore, the use of PFE offers the possibility to minimize, or even eliminate, the use of hazardous solvents, and thereby reduces waste generation [18–28].

In the field of HPLC, monolithic or rod columns represent one of the most interesting innovations. Their common characteristic is that they are constituted by one single piece of a porous material and that this piece fills the entire column. Replacing conventional columns with monolithic columns can allow shorter assay times, faster column equilibration, and larger void volume between the packed particles. Monolithic columns have also the advantages over conventional particle-columns such as higher flow rates at lower backpressures [29,30].

In this study, a PFE system (accelerated solvent extraction, ASE^{TM}) was utilized for the extraction of anthocyanin-based pigment from red cabbage. The analysis of the extracts was performed by HPLC/DAD using a monolithic column.

2. Experimental

2.1. Standards and solvents

Standards of cyanidin chloride, cyanidin-3-*O*-glucoside chloride, cyanidin-3-*O*-galactoside chloride, cyanidin-3-*O*-rhamnoside, cyanidin-3-*O*-rutinoside chloride and cyanidin-3,5-di-*O*-glucoside chloride (HPLC grade) were obtained from Extrasynthese (Geney, France). Formic acid was purchased from Sigma Aldrich (St. Louis, MO). Acetonitrile (HPLC grade) and ethanol were from Merck AG (Darmstadt, Germany). Distilled water was obtained from a purification system (Milli-Q; Millipore, Bedford, MA) and nitrogen (99.996 vol.%) was from AGA, Stockholm, Sweden.

2.2. Extraction procedure

A Dionex accelerated solvent extractor (ASE-200®) was used for the study. First, a simple homogenization procedure was used [31] for cutting in small pieces approximately 100 g red cabbage leaves with a knife, and then homogenized with a Philips cucina TYPE HR1744 blender. A portion of homogenized fresh red cabbage sample was placed into 11 mL extraction cells containing a cellulose paper filter at the bottom. The cell containing the sample was filled with extraction solvent, pressurized, and then heated. By operating the ASE system at zero pre-heating time and one extraction cycle, approximately 5–6 min was required to heat the sample and solvent from ambient temperature to the desired temperature, and a short static extraction (1–5 min) was then performed. Hence, the extraction time listed throughout this article includes a pre-heating time of 5–6 min. The cell was thereafter rinsed with fresh extraction solvent (80% of the void volume) and purged with a flow of nitrogen (1.0 MPa during 90 s). The volume of each extract was adjusted to 25 mL with the extraction solvent. The extraction solvent was a mixture of water, ethanol and formic acid, in which ethanol was kept at 5 vol.%, and formic acid was varied between 0 and 5 vol.% (Table 1). To determine the effects of sample amount (amount), extraction temperature (temp.), extraction time (time) and solvent acidity (formic acid) on the recovery of anthocyanins, the 20 experiments listed in Table 1 were performed as described above. All the extractions were performed in triplicate. The temperature range employed (80–120 °C) was decided after preliminary studies had shown that higher temperatures (>120 °C) caused degradation, and lower temperatures (<80 °C) gave poor extraction efficiency of the pigments; and by considering literature data about pressurized fluid extraction of relatively polar antioxidants and sensitive analytes [15,17,20–25]. Ethanol vol.% was decided to be 5% after preliminary tests, and by considering literature where small vol.% of organic solvent resulted in increased recovery of similar analytes [20,21,24,25]. Furthermore, it is certainly advantageous to have the same vol.% of organic solvent with the first gradient of the chromatographic run. For comparison with PFE extraction, 3 g of homogenized red cabbage were extracted with 20 mL of water/ethanol/formic acid (94/5/1, v/v/v) for 30 or 60 min at 10 °C (control extractions); or with 2× 50 mL of water/ethanol/formic acid (29/70/1, v/v/v)

Table 1
The experimental design of red cabbage's anthocyanins extraction

Experiment	Temp. (°C)	Amount (g)	Time (min)	Formic acid (vol.%)
1	80	3	6	0
2	100	3	6	0
3	120	3	7	0
4	80	1	6	0
5	100	1	6	0
6	120	1	7	0
7	80	2	6	0
8	100	2	6	0
9	120	2	7	0
10	80	3	8	0
11	100	3	8	0
12	80	3	10	0
13	100	3	10	0
14	120	3	11	0
15	80	3	6	1
16	100	3	6	1
17	120	3	7	1
18	80	3	6	5
19	100	3	6	5
20	120	3	7	5

for 60 min at 10 °C (conventional ethanol extraction). All extractions were performed in triplicate. Following extraction, samples were centrifuged (Beckman J21) at 5000 × *g* for 10 min at 5 °C, and the supernatants were analyzed.

2.3. HPLC/DAD

The HPLC system used was a VWR Hitachi ELITE LaChrom (Merck-Hitach, Tokyo, Japan), equipped with an L-2130 pump, an L-2200 autosampler, an L-2300 column oven and an L-2455 DAD. The column used was a Chomolith Performance RP-18e 100 mm × 4.6 mm i.d. (Merck, KGaA, Darmstadt, Germany), operating at 27 °C and with a flow rate of 4 mL/min. The injected volume was optimized to 40 μL, so as to have the highest loop volume (and therefore the highest analytical signal) but still maintain good resolution factors for all the peaks. Precision/injection repeatability test (expressed as relative standard deviation, R.S.D., in %) was performed by six ($n = 6$) replicate injections of cyanidin-3,5-di-*O*-glucoside standard solution at a concentration of 50 μg/mL. These tests showed good precision in peak area (R.S.D. < 2%) and peak retention time ±2%. The mobile phase was a multistep linear solvent gradient system consisting of (A) 5% formic acid (aq.) and (B) acetonitrile, optimized to achieve the best resolution. The optimal elution profile turned out to be: 0 min 95% A, 0–2 min 94% A, 2–3 min 93% A, 3–4 min 93% A, 4–5 min 89% A, 5–8 min 88% A, 8–10 min 87% A, 10–12 min 87% A, 12–13 min 87% A, 13–14 min 86% A, 14–15 min 86% A, 15–18 min 82% A, 18–19 min 20% A, 19–20 min 20% A, 20–21 min 95% A, and 21–23 min 95% A.

2.4. Compound quantification

Quantification of individual anthocyanins was performed by HPLC/DAD using a five-point regression curve ($r^2 = 0.998$) in the range of 1–200 μg/mL on the basis of the cyanidin-3,5-di-*O*-glucoside standard and determination at 520 nm. Individual and total concentrations were calculated and expressed as micrograms of cyanidin-3,5-di-*O*-glucoside equivalents per gram of fresh red cabbage.

2.5. Statistical evaluation

All statistical analyses were performed using analyses of variance (ANOVA) with consequent Experimental Design (DOE). 'Statistica for Windows' software was used to calculate the effects of the extraction conditions (temperature, extraction time, amount of sample, and formic acid concentration) by a 3^2 full factorial design, on the recovery of anthocyanins (StatSoft). The data took into consideration were single-peak quantification results for 18 of the total 24 anthocyanins in the extract, which concentrations were above the limit of detection (noise/signal ~1/10). This strategy of not just observing the total amount of anthocyanins, but rather single species, enables the evaluation of discriminative degradation of certain anthocyanin species.

Table 2
Chromatographic, spectroscopic and significance of the variables in every peak regarding their *p* values

Peak	Rf (min)	λ_{vis} (nm)	λ_{acyl} (nm)	E_{440}/E_{vis}	E_{acyl}/E_{vis}	Temp	Amount	Time	Formic acid
1[a]	2.28	514		17		***	NS	***	***
2[a]	2.82	514		17		***	NS	*	*
3[a]	3.37	530	272	17	55[b]	***	NS	**	***
4	3.59	514		17					
5[a]	4.09	528	294	19	60[b]	***	NS	**	***
6[a]	4.22	528	332	17	60[b]	NS	NS	*	***
7	5.21	528	330	19	98[c]				
8	5.65	532	n.i	19					
9[a]	6.08	522	n.i.	20		NS	NS	NS	NS
10[a]	6.79	528	336	16	95[c]	NS	NS	NS	NS
11[a]	7.03	522	286	19	57[b]	**	NS	NS	***
12[a]	7.91	536	296	19	106[c]	NS	*	NS	NS
13[a]	8.45	538	326	20	92[c]	***	NS	***	***
14[a]	8.76	536	326	16	92[c]	NS	NS	NS	NS
15[a]	10.68	523	288	16	56[b]	**	NS	NS	NS
16[a]	11.37	525	300	17	63[b]	***	NS	**	***
17[a]	13.46	526	324	21	101[c]	***	NS	*	***
18[a]	14.18	530	324	16	100[c]	***	NS	*	***
19[a]	14.91	536	324	23	103[c]	NS	NS	*	***
20	15.47	530	329	24	120[c]				
21[a]	15.92	524	327	19	126[c]	NS	NS	NS	NS
22	16.38	538	330	21	130[c]				
23[a]	16.62	538	330	18	110[c]	NS	NS	NS	NS
24	17.73	530	329	18	110[c]				

NS: not significant; ***<0.1% significance; **<1% significance; *<5% significance.

[a] Peaks used to the statistical evaluation. n.i.: not identified. The absorption maxima λ_{vis} and λ_{uv} are due to the presence of the anthocyanin chromophore while λ_{acyl} is due to the chromophore of the acylating aromatic group, and E_{vis} and E_{acyl} are the absorptivities at the corresponding maxima while E_{440} is the absorptivity at 440 nm. All anthocyanins are biocides (E_{440}/E_{vis} between 15 and 24 %).

[b] Monoacylated anthocyanins.

[c] Diacylated anthocyanins.

3. Results and discussion

A typical chromatographic profile of red cabbage extract (Fig. 1) shows the peaks of anthocyanins examined in the present study. Using peak spectral characteristic λ_{440}, λ_{vis}, λ_{acyl}, and their corresponding absorptivities E_{440}, E_{vis}, E_{acyl} (Fig. 1 and Table 2), it was possible to identify the anthocyanins as either mono- or biosides (i.e. a E_{440}/E_{vis} ratio of 29–35% indicating a monoside and a ratio of 15–24% indicating a bioside) and to determine the degree of the aromatic acylation (i.e. an E_{acyl}/E_{vis} ratio of 53–69% indicating monoacylation and a ratio of 98–128% indicating diacylation) [6,32]. The absorption maxima λ_{vis} and λ_{uv} are due to the presence of the anthocyanin chromophore while λ_{acyl} is due to the chromophore of the acylating aromatic group, and E_{vis} and E_{acyl} are the absorptivities at the corresponding maxima while E_{440} is the absorptivity at 440 nm [6,32]. Our data show that all anthocyanins seem to be glycosylated in the positions 3 and 5 (biosides), and that anthocyanins 3, 5, 6, 11, 15, 16 are monoacylated, 7, 10, 12–14, 17–24 are diacylated and 1, 2, 4 are not acylated at all (Fig. 1 and Table 2). Our obtained results on glycosylation, are in accord with the literature, where also mass spectrometry has been used as a detector for the identification of the red cabbage anthocyanins [5,6,8]. Hence, our results demonstrate how important role UV–vis spectra can play in the identification of anthocyanins; not only in terms of glycosylation but also regarding acylation.

The influence of extraction temperature, extraction time, amount of sample, and formic acid concentration on the recovery of anthocyanins is shown in the three-dimensional response surface graphs in Fig. 2. According to these graphics all variances (temperature, extraction time, amount of sample, and formic acid concentration) seem to influence the desirability to obtain the most representative chromatogram, by considering the yield of every single anthocyanin peak as discussed above. In particular, these graphs show that high desirability, within the experimental design values, has been achieved under short extraction time, medium temperature, low concentration of formic acid, and medium to high amount of sample. The significance of every

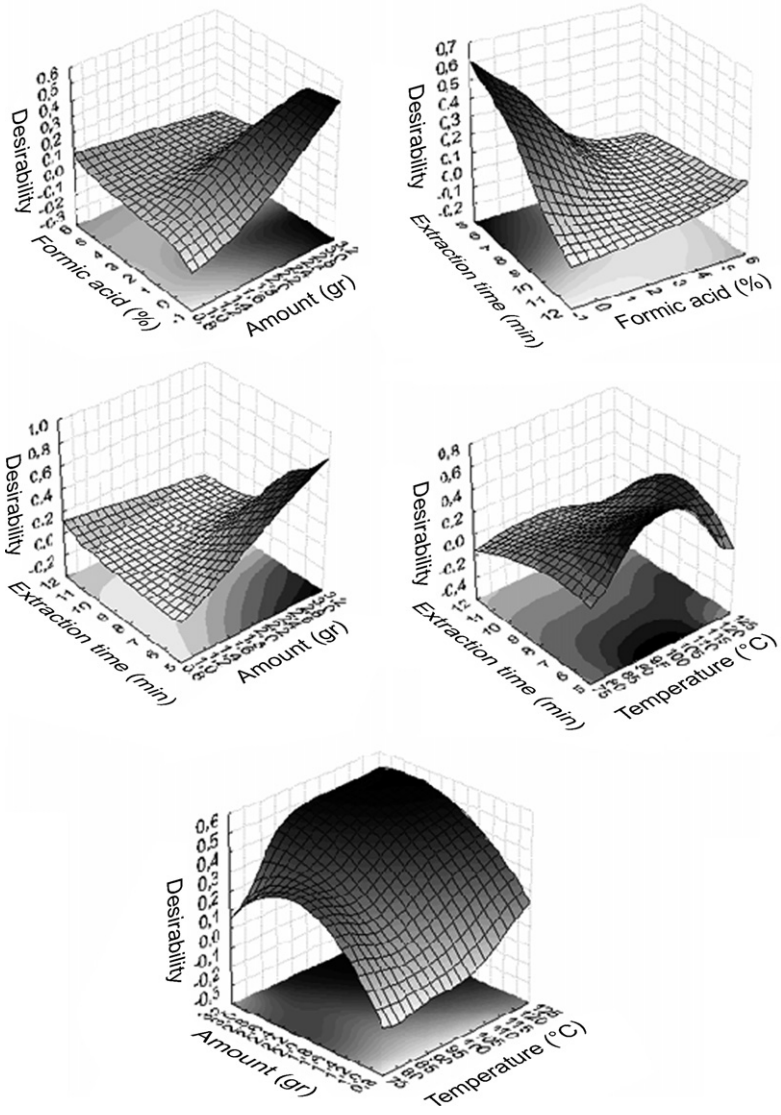

Fig. 2. Three-dimensional response surfaces of the influence of the extraction parameters studied.

extraction parameter in every peak yield is reported in Table 2. In general, it seems that temperature and formic acid concentration influence the extraction yield the most, and that the amount of sample affects less. The confrontation between the statistical significance of the variances and the UV–vis data shows that all 'non-acylated' and monoacylated anthocyanins are influenced by changing the values of the extraction parameters. However, only three of the nine diacylated anthocyanins seem to be significantly affected (Table 2). This outcome could be explained by the fact that high acylation enforces the stability of these pigments [16]. The ANOVA analysis performed to predict the optimum values for the variances, in order to obtain the most representative chromatogram, gave as best conditions, 99 °C extraction temperature, 7 min extraction length (including 5 min heat-up time), 2.5 g sample amount, and 1 vol.% of formic acid (Fig. 3).

The use of a monolithic column offered the possibility to obtain separation of 24 anthocyanins in a very short time (18 min) (Fig. 1). Moreover, the fast equilibration of the monolithic column also resulted in higher sample-throughput. It should be taken into consideration that red cabbage is one of the most complicated sample tissues regarding its anthocyanic profile, as compared to other fruits and vegetables [8].

The methods reported in the literature, for the analysis of complex mixtures of anthocyanins required more than 30 min of extraction and sample preparation, and more than 70 min of liquid chromatography separation time [5,6,8]. By using a pressurized solvent extraction method and a monolithic column coupled to a diode array detector, the total time of extraction and analysis was less than 30 min. In addition, the large volume of injection (40 μL) and the non-necessity of any sample pre-treatment make the analysis not only faster but also more representative with respect to the total extract's volume. The high volume of injection, with respect to the conventional column chromatography, is a significant advantage of the monolithic column, which is also required due to the high flow rate (4 mL/min in our case). The comparison of the optimized PFE method, with the control and conventional non-PFE methods used in the present study, showed that the efficiency of the method is comparable with the conventional one, fact already mentioned [15,17,20–26]; and more efficient with respect to the control methods. The total amount of anthocyanins, per gram of fresh red cabbage, with the optimized PFE method were 662 μg/g (±3); with the 30 and 60 min control extraction were 242 μg/g (±8) and 302 μg/g (±5), respectively; and 680 μg/g (±11) when the conventional ethanol extraction was used. At last, but not least important, the use of pressurized hot solvent for the extraction of the anthocyanins, permit to use relatively small quantity of extraction solvent, which to the biggest part was water (94 vol.%), together with small quantities of ethanol (5 vol.%) and formic acid (1 vol.%); a fact that makes this new extraction method more environmental friendly than most conventional ones.

In conclusion, this work reports the results of a novel and fast protocol for the analysis of red cabbage's anthocyanins, using pressurized solvent extraction and monolithic column separation technology. The combination of these two relatively new techniques seems promising for the challenging extraction and analysis of anthocyanins in fruits and vegetables.

To improve the method even further, the ethanol concentration should be optimized, and other solvents should be tested as well. Furthermore, an extraction system that uses pre-heated solvents (before the solvent enters the extraction cell) would speed up the extraction time as well as minimize potential degradation of labile anthocyanin species. Finally, monolithic column

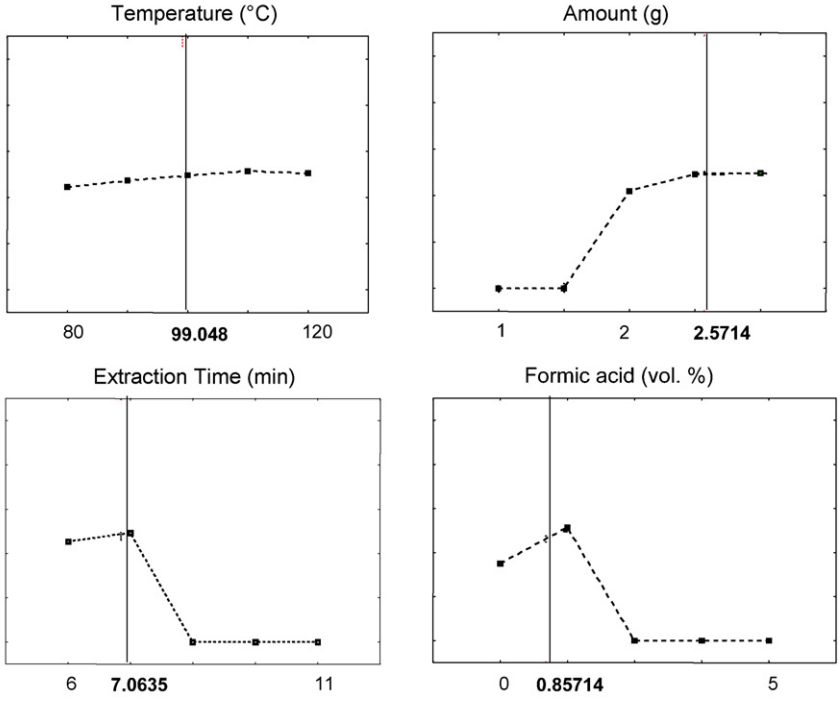

Fig. 3. Profiles of the predict values and desirability of the extraction parameters.

of smaller inner diameter in combination with both DAD and tandem MS/MS detection would further improve the analytical method.

Acknowledgments

Panagiotis Arapitsas acknowledges the Marie Curie Fellowship for a 5-month grant (contract number: HPMT-CT-2001-00419); VWR International in Solna, Sweden, for lending us the LaChrom Elite HPLC system and the monolithic column; and also appreciate the discussions with Alvaro J. Santos-Neto. Charlotta Turner acknowledges the Swedish Research Council for Environment, Agricultural Sciences and Spatial Planning (FORMAS, 209-2006-1346); the Swedish Research Council (VR, 2006-4084); the Swedish International Development Cooperation Agency (SIDA, SWE-2005-473); and the Swedish Foundation for Strategic Research (SSF, 2005:0073/13).

References

[1] G. Cheney, J. Am. Diet. Assoc. 26 (1950) 668.
[2] D. Cooke, W.P. Steward, A. Gescher, T. Marczylo, Eur. J. Cancer 41 (2005) 1931.
[3] J. Singh, A.K. Upadhyay, A. Bahadur, B. Singh, K.P. Singh, M. Rai, Sci. Hortic. 108 (2006) 233.
[4] K.A. Steinmetz, J.D. Potter, J. Am. Diet. Assoc. 96 (1996) 1027.
[5] C.S. Charron, B.A. Clevidence, S.J. Britz, J.A. Novotny, J. Agric. Food Chem. 55 (2007) 5354.
[6] M. Dyrby, N. Westergaard, H. Stapelfeldt, Food Chem. 72 (2001) 431.
[7] X. Wu, G.R. Beecher, J.M. Holden, D.B. Haytowitz, S.E. Gebhadt, R.L. Prior, J. Agric. Food Chem. 52 (2004) 4026.
[8] X. Wu, R.L. Prior, J. Agric. Food Chem. 53 (2005) 3101.
[9] G. Mazza, E. Miniati, Anthocyanins in Fruit, Vegetables, and Grains, CRC Press, Boca Raton, FL, 1993, p. 362.
[10] J. Kong, L. Chia, N. Goh, T. Chia, R. Brouillard, Phytochemistry 64 (2003) 923.
[11] J.E. Cacace, G. Mazza, J. Agric. Food Chem. 50 (2002) 5939.
[12] I.L.F. Nielsen, G.R. Haren, E.L. Magnussen, L.O. Dragsted, S.E. Rasmussen, J. Agric. Food Chem. 51 (2003) 5861.
[13] E. Revilla, J. Ryan, G. Mertin-Ortega, J. Agric. Food Chem. 46 (1998) 4592.
[14] F.C. Stintzing, A.S. Stintzing, R. Carle, B. Frei, R.E. Wrolstad, J. Agric. Food Chem. 50 (2002) 6172.
[15] Z.Y. Ju, L.R. Howard, J. Food Sci. 70 (2005) 270.
[16] R. Brouillard, S. Chassaing, A. Fougerousse, Phytochemistry 64 (2003) 1179.
[17] X. Wu, H.E. Pittman, R.L. Prior, J. Agric. Food Chem. 54 (2006) 583.
[18] C. Turner, Modern Extraction Techniques—Food and Agricultural Samples, American Chemical Society Press, 2006, ISBN13: 9780841239401, pp. 3–19.
[19] C. Turner, P. Turner, G. Jacobson, K. Almgren, M. Waldebäck, P. Sjöberg, E. Nordberg Karlsson, K.E. Markides, Green Chem. 8 (2006) 949.
[20] E.S. Ong, J.S.H. Cheong, D. Goh, J. Chromatogr. A 1112 (2006) 92.
[21] J. Kronholm, K. Hartonen, M. Riekkola, Trends Anal. Chem. 26 (2007) 396.
[22] Z. Pineiro, M. Palma, C.G. Barroso, J. Chromatogr. A 1026 (2004) 19.
[23] M. Herrero, P.J. Martin-Alvarez, F. Javier Senorans, A. Cifeuentes, E. Ibanez, Food Chem. 93 (2005) 417.
[24] E.S. Ong, S.M. Len, Anal. Chim. Acta 482 (2003) 81.
[25] M. Garcìa-Marino, J.C. Rivas-Gonzalo, E. Ibáñez, C. Garcìa-Moreno, Anal. Chim. Acta 50 (2006) 44.
[26] J.W. King, R.D. Grabiel, U.S. Patent 7,208,181 B1 (2007).
[27] B.E. Richer, B.A. Jones, J.L. Ezzel, N.P. Porter, N. Avdalovic, C. Pohl, Anal. Chem. 68 (1996) 1033.
[28] G. Isaac, M. Waldebäck, U. Eriksson, G. Odham, K.E. Markides, J. Agric. Food Chem. 53 (2005) 5506.
[29] C. Repollès, J.M. Herrero, C. Ràfols, J. Chromatogr. A 1131 (2006) 51.
[30] F. Chinnici, A. Gaiani, N. Natali, C. Riponi, S. Galassi, J. Agric. Food Chem. 52 (2004) 3.
[31] Z.Y. Zhang, X.J. Liu, X.Y. Yu, C.Z. Zhang, X.Y. Hong, Food Control 18 (2007) 723.
[32] V. Hong, R.E. Wrolstad, J. Agric. Food Chem. 38 (1990) 708.

Available online at www.sciencedirect.com
ScienceDirect
Talanta 74 (2008) 1511–1519
Talanta
www.elsevier.com/locate/talanta

Determination of total and oxidized glutathione in human whole blood with a sequential injection analysis system

André R.T.S. Araujo, M. Lúcia M.F.S. Saraiva *, José L.F.C. Lima

REQUIMTE, Departamento de Química-Física, Faculdade de Farmácia da Universidade do Porto, Rua Aníbal Cunha, 164, 4099-030 Porto, Portugal

Received 1 June 2007; received in revised form 25 September 2007; accepted 28 September 2007
Available online 4 October 2007

Abstract

This work reports the development of a simple, robust, automated sequential injection analysis (SIA) system for the enzymatic determination of total (tGSH) and oxidized (GSSG) glutathione in human whole blood. The reduced (GSH) glutathione concentration is then obtained as the difference between the tGSH and GSSG concentrations. The determination was based on the DTNB–GSSG reductase recycling assay, which couples the specificity of the GSSG reductase (GR) with an amplification of the response to glutathione, followed by spectrophotometric detection of the 2-nitro-5-thiobenzoic acid (TNB) formed ($\lambda = 412$ nm). The implementation of this reaction in a SIA flow system with an in-line dilution strategy permitted the necessary distinct application ranges for tGSH and for GSSG. It also guaranteed the exact timing of fluidic manipulations and precise control of the reaction conditions.

The influence of parameters such as reagents concentration, temperature, pH, flow rate of the carrier buffer solution, as well as reaction coil length, etc., on the sensitivity and performance of the SIA system were studied and the optimum reaction conditions subsequently selected. Linear calibration plots were obtained for GSH and GSSG concentrations up to 3.00 and 1.50 μM, with detection limits of 0.031 and 0.014 μM, respectively. The developed methodology showed good precision, with a relative standard deviation (R.S.D.) < 5.0% ($n = 10$) for determination of both glutathione forms. Statistical evaluation showed good compliance, for a 95% confidence level, between the results obtained with the SIA system and those furnished by the comparison batch procedure.
© 2007 Elsevier B.V. All rights reserved.

Keywords: Whole blood; Total and oxidized glutathione; Reduced glutathione; Glutathione reductase; SIA; In-line dilution

1. Introduction

The widespread distribution of glutathione and its role in protection against oxidative stress, detoxification of xenobiotics and modulation of enzyme activity by disulfide interchange [1] have aroused continuous interest in analytical methods for this intracellular low-molecular-weight thiol, which is involved in a multitude of cellular functions.

In cells, oxidation of reduced glutathione (GSH), the predominant form, leads to the formation of glutathione disulfide (oxidized glutathione, GSSG). Intracellular glutathione is effectively maintained in the reduced state by a ubiquitous and crucial flavoenzyme, GSSG reductase (GR), linked to the NADPH/$NADP^+$ system [2]. When mammalian cells are exposed to increased oxidative stress, the ratio of GSH/GSSG decreases due to the accumulation of GSSG [3]. On this basis, the reduced glutathione/oxidized glutathione ratio (GSH/GSSG ratio) is used to evaluate oxidative stress status in biological systems. Oxidative stress has been recognized in different chronic diseases and has been assessed by blood GSSG levels [4]. A decrease in GSH concentrations has been implicated in several pathological conditions, such as diabetes, alcoholic liver disease, AIDS, cataractogenesis, rheumatoid arthritis, muscular dystrophy, amyotrophic lateral sclerosis, Alzheimer disease, respiratory distress syndrome, acute hemorrhagic gastric erosions, xenobiotic-induced oxidative stress and toxicity and aging [5].

Numerous methods are available for measuring GSH and GSSG in biological samples (Table 1), but few are suitable for direct analysis in routine use.

A number of sensitive and specific high-performance liquid chromatography (HPLC) procedures are available for the

* Corresponding author. Tel.: +351 22 2078939/87132; fax: +351 22 2004427.
E-mail address: lsaraiva@ff.up.pt (M.L.M.F.S. Saraiva).

0039-9140/$ – see front matter © 2007 Elsevier B.V. All rights reserved.
doi:10.1016/j.talanta.2007.09.028

Table 1
Comparison between different methodologies for glutathione assay in biological samples

Methodologie	Detection	Biological sample	Compounds	Linear range (μM)	Detection limit (μM)	Time analysis	Ref.
HPLC	Spectrophotometry (ultraviolet)	Human blood	GSH GSSG	50–1500 2–500	0.5	Derivatization/run time 24 min	[6]
HPLC	Electrochemistry and fluorometry	Plasma	GSH GSSG	0–10 0–0.8	0.001 0.008	Derivatization/run time 14 min	[7]
HPLC	Mass spectrometry	Human blood	GSH GSSG	250–2000 6.25–100	–	Derivatization/run time 6 min	[8]
MEKC	Spectrophotometry (ultraviolet)	Plasma	GSH GSSG	16–81 8–40	0.8 0.4	Run time 20 min	[10]
Electrochemistry	Amperometry	Human blood	GSH	2–500	2	Signal reaching 35 s	[11]
NMR	Double quantum coherence transfer ^{1}H NMR	Rabbit blood	GSH	1000–50,000	–	20 min	[12]
Capillary electrophoresis	Fluorometry	Plasma	GSH GSSG	0.22–45.00	0.046 0.012	Derivatization/migration time 6 min	[13]
Chemiluminescence (CL)	Chemiluminometry	Rabbit blood and rat brain microdialysate	GSH	4.0×10^{-3} - 0.4	5.0×10^{-4}	CL reaction 10 s	[14]
Non-enzymatic	Fluorometry	Rat blood and liver homogenates	GSH	0.065–32.5	0.065	Reaction period 15–20 min	[15]
Enzymatic (GSSG reductase)	Spectrophotometry (visible)	Human blood, saliva and urine and rat plasma, liver and kidney homogenates	tGSH GSSG	3.25×10^{-3} - 3.25×10^{-2}	–	Derivatization/color development 6 min	[17]
Enzymatic (GSH transferase)	Spectrophotometry (ultraviolet)	Perfused livers	GSH	1–25	0.3	End-point reaching 5 min	[18]
Flow-injection analysis	Spectrophotometry (visible)	Rat hepatocytes	tGSH GSSG	– 0.0–7.5	0.05	Derivatization/residence time 235 s	[19]

determination of GSH and/or GSSG. However, the procedures involved are time consuming, requiring a long sample preparation with pre- or post-column derivatization [6] and have a low sampling throughput due to the sequential mode in analytical runs. Sometimes these procedures require a special apparatus for electrochemical [7] or mass spectrometry [8] detections due to the very poor and non-specific spectrophotometric or fluorescence properties of the GSSG. In some cases an overestimation of GSSG is obtained, caused by oxidation of GSH during the alkalization and derivatization of samples before sample injection [9].

Other methods have also been proposed for glutathione determination, including micellar electrokinetic capillary electrophoresis (MEKC) [10], electrochemistry [11], nuclear magnetic resonance (NMR) [12], fluorescence [13] and chemiluminescence-based methods [14].

Enzymatic assays are advantageous as high specificity is guaranteed, contrary to other methods that involve a non-specific derivatization of the GSH sulfhydryl group [15]. Enzymatic methods basically fall into two categories: 5,5′-dithiobis(2-nitrobenzoic acid) (DTNB)–GSSG reductase recycling assay (first reported by Owens and Belcher [16] and later modified by Tietze [17]) and the glutathione-*S*-transferase 1-chloro-2,4-dinitrobenzene (CDNB) endpoint method [18]. The endpoint method only measures GSH and is more precise but less sensitive than the recycling assay. However, the disadvantage of the recycling assay is that it is laborious and time consuming for a large number of samples. An attempt at automation was proposed by Redegeld et al. [19], in which GSH and GSSG were determined in rat hepatocytes by flow-injection analysis, where the oxidized form was analyzed after alkylation of the reduced form with *N*-ethylmaleimide (NEM). The principles of that method are identical to the proposed sequential injection analysis method.

The present work is aimed to automate the spectrophotometric determination of tGSH and GSSG in whole blood using sequential injection analysis (SIA). Automation resorting to SIA [20] was regarded as the advantageous tool for its implementation as the exact metering of small volumetric volumes and economical characteristics [21], inherent to this technique, are essential for the purposes of this work. Since all manipulations are computer controlled, reproducibility is guaranteed in all operations and thereby equal conditions in all determinations are assured.

The methodology chosen is based on the DTNB–GSSG reductase recycling assay which has been accepted as routine for the determination of glutathione in biological fluids like blood samples [22]. This method responds to both GSH and GSSG so the tGSH (GSH and GSSG) and GSSG must be determined separately. Furthermore, GSSG is analyzed after treatment of the GSH with 1-methyl-2-vinyl-pyridinium trifluoromethane sulfonate (M2VP), which does not show an inhibiting effect on GSSG reductase activity, contrarily to NEM, and presents a rapid rate of derivatization. GSH concentration is calculated by subtraction of the GSSG level from the tGSH level.

2. Experimental

2.1. Reagents and solutions

All chemicals used were of analytical reagent grade with no further purification and water from a MilliQ plus system with specific conductivity of less than 0.1 $\mu S\,cm^{-1}$ was used throughout.

L-Glutathione reduced (GSH), L-glutathione oxidized disodium salt (GSSG), 5,5′-dithiobis(2-nitrobenzoic acid) (DTNB), ethylenediaminetetraacetic acid (EDTA) dipotassium salt dihydrate and meta-phosphoric acid (MPA) were purchased from Fluka. 5-Sulfosalicicylic acid dihydrate (SSA), GSSG Reductase (E.C.1.6.4.2, ammonium sulphate suspension, from Bakers Yeast, 160 U/mg protein) and β-nicotinamide adenine dinucleotide 2′-phosphate reduced tetrasodium salt (NADPH) were obtained from Sigma–Aldrich. Potassium dihydrogen phosphate (KH_2PO_4) was supplied by Riedel-de-Haën and potassium hydroxide from Merck. 1-Methyl-2-vinyl-pyridinium trifluoromethane sulfonate (M2VP) was obtained from OxisResearch (Portland, OR).

Buffer solution was prepared with 100 mM KH_2PO_4, 1 mM dipotassium EDTA and pH was adjusted to 7.0 by addition of potassium hydroxide solution. Solutions of 3 mM DTNB and 1.2 mM NADPH were prepared daily in the buffer solution. A stock solution of 2 mM was daily prepared by dissolving appropriate amount of glutathione in buffer solution and working standards of GSH and GSSG were obtained from this stock solution by serial dilution. A 5 U/mL GSSG reductase solution was prepared in buffer solution on the preceding day of use, being frozen at −20 °C and defrosted at 25 °C until used. The DTNB solution was maintained at room temperature and the NADPH and GSH or GSSG standards were placed on ice. All of these solutions were shielded from light throughout use.

2.2. Sample collection and processing

Blood samples were obtained from healthy adult volunteers. Venous blood was collected into tubes containing EDTA as an anticoagulant. Aliquots of 50 or 100 μL were added to the bottom of a microcentrifuge tube for determination of total GSH and GSSG, respectively. For GSSG analysis, 10 μL of the thiol-blocking agent M2VP was previously added, to avoid the auto-oxidation of GSH to GSSG [23]. Thereafter, samples were frozen at −70 °C and processed after up to 30 days of storage. Processing methods included defrosting and a protein precipitation step with freshly prepared, cold 5% (w/v) meta-phosphoric acid. The mixture was vortexed and centrifuged at 14,000 rpm for 10 min at 4 °C. The resultant acid–soluble supernatants were analyzed directly in the SIA system or diluted in buffer and analyzed by the comparison batch procedure.

2.3. Apparatus

The analytical SIA flow system comprised a Gilson Minipuls 3 (VilliersleBel, France) peristaltic pump, equipped with a 1.02 mm i.d. Gilson PVC pumping tube. This pump was

connected to the central channel of a 10-port, electrically activated selection valve (Valco, Vici C25-3180D, Houston, USA). Omnifit PTFE tubing (0.8 mm i.d.) and Gilson end-fittings and connectors were used to assemble the different manifold parts.

The starting position of the peristaltic pump at the beginning of each cycle was controlled in order to guarantee reproducibility in the aspirated and propelled volumes. For this reason, an NResearch 161 T031 solenoid valve (W. Caldwell, NJ, USA) was used, with a magnet and a reed relay fixed on the rotor and on the top edge of the pump's fixed bar, respectively. When both elements were in close proximity, the reed relay was activated, allowing the electrical current flow. The signal detected by the computer set the beginning of each step of the analytical cycle from a fixed position of the peristaltic pump. The solenoid valve, placed between the pump and the holding coil, was activated enabling the solutions to flow through the holding coil. At the end of the cycle, the peristaltic pump returned to the initial position. During this time, the carrier solution flowed in closed circuit, by inactivation of the solenoid valve.

The reaction coil was placed in a water bath (G.L.F., West Germany) thermostatically controlled at 25 °C through the help of an immersion cooler (Haake, Model EK20, Thermo Electron Corporation).

A Jenway Model 6300 visible range spectrophotometer equipped with a flow-through cell from Hellma (80 μL, ref. 178.710QS) was used as detection system and the monitoring wavelength was set at 412 nm. Analytical signals were recorded on a strip chart recorder (Linseis, L 250 E) or acquired.

The SIA flow system was controlled by means of a microcomputer equipped with an interface card (Advantech Corp., PCL 711B, San Jose, CA). Software was developed in QuickBasic 4.5 (Microsoft) and permitted operation of the peristaltic pump, solenoid valve and multiposition selection valve, enabling the run-time definition of all analytical parameters to be made like flow rate, flow direction, sample volume, reagents volume, valve positioning, etc., as well as data acquisition and processing.

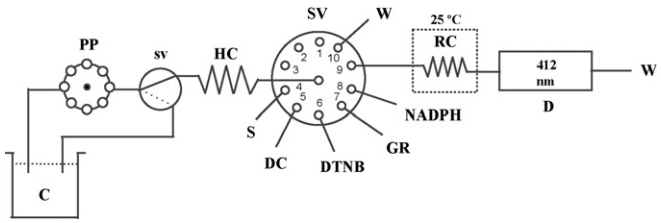

Fig. 1. Flow manifold for determination of reduced and oxidized glutathione in whole blood: C—carrier (propulsion flow rate of 1.90 mL min^{-1}), 100 mM phosphate buffer pH 7.0; PP—peristaltic pump; sv—solenoid valve; HC—holding coil; SV—selection valve; DC—dilution coil; S—standard/sample; DTNB = 3.0 mM DTNB solution; GR = 5.0 U/mL enzyme solution (immersed in a water bath thermostatically controlled at 25 °C); NADPH = 1.2 mM NADPH solution; RC—reaction coil (fixed in the same water bath); D—spectrophotometric detector; W—waste.

A Perkin-Elmer, Lambda 45 UV–VIS spectrophotometer was used to perform the determinations by the comparison test kit and the measurements were taken at 412 nm.

2.4. Manifold and procedure

System components were arranged as shown schematically in Fig. 1. The holding coil (HC) and reaction coil (RC) were 1.50 and 3 m length, both of which had a figure eight-shaped configuration. The flow protocol and timing sequence for the GSH or GSSG quantification in whole blood is listed in Table 2.

The recycling assay began with the aspiration of sample/standard to the holding coil (Step a) followed by DTNB, enzyme and NADPH solutions (Steps b–d). After flow reversal, the four-stacked zones were sent through the reaction coil (Step e) to the thermostatically controlled bath where the flow was stopped (Step f). After a pre-set time period the pump was reactivated and the reaction zone sent through the detector towards

Table 2
Protocol sequence for determination of reduced or oxidized glutathione in whole blood

Step	Valve position	Operation time (s)	Flow rate (mL min^{-1})	Volume (μL)	Description
D1	4	3	0.50	25	Aspirate GSH sample to HC
		6		50	Aspirate GSSG sample to HC
D2	5	8.70	2.00	290	GSH sample dilution
		5.85		195	GSSG sample dilution
a	4/5	15	0.80	200	Aspirate diluted sample/standard to HC
b	6	3.75	0.80	50	Aspirate 3.0 mM DTNB solution to HC
c	7	3.75	0.80	50	Aspirate 5.0 U/mL GR enzyme solution to HC
d	8	3.75	0.80	50	Aspirate 1.2 mM NADPH solution to HC
e	9	37	1.90	1172	Dispense HC content towards the RC
f	9	120	–	–	Stop period
g	9	81	1.90	2565	Signal acquisition and dispense carrier to wash flow cell

the flow cell, where the signal was acquired, after which the content of the flow cell was washed out (Step g).

Whenever a sample after the amplification reaction did not achieve the linearity range, the dilution phase was activated, which includes the aspiration of sample to the holding coil and its propulsion to the dilution coil (Fig. 1, DC) (Table 2, Steps D1–D2). Thereafter, the 200 μL of diluted sample in the analytical cycle was aspirated from the dilution coil.

2.5. Comparison batch procedure

No reference method has yet been defined, either for sample preparation or for glutathione measurement, in whole blood. Therefore as Assay Kits are commonly used in clinical laboratories, the determination of GSH and GSSG in whole blood was carried out using the Colorimetric Determination of Reduced and Oxidized Glutathione, Bioxytech GSH/GSSG-412 assay kit (catalog number 21040). In this way, both forms of glutathione were evaluated spectrophotometrically according to Tietze [17], by using reaction rate determinations of 3 min and calibration curves of the included GSSG standards.

3. Results and discussion

With the combined use of the GSSG reductase and DTNB, a glutathione recycling system is achieved (Fig. 2). GSH is oxidized by DTNB to give GSSG with formation of 2-nitro-5-thiobenzoic acid (TNB) in the thiolate anion form, which is a yellow coloured product. GSH is generated from GSSG by the action of the highly specific GSSG reductase and its cofactor NADPH and reacts with DTNB again to produce TNB. The TNB formed ($\lambda = 412$ nm) is proportional to the sum of GSH and GSSG present.

The amplification factor was evaluated, resorting to the comparison between the slopes of calibration curves obtained when using the enzymatic recycling reaction (Abs (A.U.) $= 0.1231 C_{GSH}$ (μM) $+ 0.097$, $R^2 = 0.9989$) and the stoichiometric mode (Abs (A.U.) $= 0.0044 C_{GSH}$ (μM) $+ 0.050$, $R^2 = 0.9956$) obtained by the GSH and DTNB reaction (lacking GSSG reductase and its cofactor NADPH). The difference between both intercepts (0.097 and 0.050) is due to the presence of glutathione reductase and NADPH in the amplification reaction. Then, a higher blank signal is observed when the enzymatic recycling reaction is used, because there is reduction of DTNB by glutathione reductase [24]. It was verified that in the stoichiometric mode, the response to GSH was 1/28th the response obtained in the enzymatic recycling reaction. Therefore, this recycling reaction improves the sensitivity of the total glutathione detection method.

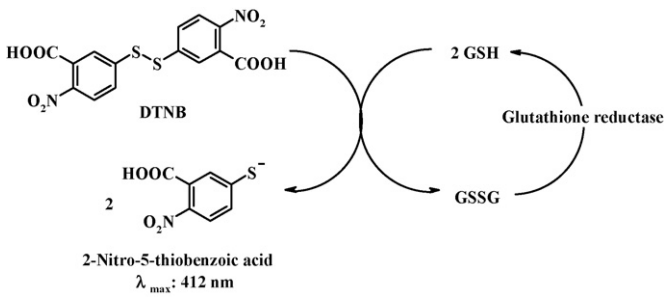

Fig. 2. The DTNB–GSSG reductase recycling system.

Table 3
Range of values used in the study of system parameters and selected values for its operation

Parameter	Range	Selected value
Enzyme concentration (U/mL)	0.4–5.0	5.0
NADPH concentration (mM)	0.4–1.6	1.2
DTNB concentration (mM)	1.5–3.0	3.0
Sample volume (μL)	50–300	200
Temperature (°C)	Ice bath—30	25
Phosphate buffer concentration (mM)	100–400	100
Carrier buffer pH	6.5–8.5	7.0
Time period of stopped flow in RC (s)	0–200	120
Propulsion carrier flow rate (mL min^{-1})	0.70–2.86	1.90

3.1. Optimization of the sequential injection system

Given the low levels of GSSG present in blood samples, the system had to be optimized accordingly. Therefore, in selecting the final conditions for the determination of total GSH and GSSG in blood samples, the influence of several parameters on the sensitivity of GSSG determination was evaluated. The studied range of parameters and final conditions selected are summarised in Table 3.

Another aim of the proposed SIA methodology was to obtain an economical one. Regarding that and given the significant cost difference between glutathione standards (GSH and GSSG), the optimization studies were carried out using GSH standards. Besides that it was tested different mixtures of GSH and GSSG and the results obtained showed compliance with known amounts of GSH and GSSG added. This evidence strengthened the fact of the reduction of one molecule of GSSG generates two molecules of GSH the response to GSSG should be twice as high as the response to GSH at equimolar concentration.

After preliminary experiments the following operating conditions were used as start values for the univariate optimization of the chemical and physical parameters: GSH standards up to 20 μM; a buffer flow rate of 0.70 mL min^{-1}; pH 7.5; a reaction coil length of 75 cm (i.d. 0.8 mm) and equal volume (50 μL) of DTNB, GR and NADPH.

3.1.1. Chemical and physical parameters

The four solutions involved in this reaction were drawn into the holding coil (HC) in the following order: sample/standard, DTNB, enzyme and NADPH. Although a complete overlap of the four zones had already been achieved on passage through the detector, sample and DTNB should be aspirated first as this minimises the physical dispersion of enzyme and NADPH. Regarding DTNB it was observed a decrease of the analytical signal of around 15% when it was first drawn into the holding coil. Consequently, the sample/standard large plug was then initially aspirated followed by the DTNB and the other two reagents were added to this mixture to enable the amplification reaction to begin.

GSSG reductase (GR) concentration was studied between 0.4 and 5.0 U/mL and an increment of signal was observed in all range. It was then established 5.0 U/mL as a limiting concentration for the GSSG reductase and then it was evaluated the concentration of its cofactor NADPH (0.4–1.6 mM) as the extent of the recycling reaction and therefore the increment in analytical signal, depends on the relationship between these two parameters. An increase in enzyme activity of about 30% up to 1.2 mM NADPH was observed. The differences obtained with higher concentrations (only 2% between 1.2 and 1.6 mM NADPH) did not justify its use. Therefore, for further experiments 1.2 mM NADPH was chosen.

Calibration curves were then established with different DTNB concentrations (1.5–3.0 mM) and it was verified that the rate of formation of TNB was around 20% higher using 3.0 mM DTNB, despite a linearity loss for values greater than 10 μM GSH. To take advantage of another increment in DTNB concentration, it would be necessary to simultaneously increase the other reagents involved, since an enzymatic recycling system was used. A 3.0 mM DTNB solution was then selected.

The background signal, which is due to the slow reduction of DTNB by glutathione reductase [24], affected the quantification limit obtained, with a non-significant difference between the 0.5 μM GSH standard and the blank signals. This could limit the evaluation of GSSG values in certain blood samples. Therefore, and considering that an increment in sample volume is an effective way of increasing sensitivity [25], different values of sample volume were then tested between 50 and 300 μL. Using a 50 μL sample, the difference between the 0.5 μM GSH standard and the blank signal was irrelevant but there was a gain in sensitivity of about 40% until 200 μL, the value which was chosen for further experiments.

Glutathione reductase activity is pH dependent and for that reason the influence of buffer composition was investigated. Buffer was initially prepared as described in Ref. [2]. Both KH_2PO_4 concentration and pH value of the buffer solution were then evaluated. KH_2PO_4 concentration was studied between 100 and 400 mM. For GSH between 0.50 and 10.00 μM, calibration curves were established at a pH of 7.5. An increase in potassium phosphate concentration resulted in an analytical signal decrease, probably justified by an ionic strength increase in environment reaction, resulting in an inhibiting effect on GR activity. Calibration curves for pH values between 6.5 and 8.5 were therefore established and maximum sensitivity was obtained at a pH of 7.0. For a pH of 6.5, the sensitivity was 39.2% lower than that found at pH 7.0 and its value decreased for pH values higher than 7.0 (3.1% and 18.6%, for pH values of 7.5 and 8.5, respectively). Therefore, when all solutions were dissolved in a buffer of pH 7.0, an increase in sensitivity of the method was achieved with reduction of the linear range (up to 3.00 μM GSH). Therefore, a buffer pH equal to 7.0 was used throughout and the pH of the samples was adjusted to 7.0 to avoid fluctuations from optimum pH in the sequential injection system.

Enzyme activity was also shown to be temperature-dependent. For the different conditions tested, immersed in an ice bath or fixed in a thermostated bath at 25 and 30 °C, an increase in activity up to 25 °C was observed with higher and repeatable analytical signals.

In flow systems, the analytical signal is generally acquired before chemical equilibrium is attained and the reaction extension is conditioned by the reaction coil's characteristics and flow rates used [26]. In this reaction, a complete four-reagent-zone overlapping was obtained with a 300-cm, figure eight-shaped reaction coil.

The propulsion carrier flow rate was varied from 0.70 to 2.86 mL min^{-1} and an absorbance increase was noticed while decreasing flow rate, although not sufficient to obtain the desired sensitivity probably because of the concomitant increase of physical dispersion. It was obvious that one should obtain a condition that originated at the same time the cease of the dispersion and a longer time for the reaction to proceed. So, it was implemented a stopped flow period in the thermostatically controlled bath before the reaction zone reached the detector. Although the sensitivity increased with time, a 120 s stop-time was selected and a carrier flow rate of 1.90 mL min^{-1} was established as a compromise between sampling rate and sensitivity, to permit the determination of GSH and GSSG in the concentration ranges present in the whole blood samples.

3.2. Analysis of whole blood samples

Initially and in a pre-analytical phase, the 5-sulfosalicicylic acid (5%, w/v) [27] which was frequently used in the protein precipitation step was considered for use. However, it was abandoned since this type of acid gave rise to higher glutathione values compared to the known amounts of glutathione added to whole blood samples (recovery experiments). It was thought that this occurrence was due to the formation of complexes by reaction of the serum and hemoglobin iron [28] with sulfosalicicylic acid during sample processing, which exhibits absorption at the wavelength used (412 nm) [29]. On this basis, meta-phosphoric acid was selected for the deproteinization step [30] which is very important since it avoids GSH and GSSG degradation, catalyzed by γ-glutamyltransferase and prevents oxidation of GSH [23].

Before titrating GSSG by the recycling assay, samples should be submitted to an appropriate scavenging GSH reagent, such as *N*-ethylmaleimide (NEM) [2] or 2-vinylpyridine [31]. On the proposed methodology, the samples were treated with a derivate of 2-vinylpyridine (2VP), 1-methyl-2-vinyl-pyridinium trifluoromethane sulfonate (M2VP), which rapidly scavenges GSH (in less than 1 min) and does not exhibit an inhibiting effect on GSSG reductase activity [32]. Therefore, no procedure was required for removal of the thiol-blocking residual reagents prior to the recycling reaction, in contrast to when NEM was used, and this derivatization shows a rapid rate of reaction, the opposite of the 2-vinylpyridine (which may allow for some degree of auto-oxidation during this slow derivatization reaction). For comparison purposes, the GSSG levels were estimated using the 2VP as thiol-blocking reagent and using our M2VP-based assay. A five-fold overestimation of GSSG levels was observed using the neat 2VP compared to that estimated by the use of the 2VP derivate.

Regarding the different values of GSH and GSSG concentrations present in whole blood (approximately 1 mM for GSH [33] and GSSG at low micromolar [9]) and the variability between samples, an in-line dilution procedure in the SIA system was developed to be used whenever it was necessary to adjust the concentrations of GSH and GSSG present in the samples to the linear concentration range obtained. For this purpose, and considering that the use of the multiposition selection valve offers easy and feasible alternatives to perform in-line sample pre-treatments, a procedure was developed whereby, with only small alterations in the analytical cycle, it was possible to carry out a quick in-line dilution of the samples, inside the automatic system before their analysis. This in-line dilution procedure was carried out by analysing a section of the concentration gradient generated in a dedicated tube of the selection valve (dilution coil) [34]. The dilution was then carried out in a dilution coil, placed in one of the inlets of the selection valve (Fig. 1, DC) and adding two steps to the analytical sequence, corresponding to Steps D1–D2 in Table 2. The degree of dilution in this kind of situation depends on: sample volume (amount of sample aspirated via the sample port to the holding coil), transfer volume (includes the sample volume and carrier solution transferred from the holding coil to the dilution coil) and analysis volume (volume of the aliquot taken from the dilution coil to the holding coil) [35]. These three parameters were studied and optimized to achieve dilution degrees of 60 and 6 for GSH and GSSG samples, respectively. Analysis volume had previously been established as 200 μL. The gradient concentration profile formed in the dilution coil and consequently the slice corresponding to this 200 μL, resulted from the combined effect between the sample volume utilized and the dispersion of this sample zone in the carrier on the way to the dilution coil. The desired dilution degrees were obtained with a good repeatability using sample volumes of 25 or 50 μL and a transfer volume of 290 or 195 μL, for tGSH and GSSG samples, respectively. Other dilution degrees if necessary could be obtained by changing only the transfer volume (Fig. 3). All dilution studies were developed by comparing the results obtained with standards made by manual volumetric dilution.

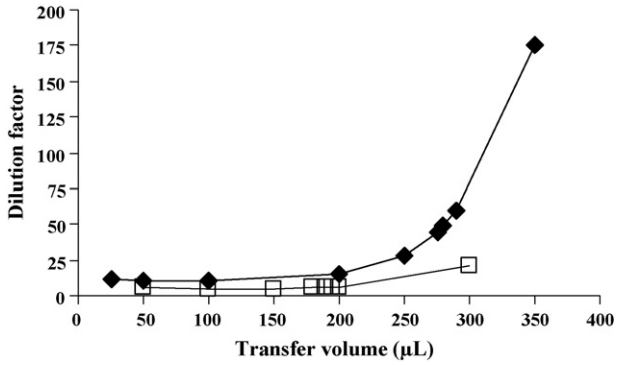

Fig. 3. Influence of transfer volume to the dilution coil on the dilution factor, using 25 μL (♦) and 50 μL (□) of sample. Dilution factor: dilution level obtained by calculating the ratio between the analytical signals obtained with and without dilution.

3.3. Interferences

Reducing agents such as ascorbic acid, β-mercaptoethanol, dithiothreitol and cysteine, or thiol reactive compounds could interfere with the glutathione assay. Therefore, SH compounds, reducing agents and SH reactive materials should be avoided during sample preparation since they can react with DTNB [19].

The GSH analogues in buffer solution were tested and the interference calculated by comparing their response with the one obtained for the GSH standard, by means of the GSH calibration curve established. The values were expressed as a percentage of the GSH standard. A compound was considered interferent when it originates a variation in the response of >5% in relation to the response obtained for the GSH standard at the same concentration. The tested analogues and the respective obtained interference values were: cysteine (4.83%), ascorbic

Table 4
Results obtained by the proposed SIA methodology and the comparison batch procedure for the determination of total glutathione (tGSH) and oxidized glutathione (GSSG) in whole blood samples

Samples	SIA		Comparison procedure		Relative error (%)	
	tGSH[a] (mM)	GSSG[a] (μM)	tGSH[b] (mM)	GSSG[b] (μM)	tGSH	GSSG
1	0.80 (±0.01)	0.99 (±0.07)	0.83 (±0.02)	1.0 (±0.1)	−3.1	−3.9
2	0.655 (±0.004)	2.6 (±0.2)	0.66 (±0.02)	2.9 (±0.2)	−0.2	−10.1
3	0.79 (±0.01)	1.28 (±0.01)	0.766 (±0.005)	1.06 (±0.05)	+3.3	+20.8
4	0.81 (±0.01)	7.6 (±0.3)	0.78 (±0.01)	7.6 (±0.1)	+3.4	+1.1
5	0.910 (±0.007)	5.48 (±0.07)	0.89 (±0.01)	5.2 (±0.2)	+2.4	+4.6
6	0.759 (±0.009)	1.4 (±0.2)	0.77 (±0.01)	1.4 (±0.2)	−1.6	+0.7
7	0.826 (±0.005)	1.5 (±0.3)	0.81 (±0.02)	1.51 (±0.08)	+1.8	+1.3
8	0.77 (±0.02)	1.0 (±0.3)	0.78 (±0.02)	1.0 (±0.4)	−2.2	+5.1
9	0.89 (±0.01)	8.2 (±0.4)	0.92 (±0.02)	8.6 (±0.1)	−3.2	−3.9
10	0.805 (±0.009)	7.3 (±0.2)	0.78 (±0.01)	7.4 (±0.2)	+3.4	−1.4
11	0.69 (±0.02)	7.5 (±0.2)	0.670 (±0.003)	7.8 (±0.2)	+3.0	−4.6
12	1.04 (±0.01)	1.3 (±0.2)	1.018 (±0.007)	1.08 (±0.07)	+2.4	+22.2
13	0.693 (±0.002)	1.55 (±0.07)	0.71 (±0.01)	1.51 (±0.01)	−2.9	+2.6
14	0.96 (±0.01)	0.48 (±0.06)	0.97 (±0.01)	0.50 (±0.05)	−0.9	−4.0

[a] Mean and standard deviation of three consecutive determinations.
[b] Mean and standard deviation of two consecutive determinations.

Table 5
Parameters of the equation $C_p = C_0 + SC_c$ for comparing the results (μM) obtained by the proposed SIA methodology (C_p) and the comparison batch procedure (C_c) and the results of the Students' *t*-test

	C_0[a]	S[a]	r[b]	$t_{0.05}$ Calculated	$t_{0.05}$ Tabulated
Total GSH	8 (±105)	1.0 (±0.1)	0.9797	0.53	2.16
GSSG	0.1 (±0.2)	0.97 (±0.03)	0.9984	0.33	2.16

[a] The values in parentheses are the limits at the 95% confidence.
[b] Correlation coefficient.

acid (2.32%), *N*-acetylcysteine (5.93%), dithiothreitol (9.94%), penicillamine (6.53%) and β-mercaptoethanol (6.14%).

Most of the nonprotein thiol in biological samples is GSH [36] and therefore testing equal concentrations of GSH analogues and GSH implies that extreme conditions are taken into account. It was verified that for the referred concentrations, there was no significant interference from either ascorbic acid or cysteine (endogenous analogues). Therefore, even cysteine does not affect the determination of GSH despite it is being the second most abundant thiol-containing compound in whole blood [36]. This leads to the successful use of the proposed method for the direct and selective determination of GSH in whole blood in the presence of cysteine.

For non-endogenous analogues, it was observed that they could interfere in the glutathione assay.

3.4. Figures of merit

Under the optimised conditions, the calibration curves (Abs (A.U.) = 0.123 (±0.002)C_{GSH} (μM) + 0.097 (±0.003), $R^2 = 0.9989$; Abs (A.U.) = 0.245 (±0.003)C_{GSSG} (μM) + 0.098 (±0.002), $R^2 = 0.9994$) obtained, showed linear responses in concentration ranges of 0.00–3.00 and 0.00–1.50 μM for GSH and GSSG, respectively, being quite appropriate for determination in human whole blood.

It was observed that GSH and GSSG give the same standard curve when expressed on the basis of GSH equivalents, in agreement with previous results [16,17]. This linearity range was perfectly compatible with the determination of total glutathione and glutathione disulfide in whole blood. The detection limit was estimated [37] as three times the standard deviation of 10 blank measurements and values of 0.031 μM for GSH and 0.014 μM for GSSG were obtained.

The repeatability of the SIA procedure was estimated by calculating the relative standard deviation (R.S.D.) from 10 consecutive injections of whole blood samples. Values of 4.4% for GSSG samples (2.05 μM) and 1.5% for tGSH samples (810.93 μM) were obtained, showing small differences over a significant range of concentrations.

The time required for a complete analytical cycle is the sum of the time required for each step and for proper valve port selection. Almost 280 s were required to complete an analytical cycle and hence the determination rate equated to about 13 determinations per hour.

3.5. Validation of the proposed system

To evaluate the accuracy of the proposed system for the determination of tGSH and GSSG, 14 human whole blood samples (after treatment as already described—Sections 2.2 and 3.2) were simultaneously assayed by the comparison batch procedure and by the sequential injection analysis (SIA) methodology (Table 4).

When looking at the results for individual samples, relative errors were higher than 5% for three GSSG samples, despite the absolute deviation correspondents between the reference procedure and the proposed methodology being lower than 0.29 μM (Table 4).

For comparison purposes, linear relationships for the two methods (C_p (μM) = $C_0 + SC_c$ (μM)) were established, either to tGSH or GSSG (Table 5). From this table, it is clear that the estimated intercept and slope do not differ significantly (according to the limits of the 95% confidence intervals observed) from values 0 and 1, respectively. Thus, there is no evidence of systematic differences between the two sets of results [37] obtained by the proposed methodology and by the comparison procedure.

Furthermore, when a paired *t*-test was performed on the data obtained for total glutathione and oxidized glutathione, *t* values of 0.53 and 0.33 were obtained, respectively. The comparison between those values with the critical value tabulated $t = 2.16$ illustrates the absence of statistical differences for the results at the 95% confidence level, obtained by the two methodologies for both total and oxidized glutathione.

4. Conclusions

The proposed SIA methodology was successfully applied to the determination of total and oxidized glutathione in human whole blood, with results comparable to those obtained by the comparison batch procedure and resorting to only a small amount of blood sample and enzyme consumed. Furthermore the developed in-line dilution strategy enables distinct concentrations of the analytes to be determined as several dilution degrees are made available by just changing the time (Step D2—Table 2) in the analytical cycle.

When comparing the two methodologies, a time saving advantage is seen in the developed SIA system, since the comparison batch procedure includes a 5 min-incubation period and 3 min kinetic measurement, in addition to the time spent on addition of the reagents to the cuvettes. Furthermore, rigorous time control is inherent during each assay in the flow system, which is difficult to ensure when analysis in series of different samples are carried out on the comparison procedure. Moreover, the developed methodology if coupled to a sampler, is fully automated and can work for long periods of time.

Compared to other previously described methods for glutathione determination in biological samples, the automatic SIA

system using an enzymatic recycling reaction seems to be most appropriate for this purpose. The developed flow methodology combines the advantages of SIA, with the specificity (guaranteed by the GSSG reductase, which is an important factor given the complexity of the whole blood matrix) and selectivity (GSSG determination after rapid and efficient derivatization of the GSH with M2VP) provided by the DTNB–GSSG reductase recycling reaction. In electrochemistry-based methods, selectivity is not guaranteed [11] and nuclear magnetic resonance does not allow for discrimination between GSH and GSSG [12]. The proposed methodology has a quick sample processing, given the very short time required to ensure full derivatization of GSH (less than 1 min), in contrast to the long derivatization times of some HPLC methods [6]. Using the micellar electrokinetic capillary electrophoresis-based methods, derivatization was not required [10], whereas the detection limits reported were higher than those achieved here. With this SIA system, it was possible to accurately determine the GSH and GSSG concentrations in whole blood, with detection limits comparable to those obtained with other methods [13]. The proposed system can be applied to other biological samples like plasma or isolated erythrocytes, after some modifications in processing the samples.

The proposed SIA methodology fulfils experimental and clinical requirements for the direct measurement of total GSH and GSSG in whole blood samples, allowing the GSH/GSSG ratios to be determined. It could be a choice for implementation in routine assessment of glutathione as an alternative to the conventional batch procedures and represent a useful tool as biomarker of health status/disease risk in humans.

Acknowledgments

A.R.T.S.A. thanks FCT and FSE (III Quadro Comunitário de Apoio) for the Ph.D. grant (SFRH/BD/23029/2005).

References

[1] A. Meister, in: D. Dolphin, R. Poulson, O. Avramovic (Eds.), Glutathione—Chemical, Biochemical and Medical Aspects, Part A, John Wiley and Sons, New York, 1989.
[2] T.P.M. Akerboom, H. Sies, Methods in Enzymology, Assay of Glutathione, Glutathione Disulfide and Glutathione Mixed Disulfides in Biological Samples, vol. 77, Academic Press, New York, 1981, p. 373.
[3] S.I. Baskin, H. Salem, Oxidants, Antioxidants and Free Radicals, Taylor & Francis, Washington, 1997, pp. 173–174.
[4] B.J. Mills, J.P. Richie Jr., C.A. Lang, Anal. Biochem. 222 (1994) 95.
[5] A. Pastore, G. Federici, E. Bertini, F. Piemonte, Clin. Chim. Acta 333 (2003) 19.
[6] D. Giustarini, I. Dalle-Donne, R. Colombo, A. Milzani, R. Rossi, Free Radic. Biol. Med. 35 (2003) 1365.
[7] A.K. Sakhi, K.M. Russnes, S. Smeland, R. Blomhoff, T.E. Gundersen, J. Chromatogr. A 1104 (2006) 179.
[8] J.P. Steghens, F. Flourié, K. Arab, C. Collombel, J. Chromatogr. B 798 (2003) 343.
[9] R. Rossi, A. Milzani, I. Dalle-Donne, D. Giustarini, L. Lusini, R. Colombo, P. Di Simplicio, Clin. Chem. 48 (2002) 742.
[10] K. Havel, K. Pritts, T. Wielgos, J. Chromatogr. A 853 (1999) 215.
[11] F. Ricci, F. Arduini, C.S. Tuta, U. Sozzo, D. Moscone, A. Amine, G. Palleschi, Anal. Chim. Acta 558 (2006) 164.
[12] R.P. Mason, G.H. Cha, G.H. Gorrie, E.E. Babcock, P.P. Antich, FEBS Lett. 318 (1993) 30.
[13] J. Zhang, Z. Hu, X. Chen, Talanta 65 (2005) 986.
[14] S. Wang, H. Ma, J. Li, X. Chen, Z. Bao, S. Sun, Talanta 70 (2006) 518.
[15] V.H. Cohn, J. Lyle, Anal. Biochem. 14 (1966) 434.
[16] C.W.I. Owens, R.V. Belcher, Biochem. J. 94 (1965) 705.
[17] F. Tietze, Anal. Biochem. 27 (1969) 502.
[18] R. Brigelius, C. Muckel, T.P.M. Akerboom, H. Sies, Biochem. Pharmacol. 32 (1983) 2529.
[19] F.A.M. Redegeld, M.A.J. van Opstal, E. Houdkamp, W.P. van Bennekom, Anal. Biochem. 174 (1988) 489.
[20] J. Ruzicka, G.D. Marshall, Anal. Chim. Acta 237 (1990) 329.
[21] E.H. Hansen, J. Environ. Sci. Heal. 40 (2005) 1507.
[22] V.F. Fairbanks, G.G. Klee, in: N.W. Tietz (Ed.), Fundamental of Clinical Chemistry, Saunders, Philadelphia, PA, 1987.
[23] D.P. Jones, J.L. Carlson, P.S. Samiec, P. Sternberg Jr., V.C. Mody Jr., R.L. Reed, L.A.S. Brown, Clin. Chim. Acta 275 (1998) 175.
[24] S.K. Srivastava, E. Beutler, Anal. Biochem. 25 (1968) 70.
[25] T. Gübeli, G.D. Christian, J. Ruzicka, Anal. Chem. 63 (1991) 2407.
[26] R.E. Taljaara, J.F. van Staden, Lab. Robotics Automat. 10 (1998) 325.
[27] M.E. Anderson, Methods in Enzymology, Determination of Glutathione and Glutathione Disulfide in Biological Samples, vol. 113, Academic Press, New York, 1983, pp. 548–550.
[28] J.H. Jandl, Blood—Textbook of Hematology, second ed., Little, Brown and Company, Boston, 1996, p. 298.
[29] R.T. Foley, R.C. Anderson, J. Am. Chem. Soc. 70 (1948) 1195.
[30] D.C. Stempak, S. Dallas, J. Klein, R. Bendayan, G. Koren, S. Baruchel, Clin. Pharmacol. Ther. 67 (2000) 116.
[31] O.W. Griffith, Anal. Biochem. 106 (1980) 207.
[32] Colorimetric Determination of Reduced and Oxidized Glutathione, Bioxytech GSH:GSSG-412 Assay, OxisResearch, Portland, OR, US Patent 5,543,298.
[33] J.P. Richie Jr., L. Skowronski, P. Abraham, Y. Leutzinger, Clin. Chem. 42 (1996) 64.
[34] J.F. Van Staden, R.E. Taljaard, Fresenius J. Anal. Chem. 357 (1997) 577.
[35] A. Baron, M. Guzman, J. Ruzicka, G.D. Christian, Analyst 117 (1992) 1839.
[36] P.C. Jocelyn, Biochemistry of the SH Group, Academic Press, New York, 1973, p. 10.
[37] J.C. Miller, J.N. Miller, Statistics and Chemometrics for Analytical Chemistry, fourth ed., Pearson Education, England, 2000, pp. 48–50, 120–123.

Available online at www.sciencedirect.com
ScienceDirect
Talanta 74 (2008) 1201–1210
Talanta
www.elsevier.com/locate/talanta

Application of multivariate curve resolution alternating least squares (MCR-ALS) to the quantitative analysis of pharmaceutical and agricultural samples

T. Azzouz, R. Tauler*

Department of Environmental Chemistry, IIQAB-CSIC, Jordi Girona 18, Barcelona 08034, Spain

Received 13 April 2007; received in revised form 13 August 2007; accepted 24 August 2007
Available online 30 August 2007

Abstract

Application of multivariate curve resolution alternating least squares (MCR-ALS), for the resolution and quantification of different analytes in different type of pharmaceutical and agricultural samples is shown. In particular, MCR-ALS is applied first to the UV spectrophotometric quantitative analysis of mixtures of commercial steroid drugs, and second to the near-infrared (NIR) spectrophotometric quantitative analysis of humidity and protein contents in forage cereal samples. Quantitative results obtained by MCR-ALS are compared to those obtained using the well established partial least squares regression (PLSR) multivariate calibration method.
© 2007 Published by Elsevier B.V.

Keywords: Forage analysis; NIR spectroscopy; MCR-ALS; PLSR

1. Introduction

In this work, direct quantitative spectrophotometric determination of mixtures of analytes in two types of samples is investigated. First, mixtures of pharmaceutical products in drug samples are analyzed by UV–vis spectrophotometry. This technique is a rapid and inexpensive analytical technique and as such is highly suitable for control analyses of pharmaceutical preparations. However, the lack of selectivity of UV–vis absorption measurements hinders its general application in the presence of strongly overlapped absorption bands of the different sample components. Pharmaceutical preparations are usually mixtures of the active principles and of various excipients absorbing in the same spectral region. The development of multivariate calibration methods based on the mathematical resolution of multivariate signals can allow their rapid resolution and quantification. The second type of samples studied in this work are forage (cereal) agricultural samples analyzed by near-infrared (NIR) spectroscopy. This technique has gained wider acceptance in different fields, due to its advantages over other analytical spectroscopic techniques. One of the best advantages of NIR spectroscopy is the possibility of working in reflectance mode and the use of fibre optical probe modules easily coupled to the spectrophotometer. This allows measurements of solid and liquid samples with little sample pretreatment, the implementation of continuous methodologies, the fast acquisition of spectra and the prediction of both physical and chemical parameters from the same sample. Near-infrared spectrophotometry (NIRS) is a non-destructive technique, very fast and easy to implement, without needing reagents and without wastes produced. Once calibrated, NIRS is simple to operate and it is well suited for the determination of the major components in many types of samples, such as protein and water contents in food and forage samples. Multivariate calibration methods like partial least squares regression (PLSR) have been frequently used to extract analytical information from UV–vis and NIR spectra.

Since in general it is very difficult to have completely selective analytical signals for every analyte of interest in a multicomponent sample, their physical separation by chromatographic methods or by any other analytical separation methods, or their mathematical resolution using chemometric methods is a preliminary step necessary for their quantitative determination, especially in the analysis of complex natural samples. Apart from the well known multivariate calibration methods

* Corresponding author.
E-mail address: rtaqam@iiqab.csic.es (R. Tauler).

0039-9140/$ – see front matter © 2007 Published by Elsevier B.V.
doi:10.1016/j.talanta.2007.08.024

like PLSR [1,2] other chemometric methods exist that allow for the direct mathematical analysis of the different components in evolving mixture systems (*Evolving Factor Analysis*, EFA) [3], for the detection of the more selective variables (SIMPLISMA [4–6]) or for the resolution of the components simultaneously present in a particular data window (*Window Factor Analysis method* [7]). The multivariate curve resolution alternating least squares (MCR-ALS) method proposed in this work [8–13] has been shown to provide an improved resolution compared to other methods and to allow quantitative determinations in the analysis of complex mixtures using spectroscopic means. MCR-ALS has been applied to the study of complex industrial evolving processes [14], to the investigation of multiequilibria systems using spectroscopic titrations (fluorescence, UV–vis absorption, etc.) [15], to the resolution of multiple coeluted peaks in chromatography [10], to the resolution and quantification of mixtures in flow injection analysis [16], to the resolution of the different components in kinetic reactions and processes [17], to the resolution of spectroscopic images [18], to multidimensional spectroscopy [19], to electrophoretic studies of amino acids [20], to voltammetric studies of metal complexes [21–23], to studies of conformational changes of polynucleotide [24] and protein folding processes [25], and to the resolution and apportionment of environmental sources of contamination [26]. In this work, the use of MCR-ALS is proposed for the quantitative determination of mixtures of analytes using first order spectrophotometric data (UV–vis and NIR absorption spectrophotometric data). A *correlation constraint* introduced in a previous work for the analysis of mixtures of metal ions analyzed by voltammetry [22] is extended in this work to establish alternating least squares (ALS) multivariate calibration models for the quantitative determination of analyte mixtures using UV and NIR spectrophotometric data. The results obtained using MCR-ALS with this new correlation constraint are then compared to those obtained using the nowadays well established PLSR multivariate calibration [37].

2. Experimental

2.1. Reagents and solutions

The following reagents and solutions were used:

- Acetonitril (Carlo Erba) for HPLC.
- Methanol (Panreac) was used for the synthetic preparation of standard, synthetic mixture and drug samples.
- Etinilestradiol (Sigma), minimum 98% (HPLC).
- Levonorgestrel (Sigma), minimum 98% (HPLC).

2.2. Pharmaceutical products

Concentrated stock solutions of etinilestradiol and levonorgestrel were prepared in methanol. From these stock solutions, 25 synthetic mixtures were prepared from which 15 samples were used as a calibration data set, and the remaining samples were used as external validation data set. The concentration range of etinilestradiol was between 3 and 31 mg/l, and for levonorgestrel between 3 and 20 mg/l. Etinilestradiol and levonorgestrel were analyzed in commercial drugs: Microgynon, Neogynona and Triagynon (ochre and brown color). From 30 original drug samples, 20 were used as a calibration data set, and the remaining samples were used as external validation data set.

The procedure used to prepare the drug samples was the following: for each drug around 20 tablets were weighted, grinded and homogenized. Methanol was used as dissolvent. Drug samples were placed in an ultrasounds bath and then centrifuged. UV–vis spectra were recorded, using methanol as a blank. Concentrations of the two analytes in these drug samples were estimated by high performance of liquid chromatography (HPLC). Chromatographic determinations were performed using diode array UV–vis, Hewlett Packard detector. The column used is a reversed phase Spherisorb ODS-2 C18 column (15 cm long × 0.4 cm i.d., 5 μm particle size) with a C18 precolumn. The mobile phase composition used for the chromatographic determinations was acetonitril/H_2O (40/60) (v/v). A flow rate of 1.2 ml/min was used.

2.3. Forage samples

Different analytes in Ray-Grass forage samples were determined. The experimental procedure used before analyzing the Ray-Grass samples by means of NIR spectrophotometry was rather simple: samples were grinded, milled, homogenized, put in a capsule and directly measured by NIR spectrophotometry. Spectra from 125 samples were selected randomly for calibration, and spectra from other 46 samples were used for validation. Calibration samples were selected randomly trying to cover all the observed spectral data variance. If one of the selected validation samples resulted to be outside of the range covered by the calibration samples, it was exchanged by a calibration sample within the calibration range.

Humidity reference concentrations were estimated from the sample weight loss after oven drying at 103 °C for 4 h [27]. Some volatile compounds apart from water could evaporate decreasing sample total weight and causing excess errors, while other compounds may be oxidized, increasing the sample total weight and causing defect errors. Weight errors will depend on the compensation of these two effects. Protein reference concentrations have been estimated from nitrogen content analyzed using Kjeldhal method [28,29] and multiplied by a factor equals to 6.25 (which is derived from the fact that proteins of forages have an average content of nitrogen equals approximately to 15%). The humidity concentration range was between 4.86 and 13.33% (w/w), and for protein between 6.53 and 21.70% (w/w).

2.4. Instrumentation

UV–vis spectrophotometric determinations were performed by a Hewlett-Packard (Waldbronn, Germany) HP8452A diode array spectrophotometer. The instrument's bundled software HP 89530 MS-DOS UV–vis includes facilities for controlling, acquiring and processing spectra. In Fig. 1, the normalized

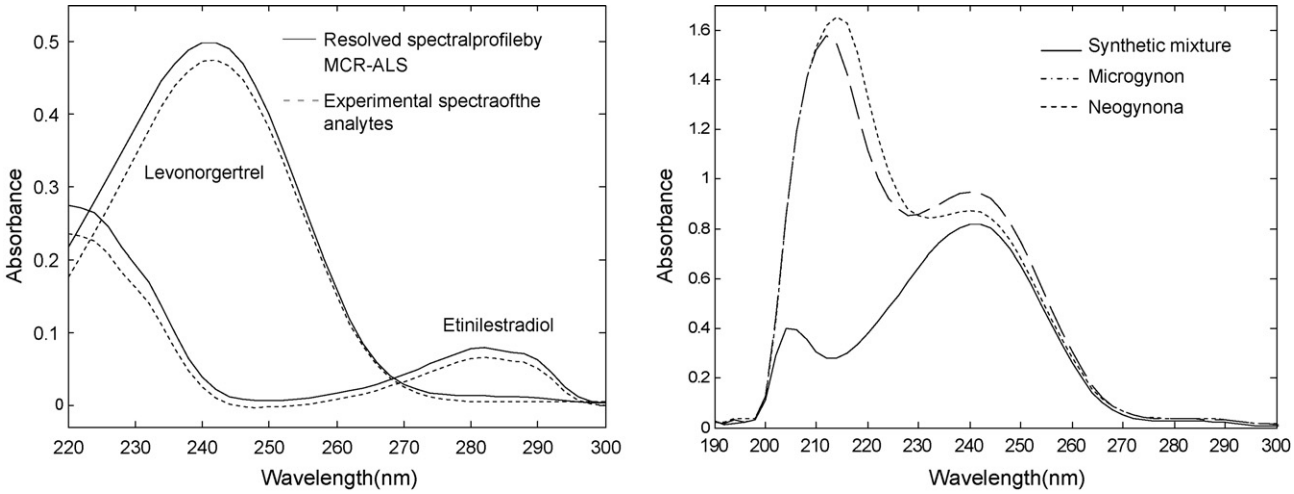

Fig. 1. Spectra of etinilestradiol and levonorgestrel analytes (left) and spectra of a synthetic mixture of them and of Microgynon and Neogynona drugs (right).

experimental spectra of etinilestradiol and levonorgestrel are presented (left), as well as spectra of the synthetic and commercial drug mixtures of them (right).

- Ultrasounds Bath, Selecta 0.61.
- Centrifuge, Arlesa model Digicen.
- NIR spectrophotometric determinations were performed using NIRSystems 6500 FOSS spectrophotometer. Each of the spectra finally considered is an average of 32 diffuse reflectance spectra. Sample containers were rectangular cups. The wavelength interval was 1100–2500 nm with 2 nm resolution. In Fig. 2, the obtained spectra of Ray-Grass samples are shown. Laboratory temperatures were always kept between 20 and 25 °C and relative humidity was always between 45 and 65%.

3. Chemometric methods

3.1. Multivariate curve resolution alternating least squares (MCR-ALS)

The first step of this chemometric data analysis procedure is to build up the data matrix, **D**. In the rows of this data matrix are the different individual spectra measured for the different analyzed samples and in the columns the absorbance (UV–vis) or Log 1/*R* (NIRS) measured values at each spectral wavelength. First a rough estimation of the possible number of components is obtained using different methods like principal component analysis (PCA) [2,5,13]. A bilinear relation between the experimental data, the concentrations and the pure spectra of the components is assumed, of analogous structure to the generalized law of Lambert–Beer [30], where the individual responses of each analyte or component are additive. In matrix form, this bilinear model is expressed in the following way:

$$\mathbf{D} = \mathbf{C}\mathbf{S}^{\mathrm{T}} + \mathbf{E} \quad (1)$$

where $\mathbf{D}(I,J)$ is the matrix of experimental data, of dimensions I samples (spectra) by J wavelengths; $\mathbf{C}(I,K)$ is the matrix of concentration profiles of the different K analytes presents in the samples; $\mathbf{S}^{\mathrm{T}}(K,J)$ is the spectra matrix, whose K rows contain the pure spectra associate with the K species present in the samples; $\mathbf{E}(I,J)$ is the matrix associated to the experimental error. The resolution of experimental spectral data matrix **D** consists of the following steps, which are summarized in Fig. 3.

To initiate the iterative ALS procedure, an initial estimation is needed for the spectral or concentration profiles for each species. Different methods are used for this purpose like evolving factor analysis [1–3] or the determination of the purest variables [4–6]. In this work, initial estimations based on purest variables were preferred. If the initial estimations are the spectral profiles, the unconstrained least squares solution for the concentration profiles can be calculated from the expression:

$$\mathbf{C} = \mathbf{D}(\mathbf{S}^{\mathrm{T}})^{+} \quad (2)$$

where $(\mathbf{S}^{\mathrm{T}})^{+}$ is the pseudoinverse matrix of the spectra matrix $\mathbf{S}^{\mathrm{T}}$, which is equal to $\mathbf{S}(\mathbf{S}^{\mathrm{T}}\mathbf{S})^{-1}$, when $\mathbf{S}^{\mathrm{T}}$ is of full rank [31]. If the initial estimations are the concentration profiles, the unconstrained least squares solution for the spectra can be calculated

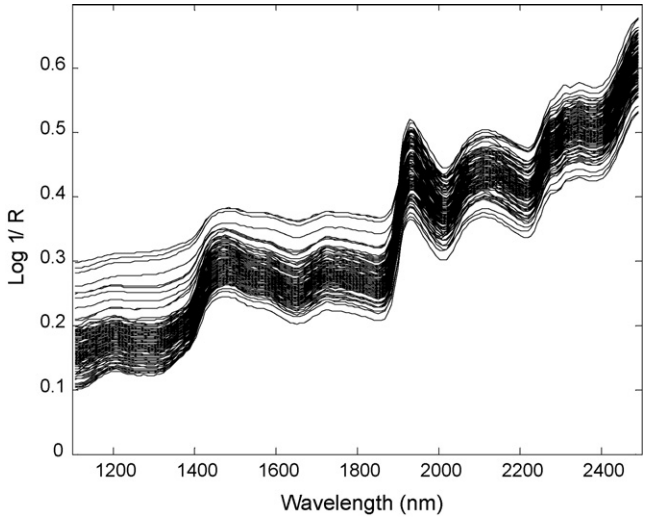

Fig. 2. NIR spectra of Ray-Grass calibration samples.

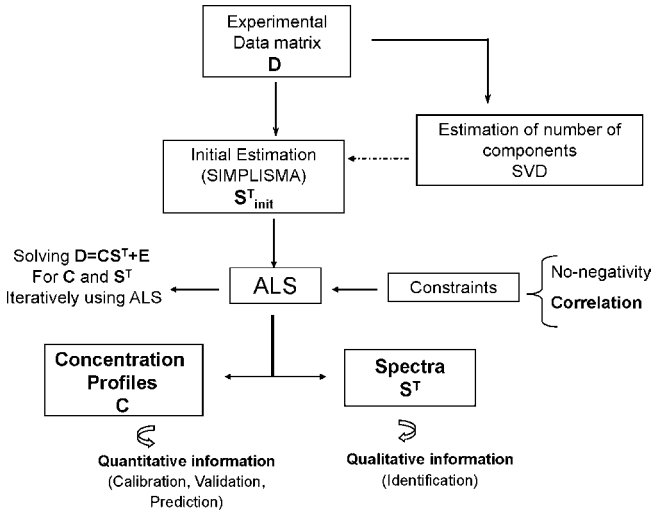

Fig. 3. Scheme of step of the resolution process in MCR-ALS method. See Section 3.1.

from the expression:

$$\mathbf{S}^{\mathrm{T}} = \mathbf{C}^{+}\mathbf{D} \tag{3}$$

where $\mathbf{C}^{+}$ is pseudoinverse of matrix $\mathbf{C}$ ($\mathbf{C}^{+} = (\mathbf{C}^{\mathrm{T}}\mathbf{C})^{-1}\mathbf{C}^{\mathrm{T}}$, when $\mathbf{C}$ is of full rank) [31]. Both steps can be implemented in an alternating least squares cycle so that in each iteration new matrices of $\mathbf{C}$ and $\mathbf{S}^{\mathrm{T}}$ are then obtained. However, during these iterative calculations, a series of constraints with the purpose of giving solutions with physical meaning and of limiting their possible number are applied [11,12]. Iterations continue until an optimal solution is obtained that fulfils the constraints postulated and the established convergence criteria. Constraints applied in this work are only described briefly.

3.1.1. Nonnegativity concentration constraint

This is a general constraint used in curve resolution methods [32–36]. It is applied to the concentration profiles, due to the fact that the concentrations of the chemical species are always positive values or zero.

3.1.2. Nonnegativity spectra constraint

The application of this constraint depends on what instrumental technique is used for detection. In the case of UV–vis or NIR spectra, the intensity of the radiation absorbed or reflected by the sample never takes negative values.

3.1.3. Correlation constraint

This constraint has been introduced for the simultaneous quantitative analysis of mixtures of metal ions using voltammetric analysis and it implies [22] the establishment of calibration models for MCR-ALS, to be used for the quantitative determination of the analytes in the presence of unknown interferences. In this work, this constraint is extended to quantitative analysis

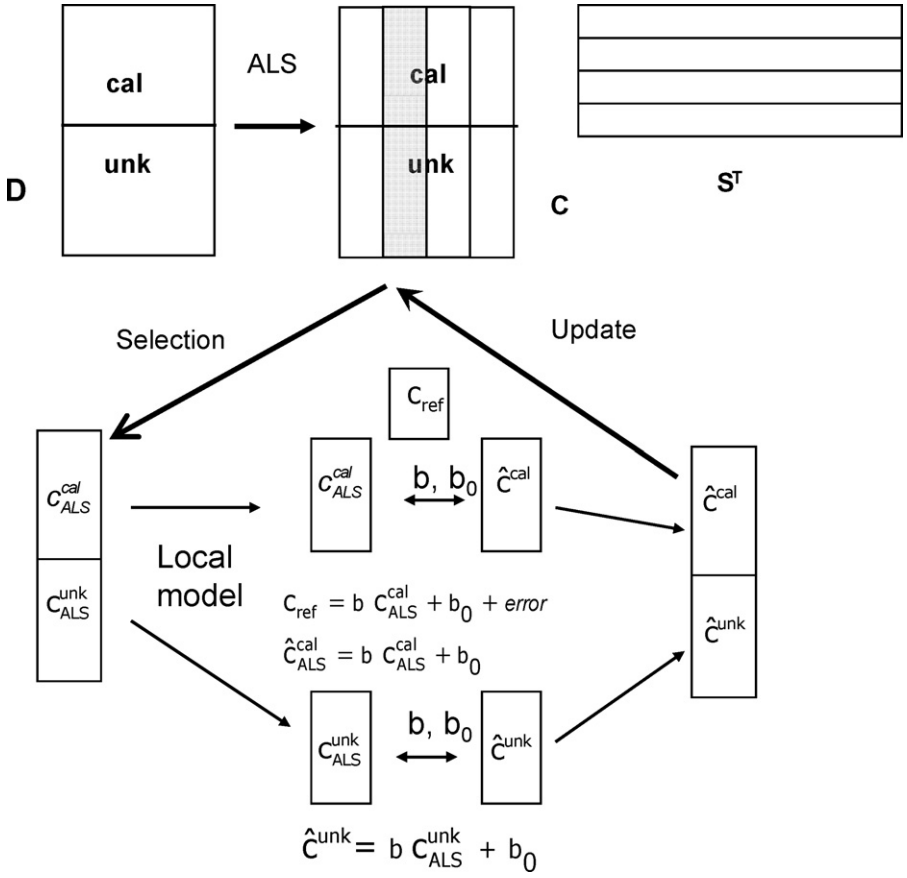

Fig. 4. Detailed description of the correlation constraint. See Section 3.1.

of spectral data in the simultaneous analysis of different analytes in samples of increasing complexity, including forage samples. This correlation constraint is explained in detail in Fig. 4, and it consists, of a series of steps performed during each iteration of the ALS optimization. Concentrations of a particular analyte in calibration samples, $\mathbf{c}_{\mathrm{ALS}}^{\mathrm{cal}}$, obtained by ALS at each iteration are correlated with previously known reference concentration values of the analyte $\mathbf{c}^{\mathrm{ref}}$ in these samples. A local linear model between the values $\mathbf{c}_{\mathrm{ALS}}^{\mathrm{cal}}$ and $\mathbf{c}^{\mathrm{ref}}$, is then built up so that:

$$\mathbf{c}^{\mathrm{ref}} = b\mathbf{c}_{\mathrm{ALS}}^{\mathrm{cal}} + b_0 + \mathbf{e}^{\mathrm{ref}} \tag{4}$$

where, b and b_0 are then the slope and offset values which better fit $\mathbf{c}_{\mathrm{ALS}}^{\mathrm{cal}}$ to $\mathbf{c}^{\mathrm{ref}}$, obtained by least squares linear regression, and $\mathbf{e}^{\mathrm{ref}}$ is the error in the reference concentrations (not modeled) The corresponding concentration values of these calibration samples calculated using this local model are:

$$\hat{\mathbf{c}}^{\mathrm{cal}} = b\mathbf{c}_{\mathrm{ALS}}^{\mathrm{cal}} + b_0 \tag{5}$$

And in order to predict the unknown concentration of the analyte in the new prediction samples $\hat{\mathbf{c}}^{\mathrm{unk}}$, the equation used is:

$$\hat{\mathbf{c}}^{\mathrm{unk}} = b\mathbf{c}_{\mathrm{ALS}}^{\mathrm{unk}} + b_0 \tag{6}$$

where b and b_0 are the values obtained previously in the calibration step from $\mathbf{c}^{\mathrm{ref}}$, and $\mathbf{c}_{\mathrm{ALS}}^{\mathrm{unk}}$ are the concentrations of the samples predicted by ALS. Each ALS iteration is then completed after updating the obtained values of prediction (i.e., by substitution of $\mathbf{c}_{\mathrm{ALS}}^{\mathrm{unk}}$ by $\hat{\mathbf{c}}^{\mathrm{unk}}$).

3.2. Partial least squares regression (PLSR)

PLSR method has been widely used in chemometrics to regression problems with highly correlated variables as it is often encountered in spectroscopy [37,38]. This regression method is based on a prediction model for the analyte concentration in the samples using efficiently the information contained in both data blocks, the spectroscopic data block (**D** matrix) and the concentrations data block (**c** vector). **D** and **c** were mean-centered prior to decomposition in factors. The PLSR algorithm selects successive orthogonal factors that maximize the covariance between spectra (**D** matrix) and analyte concentration (**c** vector). The objective of fitting a PLSR model, is to find a few number of PLSR factors that explain most of the covariation between both data blocks. Briefly, PLSR decomposes **D** and **c** into factor scores (**T**) and factor loadings (**P** and **q**) according to:

$$\mathbf{D} = \mathbf{T}\mathbf{P}^{\mathrm{T}} + \mathbf{E} \tag{7}$$

$$\mathbf{c} = \mathbf{T}\mathbf{q} + \mathbf{f} \tag{8}$$

where **T** is the scores matrix, $\mathbf{P}^{\mathrm{T}}$ and **q** are the matrix and vector loadings describing the variance in **D** and **c**, respectively, and **E** and **f** are the residuals in **D** and **c**, respectively. This decomposition is performed simultaneously and in such a way that the first few factors should explain most of the covariation between **D** and **c**. The remaining factors resemble noise and can thus be ignored, hence the addition of residuals **E** and **f**.

3.3. Validation of results

In order to asses the quality of multivariate calibration models (from PLSR and MCR-ALS), it is convenient to do their validation using new samples not used during the calibration step. In this work, external validation was performed using a set of independent samples, whose spectra were not used to build the calibration model. From the whole original data set, a number of representative samples were selected for the calibration set. The remaining samples were then only used to validate the model.

The following expressions were used to express the validation results:

Root mean square error of prediction (RMSEP)

$$\mathrm{RMSEP} = \sqrt{\frac{\sum_{i=1}^{n}(\mathbf{c}_i - \hat{\mathbf{c}}_i)^2}{n}} \tag{9}$$

Standard error of prediction (SEP)

$$\mathrm{SEP} = \sqrt{\frac{\sum_{i=1}^{n}(\mathbf{c}_i - \hat{\mathbf{c}}_i - \mathrm{Bias})^2}{n-1}} \tag{10}$$

Bias (is a meaning of systematic error)

$$\mathrm{Bias} = \frac{\sum_{i=1}^{n}(\mathbf{c}_i - \hat{\mathbf{c}}_i)}{n} \tag{11}$$

In all these expressions, $\mathbf{c}_i$ and $\hat{\mathbf{c}}_i$ are, respectively, the known and calculated analyte concentration in sample i, and n is the total number of samples considered in the validation. Also in order to evaluate the quality of the obtained results of the concentrations predicted by the application of the MCR-ALS or PLS models, for a particular analyte using n samples, the relative error in the predicted concentrations, in percentage (RE%), was calculated as:

$$\mathrm{RE}\,(\%) = 100\sqrt{\frac{\sum_{i=1}^{n}(\mathbf{c}_i - \hat{\mathbf{c}}_i)^2}{\sum_{i=1}^{n}\mathbf{c}_i^2}} \tag{12}$$

3.4. Chemometrics software

Data processing and PLS calibration calculations were carried out using commercial software packages: PLS Toolbox software version 2.1 (Eigenvector research, WA, USA) in MATLAB computer and visualization environment (The Mathworks, MA, USA), and UNSCRAMBLER software version 6.11 (CAMO A/S, Trondheim, Norway, 1986–1997). Multivariate curve resolution (MCR-ALS) has been implemented in MATLAB and it is available in Internet. See Ref. [13] for further details.

4. Results and discussion

4.1. MCR-ALS resolution and quantification of etinilestradiol and levonorgestrel steroids on commercial drugs analyzed by UV spectrophotometry

MCR-ALS has been applied first to synthetic experimental mixture samples for the resolution and quantification of steroids. Results were compared to those obtained by application of PLSR. Different wavelength intervals were investigated.

In Fig. 1, spectral profiles obtained by MCR-ALS are given. They are in agreement with the spectra of etinilestradiol and levonorgestrel pure standards. In contrast to MCR-ALS, PLS regression does not provide direct estimation of the pure spectra of the components of the mixture, although PLS loadings and weights may be interpreted in relation to the more relevant spectral features of the components present in the analyzed mixtures, specially for those for which the quantitative analytic information is available during the calibration step.

Quantitative results obtained by ALS and PLS methods for the different wavelength intervals are compared in Table 1.

Errors in Table 1 are obtained for external validation samples of synthetic mixtures. Number of components used in the calibration model was two in both cases, either for etinilestradiol or levonorgestrel. Constraints used in ALS optimization were non-negativity (for concentration and spectra profiles) and the new correlation constraint proposed in this work. Quantification errors obtained by MCR-ALS are in all the cases of the same order of magnitude than those obtained by application of PLSR. Bias in the case of etinilestradiol is higher than the bias obtained for levonorgestrel, which might be due to the lower concentrations used for this analyte in the mixtures. In the case of etinilestradiol the 230–300 nm interval gave the optimal quantification results and for levonorgestrel the best interval was 220–300 nm. Once the wavelength interval was chosen for the analysis of the two analytes in their synthetic mixtures, commercial drugs were analyzed using the same conditions.

Table 1
Figures of merit in the quantitative analysis of etinilestradiol and levonorgestrel analytes in synthetic mixtures using UV spectrophotometry (at different wavelength ranges) and PLS and MCR-ALS multivariate calibration methods

	RMSEP	SEP	Bias	RE (%)	r^2
Etinilestradiol					
220–300 nm					
ALS	0.738	0.486	0.581	3.316	0.9996
PLS	0.721	0.480	0.564	3.242	0.9996
230–300 nm					
ALS	0.616	0.395	0.493	2.769	0.9997
PLS	0.610	0.399	0.483	2.742	0.9997
250–300 nm					
ALS	0.591	0.371	0.478	2.655	0.9994
PLS	0.645	0.383	0.536	2.897	0.9994
Levonorgestrel					
220–300 nm					
ALS	0.098	0.073	0.070	0.784	0.9999
PLS	0.093	0.072	0.065	0.749	0.9999

RMSEP is root mean square error of prediction (Eq. (9)); SEP is standard error of prediction (Eq. (10)); Bias is a systematic error (Eq. (11)); r^2 is coefficient of correlation between calculated and actual concentration values of the analyzed compounds; RE% is the relative error in the predicted concentrations, in percentage (Eq. (12)). See text.

In Table 2 (upper part), results of the quantification of etinilestradiol and levonorgestrel steroids in Microgynon, commercial drug are given. Quantification of etinilestradiol in Microgynon resulted to be better in the 250–300 nm wavelength interval than in 220–300 nm range (see below), using three components, either for PLSR or MCR-ALS. Obtained errors were of the same order for MCR-ALS and PLSR. These errors were slightly higher than those obtained for synthetic mixtures, which is reasonable, since in synthetic mixtures no excipient interferences were present. Also since etinilestradiol is a minor component, it was more affected by the presence of these interferences. For levonorgestrel, rather good quantification results were obtained at the same wavelength intervals than with syn-

Table 2
Figures of merit in the quantitative analysis of etinilestradiol and levonorgestrel analytes, in Microgynon, Neogynona and Triagynon (brown and ochre) commercial drugs, using UV spectrophotometry (at different wavelength ranges) and PLS and MCR-ALS methods

	Etinilestradiol (250–300 nm)					Levonorgestrel (220–300 nm)				
	RMSEP	SEP	Bias	RE (%)	r^2	RMSEP	SEP	Bias	RE (%)	r^2
Microgynon										
ALS	0.149	0.086	0.129	4.534	0.9919	0.284	0.279	0.150	1.723	0.9998
PLS	0.143	0.081	0.125	4.366	0.9931	0.282	0.278	0.146	1.706	0.9998
Neogynona										
ALS	0.062	0.073	0.017	1.856	0.9963	0.184	0.226	0.002	1.007	0.9979
PLS	0.088	0.075	0.063	2.642	0.9964	0.200	0.229	−0.071	1.094	0.9980
Triagynon (brown)										
ALS	0.439	0.304	−0.361	4.457	0.9907	0.685	0.522	−0.551	3.747	0.9947
PLS	0.422	0.289	−0.349	4.287	0.9906	0.704	0.528	−0.557	3.856	0.9936
Triagynon (ochre)										
ALS	0.092	0.064	6.38é$^{-2}$	2.909	0.9921	0.165	0.206	−3.21e^{-3}	1.226	0.9970
PLS	0.124	0.071	1.09e^{-1}	3.927	0.9873	0.159	0.181	−6.0ê$^{-2}$	1.183	0.9986

See Table 1 for the meaning of RMSEP, SEP, bias, r^2 and RE (%).

thetic mixtures (220–300 nm), either using MCR-ALS or PLSR, using three components in each case.

In Table 2 (middle part), results in the quantification of the same analytes in Neogynona drug are given. The optimal interval for the quantification of etinilestradiol in Neogynona commercial drug was the same than for the quantification of Microgynon (250–300 nm). The use of the more restricted 250–300 nm spectral range for the analysis of these two commercial drugs instead of the 220–300 nm spectral range used during the analysis of the synthetic mixtures was due to the presence of drug interferences (excipient) that also absorb in the 220–250 nm spectral range. The inclusion of the 220–250 range would affect negatively the quantification of etinilestradiol in the commercial drugs. So, finally the 250–300 nm spectral range was considered to be the best one for the quantification of this analyte. Obtained errors were of the same order for MCR-ALS and for PLSR, and a little higher than for the synthetic mixtures. For levonorgestrel also a good quantification was obtained in the same wavelengths interval than for synthetic mixtures (220–300 nm), either for MCR-ALS or for PLSR. The number of components used to explain the model for each analyte, were in this case (like for Microgynon) three components, either for PLSR or MCR-ALS.

And finally, also in Table 2 (lower part), obtained results for the quantification of the two steroids in Triagynon (brown and ochre color), using MCR-ALS and PLS are also given. Optimal wavelength interval for the quantification of etinilestradiol in Triagynon (ochre and brown color pills) was at 250–300 nm, and obtained errors were of the same order for MCR-ALS and for PLSR. For levonorgestrel, the optimal quantification was obtained in the wavelength interval of 230–300 nm, either for MCR-ALS or for PLSR. The number of components used to explain the model, for each analyte, was again three components, either for PLSR or for MCR-ALS.

Differences observed in the results obtained in all cases by application of MCR-ALS or PLSR were considered to be little significant. A deeper interpretation of these small differences would require the study of a larger number of samples with a better control of the factors that can influence these small differences. Nevertheless, it is possible to conclude that at least in the analysis of synthetic mixtures and in the analysis of the investigated commercial drugs, MCR-ALS provided quantitative results of similar quality to those provided by the application of PLSR. The obvious advantage of MCR-ALS compared to PLSR is, however, that MCR-ALS recovers the qualitative information as well, including the pure spectra of the components (Fig. 1), and also of the interferents, allowing their possible identification/confirmation.

4.2. MCR-ALS resolution and quantification of humidity and protein content on natural samples (Ray-Grass) analyzed by NIR spectrophotometry

NIR spectroscopy has been widely applied as an analytical technique in the agricultural food sector, using partial least squares (PLS) to develop calibration equations for the determination of the humidity and protein content [39–41]. In this work, MCR-ALS and PLS methods have been applied and compared in the analysis of natural Ray-Grass forage samples using NIR spectrophotometry, with the purpose of obtaining both qualitative and quantitative information of the humidity and protein present in these samples. Obviously, in this case, difficulties for a proper calibration will be more important because of the larger contribution of unknown physical contributions and chemical interferents in the measured NIR spectra of the analyzed forage samples. This example will probably illustrate the limits of the use of the proposed MCR-ALS method for quantitative determinations of natural samples using first order spectrophotometric data. Comparison of MCR-ALS results with PLSR results is pertinent since this is a much extended method used for calibration of NIR spectrophotometric data [37].

In Table 3, obtained results in the quantification of humidity and protein in Ray-Grass forage samples using NIR spectrophotometric data and MCR-ALS and PLS are given. A summary of prediction errors for these two analytes, using different number

Table 3
Figures of merit in the quantitative analysis of humidity and protein analytes in Ray-Grass samples using NIR spectrophotometry and PLS and MCR-ALS methods

Number of factors	RMSEP		SEP		Bias		r^2		RE (%)	
	ALS	PLS	ALS	PLS	ALS	PLS	ALS	PLS	ALS	PLS
Humidity										
5	0.391	0.313	0.370	0.316	0.045	0.008	0.962	0.973	4.383	3.721
6	0.369	0.301	0.370	0.305	0.046	0.009	0.962	0.975	4.387	3.585
7	0.358	0.307	0.360	0.311	0.043	0.006	0.964	0.974	4.260	3.654
8	0.361	0.289	0.363	0.292	0.030	0.008	0.963	0.977	4.287	3.432
9	0.285	0.313	0.289	0.313	0.004	0.004	0.977	0.973	3.394	3.724
10	0.286	0.269	0.290	0.268	−0.005	0.004	0.977	0.980	3.406	3.199
Protein										
5	1.286	0.789	1.300	0.797	0.013	0.026	0.957	0.984	7.656	4.695
6	0.808	0.724	0.816	0.730	0.046	0.061	0.983	0.986	4.813	4.314
7	0.841	0.623	0.850	0.628	0.002	0.049	0.982	0.990	5.008	3.711
8	0.871	0.560	0.880	0.555	0.003	0.011	0.980	0.992	5.184	3.334
9	0.973	0.559	0.981	0.559	0.074	0.083	0.976	0.992	5.792	3.327
10	0.748	0.559	0.755	0.560	0.050	0.070	0.986	0.992	4.45	3.327

See Table 1 for the meaning of RMSEP, SEP, Bias, r^2 and RE (%).

of factors for PLS and MCR-ALS are given. The optimal number of components was selected in each case by considering the minimal RMSEP values. Errors in Table 3 are calculated for external validation samples. In the case of the PLSR method, results shown in Table 3 correspond to the application of the model to mean centered spectra. And in the case of the MCR-ALS, results shown in Table 3 correspond to data without any data pretreatment. Constraints applied during the ALS optimization were non-negativity (for concentration and spectra profiles) and the new correlation constraint discussed in this work.

According to results shown in Table 3, it is difficult to decide about the optimal number of components for the determination of humidity. Whereas in the determination of humidity by PLS, six components gave a first minimum of RMSEP (0.301) and of relative error RE (%) (3.58) in the case of MCR-ALS, seven components were needed from RMSEP (0.358) and RE% (4.26%) values. This first selection of components should be considered rather parsimonious since lower RMSEP and RE% values could still be obtained (Table 3) if a larger number of components were considered, for both PLS and ALS. However, since these differences were not large, this first selection estimation was considered good enough for the purposes of this comparative work. For protein, the best number of components was eight factors for PLS and six factors for MCR-ALS. Prediction errors (RMSEP) were 0.560 and 0.808 for PLS and MCR-ALS, respectively. In this case, PLSR clearly outperformed MCR-ALS. This improvement was probably due to the possibility to incorporate a larger number of components in PLSR models compared to MCR-ALS models. MCR-ALS could not resolve more components as PLSR for a better quantification of protein because of the intrinsic difficulties resolving minor components by MCR-ALS, whereas they could still have some effect improving quantitative estimations in PLSR. On the other hand, if RMSEP values are compared using the same number of factors, for PLS and MCR-ALS, some differences in the prediction error results are always encountered which can be due to the fact that PLS, maximizes relevant information in the first factors, and fits better calibration and validation data. In Fig. 5, regression of humidity and protein contents predicted by MCR-ALS and PLS versus the concentration reference values, using the optimal number of factors in each case, are given. In caption of Fig. 5 results of the elliptic joint confidence region F test [42] for the slope and the intercept of these regressions are given. This test considers that if no systematic errors are present, the theoretical point intercept should be zero and the theoretical slope should be equal to one and that their uncertainties should be located inside the corresponding

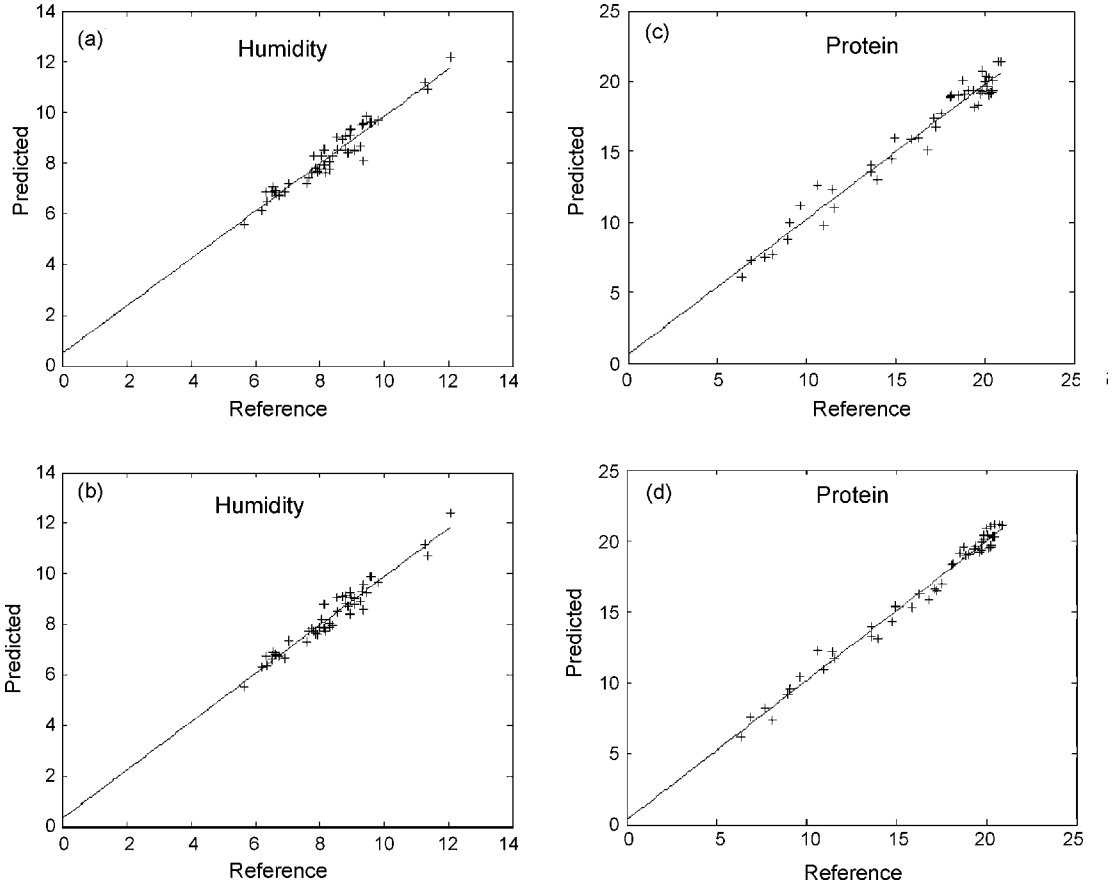

Fig. 5. Humidity and protein concentrations values predicted by MCR-ALS and PLS models vs. concentration reference values in validation samples. (a) Humidity values predicted by MCR-ALS vs. their reference values ($F = 0.18$, $\alpha = 0.91$), (b) humidity predicted values by PLSR vs. their reference values ($F = 0.24$, $\alpha = 0.87$), (c) protein predicted values by MCR-ALS vs. reference values of protein ($F = 0.43$, α=0.73), (d) protein predicted values by PLSR versus reference values of protein ($F = 2.06$, $\alpha = 0.12$). In parenthesis, calculated F values and significance levels for the regression slope and offset confidence region test (see Ref. [42]) are given. Tabulated F value at the same degrees of freedom ($\nu_1 = 2 + 1 = 3$ and $\nu_2 = 46 - 2 - 1 = 43$) and $\alpha = 0.05$ significance level is $F = 2.82$.

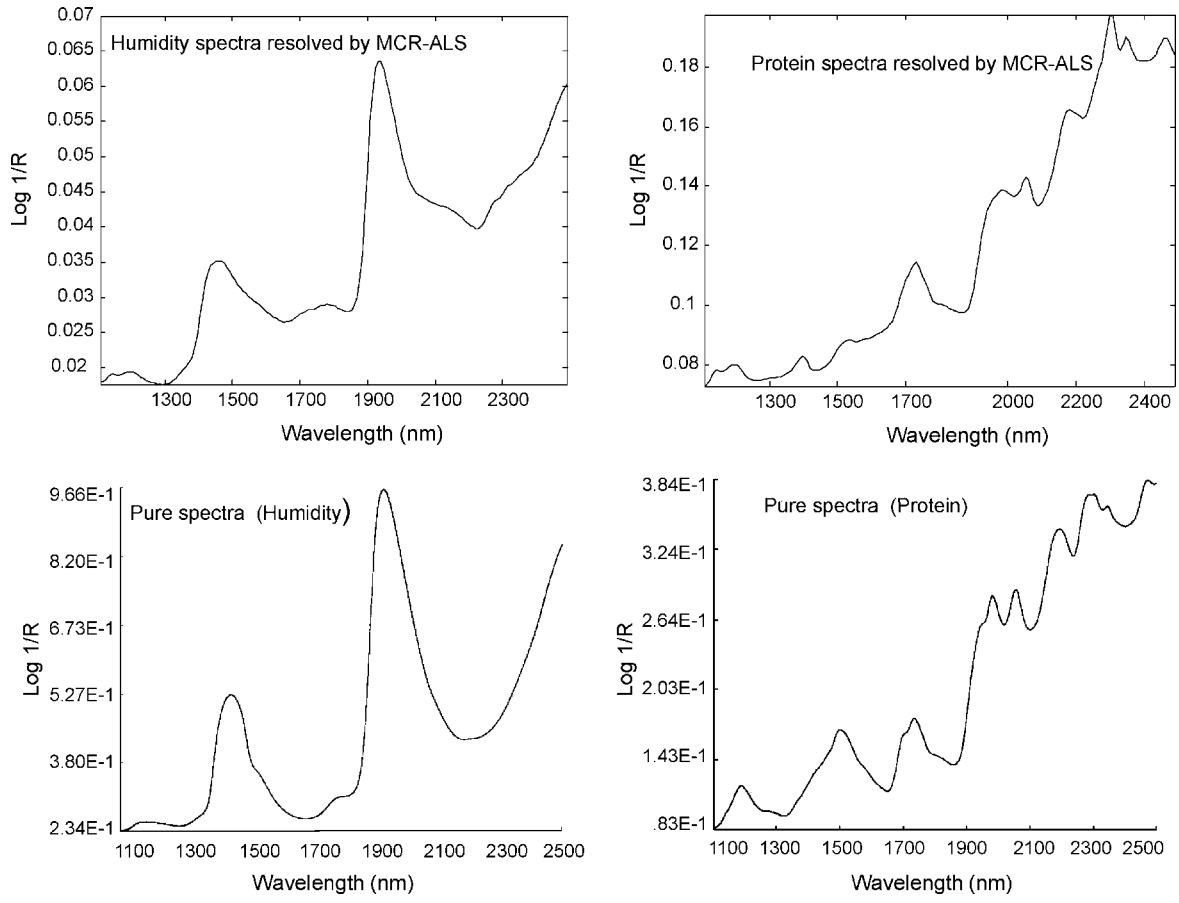

Fig. 6. Pure spectra of moisture and protein estimated by MCR-ALS (two top plots) and the same pure spectra of moisture and protein taken from the literature [43].

elliptic joint confidence region. In all cases, F test confirmed the adequacy of the postulated models.

Nevertheless and in general, the determination of humidity and protein in Ray-Grass forage samples using MCR-ALS were also rather good and close to the optimal ones obtained by PLSR. This is especially relevant if it is taken into account the intrinsic difficulties inherent to MCR-ALS to properly resolve and quantificate components contributing very little to the measured spectroscopic signal and also to the fact that neither sample nor spectra pretreatment was performed using MCR-ALS. NIR spectra resolved for humidity and protein using this method are given in Fig. 6. Humidity spectra show clearly the characteristic water bands at 1450 and 1940 nm. Protein spectra gave the characteristic bands at 2050 and 2180 nm. In general, the variations in the content of N in forages caused a change in the form of the bands located between 2000 and 2200 nm. In both cases (humidity and protein), spectra resolved by MCR-ALS were very similar to NIR spectra previously reported in the literature for humidity and protein in forages [43] (see lower part of Fig. 6).

5. Conclusions

The predictive capability of MCR-ALS using the new correlation constraint for a particular analyte in presence of interferences in unknown mixtures and natural samples, was in general comparable to the results obtained using PLSR calibration approaches. The main advantage of using MCR-ALS instead of PLSR is, however, the simultaneous recovery of qualitative information (spectra confirmation) about the analyte and possible unknown intereferents. In this work, we have presented a preliminary contribution to this problem and further work is needed to confirm the results here obtained.

References

[1] H. Gampp, M. Maeder, C. Meyer, A.D. Zuberbühler, Talanta 33 (1986) 943.
[2] M. Maeder, A. Zilian, Chemometr. Intell. Lab. 3 (1988) 205.
[3] M. Maeder, Anal. Chem. 59 (1987) 527.
[4] W. Windig, J. Guilment, Anal. Chem. 63 (1991) 1425.
[5] W. Windig, D.A. Stephenson, Anal. Chem. 64 (1992) 2735.
[6] W. Windig, C.E. Heckler, F.A. Agblevor, R.J. Evans, Chemometr. Intell. Lab. 14 (1992) 195.
[7] E.R. Malinowski, J. Chemometr. 6 (1992) 29.
[8] R. Tauler, A. Izquierdo-Ridorsa, E. Cassasas, Chemometr. Intell. Lab. 18 (1993) 293.
[9] R. Tauer, A. Izquierdo-Ridorsa, R. Gargallo, E. Casassas, Chemometr. Intell. Lab. 27 (1995) 163.
[10] R. Tauler, D. Barceló, Trends Anal. Chem. 12 (1993) 319.
[11] R. Tauler, A. Smilde, B.R. Kowalski, J. Chemometr. 9 (1995) 31.
[12] R. Tauler, J. Chemometr. 16 (2002) 117.
[13] J. Jaumot, R. Gargallo, A. de Juan, R. Tauler, Chemometr. Intell. Lab. 76 (2005) 101.
[14] R. Tauler, B. Kowalski, S. Fleming, Anal. Chem. 65 (1993) 2040.

[15] J. Saurina, S. Hernández-Cassou, R. Tauler, Anal. Chem. 67 (1995) 3722.
[16] J. Saurina, S. Hernandez-Cassou, Anal. Chim. Acta 438 (1/2) (2001) 335.
[17] A. de Juan, M. Maeder, M. Martínez, R. Tauler, Chemometr. Intell. Lab. 54 (2000) 123.
[18] A. de Juan, R. Dysson, C. Marcolli, M. Rault, R. Tauler, M. Maeder, Trends Anal. Chem. 23 (2004) 70.
[19] J. Jaumot, R. Gargallo, N. Escaja, C. Gonzalez, E. Pedroso, R. Tauler, Nucleic Acid Res. 30. (2002).
[20] R.M. Latorre, J. Saurina, S. Hernández-Cassou, Electrophoresis 21 (2000) 563.
[21] M.S. Díaz-Cruz, J. Mendieta, R. Tauler, M. Esteban, Anal. Chem. 71 (1999) 4629.
[22] M.C. Antunes, J.E.J. Simao, A.C. Duarte, R. Tauler, Analyst 127 (6) (2002) 809.
[23] M.J. López, C. Ariño, S. Diaz-Cruz, J.M. Díaz-Cruz, R. Tauler, M. Esteban, Environ. Sci. Technol. 37 (2003) 5609.
[24] M. Vives, R. Tauler, V. Moreno, R. Gargallo, Anal. Chim. Acta 446 (2001) 439.
[25] S. Navea, A. de Juan, R. Tauler, Anal. Chem. 75 (2003) 5592.
[26] E. Peré-Trepat, M. Petrovic, D. Barceló, R. Tauler, Anal. Bioanal. Chem. 378 (2004) 642.
[27] AFNOR association Francaise de Normalization 82411. NF V18-109 (1982). "Determination de la teneur en eau".
[28] A. Vogel, A Textbook of Quantitative Inorganic Analysis including elementary instrumental analysis, fourth ed., Longman Group Ltd., London, 1978.
[29] AOAC Official Method, 11, Crude Protein in Animal Feed, Forage, Grain, and Oilseeds, Block Digestion using Copper Catalyst, Steam Distillation into Boric Acid, AOAC International, Gaithersburg, MD, 2001.
[30] D.A. Skoog, D.M. West, F.J. Holler, Fundamentals of Analytical Chemistry, 7th Sanders Coll. Pub., 1995.
[31] G.H. Golub, C.F. Van Loan, Matrix computation, second ed., The Johns Hopkins University Press, Baltimore, 1989, ISBN 0-8018-3739-1.
[32] H.W. Lawton, F.A. Sylvestre, Technometrics 13 (1971) 617.
[33] O.S. Borgen, B.R. Kowalski, Anal. Chim. Acta 174 (1985) 1.
[34] B.G.M. Vandeginste, W. Derks, G. Kateman, Anal. Chim. Acta 173 (1985) 253.
[35] E. Spjotvoll, H. Martens, R. Volden, Technometrics 3 (1982) 173.
[36] D. Macnaughtan, L.B. Rogers, G. Wernimont, Anal. Chem. 44 (1972) 1421.
[37] H. Martens, T. Naes, Multivariate Calibration, Wiley, New York, 1991.
[38] R. de Carvalho, M. del Nogal Sĭanchez, J. Wattoom, R.G. Brereton, Talanta 68 (2006) 1190.
[39] J.S. Shenk, J. Workman, M.O. Westerhaus, in: D.A. Burns, E.W. Ciurczak (Eds.), Handbook of Near Infrared Analysis, Marcel Dekker, New York, 1992.
[40] D. Cozzolino, I. Delucchi, M. Kholi, D. Vázquez, Agricultura Técnica 66 (2006) 370.
[41] P.L. Bras, A.S. Bernandino, J.A. Lopez, J.C. Menezes, Chemometr. Intell. Lab. 75 (2005) 91.
[42] N. Drapper, H. Smith, Applied Regression Analysis, second ed., Wiley, New York, 1981.
[43] I. Murray, P.C. Williams, Near Infrared Technology in the Agricultural and Food Industries, American Association of Cereal Chemists, Minnesota, 1987 (Chapter 2).

Available online at www.sciencedirect.com
ScienceDirect
Talanta 74 (2008) 1505–1510
Talanta
www.elsevier.com/locate/talanta

An alcohol oxidase biosensor using PNR redox mediator at carbon film electrodes

Madalina M. Barsan, Christopher M.A. Brett *

Departamento de Química, Universidade de Coimbra, 3004-535 Coimbra, Portugal

Received 30 May 2007; received in revised form 27 September 2007; accepted 28 September 2007
Available online 2 October 2007

Abstract

A new amperometric biosensor for ethanol monitoring has been developed and optimised. The biosensor uses poly(neutral red) (PNR), as redox mediator, which is electropolymerised on carbon film electrodes and alcohol oxidase (AlcOx) from *Hansenula polymorpha* as recognition element, immobilised by cross-linking with glutaraldehyde (GA) in the presence of bovine serum albumin (BSA) as carrier protein. Optimisation of variables affecting the system was performed and, for chronoamperometric measurements, a potential of −0.300 V versus saturated calomel electrode was chosen in 0.1 M sodium phosphate buffer saline at pH 7.5. The optimised biosensor showed a good sensitivity of 171.8 ± 14.8 nA mM^{-1} and the corresponding detection limit (signal-to-noise-ratio = 3) of 29.7 ± 1.5 μM. Stability studies showed a good preservation of the bioanalytical properties of the sensor, 57.6% of its initial sensitivity remaining after 3 weeks (the sensor was used two to three times per week). No significant interferences were found from compounds usually present in wine. The biosensor was used for the determination of ethanol in Portuguese red and white wines.
© 2007 Elsevier B.V. All rights reserved.

Keywords: Alcohol oxidase; Electrochemical enzyme biosensor; Poly(neutral red); Ethanol determination

1. Introduction

The determination of ethanol is important in food technology, fermentation and wine industries as well as in clinical chemistry: blood, serum and urine analysis. It is thus of much interest to develop fast and accurate procedures for ethanol determination. A variety of methods and strategies for the determination of this analyte has been reported, including gas chromatography [1], liquid chromatography with biosensor detection [2], refractometry [3] and spectrophotometry, both based on NADH detection. These methods, routinely used in industry, are slow, relatively expensive and need well-trained operators. Biosensors are versatile analytical tools, offering an attractive alternative for ethanol determination. For this purpose, a large variety of different biosensors have been proposed, using mainly alcohol oxidase (AlcOx) [4–6], NAD^+-dependent alcohol dehydrogenase (AlcDh) [7–9] or PQQ-containing alcohol dehydrogenase [10].

Alcohol oxidase is the key enzyme for methanol metabolism in metylotrophic yeast species, including *Pichia pastoris*, *Hansenula polymorpha* and *Candida boidinii*. The enzyme catalyses the first step of methanol catabolism, namely its oxidation to formaldehyde with concomitant production of hydrogen peroxide. In vivo, the protein is compartmentalized into special cell organelles, termed peroxisomes [11]. It is a homooctameric flavoprotein consisting of eight identical subunits, each containing flavin adenine dinucleotide (FAD) as a prosthetic group [12]. Considering this, alcohol oxidase-based biosensors have an advantage when compared with those that use alcohol dehydrogenase as biorecognition element, because the latter need the cofactor to be added to the sample or to be immobilised on the sensor surface. Since AlcOx enzyme enzymatically converts all primary alcohols and formaldehyde [13] it exhibits a lack of selectivity to ethanol. However, this should not be a problem in the use of such a biosensor for analysis of ethanol in natural samples such as wine, since ethanol is present in much higher concentrations. The main problem of AlcOx-based biosensors is their limited stability. For this reason, Gibson et al. conducted several stabilisation studies of AlcOx in the dry state using a combination of polyelectrolytes and sugar derivatives [14–16].

* Corresponding author. Tel.: +351 239 835295; fax: +351 239 835295.
E-mail address: brett@ci.uc.pt (C.M.A. Brett).

0039-9140/$ – see front matter © 2007 Elsevier B.V. All rights reserved.
doi:10.1016/j.talanta.2007.09.027

In this work the development of a novel AlcOx biosensor based on carbon film electrodes made from electrical resistors is reported [17], these electrodes having been previously characterized for use in electroanalysis [18,19]. In previous work, carbon film electrodes were used as substrates for various biosensor assembly constructions, using as redox mediators ferrocene, hexacyanoferrates and polymerized phenazine dyes [20–27]. In the latter case, the biosensor assembly was prepared by immobilising the enzyme by cross-linking with glutaraldehyde in the presence of bovine serum albumin on the top of poly(neutral red) (PNR) modified carbon film electrodes. Neutral red was found to be a convenient artificial enzyme substrate and has been recently used as a starting material for the preparation of electropolymerised films of PNR that can function as redox mediators in biosensors [20]. The chemical structure of NR, with an amino functionality located on heteroaromatic phenazine ring, makes it amenable to electropolymerisation. The monomer can be polymerized from neutral aqueous solutions producing stable redox-active layers [28,29]. The main advantage of this new biosensor is the fact that PNR can mediate the enzymatic reaction catalyzed by AlcOx, since a lot of previous attempts to mediate this enzyme have failed [5–8]. It is well known that AlcOx is incompatible with most free-diffusing mediators, which makes it extremely difficult to design electron-transfer pathways between the redox active centre of the enzyme (the enzymatic cofactor) and the electrode, at low potentials. In addition, the active site of the enzyme is deeply buried within the octameric protein shell, preventing any direct electron transfer in the absence of a suitable redox mediator [30].

Optimisation of experimental conditions has been carried out and the analytical parameters for the determination of ethanol determined for several biosensor assemblies, which contain different amounts of immobilised enzyme. The operational and storage stability of the biosensor were also evaluated.

2. Experimental

2.1. Reagents

Alcohol oxidase (AlcOx, EC 1.1.3.13, 7.7 units/mg solid extracted from methylotrophic yeast *Hansenula* sp.), glutaraldehyde (GA) 25% (v/v), bovine serum albumin (BSA), L-ascorbic acid and DL-lactic acid were from Sigma, Germany. Ethanol, methanol, 2-propanol, DL-malic acid and citric acid monohydrate were obtained from Merck, Germany. Neutral red (65% dye content) and sodium phosphate monobasic monohydrate were from Sigma–Aldrich, Germany. Di-sodium hydrogenphosphate-2-hydrate, potassium hydrogenphosphate, sodium chloride and acetic acid were from Riedel-de Haën, Germany. Di-potassium hydrogenphosphate-3-hydrate was from Panreac, Spain. Potassium chloride and oxalic acid was from Fluka, Switzerland and tartaric acid was from JMUP, Portugal.

For electrochemical experiments, the supporting electrolyte was sodium phosphate buffer saline (NaPBS) (0.1 M phosphate buffer + 0.05 M NaCl and pH 6.0, 6.5, 7.0, 7.5 and 8.0). Polymerisation of neutral red was carried out in an electrolyte composed of 0.025 M potassium phosphate buffer solution and 0.1 M KNO_3 (pH 5.5).

Millipore Milli-Q nanopure water (resistivity > 18 MΩ cm) was used for preparation of all solutions. Experiments were performed at room temperature (25 ± 1 °C).

2.2. Apparatus

Batch experiments were performed in a three-electrode electrochemical cell of volume 10 cm^3, containing the enzyme modified carbon film resistor as working electrode, a platinum foil counter electrode and a saturated calomel electrode (SCE) as reference.

All electrochemical measurements were performed using a computer-controlled μ-Autolab Type II potentiostat–galvanostat running with general purpose electrochemical system (GPES) for Windows Version 4.9 software (EcoChemie, Utrecht, The Netherlands).

The pH measurements were carried out with a CRISON 2001 micro-pH meter at room temperature.

2.3. Electrode and mediator film preparation

Carbon film cylindrical electrodes were made from carbon film electrical resistors (2 Ω resistance) of length 6 mm and diameter 1.5 mm, as described elsewhere [18]. The exposed geometric area was ∼0.20 cm^2. Before use, the electrodes were electrochemically pre-treated by cycling the potential between 0.0 V and +1.0 V versus SCE in 0.025 M potassium phosphate buffer solution, pH 5.5, in order to decrease the background currents and to increase the potential window.

The preparation of poly(neutral red) films was carried out by cyclic voltammetry from a solution containing 1 mM monomer dye in 0.025 M KPB + 0.1 M KNO_3, pH 5.5. The potential was cycled from −1.0 to 1.0 V versus SCE at a scan rate of 50 mV s^{-1} for 15 cycles [24–26].

Alcohol oxidase was immobilised using cross-linking with glutaraldehyde (GA). Three different enzyme solutions were prepared, by mixing the enzyme together with BSA in 0.1 M NaPBS, pH 7.0 and the concentrations were: 1% AlcOx + 4% BSA, 3% AlcOx + 4% BSA and 5% AlcOx + 10% BSA. A volume of 10 μl of enzyme solution was then mixed with 5 μl GA (2.5%, v/v diluted in water). Of this mixture, 10 μl was dropped onto the electrode surface and left to dry at room temperature during 1 h.

All biosensors were tested in a batch cell. Amperometric measurements were performed at fixed potential, after stabilisation of the current baseline, with injection of alcohol into 0.1 M NaPBS solution in which the biosensor was immersed. Experiments were done under continuous stirring conditions.

3. Results and discussion

3.1. Optimisation of the PNR/AlcOx biosensor

The optimisation of variables affecting the AlcOx-based biosensor system, prepared as described in Section 2, was per-

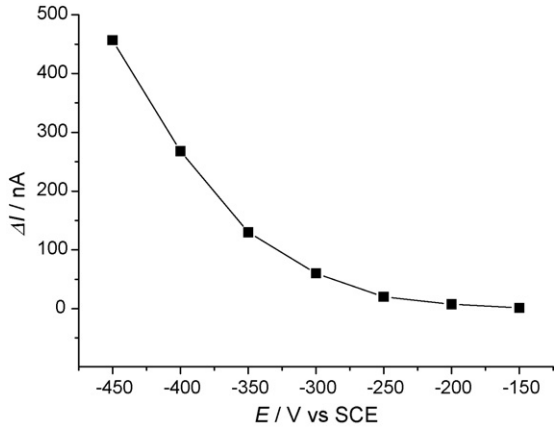

Fig. 1. Dependence of PNR/AlcOx biosensor response on applied potential; measurements performed in 0.1 M NaPBS and pH 7.0.

formed with respect to applied potential and with respect to buffer pH.

The effect of applied potential on the amperometric response of the PNR/AlcOx modified electrode as a function of alcohol concentration was studied using an enzyme solution containing 5% AlcOx and 10% BSA for biosensor construction. Experiments were done by injection of 0.40 mM ethanol after baseline stabilisation for each applied potential. The results obtained are presented in Fig. 1 and show that at, all applied potentials, oxidation processes occur at the electrode. This can be explained by a direct electronic communication between PNR and the enzyme cofactor, flavine adenine dinucleotide, so that the reduced form of the redox active prosthetic group of the AlcOx ($FADH_2$), which is formed during the enzymatic oxidation of ethanol, is then reoxidized at the PNR film. In this way, at the electrode, the PNR mediator will be oxidized and the registered biosensor response is an anodic change in current. The proposed mechanism is presented in Scheme 1a. At −0.45 V and −0.40 V versus SCE, potentials closer to the formal potential of the FAD/$FADH_2$ couple ($E^{0'}_{FAD/FADH_2} \cong -0.45$ V vs. SCE), the biosensor response is much higher when compared with that recorded at more positive applied potentials. At these potentials, it is clear that the energetics of the redox processes is facilitated. Nevertheless, a potential of −0.30 V was selected as working potential for subsequent studies with the aim of minimising possible interferences.

In order to prove that PNR acts as electron acceptor from $FADH_2$, chronoamperometry was performed at a PNR/AlcOx biosensor at −0.3 V versus SCE, in deoxygenated buffer with injection of deoxygenated ethanol solution, after the same biosensor had been previously tested in the presence of oxygen. The biosensor characteristics were compared, and in the absence of oxygen the biosensor sensitivity increased by 21.6%. This means that PNR replaces O_2 as the electron shuttle. Low oxygen solubility in aqueous solutions and the difficulty associated with controlling the O_2 partial pressure are disadvantages of electrochemical biosensors based on O_2 or H_2O_2 detection. The replacement of O_2 by PNR is the main advantage of this new reported biosensor assembly, since almost all reported biosensors based on AlcOx function through hydrogen peroxide

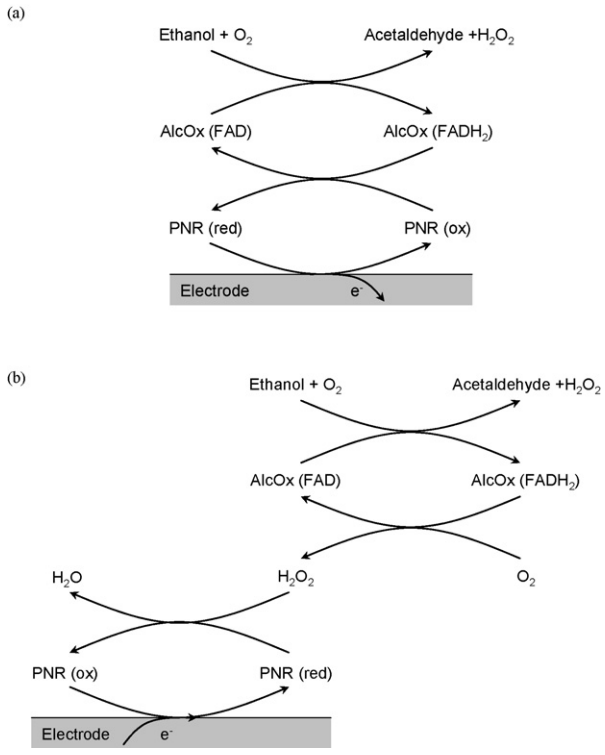

Scheme 1. Proposed reaction mechanism at PNR/AlcOx biosensor at (a) −0.30 V vs. SCE (b) applied potentials more negative than −0.35 V vs. SCE.

detection. By eliminating the dependence on the presence of O_2, the enzymatic reaction is facilitated which improves the sensor performance. As already reported [27], we assume that, in the presence of dissolved oxygen, there is a competition between the oxidation of $FADH_2$ and hydrogen peroxide reduction at the mediator film, see Scheme 1a and b. Thus, the increase of the biosensor response in the absence of dissolved oxygen, which is an anodic change in current, is explained by the absence of the competing reduction reaction of H_2O_2, since, presumably, in the absence of O_2, no H_2O_2 is formed.

A study of the influence of the pH of the 0.1 M NaPBS on biosensor response was performed at −0.30 V versus SCE. The buffer solution pH values were chosen in the range of 6–8, since it is known that the pH of AlcOx extracted from *Hansenula* sp. is 5.5–8.5 [31]. The results show an increase in the analytical signal up to pH 7.5, above which the signal decreases (Fig. 2). Also, previous studies have shown that the highest enzyme activities and stabilities are achieved at physiological pH values [16].

In order to find the optimal amount of enzyme within the biosensor membrane, placed on top of the PNR film, three different enzyme solutions were used to construct the biosensor, containing AlcOx in the concentrations at 1, 3 and 5%, as mentioned in Section 2. These biosensors were then used for the amperometric determination of ethanol under the previously optimised conditions. Calibration curves are presented in Fig. 3 and analytical data obtained from analysis of the curves are given in Table 1. The sensitivity continuously increased with increase in enzyme concentration, by a factor of 5.4 when the

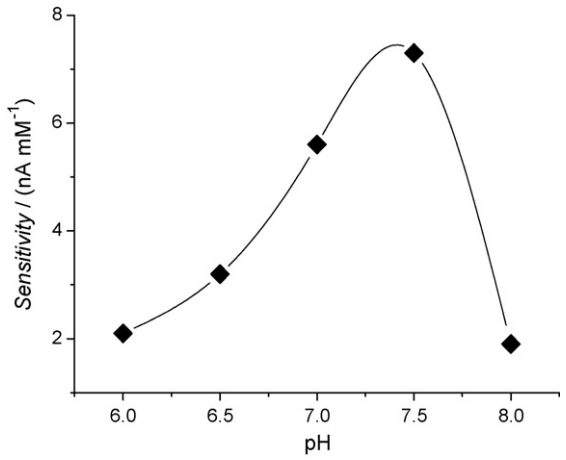

Fig. 2. The influence of buffer pH on the PNR/AlcOx biosensor sensitivity; measurements performed in 0.1 M NaPBS by chronoamperometry at −0.30 V vs. SCE.

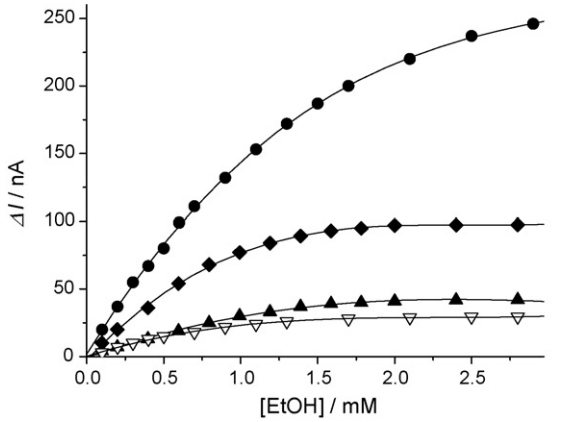

Fig. 3. Calibration curves recorded at AlcOx biosensors at −0.30 V vs. SCE in 0.1 M NaPBS pH 7.5: PNR/AlcOx with (▲) 1%, (♦) 3% and (●) 5% AlcOx; (▽) 1% AlcOx without PNR mediator.

enzyme concentration is increased from 1% to 5%. However, at the same time, the linear range becomes smaller with an increase in enzyme concentration and the limit of detection changes from 26 μM to 44 μM (calculated as three times the signal-to-noise ratio). Apparent Michaelis–Menten constants were calculated from Lineweaver–Burk plots. Since the biosensor constructed by using 5% enzyme solution showed a much higher sensitivity, it was chosen for performing further experiments.

A comparison of the analytical performances of the AlcOx biosensor assembly (1% enzyme concentration), with and without PNR mediator, was done, see Fig. 3. It was observed that using PNR as mediator, the sensitivity increases significantly by a factor of nearly 5. Additionally, the linear range was extended from 0.4 mM to 0.6 mM, and the limit of detection decreased from 45 μM to 26 μM.

3.2. Analytical properties of the PNR/AlcOx biosensor

3.2.1. Reproducibility of the sensor

In order to examine the reproducibility of the biosensor, the amperometric response to ethanol at three different PNR/AlcOx modified electrodes was recorded under the same experimental conditions. The biosensors showed a linear range up to 0.7 ± 0.1 mM (R.S.D. = 4.3%) and the corresponding detection limit (signal-to-noise-ratio = 3) was 29.7 ± 1.5 μM with a R.S.D. of 5.2% ($n = 3$). The biosensor sensitivity was 171.8 ± 14.8 nA mM^{-1}, and a R.S.D. of 8.6% was obtained. The initial biosensor sensitivity is usually lower when compared with other reported AlcOx-based biosensors [32–34]; nevertheless, stability studies demonstrated a very small decrease of this initial sensitivity value, as will be shown. Most biosensor assemblies based on AlcOx consist in bi-enzyme architectures where, together with the AlcOx, a peroxidase is used for hydrogen peroxide detection at low operating potentials. Redox hydrogels are commonly used for this type of biosensor construction, but since this procedure implies manual mixing of both enzymes together with the cross-linker, problems may appear in the optimisation procedure and reproducibility of these one-layer bi-enzyme biosensors [35,36]. The advantages of this newly developed biosensor assembly consist in the simplicity in the construction procedure and good reproducibility (see the analytical parameters above).

Another advantage of these new AlcOx-based biosensors is that they can be used for online measurements in a specially

Table 1
Analytical data obtained from ethanol calibration curves at AlcOx-based biosensors

Enzyme (%)	Linear range (mM)	Sensitivity (nA mM^{-1})	Correlation coefficient (R^2)	Limit of detection (μM)	K_M^{app} (mM)
1	0–1.0	29.2	0.999	35	2.0
3	0–0.8	84.0	0.999	44	2.4
5	0–0.6	156.3	0.999	26	2.1

Table 2
Analytical data obtained from calibration curves at AlcOx-based biosensors (5% enzyme concentration) for three different alcohols; experimental conditions as in Fig. 3

Aliphatic alcohol	Sensitivity (nA mM^{-1})	Correlation coefficient (R^2)	Limit of detection (μM)	K_M^{app} (mM)
Methanol	144	0.997	53	2.0
Ethanol	139	0.999	25	2.1
1-Propanol	53	0.999	22	2.2

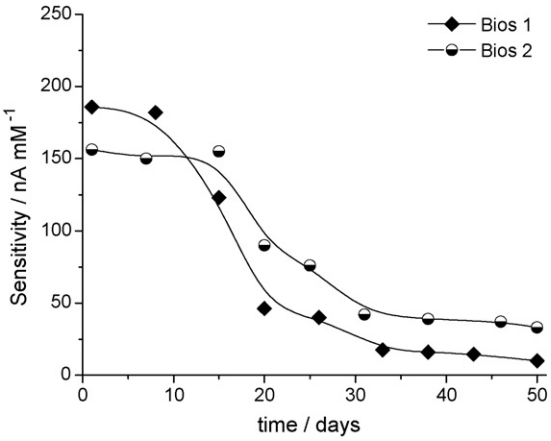

Fig. 4. Operational stability of two different PNR/AlcOx biosensors.

designed cylindrical flow cell, already used for the determination of glucose in flow analysis [26]. Thus, the sensors showed a sufficiently good, reproducible behaviour and can be used for measurements of ethanol.

Kinetic studies of the immobilised enzyme were also carried out. The apparent Michaelis–Menten constant was calculated from the Lineweaver–Burk plots and the value obtained was 1.96 ± 0.12 mM (R.S.D. = 5.7% and $n = 3$).

3.2.2. Selectivity of the sensor

Similar experiments were carried out for two other short chain aliphatic alcohols: methanol and 1-propanol and the analytical parameters obtained were compared. Table 2 summarizes the analytical parameters calculated from the calibration curves recorded for each alcohol. As expected, see [8], on increasing the length of aliphatic alcohol chain, the sensitivity of the biosensor decreases while the apparent Michaelis–Menten constant increases.

3.2.3. Stability of the sensor

The PNR/AlcOx biosensor was stored in 0.1 M NaPBS buffer pH 7.0, at 4° C when not in use. In order to check the storage stability, a chronoamperogram of the sensor was registered after 6 weeks of storage in the above-mentioned buffer. The sensitivity of the sensor decreased only by about 12% from the initial value after 6 weeks, which means that the enzyme layer is well attached on the PNR modified electrode.

The operational stability of the enzyme electrode was also tested. For this purpose, calibration curves were recorded three times per week: results are shown in Fig. 4. After 2 weeks of use, biosensor sensitivity decreases by only 0.8% in the case of one biosensor and by 33.8% in the case of the other tested biosensor. However, after 50 days of repeated use the sensitivity continues to decrease, maintaining 21.2% and 5.4%, respectively of the initial sensitivity. This is very promising achievement with respect to the stability of the sensor, since it is well known from previous studies that AlcOx has a poor long-term stability which was the main disadvantage of previous biosensors [6,8,32].

Table 3
Interference of some compounds, molar ratio of 2:1 interferent:ethanol, on the response to ethanol at PNR/AlcOx biosensors

Compound	Response of the biosensor in the presence of the interferent compound
Ascorbic acid	96.7
Acetic acid	100.0
Lactic acid	106.3
Malic acid	97.5
Oxalic acid	103.7
Citric acid	97.3
Tartaric acid	96.5

Table 4
Ethanol analysis in wines

Wine	Ethanol (% v/v)	
	Value declared by the producer	Biosensor
Red wine 1	12.5	13.0 ± 0.2
Red wine 2	13	13.2 ± 0.1
White wine	12	12.3 ± 0.2

3.3. Interferences

There are many easily oxidizable species present in natural samples, the most important of which are ascorbic and tartaric acids, in the case of wine. Since the purpose of this work was to use the biosensors for ethanol determination in wine, a study of interferences from compounds usually present in wine was needed. Several acids were examined as possible interferents that may affect ethanol determination in wine. The high level of selectivity towards common interferences provides the possibility to use this device in clinical, environmental and food control. The results obtained are presented in Table 3. At the PNR/AlcOx biosensor, at −0.3 V versus SCE, quite small anodic currents were registered due to the oxidation of lactic acid and oxalic acid. The other acids are reduced at the electrode, but also small currents were recorded, even in the case of ascorbic and tartaric acids, in the presence of which the biosensor response to ethanol decreases by 3.5% and 3.3%, respectively at a 2:1 ratio of interferent:ethanol.

3.4. Ethanol analysis in natural samples

The performance of the biosensor for practical applications in the analysis of natural samples was demonstrated by performing the determination of the alcohol content in red and white wines, estimated in terms of ethanol concentration. The samples, as described in Section 2, required only a simple dilution step, in order to fit the linear range of the calibration curve.

The alcohol content of three types of wine was measured and is displayed in Table 4. The biosensor accuracy was assessed by comparison with the results given by the wine producers.

4. Conclusions

Alcohol oxidase from *Hansenula* sp. has been immobilised by cross-linking with glutaraldehyde in the presence of bovine serum albumin on PNR modified carbon film electrodes. After optimisation of experimental parameters, the biosensor has a detection limit of 30 μM and a sensitivity of 172 nA mM^{-1}. The reproducibility is good as well as the operational and storage stability. All these characteristics make the PNR-mediated AlcOx biosensor a good alternative to other determination methods for ethanol in clinical, industry and food analysis.

Acknowledgements

Financial support from European Project HPRN-CT-2002-00186 is gratefully acknowledged as well as from Fundação para a Ciência e a Tecnologia (FCT), ICEMS (Research Unit 103). MMB thanks FCT for a PhD grant (SFRH/BD/27864/2006).

References

[1] G. Schmitt, R. Aderjan, Blutalkohol 41 (2004) 299.
[2] H. Lieden, A.R. Vijayakumar, L. Gorton, G. Marko-Varga, J. Pharm. Biomed. Anal. 17 (1998) 1111.
[3] A.I. Pen'kovskii, A.V. Gusighin, E.I. Federov, R.I. Volkov, M.I. Filatov, R.A. Salina, L.A. Nikolaeva, D.D. Khamelin, V.I. Vereshchagin, Patent Appl.: RU 2001-134083 2001 1213. CAN 141:410165 (2004).
[4] L.V. Shkotova, A.P. Soldatkin, M.V. Gonchar, W. Schuhmann, S.V. Dzyadevych, Mater. Sci. Eng. C 26 (2006) 411.
[5] I.S. Alpeeva, A. Vilkanauskyte, B. Ngounou, E. Csöregi, I.Y. Sakharov, M. Gonchar, W. Schuhmann, Mikrochim. Acta 152 (2005) 21.
[6] O. Smutok, B. Ngounou, H. Pavlishko, G. Gayda, M. Gonchar, W. Schuhmann, Sens. Actuator B: Chem. 113 (2006) 590.
[7] R. Antiochia, I. Lavagnini, Anal. Lett. 39 (2006) 1648.
[8] D. Carelli, D. Centonze, A. De Giglio, M. Quinto, P.G. Zambonin, Anal. Chim. Acta 565 (2006) 27.
[9] K. Svensson, L. Bülow, D. Kriz, M. Krook, Biosens. Bioelectron. 21 (2005) 705.
[10] J. Razumienė, V. Gurevičienė, A. Vilkanauskytė, L. Marcinkevičienė, I. Bachmatova, R. Meškys, V. Laurinavičius, Sens. Actuator B: Chem. 95 (2003) 378.
[11] P. Ozimek, M. Veenhuis, I.J. van der Klei, FEMS Yeast Res. 11 (2005) 975.
[12] H.R. Waterham, K.A. Russel, Y. De Vries, J.M. Cregg, Cell Biol. 139 (1997) 1419.
[13] S.V. Shleev, G.P. Shumakovich, O.V. Nikitina, O.V. Morozova, H.M. Pavlishko, G.Z. Gayda, M.V. Gonchar, Biochemistry (Moscow) 71 (2006) 245.
[14] T.D. Gibson, J.N. Hulbert, S.M. Parker, Biosens. Bioelectron. 7 (1992) 701.
[15] T.D. Gibson, J.N. Hulbert, Anal. Chim. Acta 279 (1993) 185.
[16] A.M. Azevedo, J.M.S. Cabral, D.M.F. Prazer, T.D. Gibson, L.P. Fonseca, J. Mol. Catal. B: Enzym. 27 (2004) 37.
[17] C.M.A. Brett, L. Agnes, H.D. Liess, Electroanalysis 13 (2001) 765.
[18] O.M.S. Filipe, C.M.A. Brett, Electroanalysis 16 (2004) 994.
[19] C. Gouveia-Caridade, C.M.A. Brett, Electroanalysis 17 (2005) 549.
[20] R. Pauliukaite, C.M.A. Brett, Electrochim. Acta 50 (2005) 4973.
[21] M.E. Ghica, C.M.A. Brett, Anal. Lett. 38 (2005) 907.
[22] M. Florescu, C.M.A. Brett, Talanta 65 (2005) 306.
[23] S. De Luca, M. Florescu, M.E. Ghica, A. Lupu, G. Palleschi, C.M.A. Brett, D. Compagnone, Talanta 68 (2005) 171.
[24] M.E. Ghica, C.M.A. Brett, Electroanalysis 18 (2006) 748.
[25] M.E. Ghica, C.M.A. Brett, Anal. Lett. 39 (2006) 1527.
[26] M.M. Barsan, J. Klinčar, M. Baltič, C.M.A. Brett, Talanta 71 (2007) 1893.
[27] R. Pauliukaite, M.E. Ghica, M.M. Barsan, C.M.A. Brett, J. Solid State Electrochem. 11 (2007) 899.
[28] A.A. Karyakin, E.E. Karyakina, H.L. Schmidt, Electroanalysis 11 (1999) 149.
[29] A.A. Karyakin, O.A. Bobrova, E.E. Karyakina, J. Electroanal. Chem. 399 (1995) 181.
[30] J. Greisler, S. Ghisla, P. Kroncek, J. Biochem. 160 (1986) 93.
[31] http://www.sigmaaldrich.com/catalog/search/ProductDetail/SIGMA/A0438.
[32] N.G. Patel, S. Meier, K. Camman, G.C. Chemnitius, Sens. Actuator B: Chem. 75 (2001) 101.
[33] H. Gülce, A. Gülce, M. Kavanoz, H. Coşkun, A. Yildiz, Biosens. Bioelectron. 17 (2002) 517.
[34] F. Mizutani, S. Yaruki, S. Iijiama, Anal. Sci. 13 (1997) 83.
[35] N. Peña, R. Tárrega, A.J. Raviejo, J.M. Pingarrón, Anal. Lett. 35 (2002) 1935.
[36] J. Castillo, S. Gáspár, I. Sakharov, E. Csöregi, Biosens. Bioelectron. 18 (2003) 705.

Available online at www.sciencedirect.com
ScienceDirect
Talanta 74 (2008) 1313–1320
Talanta
www.elsevier.com/locate/talanta

Molecular iodine preconcentration and determination in aqueous samples using poly(vinylpyrrolidone) containing membranes

P.R. Bhagat [a], A.K. Pandey [b], R. Acharya [b], A.G.C. Nair [b], N.S. Rajurkar [a], A.V.R. Reddy [b,*]

[a] *Department of Chemistry, University of Pune, Pune 411007, India*
[b] *Radiochemistry Division, Bhabha Atomic Research Centre, Trombay, Mumbai 400085, India*

Received 27 June 2007; received in revised form 30 August 2007; accepted 30 August 2007
Available online 4 September 2007

Abstract

Membranes for preconcentration of molecular iodine were developed by two different routes: (i) UV-grafting of 1-vinyl-2-pyrrolidone in the pores of microporous poly(propylene) host membrane (grafted membrane), and (ii) physical immobilization of preformed poly(vinylpyrrolidone) (PVP) in a plasticized cellulose triacetate matrix to form the polymer inclusion membrane (PVP-PIM). The UV-grafted PVP-membrane was found to be hydrophilic (water uptake capacity = 166 wt.%), while the PVP-PIM was found to be highly hydrophobic (≈2 wt.%). PVP-PIM was found to uptake only I_2 from aqueous sample whereas I_2 and I_3^- were sorbed in the grafted membrane. This selectivity of PVP-PIM towards I_2 was attributed to its hydrophobicity that allows only neutral I_2 to interact with PVP in the membrane matrix. Thus, the selective preconcentration and quantitative determination of I_2 in aqueous sample was carried out using PVP-PIM. As PVP-PIM was optically transparent, the characteristic absorbance of PVP–I_2 complex (λ_{max} = 361 nm) could be used for quantitative determination of I_2 in the membrane. The instrumental neutron activation analysis (INAA) of the I_2-loaded PIM samples indicated that 82% could be sorbed into the PIM samples from the solution within 10 min of equilibration time. This membrane was applied to I_2 determinations in the samples of ^{131}I radiotracer. The concentration level of iodine species in these samples were in sub-ppb level. Therefore, these samples were ideal for testing the preconcentration efficiency of the membrane towards I_2 by monitoring the radioactivity of ^{131}I. The amounts of I_2 in the aqueous samples were standardized by conventional solvent extraction of I_2 with the chloroform for validating the preconcentration efficiency of PVP-PIM. The detection limit of I_2 in aqueous samples by INAA hyphenated with PVP-PIM was found to be 0.3 ppb for a sample size of 25 mL.
© 2007 Elsevier B.V. All rights reserved.

Keywords: Molecular iodine; Poly(vinylpyrrolidone); Polymer inclusion membrane; Grafted membrane; Neutron activation analysis

1. Introduction

Iodide, organic iodine, molecular iodine and iodate, are the major species of iodine that may be present in food, drinking water, and seawater [1]. Iodate or iodide is added to the table salt and other food products for supplementing the dietary intake of iodine [2]. Molecular iodine is an important bactericide and is added to drinking water as a disinfectant [3]. Iodine is one of the fission products generated in a nuclear reactor and can enter into the reactor water [4]. The I_2 is also an important reactant or product in many chemical reactions that are used for analytical applications. For example, an optical chemical sensor responsive to selenium has been developed based on the generation of I_2 by reacting selenite with potassium iodide and quantifying I_2 with a color indicator variamine blue [5]. There are several methods based on conventional techniques that can be used for the determination of total iodine, iodide or iodate in solid or aqueous samples [1,6]. The determination of molecular iodine by other conventional techniques is difficult due to its volatile nature. This can lead to losses during its determination which can be prevented by complexation in the functionalized solid phase. Thus, development of reliable methods for the determination of total iodine and iodine species such as I^-, IO_3^-, I_3^-, and I_2 in different matrices is of considerable importance. The selective preconcentration of the analyte can be used not only to enhance the sensitivity of the conventional analytical techniques but also to discriminate different chemical species of an element existing in the samples [7]. Solid-phase extraction

* Corresponding author. Tel.: +91 22 25593862; fax: +91 22 25505150/1.
E-mail address: avreddy@barc.gov.in (A.V.R. Reddy).

0039-9140/$ – see front matter © 2007 Elsevier B.V. All rights reserved.
doi:10.1016/j.talanta.2007.08.035

has become a preferred method for the preconcentration of the analyte due to its effectiveness, and possibility of quantifying the analyte directly on the solid extracting medium. Particle-packed cartridges or discs, polymer-coated fibers, or membranes are generally used for the solid-phase extraction [8]. Solid-phase microextraction coupled with gas chromatography or mass spectrometry has been reported for the determination of iodine in pharmaceuticals, iodized salt, milk powder, and vegetables [9].

Membrane based preconcentration method has an advantage in analytical applications wherein direct quantification of preconcentrated species in the membrane is possible either by methods like neutron activation analysis (NAA) [10], X-ray fluorescence based methods [11] and electrochemical methods [12] or by spectrophotometry after immobilizing a suitable color indicator in the membrane matrix [13]. The analyte selective membrane is the heart of many chemical sensor designs [13–15]. Since iodine exists in different chemical forms in food and water matrices, it is of great interest to develop species based separation procedures. A scheme for the determination of low levels of I^- and total iodine in the milk and milk powder samples with iodide selective membrane followed by its determination by instrumental NAA has been developed in our laboratory [16]. However, it is difficult to selectively separate I^- and IO_3^- from the samples like salt or seawater due to the presence of huge excess of Cl^- ions [6]. Although INAA gives total iodine content irrespective of the species present in a sample it is complicated due to production of high radioactivity of the activation products of other elements like sodium and chlorine during neutron irradiation of samples like salt [17]. One of the effective ways of preconcentration of I^- or IO_3^- could be conversion of these iodine species to molecular iodine that can easily be separated by the molecular iodine selective sorbents [18].

Iodine-sensitive optode has been developed based on fluorescence quenching of 9-ethyl-3-carbazylidene carbazole hydrazone with I_2 [19]. The matrix formed by poly(vinyl chloride) plasticized with bis(2-ethylhexyl) sebacate is hydrophobic and its hydrophobicity may be responsible for the transfer of I_2 from the aqueous medium to membrane matrix in the absence of any complexing reagent for I_2 in this optode. Iodine shows a strong tendency to form charge transfer complexes even with the weak electron donors. Poly(vinylpyrrolidone) (PVP) is known to form complexes with I_2 and I_3^-, although structure of PVP–I_2 complex is not well understood [20]. The solid sorbents have been prepared by impregnating polystyrene–divinylbenzene disk with PVP for the determination of iodine by direct diffused reflectance measurements of the membranes [18,21]. Lubbad et al. have proposed another method of membrane preparation that involves impregnation of monolithic polymer-coated nylon disk with PVP for I_2 determination using diffuse reflection spectroscopy [22]. Antibacterial membrane has been prepared by the photografting of 1-vinyl-2-pyrrolidone on the surface of poly(propylene) [3].

In the present work, PVP has been anchored in the membrane matrix by two different routes. Preformed PVP has been immobilized in a plasticized cellulose triacetate matrix (polymer inclusion membrane). In another route, the monomer 1-vinyl-2-pyrrolidone has been grafted in the pores of a poly(propylene) microporous membrane (grafted membrane). These two PVP-membranes have been characterized in terms of: (i) quantitative uptake of I_2, (ii) sorption kinetics of I_2 in the membrane from the aqueous media, and (iii) stability of PVP–I_2 complex formed in the membrane. UV–vis absorbance spectra of the iodine solution were recorded before and after equilibration with the membrane sample to identify the uptake of iodine species (I_2 or I_3^-) sorbed in the membrane samples. The radiotracer ^{131}I in iodide form was used to estimate the sorption of I^- in the membrane sample. Since polymer inclusion membrane (PVP-PIM) was having good optical properties, the formation of PVP–I_2 complex in this membrane was studied by monitoring its characteristic absorbance maximum ($\lambda_{max} = 361$ nm). The amount of I_2 sorbed in the membrane samples from the equilibrating aqueous solution was determined by INAA. In order to explore potential applications of the PVP-membrane in the real samples, the membrane was applied for the quantitative determination of iodine (^{131}I in the form of I_2) in samples of nuclear reactor water. The amount of I_2 in ^{131}I radiotracer sample was also determined using PVP-membrane. The selection of these samples for studying the applications of PVP-membrane was based on the fact that the concentrations of I_2 in these samples were in sub-ppb level.

2. Experimental

2.1. Reagents and apparatus

Analytical reagent grade chemicals (dichloromethane, chloroform, carbon tetrachloride, KI, NaCl, KIO_3, H_2SO_4) and deionized water (18 MΩ/cm, Gradient A-10 model, Milli-Q USA) were used throughout the present studies. Cellulose triacetate (CTA) (molecular weight 72,000–74,000, acetyl value = 43.2%, Alfa Biochem), poly(vinylpyrrolidone) (PVP) ($M_w = 44{,}000$, BDH), 1-vinyl-2-pyrrolidone, methylene bis acrylamide (Aldrich), α,α-dimethoxy-α-phenyl acetophenone (Fluka) 2-nitrophenyloctylether (NPOE) (Fluka), tri-(2-ethylhexyl) phosphate(THEP) (Koch), and dioctyl phthalate (DOP) (BDH) were used as obtained. Standard volumetric iodine solution (0.05 mol L^{-1}, Merck) was used to prepare solutions containing known amounts of iodine by appropriate dilution with deionized water. Carrier free ^{131}I radiotracer, in the form of KI dissolved in aqueous solution, was obtained from the Board of Radiation and Isotope Technology, Mumbai, India. The membrane samples loaded with I_2 were irradiated with neutrons (flux = 5×10^{11} n cm^{-2} s^{-1}) in the APSARA reactor, BARC, Mumbai, India. The γ-activities of ^{128}I (produced by neutron activation) and ^{131}I (radiotracer) were monitored by using either a HPGe detector or a well-type NaI(Tl) detector based gamma ray spectrometer. All the samples and standards containing radioactivity were counted in identical sample-detector geometry. UV–vis spectra of aqueous solution and membrane samples were recorded using UV–vis Spectrophotometer (V-530, JASCO, Japan). The thickness of the membrane samples was measured using a digital micrometer (Mitutoy, Japan) with a precision of ±1 μm.

2.2. Preparation of polymer inclusion membrane (PVP-PIM)

The preparation of PVP-PIM is described briefly here and details can be found in [16]. A solution of cellulose triacetate (CTA) was prepared by dissolving CTA (0.2 g) and PVP (0.05 g) in 10 mL of dichloromethane. A separate solution in dichloromethane (5 mL) containing a known amount (0.6 g) of a plasticizer (DOP/NPOE/TEHP) was prepared. The amounts of PVP, plasticizer and CTA were optimized by varying their amount in casting solution to get a homogenous membrane with minimum thickness but sufficient mechanical strength required for handling. A casting solution was prepared by mixing the two solutions, homogenizing by ultrasonication for two min and spread on a leveled 9-cm diameter Petri dish. After the evaporation of chloroform and dichloromethane, the transparent homogeneous membrane was peeled off from the Petri dish. The membrane was thoroughly washed with water to remove soluble component, if any.

2.3. Preparation of grafted membrane

The monomer, 1-vinyl-2-pyrrolidone (VP) (0.4 g) along with a cross-linker, methylene bis acrylamide (MBA), and an UV initiator (α,α-dimethoxy-α-phenyl acetophenone) were dissolved in 2 mL tetrahydrofuran (THF) and dimethylformamide (DMF) mixture (1:1). The amounts of cross-linker and monomer were adjusted in the polymerization solution to get 5 mol% cross-linking. The amount of UV initiator was taken as 1 wt.%. For grafting of VP, the microporous host poly(propylene) membrane (6 cm × 6 cm area, 60% porosity, 0.2 μm pore size and 59 μm thickness) was soaked in the polymerizing solution for overnight, and sandwiched between two transparent polyester sheets to prevent any possible loss of grafting solution filled in the pores. Care was taken to remove excess of grafting solution and air bubbles trapped between membrane and polyester sheet covering the membrane surface. Finally, the sandwiched membrane was exposed to 365 nm UV light in a multilamp photoreactor (Heber Scientific, model No. HML-SW-MW-LW-888) for a period of 20 min. After irradiation in the photoreactor, the membrane was washed thoroughly with THF, methanol and distilled water to remove the ungrafted components. The membrane was then dried under vacuum and its weight was recorded. The extent of grafting was obtained from the difference in weights of the membrane after and before grafting. The water uptake capacity was determined from the difference between the weights of wet and dry membrane samples of same size. The weight of the wet membrane was obtained by equilibrating the membrane in deionized water for 24 h. The membrane sample was dried for 8–10 h under vacuum and weighed to obtain weight of the dry membrane.

2.4. Sorption of I_2 in membrane

The sorption of I_2 in the membrane was studied by equilibrating the membrane samples with 25 mL of I_2 stock solution for 30 min with constant stirring. The amount of I_2 sorbed in the membrane samples was monitored by recording UV–vis spectra of 3 mL of I_2 solution taken before and after equilibration of the membrane. The UV–vis spectra of the I_2-loaded PVP-PIM samples were also recorded by mounting these on to the inside wall of a (1 cm × 1 cm × 3 cm) quartz cell. For kinetics experiment, the membrane sample was equilibrated for a fixed time period with a solution containing a known amount of iodine, and change in characteristic absorbance of PVP–I_2 complex at 361 nm was monitored. The effect of temperature on the stability of the PVP–I_2 complex in the membrane was studied by placing a membrane sample loaded with a known amount of iodine in a constant temperature bath at 40 °C. The absorbance of the PVP–I_2 complex in the membrane was monitored at 361 nm as a function of residence time at this temperature.

^{131}I radiotracer was used to study the uptake of I^- by the membrane from the equilibrating aqueous solution. Relative method of INAA was used for the determination of concentration of I_2 using the procedure described elsewhere [16]. The I_2-loaded membrane samples were neutron irradiated for 30 min in APSARA reactor along with iodine standard. The elemental standards for iodine were prepared by drying required volume of solution containing known amounts of KI or KIO_3 on Whatman-41 filter paper having same dimensions as that of the membrane samples. The samples and the standards were doubly sealed in separate polythene packets and doubly sealed in one packet for neutron irradiation. The radioactivity of ^{128}I ($E_\gamma = 442.9$ keV and $t_{1/2} = 25$ min) produced in the membrane samples and iodine elemental standards was assayed by γ-ray spectrometry. The amounts of iodine in the membrane samples were determined by the standard comparison method.

2.5. Determination of I_2 in water from nuclear power reactor

Samples of water used in primary heat transfer system of Nuclear Power Plant, Tarapur, India were taken for iodine speciation studies. The pH of this water was 6.5. The extent of ^{131}I (a fission product) present as I_2 was determined using PVP-PIM. In order to determine iodide, an iodide-selective membrane, prepared by immobilizing aliquat-336 (a liquid anion-exchanger) in the DOP-plasticized cellulose triacetate matrix (ALI-PIM), was used. Details of the ALI-PIM are described elsewhere [16]. The samples of PVP-PIM (3 cm × 9 cm) and ALI-PIM (3 cm × 9 cm) were equilibrated in 100 mL of reactor water separately for overnight. The radioactivity of ^{131}I in reactor water was monitored, before and after equilibration with the membrane, by γ-ray spectrometry in an appropriate geometry for determining the uptake of ^{131}I species by the membrane sample. The uptake of ^{131}I species by the membrane was also confirmed by γ-counting of the membrane samples equilibrated with the reactor water.

2.6. Determination of molecular iodine in ^{131}I radiotracer

In order to determine molecular I_2 present in ^{131}I radiotracer, obtained from BRIT, 5 mL of deionized water was spiked with a known amount of radioactivity of ^{131}I tracer (50 μL in KI form). This solution was equilibrated with 1 cm × 3 cm sample

of PVP-PIM at room temperature with stirring for overnight. After equilibration, the membrane sample was taken out and the radioactivity of ^{131}I in the membrane sample was assayed. The total radioactivity of ^{131}I in equilibrating solution was also measured before and after equilibration with the membrane sample.

The solvent extraction of I_2 was also carried out using CCl_4, which is known to extract I_2 from aqueous solution. In this experiment, a known amount of activity of the tracer (50 μL) was added to 2 mL of distilled water, and to this solution 2 mL of CCl_4 was added. The aqueous and organic phases were thoroughly mixed by vigorous shaking, and then allowed to settle. I_2 extraction was repeated two to three times to ensure complete extraction of iodine from aqueous to organic phase (CCl_4). From each phase, 1 mL solution was taken to measure the radioactivity of ^{131}I in the organic (in I_2 form) and aqueous (I^- and other iodine species) phases.

3. Results and discussion

3.1. Formation and characterization of PVP-membranes

Poly(vinylpyrrolidone) (PVP) is known to form a stable complex with I_2 [20], therefore PVP was selected for complexation with I_2. PVP was immobilized in the membrane by two different routes. The first one involves physical immobilization of preformed PVP in the plasticized cellulose triacetate (CTA) matrix. The choice of CTA was based on the fact that it can be plasticized with 70–80 wt.% of NPOE, TEHP or DOP [10]. In this polymer inclusion membrane (PIM), the plasticizer also acts as a medium for the diffusion of the analyte in the membrane matrix [23]. In the present work, preformed PVP was immobilized in the plasticized CTA. Three different plasticizers, i.e. NPOE, TEHP and DOP were used to plasticize CTA. The compositions of the PVP containing PIMs (PVP-PIMs) are given in Table 1. The PVP-PIMs made up of CTA + PVP and CTA + PVP + DOP were found to be transparent and could uptake I_2 from the equilibrating solution. Therefore, these two PVP-PIMs were subjected to further studies.

The grafted membranes were prepared by pore-filled method [24]. In this method, a grafting solution containing a monomer, cross-linker and UV-initiator is filled in the pores of a microporous poly(propylene) membrane. The grafting solution is held in the pores (size 0.2 μm in the present case) of membrane by capillary force. In the present work, 1-vinyl-2-pyrrolidone (VP) was polymerized in poly(propylene) membrane with methylene bis acrylamide (MBA) cross-linker. The ratio of MBA to VP was kept as 5 mol%. The grafting of VP in poly(propylene) membrane was found to be 75 wt.%. The thickness of the membrane did not change (60 μm) after UV-grafting indicating that PVP was contained within the pores of poly(propylene) membrane, which provides containment to PVP-gel. The membranes prepared by this route were opaque, and readily sorbed water and I_2 from the equilibrating solution.

3.2. Preconcentration of I_2 in PVP-membranes

The solution chemistry of iodine is very complex as it hydrolyses in aqueous medium to form a variety of inorganic species, e.g. I^-, I_2, I_3^-, and HOI [25]. However, PVP is known to form complex only with I_2 and I_3^- in aqueous medium [20]. Both the membranes developed in the present work were not found to sorb I^- and IO_3^-. It was also observed that the membrane did not sorb I_2 significantly in the PIM prepared without PVP. In order to study the uptake of I_2 and I_3^-, the membrane samples were equilibrated with iodine solution of known concentration. The absorbance spectrum of the iodine solution before equilibration with the membrane showed three distinct peaks corresponding to I_2 (460 nm) and I_3^- (290 nm and 350 nm) (Fig. 1) as observed by Gazda et al. [21]. As can be seen from Fig. 1, all the absorbance peaks corresponding to I_2 and I_3^- disappeared in the absorbance spectrum of iodine solution equilibrated with PVP-grafted membrane. This indicated that PVP anchored in poly(propylene) membrane by UV-grafting formed complex with both I_2 and I_3^-. In the case of PVP anchored in the DOP-plasticized CTA matrix (PVP-PIM), only absorbance peak corresponding to the I_2 (460 nm) disappeared in the spectrum of solution equilibrated with the PVP-PIM. In all the cases, the membrane samples were equilibrated for 1 h with the iodine solution from the same stock solution. The comparison of absorbance spectra of solution before and after equilibration with PVP-PIM seems to suggest that there is a slight decrease in the intensities of peaks corresponding to I_3^-. In order to study the variation of intensity of I_3^- peaks in iodine solution as a function of equilibration time with PVP-PIM, the absorbance spectra of the solution were recorded at different time intervals. It was observed that absorbance corresponding to I_3^- decreased up to 5 min equilibration time, thereafter absorbance of I_3^- peaks did not change during prolonged equilibration of solution with PVP-PIM. This seems to suggest that there is a significant difference in the interaction of molecular I_2 and iodine species (mainly I_3^-) with PVP anchored in the PVP-PIM and the grafted membrane.

The water uptake capacity of the grafted membrane was found to be 166 wt.%, while water uptake capacity of PVP-PIM was negligible (>2 wt.%). The PVP is hydrophilic in nature therefore it makes the porous polypropylene matrix to readily sorb water in high amount. However, the presence of a plasti-

Table 1
Compositions of PVP-polymer inclusion membranes (PVP-PIM)

Type of plasticizer	CTA (wt.%)	PVP (wt.%)	Plasticizer (%)	Thickness (μm)	Optical quality	I_2 sorption
–	80 ± 1	20 ± 1	0	10 ± 1	Transparent	Yes
DOP	23 ± 1	6 ± 1	71 ± 1	50 ± 2	Transparent	Yes
NPOE	23 ± 1	6 ± 1	71 ± 1	49 ± 2	Transparent	No
THEP	23 ± 1	6 ± 1	71 ± 1	50 ± 3	Opaque	Yes

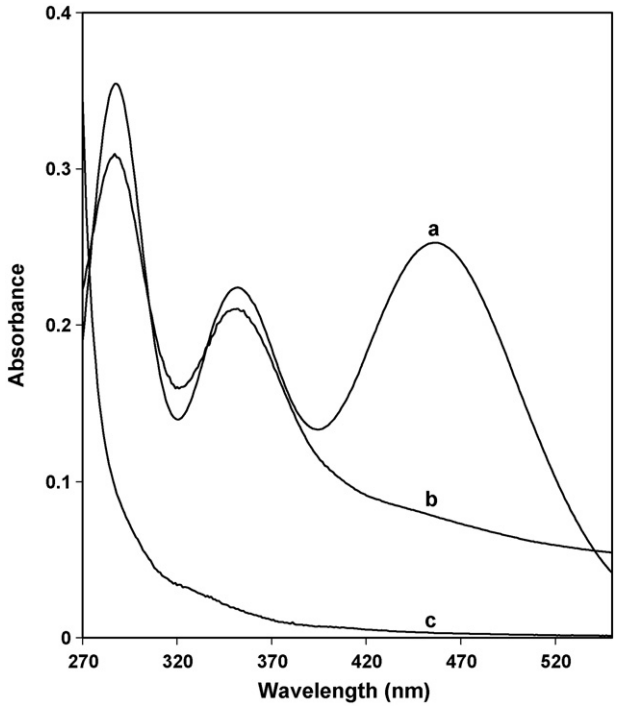

Fig. 1. Absorbance spectra of iodine solution: (a) before equilibration with membrane, (b) after equilibration with PVP containing polymer inclusion membrane, and (c) after equilibration with VP-grafted poly(propylene) membrane. The absorbance peaks shown in the spectra correspond to I_2 (460 nm) and I_3^- (290 nm and 350 nm) in solution without equilibration and equilibration with membrane samples for 1 h with constant stirring.

cizer (DOP) and CTA, which are hydrophobic and have a low dielectric constant, make the nonporous PVP-PIM hydrophobic in nature [23]. This would give rise to a barrier for transfer of I_3^- from aqueous medium (high dielectric constant) to PVP-PIM matrix (low dielectric constant). However, I_3^- would not face any barrier in the hydrophilic matrix of grafted membrane and thus would be able to interact with PVP to form complex. I_2 unlike I_3^-, is neutral and highly soluble in nonaqueous solvents. Thus, I_2 molecules in the equilibrating solution can interact easily with PVP anchored in both kinds of membranes. This is similar to PVP interactions with iodine species reported in solid or nonaqueous solution [20]. PVP-PIM appears to be having distinct advantages over UV-grafted membrane for preconcentration and determination of molecular iodine due to the facts that (i) it does not sorb I_3^-, (ii) it has good optical property with an absorbance of peak (λ_{max} = 361 nm) corresponding to PVP–I_2 complex, which can be used for the quantitative determination of I_2 held in the membrane, and (iii) PVP-PIM's are easy to prepare as it requires only controlled evaporation of solvent (CH_2Cl_2/$CHCl_3$) from casting solution containing PVP, DOP and CTA on flat bottom Petri dish. Therefore, PVP-PIM was subjected to further study for quantitative preconcentration of I_2 and its determination from the aqueous medium.

3.3. Tuning of the properties of PVP-PIM

The recorded UV–vis absorbance spectra before and after equilibrating PVP-PIM with I_2 solution are given in Fig. 2. As

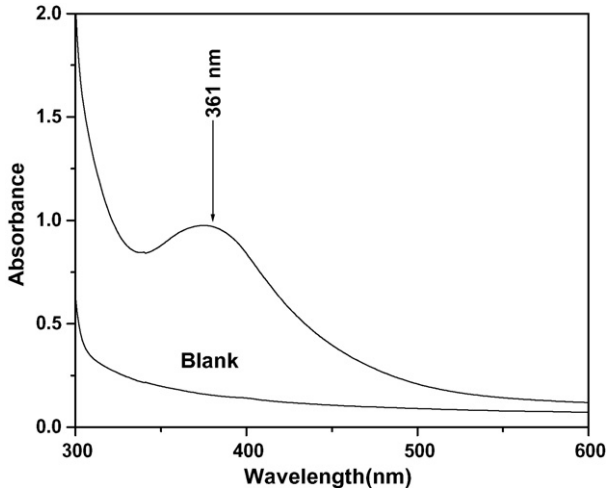

Fig. 2. Absorbance spectrum of polymer inclusion membrane (CTA + DOP + PVP) sample (1 cm × 2 cm) equilibrated with iodine solution and blank, respectively. The absorbance at λ_{max} = 361 nm corresponds to PVP–I_2 complex formed in the membrane sample.

can be seen from Fig. 2, a new peak appeared in the UV–vis absorbance spectrum of PVP-PIM sample equilibrated with I_2 solution. This absorbance peak at λ_{max} = 361 nm corresponds to PVP–I_2 complex formed in the membrane. In order to study the I_2 uptake in unplasticized and plasticized PVP-PIM, the samples of CTA + PVP and CTA + DOP + PVP were equilibrated with well-stirred solutions containing varying amounts of I_2 for 1 h. The compositions of these PVP-PIMs are given in Table 1. The measured absorbance as a function of the amount of iodine is plotted in Fig. 3. As seen from Fig. 3, the absorbance in PVP-PIM samples at 361 nm varies linearly as a function of I_2 concentration in the equilibrating solution. The absorbance varies linearly with the amount of iodine up to 100 μg in the case of sample of

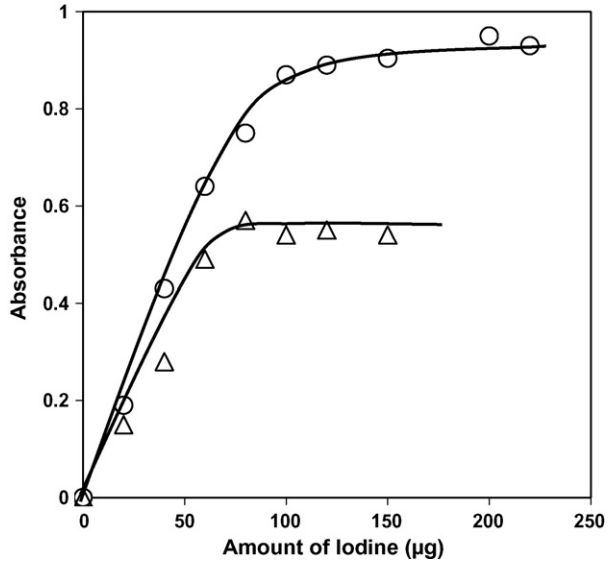

Fig. 3. Variations of absorbance in PVP-PIM samples (1 cm × 2 cm) at 361 nm as a function of I_2 concentration in the equilibrating solution. The symbols △ and ◯ represent PVP-PIM made up of CTA + PVP and CTA + DOP + PVP, respectively.

PIM containing CTA + DOP + PVP and ≈60 μg I_2 in the case of sample of PIM made up of CTA + PVP. Both the membrane samples were having almost same amounts of PVP and the area of both the membrane samples were same (1 cm × 2 cm). The difference in I_2 uptake capacities of the plasticized and unplasticized membranes can be attributed to the plasticizer DOP that constitutes the liquid fraction in the membrane. Thus, DOP would make PVP in the membrane matrix more accessible to I_2 in equilibrating solution. This might have facilitated the I_2 uptake capacity of the PVP-PIM.

The rate of sorption of I_2 in PVP-PIM samples was studied by equilibrating the membrane samples with well stirred 25 mL solution containing 100 μg of I_2 for a specified time period, and monitoring the absorbance of PVP–I_2 complex (λ_{max} = 361 nm) in the membrane. Three types of membrane samples were studied for kinetics of I_2 sorption, namely: (a) unplasticized PVP-PIM with 10 μm thickness, (b) DOP-plasticized PVP-PIM membrane with 50 μm thickness, and (c) DOP-plasticized PVP-PIM membrane with 30 μm thickness. The compositions of PVP-PIM were same as that given in Table 1. The thickness of the plasticized membrane was reduced by taking half of the amounts of CTA and DOP used in the preparation of 50 μm plasticized PVP-PIM. However, the amount of PVP was kept same in all the membranes. It is evident from Fig. 4 that the absorbance of PVP–I_2 complex (361 nm) reached an optimum value after equilibration times in following order: unplasticized PVP-PIM (≈5 min) < DOP plasticized PVP-PIM (≈10 min) < DOP plasticized PVP-PIM (≈25 min). It is interesting to note from Fig. 4 that the values of optimum absorbance in these I_2-loaded membrane samples are in the reverse order. This indicated that I_2 sorption in unplasticized PVP-PIM is predominantly surface sorption (faster I_2 sorption kinetics and lower I_2 uptake capacity). In plasticized PVP-PIM, the I_2 sorption was diffusion controlled based on the fact that reduction in thickness from 50 to 30 μm resulted in the decrease in the equilibration time with almost same absorbance of PVP–I_2 complex (Fig. 4).

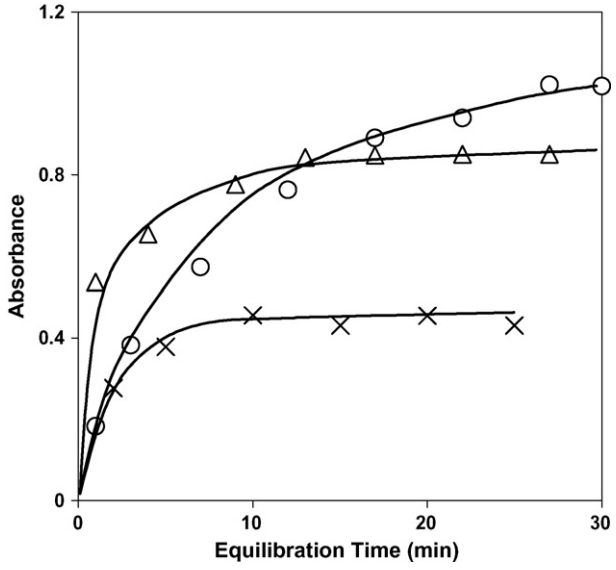

Fig. 4. Variations of absorbance at 361 nm in PVP-PIM samples as a function of equilibration time in well-stirred solution containing 100 μg of I_2 in 25 mL. The symbols ×, △, and ◯ represent PVP-PIM containing CTA + PVP (thickness = 10 μm), CTA + DOP + PVP (thickness = 30 μm) and CTA + DOP + PVP (thickness = 50 μm), respectively.

3.4. Quantification of I_2 in the PVP-PIM

In order to study the quantitative uptake of I_2, the PVP-PIM samples were equilibrated with solutions containing known amounts of I_2 and subjected to INAA. During neutron irradiation of the membrane samples, it is likely that the sample would experience slightly higher temperature than with ambience. For example, the temperature in the irradiation position of APSARA reactor is about 35 °C. In order to study the stability of PVP–I_2 complex in the reactor environment, the membrane sample was loaded with a known amount of I_2 and then kept for 2 h at 40 °C temperature and periodically the absorbance was measured. It was observed that absorbance of PVP–I_2 complex did not change significantly during a period of 2 h. This indicated that PVP–I_2 complex held in the membrane is stable up to 40 °C and is reliable for analytical applications. The amount of I_2 sorbed in PVP-PIM was determined by INAA and found to vary linearly as a function of the amount of I_2 in the equilibrating solution. As mentioned in Section 3.3, it was observed that the amount of I_2 preconcentrated in the membrane sample is fairly linear up to 100 μg. This experiment indicated that extraction efficiency of PVP-PIM towards I_2 was 82 ± 3%. In order to understand lower but constant extraction efficiency (82%) of PVP-PIM towards I_2, the concentrations of I_2 and I_3^- in the equilibrating solution were calculated from the absorbance at their characteristic λ_{max} values and using respective molar absorptivity values reported in literature [21]. These molar absorptivity values may not be highly reliable for quantitative determination but provide approximate concentrations of I_2 and I_3^- in the equilibrating solution. Thus estimated amounts of I_2 and I_3^- in the stock solution were found to be approximately 80% and 2% of total iodine, respectively. The remaining amount of I_2 may be undergoing hydrolysis forming species like I^- and HOI, which are not sorbed into the membrane. This was not further examined. This indicated that iodine existing in solution as I_2 was sorbed in the membrane sample quantitatively.

3.5. Applications of PVP-PIM for the I_2 determination

The detection limit of iodine in equilibrating solution by INAA hyphenated with PVP-PIM was calculated to be 0.3 ppb for a sample size of 25 mL by Currie method [26]. In the preconcentration based analysis methods volume of the sample used for preconcentration is important to calculate detection limits achievable for the target analyte by the chosen method. The membrane developed in the present work has good optical properties and therefore spectrophotometry can be used for quantification of I_2 held in the membrane. The detection limit obtained by spectrophotometry based on 3σ value of the blank was found to be 0.4 ppm from 25 mL. It may not be out of place to state that the detection limit of iodine reported by membrane based diffuse reflectance spectroscopy was reported to be 0.1 ppm [18]. Considering these aspects INAA stands

Table 2
Uptake of iodine species from nuclear reactor water samples (100 mL) in the PVP-PIM developed in the present work and I^- selective membrane formed by immobilizing Aliquat-336 (anion-exchanger) in plasticized cellulose triacetate membrane (ALI-PIM)

Membrane	Iodine species sorbed in membrane	Radioactivity of ^{131}I in solution before equilibration (counts/s)	Radioactivity of ^{131}I in solution after equilibration with membrane (counts/s)	Radioactivity of ^{131}I in membrane (counts/s)	Uptake of Iodine species in membrane (%)
ALI-PIM	I^-	36.4 ± 0.4	3.5 ± 0.1	85.9 ± 0.5	90.2 ± 0.2
PVP-PIM	I_2	25.6 ± 0.3	24.2 ± 0.3	4.4 ± 0.1	5.5 ± 0.3

comparatively better as compared to other techniques for the determination of I_2. Irrespective of the detection methods, the PVP-PIM showed high selectivity for preconcentration of molecular I_2 from aqueous solutions. The efficiency of PVP-PIM was further studied by applying it to the preconcentration of radioiodine present in nuclear reactor water and ^{131}I radiotracer.

3.5.1. Iodine species determination in nuclear reactor water

The major chemical species of radioiodine in reactor water during normal operation and reactor shutdown of boiling water reactor (BWR) were reported to be I^- and $IO_3{}^-$, respectively [4]. Iodine-131 has a long half life (8.02 days) with a cumulative fission yield of 2.88% in the thermal neutron fission of ^{235}U. Therefore, ^{131}I is a good radiotracer for the determination of radioiodine species present in the nuclear reactor water. In order to study the major iodine species existing in the reactor water, the samples of PVP-PIM and ALI-PIM (aliquat-336 immobilized in DOP plasticized CTA) were equilibrated overnight with 100 mL of reactor water to preconcentrate I_2 and I^-, respectively. The uptake of ^{131}I in the membrane samples were monitored by γ-spectrometry of reactor water before and after equilibration of membranes. For this, both ALI-PIM and PVP-PIM were used and results are shown in Table 2. After equilibration with membranes, the radioactivity of ^{131}I in reactor water was reduced to background indicating quantitative sorption of ^{131}I in the membrane samples. The radioactivity of ^{131}I in ALI-PIM indicated that the major species of radioiodine existing in the reactor water was I^-. The amount of I_2 sorbed in PVP-PIM was found to be 5.5 ± 0.3% of the total ^{131}I present in the nuclear reactor water. Iodide was also found to be the major chemical form of radioiodine in the BWR reactor water by Lin [4]. This was attributed to reduction of I_2 by traces of impurities present in the reactor water. Following reactor shutdown, I^- form of radioiodine changed to other form like $IO_3{}^-$ as a consequence of β^- decay as well as radiation induced oxidation of iodide ions.

3.5.2. Iodine determination in $^{131}I^-$ radiotracer

^{131}I radiotracer may contain traces of molecular iodine in it. Therefore, the preconcentration ability of PVP-PIM at sub-ppb concentration of $^{131}I_2$ in large excess of $^{131}I^-$ was studied. The ^{131}I radiotracer solution was equilibrated with PVP-PIM. For comparison, solvent extraction of I_2 was also carried out using CCl_4. The ratios of I_2 to total iodine in ^{131}I radiotracer were found to be 0.003 ± 0.001 and 0.002 ± 0.001 by extraction of I_2 by CCl_4 and PVP-PIM, respectively. The good agreement in I_2 content obtained in ^{131}I by PVP-PIM with that obtained by solvent extraction provide validation to the preconcentration efficiency of the PVP-PIM.

4. Conclusions

The present study clearly indicates that the poly (vinylpyrrolidone) immobilized in the hydrophobic matrix, formed by cellulose triacetate plasticized with dioctylphthalate, interacts only with molecular iodine. Hydrophilic 1-vinyl-2-pyrrolidone grafted membrane was found to uptake both I_2 and $I_3{}^-$. The absorbance of poly(vinylpyrrolidone)–I_2 complex in the polymer inclusion membrane (PVP-PIM) at characteristic wavelength (λ_{max} = 361 nm) could be used for quantitative determination of I_2 in the membrane. The neutron activation analysis indicated that the uptake of I_2 in the samples of PVP-PIM is quantitative (82%) and remained constant up to 100 μg I_2 preconcentrated in the 2 cm × 1 cm membrane sample. However, the equilibration time required for preconcentration of I_2 in PVP-PIM was higher (within 10 min) than that achieved with other PVP containing substrates (within 60 s) reported in the literature [18,21,22]. This was due to the difference in the procedures used for preconcentrating I_2 in the PVP containing substrates. The applications of PVP-PIM for radioiodine determinations in the water from nuclear reactor and ^{131}I radiotracer solutions indicated that detection limit of present methodology using radioanalytical technique for iodine determination in aqueous sample is in sub-ppb range.

Acknowledgements

The authors thank Dr. V.K. Manchanda, Head, Radiochemistry Division, Bhabha Atomic Research Centre (BARC), Prof. R. S. Kusurkar, Head, Dept. of Chemistry, Pune University and Prof. B.S.M. Rao, Former Head Dept. of Chemistry, Pune University for their constant support and encouragement. One of the Authors (P.B.) thanks Board of Research in Nuclear Sciences (BRNS), DAE, India for the financial assistance to the project under BARC-Pune University MoU.

References

[1] (a) E.A. Crecelius, Anal. Chem. 47 (1975) 2034;
(b) L. Maros, M. Káldy, S. Igaz, Anal. Chem. 61 (1989) 733;
(c) K. Yokota, K. Fukushi, N. Ishio, N. Sasayama, Y. Nakayama, S. Takeda, S. Wakida, Electrophoresis 24 (2003) 2244;
(d) F. Gu, A.A. Marchetti, T. Straume, Analyst 122 (1997) 535;

(e) J.S. Edmonds, M. Morita, Pure Appl. Chem. 70 (1998) 1567.
[2] (a) J. Jakmunee, K. Grudpan, Anal. Chim. Acta 438 (2001) 299;
(b) Z. Xie, J. Zhao, Talanta 63 (2004) 339;
(c) M.G. Karmarkar, S. Ranganathan, Indian J. Med. Res. 123 (2006) 531.
[3] C.M. Xing, J.P. Deng, W.T. Yang, J. Appl. Polym. Sci. 97 (2005) 2026.
[4] C.C. Lin, J. Inorg. Nucl. Chem. 42 (1980) 1093.
[5] L. dlC.Coo, I.S. Martinez, Talanta 64 (2004) 1317.
[6] (a) S.D. Kumar, B. Maiti, P.K. Mathur, Talanta 53 (2001) 701;
(b) O. Agrawal, G. Sunita, V.K. Gupta, Talanta 49 (1999) 923;
(c) C. Pasha, B. Narayana, Acta Chim. Slov. 53 (2006) 77;
(d) G.T.F. Wong, P.G. Brewer, Anal. Chim. Acta 81 (1976) 81;
(e) H.-S. Shin, Y.-S. Oh-Shin, J.-H. Kim, J.-K. Ryu, J. Chromatogr. A 732 (1996) 327;
(f) A.-H. Liang, Z.-L. Jiang, B.-M. Zhang, Q.-Y. Liu, J. Lan, X. Lu, Anal. Chim. Acta 530 (2005) 131;
(g) F.C. Pereira, L.M. Moretto, M.D. Leo, M.V.B. Zanoni, P. Ugo, Anal. Chim. Acta 575 (2006) 16;
(h) P. Bermejo-Barrera, M. Aboal-Somoza, A. Bermejo-Barrera, J. Anal. At. Spectrom. 14 (1999) 1009.
[7] S.T. Griffin, S.K. Spear, R.D. Rogers, J. Chromatogr. B 807 (2004) 151.
[8] D.E. Raynie, Anal. Chem. 78 (2006) 3997.
[9] (a) P. Das, M. Gupta, A. Jain, K.K. Verma, J. Chromatogr. A 1023 (2004) 33;
(b) K. Ito, E. Shoto, H. Sunahara, J. Chromatogr. 549 (1991) 265.
[10] Y.M. Scindia, A.K. Pandey, A.V.R. Reddy, S.B. Manohar, Anal. Chem. 74 (2002) 4204.
[11] A. Sachdeva, S. Sodaye, A.K. Pandey, A. Goswami, Anal. Chem. 78 (2006) 7169.
[12] A. Rouhollahi, M. Shamsipur, Anal. Chem. 71 (1999) 1350, and references therein.
[13] Y.M. Scindia, A.K. Pandey, A.V.R. Reddy, S.B. Manohar, Anal. Chim. Acta 515 (2004) 311;
(b) E. Pretsch, P. Bühlmann, E. Bakker, Chem. Rev. 98 (1998) 1593.
[15] S. Sodaye, R. Tripathi, A.K. Pandey, A.V.R. Reddy, Anal. Chim. Acta 514 (2004) 159.
[16] P.R. Bhagat, A.K. Pandey, R. Acharya, A.G.C. Nair, N.S. Rajurkar, A.V.R. Reddy, Talanta 71 (2007) 1226.
[17] Y. Serfor-Armah, B.J.B. Nyarko, J. Holzbecher, E.H.K. Akaho, E.K. Osae, A. Chatt, J. Radioanal. Nucl. Chem. 256 (2003) 259.
[18] M.P. Arena, M.D. Porter, J.S. Fritz, Anal. Chem. 74 (2002) 185.
[19] C.X. Jiao, Q. Shen, S.-Y. Huan, G.-L. Shen, R.-Q. Yu, Anal. Chim. Acta 528 (2005) 229.
[20] (a) R.F. Cournoyer, S. Siggia, J. Polym. Sci. Polym. Chem. 12 (1974) 603;
(b) H.-U. Schenck, P. Simak, E. Haedicke, J. Pharm. Sci. 68 (1979) 1505;
(c) D.L.A. de Faria, H.A.C. Gil, A.A.A. Queiroz, J. Mol. Struct. 479 (1999) 93.
[21] D.B. Gazda, R.J. Lipert, J.S. Fritz, M.D. Porter, Anal. Chim. Acta 510 (2004) 241.
[22] S. Lubbad, S.A. Steiner, J.S. Fritz, M.R. Buchmeiser, J. Chromatogr. A 1109 (2006) 86.
[23] Y.M. Scindia, A.K. Pandey, A.V.R. Reddy, J. Membr. Sci. 249 (2005) 143.
[24] P.K. Pujari, D. Sen, G. Amarendra, S. Abhaya, A.K. Pandey, D. Dutta, S. Mazumder, Nucl. Intsr. Meth. B 254 (2007) 278.
[25] J.D. Burger, H.A. Liebhafsky, Anal. Chem. 45 (1973) 600.
[26] L.A. Currie, Anal. Chem. 40 (1968) 586.

Available online at www.sciencedirect.com
ScienceDirect
Talanta 74 (2008) 1392–1399
Talanta
www.elsevier.com/locate/talanta

Multivariate optimization of a liquid–liquid extraction of the EPA-PAHs from natural contaminated waters prior to determination by liquid chromatography with fluorescence detection

Daniel Mares Brum [a], Ricardo J. Cassella [a,b], Annibal D. Pereira Netto [a,b,*]

[a] *Programa de Pós-Graduação em Química, Instituto de Química, Universidade Federal Fluminense, Outeiro de São João Batista s/n, 24020-150 Niterói, RJ, Brazil*
[b] *Departamento de Química Analítica, Instituto de Química, Universidade Federal Fluminense, Outeiro de São João Batista s/n, 24020-150 Niterói, RJ, Brazil*

Received 22 June 2007; received in revised form 14 September 2007; accepted 17 September 2007
Available online 21 September 2007

Abstract

This paper reports the multivariate optimization of a liquid–liquid extraction procedure for the determination of 15 EPA-polycyclic aromatic hydrocarbons (PAHs) by high-performance liquid chromatography with fluorescence detection. A Doehlert design was used to find optimum conditions for the procedure through Response Surface Methodology. Three variables (total volume of hexane, number of extraction steps and duration of such steps) were elected as factors in the optimization study. A principal component analysis (PCA) was run with optimized data, resulting in four groups of PAHs, ordered according to their molecular weight. Final working conditions were established in order to achieve a more robust methodology in relation to all fifteen PAHs under study. Best results could be observed when 77 mL of hexane were divided in four consecutive extraction steps with 18 min each. These experimental conditions were applied in the analysis of a spiked river water sample, and the recoveries varied between 80.9 and 106%, with an average value of 97.1 ± 6.8%. The application of the methodology to river water showed that the method has a good average precision for the studied PAHs.
© 2007 Elsevier B.V. All rights reserved.

Keywords: Liquid–liquid extraction; Multivariate optimization; Doehlert matrix; Polycyclic aromatic hydrocarbons

1. Introduction

Polycyclic aromatic hydrocarbons (PAHs) are organic pollutants of concern since many of them and PAH mixtures exhibit mutagenic and/or pro-carcinogenic properties to humans and experimental animals [1–4]. PAHs are ubiquitous and their formation, sources and fate have been extensively reviewed [4,5]. There are three major exposure PAH pathways to human beings: (a) ingestion of contaminated food and/or water; (b) inhalation; (c) dermal contact [3,4].

There is concern in the determination of PAHs in water since many natural water bodies are used as potable water supplies after treatment. Many environmental agencies have adopted very low levels of PAHs for potable and natural waters. For example, USEPA [6] has proposed a maximum concentration limit (MCL) of 0.2 $\mu g\,L^{-1}$ for benzo[*a*]pyrene in drinking water. The Brazilian Health Ministry has adopted an MCL of 0.7 $\mu g\,L^{-1}$ for benzo[*a*]pyrene in drinking water [7]. Indeed the Brazilian Agency CONAMA [8] has adopted an MCL of 0.05 $\mu g\,L^{-1}$ for benzo[*a*]pyrene and seven other PAHs in fresh water (Table 1).

There are many sources of PAHs to natural waters and they include: (a) urban and rural runoff; (b) petroleum spill during transportation, refining and offshore oil-well drilling; (c) wastewater of industrial activities; (d) atmospheric deposition; (e) leachate from solid waste dumps [4,9,10].

The determination of PAHs in water is generally performed by chromatographic techniques after PAH extraction from samples. High resolution gas chromatography with mass spectrometry detection (HRGC-MS) or flame ionization detection and high-performance liquid chromatography (HPLC) with fluorescence detection have been used for PAH determination following their extraction from water and other media.

* Corresponding author. Tel.: +55 21 2629 2221; fax: +55 21 2629 2143.
E-mail address: annibal@vm.uff.br (A.D. Pereira Netto).

0039-9140/$ – see front matter © 2007 Elsevier B.V. All rights reserved.
doi:10.1016/j.talanta.2007.09.013

Table 1
Maximum concentration limits (MCL; $\mu g\,L^{-1}$) for fresh and drinking water, according to Brazilian legislation and to EPA

PAHs	CONAMA 357[a] (2005) Fresh water[d]	MS-518[b] (2004) Drinking water	USEPA[c] (2003) Drinking water
Benz[*a*]anthracene	0.05	NR[e]	NR
Chrysene	0.05	NR	NR
Benzo[*a*]pyrene	0.05	0.7	0.2
Benzo[*k*]fluoranthene	0.05	NR	NR
Benzo[*b*]fluoranthene	0.05	NR	NR
Indene[1,2,3-*c*,*d*]pyrene	0.05	NR	NR
Dibenz[*a*,*h*]anthracene	0.05	NR	NR

[a] Brazilian Environment Ministry.
[b] Brazilian Health Ministry.
[c] United States Environmental Protection Agency.
[d] Simplified treatment and disinfection required before human consumption.
[e] Indicates a not regulated MCL.

Liquid–liquid extraction (LLE) and solid phase extraction (SPE) are techniques of choice for PAH extraction from water and wastewater [9–11]. However, many different LLE conditions of PAHs from water appear in the literature [10,12,13].

In order to optimize the conditions of liquid–liquid extraction of PAHs from natural waters a multivariate optimization was employed. Multivariate optimizations are considered more efficient than the univariate processes since the influences of several parameters of an experimental procedure can be evaluated simultaneously with a fewer number of experiments. Most of these multivariate strategies are based on the Response Surface Methodology (RSM), a multivariate technique that fits mathematically the experimental domain studied in the theoretical design through a response function [14,15]. It presents, in general, two distinct steps: (i) modeling and (ii) drifting of the surface. Such steps must be repeated as many times as necessary, until the optimum working region is achieved.

Second order designs like Central Composite, Box-Behnken or Doehlert matrix have been employed to determine the real function established among analytical response and the factors chosen for experimental evaluation [16]. The great advantage observed in the use of these designs is the low number of experiments (N) required to built the models, which can be expressed as $N = k^2 + k + 1$, where k is the number of variables under study.

The most prominent advantage of the Doehlert design is its high efficiency value (ϕ). Such value can be determined by dividing the number of coefficients of the quadratic equation (p) by the number of experiments (N) required to the design [17]. A Doehlert design with three factors ($k = 3$) requires 13 experiments to be completed. As in this case p is 10, the efficiency value is equal to 0.77. On the other hand, for Central Composite designs with the same number of factors ($k = 3$), N is 15, p is 10 and then a lower efficiency value (ϕ) of 0.67 is obtained.

For second order models, the experimental data fit Eq. (1) when the optimization design has three variables (X_1, X_2 and X_3) and one experimental response (Y):

$$(Y) = b_0 + b_1(X_1) + b_2(X_2) + b_3(X_3) + b_4(X_1)(X_1) + b_5(X_2)(X_2) + b_6(X_3)(X_3) + b_7\,(X_1)(X_2) + b_8(X_1)(X_3) + b_9(X_2)(X_3) \quad (1)$$

where (Y) is the experimental response to be optimized, (b_0) is the constant term, (b_1), (b_2) and (b_3) are coefficients of the linear terms, (b_4), (b_5) and (b_6) are coefficients of the quadratic terms and (b_7), (b_8), and (b_9) are coefficients of interaction between the three factors.

In order to characterize the response function, the Lagrange criterion can be applied. According to this criterion, the quadratic equations only show one critical point when the determinants Δ_1, Δ_2 and Δ_3 (see Table 2), obtained from derivation of function Y in terms of X_1, X_2 and X_3, comprises one of the following situations:

- If $\Delta_2 = 0$, there is no information about presence of relative minimum or maximum;
- If $\Delta_1 < 0$; $\Delta_2 > 0$; $\Delta_3 < 0$, there is a relative maximum in the response surface;
- If $\Delta_1 > 0$; $\Delta_2 > 0$; $\Delta_3 > 0$, there is a relative minimum in the response surface;
- If none of above situations is present, then there is a saddle point in the response surface. This point can be defined as the critical point of a surface response, which presents maximum response for levels of some variables and simultaneously minimum response for levels of other variables.

The application of Doehlert design for processes optimization was firstly proposed in 1970 [18]. However, its application in Analytical Chemistry has occurred only 19 years later, with the optimization of a chromatographic separation [19]. Since then a growing interest in this subject can been noted in the lit-

Table 2
Formula of the determinants used for the characterization of response surfaces

Determinant	Formula
Δ_3	$\begin{vmatrix} (\delta^2Y/\delta X_1^2) & (\delta^2Y/\delta X_2\delta X_1)^2 & (\delta^2Y/\delta X_3\delta X_1)^2 \\ (\delta^2Y/\delta X_1\delta X_2)^2 & (\delta^2Y/\delta X_2^2) & (\delta^2Y/\delta X_3\delta X_2)^2 \\ (\delta^2Y/\delta X_1\delta X_3)^2 & (\delta^2Y/\delta X_2\delta X_3)^2 & (\delta^2Y/\delta X_3^2) \end{vmatrix}$
Δ_2	$\begin{vmatrix} (\delta^2Y/\delta X_1^2) & (\delta^2Y/\delta X_2\delta X_1)^2 \\ (\delta^2Y/\delta X_1\delta X_2)^2 & (\delta^2Y/\delta X_2^2) \end{vmatrix}$
Δ_1	$\lvert(\delta^2Y/\delta X_1^2)\rvert$

erature, especially regarding to the optimization of procedures that involve two experimental variables [20–25]. On the other hand, multivariate optimization of procedures involving more than two variables is not widespread [26]. Among these works, some of them regarding to optimization of sample preparation procedures can be highlighted. A three variable Doehlert matrix was used to optimize a focused microwave assisted digestion procedure applied to food samples for Fe, Mn and Zn determination by FAAS [26]. Recently, Soriano et al. [27] employed a similar treatment to optimize the extraction of selected metals from multivitamin/multimineral supplements aiming their determination by FAAS.

Doehlert design was applied in the optimization of solid-phase microextraction of organochlorine pesticides from water followed by gas chromatography with electron-capture detection [28]. Conditions of headspace solid-phase microextraction of chloroanisoles [29] and of chlorophenols [30] from red wine were also optimized by using this multivariate design.

Present work describes the multivariate optimization of a procedure for liquid–liquid extraction of selected PAHs present in natural contaminated water followed by their determination by HPLC-fluorescence. All optimization was performed by Response Surface Methodology using a Doehlert matrix for three variables. As far as we are concerned this is the first time that this model is applied to the extraction of PAHs.

2. Experimental

2.1. Chemicals and reagents

A standard solution containing all 16 EPA target PAHs at concentrations of 0.2 mg/mL (AccuStandard, CT, USA) and solid PAHs from Sigma (MO, USA), Aldrich Chemical Co. (WI, USA) or AccuStandard, (CT, USA) were employed.

Hexane (Tedia, RJ, Brazil) and acetonitrile (Tedia, RJ, Brazil) were used. Ultra-pure water was prepared through a Millipore Milli-Q System (MA, USA).

Table 3
Elution gradient used for PAH separation

Time (min)	Acetronitrile (%)	Water (%)
0	50	50
10	50	50
20	85	15
25	85	15
28.5	95	5
30	50	50

2.2. Glassware decontamination

Due to the low levels of interest, glassware was carefully cleaned and decontaminated. Firstly, all glassware was rinsed with a solvent (ACS Analytical Grade acetone or methanol) to remove residues and organic contaminants. After removing the organic solvent, glassware was rinsed with water and immersed for 12 h in a Neutral Extran solution (Merck, Brazil) that was removed with distilled water. Glassware was rinsed several times with ultra-pure water (Millipore) and baked overnight at 250 °C.

2.3. Sample collection

River water samples were collected from an environment with known industrial contamination. They were collected and conserved as recommended by NBR 13895 [31]. Around 1000 mL of water were sampled and transported to the laboratory under refrigeration ($T < 4$ °C) and kept at this temperature until analysis. Samples were collected and maintained in amber 1 L flasks without headspace. They were always processed within 1 or 2 days after collection.

2.4. PAH extraction

PAHs were extracted from water samples by liquid–liquid extraction and analyzed by HPLC-FLUO. Water samples (300 mL) were extracted in erlenmeyer flasks under magnetic

Table 4
Excitation and emission wavelengths employed for PAH detection and figures of merit of the analytical method

PAHs	Maximum excitation wavelengths (nm)	Maximum mission wavelengths (nm)	LOD (ng L^{-1})[a]	LOQ (ng L^{-1})[a]	Correlation coefficients
Naphthalene	224	332	0.10	0.33	1.0000
Acenaphthene	230	336	0.033	0.11	1.0000
Fluorene	230	316	0.13	0.43	1.0000
Phenanthrene	252	364	0.033	0.11	1.0000
Anthracene	252	404	0.033	0.11	1.0000
Fluoranthene	252	452	0.033	0.11	0.9999
Pyrene	238	388	0.033	0.11	0.9999
Benz[*a*]anthracene	238	396	0.033	0.11	1.0000
Chrysene	238	376	0.067	0.22	0.9999
Benzo[*b*]fluoranthene	268	447	0.13	0.43	1.0000
Benzo[*k*]fluoranthene	268	432	0.033	0.11	1.0000
Benzo[*a*]pyrene	268	412	0.033	0.11	0.9999
Dibenz[*a*,*h*]anthracene	292	400	0.033	0.11	1.0000
Benzo[*g*,*h*,*i*]perilene	292	420	0.067	0.22	1.0000
Indene[1,2,3-*c*,*d*]pyrene	300	500	0.067	0.22	0.9999

[a] Considering the extraction of 300 mL of water.

Table 5
Experimental planning for PAH extraction according to Doehlert design

Experiment number	Total volume of hexane (V, mL)	Extraction step time (t, min)	Extraction steps (n)
1	80	10	3
2	80	20	3
3	70	15	4
4	60	10	2
5	60	20	2
6	50	5	3
7	50	15	3
8	50	25	3
9	40	10	4
10	40	20	4
11	30	15	2
12	20	10	3
13	20	20	3

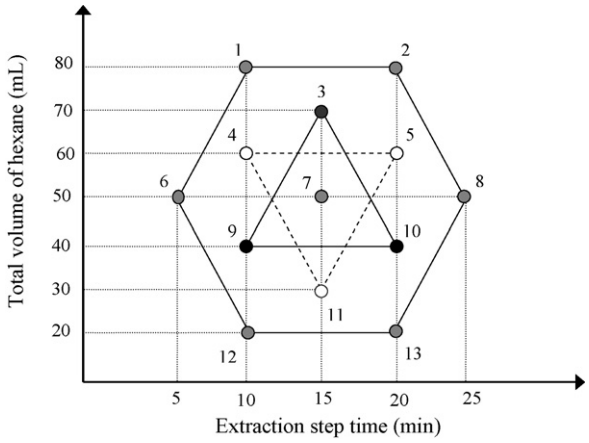

Fig. 1. Plane projection of the Doehlert design employed in this work. White, gray and black circles represent experiments with 2, 3 and 4 extraction steps (n), respectively.

stirring with variable volumes of hexane, time and number of extraction steps, according to the Dohelert design. Due to the lowest density of hexane and to the shape of the extraction flasks, the extracts could be easily drawn and transferred to pear-shaped evaporation flasks. Combined extracts were concentrated in rotary evaporator at temperatures below 40 °C. Concentrated extracts were made up to a final volume of 1 mL with acetonitrile, transferred to 2 mL vials and kept in freezer until analysis. When necessary they were diluted with acetonitrile before injection into the chromatographic system in order to fit linear range of the method.

In order to carry out the experiments designed in the multivariate experimental planning, solutions containing known PAH concentrations were prepared in the laboratory with pure water.

A recovery study was performed by spiking a contaminated river water sample with 25 $\mu g\,L^{-1}$ of each PAH. Once verified the accuracy of the procedure, at the experimental conditions established, it was applied in the determination of PAHs in more two samples of river waters containing variable concentrations of the analytes.

2.5. PAH determination

Qualitative and quantitative analysis of PAHs were performed by high-performance liquid chromatography with fluorescence detection (HPLC-FLUO). The HPLC consisted of a quaternary pump, an automated injector, a column oven and a fluorescence detector (all Agilent 1100 Series, USA). Chromatographic conditions (mobile phase composition and flow-rates) were evaluated and optimized using a reversed-phase column (Vydac 201TP54, 4.6 mm; 25 cm; 5 μm) and a guard column of the same characteristics (10 mm). The gradient shown in Table 3 allowed the best resolution of the studied PAHs. Excitation and emission wavelengths used for PAH detection are shown in Table 4.

3. Results and discussion

The first step of this work was the implementation of chromatographic conditions for determination of the studied PAHs. For this purpose, analytical curves in the range of 0.5–15 $\mu g\,L^{-1}$

Table 6
PAH recoveries (%) in the 13 experiments performed according to the Doehlert design

PAHs	Experiment number												
	1	2	3	4	5	6	7	8	9	10	11	12	13
Naphthalene	101	92.6	96.7	89.5	96.5	86.9	99.5	95.4	102	88.5	82.4	1.79	40.8
Acenaphthene	101	101	97.7	101	99.7	95.7	101	100	100	91.2	92.2	4.24	73.0
Fluorene	80.4	95.3	87.0	93.6	84.6	83.8	91.1	86.8	83.8	66.4	71.0	15.2	83.4
Phenanthrene	102	99.3	98.5	98.3	105	95.5	100	95.5	98.2	101	99.4	95.2	93.4
Anthracene	99.0	97.4	93.7	92.6	102	94.2	98.5	98.4	100	91.1	88.8	95.0	95.7
Fluoranthene	99.0	102	97.8	104	94.0	99.0	99.1	98.4	100	97.8	91.9	77.3	85.3
Pyrene	102	97.9	98.1	93.1	96.2	91.9	99.7	88.6	92.7	94.6	86.2	76.1	84.4
Benz[*a*]anthracene	103	98.6	98.6	92.3	93.3	96.9	101	99.6	95.5	103	94.5	96.2	102
Chrysene	99.8	99.1	90.5	94.5	102	90.0	94.0	92.1	97.7	95.4	90.6	86.8	78.6
Benzo[*b*]fluoranthene	107	99.6	97.6	97.9	100	96.0	99.0	94.7	97.8	101	95.9	86.0	82.0
Benzo[*k*]fluoranthene	103	96.5	93.6	102	102	92.0	92.8	95.7	90.4	93.3	90.4	89.0	85.7
Benzo[*a*]pyrene	103	102	97.6	100	102	91.7	97.2	94.2	99.7	92.2	93.6	88.2	83.4
Dibenz[*a*,*h*]anthracene	98.0	101	98.8	96.0	99.2	98.3	101	97.3	91.6	92.9	88.7	83.3	81.0
Benzo[*g*,*h*,*i*]perilene	98.8	99.1	97.4	91.2	97.2	84.5	100	99.6	89.2	93.7	95.3	76.8	83.0
Indene[1,2,3-*c*,*d*]pyrene	100	99.6	99.0	99.8	94.6	99.0	99.4	101	99.7	70.5	85.3	80.5	75.3

Table 7
Coefficients (b_0–b_9) for the studied PAHs

PAHs	Coefficients of individual extraction models										
	b_0	b_1	b_2	b_3	b_4	b_5	b_6	b_7	b_8	b_9	R
Naphthalene	−177.7	5.84	−0.043	12.51	−0.083	2.55	3.03	−0.080	0.201	−1.837	0.94
Acenaphthene	−133.5	5.26	−0.033	12.02	−0.027	−8.96	3.50	−0.115	0.211	−1.544	0.90
Fluorene	−167.2	4.01	−0.023	10.78	−0.058	39.4	−4.50	−0.089	0.089	−1.270	0.82
Phenanthrene	74.52	0.44	−0.001	2.01	−0.042	−1.45	1.20	−0.001	−0.070	−0.209	0.86
Anthracene	−15.85	0.79	−0.001	3.81	−0.022	42.4	−3.16	−0.004	−0.178	−0.954	0.97
Fluoranthene	64.42	1.46	−0.009	−0.48	−0.004	−3.87	0.41	−0.009	−0.053	0.326	0.91
Pyrene	−26.83	1.62	−0.008	4.69	−0.095	27.1	−3.04	−0.020	−0.066	−0.265	0.98
Benz[*a*]anthracene	36.29	0.34	−0.001	1.42	−0.029	26.9	−4.36	−0.017	−0.005	0.173	0.96
Chrysene	49.45	0.96	−0.002	1.37	−0.029	3.81	2.09	0.012	−0.230	−0.366	0.90
Benzo[*b*]fluoranthene	60.75	1.01	−0.005	1.37	−0.037	−1.98	0.99	−0.005	−0.061	−0.040	0.88
Benzo[*k*]fluoranthene	89.89	0.74	0.001	−0.29	0.010	−9.51	2.23	−0.006	−0.167	0.098	0.95
Benzo[*a*]pyrene	57.91	0.72	−0.002	2.10	−0.042	1.18	1.55	0.006	−0.110	−0.401	0.96
Dibenz[*a*,*h*]anthracene	34.33	1.04	−0.010	0.46	−0.028	19.7	−3.61	0.009	0.038	−0.004	0.99
Benzo[*g*,*h*,*i*]perilene	18.27	0.94	−0.010	4.05	−0.082	12.1	−2.92	−0.010	0.148	−0.173	0.95
Indene[1,2,3-*c*,*d*]pyrene	−7.374	0.98	−0.012	2.35	0.005	40.8	−5.59	0.008	0.155	−1.119	0.92

were built up utilizing standard solutions containing the 15 PAHs under study. The analytical curves (derived from least-square regression) presented excellent correlation coefficients, showing the good relationship between concentrations and fluorescence intensity in the studied range and they were employed for the determination of detection and quantification limits for each PAH. The analytical figures of merit of each PAH are shown in Table 4.

The quantification limits verified in the established experimental conditions were sufficiently low to allow PAH determination in concentrations lower than the Brazilian regulation limits for drinking and fresh water [7,8]. Moreover, in order to put our data and Brazilian legislation into a perspective, Table 1 shows a comparison between the MCL for PAHs in fresh and drinking water, according to the Brazilian legislation [7] and the values adopted for drinking water by USEPA [6].

3.1. Optimization strategy

Optimization of the extraction procedure was performed by employing a Response Surface Methodology based on a Doehlert matrix. Hexane was the solvent of choice due to its lowest density when compared to water and magnetic stirring was adopted in order to allow multiple sample processing.

For the Doehlert design, when three variables are considered, the solid obtained presents a cuboctahedron geometry, which is produced through a uniform distribution of points over the whole experimental region. Cuboctahedron is a geometrical solid with eight vertices symmetrically truncated producing eight equilateral triangles whose edges are equal to those of the remaining squares. Fig. 1 presents the plane projection of the design employed in this work with the actual levels of the variables taken. As can be seen, the experimental variables evaluated were total volume of hexane (V), extraction step time (t) and number of extraction steps (n). The number of levels for these variables were established according to the geometry of the design employed, which resulted in a study with seven levels for V, five levels for t and three levels for n, totaling 13 experiments. Total volume of hexane was varied between 20 and 80 mL, the extraction step time (t) between 5 and 20 min and the number of extraction steps (n) between 2 and 4. Table 5 shows the numbered experiments designed for these variables according to Doehlert matrix and Table 6 presents the extraction efficiency obtained for the individual PAHs in each experiment. Obtained data were modeled by using Statistica for Windows (Version 6) software employing the Experimental Design module. Triplicates at the central point were carried out in order to estimate experimental variance.

In order to attain the effect of each variable on the response, they were coded in order to eliminate the influence of their different magnitudes on such evaluation. The codification was performed by application of the following relation:

$$U_i = \frac{(X_i - X_i^0)}{\Delta X_i}$$

where U_i is the coded value of the variable, X_i^0 is the real value of the variable at the center of the experimental domain and ΔX_i the step of variation of the real value.

The extraction efficiencies of each PAH fit in functions that can be described by a general equation (Eq. (1)), containing 10 coefficients (b_0–b_9) to be determined for each individual PAH. The coefficients b_0–b_9 obtained for each PAH are shown in Table 7 as well as the correlation coefficients obtained for each model when predicted and experimental values were compared. For example, in the case of benzo[*a*]pyrene (BaP) the correspondent equation may be written as:

$$\%E_{BaP} = 57.91 + 0, \quad 72V - 0.002V^2 + 2.10t - 0.042t^2 + 1.18n - 1.55n^2 + 0.006Vt - 0.110Vn - 0.401tn \quad (2)$$

Table 8
Critical conditions calculated for each PAH after application of the Doehlert design experiments

PAHs	Total volume of hexane (V, mL)	Extraction step time (t, min)	Extraction steps (n)
Naphthalene	59	17	3
Acenaphthene	62	15	3
Fluorene	61	16	3
Phenanthrene	64	14	4
Anthracene	64	11	3
Fluoranthene	64	13	3
Pyrene	70	13	3
Benz[*a*]anthracene	66	15	3
Chrysene	61	14	4
Benzo[*b*]fluoranthene	73	12	3
Benzo[*k*]fluoranthene	71	14	4
Benzo[*a*]pyrene	77	12	4
Dibenz[*a*,*h*]anthracene	65	18	3
Benzo[*g*,*h*,*i*]perilene	63	18	3
Indene[1,2,3-*c*,*d*]pyrene	65	18	3

3.2. Determination of the critical points

The coordinates of the critical points (V^c, n^c and t^c) for each individual PAH were calculated by solving the equations system obtained by deriving the response function in terms of each variable established for the design, as follows:

$$\frac{\delta Y}{\delta V} = 0; \quad \frac{\delta Y}{\delta n} = 0 \quad \text{and} \quad \frac{\delta Y}{\delta t} = 0$$

where Y represents the extracted percentage of each PAH.

From the application of such derivates, a system with three variables and three linear equations was obtained for each PAH. Although the values of Δ_1, Δ_2 and Δ_3 demonstrated that most of surfaces obtained presented saddle points [32], the resolution of this system to find critical conditions was performed by applying the least-squares methodology and solving Eq. (3):

$$A^{-1}B = \begin{bmatrix} V^c \\ n^c \\ t^c \end{bmatrix} \tag{3}$$

where A^{-1} is the inverse matrix of the coefficients of the linear equations obtained by derivation of the surface functions and B is the matrix containing the independent terms, with inverse signal, of the same linear equations.

The values of the variables found for the critical point can be considered the optimum values for each variable, since they represent the point of the function where the extraction of each PAH is maximized and, this way, should be used in the experimental procedure for the extraction of the studied PAHs from water. The application of such calculation method led to the results shown in Table 8. For example, our results showed that best conditions for benzo[*a*]pyrene are a total volume of 77 mL of hexane divided in three extraction steps of 12 min each. However, the best individual conditions led to partial or total extraction of the other PAHs. Indeed for the evaluation of 15 PAHs this fact has to be considered since the set of experimental conditions has to be sufficiently robust to allow quantitative extraction of all PAHs of interest.

As can be seen from the presented results (Table 7) models with correlation coefficients between 0.82 and 0.99 were found, indicating that they can have a good prediction capability in relation to experimental conditions employed. Moreover, all critical conditions were located inside the experimental region tested showing the robustness of the chosen conditions and also of the planning.

According to Pareto analysis, performed with normalized variables, the most important variable for the extraction of all PAHs was the total volume of hexane employed in the extraction.

Table 9
Concentrations of the studied PAHs in a contaminated river water sample (S1) and percentage recoveries of the studied PAHs in the maximum optimized conditions

PAHs	Concentration in the sample (ng L^{-1})	Concentration found in the spiked sample (ng L^{-1})	Recovery (%)
Naphthalene	95.6 ± 1.2	175 ± 29	95.1
Acenaphthene	3.14 ± 1.4	107 ± 1	91.0
Fluorene	18.0 ± 0.7	85.4 ± 12.8	80.9
Phenanthrene	88.5 ± 3.3	173 ± 3	101
Anthracene	25.8 ± 0.9	106 ± 6	96.0
Fluoranthene	432 ± 14	506 ± 9	88.2
Pyrene	431 ± 10	513 ± 5	97.7
Benz[*a*]anthracene	183 ± 9	264 ± 9	97.4
Chrysene	158 ± 18	247 ± 3	106
Benzo[*b*]fluoranthene	477 ± 3	565 ± 2	106
Benzo[*k*]fluoranthene	92.6 ± 2.7	178 ± 12	103
Benzo[*a*]pyrene	390 ± 32	476 ± 5	103
Dibenz[*a*,*h*]anthracene	17.5 ± 0.6	96.8 ± 20.0	95.2
Benzo[*g*,*h*,*i*]perilene	141 ± 5	220 ± 9	95.0
Indene[1,2,3-*c*,*d*]pyrene	281 ± 1	365 ± 8	101

Data refer to three independent determinations.

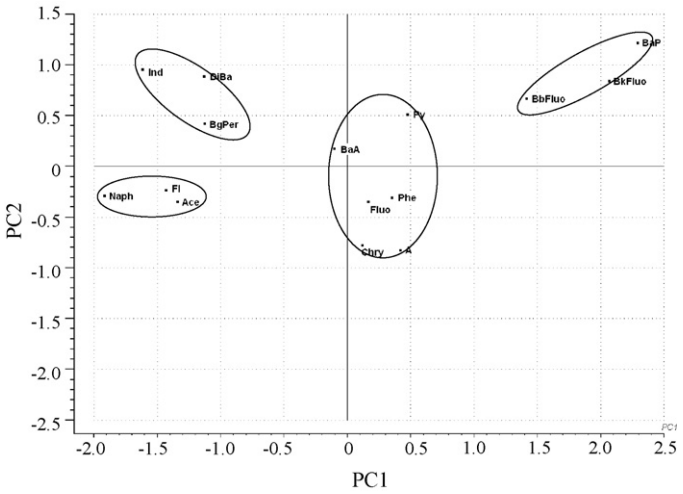

Fig. 2. PCA considering the best extraction conditions for the studied PAHs.

3.3. Principal component analysis

As can be seen from Table 8, each PAH showed a proper set of optimized conditions. So, in order to group the PAHs according to these optimized extraction conditions, a principal component analysis (PCA) was applied considering data presented in Table 8. The results obtained in the PCA analysis are shown in Fig. 2. Such results showed that PAH can be separated in four different groups according to their similar extraction conditions. It is important to remark that this classification clearly followed the molecular weight of the substances.

The first group contained the three lightest studied PAHs (namely naphthalene, acenaphthene and fluorene) and its main characteristic was the lower volume of solvent required to achieve maximum extraction from samples. The second group was composed by phenanthrene, anthracene, fluoranthene, pyrene, benz[*a*]anthracene and chrysene. For this group it seems that there are no singular characteristic to explain this clustering, since various extraction conditions were observed for all PAHs in terms of all variables. The third group was formed by benzo[*b*]fluoranthene, benzo[*k*]fluoranthene and benzo[*a*]pyrene and its main feature was the highest volume of hexane required to obtain maximum extraction. Finally, the fourth and last group was composed by the heaviest PAHs, which present as main characteristic the necessity of higher extraction times to allow maximum extraction.

With the information provided by the PCA is possible to conclude that each group of PAHs can be conveniently extracted from water samples by application of specific liquid–liquid extraction experimental conditions. Therefore, lower volume of hexane and lower time can be used in the determination of the lightest PAHs when compared with the higher volume of solvent needed to achieve quantitative recovery of the heaviest PAHs. This information can be used for saving reagent and time in this kind of analysis.

Table 10
Concentrations (means ± standard deviations) of the studied PAHs in two river water samples collected before (S2) and after (S3) a factory effluent discharge point

PAHs	S2 (ng L^{-1})	S3 (ng L^{-1})
Naphthalene	4.46 ± 0.04 (0.9)[a]	61.9 ± 3.2 (5.2)
Acenaphthene	0.87 ± 0.01 (1.1)	22.0 ± 0.7 (3.2)
Fluorene	1.05 ± 0.01 (1.0)	30.4 ± 0.6 (2.0)
Phenanthrene	6.30 ± 0.24 (3.8)	177 ± 2 (1.1)
Anthracene	0.19 ± 0.01 (5.3)	12.8 ± 1.0 (7.8)
Fluoranthene	5.53 ± 0.12 (2.2)	791 ± 3 (0.4)
Pyrene	3.10 ± 0.05 (1.6)	417 ± 1 (0.2)
Benz[*a*]anthracene	<LOD	29.0 ± 1.6 (5.5)
Chrysene	1.17 ± 0.03 (2.6)	114 ± 1 (0.9)
Benzo[*b*]fluoranthene	<LOD	88.7 ± 2.2 (2.5)
Benzo[*k*]fluoranthene	0.22 ± 0.01 (4.5)	25.2 ± 0.8 (3.2)
Benzo[*a*]pyrene	<LOD	54.3 ± 2.5 (4.6)
Dibenz[*a*,*h*]anthracene	0.22 ± 0.03 (14)	3.0 ± 0.2 (6.7)
Benzo[*g*,*h*,*i*]perilene	<LOD	27.9 ± 2.0 (7.2)
Indene[1,2,3-*c*,*d*]pyrene	<LOD	46.0 ± 1.6 (3.5)

Data refer to three independent determinations.
[a] Relative standard deviations (%).

4. Application to river water samples

How different optimized conditions were observed for the liquid–liquid extraction of each PAH, the main problem was to select only one set of experimental conditions for the determination of all 15 PAHs under study since it is not possible to run individual samples under the different experimental conditions of each PAH group. In this context, in order to employ only one experimental condition in which all PAHs could be quantitatively extracted, the set of conditions chosen comprised the maximum values obtained for each variable considering all PAHs. Therefore, a total volume of 77 mL of hexane, divided into four extraction steps of 18 min each were established as experimental conditions for liquid–liquid extraction. The obtained results are shown in Table 9.

In order to evaluate the accuracy of the developed procedure, these maximum experimental conditions were employed for the evaluation of the recovery rates obtained in the analysis of a river water sample. For this purpose 300 mL of the sample were spiked with 1 mL of a solution containing 25 μg L^{-1} of each PAH, resulting in a final spiked concentration of 83.3 ng L^{-1}. Recoveries for the studied PAHs varied between 80.9 and 106 with a mean value of 97.1 ± 6.8% (Table 9). Such recoveries were considered suitable for analytical quantitative work.

Furthermore, the developed methodology was applied in the determination of PAHs in two river water samples collected before (S2) and after (S3) an aluminum factory effluent discharge point. The results obtained in the sample analysis are presented in Table 10. As expected the sample collected before the discharge point presented lower individual PAH concentrations when compared to the sample collected after that point. It is important to remark that all relative standard deviations were situated between 0.2 and 14% showing the suitable precision of the methodology.

5. Conclusions

The Doehlert design approach proved to be a rapid, economical and efficient way to optimize the experimental conditions for the liquid–liquid extraction of fifteen EPA-PAHs from water samples.

Although different extraction conditions were obtained for each PAH, the application of a PCA showed that the studied PAHs could be grouped according to the optimized conditions. Moreover, it was shown that the presence of PAHs in each group was dependent on their molecular weight.

The application of the optimized conditions led to a mean recovery of $97.1 \pm 6.8\%$ proving that they are sufficiently robust for PAHs determination in contaminated river water. Relative standard deviations were always better than 14% in the analysis of real samples proving that the developed methodology presents an adequate precision for PAH determination in this kind of sample.

Acknowledgements

The authors are thankful to CNPq (Conselho Nacional de Desenvolvimento Científico e Tecnológico), CAPES (Coordenação de Aperfeiçoamento de Pessoal de Nível Superior) and FINEP (Financiadora de Estudos e Projetos) for the grants and fellowships, and for financial support.

References

[1] IARC – International Agency for Research on Cancer. Complete list of agents, mixtures and exposures evaluated and their classification, 2006, http://www.iarc.fr.
[2] P. Boffetta, N. Jourenkova, P. Gustavsson, Cancer Causes Control 8 (1997) 444.
[3] A.D. Pereira Netto, J.C. Moreira, A.E.X.O. Dias, G. Arbilla, L.F.V. Ferreira, A.S. Oliveira, J. Barek, Química Nova 23 (2000) 765.
[4] International Programme on Chemical Safety, Selected Non-Heterocyclic Polycyclic Aromatic Hydrocarbons, World Health Organization, Geneva, 1998.
[5] T. Vo Dinh, J. Fetzer, A.D. Campiglia, Talanta 47 (1998) 943.
[6] United States Environmental Protection Agency. National Primary Drinking Water Standards, 2003, http://www.epa.gov/safewater.
[7] Brazilian Health Ministry. Portaria MS 518, Brasília, Brazil, 2004.
[8] Brazilian Environment Ministry. Resolução CONAMA 357, Brasília, Brazil, 2005.
[9] E. Manoli, C. Samara, Trends Anal. Chem. 18 (1999) 417.
[10] A.D. Pereira Netto, C.L.S. Sisinno, J.C. Moreira, G. Arbilla, M. Dufrayer, Bull. Environ. Contam. Toxicol. 68 (2002) 148.
[11] D.A. Azevedo, E. Gerchon, E.O. Reis, J. Braz. Chem. Soc. 15 (2004) 292.
[12] E. Manoli, C. Samara, Chromatographia 43 (1996) 135.
[13] G.M. Titato, F.M. Lancas, J. Liquid Chromatogr. Relat. Technol. 28 (2005) 3045.
[14] G.E.P. Box, W.G. Hunter, J.S. Hunter, Statistics for Experimenters, Wiley, NewYork, USA, 1978.
[15] B.B. Neto, I.S. Scarminio, R.E. Bruns, Como Fazer Experimentos, Editora da Unicamp, Campinas, Brazil, 2001.
[16] D.C. Montgomery, Design and Analysis of Experiments, fourth ed., Wiley, New York, USA, 1997.
[17] A.M.G. Campaña, L. Cuadros, A.L. González, F.A. Barrero, M.R. Ceba, Anal. Chim. Acta 348 (1997) 237.
[18] D.H. Doehlert, Appl. Stat. 19 (1970) 231.
[19] Y. Hu, D.L. Massart, J. Chromatogr. 485 (1989) 311.
[20] M. Nechar, M.F.M. Molina, L.C. Rodriguez, J.M. Bosque-Sendra, Anal. Chim. Acta 316 (1995) 185.
[21] D. Gazquez, M. Sanchez-Vinas, M.G. Bagur, G. Garcia, J. Anal. At. Spectrom. 13 (1998) 105.
[22] M. Zougagh, P.C. Rudner, A.G. Torres, J.M.C. Pavon, J. Anal. At. Spectrom. 15 (2000) 1589.
[23] S.L.C. Ferreira, H.C. Santos, M.S. Fernandes, M.S. Carvalho, J. Anal. At. Spectrom. 17 (2002) 115.
[24] S.L.C. Ferreira, A.S. Queiroz, M.S. Fernandes, H.C. Santos, Spectrochim. Acta Part B 57 (2002) 1939.
[25] R.J. Cassella, O.D. SantAna, R.E. Santelli, Spectrochim. Acta Part B 57 (2002) 1967.
[26] R.E. Santelli, M.A. Bezerra, O.D. SantAna, R.J. Cassella, S.L.C. Ferreira, Talanta 68 (2006) 1083.
[27] S. Soriano, A.D. Pereira Netto, R.J. Cassella, Anal. Bioanal. Chem. 387 (2007) 1113.
[28] C. Aguilar, A. Penalver, E. Pocurull, J. Ferre, F. Borrull, R.M. Marce, J. Chromatogr. A 844 (1999) 425.
[29] A. Martinez-Urunuela, J.M. Gonzalez-Saiz, C. Pizarro, J. Chromatogr. A 1056 (2004) 49.
[30] A. Martinez-Urunuela, J.M. Gonzalez-Saiz, C. Pizarro, J. Chromatogr. A 1048 (2004) 141.
[31] ABNT – Associação Brasileira de Normas Técnicas. Construção de poços de monitoramento e de amostragem – NBR 13895. Rio de Janeiro, Brazil, 1997.
[32] S.L.C. Ferreira, W.N.L. Santos, C.M. Quintella, B.B. Neto, J.M. Bosque-Sendra, Talanta 63 (2004) 1061.

Available online at www.sciencedirect.com
ScienceDirect
Talanta 74 (2008) 1700
Talanta
www.elsevier.com/locate/talanta

Erratum

Erratum to "Determination of polycyclic aromatic hydrocarbons (PAHs) in particulate matter collected with low volume samplers" [Talanta 72 (4) (2007) 1357–1361]

Paolo Bruno, Maurizio Caselli, Gianluigi de Gennaro *, Maria Tutino

Dipartimento di Chimicâ, Universita Degli Studi di Bari, via Orabona 4, 70126 Bari, Italy

Available online 13 July 2007

The publisher regrets that during the processing of the above paper errors occurred in Tables 8 and 9
The correct parts are:

Table 8
PAHs measured concentrations (ng/m^3) for each half of filter.

Table 9

Compounds	Bari concentration (ng/m^3)	S.D.	Taranto concentration (ng/m^3)	S.D.
BaA	0.47	0.30	1.90	2.84
BbF	1.33	0.82	3.91	5.26
BkF	0.41	0.22	1.34	1.82
BaP	0.56	0.41	2.05	2.90
Ip	0.79	0.56	2.41	3.28
BgP	1.07	0.75	2.30	2.74
DbA	0.13	0.08	0.55	0.79

DOI of original article:10.1016/j.talanta.2007.01.043.
* Corresponding author. Tel.: +39 0805442023; fax: +39 0805442023.
E-mail address: giangi@chimica.uniba.it (G. de Gennaro).

0039-9140/$ – see front matter © 2007 Elsevier B.V. All rights reserved.
doi:10.1016/j.talanta.2007.06.003

Available online at www.sciencedirect.com
ScienceDirect
Talanta 74 (2008) 1281–1286
Talanta
www.elsevier.com/locate/talanta

Impact of malolactic fermentation on low molecular weight phenolic compounds

M.J. Cabrita, M. Torres, V. Palma, E. Alves, R. Patão, A.M. Costa Freitas *

Laboratório de Enologia, Instituto de Ciências Agrárias Mediterrânicas, Universidade de Évora, Ap 94 7002-554 Évora, Portugal

Received 19 April 2007; received in revised form 23 August 2007; accepted 30 August 2007
Available online 8 September 2007

Abstract

A reversed phase liquid chromatography-DAD method is proposed for analysis of major non-flavonoid phenolic compounds in wines. The method employed a mixture of acetic acid, water and methanol as eluents and was used to evaluate the impact of malolactic fermentation in low molecular phenolic compounds.

The wines analyzed underwent different treatments, like the addition of a pectolytic enzyme or lysozyme, and the way malolactic fermentation was carried out—spontaneously or with the inoculation of two different commercial lactic bacteria.

The main result observed was the disappearance of hydroxycinnamoyltartaric acids and the increase of resultant free forms, regardless the way malolactic fermentation was carried out.
© 2007 Elsevier B.V. All rights reserved.

Keywords: HPLC-DAD; Malolactic fermentation; Non-flavonoid compounds

1. Introduction

The importance of phenolic compounds in wine is very well established due to their influence in colour, flavour and astringency [1,2]. Non-flavonoid compounds include benzoic, cinnamic acids and aldehydes, usually named low molecular weight phenols. Although being present in small amounts in wines they play an important role in sensory quality and may contribute, through an additive effect, to bitterness and harshness, specially cinnamic acids [3].

There are two main groups of phenolic acids: hydroxybenzoic acids and hydroxycinnamic acids. Hydroxybenzoic acids (C6–C1) have a general structure derived from benzoic acid and they differ according to hydroxylation and methoxylation of the aromatic ring.

Hydroxycinnamic acids (C6–C3) derive from cinnamic acid. Both groups are commonly present in grapes and wines, sometimes in the form of tartaric acid esters [4].

Hydroxycinnamic acids such as *p*-coumaric, ferulic or caffeic acid are also important, as they can be decarboxylated by a number of microbiological species, into ethyl-phenols considered as off-flavours [5]. Cinnamic acids are also involved in co-pigmentation process with anthocyanins, which affect the colour of red wines [6].

They are usually esterified with tartaric acid as hydroxycinamic tartaric esther known as caftaric acid, fertaric acid and coutaric acid. The yeast *Dekkera bruxellensis* is mainly responsible for *p*-coumaric and ferulic acid decarboxylation and reduction to 4-ethylphenol and 4-ethylguaiacol, although other microorganisms, like lactic acid bacteria, also appear to be able to undertake this pathway. The capacity of lactic acid bacteria to produce volatile phenols from ferulic acid was observed to be much lower than its capacity to produce volatile phenols from *p*-coumaric acid [7]. Recently 4-ethylcathecol was found in wine, this compound is expected to result from the decarboxylation and reduction of caffeic acid (data not published) Sinapic acid, that exists in small amounts in wines, can lead to 4-ethyl syringol but this compound is not considered to be sensorially relevant [8].

Malolactic fermentation (MLF), the enzymatic decarboxylation of L-malic to L-lactic acid and CO_2, is an important secondary fermentation carried out by lactic acid bacteria (LAB) during the vinification of red wines. In addition to the deacidification, the MLf is considered to contribute to complexity of

* Corresponding author. Tel.: +351 266 760 934/800; fax: +351 266 760 828.
E-mail address: afreitas@uevora.pt (A.M. Costa Freitas).

0039-9140/$ – see front matter © 2007 Elsevier B.V. All rights reserved.
doi:10.1016/j.talanta.2007.08.045

Table 1
Parameters for the calibration of low molecular weight phenolic compounds

Compound	RT ± S.D. (min)	λ (nm)	Equation	r^2	Linear range (mg/L)
Gallic acid	5.95 ± 0.13	280	$y = 57.573x + 4.55$	0.9998	5.5–93.5
Protocatechuic acid	11.53 ± 0.23	254	$y = 60.156x + 1.20$	0.9976	0.5–10
Protocatechuic aldehyde	16.64 ± 0.29	280	$y = 109.97x + 19.76$	0.9886	0.5–10
Vanillic acid	26.69 ± 0.38	254	$y = 55.629x + 6.69$	0.9968	0.5–10
Caffeic acid	28.09 ± 0.50	320	$y = 124.69x - 67.94$	0.9977	5–105
Syringic acid	32.33 ± 0.34	280	$y = 64.62x - 23.64$	0.9908	4.9–24.9
p-Coumaric acid	39.23 ± 0.59	320	$y = 144.67x - 42.31$	0.9975	5–105
Ferulic acid	45.65 ± 0.64	320	$y = 97.925 + 29.98$	0.9979	0.5–10

RT ± S.D.: retention time ± estimated standard deviation ($n = 3$); λ (nm): quantification wavelength; r^2: determination coefficient.

the flavour and to confer a degree of microbiological stability to the wine. Aiming to improve also organoleptic properties such as colour stability and smoothness, winemakers have introduced different ways to perform this fermentation including the addition of commercial lactic bacteria or the use of oak barrels. Spontaneous MLF commonly occurs after alcoholic fermentation when wine conditions are favourable for the growth of lactic acid bacteria, however spontaneous MLF is unpredictable, hence the importance of using commercial starters.

Regarding low molecular weight phenolic compounds it is known that some phenolic acids can inhibit the growth of lactic acid bacteria [9] while others can stimulate malolactic fermentation carried out by *Oenococus oeni* [10–12]. During this process hydroxycinnamic acids and their derivatives are the main compounds modified. The decrease in the concentration of *trans*-caftaric and *trans-p*-coutaric acids until disappearance, along with an increase in the corresponding free forms, *trans*-caffeic and *trans-p*-coumaric acids could be linked to lactic acid bacteria metabolism [13].

Various different chromatographic methods have been employed for the separation of low molecular weight phenolic compounds in wines. Wine sample analysis can be performed by direct injection [14] or include a sample preparation step like liquid–liquid [13,15–17] or solid phase extraction [18–21]. A new solid supported liquid–liquid extraction using diatomaceous earth has been recently proposed, being an environmentally friendly low-cost sample preparation method which proved to be reproducible and yielding high recoveries [22].

For separation almost every methods use a reversed phase C18 column with a binary solvent system, a combination of acetic [23,24] or formic acid [15,17] with a dilute polar organic solvent as acetonitrile [23,24] or methanol [15,17,21]. Detection is usually achieved using UV–vis or DAD detectors, and occasionally using mass detection methods [25] that lead to a more reliable compound identification. Very rarely fluorescence detection is used [26].

Analysis times are usually long, reaching 100 min or more, thus limiting the number of analyses that can be carried out in a given period. We propose a chromatographic method that in 46 min provides good separartion of the 11 compounds being studiedensuring high resolution ($R > 1$, 5 for almost compounds studied). When applied to red wine samples obtained before and after malolactic fermentation it has allowed the understanding of the effect of malolactic fermentation on low molecular weight phenolic compounds.

2. Experimental

2.1. Samples

Red grapes of *Vitis vinifera* L.,c.v. Trincadeira were picked up during 2004 harvest at commercial maturity. Three sets of microvinifications, with three replications, were done according to the scheme presented in Fig. 1. After crushing and destemming, grapes and musts were placed in stainless steel containers of 80 L capacity occupying only 50 L, treated with sulfur dioxide (150 mg/L SO_2), inoculated with active dry yeast (Fermol A3B, AEB, Brescia, Italy) and nutrients Fermoplus Ecorcell (AEB, Brescia, Italy) according to manufacturer's instructions. The first set (D1, D2 and D3) suffered no other treatment, to the second set (D4, D5 and D6) lysozyme (lysocid) was added and to the third set (D6, D7 and D8) a pectolitic enzyme (Endozym Rouge) was added. The fermenting musts were punched down twice a day, and were pressed after 7 days of pomace contact, when specific gravity fell under 1000. Both press and free run wines were assembled, and at this point, each vinification tank was split in three to allow malolactic fermentation to undergo spontaneously (control, no inoculation of lactic bacteria) or carried out by two different commercial preparations of lactic acid bacteria, Biolact Acclimatée (BL1) and Biolact Acclimatée 4R (BL2). All enological products were from AEB (Brescia, Italy)

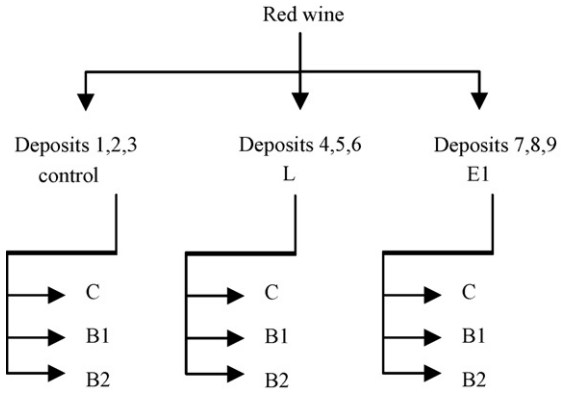

Fig. 1. Vinification scheme—C: control; L: lysocid; E: E. Rouge; B1: biolact acclimatée; B2: biolact acclimatée 4R.

and were added as recommended by suppliers. We obtained a total of 27 wines.

2.2. Reagents and standards

The water employed was previously purified in a Mili-Q system (Millipore, Bedford,MA). HPLC grade methanol was from MercK (Darmstadt, Germany). Phenolic compounds: gallic acid, gentisic acid, protocatechuic acid, protocatechuic aldehyde, (+)-catechin, syringic acid, vanillic acid and ferulic acid were supplied by extrasynthese (Genay, France). Caffeic acid and *p*-coumaric acid were from Sigma–Aldrich (St. Louis, MO).

2.3. Phenolic compound's extraction

A liquid–liquid extraction was performed: 5 mL of wine with pH adjusted to 2 were extracted twice with 5 mL of diethyl ether for ten minutes. The organic phase was dried over Na_2SO_4, the solvent was evaporated under nitrogen, the dry residue obtained was dissolved in methanol–water (1:1, v/v) and filtered through a 0.45 μm Nylaflo membrane filter (Gelman) before being injected into the chromatograph. All samples were extracted in duplicate and results are expressed as the mean value.

A recovery study on the liquid–liquid extraction was performed using a spiked wine sample. In order to provide information that allows us a better discussion on the results obtained. Recovery percentages found were—gallic acid: 60%; protocatechuic acid: 45%; protocatechuic aldehyde: 37%; vanillic acid: 33%; caffeic acid: 36%; syringic acid: 54%; *p*-coumaric acid: 37%; ferulic acid: 33%.

Malovaná et al. [16] evaluate SPE and LLE for the analysis of several wine phenolic compounds, and the list of the compounds studied now is very similar to that studied before. Ethyl acetate and diethyl ether were reportedly used to extract the wine samples and, although the results obtained with both solvents were very similar, diethyl ether yields were slightly better.

2.4. Instrumentation and conditions

Twenty microlitres of each extract were separated on a Superpher® 100, C18 (5 μm packing, 250 mm × 4.6 mm i.d.) (Merck, Germany) column using a Hewllet Packard 1050 equipment with a Hewllet Packard Diode Array 1100 detector.

Flow rate was 1 mL/min. The mobile phase was—solvent A: water:acetic acid (98:2, v/v), solvent B: water:methanol:acetic acid (68:30:2, v/v), and solvent C: methanol for column wash at the end of each day. A gradient program was adopted as follows for solvent A: from 95% to 70% (12 min); from 70% to 45% (15 min); from 45% to 23% (6 min); isocratic for 9 min; from 23% to 5% (5 min); from 5% to 0% (3 min); isocratic for 5 min, and a post-run of 5 min for re-equilibration of the initial gradient.

The detection wavelengths were 280, 254, and 320 nm and the UV–vis spectra (scanning from 190 to 400 nm) were recorded for all peaks.

Phenolic compounds were identified by comparison of elution order, retention times and the spectral UV–vis with those of standards and quantified by the external standard method (Table 1).

Caftaric, coutaric and fertaric acids were isolated from wine according to [27] to help identification by comparison with spectral UV–vis, and were quantified as their corresponding free forms.

2.5. Malic and lactic acid determination

Malolactic fermentation was followed through the determination of malic and lactic acid in deposits 1, 2 and 3, according to the methodology previously reported [28] and using the same equipment with a LichroCART® 250-4 Superspher® RP 18 endcapped (5 μm packing, 250 mm × 4.6 mm i.d.) (Merck, Germany) column. The mobile phase was fosforic acid (5×10^{-3} M), flow 0.7 mL/min and detection was done at 210 nm. Sample preparation includes an extraction in a Sep-Pak® cartridge C18 300 g (Waters, Milford; MA, USA) of wine diluted 1:2 with fosforic acid 1N, and recovered with fosforic acid 5×10^{-3} M. Calibration curves were established for the two acids from 4 to 0.1 g/L, with correlation coefficients of 0.999 and 0.998 for malic and lactic acids.

2.6. Statistical analysis

Differences in phenolic compounds present in wine before and after FML realized under different conditions (C, B1 and B2) were assessed by one-way analysis of variance (ANOVA); mean comparisons were performed using Fischer's multiple comparison test at the 95% confidence level. Analyses were accomplished using NCSS 6.0 software.

3. Results and discussion

Malic acid consumption in deposits 1, 2 and 3 (control) is shown in Fig. 2. The graphics show that during the sampling period the malic acid content drops below the method's detection limit, regardless the inoculation or not (control) of lactic bacteria (B1 and B2). The disappearance of malic acid seems to be more related to each wine characteristics (from deposits 1, 2 or 3) then with the addition or not of a lactic bacteria. Regardless the addition or not of lactic bacterias, the content of malic acid begins to disappear first in wine from deposit 3 than in wine from deposit 1 and last in wines from deposit 2.

Fig. 3 illustrates the chromatogram obtained from a red wine sample before malolactic fermentation and Fig. 4 presents the chromatogram of a sample after malolactic fermentation.

Tables 2–4 show the content of phenolic compounds in wine samples collected before and after malolactic fermentation, from the control set, the set treated with lysozyme and the set treated with pectolytic enzyme. If results from deposit 2 are ignored, most marked changes observed in all other samples before and after malolactic fermentation involve the tartaric esters of

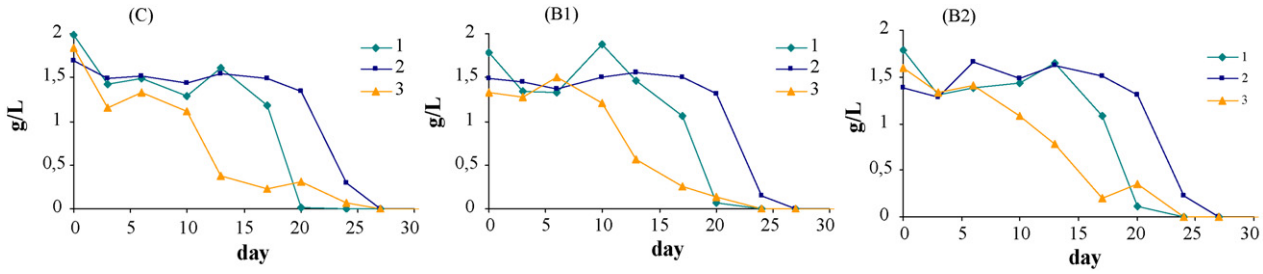

Fig. 2. Acid malic disappearance during malolactic fermentation in control wine from deposits 1, 2 and 3.

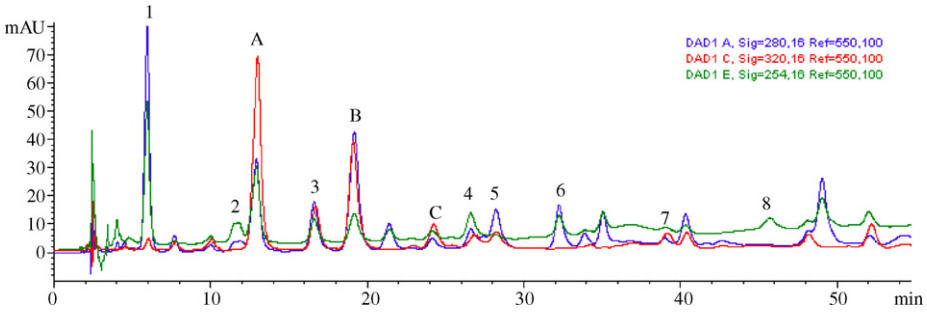

Fig. 3. Chromatogram obtained from a sample of red wine before malolactic fermentation—1: gallic acid, 2: protocatechuic acid, 3: protocatechuic aldehyde, 4: vanillic acid, 5: caffeic acid, 6: syringic acid, 7: *p*-coumaric acid, 8: ferulic acid. A: caftaric acid, B: coutaric acid, C: fertaric acid.

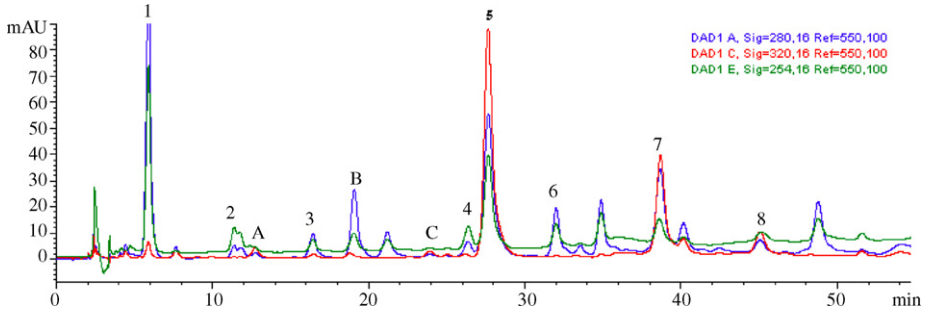

Fig. 4. Chromatogram obtained from a sample of red wine after malolactic fermentation—1: gallic acid, 2: protocatechuic acid, 3: protocatechuic aldehyde, 4: vanillic acid, 5: caffeic acid, 6: syringic acid, 7: *p*-coumaric acid, 8: ferulic acid. A: caftaric acid, B: coutaric acid, C: fertaric acid.

Table 2
Phenolic compounds (mg/L) in control wine samples (D1, D2 and D3) before and (D1 and D3) after malolactic fermentation (mean ± S.D.) (D2)

Compound	Before MLF		After MLF	
	Initial wine	Control (D2)	Lactic bacteria 1 (D2)	Lactic bacteria 2 (D2)
Gallic acid	7.19 a ± 0.05	8.41 b ± 0.59 (8.68)	8.75 b ± 0.08 (8.62)	8.63 b ± 0.53 (9.06)
Protocatechuic acid	1.32 ± 0.30	1.30 ± 0.13 (1.20)	1.28 ± 0.04 (1.43)	1.24 ± 0.08 (1.04)
Caftaric acid	4.10 b ± 0.51	0.25 a ± 0.01 (3.02)	0.24 a ± 0.09 (3.19)	0.29 a ± 0.05 (3.21)
Protocatechuic aldehyde	1.13 b ± 0.06	0.55 a ± 0.10 (1.11)	0.55 a ± 0.04 (1.12)	0.51 a ± 0.05 (1.16)
Coutaric acid	0.85 b ± 0.08	0.12 a ± 0.01 (0.60)	0.06 a ± 0.01 (0.63)	0.06 a ± 0.01 (0.61)
Fertaric acid	0.40 a ± 0.07	0.06 b ± 0.01 (0.67)	0.07 b ± 0.01 (0.68)	0.11 b ± 0.01 (0.65)
Vanillic acid	1.13 ± 0.18	1.16 ± 0.29 (1.35)	1.14 ± 0.13 (1.27)	0.87 ± 0.18 (1.31)
Caffeic acid	0.47 a ± 0.05	6.90 b ± 0.25 (3.28)	7.05 b ± 0.21 (2.88)	6.80 b ± 0.79 (2.85)
Syringic acid	1.75 a ± 0.17	2.36 b ± 0.41 (2.55)	2.36 b ± 0.05 (2.50)	2.05 ab ± 0.06 (2.52)
p-Coumaric acid	0.24 a ± 0.04	2.31 b ± 0.24 (0.77)	2.46 b ± 0.33 (0.73)	2.26 b ± 0.20 (0.78)
Ferulic acid	nd a	0.95 b ± 0.04 (0.21)	0.95 b ± 0.03 (0.16)	0.86 b ± 0.11 (0.40)

Note: As D2 deposit behaved differently, their content of phenolic compounds are presented in parentisis and mean value and S.D. account for deposit D1 and D3 only. Different letters in a row denote a significant difference with 95% confidence level in the Fisher's LSD multiple comparison test.

Table 3
Phenolic compounds (mg/L) in lysozyme wine samples (D4, D5 and D6) before and after malolactic fermentation (mean ± S.D.)

Compound	Before MLF		After MLF	
	Initial wine	Control	Lactic bacteria 1	Lactic bacteria 2
Gallic acid	6.64 a ± 0.42	7.00 ab ± 0.58	7.36 ab ± 0.26	7.95 b ± 1.00
Protocatechuic acid	1.03 a ± 0.11	1.14 ab ± 0.19	1.21 ab ± 0.08	1.31 b ± 0.19
Caftaric acid	3.71 b ± 0.56	0.27 a ± 0.16	0.22 a ± 0.38	0.30 a ± 0.16
Protocatechuic aldehyde	1.20 b ± 0.08	0.50 a ± 0.05	0.51 a ± 0.10	0.59 a ± 0.09
Coutaric acid	0.72 b ± 0.21	0.08 a ± 0.07	0.09 a ± 0.15	0.11 a ± 0.08
Fertaric acid	0.71 b ± 0.08	0.06 a ± 0.08	0.05 a ± 0.08	0.13 a ± 0.07
Vanillic acid	1.27 ± 0.08	1.05 ± 0.09	1.19 ± 0.10	1.29 ± 0.23
Caffeic acid	0.59 a ± 0.01	6.64 b ± 0.58	7.18 b ± 0.34	7.43 b ± 0.76
Syringic acid	1.99 ± 0.15	2.07 ± 0.34	2.16 ± 0.09	2.35 ± 0.49
p-Coumaric acid	0.30 a ± 0.07	2.15 b ± 0.13	2.42 bc ± 0.05	2.63 c ± 0.35
Ferulic acid	nd a	0.75 b ± 0.15	0.84 b ± 0.18	0.94 b ± 0.29

Different letters in a row denote a significant difference with 95% confidence level in the Fisher's LSD multiple comparison test.

hydroxycinnamic acids and their derivatives. The concentration of tartaric esters of hydroxycinnamic acids seems to drop until almost total disappearance. This results in a rise of the corresponding free forms, caffeic, *p*-coumaric and ferulic acids. Similar results were already described [13].

In all wines under study, the content of non-coloured phenolic compounds in samples before malolactic fermentation ranges from 18.40 to 23.53 mg/L after malolactic fermentation. The difference is mainly due to changes in content of tartaric esters of hydroxycinnamic and the corresponding free forms. In samples before malolactic fermentation mean value of caftaric, coutaric and fertaric acids is 5.33 mg/L and after malolactic fermentation this values drops to a mean value of 0.46 mg/L. Again considering all samples the mean value for caffeic, *p*-coumaric and ferulic acids ranges from 0.98 to 10.24 mg/L before and after malolactic fermentation. These values also seems to indicate that there is additional sources of caffeic, *p*-coumaric and ferulic acids in wines, that probably came from the hydrolysis of cinnamoyl-glucoside anthocyanins as well as from other hidroxycinnamics derivates by lactic bacteria enzymatic activity [13]. It was not observed any impact on these compounds by the use of the enzyme or the lysosyme.

In all samples studied, caffeic acid is the most abundant free form of cinnamic acid. The importance of this free acid in red wine is the possibility of its conversion into volatile phenols such as 4-ethylphenol and 4-ethylguaiacol, from *p*-coumaric acid and from ferulic acid, that have a huge negative impact on wine aroma.

Gallic acid content also increases with malolactic fermentation in all wines, while protocatechuic aldehyde content decreases. The contents of vanillic, syringic and protocatechuic acids remains almost the same after malolactic fermentation.

The differences observed in deposit 2 seem to be related with the slower disappearance of malic acid also observed in this deposit, regardless the inoculation or not wit lactic bacteria, as shown in Fig. 2. Although it is not easy to explain the different behaviour of deposit 2, results obtained seem to indicate that the degradation of hydroxycinnamic acids is preceded by malic acid degradation. This is a very interesting result as it can indicate that measuring the malic acid conversion into lactic acid may be insufficient data to conclude about the end of malolactic fermentation.

Quantitatively there is no significant difference between wines regarding the use of different lactic bacteria. The use of lysozyme had no influence on malolactic fermentation or in the content of the compounds studied, probably from the fact that the enzyme was added at the beginning of alcoholic fermentation instead of at the end of it.

Table 4
Phenolic compounds (mg/L) in enzyme wine samples (D7, D8 and D9) before and after malolactic fermentation (mean ± S.D.)

Compound	Before MLF		After MLF	
	Initial wine	Control	Lactic bacteria 1	Lactic bacteria 2
Gallic acid	7.50 a ± 0.33	8.90 b ± 0.70	7.60 a ± 0.42	7.73 a ± 0.28
Protocatechuic acid	0.92 ± 0.05	0.99 ± 0.12	0.86 ± 0.13	0.96 ± 0.04
Caftaric acid	4.04 b ± 0.23	0.39 a ± 0.23	0.33 a ± 0.16	0.22 a ± 0.00
Protocatechuic aldehyde	0.83 b ± 0.04	0.51 a ± 0.10	0.41 a ± 0.08	0.44 a ± 0.12
Coutaric acid	0.73 b ± 0.06	0.15 a ± 0.04	0.12 a ± 0.03	0.09 a ± 0.01
Fertaric acid	0.71 b ± 0.07	0.16 a ± 0.09	0.12 a ± 0.07	0.07 a ± 0.00
Vanillic acid	1.05 ab ± 0.07	1.22 b ± 0.22	0.96 b ± 0.09	1.00 ab ± 0.04
Caffeic acid	1.05 a ± 0.07	7.09 b ± 0.35	6.84 b ± 0.83	7.23 b ± 0.34
Syringic acid	1.34 a ± 0.13	1.89 b ± 0.21	1.52 ab ± 0.17	1.65 ab ± 0.28
p-Coumaric acid	0.30 a ± 0.02	2.52 b ± 0.25	2.43 b ± 0.29	2.43 b ± 0.08
Ferulic acid	nd a	0.64 b ± 0.12	0.73 b ± 0.15	0.72 b ± 0.12

Different letters in a row denote a significant difference with 95% confidence level in the Fisher's LSD multiple comparison test.

Some authors have observed some changes in the content of phenolic aldehydes and acids [21] or total polyphenols [29] by the use of commercial pectolitic enzymes. In this study any significant changes were observed in wines fermented in the presence of the commercial enzyme, except for caffeic acid that showed higher concentration values in these wines before malolactic fermentation. This could be related with the phenol esterase side activity present in this enzyme [30]. Syringic acid content did not increase in wines treated with the enzyme. Again it can be related to side activity of the commercial enzyme used, in this case, the lack of β-glucosidase activity, as it is known that syringic acid arises from B-ring of malvidin-3-glucoside upon its degradation [31]. Vanillic and siringic acids content are very similar in all wines because their presence in wines is not related to yeast metabolism but to the extraction from solid parts of grapes by alcohol and depends on the alcohol content [32] that in this wines were the same.

4. Conclusions

The obtained data show that hydroxycinnamic acids and their derivatives were the main compounds modified by malolactic fermentation, independently of the use or not of commercial lactic bacterias. In fact it seems clear that the decrease in concentration of caftaric, coutaric and fertaric acids, and the increase in concentration of caffeic, *p*-coumaric and ferulic acids are linked to lactic acid bacteria metabolism, as previously stated by Hernández and co-workers[33] that have shown that *trans*-caftaric and *trans*-coutaric acids are substrates of lactic acid bacteria witch can exhibit cinnamoyl esterase activities during malolactic fermentation, increasing the concentration of hydroxycinnamic acids.

Results also seem to indicate that the use of lysozyme in grapes, prior to alcoholic fermentation have no effect on malolactic fermentation development. Also the enzyme used in this work had no significant impact on non-coloured phenolic composition of these red wines.

Acknowledgments

Authors wish to thanks AEB Bioquímica Portuguesa for kindly providing the enological products, and Fundação para a Ciência e a Tecnologia, Ministério da Ciência, Tecnologia e Ensino Superior and Programa Operacional Ciência e Inovação 2010 (POCI 2010) for financial support (Projects POCI/AGR 56771 and POCI/AGR 55432).

References

[1] V.L. Singleton, P. Esau, Academic Press New York, 1969.
[2] J.L. Robichaud, A.C. Noble, J. Sci. Food Agric. 53 (1990) 343–353.
[3] V.L Singleton, A.C. Noble, Phenolic, sulfur and nitrogen compounds in food flavors, in: ACS Symposium Series 26, 1976, pp. 47–70.
[4] I. Biudic-Leto, T. Lovric, Food Technol. Biotechnol. 40 (2002) 221–225.
[5] D.A.N. Edlin, A. Narbad, N.J. Gasson, J.R. Dickinson, D. Lloyd, Enzyme Microbial. Technol. 22 (1998) 232–239.
[6] R. Brouillard, O. Dangles, Food Chem. 51 (1994) 365–371.
[7] J.A. Couto, F.M. Campos, A.R. Figueiredo, T.A. Hogg, Am. J. Enol. Vitic 57 (2) (2006) 166–171.
[8] T. Heresztyn, Arch. Microbiol. 146 (1986) 96–98.
[9] D. Stead, J. Appl. Bacteriol. 75 (1993) 135–141.
[10] N. Vivas, L. Bellemère, A. Lonvaud-Funel, Y. Glories, M. Augustin, Revue Française D'enologie 149 (1994) 37–42.
[11] N. Vivas, L. Bellemère, A. Lonvaud-Funel, Y. Glories, M. Augustin, Revue Française D'enologie 151 (1995) 39–45.
[12] N. Vivas, A. Lonvaud-Funel, Y Glories, Food Microbiol. 14 (1997) 291–300.
[13] T. Hernández, I. Estrella, D. Carlavilla, P.J. Martýn-Alvarez, M.V Moreno-Arribas, Anal. Chim. Acta 563 (2006) 116–125.
[14] A.F. Recamales, A. Sayago, M.L. González-Miret, D. Hernanz, Food Res. Int. 39 (2006) 220–229.
[15] R. Ramos, P.B. Andrade, R.M. Seabra, C. Pereira, M.A. Ferreira, M.A. Faia, Food Chem. 67 (1999) 39–44.
[16] S. Malovaná, F.J.G. Montelongo, J.P. Pérez, M.A. Rodrígues-Delgado, Anal. Chim. Acta 428 (2001) 245–253.
[17] L.R. Silva, P.B. Andrade, P. Valentão, R.M. Seabra, M.E. Trujillo, E. Velázquez, Food Chem. 89 (2005) 185–189.
[18] R. Di Stefano, M.C. Cravero, Sci. des Aliments 12 (1992) 139–144.
[19] D.A. Guillén, F. Merello, C.G. Barroso, J.A. Pérez-Bustamante, J. Agric. Food Chem. 45 (1997) 403–406.
[20] C.Y. Lee, A. Jaworski, Am. J. Enol. Vitic. 38 (1987) 277–281.
[21] I. Revilla, M.L Gonzáles-San José, Food Chem. 80 (2003) 205–214.
[22] F. Nave, M.[a].J. Cabrita, C.T Costa, J. Chromatogr. A (2007) 07–861.
[23] M. Del Alamo, I.N. Domínguez, L.M.C. Cárcel, L.N. Gracia, Anal. Chim. Acta (2004).
[24] C. Proestos, A. Bakogiannis, C. Psarianos, A.A. Koutinas, M. Kanellaki, M. Komaitis, Food Control 16 (2005) 319–323.
[25] S. Pérez-Magarino, I. Revilla, M.L. González-SanJosé, S. Beltrán, J. Chromatogr. A 847 (1999) 75–81.
[26] M.A. Rodrígues-Delgado, G. González-Hernández, J.E. Conde-González, J.P. Pérez-Trujillo, Food Chem. 78 (2002) 523–532.
[27] V.L. Singleton, C.F. Timberlake, A.G.H. Lea, J. Sci. Food Agric. 29 (1978) 403–410.
[28] P. Cane, L'enotecnico 26 (1990) 69–72.
[29] F. Pardo, M.R. Salinas, G.L. Alonso, G. Navarro, M.D. Huerta, Food Chem. 67 (1999) 135–142.
[30] A. Parley, Ph D Thesis, University of Lincoln, New Zeland, 1997.
[31] A.B. Bautista-Ortín, A. Martinez-Cutillas, J.M. Ros-Garcia, J.M. López-Roca, E. Gómez-Plaza, Int. J. Food Sci. Technol. 40 (2005) 867–878.
[32] R. Di Stefano, M.C. Cravero, Riv. Vitic. Enol. 43 (1990) 47–53.
[33] T. Hernández, I. Estrella, M. Pérez-Gordo, E.G. Alegría, C. Tenorio, F. Ruiz-Larrrea, Moreno-Arribas, M.V. J. Agric. Food Chem. 55 (2007) 5260–5266.

Available online at www.sciencedirect.com
ScienceDirect
Talanta 74 (2008) 1287–1298
Talanta
www.elsevier.com/locate/talanta

Biosensor analysis for the kinetic study of polyphenols deterioration during the forced thermal oxidation of extra-virgin olive oil

Luigi Campanella [a], Adriano Nuccilli [a], Mauro Tomassetti [a,*], Stefano Vecchio [b]

[a] *Department of Chemistry, "La Sapienza" University of Rome, P.le A. Moro 5, I-00185 Rome, Italy*
[b] *Department of Chemical Engineering (I.C.M.A.), "La Sapienza" University of Rome, Via del Castro Laurenziano 7, I-00161 Rome, Italy*

Received 27 April 2007; received in revised form 28 August 2007; accepted 30 August 2007
Available online 5 September 2007

Abstract

The process of artificial rancidification of extra-virgin olive oil due to heating in an oxidizing atmosphere was studied by testing an actual kinetic model of the process and monitoring the thermal oxidative degradation of the polyphenols contained in it. To this end, a series of oxidative degradation experiments were carried out on extra-virgin olive oil samples under isothermal conditions at 98, 120, 140, 160, and 180 °C using a thermostatic silicon oil bath. The experimental procedure used in this study carefully followed the recommendations regarding the study of olive oil rancidification set out in the AOM procedure. The change in polyphenol concentration with time was monitored at selected temperatures using a tyrosinase biosensor operating in an organic phase (*n*-hexane). The activation energy for the polyphenol degradation process determined using the MacCallum method was found to be practically constant throughout most of the process.

Furthermore, the application of the so-called "model-fitting" method to this process enabled the specific constant rates to be determined at the above-mentioned selected temperatures. In addition, a confirmation of the activation energy value was obtained by the "model-fitting" method and the algorithm of the kinetic model equation best-fitting the experimental curve representing the whole process was checked.

Finally, further very interesting observations were made, for instance, the half-life concentration values of polyphenols at selected temperatures between 98 and 180 °C.
© 2007 Elsevier B.V. All rights reserved.

Keywords: Extra-virgin olive oil; Artificial rancidification; Tyrosinase biosensor; Kinetic analysis

1. Introduction

As part of a dietary tradition linked to the territory, olive oil represents one of the fundamental products of Mediterranean agriculture; it has undisputed food value due to its chemical composition, as well as its distinctive (organoleptic) features, enhanced by its everyday use as a condiment [1].

At the international level the importance of extra-virgin olive oil (EVOO) is universally recognized in the food, agricultural and industrial sectors. Italy plays a leading role as far as EVOO is concerned both as regards quantity (it is the second world producer after Spain) and quality, i.e. large number of DOP "denominazione di origine protetta" trade-marks (in English, PDO "protected designation of origin") trade-marks recognized within the European Union [2].

The consumption of olive oil is linked mainly to its alimentary use. Nevertheless, mention should also be made of its use in medicine, recommended already in ancient times and today for its anti-oxidative capacity and for the prevention of cardio-circulatory diseases [3].

One fundamental aspect of EVOO is the proper conservation of the product, as in the case of all fats [4].

The study of the phenomena and auto-oxidative kinetics underlying the rancidification of the product is therefore of great importance [5–7]. In a recent research [8] we studied the process of artificial rancidification of EVOO, at the same time determining both the variation in the more traditional index which is the result of the peroxide value (PV) and that of a more innovative index determined by the concentration of the "total polyphenols" (expressed in mol l^{-1} of phenol), however polyphenols

* Corresponding author. Tel.: +39 06 49913722; fax: +39 06 490631.
E-mail address: mauro.tomassetti@uniroma1.it (M. Tomassetti).

0039-9140/$ – see front matter © 2007 Elsevier B.V. All rights reserved.
doi:10.1016/j.talanta.2007.08.036

are known to be the main natural anti-oxidant contained in abundance in the EVOO [9,10]. In this research, EVOO rancidification was studied by subjecting the oil to an isothermal process of artificial oxidation. In order to artificially oxidize the EVOO test samples, the AOM (Active Oxygen Method) of the American Oil Chemist Society [11] was employed; the oxidative process was therefore conducted at 98 °C, under a constant air flow.

The EVOO rancidification process rate displayed good inverse correlation between the two indexes considered regarding the total polyphenols concentration, as well as the PV values. However, in this preliminary research [8] no considerations regarding kinetic degradation could be made. Furthermore, in literature, kinetic data on this process are both incomplete and scarce [12,13]. To fill this gap, in the present research the kinetic parameters of the process were determined through an isothermal study carried out at different temperatures (between 98 and 180 °C). This also allowed important considerations to be made concerning the stability of EVOO at the high temperatures (180 °C) to which EVOO is sometimes subjected, for example in the frying process.

2. Experimental

2.1. Materials

Silicon oil 350 Cps (Crual srl); *n*-hexane RPE (Carlo Erba Reagents); phenol RPE (Carlo Erba Reagents); Kappa-Carrageenan (Fluka); dialysis membrane (art. D-9777) (Sigma–Aldrich); gas permeable membrane in PTF (YSI model 5775, Yellow Springs); monobasic and dibasic potassium phosphate RPE (Carlo Erba Reagents); tyrosinase (EC 1.14.18.1) from mushroom 3216 U/mg (Fluka); potassium chloride supplied by Riedel-de Haen (Seelze, Germany); chloroform RPE (Carlo Erba Reagents); tyrosol (Sigma–Aldrich); vanillin (Sigma–Aldrich); caffeic acid (Extrasynthese); ferulic acid (Extrasynthese); oleuropein (Extrasynthese); glyceryl trioleate (solvent) about 65% (w/w) (Sigma–Aldrich); commercial extra-virgin olive oil, purchased from local shops and produced by the most important industrial Italian olive oil producer firms, was contained in sealed glass bottles.

2.2. Instruments

The degradation of the polyphenols contained in the sample examined in this study took place in a silicon oil-based thermostatic bath (Fig. 1) (with temperature ranging from 0 to 250 °C and an associated uncertainty of ±0.1 °C), in an air stream of 140 ml min^{-1} produced by a Unistar mod. AIR 1000–1 pump. The transducer employed for the biosensor determination of the polyphenols in EVOO samples was an amperometric electrode for oxygen supplied by Universal Sensor Inc., New Orleans (USA), Mod. 4000-1. Measurements were performed using a potentiostat supplied by Radelkis Mod. OP 960. The current signal was converted into potential and read off on a Mitek multimeter mod. MK 5001, connected to an Amel analog recorder, mod. 868.

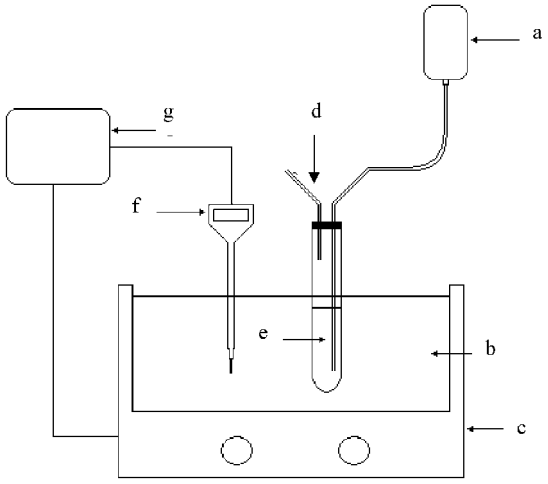

Fig. 1. Apparatus used to study the isothermal degradation of extra-virgin olive oil samples under in an oxidizing atmosphere at different temperatures between 98 and 180 °C. (a) Stream of air pump; (b) silicon oil; (c) adjustable heating device for the constant-temperature chamber; (d) overflow tube; (e) extra-virgin olive oil sample in a pyrex tube with a perforated Teflon plug; (f) vertex thermometer; and (g) electronic temperature controller.

The sample under investigation was added to the initial solution (10 ml *n*-hexane) contained in a constant-temperature chamber at 23 ± 0.2 °C and kept under stirring using an Amel magnetic stirrer, mod. 291/lf.

3. Methods

3.1. Artificial rancidification process

The artificial oxidation of the EVOO was obtained by placing the sample in a pyrex glass tube (containing 25 ml of sample under a constant stream of air at 140 ml min^{-1}) immersed in a silicon oil thermostatic bath both at 98 °C, according to the method proposed by the AOM [11], and at the following set temperatures of 120, 140, 160, and 180 °C, using the apparatus illustrated in Fig. 1. During the artificial rancidification process under isothermal conditions at the above-mentioned selected temperatures, fixed amounts of the sample contained in the test glass tube were collected at regular time intervals and immediately analyzed. The determination of the pool of polyphenols was carried out using an enzymatic tyrosinase biosensor both on the pure EVOO sample and on the degraded samples [8,14].

3.2. Tyrosinase OPEE

The biosensor method adopted was based on the oxidation of phenol to quinone catalyzed by the tyrosinase enzyme. The recorded signal was proportional to the variation of the partial vapor pressure of oxygen dissolved in solution, which was consumed in the course of the enzymatic reaction (1):

$$\text{phenol} + O_2 \xrightarrow{\text{tyrosinase}} o\text{-quinone} + H_2O \quad (1)$$

For this purpose, a tyrosinase biosensor made of polytetrafluoroethylene (PTFE) capable of measuring the decrease in

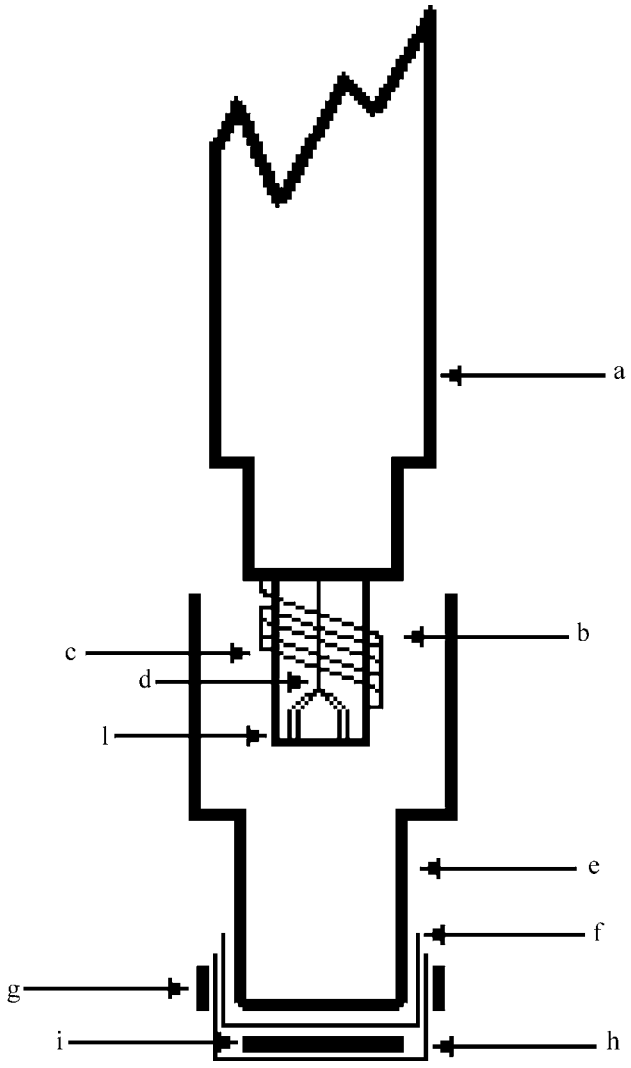

Fig. 2. Scheme of the tyrosinase biosensor used: (a) external structure of the electrode; (b) internal solution (phosphate buffer 0.067 mol l^{-1} at pH 6.6 and KCl 0.1 mol l^{-1}); (c) reference inner electrode: Ag/AgCl (anode); (d) Pt electrode (cathode); (e) Teflon cap; (f) gas-permeable membrane; (g) Teflon O-ring; (h) dialysis membrane; (i) tyrosinase immobilized in Kappa-Carrageenan gel; and (l) glass insulator.

dissolved oxygen concentration due to the oxidation of a phenolic compound to a *o*-quinone operating in *n*-hexane was used (this kind of biosensor is usually denoted as an organic phase enzyme electrode, OPEE) (Fig. 2). The variation of the signal recorded is proportional to the species reduced at the cathode (O_2), the amount of which depends on the concentration of the oxidized phenols in the sample. The decision to carry out the determination of the polyphenols in an organic solvent (*n*-hexane) was based on the very high solubility of the oil matrix in this organic solvent and to its very low solubility in aqueous solution [8,15].

The tyrosinase enzyme was immobilized in a Kappa-Carrageenan gel [16,17] prepared as follows: 3.75 mg of tyrosinase (3216 U mg^{-1}) was placed in an Eppendorf vial and dissolved in 100 μl of phosphate buffer 0.06 mol l^{-1} at pH 7. To obtain the enzyme membrane 50 μl of the enzyme solution was added to each disk of Kappa-Carrageenan, which was then stored for 48 h, at 4 °C.

The gel disk containing the enzyme was sandwiched between a PTFE membrane and a dialysis membrane; the whole assembly was fixed to the electrode head by a PTFE O-ring, as shown in Fig. 2.

3.3. Polyphenol measurement

At selected time intervals the oil samples to be analyzed were taken from the pyrex glass tube, where they had previously undergone thermal degradation under isothermal conditions at each of the above-mentioned five temperatures. These samples were placed in an Eppendorf vial which was cooled very rapidly by dipping it in cold water. Before performing the measures, both in order to reduce the viscosity of the sample in the successive preparations and to facilitate its immediate dissolution in the organic solvent (*n*-hexane) in which the measure was performed, the samples were diluted using the same solvent (*n*-hexane) in the ratio of (1:4 v/v).

The biosensor measurement was carried out under constant magnetic stirring in a glass cell thermostated at 23 °C and containing 10 ml of *n*-hexane, in which the bionsensor was immersed for the time necessary to achieve a stable signal [8]. When the signal of the biosensor immersed in *n*-hexane became stabilized, 25 μl of a standard solution of phenol 10^{-3} mol l^{-1} in *n*-hexane were added and the corresponding signal variation measured. When the new stationary state was reached, a second addition of 25 μl of the standard solution of phenol was made and after the new corresponding variation of the signal had been recorded, a further addition of 50 μl of the *n*-hexane solution of the oil sample, diluted (1:4 v/v), was made as described in a previous section and the corresponding variation of the signal was measured after the last addition. The polyphenol concentration in the sample examined was obtained using the following algorithm:

$$C_{\mathrm{EVOO}} = \left[\frac{\Delta S_{\mathrm{EVOO}}(\mu \mathrm{l}_{\mathrm{EVOO}})}{\Delta S_{\mathrm{standard}}(\mu \mathrm{l}_{\mathrm{standard}})}\right] C_{\mathrm{standard}} \times 4 \quad (2)$$

where 4 is the multiplier factor due to dilution and ΔS is the recorded signal variation, respectively, for EVOO and for the reference standard solution of phenol in *n*-hexane. The C_{EVOO} thus obtained, expressed in mol l^{-1} of phenol, clearly represents an index of the total polyphenols concentration in the sample.

3.4. Preparation of synthetic mixture of polyphenols

The lack of quantitative kinetic data available in literature concerning the thermal oxidative degradation process of polyphenols contained in EVOO led us to investigate a comparison system consisting in a synthetic mixture (SM) of five of the more readily available polyphenols contained in the EVOO dissolved in glyceryl trioleate. The composition of this mixture is shown in Table 1. Also this mixture was subjected to an isothermal degradation process at the same temperatures and in the same experimental conditions as used for the EVOO and analyzed with the biosensor method described above in order to

Table 1
Composition of the synthetic mixture (SM) of polyphenols in glyceryl trioleate

Compounds	MW	C (mol l^{-1})
Tyrosol	138	1.1
Vanillin	152	3.1
Caffeic acid	180	4.4
Ferulic acid	194	2.5
Oleuropein	540	1.4

evaluate quantitatively the kinetics of the polyphenol degradation process and to compare it with the same process occurring in the EVOO sample.

3.5. MacCallum method

The MacCallum method [18] was selected for this study from among the several kinetic methods reported in literature. It enables the activation energy related to the process to be determined by carrying out isothermal experiments at different pre-fixed temperatures using the following equation:

$$\ln(t_{iso})_\alpha = a + \frac{b}{(T_{iso})_\alpha} \quad (3)$$

where t_{iso} is the time necessary to achieve a given degree of conversion α under isothermal conditions at a given temperature T_{iso}. The kinetic parameters (pre-exponential factor, A and activation energy, E_a) are calculated from the regression parameters of Eq. (3) via the following relation: $a = \ln[f(1-\alpha) - \ln A]$ and $b = E_a/R$, where $f(1-\alpha)$ is a function representing the fraction of the sample not converted during the isothermal degradation process and R is the gas constant. From the slope b of Eq. (3), calculated at each degree of conversion α, the corresponding activation energy value is derived for the process considered. The time dependence of the degree of conversion at each isothermal temperature enables the $\ln(t_{iso})_\alpha$ values corresponding to given $(T_{iso})_\alpha$ values to be derived at selected α values ranging from 0 to 0.20, in accordance with the recommended literature interval for the application of the method [18]. Moreover, this method requires the construction of interpolated α_i *versus* t_i curves based on the experimental data at each T_{iso} in order to determine the time values necessary to achieve pre-fixed α values.

3.6. "Model-fitting" method

In order to complete the kinetic data and to validate more satisfactorily the results obtained using the above-mentioned method, another method denoted as "model-fitting" [19] was also applied to the experimental data obtained using the tyrosinase biosensor. This method was used to seek the "model function" that represents the best equation for describing the process; it also enabled the most important kinetic parameters of the process considered to be determined. It involved selecting from among the most suitable kinetic models described by appropriate mathematical functions the one that shows the best (linear) fit with the experimental data. To this end, the mathematical expressions of the most common differential and integral model functions ($f(\alpha)$ and $g(\alpha)$, respectively) found in literature [19] are given in Table 2. Since only the actual integral function $g(\alpha)$, which represents the process examined, depends linearly on time, according to the following relationship [19]:

Table 2
Most commonly used differential $f(\alpha)$ and integral $g(\alpha)$ model functions of the degree of conversion $\alpha = ((C_i - C_t)/(C_i - C_f))$, which are used to describe the degradation process examined

Reaction model	$f(\alpha)$	$g(\alpha) = kt$
P1	$4\alpha^{3/4}$	$\alpha^{1/4}$
A1.5	$1.5(1-\alpha)(-\ln(1-\alpha))^{1/3}$	$(-\ln(1-\alpha))^{2/3}$
A2	$2(1-\alpha)(-\ln(1-\alpha))^{1/2}$	$(-\ln(1-\alpha))^{1/2}$
A3	$3(1-\alpha)(-\ln(1-\alpha))^{2/3}$	$(-\ln(1-\alpha))^{1/3}$
A4	$4(1-\alpha)(-\ln(1-\alpha))^{3/4}$	$(-\ln(1-\alpha))^{1/4}$
B1	$\alpha(1-\alpha)$	$\ln(\alpha/(1-\alpha))$
R2	$2(1-\alpha)^{1/2}$	$1-(1-\alpha)^{1/2}$
R3	$3(1-\alpha)^{1/3}$	$1-(1-\alpha)^{1/3}$
D1	$1/2\alpha$	α^2
D2	$(-\ln(1-\alpha))^{-1}$	$(1-\alpha)\ln(1-\alpha)+\alpha$
D3	$1.5(1-(1-\alpha)^{1/3})^{-1}(1-\alpha)^{1/3}$	$(1-(1-\alpha)^{1/3})^2$
D4	$1.5((1-\alpha)^{1/3}-1)^{-1}$	$1-(2\alpha/3)-(1-\alpha)^{2/3}$
F1	$(1-\alpha)$	$-\ln(1-\alpha)$
F2	$(1-\alpha)^2$	$1/(1-\alpha)-1$
F3	$0.5(1-\alpha)^3$	$1/(1-\alpha)^2-1$

$$g(\alpha) = \int_0^\alpha \frac{d\alpha}{f(\alpha)} \quad (4)$$

A plot of the $g(\alpha)$ values *versus* time values corresponding to the fixed α value was made at each isothermal temperature. At each isothermal temperature the $g(\alpha)$ values were obtained by inserting in the expressions reported in Table 2 the regression α values (obtained from non-linear regression of the $\alpha = f(t)$ experimental values) for the thermal degradation of both EVOO and SM. The selection of the best $g(\alpha)$ function was obtained from the best linear fit of the $g(\alpha)$ *versus* t curves. Once the best $g(\alpha)$ function was selected, the specific rate constant k_{iso} values at each isothermal temperature were obtained from the slopes of the corresponding "best-fitting" $g(\alpha)$ *versus* t regression line. The temperature dependence of the specific rate constants is usually represented by the Arrhenius equation [20]:

$$\ln k_{iso} = c - \frac{b}{T_{iso}} \quad (5)$$

where $c = \ln A$ and $b = E_a/R$. Thus, by applying the linear regression to the Arrhenius equation, the pre-exponential factor $\ln A$ and the activation energy E_a were determined, respectively, from the intercept and the slope of the corresponding regression line as far as the best linear-fitting model function was concerned.

4. Results and discussion

4.1. Kinetic analysis of polyphenol degradation using the MacCallum method

Once the samples of EVOO and of SM had been subjected to the isothermal oxidative degradation process, at the different

Table 3
Concentration values in the "total polyphenols" of the extra-virgin olive oil (EVOO) sample for selected time values during the degradation as obtained by isothermal measurements at different temperatures using the tyrosinase biosensor

T (°C)	t (min)	C ($\times 10^3$ mol l^{-1})	t (min)	C ($\times 10^3$ mol l^{-1})	t (min)	C ($\times 10^3$ mol l^{-1})
98	0	2.00	480	0.47	1980	0.26
	10	1.96	1080	0.45	2820	0.23
	20	1.94	1380	0.42	3120	0.18
	30	1.40	1620	0.38	3360	0.13
	60	0.81	1800	0.29	3600	0.05
	120	0.77				
120	0	2.00	30	1.07	450	0.25
	3	1.95	60	0.94	570	0.21
	6	1.82	90	0.91	720	0.18
	10	1.79	150	0.59	840	0.15
	15	1.46	210	0.52	960	0.08
	20	1.28	330	0.41		
140	0	2.00	30	0.95	450	0.21
	3	1.86	60	0.87	570	0.15
	6	1.60	90	0.86	720	0.13
	10	1.54	150	0.53	840	0.11
	15	1.31	210	0.48	960	0.04
	20	1.12	330	0.40		
160	0	2.00	15	1.17	90	0.51
	3	1.67	20	1.01	210	0.30
	6	1.36	30	0.90	330	0.18
	10	1.35	60	0.67	450	0.07
180	0	2.00	15	0.61	90	0.26
	3	1.56	20	0.56	120	0.18
	6	0.71	30	0.41	210	0.11
	10	0.67	60	0.27		

S.D. $\leq 0.04 \times 10^{-3}$ mol l^{-1}.

pre-set temperatures, that is, at 98, 120, 140, 160, and 180 °C, the "total polyphenols" concentrations in the EVOO and in the SM were determined as a function of the heating time. The relevant experimental values found have been summarized in Tables 3 and 4. The comparison of degradation trends at the same temperatures is shown graphically in Fig. 3; the concentration of the "total polyphenols" as a function of heating time does not appear significantly different for the EVOO and the SM samples. It may thus be stated that the SM, although made up of a polyphenol mixture that is simpler than that contained in the EVOO, proves to be sufficiently representative of the EVOO samples. On the other hand, further confirmation was obtained by observing the time trends of total polyphenols disappearance in the EVOO and in the SM at the five different temperatures examined, shown in Fig. 4, which were very similar. This also confirms that it is correct to affirm that the trend observed for the degradation process of EVOO may essentially be ascribed to the degradation of the total polyphenols contained therein.

Moreover, comparison of the histograms illustrated in Fig. 4 allows some more interesting results to be harvested, as may be inferred from the trends shown in Fig. 3, such as the time required to achieve complete disappearance of the polyphenols, (A) in the EVOO and (B) in the SM, at the different temperatures considered. For example, at 100 °C, about 60–65 h are necessary, while at 180 °C only about 6–7 h are required. This

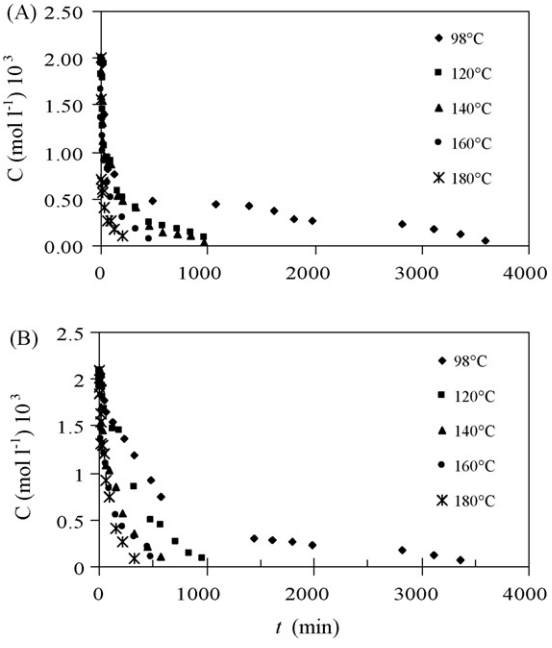

Fig. 3. Total polyphenol concentration trend in (A) extra-virgin olive oil and (B) synthetic polyphenols mixture concentration trend in glyceryl trioleate as a function of time for isothermal measurements at different temperatures.

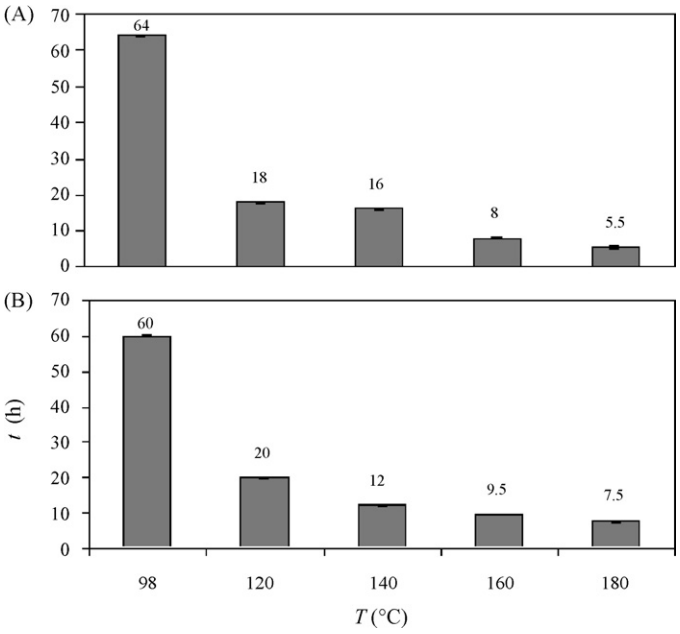

Fig. 4. Time taken to achieve complete disappearance of total polyphenols in extra-virgin olive oil and in the synthetic mixture in glyceryl trioleate due to the isothermal heating at different temperatures. (A) Extra-virgin olive oil and (B) synthetic mixture in glyceryl trioleate.

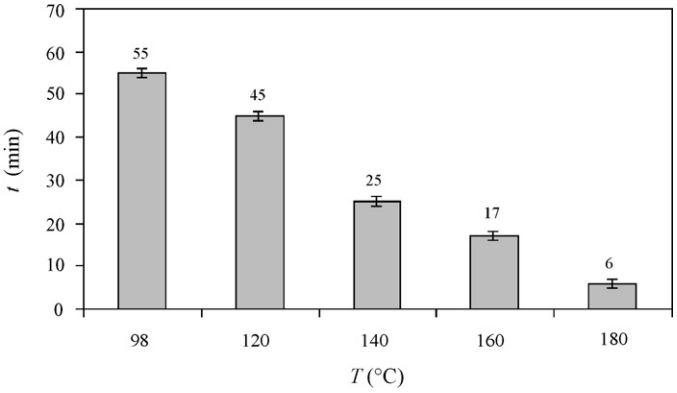

Fig. 5. Half-life values for total polyphenols concentration in extra-virgin olive oil samples at the different isothermal temperatures considered.

is because the polyphenols disappear completely both from the EVOO and from the SM subjected to the artificial rancidification process under the same conditions as prescribed by the AOM method [11], although of course individually at each of the five different temperatures considered. Also of great interest are the values of the polyphenol concentration half-life of the EVOO at the different isothermal heating temperatures considered, shown as a histogram in Fig. 5. The half-life is seen to decrease almost constantly between 100 and 180 °C, plunging from about 1 h to about 5 min on going from the

Table 4
Concentration values in the "total polyphenols" of the synthetic mixture (SM) sample for selected time values during the degradation as obtained by isothermal measurements at different temperatures using the tyrosinase biosensor

T (°C)	t (min)	C ($\times 10^3$ mol l^{-1})	t (min)	C ($\times 10^3$ mol l^{-1})	t (min)	C ($\times 10^3$ mol l^{-1})
98	0	2.09	120	1.55	1620	0.29
	10	2.05	240	1.36	1800	0.26
	20	2.02	330	1.18	1980	0.23
	30	1.94	480	0.92	2820	0.18
	45	1.78	570	0.74	3120	0.13
	60	1.65	1440	0.31	3360	0.07
120	0	2.09	45	1.69	570	0.45
	3	2.03	120	1.48	720	0.26
	6	1.98	180	1.45	840	0.15
	10	1.95	330	0.85	960	0.08
	30	1.80	480	0.50		
140	0	2.09	20	1.54	210	0.56
	3	2.02	30	1.46	330	0.36
	6	1.96	60	1.09	450	0.22
	10	1.94	90	1.02	570	0.10
	15	1.71	150	0.85		
160	0	2.09	20	1.37	150	0.55
	3	1.97	30	1.31	210	0.43
	6	1.92	45	1.20	330	0.32
	10	1.83	60	1.10	450	0.22
	15	1.48	90	0.83	480	0.10
180	0	2.09	20	1.32	90	0.75
	3	1.92	30	1.30	150	0.40
	6	1.84	45	1.20	210	0.26
	10	1.63	60	0.92	330	0.09
	15	1.55				

S.D. $\leq 0.04 \times 10^{-3}$ mol l^{-1}.

first to the second temperature. Finally, it should be noted how the temperature to which the oil is heated is the decisive factor, as it determines polyphenol persistence time and therefore the time of rancidification of the extra-virgin olive oil.

In order to determine the energy of activation of the EVOO and SM degradation processes, first of all the MacCallum method [18] was applied. To this end, a set of values of the natural logarithm of t (i.e. $\ln t$) were determined that corresponded to pre-established values of the conversion degree α, over the interval $\alpha \leq 0.20$, for each of the temperatures considered (see Fig. 6 and Table 5). After inserting these values in Eq. (3), and performing the linear regressions of each ($\ln t_{iso}$ *vs.* $1/T_{iso}$) set of data using the least squares method at the five different isothermal temperatures considered, the values of the activation energy (E_a) corresponding to the different α values selected were drawn from the value of the slope of the straight line obtained (Fig. 7) and have been set out in Table 6. The associated errors were obtained starting with the error on the slope (b) of the regression reported in Table 6. Observing the behaviour of the values of the activation energy of the EVOO and of the SM at the different a values considered, which are shown graphically in Fig. 8, it can be concluded that the E_a values, at least over the range of α values examined, can be considered constant within the limits of experimental error. For this reason the mean activation energy values (38.0 ± 0.8 and 33.8 ± 0.1 kJ mol^{-1}, respectively, for the thermal degradation of the EVOO and of the SM), which are also reported, together with their standard deviations, in Table 6, can be considered constant for all the first part (i.e. about a quarter of the entire process) and as likely to be representative of the entire degradation process.

4.2. Kinetic analysis of polyphenol degradation using the model-fitting method

As neither the values of the kinetic constants nor the mathematical model representing the mechanism of the degradation process were obtained via the previous method, and in order to stress the value of the results of the activation energy achieved, it was decided to apply another kinetic method, namely the "model-fitting" method [19], by processing the data reported in Tables 3 and 4. First of all, to this end, the values of the degree of conversion for the entire isotherm degradation process of the EVOO and of the SM at the five temperatures selected (see Tables 7 and 8) were computed; these values have

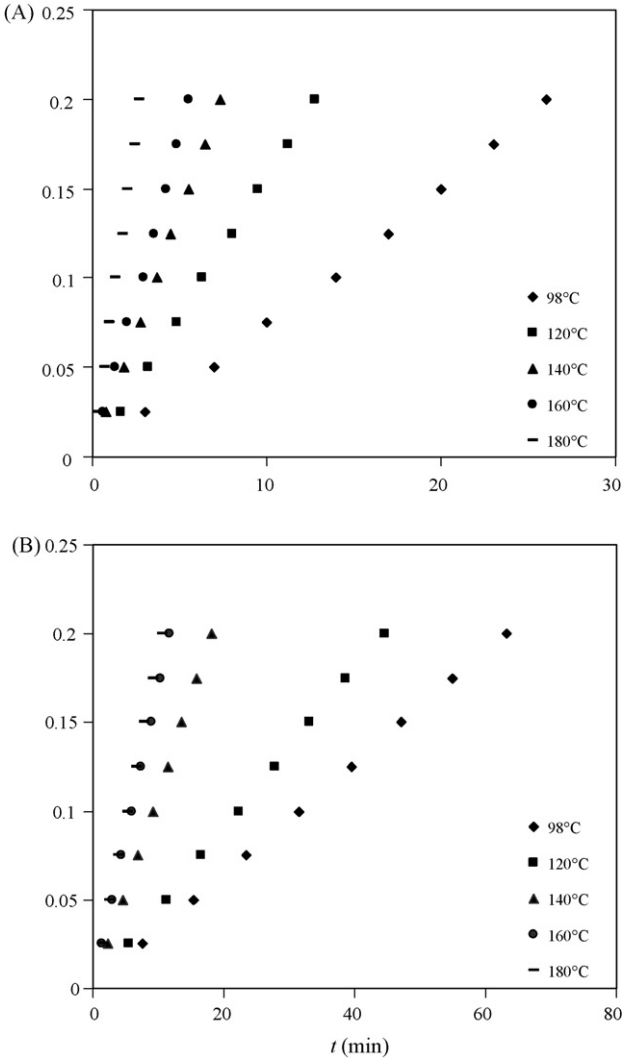

Fig. 6. Regression degree of conversion (α) values obtained from the linear fit of experimental data regarding total polyphenols degradation in (A) extra-virgin olive oil and (B) the synthetic mixture at different isothermal temperatures during heating over the range $0.025 \leq \alpha \leq 0.200$.

Table 5
$\ln t$ (min) values for selected values of the degree of conversion $\alpha = ((C_i - C_t)/(C_i - C_f))$, obtained by isothermal measurements corresponding to defined temperatures

α	EVOO					SM				
	98 °C	120 °C	140 °C	160 °C	180 °C	98 °C	120 °C	140 °C	160 °C	180 °C
0.025	1.099	0.470	−0.223	−0.511	−1.204	2.015	1.705	0.789	0.337	0.262
0.050	1.946	1.163	0.588	0.262	−0.431	2.741	2.425	1.504	1.065	0.956
0.075	2.303	1.569	1.030	0.693	−0.051	3.157	2.803	1.932	1.482	1.361
0.100	2.639	1.841	1.308	1.065	0.262	3.447	3.100	2.230	1.775	1.668
0.125	2.833	2.079	1.504	1.253	0.531	3.676	3.325	2.434	2.002	1.887
0.150	2.996	2.251	1.705	1.447	0.693	3.852	3.503	2.610	2.186	2.067
0.175	3.136	2.416	1.872	1.569	0.876	4.007	3.656	2.766	2.332	2.219
0.200	3.258	2.549	1.988	1.705	0.993	4.146	3.798	2.901	2.468	2.361

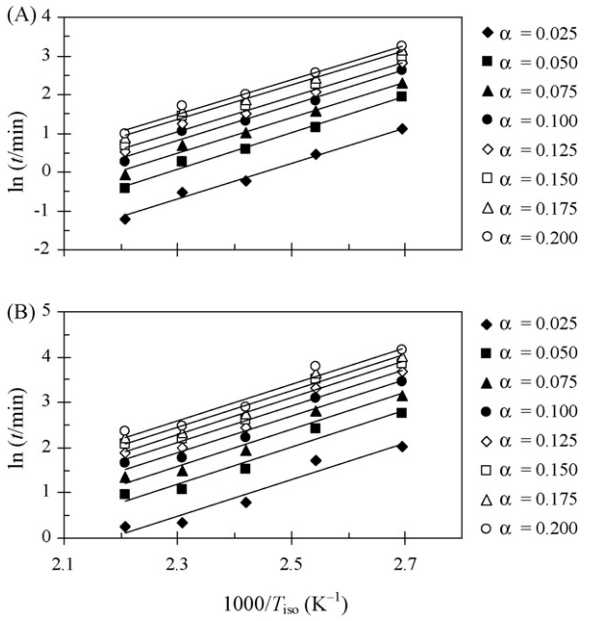

Fig. 7. Linear trend of the $\ln(t_{iso})_\alpha$ values as a function of T_{iso}^{-1} at the given values of the degree of conversion (α) for the thermal degradation of (A) extra-virgin olive oil and (B) synthetic mixture of polyphenols in glyceryl trioleate.

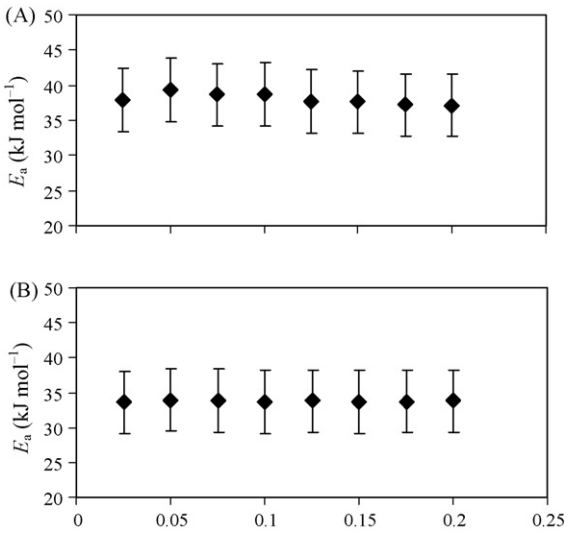

Fig. 8. Activation energy trends found for the thermal degradation of (A) the extra-virgin olive oil and (B) the synthetic mixture of polyphenols in glyceryl trioleate as a function of the degree of conversion α.

been shown graphically in Fig. 9. Lastly, the trends obtained for the corresponding regression values of conversion degree α are shown in Fig. 10. Hence, by reporting the values of $g(\alpha)$, calculated starting from the regression values of α represented in Fig. 10 as a function of the time values t_α. For each of the equations corresponding to the various kinetic models considered (reported in Table 2) and for each of the five different temperatures of degradation examined, trends were obtained (see, for example, those reported in Fig. 11) that were found to have different degree of linearity, depending on the greater or lesser correspondence between the trends of the experimental data and the kinetic model used to represent them. The slopes of the values for the straight line representing the best fit of these behaviours provide the values of the kinetic constants (k) at the five different temperatures at which the isotherms of Fig. 10 were obtained. The selection of the model that best represents the kinetic behaviour of the thermal degradation of the polyphenols among all the kinetic models considered, both for the EVOO and for the SM in glyceryl trioleate, was carried out by determining the values of the correlation coefficients r^2 calculated for all the (more or less straight-line) curves obtained by inserting the expressions given in Table 2 in Eq. (4). In Table 9 the values of r^2 for all the kinetic models and for all the temperatures considered have been reported and compared. This table indicates that for the degradation of polyphenols in extra-virgin olive oil the most representative kinetic model was the one marked in Table 9 with the abbreviation F2, while, for the degradation of the "total polyphenols" in glyceryl trioleate, two models proved to be

Table 6
Slope and intercept values of the linear regressions applied to the MacCallum equation for the isothermal degradation of the "total polyphenols" in both the extra-virgin olive oil (EVOO) and synthetic mixture (SM) samples

α	EVOO				SM			
	a[a]	b[b] ($\times 10^3$ K)	r^2	E_a (kJ mol^{-1})	a[a]	b[b] ($\times 10^3$ K)	r^2	E_a (kJ mol^{-1})
0.025	−11.2 ± 0.9	4.6 ± 0.4	0.9886	37.9 ± 3.0	−9.5 ± 1.4	4.0 ± 0.6	0.9499	33.6 ± 4.8
0.050	−10.8 ± 0.8	4.7 ± 0.3	0.9899	39.3 ± 2.7	−8.1 ± 1.4	4.1 ± 0.6	0.9515	33.9 ± 4.7
0.075	−10.2 ± 0.9	4.6 ± 0.4	0.9868	38.6 ± 3.2	−7.6 ± 1.2	4.1 ± 0.5	0.9515	33.8 ± 4.3
0.100	−9.9 ± 1.2	4.6 ± 0.5	0.9771	38.6 ± 4.0	−7.2 ± 1.3	4.0 ± 0.5	0.9514	33.6 ± 4.3
0.125	−9.4 ± 1.0	4.5 ± 0.4	0.9841	37.7 ± 3.4	−7.7 ± 1.3	4.1 ± 0.5	0.9527	33.8 ± 4.4
0.150	−9.2 ± 1.0	4.5 ± 0.4	0.9819	37.6 ± 3.6	−7.5 ± 1.3	4.0 ± 0.5	0.9547	33.7 ± 4.4
0.175	−8.9 ± 0.8	4.5 ± 0.3	0.9881	37.2 ± 2.9	−7.4 ± 1.3	4.1 ± 0.5	0.9461	33.8 ± 4.4
0.200	−8.8 ± 0.9	4.5 ± 0.4	0.9864	37.1 ± 3.2	−7.3 ± 1.3	4.1 ± 0.5	0.9412	33.8 ± 4.5
				38.8 ± 0.8[c]				33.8 ± 0.1[c]

E_a = activation energy.
[a] $a = \ln[f(1-\alpha)] - \ln A$, where $f(1-\alpha)$ is a function representing the degree of degradation trend.
[b] $b = E_a/R$.
[c] Average.

Table 7
Degree of conversion (α) values for the thermal degradation of the "total polyphenols" of the extra-virgin olive oil (EVOO) sample obtained by isothermal measurements at different temperatures

T (°C)	t (min)	α	t (min)	α	t (min)	α
98	0	0.00	480	0.76	2820	0.88
	10	0.02	1380	0.77	3120	0.91
	20	0.03	1620	0.81	3360	0.94
	30	0.30	1800	0.86	3600	0.97
	60	0.60	1980	0.87	3840	1.00
	120	0.62				
120	0	0.00	30	0.55	450	0.88
	3	0.07	60	0.56	570	0.90
	6	0.09	90	0.86	720	0.91
	10	0.11	150	0.74	840	0.93
	15	0.27	210	0.76	960	0.96
	20	0.49	330	0.80		
140	0	0.00	30	0.53	330	0.90
	3	0.17	60	0.55	450	0.93
	6	0.20	90	0.71	570	0.94
	10	0.23	150	0.74	720	0.98
	15	0.41	210	0.79	840	1.00
	20	0.47				
160	0	0.00	15	0.34	90	0.74
	3	0.02	20	0.36	210	0.85
	6	0.32	30	0.53	330	0.91
	10	0.32	60	0.67	450	0.97
180	0	0.00	15	0.70	90	0.89
	3	0.22	20	0.72	120	0.91
	6	0.65	30	0.80	210	0.95
	10	0.67	60	0.87		

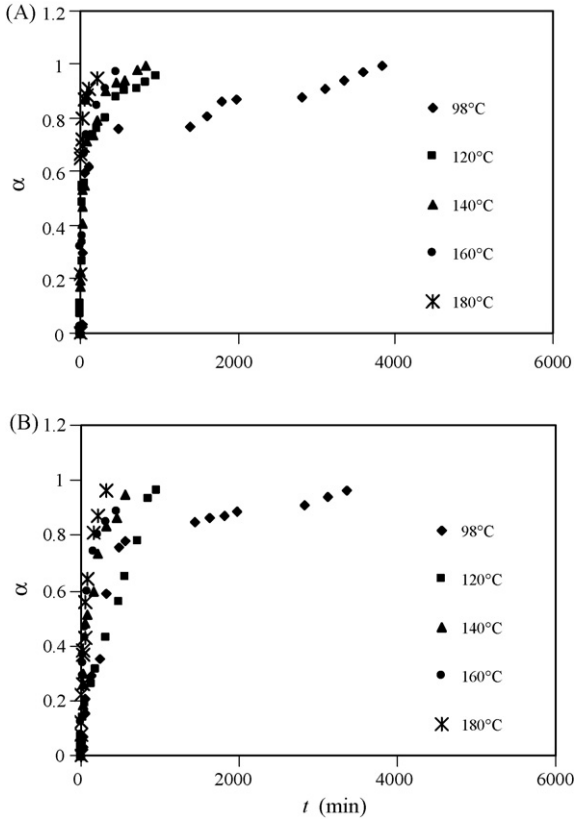

Fig. 9. Trend of the degree of conversion (α) values for the thermal degradation of total polyphenols pool under isothermal conditions at different temperatures in (A) extra-virgin olive oil and (B) synthetic mixture of polyphenols in glyceryl trioleate. R.S.D. $\leq 2\%$.

equally significant, that is, the ones indicated with the abbreviations D2 and F1 (see the corresponding equations reported in Fig. 11).

As stated previously, the slopes of the $g(\alpha)$ *versus* t lines represent the specific constant rates k_{iso} related to the five given T_{iso} values. The resulting k_{iso} values for the thermal degradation of polyphenols contained in the EVOO at 98, 120, 140, 160, and 180 °C related to the "model function" F2, which shows the best linear fit (Table 9), are displayed as a histogram in Fig. 12. It should be noted that at 180 °C k_{iso} is about 20 times greater than at 98 °C. However, once the specific constant rates have been determined for the most suitable model functions (F2 for thermal degradation of EVOO and D2 and F1 for that of SM in glyceryl trioleate, as emerged from the comparison of values in Table 9), single activation energy (E_a) values for the polyphenol degradation process over the temperature range of 98–180 °C were easily obtained from the slope of the logarithmic form of the Arrhenius equation (Eq. (5)).

The $\ln k_{iso}$ values used in Eq. (5) for the thermal degradation of both EVOO and SM in glyceryl trioleate at the five T_{iso} temperatures considered are summarized in Table 10 for the most probable "model functions". The E values thus obtained referred to the thermal degradation of polyphenols in EVOO, as described by the F2 model function, and SM to polyphenol degradation in glyceryl trioleate, as described by the D2 and F1 model functions presented, are 36 ± 4 and

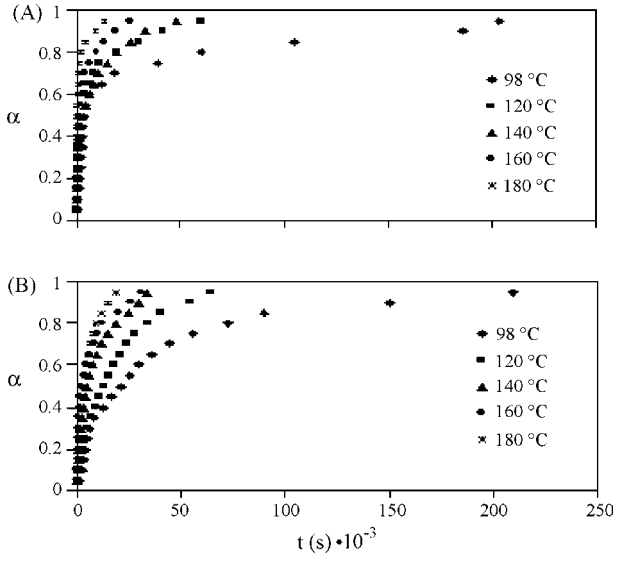

Fig. 10. Trend of the regression α values for the thermal degradation of total polyphenols under isothermal conditions at different temperatures in (A) extra-virgin olive oil and (B) synthetic mixture of polyphenols in glyceryl trioleate. The isothermal experiments were carried out at selected temperatures.

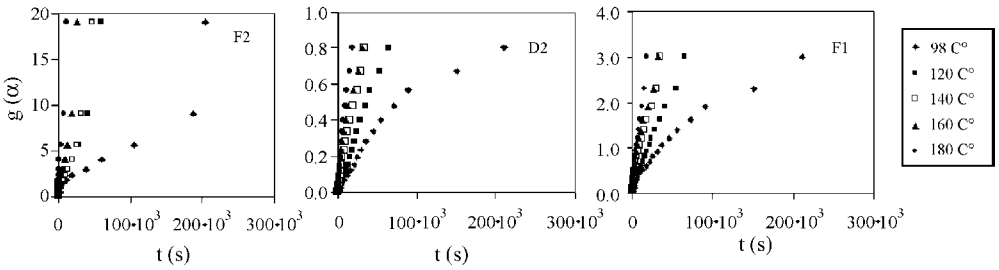

Fig. 11. Trend of the values of the integral function $g(\alpha)$ as a function of time t for the most suitable selected model functions (F2, D2 and F1) at the different selected temperatures for the thermal degradation of total polyphenols contained in extra-virgin olive oil and in the synthetic mixture in glyceryl trioleate.

Table 8
Degree of conversion (α) values for the thermal degradation of the "total polyphenols" of the synthetic mixture (SM) sample obtained by isothermal measurements at different temperatures

T (°C)	t (min)	α	t (min)	α	t (min)	α
98	0	0.00	120	0.29	1620	0.86
	10	0.02	240	0.35	1800	0.87
	20	0.03	330	0.59	1980	0.89
	30	0.07	480	0.76	2820	0.91
	45	0.15	570	0.78	3120	0.94
	60	0.21	1440	0.85	3360	0.96
120	0	0.00	45	0.19	570	0.65
	3	0.03	120	0.26	720	0.78
	6	0.06	180	0.31	840	0.93
	10	0.07	330	0.43	960	0.96
	30	0.14	480	0.56		
140	0	0.00	20	0.26	210	0.73
	3	0.03	30	0.30	330	0.83
	6	0.06	60	0.48	450	0.86
	10	0.07	90	0.51	570	0.95
	15	0.18	150	0.60		
160	0	0.00	20	0.34	150	0.74
	3	0.06	30	0.37	210	0.80
	6	0.08	45	0.43	330	0.85
	10	0.12	60	0.47	450	0.89
	15	0.29	90	0.60		
180	0	0.00	20	0.37	90	0.64
	3	0.08	30	0.38	150	0.81
	6	0.12	45	0.43	210	0.87
	10	0.22	60	0.56	330	0.96
	15	0.26				

38 ± 6 or $38 \pm 5\,\mathrm{kJ\,mol^{-1}}$, respectively. A comparison of the activation energy values found for the thermal degradation processes in both EVOO and SM, obtained using the MacCallum and model-fitting kinetic methods, is presented in Table 11. It may be observed that the agreement among the E_a values found for EVOO ($36 \pm 4\,\mathrm{kJ\,mol^{-1}}$) is reasonably good if compared with that obtained for the synthetic mixture of polyphenols (SM) ($38.8 \pm 0.8\,\mathrm{kJ\,mol^{-1}}$). This result confirms that the MacCallum method applied in this study is able to provide realistic kinetic data not only for relatively simple synthetic mixtures but also for real complex samples like extra-virgin olive oil. On the other hand, in the case of the SM the most realistic E_a value (closer to that of EVOO) seems to be that obtained with the model-fitting method, even if the precision is higher for the values calculated by the MacCallum method.

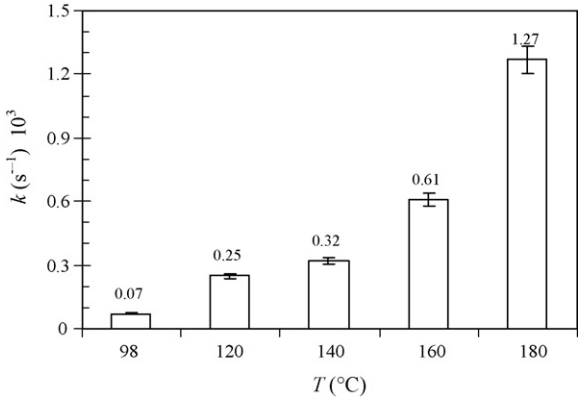

Fig. 12. Trend of the kinetic constant k_{iso} values as a function of temperature for the thermal degradation of total polyphenols in extra-virgin olive oil according to the F2 model function.

Table 9
r^2 values for the $g(\alpha)$ *vs.* t linear equations at the different temperatures considered for both the extra-virgin olive oil (EVOO) and the synthetic mixture (SM) samples

$g(\alpha)$	r^2 values for EVOO					r^2 values for SM				
	98 °C	120 °C	140 °C	160 °C	180 °C	98 °C	120 °C	140 °C	160 °C	180 °C
P1	0.3589	0.3991	0.4939	0.4476	0.2969	0.4826	0.6615	0.6106	0.5077	0.6080
A1.5	0.7445	0.795	0.8763	0.8342	0.6755	0.8573	0.9656	0.9373	0.8793	0.9428
A2	0.6788	0.7289	0.8182	0.7726	0.6067	0.7996	0.9305	0.8965	0.8244	0.8996
A3	0.6045	0.6534	0.7476	0.7003	0.5324	0.7306	0.8799	0.8399	0.7564	0.8415
A4	0.5649	0.6128	0.7081	0.6607	0.4941	0.6925	0.8487	0.8060	0.7180	0.8070
B1	0.5988	0.6476	0.7361	0.6933	0.5349	0.7249	0.8660	0.8220	0.7440	0.8268
R2	0.6970	0.7455	0.8388	0.7890	0.6133	0.8113	0.9453	0.9208	0.8464	0.9190
R3	0.7501	0.7988	0.883	0.8382	0.6725	0.8579	0.9701	0.9481	0.8876	0.9498
D1	0.7288	0.7746	0.8688	0.8152	0.6315	0.8289	0.9581	0.9491	0.8772	0.9411
D2	0.8280	0.8711	0.9421	0.9022	0.7441	**0.9091**	**0.9906**	**0.9871**	**0.9459**	**0.9858**
D3	0.5855	0.6333	0.7398	0.6825	0.4964	0.7093	0.8780	0.8481	0.7514	0.8412
D4	0.7288	0.7746	0.8688	0.8152	0.6315	0.8289	0.9582	0.9491	0.8772	0.9411
F1	0.8454	0.8948	0.9541	0.9229	0.7912	**0.9388**	**0.9956**	**0.9762**	**0.9501**	**0.9880**
F2	**0.8797**	**0.9400**	**0.9142**	**0.9272**	**0.9587**	0.9477	0.8276	0.7953	0.8699	0.8467
F3	0.6833	0.7604	0.7073	0.7300	0.8478	0.7637	0.5844	0.5379	0.6370	0.6057

The most significant models and the related r^2 values are given in bold.

Table 10
ln k values for the thermal degradation of both extra-virgin olive oil (EVOO) and synthetic mixture (SM) in glyceryl trioleate obtained using the most probable model functions selected from the best linear fits of $g(\alpha)$ *vs.* t in Table 9

T_{iso} (°C)	ln k (min^{-1})		
	EVOO	SM	
	F2	D2	F1
98	−8.93	−12.39	−11.17
120	−8.23	−11.24	−10.04
140	−8.03	−10.67	−9.48
160	−7.40	−10.58	−9.37
180	−6.67	−10.01	−8.81

Table 11
Comparison of the activation energy (E_a) values for the thermal degradation of the total polyphenols contained in both the extra-virgin olive oil (EVOO) and the synthetic mixture (SM) obtained using the two kinetic methods proposed

	E_a (kJ mol^{-1})	
	MacCallum method	Model-fitting method
EVOO	38.8 ± 0.8	36 ± 4[a]
SM	33.8 ± 0.1	38 ± 6[b]
		38 ± 5[c]

The associated uncertainties are standard deviations.
[a] Values obtained taking into account the reaction model F2.
[b] Values obtained taking into account the reaction model D2.
[c] Values obtained taking into account the reaction model F1.

5. Conclusions

As described in the previous section, for the purpose of monitoring the rancidification process of the extra-virgin olive oil carried out isothermally at different temperatures (98, 120, 140, 160, and 180 °C), the "total polyphenols" concentration was determined at regular time intervals. Polyphenol determination using the tyrosinase OPEE proved to be particularly suitable for the purpose of the present research as it allowed the analysis to be carried out more rapidly (only a few minutes) than when using other chemical methods, such as Folin Ciocalteu's [21].

The good solubility of the oily sample in *n*-hexane, i.e. the solvent used to carry out the measurement, allowed the problems of inaccuracy often encountered when using other methods [21] to analyse oily matrixes due to the low solubility of the oil in aqueous medium to be overcome successfully. Moreover, the solvent selected for carrying out the biosensor measurement, i.e. *n*-hexane, was found to be particularly suitable, also from a theoretical point of view, for carrying out measurements using an enzymatic biosensor; indeed, if the value of an index for hydrophobicity measurement, i.e. $\log p = 3.5$ (p is the distribution coefficient of the solvent used in a standard two-phase octanol/water system) and the value of the dielectric constant of this solvent (1.89) are considered, it is immediately evident that the first value is sufficiently high and the second sufficiently low to ensure a high enzymatic activity and therefore a good response by the (tyrosinase) biosensor [22,23].

Finally, the study of the thermal degradation in an oxidising atmosphere of the polyphenols contained in the extra-virgin olive oil was carried out isothermally at five different temperatures. This allowed both the kinetic model to be identified and the activation energy (E_a) to be calculated, which was found to be in the order of 38 kJ mol^{-1}. Furthermore, this value remains constant (and so also the degradation mechanism does not change) at least throughout whole of the first part, i.e. for practically a quarter, of the entire process. The value of E_a found was obtained for the thermal degradation of a typical commercial extra-virgin olive oil of good quality. Therefore, it can be considered valid in all likelihood way for the most commonly used commercial extra-virgin olive oils, most of which have common standard characteristics and are consequently very similar to each other. Naturally, in the case of extra-virgin olive oils obtained from very particular cultivars it cannot be stated that the value of E_a thus derived can be considered strictly representative also of the thermal degradation of this particular oil sample. From an applicative point of view, some significant aspects of the rancid-

ification process have been displayed: for instance it was found that, at 98 °C, the polyphenols disappear completely in about 60 h, while, at 180 °C, they disappear in about 6 h only; moreover, at 98 °C their concentration is halved after about 50 min, while at 180 °C it is halved in only 6 min. Finally, the kinetic study showed that the value of the kinetic constant of the process at 180 °C is about 20 times higher than at 98 °C.

It may thus be concluded that the temperature at which this important foodstuff is used is a crucial factor in establishing the maximum time for which it can be used safely for the cooking of food.

Acknowledgement

This work was financially supported by MIUR, Co-funded project Prin 2005.

References

[1] A. Kiritsakis, P. Markakis, Adv. Food Res. 31 (1987) 453–482.
[2] CE 2006 Regolamento (CE) N. 510/2006 del Consiglio del 20 Marzo 2006, Gazzetta ufficiale dell'Unione Europea in date March 31, 2006, L 93/12.
[3] L.A. Ferrara, Nutr. Metab. Cardiovasc. Dis. 10 (3) (2000) 109–110.
[4] H.J. Nieschlag, J.W. Hagemann, J.A. Rothfus, Anal. Chem. 46 (14) (1974) 2215–2217.
[5] B. Kowalski, Thermochim. Acta 184 (1991) 49–57.
[6] L. Gennaro, A. Piccioli Bocca, D. Modesti, R. Masella, E. Coni, J. Agric. Food Chem. 46 (11) (1998) 4465–4472.
[7] G.M. Montiel, J.R. Avanza, Inform. Tecnol. 12 (6) (2001) 43–46.
[8] L. Campanella, G. Favero, M. Pastorino, M. Tomassetti, Biosens. Bioelectron. 14 (1999) 179–186.
[9] L.Cerrettani, A. Bendini, D. Mencarelli, G. Caramia, Il Chimico Italiano, N 3\4, lugl./ag./set., 2006, pp. 1–3.
[10] A. Bianco, F. Buiarelli, G. Cartoni, F. Coccioli, R. Jasonowska, P. Margherita, J. Sep. Sci. 26 (2003) 417–424.
[11] AOCS, Method Cd 12-57, in: Official and Tentative Method of the American Oil Chemist's Society, vol. 1, 3rd ed., 1964, pp. 1–4.
[12] E. Pagliarini, B. Zanoni, G. Giovannelli, J. Agric. Food Chem. 48 (2000) 1345–1351.
[13] J. Dweck, C.M.S. Sampaio, J. Therm. Anal. Cal. 75 (2004) 385–391.
[14] L. Campanella, G. Favero, A. Fortuney, M.P. Sammartino, M. Tomassetti, Life Chem. Rep. 11 (1994) 363–371.
[15] L. Campanella, G. Favero, M.P. Sammartino, M. Tomassetti, Polyphenols Actualites 14 (1996) 9–12.
[16] L. Campanella, G. Favero, M.P. Sammartino, M. Tomassetti, J. Mol. Catal. B: Enzym. 7 (1997) 101–113.
[17] L. Campanella, G. Favero, M.P. Sammartino, M. Tomassetti, Anal. Chim. Acta 426 (2001) 235–247.
[18] L. Abate, I. Bianco, O. Motta, A. Pollicino, A. Recca, Polym. Degrad. Stabil. 75 (2002) 465–471.
[19] F. Rodante, S. Vecchio, M. Tomassetti, J. Pharm. Biomed. Anal. 29 (2002) 1031–1043.
[20] S. Vecchio, F. Rodante, M. Tomassetti, J. Pharm. Biomed. Anal. 24 (2001) 1111–1123.
[21] A. Vazquez Roncero, C. Janer Della Valle, M.L. Janer Della Valle, Grassa Aceites 24 (1973) 350–357.
[22] L. Campanella, G. Favero, M.P. Sammartino, M. Tomassetti, Talanta 41 (1994) 1015–1023.
[23] L. Campanella, G. Favero, M.P. Sammartino, M. Tomassetti, Talanta 46 (1998) 595–606.

Available online at www.sciencedirect.com
ScienceDirect
Talanta 74 (2008) 1520–1526
Talanta
www.elsevier.com/locate/talanta

Characterization of mercury species in soils by HPLC–ICP-MS and measurement of fraction removed by diffusive gradient in thin films

I. Cattani [a,b,*], S. Spalla [a,c], G.M. Beone [a,c], A.A.M. Del Re [a,b], R. Boccelli [a,b], M. Trevisan [a,b]

[a] *Institute of Agricultural and Enviromental Chemistry, Catholic University of Sacre Heart, Via Emilia Parmense 29100, Piacenza, Italy*
[b] *Division of Vegetable Chemistry, Catholic University of Sacre Heart, Via Emilia Parmense 29100, Piacenza, Italy*
[c] *Division of Soil Chemistry, Catholic University of Sacre Heart, Via Emilia Parmense 29100, Piacenza, Italy*

Received 7 June 2007; received in revised form 25 September 2007; accepted 28 September 2007
Available online 2 October 2007

Abstract

The properties and behaviour of Hg depend on both the oxidation state and the chemical form: the bioavailability, toxicity, persistence and accumulation of mercury in the food web are strongly influenced by chemical speciation. The present work aims to determine the chemical forms of mercury present in soil and to evaluate the fraction of mercury in soil solution available to plants. In order to do this, we analyzed eight samples of contaminated soils with Hg concentrations ranging from 1.31 to 21.7 mg kg^{-1}, collected from different depths (0–10 and 40–50 cm) close to an abandoned industrial site in Val Basento (southern Italy). Two innovative analytical techniques were used: HPLC–ICP-MS and diffusive gradient in thin films (DGT). The analytical procedure was validated using ERM 580-certified sediment and spiked samples in the case of HPLC–ICP-MS, and by a performance test in the case of DGT. In all samples, the only species found in soil and soil solution was $MeHg^+$ and Hg^{2+}. In soil, the $MeHg^+/Hg_{tot}$ ratio ranged from 0.05% to 0.82%; total mercury in soil solution was less than 0.01% of total mercury in soil. The percentage of $MeHg^+$ in soil solution varied considerably (from 0% to 50%), with a maximum concentration of 0.02 mg L^{-1}. The root available concentration evaluated by DGT is comparable to the total mercury content of the soil solution measured by HPLC–ICP-MS. The DGT results suggest that all mercury in solution is available for uptake in DGT, and that mercury is supplied from soil to solution. However, for all samples the soluble and root available (DGT-labile) fractions of mercury are generally very low with respect to the total mercury concentration. This study confirmed that both HPLC–ICP-MS and DGT techniques are suitable tools for the estimation of Hg root availability and in assessing the risk from contaminated soils.
© 2007 Elsevier B.V. All rights reserved.

Keywords: Mercury; Methylmercury; Speciation; HPLC–ICP-MS; DGT; Root availability

1. Introduction

Mercury (Hg) is naturally ubiquitous in the earth's crust, present in rocks, soils and sediments. An unpolluted soil may contain up to 200 μg kg^{-1} Hg [1]. Higher concentrations in soil may result from the proximity of abandoned mines, geogenic processes, industrial discharges, organic (aryl) mercury compounds used in agriculture and the atmospheric deposition [2]. The element Hg is stable, but its various forms undergo many chemical, biological and photochemical reactions [3]: inorganic forms may be biologically transformed to organic (e.g. methyl- and ethyl-mercury) forms. Both organic and inorganic mercury may be converted to the very volatile elemental Hg, to the insoluble sulphide, or strongly complexed with inorganic and organic ligands. There are three oxidation states of mercury: elemental (Hg^0), mercurous (Hg^{1+}) and mercuric (Hg^{2+}). The mercurous form is not stable and is readily oxidized or reduced. The properties and behaviour of Hg depend on both the oxidation state and the chemical form. Hg^{2+} tends to be methylated by anaerobic (mostly by sulfate reducing [4,5], by iron-reducing [6] and within certain limits by methane producing bacteria) and sometimes by aerobic bacteria, normally in aquatic environments. Methyl Hg compounds may be demethylated by bacterial action [7]. Weber [8], Rogers [9] and Van Faassen [10] also found slight methylation in soil due to abiotic factors.

* Corresponding author at: Institute of Agricultural and Environmental Chemistry, Division of Vegetable Chemistry, Catholic University of Sacre Heart, Via Milano 24, 26100, Cremona, Italy. Tel.: +39 0372 499124; fax: +39 0372 499122.
E-mail address: ilenia.cattani@unicatt.it (I. Cattani).

0039-9140/$ – see front matter © 2007 Elsevier B.V. All rights reserved.
doi:10.1016/j.talanta.2007.09.029

Mobilization of Hg in soil may occur as a result of volatilization, leaching or plant uptake. Volatilization from soil and plants often represents a considerable route of loss, whereas soluble forms are stabilized by humic acid containing sulphur. The chemical speciation of mercury in soil, water and soil solution strongly influences its bioavailability and toxicity to living organisms, as well as its persistence and accumulation in the food web. Methylmercury (CH_3Hg^+) is the most common organomercurial in the environment (compared to the rarer ethyl-mercury and phenyl-mercury). CH_3Hg^+ is 10–100 times more toxic than inorganic Hg [11–13]. Ratio between CH_3Hg^+ and Hg^{2+} in runoff waters transported to lakes has been proposed as a predictor of accumulation in fish [14], whereas ratio CH_3Hg^+ and Hg^{2+} in soil has been proposed as indicator of sites suitable for scarce drainage. In the slowly draining soils, soil pores are filled with water rather than air and the availability of oxygen is limited: this may consequently effect methylation reactions [15].

The development of techniques for the speciation of Hg has primarily been focused on seafood analysis following the poisoning accident at Minamata (Japan). At the beginning of the 1990s [16], increasing interest in other environmental matrices prompted the development of other techniques, such as GC-AAS following ethylation [17], GC-atomic emission detector (AED) [18,19] and distillation followed by GC-atomic fluorescence spectrometry (AFS) [20,21]. More sophisticated techniques have been developed, but these have yet to be included into routine analysis, e.g. HPLC–ICP-MS and isotope dilution-ICP-MS. Few studies have been conducted concerning Hg contamination in agrarian soil: most studies consider soils from abandoned Hg mines [13,22,23] or peat soils [15,24]. In this work separation of inorganic Hg from organic Hg compounds was performed by HPLC. The main detection systems are fluorescence, plasma techniques and atomic absorption techniques. In our case was used ICP-MS for its very low detection limit. The main advantage of coupling HPLC and ICP-MS is that sample manipulation was reduced to the minimum [25].

The diffusive gradient in thin films (DGT) technique [26,27], developed for in situ determination of kinetically labile metal species in aquatic systems, has been recently proposed as a means by which to measure concentrations of trace metals in natural waters and to estimate their concentrations in soil pore water [28,29]. The technique consists of a diffusive layer (hydrogel) placed on top of a selective binding phase (resin–gel). Both are sealed in a plastic unit. The DGT is then exposed to the solution to be analyzed. Dissolved heavy metal species diffuse through the hydrogel and accumulate in the resin–gel. Chelex-100, with iminodiacetic groups, and Spheron-Thiol, with sulphydrilic groups, have recently been recommended as possible tools to capture the various mercury species and to distinguish between mercury complexes with different stabilities [30]. When exposed to a soil solution, a DGT device provides an indirect measure of the maximum potentially available concentration of pollutants in soil water, and consequently an estimation of potential uptake by plants [31]. For this reasons, in this work we use the expression 'root available' to signify the fraction of Hg which is not complexed with organic species in solution or absorbed to soil particles and free to cross the root plant membrane for the assimilation (DGT-labile fraction).

The objective of this work was the analysis of total and methylmercury in multiple contaminated soils and a characterization by HPLC–ICP-MS of the species found in their soil solution, a description of the analytical method used for the characterization and a quantitation of the fraction of the mercury species removed from the soil solution by the DGT device.

2. Experimental

2.1. Soil

Soil samples were collected close to an abandoned industrial area of Val Basento (southern Italy) where Hg pollution was generated by chlor-alkali plants. Soil samples, from the topsoil (0–10 cm) and from a depth of 40–50 cm, were passed through a 2 mm mesh sieve. Soil properties, including pH, texture, cation exchange capacity (CEC) and organic matter (OM) (Table 1), were determined using official analytical methods [32].

2.2. Hg species

Before analysis soil samples were dried by lyophilization. Total Hg was measured using an atomic absorption spectrometer Advanced Mercury Analyzer (AMA 254, FKV) based on combustion of the sample in oxygen atmosphere and amalgamation preconcentration.

The extraction for analysis by HPLC–ICP-MS was performed following the methodology described by Chen et al. [33] with some changes. Methylmercury chloride and ethyl mercuric chloride were obtained from Riedel-de-Haen; mercury(II) chloride and mercury(I) nitrate were obtained from Sigma–Aldrich.

Table 1
Selected properties of the soil samples (CEC = cation exchange capacity, OM = organic matter)

Sample	Sand ($g\,kg^{-1}$)	Silt ($g\,kg^{-1}$)	Clay ($g\,kg^{-1}$)	pH	CEC ($cmol_{(+)}\,kg^{-1}$)	OM ($g\,kg^{-1}$)
P1 0–10 cm	573	247	180	8.2	11.1	14.6
P1 40–50 cm	580	264	156	8.2	11.4	18.2
P2 0–10 cm	310	413	277	8.5	13.5	17.2
P2 40–50 cm	694	186	121	8.9	6.4	6.5
P3 0–10 cm	280	493	228	8.2	13.2	10.7
P3 40–50 cm	403	392	205	8.5	11.8	11.7
P4 0–10 cm	671	206	123	7.9	12.3	48.2
P4 40–50 cm	555	297	148	8.5	12.3	10.1

Table 2
Working parameters for HPLC

HPLC (Agilent series 1100)	
Column	ZORBAX Eclipse XDB-C18, 2.1-mm i.d. × 50 mm, 5 μm
Mobile phase	0.06 M ammonium acetate, 3% (v/v) methanol, 0.1% 2-mercaptoethanol, pH 6.8
Flow rate	0.35 mL min^{-1}
Injection volume	100 μL

Reagent water was ultrapure, deionized (18 MΩ-cm resistance, Millipore® system); subpure HCl was obtained using a sub-boiling system (Milestone mod. Subpure). 1000 mg L^{-1} stock solutions of methylmercury chloride and ethylmercury chloride were prepared by dissolving them in methanol (Merck). One thousand milligrams per liter stock solution of mercury(II) chloride and mercury(I) nitrate were prepared by dissolving them in 5% HNO_3 sub-boiled. The working solutions were obtained by diluting the stock solutions in 0.06 M ammonium acetate and 0.1% 2-mercaptoethanol at pH 6.8. Standard preparation, extraction and measurements were performed on the same day. One gram of soil was mixed with 9 ml HCl acid (7.6%, w/v) and 1 ml mercaptoethanol (10%, w/v) in a polycarbonate bottle. The mixture was placed in an ultrasonic bath for 45 min, with addition of ice to avoid an excessive warming of the bath water, and then centrifuged for 5 min at 3000 rpm. Following centrifugation, 2 ml of the supernatant was transferred to a 50 ml polyethylene terephthalate (PET) bottle with 15 ml of Milli-Q water. Ammonia (10%, w/v) was used to adjust the pH of the solution to pH 6.8. Finally, pure water was added to give a final solution weight of 20.0 g. The solution was then filtered through a 0.45-μm membrane before HPLC–ICP-MS analysis. The operating conditions of ICP-MS and HPLC are summarized in Table 2. The column was chilled at 4 °C in order to improve peak resolution.

LC was chosen as a separation technique because it is extremely versatile, it applies to separation of non-volatile compounds, it is easy to interface to detectors such as ICP-MS and a minimum sample preparation is required. In a first step, LC was used in the operating conditions described by Chen et al. [27]. Afterwards, as the very large difference between the concentrations of Hg species ($MeHg^+$ and Hg^{2+}) in the soil extracts was found to compromise the separation and consequently the analyte identification, the method was modified. The methanol percentage in the mobile phase was changed and the column was chilled at 4 °C in order to improve the peak resolution. The operating conditions of HPLC are summarized in Table 2. The low amount of methanol in the mobile phase (3%, v/v) allowed to work with ICP-MS without any oxygen addition. The *m/z* signal was 202, the sampling depth was 4.5 mm and the spray chamber was chilled to −4 °C. Figs. 1 and 2 show typical chromatograms obtained by HPLC–ICP-MS for standards of inorganic and organic Hg species.

One of the main problems in speciation studies is the possibility of interconversion between different chemical forms of the element. Concerning the exposed analytical procedure, a interconversion could occur during the extraction or the separation by LC. The matrix for verification of the accuracy should be

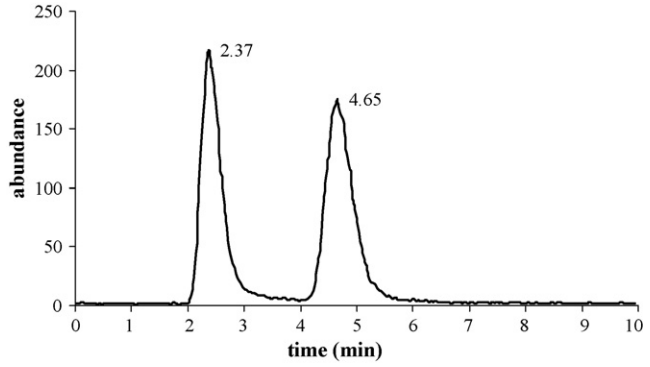

Fig. 1. HPLC–ICP-MS TIC of inorganic Hg species standards: Hg^+ 2.37 min, Hg^{2+} 4.65 min and 1 μg L^{-1}.

the most similar to the analyzed samples. An estuarine sediment (ERM 580) was selected because it is the most similar to the CRM soil, it is available on the market and certified for the concentration of $MeHg^+$ and total Hg. To verify the accuracy, spike additions were carried out from the stock solutions on both the certified sediment and the soil samples 24 h before the extraction. The extraction was realized in order to assure a complete recovery of the organic forms of Hg, which are the most easily to extract without leading to any interconversion [34]. Addition of Hg^{2+} (20 μg as Hg), $MeHg^+$ (30 ng as Hg) and of $EtHg^+$ (30 ng as Hg) were achieved separately, to monitor any possible interconversion between Hg species. The analytical precision was verified by replicate measurement (three injections of a single sample) whereas the procedural precision was assessed by analysing 15 replicate subsamples of ERM 580 on three different working days. Each six injections, to exclude any instrumental

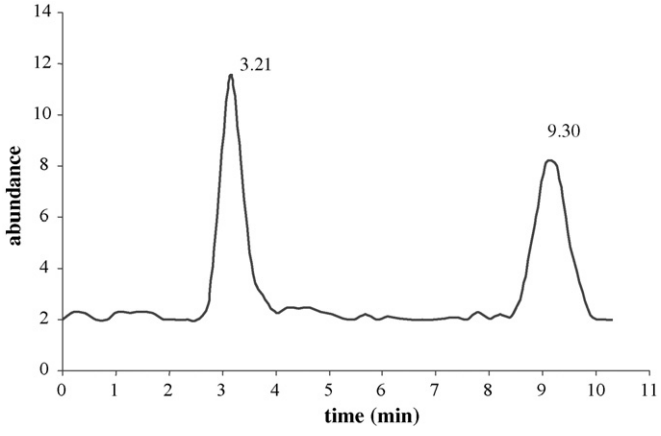

Fig. 2. HPLC–ICP-MS TIC of organic Hg species standards: $MeHg^+$ 3.21 min, $EtHg^+$ 9.30 min and 40 ng L^{-1}.

drift and to check the analyte retention time, measurement of the intermediate calibration standard were realized.

2.3. Hg species and availability in soil solution

Rhizon soil moisture samplers (Rhizosphere Research Products, Wageningen, The Netherlands) were used to extract soil solution from 400 g of each soil. Extractions were performed in triplicate. The samplers comprise 5 cm of inert porous plastic tubing (2.5 mm diameter), capped with nylon wire at one end and connected to 30 cm long PVC/PE tubing, joined to a female lock. The capped end was inserted into each plastic (PET) pot of soil during filling. During the experiment soil humidity was maintained at 100% of WHC by adding deionized water. After 48 h of water equilibration, a syringe needle was connected to the female lock and inserted into a 10 ml glass vacuum tube in order to extract the soil pore water by vacuum. Temperature varied between 23 and 24 °C during the experiment. The root available mercury concentration in soil solution (Hg_{DGT}) was measured by the DGT units, supplied by DGT Research Ltd. (Lancaster, UK, web: http://www.dgtresearch.com). The DGT devices consist of a resin layer placed on top of a piston, which is then overlain by a diffusive gel followed by a 140 μm thick, 0.45 μm pore size polysulfone filter membrane. The devices were deployed directly in the soil samples by placing each one in the same container as soil solution extraction, in triplicate and for 24 h. The devices were removed immediately before the soil solution extraction. Hg bound by the resin was directly measured by AMA 254. Dočekalová and Divis [30] recently reported agarose gel as the best diffusive medium, and both Chelex-100 and Spheron-Thiol as possible chelating resins for mercury measurements, able to distinguish between various species and between complexes with different stabilities. As a consequence, we tested the DGT performance [27] of the two different resin–gels and one diffusive gel (agarose). For this purpose, we prepared four different test solutions, each of 100 ng mL^{-1}, from stock standard solutions of Hg^{2+}, CH_3Hg^+ and $CH_3CH_2Hg^+$.

Following 24 h exposure to the test solutions, the mass of Hg accumulated by the resin was analyzed by AMA 254 by placing the resins directly in the instrument. The concentration of Hg at the beginning and end of the experiment was controlled in each solution. Hg_{DGT} was calculated using the equation provided by DGT Research Ltd. ($M = m\Delta g/DtA$, where M, the free metal concentration (μg cm^{-3}) is calculated by taking into account, m the metal mass (μg) captured on the chelating resin, Δg, the thickness of the diffusion gel layer, D the diffusion coefficient of the metals in the hydrogel ($cm^2\ s^{-1}$), t the deployment time (s) and A is the area of the DGT device exposed to the sample solution (cm^2).

For all species tested, the discrepancy between Hg_{DGT} and the immersion solution concentration was acceptable only for Spheron-Thiol DGT (the recovery for Chelex-100 ranged from 50% to 58%, for Spheron-Thiol from 83% to 97%). DGT with Spheron-Thiol as chelating resin were therefore deployed in this experiment.

Statistical analysis of the results was performed using SAS System [35].

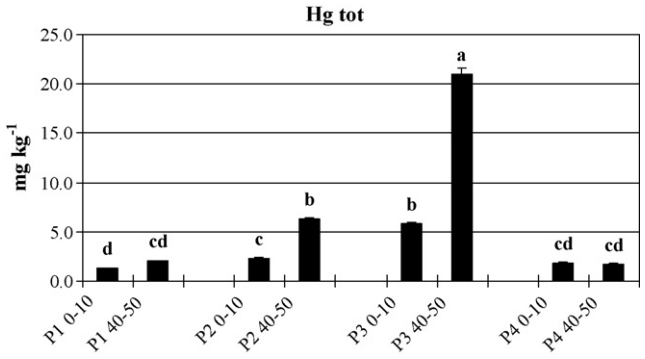

Fig. 3. . Total Hg concentrations (mean of three values) measured in each experimental soil. Values with the same letters are not significantly different according to the Duncan test ($p < 0.01$).

3. Results and discussion

3.1. Soil

All soil samples were of alkaline pH (Table 1), lower than that found by Hempel et al. [36] in 46 samples collected in East Germany, and similar to that reported by Neculita et al. [37] for three samples collected from former industrial areas, all contaminated from chlor-alkali plants, in The Netherlands, Belgium and France. The organic carbon content of all soils was below 20 g kg^{-1}, with the exception of P4 0–10. The particle size distribution was consistent with the low cation exchange capacity. The soil texture would tend to hinder Hg retention in the experimental soils, whereas the ligand in the organic matter was enough for complexing all the Hg present. All soils were contaminated, with total Hg concentrations ranging from 1.31 to 5.82 mg kg^{-1} in the upper layer and from 1.72 to 21.00 mg kg^{-1} in the lower layer (Fig. 3). Analysis of variance (ANOVA) and post hoc analysis with Duncan grouping were performed in the same way for Fig. 7 as it was for Fig. 3 using SAS [35]. Significant differences (at $p < 0.01$) between the groups are indicated by different letters.

Fig. 4 shows a typical chromatogram obtained by HPLC–ICP-MS for a soil sample. The technique showed good separation and sensitivity for all of the species investigated (Hg^{2+}, CH_3Hg^+ and $CH_3CH_2Hg^+$). Concentration of Hg in the method blank was always below the DL. After the

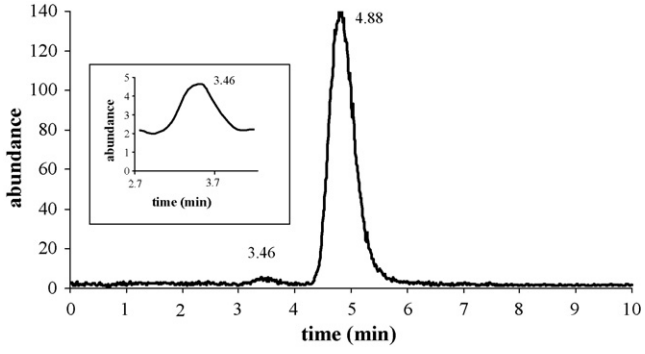

Fig. 4. HPLC–ICP-MS chromatograms of methyl Hg (3.46 min) and inorganic Hg(II) (4.88 min) in a soil sample.

extraction, which kept Hg in solution as a free ion only, mercury species in solution, the only organic form identified was $MeHg^+$ and the only inorganic form of mercury identified was Hg^{2+}. Analyte peaks were well resolved and baseline noise was low with respect to peaks obtained during analysis of the reference material ERM 580. The mean $MeHg^+$ concentration in ERM 580, measured on three different days, was $76.5 \pm 4.1\ \mu g\ kg^{-1}$ ($n = 15$), and was not statistically different ($\alpha = 0.05$) from its certified value ($75.5 \pm 3.7\ \mu g\ kg^{-1}$). Spike additions performed on both CRM and P3 soil sample confirmed a quantitative recovery (always between 80% and 120%) without any interconversion. Detection limits of all the species of Hg species investigated by HPLC–ICP-MS were lower than $15\ ng\ L^{-1}$.

Total Hg analyzed with AMA was 105% of the certified value ($132 \pm 3\ mg\ kg^{-1}$). The R.S.D. for total mercury was 2.7%.

The $MeHg^+$ concentration and total Hg concentration in each soil are compared in Fig. 5. The $MeHg^+/Hg_{tot}$ ratio varies between 0.05% and 0.82%. These values are very much smaller than those reported by Skyllberg et al. [15] for peat soils, and similar to or greater than those reported by Maserti and Ferrara [38] and Bloom et al. [39] for similarly polluted sites. There appears to be little relationship between $MeHg^+$ and Hg_{tot}. This can be attributed to the fact that many factors in addition to total Hg influence the transformation mechanisms of Hg to its various species [13].

The ratios of $MeHg^+$ to Hg_{tot} observed in the present study are difficult to explain. Hg methylation occurs predominantly in reduced sediments, and depends on the sulphur speciation (uptake of HgS^0 by sulphur reducing bacteria) and the redox potential [40]. The site from which the samples were collected is predominantly dry—rainfall is scarce and the soil is well drained. We can only suppose that other unknown factors influence methylation reactions in soils from this site. Generally, $MeHg^+$ concentrations were not depth dependent, but varied between samples depending upon the level of contamination. The ratios $MeHg^+/Hg_{tot}$, however, seem to depend on depth as if methylation took place mostly in the upper layers. The highest concentrations of $MeHg^+$ were measured in the most contaminated sample (P3).

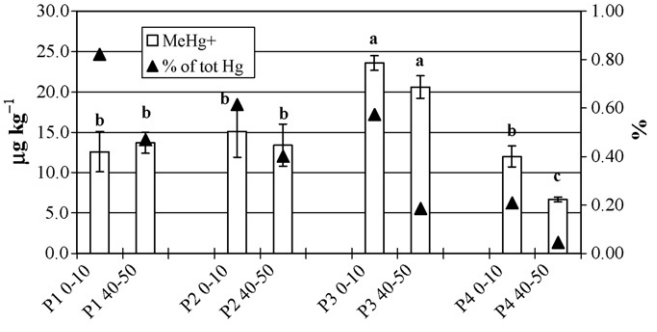

Fig. 5. $MeHg^+$ concentrations (mean of three values) measured in each experimental soil. Values with the same letters are not significantly different according to the Duncan test ($p < 0.01$). Black triangles show the $MeHg^+/Hg_{tot}$ ratio as percentage.

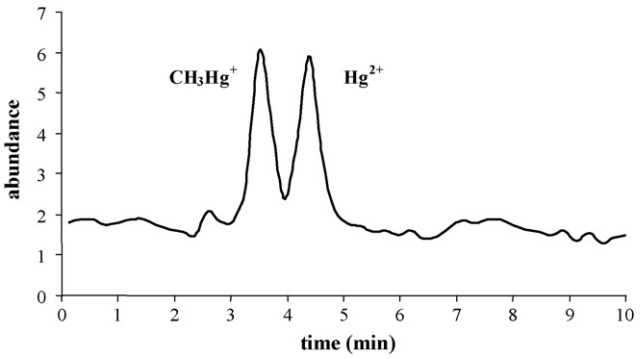

Fig. 6. HPLC–ICP-MS chromatogram of methyl Hg and inorganic Hg(II) in a soil solution sample, collected by a Rhizon sampler.

3.2. Soil solution

A representative HPLC–ICP-MS chromatogram of a soil solution sample, collected by a Rhizon sampler, is shown in Fig. 6.

As was the case for soil, only two Hg species ($MeHg^+$ and Hg^{2+}) were identified in the soil solution. Some authors [22,37] have employed sequential extraction methods to evaluate the mobility of Hg in soil, without identifying the individual species of Hg. The technique used in the present work is innovative in this sense. The soluble fraction accounts for only 0.01% of total Hg (Fig. 7): this small percentage corresponds to very low concentrations of $MeHg^+$ or Hg^{2+} (0.15 and $0.30\ \mu g\ L^{-1}$, respectively).

The mobile fraction and the ratio of inorganic/organic forms vary between samples. The concentration of Hg^{2+} is highest in P3 40–50, whilst $MeHg^+$ is undetectable in this sample, which also has the greatest concentration of total Hg. The sum of concentrations of Hg^{2+} and $MeHg^+$ is less than $0.1\ \mu g\ L^{-1}$ for four samples, where the ratio of inorganic/organic forms is about 1/1. In most cases, the ratio $MeHg^+/Hg_{tot}$ in soil solution ranges from 30% to 50%. By comparison, Skyllberg et al. [15] reported a range of 1.6% to 8.5% in samples collected from a small boreal forest catchment, whilst Heyes et al. [41] reported values of 1–26% for peat soils. $MeHg^+$ concentrations are weakly dependent on soil depth and on the sample: high values were obtained for one of the less polluted samples, P1. Concentrations of $MeHg^+$ do not appear to be correlated with Hg^{2+} in solution.

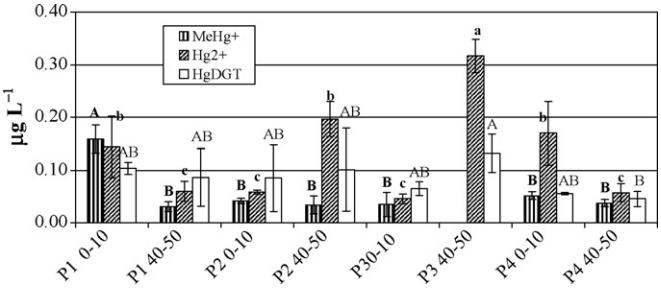

Fig. 7. $MeHg^+$, Hg^{2+} and Hg_{DGT} concentrations (mean of three values) measured in the soil solution of each sample. Hg_{DGT} indicates the root available concentration. Values with the same letters are not significantly different according to the Duncan test ($p < 0.01$).

The methylation process is largely anaerobic and in general it takes place more likely in soil than in solution, so the very low amount of Hg^{2+} in solution appears to be a not significant source for methylation compared to Hg^{2+} in soil. Possible explanations for the diverse behaviour observed in the different experimental soils may include: the dependence of mobility on the ratio of chlorides to total Hg, as suggested by Neculita et al. [42], the different binding capacity of the S groups of humic and fulvic acids for $MeHg^+$ [24,42] or, in general, the well recognised role of organic matter in mobility and transport in aquatic systems [43].

The Hg_{DGT} values are similar for all samples, regardless of the sampling point and the degree of contamination. Hg_{DGT} concentrations in soil solution (Fig. 7) range from 50% to 100% of the total Hg, indicating that, even if the concentration of Hg in soil solution is low, it is, for the most part, DGT-labile or even available. In the case of DGT deployment, the ratio Hg_{DGT}/Hg in soil solution represents the supply of Hg accumulated by DGT from soil to solution [44]. If the resupply is sufficiently fast to maintain the pore water concentration adjacent to the DGT device at close to its initial value (*sustained case* or *partial case-steady state* [44]), it will be a linear increase of the accumulation of Hg mass by DGT with time. On the contrary, if the rate of resupply is slow, the accumulation by DGT significantly depletes the small available pool of sorbed metal. The resupply therefore cannot be sustained, and pore water concentrations become depleted further into the sediment (*diffusive case* or *partial case-nonsteady state*). The experimental results imply that Hg in solution is rapidly replenished from the solid phase, where it is prevailingly free and not complexed. The values obtained for soil solution suggest that for most soils there is a substantial reservoir of organic Hg in the soil that can be rapidly supplied to the soil solution if there is removal of Hg by, for example, biological uptake.

It is important to highlight the agreement, within one order of magnitude, of the results of HPLC–ICP-MS and DGT analysis, as this is an important element for the cross validation of the two pioneering techniques.

In this work we have examined two innovative techniques for the determination of various chemical forms of mercury in soil and for the evaluation of root availability. The HPLC–ICP-MS technique proved suitable for the separation and determination of inorganic (Hg^+, Hg^{2+}) and organic forms ($MeHg^+$, Hg^{2+}) of mercury. The speciation procedure was validated using ERM 580-certified sediment and spiked samples. Extraction by HCl 2-mercaptoethanol and ultrasound followed by HPLC–ICP-MS analysis gave a quantitative recovery of the organic forms of Hg ($MeHg^+$ and $EtHg^+$). The proposed method was confirmed as simple, sufficiently sensitive, rapid and reproducible. Unlike GC methods, it does not require any preconcentration or derivatization. The root availability of Hg, a parameter not yet thoroughly investigated, was estimated by the speciation of soil solution collected by Rhizon soil samplers and the deployment of DGT devices containing a Spheron-Thiol resin, set up and tested specifically for this purpose. These two approaches allowed the collection of complementary information. The DGT technique allowed the estimation of the maximum potential root availability, whilst soil solution analysis permitted the identification of the different chemical forms of mercury. On the basis of our data, we can affirm that the Spheron-Thiol DGT proposed by Dočekalová and Divis [30] may be suitable for the evaluation of the availability of Hg in soil solution. Nevertheless, it is not currently possible to obtain a speciation of the Hg bound by the gel–resin. On the contrary, the HPLC–ICP-MS technique is highly appropriate for this purpose, but cannot be used directly in the field and does not provide an assessment of resupply of Hg from soil to solution. In conclusion, in this study HPLC–ICP-MS and DGT techniques were confirmed as suitable tools for the estimation of Hg root availability and risk from contaminated soils.

All the results reported in this work demonstrate that Hg was largely unavailable. $MeHg^+$ was found in low concentrations and this species, due to its high availability, is the most important from the perspective of environmental risk [45]. The low availability of Hg to plants and to environment is a further interesting outcome of this study.

Acknowledgements

This research was conducted in the framework of the project PRIN 2005 “Chemical, physical and biological innovative methods for the characterization and the reclamation of a heavy metal contaminated soil (MICROS)” and the authors wish to acknowledge the financial support of the Ministry of University and Research of Italy.

References

[1] D.C. Adriano, Trace Elements in Terrestrial Environment; Biogeochemistry, Bioavailability and Risks of Metals, Springer, New York, 2001, pp. 866.
[2] W.F. Fitzgerald, D.R. Engstrom, R.P. Mason, E.A. Nater, Environ. Sci. Technol. 32 (1998) 1–7.
[3] C.C. Gilmour, E.A. Henry, R. Mitchell, Environ. Sci. Technol. 26 (1992) 2281–2287.
[4] G. Compeau, R. Bartha, Appl. Environ. Microbiol. 50 (1985) 498–502.
[5] G. Kaiser, G. Tölg, in: O. Hutzinger (Ed.), The Handbook of Environmental Chemistry, vol. 3, Part A, Springer-Verlag, New York, 1980, pp. 1–58.
[6] E.J. Fleming, E.E. Mack, P.G. Green, D.C. Nelson, Appl. Environ. Microb. 72 (2006) (2006) 457–464.
[7] R.S. Oremland, C.W. Culbertson, M.R. Winfrey, Appl. Environ. Microbiol. 57 (1991) 130–137.
[8] J.H. Weber, Chemosphere 26 (1993) 2063–2077.
[9] R.D.J. Rogers, Environ. Qual. 6 (1977) 463–467.
[10] H.G. Van Faassen, Plant Soil 44 (1975) 505–509.
[11] National Academy of Science. An assessment of Mercury in the Environment, National Research Council, Washington, DC, 1978, pp. 185.
[12] J.O. Nriagu, The Biogeochemistry of Mercury in the Environment, Elsevier, Amsterdam, 1979, pp.706.
[13] M. Horvat, N. Nolde, V. Fajon, V. Jereb, M. Logar, S. Lojen, R. Jacimovic, I. Falnoga, Q. Liya, J. Faganeli, D. Drobne, Sci. Total Environ. 304 (2003) 231–256.
[14] Y.H. Lee, A. Iverfeldt, Water Air Soil Pollut. 56 (1991) 309–321.
[15] U. Skyllberg, J. Qian, W. Frech, K. Xia, W.F. Bleam, Biogeochemistry 64 (2003) 53–76.
[16] P. Quevauviller, M. Filippelli, M. Horvat, Trends Anal. Chem. 19 (2000) 157–166.
[17] S. Rapsomanikis, Analyst 119 (1994) 1429–1439.

[18] Y. Liu, V. Lopez-Avila, M. Alearaz, W. Beckert, J. High Resolution Chromatogr. 17 (1994) 527–536.
[19] A.M. Carro-Diaz, R.A. Lorenzo-Ferreira, R. Cela-Torrijos, J. Chromatogr. A 683 (1994) 242–252.
[20] K.C. Bowles, S.C. Apte, Anal. Chim. Acta 419 (2000) 145–151.
[21] L. Liang, M. Horvat, N.S. Bloom, Talanta 41 (3) (1994) 371–379.
[22] R. Fernández-Martínez, J. Loredo, A. Ordóñez, M.I. Rucandio, Sci. Total Environ. 346 (2005) 200–256.
[23] G. Qiu, X. Feng, S. Wang, L. Shang, Appl. Geochem. 20 (2005) 627–638.
[24] J. Qian, U. Skyllberg, W. Frech, W.F. Bleam, P.R. Bloom, P.E. Petit, Geochim. Cosmochim. Acta 22 (2002) 3873–3885.
[25] C.F. Harrington, Trends Anal. Chem. 19 (2000) 167–179.
[26] W. Davison, H. Zhang, Nature 367 (1994) 546–548.
[27] H. Zhang, W. Davison, Anal. Chem. 67 (1995) 3391–3400.
[28] H. Zhang, W. Davison, R.J.G. Mortimer, M.D. Krom, P.J. Hayes, I.M. Davies, Sci. Total Environ. 296 (2002) 175–187.
[29] P. Diviš, H. Dočekalová, V. Smetková, Chem. List. 97 (2003) 1184–1189.
[30] H. Dočekalová, P. Diviš, Talanta 65 (2005) 1174–1178.
[31] H. Zhang, F.J. Zhao, B. Sun, W. Davison, S.P. McGrath, Environ. Sci. Technol. 35 (2001) 2602–2607.
[32] SSIS, in: P. Sequi (Ed.), Collana di metodi analitici per l'agricoltura, a cura di Pietro Violante, Soil Science Italian Society, Franco Angeli, Bologna, 2000, p. 536.
[33] D. Chen, M. Jing, X. Wang, Determination of Methyl Mercury in Water and Soil by HPLC–ICP-MS, Agilent Technologies, 2005, pp. 8.
[34] EPA 3200 Rev. 0 (2005) pp. 28.
[35] S.A.S. Institute, SAS/STAT user's guide. Version 6, vols. 1 and 2, 4th ed., SAS Inst., Cary, NC, 1996.
[36] M. Hempel, C. Wilken, C. Geilhufe, I. Richter-Politz, in: W.J. Van der Brink, R. Bosman, F. Arendt (Eds.), Transformation of Elemental Mercury to Organic Mercury Species at Sites of Former Caustic Soda Plants in East-Germany, Contaminated soils, Kluwer Academic Publ., The Netherlands, 1995, pp. 505–506.
[37] C. Neculita, G.J. Zagury, L. Deschênes, J. Environ. Qual. 34 (2005) 255–262.
[38] B.E. Maserti, R. Ferrara, Water Air Soil Pollut. 56 (1991) 15–20.
[39] N.S. Bloom, E. Preus, J. Katon, M. Hiltner, Anal. Chim. Acta 479 (2003) 233–248.
[40] J.M. Benoit, C.C. Gilmour, R.P. Mason, A. Heyes, Environ. Sci. Technol. 33 (1999) 951–957.
[41] A. Heyes, T.R. Moore, J.W.M. Rudd, J.J. Dugoua, Can. J. Fish Aquat. Sci. 57 (2000) 2211–2222.
[42] H. Hintelmann, P.M. Welbourn, R.D. Evans, Environ. Sci. Technol. 31 (1997) 489–495.
[43] S.M. Ullrich, T.W. Tanton, S.A. Abdrashitova, Environ. Sci. Technol. 31 (2001) 241–293.
[44] M.P. Harper, W. Davison, W. Tych, Environ. Modell. Softw. 15 (2000) 55–66.
[45] D. Wallschläger, M.V.M. Desai, M. Spengler, P.F. Sanders, J. Environ. Qual. 25 (1996) 837–844.

Available online at www.sciencedirect.com
ScienceDirect
Talanta 74 (2008) 1330–1336
Talanta
www.elsevier.com/locate/talanta

Amperometric immunosensors based on layer-by-layer assembly of gold nanoparticles and methylene blue on thiourea modified glassy carbon electrode for determination of human chorionic gonadotrophin

Rong Chai, Ruo Yuan *, Yaqin Chai, Chaofeng Ou, Shurui Cao, Xuelian Li

Chongqing Key Laboratory of Analytical Chemistry, College of Chemistry and Chemical Engineering, Southwest University, Chongqing 400715, China

Received 15 May 2007; received in revised form 30 August 2007; accepted 31 August 2007
Available online 14 September 2007

Abstract

Nano-Au and methylene blue (MB) were assembled layer-by-layer (LBL) into films on the glassy carbon electrode modified by thiourea for detection of human chorionic gonadotrophin (HCG). The electrode modification process was characterized by cyclic voltammetry (CV), electrochemical impedance spectroscopy (EIS) and scanning electron micrograph (SEM). The factors influencing the performance of the amperometric immunosensor were studied in detail. Tests performed with this immunosensor showed good linearity, the working range for the system was 1.0–100.0 mIU/mL with a detection limit of 0.3 mIU/mL at 3σ. Moreover, the studied immunosensor exhibited high sensitivity and long-term stability. The present work supplied a promising test method for clinical immunoassay.
© 2007 Elsevier B.V. All rights reserved.

Keywords: Immunosensor; Thiourea; Layer-by-layer (LBL); Gold nanoparticles (nano-Au); Human chorionic gonadotrophin

1. Introduction

Immunoassays based on the specific antigen–antibody complexation for analytical purposes have been successfully applied to many fields including food industry [1], environmental protection [2,3] and clinical control [4–6]. Electrochemical immunosensors offer good possibilities for sensitive detection of unlabeled proteins (direct detection). Recently, a wide range of immunosensors based on electrochemical transducers have been developed, such as potentiometric [7,8], amperometric [9], conductimetric [10] and impedimetric [11]. Among these, amperometric immunosensors gain growing attention owing to a relatively low detection limit and high sensitivity. Moreover, the addition of mediator such as dyes [12], potassium hexacyanoferrates [13], ferrocene and its derivatives [14] in the analyte solution is of great satisfaction because it leads to a more complex immunoassay system and increases the analytical time and expense, so it would be available to construct amperometric immunosensors through immobilizing a mediator onto the electrode surface [15].

Self-assembly molecular (SAMs) have demonstrated their superiority over other surface modification techniques, owing to its simplicity, versatility, and the establishment of a high level of order on a molecular scale [16–18]. It is very attractive for tailoring surfaces with desired properties with the expectation of the high organization and homogeneity, together with its molecular dimension. Recently, gold nanoparticles (nano-Au) has gained much attention for studying in analytical chemistry which possesses tremendous specific surface area and good biocompatibility [19,20]. It can strongly absorb proteins without loss of their biological activity [21]. Among SAMs, layer-by-layer (LBL) assembly method is based on electrostatic adsorption of oppositely charged substance from their solution in alternate steps and has many advantages compared with other film-forming approaches. So it is a rich, versatile, low-cost, and easy-operation method [22,23]. The major stabilizing interaction is usually supposed to be electrostatic. Mechanically stable films which are constructed by layer-by-

* Corresponding author. Tel.: +86 23 68252277; fax: +86 23 68254000.
E-mail address: yuanruo@swu.edu.cn (R. Yuan).

0039-9140/$ – see front matter © 2007 Elsevier B.V. All rights reserved.
doi:10.1016/j.talanta.2007.08.046

layer film self-assembly, have been successfully designed for optics, electroactive, enzyme-catalyzed synthesis, biosensor and biochemical studies of proteins [24,25].

Human chorionic gonadotropin (HCG) secreted by the trophoblastic cells of placenta chorionic vesicle to promote the development of the sexual gland, is an important diagnostic marker of pregnancy and one of the most important carbohydrate tumor markers. It frequently appears in the serum and urine of human at extremely low concentrations and high levels of HCG predict a high risk for prostate cancer. Thus, serum or urine HCG level has been used to diagnose many diseases related to pregnancy and seminal system such as the early pregnancy, the hydatid pregnancy, the trophoblastic cancer and the orchic teratoma, etc. [26].

Recently, some immunosensors based on various nanoparticles such as Au nanoparticles, Ag nanoparticles and TiO_2 nanoparticles, etc., have been reported in our laboratory [27–29]. In this experiment, nano-Au and methylene blue (MB) were carried out alternatively on thiourea (TU) modified glassy carbon electrode by LBL assembly. The desired number of nano-Au/MB films with sufficient nano-Au on it was obtained, which is based on the electrostatic interaction between positively charged mediator MB and negatively charged nano-Au. Finally, human chorionic gonadotropin antibody (anti-HCG) and BSA were adsorbed onto the surface of the nano-Au layer successively. The anti-HCG/{nano-Au/MB}$_n$/TU multilayer films-modified immunosensors were used for the determination of HCG and showed high sensitivity, good stability and reproducibility. Furthermore, the immunosensors had the high surface area of the nanoparticles for loading anti-HCG. The novel immobilization approach for binding of anti-HCG was simple and effective. So, it would be a potential application on clinical determination of HCG level.

2. Experimental

2.1. Reagent and materials

HCG and anti-HCG were purchased from Biocell Company (Zhengzhou, China). Thiourea (TU), bovine serum albumin (BSA, 96–99%), methylene blue, gold chloride ($HAuCl_4$) and sodium citrate were obtained from Sigma Chemical Co. (St. Louis, MO, USA). All chemicals and solvents used were of analytical grade and were used as received. Double distilled water was used throughout this study. Phosphate-buffered solutions (PBS, 0.1 mol/L) at various pH were prepared by using the stock solutions of Na_2HPO_4, NaH_2PO_4 and 0.1 mol/L KCl, then adjusting the pH with 0.1 mol/L NaOH and H_3PO_4. Gold nanoparticles were produced by reducing gold chloride tetrahydrate with citric acid at 100 °C for half an hour [30,31]. The size of the prepared Au colloids was about 16 nm, which was estimated from transmission electron microscopy (the graph not shown). The prepared nano-Au was stored at 4 °C in a dark bottle. The HCG was stored in the frozen state, and its standard solutions were prepared daily with double distilled water as in use.

2.2. Apparatus

Cyclic voltanmmetric (CV) measurements were carried out with a CHI 610A electrochemistry workstation (Shanghai CH Instruments Co., China). The CV experiments were performed in a conventional electrochemical cell containing a three-electrode system where bare or modified glassy carbon electrode ($\Phi = 4$ mm) was used as a working electrode, platinum wire as an auxiliary electrode and a saturated calomel as a reference electrode (SCE). The pH measurements were made with a pH meter (MP 230, Mettler-Toledo Switzerland) and a digital ion analyzer (Model PHS-3C, Dazhong Instruments, Shanghai, China). The size of nano-Au was estimated from transmission electron microscopy (TEM) (H600, Hitachi Instrument, Japan). The image of the{nano-Au/MB}$_5$ films and anti-HCG/{nano-Au/MB}$_5$ films on the glassy carbon electrodes surface were characterized by scanning electron microscopy (SEM) (JSMT220, Japan). Impedance measurements of the electrodes were carried out with a Model IM6e (ZAHNER Elektrick Co., Germany), and were performed in a background solution of 5.0×10^{-3} mol/L $K_3Fe(CN)_6 + K_4Fe(CN)_6$ at 25 °C. The frequency range is at 100 mHz–10 KHz at 220 mV versus SCE.

2.3. Preparation of the immunosensor

Glassy carbon electrode (GCE) ($\Phi = 4$ mm) was used for electrochemical measurement. It was polished carefully with α-Al_2O_3 powder of 0.3 and 0.05 μm respectively, to a mirror-like surface, then cleaned through sonication in bi-distilled water and ethanol for 5 min and dried in air. The cleaned electrode was treated with cyclic scanning in the potential rang of −1.4 to 0.2 V at 0.10 V s^{-1} for 10 cycles in 0.25 mol/L thiourea. After being modified by thiourea, glassy carbon electrode was thoroughly rinsed with distilled water and alternately immersed in nano-Au at 4 °C overnight and 1.0×10^{-4} mol/L MB solution at room temperature for 4 h. The above procedure was repeated to obtain the desired number of sandwiched nano-Au/MB. Then, the{nano-Au/MB}$_n$ multilayer modified electrode was immersed in 0.5 mL anti-HCG solution at 4 °C for about 12 h. After the resulting electrode was incubated in BSA solution about 4 h at 4 °C in order to block possible remaining active sites of the nano-Au monolayer and avoid the non-specific absorption. The final structure of the modified electrode is expressed as anti-HCG/{nano-Au/MB}$_5$/nano-Au/thiourea/GC electrode. The schematic diagram of the stepwise self-assemble procedure of the immunosensor was shown in Scheme 1.

2.4. Experimental measurements

The cyclic voltanmmetric (CV) experiments were performed in a conventional electrochemical cell and the potential swept from −0.7 to 0.2 V (versus SCE) with a sweeping rate of 100 mV/s in 0.1 mol/L PBS of pH 6.5 solution at room temperature. All measurements were carried out at a temperature of 25 °C. The incubating buffer was PBS containing various concentrations of HCG (pH 7.0) at 25 °C. When the immunosensor was incubated into the solution for 40 min, the immunoreac-

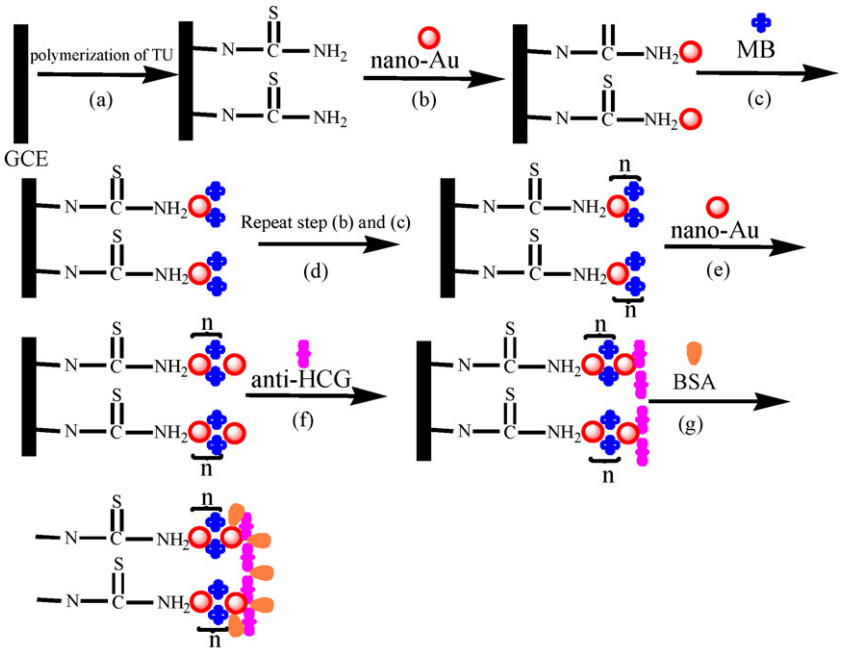

Scheme 1. Schematic illustration of the stepwise immunosensor fabrication process: (a) successive CV scanning of TU film; (b) self-assembly of nano-Au monolayer; (c) fabrication of $\{\text{nano-Au/MB}\}_n$ multilayer films, n denotes the number of the layers; (f) anti-HCG loading; (g) blocking with BSA.

tion was performed. The detection of HCG level is based on the charges of amperometric reduction current response (ΔI) before and after the immunoreaction.

3. Results and discussion

3.1. Electrochemical characterization of the $\{$nano-Au/MB$\}_n$/nano-Au/thiourea-modified glassy carbon electrode

Cyclic voltammetry (CV) was used to immobilize thiourea (TU) onto surface of pretreated GCE. The experiment result indicated that TU could be immobilized onto surface of the pretreated GCE at the range of −1.4 to 0.2 V at 0.10 V s^{-1} for 10 cycles in 0.25 mol/L thiourea. It could be seen that a white film was constructed on the surface of the pretreated GCE. Thiourea (NH_2CSNH_2) has two amino groups (R-NH_2) that the one can be immobilized onto surface of the pretreated GCE through cyclic voltammetry, which is similar to the previous reports [32] and the other can be used for coupling of gold nanoparticles. As we all know, some functional groups such as cyano (–CN), mercapto (–SH), and amino (–NH_2) groups have a high affinity for Au. Therefore, nano-Au could be immobilized on thiourea (TU) modified glassy carbon electrode via covalent bonds between gold nanoparticles (nano-Au) and the –NH_2 groups of the thiourea.

Electrochemical impedance spectroscopy (EIS) has been proven to be one of the most powerful tools for probing the features of surface-modified electrodes [33]. Fig. 1 shows the electrochemical impedance of the bare GCE (a), TU/GCE (b) and nano-Au/TU/GCE (c) in 5.0×10^{-3} mol/L $K_3Fe(CN)_6 + K_4Fe(CN)_6$ at 25 °C. It can be seen that the bare glassy carbon electrode exhibited an almost straight line (Fig. 1a), which was characteristic of a diffusional limiting step of the electrochemical process. It is obvious that change of electrochemical impedance occurred after TU bound to surface of bare GCE (Fig. 1b), indicating that the TU film obstructed electron-transfer of the electrochemical probe. When the negatively charged nano-Au was absorbed on thiourea modified glassy carbon electrode, the interfacial resistance increased highly (Fig. 1c). It shows that the nano-Au could be adsorbed on the TU film. Methylene blue is positively charged in pH 6.5 PBS buffer and can be easily absorbed by the charged negatively gold nanoparticles as a result of the adsorption of citrate in the fabrication process to obtain the desired number of $\{$nano-Au/MB$\}_n$ mutilayer films. Fig. 2 shows the CVs of

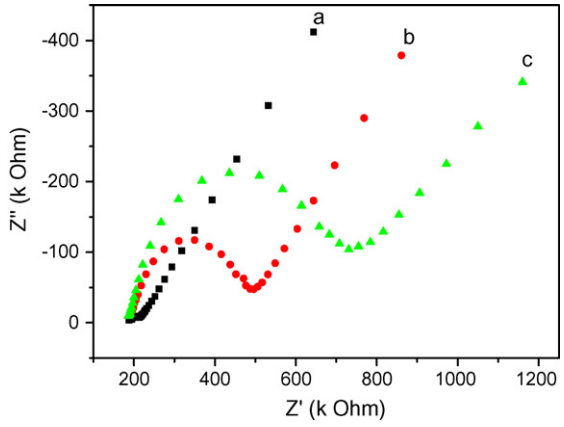

Fig. 1. AC impedance of bare GCE (a), TU/GCE (b) and nano-Au/TU/GCE (c) measured in 5.0×10^{-3} mol/L $K_3Fe(CN)_6 + K_4Fe(CN)_6$ solution under room temperature.

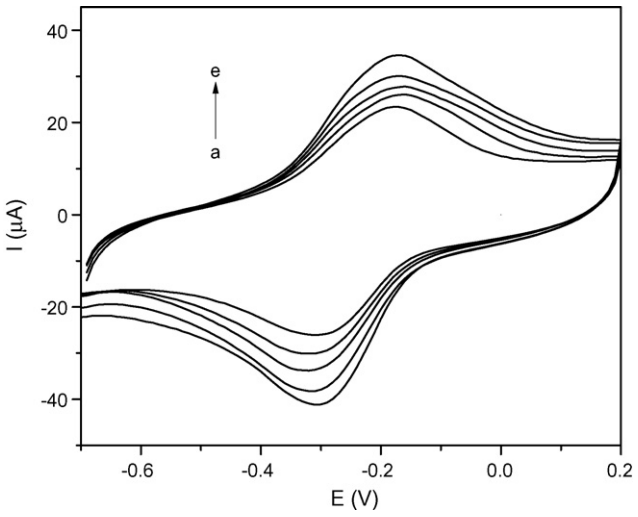

Fig. 2. Cyclic voltammogramms of the $\{$nano-Au/MB$\}_n$ multilayered: (a) $n=1$, (b) $n=2$, (c) $n=3$, (d) $n=4$ and (e) $n=5$. All the measurements were carried out in 0.1 mol/L pH 6.5 PBS solution. Potential scan rate was 100 mV/s.

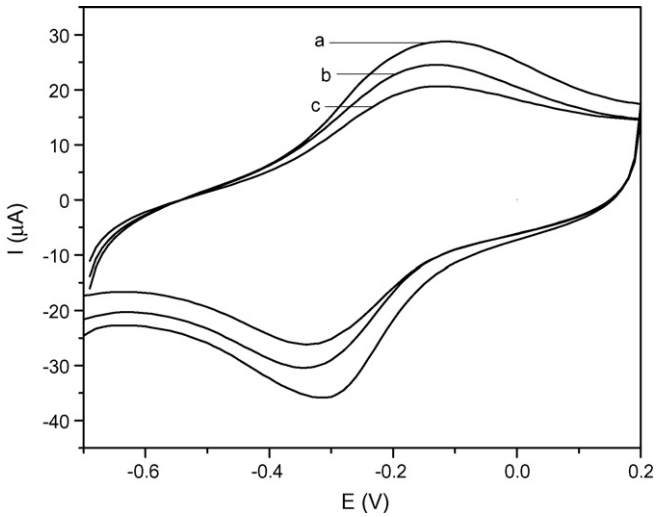

Fig. 3. Cyclic voltammogramms of the modified electrode measured in 0.1 mol/L pH 6.5 PBS solution: (a)$\{$nano-Au/MB$\}_5$/nano-Au/thiourea-modified GCE; (b) anti-HCG immobilized electrode; (c) the HCG electrode incubated in 50 mIU/mL HCG.

$\{$nano-Au/MB$\}_n$ mutilayer films with different layer numbers ($n=1$–5). With the layer number of $\{$nano-Au/MB$\}_n$ increased from 1 to 5, the peak currents also increased. When the layers was over 5, $\{$nano-Au/MB$\}_n$ layers gave nearly the same response as the 5th layer which indicated a saturation was reached after five times of alternately adsorption. Therefore, the films of $\{$nano-Au/MB$\}_5$ was adopted in the subsequent work.

3.2. Electrochemical characterization of the HCG/anti-HCG/$\{$nano-Au/MB$\}_5$/nano-Au/thiourea-modified glassy carbon electrode

Fig. 3 showed the CVs of $\{$nano-Au/MB$\}_5$/nano-Au/thiourea-modified electrode (Fig. 3a), anti-HCG immobilized electrode (Fig. 3b) and the HCG electrode incubated in 50 mIU/mL HCG (Fig. 3c) in a background solution of 0.1 mol/L pH 6.5 PBS buffer. We can find the peak currents decrease after anti-HCG was adsorbed on the nano-Au monolayer because the membrane became less conductive. When the modified immunosensor was incubated in 50 mIU/mL HCG, the peak currents decrease dramatically because the antigen–antibody reaction and form anti-HCG/HCG immunocomplex, which acts as the inert electron and mass transfer blocking layer. In order to further confirm the assembly of nano-Au and anti-HCG on the electrode, the scanning electron micrographs (SEMs) of $\{$nano-Au/MB$\}_5$ film and anti-HCG/$\{$nano-Au/MB$\}_5$ film was performed. The results are shown in Fig. 4. The SEM image of $\{$nano-Au/MB$\}_5$ film (Fig. 4a) clearly shows the presence of numerous bright particles, well-distributed gold nanoparticles, suggesting MB can be easily absorbed by gold nanoparticle to obtain the desired number of $\{$nano-Au/MB$\}_5$ mutilayer films. When anti-HCG was immobilized in $\{$nano-Au/MB$\}_5$ films, the structure kept being uniform and porous, and bright particles of anti-HCG were observed (Fig. 4b), which resulted in a good amperometric response.

The CVs of the resulting immunosensor in 0.1 mol/L pH 6.5 PBS at different scan rates were shown in Fig. 5. Both the anodic and cathodic peak currents increased linearly with scan rates in the range of 10–300 mV/s, as shown in the inset of Fig. 5, suggesting a surface-controlled electrochemical behavior.

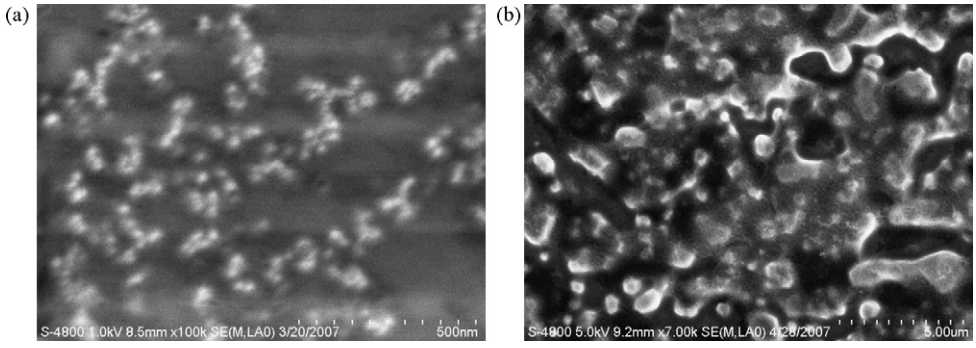

Fig. 4. Scanning electron micrographs of the glassy carbon electrodes coated with (a) $\{$nano-Au/MB$\}_5$ films and (b) anti-HCG/$\{$nano-Au/MB$\}_5$ films.

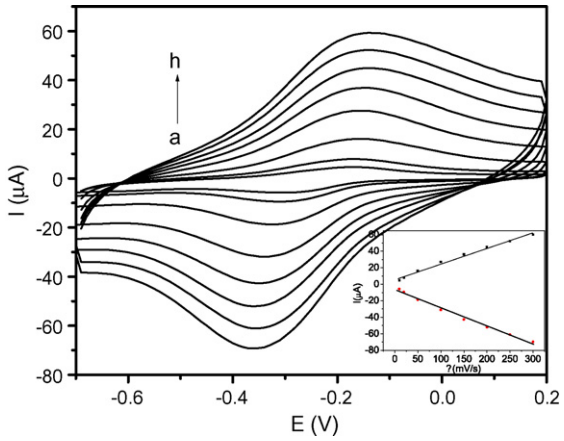

Fig. 5. Cyclic voltammogramms of the immunosensor at different scan rates (from a to h): 10, 20, 50, 100, 150, 200, 250 and 300 mV/s measured in 0.1 mol/L pH 6.5 PBS solution under room temperature. All potentials are given vs. SCE. The inset is the dependence of redox peak currents on the potential sweep rates.

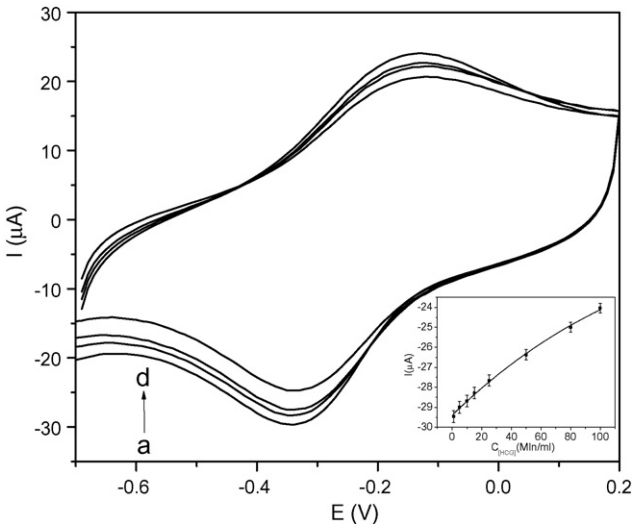

Fig. 6. Cyclic voltammogramms of anti-HCG immobilized electrode with different concentrations of the HCG. (a: 1, b: 15, c: 25, d: 100 mIU/mL). The insert shows calibration plots of the cathodic peak current response vs. concentration of HCG.

3.3. The effect of pH on the immunoreaction

The CVs of the immunosensor in 0.1 mol/L PBS buffer at different pH was studied from 4.0 to 8.5. The experimental results show that the maximum current response occurs at 6.5. Thus, 0.1 mol/L pH 6.5 PBS buffer was selected in our test.

3.4. Incubation time of immunosensor

The effect of incubation time on response current of the immunosensor was studied in the 0.1 mol/L PBS (pH 7.0) containing 80 mIU/mL HCG solution. It was found with the increasing incubation time, the response current was rapidly down and reached a plateau at about 40 min which indicated an equilibration state was reached. Therefore, the incubation time of 40 min was adopted in the subsequent work.

3.5. Detection of HCG

The Fig. 6 shows the CVs of the anti-HCG/{nano-Au/MB}$_5$/nano-Au/thiourea-modified glassy carbon electrode with different concentrations of the HCG. The insert in Fig. 6 shows that the cathodic peak current response of CVs were proportional to the concentration of HCG in the range from 1.0 to 100.0 mIU/mL. The linear regression equation was $I = 0.053C_{HCG} - 29.206$ and correlation coefficient of 0.9960 with a detection limit of 0.3 mIU/mL at 3σ.

3.6. Repeatability and stability of the immunosensor

In this paper, the regeneration of the prepared immunosensor was immersed in a stirred 4 M urea solution for about 5 min. The current response error of the renewable electrode was 4.1% (eight regenerations and measurements). The stability of the successive assays was studied. A relative standard deviation (R.S.D.) of 3.6% was acquired when the electrode was repeated ten times of consecutive measurements. The storage stability of the immunosensor was also investigated over a 60-day period. When the HCG electrode was stored at 4 °C and measured intermittently (every 5 days), it retained 93.8% of its initial amperometric value within 60 days. The good stability may be explained by nano-Au had no effect on immunoprotein activity and antibody molecules were attached firmly on the surface of colloidal Au.

3.7. Selectivity

The effect of substances that might interfere with the response of the HCG immunosensor system was also studied. The immunosensor was incubated in 50 mIU/mL HCG solutions containing separately hepatitis B surface antigen, carcinoembryonic antigen (CEA) and α-1-fetoprotein (AFP). The relative standard deviation of amperometric reduction current response obtained for each interfering substance were between 3.10 and 3.98%. The R.S.D. of amperometric reduction current for lower concentration of HCG (1.0 mIU/mL) response obtained for each interfering substance were less than 3.6%. These results suggested that the selectivity of the immunosensor was satisfactory.

Fig. 7 showed the CVs of the electrode without immobilized anti-HCG, the electrode without immobilized anti-HCG added with 50 mU/mL HCG, the electrode with immobilized anti-HCG and the electrode with immobilized anti-HCG added with 50 mU/mL HCG in 0.1 mol/L PBS of pH 6.5 solution at room temperature. Fig. 7a showed the CV of the electrode blocked by bovine serum albumin (BSA) without immobilized anti-HCG. Fig. 7b showed the CV of the electrode blocked by BSA without immobilized anti-HCG added with 50 mIU/mL HCG. Fig. 7c showed the CV of the electrode blocked by BSA with immobilized anti-HCG and Fig. 7d showed the CV of the electrode blocked by BSA with immobilized anti-HCG added with 50 mIU/mL HCG. We found that the charges of amperometric reduction current response (ΔI_1) of the immunosensor without immobilized anti-HCG is much more smaller than the amper-

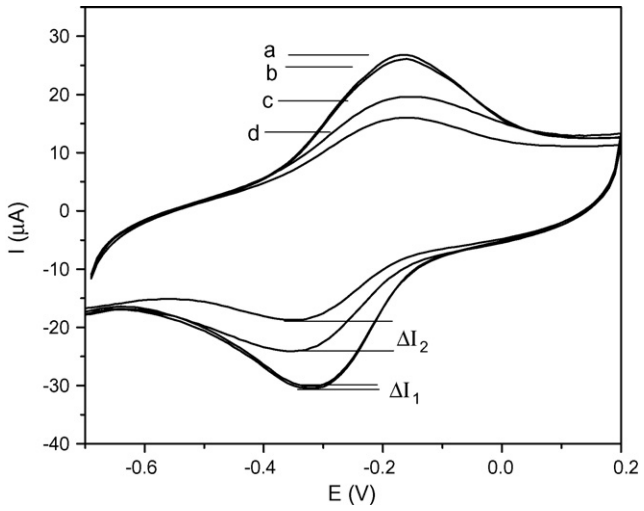

Fig. 7. Cyclic voltammogramms of the electrode without immobilized anti-HCG, the electrode without immobilized anti-HCG added with 50 mIU/mL HCG, the electrode with immobilized anti-HCG and the electrode with immobilized anti-HCG added with 50 mIU/mL HCG in 0.1 mol/L PBS of pH 6.5 solution at room temperature.

Table 1
Application of the immunosensor in serum sample

	Serum samples				
	1	2	3	4	5
This method (mIU/mL)	2.1	3.7	13.5	65.5	87.0
Acesss™ (mIU/mL)	2.0	4.0	13.6	60.7	88.5
Relative deviation (%)	5.0	−7.5	−0.7	7.9	−1.7

ometric reduction current response (ΔI_2) of the immunosensor with immobilized anti-HCG. Thus, there is almost no amperometric reduction current response of immunosensor without immobilized anti-HCG added with 50 mIU/mL HCG. Moreover, it showed that the studied immunosensor exhibited good selectivity.

3.8. Application of the immunosensor in serum sample

In order to demonstrate the possibility of the proposed immunosensor to be applied for clinical analysis, five serum samples with different infection degrees from hospital were examined with this method and Access™ analyzer, a commonly used analyzer in clinic laboratory. The results were listed in Table 1. It was found that there is a good correlation between the results given by two methods. The relative deviations between two methods were in the range of −7.5 to 7.9%. Thus, the present method could satisfy the requirements for determining HCG in human serum in clinical laboratory.

4. Conclusions

In this paper, we described a new strategy for developing an amperometric immunosensor based on layer-by-layer self-assembly of nano-Au and methylene blue on the glassy carbon electrode modified by thiourea for detection of human chorionic gonadotrophin (HCG). Thiourea (NH_2CSNH_2) has two amino groups (R-NH_2) that the one can be immobilized onto surface of the pretreated GCE through cyclic voltammetry and the other can be used for coupling of gold nanoparticles, while nano-Au has a large surface area to increase the immobilization amount of antibody. The immunosensor system could provide high sensitivity, low detection limit, good selectivity and specificity for the assay of HCG.

Acknowledgement

Financial support of this work was provided by the National Natural Science Foundation of China (20675064), the Natural Science Foundation of Chongqing City, China (No. CSTC-2004BB4149, 2005BB4100) and High Technology Project Foundation of Southwest University (No. XSGX02).

References

[1] E. Martlbauer, E. Usleber, E. Schneider, R. Dietrich, Analyst 119 (1994) 2543.
[2] M.C. Hennion, D. Barcelo, Anal. Chim. Acta 362 (1998) 3.
[3] A.G. Miguel, P. Rosa, M. Angel, Trends Anal. Chem. 18 (1999) 204.
[4] N. Isao, I. Sakiko, S. Nobuko, K. Hidenobu, M. Hiroshi, A. Yoshihiro, O. Masahisa, Clin. Chem. 37 (1991) 1639.
[5] A.K. Paul, G. Gisele, Anal. Biochem. 268 (1999) 173.
[6] J. Wang, Anal. Chem. 71 (1999) 328R.
[7] D.P. Tang, R. Yuan, Y.Q. Chai, X. Zhong, Y. Liu, J.Y. Dai, Biochem. Eng. J. 22 (2004) 43.
[8] R.F. Taylor, I.G. Marenchic, R.H. Spencer, Anal. Chim. Acta 249 (1991) 67–90.
[9] A. Ramanaviciene, A. Ramanavocous, Biosens. Bioelectron. 20 (2004) 1076.
[10] K. Yagiuda, A. Hemmi, S. Ito, Y. Asano, Biosens. Bioelectron. 11 (1996) 703.
[11] D.P. Tang, R. Yuan, Y.Q. Chai, J.Y. Dai, X. Zhong, Y. Liu, Bioelectrochemistry 65 (2004) 15.
[12] V. Ganesan, S.A. John, R. Ramaraj, J. Electroanal. Chem. 502 (2001) 167.
[13] B.P. Simón, E. Fàbregas, Biosens. Bioelectron. 19 (2004) 1131.
[14] J. Razumiene, R. Meškys, V. Gureviėiene, V. Laurinaviėius, M.D. Reshetova, A.D. Ryabov, Electrochem. Commun. 2 (2000) 307.
[15] B.Q. Wang, S.J. Dong, Talanta 51 (2000) 565.
[16] L.A. Godinez, Res. Soc. Quim. Mex. 43 (1999) 219.
[17] A. Ulman, An Introduction to Ultrathin Organic Films from Langmuir-Blodgett to Self-Assembly, Academic Press, New York, 1991.
[18] J.D. Swalen, D.L. Allara, J.D. Andrade, E.A. Chandross, S. Graoff, J. Israelachvili, T.J. McCarthy, R. Murray, R.F. Pease, J.F. Rabolt, K.J. Wynne, H. Yu, Langmuir 3 (1987) 932.
[19] L. Wang, E. Wang, Electrochem. Commun. 6 (2004) 225.
[20] S.Y. Xu, X.Z. Han, Biosens. Bioelectron. 19 (2004) 1117.
[21] M.A. Hyatt, Colloidal Gold: Principles, Methods and Applications, vol. 3, Academic Press, New York, 1989.
[22] G. Decher, Science 277 (1997) 1231.
[23] Y. Lvov, in: Y. Lvov, H. Mohwald (Eds.), Protein Architecture: Interfacing Molecular Assemblies and Immobilization Biotechnology, Marcel Dekker, New York, 2000, pp. 125–166.
[24] J.F. Rusling, in: Y. Lvov, H. Mohwald (Eds.), Protein Architecture: Interfacing Molecular Assemblies and Immobilization Biotechnology, Marcel Dekker, New York, 2000, pp. 337–354.
[25] J.F. Rusling, Z. Zhang, in: R.W. Nalwa (Ed.), Handbook of Surfaces and Interfaces of Materials, vol. 5: Biomolecules, Biointerfaces, and Applications, Academic Press, San Diego, CA, 2001, pp. 33–71.
[26] B. Steven, K. Galina, O. John, Arch. Med. Res. 32 (2001) 635.

[27] Y. Zhuo, R. Yuan, Y.Q. Chai, D.P. Tang, Y. Zhang, X.L. Li, N. Wang, Q. Zhu, Electrochem. Commun. 7 (2005) 355.
[28] Q. Zhu, R. Yuan, Y.Q. Chai, N. Wang, Y. Zhuo, Y. Zhang, X.L. Li, Electrochim. Acta 51 (2006) 3763.
[29] Y.T. Shi, R. Yuan, Y.Q. Chai, M.Y. Tang, X.L. He, Electrochim. Acta 52 (2007) 3518.
[30] G. Frens, Phys. Sci. 241 (1973) 20.
[31] B.V. Enustun, J.J. Turkevich, J. Am. Chem. Soc. 85 (1963) 3317.
[32] W. Limbut, P. Kanatharana, B. Mattiasson, Anal. Chim. Acta 561 (2006) 55.
[33] Z.L. Cheng, E.K. Wang, X.R. Yang, Biosens. Bioelectron. 16 (2001) 179.

Available online at www.sciencedirect.com
ScienceDirect
Talanta 74 (2008) 1547–1555
Talanta
www.elsevier.com/locate/talanta

Evaluation of semiquantitative analysis mode in ICP-MS

Heidi Chen [a,*], Ewa Dabek-Zlotorzynska [a], Pat E. Rasmussen [b], Nouri Hassan [b,1], Monique Lanouette [b]

[a] *Analysis and Air Quality Division, Environmental Science and Technology Centre, Environment Canada, 335 River Road, Ottawa, Ontario, Canada K1A 0H3*
[b] *Environmental Health Sciences Bureau, AL0803C, Health Canada, 50 Columbine Driveway, Ottawa, Ontario, Canada K1A 0K9*

Received 6 July 2007; received in revised form 27 September 2007; accepted 28 September 2007
Available online 7 October 2007

Abstract

Semiquantitative analysis mode in inductively coupled plasma mass spectrometry (ICP-MS) has been popularly used for fast screening purposes. Although the benefit of it has been studied by many researchers, its performance of application in real-world routine analyses has not been reported.

In this study, we evaluated the reliability of semiquantitative analysis mode through inter-laboratory comparison using two different ICP-MS systems with one multi-element calibration standard. The suitability of semiquantitative analysis mode in routine analysis laboratory was demonstrated by evaluating its application in different laboratories and in real production laboratory practices. Twenty one elements were measured, namely, Be, B, Al, Ti, V, Cr, Mn, Co, Ni, Cu, Zn, As, Sr, Mo, Ag, Cd, Sn, Sb, Ba, Tl, and Pb in various fresh water reference samples. Good results concerning accuracy (relative percentage error within 10%) and reproducibility (relative standard deviation lower than 5%) were obtained in more than 90% analyzed samples at concentrations equal to or greater than 10 times the detection limit (DL). Semiquantitative analysis mode also enabled the determination of elements that are not present in the calibration standard. The results demonstrated the potential of semiquantitative analysis mode as a reliable approach in routine laboratory determination of simple matrices, where high throughput and cost-effectiveness are desired, as well as in emergency situations where speed of analysis is critical and quite often limited sample information is available.
© 2007 Elsevier B.V. All rights reserved.

Keywords: Semiquantitative analysis mode; ICP-MS; Inter-laboratory comparison; Routine laboratory analysis

1. Introduction

Inductively coupled plasma mass spectrometry (ICP-MS) has become a popular technique in multi-element analysis since the first commercial instrument became available in 1980s. Semiquantitative analysis by ICP-MS has proven to be a powerful tool for fast screening, in addition, it does not require the element of interest to be present in the calibration standard [1,2], making it especially useful for the analysis of unknown samples.

Typically, the accuracy of quantitative analysis is better than 10% and semiquantitative analysis is between 30% and 50% [3]. An early version of semiquantitative analysis software was critically investigated by Amarasiriwardena et al. [4], where selected elements with known concentrations (internal references) were used to perform external calibration and as internal standards to reduce matrix mismatch problems and compensate for instrument drift during the analysis. The best accuracy was achieved when the response table was divided into three groups based on relative atomic mass, with one internal reference per group. The accuracy was found to be within 30% for a variety of certified reference materials with different matrices.

Semiquantitative analysis by ICP-MS involves the use of a pre-determined response factor for each element, which is defined as ion counts per unit concentration. Many instruments provide semiquantitative analysis software containing a database or table of the response factors for all elements that can be determined by ICP-MS. Some ICP-MS instruments are equipped with a semiquantitative analysis mode that enables the removal of spectral interference contribution by interpreting the whole spectrum.

* Corresponding author.
E-mail address: Chen.H@forces.gc.ca (H. Chen).
[1] Current address: Worsfold Water Quality Centre, Trent University, 1600 West Bank Drive, Peterborough, Ontario, Canada K9J 7B8.

0039-9140/$ – see front matter © 2007 Elsevier B.V. All rights reserved.
doi:10.1016/j.talanta.2007.09.037

It has been reported that by using the semiquantitative analysis mode in ICP-MS, an accuracy better than 30% can be achieved without any external calibration [5]. However, accuracy can be improved by updating the element response factors prior to analysis through the measurement of a multi-element standard solution. A typical semiquantitative analysis mode uses a one-point or two-point calibration (usually with a blank as one calibration point). The multi-element standard solution may contain a few elements that cover the mass range to be analyzed, however, the presence of more elements in the calibration standard may result in a better accuracy. Matrix matching and introduction of internal standard(s) and/or internal calibration may also improve the accuracy of the analysis. Levels of accuracy equal to or better than 10% have been reported for some elements in biological standard reference materials [6] and in drinking water certified reference material [7] with some of these approaches using semiquantitative analysis mode. Better results were reported when using a molar response curve instead of commercial software offered by instrument manufacturers [8–10]. By comparing the uncertainities of semiquantitative and quantitative analysis results, Laborda et al. [11] found that the quality of semiquantitative results, in terms of measurement uncertainty, are equal to or even better than those obtained by quantitative analyses over a wide concentration range (0.01–100 $\mu g\,L^{-1}$). It has been reported that the number of calibration standards used in ICP-MS is not critical to the quality of the results [12].

The objective of this work was to evaluate and demonstrate the potential of semiquantitative analysis as a reliable routine analysis tool for trace metals in simple environmental samples through inter-laboratory comparison of results on a few natural water certified reference materials. The results from one of the laboratories were obtained under real production laboratory practices, and the method was applied to inter-laboratory proficiency testing program samples. The ICP-MS instruments are different between the two laboratories involved in the comparison, as is the semiquantitative analysis software, one using a one-point calibration, the other using a two-point calibration.

2. Experimental

2.1. Apparatus

2.1.1. Environment Canada laboratory

Measurements were made using an Agilent Technologies 7500c ICP-MS system (Agilent Technologies, Wilmington, DE, USA) equipped with an octopole collision/reaction cell, the Agilent 7500 ICP-MS ChemStation software, a Babington nebulizer, a Peltier cooled (2 °C) quartz Scott-type double pass spray chamber and an Agilent I-AS integrated autosampler. The instrument was optimized daily in terms of sensitivity (Li, Y, and Tl), level of oxide (Ce) and doubly charged ion (Ce) using a tuning solution containing 10 μg/L of Li, Y, Tl, Ce, and Co in 2% HNO_3 (w/v), standard optimization procedures and criteria specified in manufacturer's manual were followed, and the typical operating conditions are summarized in Table 1.

Table 1
Optimum operating conditions

	Agilent 7500c	ELAN DRC (II)
Operation parameters		
RF power (W)	1300–1500	1100
Plasma gas flow (L/min)	15	15
Nebulizer gas flow (L/min)	1.00–1.12	0.88–0.92
Auxiliary gas flow (L/min)	0.9	1.2
Sample uptake rate (mL/min)	0.35	1
RPq		0.25
Data acquisition		
Acquisition mode	Peak hopping	
Integration time (s)	0.1–0.3/point	
Peak pattern (SemiQ)	6 points/peak	
Peak pattern (FullQ)	3 points/peak	
Repetition	3 (SemiQ), 5 (FullQ)	
Acquisition mode		Peak hopping
Dwell time (ms)		50
Sweeps/Reading		10
Readings/Replicate		1
Number of replicates		3

2.1.2. Health Canada laboratory

Measurements were made using a Perkin-Elmer SCIEX ELAN DRC (II) Axial Field Technology (SCIEX, Concord, ON, Canada) equipped with ELAN Version 2.4 Software, a Meinhard quartz nebulizer, a cyclonic quartz spray chamber, and an AS93Plus autosampler (Perkin-Elmer). The instrument was optimized daily in terms of sensitivity, level of oxide and doubly charged ion using a tuning solution (details in Section 2.2). Standard optimization procedures and criteria specified in manufacturer's manual were followed. Typical operating conditions are summarized in Table 1.

2.2. Reagents and standards

2.2.1. Environment Canada laboratory

Double-deionized water (18 MΩ cm) (Millipore, Milli RO-15 Super-Q systems, Bedford, MA, followed by Barnstead, Nanopure Diamond™) was used throughout the work. High purity concentrated HNO_3 was obtained by purifying concentrated HNO_3 (70%, w/v) (Fisher, ACS Plus, Ottawa, Canada) with duoPUR Subboiling Distillation System (Milestone, Sorisole, BG, Italy). The multi-element calibration standards for multi-point (level) calibration were prepared by mixing *Plasma*CAL Calibration Standard 1–5 (multi-element standards with assorted concentrations) and 1000 mg/L Sn single element calibration solution (SCP Science, Baie D'Urfé, QC, Canada). The multi-element calibration standard for single-point calibration (100 μg/L) was prepared from 10 mg/L multi-element *Plasma*CAL ICP-MS Verification Standard 1 and 2 (SCP Science), or from 100 mg/L multi-element CLÅRITAS PPT® Instrument Calibration Standard 2 (SPEX CertiPrep, Inc., Metuchen, NJ, USA). The internal standard solution of 1 mg/L of Sc, Y, Rh, In, Tb, Ho and Bi in 5% (v/v) HNO_3 was prepared from 100 mg/L *Plasma*CAL single Internal Standard Stock solutions (SCP Science). Tuning solution for the Agilent 7500c (10 μg/L of Li, Y, Ce and Tl in 2% (w/v) HNO_3) was either purchased

Table 2
Detection limits

Isotope	Integration time EC (s)	EC FullQ (μg/L) ($n=7$)	EC SemiQ (μg/L) ($n=21$)	Element	Dwell time HC (s)	HC TotalQ (μg/L) ($n=8$)
^{9}Be	0.2	0.004	0.007	Be	0.05	0.002
^{11}B	0.1	0.07	0.09	B	n/a	n/a
^{27}Al	0.01	0.06	0.1	Al	0.05	0.3
^{47}Ti	0.1	n/a	0.08	Ti	n/a	n/a
^{51}V	0.1	0.005	0.04	V	0.05	n/a
^{53}Cr	0.1	0.02	0.1	Cr	0.05	0.06
^{55}Mn	0.1	0.007	0.01	Mn	0.05	0.01
^{59}Co	0.2	0.003	0.005	Co	0.05	0.004
^{60}Ni	0.2	0.004	0.01	Ni	0.05	n/a
^{65}Cu	0.1	0.01	0.02	Cu	0.05	0.01
^{66}Zn	0.3	0.3	0.3	Zn	0.05	0.1
^{75}As	0.3	0.01	0.09	As	0.05	0.004
^{88}Sr	0.1	n/a	0.008	Sr	0.05	0.01
^{95}Mo	0.2	0.006	0.008	Mo	n/a	n/a
^{107}Ag	0.2	0.2	0.1	Ag	0.05	0.03
^{111}Cd	0.3	0.003	0.006	Cd	0.05	0.003
^{118}Sn	0.1	0.006	0.01	Sn	n/a	n/a
^{121}Sb	0.1	0.009	0.02	Sb	n/a	n/a
^{137}Ba	0.1	0.02	0.02	Ba	0.05	0.01
^{205}Tl	0.1	0.003	0.007	Tl	0.05	0.003
Pb	0.1	0.007	0.03	Pb	0.05	0.004

from Agilent Technologies (Wilmington, DE, USA), or prepared from 1000 μg/mL *Plasma*CAL single element standards (SCP Science). All standard and sample preparation and transfer were carried out in a PURIFIER® Trace Metal Work Station (Labconco Corporation, Kansas City, MO, USA) which is a total exhaust clean bench that provides Class-100 air.

2.2.2. Health Canada laboratory

Deionized distilled water (18.2 MΩ cm) (Milli-Q Element, Bedford, MA, USA) was used throughout the study. Ultra pure concentrated HNO_3 (70%, w/w) was obtained from Seastar Chemicals Inc., Sidney, BC. The calibration standards were prepared using *Plasma*CAL single element standards, and a mixed internal standard solution (25 μg/L for all elements except for Li, which was 50 μg/L) was prepared using Sc, In, Ho, Tb, Th and Tl CLÅRITAS PPT® standards and Li, Rh, Re, and Y *Plasma*CAL standards. The internal standard solution also contained 0.01% Triton X-100 (OmniPur EM SCIENCE, MERCK KGaA, Damstadt, Germany). The Elan 6100 DRC ICP-MS Sensitivity Detection Limit Solution was used as the tuning solution and contained 1.0 μg/L Be, Co, In, U, Mg, Rh, Pb, Na, Fe, Ca, K, Ba, Ce in 0.5% (v/v) HNO_3 and was purchased from Perkin-Elmer Ltd. (ON, Canada) where In, Mg, Pb and U are verified for sensitivity, Ce for oxide levels and Ba for double charged ions.

2.2.3. Certified reference materials

The Certified Reference Materials (CRMs) used in this study include: SLRS-4 (River Water Reference Material for Trace Metals, National Research Council, Ottawa, ON, Canada), TM24.2 (a Low Level Fortified Standard for Trace Elements made in filtered and diluted Lake Ontario water, National Water Research Institute, Environment Canada), TMDWS (a Trace Element Fortified Sample made in filtered and diluted Lake Ontario water, National Water Research Institute, Environment Canada), and a NIST1640 Standard Reference Material (SRM) (Natural Fresh Water, National Institute for Science and Technology, Gaithersburg, MD, USA).

2.3. Data acquisition

2.3.1. Environment Canada laboratory

Data were acquired using Agilent SemiQuant software for a one-point calibration, and FullQuant software for a multi-point (level) calibration. Be, B, Al, Ti, V, Cr, Mn, Co, Ni, Cu, Zn, As, Sr, Mo, Ag, Cd, Sn, Sb, Ba, Tl, and Pb were measured. The isotopes measured for each element are shown in Table 2. The SemiQuant Mode can provide one-point calibration with or without blank subtraction, the former being equivalent to a two-point calibration. In this study, a one-point calibration was used, where a single multi-element calibration standard (100 μg/L) was analyzed before sample analysis to update the response factors. For FullQuant Mode, a 7–8-level calibration was used (7-level calibration for Be, Cd, Mn, Pb and Zn, and Ag, B, Sb and Tl, and 8-level calibration for the rest of the elements). The determination of calibration levels was based on the effort to cover as wide a concentration range as possible, while avoiding possible memory effect caused by some elements at high concentrations, such as Ag, Tl and Pb, presented in different groups (standards) of elements. Analysis in both SemiQuant and FullQuant Modes were carried out with internal standard (Sc, Y, In and Ho) correction to compensate for instrumental drift during the analysis, and to reduce some matrix effect. The internal standard correction was performed by updating the mass response curve against the measured internal standard values. The internal standard solution was added on-line using Agilent on-line ISTD addition kit (Agilent Technologies, Wilmington, DE, USA). The effective concentration of the 1 mg/L internal standards after mixing with

the analytes was about 50 μg/L. Pb was determined using the sum of the intensities for its three major isotopes (^{206}Pb, ^{207}Pb and ^{208}Pb) to account for isotopic variation in the samples and standards.

2.3.2. Health Canada laboratory

Data were acquired using Perkin-Elmer ELAN TotalQuant, and Quantitative Analysis Method. TotalQuant was used for a two-point calibration with a blank value as one-point, it was calibrated with a 100 μg/L multi-element standard and a calibration blank solution. Quantitative Analysis Method was used for multi-point (level) calibration, it was carried out using an eight-level calibration (0.05, 0.1, 0.5, 5, 10, 50, 100, 500 μg/L). The TotalQuant software does not provide results related to specific isotopes. The internal standards were selected so that they are within 50 amu of the analyte and are not present in the analyte matrix. Li, Sc, Ho and Th were used as internal standard for analyses by TotalQuant Mode, while Y, In, Re and Rh were used for analyses conducted with Quantitative Analysis Method. The internal standard was applied on-line to each blank, calibration standard and sample using a flow/mixing Tee-connector from Pulse instrumentation (part number 116-B332-01), where the internal standard is pumped at 20 rpm using 0.38 mm inside diameter PVC pump tubing (part number 116-0549-04; orange-green; Pulse Instrumentation) and 0.76 mm inside diameter PVC sample pump tubing (part number 116-0549-070; black-black; Pulse Instrumentation).

3. Results and discussion

3.1. Detection limits

The detection limits (DLs) and the corresponding dwell time for the one or two-point calibration and multi-point calibration are shown in Table 2, and in both laboratories were calculated as three times standard deviation of the blanks.

For routine laboratory practices, variation of blank preparation and measurement between days is very important and should be taken into consideration when detection limit is calculated. Therefore, the DLs from the Environment Canada laboratory using SemiQuant Mode were obtained by analyzing seven replicate analyses per run (day) of the blank (1% HNO_3, v/v), each from a different autosampler vial, and ran for three non-consecutive days, using a 10 μg/L multi-element solution as calibration standard. The DLs using FullQuant Mode were obtained by analyzing seven replicates of the blank (1% HNO_3, v/v), each from a different autosampler vial.

The DLs from the Health Canada laboratory from TotalQuant Mode were obtained by analyzing eight blanks (1% HNO_3, v/v) on different days, using a 10 μg/L multi-element solution as calibration standard.

The DLs listed in Table 2 are for information only, and DL comparison between the two laboratories should not be made as they were obtained from different instruments, different software and by different approaches.

3.2. Accuracy

3.2.1. Analysis of CRMs and SRM samples

The accuracy of the analyses using one or two-point calibration was evaluated first through inter-laboratory (Environment Canada and Health Canada laboratories) comparison of results obtained by analyzing various CRMs (SLRS-4, TM24.2, TMDWS) and SRM (NIST1640) samples. Relative percentage error (RPE) was used to represent the accuracy of the results, which was calculated as follows:

$$\text{RPE} = 100\,(\text{measured value} - \text{certified value})/\text{certified value}$$

Mean values of RPEs of TMDWS (Environment Canada laboratory only), SLRS-4, TM24.2, and NIST1640 samples were plotted against the ratio of concentration over DL (c/DL) (Fig. 1). Results for samples at concentrations lower than three times DL are not shown in the graph. A larger variation in RPEs was observed for samples at concentrations lower than 10 times DL. At higher concentration (≥10 DL), about 90% of the results agreed within ±10% of the target values; and 98% of the results agreed within ±15% of the target values. Similar to the observation by Almeida and Vasconcelos [13] and Amarasiriwardena et al. [6], some elements showed worse results (RPE worse than 10%) than others. For example, RPE worse than 10% was obtained by Environment Canada laboratory for Be, Sr, Sb, Sn and Zn; and for Be, Ag and Zn by Health Canada laboratory. It was interesting to observe that both instruments gave results with RPE >10% on Be and Zn in TM24.2, indicating the worse RPE was possibly associated with matrices. The results and their associated uncertainties at 95% confidence limit are shown in Tables 3–6.

Paired *t*-tests were performed to compare the results (covering all elements and CRMs and SRM) obtained by SemiQuant or TotalQuant to the certified values. No significant difference was found, at 95% confidence level, between the certified values and the SemiQuant or TotalQuant results.

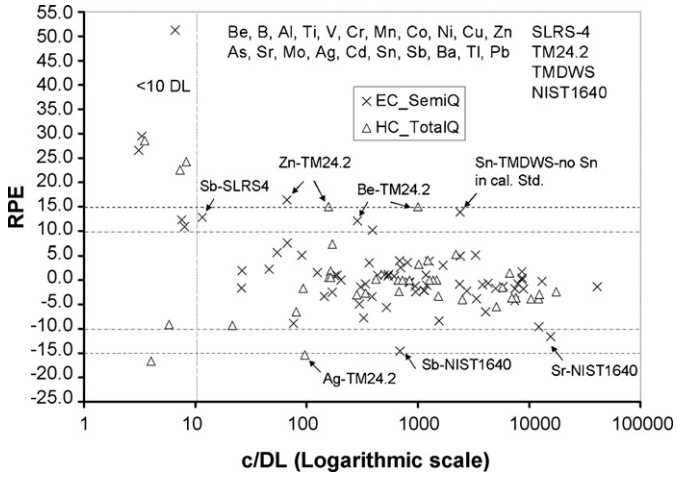

Fig. 1. Accuracy (relative percentage error) of semiquantitative analysis mode of three certified reference materials and one standard reference material from Environment Canada (EC_SemiQ) and Health Canada (HC_TotalQ) laboratories as a function of the ratio of the certified concentration (c) of each element to their respective detection limits (DLs).

Table 3
Inter-laboratory comparison on results of SLRS 4 obtained from semi and full quantitative analysis modes (95% confidence level)

Element	Certified value (μg/L)	EC_FullQ (μg/L) ($n=3$)	EC_SemiQ (μg/L) ($n=37$)	HC_FullQ (μg/L) ($n=3$)	HC_TotalQ (μg/L) ($n=3$)
Be	0.007 ± 0.002	<DL	<DL	0.010 ± 0.002	0.009 ± 0.002
Al	54 ± 4	52 ± 2	54.5 ± 0.9	55 ± 2	55 ± 2
V	0.32 ± 0.03	0.37 ± 0.07	0.355 ± 0.005	0.33 ± 0.02	0.34 ± 0.05
Cr	0.33 ± 0.02	0.29 ± 0.05	0.43 ± 0.02	0.35 ± 0.02	0.30 ± 0.05
Mn	3.37 ± 0.18	3.36 ± 0.12	3.34 ± 0.04	3.38 ± 0.20	3.28 ± 0.05
Co	0.033 ± 0.006	0.059 ± 0.003	0.050 ± 0.002	0.042 ± 0.005	0.041 ± 0.010
Ni	0.67 ± 0.08	0.73 ± 0.05	0.72 ± 0.01	0.63 ± 0.02	0.80 ± 0.15
Cu	1.81 ± 0.08	1.83 ± 0.11	1.90 ± 0.03	1.84 ± 0.02	1.82 ± 0.20
Zn	0.93 ± 0.10	1.12 ± 0.13	1.18 ± 0.02	1.06 ± 0.10	1.14 ± 0.32
As	0.68 ± 0.06	0.9 ± 0.5	0.76 ± 0.01	0.76 ± 0.07	0.73 ± 0.05
Sr	26.3 ± 3.2	n/a	27.6 ± 0.3	27.0 ± 0.5	27.7 ± 0.5
Mo	0.21 ± 0.02	0.21 ± 0.02	0.214 ± 0.005	0.240 ± 0.007	n/a
Cd	0.012 ± 0.002	n/a	0.020 ± 0.004*	0.014 ± 0.002	0.010 ± 0.002
Sb	0.23 ± 0.04	0.26 ± 0.15	0.26 ± 0.01	0.26 ± 0.01	n/a
Ba	12.2 ± 0.6	12.5 ± 1.0	12.3 ± 0.2	12.8 ± 1.0	12.6 ± 0.5
Pb	0.086 ± 0.007	0.12 ± 0.08	0.099 ± 0.002	0.084 ± 0.002	0.078 ± 0.005

* $n=16$.

The effect of the presence/absence of analyte in calibration standard was studied. Two types of calibration standards were used for SemiQuant Mode analysis, one without Sn and Sb, and the other one without B. The CRMs were analyzed using both types of calibration standard and the results are shown and compared in Tables 7a and 7b. Regardless of the presence of Sn, Sb or B in the calibration standard, all RPEs were below 10% with the exception of Sb in SLRS-4, where the concentration is just above 10 DL. Statistical analyses have shown that, at 95% confidence level, the absence or presence of B and Sb in the calibration standard did not make a significant difference in the results of all applicable CRMs. While the same conclusion was obtained for Sn in TM 24.2, a significantly better result in TMDWS was obtained when Sn was present in the calibration standard. It is not clear why it happened in this case, but in general, satisfying results were obtained regardless the presence or absence of the analyte in the calibration standard. Despite the problem with Sn results, semiquantitative analysis mode is advantageous over full quantitative analysis mode in analyzing samples with limited information since it has the unique feature to provide information on analytes that are not present in calibration standard, and our work demonstrated that quality results on these analytes could be achieved.

3.2.2. *Comparison of SemiQuant/TotalQuant Mode with FullQuant Mode on CRMs and SRM determination*

The results from SemiQuant and TotalQuant for SLRS-4, TM24.2 and NIST1640 samples were then compared to those obtained by multi-point calibration using FullQuant Mode (Tables 3–6). The RPEs plotted against c/DL at concentrations

Table 4
Inter-laboratory comparison on results of TM 24.2 obtained from semi and full quantitative analysis modes (95% confidence level)

Element	Certified value (μg/L)	EC_FullQ (μg/L) ($n=3$)	EC_SemiQ (μg/L) ($n=48$)	HC_TotalQ (μg/L) ($n=3$)
Be	2.0 ± 0.03	2.0 ± 0.2	2.24 ± 0.05	2.3 ± 0.2
Al	30.6 ± 0.6	28.9 ± 1.3	30.2 ± 0.6	30.1 ± 2.0
V	6.8 ± 0.1	7.1 ± 0.5	6.6 ± 0.1	6.6 ± 0.5
Cr	4.6 ± 0.1	4.6 ± 0.1	4.70 ± 0.05	4.3 ± 0.5
Mn	8.4 ± 0.1	8.6 ± 0.4	8.4 ± 0.1	8.4 ± 1.0
Co	5.9 ± 0.1	6.1 ± 0.3	5.96 ± 0.05	5.9 ± 0.5
Ni	5.0 ± 0.1	5.2 ± 0.3	5.06 ± 0.04	4.6 ± 0.2
Cu	7.3 ± 0.1	7.8 ± 0.3	7.56 ± 0.06	7.3 ± 0.7
Zn	20 ± 0.5	27 ± 4	23.3 ± 0.5	23 ± 2
As	4.9 ± 0.1	5.4 ± 0.5	5.18 ± 0.05	5.1 ± 0.5
Sr	69 ± 0.5	n/a	69.1 ± 0.6	68 ± 8
Mo	5.6 ± 0.1	6.1 ± 0.6	5.74 ± 0.06	n/a
Ag*	2.6	2.6 ± 0.1	2.56 ± 0.03	2.2 ± 1.5
Cd	4.1 ± 0.04	4.4 ± 0.3	4.26 ± 0.04	4.1 ± 0.1
Sn*	3.9	4.2 ± 0.1	4.3 ± 0.1	3.8 ± 0.2
Sb	2.5 ± 0.06	2.6 ± 0.1	2.54 ± 0.05	n/a
Ba	8.7 ± 0.1	8.7 ± 0.8	8.8 ± 0.1	8.7 ± 0.7
Tl	3.8 ± 0.06	3.7 ± 0.6	3.84 ± 0.06	3.8 ± 0.2
Pb	6.1 ± 0.1	5.6 ± 1.3	6.10 ± 0.07	5.9 ± 0.1

* Value for information only.

Table 5
Inter-laboratory comparison on results of NIST 1640 obtained from semi and full quantitative analysis modes (95% confidence level)

Element	Certified value** μg/kg (μg/L)	EC_FullQ (μg/L) ($n=4$)	EC_SemiQ (μg/L) ($n=5$)	HC_FullQ (μg/L) ($n=3$)	HC_TotalQ (μg/L) ($n=3$)
Be	34.94 (34.99) ± 0.41	36.0 ± 1.8	34.4 ± 1.4	35.3 ± 3.7	34.1 ± 7.2
B	301.1 (301.6) ± 6.1	320 ± 15	290.0 ± 8.8	306.3 ± 3.7	n/a
Al	52.0 (52.1) ± 1.5	50.5 ± 1.5	49.2 ± 1.4	52.4 ± 2.0	52.4 ± 4.5
V	12.99 (13.01) ± 0.37	13.83 ± 0.44	12.00 ± 0.00	13.0 ± 0.5	12.9 ± 1.7
Cr	38.6 (38.7) ± 1.6	37.8 ± 1.4	37.4 ± 1.1	38.1 ± 2.5	37.8 ± 1.5
Mn	121.5 (121.7) ± 1.1	125.8 ± 2.2	110.0 ± 0.0	123.5 ± 7.4	117.1 ± 0.5
Co	20.28 (20.31) ± 0.31	21.14 ± 0.46	19.00 ± 0.88	20.5 ± 2.0	19.2 ± 1.5
Ni*	27.4 (27.4) ± 0.8	27.8 ± 0.4	26.8 ± 1.0	27.5 ± 1.2	26.9 ± 2.0
Cu*	85.2 (85.3) ± 1.2	87.5 ± 2.1	84.8 ± 1.6	83.1 ± 5.5	81.9 ± 3.5
Zn*	53.2 (53.3) ± 1.1	55.1 ± 0.5	53.8 ± 1.0	53.7 ± 2.0	53.4 ± 2.0
As	26.67 (26.71) ± 0.41	26.9 ± 1.5	25.4 ± 1.1	26.9 ± 3.0	27.1 ± 0.7
Sr	124.2 (124.4) ± 0.7	n/a	110.0 ± 0.0	122.7 ± 2.2	119.6 ± 5.0
Mo	46.75 (46.82) ± 0.26	48.3 ± 1.9	46.2 ± 2.0	45.6 ± 1.7	n/a
Ag	7.62 (7.63) ± 0.25	7.3 ± 1.4	6.4 ± 1.7	n/a	7.4 ± 0.5
Cd	22.79 (22.82) ± 0.96	23.87 ± 0.41	22.6 ± 1.1	23.0 ± 0.99	22.0 ± 2.0
Sb	13.79 (13.81) ± 0.42	n/a	11.80 ± 0.56	13.70 ± 0.15	n/a
Ba	148.0 (148.2) ± 2.2	152.9 ± 2.2	142.0 ± 5.6	150.2 ± 4.0	144 ± 12
Pb	27.89 (27.93) ± 0.14	28.9 ± 1.1	26.8 ± 1.4	27.20 ± 0.99	26.90 ± 2.5

* Reference value.
** Values in parenthesis are in μg/L, converted from the certified values using $d = 1.0015$ g/cm^3 (g/ml).

greater than 3 DL are shown in Figs. 2 and 3. Better agreement between results was observed for analytes at concentration higher than 10 DL. The accuracy of results obtained from FullQuant Mode was not noticeably better than that obtained by SemiQuant/TotalQuant Mode, as the RPEs of both multi- and one/two-point calibration are mostly within ±10%. One exception was Zn (as marked in Fig. 2, Zn), where RPE from FullQuant Mode is significantly worse (higher), probably due to random contamination. Almeida and Vasconcelos [13] observed a slight negative bias for semiquantitative mode (TotalQuant Mode) results compared to quantitative mode, which was also observed in this study, but only at high concentrations (above 1000 DL) as can be seen in Fig. 2. This may be due to a minor negative bias in pulse/analogue correction factor.

Table 6
Results of TMDWS obtained from semiquantitative analysis mode (95% confidence level)

Element	Certified value (μg/L)	EC_SemiQ (μg/L) ($n=26$)
Be	11.8 ± 0.214	12.2 ± 0.3
B*	86	84 ± 2
Al	155 ± 2.22	142 ± 2
Ti*	15	15.2 ± 0.2
V	45.5 ± 0.501	44.5 ± 0.4
Cr	94.8 ± 0.951	93.6 ± 0.9
Mn	86.2 ± 0.970	86.6 ± 1.0
Co	65.2 ± 0.746	65.0 ± 0.7
Ni	78.9 ± 0.900	78.3 ± 0.7
Cu	178 ± 1.81	175 ± 2
Zn	379 ± 5.19	394 ± 4
As	72.5 ± 1.26	75.1 ± 1.0
Sr	326 ± 3.77	322 ± 3
Mo	68.6 ± 0.757	69.8 ± 0.5
Ag	14.4 ± 0.281	13.9 ± 0.2
Cd	14.2 ± 0.151	14.1 ± 0.2
Sn*	24	27.3 ± 0.5** 25.2 ± 0.3***
Sb	16.7 ± 0.285	16.6 ± 0.3
Ba	149 ± 1.56	146 ± 2
Tl	8.4 ± 0.195	8.3 ± 0.1
Pb	34.2 ± 0.355	33.5 ± 0.3

* Values for information only.
** Determined by using calibration standard without Sn.
*** Determined by using calibration standard containing Sn.

In a routine analysis laboratory, quality of results (accuracy and reproducibility) is important, but analysis time and cost is also important, and similarly, rapid screening is critical in an emergency situation. When using unweighted linear regression for a multi-point calibration (with at least three calibration points), the best results are obtained when sample signals are interpolated close to the center of the calibration interval and this interval is adequately narrow [11]. In other words, a carefully and properly designed calibration is required to achieve the best results, or else multiple data re-processing would be needed when substantially more calibration points are allowed to cover the whole concentration range. Therefore, it is time consuming to apply these strategies for multi-element determination where elements may be at very different concentration levels, and/or for a series of samples present at very different concentration levels. Although weighted linear regression for a multi-point calibration is more advantageous over unweighted linear regression, it is more so for the determination of analytes at low concentrations. On the other hand, one or two-point calibration offered comparable results to multi-point calibration, while only requiring one calibration standard and no data reprocessing. As a result, it is time and cost-effective. Since the dwell time used was the same for SemiQuant and FullQuant Mode, the analysis time (including rinsing in between samples) for each sample was not very different, however, the total time it takes using SemiQuant Mode is much shorter than FullQuant Mode. For example, to analyze 50 samples of about 50 elements, preparation and analysis of the calibration standards and samples took about 30 min less using SemiQuant Mode. However,

Table 7a
Comparison of results on B, Sn, and Sb when they were present in calibration standards

CRM	Element	Certified value (μg/L)	Results* (μg/L)	*N*	Relative error (%)
TMDWS	B	86**	86 ± 3	9	−0.3
TM24.2	Sn	3.9**	4.27 ± 0.07	16	9.5
TMDWS	Sn	24**	25.2 ± 0.3	16	4.9
SLRS4	Sb	0.23 ± 0.04	0.264 ± 0.009	16	15
TM24.2	Sb	2.5 ± 0.06	2.58 ± 0.03	16	3.3
TMDWS	Sb	16.7 ± 0.285	16.4 ± 0.2	16	−1.9

* Uncertainties associated with the results are based on 95% confidence interval.
** Values for information only.

Table 7b
Comparison of results on B, Sn, and Sb when they were absent in calibration standards

CRM	Element	Certified value (μg/L)	Results* (μg/L)	*N*	Relative error (%)
TMDWS	B	86**	83 ± 2	16	−3.6
TM24.2	Sn	3.9**	4.3 ± 0.1	20	11
TMDWS	Sn	24**	27.3 ± 0.5	9	14
SLRS4	Sb	0.23 ± 0.04	0.26 ± 0.01	21	11
TM24.2	Sb	2.5 ± 0.06	2.51 ± 0.08	20	0.2
TMDWS	Sb	16.7 ± 0.285	17.1 ± 0.5	9	2.5

* Uncertainties associated with the results are based on 95% confidence interval.
** Values for information only.

after the analysis by FullQuant Mode, calibration curve has to be evaluated on each element analyzed, re-processing data is typically necessary, and this took at least 1 h to complete the task. Therefore, in total, it took at least 1 h and half less when using SemiQuant Mode to perform the analysis. This has not counted for the fact that the judgment of calibration curve verification can be analyst dependent, this could therefore contribute to a worse reproducibility and consistency of results.

3.3. Reproducibility

Fig. 4 shows the percentage relative standard deviation (RSD%) of the SemiQuant results from the Environment Canada laboratory (SemiQ, solid diamond) and the Health Canada laboratory (TotalQ, open triangle) plotted against c/DL. The RSDs obtained from the Environment Canada laboratory (SemiQuant) covered a 5-month period of routine analysis using calibration

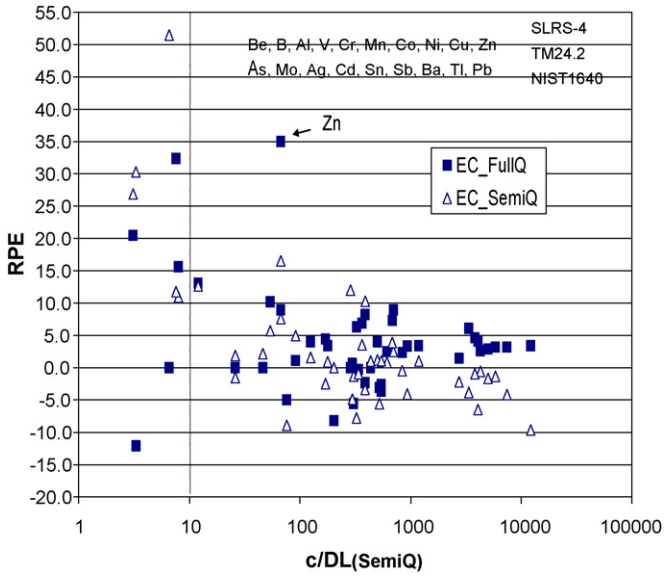

Fig. 2. Accuracy (relative percentage error) comparison of semiquantitative and full quantitative analysis modes of two certified reference materials and one standard reference material obtained by the Environment Canada laboratory as a function of the ratio of the certified concentration (c) of each element to their respective detection limits (DLs).

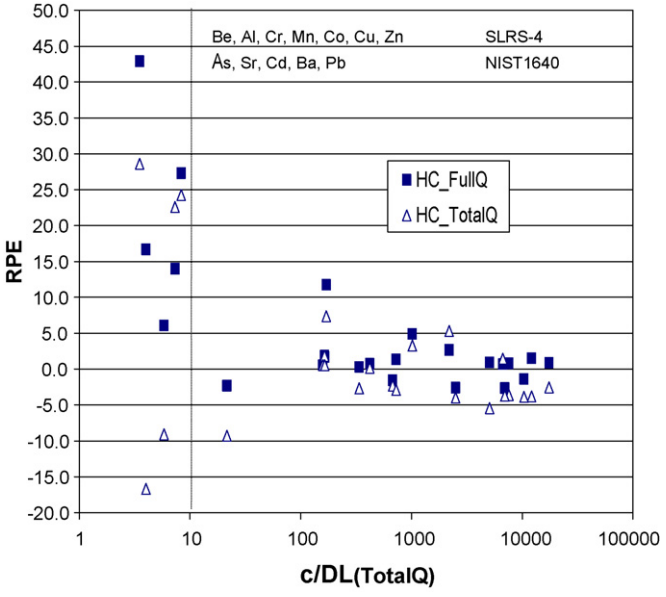

Fig. 3. Accuracy (relative percentage error) comparison of semiquantitative and full quantitative analysis modes for determining one certified reference material and one standard reference material obtained by the Health Canada laboratory as a function of the ratio of the certified concentration (c) of each element to their respective detection limits (DLs).

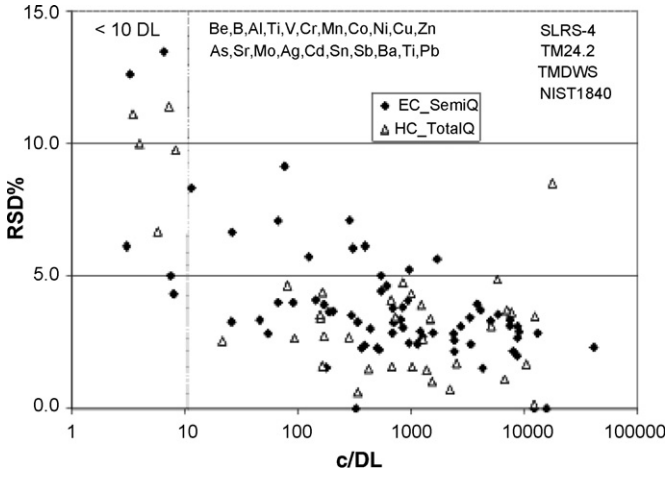

Fig. 4. Reproducibility (percentage relative standard deviation) of semiquantitative analysis mode of three certified reference materials and one standard reference material from Environment Canada (EC_SemiQ) and Health Canada (HC_TotalQ) laboratories as a function of the ratio of the certified concentration (c) of each element to their respective detection limits (DLs).

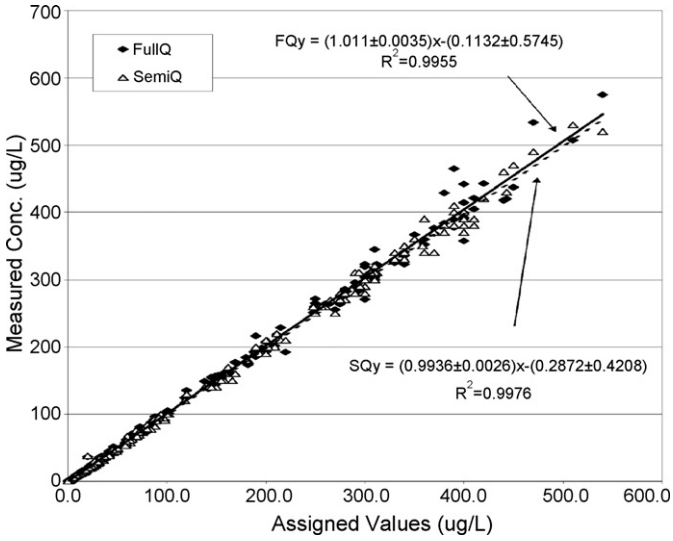

Fig. 5. Comparison of semiquantitative and full quantitative analysis modes results obtained by Environment Canada laboratory on Interlaboratory Proficiency Testing Program samples with respect to the assigned concentrations.

standards from two different sources in which the number and type of elements are slightly different. The RSDs from the Health Canada laboratory (TotalQuant) were calculated from results obtained in 1 month. Overall, good reproducibility (RSD lower than 10%) was obtained by both laboratories. Apparently, the RSDs within a shorter period of analysis (1 month) could be 5% or better.

3.4. Analysis of inter-laboratory proficiency testing (PT) program samples

To further evaluate the performance of SemiQuant Mode, two batches (10 samples per batch) of fortified fresh water samples were analyzed by the Environment Canada laboratory, in participation of a National Water Research Institute Ecosystem Interlaboratory Proficiency Testing Program (FPTM Study 0083 and 0084). Fig. 5 shows that the results obtained by SemiQuant matched the assigned values well (slope 0.9936) compared to those obtained by FullQuant (slope 1.011). It appeared that the spread for the multi-point calibration (FullQuant) was greater than that for the single-point calibration (SemiQuant) at higher concentrations (≥400 DL), demonstrating that SemiQuant is advantageous over FullQuant in analysis over a large concentration range.

In summary, both laboratories used a 100 μg/L calibration standard when using SemiQuant and TotalQuant Mode; the Environment Canada laboratory used a single standard, and the Health Canada laboratory used a blank and a standard for calibration. Overall, the results obtained demonstrated satisfactory accuracy for elements present at concentrations within and above the calibration standard concentration 100 μg/L (e.g., B, Mn, Sr and Ba in NIST1640, Al, Cu, Zn, Sr, and Ba in TMDWS) in the analysis of CRMs, SRM and FPTM study samples. Results from both laboratories showed that when element concentration is greater than 10 times DL, more reproducible results were obtained and accuracy equal to or better than 10% could be achieved. This observation indicated that a quantitation limit of 10 DL seems to be more appropriate than the conventional 10 times the standard deviation (S.D.), at least in our applications on fresh water sample analyses.

4. Conclusions

The reliability of semiquantitative analysis mode in ICP-MS was evaluated by inter-laboratory comparison using CRMs and a SRM, of which the matrices are natural or fortified fresh water. The results were obtained from two different ICP-MS instruments and different semiquantitative analysis software, SemiQuant and TotalQuant, using slightly different calibration protocols: one used a single standard, and the other used a blank and a standard for calibration. Results from two laboratories demonstrated that regardless of the difference of semiquantitative software from different ICP-MS instruments, and regardless of the fact that the analyses were performed in different laboratories, by different analysts, semiquantitative analysis mode could be a reliable and robust alternative to full quantitative mode in routine laboratory practices and emergency situations where rapid screening is required and limited sample information is available. Compared to full quantitative analysis mode, semiquantitative analysis mode allows not only higher sample throughput by simplifying experiment preparation and data re-processing, but also uniquely provides quality results of analytes that are not present in the calibration standard.

Acknowledgements

NH is grateful for financial support in the form of an NSERC visiting fellowship. Thanks go to Marc Chénier (Health Canada) for his assistance.

References

[1] G. Woods, E. McCurdy, S. Wilbur, Interference-free semiquantitative analysis using the 3 Agilent 7500ce ICP-MS, Agilent Application Note 5989-1492EN, 2004.

[2] R.D. Ediger, Totalquant: the answer to the real question. Perkin-Elmer/Sciex, circa Perkin-5 Elmer Corporation, Technical Note TSMS-9, 1997.

[3] H.E. Taylor, R.A. Huff, A. Montaser, Novel applications of ICPMS, in: A. Montaser (Ed.), Inductively Coupled Plasma Mass Spectrometry, Wiley-VCH, New York, 1998, pp. 681–807.

[4] C.J. Amarasiriwardena, B. Gercken, M.D. Argentine, R.M. Barnes, J. Anal. At. Spectrom. 5 (1990) 457.

[5] S. Wilbur, Am. Lab. News 36 (2004) 20.

[6] D. Amarasiriwardena, S.F. Durrant, A. Lásztity, A. Krushevska, M.D. Argentine, R.M. Barnes, Microchem. J. 56 (1997) 352.

[7] J. Soldevila, M.E. Himri, A. Pastor, M. de la Guardia, J. Anal. At. Spectrom. 13 (1998) 803.

[8] J.I. García Alonso, M.G. Camblor, M. Montes Bayón, J.M. Marchante-Gayón, A. Sanz-Medel, J. Mass Spectrom. 32 (1997) 556.

[9] M. Montes Bayón, J.I. Garcia Alonso, A. Sanz-Medel, J. Anal. At. Spectrom. 13 (1998) 1027.

[10] M. Montes Bayón, J.I. Garcia Alonso, A. Sanz-Medel, J. Anal. At. Spectrom. 13 (1998) 277.

[11] F. Laborda, J. Medrano, J.R. Castillo, J. Anal. At. Spectrom. 16 (2001) 732.

[12] F. Laborda, J. Medrano, J.R. Castillo, J. Anal. At. Spectrom. 19 (2004) 1434.

[13] C.M. Almeida, M.T.S.D. Vasconcelos, Anal. Chim. Acta 463 (2002) 165.

Available online at www.sciencedirect.com
ScienceDirect
Talanta 74 (2008) 1132–1140
Talanta
www.elsevier.com/locate/talanta

The application of BTEM to UV–vis and UV–vis CD spectroscopies: The reaction of $Rh_4(CO)_{12}$ with chiral and achiral ligands

Shuying Cheng [a], Feng Gao [b], Karl I. Krummel [a], Marc Garland [a,b,*]

[a] *Department of Chemical and Bimolecular Engineering, National University of Singapore, 4 Engineering Drive 4, Singapore 117576, Singapore*
[b] *Institute of Chemical and Engineering Sciences, 1 Pesek Road, Jurong Island, Singapore 627833, Singapore*

Received 10 July 2007; received in revised form 17 August 2007; accepted 17 August 2007
Available online 23 August 2007

Abstract

Two different organometallic ligand substitution reactions were investigated: (1) an achiral reactive system consisting of $Rh_4(CO)_{12} + PPh_3 \rightleftharpoons Rh_4(CO)_{11}PPh_3 + CO$ in *n*-hexane under argon; and (2) a chiral reactive system consisting of $Rh_4(CO)_{12} + (S)$-BINAP $\rightleftharpoons Rh_4(CO)_{10}$BINAP $+ 2CO$ in cyclohexane under argon. These two reactions were run at ultra high dilution. In both multi-component reactive systems the concentrations of all the solutes were less than 40 ppm and many solute concentrations were just 1–10 ppm. In situ spectroscopic measurements were carried out using UV–vis (Ultraviolet–visible) spectroscopy and UV–vis CD spectroscopy on the reactive organometallic systems (1) and (2), respectively. The BTEM algorithm was applied to these spectroscopic data sets. The reconstructed UV–vis pure component spectra of $Rh_4(CO)_{12}$, $Rh_4(CO)_{11}PPh_3$ and $Rh_4(CO)_{10}$BINAP as well as the reconstructed UV–vis CD pure component spectra of $Rh_4(CO)_{10}$BINAP were successfully obtained from BTEM analyses. All these reconstructed pure component spectra are in good agreement with the experimental reference spectra. The concentration profiles of the present species were obtained by performing a least square fit with mass balance constraints for the reactions (1) and (2). The present results indicate that UV–vis and UV–vis-CD spectroscopies can be successfully combined with an appropriate chemometric technique in order to monitor reactive organometallic systems having UV and Vis chromophores.
© 2007 Elsevier B.V. All rights reserved.

Keywords: BTEM; Spectral reconstruction; $Rh_4(CO)_{12}$; BINAP; UV–vis and UV–vis CD spectroscopy

1. Introduction

Rhodium complexes are frequently used as catalyst precursors for hydroformylation, hydrogenation, cyclotrimerization, etc. [1]. This group of complexes is one of the most extensively studied in organometallic chemistry [2]. A rather large variety of achiral and chiral ligands have been used to modify the reactivity and selectivity of rhodium in catalytic reactions. In particular, mono-dentate and bi-dentate ligands are widely used to generate new mono-nuclear and poly-nuclear rhodium complexes.

The tetranuclear rhodium complex $Rh_4(CO)_{12}$ is a well known and widely used catalyst precursor [1]. It has been shown that $Rh_4(CO)_{12}$ readily reacts with 1 equivalent triphenyl phoshine at room temperature to give the corresponding mono-substituted product Eq. (1) [3]. Alternately, it is known that disubstitution can occur when 2 equivalents of triphenyl phoshine are used [3]. In the present contribution, 1 equivalent of (*S*)-BINAP, a chiral bidentate phosphine [4], will be used Eq. (2). The polynuclear metal cluster $Rh_4(CO)_{12}$ has a very strong red color and all known derivatives are also highly colored. Since it is a chiral naphthalene derivative, (*S*)-BINAP has both intense UV and UV-CD spectra.

$$Rh_4(CO)_{12} + PPh_3 \rightleftharpoons Rh_4(CO)_{11}PPh_3 + CO \quad (1)$$

$$Rh_4(CO)_{12} + (S)\text{-BINAP} \rightleftharpoons Rh_4(CO)_{10}\text{BINAP} + 2CO \quad (2)$$

Organometallics are frequently characterized by NMR [5–7] and FTIR [8–12]. NMR typically requires high solute concentrations, on the order of many milligrams per milliliter. FTIR

* Corresponding author. Tel.: +65 6796 3947; fax: +65 6316 6185.
E-mail address: marc_garland@ices.a-star.edu.sg (M. Garland).

0039-9140/$ – see front matter © 2007 Elsevier B.V. All rights reserved.
doi:10.1016/j.talanta.2007.08.019

analysis can frequently be performed at much lower concentrations or even in situ during catalytic reactions (in the ppm range). Since the molar absorptivities of chromophores in the UV–vis are typically orders of magnitude greater than fundamental vibrations in the IR, UV–vis has the potential for characterizing chromophore-containing organometallics at much lower concentrations. Electronic circular dichroism (ECD) spectroscopy, which measures the difference in absorbance of right- and left-circularly polarized light by a substance, is also a valuable tool to monitor chiral organometallic complexes, particularly complexes of biological and medical importance [13]. Since the phenomenon of electronic circular dichroism spectroscopy is normally many orders of magnitude greater than either vibrational circular dichroism or Raman Optical Activity (ROA), ECD holds the potential for detecting chiral organometallics possessing chromophores at very low concentrations.

Many techniques have been proposed for UV/UV-CD spectroscopic data analysis of multi-component solutions in order to reconstruct the pure component spectra. Basically, the main idea of these methods is to first determine the basis vectors associated with the observed UV/UV-CD spectroscopic data. The most generally used decomposition techniques include principal component analysis (PCA) [14], singular value decomposition (SVD) [15–18] and non-linear iterative partial least-squares (NIPALS) [19]. These basis vectors are then transformed to give the spectral estimates of the pure components in the mixture. Examples include; (1) a self-modelling curve resolution (SMCR) technique based on principal component analysis (PCA) and non-negativity constraints to resolve a two-component mixture system measured using UV/vis spectroscopy introduced by Lawton and Sylvester [14]. (2) A computer-assisted target factor analysis (CAT) algorithm, where SVD was applied to the abstract factor analysis and simple-to-use interactive self-modelling mixture analysis (SIMPLISMA) was applied to optimize UV–vis spectral estimates of the components [20]. (3) A singular value decomposition analysis was applied to a large set of UV-CD spectra measured from a metalloprotein [15].

Although, other SMCR methods have been proposed and implemented, some serious problems remain for spectral resolution of UV–vis data [14–20]. In particular, UV–vis spectra are normally very broad with few distinct features. Moreover, there is often a very high degree of spectral overlap between the spectra of different species. In addition, a prior information of some sort is often needed for spectral reconstruction, i.e. an estimate of the number of species present and/or an estimate of the concentrations of the species present.

In the present contribution band-target entropy minimization (BTEM) is applied to UV–vis data from reactions (1) and (2) in order to reconstruct the pure component spectra. Furthermore, BTEM is successfully applied to the UV–vis-CD data as well to reconstruct the circularly polarized pure component spectra. Although BTEM has been successfully applied to many spectroscopic data sets with non-negative localized signals, i.e. FTIR, Raman, NMR, this is the first time it has been applied to broad UV–vis data. In addition, this is the first application of BTEM to UV–vis-CD spectra which possess both positive and negative parts.

2. Computational section

2.1. Inverse problems and system identification

Both multi-component UV–vis and UV–vis CD measurements obey the Bouguer–Lamber–Beer law in the low concentration range. Consequently, they can be modeled as follows:

$$A_{k\times\nu} = l_{k\times k} C_{k\times s} a_{s\times\nu} + e_{k\times\nu} \tag{3}$$

$$\Delta A_{k\times\nu} = l_{k\times k} C_{k\times s} \Delta\varepsilon_{s\times\nu} + \left[e_{k\times\nu}\right]_{CD} \tag{4}$$

where

$$\Delta\varepsilon = \varepsilon_{\mathrm{L}} - \varepsilon_{\mathrm{R}} \tag{5}$$

In the above equations, $A_{k\times\nu}$ is an absorbance matrix, $C_{k\times s}$ a concentration matrix, $a_{s\times\nu}$ a pure component spectral matrix, ΔA the difference between absorbance of left circularly polarized (LCP) and right circularly polarized (RCP) light, ε_{L} and ε_{R} the molar extinction coefficients for RCP and LCP light, l the path length, subscript k the number of measurements (spectral pattern), subscript s the number of the observed species, subscript ν the number of data channels, subscript CD refers to polarized data and $e_{k\times\nu}$ is error, i.e. the experimental noise and model non-linearity.

In multi-component spectroscopic data analysis, there are three frequent major tasks: (1) determine the number of observable species "s" present (2) determine the pure component spectra of the observable species, i.e. $a_{s\times\nu}$ and $\Delta\varepsilon_{s\times\nu}$ and (3) determine the concentrations $C_{k\times s}$ of all observable species present. These inverse problems are typically ill posed. In order to constrain the problems and hence obtain meaningful solutions, various constraints are usually imposed. Non-negativity in concentrations and non-negativity in pure component spectra $a_{s\times\nu}$ are the most frequently used. Since CD spectra possess both positive and negative parts, a non-negativity constraint cannot be imposed on $\Delta\varepsilon_{s\times\nu}$.

2.2. Band-target entropy minimization (BTEM)

The main system identification task is pure component spectral estimation. Self-modeling curve resolution (SMCR) comprises a family of chemometric techniques which target the reconstruction of pure component spectra from mixture spectroscopic data [21–24]. Band-target entropy minimization, a SMCR technique, was developed to reconstruct the pure component spectra from mixture spectroscopic data without any a priori information such as the number of significant factors present (a priori information is indispensable for many other self-modeling curve resolution methods) [25–29]. In BTEM, the entropy minimization concept is used in the objective function and optimization is performed using Simulated Annealing to give the simplest spectral patterns. Some frequently encountered difficulties in signal processing, such as spectral nonlinearities

arising from shifting band position and changing band shapes, are easily accommodated by the BTEM algorithm. Another important advantage of BTEM is that it can be used to retrieve a pure component with very low concentration (very low signal intensity).

The first step in BTEM is to perform singular value decomposition (SVD) in order to decompose the experimental UV absorbance data, $A_{k\times\nu}$, into three matrices according to Eq. (6), where $U_{k\times k}$ and $\mathrm{V}^{\mathrm{T}}_{\nu\times\nu}$ are the left singular vectors and right singular vectors which form an orthonormal basis, and $\Sigma_{k\times\nu}$ is the corresponding singular value of matrix. The UV–vis-CD data $\Delta A_{k\times\nu}$ can be decomposed in a similar manner Eq. (7).

$$A_{k\times\nu} = U_{k\times k}\Sigma_{k\times\nu}\mathrm{V}^{\mathrm{T}}_{\nu\times\nu} \tag{6}$$

$$\Delta A_{k\times\nu} = \left[U_{k\times k}\Sigma_{k\times\nu}\mathrm{V}^{\mathrm{T}}_{\nu\times\nu}\right]_{CD} \tag{7}$$

The first several row vectors of $\mathrm{V}^{\mathrm{T}}_{\nu\times\nu}$ will consist of meaningful spectral features while the rest will consist primarily of noise. The BTEM algorithm searches the subspace of z basis vectors for the simplest underlying patterns. This is achieved by transforming the abstract right singular vectors in $\mathbf{V}^{\mathrm{T}}$ into pure component spectra estimates, $\hat{a}$ for UV–vis data and $\Delta\hat{\varepsilon}$ for UV–vis-CD data, one-at-a-time using Eqs. (8) and (9).

$$\hat{a}_{1\times\nu} = T_{1\times z}\mathbf{V}^{\mathrm{T}}_{z\times\nu} \tag{8}$$

$$\Delta\hat{\varepsilon}_{1\times\nu} = \left[T_{1\times z}\mathbf{V}^{\mathrm{T}}_{z\times\nu}\right]_{CD} \tag{9}$$

The z transformation elements $T_{1\times z}$ are determined using a non-linear optimization. The objective function Eq. (10) includes two terms: information entropy function (H) and penalty function (P) for non-negativity of the estimated spectra $A_{k\times\nu}$ and their corresponding concentrations:

$$F_{\mathrm{obj}} = H + P \tag{10}$$

In turn, the information entropy function is given by Eq. (11) where h_ν is a discrete probability distribution function and the exponent m is the degree of spectrum differentiation. In the present study, both the first and second derivative were used in the BTEM analyses. These provided good spectral reconstruction for bands having shoulders and for those with severe overlap.

$$H = -\sum h_\nu \ln h_\nu \tag{11}$$

$$h_\nu = \frac{|\hat{a}^m_\nu|}{\sum_\nu |\hat{a}^m_\nu|} \quad \text{or} \quad h_\nu = \frac{|\Delta\hat{\varepsilon}^m_\nu|}{\sum_\nu |\Delta\hat{\varepsilon}^m_\nu|} \tag{12}$$

3. Experimental

3.1. General information

All solution preparations and transfers were carried out under argon (99.999%, Soxal, Singapore) atmosphere using standard Schlenk techniques [30]. The argon was further purified before use by passing it through a deoxy and zeolite column to reduce the trace oxygen and water, respectively. The solvents *n*-hexane and cyclohexane (>99.6%, Fluka) were refluxed over sodium–potassium alloy under argon atmosphere. Purified nitrogen (99.999%, Saxol, Singapore) was used to purge the 2250 Shimadzu UV–vis spectrometer and Jasco-810 UV–vis spectropolarimeters.

The metal complex tetrarhodium dodecacarbonyl, $Rh_4(CO)_{12}$ (98%) and the chiral ligand (*S*)-(−)-2,2′-bis (diphenylphosphino)-1,1′-binaphthyl, (*S*)-BINAP (97%) from Strem chemicals (Newport, MA) and the achiral ligand triphenylphosphine, PPh_3 (>99%) from Merck were used as received.

3.2. Equipmental setup

A schematic diagram of the experimental setup is shown in Fig. 1. The two semi-batch ligand substitutions (i) $Rh_4(CO)_{12}$ with PPh_3, and (ii) $Rh_4(CO)_{12}$ with (*S*)-BINAP were performed in a Schlenk tube equipped with magnetic stirring. A rubber septum was used at the top of the Schlenk tube in order to insert transfer lines and in order to inject perturbations during the semi-batch runs. The liquid phases was circulated to a quartz cuvette with 1.0 cm path length using a Teflon membrane pump (Cole Parmer) at the flow rate of 5 ml/min via Teflon tubes of 1/16 in. outer diameter. The quartz cuvette was fixed in a stainless steel cell holder and placed in the cell chamber of UV spectrometer. For any particular experiment, either the Shimadzu UV-2550 spectrometer or the Jasco-810 spectropolarimeter was used. Experiments were run at ambient temperature circa 298 K.

The entire system was cleaned with anhydrous solvent (*n*-hexane/cyclohexane) prior to experiments. Furthermore, the reactions were carried out under argon in order to avoid of the degradation of $Rh_4(CO)_{12}$, PPh_3, (*S*)-BINAP and the resulting metal complexes.

3.3. In situ spectroscopic measurements

Fifty milliliters *n*-hexane and 50 ml cyclohexane were used as solvent for the reactions (1) and (2), respectively. Both semi-batch reactions were performed in a similar manner. For example, in the ligand substitution reaction (1) first, 50 ml of *n*-hexane was transferred to the Schlenk tube under argon and the stirrer was turned on. The pressure was controlled

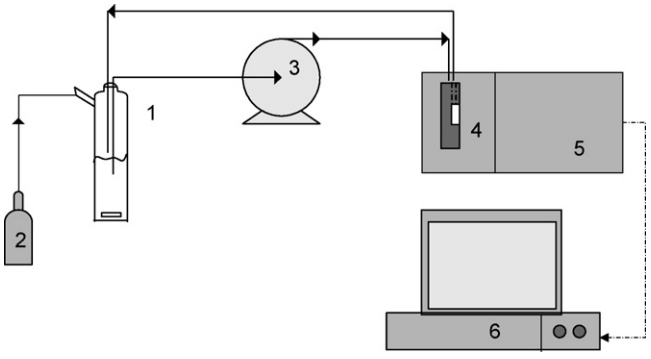

Fig. 1. Schematic of experimental configuration: (1) Schlenk tube; (2) argon tank; (3) pump; (4) quartz cell; (5) UV–vis spectrometer; (6) data acquisition.

Table 1
Experimental design for ligand substitution reaction indicating the individual perturbation steps

Index	Experiment 1: $[Rh_4(CO)_{12}]$ with PPh_3		Experiment 2: $[Rh_4(CO)_{12}]$ with (*S*)-BINAP	
	Perturbation	Spectra #	Perturbation	Spectra #
1	Solvent: *n*-hexane	1–2	Solvent: cyclohexane	1–2
2	Add 100 μl $[Rh_4(CO)_{12}]$	3–4	Add 100 μl $[Rh_4(CO)_{12}]$	3
3	Add 100 μl $[Rh_4(CO)_{12}]$	5–6	Add 200 μl $[Rh_4(CO)_{12}]$	4
4	Add 50 μl PPh_3	7–8	Add 200 μl $[Rh_4(CO)_{12}]$	5
5	Add 100 μl PPh_3	9–10	Add 50 μl (*S*)-BINAP	6-7
6	Add 250 μl $[Rh_4(CO)_{12}]$	11–12	Add 50 μl (*S*)-BINAP	8
7	Add 250 μl $[Rh_4(CO)_{12}]$	13–14	Add 50 μl (*S*)-BINAP	9
8	Add 200 μl PPh_3	15–17	Add 100 μl (*S*)-BINAP	10
9	Add 250 μl PPh_3	18–19	Add 100 μl (*S*)-BINAP	11–12

at just over 0.1013 MPa of argon. After the *n*-hexane solvent was circulated through the entire system, the UV–vis spectra in the quartz cuvette were collected. A stock solution of *n*-hexane with $Rh_4(CO)_{12}$ (ca. 27.5 mg in 20 ml) was prepared and a predetermined amount was injected into the Schlenk tube under argon. Typically, after each perturbation the solution was circulated for circa 10 min to achieve solution homogeneity. Then the UV–vis spectra of the $Rh_4(CO)_{12}$/*n*-hexane solution in the quartz cuvette were collected. A stock solution of *n*-hexane with PPh_3 (ca. 8.4 mg in 20 ml) was prepared and a predetermined amount was injected into the Schlenk tube under argon. After equilibrium, the UV–vis spectra of the reactive system were collected. The perturbation steps in each experiment correspond to the experimental design as shown in Table 1.

In a similar manner, a stock solution of 13.5 mg (*S*)-BINAP dissolved in 20 ml cyclohexane and a stock solution of 31.5 mg of $Rh_4(CO)_{12}$ dissolved in 20 ml cyclohexane were prepared for the ligand substitution reaction (2). The corresponding experimental design is also shown in Table 1.

All the UV–vis and/or CD spectra were recorded at scanning speed of 200 nm/min in the range of 800–200 nm. Since $Rh_4(CO)_{12}$ reacts with PPh_3 almost instantaneously, most of these spectra were collected under nearly full transformation of PPh_3, i.e. where the equilibrium is shifted to the far right in Eq. (1). Similarly, $Rh_4(CO)_{12}$ reacted rapidly with (*S*)-BINAP, most of these spectra were collected under nearly full transformation of (*S*)-BINAP, i.e. where the equilibrium is shifted to the far right in Eq. (2).

4. Results and discussion

4.1. Ligand substitution of $Rh_4(CO)_{12}$ with PPh_3

4.1.1. Experimental data

The ligand substitution of $Rh_4(CO)_{12}$ with the achiral ligand PPh_3 was carried out in *n*-hexane under argon atmosphere. The in situ spectroscopic measurements were performed using the Shimadzu UV-2550 spectrometer. A total of 19 UV–vis spectra were obtained from this experiment as shown in Fig. 2. These measurements show absorbance from the solvent, $Rh_4(CO)_{12}$ and the cluster. A few spectral maxima and shoulders are seen, i.e. at 305, 380 nm, etc. All spectral features are broad, as expected for UV–vis spectra. Two spectral step changes, one at 420 nm and the other at 540 nm are also observed. These are due to the optical filter changes.

4.1.2. Singular value decomposition (SVD)

The 19 UV–vis spectra were first consolidated into a single matrix. The spectra preconditioning, namely background subtraction, was performed on the consolidated absorbance data matrix and then singular value decomposition (SVD) was employed to decompose this preconditioned absorbance data matrix to obtain the right singular vectors, the orthonormal matrix V^T. The first 6 right singular vectors and 19th vector are shown in Fig. 3.

The first 3 right singular vectors in Fig. 3 show meaningful signals although the bands are quite broad. These bands are significant spectral features associated with the metal carbonyl and metal complex. The 4th and 5th right singular vectors still show some absorbance bands, however, there is a considerable contribution from noise. The 6th to the 19th right singular vectors can be considered to be primarily white noise. Since all meaningful spectral features are seen in the first five right singular vectors, only vectors 1–5 were used in the following BTEM analysis.

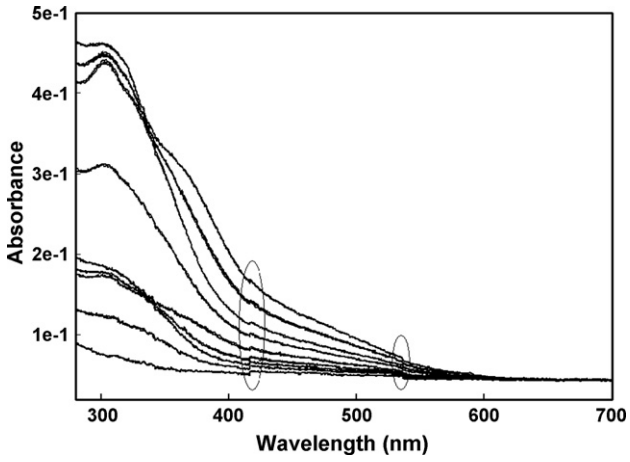

Fig. 2. UV–vis reaction spectra of the ligand substitution reaction of $Rh_4(CO)_{12}$ with PPh_3 (under argon) involving 9 perturbation steps. The ovals highlight the areas where filter changes occur.

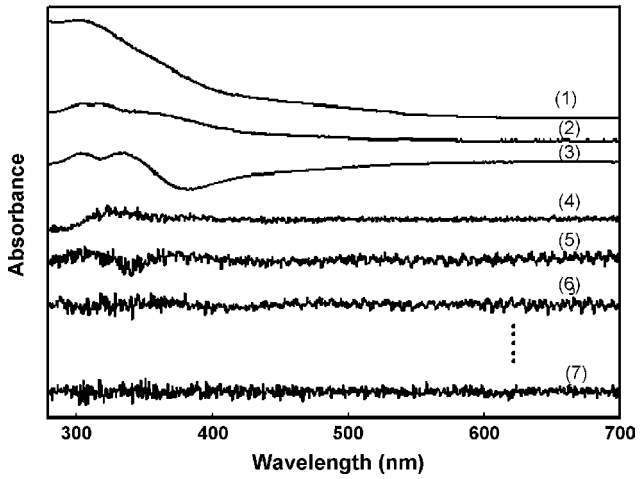

Fig. 3. Seven right singular vectors of the V^T matrix for the consolidated data set from the ligand substitution reaction of $Rh_4(CO)_{12}$ with PPh_3 (Experiment 1): (1)–(6) first six right singular vectors; (7) 19th right singular vector.

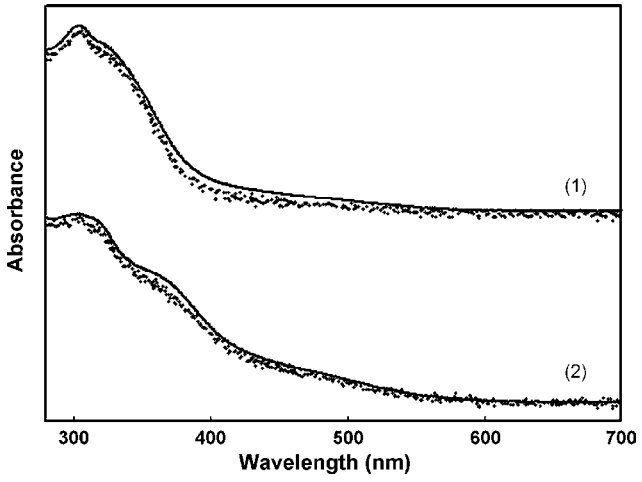

Fig. 4. Solid lines: recovered pure component spectra obtained by BTEM: (1) $Rh_4(CO)_{12}$ and (2) $Rh_4(CO)_{11}$ PPh_3; dotted lines: UV–vis experiment reference spectra: (1) $Rh_4(CO)_{12}$ and (2) $Rh_4(CO)_{11}$ PPh_3.

4.1.3. Spectral reconstruction using BTEM

The 5 right singular vectors from the experimental absorbance data were transformed to pure component spectra using BTEM analysis. Two estimated spectral patterns could be successfully reconstructed from the BTEM analysis. These are the estimated UV–vis pure component spectra of $Rh_4(CO)_{12}$ and the product $Rh_4(CO)_{11}PPh_3$. Fig. 4 compares the estimated UV–vis spectra with the experimental reference spectra. Both estimated spectra are in quite good agreement with the experimental reference spectra.

More right singular V^T vectors (up to 19 V^T vectors) were used in other analyses, however, no additional meaningful spectra patterns were obtained. Since $Rh_4(CO)_{12}$ reacts instantaneously with PPh_3 and since Eq. (1) is shifted to the far right, the analysis indicates that little or no free PPh_3 was present in these spectra (note that PPh_3 has a broad chromophore from 200 to 300 nm due to the phenyl groups).

4.1.4. Concentrations profiles

The relative concentration profiles of the reactants were calculated by a least squares fit of the estimated UV–vis spectra onto the original experimental UV–vis absorbance spectra. Since the present experiments were conducted at PPh_3:$Rh_4(CO)_{12}$ ratios less than 0.7 the presence of the di-substituted product $Rh_4(CO)_{10}(PPh_3)_2$ can be neglected [31]. Furthermore, the mono-substituted product was totally soluble in *n*-hexane in the range of concentration used in this study (less than 5 ppm). Accordingly, the mass balance from the experimental design was used as a constraint in order to determine the calibrations for both $Rh_4(CO)_{12}$ and $Rh_4(CO)_{11}PPh_3$. Fig. 5 compares the concentration profiles of $Rh_4(CO)_{12}$ and $Rh_4(CO)_{11}PPh_3$ obtained from the experimental design with those obtained from the spectroscopic measurements. It is clearly seen that satisfactory concentration profiles for both $Rh_4(CO)_{12}$ and the product $Rh_4(CO)_{11}$ PPh_3 are obtained. However, some discrepancy appears as more and more perturbations are made. This increasing discrepancy is probably due to accumulation of error during the experimental procedure, either from systematic error during injection and/or the slow loss of hexane through the septum (it is very volatile).

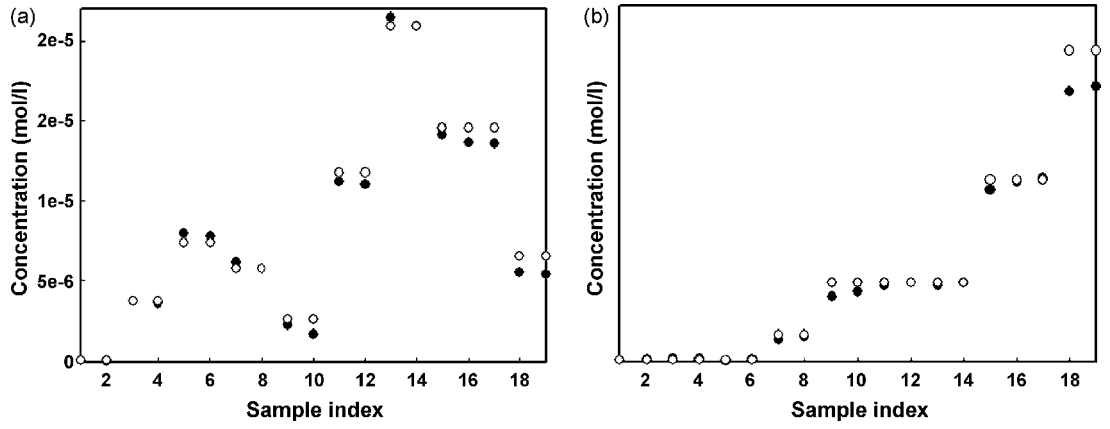

Fig. 5. Comparison of the concentration profiles from recovered UV–vis pure component spectra (●) and experiment design (◯). Profiles for (a) $Rh_4(CO)_{12}$ and (b) $Rh_4(CO)_{11}$ PPh_3.

4.2. Ligand substitution of $Rh_4(CO)_{12}$ with (S)-BINAP

The ligand substitution of $Rh_4(CO)_{12}$ with the chiral bidentate ligand (*S*)-BINAP was carried out in cyclohexane under an argon atmosphere. This reaction was carried out in a semi-batch mode by introducing perturbations of (*S*)-BINAP into reactive system. The concentrations of all the reactants involved in this reaction were less than 20 ppm and the concentration of the product $Rh_4(CO)_{10}$BINAP was less than 10 ppm. The in situ spectroscopic measurements were performed using the UV Jasco-810 spectropolarimeter. A total of 12 UV–vis spectra and 12 UV–vis-CD spectra were obtained simultaneously from the above experiment.

4.2.1. UV–vis experimental data set

4.2.1.1. Experimental data. The 12 UV–vis spectra from the above experiment in the range of 700–280 nm are shown in Fig. 6. Since all spectra are below circa 2 absorbance units, these spectra were taken in a more-or-less linear instrument response region. In the high nm range, the UV–vis spectra are rather featureless and correspond primarily to the instrument function. The primary signals of interest are all below 500 nm. At the reagent concentrations used, significant changes are seen in the region of circa 280–500 nm during the semi-batch experiment. Since none of the experimental spectra have absorbance above circa 1.5, rather strict additivity of component spectra should exist, and the bilinear form of the Bouguer–Lamber–Beer law should remain valid.

4.2.1.2. Singular value decomposition. A total of 12 UV–vis spectra were first consolidated into a single matrix. To minimize the effects of the solvent and cuvette signals on the spectral analysis, spectral preconditioning was performed. This background subtraction resulted in a new consolidated absorbance data matrix. Next, singular value decomposition (SVD) was employed to decompose this preconditioned absorbance data matrix to give the right singular vectors, the orthonormal matrix V^T. The first 6 right singular vectors and 12th vector are shown in Fig. 7.

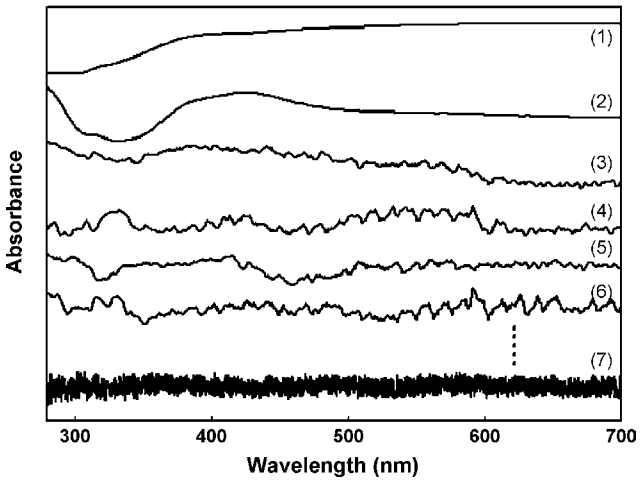

Fig. 7. Seven right singular vectors of the V^T matrix for UV–vis consolidated data set from the ligand substitution reaction of $Rh_4(CO)_{12}$ with (*S*)-BINAP (Experiment 2): (1)–(6) first six right singular vectors; (7) 12th right singular vector.

The first 2 right singular vectors in Fig. 7 show significant spectral features with the very broad bands associated with the metal carbonyl and metal complex. The 3rd to 6th right singular vectors still show some absorbance bands, however, there is a considerable contribution from noise. The 12th right singular vectors can be considered to be white noise. Since prominent spectra features can be observed only in the first six right singular vectors, these will be used in the following BTEM analysis.

4.2.1.3. Spectral reconstruction using BTEM. BTEM analysis was performed using the first 6 right singular vectors from the preconditioned UV–vis absorbance data in order to reconstruct the pure component spectra involved in the reaction. The noticeable spectral extrema in the first 6 right singular vectors

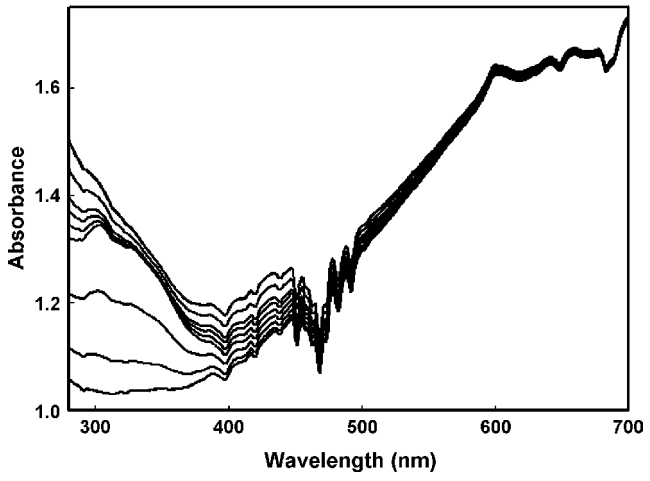

Fig. 6. UV–vis reaction spectra of the ligand substitution reaction of $Rh_4(CO)_{12}$ with (*S*)-BINAP (under argon) involving 9 perturbation steps.

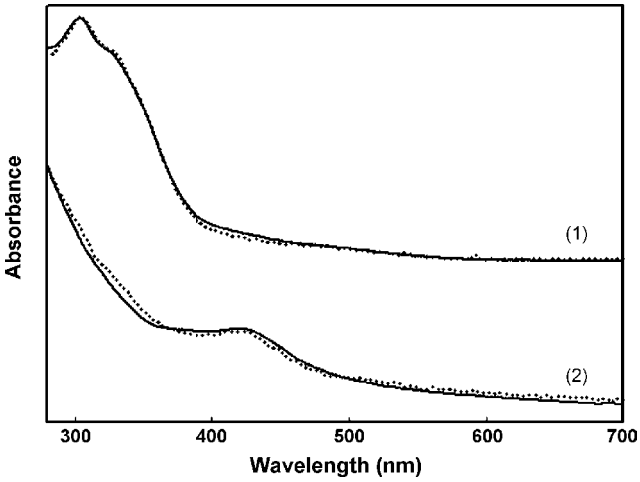

Fig. 8. Solid lines: recovered pure component spectra obtained by BTEM: (1) $Rh_4(CO)_{12}$ and (2) $Rh_4(CO)_{10}$ BINAP; dotted lines: UV–vis experiment reference spectra: (1) $Rh_4(CO)_{12}$ and (2) $Rh_4(CO)_{10}$BINAP.

were used as targets. Two estimated UV–vis spectral patterns, from $Rh_4(CO)_{12}$ and the product $Rh_4(CO)_{10}$BINAP, could be successfully reconstructed from the BTEM analysis. Fig. 8 compares the estimated UV–vis spectra with the experimental reference spectra. Both estimated spectra are in quite good agreement with the experimental reference spectra.

4.2.1.4. Concentrations profiles. An estimate of the relative concentration profiles of the reactants was calculated by a least squares fit of the estimated UV–vis spectra onto the original experimental UV–vis absorbance spectra. Further quantitative spectroscopic analysis was performed using the mass balances from the experimental design as a constraint and assuming that only reaction (2) occurs. The quantitative analysis resulted in two concentration profiles for $Rh_4(CO)_{12}$ and the product $Rh_4(CO)_{10}$BINAP as shown in Fig. 9. It is clearly seen that satisfactory concentration profiles of both $Rh_4(CO)_{12}$ and the product $Rh_4(CO)_{10}$BINAP were obtain from the quantitative analysis, at least for the first 10 steps of the semi-batch reaction.

The 10th step corresponds to a (*S*)-BINAP:$Rh_4(CO)_{12}$ ratio of circa 0.5. In the 11th and 12th step higher ratios of (*S*)-BINAP:$Rh_4(CO)_{12}$ up to 2:3 were used. In these last two steps, some discrepancy occurs between the estimated and experimental design concentrations. This result appears to indicate that some non-negligible side reactions are occurring. The formation of small amounts of a di-substituted product $Rh_4(CO)_8(BINAP)_2$ and/or a dinuclear species of the stoichiometry $Rh_2(CO)_6$BINAP are the most likely candidates.

4.2.2. UV–vis CD experimental data set

4.2.2.1. Experimental data. The 12 UV–vis CD spectra from the above experiment in the range of 225–425 nm are shown in Fig. 10. These spectra show (1) a non-flat and non-zero baseline (at least in the region of <300 nm) due to the instrument function and (2) pronounced CD features at circa 235, 265 and 320 nm. In addition, these CD spectra have considerably lower S/N ratios compared to the unpolarized UV–vis measurements.

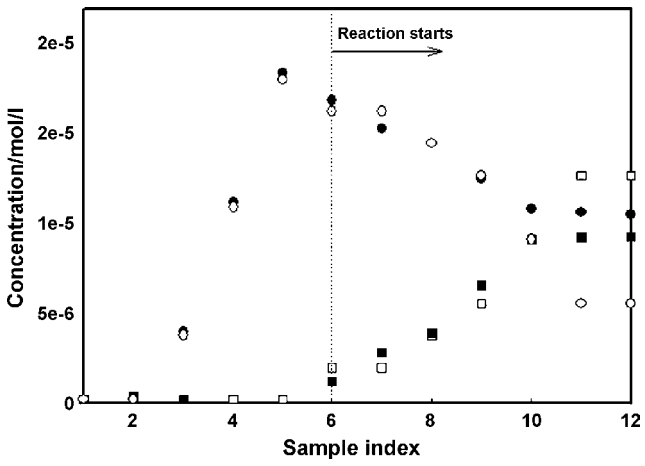

Fig. 9. Comparison of the concentration profiles from recovered UV–vis pure component spectra (solid symbols) and experiment design (open symbols). Profiles for: (●) $Rh_4(CO)_{12}$ and (■) $Rh_4(CO)_{10}$ BINAP.

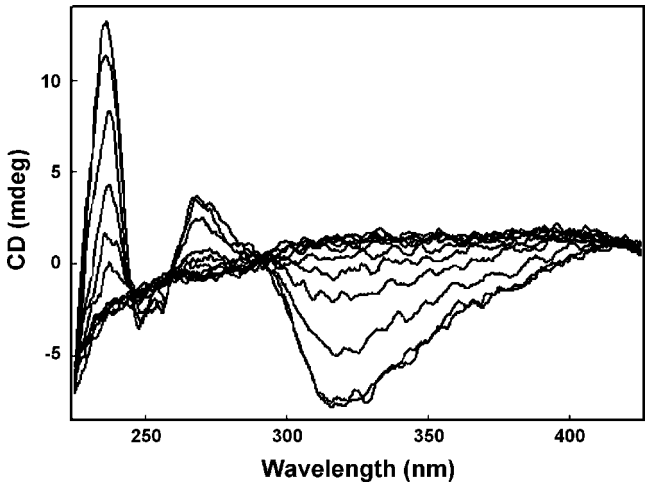

Fig. 10. UV–vis CD reaction spectra of the ligand substitution reaction of $Rh_4(CO)_{12}$ with (*S*)-BINAP (under argon) involving 9 perturbation steps.

4.2.2.2. Singular value decomposition. No base-line correction was performed with the 12 UV–vis CD spectra, however, they were smoothed with the Savitzky–Golay smoothing algorithm. Subsequently, the smoothed spectra were consolidated into a single matrix. Next, singular value decomposition was employed to decompose this CD data matrix to give the right singular vectors, the orthonormal matrix V^T. The first 6 right singular vectors and 12th vectors are shown in Fig. 11.

The first 2 right singular vectors in Fig. 11 show significant spectral features associated with the instrument function and the chiral metal complex. The 3rd to 6th right singular vectors still show some features, however, there is a considerable contribution from noise. The 12th right singular vector can be considered to be more-or-less white noise. Most of the prominent spectral features are embedded in the first six right

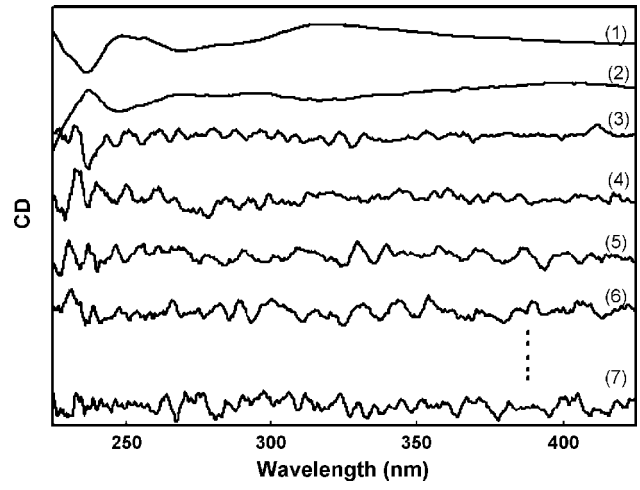

Fig. 11. Seven right singular vectors of the V^T matrix for UV–vis CD consolidated data set from the ligand substitution reaction of $Rh_4(CO)_{12}$ with (*S*)-BINAP (Experiment 2): (1)–(6) first six right singular vectors; (7) 12th right singular vector.

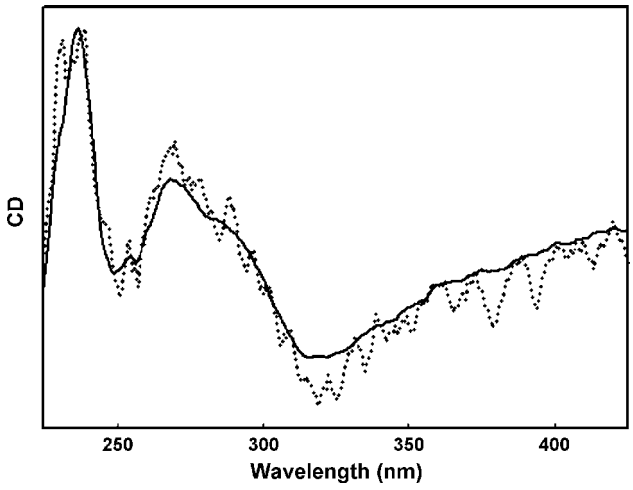

Fig. 12. Recovered pure component spectra obtained by BTEM: $Rh_4(CO)_{10}$ BINAP, solid line and UV–vis CD experiment reference spectra: $Rh_4(CO)_{10}$ BINAP, dotted line.

singular vectors and these will be used in the following BTEM analysis.

4.2.2.3. Spectral reconstruction using BTEM. The first 6 right singular vectors were used to reconstruct the pure component ECD spectrum of the chiral metal complex $Rh_4(CO)_{10}$BINAP. The noticeable spectral extrema in the first 6 right singular vectors were used as targets. Fig. 12 compares the estimated UV–vis CD spectrum with the experimental reference spectrum. This result indicates that the BTEM algorithm can be used to obtain accurate CD pure component spectra, i.e. spectra with both positive and negative parts.

4.2.2.4. Concentration profiles. The estimated relative concentration profiles of the reactants were computed by least squares fit of the estimated UV–vis CD spectra onto the original experimental UV–vis CD spectra. Further quantitative spectroscopic analysis was performed using the mass balances to constrain the numerical solution, assuming that only reaction (2) occurs. The quantitative analysis resulted in the concentration profile for the product $Rh_4(CO)_{10}$ BINAP. Fig. 13 compares the estimated concentration profile of the product $Rh_4(CO)_{10}$ BINAP obtained from (i) the UV–vis CD experimental data set with (ii) the UV–vis experimental data set and (iii) the experimental design 'real' concentration profile. The 3 concentration profiles of the product $Rh_4(CO)_{10}$ BINAP are in very good agreement. The only exception involves the last 2 steps, 11 and 12, which might be associated with the formation of small amounts of a disubstituted product $Rh_4(CO)_8(BINAP)_2$ and/or a dinuclear species of the stoichiometry $Rh_2(CO)_6$BINAP.

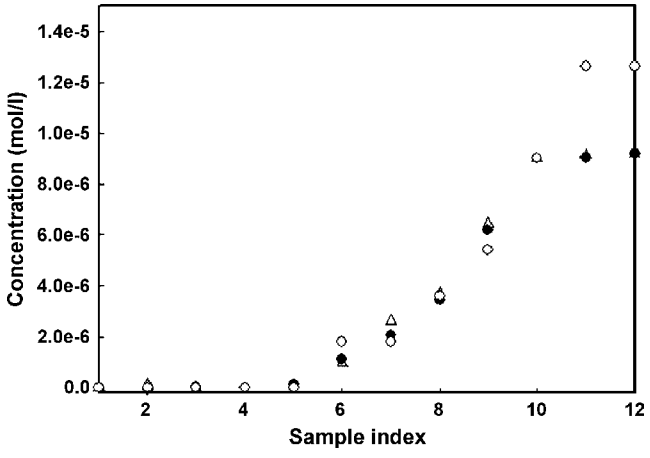

Fig. 13. Comparison of $Rh_4(CO)_{10}$ BINAP concentration profile determined from recovered UV–vis CD pure component spectra (●),UV–vis pure component spectra (△) and experiment design (◯).

5. Conclusions

The present results demonstrate that spectral reconstruction for organometallic reactive systems can be achieved by the application of UV–vis/UV–vis CD spectroscopy combined with a reliable and effective chemometric technique, namely, the BTEM algorithm. Moreover, the present results suggest that much more complex systems can be studied. Since the BTEM algorithm has been previously shown to be effective with systems containing 10 or more species (using FTIR, Raman, etc.), analysis of complex reactive systems using UV–vis/UV–vis CD spectroscopy appears possible in the near future.

Acknowledgment

The authors wish to thank the Institute of Chemical and Engineering Sciences for support of this research.

References

[1] R. Dickson, Homogeneous Catalysis with Compounds of Rhodium and Iridium, Springer, New York, 1985.
[2] J.E. Macintyre (Ed.), Dictionary of Organometallic Compounds, vol. 3, second ed., Chapman & Hall, London, 1995, pp. 3197–3397.
[3] R. Whyman, J. Chem. Soc. Dalton Trans. 13 (1972) 1375.
[4] J. Seyden-Penne, Chiral Auxiliaries and Ligands in Asymmetric Synthesis, Wiley-Interscience, New York, 2004.
[5] M. Stichelberger, D. Desbouis, V. Spiwok, L. Scapozza, P.A. Schubiger, R. Schibli, J. Organomet. Chem. 692 (2007) 1255.
[6] B.T. Heaton, L. Strona, J. Jonas, T. Eguchi, G.A. Hoffman, J. Chem. Soc. Dalton Trans. (1982) 1159.
[7] P.J. Dyson, J.S. Mclndoe, Transition Metal Carbonyl Cluster Chemistry, Gordon and Breach Science Publishers, Amsterdam, 2000.
[8] P.S. Braterman, Metal Carbonyl Spectra, Academic Press, 1975.
[9] W. Chew, E. Widjaja, M. Garland, Organometallics 21 (2002) 1982.
[10] C. Li, E. Widjaja, M. Garland, J. Am. Chem. Soc. 125 (2003) 5540.
[11] P.C. Ford, J.S. Bridgewater, B. Lee, Photochem. Photobiol. 65 (1997) 57.
[12] S.M. Massick, T. Buttner, P.C. Ford, Inorg. Chem. 42 (2003) 575.
[13] S. Eriksson, S.K. Kim, M. Kubista, B. Nordtn, Biochemistry 32 (1993) 2987.
[14] W.H. Lawton, E.A. Sylvester, Technometrics 13 (1971) 617.
[15] T. Konno, Protein Sci. 7 (1988) 975.
[16] P. McPhie, R.I. Shrager, Arch. Biochem. Biophys. (1992) 293.
[17] N. Sreerama, R.W. Woody, J. Mol. Biol. 242 (1994) 497.
[18] D.W. McMullen, S.R. Jaskunas, I.J. Tinoco, Biopolymers 5 (1967) 589.
[19] L. Antonov, G. Gergov, V. Petrov, M. Kubista, J. Nygren, Talanta 49 (1999) 99.

[20] G. Meinrath, S. Lis, Fresenius J. Anal. Chem. 369 (2001) 124.
[21] R.M. Wallance, J. Phys. Chem. 64 (1960) 899.
[22] W. Windig, J. Guilment, Anal. Chem. 63 (1991) 1425.
[23] W. Windig, Chemom. Intell. Lab. Syst. 36 (1997) 3.
[24] R. Tauler, I. Marques, E. Casassas, J. Chemom. 12 (1998) 55.
[25] C. Srilakshmi, E. Widjaja, M. Garland, B.G. Anderson, J. Raman Spectrosc. 38 (2007) 349.
[26] S.Y. Cheng, D. Rajaratham, M.L. Tan, M. Garland, Appl. Spectrosc. 60 (2006) 521.
[27] C. Li, L. Guo, M. Garland, Organometallics 23 (2004) 2201.
[28] C. Li, E. Widjaja, M. Garland, J. Catal. 213 (2003) 126.
[29] L.R. Ong, E. Widjaja, R. Stanforth, M. Garland, J. Raman Spectrosc. 34 (2003) 282.
[30] D.F. Shriver, M.A. Drezdzon, The Manipulation of Air-Sensitive Compounds, Wiley, New York, 1986.
[31] M. Tjahjono, A.D. Allian, M. Garland, Dalton Trans. 12 (2006) 1505.

Available online at www.sciencedirect.com
ScienceDirect
Talanta 74 (2008) 1175–1183
Talanta
www.elsevier.com/locate/talanta

Sediment extraction and clean-up for organic phosphorus analysis by electrospray ionization tandem mass spectrometry

Heidi De Brabandere [a], Rolf Danielsson [a], Per J.R. Sjöberg [a], Joakim Ahlgren [a], Emil Rydin [b], Monica Waldebäck [a,*]

[a] *Department of Physical and Analytical Chemistry, Uppsala University, Box 599, 751 24 Uppsala, Sweden*
[b] *Department of Limnology, Uppsala University, Norbyvägen 20, 752 36 Uppsala, Sweden*

Received 15 February 2007; received in revised form 13 August 2007; accepted 24 August 2007
Available online 2 September 2007

Abstract

A method to prepare NaOH sediment extracts for organic P compound analysis with electrospray ionization tandem mass spectrometry (ESI-MS-MS) was developed on natural samples. Ion exchange, rotary evaporation and mass cut-off filtering proved to be suitable for sample preparation. Samples were analyzed with ESI-MS-MS, and reproducibility and repeatability of the method was calculated. In addition, ^{31}P-nuclear magnetic resonance spectroscopy (^{31}P NMR) was used to measure recovery of different P compound groups such as orthophosphate (Ortho-P), orthophosphate monoesters (Monoester-P), orthophosphate diesters (Diester-P) and pyrophosphates (Pyro-P).

The developed sample preparation method resulted in an easy-to-spray liquid for the ESI-MS-MS instrumentation. The overall P recovery was 65% and ^{31}P NMR showed that Diester-P, possibly in the form of DNA, was apparently lost through the filtering step most likely due to their size. Variances in the total intensities of the MS scans (relative standard deviation (R.S.D.) 35–54%) were for about 50% due to repeated MS runs. Covariances of the peaks in the MS spectra were calculated to be for about 30% due to the sample preparation procedure. Finally, with the ESI-MS-MS approach, 11 peaks in the mass spectra were found likely to represent phosphate containing compounds.
© 2007 Elsevier B.V. All rights reserved.

Keywords: Organic phosphorus; Sediment; Sample preparation; ESI-MS-MS; ^{31}P NMR

1. Introduction

Phosphorus (P) is a key element for primary production in aquatic systems, and is thus in many cases a regulator of trophic status. In lakes, the primary source of P is the drainage area. However, P available for lake primary production is also heavily dependent on recycling of P, either within the water column or after sedimentation. Sediment P may either be buried permanently or recycled into the water column. Although organic P most likely constitutes a major proportion of sediment P [1], most studies have focused on inorganic P forms [2–5], which may be due to the limitations of the currently used analytical techniques for extraction and identification of organic P forms in sediments. Studies that have focused on the organic P part in sediments, have in most cases only been able to identify groups of organic P compounds (i.e. phosphate monoesters, phosphate diesters, polyphosphates, pyrophosphate, orthophosphate), most often using the ^{31}P-nuclear magnetic resonance (^{31}P NMR) technique [6–11]. However, a few studies have focused entirely on individual organic P compounds. Suzumura and Kamatani [12] extracted inositol phosphates by hypobromite oxidation followed by isolation with anion exchange chromatography and analysis with ^{1}H NMR and gas chromatography (GC). The phospholipid phosphatidylcholine, isolated from sediment pore waters and extracts, has been analyzed with chemiluminescence via an enzymatic reaction [13]. Additionally, several sediment phospholipids were identified via a flow-blending extraction combined with liquid chromatography electrospray ionization tandem mass spectrometry (LC-ESI-MS-MS) [14].

To gain a deeper understanding of the sediment P turnover, it would be of interest to characterize all the individual organic P compounds in a sediment sample. Since existing methods focus either on groups of organic P compounds or on one specific P

* Corresponding author. Tel.: +46 18 4713679; fax: +46 18 4713692.
E-mail address: monica.waldeback@kemi.uu.se (M. Waldebäck).

0039-9140/$ – see front matter © 2007 Elsevier B.V. All rights reserved.
doi:10.1016/j.talanta.2007.08.030

compound, there is a need for analytical methods that determine and characterize several individual P containing compounds simultaneously.

Mass spectrometry (MS) detects ions with specific mass over charge ratios with high selectivity and sensitivity. In related studies, electrospray ionization (ESI) as ion source has been combined with a number of analyzers utilizing different types of mass analyzers. For instance, ESI-MS was applied to identify dissolved organic matter (DOM) [15]. In an attempt to characterize organic phosphorus in natural waters, ESI-Fourier transform ion cyclotron resonance-MS (ESI-FTICR-MS) was used [16,17]. Finally, as previously mentioned, phospholipids in sediments have been determined with ESI-MS-MS [14]. The popularity of ESI is based on its 'soft' ionization, allowing compounds to be observed with minimum fragmentation, which facilitates the characterization of entire compounds. With tandem mass spectrometry (MS-MS) it is possible to detect parent ions of selected fragments after collision induced dissociation (CID). This technique was applied in the determination of phosphopeptides [18,19].

A general drawback of ESI is the need of relatively clean samples, free from salts that may result in ion suppression during the ionization process. This study therefore focuses on the development of a sample preparation method for the sediment sample, enabling characterization of sediment organic P compounds with ESI-MS-MS. This is an important step towards the ultimate goal to identify all the organic P compounds in a lacustrine sediment extract.

2. Experimental

2.1. Sampling

All sediment samples were taken in Lake Erken, a moderately eutrophic lake in Sweden. The surface area is 24 km^2 and mean and maximum depth is 9 and 21 m, respectively. The drainage area (137 km^2) is mostly forested and consists of nutrient rich glacial and post-glacial clay deposits. Total P (TP) in the lake water is on average 27 $\mu g\,L^{-1}$ and in the surface sediment between 1.5 and 3.0 mg $P\,g^{-1}$ DW [20]. During summer stratification, bottom water occasionally turns anoxic. The lake has been well examined, and has ever since the measurements started in 1930, been moderately eutrophic. This, together with the fact that the small number of inhabitants and size of the farmland in the area has been constant for at least a century, makes this a stable system concerning external P load. The sediment samples were collected with a core sampler (Willner sampler) at a depth of 17 m within the same accumulation bottom area of the lake in October 2005. In Fig. 1, a summary of the sampling, extraction and analysis procedure is shown. The upper two centimeters of four sediment cores were collected and pooled in order to obtain samples ('a–d') that are representative for the area (Fig. 1). Samples were extracted (NaOH, described in more detail below) followed by clean-up (ion exchange, concentration and filtering) immediately after sampling and were then kept frozen until analysis.

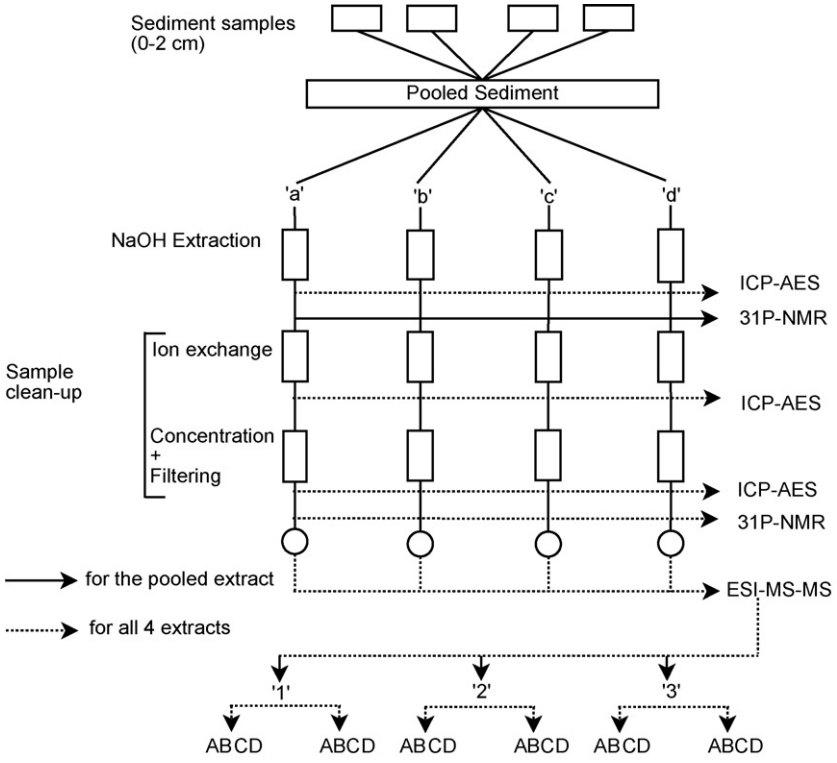

Fig. 1. Overview on samples and measurements.

2.2. Extraction

In this study, sodium hydroxide (NaOH) was chosen as extractant for sediment organic P since it is well established in this area [10,11,21]. The use of NaOH originates from a sequential fractionation method according to Psenner and Pucsko [22]. First of all, the wet sediment was, via stirring and pouring, divided into four replicate sediment samples ('a–d'), each weighing about 12 g. From each sediment sample, P compounds were extracted with 0.1 mol L^{-1} NaOH (p.a., EKA Bohus. Sweden). The wet sediment was mixed with the solvent at a 1:3 (w/v) ratio. After 16 h of extraction at room temperature, the NaOH extract was collected following centrifugation (4302 relative centrifugal force (RCF), Sigma 4-15 Laboratory Centrifuges, LABEX Instrument AB, Sweden).

2.3. Sample clean-up

To prevent ion suppression in the ESI interface, Na ions were removed from the extract by an ion exchange method, using a strongly acidic cation exchange resin with sulfonic acid as functional groups (Dowex50W®, The Dow Chemical Co., USA). The capacity of this resin was 2.6 mmol H^+ g^{-1} resin which enabled 1.5 g of the resin to handle 20 mL of NaOH sediment extract. The flow rate through the column (diameter 1.0 cm and height 1.7 cm) was 1 mL min^{-1}. After applying the extract, the resin was rinsed four times with 5 mL NH_3 solution (0.64 mol L^{-1}, p.a. 25%, Merck) and captured in the same vial as the initial extract. Despite ESI-MS-MS having a good sensitivity, the P compounds needed to be concentrated to obtain a good signal to noise ratio. Therefore, the eluent was concentrated from 80 to 3.2 g sample (concentration factor 25) with rotary evaporation at ambient temperature and under air atmosphere. Large particles were removed by centrifugation at 10,000 RCF during 10 min (Sigma-Labozentrifugen 2K15, LABEX Instrument AB, Sweden). The obtained viscous liquid was run through two different mass cut-off filters (Microsep™ Centrifugal Devices, VWR, Pall* Life Sciences). The filters had a volume of 3.5 mL and a molecular weight cut-off (MWCO) of 100 kDa (maximum centrifugal force is 1000 RCF) and 3 kDa (maximum centrifugal force is 4302 RCF). A non-viscous, easy-to-spray liquid was obtained after the last filtration step.

To enable statistical evaluation of both the sample preparation method (extraction and clean-up) and the ESI-MS-MS studies, four replicate samples were prepared according to the proposed sample preparation method (Fig. 1). These four replicates were divided into three subsamples ('1–3') to enable MS measurements of these replicates on three different days. Since it has been shown that freezing extracts does not alter their P composition [9], all the samples were frozen until measurements.

2.4. Inductive coupled plasma atomic emission spectroscopy (ICP-AES) measurements

To calculate amounts of total sediment P (TP), sediment water content was determined after drying over night at 105 °C. After acid hydrolysis at high temperature (340 °C), the TP content in the pooled sediment was measured with ICP-AES. The total P and sodium (Na) concentrations of the NaOH extracts were measured with ICP-AES before sample clean-up, after ion exchange and after the concentration and filtering step (see Fig. 1). The losses could then be calculated. The ICP instrument was a Spectroflame-P ICP (Spectro Analytical Instruments) equipped with an Alitea-pump (0–50 rpm). Na and P were measured on wavelengths 330.2 and 178.2 nm, respectively.

2.5. Nuclear magnetic resonance spectroscopy (NMR) measurements

The P containing compound groups (i.e. phosphate monoesters, phosphate diesters, polyphosphates, pyrophosphate, orthophosphate) in the extracts were measured with ^{31}P NMR, and from the peak areas of each compound group the concentrations were calculated. By making ^{31}P NMR measurements before and after sample clean-up, losses could be calculated. The four NaOH extracts before sample clean-up were divided into one part for NMR measurement (4 samples, 'a–d' pooled and concentrated 25 times to one NMR sample) and one part to undergo sample clean-up (see Fig. 1). Before the ^{31}P NMR measurements the samples were centrifuged at 10,000 RCF. They were then mixed (4:1, v/v) with a dithionite solution (0.11 M $NaHCO_3$ and 0.11 M $Na_2S_2O_4$) in order to reduce Fe(III) to Fe(II), as the paramagnetic Fe(III) otherwise would interfere with the NMR runs [23]. ^{31}P NMR spectra were then recorded on a Varian XL-300 instrument at 121.4 MHz and ambient temperature. An amount of D_2O sufficient to obtain a stable lock signal was added to the samples, and spectra were recorded using a 72° observe pulse, an acquisition time of 0.4 s, a relaxation delay of 0.2 s and between 70,000 and 100,000 transients (12–17 h) were acquired. Chemical shifts were indirectly referenced to external 85% H_3PO_4 (at $\delta = 0.0$) via the lock signal. Data were processed using a line broadening of 5–20 Hz.

To obtain peak areas, peaks in the raw spectrum were fitted with Lorentzian line shape using the deconvolution subroutine of the NMR software (Vnmr 6.1C, Varian Inc., Palo Alto, CA, USA). From these peak areas the contribution of the individual compound groups were calculated and related to TP detected in the extracts with ICP-AES.

2.6. ESI-MS-MS studies

After sample preparation (Fig. 1), the four extracts ('a–d') were mixed in a 1:1 (v/v) with MeOH before direct infusion into the mass spectrometer (PE SCIEX API III+). A Harvard apparatus pump with a Hamilton syringe of 250 μL handled the direct infusion of the extract via a fused silica capillary (50 μm i.d.) into the electrospray ionization source. The flow rate was 5 μL min^{-1}. For monitoring and viewing of the data LC2-tune (PE-SCIEX) and Multiview software were used, respectively. Measurements were made in negative ion mode, and consisted of scanning the parent ions of mass over charge (m/z) 97 and 79 that correspond, respectively, to the dihydrogenphosphate ($[H_2PO_4]^-$) and phosphite ($[PO_3]^-$) ion. Spectra were recorded in duplicate at two collision energy levels, 20 (low) and 40 (high)

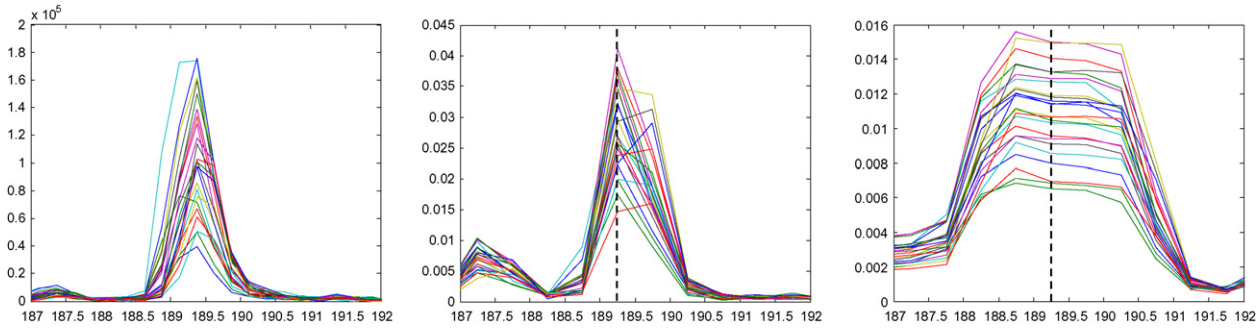

Fig. 2. Selected peak around $m/z = 189.25$ for set-up B (parents of m/z 79 at high collision energy). (Left panel) Raw data (m/z resolution 0.25), total intensities. (Mid panel) Binned (m/z resolution = 0.5) and normalized intensities (unit total sum); maximum average at m/z 189.25. (Right panel) As mid panel but 'blurred' by ± 2 bin ($m/z \pm 1$) to be evaluated at m/z 189.25.

eV. The four different instrument settings were thus: (A) parent 79, low energy; (B) parent 79, high energy; (C) parent 97, low energy and (D) parent 97, high energy. The dwell time was 5 ms and the step size for m/z was 0.25. For each set of settings, 10 scans were recorded in multiacquisition mode (MCA) resulting in one spectrum with mass range m/z 75–600. The four extracts ('a–d') were each analyzed at three different occasions ('1–3') with two MS runs as shown in Fig. 1. Twenty-four MS spectra originating from the same pooled sediment sample were made and in total 96 spectra were acquired from the four samples.

3. Evaluation of the ESI-MS-MS data

The aim of the data analysis was to assess the variations between the spectra induced by different extractions, different occasions of MS analysis as well as repeated MS runs. The analysis was performed independently for the four MS-MS set-ups (A–D) and with respect to: (i) total ion counts, (ii) most abundant peaks and (iii) prominent peak patterns as described below.

3.1. Quantitation of the MS runs

Large peak intensity variations occurred between the different runs and the sum of the intensities for all peaks was taken as a first quantitative measure of each spectrum. By normalization to unit sum within each spectrum, i.e. dividing with the total sum of intensities in the spectrum, the individual peaks can be evaluated without influence of common variations caused by, e.g., changes in the ESI conditions. However, possible m/z shifts between the spectra may also result in large variations in the intensity values for a selected m/z value. Fig. 2 shows a part of the raw data from set-up B in the left panel, the 24 spectra around m/z 198 with step size 0.25 (the data points are drawn halfway between the m/z steps). As a first step to reduce the m/z shifts, the data were binned to m/z resolution 0.5 by summing the intensities for two consecutive m/z steps. The resulting spectra, normalized to unit sum, are shown in the mid panel of Fig. 2. The average of the binned and normalized spectra was calculated for each set-up, representing the mean ESI-MS-MS result. For the selected peak in Fig. 2, the maximum average relative intensity occurs at m/z 189.25, which was taken as the peak position. To further reduce the influence of the m/z shifts, 'blurred' versions of the spectra were produced; for each data point (m/z value) the mean value was taken for the intensities including two neighboring data points on each side resulting in broadened flat peaks (Fig. 2, right panel). Together the binning and 'blurring' comprise a summing window of m/z 2.5, which accounts for the peak width as well as possible peak shifts. Thus the peak level for the 'blurred' spectra represents the individual peak areas, and despite the original variations in peak position there is a single m/z value that can be used for comparable peak quantitation (the 'blurred' intensity value).

From the average spectrum, the peak positions for the 20 most intense peaks were identified for the 4 different set-ups as shown in Fig. 3. The top three peaks were selected for comparison based on individual peaks within each set-up, but one should also take the covariation between the peaks into account. Covarying peaks imply underlying variation patterns that involve several ions, and such more systematic variations will stand out more clearly in comparison with the unavoidable random variations for individual peaks. Hence, principal component analysis (PCA) was applied to the values for the 20 selected peaks with each instrumental set-up, resulting in a rather small number of scores for each run. The score values are linear combinations of the 20 peak values, selected sequentially to describe as much as possible of the peak variations. In this work the first three principal components were retained, accounting for more than two-thirds of the variations with each set-up. Moreover, these components will especially capture variation that is common for several variables (peaks) and therefore be more related to common sources of variation. The differences between the four extracts and the three occasions, as well as between replicate runs, were visualized by score plots.

3.2. Analysis of variance (ANOVA)

A two-way ANOVA determined to which extent the variations were due to differences between extracts, between occasions and between replicate runs. Variance estimates for these different sources of variation were calculated and checked for significance. The sum of the three variances was taken as a measure of the reproducibility, expressed as the relative standard deviation (R.S.D.) and reported together with

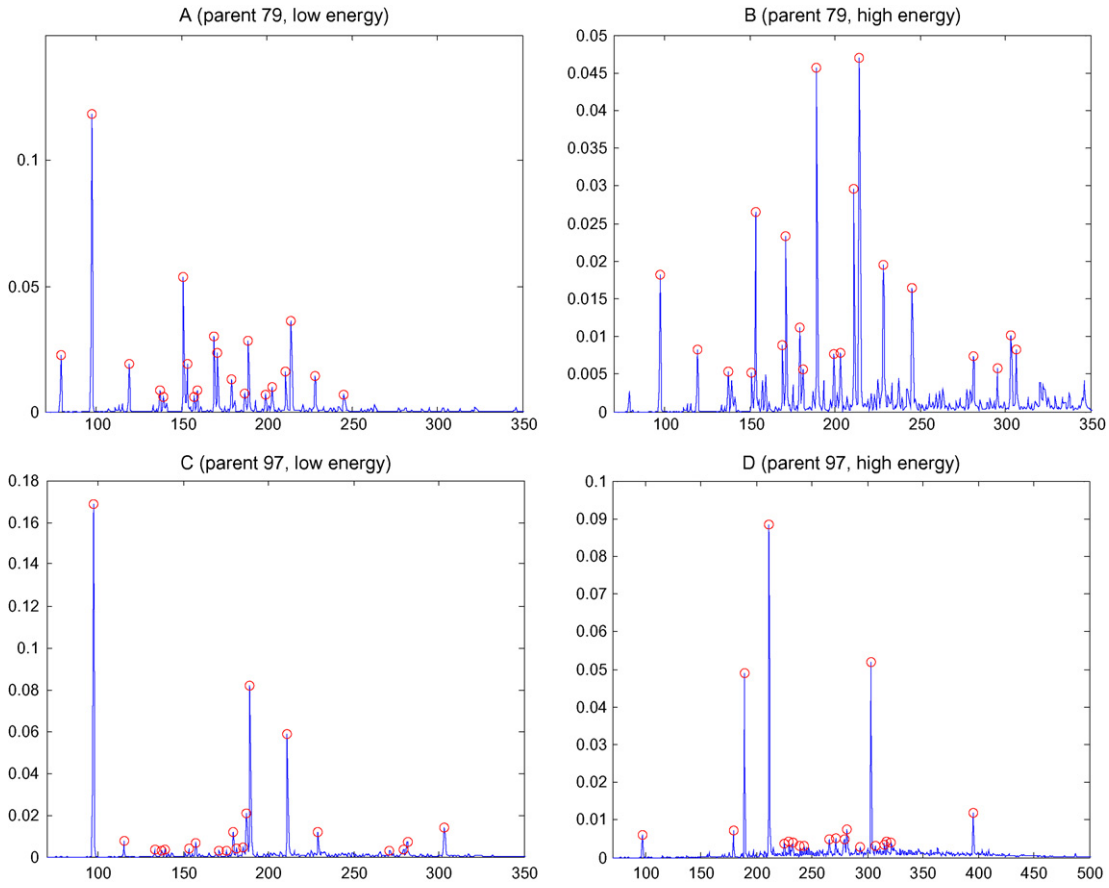

Fig. 3. The average spectra and the 20 most abundant peaks from the 4 ESI-MS-MS set-ups (A–D). (Vertical axes) Relative abundance (scaled to unit sum). (Horizontal axes) Mass over charge (m/z). Note the different m/z scale for D.

the percentage variance contributions from the three sources. These measures were calculated for the total ion count as well as the three dominant peaks for each set of instrumental conditions (A–D). The multivariate variation patterns were analyzed by the same ANOVA treatment of the score values for one principal component at a time, as these could be regarded as independent latent variables. The significance was used as guidance for selection of the most informative score plots.

3.3. Software

For general data treatment and basic calculations, Microsoft Excel was used. ANOVA was performed with Minitab 14 (Minitab Inc., State College, PA, USA) and multivariate data analysis with The Unscrambler 7.6 (ASA Camo, Oslo, Norway).

4. Results and discussion

4.1. Extraction

The TP concentration in the sediment was 1.99 mg g^{-1} DW and the concentration of P extracted with NaOH was 0.37 mg g^{-1} DW P (Table 1). According to the fractionation scheme in Psenner and Pucsko [22], the extracted part should contain the major part of the organic P present in the sediment. It should be kept in mind though that NaOH most likely hydrolyzes some of the organic P compounds and the extract will thus not exactly represent what is present in the sediment [24]. Hupfer et al. [6] suggests the use of NaOH–EDTA to decrease this hydrolyzing process because metal ions likely to catalyze the degradation process will be inactivated by the complexing agent EDTA. Moreover, P compounds are most commonly bound to sediment via adsorption to Fe or Al oxides. Since EDTA will chelate Fe ions it will enable the release of the P compounds into solution and will thus increase the overall P yield of the extraction. However, since EDTA causes ion suppression in the ESI-interface and is more difficult than sodium ions to clean from the extract, NaOH was preferred in this study. Even though this results in a lower overall P yield [24], a bet-

Table 1
The total sediment P concentration (mg g^{-1} dry sediment weight) and the total P concentrations (mg g^{-1} dry sediment weight) for the four extracts ('a–d') as measured with ICP-AES; before sample clean-up (NaOH extract), after ion exchange and after the concentration and filtering steps

	'a'	'b'	'c'	'd'	Average
Sediment	1.99	1.99	1.99	1.99	1.99
NaOH extract	0.44	0.34	0.35	0.35	0.37
After ion exchange	0.62	0.34	0.41	0.34	0.43
Concentrated and filtered	0.30	0.21	0.21	0.22	0.24

Table 2
Concentration (mg g^{-1} dry sediment weight) and relative composition (percentage within brackets) of the P compounds measured by ^{31}P NMR for the pooled extract after NaOH extraction and the four extracts ('a–d') after sample clean-up

	Pooled	'a'	'b'	'c'	'd'	Average	Recovery (%)
Ortho-P	0.19 (52)	0.17 (56)	0.12 (56)	0.12 (58)	0.14 (65)	0.14 (59)	72
Monoesters	0.078 (21)	0.069 (23)	0.051 (24)	0.049 (23)	0.033 (15)	0.050 (21)	65
P-lipids	0.016 (4)	0.027 (9)	0.019 (9)	0.018 (9)	0.011 (5)	0.019 (8)	120
Pyro-P	0.050 (14)	0.037 (12)	0.024 (11)	0.023 (11)	0.031 (14)	0.028 (12)	85
DNA	0.034 (9)	<l.o.d.	<l.o.d.	<l.o.d.	<l.o.d.	<l.o.d.	–

For the latter, also the average results are given. The P recovery during sample preparation is calculated for the individual P compounds using the average results; l.o.d., limit of detection.

ter resolution in identification of unknown organic P sediment compounds was gained. The main objectives of the subsequent sample clean-up were: (i) to reduce sodium ions coming from the extractant, (ii) to concentrate the sample and (iii) to obtain a non-viscous easy-to-spray liquid representative for the original extract.

4.2. Sample clean-up and recoveries

On average about one-third of the P contents are lost in the sample preparation steps following the extraction with NaOH (Table 1). Using ion exchange as a method for reducing Na ions resulted in no detectable P losses (Table 1) while the sodium amount decreased 80% (from 22,300 ppm Na in the extract to 4500 ppm Na after sample clean-up). Losses of P compounds occurred mainly during concentration and filtering. The filters were chosen according to their mass cut-off abilities. Hence, besides obtaining an easy-to-spray sample, the compounds retrieved in the filtrate did not exceed a certain mass, narrowing the mass window for MS-analysis and simplifying the spectra. Pre-studies showed that $66 \pm 1\%$ of the organic P compounds in the extract had a molecular weight lower than 3 kDa. The relative losses, including P compounds larger than 3 kDa, in the presented study were highly reproducible between the individual extracts (Table 1), which indicates quantitative total P recovery (about 65%) during sample clean-up.

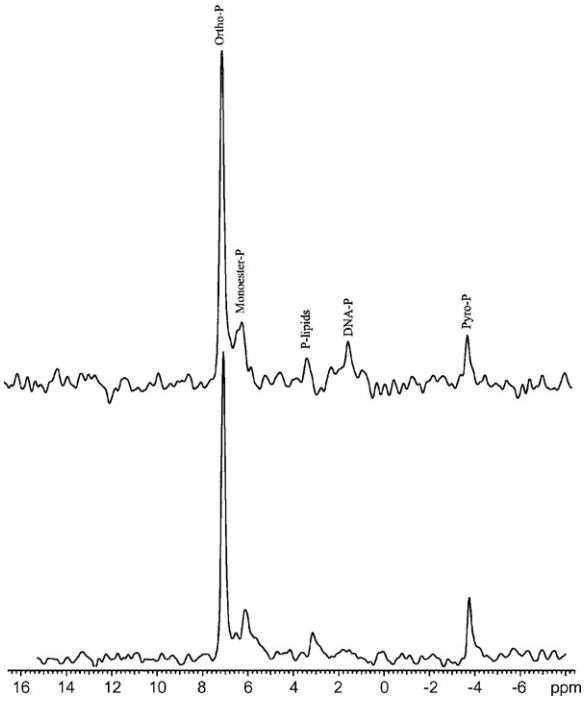

Fig. 4. ^{31}P NMR spectra on the NaOH-extract (upper) and on the extract after complete sample preparation (lower). DNA-P is below the limit of the detection for the latter one.

In terms of individual P compound groups, there were reasonable recoveries of Ortho-P (72%), Monoester-P (65%), P-lipids (120%) and Pyro-P (57%) with the applied sample preparation procedure (Table 2). Note that Diester-P, most likely DNA-P was below the detection limit after the proposed sample preparation method (Fig. 4). Additional measurements showed that DNA mainly disappeared after the mass cut-off filtering step, indicating that DNA does not pass through the 3 kDa mass cut-off filter. It is thus likely to assume that these compounds are too large to pass the filter due to their shape and size. The absence of polyphosphates in the NaOH extract (Table 2) was not surprising. Due to the overall lower P yield because of only using NaOH instead of EDTA–NaOH as main extractant and most probably in combination with alkali induced hydrolysis as previously mentioned [24], it is likely that the polyphosphate level dropped under the limit of detection for ^{31}P NMR.

Except for DNA, the extract after the sample preparation procedure was representative for the original extract (showing a similar P composition). In addition the proposed procedure provided an easy-to-spray sample compatible with ESI-MS-MS.

Table 3
Total intensities for the spectra of the different instrumental set-ups A–D

	A	B	C	D
Mean	4379983	3821900	4117192	1240883
R.S.D. (%)	35	43	38	54
Extract (%)	34**	10	28*	6
Occasion (%)	33**	44**	19*	23*
Replicate (%)	33	46	53	71

Mean intensity and relative standard deviation (R.S.D.) for $n = 24$. The variance components due to extract, occasion and replicate were assigned by ANOVA and reported in percentage of the total variance. Statistical significance noted by ($^{*}p < 0.05$), ($^{**}p < 0.01$).

Table 4
Variations in relative intensity for the three most intense peaks of each dataset (A–D)

	A			B			C			D		
m/z	97	151	214	214	189	211	97	189	211	211	303	189
R.S.D. (%)	10	17	10	12	21	14	13	24	13	13	26	28
Extract (%)	28*	7	21	0	49**	30*	0	62***	14	9	67***	30*
Occasion (%)	12	17	12	31*	0	11	18	0	0	0	0	0
Replicate (%)	60	76	67	69	51	59	82	38	86	91	33	70

The position (*m/z*) and the relative standard deviation (R.S.D.) is given together with the relative variance contributions due to extract, occasion and replicate. Statistical significance noted by ($^{*}p<0.05$), ($^{**}p<0.01$) and ($^{***}p<0.001$).

Table 5
Variations in the scores for the three first principal components (PCs) of each dataset (A–D)

	A			B			C			D		
PC number	1	2	3	1	2	3	1	2	3	1	2	3
Expl. var. (%)	41	15	12	40	16	10	39	17	13	32	15	14
Extract (%)	79***	6	5	70***	8	0	73***	0	0	74***	7	5
Occasion (%)	0	51**	19	4	47**	44**	0	0	47**	0	61***	32**
Replicate (%)	21	43	76	26	45	56	27	100	53	26	31	42

For each PC the amount of explained variation (expl. var.) is given together with the relative variance contributions due to extract, occasion and replicate. Statistical significance noted by ($^{**}p<0.01$) and ($^{***}p<0.001$).

4.3. Analysis of phosphate groups with ESI-MS-MS measurements: reproducibility and repeatability

As a first step the total intensities, for all parent ions within *m/z* 75–600, are considered. Their variation, expressed in R.S.D. values, was in the range of 35–54% (Table 3). These values were then further analyzed by ANOVA. Less than a third of the variation was due to the sample preparation, where the significant results (set-ups A and C) could be referred to a low mean value of the intensity for sample 'a'. On the other hand, it could be noted that extract 'a' showed the highest recovery based on the ICP-AES analysis of total P (Table 1). However, most of the variation in the total intensities of the MS spectra was associated with variations in the measurement conditions, partly between measurement occasions (with means ordered as '1' < '3' < '2') but mostly between mere replicate runs.

The 'blurred' intensities (cf. Section 3.1) were compiled for the 20 most intense peaks in each dataset, providing a set of variables (relative intensities for the dominant peaks) that could be analyzed by ANOVA in the same way as the total intensities. The ANOVA results for the three most dominant peaks in each dataset are given in Table 4. The selected peaks may easily be identified in Fig. 3. The over-all variation for these individual peaks corresponds to a R.S.D. value in the range 10–26%, with pure replication (repeated runs) as the major source. For some of the peaks (*m/z* 189 and *m/z* 303), however, there are significant differences between the extracts even at the lowest significant level ($\alpha<0.001$). The single case of significance (at $\alpha<0.05$) for the occasion factor could be disregarded; due to the multiple significance test such results are quite likely to occur by chance.

Table 5 shows the ANOVA results for the first three principal components (PCs) for each instrumental set-up. PC1, explaining about 40% of the total variance, is mostly related to differences between the four extracts, i.e. due to sample preparation. Such differences account for 70–80% of the PC1 variance, which is

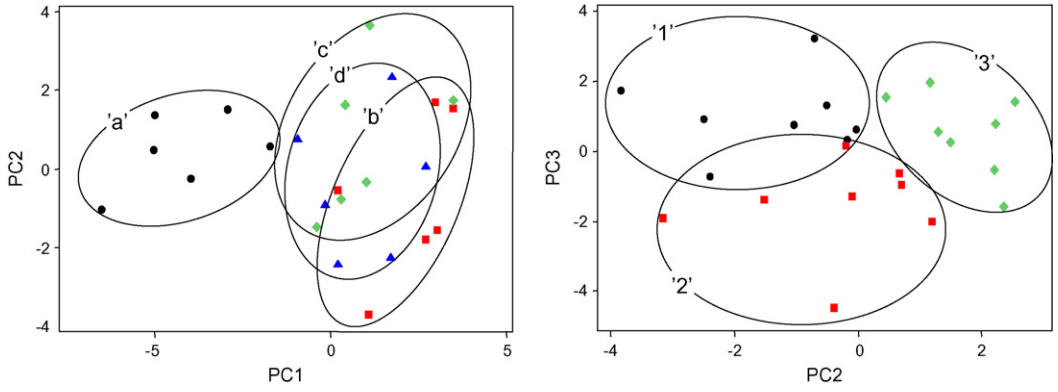

Fig. 5. Score plots from PCA of the 20 most intense peaks (cf. Fig. 1 and Table 3). (Left panel) PC1 and PC2 for set-up A (parents of *m/z* 79 at low collision energy) indicating the significant variation between extracts ('a' differing from 'b', 'c' and 'd'). (Right panel) PC3 and PC2 for set-up D (parents of *m/z* 97 at high energy) with clustering according to occasions '1', '2' and '3'.

highly significant for all set-ups ($\alpha < 0.001$). Also the different occasions give rise to significant variations, although in higher principal components (PC2 and/or PC3). With two-dimensional score plots, each run is represented as a point and by proper labeling the systematic variation due to samples and occasions are visualized.

In Fig. 5 (left panel), the PC1/PC2 scores are plotted for dataset A with extract ('a–d') as labels. Again it is found that extract 'a' is different from extracts 'b–d', forming a clearly separated cluster. To illustrate the difference between occasions, a score plot of PC2/PC3 for dataset D was chosen (Fig. 5, right panel). Here the three occasions ('1–3') cluster separately.

The variation between the extracts can partially be explained by the differences between the four sediment samples obtained from the pooled sediment (Fig. 1). Since the sediment is a mixture of particles and pore water, continuous stirring is necessary to keep a homogenous sample. As soon as we stop stirring and start to pour the sediment into four different vials, the sediment particles will start to sink. These problems could therefore result in variations between the four sediment samples because some of them will contain a higher ratio of particles to pore water than others. Assuming that the organic phosphorus compounds are attached to the particles, differences will occur in the composition of the extracted compounds and thus in the composition of the MS spectra. Not only does the amount of particles differ also the shape and size of the particles most likely varies. This results in different amounts of P compounds attached to the sediment particle surface and thus again, different amounts of extracted P compounds.

To summarize this section, it was found (Table 3) that there is rather large variation in total intensity (R.S.D. 35–54%). Of the estimated variance components, about one-half represents repeatability (mere replicates). As for reproducibility, the remaining half was divided between the extracts (sample preparation) and the occasions of analysis (measurement conditions), with the contribution of the latter somewhat higher. The relative intensities for the three most intense peaks in each dataset were analyzed in the same way by ANOVA, and Table 4 shows that replicate runs are the dominating source of variation. Due to correlation between different peaks (parent ions) the scores from PCA will emphasize the influence of the underlying experimental factors, and for all the set-ups the sample preparation (extract) caused the major part of the total variance in PC1 (Table 5, also visualized in Fig. 5, left panel). Also, all three occasions clustered separately as shown in Fig. 3 (right panel).

4.4. Parent ions with phosphate groups according to ESI-MS-MS

Fig. 3 shows the average spectrum for each experimental set-up (A–D) measured with ESI-MS-MS. We assume that *m/z* 79 and 97 represent the ions phosphite and dihydrogenphosphate, respectively. However, it cannot be ruled out completely that other ions than dihydrogenphosphate and phosphite are detected at the same *m/z* and thus also result in certain parent ions. When looking for parent ions of *m/z* 97 (dihydrogenphosphate) it is advantageous that phosphate ions can fragment into phosphite ions in the collision cell. This can be seen in Fig. 3 (set-up A), where phosphate ions (*m/z* 97) actually appear as parent ions of *m/z* 79. Therefore, peaks that occur in the parent ion spectrum of both *m/z* 79 and 97 are more likely to represent phosphate containing compounds than peaks that occur only in the *m/z* 97 parent ion spectrum. From Table 6, it is thus reasonable to assume that *m/z* 137, 139, 153, 157, 171, 179, 187, 189, 211, 281 and 303 represent phosphate containing ions since they occur in both the parent ion spectra of *m/z* 79 and 97. However, it must be kept in mind that peaks that only occur as parents of *m/z* 97 still might represent phosphate containing ions.

The information from the two collision energy levels indicates that larger parent ions require higher energy to produce the

Table 6
m/z values for the 20 most intense peaks for each instrumental set-up A–D

Parents of 79		Parents of 97	
A, 20 eV[a]	B, 40 eV[a]	C, 20 eV[a]	D, 40 eV[a]
79.0			
97.0	97.0	97.0	
		115.0	
119.0	119.0		
		133.0	
137.0	137.0	137.0	
139.0		139.0	
151.0	151.0		
153.0	153.0	153.0	
157.0		157.0	
159.0			
169.0	169.0		
171.0	171.0	171.0	
		175.0	
179.0	179.0	179.0	179.0
	181.0	181.0	
		185.0	
187.0		187.0	
189.0	189.0	189.0	189.0
199.0	199.0		
203.0	203.0		
211.0	211.0	211.0	211.0
214.0	214.0		
			225.0
228.0	228.0		
		229.0	229.0
			232.5
			239.0
			243.0
245.0	245.0		
			265.5
		271.0	271.0
		279.0	279.0
	281.0	281.5	281.5
			293.5
	295.0		
	303.0	303.0	303.0
	306.0		
			307.0
			315.0
			317.0
			321.0
			395.0

[a] Collision energy.

characteristic fragments for phosphate containing compounds. This is shown in Fig. 3, where there are relatively more peaks in the *m*/*z* range beyond 250 for the high energy spectra compared to the low energy spectra. Work is currently in progress to explore if this observation also can be utilized for differentiation of mono- and di-phosphate esters.

5. Conclusions

The proposed method obtained the three pre-set goals of reducing sodium ions, concentration and an easy-to-spray liquid representative for the original extract. With the causes of variations in mind, eleven different masses were found to most likely represent phosphate containing compounds. To gain further knowledge about turnover rates of the different P compounds, which is of interest in an ecological perspective, it will be highly desirable to verify the performance of the proposed methods with different sediments, especially sediments representing different age. To determine turnover rates it is necessary to secure the quality of the quantitative information by investigating possible matrix effects. Future work should include a separation step prior to MS analysis. The implementation of a separation step will also contribute to a reduction in sample complexity and thereby further enhance the possibility to identify individual P compounds.

References

[1] B.L. Turner, B.J. Cade-Menun, L.M. Condron, S. Newman, Talanta 66 (2005) 294.
[2] A. Hieltjes, L. Lijklema, J. Env. Qual. 9 (1980) 405.
[3] H. Golterman, Hydrobiologia 335 (1996) 87.
[4] E. Rydin, Water Res. 4 (2000) 2037.
[5] K. Reitzel, J. Hansen, H.S. Jensen, F.Ø. Andersen, K.S. Hansen, Hydrobiologia 506–509 (2003) 781.
[6] M. Hupfer, R. Gachter, H. Rüegger, Limnol. Oceanogr. 40 (1995) 610.
[7] L.L. Clark, E.D. Ingall, R. Benner, Nature 393 (1998) 426.
[8] A. Paytan, B.J. Cade-Menun, K. McLaughlin, K.L. Faul, Mar. Chem. 82 (2003) 55.
[9] M. Hupfer, B. Rube, P. Schmieder, Limnol. Oceanogr. 49 (2004) 1.
[10] J. Ahlgren, L. Tranvik, A. Gogoll, M. Waldeback, K. Markides, E. Rydin, Env. Sci. Technol. 39 (2005) 867.
[11] K. Reitzel, J. Ahlgren, H. De Brabandere, M. Waldebäck, A. Gogoll, L. Tranvik, Biogeochemistry 82 (2007) 15.
[12] M. Suzumura, A. Kamatani, Geochim. Cosmochim. Acta 57 (1993) 2197.
[13] N. Amini, I. McKelvie, Talanta 66 (2005) 445.
[14] K.G. Zink, K. Mangelsdorf, Anal. Bioanal. Chem. 380 (2004) 798.
[15] S.P. Seitzinger, H. Hartnett, R. Lauck, M. Mazurek, T. Minegishi, G. Spyres, R. Styles, Limnol. Oceanogr. 50 (2005) 1.
[16] J.M. Llewelyn, W.M. Landing, A.G. Marshall, W.T. Cooper, Anal. Chem. 74 (2002) 600.
[17] W.T. Cooper, J.M. Llewelyn, G.L. Bennett, V.J.M. Salters, Talanta 66 (2005) 348.
[18] M. Edelson-Averbukh, R. Pipkorn, W.D. Lehmann, Anal. Chem. 78 (2006) 1249.
[19] M.J. Huddleston, R.S. Annan, M.F. Bean, S.A. Carr, J. Am. Soc. Mass Spectr. 4 (1993) 710.
[20] E. Rydin, A.-K. Brunberg, Arch. Hydrobiol. Spec. Issues Adv. Limnol. 51 (1998) 157.
[21] E.D. Ingall, P.A. Schroeder, R.A. Berner, Geochim. Cosmochim. Acta 54 (1990) 2617.
[22] R. Psenner, R. Pucsko, Adv. Limnol. 30 (1988) 43.
[23] A.M. Vassallo, M.A. Wilson, P.J. Collin, J.M. Oades, A.G. Waters, R.L. Malcolm, Anal. Chem. 59 (1987) 558.
[24] J. Ahlgren, H. De Brabandere, K. Reitzel, E. Rydin, A. Gogoll, M. Waldebäck, J. Env. Qual. 26 (2007) 892.

Available online at www.sciencedirect.com
ScienceDirect
Talanta 74 (2008) 1378–1384
Talanta
www.elsevier.com/locate/talanta

The use of microemulsion for determination of sodium and potassium in biodiesel by flame atomic absorption spectrometry

Alexandre de Jesus, Márcia M. Silva *, Maria Goreti R. Vale

Instituto de Química, Universidade Federal do Rio Grande do Sul, Av. Bento Gonçalves 9500, CP 15003, CEP 91501-970, Porto Alegre-RS, Brazil

Received 8 September 2007; received in revised form 13 September 2007; accepted 13 September 2007
Available online 19 September 2007

Abstract

A new method for F AAS determination of sodium and potassium in biodiesel using water-in-oil microemulsion as sample preparation is proposed. The method was investigated for biodiesel produced from different sources, as soybean, castor and sunflower oil and animal fat and was also applied for vegetable oils. The optimized condition for microemulsion formation was 57.6% (w/w) of *n*-pentanol, 20% (w/w) of biodiesel or vegetable oil, 14.4% (w/w) of Triton X-100 and 8% (w/w) of water (aqueous standard of KCl or NaCl in/or diluted HNO_3). The optimized instrumental parameters were: aspiration rate of 2 mL min^{-1} and the flame composition of 0.131 of C_2H_2/air ratio. For comparison purpose, the determination of sodium and potassium were also carried out according to European norms (EN 14108 and EN 14109, respectively). These norms are applied for determination of sodium and potassium in fatty acid methylic ester samples and consist in the sample dilution using organic solvent and determination by F AAS. The stability of microemulsified aqueous standards and samples was investigated and it was found to be stable for at least 3 days while the organic standard diluted with xylene showed a decrease around of 15% in the analytical signal in 1 h. The limits of detection were 0.1 μg g^{-1} and 0.06 μg g^{-1} and the obtained characteristic concentrations were 25 μg L^{-1} and 28 μg L^{-1} for sodium and potassium, respectively. The proposed method presented two times better limits of detection and better precision (0.4–1.0%) when compared with the dilution technique (1.5–4.5%). The accuracy of the method was evaluated through recovery tests and comparison with the results obtained by dilution technique. The recoveries ranged from 95% to 115% for biodiesel and 90% to 115% for vegetable oil samples. Comparison between the results obtained for biodiesel by both methods showed no significant differences at the 95% confidence level according to a Student's *t*-test. This study shows that the proposed method based on microemulsion as sample preparation can be applied as an efficient alternative for sodium and potassium determination in biodiesel samples.
© 2007 Elsevier B.V. All rights reserved.

Keywords: Sodium and potassium determination; Biodiesel; Microemulsions; Flame atomic absorption spectrometry

1. Introduction

With the constant exhaustion of the petroleum sources, the use of alternative sources of energy becomes essential. The fatty acid alkyl esters derived from vegetable oils or animal fats (biodiesel or B100) reveals a promising renewable source of energy [1]. The use of biodiesel presents many advantages: it is a renewable source of energy, it is energy efficient, displaces petroleum derived diesel fuel, reduces global warming gas emissions, reduces tailpipe emissions including air toxics and recycled cooking grease could be used for biodiesel production [2]. In tropical countries with large territorial areas as Brazil, the cultivation of vegetable oil sources to produce biodiesel could also achieve an economic up-scale, besides of hindering the rural exodus [3].

In the biodiesel manufacture process, that consists in the transesterification of oils or fats (from plants or animals) with short chain alcohols (methanol or ethanol), sodium or potassium hydroxide are used as catalysts. However the presence of potassium or sodium in the end product results in the formation of insoluble soap and consequently deposit formation in the vehicles filters [4]. Thus the residual catalyst should be removed from the biodiesel through successive washes with water, after what the quantification of these metals becomes necessary to assure the quality of the product. The determination of sodium and potassium in fatty acid methylic ester samples, according

* Corresponding author. Tel.: +55 51 3308 6278; fax: +55 51 3308 7304.
E-mail address: mmsilva@iq.ufrgs.br (M.M. Silva).

0039-9140/$ – see front matter © 2007 Elsevier B.V. All rights reserved.
doi:10.1016/j.talanta.2007.09.010

to Europeans norms (EN 14108 and EN 14109) [5,6] consist of sample dilution with organic solvent (xylene, cyclohexane or petroleum ether) and determination by flame atomic absorption spectrometry (F AAS). Nowka proposed the use of flame emission spectrometry for determination (F AES) of these elements in biodiesel samples after dilution with kerosene [7]. By the application of a supplementary oxidant (atmospheric oxygen) it was possible to eliminate the optical background observed in potassium analysis, allowing the interference free determination of both elements in the biodiesel fuel samples. The use of inductively coupled plasma optical emission spectrometry (ICP OES) has been proposed by Edlund et al. [8] for analyses of biodiesel samples diluted with kerosene. The application of cold argon-oxygen plasma enables Na and K determination at $\mu g\,kg^{-1}$ concentrations in biodiesel due to reduction of background emission of carbon and carbon compounds.

Despite of its simplicity the methods based on dilution with organic solvents as kerosene present the following disadvantages: low stability of the analyte in the diluted standards or samples, calibration curves prepared with high-cost organometallics standards, handling of some organic solvents with conventional laboratory equipment is difficult, moreover, several organic solvents present carcinogenic effects. The use of ethanol as solvent for diluting biodiesel samples was proposed by Santos et al. [9] for determination of Ca, P, Mg, K and Na by ICP OES. This solvent allowed the use of aqueous standard for calibration overcoming some disadvantages cited above. By using a supplementary oxygen flow to decrease the background and Y as internal standard, recoveries in the range from 82% to 114% for all analytes were obtained.

The use of emulsion and microemulsion as sample preparation has been applied for trace metal determination in petroleum derivates such as automotive fuels, as reported in recent reviews [10,11]. Microemulsions are thermodynamically stable systems composed of water, oil and surfactant, and, in some cases, an alcohol can be added as co-surfactant [12–15]. Microemulsions are apparently homogeneous under visual observation, but in fact they are nanoheterogeneous, i.e., systems formed of particles with diameters in the order of 5–100 nm suspended in a continuous phase [16–18]. This technique allows the use of aqueous standards for calibration instead of expensive and instable organometallic standards. The microemulsion sample preparation has been used with the main atomic spectrometric techniques such as electrothermal atomic absorption spectrometry (ET AAS) [19–23], inductively coupled plasma optical emission spectrometry (ICP OES) [24], and inductively coupled plasma mass spectrometry (ICP-MS) [25,26]. Due to their inherently low sensitivity the use of F AAS and F AES for these applications is quite reduced. Du et al. utilized microemulsion for the determination of chromium naphthenate in gasoline by F AAS [27]. These authors found high-nebulization efficiency and stable combustion of the flame when the microemulsions were analyzed. Another advantage reported was the use of aqueous standard of chromium to prepare the microemulsion for calibration.

The use of microemulsion as sample preparation for biodiesel analysis, to the best of our knowledge, has not been described yet. However the microemulsion formation with vegetable oils has been investigated by some authors. Mendonça et al. proposed a water-in-oil microemulsion with vegetable oils as medium for electrochemical measurements [28] and as background electrolyte in reverse microemulsion electrokinetic capillary chromatography [29]. The use of emulsions as sample preparation for the determination of trace metals in vegetable oils by ICP OES [30,31], ICP-MS [32,33] and F AAS [33] have been also proposed.

The goal of this work was to investigate the use of microemulsions as sample preparation for a routine and reliable determination of sodium and potassium in biodiesel and vegetable oil. The expected advantage of this procedure would be the higher stability and easily handle of sample and standard microemulsions, as well as no need of using organometallic standards and carcinogenic solvents. The composition of microemulsion, the stability of the standards and samples and optimization of the instrument parameters were investigated. Emphasis was also given to comparison with the standard method of dilution of sample with organic solvent.

2. Experimental

2.1. Instrumentation

All measurements were carried out using a model AAS 6 Vario atomic absorption spectrometer (Analytik Jena AG, Jena, Germany). Sodium and potassium hollow cathode lamp (Photron, Australia) operating at 7 mA and 6 mA, respectively, were used as the radiation source. The primary resonance lines of sodium (589.0 nm) and potassium (766.5 nm) were used with a bandwidth of 0.8 nm for both metals. The acetylene flow rates and the burner height were adjusted in order to obtain the maximum absorbance signal.

A Europe balance (Gibertini, Italy) with an accuracy of 0.0001 g was used for weighing the samples and reagents.

2.2. Reagents and samples

Analytical grade reagents were used throughout. Distilled, deionized water (DDW) with a specific resistivity of 18.2 MΩ cm from a Milli-Q water purification system (Millipore, Bedford, MA, USA), was used for the preparation of the solutions and microemulsions. All containers and glassware were soaked in $3\,mol\,L^{-1}$ nitric acid for at least 24 h and rinsed three times with DDW before use. The nitric acid (Merck, Germany) used for microemulsion preparation was further purified by sub-boiling distillation in a quartz sub-boiling still (Kürner Analysentechnik, Rosenheim, Germany). The surfactant Triton X-100 (Union Carbide, United States) and the alcohols propanol, *n*-butanol and *n*-pentanol (Merck, Darmstadt, Germany) were used for microemulsion preparation. Base mineral oil (High Purity Standards, Charleston, USA) was used in the microemulsions and in the dilution techniques to simulate the oil phase in the standards for calibration. Aqueous stock solutions ($1000\,mg\,L^{-1}$) were prepared from of sodium and potassium chlorides (Acros, USA). Xylene (Nuclear, Brazil) as

Table 1
Biodiesel samples characteristics

Samples	Oil	Catalyst	Alcohol
R-02	Soybean	KOH	Ethanol
S-01	Animal fat	KOH	Ethanol
S-02	Animal fat	KOH	Methanol
E-01, C-32	Soybean	NaOH	Ethanol
B-09, B-13, B-14, B-40	Castor bean	KOH/NaOH	Methanol
B-48	Sunflower	NaOH	Methanol
C-01, C-04, D-01, I-01, J-02	Soybean	KOH	Methanol
B15, C-57, C-64, C-74	Soybean	NaOH	Methanol

solvent and sodium and potassium organometallic standards, the salts sodium cyclohexanebutirate ($1.000\,mg\,g^{-1} \pm 0.008$) and potassium cyclohexanebutirate ($1.001\,mg\,g^{-1} \pm 0.003$) purchased from Specsol (São Paulo, Brazil), were used for the determination of sodium and potassium according to EN 14108 and EN 14109.

Biodiesel samples obtained from different sources were analyzed and the characteristics of these samples are shown in Table 1. The samples S-01, S-02 and the B series are commercial samples obtained from producers and all others were obtained from research groups that are working in development of production of biodiesel at Federal University of Rio Grande do Sul and at a research center CIENTEC, Porto Alegre, Brazil. Another sample named H-23 provided by PETROBRAS, Rio de Janeiro, Brazil, was also analyzed. This sample is not a biodiesel, but a fuel obtained from vegetable oil called H-Bio, still in development by PETROBRAS. Unfortunately, additional information was not provided. Some vegetable oils (soybean, sunflower and rapeseed) obtained from local market were also analyzed.

2.3. Microemulsion preparation and analysis

For the microemulsion preparation the biodiesel or vegetable oil sample was first mixed with surfactant (Triton X-100) and co-surfactant (the alcohols propanol, *n*-butanol or *n*-pentanol), after which the water phase ($1.4\,mol\,L^{-1}$ HNO_3) was added. The microemulsion was obtained when a single transparent phase was formed. The mass proportion adopted for microemulsion preparation for biodiesel analysis was 57.6% of *n*-pentanol or *n*-butanol, 20% of biodiesel or vegetable oil, 14.4% of Triton X-100 and 8% of water ($1.4\,mol\,L^{-1}$ HNO_3). The microemulsions were prepared in volumetric flasks of 5 mL. For the calibration standards, 20% (w/w) of base oil was used in the microemulsion to simulate the biodiesel or vegetable oil phase. The standards were prepared from a NaCl or KCl stock solution of $100\,mg\,kg^{-1}$ pipetting, into the aqueous phase, the volume to give concentrations in the range of 0.0–4.0 $mg\,L^{-1}$ in 5 mL.

The aspiration rate and fuel/oxidant ratio were optimized before analysis.

In order to investigate the matrix effect, the microemulsified samples of biodiesel and vegetable oil were spiked with inorganic standards. The standard was added within the aqueous phase of the microemulsion.

2.4. Determination of sodium and potassium according to EN 14108 and EN 14109

As there is no certified reference material for biodiesel, the accuracy of the proposed method was evaluated comparing the obtained results with those obtained by using European norm EN 14108 and EN 14109. These norms are adopted for the determination of sodium and potassium in fatty acid methylic ester samples or B100 by the Brazilian regulations. These methods consist in the sample dilution with organic solvents (xylene, cyclohexane or petroleum ether) and determination by F AAS. In this work xylene was used as organic solvent for dilution of the samples and organometallic standards for calibration. The standards were prepared from a stock solution of $100\,mg\,kg^{-1}$, pipetting the volume to give concentrations in the range of 0.0–2.0 $mg\,L^{-1}$ in 10 mL volumetric flasks, and base oil was added for adjustment of the viscosity. The samples were prepared weighing 0.4 g and 1.0 g of sample for the determination of sodium and potassium, respectively, in a volumetric flask of 10 mL, and then diluted with xylene. The standards and samples were analyzed immediately after the dilution.

The aspiration rate and fuel/oxidant ratio were optimized before analysis.

The matrix effect was also investigated for this method. The biodiesel and vegetable oil samples were spiked with organometallic standards and then diluted with xylene.

3. Results and discussion

3.1. Microemulsion formation

A system based on oil-in-water (O/W) microemulsion, mainly with a large amount of water, is very advantageous in order to reduce the costs and because it is similar to aqueous solutions, being much simpler to obtain optimized instrument parameters for analysis without drastic changes after aqueous solutions analysis. Calibration against aqueous standards could also be expected. Therefore, we tried first to use large amount of water to obtain the microemulsion, but the hydrophobic phase (biodiesel or vegetable oil) not exceeding 20% in mass was not stabilized when more than 8% (w/w) of water was used and the emulsion formation was achieved. Although emulsions have been used for determination of trace metals in vegetable oils and fats by techniques based on nebulization systems for sample introduction [30,32,33], emulsions are unstable and the separation between phases takes place after a short period of time, requiring agitation to maintain the stability of the system during the analysis. To avoid this inconveniency, in this work the use of water-in-oil (W/O) microemulsion was chosen, using a maximum of 8% (w/w) of water. The water phase was also used to introduce the inorganic standard in the microemulsions prepared for calibration. Nitric acid was also introduced into this phase as it is very important to improve the stability of the analyte in the microemulsified samples and standards.

The use a relatively large amount of co-surfactant for the hydrophobic phase stabilization is related in the literature [34]. The formation of microemulsion was achieved using either

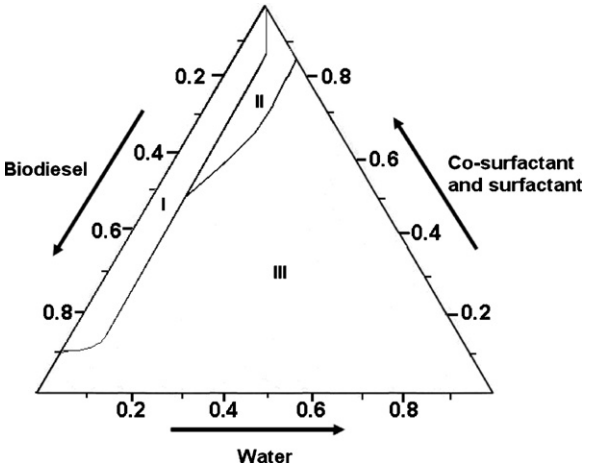

Fig. 1. Phase diagram of biodiesel/water/Triton X-100 and *n*-pentanol mixtures at 25 °C. Region I: microemulsion with *n*-butanol or *n*-pentanol; region II: microemulsion with *n*-buthanol; region III: emulsion.

n-butanol or *n*-pentanol as co-surfactant. The use of Triton X-100 was chosen because most of ionic surfactants frequently presents alkali metal contaminations. The microemulsion formation was achieved for surfactant/co-surfactant ratios in the range of 1:1–1:8, considering the percentage of water not exceeding 8% in mass. Concerning the amount of biodiesel, it was possible to stabilize up to 90% (w/w) of sample. The use of a maximum amount of sample in the microemulsion is desirable to increase the analysis sensitivity, but it also increases the viscosity, reducing the nebulization efficiency. Therefore the amount of 20% (w/w) was adopted. In Fig. 1 the obtained pseudo-ternary diagram for the microemulsion is shown. The mass proportion adopted for microemulsion preparation for biodiesel analysis was 57.6% of *n*-pentanol or *n*-butanol, 20% of biodiesel, 14.4% of Triton X-100 and 8% of water (NaCl or KCl aqueous standard in/or diluted nitric acid). This composition was also efficient for the microemulsion formation with vegetable oil or mineral oil (replacing the biodiesel).

3.2. Optimization of instrumental parameters

The optimization of fuel/oxidant ratio and aspiration rate was carried out with organometallic sodium standard diluted in xylene and with the microemulsified sodium chloride standard. For both medium 1.0 mg L^{-1} of sodium were used. The best sensitivity and stability of measurements for the dilution technique were obtained using the minimum fuel/oxidant ratio (0.061). In this condition the fuming and strongly reducing yellow flame is attenuated significantly, decreasing the instability of the absorption measurements. For the microemulsion system the stability of absorption measurements were not greatly affected and the best sensitivity was obtained using the fuel/oxidant ratio of 0.131.

The aspiration rate that gave the best sensitivity for dilution with xylene was also the minimum allowed in our equipment (2.8 mL min^{-1}) for this solution. On the other hand, for the microemulsion system that is much more viscous than the xylene solution the aspiration rate of 2 mL min^{-1}, that is not the minimum, gave the best sensitivity.

These optimizations were also carried out for potassium standards using 2 mg L^{-1} in both medium and very similar results were obtained for this element. Then the conditions described above were adopted for both elements.

3.3. Stability studies

An important part of a routine procedure is that the sample and the calibration solutions remain stable at least for a few hours so that the analysis can be carried out once the solutions or microemulsions have been prepared. First the stability of sodium and potassium organometallic standards (sodium and potassium cyclohexanebutirates) and samples diluted in xylene were investigated.

As can be seen in Fig. 2 the analytical signal for potassium in the standard solution and in the sample decreased about 10% in 1 h, reaching about one third of its initial value over 8 h, i.e., within a typical working day. This drop in sensitivity was reported before for nickel organometallic standard diluted with xylene [35], due to adsorption of the metal in the flasks and tubes used for analyses. In relation to sodium stability the decrease of analytical signal was also observed, but not as strong as for potassium (Fig. 2). These results confirm the necessity of immediate analysis of standards and samples after the dilution with organic solvents, as recommended by EN 14108 [5] and EN 14109 [6].

On the other hand, the absorbance signal for sodium and potassium in microemulsified inorganic standards (sodium and potassium chlorides) and biodiesel samples, using either *n*-pentanol or *n*-butanol as co-surfactant, did not change significantly over 3 days for potassium and at least 5 days for sodium, as showed in Fig. 3. Higher stability for a number of elements

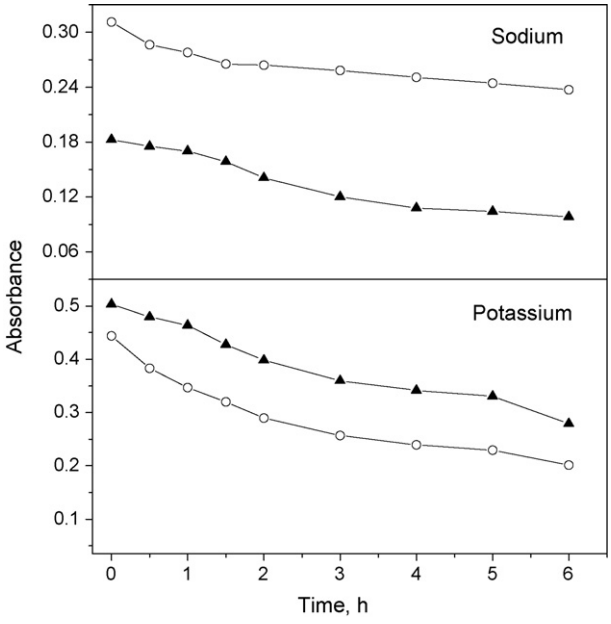

Fig. 2. Variation of the absorbance over time for potassium and sodium in: (○) standard solutions (2 mg K L^{-1} and 1 mg Na L^{-1} from cyclohexanebutirate salt) and (▲) biodiesel sample (B-13 for K and C-74 for Na), diluted with xylene.

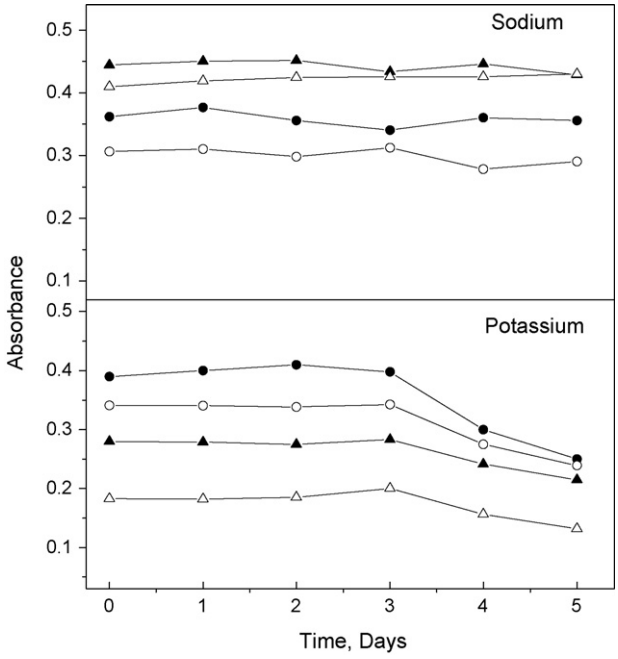

Fig. 3. Variation of the absorbance over time for potassium and sodium in microemulsions: (circles) standard (2 mg K L^{-1} and 1 mg Na L^{-1} as chloride) and (triangles) biodiesel sample (B-13 for K and C-74 for Na). Open symbols: *n*-pentanol; close symbols: *n*-butanol.

in microemulsions of petroleum derivates has been reported in the literature [19,23,24]. This high-stability found in this work together with the use of inorganic standard for calibration, make this sample preparation more suitable for routine application.

3.4. Figures of merit

Using the optimized conditions for each situation, calibration curves were established using: (i) organometallic standards diluted with xylene and (ii) microemulsion with inorganic standards and *n*-pentanol. For comparison purpose the conventional calibration curves with aqueous standards (NaCl and KCl) were also performed and the following equations were obtained: $A = 0.3896c - 0.0025$ ($R^2 = 0.9981$) for sodium and $A = 0.3449c + 0.0097$ ($R^2 = 0.9991$) for potassium. Comparing the sensitivity of these curves with those of the microemulsions and dilution techniques, shown in Table 2, it can be concluded that, as expected, the aqueous standards cannot be used for calibration.

All calibration curves for both techniques were linear up to 5.0 mg L^{-1}. Comparing the sensitivity of the curves it can be seen that the dilution techniques showed better sensitivity, as reflected in the characteristic concentration (C_0). However the microemulsion technique presented two times better limits of detection and quantification (LOD and LOQ). This feature is due the higher amount of sample used for microemulsion preparation but also due to the lower fluctuation in the signal measurements which reflected also in a better relative standard deviation (R.S.D.) for this technique, as shown in Table 2. Even so, the LODs found in this work were almost 10 times higher than the LODs obtained by ICP OES under especial conditions [8]. However, it should be stressed that the value found in this work is comfortably lower than the maximum levels of 10 mg kg^{-1} for sodium plus potassium in biodiesel established by the Brazilian regulations.

Table 3
Determination of sodium in biodiesel samples by F-AAS

Samples	Na concentration (mg kg^{-1}) (mean ± S.D., $n = 3$)	
	Reference method (EN 14108)	Proposed method (microemulsion)
S-02	0.73 ± 0.03	0.71 ± 0.03
B-13	1.9 ± 0.1	1.9 ± 0.2
B-15	0.5[a]	0.4 ± 0.03
B-40	1.1 ± 0.02	1.1 ± 0.2
C-32	39.7 ± 0.5	36.2 ± 0.4
C-57	1.1 ± 0.1	0.94 ± 0.01
C-64	1.3 ± 0.1	1.2 ± 0.3
C-74	1.6 ± 0.2	1.5 ± 0.1
H-23	1.6[a]	1.1 ± 0.01

[a] Results provided by Atomic Absorption Laboratory at Pontifical Catholic University (PUC) of Rio de Janeiro, Brazil.

3.5. Analytical results

In order to obtain information on the accuracy of the results for biodiesel and vegetable oils by the proposed method, the samples were also analyzed by the adopted norms (EN 14108 and EN 14109). The results obtained for sodium and potassium in biodiesel samples obtained from different sources are summarized in Tables 3 and 4. It should be stressed that the samples R-02, C-01 and D-01 that presented relatively high-potassium concentrations, and C-32 that presented high-sodium concentration, were obtained from research groups that are working in a development of production of biodiesel, i.e., it is not a commercial biodiesel. The three vegetable oil samples analyzed presented no measurable sodium and potassium concentrations, considering the LOD of both methods. The paired *t*-test was

Table 2
Analytical figures of merit for the determination of sodium and potassium in biodiesel by F AAS using microemulsion and dilution with xylene methods

Analyte	Method	Linear regression equation	R	C_0 (μg L^{-1})	LOD ($n = 10$) (μg g^{-1})	LOQ ($n = 10$) (μg g^{-1})	R.S.D. ($n = 10$) (%)
Sodium	Dilution with xylene	$A = 0.2172c + 0.0036$	0.9965	21	0.2	0.6	2.0–4.0
	Microemulsion	$A = 0.1732c + 0.0040$	0.9993	25	0.1	0.3	0.4–1.0
Potassium	Dilution with xylene	$A = 0.2237c - 0.0053$	0.9993	22	0.13	0.4	1.5–4.5
	Microemulsion	$A = 0.1562c + 0.0099$	0.9997	28	0.06	0.2	0.6–1.0

R: correlation factor, C_0: characteristic concentration, LOD: limit of detection, LOQ: limit of quantification, R.S.D.: relative standard deviation.

Table 4
Determination of potassium in biodiesel samples by F-AAS

Samples	K concentration (mg kg^{-1}) (mean ± S.D., n = 3)	
	Reference method (EN 14109)	Proposed method (microemulsion)
R-02	12.1 ± 0.64	11.5 ± 0.06
S-01	3.08 ± 0.14	3.16 ± 0.03
E-01	<0.4	0.29
B-09	<0.4[a]	<0.2
B-13	3.10[a]	3.00 ± 0.03
B-14	0.94[a]	0.74 ± 0.01
B-48	<0.4[a]	<0.2
C-01	172 ± 17	156 ± 1.5
C-04	0.9 ± 0.03	1.1 ± 0.1
D-01	10.1 ± 0.6	10.2 ± 2.6
I-01	4.9 ± 0.4	4.9 ± 0.04
J-02	1.6 ± 0.03	1.7 ± 0.4

[a] Results provided by Atomic Absorption Laboratory at Pontifical Catholic University (PUC) of Rio de Janeiro, Brazil.

applied to the data of Tables 3 and 4 and showed that the results of both methods are not significantly different at the 95% confidence level.

In addition, some biodiesel samples obtained from different sources (soybean, castor bean and animal fat) and three vegetable oil samples were spiked with sodium and potassium standards, as described in Sections 2.3 and 2.4. This study is important particularly for vegetable oil analysis by the proposed method and also by the European norm, once it was not possible to compare the results due to the low concentration of sodium and potassium in these samples. The spike recoveries obtained for dilution and microemulsion methods, which are shown in Tables 5 and 6, indicate the absence of matrix effects in the analysis of biodiesel samples for both elements and in the analysis of vegetable oils for potassium. However the recoveries of sodium in the vegetable oil samples, were satisfactory for the dilution technique but not for microemulsion. The recoveries of sodium obtained using the sample preparation condition described in the experimental Section 2.3, i.e., 20% (w/w) of vegetable oil, varied from 72% to 79%. The measurement of the viscosity of the microemulsions prepared with vegetable oil and with base oil, used to simulate the oil phase in the standards, showed significant differences (7.7 and 6.6 cP, respectively). By reducing the amount of sample to 16% (w/w) this difference

Table 5
Recovery tests for sodium carried out with dilution with xylene and microemulsions (n = 3)

Samples	EN 14108		Microemulsion	
	Spike (mg L^{-1})	Recovery (%)	Spike (mg L^{-1})	Recovery (%)
S-02	1.0	96 ± 1.5	0.25	108 ± 4.0
B-13	0.75	96 ± 4.6	0.75	96 ± 2.5
C-57	1.0	107 ± 0.1	1.0	95 ± 6.1
Soybean oil	0.25	87 ± 1.2	0.25	105 ± 3.0[a]
Sunflower oil	0.75	96 ± 1.1	0.75	90 ± 2.0[a]
Rapeseed oil	1.0	97 ± 4.1	1.0	91 ± 1.0[a]

[a] Recovery obtained using 16% (w/w) of vegetable oil.

Table 6
Recovery tests for potassium carried out with dilution with xylene and microemulsions (n = 3)

Samples	EN 14109		Microemulsion	
	Spike (mg L^{-1})	Recovery (%)	Spike (mg L^{-1})	Recovery (%)
C-04	2.0	96 ± 1.5	3.0	105 ± 5.4
B-13	2.0	98 ± 4.0	1.0	101 ± 1.8
S-01	1.0	95 ± 0.2	2.0	113 ± 0.8
Soybean oil	2.0	98 ± 1.3	4.0	98 ± 3.9
Rapeseed oil	3.0	93 ± 0.5	3.0	95 ± 0.7
Sunflower oil	2.0	92 ± 1.5	2.0	115 ± 1.4

was reduced (6.9 cP). In this condition the obtained recoveries varied form 90% to 105%, as shown in Table 5. The most interesting result is that this effect was not observed for potassium. The repetition of the recovery test with 20% (w/w) of vegetable oils for potassium for confirmation showed results similar to those presented in Table 6. These results indicate that the effect of viscosity for potassium is not very critical, not requiring the adjustment of the viscosity. Nevertheless special care should be taken when trying to apply this technique to other kind of vegetable oils such as castor oil, palm, etc., that present higher viscosities.

The overall result was very satisfactory for routine application, and good agreement was observed comparing the proposed method and the adopted method, showing that the proposed method could be used for the purpose.

4. Conclusion

The new proposed method based on the microemulsion was shown to be an efficient alternative for determination of sodium and potassium in biodiesel samples. This simple and fast method of sample preparation, with higher stability of the standards and samples together with the use of inorganic standard for calibration and lower limits of detection, make this sample preparation more suitable for routine application than the dilution with organic solvents. The recovery tests suggested that the method can be also applied for determination of sodium and potassium in vegetable oils, after adjustment of the viscosity for sodium. It might be assumed that this procedure could also be applied for the determination of other trace elements of interest in biodiesel, as long as their concentration is within the working range of the technique.

Acknowledgements

The authors are grateful to Fundação de Amparo a Pesquisa do Rio Grande do Sul—FAPERGS (process no. 04/1047.5), Financiadora de Estudos e Projetos (Convênio FINEP No. 01.04.0842.00) for financial support. A.J., M.G.R.V., M.M.S. thank to Conselho Nacional de Desenvolvimento Científico e Tecnológico (CNPq) for their scholarships. We would like to thank Mariana da Silva Assis and Tamara dos Santos Castilhos for their careful experimental work. We also thank Márcia Mar-

tinelli, Renato Cataluña, Elina Caramão and Reinaldo Calixto Campos for donation of samples.

References

[1] H. Fukuda, A. Kondo, H. Noda, J. Biosci. Bioeng. 92 (2001) 405.
[2] K.S. Tyson, Biodiesel: Handling and Use Guideline, US Department of Energy, 2005.
[3] A.C. Pinto, L.L.N. Guarieiro, M.J.C. Rezende, N.M. Ribeiro, E.A. Torres, W.A. Lopes, P.A.P. Pereira, J.B. Andrade, J. Braz. Chem. Soc. 16 (2005) 1313.
[4] Visão da OEM – Qualidade – especificação programa de testes para o uso da mistura diesel/biodiesel, http://www.unifacs.br/acontece/QUALICOM.htm.
[5] BS EN 14108, Fat and oil derivatives—fatty acid methyl esters (FAME), 2003.
[6] BS EN 14109, Fat and oil derivatives—fatty acid methyl esters (FAME), 2003.
[7] R. Nowka, GIT Labor-Fachzeitschrift 47 (2003) 518.
[8] M. Edlund, H. Visser, P. Heitland, J. Anal. Atom. Spectrom. 17 (2002) 232.
[9] E.J. dos Santos, A.B. Herrmann, E.S. Chaves, W.W.D. Vechiatto, A.C. Schoemberger, V.L.A. Frescura, A.J. Curtius, J. Anal. Atom. Spectrom. 22 (2007) 1300.
[10] C.P. Lienemann, Oil Gas Sci. Technol. Rev. IFP 60 (6) (2005) 951.
[11] M.G.A. Korn, D.S.S. Santos, B. Welz, M.G.R. Vale, A.P. Teixeira, D.C. Lima, S.L.C. Ferreira, Talanta 73 (2007) 1.
[12] J.F.N. Ortí, R.M.V. Camañas, G.R. Ramos, Anal. Chim. Acta 387 (1999) 127.
[13] A. Radomska, R. Dobrucki, Int. J. Pharm. 196 (2000) 131.
[14] H. Wennerström, O. Söderman, U. Olsson, B. Lindman, Colloids Surf. A 13 (1997) 123.
[15] T.N.C. Dantas, A.C. Da Silva, A.A.D. Neto, Fuel 75 (2001) 75.
[16] S.P. Moulik, L.G. Digout, W.M. Alylward, R. Palepu, Langmuir 16 (2000) 3101.
[17] J. Klier, C.J. Tucker, T.H. Kalantar, D.P. Green, Adv. Mater. 12 (2000) 1751.
[18] S.G. Dixit, A.R. Mahadeshwar, S.K. Haram, Colloids Surf. A 133 (1998) 69.
[19] R.Q. Aucélio, A.J. Curtius, B. Welz, J. Anal. Atom. Spectrom. 15 (2000) 1389.
[20] R.Q. Aucélio, A.J. Curtius, J. Anal. Atom. Spectrom. 17 (2002) 1.
[21] R.Q. Aucélio, A. Doyle, B.S. Pizzorno, M.L.B. Tristão, R.C. Campos, Microchem. J. 78 (2004) 21.
[22] W.N.L. Santos, F.S. Dias, M.S. Fernandes, M.V. Rebouças, M.G.R. Vale, B. Welz, S.L.C. Ferreira, J. Anal. Atom. Spectrom. 20 (2005) 127.
[23] M.N.M. Reyes, R.C. Campos, Spectrochim. Acta B 60 (2005) 615.
[24] A.L. Molinero, J.R. Castillo, Anal. Lett. 31 (1998) 903.
[25] H.M. Al-Swaidan, Talanta 43 (1996) 1313.
[26] H.M. Al-Swaidan, Anal. Lett. 27 (1994) 145.
[27] B. Du, Q. Wei, S. Wang, W. Yu, Talanta 44 (1997) 1803.
[28] C.R.B. Mendonça, C.I.D. Bica, C.M.S. Piatinicki, J. Braz. Chem. Soc. 14 (4) (2003) 628.
[29] C.R.B. Mendonça, C.I.D. Bica, C.M.S. Piatnicki, E.F. Simó-Alfonso, G. Ramis-Ramos, Electrophoresis 26 (2005) 858.
[30] M. Murilo, M. Benzo, E. Marcano, C. Gomez, A. Garaboto, C. Marin, J. Anal. Atom. Spectrom. 14 (1999) 815.
[31] R.M. Souza, B.M. Mathias, C.L.P. Silveira, R.Q. Aucélio, Spectrochim. Acta B 60 (2005) 711.
[32] J.R. Castillo, M.S. Jiménez, L. Ebdon, J. Anal. Atom. Spectrom. 14 (1999) 1515.
[33] M.S. Jiménez, R. Velarte, M.T. Gomez, J.R. Castillo, Atom. Spectrosc. 25 (2004) 1.
[34] T.P. Hoar, J.H. Schulman, Nature 152 (1943) 102.
[35] M.G.R. Vale, I.C.F. Damin, A. Klassen, M.M. Silva, B. Welz, A.F. Silva, F.G. Lepri, D.L.G. Borges, U. Heitmann, Microchem. J. 77 (2004) 131.

Available online at www.sciencedirect.com
ScienceDirect
Talanta 74 (2008) 1630–1634
Talanta
www.elsevier.com/locate/talanta

Determination of potassium ions in biodiesel using a nickel(II) hexacyanoferrate-modified electrode

Michelle de Souza Castilho *, Nelson Ramos Stradiotto

Departamento de Química Analítica, UNESP, Araraquara, SP, Brazil

Received 15 June 2007; received in revised form 4 October 2007; accepted 9 October 2007
Available online 22 October 2007

Abstract

In this work, nickel hexacyanoferrate-modified electrode was developed to determine potassium ions in biodiesel by potentiometry. The modified electrodes exhibit a linear response to potassium ions in the concentration range of 4.0×10^{-5} to 1.0×10^{-2} mol L^{-1}, with a detection limit of 1.9×10^{-5} mol L^{-1}, and a near-Nernstian slope (53–55 mV per decade) at 25 °C. The method developed in this work was compared with flame photometry and the potassium concentration found in biodiesel showed that the modified electrode method gives results similar to those obtained by flame photometry.
© 2007 Elsevier B.V. All rights reserved.

Keywords: Biodiesel; Modified electrodes; Nickel(II) hexacyanoferrate; Potassium ions

1. Introduction

Biodiesel [1] is defined as fatty acid methyl or ethyl esters from vegetable oils or animal fats and they are used as fuel in diesel engines and heating systems. In this context, biodiesel shows the following general advantages: an alternative to petroleum-based fuel, which implies lower dependence on foreign imports of crude oil; a reduction in greenhouse gas emissions in line with the Kyoto Protocol agreement, and it is a renewable fuel. It also gives lower harmful emissions, which is very advantageous in environmentally sensitive areas such as large cities and mines. It is a biodegradable and non-toxic fuel, being inoffensive to reservoirs, lakes, marine life and other environmentally sensitive places.

There are several choices [2] of vegetable oil sources. In Brazil, soybean oil is a source that is already scaled up for biodiesel production. Nevertheless, other sources, such as sunflower, peanut, cotton, palm oil, coconut, babassu and, especially, castor oil may be used in the near future, once their cultivation achieves an economic up-scaling. The alcohol in general usage is methanol. In Brazil, ethanol from sugar cane has great potential as an alcohol source, since it unites its non-toxicity with a ready availability.

Fatty acid methyl esters are products of the transesterification of vegetable oils and fats with methanol in the presence of a suitable catalyst. The transesterification reaction can be catalyzed by both homogeneous and heterogeneous catalysts. In turn, the homogeneous catalysts include alkalis and acids. The most commonly used alkali catalysts are sodium hydroxide, sodium methoxide and potassium hydroxide.

Rarely any chemical reaction in biodiesel production, including its transesterification, is completed and usually the products of the reaction (alkyl esters) are contaminated. The contaminants to be considered include water, free glycerin, bound glycerin, alcohol, free fatty acids, soaps, and residual catalyst. The presence of inorganic contaminants is related to the efficiency of the wash.

The potassium existing in the catalyst is very important for the reaction, but its presence in the biodiesel [3] can form deposits in fuel-injection system components, and poison emission control after-treatment systems.

According to American legislation provided by the American Society for Testing and Materials (ASTM International) Standards and European Biodiesel Standards [4], a maximum level of 5 mg kg^{-1} of potassium and sodium in biodiesel samples has been established. Standard method for determination of

* Corresponding author. Tel.: +55 16 3301 6621; fax: +55 16 3322 7932.
E-mail address: michcast@iq.unesp.br (M. de Souza Castilho).

0039-9140/$ – see front matter © 2007 Elsevier B.V. All rights reserved.
doi:10.1016/j.talanta.2007.10.027

potassium in biodiesel according to European standard EN 14109 [5] is the flame atomic absorption spectrometry (AAS) at 766.5 nm for potassium.

The potassium ions have been determined in several matrices using different techniques such as, thermogravimetry [6], inductively coupled plasma-atomic emission spectrometry [7], turbidimetric in-flow injection analysis [8,9], spectrophotometry [10], chromatography [11] and electroanalytical methods [12–29].

Some of the electroanalytical methods found in literature are significantly important such as those that use hexacyanoferrate-modified electrodes, which have been used as ion-selective electrodes [12–25]. Eftekhari [24] used a chemically modified electrode with silver hexacyanoferrate as a potentiometric sensor for the determination of the potassium ion over a wide range of concentrations, from 8.0×10^{-5} to 1.0 mol L^{-1}, with a low detection limit of 4.0×10^{-5} mol L^{-1}. The potassium-selective electrode has a relatively short response time. It has good sensitivity with a near-Nernstian slope of 53–57 mV per decade and good selectivity in the presence of possible interferences.

Mortimer et al. [25] developed a nickel hexacyanoferrate-modified electrode as a potentiometric sensor for the determination of potassium ions. The modified electrode exhibit a linear response to potassium ions in the concentration range of 1.0×10^{-3} to 2.0 mol L^{-1}, with a near-Nernstian slope (45–49 mV per decade) at 25 °C. The nickel hexacyanoferrate electrode exhibits good response to alkaline metals and its electrochemical behavior is a consequence of the size and shape of the ion [26,27].

Huang et al. [28] developed a method for the simultaneous determination of sodium and potassium by adsorption voltammetry using a hanging mercury-drop electrode. After dibenzo-18-crown-6 is added to the test solution, K^+ may form a complex with it. The complex is reduced at the hanging mercury-drop electrode, and gives a new reductive peak at −1.80 V, which is more negative than the reductive peak of Na^+. The current of the two peaks are proportional to the concentration of Na^+ and K^+. The sodium concentration detection range was 1.0×10^{-8} to 1.0×10^{-6} mol L^{-1}, and the potassium concentration detection range was 2.0×10^{-9} to 4.0×10^{-6} mol L^{-1}. The detection limits are 5.0×10^{-9} and 6.0×10^{-10} mol L^{-1} for sodium and potassium ions, respectively.

The potassium is determined in biodiesel using flame atomic emission spectrometry and using ICP optical emission spectrometry [30,31]. These methods of analysis show low standard deviations and good reproducibility, but involve costly equipments and long time of analysis.

Edlund et al. [30] developed a method for the determination of Ca, Cl, K, Mg, Na and P in biodiesel samples using ICP optical emission spectrometry. This was investigated using a new ICP spectrometer with CCD detectors and radial plasma viewing. The limits of detection for sodium and potassium after the dilution of biodiesel with kerosene are 1.4 and 7.1 μg kg^{-1}, respectively.

Recently, Nowka [31] determined alkali metal elements in biodiesel using flame atomic emission spectrometry. For different samples of biodiesel, concentrations of 0.09–1.21 mg kg^{-1} potassium and 1.24–4.85 mg kg^{-1} sodium were detected. These results correlated well with results achieved using other measurement techniques.

Present tends see biodiesel as an important alternative fuel. But residual alkali metals, such as potassium, can form deposits in fuel-injection system components and poison emission control after-treatment systems [32]. Along with these problems, the official method of analysis involves costly equipment. Thus, the objective of the present project is to develop an alternative cost-effective electroanalytical methodology for potassium determination in biodiesel.

2. Experimental

2.1. Reagents and apparatus

All chemicals were of analytical grade and the solutions were prepared using deionized water from Milli-Q (Millipore, USA). KCl (Merck), $NaNO_3$ (Mallinckrodt), $K_3Fe(CN)_6$ (Merck), HCl (Merck) and $Ni(NO_3)_2$ (Merck) were used without further purification.

Voltammetric measurements were carried out using a potentiostat from Auto-Lab, Model PGSTAT 30. A conventional electrochemical cell of 25 mL was employed, using a system of three electrodes: a glassy carbon disk, $A = 0.07$ cm^2, used as the working electrode, a platinum wire used as an auxiliary electrode and a saturated calomel electrode (ECS) as reference. The glassy carbon electrode was polished to a mirror finish with alumina (0.5 μm), and then rinsed thoroughly with water. Dry nitrogen was passed through the solution to remove oxygen and was kept flowing over the solution during runs. The potentiometric measurements were carried out using a Crison GLP pH-meter.

2.2. Electrode modification

Nickel(II) hexacyanoferrate (NiHCF) films were prepared by voltammetric cycling of the glassy carbon electrode in a solution of 1.0 mol L^{-1} $NaNO_3$ containing 1.0×10^{-3} mol L^{-1} $K_3Fe(CN)_6$ and 1.0×10^{-3} mol L^{-1} $Ni(NO_3)_2$ in an oxygen-free solution. For the film formation, 20 successive potential cycles from 0.0 to 0.8 V (vs. ECS) were carried out using a scan rate of 100 mV s^{-1}.

The biodiesel samples of soy oil analyzed were obtained from the Paraná Technological Institute (TECPAR) in Brazil.

2.3. Analytical procedure

Before the potentiometric measurements, the nickel hexacyanoferrate-modified electrode was conditioned at 0.7 V against an SCE for 10 min in a 1.0 mol L^{-1} KCl solution. Electrode potentials were recorded after the working and reference electrodes had been immersed in the sample solution for 2 min.

The potentiometric measurements were carried out in 0.1 mol L^{-1} HCl solution to maintain the ionic strength constant.

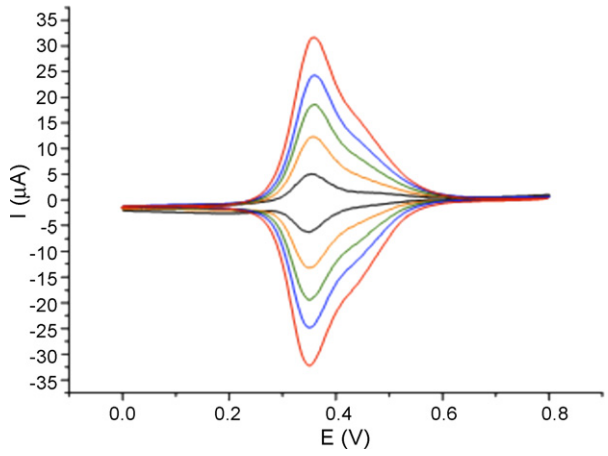

Fig. 1. Formation of the NiHCF-modified glassy carbon electrode in 1.0 mol L^{-1} $NaNO_3$ containing 1.0×10^{-3} mol L^{-1} $K_3Fe(CN)_6$ and 1.0×10^{-3} mol L^{-1} $Ni(NO_3)_2$ ($\nu = 100$ mV s^{-1}).

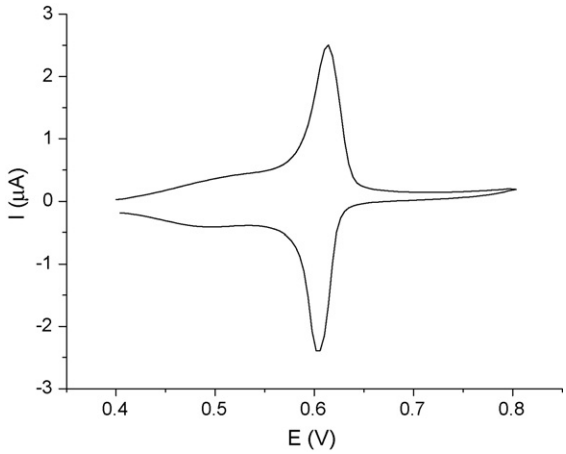

Fig. 2. Cyclic voltammogram of the NiHCF-modified electrode in 0.5 mol L^{-1} KCl. Scan rate 100 mV s^{-1}.

3. Results and discussion

3.1. Nickel hexacyanoferrate film formation

Nickel hexacyanoferrate complexes [33] have a cubic framework structure in which metals atoms are linked by cyanide units. Iron and nickel alternate between themselves at the vertices of the cube. The cyano groups are oriented in such a way that all iron atoms are coordinated exclusively to carbon and all nickel atoms to nitrogen. The sites at the cube center are occupied by alkali metal cations as necessary to guarantee charge neutrality.

Fig. 1 illustrates the film formation of NiHCF on the glassy carbon electrode by repetitive potential cycling from 0.0 to 0.8 against SCE in an oxygen-free 1.0 mol L^{-1} $NaNO_3$ solution containing 1.0×10^{-3} mol L^{-1} $K_3Fe(CN)_6$ and 1.0×10^{-3} mol L^{-1} $Ni(NO_3)_2$ having scan rate of 100 mV s^{-1}.

The transfer of NiHCF-modified electrodes to pure 1.0 mol L^{-1} KCl supporting electrolyte gave a single pair of redox peaks (0.36 V) represented by the following equation:

$$K^+Ni^{2+}[Fe^{III}(CN)_6] + K^+ + é \rightarrow (K^+)_2Ni^{2+}[Fe^{II}(CN)_6] \quad (1)$$

Different NiHCF film excess superficial were prepared varying the number of cycles (Table 1) as the excess superficial depends on the number of cycles the electrode is submitted to. The best slope (55 mV) and lowest detection limit (1.9×10^{-5} mol L^{-1}) were attained after 20 cycles.

3.2. The influence of potassium

Fig. 2 represents a cyclic voltammogram of the NiHCF-modified electrode in 0.5 mol L^{-1} KCl, having a scan rate 100 mV s^{-1}. The cyclic voltammogram exhibits a well-defined anodic peak at 0.61 V (I_{pa}) and a cathodic peak at .0.61 V (I_{pc}). Where the relation I_{pa}/I_{pc} is equal to unity and $|E_{pa} - E_{pc}| \approx 0$ at any studied scan rate (20–200 mV s^{-1}), indicating a rapid and reversible charge transfer to the surface-confined redox species.

Successive potential scanning in KCl showed that, after 100 cycles, there was a decrease of only 3% in the current and demonstrated a good lifetime (approximately 10 days), indicating good stability of the NiHCF-modified electrodes.

3.3. Potentiometric response to potassium ions

The potentiometric response of the NiHCF-modified electrode to potassium ions was tested by measuring the electrode potentials for a series of standard solutions of KCl (Fig. 3). The average slope was 55 mV per decade, slightly lower than the Nernstian value. The detection limit was calculated according to IUPAC recommendations [34] and was 1.9×10^{-5} mol L^{-1}. The modified electrode exhibited a linear response to potassium ions in the concentration range of 4.0×10^{-5} to 1.0×10^{-2} mol L^{-1}. All the measurements were accomplished in 0.1 mol L^{-1} HCl solution to maintain the ionic strength constant.

Table 1
Effect of the film thicknesses on the potentiometric response to the potassium ion

Film excess superficial (nmol cm^{-2})	Linear range (mol L^{-1})	Detection limit (mol L^{-1})	Slope (mV)
1.5	2.0×10^{-5} to 1.0×10^{-2}	1.9×10^{-5}	47
2.8	6.0×10^{-5} to 1.0×10^{-2}	2.1×10^{-5}	48
6.8	4.0×10^{-5} to 1.0×10^{-2}	1.9×10^{-5}	55
10.0	7.0×10^{-5} to 1.0×10^{-2}	2.2×10^{-5}	54

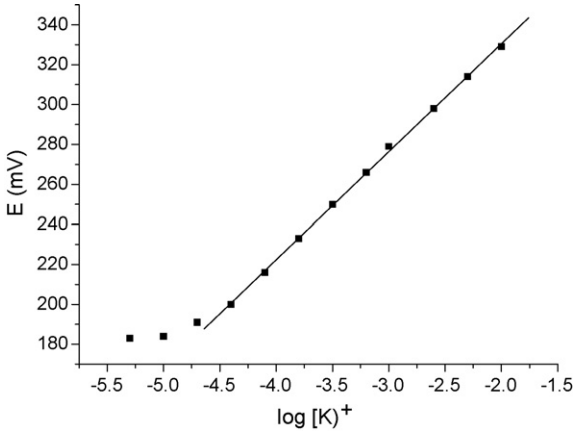

Fig. 3. Potentiometric response to the potassium ion (in HCl 0.1 mol L^{-1}) using NiHCF film having excess superficial of 6.8 nmol cm^{-2}.

3.4. Selectivity of the potassium-selective electrode

The selectivity coefficients for potassium determination based on the directly modified NiHCF-film electrode was evaluated using the fixed interference method recommended by IUPAC [35]. In this method, the potential of a cell comprising an ion-selective electrode and a reference electrode is measured in solutions, which have a constant level of interference (a_B) and varying primary ion activity (a_A). The potential values obtained are plotted vs. the activity of the primary ion. The intersection of the extrapolation of linear portions of this curve will indicate the value of a_A which is to be used to calculate $K^{pot}_{A,B}$ from the following equation:

$$K^{pot}_{A,B} = a_A/(a_B)Z_A/Z_B \quad (2)$$

where both z_A and z_B have the same sign, either positive or negative.

The interfering ion concentration was kept constant (1.0×10^{-3} mol L^{-1}) and the potassium concentration was varied. The selectivity coefficients for the electrode are listed in Table 2. For isovalent ions, a value of $K^{pot}_{A,B} < 1$ univocally indicates a preference of the electrode for the primary ion and $K^{pot}_{A,B} > 1$ a preference for the interfering ion. The results clearly show a high selectivity for potassium, except in the presence of NH_4^+ whose $K^{pot}_{A,B}$ value shows that this cation provokes a significant interference due to its hydrated diameter.

The other cations that could be present in the biodiesel are magnesium and calcium. However analyzing the nickel hexacyanoferrate structure [33], just alkali metal cations can occupy the sites at the cube center to guarantee charge neutrality. This is a consequence of the zeolitic structure of the nickel hexacyanoferrate characterized by channels whose characteristics constitute the driving force for ion discrimination: the size and shape of ion are the limiting factor in order to be inserted into the structure.

Table 2
Potentiometric selectivity coefficient of the NiHCF-modified film electrode

Interfering ion	$K^{pot}_{A,B}$
Sodium	1.0×10^{-2}
Lithium	8.9×10^{-3}
Ammonium	5.0×10^{-1}

Table 3
Potassium ion concentration (mg kg^{-1} of biodiesel) obtained by different analytical methods (three assays ($n = 3$))

Method	Biodiesel sample (mg kg^{-1})
Potentiometry	0.96 ± 0.06
Flame photometry	0.93 ± 0.04

3.5. Determination of potassium ion in biodiesel sample

The potassium ion was determined in biodiesel sample. Firstly, liquid–liquid extraction was done using HCl 0.1 mol L^{-1}. The potentiometric measurements were accomplished in an aqueous extract using the standard addition method implementing the NiHCF-modified electrode, which had a film thickness of 6.8 nmol cm^{-2}. The method developed in this work was compared with flame photometry and the results obtained are reported in Table 3. Analyzing the results obtained it is possible to verify that the potassium concentration in the biodiesel sample is below the maximum level provided by ASTM and European Biodiesel Standards (5 mg kg^{-1}) [4]. Both methods showed good reproducibility and low standard deviations. However, the potentiometric method has the advantages of being easy to operate and cost effective.

Acknowledgements

The authors gratefully acknowledge the financial support from CAPES, CNPq and Paraná Technological Institute (TECPAR).

References

[1] G. Vicente, M. Martinez, J. Aracil, Bioresour. Technol. 92 (2004) 297.
[2] A.C. Pinto, et al., J. Braz. Chem. Soc. 16 (2005) 1313.
[3] Test Specifications for Biodiesel Fuel. Available in: http://www.gsa.gov/gsa/cm_attachments/GSA_DOCUMENT/ema_R2B-x17_0Z5RDZ-i34K-pR.pdf.
[4] G. Knothe, J. Am. Oil Chem. Soc. 83 (2006) 823.
[5] EN 14 109, Fat and Oil Derivatives—Fatty Acid Methyl Esters (FAME), Determination of Potassium Content by Atomic Absorption, European Committee for Standardization, Brussels, Belgium, 2003.
[6] D. Adamczyk, A. Cyganski, Chem. Anal. 49 (2004) 317.
[7] Y.H. Li, H. Vansickle, Atom. Spectrosc. 25 (2004) 21.
[8] S. Vicente, E.P. Borges, F.B. Reis, E.A.G. Zagatto, Anal. Chim. Acta 438 (2001) 3.
[9] J.R.D. Torres, M. Tubino, Anal. Lett. 27 (1994) 1625.
[10] V.I. Dvorkin, Y.G. Gorbunova, V.I. Zhilov, G.Y. Sitnikova, A.Y. Tsivadze, J. Anal. Chem. 57 (2002) 552.
[11] Q. Xu, K. Tanaka, M. Mori, M.I. Helaleh, H. Toada, W. Hu, K. Hasebe, Chromatographia 57 (2003) 19.
[12] D. Engel, E.W. Grabner, Berichte der Bunsengesellschaft fuer Physikalische Chemie 89 (1985) 982.
[13] C.A. Nitin Bagkar, P.A. Betty, K. Hassan, J.R. Kahali, Thin Solid Films 497 (2006) 259.
[14] K.N. Thomsen, R.P. Baldwin, Anal. Chem. 61 (1989) 2598.
[15] V. Krishnan, A.L. Xidis, V.D. Neff, Anal. Chim. Acta 239 (1990) 7.

[16] K.C. Ho, C.L. Lin, Sens. Actuator B 76 (2001) 512.
[17] J.J. Xu, H.Q. Fang, H.Y. Chen, J. Electroanal. Chem. 426 (1997) 139.
[18] A. Khandar, A.L. Shabanov, R. Medzhidi, G.G. Asadov, C.I. Mamedov, J. Anal. Chem. 58 (2003) 183.
[19] M. Mascini, G. Marrazza, Anal. Chim. Acta 231 (1990) 125.
[20] C. Diaz, J.C. Vidal, J. Galban, M.L. Uruarte, J. Lanaja, Microchem. J. 39 (1989) 289.
[21] E.K. Quagraine, V.P.Y. Gadzekpo, Discov. Innov. 10 (1998) 41.
[22] V.V. Egorov, Y.F. Lushchik, N.M. Khrol, M.I. Suboch, N.N. Golenya, Ind. Lab. 55 (1989) 1234.
[23] H.A. Arida, R.F. Aglan, Anal. Lett. 23 (2003) 895.
[24] A. Eftekhari, Anal. Lett. 36 (2003) 263.
[25] R.J. Mortimer, P.J.S. Barbeira, A.F.B. Sene, N.R. Stradiotto, Talanta 49 (1999) 271.
[26] M. Pyrasch, A. Toutianoush, W. Jin, J. Schnepf, B. Tieke, Chem. Mater. 15 (2003) 245.
[27] W. Jin, A. Toutianoush, M. Pyrasch, J. Schnepf, H. Gottschalk, B. Tieke, J. Phys. Chem. B 107 (2003) 12062.
[28] H.L. Huang, L.Z. Wang, C.S. MA, X.L. Zhang, C.X. Liu, Chem. Lett. 3 (1997) 227.
[29] I.E. Stas, I.A. Nedyakina, B.P. Shipunov, J. Anal. Chem. 58 (2003) 959.
[30] M. Edlund, H. Visser, P. Heitland, J. Anal. Atom. Spectrom. 14 (2002) 232.
[31] R. Nowka, GIT Labor-Fachzeitschrift 47 (2003) 518.
[32] Test Specifications for Biodiesel Fuel. Available in: http://www.enginemanufacturers.org/admin/library/upload/924.pdf.
[33] M. Giorgetti, E. Scavetta, M. Berretoni, D. Tonelli, Analyst 126 (2001) 2168.
[34] R.P. Buck, E. Lindner, Pure Appl. Chem. 66 (1994) 2527.
[35] Y. Umezawa, K. Umezawa, H. Sato, Pure Appl. Chem. 67 (1995) 507.

Available online at www.sciencedirect.com
ScienceDirect
Talanta 74 (2008) 1321–1329
Talanta
www.elsevier.com/locate/talanta

Method development for the determination of lead in wine using electrothermal atomic absorption spectrometry comparing platform and filter furnace atomizers and different chemical modifiers

Morgana B. Dessuy [a], Maria Goreti R. Vale [a,*], Anderson S. Souza [b], Sérgio L.C. Ferreira [b], Bernhard Welz [b], Dmitri A. Katskov [c]

[a] *Instituto de Química, Universidade Federal do Rio Grande do Sul, Av. Bento Gonçalves 9500, 91501-970 Porto Alegre, RS, Brazil*
[b] *Instituto de Química, Universidade Federal da Bahia, Campus Universitário de Ondina, 40170-290 Salvador, BA, Brazil*
[c] *Department of Chemistry and Physics, Tshwane University of Technology (TUT), Private Bag X680, Pretoria 0001, South Africa*

Received 24 July 2007; received in revised form 29 August 2007; accepted 30 August 2007
Available online 16 September 2007

Abstract

A method has been developed for the determination of lead in wine by electrothermal atomic absorption spectrometry without any sample preparation and calibration against aqueous standards, using 7.5 μg Pd as a chemical modifier. The results obtained for seven wines using the proposed method and an acid digestion procedure did not show any significant difference using a Student's *t*-test. Atomization in a transversally heated filter atomizer (THFA) was compared with atomization in a conventional transversally heated platform furnace. The former provided a 2.6-fold higher sensitivity, improving the characteristic mass from 34 to 12 pg and a 1.6-fold better limit of detection (0.3 μg L^{-1} compared to 0.5 μg L^{-1}) for aqueous solutions using the same injection volume of 20 μL. However, the average precision, expressed as the relative standard deviation for the determination of lead in wine under routine conditions was improved from 4.6% with platform atomization to 0.6% in the THFA. The lead content found in seven arbitrarily chosen white and red wines, five from Brazil, one from Chile and one from Spain, ranged from 6 to 60 μg L^{-1} Pb with an average content of 11.4 μg L^{-1} Pb for the wines from South America.
© 2007 Elsevier B.V. All rights reserved.

Keywords: Lead; Wine; Electrothermal atomic absorption spectrometry; Filter atomizer; Palladium modifier

1. Introduction

Wine has been a widely consumed beverage in many parts of the world for thousands of years with very obvious commercial value and social importance. The current worldwide production and consumption is more than 2×10^{10} L $year^{-1}$ [1], which underlines the economic importance of this beverage. Several studies have shown that the moderate consumption of wine, especially red wine, improves health and longevity [2,3]. Wine is a complex sample containing organic as well as inorganic substances in an ethanol-aqueous solution. The metal content in wine can be attributed to natural sources and/or to contamination during the wine-making process. The analysis of trace metals in wine is of great importance for quality and authenticity control, metals bioavailability and toxicity, and is nowadays routinely carried out in most enological laboratories. A recent review article summarizes the analytical methods used for the determination of trace metals in wine [1].

Lead contamination of wine is a problem dating back to ancient times. The Romans were known to use lead vessels for storage purposes and lead acetate as sweetener to improve acid-tasting wines [4]. Lead alloys have been widely used in wine cellars due to the ease with which this metal can be mechanically formed. An excess of ingested lead may present a real health hazard, affecting both the nervous system and the biosynthesis of hemoglobin [5]. It has been estimated that 70% of the lead intake of humans comes from food and drinks, and wine is the alcoholic beverage that shows the highest level of lead [1]. In response to this health concern, the threshold limit value of

* Corresponding author. Tel.: +55 51 3308 6278; fax: +55 51 3308 7304.
E-mail address: mgrvale@iq.ufrgs.br (M.G.R. Vale).

0039-9140/$ – see front matter © 2007 Elsevier B.V. All rights reserved.
doi:10.1016/j.talanta.2007.08.048

lead in wine has been reduced progressively, and is at present between 200 and 300 μg L^{-1}, depending on national legislation [6]. Although, depending on the origin, particularly red wines have been found that clearly exceeded these limits [7] with lead levels even higher than 1000 μg L^{-1} [8], most wines nowadays are within the above limits [9,10]. On the other hand there is indication that wines from South America show significantly lower lead contents than European wines [11–13]. There is clearly an increasing demand for a rapid, reliable and sensitive method for the routine determination of lead in wine.

Electrochemical techniques have been widely described in the literature for the determination of lead in wine; however, voltammetry requires complete sample mineralization to decompose interfering substances, which makes it labor-intensive. Potentiometric stripping analysis, in contrast, has been reported to make possible a determination directly in the wine without or with only a minimum sample preparation [9,10,14,15]. Similar performance has recently been reported for anodic stripping voltammetry using a thick-film modified electrode [16].

The inductively coupled plasma (ICP)-based optical emission (OES) and mass spectrometric (MS) techniques suffer from severe matrix effects, which cannot be removed by simple dilution or matrix matching because of the very much different matrix composition of different wines [17]. Decomposition of the sample matrix was necessary for a determination by ICP-MS, and it was found that UV-irradiation provided more precise results than high-pressure microwave digestion [17]. It has been demonstrated that exact-matching isotope dilution can solve the problem for ICP-MS and provide accurate results [18,19], however, this cannot be considered a routine technique. Although direct determination of mineral components in wine by ICP OES has been described [20], this technique suffers not only from serious matrix effects, but also from a lack of sensitivity [21].

Flame atomic absorption spectrometry (FAAS) has been applied occasionally for the determination of lead in wine; however, this technique is not sensitive enough and requires a prior digestion and pre-concentration step. Fernandes et al. [22] used a block digester and an open-vessel microwave system and found that C-18 bonded silica was most efficient in extracting lead as diethyl-dithiophosphate complex in a flow-injection system. Tarley et al. [23] proposed modified rice husks as a natural solid adsorbent for the same purpose. Hydride generation (HG) AAS has also been proposed for the determination of lead in wine [7,24]. However, although this technique offers sufficient sensitivity, it also requires mineralization of the sample, as lead has to be present in ionic form for HG. Karadjova et al. [25] proposed HG atomic fluorescence spectrometry for the determination of lead in wine in the presence of HCl and $K_3[Fe(CN)_6]$ and found that no prior digestion of the wine was necessary.

The technique of choice for the determination of lead among the atomic spectrometric techniques appears to be electrothermal AAS (ET AAS) due to its high sensitivity and tolerance of inorganic and organic matrices, which should make possible a direct determination of lead in wine. Nevertheless some kind of sample pretreatment has been used in most of the procedures using this technique. Buldini et al. [26] used an oxidative UV photolysis and Capelo et al. [27] used a focused ultrasound treatment with HNO_3 and H_2O_2, which they found much more efficient than a microwave-assisted digestion. Freschi et al. [13] only used a 1 + 1 dilution of wine with 0.028 mol L^{-1} HNO_3 and 5 μg Pd + 3 μg Mg as chemical modifiers, which was injected directly into the graphite tube. The formation of carbonaceous residues inside the atomizer was avoided by the use of a two-step pyrolysis at 400 and 600 °C. Karadjova et al. [28] also used a 1 + 1 dilution of the wine with 0.2 mol L^{-1} HNO_3; however, due to matrix effects they had to use the analyte addition technique for calibration, which made the procedure laborious and time consuming. Fernandes et al. [29] investigated the application of bismuth as an internal standard for the determination of lead in wines and found a significant improvement in accuracy and precision compared to external calibration. This application obviously requires a simultaneous atomic absorption spectrometer, which is not commercially available nowadays.

Obviously the direct determination of lead in wine using ET AAS, which has actually not yet been described in the literature, would require careful optimization of the temperature program and the strict application of the stabilized temperature platform furnace (STPF) concept [30], including the selection of proper chemical modifiers. A variety of modifiers has been proposed for the determination of lead besides the 'classical' mixture of palladium and magnesium nitrates [31], including organic acids, such as citric or ascorbic acid, either alone [32,33] or in combination with palladium [34–36]. A different approach is the use of 'permanent' chemical modifiers, mostly platinum group metals, such as Rh, Ru and Ir, which are applied as kind of a surface coating to graphite tubes or platforms [37] mainly in order to simplify the analytical procedure and to avoid contamination introduced by the modifier [38].

The goal of this work has been to develop a procedure for the determination of lead in wine using ET AAS that does not require any sample preparation after optimization of the temperature program and selection of the best chemical modifier. A transversely heated filter atomizer (THFA) has been included in the investigation in addition to a conventional transversely heated graphite tube with integrated platform (THPA), because the former atomizer has been reported to reduce background absorption significantly and does not require chemical modifiers [39–43]. A conventional acid digestion procedure was included in the investigation for validation in addition to the usual spike recovery tests, as no certified reference material for wine is available.

2. Experimental

2.1. Instrumentation

All measurements were carried out using a Model AAS 5 EA atomic absorption spectrometer (Analytik Jena AG, Jena, Germany), equipped with a transversely heated graphite tube atomizer and a deuterium background correction. A NARVA hollow cathode lamp of lead (GLE, Berlin, Germany) was used as the radiation source with a current of 5.5 mA (wavelength 283.3 nm, spectral bandwidth 0.8 nm). The spectrometer was

Table 1
Temperature program for the determination of Pb using transversely heated graphite tubes with PIN platform

Stage	Temperature (°C)	Ramp (°C s^{-1})	Hold time (s)
Drying 1	110	15	10
Drying 2	120	10	15
Drying 3	140	5	10
Pyrolyses	900	100	30
Atomization	2000	FP[a]	6
Cleaning	2300	FP[a]	5

[a] FP = full power.

interfaced to an IBM PC/AT compatible computer. Commercially available transversely heated pyrolytic graphite coated tubes with PIN platform (Analytik Jena Part No. 407-A81.025) and experimental THFA tubes made at Department of Chemistry and Physics, Tshwane University of Technology, Pretoria, South Africa similar to those described in Ref. [39] were used for the determinations. Both tubes had exactly the same outer dimensions and could be used in the atomizer unit of the AAS 5 EA without any modification. An MPE 5 furnace autosampler (Analytik Jena) was used for sample introduction. Argon with a purity of 99.996% (White Martins, São Paulo, Brazil) was used as the purge gas with a flow rate of 2.0 L min^{-1} during all stages, except during atomization, when the flow was stopped. Integrated absorbance, A_{int}, was used exclusively for signal evaluation and quantification. The optimized graphite furnace temperature program used for all determinations is given in Tables 1 and 2 for the two types of atomizer tubes. A significantly greater sample volume could have been introduced into the THFA if the temperature during sample injection would have been increased to 120 °C (hot injection); however, this option has not been used as no further increase in sensitivity was necessary for the present application.

2.2. Reagents

Analytical grade reagents were used throughout. Nitric acid (Merck, Darmstadt, Germany) used in this work was further purified by sub-boiling distillation in a quartz sub-boiling still (Kürner Analysentechnik, Rosenheim, Germany). Distilled, deionized water (DDW) with a specific resistivity of 18 MΩ cm, from a Milli-Q water purification system (Millipore, Bedford, MA), was used for the preparation of the samples and standards. All containers and glassware were soaked in 1.4 mol L^{-1} nitric acid for at least 24 h and rinsed three times with DDW before use.

Table 2
Temperature program used for the determination of Pb using the THFA

Stage	Temperature (°C)	Ramp (°C s^{-1})	Hold time (s)
Sampling[a]	100	5	10
Drying	110	5	10
Pyrolysis	900	300	30
Atomization	2000	FP[b]	6
Cleaning	2300	FP[b]	5

[a] Samples were introduced in this stage.
[b] FP = full power.

The lead stock solution (1000 mg L^{-1} in 0.014 mol L^{-1} nitric acid) was prepared from $Pb(NO_3)_2$ (Merck). The working standards were prepared by serial dilutions of the stock solution in 0.014 mol L^{-1} nitric acid.

The following chemical modifier solutions were used (all solutions and reagents from Merck):

Palladium modifier stock solution 10.0 ± 0.2 g L^{-1} Pd in 15% (v/v) HNO_3; the palladium modifier solution added to samples and standards was prepared by diluting 0.5 mL of this stock solution to 10 mL with DDW, resulting in a final concentration of 0.75% (v/v) HNO_3.
Magnesium modifier stock solution 10.0 ± 0.2 g L^{-1} Mg in 17% (v/v) HNO_3; the Pd + Mg modifier solution was prepared by mixing 0.5 mL of palladium modifier stock solution and 0.3 mL of magnesium modifier stock solution and diluting to 10 mL with DDW; the acid concentration in the final solution was 0.5%.
Iridium stock solution of 1000 mg L^{-1} Ir in 8% HCl was used as provided.
Ruthenium stock solution of 1000 mg L^{-1} Ru in 8% HCl was used as provided.
Ascorbic and citric acid, 2% (m/v), were prepared by dissolving the solid reagent in water.

2.3. Permanent chemical modifiers

Iridium or Ru was deposited on the platform by injecting 10 times 40 μL of 1000 mg L^{-1} Ir or Ru standard solution and submitting the tube after each injection to the first four stages of the temperature program shown in Table 3. After the last treatment, when a total of 400 μg of Ir or Ru had been applied, the full program was executed. An Ar gas flow of 2 L min^{-1} was maintained throughout all program stages.

2.4. Samples

Seven commercial wine samples, three white wines and four red wines were analyzed. All samples were purchased at a local super market. In detail the following wine samples have been investigated: Sauvignon Blanc, white (Vinã Concha y Toro, Chile); Semilon, white (Bacardi Martín do Brasil, Brazil); Chardonnay, white (Cooperativa Vinícola Aurora, Brazil); Merlot, red (Bacardi Martín do Brasil, Brazil); Cabernet Franc, red

Table 3
Temperature program for treatment of the platform with permanent modifiers; argon gas flow 2 L min^{-1} in all program stages

Stage[a]	Temperature (°C)	Ramp (°C s^{-1})	Hold time (s)
1	130	20	40
2	160	20	50
3	1000	100	25
4	1400	200	5
5	2000	1000	5

[a] Program stages 1–4 were repeated after each injection of a modifier solution; the full program was executed only after the 10th injection.

(Bacardi Martín do Brasil, Brazil); Cabernet Sauvignon, red (Adega Bianchetti Tedesco, Brazil); Monastrell, red (Salvador Poveda Monóvar, Spain).

2.5. Sample preparation

For the acid digestion that has been carried out for comparison 20 mL of wine sample was digested in digester block at 150 °C with the addition of 6 mL of concentrated nitric acid, added in three aliquots of 2 mL. The mixture was evaporated to a minimum volume of 5 mL, and 4 mL of 30% (v/v) hydrogen peroxide (Merck) were added to complete the digestion. The solution was heated to boiling and the residues were diluted with DDW to a final volume of 10 mL [44,45].

2.6. Procedure

20 μL of standard or sample was introduced into the furnace (THPA or THFA) with 15 μL of Pd modifier solution (0.05%, m/v). For THFA all standards and samples were injected while temperature of furnace was kept at 100 °C. Aqueous standards were used for calibration and all samples were analyzed in triplicate. All standards for THFA were prepared in 13% (v/v) of ethanol in order to facilitate sample introduction (lower surface tension).

3. Results and discussion

3.1. Organic acids as modifiers for lead

Our first investigations went into the direction of organic acids as chemical modifiers for lead, and the wine sample Monastrell was chosen for these experiments because of its elevated lead content. Fig. 1 shows the absorbance signals for lead and for the background without a modifier and in the presence of the two organic acids, respectively. It is obvious that there is very little difference in the lead and the background absorbance without or with the two modifiers. A non-symmetric double peak that is most likely due to different atomization mechanisms or due to different lead species is formed in all cases, as has been reported previously for this element [46]. The background absorption also did not change significantly, but apparently it could be corrected without problems. A change of the modifier mass between 20 and 200 μg had no significant influence on the overall pattern. The A_{int} for lead remained essentially the same in all situations without or with an organic acid modifier.

The A_{int} for lead increased by almost 50% when 10 μg Pd was added as a modifier, compared to the situation without or with the organic acid modifiers and the absorbance signal for lead became a single symmetric peak, demonstrating the modifier action, as shown in Fig. 2A. The background absorption also changed, but could be corrected without problems. The addition of an organic acid to the palladium had essentially no effect, as can be seen in Fig. 2B for citric acid, as neither the A_{int} nor the background changed significantly. Similar experiments have been carried out for the Pd + Mg modifier with essentially the same result. The addition of Mg shifted the absorbance signal of lead to earlier appearance but did not change the A_{int}; the addition of citric acid had no significant influence either.

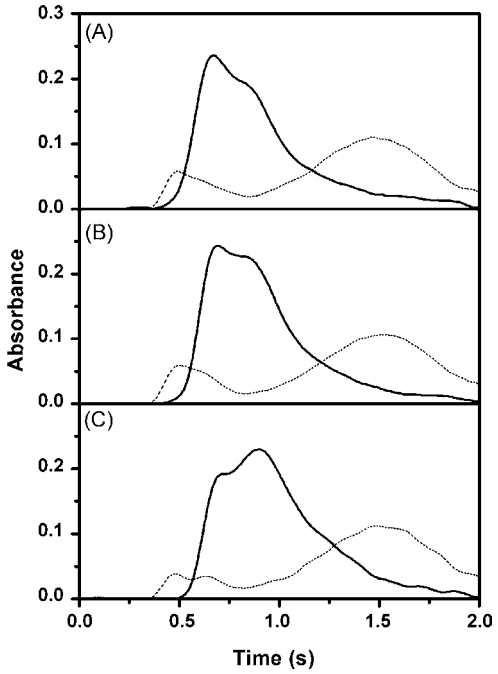

Fig. 1. Absorbance signals for lead (—) and background (- - -) using 20 μL of Monastrell wine; T_p = 500 °C, T_a = 1800 °C; (A) without a modifier; (B) addition of 100 μg ascorbic acid; (C) addition of 100 μg citric acid as the modifier.

In order to conclude this investigation we carried out a factorial design with tree variables, the mass of palladium modifier (between 2.5 and 7.5 μg), the mass of citric acid (between 50 and 150 μg), and the pyrolysis temperature (between 700 and 900 °C). The result of the Pareto diagram, which is not shown here, clearly indicated that only the mass of palladium had a significant and positive influence, whereas neither the amount of citric acid nor the pyrolysis temperature or any of the combinations of the above factors had a significant influence. After these results we decided not to further investigate organic acids as modifiers, as they either do not have any positive effect on lead atomization in the wine matrix or the wine matrix already contained sufficient similar substances, so that their addition was not necessary.

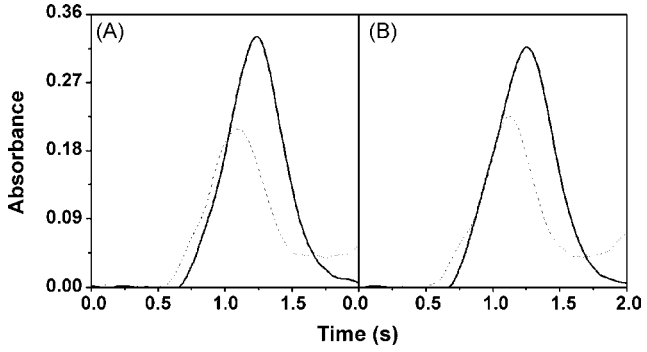

Fig. 2. Absorbance signals for lead (—) and background (- - -) using 20 μL of Monastrell wine; T_p = 650 °C. T_a = 2000 °C; (A) 10 μg Pd modifier; (B) 10 μg Pd and 50 μg citric acid as the modifiers.

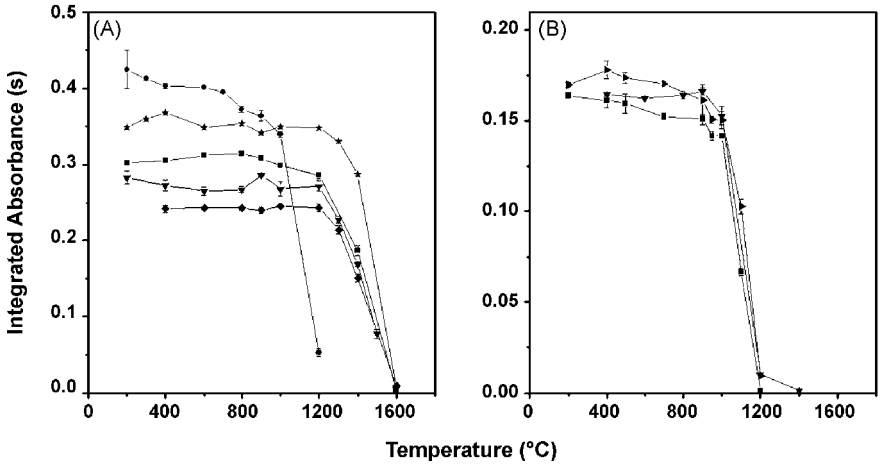

Fig. 3. Pyrolysis curves for (A) 2 ng Pb in aqueous solution and (B) 20 μL of Monastrell wine using different chemical modifiers; (▼) 7.5 μg Pd; (●) 400 μg Ru as permanent modifier; (⋆) 400 μg Ir as permanent modifier; (■) 5 μg Pd + 3 μg Mg; (♦) 7.5 μg Pd with the addition of 13% (v/v) ethanol; (►) 7.5 μg Pd + 50 μg citric acid; T_a = 2000 °C.

3.2. Platinum-group metals as modifiers

In the next step we investigated several platinum-group metals both as conventional and as permanent modifiers. An optimization of the palladium mass used as a conventional modifier, added together with each sample or standard showed that for aqueous solutions there was no change in sensitivity between 5 and 15 μg Pd, however, an increase in A_{int} was observed for lead in wine when the modifier mass was increased to 7.5 μg Pd. Hence, this modifier mass was used in further experiments. Fig. 3A shows the pyrolysis curves for this modifier obtained for aqueous calibration solutions and solutions containing 13% ethanol in order to simulate the wine matrix. In addition the traditional modifier of 5 μg Pd + 3 μg Mg and the two permanent modifiers, Ir and Ru (400 μg each) have been investigated. Essentially all the modifiers could stabilize lead up to about 1200 °C except for Ru as a permanent modifier, which exhibited a slight loss of sensitivity already above 700 °C and dramatic losses above 1000 °C. The highest sensitivity among the other modifiers was provided by the Ir permanent modifier, however, a pronounced double peak was observed for lead in wine with this modifier, similar to that obtained without a modifier or with the organic acids, as shown in Fig. 1, which indicated some stabilization problems. It is interesting to note that a single, symmetric atomization peak, similar to that shown in Fig. 2 for the Pd modifier was observed when 10 μg Ir was added to the wine sample. This means that the stabilization problem for lead is not due to the use of Ir, but due to its application as a permanent modifier. The same phenomenon was actually observed for the Ru modifier, so that permanent modifiers were no longer considered in this work.

Among the pyrolysis curves for the palladium-based modifiers a slightly higher sensitivity was obtained for the Pd + Mg modifier compared to Pd alone when aqueous solutions were considered; however, the background absorbance was about three times higher for the mixed modifier when a wine sample was analyzed. The addition of 13% ethanol to the standards caused a slight loss of sensitivity and a significant deterioration of precision. The pyrolysis curves for lead in the Monastrell wine sample using palladium alone or mixed with citric acid or magnesium are shown in Fig. 3B. There is no significant difference between the three pyrolysis curves, so that the use of the simplest modifier, i.e. palladium alone was selected in further experiments. In contrast to aqueous standards, all modifiers could stabilize lead only up to 900 °C, so that this pyrolysis temperature has been chosen for future investigations.

The linear regression equations for lead in the presence of the three palladium-based modifiers are shown in Table 4 together with the limits of detection (LOD) and quantification (LOQ), which are defined as three times and ten times the standard deviation of a blank solution (n = 10) divided by the slope of the calibration curve. It is obvious that the best LOD was obtained with the Pd + Mg mixed modifier; however, these values have been obtained with aqueous solutions, and they would obviously deteriorate for wine samples, particularly in view of the three times higher background absorbance observed with this

Table 4
Linear regression equations of the calibration curves for 0.5–4.0 ng Pb, using a PIN platform atomizer, in aqueous solution in the presence of Pd + Mg and Pd only as the modifier, and for a 13% (v/v) ethanolic solution in the presence of Pd

Modifier	Regression equation	R	LOD (pg)	LOQ (pg)
5 μg Pd + 3 μg Mg	$A = 0.1572m$ (ng) + 0.0111	0.9999	5.2	17
7.5 μg Pd aqueous	$A = 0.1257m$ (ng) + 0.0105	0.9999	9.7	32
7.5 μg Pd 13% ethanol	$A = 0.1142m$ (ng) + 0.0118	0.9999	20	66

R = correlation coefficient; LOD = limit of detection; LOQ = limit of quantification; for definition see text; T_p = 900 °C, T_a = 2000 °C.

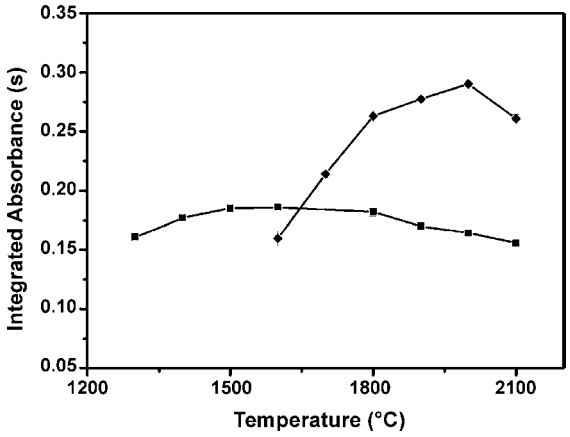

Fig. 4. Atomization curves (♦) for 2 ng Pb in 20 μL of aqueous solution and (■) for 20 μL of Monastrell wine using 7.5 μg Pd as a chemical modifier; T_p = 900 °C.

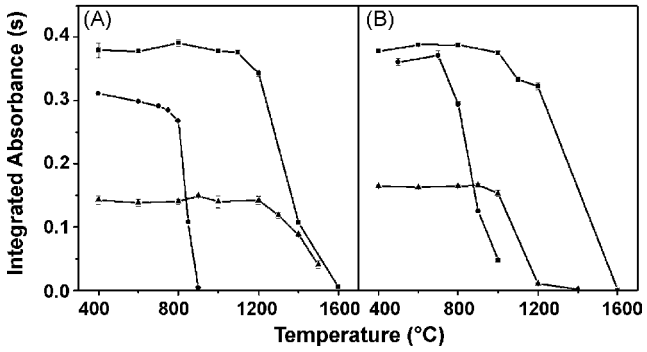

Fig. 5. Pyrolysis curves for (A) 1 ng Pb in aqueous solution and (B) in 20 μL of Monastrell wine; (▲) platform atomizer with 7.5 μg Pd modifier; (●) THFA without modifier (aqueous standards with 13% ethanol); (■) THFA with 7.5 μg Pd modifier (aqueous standards with 13% ethanol); T_a = 2000 °C.

modifier. It is also obvious that the addition of ethanol to the aqueous standards deteriorated the LOD and LOQ for lead significantly. Therefore the above-mentioned conditions have been chosen for further experiments.

During the optimization of the atomization temperature it was observed that lead in an aqueous solution behaved significantly different from lead in wine, as shown in Fig. 4 in the presence of 7.5 μg Pd as the modifier. For lead in an aqueous solution the A_{int} increased to a maximum at 2000 °C and decreased at higher atomization temperatures, which is typical for volatile analytes. For lead in wine, in contrast, essentially the same A_{int} was obtained for atomization temperatures between 1400 and 2000 °C. The only explanation for this phenomenon is that lead is present in wine in a different chemical form (which is well known) and that this compound is stabilized according to a different mechanism that makes possible quantitative atomization already at significantly lower temperatures. A detailed investigation of these mechanisms is obviously beyond the scope of this work. Based on these results, 7.5 μg Pd was used as the modifier in our future experiments with a pyrolysis temperature of 900 °C and an atomization temperature of 2000 °C.

3.3. Evaluation of the filter atomizer

In the case of the THFA the solution for measurement has to be introduced into a ring cavity that is loosely filled with a carbon fiber. In order to facilitate sample introduction the furnace was heated to 100 °C during injection (see Table 2) and 13% (v/v) ethanol was added to all aqueous solutions in order to reduce the surface tension. The wine samples were introduced into the

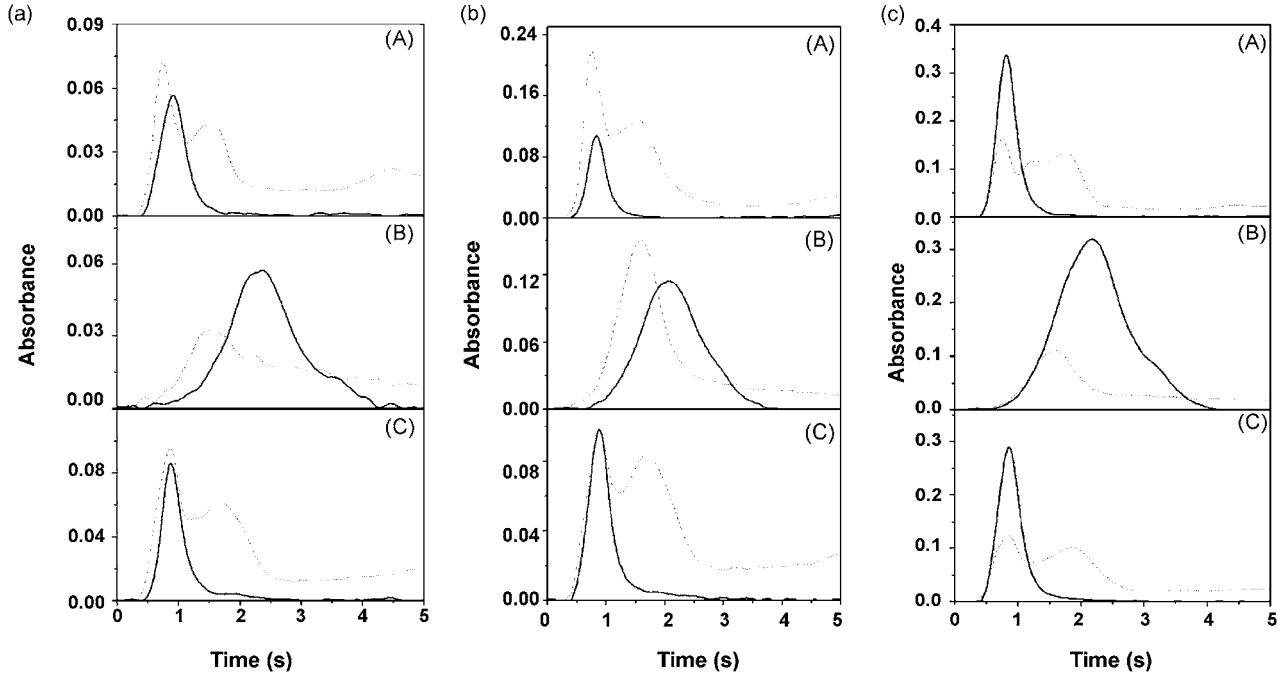

Fig. 6. Absorbance signals for lead (—) and background (- - -) using 20 μL of (a) Chardonnay, (b) Merlot and (c) Monastrell; (A) untreated wine, PIN platform atomizer; (B) untreated wine, THFA; (C) digested wine, PIN platform atomizer.

preheated furnace without any further treatment. A significantly greater sample volume could actually be introduced into the filter furnace using an injection temperature ≥120 °C; however, this option has not been used in this work as no additional increase in sensitivity was necessary for the proposed application. The pyrolysis curves for 1 ng Pb in aqueous/13% ethanol solution and in the Monastrell wine sample without and with the addition of 7.5 μg Pd as a chemical modifier are shown in Fig. 5 in comparison to the curves obtained for the same solutions in the conventional platform furnace. The most obvious effect is the significant increase in sensitivity that was obtained with the THFA, which is due to the reduced diameter of the absorption volume. The second observation is that without the addition of a modifier the increase in sensitivity was different for aqueous standards and for the wine sample and that only a pyrolysis temperature of 700 °C could be used. With the addition of 7.5 μg Pd as a chemical modifier lead was stabilized up to about 1100 °C in aqueous solution and 1000 °C in the wine sample, i.e. values similar to those found for the platform furnace. A pyrolysis temperature of 900 °C, the same as with the platform furnace, was therefore used in further experiments.

Fig. 6 shows the absorbance signals for lead and background obtained for three wine samples, one white and two red wines, using the THPA, the THFA and the digested wine samples with the platform furnace. A comparison of the signals for the undigested and the digested wines obtained in the platform furnace shows that there is very little difference in the shape and size of both, the lead absorption signal and the background absorbance. This shows that the organic matrix is efficiently destroyed and/or removed in the pyrolysis stage and the background is essentially due to the inorganic constituents of the wine. A comparison of the platform furnace and the THFA shows a very significant broadening of the lead absorption signal, which results in the observed increase in the integrated absorbance, and an equally significant reduction in the background absorbance; both effects are according to expectation.

3.4. Analysis of wine samples

The seven wine samples were analyzed without any sample preparation with the addition of 7.5 μg Pd as a chemical modifier in the platform atomizer and in the THFA using aqueous standards for calibration in the former and aqueous standards with 13% ethanol in the latter atomizer. The digested wine samples were only analyzed in the platform atomizer also using aqueous standards for calibration. The results are shown in Table 5. All values were compared using a paired Student's *t*-test, and there was no significant difference in the results for undigested and digested wine samples using the platform atomizer, between the undigested samples using platform and filter atomizer, and between the results obtained for digested samples and those for undigested samples using THFA, all on a 99% confidence level. This shows that accurate results can be obtained for lead in wine without any sample pretreatment using the proposed procedure.

Table 5
Determination of lead in wine samples without sample preparation using a platform (THPA) and a filter atomizer (THFA), and after acid digestion using a platform atomizer; calibration against aqueous standards (in the THFA with the addition of 13% ethanol); 7.5 μg Pd as chemical modifier; pyrolysis temperature 900 °C; atomization temperature 2000 °C; all values average and standard deviation of $n = 3$

Wine sample	Found concentration (μg L^{-1} Pb)		
	THPA digested	THPA undigested	THFA undigested
Sauvignon Blanc	16 ± 0.36	16 ± 0.14	19 ± 0.09
Semillon	6.0 ± 0.22	7.1 ± 0.18	8.0 ± 0.06
Chardonnay	8.4 ± 1.3	7.9 ± 0.17	9.5 ± 0.25
Merlot	13 ± 0.25	12 ± 0.05	14 ± 0.05
Cabernet Franc	11 ± 0.87	12 ± 0.21	15 ± 0.07
Cabernet Sauvignon	10 ± 0.57	8.7 ± 0.29	11 ± 0.10
Monastrell	46 ± 2.4	47 ± 0.8	60 ± 0.02

The lead concentration found in all the investigated wine samples was clearly below the lowest threshold limit of 200 μg L^{-1}. With one exception (Monastrell from Spain) the lead content was more than one order of magnitude lower than this limit with an average of 11.7 μg L^{-1} for the wines from South America. There is also no significant difference in the lead content between white and red wines. This is in contrast to the findings of others, who reported values of 324–477 μg L^{-1} Pb in German red wines [7], 4–254 μg L^{-1} Pb in German white and red wines [9], 130–270 μg L^{-1} Pb in Yugoslav white and red wines [10] and up to 1125 μg L^{-1} Pb in Spanish wines [8]. Although obviously not enough samples have been investigated in this work to allow general conclusions, our results appear to be in agreement with the values reported by others for South American wines, such as contents of 6–57 μg L^{-1} Pb in wines from Uruguay [11], or values of 10.3–55 μg L^{-1} Pb in white and red wines from Brazil [13], but also for wines from Macedonia [25,28].

Table 6
Comparison of the figures of merit obtained for the determination of lead in a commercial PIN platform atomizer (THPA) and the THFA; aqueous standards with 7.5 μg Pb as chemical modifier

Parameter	THPA	THFA
Regression equation	$A = 0.1257m$ (ng) + 0.0105	$A = 0.3373m$ (ng) + 0.0213
Correlation coefficient R	0.9999	0.9998
Characteristic mass, m_0 (pg)	34	12
LOD (μg L^{-1})	0.48	0.29
LOD (pg)	9.7	5.9
LOQ (μg L^{-1})	1.6	1.0
LOQ (pg)	32	20

3.5. Figures of merit

A comparison of the figures of merit obtained with the platform and the filter atomizer for aqueous standards is shown in Table 6. The sensitivity, expressed as the slope of the analytical curve, is more than a factor of 2.5 better in the THFA, compared to the platform atomizer, but the limits of detection and quantification were only better by a factor of 1.6. On the other hand, this improvement in sensitivity and LOD does not reflect the real improvement brought about by the THFA, as these data were obtained with aqueous solutions. A much more interesting comparison is that of the average repeatability of the signals obtained in the seven undigested wine samples under routine conditions, i.e. with three replicates each. The average repeatability, expressed as the relative standard deviation (R.S.D.) obtained with the PIN platform atomizer was 4.6%, whereas that obtained with the THFA was 0.6%. This dramatic improvement is most likely to a great extent due to the significantly lower background absorbance and hence an improved signal-to-background ratio in the latter atomizer. This improvement in R.S.D. would most likely also have resulted in significantly lower LOD for lead in wine; however, the lead content in all the investigated wine samples was too high to determine a realistic LOD or LOQ.

Spike recovery tests were carried out with one white and one red wine as no certified reference material is available for wine or any substance of comparable composition. The addition of $50\,\mu g\,L^{-1}$ Pb to the Sauvignon Blanc resulted in an average recovery of $108 \pm 1\%$ using the platform atomizer and of $108 \pm 2\%$ using the THFA; the same addition to the Mostarell resulted in an average recovery of $98 \pm 1\%$ using the platform atomizer and of $103 \pm 3\%$ using the THFA.

4. Conclusion

A method has been developed for the determination of lead in wine using ET AAS without any sample preparation, except the addition of 7.5 μg Pd as a chemical modifier, and calibration against aqueous standards. Sensitivity, accuracy and precision were adequate for the purpose of a routine method. It might be assumed that other trace elements in wine could be determined in a similar way after careful program optimization. The THFA provided improved sensitivity and significantly better R.S.D. values for the analysis of real samples, most likely because of the much better signal-to-background ratio. Our results confirmed the findings of others that the lead content in wines from South America is roughly an order of magnitude lower than in wines from Europe, although the number of samples investigated in this work might not be representative. A detailed investigation of the reasons for this difference would certainly be worthwhile, as the outcome of this study might help to show ways to lower the lead content in European wines as well. This aspect is of particular interest, as it is kind of accepted that lead is introduced mostly during wine processing and – except for some isolated cases – not from environmental sources [1,46,47].

Acknowledgements

The authors are grateful to Conselho Nacional de Desenvolvimento Científico e Tecnológico (CNPq), to Coordenação de Aperfeiçoamento de Pessoal de Nível Superior (CAPES) and Fundo de Amparo à Pesquisa do Estado da Bahia (FAPESB) for financial support and fellowships. M.G.R.V., M.B.D. and S.L.C.F. have research scholarships from CNPq and B.W. has a research scholarship from FAPESB. The authors are also grateful to Analytik Jena dor the donation of an atomic absorption spectrometer.

References

[1] K. Pyrzyńska, Crit. Rev. Anal. Chem. 34 (2004) 69.
[2] D.M. Goldberg, I.L. Bromberg, Clin. Chim. Acta 246 (1996) 14.
[3] M. Gronbaek, M. Deis, T.I. Sorensen, U. Becker, P. Schnohr, P. Jensen, Br. Med. J. 10 (1995) 1165.
[4] A. Kaufmann, Food Addit. Contam. 15 (1998) 437.
[5] T. Nielsen, K.A. Jensen, P. Grandjean, Nature 274 (1978) 602.
[6] M. Aceto, O. Abollino, M.C. Bruzzoniti, E. Mentasti, C. Sarzanini, M. Malandrino, Food Addit. Contam. 19 (2002) 126.
[7] M.M. Castiñeira, R. Brandt, A. van Bohlen, N. Jakubowski, Fresenius J. Anal. Chem. 370 (2001) 553.
[8] C.M. Mena, C. Cabrera, M.L. Lorenzo, M.C. Lopez, J. Agric. Food. Chem. 45 (1997) 1812.
[9] P. Ostapczuk, H.R. Eschnauer, G.R. Scollari, Fresenius J. Anal. Chem. 358 (1997) 723.
[10] Z.J. Suturovic, N.J. Marjanovic, Nahrung-Food 42 (1998) 36.
[11] M.E.R. Huguet, At. Spectrosc. 25 (2004) 177.
[12] R. Lara, S. Cerutti, J.A. Salonia, R.A. Olsina, L.D. Martinez, Food Chem. Toxicol. 43 (2005) 293.
[13] G.P.G. Freschi, C.S. Dakuzaku, M. de Moraes, J.A. Nóbrega, J.A. Gomes Neto, Spectrochim. Acta Part B 56 (2001) 1987.
[14] A.M. Green, A.C. Clark, G.R. Scollary, Fresenius J. Anal. Chem. 358 (1997) 711.
[15] O. Mikkelsen, C. Nordhei, S.M. Skogvold, K.H. Schroder, Anal. Lett. 37 (2004) 2925.
[16] K.Z. Brainina, N.Y. Stozhko, G.M. Belysheva, O.V. Inzhevatova, L.I. Kolyadina, C. Cremisini, M. Galletti, Anal. Chim. Acta 514 (2004) 227.
[17] I.I. Stewart, J.W. Olesik, J. Anal. Atom. Spectrom. 13 (1998) 1313.
[18] R.B. Myors, R. Hearn, L.G. Mackay, J. Anal. Atom. Spectrom. 20 (2005) 216.
[19] S. Augagneur, B. Medina, F. Grousset, Fresenius J. Anal. Chem. 357 (1997) 1149.
[20] G. Thiel, K. Danzer, Fresenius J. Anal. Chem. 357 (1997) 553.
[21] H. Eschnauer, L. Jakob, H. Meierer, R. Neeb, Mikrochim. Acta 3 (1989) 291.
[22] A.P. Fernandes, M. de Moraes, J.A. Gomes Neto, Atom. Spectrosc. 24 (2003) 179.
[23] C.R.T. Tarley, S.L.C. Ferreira, M.A.Z. Arruda, Microchem. J. 77 (2004) 163.
[24] W. Chuachuad, J.F. Tyson, J. Anal. Atom. Spectrom. 20 (2005) 282.
[25] I.B. Karadjova, L. Lampugnani, A. D'Ulivo, M. Onor, D.L. Tsalev, Anal. Bioanal. Chem. 388 (2007) 801.
[26] P.L. Buldini, S. Cavalli, J.L. Sharma, J. Agric. Food Chem. 47 (1999) 1993.
[27] J.L. Capelo, S. Catarino, A.S. Curvelo-Garcia, M. Vaiao, JAOAC Int. 88 (2005) 585.
[28] I. Karadjova, J. Cvetković, T. Stafilov, S. Arpadjan, Central Eur. J. Chem. 5 (2007) 739.
[29] K.G. Fernandes, M. de Moraes, J.A. Gomes Neto, J.A. Nóbrega, P.V. Oliveira, Analyst 127 (2002) 157.
[30] W. Slavin, D.C. Manning, G.R. Carnrick, Atom. Spectrosc. 2 (1981) 137.
[31] G. Schlemmer, B. Welz, Spectrochim. Acta Part B 41 (1986) 1157.
[32] J.Y. Cabon, A. Le Bihan, Spectrochim. Acta Part B 51 (1996) 1245.

[33] J.C.P. De Mattos, A.M. Nunes, A.F. Martins, V.L. Dressler, E.E.M. Flores, Spectrochim. Acta Part B 60 (2005) 687.
[34] L.M. Voth-Beach, D.E. Schrader, J. Anal. Atom. Spectrom. 2 (1987) 45.
[35] P. Bermejo-Barrera, J. Moreda-Pineiro, A. Moreda-Pineiro, A. Bermejo-Barrera, J. Anal. Atom. Spectrom. 13 (1998) 777.
[36] O. Acar, Z. Kilic, A.R. Turker, Food Chem. 71 (2000) 117.
[37] D.L. Tsalev, V.I. Slaveykova, L. Lampugnani, A. D'Ulivo, A.R. Georgieva, Spectrochim. Acta Part B 55 (2000) 473.
[38] J.B.B. da Silva, M.A.M. da Silva, A.J. Curtius, B. Welz, J. Anal. Atom. Spectrom. 14 (1999) 1737.
[39] D.A. Katskov, P.J.J.G. Marais, P. Ngobeni, Spectrochim, Acta Part B 53 (1998) 671.
[40] A. Anselmi, P. Tittarelli, D.A. Katskov, Spectrochim. Acta Part B 57 (2002) 403.
[41] P. Ngobeni, C. Canário, D.A. Katskov, Y. Thomassen, J. Anal. Atom. Spectrom. 18 (2003) 762.
[42] C. Canário, P. Ngobeni, D.A. Katskov, Y. Thomassen, J. Anal. Atom. Spectrom. 19 (2004) 1468.
[43] C. Canário, D.A. Katskov, J. Anal. Atom. Spectrom. 20 (2005) 1386.
[44] D. Bellido-Milla, J.M. Moreno-Perez, M.P. Hernandez-Artiga, Spectrochim. Acta Part B 55 (2000) 855.
[45] V.A. Lemos, M. de la Guardia, S.L.C. Ferreira, Talanta 58 (2002) 475.
[46] S. Imais, Y. Hayashi, Anal. Chem. 63 (1991) 772.
[47] S. Galani-Nikolakaki, N. Kallithrakas-Kontos, A.A. Katsanos, Sci. Total Environ. 285 (2002) 155.

Available online at www.sciencedirect.com
ScienceDirect
Talanta 74 (2008) 1562–1567
Talanta
www.elsevier.com/locate/talanta

Comparison between the electrocatalytic properties of different metal ion phthalocyanines and porphyrins towards the oxidation of hydroxide

Karolien De Wael *, Annemie Adriaens

Ghent University, Department of Analytical Chemistry, Krijgslaan 281 S12, B-9000 Ghent, Belgium

Received 24 July 2007; received in revised form 17 September 2007; accepted 28 September 2007
Available online 2 October 2007

Abstract

This work reports on the electrocatalytic oxidation of hydroxide using different central metal ion phthalocyanines and porphyrins immobilized on gold electrodes. The apparent electrocatalytic activity of cobalt phthalocyanine or porphyrin modified electrodes was found to be the greatest among the present series of metal ion macrocycles investigated. Copper and unmetallated phthalocyanine or porphyrin modified electrodes show no electrocatalytic behaviour towards hydroxide, such as bare gold. A possible mechanism for the enhanced reactivity of cobalt ion macrocycles towards the oxygen evolution is given. It is also stated that the electrocatalytic activity towards an adsorbate involves several aspects, such as the coordination state of the central metal ion, the nature of the ligand, the stability of the complexes, the number of d electrons, the energy of orbitals and the strength of the bonding between the central metal ion and the axial ligand.
© 2007 Elsevier B.V. All rights reserved.

Keywords: Modified electrode; Electrocatalysis; Phthalocyanines; Porphyrins; Hydroxide; Oxygen evolution

1. Introduction

Most studies in electrocatalysis are focused on the electroformation and reduction of oxygen, because of their use in many electrochemical devices such as water electrolysis, fuel cells, ... [1,2]. The evolution of oxygen is important in the field of photosynthesis and in the functioning of electrolysers which may by the basis of the production of hydrogen as a clean fuel [3]. The anodic oxygen electrode reaction is known for its high activation overpotential in aqueous solutions resulting in substantial energy losses. Therefore, it is desired to limit the oxygen overvoltages as much as possible.

A series of papers is devoted to the voltammetric determination of hydroxide ions with formation of oxygen in aqueous solutions by using micro-electrodes or rotating disc electrodes [4–6]. In these cases, the concentration of bases can be determined by direct oxidation of hydroxide ions. The potential at which this oxidation occurs varies between 1.1 and 1.4 V vs. SCE. Another approach to reduce the oxygen overvoltages, is the use of electrocatalysts. Some semiconducting oxides, such as $NiCo_2O_4$, give quite good performance towards hydroxide, but the best anodes described in literature seem to be those based on Ir/RuO_2 coatings of Ti which give current densities at an overpotential of 200 mV [7,8].

As phthalocyanines and porphyrins can act as an electron transfer mediator for several compounds [2], they are potential species for the electroanalytical determination of the OH^- ion concentration. Phthalocyanines and their derivatives have been widely used as dyestuffs and colours. Nowadays they are also commonly used in high-tech applications, such as photovoltaic, electronic and sensing devices [9–12]. Porphyrins are widespread compounds in nature. They are important for several mechanisms in life: they catalyse enzymatic reactions and are, for instance, responsible for the oxygen transport in the human body [13]. These complexes are among the most common and best-known bioinorganic compounds: chlorophylls, cobalamins, hemoglobin, ... [14,15]. The major characteristics of phthalocyanines and porphyrins are their thermal and chemical stability and their extensive redox chemistry. The extensive π system of phthalocyanine and porphyrins causes very sta-

* Corresponding author. Tel.: +32 9 264 48 20; fax: +32 9 264 49 60.
E-mail address: Karolien.DeWael@UGent.be (K. De Wael).

0039-9140/$ – see front matter © 2007 Elsevier B.V. All rights reserved.
doi:10.1016/j.talanta.2007.09.034

ble complexes with a variety of metal ion. The central metal ion of these macrocycles binds one or two axial ligands and undergoes either metal centered, macrocycle centered and/or axial ligand centered redox reactions. The immobilization of these compounds on an electrode surface can lead to modified electrodes with electrocatalytic properties [16]. Transition metal complexes of macrocyclic ligands, including phthalocyanines and porphyrins, have been widely described as catalysts for oxygen reduction [2]. The use of these compounds for oxygen evolution was already published for carbon electrodes but not for gold [17]. In the former situation, no peak shaped processes was observed thus lacking analytical purposes. The successful use of transition metal ions phthalocyanines and porphyrins as catalysts can be related to the fact that these compounds have unpaired d electrons and unfilled d orbitals which are available to form bonds with the adsorbate in axial position. In the literature, the electrocatalytic activity is most of the time expressed as a function of the number of d electrons of the metal ion in the phthalocyanine or porphyrin ring [2,17–19].

In this paper, we will show that some phthalocyanines and porphyrins immobilized on gold electrodes exhibit enhanced reactivity towards the oxygen evolution. The influence of the nature of the central metal ion on the electrocatalytic behaviour is investigated in detail. It is proven that not only the number of d electrons of the central metal ion is linked to the electrocatalytic activity of the macrocycle. Electrocatalysing the oxidation of hydroxide opens up new perspectives for its analytical application, especially in sensor development to monitor the hydroxide concentration during processing.

2. Experimental

A saturated calomel reference electrode (SCE, Radiometer, Copenhagen) with two compartments from Radiometer and a carbon counter electrode were used. The working electrodes were gold electrodes from BASi (West Lafayette, USA) (diameter 1.6 mm) and were pretreated by mechanical and electrochemical polishing. Before its first use, the electrode surface was scoured briefly on 1200 grit SiC-emery paper to obtain a fresh surface. To smoothen this relatively rough surface, it was further subjected to sequential polishing on a polishing cloth covered with alumina (Buehler, Illinois, USA) powder of 1, 0.3 and 0.05 μm particle size for respectively 5, 10 and 20 min. To remove any adherent Al_2O_3 particles, the electrode surface was rinsed thoroughly with doubly deionised water and cleaned in an ultrasonic bath (Branson 3210) for 2 min. Finally, the electrode was pretreated electrochemically by scanning it in a Na_2HPO_4/NaOH buffer solution (pH 12, purchased from Riedel-de Haën) between −1.2 and 0.6 V vs. SCE until 5 subsequent scans were identical. The scan rate for all cyclic voltammetric experiments was 50 mV s^{-1}.

A PGSTAT20 potentiostat (ECO Chemie, The Netherlands) controlled by GPES 4.9 software package running on a Pentium II computer (Eknadata) was used to obtain the voltammetric data. Measurement of the pH of the solution was done using a Model 420A Orion Benchtop pH-meter. The phthalocyanine compounds, more specific Co(II) tetrasulphonated phthalocyanine

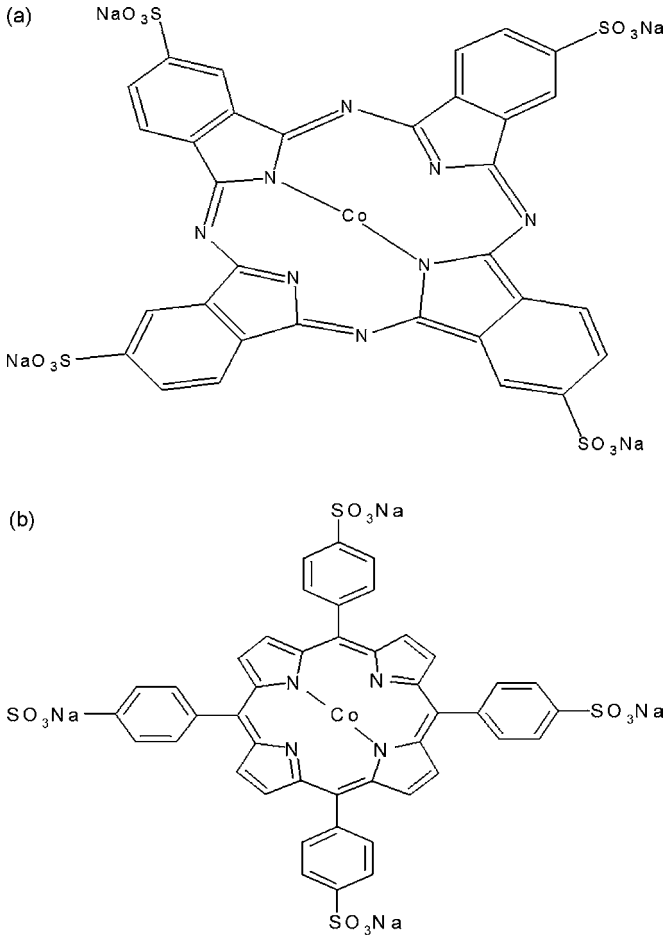

Fig. 1. Molecular structure of Co(II) tetrasulphonated phthalocyanine sodium salt (CoTSPc) (a) and 5,10,15,20-tetrakis(4-sulphonatophenyl)porphyrin-Co(II) tetrasodium salt (CoTSPor) (b).

sodium salt (CoTSPc, Fig. 1a), 3,4′,4″,4‴Cu(II) tetrasulphonated phthalocyanine sodium salt (CuTSPc) and Fe(III) tetrasulphonated phthalocyanine sodium salt (FeTSPc) were purchased respectively from Sigma–Aldrich (USA), Rhodes University of Grahamstown, Eastern Cape (South Africa) and Midcentury (Posen, USA). The porphyrin compounds were purchased from Porphyrin Systems (Lübeck, Germany): 5,10,15,20-tetrakis(4-sulphonatophenyl)porphyrin-Co(II) tetrasodium salt (CoTSPor, Fig. 1b), 5,10,15,20-tetrakis-(4-carboxyphenyl)-porphyrin-Co(II) (CoTCPor), 5,10,15,20-tetrakis-(4-carboxyphenyl)-porphyrin-Cu(II) (CuTCPor), 5,10,15,20-tetrakis-(4-sulphonatophenyl)-porphyrin-Mn(III) chloride (Mn-TSPor) and 5,10,15,20-tetrakis-(4-carboxyphenyl)-21,23H-porphyrin (H_2TCPor). Sodium hydroxide (NaOH) and sodium sulphate (Na_2SO_4) were purchased from Sigma–Aldrich. Before each experiment, pure nitrogen was bubbled through the cell solution for 20 min.

Electrode modification was performed by recording successive cyclic voltammetric scans (60 scans) in a potential window from −1.2 to 0.6 V vs. SCE in a Na_2HPO_4/NaOH pH 12 buffer solution containing 1×10^{-3} mol L^{-1} phthalocyanine or porphyrin. After each modification procedure, the electrode was immersed in a Na_2HPO_4/NaOH pH 12 buffer solution (not con-

taining phthalocyanine or porphyrin) while voltammetric scans were taken in order to study the electrochemical behaviour of the modified electrode.

3. Results and discussion

3.1. Oxidation of hydroxide at several phthalocyanine or porphyrin modified gold electrodes

Fig. 2 shows the current–potential behaviour of a bare gold electrode (1) and different phthalocyanine or porphyrin modified gold electrodes (2–9) in a Na_2HPO_4/NaOH buffer solution containing 0.01 mol L^{-1} hydroxide. A detailed explanation of all electrochemical processes related to the phthalocyanine or porphyrin can be found in literature [20–22]. Only the oxidation process in the potential region of 0.7–1.2 V vs. SCE and the reduction peak that starts at −0.1 V vs. SCE are relevant for this study. The latter is the reduction of dissolved oxygen. As the buffer solution is saturated with nitrogen before and during the electrochemical experiment, the oxygen must be formed during the electrochemical scanning process. It is clear that the oxygen reduction only occurs when there is an oxidation peak in the potential region of 0.7–1.2 V vs. SCE. This redox reaction can be explained as the electrocatalytic oxidation of hydroxide with formation of oxygen [23]:

$$4OH^- \rightleftarrows O_2 + 2H_2O + 4e^- \quad (1)$$

Fig. 2 clearly shows that at a bare gold electrode (1) hydroxide is not electrocatalytically oxidized in the presented potential range. At 1.2 V vs. SCE, there is an increase in current indicating the beginning of the solvent oxidation and thus representing the limit of the potential range. Analogous cyclic voltammetric scans were recorded for H_2TCPor (2), CuTSPc (3) and CuTCPor (4) modified gold electrodes. None of these curves show redox processes in the potential range from 0.7 to 1.2 V vs. SCE and thus do not electrocatalyse the oxidation of hydroxide. Curves 5–8 are the first cyclic voltammograms recorded at a CoTSPor (5), CoTCPor (6), CoTSPc (7) and MnTSPor (8) modified gold electrode and clearly exhibit electrocatalytic activity towards hydroxide. The electrocatalytic properties are the best for a CoTCPor modified gold electrode which is shown by the highest current and the largest shift towards less positive potentials. The current–potential behaviour of a FeTSPc modified electrode is shown as curve 9. Only a poorly defined oxidation peak is observed, indicating a less pronounced electrocatalytic behaviour. The smaller the oxidation peak in the potential region of 0.7–1.2 V vs. SCE, the less oxygen is formed and thus the lower the reduction current corresponding to the oxygen reduction. The catalytic activity of the modified electrodes towards the oxidation of hydroxide was found to increase as follows:

$$\text{FeTSPc} < \text{MnTSPor} < \text{CoTSPc} < \text{CoTSPor} < \text{CoTCPor}$$

$$(\text{no activity} : \text{Au},\ H_2\text{TCPor},\ \text{CuTCPor},\ \text{CuTSPc})$$

Based on these observations, it can be concluded that the nature of the central metal ion has a major influence on the electrocatalytic properties of the modified electrode towards hydroxide. A hypothesis for the corresponding mechanism is given further in the text.

Electrocatalysing the oxidation of hydroxide has advantageous consequences for its analytical application, especially in sensor development to monitor the hydroxide concentration during processing. A CoTCPor modified gold electrode is selected to investigate the hydroxide oxidation in detail.

When recording successive cyclic voltammograms at a CoTCPor modified electrode in a pH 12 buffer solution, a decrease in OH^- reactivity is observed, as shown in Fig. 3a. Curves 1–6 represent some of the first 20 scans. The decrease of ca. 14 μA over 20 scans can be explained by the fact that oxygen formation slowly impairs the immobilized layer, e.g. by the formation of oxo species. The stability was also tested by sweeping the potential from 0 to 0.98 V vs. SCE (peak maximum) and holding it at 0.98 V for 760 s (the time equivalent of measuring 20 successive voltammetric scans). This amperometric experiment is shown in Fig. 3b and indicates that the current

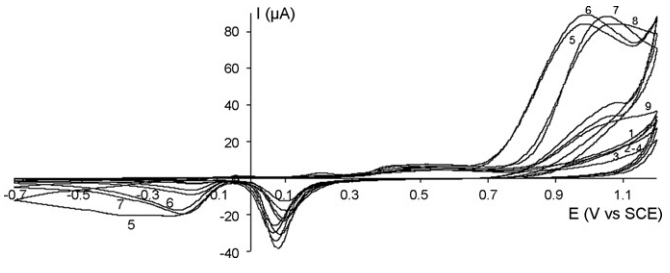

Fig. 2. Cyclic current–potential curves of different modified electrodes in a pH 12 buffer solution: a bare gold electrode (1), H_2TCPor (2), CuTSPc (3), CuTCPor (4), CoTSPor (5), CoTCPor (6), CoTSPc (7), MnTSPor (8) and FeTSPc (9) modified gold electrode.

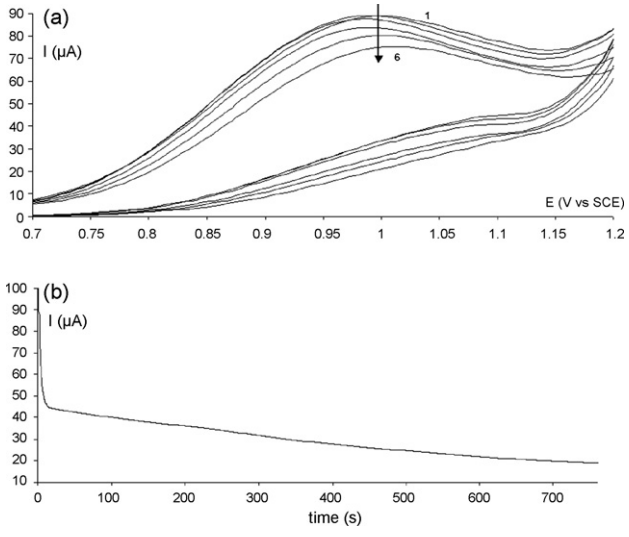

Fig. 3. (a) Successive cyclic voltammograms recorded at a CoTCPor modified electrode in a pH 12 buffer solution: scan 1 (1), 2 (2), 5 (3), 10 (4), 15 (5) and 20 (6); (b) evolution of the current as a function of time for a CoTCPor modified electrode held at a constant potential (0.98 V) during 760 s in a pH 12 buffer solution.

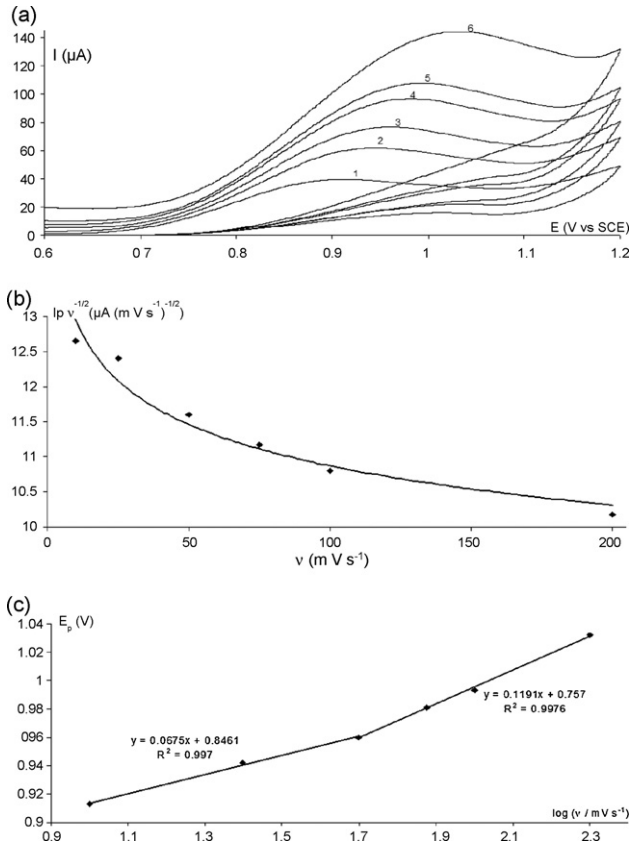

Fig. 4. (a) Oxidation of hydroxide at a CoTCPor modified electrode in a pH 12 buffer solution at different scan rates: 10 mV s^{-1} (1), 25 mV s^{-1} (2), 50 mV s^{-1} (3), 75 mV s^{-1} (4), 100 mV s^{-1} (5) and 200 mV s^{-1} (6); (b) relationship between $I_p\nu^{-1/2}$ and ν; (c) Relationship between E_p and log ν.

declines as a function of time to a much bigger extent compared to the cyclic voltammetric experiment. This decrease is caused by a continuous formation of oxygen during the amperometric experiment. In the limit, the oxygen bubbles will slow down the electron transfer and block the electrode. In contrast, when several successive voltammetric scans are recorded, the formed oxygen is reduced in the cathodic sweep.

The influence of the scan rate on the peak current was investigated to determine the nature of the process. Fig. 4a shows the oxidation of 0.01 mol L^{-1} hydroxide in a Na_2HPO_4/NaOH buffer solution over a wide range of scan rates. The half-wave potentials shift positively with increasing scan rate, characteristic for an irreversible case. When the slope of the relationship between log I_p and log ν equals 1, this corresponds to a reaction of an adsorbed species; while a slope of 0.5 rather indicates a rate determining diffusion of a species towards the electrode surface. For the described redox reaction, a slope of 0.49 is found for the relationship between log I_p and log ν, indicating a reaction of a particle in solution, i.e. hydroxide. In contrast to results obtained at gold micro-electrodes [4], the linearity is valid for all scan rates for modified electrodes. For phthalocyanine and porphyrin modified electrodes, there is no interference between the wave corresponding to the formation of gold oxides with the wave for the hydroxide oxidation. The latter is the case at gold micro-electrodes making the wave due to hydroxide oxidation

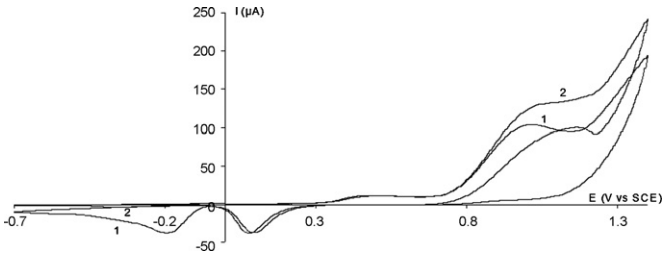

Fig. 5. Cyclic current–potential curves of a stationary (1) and a rotating (2, 76 rpm) CoTCPor modified electrode in a pH 12 buffer solution.

less defined and no longer useful for analytical purposes at high scan rates [4]. Fig. 4b represents the behaviour of $I_p\nu^{-1/2}$ as a function of the scan rate. The $I_p\nu^{-1/2}$ value increases markedly on decreasing the scan rate, characteristic for a catalytic mechanism. The oxidation peak becomes thus less pronounced with decreasing scan rate, indicating an EC_{cat} mechanism. This mechanism is usually very readily identified as it is the only one in which this behaviour occurs. Another diagnostic criterion for an EC_{cat} mechanism is proposed Fig. 4c: the variation of the peak potential E_p with the scan rate gives two linear regions suggesting that chemical reactions coupled with electrochemical steps are involved [24,25].

The presumed diffusion nature was also tested by varying both the rotation frequency and the concentration of hydroxide ions. For the latter, the reader is referred to the literature [23]. The recorded cyclic voltammograms of a stationary (curve 1) and a rotating (curve 2) CoTCPor modified electrode in a Na_2HPO_4/NaOH buffer solution, containing 0.01 mol L^{-1} hydroxide, are shown in Fig. 5. In contrast to a stationary electrode, the reduction peak of oxygen at ca. −0.15 V vs. SCE disappears when using a rotating electrode as the movement of the electrode moves the oxygen away. It is also observed that the dependence of the limiting current on the rotation speed ω satisfies the Levich equation [26]. The slope of ca. 0.5 indicates a diffusion controlled process. A value for the diffusion coefficient of OH^- ions is calculated: 4.92×10^{-5} cm^2 s^{-1}. Other values reported so far in the literature are: 6.8×10^{-5} cm^2 s^{-1}, determined by Littauer and Tsai [27], in LiOH solution at infinite dilution by the Pt rde technique, 4.62×10^{-5}, determined by Daniele et al. [28] and 5.6×10^{-5} cm^2 s^{-1}, determined by Breiter and Hoffmann [29]. In short, the calculated value for the detection limit is in good correlation with the values reported in literature.

3.2. Interaction between hydroxide and metal ion phthalocyanines or porphyrins

Only a number of the investigated transition metal ion phthalocyanines or porphyrins immobilized onto a gold electrode exhibit enhanced reactivity towards the oxygen evolution (Fig. 2). The highest activity is observed for 5,10,15,20-tetrakis-(4-carboxyphenyl)-porphyrin-Co(II) (CoTCPor). No catalytic activity was observed for unmetallated H_2TCPor: the current–potential behaviour is exactly the same as for a bare, unmodified gold electrode. This shows that ring based redox

processes are not involved in the electrocatalytic oxidation of hydroxide on phthalocyanine or porphyrin complexes immobilized on gold electrodes. The effect of ring substituents was already investigated in the past [23] and is confirmed in this work. The substituent COOH yields a slightly better activity compared to SO_3H. The dependence of the kinetics of the reaction on the nature of the central metal ion proofs the idea that the metal ion is the site where the electrocatalytic process occurs. The catalytic activity of phthalocyanine and porphyrin macrocycles is due to their ability to bind ligands axially. Interaction of an adduct, such as hydroxide, is located in an axial position, as a ligand of the metal center of the phthalocyanine or porphyrin ring. In the past, volcano-correlations have been found, when comparing the catalytic activity vs. the redox potential of the metal ion or the number of d electrons of the central metal ion [2,17–19]. It will be shown in this work that more is involved than the redox potential or the number of d electrons.

The cobalt center interacts more favourably with the oxygen atom of the hydroxide ion compared to the other metal ions. According to the perturbation theory, this implies that the orbital energy of cobalt is similar to the one of oxygen [30]. Based on studies concerning the catalytic activity of, on the one side, cobalt macrocycles towards small adducts other than hydroxide and, on the other hand, the electrocatalytic activity of cobalt oxides towards the oxygen evolution [31], the following reaction mechanism is suggested (equatorial ligands are left out) [32]:

$$Co(III)_{ads} + OH^- \rightleftarrows Co(III)(OH^-)_{ads}$$

$$Co(III)(OH^-)_{ads} \rightleftarrows [Co(II)(OH)_{ads}]^-$$

$$[Co(II)(OH)_{ads}]^- \rightleftarrows Co(III)(OH)_{ads} + e^-$$

$$Co(III)(OH)_{ads} + OH^- \rightleftarrows Co(III)_s + \tfrac{1}{2}O_2 + H_2O + e^-$$

Just before the onset of the oxygen evolution, the oxidation state of the cobalt ion is +III. In the first step, the hydroxide ion occupies the place of the axial ligand of the macrocycle followed by an internal electron shift leading to $Co(II)(OH)_{ads}$, which is, because of the applied potential, directly oxidized to $Co(III)(OH)_{ads}$ in the third step. This adsorbed species can react with another hydroxide ion resulting in the original $Co(III)_{ads}$ state and oxygen evolution. The catalytic oxidation of OH^- is due to the stabilization of the intermediate oxidized product through the formation of a covalent bond between the unpaired p electron of hydroxide and an unpaired d electron of the metal ion. This phenomenon is analogous to the one observed in the oxidation of dithiolate-metal complexes via covalent d–p bond formation [33]. The extent of this stabilization can be estimated from the negative shift of the redox potential for OH^- oxidation in the presence of a transition metal ion phthalocyanine or porphyrin.

Normal Cu(II) complexes with their d^9 configuration have the d_x^2–y^2 orbital occupied by the single electron. In d^9 systems, the octahedral configuration is unstable because of the ambiguity which results from incomplete occupation of the e_g orbital. This situation is circumvented through geometrical distortion; a lowering of the symmetry removes the orbital degeneracy (also called Jahn-Teller effect, Fig. 6). The preference of this metal ion for a square planar geometry and N ligand coordination, arises from this ligand-field effect [34]. Therefore, the probability for hydroxide to act as an axial ligand is quasi nihil and thus the oxygen evolution will not occur at copper ion phthalocyanines or porphyrins modified electrodes. A second reason for the non-catalytic properties of copper ion phthalocyanines and porphyrins is the fact that the energy of the highest occupied molecular orbital (HOMO) in transition metal ion phthalocyanines and porphyrins decreases almost linearly with the number of d electrons in the metal complex. The energy of the HOMO for copper is probably too low for an interaction between the metal ion and the oxygen. Therefore, a transfer of electron density from an oxygen orbital to d orbitals of the metal is strongly inhibited. A third reason can be derived from the proposed mechanism for hydroxide oxidation. If a hydroxide ion would bind axially towards Cu(II), in the second step Cu(I) is formed. This metal ion prefers a tetrahedral geometry [34], a state the rigid phthalocyanine or porphyrin ligand can never adapt. Therefore, further oxidation is excluded. Finally, cobalt, iron and manganese ions are rather hard ions compared to the rather soft nature of a copper ion. Therefore, the former prefer a reaction with a hard ligand, such as hydroxide. In contrast, copper prefers a complexation with a rather soft ligand such as sulfides [34,35].

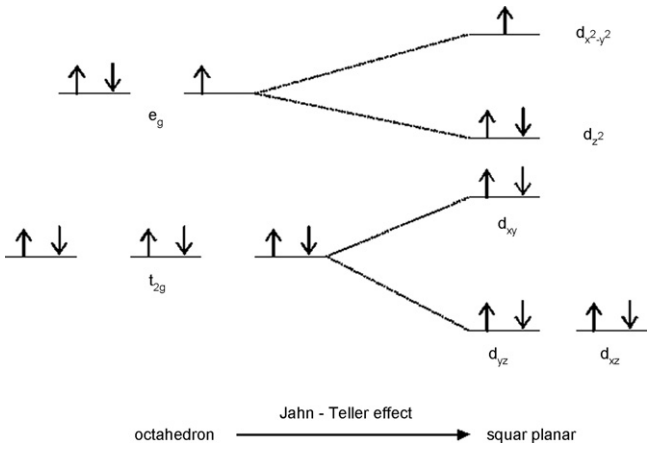

Fig. 6. Jahn-Teller effect of Cu(II).

Based on the hard–soft theory, manganese and iron complexes are expected to show some electrocatalytic behaviour towards hydroxide. Hydroxide is one of the most preferred ligands of Mn(III) next to phenolate and hydroxamate [34]. This metal ion is known as a powerful oxidizing agent and its relatively fast exchange of hydroxide or oxygen from it. The well-defined catalytic current in Fig. 1 is not a surprise because manganese ions also play an important role in photosynthesis [34]. They show crucial but until now little understood catalytic function in the mechanistically challenging oxidation of water to oxygen. The importance of manganese for the oxygen metabolism is not restricted to photosynthesis; further established examples include a manganese-containing superoxide dismutase, an azide-insensitive catalase and other peroxidases [36,37].

Iron porphyrin and its analogous derivates are well known because of their stoichiometric oxygen transport in living cells but also in a variety of catalytic biochemical processes [34]. Several small molecules can bind axially towards the iron ion. Fig. 1 shows that Fe(III)TSPc is less active compared to cobalt and manganese complexes, only a small peak can be attributed to the electrocatalytic hydroxide oxidation. This can be explained by the fact that Fe(III)TSPc probably forms a very stable adduct with hydroxide, analogous to Fe(III)EDTA [34]. The release of hydroxide in one of the last steps is slowed down resulting in a lower catalytic activity and thus oxidation peak.

Based on the above results, it is clear that the electrocatalytic activity towards an adsorbate involves lots of aspects, such as the coordination state of the central metal ion, the nature of the ligand, the stability of the complexes, the number of d electrons, the energy of orbitals, the strength of the bonding between the central metal ion and the axial ligand, ... All parameters must be taken into account to describe the catalytic activity.

4. Conclusions

This paper describes that a number of metal ion phthalocyanines or porphyrins immobilized on gold electrodes exhibit a catalytic activity towards hydroxide. A detailed electrochemical investigation of the oxidation of hydroxide at these kinds of modified electrodes is performed. It is observed that 5,10,15,20-tetrakis-(4-carboxyphenyl)-porphyrin-Co(II) (CoTCPor) appears to be the best electron transfer mediator for this oxidation reaction. A mechanism for the hydroxide oxidation is proposed as well as an explanation for the difference in catalytic activity between different metal ion phthalocyanines and porphyrins. It is clear that the electrocatalytic activity towards an adsorbate, including hydroxide, involves several aspects. All parameters must be taken into account to describe the catalytic activity.

References

[1] D. Pletcher, Industrial Electrochemistry, Chapman & Hall, New York, 1982.
[2] J.P. Dodelet, J.H. in, F. Zagal, J.P. Bedioui, Dodelet (Eds.), N_4-Macrocyclic Metal Complexes, Springer, New York, 2006 (Chapter 3).
[3] V.P. Shinkarev, C.A. Wraight, Proc. Natl. Acad. Sci. 90 (1993)1834.
[4] M.E. Abdelsalam, G. Denuault, M.A. Baldo, C. Bragato, S. Daniele, Electroanalysis 13 (2001) 289.
[5] O. Ordeig, C.E. Banks, T.J. Davies, F.J. del Campo, F.X. Munõz, R.G. Compton, Anal. Sci. 22 (2006) 679.
[6] A. Abu-Rabi, D. Jasin, S. Mentus, J. Electroanal. Chem. 600 (2007) 364.
[7] A.C.C. Tseung, S. Jasem, Electrochim. Acta 22 (1977) 31.
[8] A.J. Scarpellino, G.L. Fisher, J. Electrochem. Soc. 129 (1982) 515, 522.
[9] C.C. Leznoff, A.B.P. Lever, Phthalocyanines Properties and Applications, vol. 3, VCH Publishers, Weinheim, 1993.
[10] A.B.P. Lever, Chemtech 17 (1987) 506–510.
[11] M. Kato, Y. Nishioka, K. Kaifu, K. Kawamura, S. Ohno, Appl. Chem. Lett. 86 (1985) 196.
[12] T.A. Temofonte, K.F. Schoch, J. Appl. Chem. 65 (1989) 1350.
[13] K.M. Kadish, K.M. Smith, R. Guilard, The Porphyrin Handbook, Academic Press, New York, 2000.
[14] J.H. Fuhrhop, Angew. Chem. Int. Ed. Engl. 15 (1974) 321.
[15] D. Dolphin, The Porphyrins, vols. I–VII, Academic Press, New York, 1978.
[16] K. De Wael, P. Westbroek, E. Temmerman, Electroanalysis 17 (2005) 263.
[17] N. Chebotareva, T. Nyokong, Electrochim. Acta 42 (1997) 3519.
[18] J.H. Zagal, M. Gulppi, M. Isaacs, G. Cárdenas-Jirón, M.J. Aguirre, Electrochim. Acta 44 (1998) 1349.
[19] J.H. Zagal, S. Lira, S. Ureta-Zañartu, J. Electroanal. Chem. 210 (1986) 95.
[20] K. Peeters, K. De Wael, L. Vincze, A. Adriaens, Anal. Chem. 77 (2005) 5512.
[21] K. De Wael, K. Peeters, D. Bogaert, H. Buschop, L. Vincze, A. Adriaens, J. Electroanal. Chem. 603 (2007) 212.
[22] K. De Wael, A. Adriaens, E. Temmerman, Anal. Chim. Acta 554 (2005) 60.
[23] K. De Wael, A. Adriaens, Electrochim. Acta, accepted for publication.
[24] C.A. Caro, F. Bedioui, J.H. Zagal, Electrochim. Acta 47 (2002) 1489.
[25] K.I. Ozoemena, T. Nyokong, J. Electroanal. Chem. 579 (2005) 293.
[26] D. Pletcher, R. Greef, R. Peat, L.M. Peter, J. Robinson, Instrumental Methods in Electrochemistry, Horwood Publishing Limited, England, 2001.
[27] E.L. Littauer, K.C. Tsai, Electrochim. Acta 24 (1979) 351.
[28] S. Daniele, M.A. Baldo, C. Bragato, Anal. Chem. 71 (1999) 811.
[29] M. Breiter, K. Hoffmann, Z. Elektrochem. 64 (1960) 462.
[30] R. Hoffmann, Acc. Chem. Res. 4 (1971) 1.
[31] E.B. Castro, C.A. Gervasi, J.R. Vilche, J. Appl. Electrochem. 28 (1998) 835.
[32] C.J. Ballhausen, Introduction to Ligand Field Theory, McGraw-Hill, New York, 1962.
[33] D.T. Sawyer, G.S. Srivatsa, M.E. Bodini, W.P. Schaefer, R.M. Wing, J. Am. Chem. Soc. 108 (1986) 936.
[34] W. Kaim, B. Schwederski, Bioinorganic Chemistry: Inorganic Elements in the Chemistry of Life, second ed., John Wiley & Sons, New York, 1994.
[35] R.J.P. Williams, Coord. Chem. Rev. 100 (1990) 573.
[36] K. Wieghardt, Angew. Chem. Int. Ed. Engl. 28 (1989) 1153.
[37] G.E.O. Borgstahl, H.E. Parge, M.J. Hickey, W.F. Beyer, R.A. Hallewell, J.A. Tainer, Cell 71 (1992) 107.

Available online at www.sciencedirect.com
ScienceDirect
Talanta 74 (2008) 1344–1349
Talanta
www.elsevier.com/locate/talanta

Quality control of medicinal herbs *Fructus gardeniae*, Common Andrographis Herb and their preparations for their active constituents by high-performance liquid chromatography–photodiode array detection–electrospray mass spectrometry

Li Ding [a], Xu Biao Luo [b], Fei Tang [a], Jin Bin Yuan [a], Manli Guo [a], Shou Zhuo Yao [a,*]

[a] *College of Chemistry and Chemical Engineering, Hunan University, Changsha 410082, PR China*
[b] *College of Environmental and Chemical Engineering, Nanchang Hangkong University, Nanchang 330063, PR China*

Received 27 June 2007; received in revised form 5 September 2007; accepted 6 September 2007
Available online 12 September 2007

Abstract

Dehydroandrographolide, andrographolide and geniposide are the main active constituents of many herbal medicines, e.g., *Fructus gardeniae*, Common Andrographis Herb. They are used as the markers to control the quality of such herbal medicines and their herbal preparations. In this paper, a simple and sensitive high-performance liquid chromatographic (HPLC) method coupled with photodiode array detection (DAD) and electrospray mass spectrometry (ESI/MS) were developed to determine the three compounds simultaneously in extracts of medicinal herbs and herbal preparations produced by different companies. The extracts were separated on a C_{18} reversed phase HPLC column, with a gradient solvent system, the time for the separation of the three target analytes was 10 min. The abundance ions were recorded using selected ion monitoring (SIM) mode with *m/z* 297.3, 297.3 and 411.1 for dehydroandrographolide, andrographolide and geniposide, respectively. The limit of detection for dehydroandrographolide, andrographolide and geniposide were 20, 30 and 150 ng mL^{-1}, respectively. The proposed method was successfully applied to the determination of the contents of the compounds in related to medicinal herbs and preparations.
© 2007 Elsevier B.V. All rights reserved.

Keywords: Dehydroandrographolide; Andrographolide; Geniposide; Herbal medicine preparations; *Fructus gardeniae*; Common Andrographis Herb

1. Introduction

The herbal medicine, including the traditional Chinese medicine (TCM), has attracted more attention for their therapeutic effects. Herbal medicinal preparations, which are combined mixtures of herbal medicines, are processed to achieve better medical or therapeutic effect. In order to ensure its maximal therapeutic effect, it is necessary and important to develop a simple and sensitive quality control method for the herbal medicinal preparations [1,2].

A representative herbal medicine preparation, widely adopted for the clinical use, is that made from a combination of multiple herbal constituents of *Fructus gardeniae*, Common Andrographis Herb and *Radix ophiopogonis*. According to the Chinese pharmacopoeia, this herbal medicine preparation has the effects of dispelling hot and healing poison, cooling blood and detumescence. The bioactive compounds of geniposide, andrographolide and dehydroandrographolide are used as the markers to control quality of such herbal medicines and preparations.

F. gardeniae, with its active component of geniposide, has been used to treat jaundice, acute conjunctivitis and epistaxis. Geniposide has the anti-phlogistic and diuretic effects [3]. Common Andrographis Herb is effective for curing digestive disease, snakebite, and infections ranging from malaria to dysentery [4,5]. Andrographolide and dehydroandrographolide are the main diterpenes components in this medicinal herb, possessing immune stimulating, anti-inflammatory and liver-protective effects [6,7]. Recently, many researches show that andrographolide has hypoglycemic, choleretic and hepatoprotective activity against carbon tetrachloride (CCl_4), and

* Corresponding author. Tel.: +86 731 8821968; fax: +86 731 8821848.
E-mail addresses: dingli0824@hotmail.com (L. Ding), szyao@hnu.cn (S.Z. Yao).

0039-9140/$ – see front matter © 2007 Elsevier B.V. All rights reserved.
doi:10.1016/j.talanta.2007.09.001

dehydroandrographolide is a *in vitro* inhibitor against the human immunodeficiency virus (HIV) [8].

Several methods have been reported for determination of geniposide in herbs and herbal medicine preparations, including high-performance liquid chromatography with UV detector, mass detector (HPLC–UV, HPLC–MS) [9–12], and capillary electrophoresis (CE) [13]. For the determination of andrographolide and dehydroandrographolide in herbs, the methods of thin-layer chromatography (TLC) [14,15], high-performance liquid chromatography (HPLC) [16], liquid chromatography (LC) [17], high-speed counter-current chromatography (HSCCC) [18] and microemulsion electrokinetic chromatography (MEEKC) [19,20] were reported. Most of them are time-consuming or laborious and the retention times of andrographolide and dehydroandrographolide are longer than 10 min. Moreover, there were no studies reported on the simultaneous determination of these three compounds in herbs or herbal medicine preparations to reflect their quality or for their quality control. Thus, the development of a simple and sensitive quality control method for their simultaneous analysis is necessary and valuable.

HPLC–DAD–ESI/MS provides more structural information on the compounds and has been proven to be a powerful approach for the rapid identification and determination of the ingredients in botanic extracts and herbal medicines [21–23]. The objective of this work was to develop a simple and reliable HPLC–DAD–ESI/MS method for full quality control of herbal medicinal preparations by determining the geniposide, andrographolide and dehydroandrographolide contents, respectively. This developed method was also successfully applied to quantification of these components contained in several commercially available herbs.

2. Experimental

2.1. Materials and chemicals

Standards of geniposide, andrographolide, and dehydroandrographolide were purchased from the National Institute for the Control of Pharmaceutical and Biological Products (Beijing, China). Structures of the compounds are shown in Fig. 1. Tablets of herbal medicine preparation made from *F. gardeniae*, Common Andrographis Herb and *R. ophiopogonis* were purchased from drugstores (Changsha, China). *F. gardeniae* and Common Andrographis Herb were purchased from Chinese herbal market (Changsha, China). HPLC-grade methanol and acetonitrile were purchased from Tedia Company, Inc. (Fairfield, OH, USA). Other reagents were of analytical grade. Water was deionized in a Milli-Q water purification system (Millipore Bedford, MA, USA).

2.2. Standard solutions

Standard solutions containing geniposide (200 μg mL^{-1}), andrographolide (200 μg mL^{-1}) and dehydroandrographolide (200 μg mL^{-1}) were prepared in methanol. By diluting the standard solution, a series of standard solutions between 0.1 and 200 μg mL^{-1} were obtained. The solutions were stored in refrigerator before use.

2.3. Sample pretreatment

After removing the sugar-coat, 10 pieces of herbal medicine preparation tablets were ground and mixed homogeneously in a mortar. 0.1 g samples were weighed out. The sample was extracted with 90% methanol aqueous solution (10 mL) by sonicating for 15 min, and then centrifuged at 4024 × *g* for 5 min. The residue was again extracted with 10 mL 90% methanol aqueous solution and centrifuged. The supernatants were combined and diluted to 25 mL with 90% methanol aqueous solution. Two milliliters solutions were filtered through a 0.45 μm membrane into an HPLC vial prior to HPLC/MS analysis. Samples (0.1 g) of the pulverized *F. gardeniae* and Common Andrographis Herb were treated by sonicating in the same way as above, respectively.

2.4. HPLC–DAD–ESI/MS analysis

A Waters-600 HPLC system (Milford, MA, USA) equipped with DAD detector was interfaced to Micromass ZQ 4000 elec-

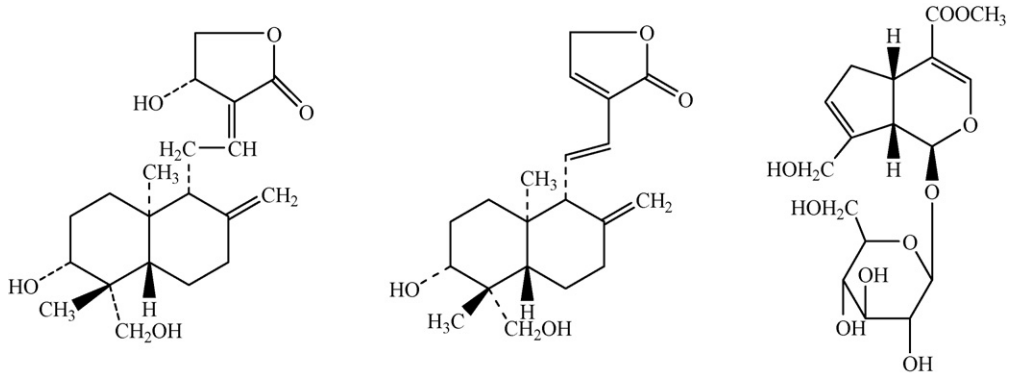

Fig. 1. Chemical structures of the three compounds.

trospray mass spectrometer (Manchester, UK). Masslynx V 4.0 software (Micromass) was used for data acquisition and processing. A symmetry column C_{18} (3.9 mm × 150 mm, 5 μm, Milford, MA, USA) was used. Mobile phase consisted of an aqueous solution of 0.1% formic acid (A) and acetonitrile (B). The gradient elution was programmed as follows: 0–2 min, 15–35% B; 2–3 min, 35–50% B; 3–5 min, 50–60% B; 5–10 min, 60% B; 10–15 min, 60–15% B. The flow rate was 1 mL/min, 20% eluent was allowed to flow into the mass spectrometer by solvent splitting. The column temperature was kept at 30 °C. The injection volume was 10 μL. UV spectra were recorded in the range of 210–400 nm, while 239.5, 226.5 and 250.5 nm were used for quantification of geniposide, andrographolide and dehydroandrographolide, respectively. ESI mass spectra were acquired in positive-ion mode by scanning over the *m/z* range of 230–450. The capillary potential was set at 4.0 kV and the cone voltage was 60 V. The temperatures of the electrospray source and desolvation were 95 and 350 °C, respectively. Nitrogen was used as both nebulizing gas and desolvation gas at flow rates of 50 and 350 L/h, respectively.

3. Results and discussion

3.1. Optimization of chromatographic separation conditions

In this work, in order to improve the peak shape and restrain the peak tailing, from the tested compounds, formic acid was selected as the mobile phase modifier. Zero%, 0.05%, 0.1%, 0.2% and 0.3% aqueous formic acid solutions were compared for their efficiency. When 0.1% formic acid solution was employed, high and narrow peaks for all the three compounds were obtained. When higher concentrations of formic acid were employed, no further improvements in the peaks shapes were observed. So 0.1% aqueous formic acid solution was selected. In order to separate the three compounds in an appropriate analysis time, various mixed gradients of 0.1% aqueous formic acid solution with acetonitrile were tested. Finally, an optimized gradient solvent system was developed. It was programmed as follows: 0–2 min, 15–35% B; 2–3 min, 35–50% B; 3–5 min, 50–60% B; 5–10 min, 60% B; 10–15 min, 60–15% B. Under the above-mentioned optimized condition, the three target analytes were baseline resolved.

The HPLC–DAD and HPLC–ESI–TIC (total ion current) chromatograms of geniposide, andrographolide and dehydroandrographolide in 10 min are shown in Fig. 2. In this work, many chemical compounds were tested as the internal standard for the MS quantification. Due to the ion suppression existed for the target analytes, low sensitivity was obtained. And suitable internal standard for MS quantification of the three analytes was not found. For the tested analytes, the sensitivity is satisfactory using UV. Using the photodiode array detector (DAD), the maximum absorption wavelength (λ_{max}) of the target peaks was obtained. 239.5, 226.5 and 250.5 nm were chosen as the optimal wavelength for simultaneous quantification of the three constituents, respectively. The MS chromatograms mainly provided the qualitative information.

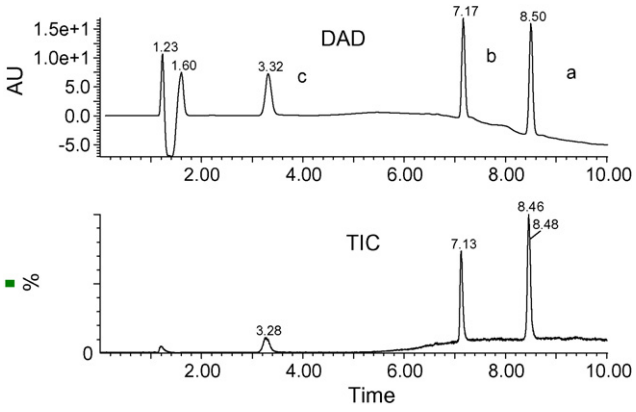

Fig. 2. The HPLC–DAD and HPLC–ESI–TIC chromatograms of the three analytes: (a) dehydroandrographolide; (b) andrographolide; (c) geniposide.

3.2. Optimization of cone voltage

In ESI mass spectrometry, cone voltage can significantly affect the signal intensity of the analytes. So the influence of cone voltage was investigated by varying the cone voltage from 15 to 100 V in this work. It was found that the maximum signal intensity of the useful fragment ions, molecular ion $[M+H]^+$ and adduct ion $[M+Na]^+$ took place at cone voltage of 60 V. At cone voltages above 60 V, the intensity of the adduct ion $[M+Na]^+$ for geniposide was increased, but for andrographolide and dehydroandrographolide, only weak molecular ions $[M+H]^+$ were obtained and more insignificant small fragment ions were produced. In this work, in order to obtain the useful fragments with high intensity, an optimum cone voltage of 60 V was chosen for analysis.

3.3. Identification of the iridoid glycosides and diterpene lactones in herbs and herbal preparations

Fig. 3 shows the positive-ion mode ESI/MS spectra for the compounds at cone voltage 60 V. The signals at *m/z* 355.3 and 333.4 in the mass spectrum of dehydroandrographolide (Fig. 4a) represents the adduct ion $[M+Na]^+$ and molecular ion $[M+H]^+$, respectively. The fragment ions at *m/z* 315.2 and 297.3 are the molecular ions losing one and two H_2O molecules, respectively. Andrographolide (Fig. 4b) shows both the molecular ion $[M+H]^+$ at 351.2 and the adduct ion $[M+Na]^+$ at *m/z* 373.2, together with the molecular ions losing one, two and three H_2O molecules at *m/z* 333.3, 315.2 and 297.3, respectively. In the mass spectrum of geniposide (Fig. 4c), the signals at *m/z* 427.1, 411.1 and 389.2 correspond to the adduct ions $[M+K]^+$, $[M+Na]^+$ and molecular ion $[M+H]^+$, respectively. The signal at *m/z* 406.3 represent the adduct ion $[M+K–H_2O]^+$. In our experiments, SIM mode was found to be more sensitive than the full-scanning mode, hence, SIM mode was used to monitor the investigated analytes, and the abundant ions at *m/z* 297.3, 297.3 and 411.1 were selected as quantifier ions for dehydroandrographolide, andrographolide and geniposide, respectively. In this way, the proposed method can be used as a simple method

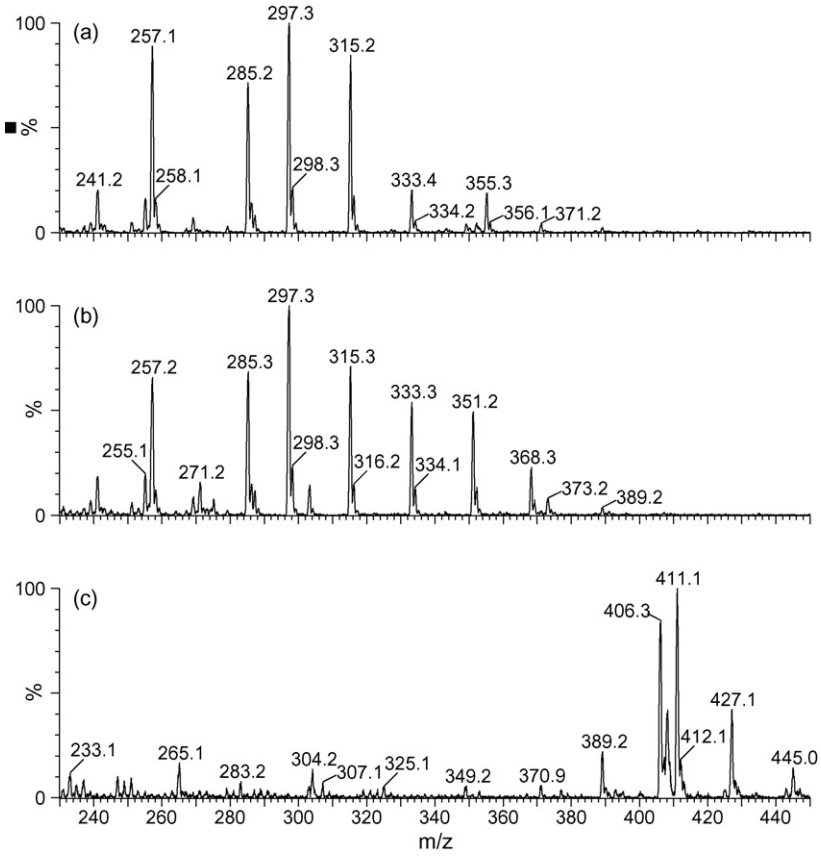

Fig. 3. The positive-ion ESI/MS spectra for the compounds at cone voltage 60 V: (a) dehydroandrographolide; (b) andrographolide; (c) geniposide.

for identification of these active ingredients in herbs and herbal medicine preparations. Their retention times, molecular ion, fragment ions, and λ_{max} (nm) are summarized in Table 1. Their HPLC–UV and HPLC–MS–SIM chromatograms are shown in Fig. 4.

3.4. Method validation

3.4.1. Response linearity and limit of detection

At least five experiments for each reference compound were conducted to construct the UV linearity calibration curves. Good linear relationships between corresponding peak areas and concentration were observed in the range of 1–200 $\mu g\,mL^{-1}$ for the three tested analytes. Correlation coefficients of all the calibration curves were found to be higher than 0.9990. The limit of detection (LOD) was measured, with the signal-to-noise ratio of 3 as criteria. The LOD for dehydroandrographolide, andrographolide and geniposide was 20, 30 and 150 $ng\,mL^{-1}$, respectively.

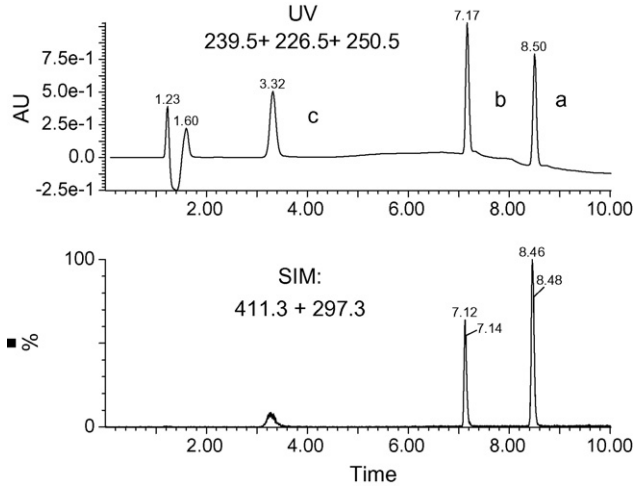

Fig. 4. The HPLC–UV and HPLC–ESI–SIM chromatograms of the three analytes: (a) dehydroandrographolide; (b) andrographolide; (c) geniposide.

Table 1
Assignment of peaks in Fig. 2

Compound	t_R (min)	m/z $[M+H]^+$	m/z fragment ion	λ_{max}(nm)
Geniposide	3.32 ± 0.03	389.2	427.1, 411.1, 406.3	239.5
Andrographolide	7.17 ± 0.01	351.2	333.3, 315.2, 297.3	226.5
Dehydroandrographolide	8.50 ± 0.02	333.4	355.2, 315.2, 297.3	250.5

3.4.2. Reproducibility

The reproducibility of the method was evaluated with a standard solution under the optimal conditions. The relative standard deviations (R.S.D.) of the intra-day reproducibility (five times in 1 day) were 1.3% for geniposide, 1.4% for andrographolide and 1.2% for dehydroandrographolide. The inter-day reproducibility (three a day on three consecutive days) was less than 2.5% for all the tested compounds.

3.4.3. Recovery

The recovery of the method was studied by calculating the mean recoveries of the analytes using the standard addition method. The reference standards were added at three different concentration levels (approximately equivalent to 0.5, 1.0 and 1.2 times of the concentration of the matrix) with three parallels at each level. The solutions were prepared in accordance with the sample preparation procedure. The recoveries of the three compounds were tested with one of the herbal medicine preparations as the matrix. The mean recovery for dehydroandrographolide, andrographolide and geniposide was 100.4%, 98.6% and 101.5%, respectively. The R.S.D. of the recoveries for dehydroandrographolide, andrographolide and geniposide were 2.8%, 2.7% and 2.5%, respectively. The results showed the recovery of the proposed method was satisfactory.

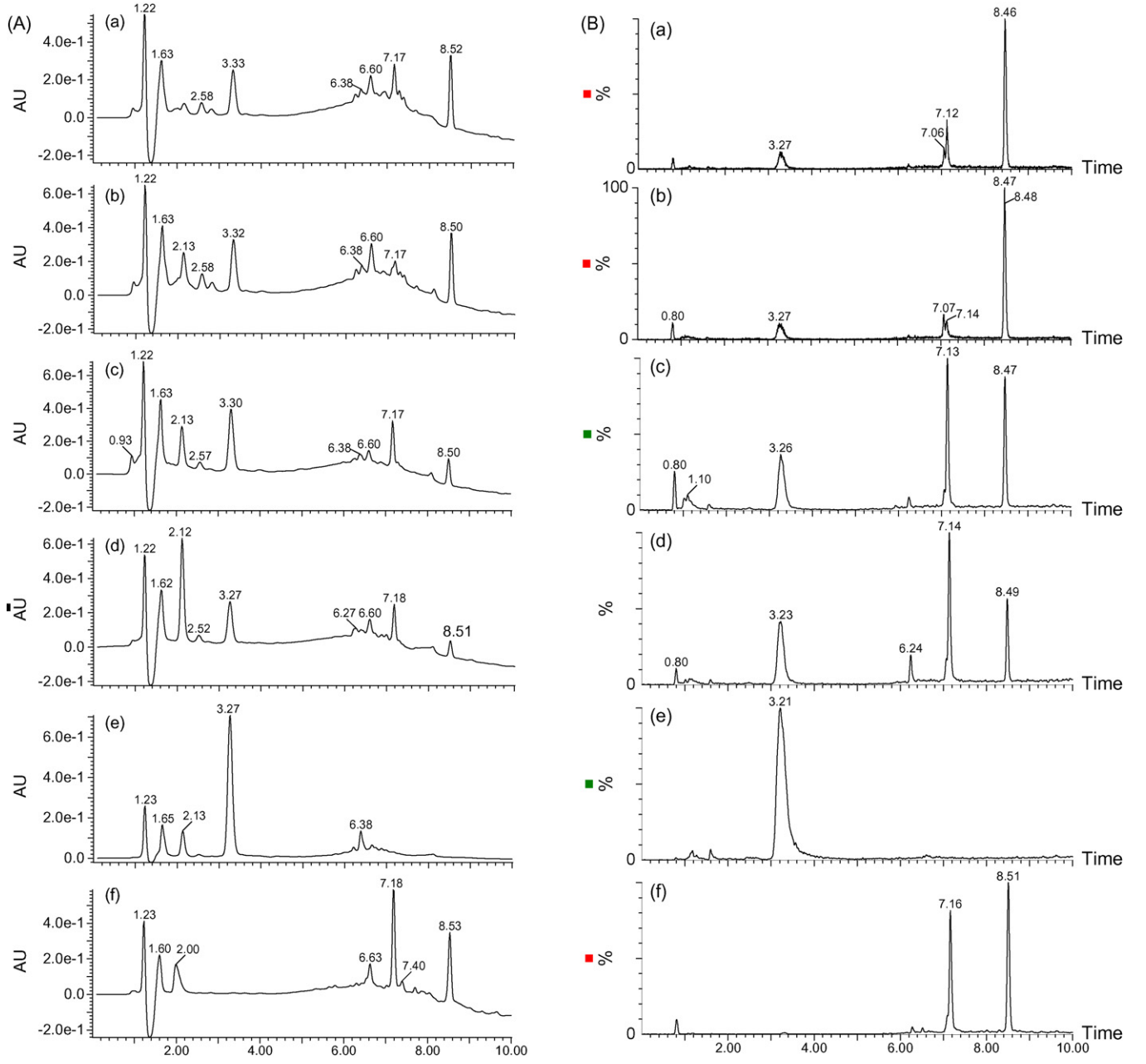

Fig. 5. The HPLC–UV (A) and HPLC–ESI–SIM (B) chromatograms of the three analytes in the real samples: (a) HM Tablets No. 1; (b) HM Tablets No. 2; (c) HM Tablets No. 3; (d) HM Tablets No. 4; (e) *Fructus gardeniae*; (f) Common Andrographis Herb.

Table 2
Determination of the three compounds in real samples ($n = 3$)

Samples	Contents determined (mg/g)[a]		
	Geniposide	Andrographolide	Dehydroandrographolide
HM Tablets No. 1[b]	4.33 ± 0.12	0.92 ± 0.05	3.27 ± 0.08
HM Tablets No. 2[b]	5.96 ± 0.17	0.96 ± 0.04	4.12 ± 0.11
HM Tablets No. 3[b]	7.99 ± 0.14	2.08 ± 0.13	1.46 ± 0.15
HM Tablets No. 4[b]	5.24 ± 0.16	1.82 ± 0.12	0.83 ± 0.10
Fructus gardeniae	31.78 ± 0.21	–	–
Common Andrographis Herb	–	4.56 ± 0.15	3.47 ± 0.18

[a] Mean ± S.D.
[b] HM Tablets: tablets of herbal medicinal preparations containing geniposide, andrographolide and dehydroandrographolide as their main active ingredients.

3.5. Sample analysis

The proposed method was applied to the analysis of practical samples. The extracts of herbal medicine preparations manufactured by four different pharmaceutical companies (Nos. 1–4) and two medicinal herbs (*F. gardeniae* and Common Andrographis Herb) were analyzed by the proposed HPLC–DAD–ESI method. Fig. 5 shows the HPLC–UV (Fig. 5A) and HPLC–ESI–SIM (Fig. 5B) chromatograms of the active compounds in the extracts. It was observed that dehydroandrographolide, andrographolide and geniposide and other unknown compounds were baseline resolved. The contents of dehydroandrographolide, andrographolide and geniposide in samples were determined using UV standard curve. The results are shown in Table 2. It is shown that the compounds contents in herbal medicine preparations produced by different factories are different. The reasons maybe caused by difference in the raw material source and process dissimilarity. So their medical effects are somewhat different. Therefore, it is necessary and critical to control the quality of the herbal medicine preparations. The developed HPLC–UV–ESI method can be used as a quality control method for the pharmaceutical factories.

4. Conclusion

In this work, a simple and reliable HPLC–DAD–ESI/MS method for simultaneous analyses of marker compounds geniposide, andrographolide and dehydroandrographolide in herbs and herbal medicine preparations have been developed. Using a gradient solvent system, these compounds were separated on a C_{18} column in only one run and the analytes were identified based on UV spectra and MS fragmentation behavior. The total analysis time only needs 10 min. The contents of geniposide, andrographolide and dehydroandrographolide in different herbal medicine preparations and herbs were accurately determined by this method, which provides a simple, convenient and effective means for quality control in pharmaceutical practice. Furthermore, this method will also be useful in further developing analytical method for other related herbal medicines.

Acknowledgements

This work was financially supported by the National Natural Science Foundation of China (Nos. 20575019 and 20335020).

References

[1] J.B. Yuan, L.H. Nie, D.Y. Zeng, X.B. Luo, S.Z. Yao, Talanta 73 (2007) 644.
[2] Q.B. Han, Y.K. Yip, N.Y. Yang, L. Wong, H.X. Xu, Talanta 73 (2007) 757.
[3] M. Harada, N. Tenmyo, M. Aburada, T. Endo, Yakugaku Zassi 94 (1974) 157.
[4] A. Leelarasamee, S. Trakulsomboon, N. Sittisomwong, J. Med. Assoc. Thailand 73 (1990) 299.
[5] D. Bensky, A. Gamble, T. Kaptchuk, Chinese Herbal Medicine Materia Medica, Revised ed., Eastland Press, Seattle, 1993, p. 95.
[6] P.K. Singha, S. Roy, S. Dey, Fitoterapia 74 (2003) 692.
[7] S. Rajagopal, R.A. Kumar, D.S. Deevi, C. Satyanarayana, R. Rajagopalan, J. Exp. Ther. Oncol. 3 (2003) 147.
[8] H.Y. Cheung, C.S. Cheung, C.K. Kong, J. Chromatogr. A 930 (2001) 171.
[9] T. Oshima, K. Sagara, T. Yoshida, Y.Y. Tong, G.D.Y.H. Chen, J. Chromatogr. 455 (1988) 410.
[10] T.R. Tsaia, T.Y. Tsengb, C.F. Chenc, T.H. Tsai, J. Chromatogr. A 961 (2002) 83.
[11] T.Q. Pham, F. Cormier, E. Farnworth, V.H. Tong, M.R. Van Calsteren, J. Agric. Food Chem. 48 (2000) 1455.
[12] S.C. Wang, T.Y. Tseng, C.M. Huang, T.H. Tsai, J. Chromatogr. B 812 (2004) 193.
[13] H.K. Wu, W.C. Chuang, S.J. Sheu, J. Chromatogr. A 803 (1998) 179.
[14] S. Saxena, D.C. Jain, M.M. Gupta, Phytochem. Anal. 11 (2000) 34.
[15] A. Srivastava, H. Misra, R.K. Verma, Phytochem. Anal. 15 (2004) 280.
[16] N. Pholphana, N. Rangkadilok, S. Thongnest, J. Satayavivad, Phytochem. Anal. 15 (2004) 365.
[17] D.C. Jain, M.M. Gupta, S. Saxena, S. Kumar, J. Pharmacol. Biomed. Anal. 22 (2000) 705.
[18] Q. Du, G. Jerz, P. Winterhalter, J. Chromatogr. A 984 (2003) 147.
[19] Y.F. Zhao, X.P. Luo, Z.D. Zhai, L. Chen, J. Pharmacol. Biomed. Anal. 40 (2006) 157.
[20] Y.F. Zhao, Y.F. Ming, H.L. Zhang, L.R. Chen, Y.M. Li, Chromatographia 62 (2005) 611.
[21] X.B. Luo, B. Chen, S.Z. Yao, J.G. Zeng, J. Chromatogr. A 986 (2003) 73.
[22] X.B. Luo, B. Chen, S.Z. Yao, Talanta 66 (2005) 103.
[23] J.J. Liu, B. Chen, S.Z. Yao, Talanta 71 (2007) 668.

Available online at www.sciencedirect.com
ScienceDirect
Talanta 74 (2008) 1337–1343
Talanta
www.elsevier.com/locate/talanta

In situ electrodeposited nanoparticles for facilitating electron transfer across self-assembled monolayers in biosensor design

Dan Du [a,*], Jiawang Ding [a], Jie Cai [b], Jianming Zhang [a], Li Liu [a]

[a] *Key Laboratory of Pesticide and Chemical Biology of Ministry of Education, College of Chemistry, Central China Normal University, Wuhan 430079, PR China*
[b] *The Technology Center of Wuhan Iron & Steel Company, Wuhan 430080, PR China*

Received 23 May 2007; received in revised form 6 September 2007; accepted 6 September 2007
Available online 14 September 2007

Abstract

Gold nanoparticles (AuNPs) were synthesized *in situ* and electrodeposited onto Au substrate. The AuNPs modified interface facilitates electron transfer across self-assembled monolayers (SAMs) of 11-mercaptoundecanoic acid (MUA). After activation of surface carboxyl groups with 1-ethyl-3-(3-dimethylaminopropyl) carbodiimide and *N*-hydroxysuccinimide, the interface displayed good stability for immobilization of biomolecules. These modification processes were characterized by contact angle measurement, cyclic voltammetry and electrochemical impedance spectra. The immobilized acetylcholinesterase (AChE), as a model, showed excellent activity to its substrate, leading to a stable AChE biosensor. Under the optimal experimental conditions, the inhibition of malathion on AChE biosensor was proportional to its concentration in two ranges, from 0.001 to 0.1 μg mL^{-1} and from 0.1 to 25 μg mL^{-1}, with detection limit of 0.001 μg mL^{-1}. The simple method showed good reproducibility and acceptable stability, which had potential application in biosensor design.
© 2007 Elsevier B.V. All rights reserved.

Keywords: Electrodeposition; Gold nanoparticles; Self-assembled monolayers; Organophosphate pesticides; Biosensor

1. Introduction

Enzymes are the most powerful molecular recognition elements in biosensing, since the sensing signal can be amplified millions of times through enzymatic reactions [1]. This signal amplification enables the design of highly sensitive biosensing systems. Amperometric enzymatic biosensors have been considered to be the most suitable for biochemical analysis due to their good selectivity, sensitivity, rapid response, miniature size, and reproducible results [2]. A combination of enzymatic reactions with the electrochemical method allows developing different enzyme-based electrochemical biosensors for sensitive and rapid determination of environmental analysis [3]. Among these, amperometric acetylcholinesterase (AChE) biosensors have shown satisfactory results for pesticides analysis based on their inhibition on AChE [4–6], in which the enzymatic activity is employed as an indicator of quantitative measurement of pesticides.

A significant challenge to develop sensitive and stable biosensors comes from the effective immobilization of enzyme to solid electrode surface [7,8]. Generally, direct adsorption of enzyme onto bare gold surface can frequently result in their denaturation and the loss of bioactivity [9]. Self-assembled monolayers (SAMs) of alkanethiols on gold substrate provide an easy method to create well-defined surfaces with controllable chemical functionality, and partly as a functionalized structure for further modification of the surface [10]. This interface has been used to anchor different functional groups in biosensors design [11,12]. For example, when the terminal group of thiolate SAMs is a carboxylic group, the modified gold surface combining the unique properties of SAMs with the carbodiimide chemistry offers a further functionalization with biomolecules, such as proteins [13,14], DNA [15], and antibody [16].

The SAMs serves partly as a barrier to prevent proteins and other ligands from coming into contact with the metal. The stable, close-packed, and well-ordered SAMs on gold electrodes usually display a very low fraction of defects [17,18]. They are strongly resistant to ion penetration, and may therefore impede the electron transfer between the electrode surface and the electroactive species in solution. To circumvent the

* Corresponding author. Tel.: +86 27 67867953.
E-mail address: dudan@mail.ccnu.edu.cn (D. Du).

0039-9140/$ – see front matter © 2007 Elsevier B.V. All rights reserved.
doi:10.1016/j.talanta.2007.09.003

drawbacks of electron transfer, a possible route consists in incorporating metal nanoparticles. Metal nanoparticles provide three important functions for electroanalysis: the roughening of the conductive sensing interface, catalytic properties, and conductivity properties [19]. Among several nano-materials, gold nanoparticles (AuNPs) have been widely used for preparation of electrochemical biosensors [20,21]. Generally, AuNPs could be easily fabricated by standard methods [22] or electrochemical technologies [23]. Compared with traditional process, electrochemical deposition is simple, the performance conditions are moderate, and it is suitable for selective deposition of films with controllable thickness [24], which provides an easy and rapid alternative for the preparation of AuNPs modified electrodes in a short time [25].

The present work is motivated by very promising applications of AuNPs facilitating electron transfer. At a constant applied potential, AuNPs were synthesized *in situ* and electrodeposited onto gold electrode surface. SAMs of 11-mercaptoundecanoic acids were then formed onto the resulting surface. After activation of surface carboxyl groups with 1-ethyl-3-(3-dimethylaminopropyl) carbodiimide and *N*-hydroxysuccinimide, the interface possessing good stability is suitable for facile immobilization of enzyme, leading to a stable AChE biosensor (Scheme 1) for quantitative measure of organophosphate pesticide. The immobilized AChE, as a model showed excellent activity to its substrate. In order to estimate the properties of the interface, several methods such as cyclic voltammetric scan and electrochemical impedance have been used to characterize and optimize the deposition conditions.

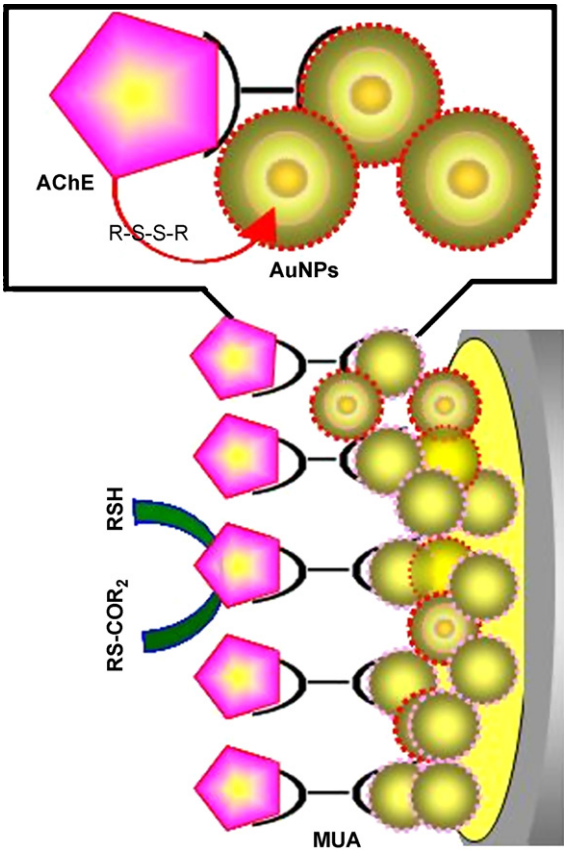

Scheme 1. Principle of AuNPs served as mediator for electron transfer across SAMs for AChE biosensor design.

2. Experimental

2.1. Reagents

Acetylthiocholine chloride (ATCl), Acetylcholinesterase (Type C3389, 500 U mg^{-1} from electric eel) and 11-mercaptoundecanoic acid (MUA) were purchased from Sigma–Aldrich (St. Louis, USA) and used as received. 1-ethyl-3-(3-dimethylaminopropyl) carbodiimide (EDC), *N*-hydroxysuccinimide (NHS) were obtained from Aldrich Chemical Company Inc. $HAuCl_4{\cdot}4H_2O$ (Au > 48%) was obtained from TreeChem.co (China). Malathion was obtained from AccuStandard (USA). $Fe(CN)_6^{4-/3-}$, phosphate buffer solution (PBS, pH 7.0) and other reagents used were of analytical reagent grade. Aqueous solution was prepared with double distilled water.

2.2. Instruments

Cyclic voltammetric measurements were performed on a Bio-analytical System (BAS, cv-50w, USA) with a conventional three-electrode system comprising platinum wire as auxiliary electrode, Ag/AgCl (3 M NaCl) as reference. AChE coupled to MUA-AuNPs modified gold electrode (AChE-MUA-AuNPs/Au) was used as working electrode. The ac impedance experiment was carried out in 5 mM $Fe(CN)_6^{4-/3-}$ with frequencies ranging from 100 kHz to 0.1 Hz with a CHI 660C electrochemical workstation. The static water contact angle was measured at 25 °C by a contact angle system OCA 20 (Dataphysics, Germany). Measurements were repeated on at least four drops.

2.3. Preparation of AChE-MUA-AuNPs/Au

Gold disk electrode with a polypropylene body (1.0 mm in diameter) was used for the electrochemical measurement. Before modification, the gold electrode was abraded with fine SiC paper, lightly polished with 0.05 μm alumina (Buhler), followed by sonication in ethanol and double distilled water for 10 min, respectively. The electrochemical pretreatment was performed in a BAS cell by cycling from a potential of −0.1 to +1.25 V versus Ag/AgCl in 0.1 M H_2SO_4 solution until a stable and reproducible gold oxidation peak at +1.1 V versus Ag/AgCl was obtained [26].

For electrochemical deposition, Time-Base mode was used. Briefly, a clean gold electrode was immersed in 0.1% $HAuCl_4{\cdot}4H_2O$ and an initial potential of +0.15 V was applied on the electrode. The resulting AuNPs-deposited gold electrode (AuNPs/Au) was immersed in 1 mM MUA for 3 h to prepare MUA monolayer modified AuNPs/Au (MUA-AuNPs/Au). After activation using 0.2 M EDC and 0.05 M NHS for 30 min, the carboxyl groups were activated to form reactive *N*-hydroxysuccinimide esters. Then 3.0 μL AChE solution

(100 mU) was dropped and dried in air at room temperature for another 2 h. After washing carefully with PBS to remove non-specifically adsorbed enzyme, the AChE-MUA-AuNPs/Au was obtained.

2.4. Measurement procedure

For measurement of malathion, the pretreated AChE-MUA-AuNPs/Au was first immersed in standard malathion solutions with different concentration for 12 min, and then transferred to the electrochemical cell of 1.0 mL pH 7.0 PBS containing 0.3 mM ATCl to study the electrochemical response by cyclic voltammetry (CV). The inhibition of malathion was calculated as follows:

$$\text{Inhibition}\,(\%) = 100 \times \frac{i_{\text{P,control}} - i_{\text{P,exp}}}{i_{\text{P,control}}}$$

where $i_{\text{P,control}}$ is the peak current of ATCl on the AChE-MUA-AuNPs/Au, $i_{\text{P,exp}}$ is the peak current of ATCl on the AChE-MUA-AuNPs/Au with malathion inhibition.

3. Results and discussion

3.1. Electrodeposition of AuNPs on gold electrode

Cyclic voltammetric measurement for gold electrodes in 0.1% $HAuCl_4{\cdot}4H_2O$ solution revealed that reduction of $AuCl_4^-$ occurred at a peak potential of +0.18 V (inset in Fig. 1). Thus, an initial potential of +0.15 V was selected for deposition of AuNPs. The obtained AuNPs/Au showed two reduction peaks differing in the reduction potential (Fig. 1a), while only one reduction peak was observed at bare gold electrode (Fig. 1b). The single reduction peak at +0.88 V (versus Ag/AgCl 3 M NaCl) was attributed to the reduction of gold surface oxide [27]. The two-reduction peak was due to the different reduction abilities of the oxidized AuNPs and the oxidized plane gold surface [28]. It is also obvious that the cathodic peak current of the AuNPs/Au was higher than that of bare gold electrode, indicating that AuNPs modified gold electrode had a larger surface area. The real surface areas of AuNPs/Au and bare gold were determined by integrating the reduction peak area of oxidized gold layer formed by CV scans from −0.2 to +1.6 V in 0.5 M H_2SO_4 [29,30] and thus the roughness factor could be estimated. The real surface area of AuNPs/Au by electrodeposition was calculated to reach 0.0564 cm^2, while the real surface area of bare gold electrode was 0.0357 cm^2. The roughness factor increased from 1.14 of bare gold electrode to 1.52 of AuNPs/Au with electrodeposition time of 120 s. Nanoparticles with deposition time of 120 s have average particle sizes in the range of 20–40 nm [26].

It has been reported that by varying the deposition time at a constant applied potential, AuNPs with different sizes and densities could be deposited onto gold electrode and the big-size gold clusters led to a much rougher electrode surface [26]. When the deposition time reaches to 180 s, big size gold clusters may form on the gold electrode surface. This packed clusters on the electrode surface would somewhat block the electron transfer. Thus, 120 s was chosen as deposition time.

3.2. Preparation of the MUA-AuNPs/Au monolayer

$Fe(CN)_6^{4-/3-}$ redox system as one of the most extensively studied redox couples in electrochemistry was used to confirm the properties and changes of deposited surface. Theoretically, the electron transfer rate or electron transfer resistance of electroactive probe on electrode surface was related to the surface properties. As seen from Fig. 2, when MUA was assembled directly on Au electrode (MUA/Au), the CV curves of $Fe(CN)_6^{4-/3-}$ probe on MUA/Au resulted in a sharp decrease in peak currents with the increase of assembling time from 1

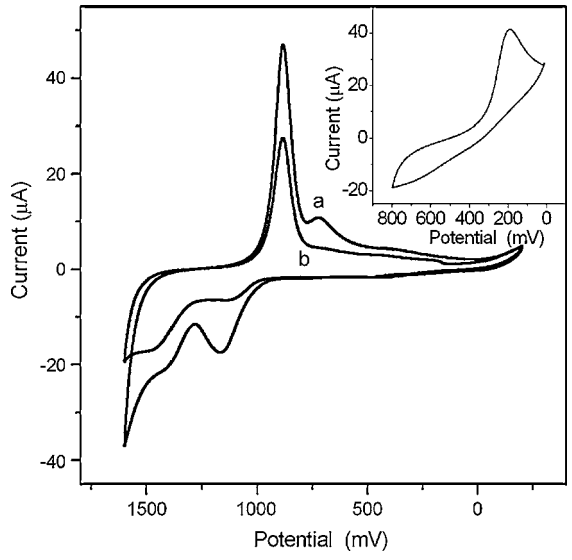

Fig. 1. Cyclic voltammograms of AuNPs/Au (a) and bare Au (b) in 0.5 M H_2SO_4. Inset: cyclic voltammograms of 0.1% $HAuCl_4{\cdot}4H_2O$ reduction.

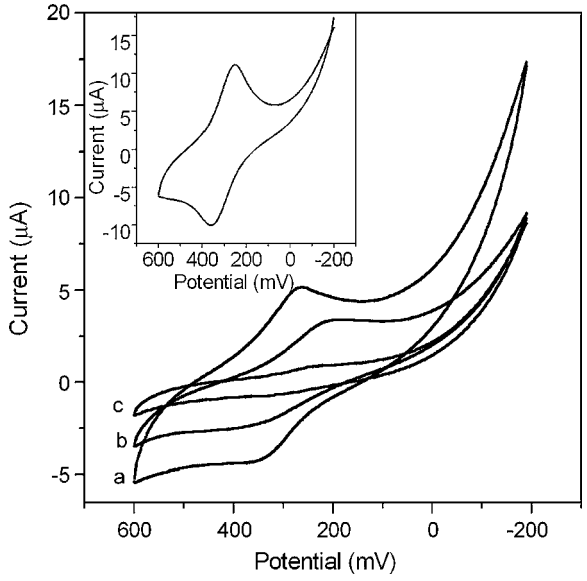

Fig. 2. Cyclic voltammograms of $Fe(CN)_6^{4-/3-}$ at MUA/Au with MUA assembling time of 1 h (a), 2 h (b) and 3 h (c). Inset: cyclic voltammogram of $Fe(CN)_6^{4-/3-}$ at MUA-AuNPs/Au with MUA assembling time of 3 h.

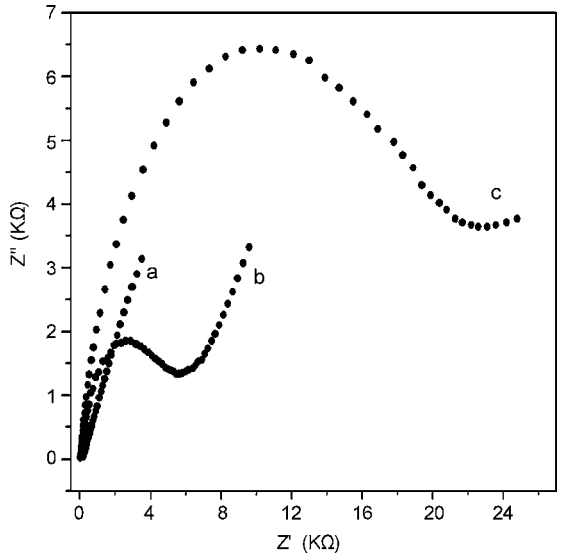

Fig. 3. Electrochemical impedance spectra of bare Au electrode (a), MUA-AuNPs/Au (b) and MUA/Au (c) in 5 mM $Fe(CN)_6^{4-/3-}$.

to 3 h. The encumbrance of the electron transfer was due to the negatively charged surface of MUA modified electrode, which blocked $Fe(CN)_6^{3-/4-}$ go through the MUA film to exchange the electron with electrode. No obvious redox peaks were observed for further assembling, indicating a close-packed and well-ordered SAMs was formed with 3 h. However, it was worthwhile mentioning that the CV of $Fe(CN)_6^{4-/3-}$ probe on MUA-AuNPs/Au displayed a significant change. A couple of redox peaks with much larger peak currents were observed (inset in Fig. 2). This phenomenon was due to the deposited AuNPs, which improved conductive sensing interface and thus circumvented the drawbacks of electron transfer across the MUA interface. The same result was also obtained in the following experiment. Therefore, MUA-AuNPs/Au was selected as support surface for biosensor design.

Furthermore, the MUA-AuNPs/Au displayed a reduction peak at −1.10 V in 0.5 M KOH. This peak was attributed to the reductive desorption of the thiolated compounds bound to gold [31,32], indicating the presence of the MUA molecule on Au surface. The reaction for reductive desorption of thiolated compounds is: $Au\text{-}SR + e^- \rightarrow Au + RS^-$ [33]. From the integration of the reductive desorption peak, the surface coverage, Γ ($\Gamma = Q/nFA$ and $A = 0.0564\,cm^2$), was calculated to be 7.63×10^{-10} mol/cm^2, which means that each molecules occupies a surface area of 21.8 A^2 on average. Following Dubois and Zegarski [34], simple alkanethiols require an area of about 21.4 A^2 if deposited as densely packed SAMs on Au. These results indicated a densely packed MUA monolayer on AuNPs modified electrode.

3.3. ac impedance measurements

Fig. 3 showed the results of electrochemical impedance spectra (EIS) on modified electrodes. The electron transfer resistances of $Fe(CN)_6^{4-/3-}$ at bare gold electrode (curve a), MUA-AuNPs/Au (curve b), and MUA/Au (curve c) were 26, 6352 and 23,145 Ω, respectively. The significant change occurred at MUA/Au, indicating that MUA monolayer introduced a barrier to electrochemical process. However, an obvious decrease in charge-transfer resistance at MUA-AuNPs/Au was clearly observed. This change might be related to electrodeposited AuNPs, which decreased the impedance of interface and resulted in the electron exchange of $Fe(CN)_6^{4-/3-}$ across the MUA SAMs. This result was in accordance with the electrochemical probe assays as detailed above.

3.4. Contact angle measurements

Contact angle measurements were carried out to confirm the properties and changes of deposited surface. As shown in Fig. 4, the bare Au and MUA/Au gave the contact angles of 72.1° and 61.4°, respectively. The MUA surface showed comparatively high hydrophilicity, which was not surprising since the terminal carboxylate group was highly polar [35]. For MUA-AuNPs/Au, the contact angle decreased to be 47.5° (Fig. 4C). The decrease in contact angle was due to roughening of the conductive sensing interface, which had a large real surface area for MUA assembling and more terminal carboxylate groups. Thus, the electrodeposited AuNPs not only improved the electro transfer, but also increased the surface hydrophilicity. This interface was suitable for facile immobilization of biomolecules.

3.5. Cyclic voltammetric behavior of AChE-MUA-AuNPs/Au

AChE, as a model, was immobilized onto MUA-AuNPs/Au surface after activation of carboxy groups in MUA molecule. As shown in Fig. 5, no peak was observed at MUA-AuNPs/Au (curve a) and AChE-MUA-AuNPs/Au (curve b) in pH 7.0 PBS. When 0.3 mM ATCl was added into PBS, the AChE-MUA-AuNPs/Au showed an irreversible oxidation peak at 859 mV (curve e), while no detectable signal was observed at MUA-AuNPs/Au (curve c). Obviously this peak

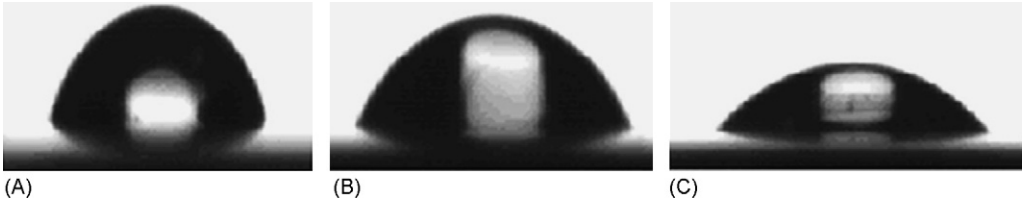

Fig. 4. Contact angle graphs of bare Au substrate (A), MUA/Au (B) and MUA-AuNPs/Au (C).

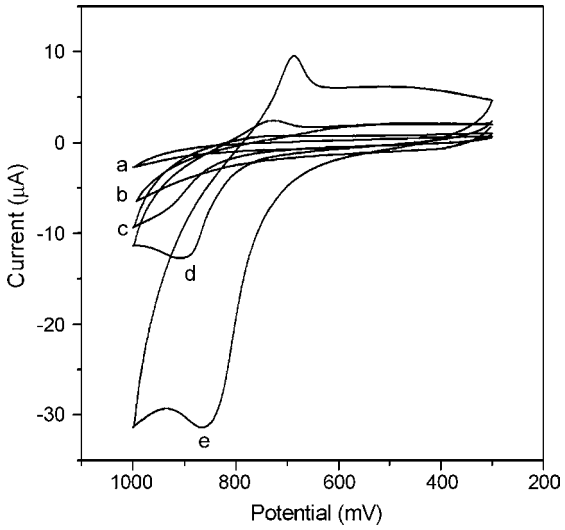

Fig. 5. Cyclic voltammograms of MUA-AuNPs/Au (a and c), AChE-MUA/Au (b) and AChE-MUA-AuNPs/Au (b and e). Supporting electrolyte: pH 7.0 PBS (a and b) and pH 7.0 PBS containing 0.3 mM ATCl (c–e).

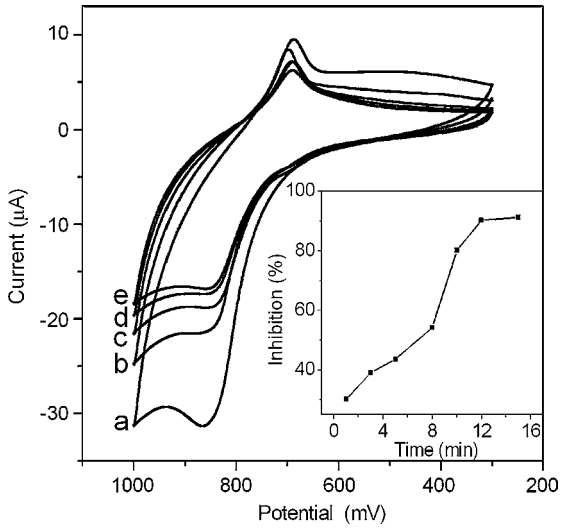

Fig. 6. Cyclic voltammograms of AChE-MUA-AuNPs/Au in pH 7.0 PBS containing 0.3 mM ATCl after inhibition with 2.0 μg mL^{-1} malathion for 1 min (a), 3 min (b), 5 min (c), 8 min (d) and 10 min (e). Inset: dependence of malathion inhibition curve on inhibition time.

came from the oxidation of thiocholine, hydrolysis product of ATCl, which was catalyzed by immobilized AChE. The reaction between AChE-MUA-AuNPs/Au electrode and ATCl substrate was a CE coupled reaction, including a chemical reaction: $EH + RS\text{-}COR_2 \rightarrow RSH + E\text{-}COR_2$ and an electrode reaction: $RSH - 2e^- \rightarrow RSSR + 2H^+$. It was interesting to compare the current responses at AChE-MUA/Au and AChE-MUA-AuNPs/Au. The peak current of ATCl on AChE-MUA-AuNPs/Au was much higher and the peak potential shifted negatively compared to those on AChE-MUA/Au electrode without AuNPs (curves d and e). These phenomena were attributed to the presence of electrodeposited AuNPs, which possessed inherent conductive properties and thus provided a conductive pathway to electron transfer and promoted electron transfer reactions at a lower potential. The produced current on AChE-MUA-AuNPs/Au reflected enzymatic activity, which could be used for organophosphate pesticides analysis involved in the inhibition action [36,37].

3.6. Effect of incubation time on response of AChE-MUA-AuNPs/Au

Upon AChE-MUA-AuNPs/Au was immersed in the standard solution of malathion at a known concentration for different time, the produced current of ATCl on AChE-MUA-AuNPs/Au decreased drastically. The decrease in peak current was related to the increase of incubation time (Fig. 6). This was because malathion as one of the organophosphate pesticide involved in the inhibition action to AChE, thus reduced the enzymatic activity to its substrate. As seen from inset of Fig. 6, malathion displayed increasing inhibition to AChE with immersing time. When the immersing time was longer than 12 min the curve trended to a stable value, indicating the binding interaction with active target groups in enzyme could reach saturation. This change tendency of peak current reflected the alteration of enzymatic activity, which resulted in the change of the interactions with its substrate. However, the maximum value of inhibition of malathion was not 100%, which was likely to attribute to the binding equilibrium between pesticide and binding sites in enzyme.

3.7. Calibration curve

Due to the notable change in voltammetric signal of the AChE-MUA-AuNPs/Au, the simple method for determination of malathion was established. With increasing malathion concentrations the produced currents of ATCl on AChE-MUA-AuNPs/Au decreased. Under the optimal experimental conditions, the malathion inhibition on AChE-MUA-AuNPs/Au was proportional to the malathion concentrations in two ranges, from 0.001 to 0.1 μg mL^{-1} and from 0.1 to 25 μg mL^{-1}, The regression equation was $I\ (\%) = 11.53 + 59.68c$ and $I\ (\%) = 15.94 + 2.40c$, with the correlation coefficients of 0.9990 and 0.9969, respectively (Fig. 7). The detection limit was 0.001 μg mL^{-1}.

To further demonstrate the practicality of the proposed method, the recovery test was studied by adding different amounts of malathion into garlic samples. Results were summarized in Table 1. The recoveries were from 96.8 to 104.7 %. The results indicated that the proposed method can be used for direct analysis of relevant samples.

Table 1
Recovery studies of malathion in garlic samples

Samples	Concentrations		Recovery (%)
	Taken (μg mL^{-1})	Found (μg mL^{-1})	
1	0.010	0.0968	96.8
2	0.200	0.197	98.5
3	2.500	2.528	101.1
4	5.000	5.235	104.7

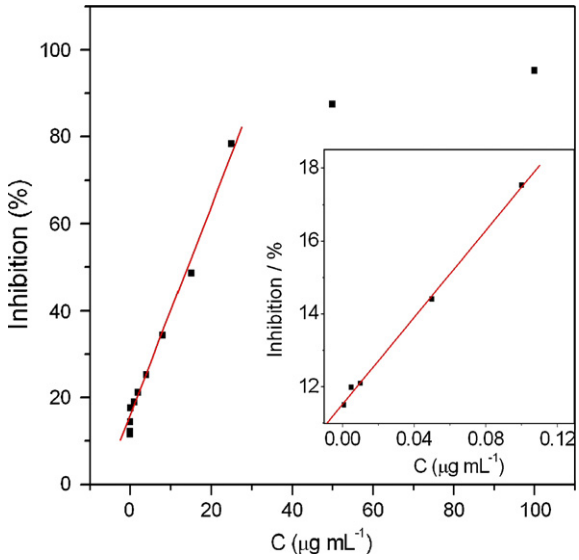

Fig. 7. Relationship between inhibition and concentration. Inset: linear relationship between inhibition and low concentration.

We are currently facing the disadvantage of the low selectivity of AChE because the degree of inhibition on AChE by organophosphate pesticide is almost the same. However, this does not necessarily compromise its value extended toward the preparation of other electrochemical sensors based on this mode. The ease of performance and the cost effectiveness of the system for malathion detection show the high potentiality in total amount of pesticide analysis. Regarding other possible interferences such the heavy metals, we can suppose that these inhibitors cannot interfere with the proposed biosensor because of its reversible inhibition on AChE.

3.8. Precision, reproducibility and stability of AChE-MUA-AuNPs/Au

The inter-assay precision was estimated by determining the response of 0.3 mM ATCl at six different electrodes, which were immersed in 0.1 μg mL^{-1} and 2.0 μg mL^{-1} malathion for 12 min, respectively. The coefficients of variation were calculated to be 2.4% and 3.1%, respectively, indicating acceptable fabrication reproducibility. The intra-assay precision of the sensors was evaluated by assaying one enzyme electrode for six replicate determinations, and the R.S.D. was 2.0% at the ATCl concentration of 0.3 mM.

When the enzyme electrode was not in use, it was stored at 4 °C in dry condition. No obvious decrease in the response to ATCl was observed in the first 10-day storage. After a 30-day storage period, the sensor retained 90% of its initial current response. It indicated that this interface provided a biocompatible microenvironment around the enzyme to stabilize its biological activity to a large extent.

4. Conclusions

We have demonstrated in this paper the application of electrodeposited nanoparticles for facilitating electron transfer across self-assembled monolayers. The presence of AuNPs not only provided a conductive pathway to promote electron transfer reactions at a lower potential, but also increased the surface hydrophilicity for immobilization of enzyme. The immobilized AChE, as a model showed excellent activity to its substrate and could be used for quantitative measure of organophosphate pesticide. The electrodeposited AuNPs combining with the unique properties of SAMs circumvented the drawbacks of electron transfer and offered a simple method for further functionalization by biomolecules. It provided a new avenue for biosensor design.

Acknowledgements

The authors are gratefully acknowledging the financial support of the National Natural Science Foundation of China (No. 20705010) and the Natural Science Foundation of Hubei Province (No. 2006ABA183).

References

[1] W. Yoshida, K. Sode, K. Ikebukuro, Anal. Chem. 78 (2006) 3296.
[2] W.W. Yang, J.X. Wang, S. Zhao, Y.Y. Sun, C.Q. Sun, Electrochem. Commun. 8 (2006) 665.
[3] L. Qian, X.R. Yang, Talanta 68 (2006) 721.
[4] M.H. Shi, J.J. Xu, S. Zhang, B.H. Liu, J.L. Kong, Talanta 68 (2006) 1089.
[5] V.B. Kandimalla, H.X. Ju, Chem. Eur. J. 12 (2006) 1074.
[6] D. Du, S.Z. Chen, J. Cai, A.D. Zhang, Talanta 74 (2008) 766.
[7] J. Haccoun, B. Piro, V. NoÃÃl, M.C. Pham, Bioelectrochemistry 68 (2006) 218.
[8] J.C. Vidal, S. Esteban, J. Gil, J.R. Castillo, Talanta 68 (2006) 791.
[9] I. Willner, N. Lapidot, A. Riklin, R. Kasher, E. Zahavy, E. Katz, J. Am. Chem. Soc. 116 (1994) 1428.
[10] S. Lofas, B. Johnsson, Chem. Commun. (1990) 1526.
[11] P.L. Schilardi, P. Dip, P.C. dos Santos Claro, G.A. Bentez, M.H. Fonticelli, O. Azzaroni, R.C. Salvarezza, Chem. Eur. J. 12 (2006) 38.
[12] L. Wang, J.Y. Bai, P.F. Huang, H.J. Wang, L.Y. Zhang, Y.Q. Zhao, Electrochem. Commun. 8 (2006) 1825.
[13] S. Balasubramanian, A. Revzin, A. Simoniana, Electroanalyst 18 (2006) 1885.
[14] X.Q. Ding, J.B. Hu, Q.L. Li, Talanta 68 (2006) 653.
[15] M.G. Cerruti, M. Sauthier, D. Leonard, D. Liu, G. Duscher, D.L. Feldheim, S. Franzen, Anal. Chem. 78 (2006) 3282.
[16] H.J. Lee, D. Nedelkov, R.M. Corn, Anal. Chem. 78 (2006) 6504.
[17] F. Cecchet, M. Marcaccio, M. Margotti, F. Paolucci, S. Rapino, P. Rudolf, J. Phys. Chem. B 110 (2006) 2241.
[18] A.I. Abdelrahman, A.M. Mohammad, T. Okajima, T. Ohsaka, J. Phys. Chem. B 110 (2006) 2798.
[19] X. Dai, O. Nekrassova, M.E. Hyde, R.G. Compton, Anal. Chem. 76 (2004) 5924.
[20] M.C. Daniel, D. Astruc, Chem. Rev. 104 (2004) 293.
[21] L. Su, L.Q. Mao, Talanta 70 (2006) 68.
[22] K.C. Grabar, R. GrWith Freeman, M.B. Hommer, M.J. Natan, Anal. Chem. 67 (1995) 735.
[23] M.S. El-Deab, T. Okajima, T.J. Ohsaka, J. Electrochem. Soc. 150 (2003) A851.
[24] P.N. Deepa, M. Kanungo, G. Claycomb, P.M.A. Sherwood, M. Collinson, Anal. Chem. 75 (2003) 5399.
[25] E. Majid, S. Hrapovic, Y.L. Liu, K.B. Male, J.H.T. Luong, Anal. Chem. 78 (2006) 762–769.
[26] C.Z. Li, Y.L. Liu, J.H.T. Luong, Anal. Chem. 77 (2005) 478.
[27] M.O. Finot, G.D. Braybrook, M.T. McDermott, J. Electroanal. Chem. 466 (1999) 234.
[28] P. Xu, S.Y. Du, S.J. Dong, E. Wang, Anal. Chem. 77 (2005) 8166.

[29] S. Trasatti, O.A. Petrii, J. Electroanal. Chem. 327 (1992) 353.
[30] G.T. Filho, L.H. Dall, L. Antonia, G. Jerkiewiez, J. Electroanal. Chem. 422 (1997) 149.
[31] C.J. Zhong, M.D. Porter, J. Am. Chem. Soc. 116 (1994) 11616.
[32] M.M. Walczak, D.D. Popenoe, R.S. Deinhammer, B.D. Lamp, C. Chung, M.D. Porter, Langmuir 7 (1991) 2687.
[33] T. Sumi, K. Uosaki, J. Phys. Chem. B 108 (2004) 6422.
[34] L.H. Dubois, B.R. Zegarski, J. Chem. Phys. 98 (1993) 678.
[35] N. Patel, M.C. Davies, M. Hartshorne, R.J. Heaton, C.J. Roberts, S.J.B. Tendler, P.M. Williams, Langmuir 13 (1997) 6485.
[36] H. Schulze, S. Vorlová, F. Villatte, T.T. Bachmann, R.D. Schmid, Biosens. Bioelectron. 18 (2003) 201.
[37] G.D. Liu, S.L. Riechers, M.C. Mellen, Y.H. Lin, Electrochem. Commun. 7 (2005) 1163.

Available online at www.sciencedirect.com
ScienceDirect
Talanta 74 (2008) 1166–1174
Talanta
www.elsevier.com/locate/talanta

Evaluation of solid-phase micro-extraction coupled to gas chromatography–mass spectrometry for the headspace analysis of volatile compounds in cocoa products

Sylvie Ducki [a,*], Javier Miralles-Garcia [a], Albert Zumbé [a,b], Antonio Tornero [a], David M. Storey [a]

[a] *Biomedical Sciences Research Institute, School of Environment and Life Sciences, University of Salford, The Crescent, Salford, M5 4WT Greater Manchester, United Kingdom*
[b] *The Chocolate Powder Company Ltd., 23 Glendon Way, Dorridge, B93 8SY Solihull, United Kingdom*

Received 14 August 2006; received in revised form 16 August 2007; accepted 24 August 2007
Available online 2 September 2007

Abstract

The aroma profile of cocoa products was investigated by headspace solid-phase micro-extraction (HS-SPME) combined with gas chromatography–mass spectrometry (GC–MS). SPME fibers coated with 100 μm polydimethylsiloxane coating (PDMS), 65 μm polydimethylsiloxane/divinylbenzene coating (PDMS-DVB), 75 μm carboxen/polydimethylsiloxane coating (CAR-PDMS) and 50/30 μm divinylbenzene/carboxen on polydimethylsiloxane on a StableFlex fiber (DVB/CAR-PDMS) were evaluated. Several extraction times and temperature conditions were also tested to achieve optimum recovery. Suspensions of the samples in distilled water or in brine (25% NaCl in distilled water) were investigated to examine their effect on the composition of the headspace. The SPME fiber coated with 50/30 μm DVB/CAR-PDMS afforded the highest extraction efficiency, particularly when the samples were extracted at 60 °C for 15 min under dry conditions with toluene as an internal standard. Forty-five compounds were extracted and tentatively identified, most of which have previously been reported as odor-active compounds. The method developed allows sensitive and representative analysis of cocoa products with high reproducibility. Further research is ongoing to study chocolate making processes using this method for the quantitative analysis of volatile compounds contributing to the flavor/odor profile.
© 2007 Elsevier B.V. All rights reserved.

Keywords: Headspace solid-phase micro-extraction (HS-SPME); Gas chromatography–mass spectrometry (GC–MS); Chocolate; Cocoa; Volatile compounds

1. Introduction

Chocolate and cocoa are amongst the most popular flavors worldwide. Unlike many other natural flavors that have one principal compound responsible for their flavor [e.g. vanilla (vanillin), banana (amyl acetate), peach (γ-undecalactone) or almond (benzaldehyde)], chocolate and cocoa flavors reside in their volatile fraction, which is composed of a complex mixture of up to 500 compounds [1] with new research continuously increasing this number [2,3]. The complexity of this flavor is obvious and thus far it has not been possible for the chemist to duplicate the flavor. It has been known for some time that the compounds that give cocoa and chocolate their flavors are N- and O-containing molecules such as pyrazines, pyrroles, furans, aldehydes and amides, which are mainly generated during the Maillard reaction [4].

The analysis of volatile fractions of cocoa and chocolate is essential to study their aromatic profile. In general, the volatile fractions have been recovered by steam distillation or solvent extraction and analyzed by GC [5]. Considering the limitations of these sampling techniques, headspace solid-phase micro-extraction (HS-SPME) emerges as an attractive alternative [6]. The technique has been reported to be relatively cheap,

Abbreviations: SPME, solid-phase micro-extraction; GC–MS, gas chromatography–mass spectrometry; PDMS, polydimethylsiloxane; DVB, divinylbenzene; CAR, carboxen; HS, headspace; NCP, natural cocoa powder; CCP, conched chocolate powder; RI, retention index.

* Corresponding author. Tel.: +44 1612954701; fax: +44 1612955111.
E-mail address: s.ducki@salford.ac.uk (S. Ducki).

0039-9140/$ – see front matter © 2007 Elsevier B.V. All rights reserved.
doi:10.1016/j.talanta.2007.08.034

solventless, fast and reproducible. SPME seems particularly appealing since it also eliminates problems associated with chemically and thermally unstable samples where generation of artifacts can be problematic as in the case of chocolate and cocoa. SPME, and HS-SPME in particular, in combination with GC and GC–MS, have been largely used in food [7,8], environmental [9] and biomedical analyses [10].

Counet et al. [11] used HS-SPME-GC–MS to analyze the flavor of 8 cocoa liquors and tentatively identified 43 compounds, of which 5 had never been associated with chocolate flavor. In each case, 2 g of the cocoa liquor was adsorbed onto a CAR-PDMS fiber for 20 min at 25 °C and deorbed for 5 min at 250 °C in the GC injector. Pini et al. [12] assessed HS-SPME-GC-FID for the analysis of the alkylpyrazine content in single-roasted cocoa liquor. The optimum recovery was obtained using the DVB/CAR-PDMS fiber when the extraction was performed at 60 °C for 45 min, following a 15 min equilibration. In related studies, they had also analyzed the pyrazine content of cocoa mass [13] and cocoa nibs [14] using a CAR-PDMS fiber under similar conditions.

The objective of this study was to investigate the use of HS-SPME-GC–MS to analyze cocoa products, such as natural cocoa powder (NCP) and conched chocolate powder (CCP). NCP is a product obtained from cocoa liquor which has been pressed hydraulically to reduce the fat content and milled into a powder [15]. CCP is a new product obtained by a similar process but using chocolate. The chocolate is prepared following the traditional process (mixing, refining and conching), then pressed hydraulically to reduce the fat content and ground into a fine powder.

In the present study, four types of SPME fibers, coated with different stationary phases (PDMS, PDMS-DVB, CAR-PDMS and DVB/CAR-PDMS), were used to examine their extraction efficiencies and compared for sensitivity. Conditions that might affect the SPME procedure, such as extraction time and temperature, were also investigated to determine the analytical performance of the selected fiber coatings.

2. Experimental

2.1. Materials

Non-alkalized natural cocoa powder (NCP) and conched chocolate powder (CCP), from West African origin, were obtained from The Chocolate Powder Company (Solihull, United Kingdom). The fat content of the NCP was 10–12%. The fat content of the CCP was 10–12% and the cocoa content was 69%. The NCP and CCP were stored in hermetic boxes at room temperature.

Analytical grade 2-methylpropanal, 3-methylbutanal, 2-methylbutanal, 2-phenyl-5-methyl-2-hexanal, 2,3-dimethylpyrazine, trimethylpyrazine, tetramethylpyrazine were purchased from Alfa Aesar (Heysham, United Kingdom) and acetone, benzyl alcohol, benzaldehyde, vanillin, caffeine and 1-(2-furanylmethyl)-1*H*-pyrrole from Sigma–Aldrich (Dorset, United Kingdom).

2.2. SPME extraction

Volatiles from the NCP and CCP samples were extracted using four fibers: 100 μm polydimethylsiloxane coating (PDMS), 65 μm polydimethylsiloxane/divinylbenzene coating (PDMS-DVB), 75 μm carboxen/polydimethylsiloxane coating (CAR-PDMS) and 50/30 μm divinylbenzene/carboxen on polydimethylsiloxane on a StableFlex fiber (DVB/CAR-PDMS). These fibers were purchased from Supelco (Bellefonte, PA, USA). Before extraction, the fibers were conditioned according to the supplier's instructions. Extractions were carried out in 10 mL PTFE/Silicone septa vials (Supelco, Bellefonte, PA, USA). Every septum was predrilled with a regular needle before sampling with the SPME fiber.

2.2.1. Selection of fiber coating

The sample (2.0 g) was placed in the vial and conditioned for 10 min at the extraction temperature, 60 °C. The extraction time was 15 min. The SPME fiber was then exposed to the headspace. The desorption time was 5 min and the temperature in the GC liner was 250 °C.

2.2.2. Selection of extraction time and temperature

The sample (2.0 g) was placed in the vial and conditioned for 10 min at the extraction temperature. The fiber was exposed for 1, 5, 10, 15 and 30 min to the headspace of the vial at four different temperatures, 25, 40, 60 and 80 °C. The desorption time was 5 min and the temperature in the GC liner was 250 °C.

2.2.3. Dry, wet and brine conditions

The sample (1.0 g) was placed in a vial (dry conditions). In a second vial the sample (1.0 g) was mixed with 4 mL of distilled water. The effect of the ionic strength was studied by substituting the water by brine (25% of NaCl in distilled water) in a third vial. In all cases the headspace extraction was carried out using the optimized conditions (T_{ext}: 60 °C; t_{ext}: 15 min). The desorption time was 5 min and the temperature in the GC liner was 250 °C.

2.2.4. Quantitative determination

The sample (2.0 g) was placed in the vial and toluene (50 μg) was added. The vial was conditioned for 10 min at the extraction temperature (60 °C). The fiber was exposed for 15 min to the headspace of the vial at the same temperature. The desorption time was 5 min and the temperature in the GC liner was 250 °C. The standard curves were obtained using 2-methylpropanal (slope: 2.5715; intercept: 0.0011; R^2: 0.9997), 3-methylbutanal (slope: 4.1238; intercept: −0.0019; R^2: 0.9997), 2-methylbutanal (slope: 16.79; intercept: −0.0149; R^2: 0.9996), 2,3-dimethylpyrazine (slope: 2.1598; intercept: 0.0175; R^2: 0.9990), trimethylpyrazine (slope: 3.7317; intercept: 0.0342; R^2: 0.9900) and tetramethylpyrazine (slope: 6.567; intercept: 0.00758; R^2: 0.9817).

2.3. Gas chromatography–mass spectrometry (GC–MS)

The analysis of volatiles extracted by HS-SPME was carried out using a Varian CP-3800 Gas Chromatograph linked to a Varian 1200L Quadrupole MS/MS. The GC was equipped with a CTC CombiPAL autosampler upgraded with a SPME analysis kit. The injector port has a deactivated glass SPME liner supplied by Supelco. The GC was fitted with a 30 m capillary column with a 0.25 mm i.d. and 1 μm FD, Factor 4 VF-5ms purchased from Varian. After absorption, the SPME fibers were introduced into the injector port of the GC (in splitless mode at 250 °C for 5 min). The volatiles extracted by the fibers were thermally desorbed and introduced in the capillary column. The GC was setup with a constant flow of 1.0 mL/min (helium), the oven temperature was programmed to start at 30 °C (5 min)–(10 °C/min)–200 °C–(25 °C/min)–280 °C (5 min). The transfer line was at 280 °C. The MS was setup with the source at 280 °C, where electronic ionization energy was −70 eV and with a 1200 V in the detector. One mass spectra scan every second was acquired. Three identical samples were prepared for each analysis. The average of their results is reported. The compounds were identified by a combination the US national Institute of Standards and Technology (NIST) 98 library of mass spectra and gas chromatographic retention indexes reported of standard compounds. Under these conditions, no sample carry-over was observed as confirmed by blank runs conducted between each analysis.

3. Results and discussion

3.1. Selection of fiber coatings

Fiber type selection is very important to define the optimum extraction conditions from the headspace. Several types of coating fibers, with a range of polarities and mechanisms, are commercially available for the analysis of volatiles of food samples [7]. PDMS-supported fibers are the best as they result in optimal long-term stability and overall performance, including chromatography, extraction characteristics and analyte recovery. These fibers are also very durable and usually retain their performance for up to 100 analytical cycles. The non-polar PDMS fiber is recommended by the supplier for the extraction of non-polar analytes, such as volatile flavor compounds but can also be applied to more-polar compounds. Mixed fiber coatings, containing DVB or CAR, increase retention capacity due to a mutually potentiating effect on extraction and distribution of the stationary phase. PDMS-DVB and CAR-PDMS have been used for the extraction of volatile low-molecular mass and polar analytes. The dual-coated fiber DVB/CAR-PDMS comprises a layer of PDMS-DVB over a layer of CAR-PDMS and is recommended for flavor and odor extraction (volatiles and semi-volatiles). The natural cocoa powder (NCP) and conched chocolate powder (CCP) were sampled using these four SPME fibers and analyzed by GC–MS, as described above. The objective was to establish which fibers reliably achieved the highest performance for the recovery of flavor compounds.

Altogether 42 compounds were extracted and identified on the basis of their mass spectra (MS) and retention indexes (RI) (Table 1). In general, the four fibers extracted compounds with RI from less than 500 (RI: 495 for acetone) to almost 1800 (RI: 1783 for caffeine). These included 9 aldehydes, 14 heterocyclic compounds, 5 ketones, 4 alcohols, 2 esters, 5 acids and 3 terpenes. Inspection of the total peak area for each fiber clearly showed that the most efficient fiber is CAR-PDMS, extracting around five times more than the PDMS-DVB and DVB/CAR-PDMS fibers and 25 times more than the PDMS fiber. Extraction with the latter fiber (total peak area = 5000–6000) was very weak compared to the other three fibers (total peak area > 200,000). Indeed very few peaks were observed on the chromatogram, with some undetected by the MS, making this fiber unsuitable for our study. The CAR-PDMS fiber presented the highest extraction (total peak area > 1,000,000) and proved to be very efficient at extracting volatiles, providing wide peaks at the beginning of the chromatogram (RI < 950). A split injection might lead to sharper peaks. However even under splitless conditions we were unable to extract most of the semi-volatiles, making this fiber undesirable for our study. Finally the PDMS-DVB and DVB/CAR-PDMS fibers resulted in similar extractions (total peak area = 200,000–300,000); the peaks were sharp and well distributed throughout the chromatogram. Both fibers would be suitable.

A number of compounds have been identified by gas chromatography-olfactometry (GC-O) as key odorant compounds in dark chocolate [2]. 2-Methylpropanal, 3-methylpropanal and 2-methylbutanal have been related to chocolate odors while trimethylpyrazine, 2,5-dimethylpyrazine and acetylpyrrole have been attributed cocoa odors. Methylpyrazine, 2,3-dimethylpyrazine, 2-ethyl-6-methylpyrazine and benzaldehyde added a hazelnut/almond note to the aroma profile of chocolate; ethylpyrazine, 3-ethyl-2,5-dimethylpyrazine and tetramethylpyrazine a roasty note. These compounds were tentatively extracted by all four fibers (Figs. 1 and 2).

In general, the PDMS fiber proved very inefficient at extracting key odorant compounds. The CAR-PDMS fiber was found to be the best fiber for the extraction of volatiles (RI < 950) while the PDMS-DVB was best at extracting semi-volatiles (RI > 950). In their study, Counet et al. [11] tentatively identified 43 flavor compounds using the CAR-PDMS fiber, only 22 of which were also extracted in our study. We attribute this difference to the matrix of the cocoa samples which has been shown to affect the composition of the headspace. Counet analyzed cocoa liquors which can contain up to 40% fat, whereas our study analyzed cocoa powders containing 10–12% fat. Interestingly, the DVB/CAR-PDMS seemed to extract both volatiles and semi-volatiles with the same efficiency. This dual-coated fiber proved to be the best fiber for the analysis of odorant compounds for both NCP and CCP because it combined the characteristics of the CAR-PDMS fiber with the addition of the properties of PDMS-DVB. The CAR layer allowed the fiber to extract the low molecular weight analytes (RI < 950), but with less efficiency than the CAR-PDMS, presumably because the layer of CAR is thinner in the dual-

Table 1
Effect of fiber type on the peak area ($\times 10^8$ area units) of natural cocoa powder (NCP) and conched chocolate powder (CCP) using HS-SPME-GC–MS[a]

No.	Compound[b]	RI	PDMS		DVB-PDMS		CAR-PDMS		DVB/CAR-PDMS	
			NCP	CCP	NCP	CCP	NCP	CCP	NCP	CCP
Volatile aldehydes and ketones										
1	Acetone[b]	495	65 ± 11	22 ± 8	1246 ± 11	243 ± 61	33,050 ± 3275	6311 ± 945	3073 ± 458	1660 ± 355
2	Methyl acetate[c]	521	18 ± 2	ND	456 ± 2	49 ± 23	14,080 ± 1648	982 ± 145	1416 ± 342	332 ± 82
3	2-Methylpropanal[b]	550	69 ± 12	66 ± 14	916 ± 12	661 ± 128	40,910 ± 5224	15,550 ± 2513	914 ± 245	1719 ± 320
4	2,3-Butanedione[c]	581	1783 ± 251	1292 ± 185	757 ± 251	562 ± 152	13,760 ± 2360	15,970 ± 2458	1908 ± 265	2925 ± 236
5	2-Butanone[c]	586	ND	ND	813 ± 145	224 ± 49	37,620 ± 5124	10,060 ± 1420	3470 ± 521	1567 ± 251
7	3-Methylbutanal[b]	653	139 ± 32	169 ± 29	3401 ± 242	3091 ± 423	77,690 ± 9423	86,430 ± 11,045	4439 ± 623	7179 ± 1366
8	2-Methylbutanal[b]	662	69 ± 14	97 ± 21	1361 ± 142	1476 ± 252	41,520 ± 6210	59,890 ± 8541	2241 ± 252	4231 ± 651
9	Pentanal[c]	696	ND	ND	304 ± 64	86 ± 26	7509 ± 845	3940 ± 687	906 ± 260	544 ± 124
10	3-Hydroxy-2-butanone[c]	707	ND	63 ± 10	1550 ± 194	1610 ± 210	19,490 ± 2180	49,900 ± 8511	1560 ± 310	4926 ± 845
12	35-Dimethyl-dihydro-furan-2-one[c]	766	11 ± 4	ND	610 ± 154	59 ± 24	5700 ± 945	2344 ± 322	583 ± 240	240 ± 62
15	Hexanal[c]	802	ND	ND	403 ± 94	57 ± 21	1221 ± 182	ND	607 ± 124	322 ± 58
Acids and alcohols										
6	Acetic acid[c]	630	1612 ± 211	1519 ± 261	29,290 ± 3250	21,460 ± 2854	389,700 ± 40,211	509,000 ± 61,525	78,310 ± 11,254	134,000 ± 21,804
11	Dimethylpropanedioic acid[c]	755	ND	ND	4875 ± 954	3125 ± 487	33,710 ± 4127	ND	2400 ± 325	3256 ± 812
13	2,3-Butanediol[c,d]	782	560 ± 102	670 ± 123	55,860 ± 5821	60,960 ± 6221	170,000 ± 22,943	276,500 ± 36,102	33,990 ± 5442	61,060 ± 12,209
14	2,3-Butanediol[c,d]	792	306 ± 51	314 ± 62	32,670 ± 4151	28,590 ± 3562	89,220 ± 12,452	123,300 ± 19,450	11,990 ± 2112	22,210 ± 3251
17	3-Methyl-butanoic acid[c]	837	185 ± 42	ND	16,180 ± 1822	15,420 ± 2511	35,600 ± 3254	92,010 ± 14,520	9667 ± 1225	14,860 ± 2524
18	2-Methyl-butanoic acid[c]	847	ND	ND	3491 ± 385	3.091 ± 520	7457 ± 1346	15,680 ± 2364	2146 ± 363	2666 ± 326
19	2-Furanmethanol[c]	854	6 ± 3	ND	439 ± 84	203 ± 38	3288 ± 651	3245 ± 458	996 ± 251	860 ± 152
30	Benzyl alcohol[b]	1048	ND	ND	256 ± 62	586 ± 154	234 ± 74	871 ± 210	118 ± 22	344 ± 54
35	Phenylethyl alcohol[c]	1133	78 ± 44	44 ± 9	6248 ± 1114	11,850 ± 1514	3158 ± 845	6628 ± 1125	5645 ± 945	7342 ± 945
36	Benzoic acid[c]	1157	17 ± 5	12 ± 4	157 ± 34	456 ± 86	106 ± 32	796 ± 124	189 ± 34	464 ± 214
39	Isopentyl benzoate[c]	1404	45 ± 11	ND	831 ± 214	166 ± 53	30 ± 15	ND	226 ± 14	61 ± 24
Pyrazines										
16	Methylpyrazine[c]	832	30 ± 13	18 ± 6	1117 ± 224	551 ± 94	17,480 ± 3254	19,690 ± 3458	3243 ± 432	4249 ± 832
20	2,5-Dimethylpyrazine[c]	921	146 ± 44	116 ± 34	8254 ± 1244	5817 ± 854	30,760 ± 1346	40,710 ± 8245	6987 ± 732	12,760 ± 1532
21	2,3-Dimethylpyrazine[b]	928	14 ± 6	ND	396 ± 85	764 ± 152	705 ± 251	ND	351 ± 122	1175 ± 232
22	Ethylpyrazine[c]	926	ND	ND	ND	ND	603 ± 124	259 ± 51	428 ± 74	1429 ± 645
27	Trimethylpyrazine[b]	1011	75 ± 21	123 ± 42	3517 ± 655	4936 ± 866	2578 ± 345	8396 ± 1257	1693 ± 645	4206 ± 532
28	2-Ethyl-6-methylpyrazine[c]	1013	2 ± 1	ND	143 ± 44	243 ± 62	106 ± 31	850 ± 53	101 ± 32	1489 ± 445
33	3-Ethyl-2,5-dimethylpyrazine[c]	1086	3 ± 1	ND	202 ± 57	824 ± 122	136 ± 42	651 ± 132	160 ± 35	690 ± 232
34	Tetramethylpyrazine[b]	1094	169 ± 54	105 ± 37	2648 ± 454	2484 ± 482	1150 ± 185	1846 ± 324	1714 ± 382	1829 ± 352
Semi-volatile aldehydes and ketones										
24	Benzaldehyde[b]	981	75 ± 34	54 ± 25	6138 ± 1032	6617 ± 1102	19,790 ± 3232	34,290 ± 4251	11,790 ± 1845	17,010 ± 2842
29	1*H*-Pyrrole-2-carboxaldehyde[c]	1018	7 ± 4	ND	424 ± 82	654 ± 148	777 ± 151	2653 ± 450	255 ± 82	624 ± 255
31	Benzeneacetaldehyde[c]	1062	33 ± 15	58 ± 34	1567 ± 284	13,780 ± 2152	164 ± 21	626 ± 122	1192 ± 355	5198 ± 1252
32	2-Acetylpyrrole[c]	1072	19 ± 6	19 ± 8	1479 ± 314	4235 ± 651	1829 ± 251	6870 ± 853	925 ± 132	2561 ± 512
37	3,5-Dihydroxy-6-methyl-2,3-dihydro-pyran-4-one[c]	1164	39 ± 21	ND	1341 ± 253	2628 ± 541	ND	ND	339 ± 82	734 ± 252
38	3,5-Dimethyl-benzaldehyde[c]	1250	ND	ND	391 ± 132	147 ± 25	47 ± 25	ND	161 ± 25	69 ± 18
40	Vanillin[b]	1419	7 ± 4	451 ± 148	699 ± 157	11,180 ± 2104	22 ± 9	777 ± 178	135 ± 34	1661 ± 258
Terpenes and others										
23	α-Pinene[c]	949	66 ± 28	ND	7478 ± 1612	ND	20,440 ± 3512	69 ± 22	6259 ± 845	ND
25	β-Pinene[c]	999	ND	ND	544 ± 126	ND	1273 ± 210	ND	287 ± 42	ND
26	35-Dimethyl-octane[c]	1007	ND	ND	4701 ± 745	ND	ND	ND	1340 ± 281	ND
41	8-Hydroxy-3-methyl-iso-chroman-1-one[c]	1565	ND	ND	106 ± 34	112 ± 35	ND	ND	22 ± 12	24 ± 18
42	Caffeine[b]	1783	170 ± 46	101 ± 54	348 ± 72	594 ± 142	ND	ND	107 ± 32	109 ± 34
Total			5816	5311	203,606	209,591	1,122,912	1,397,093	204,283	328,585

ND: compound not detected.
[a] All runs preformed with extraction at 60 °C for 15 min under dry conditions.
[b] Compound identified by GC–MS and RI using authentic compounds.
[c] Compound tentatively identified by GC–MS and RI using NIST98 database.
[d] Diastereoisomers.

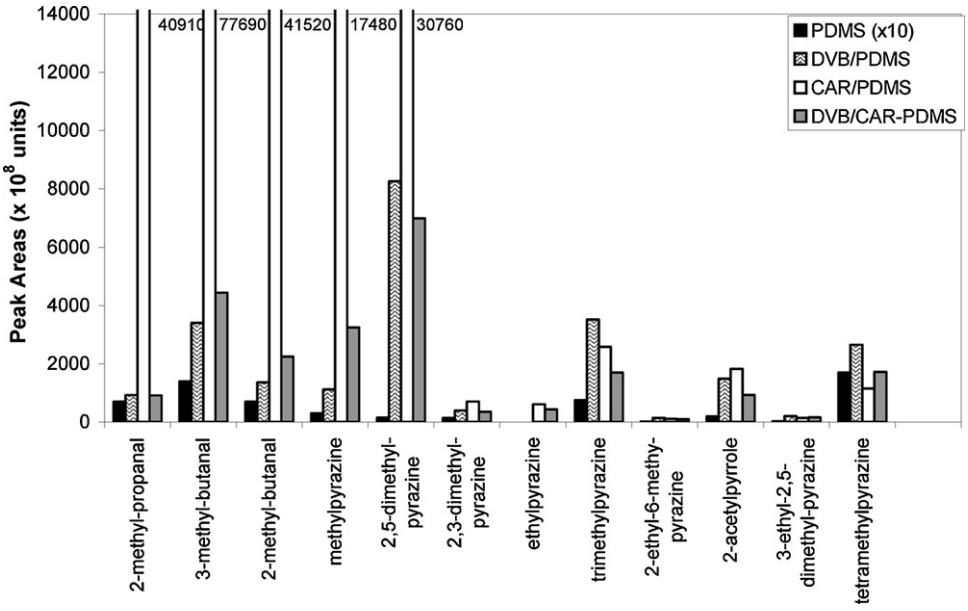

Fig. 1. Peak areas (in 10^8 area counts) of key odorant compounds identified by GC–MS extracted from NCP with four types of SPME fibers at 60 °C for 15 min.

coated fiber (75 μm in CAR-PDMS versus 30 μm in DVB/CAR-PDMS).

Furthermore, the DVB/CAR-PDMS fiber afforded high-resolution chromatograms when compared to the other fibers' chromatograms. We therefore decided to use this fiber to characterize the cocoa and chocolate products and establish their aroma and volatile profiles.

3.2. Selection of extraction time and temperature

Temperature and time of extraction are two important factors that control sample recovery by the fibers [16]. Consequently, these parameters were studied in order to establish the optimum extraction conditions. Time affects the mass transfer of the analytes onto the fiber; optimum time is required for the fiber to reach its equilibrium. Temperature directly affects how fast this equilibrium is reached, favoring the diffusion and it also has an influence on the composition of the volatile phase, increasing the ratio of compounds with low vapor pressure (semi-volatiles). A 3D representation of the extracted amount (total peak area) versus extraction times and temperatures (Fig. 3) clearly shows that the equilibrium is reached within 15 min (total peak area remains constant after that time).

The extraction was investigated at four different temperatures (25, 40, 60 and 80 °C) and the compounds extracted were divided into five main compound family: pyrazines, volatile aldehy-

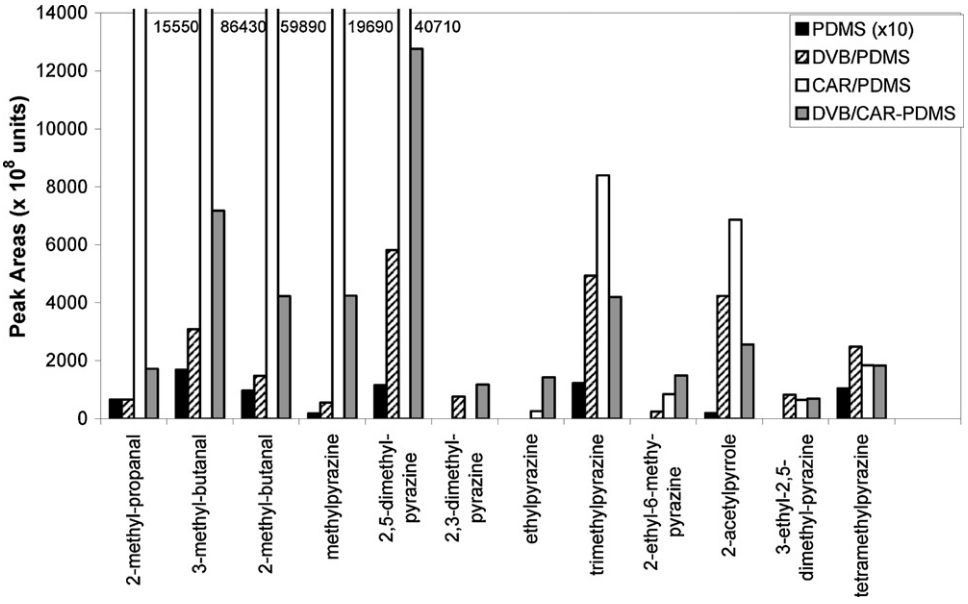

Fig. 2. Peak areas (in 10^8 area counts) of key odorant compounds identified by GC–MS extracted from CCP with four types of SPME fibers at 60 °C for 15 min.

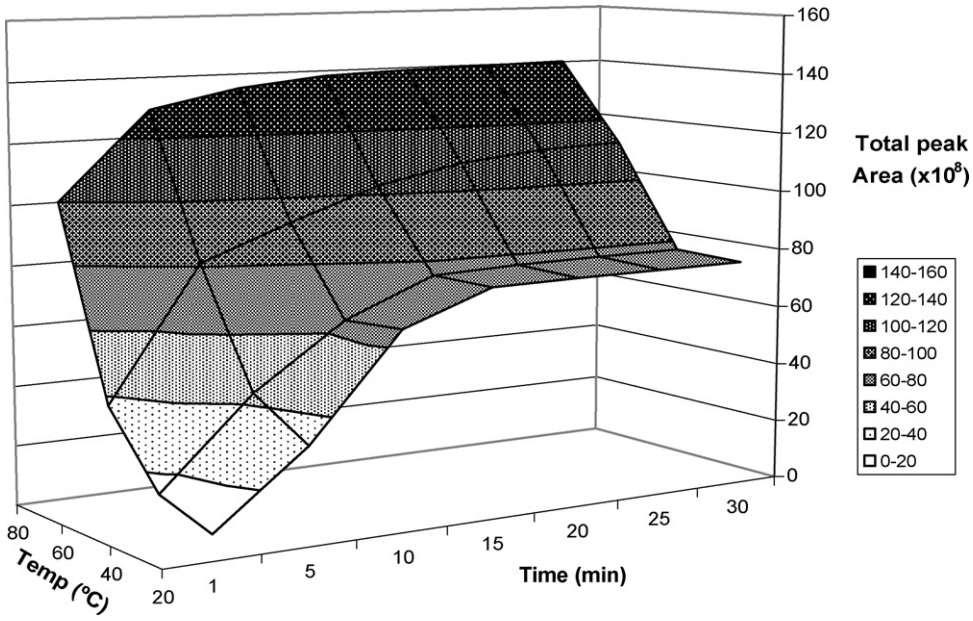

Fig. 3. Effect of extraction time and temperature on the total peak area (*x*-axis: time in min; *y*-axis: total peak area expressed in total ion counts; *z*-axis: temperature in °C). CAR/DVB-PDMS fiber was used.

des/ketones, semi-volatile aldehydes/ketones, acids/alcohols, and terpenes and others (Fig. 4).

In general, the amount extracted increases exponentially with the temperature of extraction, allowing optimum extraction at 80 °C. Nonetheless this temperature was discarded since chemical changes are likely to occur in the sample at such high temperature. The "acid and alcohol" fraction are better extracted at higher temperatures. The "pyrazine" and the "semi-volatile aldehyde and ketone" groups behave similarly at low temperatures (weak peaks) and from 60 °C their extraction efficiency is improved. Volatile compounds have a higher vapor pressure at room temperature; at 25 °C their concentration in the gas phase is higher than at higher temperatures when the presence of semi-volatiles starts to became important. On the other hand, there is a dramatic decrease in the "volatile aldehyde and ketone" family of compounds (30% at 25 °C) with increase of the temperature (only 5% at 60 °C). Peaks for 2-methylpropanal, 2-butanone or 3-methylbutanal almost disappear at 40 °C.

Augusto et al. [12] reported that the optimum extraction conditions were obtained when the cocoa liquor was extracted at 60 °C with 15 min of headspace equilibration and 45 min extraction while de Brito et al. [13] reported the extraction of cocoa mass under the same conditions. In their cases, the matrix is high in fat content (50% fat), while our cocoas are low in fat. The fat content affects the release of volatiles thus the extraction efficiency. In general, the extraction of compounds reached equilibrium within 15 min (Fig. 3). Looking at the families of compounds, the volatiles tended to be extracted within 10 min

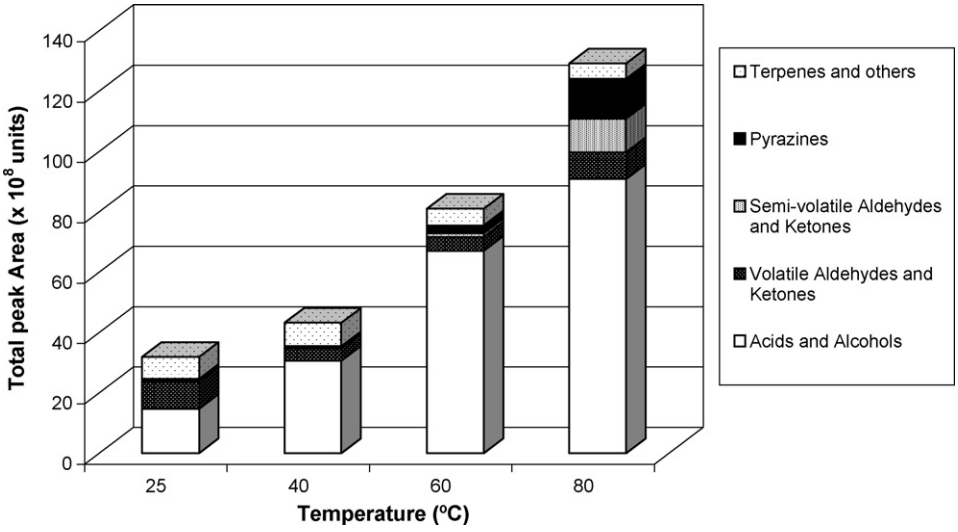

Fig. 4. Effect of extraction temperature on the extraction efficiency by main compound families (*x*-axis: temperature in °C; *y*-axis: total peak area expressed in total ion counts). DVB/CAR-PDMS fiber was used, and 5 min for extraction time.

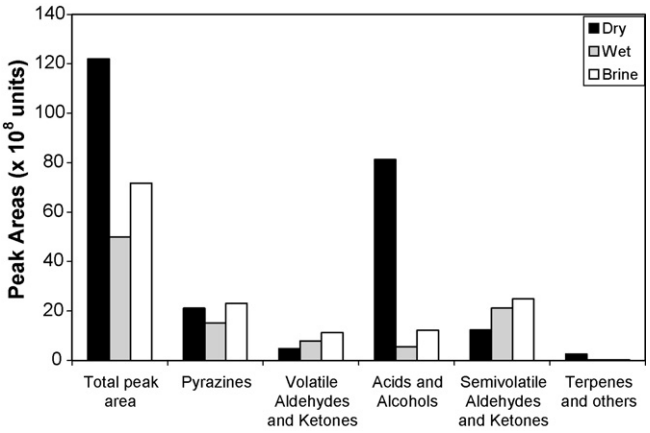

Fig. 5. Effect of dry, wet and brine conditions on the headspace compounds in NCP by SPME. CAR/DVB-PDMS fiber was used (sampling at 60 °C for 15 min).

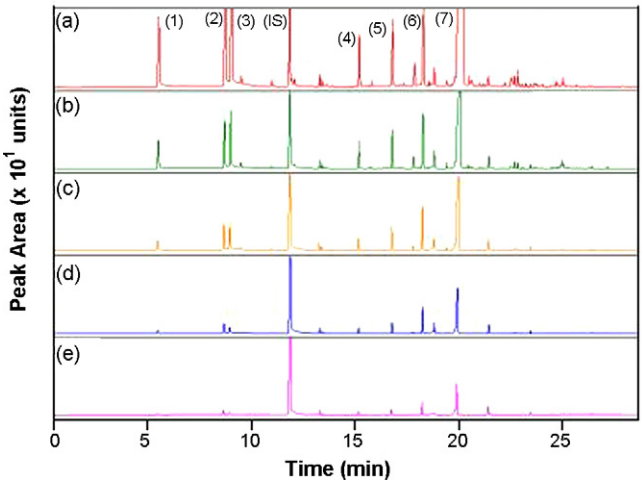

Fig. 6. HS-SPME-GC–MS chromatograms of standard mixture (Table 2) spiked with 50 μg of toluene (IS): (a) ratios as described in Table 2; (b) 1/3 dilution of (a); (c) 1/3 dilution of (b); (d) 1/3 dilution of (c); (d) 1/3 dilution of (c); peak identification: (1) 2-methylpropanal; (2) 3-methylbutanal; (3) 2-methylbutanal; (4) 2,3-dimethylpyrazine; (5) trimethylpyrazine; (6) tetramethylpyrazine; (7) 1-furfurylpyrrole. Peak area scale is the same for the five chromatograms.

but after 20 min, a decrease in the amount of volatile extracted was noticed. On the other hand, semi-volatiles took a bit longer to be extracted, i.e. 30 min. A consensus was reached to extract for 15 min which we consider to be the equilibrium for the competition between volatiles and semi-volatiles.

Taking these results into account (chromatograms available in Supporting information), the optimum conditions were chosen to be 60 °C for the extraction temperature and 15 min for the extraction time, preceded by 10 min of conditioning at the same temperature.

3.3. Study in wet, dry and brine conditions

In order to examine water and salt influence on the composition of the headspace, samples were analyzed under dry, wet and brine conditions.

In the absence of water, the amount of compounds extracted by the fiber was higher than under wet conditions (Fig. 5). Increasing the ionic strength by adding brine to the sample resulted in better extraction than in plain water, as recently reported by Pini et al. [12]. Comparing the chemical families, the largest difference was found in the "acid and alcohol" group, being the least well extracted. These results can be explained by the fact that acids and alcohols are very soluble in water, decreasing their presence in the volatile phase. The "pyrazine" group presented only weak signals in plain water which by increasing the ionic strength of the media increased significantly. The polarity of their nitrogen gives pyrazines an acceptable solubility in water, which in presence of NaCl makes them less soluble in water thus increasing their presence in the volatile fraction.

Table 2
List of compounds and their amounts in the initial solution (water 5 mL)

No.	Compound	Amount (mg)
1	2-methylpropanal	1
2	3-methylbutanal	1
3	2-methylbutanal	0.5
4	2,3-Dimethylpyrazine	1
5	Trimethylpyrazine	0.5
6	Tetramethylpyrazine	0.5
7	1-Furfurylpyrrole	0.5
IS	Toluene	0.05

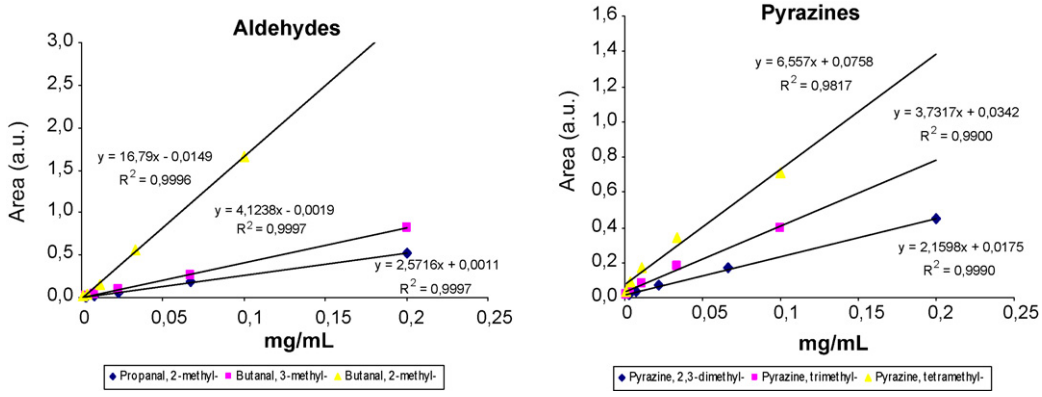

Fig. 7. Calibration curves of some representative standards obtained using SPME.

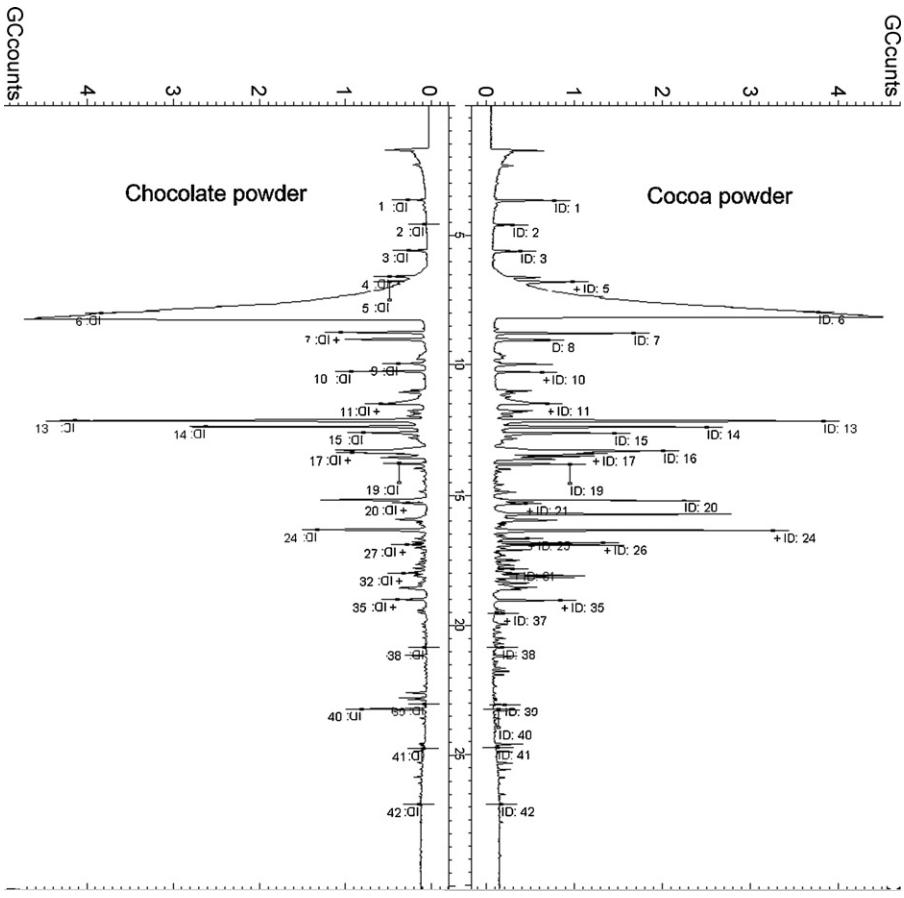

Fig. 8. Typical HS-SPME-GC–MS chromatograms of compounds extracted from chocolate (left) and cocoa (right) powders with DVB/CAR-PDMS fiber. Peak identification (see Table 1).

Three new pyrazines were tentatively identified under wet conditions, 3,5-dimethyl-2-isobutylpyrazine (RI: 1197), 2-isoamyl-6-methylpyrazine (RI: 1258) and 2,6-dimethyl-5-isopentylpyrazine (RI: 1325). These new pyrazines have longer carbon chains, increasing their hydrophobicity. As a consequence, their presence in the volatile phase is higher and can be detected. On the other hand, a few compounds could not be detected under wet conditions such as dimethylpropanedioic acid, 2,3-butanodiol and α-pinene.

3.4. Quantitative determination

Quantitative determination can be carried out by the method of internal standards which requires a calibration curve of each compound. A quantification in equivalents can also be used by using the method of the internal standard, in which ratios between the response of the individual compounds and that of the internal standard can be used (Table 2 and Figs. 6 and 7). In this case, toluene was used as an internal standard. The optimum amount of toluene added to the analyte was adjusted to 50 μg to avoid saturation of the detector and also to prevent it from masking peaks of interest. Subsequent semi-quantitative determination was accomplished with reference to the internal standard.

4. Conclusion

HS-SPME coupled to GC–MS has proven a valuable tool for analysis of volatile and semi-volatile compounds from cocoa and chocolate products. The technique is very sensitive to experimental conditions; fibre coating, temperature, extraction time, ionic conditions were shown to influence the extraction efficiency. Consequently the DVB/CAR-PDMS fibre was found to afford the most efficient extraction of both volatile and semi-volatile compounds from the analyte's headspace. An extraction temperature of 60 °C was found to be optimum to ensure efficient transfer from the headspace to the fibre while avoiding production of unwanted thermal artefacts, while an extraction time of 15 min was deemed sufficient. Although wet and ionic conditions presented slightly higher extraction efficiencies, they did not offer any significant advantage over the dry conditions. Finally quantitation of the volatile and semi-volatile fractions from cocoa and chocolate products was made possible by the method of internal standard and reproducibility was ascertained alongside.

The method is simple, sensitive, reproducible, rapid and low-cost for the evaluation of key odorant compounds found in cocoa and chocolate products (Fig. 8) and the mild conditions used for the analysis allow a good estimation of the aroma profile as

perceived by the human sensory organs (nose and tongue). This SPME method was developed to study small chemical changes that are sensorially detectable in cocoa and chocolate samples since there is an increasing interest to identify chemical modifications in the process leading to the production of cocoa liquor, cocoa powder and chocolate.

Acknowledgements

We are grateful to Dr. Ian Podmore and Dr. Laurie Cunliffe for expert technical assistance. We would also like to thank the Chocolate Powder Company (Solihull, United Kingdom) for supplying the NCP and CCP. Finally we wish to thank Natraceutical (Valencia, Spain) for initial funding of the project.

Appendix A. Supplementary data

Supplementary data associated with this article can be found, in the online version, at doi:10.1016/j.talanta.2007.08.034.

References

[1] P.S. Dimick, J.C. Hoskin, in: S.T. Beckett (Ed.), Industrial Chocolate Manufacture and Use, Blackwell Science, 2003, pp. 137–152.
[2] C. Counet, D. Callemien, C. Ouwerx, S. Collin, J. Agric. Food Chem. 50 (2002) 2385.
[3] F. Luna, D. Crouzillat, L. Cirou, P. Bucheli, J. Agric. Food Chem. 50 (2002) 3527.
[4] F.B. Whitfield, Crit. Rev. Food Sci. Nutr. 31 (1992) 1.
[5] F. Augusto, A.L.E. Lopes, C.A. Zini, Trends Anal. Chem. 22 (2003) 160.
[6] H. Lord, J. Pawliszyn, J. Chromatogr. A 885 (2000) 153.
[7] H. Kataoka, H.L. Lord, J. Pawliszyn, J. Chromatogr. A 880 (2000) 35.
[8] W. Wardencki, M. Michulec, J. Curylo, Int. J. Food Sci. Technol. 39 (2004) 703.
[9] B. Zygmunt, A. Jastrzebska, J. Namiesnik, Crit. Rev. Anal. Chem. 31 (2001) 1.
[10] T. Kumazawa, X.P. Lee, K. Sato, O. Suzuki, Anal. Chim. Acta 492 (2003) 49.
[11] C. Counet, C. Ouwerx, D. Rosoux, S. Collin, J. Agric. Food Chem. 52 (2004) 6243.
[12] G.F. Pini, E.S. de Brito, N.H.P. Garcia, A.L.P. Valente, F. Augusto, J. Brazil. Chem. Soc. 15 (2004) 267.
[13] N.N.E.S de Brito, N.H. Pezoa García, A.L.P. Valente, G.F. Pini, J. Sci. Food Agric. 82 (2002) 534.
[14] E.S. de Brito, N.H.P. Garcia, A.C. Amancio, A.L.P. Valente, G.F. Pini, F. Augusto, Int. J. Food Sci. Technol. 36 (2001) 625.
[15] A. Zumbe, N. Sanders, UK Patent US6296891 (2001).
[16] S. Vichi, A.I. Castellote, L. Pizzale, L.S. Conte, S. Buxaderas, E. Lopez-Tamames, J. Chromatogr. A 983 (2003) 19.

Available online at www.sciencedirect.com
ScienceDirect
Talanta 74 (2008) 1675–1680
Talanta
www.elsevier.com/locate/talanta

Short communication

Critical evaluation and comparison of enrichment efficiency of multi-walled carbon nanotubes, C18 silica and activated carbon towards some pesticides from environmental waters

Amjad H. El-Sheikh *, Jamal A. Sweileh, Yahya S. Al-Degs, Ahmad A. Insisi, Nancy Al-Rabady

Department of Chemistry, Faculty of Science, Hashemite University, P.O. Box 150459, Al-Zarqa 13115, Jordan

Received 31 July 2007; received in revised form 29 August 2007; accepted 10 September 2007
Available online 15 September 2007

Abstract

In this work, optimization of multi-residue solid phase extraction (SPE) procedures coupled with high-performance liquid chromatography for the determination of Propoxur, Atrazine and Methidathion from environmental waters is reported. Three different sorbents were used in this work: multi-walled carbon nanotubes (MWCNTs), C18 silica and activated carbon (AC). The three optimized SPE procedures were compared in terms of analytical performance, application to environmental waters, cartridge re-use, adsorption capacity and cost of adsorbent. Although the adsorption capacity of MWCNT was larger than AC and C18, however, the analytical performance of AC could be made close to the other sorbents by appropriate optimization of the SPE procedures. A sample of AC was then oxidized with various oxidizing agents to show that ACs of various surface properties has different enrichment efficiencies. Thus researchers are advised to try AC of various surface properties in SPE of pollutants prior to using expensive sorbents (such as MWCNT and C18 silica).
© 2007 Elsevier B.V. All rights reserved.

Keywords: Activated carbon; Multi-walled carbon nanotubes; C18 silica; Solid phase extraction; Water samples; Pesticides

1. Introduction

Solid phase extraction (SPE) is the most common technique that is used for preconcentration of analytes in environmental waters [1]. In SPE procedure, the choice of appropriate sorbent is a critical factor to obtain full recovery and high-enrichment factor. Multi-walled carbon nanotubes (MWCNTs) have been recently used as preconcentrating sorbent for many organic pollutants [2–19]. On the other hand, activated carbon (AC) is an old sorbent [20], which has been extensively used for preconcentration and sample clean-up. Sometimes it is necessary to take into account the cost of adsorbent in addition to its analytical performance. This is of great importance especially when cheaper sorbent does the job with satisfactory analytical performance. This necessitates performing comparative studies among various sorbents and then deciding which sorbent is the cheapest with appropriate analytical performance.

There are very few comparative studies in the literature among various sorbents. For example, Zhou et al. [6] conducted a comparison of the enrichment efficiency among MWCNTs, AC and C18 silica as sorbents for SPE of Atrazine and Simazine in environmental waters. However, they did not specify the type, surface properties and textural characteristics of the AC used in their study [6]. They proposed that AC did not give the expected extraction efficiency because of its large size and blank volume and less active sites for adsorption. D'Archivio et al. [21] compared different sorbents (C18 silica, graphitized carbon black) and four different polymeric sorbents. Niu et al. [22] compared the enrichment efficiency of MWCNT with C18 silica towards phenolic compounds.

In this work, we report a comparison between AC with MWCNT and C18 silica as SPE sorbents for some pesticides from environmental waters prior to their simultaneous analysis by HPLC. This type of comparisons is rare in the literature. The pesticides involved are model pesticides that have been

* Corresponding author. Tel.: +962 5 390 3333; fax: +962 5 382 6613.
E-mail addresses: amjadelsheikh3@yahoo.com, elsheikh@hu.edu.jo (A.H. El-Sheikh).

0039-9140/$ – see front matter © 2007 Elsevier B.V. All rights reserved.
doi:10.1016/j.talanta.2007.09.005

selected from various common pesticides' categories usually used in Jordan (viz. Atrazine "a triazine herbicide", Propoxur "a carbamate insecticide", Methidathion "an organophosphorus insecticide and acaricide"). One objective of this work is to reach a conclusion whether it is advantageous to use expensive sorbents (such as MWCNT and C18 silica) as SPE sorbent or not. To study the effect of surface properties of AC on its preconcentration efficiency, AC was oxidized by various sorbents to alter its properties.

2. Experimental

2.1. Chemicals

Atrazine, Propoxur and Methidathion standard material were kindly provided by Vegetarian and Agricultural Production Company/VAPCO (Al-Zarqa, Jordan) as 10 μg mL^{-1} solution in acetonitrile. Working solutions were prepared daily by appropriate dilution of the stock solutions with water. Acetonitrile, water and methanol were all of HPLC-grade purchased from TEDIA, Ohio, USA. All other solvents and reagents used were of analytical reagent grade unless stated otherwise. Multi-walled carbon nanotubes (MWCNTs) were purchased from Shenzhen Nanotechport Co. Ltd., Shenzhen, China. MWCNT was of 1–5 μm length and 40–60 nm external diameter. It was treated with nitric acid to open the tube caps. Before use, MWCNTs were dried at 80 °C for 2 h. Specific surface area of the MWCNTs, as determined by N_2 adsorption, was provided by the manufacturer and found to be 40–300 m^2 g^{-1}. Activated carbon (AC) was purchased from Sigma (untreated granular activated charcoal, 20–60 mesh, product number C3014). C18 cartridges were purchased from Supelco.

2.2. Oxidation of the AC and characterization by Boehm titrations

AC was oxidized with various oxidizing agents to study the effect of oxidation on enrichment efficiency towards the target pesticides. Details of oxidation conditions are given in Table 1. Oxidized sorbents were thoroughly washed with doubly distilled water and then dried. The produced sorbents were labelled AC-NA, AC-HP and AC-APS, which refers to AC samples oxidized with nitric acid, hydrogen peroxide and ammonium per-sulphate, respectively. AC refers to the non-oxidized AC. The determination of surface oxides was described by Boehm [23].

2.3. Apparatus

SPE cartridge was prepared by placing the adsorbent in an empty 6 mL polypropylene SPE-tube "filtration tube" (from Supelco). Polyethylene frits (from Supelco) of 20 μm porosity were used to hold the adsorbent packing in the cartridge. Solid phase extraction process was performed using a visiprep-12-port vacuum manifold (from Supelco). The outlet tip of the manifold was connected to a vacuum pump (KNF NEUBERGER D-7800, Germany) and the flow rate was maintained at 6 mL min^{-1}.

HPLC analyses of the target pesticides (Propoxur, Atrazine and Methidathion) were performed using a model 785A programmable absorbance detector and a series 200 LC pump. Separations were performed on a spherisorb ODS2 (150 mm × 4.6 mm, 5 μm) from Dr. Maisch GmbH (Germany). A MetaGuard 2.0 mm Polaris 5 μ C18-A guard column was also used. The mobile phase consisted of acetonitrile and water (60/40 (v/v)), and the flow rate of the mobile phase was set at 1.0 mL min^{-1}. Chromatographic data were acquired and processed at 210 nm using a Perkin-Elmer 1022 LC Plus system.

2.4. General SPE procedure

0.200 g of the adsorbent was packed into the SPE-cartridge and pre-conditioned with 5 mL of acetonitrile then with 5 mL water ahead of the preconcentration procedure. Next, 50 mL of the water sample solution (spiked simultaneously with 50 ng mL^{-1} of Atrazine, Propoxur and Methidathion and adjusted to pH 5) was passed through the cartridge. The cartridge was then washed with 5 mL of 10% acetonitrile aqueous solution to remove co-absorbed matrix materials. Subsequently, the retained Atrazine, Propoxur and Methidathion were eluted with 5 mL of acetonitrile. Twenty microliters of the eluent was injected into HPLC system for quantitative determination.

2.4.1. Adsorption capacity

Adsorption capacity of the sorbents towards the three pesticides was estimated in separate experiments at pH 5 (optimum pH), by passing 50 mL of 5 μg mL^{-1} of each pesticide solution

Table 1
Preparation conditions and surface oxides of AC sorbent with appropriate labelling of the oxidized adsorbents

Adsorbent abbreviation	Oxidation conditions	Boehm titrations				
		a	b	c	d	e
AC	No oxidation	1.46	0	0	0	0
AC-NA	100 mL of concentrated HNO_3, 25 °C, stirring for 24 h.	0.121	2.164	0.613	0.563	0.988
AC-APS	100 mL saturated solution of $(NH_4)S_2O_8$ in 1 M H_2SO_4, 25 °C, stirring for 18 h.	0.135	2.151	0.625	0.288	1.238
AC-HP	Mixture of 50 mL H_2O_2 and 50 mL 1 M H_2SO_4, 50 °C, stirring for 1 h.	0	2.051	0.838	0.438	0.775

a: total basic group (mmol g^{-1}), b: total acidic group (mmol g^{-1}), c: phenolic groups (mmol g^{-1}), d: lactonic groups (mmol g^{-1}), e: carboxylic groups (mmol g^{-1}).

Table 2
Summary of the experimental conditions of the three optimized preconcentration procedures using the adsorbents AC, MWCNT and C18 silica

	Optimized SPE method using AC as sorbent	Optimized SPE method using MWCNT as sorbent	Optimized SPE method using C18 silica as sorbent
Breakthrough volume (mL)	400	400	400
Mass of adsorbent (g)	0.300	0.200	0.400
Washing solvent (mL)	10 mL of 10% acetonitrile aqueous solution	10 mL of 10% acetonitrile aqueous solution	10 mL of 10% acetonitrile aqueous solution
Eluting solvent (mL)	10 mL of acetonitrile	10 mL of acetonitrile	10 mL of acetonitrile

(separately) into a 0.200 g of the sorbent packed in the cartridge and pre-conditioned as described above. The adsorbed pesticide was eluted with 20 mL acetonitrile to ensure full elution.

2.4.2. Analytical performance of the method

Four hundred milliliters of highly purified (doubly distilled de-ionized) water samples were spiked with various concentrations of the three pesticides (simultaneously): 10, 17.5, 25, 37.5, 50, 75, 100 ng mL^{-1} and then enriched using the desired sorbent according to the three optimized SPE procedures described in Section 3.1. SPE experiments were performed in five replicates ($n = 5$) and the five extracts were analyzed as separate samples.

2.5. Water samples

In this work, three types of environmental water samples were used for evaluation of the proposed SPE method; tap water, reservoir water and stream water; using grab sampling in borosilicate glass bottles. Tap water samples were taken after flowing for 10 min from various water taps in our school in different days, and then pooled and used to generate a composite tap water sample. Reservoir water composite sample was generated by collecting various samples from local household reservoirs; which are known to store water for several weeks. Stream water composite sample was generated by collecting various samples from Al-Zarqa stream from various positions at various days. Before use, all the environmental water samples were filtered through 0.45 μm micropore membranes and stored in brown glass bottles at 4 °C.

2.5.1. Application of the proposed method on real water samples

Unspiked real water samples were analyzed according to the optimum SPE procedures. Since real water samples were free of the pesticides according to our procedure, water samples were spiked with the three pesticides (simultaneously) at various concentrations according to the estimated limit of linearity. SPE experiments were performed in five replicates ($n = 5$) and the five extracts were analyzed as separate samples.

3. Results and discussion

3.1. Optimization of SPE procedures

Optimization of SPE procedure using MWCNTs, C18 and AC involved the effect of pH of water sample, washing solvent and its volume, type of eluting solvent and its volume, mass of adsorbent, and breakthrough volume. Details of the optimization process are not presented here. However, a summary of the optimized parameters for simultaneous preconcentration of the three pesticides using MWCNT and C18 silica are given in Table 2. All the three sorbents gave optimum recovery at pH 5. It is noted that the only difference among the three optimized procedures was in the mass of adsorbent required in each procedure, i.e. mass of AC required is 0.300 g; mass of MWCNT required is 0.200 g; mass of C18 silica required is 0.400 g.

3.2. Comparing the performance of the three preconcentration procedures

3.2.1. Analytical performance of the methods

Analytical parameters (linear range, detection limit, relative error range and precision) of the three SPE procedures are shown in Table 3. These results indicate that the precision of the optimized procedure by AC was very close to those obtained by the other two preconcentration procedures. The three preconcentration procedures have satisfactory precision at a very low level and the relative standard deviations %R.S.D. ($n = 5$) was always less than 4.0%. Linear ranges for the three target pesticides were estimated based on the value of the r^2 for the calibration curve. All the procedures were linear in the range 10–50 ng mL^{-1} for the three pesticides. The detection limits of the three pesticides by the three optimized preconcentration methods were close to each other. They were estimated as three times the standard deviation of the blank signal. The relative error range of Atrazine and Propoxur in the three procedures were very close to each other, but the relative error range for Methidathion in case of AC was almost double that in the other two sorbents (MWCNT and C18 silica).

3.2.2. Application of the method on real water samples

Three real environmental water samples (tap water, reservoir water and stream water) were used to validate and compare the three preconcentration methods using MWCNT, C18 silica and AC. The three target pesticides were not found in any of the real water samples by any of the three optimized methods. Thus the real water samples were spiked with the three pesticides (simultaneously) at various concentrations according to the appropriate linear ranges shown in Table 3 for each of the three optimized procedures. SPE experiments were performed in five replicates ($n = 5$) and the five extracts were analyzed as separate samples. Chromatograms from the SPE of spiked real waters using the

Table 3
Adsorption capacity of sorbents and analytical parameters ($n = 5$) of the three optimized preconcentration SPE procedures towards the target pesticides

	Optimized SPE method using AC as sorbent			Optimized SPE method using MWCNT as sorbent			Optimized SPE method using C18 silica as sorbent		
	Pr	At	Me	Pr	At	Me	Pr	At	Me
Adsorption capacity (mg g^{-1})	0.356	0.240	0.456	0.956	0.625	1.11	0.298	0.182	0.413
Linearity range (ng mL^{-1})	10–50	10–50	10–50	10–50	10–100	10–50	10–100	10–50	10–50
r^2	0.9722	0.9810	0.9997	0.9740	0.9990	0.9993	0.9947	0.9968	0.9986
Detection limit (ng L^{-1})	230	94	23	220	58	36	193	78	33
Precision, %R.S.D. range ($n = 5$)	1.9–3.5	1.1–3.6	1.5–2.7	0.39–3.0	0.21–2.8	0.30–2.5	0.75–2.7	1.2–3.1	0.95–2.9
Relative error range (%)	+1 to +8	+3 to +11	+9 to +18	−3 to +10	−2 to +10	+2 to +8	+1 to +10	+2 to +7	+5 to +10

Pr: Propoxur, At: Atrazine, Me: Methidathion.

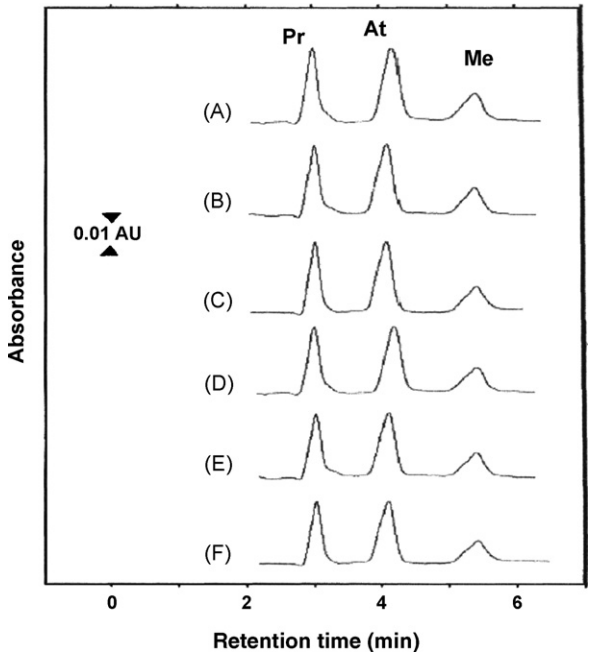

Fig. 1. Chromatograms from the three optimized SPE procedures of various environmental waters. A: reservoir water using MWCNT as sorbent, B: reservoir water using AC as sorbent, C: reservoir water using C18 silica as sorbent, D: tap water using AC as sorbent, E: stream water using AC as sorbent, F: tap water using MWCNT as sorbent. Peaks identification: Pr, Propoxur; At, Atrazine; Me, Methidathion.

three optimized SPE procedures (using AC, MWCNT and C18 silica) are presented in Fig. 1. Spike recoveries of the target pesticides in real water samples for each proposed method are shown in Table 4. It is noted that spike recovery range of the three pesticides with MWCNTs was 81–108%; with C18 silica was 60–95%; while with AC it was 70–98%.

3.2.3. Adsorption capacity and mass of adsorbent required in each optimum procedure

From Table 2, it is noted that the only difference among the three optimized procedures lies in the mass of adsorbent required in each procedure, i.e. mass of AC required is 0.300 g; mass of MWCNT required is 0.200 g; mass of C18 silica required is 0.400 g.

The adsorption capacity of the three sorbents towards the pesticides is presented in Table 3. It is noted that adsorption capacity of the adsorbents was generally in the following order: MWCNT > AC > C18 silica. It is also noted that the adsorption capacity of MWCNT is almost three times that of AC and C18 silica. This explains why 0.300 g of AC and 0.400 g of C18 silica are needed to do the same job as 0.200 g of MWCNT.

3.2.4. Cost of adsorbent

The price of C18 silica from ACROS is US$200 per 50 g, i.e. US$4 per gram. The average price of activated carbon from ACROS and Aldrich is US$75 per kg, i.e. US$0.075 per gram. The price of MWCNT varies from ∼US$20 per gram (from Aldrich) to ∼US$3 per gram (from Shenzhen Nanotechport Co.

Table 4
Spike recovery ranges of the three optimized preconcentration procedures of target pesticides in environmental waters

	Optimized SPE method using AC as sorbent			Optimized SPE method using MWCNT as sorbent			Optimized SPE method using C18 silica as sorbent		
	Pr	At	Me	Pr	At	Me	Pr	At	Me
Tap water	82–90	70–90	81–91	86–96	91–101	85–96	92–94	93–95	85–95
Reservoir water	82–98	80–96	83–92	85–107	93–108	96–104	92–99	70–94	60–87
Stream water	82–91	70–87	81–87	82–102	81–105	81–101	72–94	70–89	73–85

Pr: Propoxur, At: Atrazine, Me: Methidathion.

Ltd., China). This means that MWCNT and C18 silica may be 250 times and 50 times as expensive as AC, respectively.

3.2.5. Cartridge re-use

Experimental results indicated that the three adsorbents may be re-used over 100 times after proper cleaning and re-conditioning. However, it is not always recommended to re-use the cartridge to avoid contamination and error in the results. Additionally, re-using the cartridge necessitates consuming substantial amounts of expensive solvents for cleaning the adsorbent. For the highly expensive MWCNT sorbent, it may be worthy re-using the cartridge, but not in case of cheap sorbents, such as activated carbon.

3.3. Comparing our results with the literature

Zhou et al. [6] conducted a comparison of the enrichment efficiency of MWCNTs, AC and C18 silica as the sorbents for SPE of Atrazine and Simazine in environmental waters. They proposed that "AC did not give the expected extraction efficiency because of its large size and blank volume and less active sites for adsorption".

They did not show the type, surface and textural characteristics of the AC they used. It is recommended that researchers try AC of various chemical and textural properties in SPE of various analytes before attempting to use expensive sorbents. Our results reveal that there is a contradiction with the results obtained with Zhou et al. [6]. However, we would like here to state that adsorption characteristics of certain pollutants may vary with the surface chemistry and textural properties of AC. Thus changing the type of AC or altering the properties of AC may enhance or reduce adsorption of certain pollutants if the AC selected has appropriate properties for adsorption of those pollutants. For that purpose, it was considered reasonable to try altering the surface properties of AC by oxidation and then studying its effect on enrichment efficiency.

3.4. Effect of oxidation of AC

The aim of this section is to show that AC of various surface properties has different enrichment efficiencies. It is known [23] that oxidation of AC usually enhances the quantity of carboxyl groups on the surface of AC. Various oxidized AC sorbents (AC-NA, AC-APS and AC-HP) were used as a SPE sorbents at various pH values of the target pesticides. Results and details of the SPE experiments are shown in Fig. 2. Surface oxides of oxidized and non-oxidized ACs are presented in Table 1. It is generally noted that the non-oxidized AC and the oxidized ACs all gave the highest recoveries for the three pesticides (Propoxur, Atrazine and Methidathion) at pH 5. Comparing the percentage recovery when using the oxidized AC with the non-oxidized AC generally reveals that oxidation of the AC with various oxidizing agents reduced the recovery. This is probably due to carboxyl groups (formed upon oxidation of carbon surface) which tend to form water clusters on the micropores' openings in the AC surface [24] and thus blocking pesticides from entering the micropores. It is noted that the lowest recov-

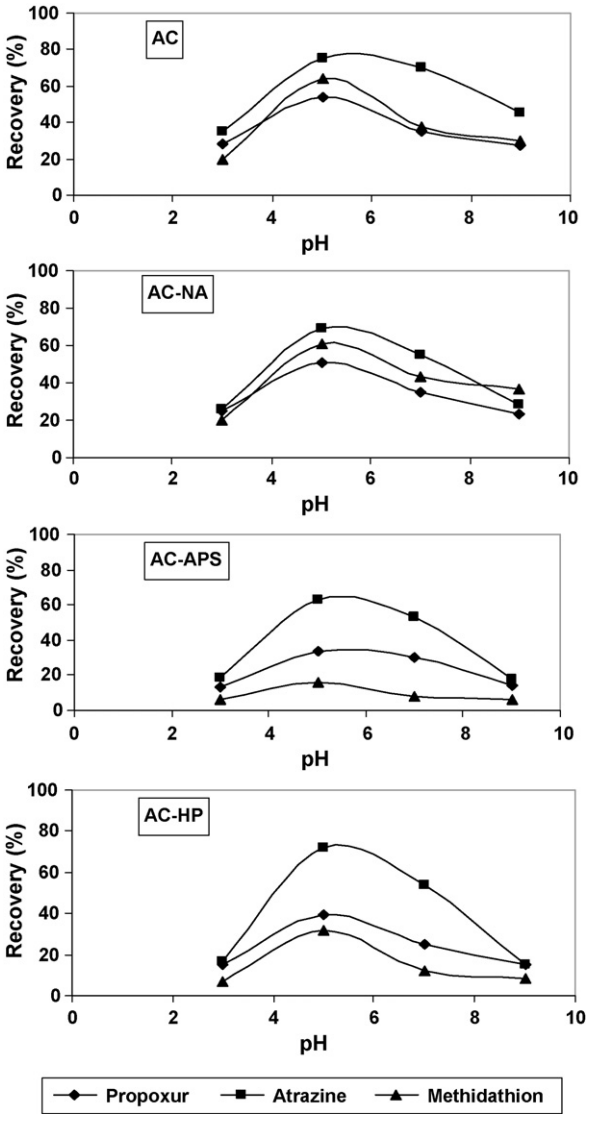

Fig. 2. Effect of oxidation of AC on percentage recovery of the pesticides from water at various pH values: 50 mL water sample spiked with 50 ng mL^{-1} of the three target pesticides; 0.200 g adsorbent; washing solvent: 5 mL of 10% acetonitrile aqueous solution; eluting solvent: 5 mL of acetonitrile.

eries of the three pesticides were obtained when AC-APS was used as preconcentrating sorbent.

4. Conclusion

Using non-oxidized AC as preconcentrating sorbent in SPE of Propoxur, Atrazine and Methidathion gave satisfactory results when applied to environmental waters. Analytical performance was comparable to those obtained with MWCNTs and C18 silica. Although MWCNT has more adsorption capacity towards the selected pesticides, however AC is superior over the other sorbents in that it is much cheaper. Thus it is not always advantageous to use expensive sorbents in SPE of analytes. It is recommended that researchers try AC of various chemical and textural properties in SPE of various analytes before attempting to use expensive sorbents. There should be a balance between cost and benefits in using the proper sorbent. Studying the effect of AC oxidation on SPE process indicated that surface chemistry may have an effect on the SPE process. For example, the generation of carboxyl groups will form water clusters that block pore openings and hinder adsorption. Therefore, to enhance the enrichment performance of AC, authors should try AC of various textural properties and surface chemistry.

Acknowledgements

The authors are grateful for the Faculty of Scientific Research for the financial support; and for VAPCO (Al-Zarqa, Jordan) for donating standard pesticides' solutions. The technical assistance of Rehab Banat, Mazen Musa, Basem Nasr-Allah and Einas Nabeeh is highly appreciated.

References

[1] E.M. Thurman, M.S. Mills, in: J.D. Winefordner (Ed.), Chemical Analysis, vol. 147, John Wiley & Sons, Inc., New York, 1998.
[2] M. Valcarcel, B.M. Simonet, S. Cardenas, B. Suarez, Anal. Bioanal. Chem. 382 (2005) 1783.
[3] A. Merkoci, Microchim. Acta 152 (2006) 155.
[4] Y.Q. Cai, G.B. Jiang, J.F. Liu, Q.X. Zhou, Anal. Chem. 75 (2003) 2517.
[5] Y.Q. Cai, G.B. Jiang, J.F. Liu, Q.X. Zhou, Anal. Chim. Acta 494 (2003) 149.
[6] Q.X. Zhou, W.D. Wang, J.P. Xiao, J.H. Wang, G.G. Liu, Q.Z. Shi, G.L. Guo, Microchim. Acta 152 (2006) 215.
[7] G. Liu, J. Wang, Y. Zhu, X. Zhang, Anal. Lett. 37 (2004) 3085.
[8] Y.Q. Cai, Y.E. Cai, S.F. Mou, Y.Q. Lu, J. Chromatogr. A 1081 (2005) 245.
[9] Q.X. Zhou, W.D. Wang, J.P. Xiao, Anal. Chim. Acta 559 (2006) 200.
[10] Q.X. Zhou, J.P. Xiao, W.D. Wang, Anal. Sci. 23 (2007) 189.
[11] R.Q. Long, R.T. Yang, J. Am. Chem. Soc. 123 (2001) 2058.
[12] S.F. Xiao, Z.H. Wang, G.A. Luo, Chin. J. Anal. Chem. 33 (2005) 261.
[13] Q.X. Zhou, Y.J. Ding, J.P. Xia, Chromatographia 65 (2007) 25.
[14] Q.X. Zhou, J.P. Xiao, W.D. Wang, Microchim. Acta 157 (2007) 93.
[15] J.X. Wang, D.Q. Jiang, Z.Y. Gu, X.P. Yan, J. Chromatogr. A 1137 (2006) 8.
[16] M. Biesaga, K. Pyrzynska, J. Sep. Sci. 29 (2006) 2241.
[17] G.Z. Fang, J.X. He, S. Wang, J. Chromatogr. A 1127 (2006) 12.
[18] F. Zheng, D.L. Baldwin, L.S. Fifield, N.C. Anheier, C.L. Aardahl, J.W. Grate, Anal. Chem. 78 (2006) 2442.
[19] P. Liang, Q. Ding, F. Song, J. Sep. Sci. 28 (2005) 2339.
[20] R. Bansal, J. Donnet, F. Stoeckli, Active Carbon, Marcel Dekker, New York, 1988.
[21] A.A. D'Archivio, M. Fanelli, P. Mazzeo, F. Ruggieri, Talanta 71 (2007) 25.
[22] H. Niu, Y. Cai, Y. Shi, F. Wei, J. Liu, S. Mou, G. Jiang, Anal. Chim. Acta 594 (2007) 81.
[23] H.P. Boehm, Carbon 40 (2002) 145–149.
[24] C. Ania, J. Parra, J. Pis, Fuel Process. Technol. 77/78 (2002) 337.

Available online at www.sciencedirect.com
ScienceDirect
Talanta 74 (2008) 1355–1362
Talanta
www.elsevier.com/locate/talanta

Electrochemical, HPLC and electrospray ionization mass spectroscopic analyses of peroxycitric acid coexisting with citric acid and hydrogen peroxide in aqueous solution

Begum Nadira Ferdousi, Md. Mominul Islam, Takeyoshi Okajima, Takeo Ohsaka *

Department of Electronic Chemistry, Interdisciplinary Graduate School of Science and Engineering, Tokyo Institute of Technology, Mail Box G1-5, 4259 Nagatsuta, Midori-ku, Yokohama 226-8502, Japan

Received 9 August 2007; accepted 9 September 2007
Available online 16 September 2007

Abstract

We successfully determined the molecular structure of peroxycitric acid (PCA) coexisting in the aqueous equilibrium mixture with citric acid (CA; 1,2,3-tricarboxylic-2-hydroxy propane) and hydrogen peroxide (H_2O_2) by a combined use of reversed-phase HPLC (RP-HPLC), potentiometric, hydrodynamic chronocoulometric (HCC) and electrospray ionization mass spectroscopic (ESI-MS) methods. Firstly, the RP-HPLC was employed to separate CA, PCA and H_2O_2 coexisting in the equilibrium mixture and the concentration of CA consumed (ΔC_{CA}) in the formation of PCA that was evidenced to be fairly stable during the RP-HPLC measurement was quantitatively measured based on the standard calibration curve of CA. Secondly, the total oxidant concentration (C_{Ox}) corresponding to peroxycarboxylic (–COOOH) group in PCA in the equilibrium mixture was determined using potentiometric measurement. The ratio of $C_{Ox}/\Delta C_{CA}$ was found to be 1.07, which indicates that only one –COOH group in CA molecule is oxidized to the corresponding –COOOH group in PCA molecule. Thirdly, using the HCC technique the diffusion coefficient of PCA, which could be electroreduced at a more positive potential by 1.0 V than the coexisting H_2O_2, was independently measured as 0.3×10^{-5} cm^2 s^{-1} and at the same time, by considering ΔC_{CA} as the concentration of PCA, the number of electrons (n) required for the reduction of PCA was determined to be 2. The result obtained from RP-HPLC and HCC, i.e., $n = 2$ which is equivalent to one –COOOH group in PCA, is in agreement with that obtained from the combination of RP-HPLC and potentiometric measurements. Finally, the structure of PCA was proposed to contain one –COOOH group with a molecular mass of 208 confirmed by negative ion ESI-MS method. A probable molecular structure of PCA was discussed.
© 2007 Elsevier B.V. All rights reserved.

Keywords: Peroxycitric acid; Potentiometric measurement; HPLC and ESI(−)-MS measurements; Equilibrium mixture; Molecular structure

1. Introduction

Peroxycarboxylic acids (POCAs) have been increasingly used as the alternative oxidants of chlorine, ozone and hydrogen peroxide (H_2O_2) for chemical processing and synthesis, bleaching and disinfection purposes [1–7,10–13]. The well-known POCA, peroxyacetic acid (PAA) coexisting with H_2O_2 and acetic acid (AA), has received FDA (food and drug approval) in 1986 and has been widely used as a cleaning-in-place oxidizer in various industries. Recently, we have first synthesized peroxycitric acid (PCA) by the reaction of citric acid (CA) and H_2O_2 in the presence of H_2SO_4 and solid superacid catalysts (Eq. (1)) [5]. The choice of CA would provide a hygienic POCA (i.e., PCA), since CA is a biological molecule and continuously produced in the human respiratory system. Moreover, PCA could be promising in using as a food preservative [6].

PCA is formed typically by an acid-catalyzed nucleophilic substitution reaction (Eq. (1)) [7]. Nevertheless, three carboxylic (–COOH) groups of CA may not be chemically equivalent towards the oxidation reaction by H_2O_2, because one –COOH group of CA is adjacent to –OH group (see Eq. (1)) as well as the pK_a values of three –COOH groups are different, i.e., 3.1, 4.6 and 6.4 [8,9]. Thus, the equilibrium mixture (Eq. (1)) may contain PCA with a unique structure (i.e., PCA1, PCA2 or PCA3) or a mixture of PCAs (i.e., PCA1, PCA2 and PCA3). Unfortunately, PCA could not be isolated from the aqueous solution. In this connection, the controversial results regarding the structures of some POCAs, e.g., peroxy-succenic and peroxy-glutaric acids

* Corresponding author. Tel.: +81 45 924 5404; fax: +81 45 924 5489.
E-mail address: ohsaka@echem.titech.ac.jp (T. Ohsaka).

0039-9140/$ – see front matter © 2007 Elsevier B.V. All rights reserved.
doi:10.1016/j.talanta.2007.09.006

synthesized from succenic and glutaric (dicaboxyalic) acids, respectively, would be mentioned [10–13]. In fact, both mono- and di-peroxy structures of peroxy-succenic and peroxy-glutaric acids have been proposed. Thus, the determination of the molecular structure of PCA in the equilibrium mixture (Eq. (1)) is not straightforward.

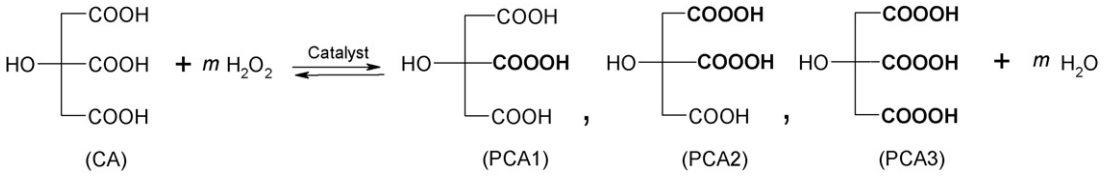

(1)

On the other hand, Klaas et al. have synthesized different POCAs including a peroxyacid from citric acid triethylester (CAT) using an enzyme catalyst (Novozyme®435) [6]. The authors did not mention the details of the determination of structure of the peroxyacid from CAT, but the obtained peroxyacid has been reported to contain one peroxycarboxylic (–COOOH) group based on a gas chromatography-mass measurement, i.e., the ultimate product may be called monoperoxycitric acid diethylester. Such conversion of one ethylester group into –COOOH group among the available three triethylester groups of CAT may be possible since the enzymatic reaction is regioselective. Nevertheless, it needs to be clarified that how many –COOH groups of CA are converted into –COOOH groups in forming PCA in the presence of acid catalyst.

Several methods, e.g., titration [14–16], UV–vis spectrophotometric [17], chromatographic [18–21], ex situ and in situ infrared spectroscopic [22–25], potentiometric [26–28] and voltammetric [29–31,33] techniques have been known for the detection of POCA in equilibrium mixture, but they are related to the total quantity of the oxidant in the solution (i.e., total amount of –COOOH groups) and thus are incapable of telling about the number of –COOOH groups of a POCA synthesized from a carboxylic acid containing more than one –COOH groups (e.g., CA). Thus, the characterization of PCA seems to be challenging, indeed. One the other hand, very recently, PCA could be successfully separated from the coexisting CA and H_2O_2 using a reversed-phase high performance liquid chromatography (RP-HPLC). Furthermore, PCA has been found to be electroreduced at a more positive potential by ca. 1.0 V than the coexisting H_2O_2 [32].

In the present study, we could successfully determine the molecular structure of PCA without isolating from the aqueous equilibrium mixture by combining RP-HPLC, potentiometric and hydrodynamic chronocoulometric (HCC) measurements. The determination of the molecular structure of PCA is definitely important from the points of view of its quantitative analysis that lacks the authentic sample required for the internal calibration as well as the ultimate goals of its synthesis and applications. In addition, this combined approach would be applicable in other cases where similar complicacy is involved in determining the structure of reaction product(s) in the equilibrium mixture. The obtained structure of PCA was further confirmed by measuring the molecular mass of PCA by a negative ion electrospray ionization mass spectroscopic [38,39] [ESI(−)-MS] technique. A discussion on the feasibility of the proposed molecular structure of PCA was also given.

2. Methodologies

As is mentioned above, PAA [29,30] and PCA are electroactive and PCA can be reduced at ca. 1.0 V more positive potential than the coexisting H_2O_2 [32]. It is also noted that in aqueous solution one –COOOH group of POCA is electroreduced to the parent –COOH group by consuming two electrons as can be expressed by Eq. (2) [29]

$$\text{–COOOH(e.g., PAA)} + 2H^+ + 2e^- \rightarrow \text{–COOH(e.g., AA)} + H_2O \quad (2)$$

Therefore, one can know the molecular structure of PCA by knowing the number of electrons (n) required for its reduction, e.g., the n values of 2, 4 and 6 correspond to one, two and three –COOOH groups in POCA, respectively.

Both voltammetric and coulometric methods would be the first choice to evaluate the value of n. The output results obtained by these techniques generally involve n, C (concentration) and D (diffusion coefficient) variables together in a single equation, i.e., two variables should be previously known to estimate the third one [34,35]. On the other hand, the hydrodynamic chronocoulometry (HCC) technique [34] that involves the fundamental equations (3)–(6) advantageously enables the determination of the value of D independently by solving Eqs. (4) and (5) without previously knowing the values of n and C.

$$Q = Q_\delta + I_L t \quad (3)$$

with

$$Q_\delta = 0.3764 n F A C \delta \quad (4)$$

$$I_L = \frac{n F A D C}{\delta} \quad (5)$$

where I_L, F and A are the Levich limiting current, Faraday constant and electrode area, respectively, and Q_δ is the charge passed in electrolysis of species contained initially in the hydrodynamic boundary layer, which has the thickness δ.

$$\delta = 1.610 D^{1/3} \nu^{1/6} \omega^{-1/2} (1 + 0.2980 Sc^{-1/3} + 0.14514 Sc^{-2/3}) \quad (6)$$

where ν is the kinematic viscosity of the solution, Sc the Schimdt number (ν/D), and ω is the electrode angular velocity ($\omega = 2\pi f$, where f is the frequency of the electrode rotation).

Here, dividing Eq. (4) by Eq. (5), we can get Eq. (7) as

$$\frac{Q_\delta}{I_L} = \frac{0.3764 \delta^2}{D} \quad (7)$$

By comparing Eq. (7) with Eq. (6), one can write

$$\frac{Q_\delta}{I_L} = 0.9757\left(\frac{\nu}{D}\right)^{1/3}\omega^{-1} \quad (8)$$

That is,

$$D = \left\{0.9757\left(\frac{I_L}{Q_\delta}\right)\omega^{-1}\right\}^3 \nu \quad (9)$$

The values of I_L, Q_δ, ω and ν in the right hand side of Eq. (9) can be obtained from the experimental conditions and results. Thus, Eq. (9) provides the value of D. Consequently, one can get the product of nC as a numerical value by comparing Eq. (9) either with Eq. (4) or Eq. (5).

Although the HCC method makes the present problem relatively simpler, this single electrochemical technique is still incapable of obtaining the value of n since the C of PCA (C_{PCA}) in the equilibrium mixture is unknown. On the other hand, C_{PCA} can be estimated from RP-HPLC measurement because the species (PCA, CA and H_2O_2) coexisting in the reaction mixture as shown by Eq. (1) could be fortunately separated. In fact, the RP-HPLC enables us to measure quantitatively the concentration of CA (C_{CA}) using the standard calibration curve of CA. If the loss in C_{CA} due to the reaction shown by Eq. (1) is assumed to convert solely into PCA, then the value of C_{PCA} can be obviously estimated by subtracting the value of the C_{CA} (final) from C_{CA} (initial) used for the formation of PCA [i.e., $\Delta C_{CA} = C_{CA}$ (initial) $- C_{CA}$ (final)]. Thus, by putting the values of ΔC_{CA} ($=C_{PCA}$) and D obtained from RP-HPLC and HCC (Eq. (9)), respectively, either into Eq. (4) or Eq. (5), we may estimate the value of n required for the reduction of one PCA molecule and hence the number of –COOOH groups in PCA.

On the other hand, the total oxidant concentration (C_{Ox}) corresponding to –COOOH groups in the PCA solution obtained by potentiometric [26,27] and cerimetric–iodometric titrations [16] would be compared with ΔC_{CA}. The ratio of $C_{Ox}/\Delta C_{CA}$ would also provide the number of –COOOH groups involved in one PCA molecule, in other words, the value of a stoichiometric factor, m in Eq. (1).

3. Experimental

3.1. Cautionary note!

POCA solutions are generally a severe irritant to eyes, skin and mucous membranes. The mixture of PCA and H_2O_2 is a strong oxidizing agent that can form explosive mixtures. Therefore, PCA solution should be handled carefully to avoid any contact, and the concentrated solution of PCA should be mixed with neither reducing agents nor organic substances, including solvents.

3.2. Chemicals and synthesis of PCA

All the chemicals were of analytical grade and the solutions were prepared or diluted with deionized water (Milli-Q, Millipore, Japan). Monohydrated CA (1,2,3-tricarboxylic-2-hydroxy propane, purity 99.5%) and HPLC grade 60.0% perchloric acid ($HClO_4$) were purchased from Kanto Chemical Co. Inc., Japan. 30.0–35.0% H_2O_2, 98.0% H_2SO_4 were available from Wako Pure Chemical Industries, Japan. The preparation of PCA was described in our previous paper [5]. Shortly, PCA was synthesized in a flat-bottomed glass vessel of 200 ml volume placed in a constant temperature bath of 4 °C. Typically, 10 ml of 2.0 M CA solution and 0.5 M H_2SO_4 acid catalyst or 10% (w/v) solid superacid catalyst (Dowex DR-2030, Aldrich Chemical Co., Japan) were taken in the reaction vessel and 10 ml of 10.0 M H_2O_2 was added dropwise with a slow stirring by magnetic stirrer over 20 min. Then the reaction mixture was allowed to stand for 2–7 days for attaining the equilibrium at room temperature (25 °C). The progress of the reaction was monitored with conventional cerimetric–iodometric titrations [16], RP-HPLC and potentiometric measurements [5]. In this study, the catalysts were removed either by RP-HPLC (H_2SO_4 catalyst) or simple filtration (solid superacid catalyst) methods, if necessary. All measurements were carried out with the equilibrium reaction mixture at appropriate dilutions.

3.3. Electrochemical instrumentations and procedures

Electrochemical measurements were carried out using a computer-controlled electrochemical system (Model: ALS/CHI 832A). The electrochemical cell for the voltammetric measurements was a conventional two-compartment Pyrex glass container with an Au ($\phi = 2.0$ mm and geometrical area: 0.0314 cm^2) working electrode, a spiral Pt-wire counter electrode and an Ag/AgCl/KCl (sat.) reference electrode. The Au electrodes were polished with aqueous slurries of successively finer alumina powder (down to 0.06 μm) and were sonicated for 10 min in Milli-Q water. The working electrode was electrochemically pretreated in N_2-saturated 0.05 M H_2SO_4 solution by repeating the potential scan in the range of −0.2 to 1.5 V until the voltammogram characteristic for the clean Au electrode was obtained. The geometrical area of Au electrode (0.0314 cm^2) was used for calculation. Before each voltammetric measurement, the solution was de-aerated with N_2 gas for 15 min.

The HCC measurements were carried out within the potential range of 0.5–0.1 V [32] that corresponds to only the reduction of PCA, as shown by the cyclic voltammetric measurement. In addition, the HCC measurements were performed by varying the electrode rotation speeds from 200 to 1600 rpm. In the calculation, the ν value of 0.0098 $cm^2\ s^{-1}$ was used [29].

The potentiometric measurement was performed using a Pt ($\phi = 1.6$ mm) indicator electrode in the potential buffer solution of triiodide (I_3^-)/iodide (I^-) redox couple [5,26,27]. I_3^- (I_2) was in situ prepared by the electrolysis of I^- (KI) at 1.0 V in 0.05 M acetate buffer solution (pH 6.0). Using the optimized Nernst equation presented for the potentiometric measurements [$\Delta E = 29.6\ \log(1 + C_{Ox}/[I_3^-])$, where ΔE and C_{Ox} are the apparent potential change at the indicator electrode and the concentration of oxidant, respectively] published elsewhere [5,26], the value of C_{Ox} (–COOOH group) was calculated using the corresponding transient potential change. All the measurements were carried out at room temperature (25 ± 2 °C).

3.4. RP-HPLC apparatus and measurement procedures

The RP-HPLC [41] measurement unit consists of mainly five parts such as pump (Model 7410, GL Science, USA), UV detector (Model 7450, GL Science, USA), column-oven (Model 7432, GL Science, USA), autosampler (Model L-7200, Hitachi, Japan) and a personal computer for data acquisition with software (EZChrome *elite*, Scientific Software, Inc., CA, USA). The used column was Intersil C8-3 [5 μm 250 × 4.6 mm i.d.] and bonded phase is $-(CH_2)_7CH_3$ group]. All the RP-HPLC measurements were carried out at optimized conditions regarding eluting solvent, additive, flow rate, column temperature and so on. The eluting solution was 3.0 mM $HClO_4$ (pH 2.5) containing 33.0 mM $NaClO_4$ additive. The flow rate of the eluting solution, the volume of the injected sample and the column temperature were 0.5 ml/min, 10 μl, and 25 °C, respectively. Each measurement was repeated thrice for confirming the reproducibility. The calibration curve for CA was constructed by measuring the chromatograms of CA solutions of various concentrations prepared by dissolving CA crystal. The peak area of the chromatogram integrated by the EZChrome *elite* software was plotted against the corresponding C_{CA}.

3.5. ESI(−)-MS measurements

Mass spectrometric analysis was performed using LC/MS/MS system (Model: API 3000, Applied Biosystems, USA) equipped with negative electrospray ionization (ESI) apparatus. The flowing solvent was acetonitrile and its flow rate was 10 μl/min. N_2 was used as nebulizing gas. The mass measurements were carried out with a negative ESI mode [37–39]. Mass spectra were acquired by scanning from mass to charge ratio (m/z) of 50–1000, and the ionization voltage and scan speed were 4000 V and 10 s, respectively.

4. Results and discussion

4.1. RP-HPLC measurement

Fig. 1 represents the typical chromatograms obtained for H_2O_2 (a), CA (b) and the equilibrium mixture of PCA, CA and H_2O_2 (c). From the obtained chromatograms (a) and (b), the retention times of H_2O_2 and CA were determined to be 6.0 and 14.0 min, respectively. In a separate measurement, it was observed that H_2SO_4 used as the acid catalyst for the synthesis of PCA (Eq. (1)) was found to elute at the retention time of H_2O_2 (data is not shown). By comparing the chromatogram (c) with those of (a) and (b), we can see that a new peak appeared with retention time of 13.3 min. In fact, this new peak corresponds to PCA in the equilibrium mixture. It can be noted that no other peak that may correspond to the by-product was observed, indicating that any loss in C_{CA} in the case of chromatogram (c) may be solely attributed to the new peak of PCA (discussed later). The mechanism of such separation of CA and PCA is beyond the scope of the present study and will be published elsewhere, but it could be noted that the areas

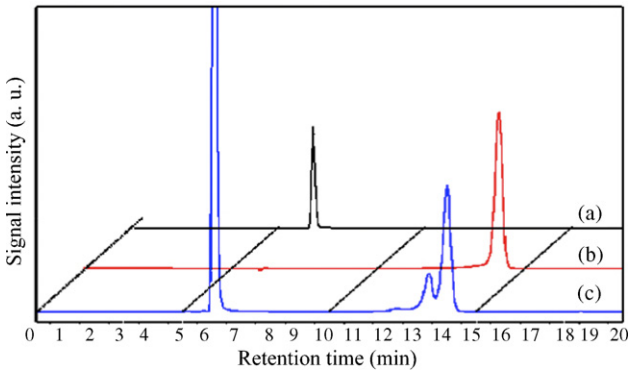

Fig. 1. RP-HPLC chromatograms obtained for 2.1 mM H_2O_2 (a), 10.0 mM CA (b) and the equilibrium reaction mixture (c). Eluting solution: 3.0 mM $HClO_4$ containing 33.0 mM $NaClO_4$ (pH 2.5), flow rate: 0.5 ml min^{-1} and the column temperature: 25 °C. The reaction mixture was allowed to stand for 3 days to attain the equilibrium in the presence of H_2SO_4 catalyst.

of the peaks of CA (A_{CA}) and H_2O_2 increased linearly with their successive standard additions. Within the necessity of this study, we will only confine our attention to the peaks of CA and PCA and several chromatograms for CA were measured by varying C_{CA} to construct a calibration curve of A_{CA} versus C_{CA}.

Fig. 2 shows the plot of A_{CA} versus C_{CA} (a) and the overlaid chromatograms of CA (b) and the reaction mixture (c). The plot of A_{CA} versus C_{CA} is a straight line passing through the

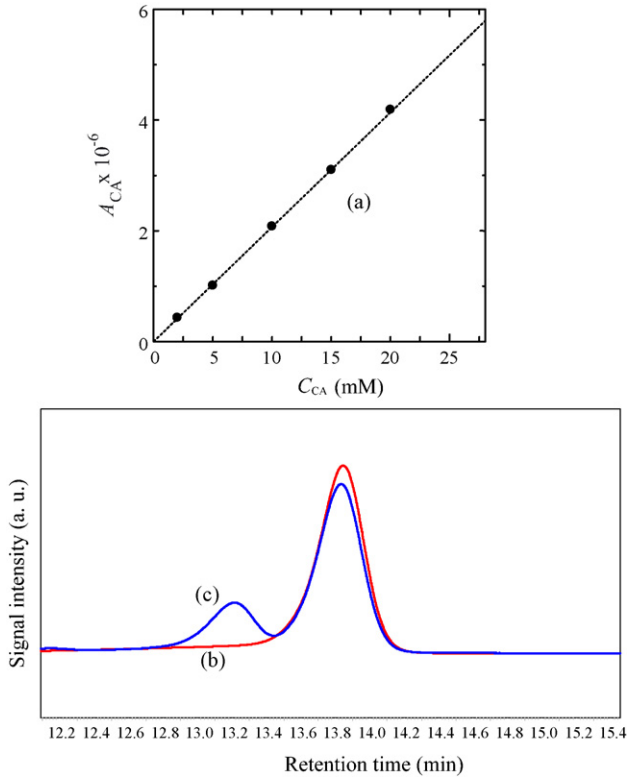

Fig. 2. A calibration curve, A_{CA} vs. C_{CA}, of CA obtained from the RP-HPLC chromatograms measured by varying the concentration of CA (a) and a comparison of chromatograms for CA measured initially (b) and after attaining the equilibrium (c). The chromatograms (b) and (c) were taken from Fig. 1.

Table 1
Analyses of reaction mixtures[a] containing PCA, CA and H_2O_2 using HPLC, HCC, potentiometric and ESI(−)-MS methods

Run	HPLC			Potentiometric C_{Ox} (M)	Average ratio of $C_{Ox}/\Delta C_{CA}$	HCC			Molecular mass of PCA
	C_{CA} (initial) (M)	C_{CA} (final) (M)	ΔC_{CA} (=C_{PCA}) (M)			D_{PCA} ($\times 10^5$/cm^2 s^{-1})	nC_{PCA} (M)	Average, $n = nC_{PCA}/\Delta C_{CA}$	
1	1.0	0.86	0.14	0.15	1.07				
2	1.0	0.86	0.14	0.15	1.07	0.3	0.285	∼2	208
3	0.95	0.80	0.15	0.16	1.06				

[a] The initial concentrations of CA and H_2O_2 were 1.0 and 5.0 M, respectively, in the presence of 0.5 M H_2SO_4 catalyst.

origin with a regression coefficient of 99.73%. From the obtained calibration curve, the values of C_{CA} (initial) and C_{CA} (final) (i.e., unreacted CA in the reaction mixture) were estimated using the values of A_{CA} (initial) and A_{CA} (final) obtained from the chromatograms (b) and (c), respectively. Then the values of C_{CA} (initial) and C_{CA} (final) were used to determine ΔC_{CA} (Table 1).

4.2. HCC measurements

Fig. 3 shows typical HCC curves obtained for the reduction of PCA coexisting with CA and H_2O_2 in aqueous acetate buffer solution (pH 4.0). The electrode potential was stepped from 0.5 to 0.1 V. In this potential range, the reduction of PCA has been characterized as an irreversible, diffusion-controlled process and the reduction of H_2O_2 does not take place [32]. Thus, the obtained charge (Q)–time (t) curves correspond to only the reduction of PCA. A linear regression for each curve was carried out over the electrolysis time domain between 1.2 and 1.5 s, where a steady-state current condition was reached. The straight line obtained by such a linear regression can be expressed by the Q–t relationship (Eq. (3)).

The plots of Q_δ versus $\omega^{-1/2}$ and I_L versus $\omega^{1/2}$ were derived from the obtained Q–t curves (Fig. 3) and the thus-obtained plots are shown in Fig. 4. According to Eqs. (4) and (5), both plots should be the straight lines passing through the origin that are practically observed in Fig. 4. The slopes of the obtained plots were estimated and compared with each other. Eventually, the value of D_{PCA} was determined to be 0.3×10^{-5} cm^2 s^{-1} (discussed above). The obtained value of D_{PCA} [32] is significantly smaller than that of CA (0.71×10^{-5} cm^2 s^{-1}) [36]. It can be noted that the diffusion coefficient of PAA (0.73×10^{-5} cm^2 s^{-1}) [29] is twofold smaller than that (1.27×10^{-5} cm^2 s^{-1}) of AA [36], suggesting that the diffusion coefficient of POCA is smaller than that of the corresponding parent acid. This fact may be reasonably acceptable since POCA has larger molecular mass than that of the parent acid. In the present case, the observed smaller D_{PCA} than that of CA [36] may also be acceptable. Here, Eq. (4) or (5)

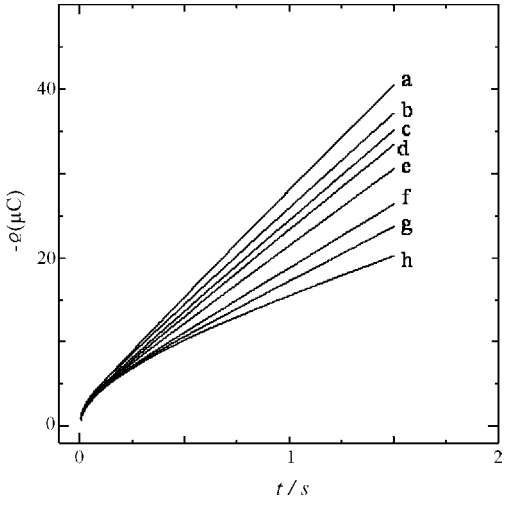

Fig. 3. Typical Q–t curves measured using HCC for the reduction of 0.8 mM PCA at a rotating Au disk electrode in N_2-saturated 0.1 M acetate buffer solution (pH 4.5) containing 0.1 M Na_2SO_4. Electrode rotation speeds: (a) 1600 rpm, (b) 1400 rpm, (c) 1200 rpm, (d) 1000 rpm, (e) 800 rpm, (f) 600 rpm, (g) 400 rpm and (h) 200 rpm. The electrode potential was stepped from 0.5 to 0.1 V.

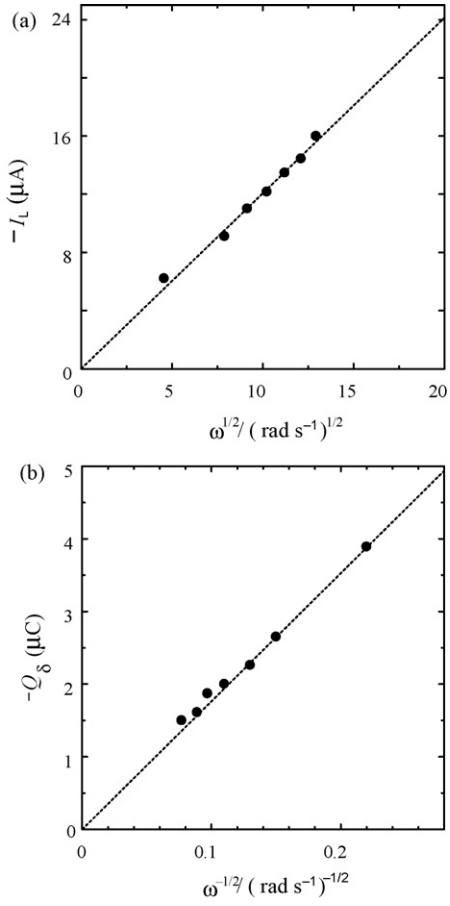

Fig. 4. The plots of (a) $-I_L$ vs. $\omega^{1/2}$ and (b) $-Q_\delta$ vs. $\omega^{-1/2}$ obtained for the reduction of PCA. Data were derived from the Q–t curves shown in Fig. 3.

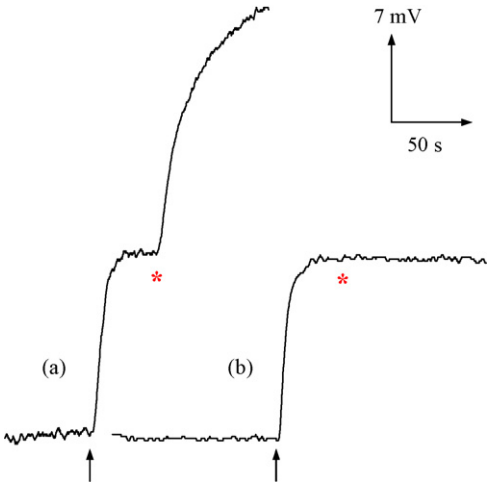

Fig. 5. Potential change of the Pt indicator electrode by the addition of 2 μl of the equilibrium reaction mixture without (a) and with (b) separation of H_2O_2 using HPLC shown in Fig. 1c into 20 ml of 0.05 M acetate buffer solution (pH 6.0) containing 0.007 mM I_3^- and 10 mM I^-. The curve (b) was measured just after the HPLC separation of the analyte (after ca. 10 min from the separation of H_2O_2). The upward arrow and the asterisk marks indicate the addition of the reaction mixture and Mo(VI) catalyst into the buffer solution, respectively.

was recalled to estimate the value of nC_{PCA} using the obtained value of D_{PCA} and all the estimated values are also summarized in Table 1.

4.3. Potentiometric measurement

Fig. 5 shows the potentiometric response obtained for the addition of the reaction mixture (a) directly and (b) after the separation of H_2O_2 using HPLC (Fig. 1) into the potential buffer solution containing the I^-/I_3^- redox couple. The measured potential–time curves (curves a and b) represent a transient potential change (ΔE) within a few seconds followed by a slow potential change (curve a), that was accelerated by adding Mo(IV) catalyst, of the indicator electrode [5]. This transient ΔE quantitatively reflects the amount of oxidant (i.e., C_{Ox}) corresponding to the –COOOH group of PCA coexisting with H_2O_2 in the reaction mixture estimated using the optimized Nernst equation [26,27]. In both measurements, the value of C_{Ox} was found to be the same, indicating that the products formed by the reaction shown in Eq. (1) are sufficiently stable within the time scale of the HPLC measurement. On the other hand, the value of C_{Ox} was also measured using cerimetric–iodometric titrations [16]. Both methods gave excellent agreement for C_{Ox}. The ratios of $C_{Ox}/\Delta C_{CA}$ were found to be 1.07 (Table 1), which is equivalent to one –COOOH group in PCA molecule.

4.4. ESI(−)-MS measurements

The typical ESI(−)-MS spectra measured for the reaction mixture containing PCA and CA (a) and only CA (b) in aqueous $HClO_4$ solution are shown in Fig. 6. In the case of spectrum a, the RP-HPLC fragment of both CA and PCA eluted in retention time range of about 12–15 min (seen in Fig. 1c) was used for the ESI(−)-MS measurement, i.e., the reaction mixture was

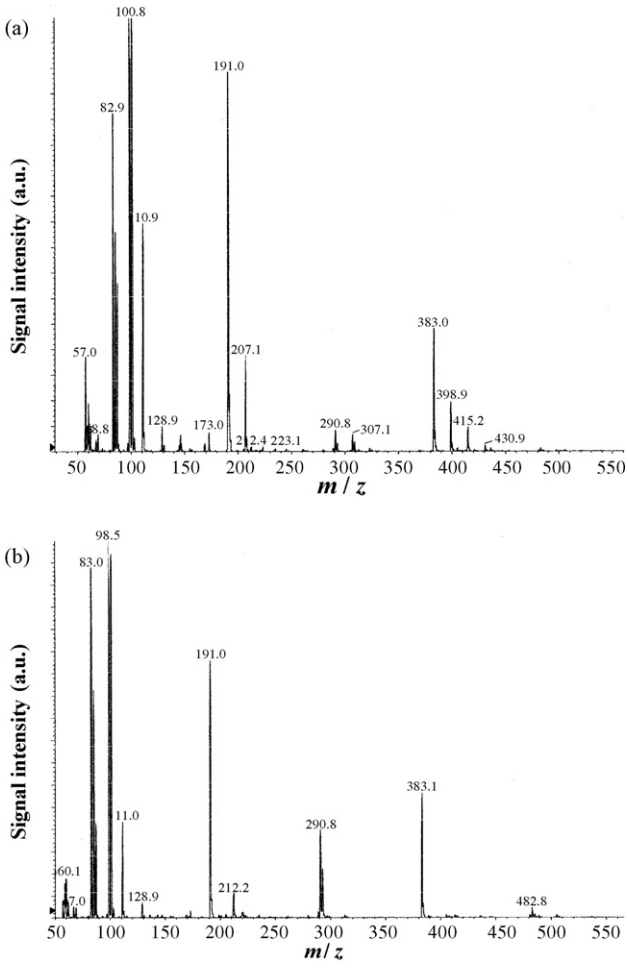

Fig. 6. ESI(−)-MS spectra obtained for (a) the reaction mixture containing PCA and CA and (b) CA in aqueous perchloric acid solution.

made free from corrosive H_2SO_4 (concentrated) catalyst as well as excess H_2O_2. Several peaks were found at m/z values larger (191.0, 207.1, 383.0, 398.9 and 415.2 with some other peaks with noise level intensities) and lower (57.0, 82.9, 100.8 and 110.9) than the molecular mass of CA ($M = 192$). In the case of CA (Fig. 6b), the peak at m/z of 191.0 was observed along with similar additional peaks. In comparison of the spectral results of the reaction mixture with CA, the peaks at m/z of 207.1, 398.9 and 415.2 were additionally observed. It is noted that the measured spectrum (Fig. 1c) was of the reaction mixture containing PCA synthesized using H_2SO_4 catalyst and the similar ESI(−)-MS spectrum was also obtained for the equilibrium mixture containing PCA, CA and H_2O_2 synthesized using the solid superacid catalyst, Dowex DR-2030 (not shown).

All the ESI(−)-MS measurements were carried out at a negative ion mode [37–39] (where $z = 1$) and the base peak of CA ($M = 192$) corresponds to the m/z value of 191.0 that is equivalent to $[M - H^+]^-$. A further analysis of the ESI(−)-MS spectrum of CA reveals that the peaks at m/z of 191.0 and 383.1 can be attributed to $[M - H^+]^-$ and 2 $[M - H^+]^-$, respectively. Similarly, in the case of spectrum a, the additional peaks at m/z of 207.1, 398.9 and 415.2 may be considered as the equivalence of $([M - H^+] + 16)^-$, (2 $[M - H^+] + 16)^-$ and

$[2\ ([M-H^+]+16)]^-$, respectively. On the other hand, in both cases the observed peak at *m/z* of 98.5 is assigned to $HClO_4$ because this peak was absent when $HClO_4$ was not contained in the measured solution, but the origin of the peaks at *m/z* of 111.0 and 83.0 is unknown and these peaks may be attributed to the fragments of CA and PCA1. However, the equivalent *m/z* values expressed above, $[M-H^+]^-$ and $2[M-H^+]^-$ correspond to CA and (CA–CA), respectively. Similarly, the observed equivalent *m/z* value, $([M-H^+]+16)^-$ can be reasonably attributed to PCA1 (see Eq. (1)) and the other equivalent *m/z* values of $(2\ [M-H^+]+16)^-$ and $[2\ ([M-H^+]+16)]^-$ obtained for the reaction mixture can also be assigned for (CA–PCA1) and (PCA1–PCA1), respectively. From the observed ESI(−)-MS results, it is clear that the PCA in the reaction mixture has a molecular mass of 208 equiv. to $([M-H^+]+16)^-$ and obviously no masses corresponding to PCA2 (224) and PCA3 (240) were found.

4.5. Molecular structure of PCA

From Table 1, it can be seen that the average ratio of $C_{Ox}/\Delta C_{CA}$, which was quantitatively determined by RP-HPLC and potentiometric measurements, is about unity. The physical meaning of such observation is that one molecule of consumed CA is equivalent to one molecule of oxidant, i.e., PCA has one –COOOH group and the value of *m* as a stoichiometric factor in Eq. (1) is 1. Such consideration can be further supported by the results obtained from a combined use of RP-HPLC and HCC methods. In this case, the value of *n* for the reduction of PCA was found to be 2, which is also equivalent to one –COOOH group in PCA molecule (Eq. (2)). Therefore, the equilibrium mixture expressed by Eq. (1) contains PCA with a unique structure of PCA1, although the other forms of PCA (PCA2 and PCA3) may be unfavorably formed via the same oxidation reaction of the other two –COOH groups of PCA1 by H_2O_2. This obtained result may be well understood by considering the inherent chemical properties of –COOH group of CA towards the chemical reaction with H_2O_2 to form PCA.

According to the viewpoint of the chemical equivalence of –COOH groups in CA, three –COOH groups may be classified into two types: the –COOH group adjacent to –OH group (first type) and the rest two –COOH groups (second type). On the contrary, three –COOH groups in CA have three distinct pK_a values (given above) and the PCA formation reaction is a nucleophilic bimolecular reaction in which the first type of –COOH group (relatively polar) should be more preferentially attacked by H_2O_2 to form PCA than those of the second type, i.e., the first type of –COOH group would be oxidized first by H_2O_2 to –COOOH group (i.e., PCA1), and then both –COOH groups of the second type.

In addition, it is known that the –OH group in alcohol can also be oxidized by H_2O_2 to form a hydroperoxide (–OOH) group. In the present case, the possibility of the oxidation of –OH group of CA by H_2O_2 to –OOH group may be neglected since this reaction is typically a unimolecular reaction in which a carbocation of CA must be formed [40], but we are not aware of the formation of carbocation of CA. From the above discussion, it can be concluded that the reaction of CA and H_2O_2 forms only PCA1, which can be strongly supported by the mass value of PCA (208) determined with ESI(−)-MS measurement, and that the obtained PCA1 may be named as 1,3-dicarboxylic-2-hydroxy-2-peroxycarboxylic propane. Moreover, the equilibrium reaction shown in Eq. (1) is not dependent on the type of acid catalysts (H_2SO_4 or solid superacid catalyst) used in preparing PCA.

5. Conclusions

The molecular structure of PCA that could not be isolated from the coexisting CA and H_2O_2, which cannot be determined using conventional analytical techniques (i.e., NMR, IR and UV–visible measurements), was successfully determined based on the combined use of the potentiometric-HPLC and HPLC–HCC measurements. From the obtained results, it was concluded that the reaction of CA and H_2O_2 in the presence of acid catalysts produces only PCA1, which was confirmed by measuring the molecular mass using ESI(−)-MS technique. The approach employed in this study may be applicable for the characterization of other peroxyacids coexisting with the parent acid and H_2O_2 in the equilibrium mixture. Similar studies on the determination of molecular structures of peroxy-succenic (and peroxy-glutaric) acids, which are of controversy [10–13], are currently under way.

Acknowledgements

The present work was financially supported by Grant-in-Aids for Scientific Research on Priority Areas (No. 417), Scientific Research (No. 12875164), and Scientific Research (A) (No. 10305064) to T. Ohsaka, from the Ministry of Education, Culture, Sports, Science and Technology of the Japanese Government, and by Venture Business Laboratory at TIT. B.N.F. is grateful for the financial supports of COE at TIT and JASSO, and also thanks the SANEYOSHI Foundation and KATOH Science Foundation, Japan, for scholarships. The authors are also grateful to Dr. Hiroko Hieda, Nitto Analytical Centre, Nitto Denko Group, Osaka, Japan, for ESI(−)-MS measurements.

References

[1] D. Swern, Chem. Rev. 45 (1949) 1.
[2] F.P. Greenspan, J. Am. Chem. Soc. 68 (1946) 907.
[3] W.E. Parker, L.P. Witnauer, D. Swern, J. Am. Chem. Soc. 79 (1957) 1929.
[4] W.E. Parker, C. Riccuti, C.L. Ogg, D. Swern, J. Am. Chem. Soc. 77 (1955) 4037.
[5] B.N. Ferdousi, M.M. Islam, M.I. Awad, T. Okajima, F. Kitamura, T. Ohsaka, Electrochemistry 74 (2006) 606.
[6] M.R.G. Klaas, K. Steffens, N. Patett, J. Mol. Catal. B: Enzym. 19–20 (2002) 499.
[7] L.V. Dulneva, A.V. Moskvin, Russ. J. Gen. Chem. 75 (2005) 1125.
[8] C. Francesco, C.D. Stefano, F.J. Millero, V.K. Sharma, J. Solution Chem. 33 (2004) 1349.
[9] R.G. Bates, G.D. Pinching, J. Am. Chem. Soc. 71 (1949) 1274.
[10] M. Dankowski, 4650612 (1986), to Degussa A.-G., Fed. Rep. Ger.
[11] G.O. Bianchetti, D. Furia, EP 0778270 (1997), to Procter and Gamble Company, USA.
[12] E George, E. Hawkins, GB 1139507 (1969), to The Distiller Company.

[13] D. Gold, S.V. Roessler, GB 905877 (1962), to Degussa A.-G.
[14] B.D. Sully, P.L. Williams, Analyst 87 (1962) 653.
[15] J. D'Ans, W. Frey, Chem. Ber. 45 (1912) 1845.
[16] F.P. Greenspan, D.G. McKellar, Anal. Chem. 20 (1948) 1061.
[17] D.M. Davies, M.E. Deary, Analyst 113 (1988) 1477.
[18] S. Effkemann, U. Pinkernell, R. Neumuller, F. Schwan, H. Engelhardt, U. Karst, Anal. Chem. 70 (1998) 3857.
[19] U. Pinkernell, S. Effkemann, U. Krast, Anal. Chem. 69 (1997) 3623.
[20] F. Di Furia, M. Prato, G. Stivanelo, Analyst 113 (1988) 793.
[21] G.T. Cairns, R.R. Diaz, K. Selby, D.J. Waddington, J. Chromatogr. 103 (1975) 381.
[22] M. Janotta, F. Vogt, H.-S. Voraberger, W. Waldhauser, J.M. Lackner, C. Stotter, M. Beutl, B. Mizaikoff, Anal. Chem. 76 (2004) 384.
[23] D. Swern, L.P. Witnauer, C.R. Eddy, W.E. Parker, J. Am. Chem. Soc. 77 (1955) 5537.
[24] P.A. Giguere, A.W. Olmos, Can. J. Chem. 30 (1952) 821.
[25] W.H.T. Davison, J. Chem. Soc. (1951) 2456.
[26] M.I. Awad, T. Ohsaka, J. Electroanal. Chem. 544 (2003) 35.
[27] M.I. Awad, T. Oritani, T. Ohsaka, Anal. Chem. 75 (2003) 2688.
[28] M.I. Awad, T. Ohsaka, Electrochem. Commun. 6 (2004) 1135.
[29] M.I. Awad, A. Denggerile, T. Ohsaka, J. Electrochem. Soc. 151 (2004) E358.
[30] M.I. Awad, C. Harnoode, K. Tokuda, T. Ohsaka, Anal. Chem. 73 (2001) 1839.
[31] R. Baron, A. Darchen, D. Hauchard, Electrochim. Acta 51 (2006) 1336.
[32] B.N. Ferdousi, M.M. Islam, T. Okajima, T. Ohsaka, Electrochim. Acta 53 (2007) 968.
[33] R.L. Donkers, F. Maran, D.D.M. Wayner, M.S. Workentin, J. Am. Chem. Soc. 121 (1999) 7239.
[34] M. Tsushima, K. Tokuda, T. Ohsaka, Anal. Chem. 66 (1994) 4551.
[35] A.J. Bard, L.R. Faulkner, Electrochemical Methods—Fundamentals and Applications, 2nd ed., Wiley, 2001, p. 159.
[36] G.L. Liu, S.P. Luo, J.D. Wang, Chem. Eng. Process. 43 (2004) 43.
[37] D. Hoffmann, J. Charette, Mass Spectroscopy—Principles and Applications A, 1996.
[38] Y. Abe-Oinishi, C. Yomota, N. Sugimoto, H. Kubata, K. Tanamoto, J. Chromatogr. A 1040 (2004) 209.
[39] S. Tanaka, R. Lio, S. Chinaka, N. Takayama, K. Hayakawa, Biomed. Chromatogr. 16 (2002) 390.
[40] A.G. Devies, R.V. Foster, A.M. White, J. Chem. Soc. (1953) 1541.
[41] R. LoBrutto, A. Jones, Y.V. Kazakevisch, H.M. McNair, J. Chromatogr. A 913 (2001) 173.

Available online at www.sciencedirect.com
ScienceDirect
Talanta 74 (2008) 1096–1103
Talanta
www.elsevier.com/locate/talanta

A multivariate study of the programmed temperature vaporization injection-gas chromatographic–mass spectrometric determination of polycyclic aromatic hydrocarbons Application to marine sediments analysis

V. Fernández-González [a,1], E. Concha-Graña [a,1], S. Muniategui-Lorenzo [a,*], P. López-Mahía [b], D. Prada-Rodríguez [b]

[a] *Department of Analytical Chemistry, University of A Coruña, Campus da Zapateira, E-15071 A Coruña, Spain*
[b] *University Institute of Environment, Pazo de Lóngora, Liáns, Oleiros, E-15179 A Coruña, Spain*

Received 13 April 2007; received in revised form 6 July 2007; accepted 30 July 2007
Available online 22 August 2007

Abstract

The trace analysis of polycyclic aromatic hydrocarbons (PAHs) in environmental matrices requires highly sensitive and selective methods. The use of large-volume injection in gas chromatography with mass spectrometry detection allows the improvement of the sensitivity. In this work, one of the most popular large-volume injectors, programmed temperature vaporization (PTV)-splitless injection, was optimized to determine 26 alkylated and non-alkylated PAHs at ultratrace levels. The injection conditions that use two different injection volumes, 10 and 25 μl, were optimized applying experimental designs. Six experimental factors that could affect the vaporization efficiency were studied. Detection limits for each assayed volume were compared with splitless injection, both in full scan and in SIM mode. An improvement of 50- and 100-fold, for 10 and 25 μl, respectively, was achieved for PAHs in comparison with splitless injection. Finally, the method that was optimized for 25 μl was applied successfully to the analysis of a certified marine sediment SRM 1941b and a real marine sediment extracted by microwave assisted extraction.
© 2007 Elsevier B.V. All rights reserved.

Keywords: Experimental designs; Large-volume injection; Marine sediments

1. Introduction

Polycyclic aromatic hydrocarbons (PAHs) are widely spread in the environment and mainly arise from the incomplete combustion of organic matter, from industrial processes and from other human activities [1]. Sixteen of these compounds are included in the *Environmental Protection Agency* (EPA) list as priority contaminants and fifteen of them have been regarded as potentially genotoxic and carcinogenic to humans by the *Scientific Committee on Food* (SCF) of the European Union [2].

Gas chromatography with mass spectrometry detection (GC–MS) has become a useful tool in PAHs analysis because it provides the simultaneous identification and quantitation of a large number of these compounds. Nevertheless, the very high sensitivity that is required for the trace or ultratrace analysis of PAHs in environmental matrices makes it necessary to improve the detection limits reached by GC–MS.

Nowadays, large-volume injection (LVI) is widely used to improve the sensitivity in the GC determination of trace analytes. This improvement could lead to the complete elimination of preconcentration steps in the analysis of samples containing trace compounds, reducing the total analysis time and loss of volatile compounds [3]. Instead of the maximum volume of approximately 2 μl that can be injected when using a conventional technique such as splitless injection, LVI injection allows us to use volumes of 10–100 μl [4].

The most popular injectors for LVI are programmed temperature vaporization (PTV) and on-column injectors. Direct on-column and large-volume on-column injection are particularly indicated to analyze thermolabile and volatile analytes.

* Corresponding author. Tel.: +34 9 81 167000; fax: +34 9 81 167065.
E-mail address: smuniat@udc.es (S. Muniategui-Lorenzo).
[1] Tel.: +34 9 81 167000; fax: +34 9 81 167065.

0039-9140/$ – see front matter © 2007 Elsevier B.V. All rights reserved.
doi:10.1016/j.talanta.2007.07.042

However, contamination of the column inlet with no-volatile sample materials is frequent in this injection technique.

After the PTV injector was initially presented in 1979 by Vogt et al. [5], the number of applications has increased significantly and many papers have been published on either the optimization of PTV parameters or their application in routine trace analysis [4,6–11]. The advantages of PTV injection over other techniques like split, splitless, and on-column injection are mainly an increase in sensitivity, a decrease in analyte discrimination during injection step, better recoveries of thermodegradable compounds and less pronounced adverse effects of non-volatiles present in the sample during the injection process [9].

Few papers have been published about the study of PTV injection for PAHs determination: most of them tackle the study by univariate procedures. For example, Vecera et al. [3] and Norlock et al. [12] applied univariate procedures to optimize PTV injection for the GC–MS determination of 16 PAHs. Recently, a multivariate study has been published for just 8 PAHs, and the optimized method was applied to monitor PAHs levels in ambient air [13]. In recent years, the interest in the study and control of hydrocarbons spills in the marine environment has increased, because they lead to sediments and biota pollution. In marine pollution monitoring programs, it is particularly interesting to analyze "source-specific marker" compounds, such as alkylated and non-alkylated PAHs, so as to characterize spilled oils and relate them to the origin sources. To our knowledge, there are no detailed studies, prior to the present one, concerning the multivariate optimization of PTV injection for the GC–MS determination of a high number alkylated and non-alkylated PAHs at trace levels.

In order to improve the sensitivity, it is necessary to optimize those variables that affect the solvent elimination efficiency during the injection; this is why we optimize a PTV-GC–MS method by means of an experimental design strategy, which reduces the number of experiences and allows for the analysis of interactions between factors. The PTV was operated in the splitless mode, i.e. the sample is introduced with the injector at a temperature below or close to the boiling point of the solvent and the split valve is closed during the evaporation step. In this mode, injection volumes between 1 and 25 μl can be injected [9]. Injection can be carried out in three different modes: at-once, speed controlled injection, and multiple injection. In the at-once mode, the sample is introduced at relatively high speed, whereas in the speed controlled injection mode the sample is introduced at a rate that is theoretically equal to the evaporation rate. This work applies the speed controlled injection mode [13].

We selected the injection volumes of 10 and 25 μl were selected because 25 is the maximum volume that can be applied when the PTV is operated in the PTV-splitless mode in a single injection. Larger sample volumes are injected normally with multiple injections of small volumes (e.g. 40 μl in 8 injections of 5 μl [14], 100 μl in 10 injections of 10 μl [15], or 50 μl in 10 injections of 5 μl [16]). High volumes are also injected when a PTV in solvent vent mode with a pre-column and a solvent vapour exit valve is used. Firstly, and in order to reduce the number of variables that require optimization, a Plackett–Burman factorial design was applied so as to determine which factors (split vent flow, injector heating rate, injection speed, splitless time, oven isothermal time, and t1: injector isothermal time and time during which the split valve is open) affect the vaporization efficiency. Then, the optimum values of the significant factors were found by a central composite design. Once the method was optimized the figures of merit were calculated and the detection and quantification limits were compared with those obtained by splitless injection.

Finally, the optimized PTV method for 25 μl of injection volume was successfully applied to the analysis of a marine sediment reference material SRM 1941b and a real marine sediment sample extracted by microwave assisted extraction (MAE).

2. Experimental

2.1. Apparatus

Gas chromatography was performed with a Thermo-Finnigan (Waltham, MA, USA) Trace GC chromatograph equipped with a GC PAL autosampler, PTV and split/splitless injectors and coupled to an ion trap mass spectrometer (Polaris Q). Xcalibur was the data processor. The system was operated in electron impact mode (EI; 70 eV). The separation was achieved with a DB-XLB column (60 m × 0.25 mm, 0.25 μm film thickness) (J&W Scientific, Folsom, CA, USA). Statgraphics Plus 4.0 for Windows (Statistical Graphics Corp., Herndon, VA, USA) software was employed for the statistics.

A Silcosteel® liner, with 2 mm of inner diameter, empty for splitless injections and glass wool packed for PTV injection was purchased from Thermo Finnigan. Microliter™ Syringes of 10 and 25 μl with 5 mm of needle length were obtained from Hamilton (Bonaduz, Switzerland).

Microwave Ethos-Sel, with media pressure rotor MPR-600/1 2S, and high purity TFM vessels from Milestone (Shelton, CT, USA) was used in the extraction of the sediment sample.

2.2. Materials

n-Hexane Unisolv and Anhydride Sodium Sulphate for organic trace analysis were purchased from Merck (Darmstadt, Germany). Acetone and Dichloromethane Romil-SpS Super Purity Solvent were obtained from Romil (Cambridge, UK). Neutral Alumina, for column chromatography, activity grade I was purchased from Sigma (St. Louis, MO, USA). Alumina was precleaned by sonication with dichloromethane and hexane and activated at 350 °C during 12 hours.

QTM PAHs Mix (2000 μg ml^{-1} in methylene chloride), containing acenaphthene, acenaphthylene, anthracene, benzo(*a*) anthracene, benzo(*a*)pyrene, benzo(*b*)fluoranthene, benzo(*g*,*h*,*i*) perylene, chrysene, dibenz(*a*,*h*)anthracene, fluoranthene, fluorene, indeno(1,2,3-*cd*)pyrene, naphthalene, phenanthrene and pyrene; and 525 Fortification Solution (acenaphthene-d10, chrysene-d12, and phenanthhrene-d10 at 2000 μg ml^{-1} each) and naphthalene-d8 (2000 μg ml^{-1}) were purchased from Supelco (Bellefonte, PA, USA). Solid standards of triphenylene, dimethylnaphthalene, benzo(*k*)fluoranthene, benzo(*e*)pyrene,

methylanthracene, methylphenanthrene, methylfluorene and methylnaphthalene were from Chem Service (West Chester, PA, USA) and Benzo(*b*)fluorene from Aldrich (Steinheim, Germany).

Reference material, SRM 1941b (Organics in Marine Sediment) was provided by the National Institute of Standards and Technology (NIST, Gaithersburg, MD, USA).

The standard solutions (0.3 μg ml^{-1}) were prepared by dilution in hexane and stored in capped amber vials at −20 °C.

2.3. Chromatographic conditions

The GC oven temperature program used was: 50 °C during 3 min (studied variable), increased at 4 °C min^{-1} to 325 °C (hold for 20 min). The mass spectrometer was operated in Full scan and in SIM mode (selected ion monitoring). Ionization voltage was set to 70 eV, transfer line temperature 300 °C and ion source temperature 250 °C. The injector program was started at 55 °C and ended at 300 °C (hold for 20 min). The heating rate was optimized in this work.

The selected conditions for GC–MS in SIM mode are showed in Table 1.

For splitless injection, the experimental conditions were: injector temperature 310 °C, empty liner (2 mm), split vent flow 20 ml min^{-1} and splitless time 0.8 min. The oven temperature program was 50 °C during 1 min then increased at 4 °C min^{-1} to 325 °C (hold for 20 min). A standard solution of 1 μg ml^{-1} in hexane was used, and the injection volume was 1 μl.

Table 1
GC–MS–SIM mode conditions for the studied PAHs, in elution order

PAHs	Quantification ion (*m*/*z*)	Confirmation ion (*m*/*z*)	Retention time (min)
Naphthalene	128	127	28.56
Methylnaphthalene	142	141	33.28
Dimethylnaphthalene	141	156	39.38
Acenaphthylene	152	153	39.34
Acenaphthene	153	154	40.52
Fluorene	166	165	43.55
Methylfluorene	165	180	45.94
Dibenzothiophene	184	152	46.98
Phenanthrene	178	176	47.68
Anthracene	178	176	47.98
Methylphenanthrene	192	191	50.59
Methylanthracene	192	191	50.86
Fluoranthene	202	101	54.15
Pyrene	202	101	55.47
Benzo(*b*)fluorene	216	–	57.93
Benzodiphenylenesulfure	234	–	61.21
Benzo(*a*)anthracene	228	226	62.73
Triphenylene	228	226	62.86
Chrysene	228	226	62.98
Benzo(*b*+*j*)fluoranthene	252	253	69.07
Benzo(*k*)fluoranthene	252	253	69.19
Benzo(*e*)pyrene	252	253	70.63
Benzo(*a*)pyrene	252	253	70.90
Dibenz(*a*,*h*)anthracene	278	279	77.13
Benzo(*g*,*h*,*i*)perylene	276	277	77.19
Indeno(1,2,3-*cd*)pyrene	276	277	79.02

Helium (99.9999%) was used as carried gas, under constant flow rate of 1 ml min^{-1}.

2.4. Extraction procedure

The validation of the optimized PTV-GC–MS method was carried out by analyzing a sediment reference material and a real marine sediment sample. Each sample of freeze dried sediments (0.5 g) was spiked with 60 μl of a 1 μg ml^{-1} fortification solution with naphthalene-d8, acenaphthene-d10, phenanthrene-d10 and chrysene-d12. The extraction was carried out by MAE with 30 ml of hexane:acetone (1:1, v/v) mixture. The microwave program began at room temperature, reached 130 °C in 10 min (held for 20 min), and finished with a cooldown of 10 min. The extracts were cleaned with a 5 g alumina (10% deactivated) column and eluted with 30 ml of a mixture of dichloromethane:hexane (20:80; v/v). Then they were concentrated in a rotary evaporator, dried under a nitrogen stream, and redissolved in 250 μl of perylene-d12 (0.25 μg ml^{-1} in hexane) before the GC–MS analysis. The isotope dilution method was utilized for quantification.

3. Results and discussion

3.1. Optimization of PTV conditions

To establish which factors are statistically significant, a Plackett-Burman $2^7 \times 3/32$ design was carried out. Six experimental factors were considered: injector heating rate, injection speed, split flow, injector isothermal time and time during which the split valve is open (t1 variable), oven isothermal time, splitless time, and a "dummy" variable, which has not influence in the experiment and is used to evaluate the standard errors of the experiments. Low and high values were selected for each factor according to previous studies about PTV systems [6,11,17]. The experimental design matrix that corresponds to the selected factors is shown in Table 2. In order to simplify this study, we selected twelve PAHs representatives of a whole range of volatilities and molecular weights. A standard solution of PAHs of 0.3 μg ml^{-1} in hexane, was used for these experiments.

Table 2
Experience matrix of the Placket–Burman design

Run	A	B	C	D	E	F	G
1	0.8	20.0	40	0.1	3.0	0.1	–
2	0.8	5.0	10	0.1	0.5	0.1	–
3	0.8	5.0	40	0.5	3.0	0.1	–
4	3.5	5.0	10	0.1	3.0	3.5	–
5	3.5	20.0	10	0.5	3.0	0.1	–
6	3.5	20.0	10	0.5	0.5	0.1	–
7	3.5	5.0	40	0.5	0.5	3.5	–
8	0.8	20.0	10	0.1	0.5	3.5	–
9	0.8	20.0	40	0.5	0.5	3.5	–
10	3.5	20.0	40	0.1	3.0	3.5	–
11	0.8	5.0	10	0.5	3.0	3.5	–
12	3.5	5.0	40	0.1	0.5	0.1	–

Factors: (A) injector heating rate (°C s^{-1}); (B) injection speed (μl s^{-1}); (C) split flow (ml min^{-1}); (D) t1 (injector isothermal time and time during the split valve is open); (E) oven isothermal time (min); (F) splitless time (min); (G) dummy.

The results were studied by analyzing the Pareto charts ($P = 95\%$). In these charts, the length of each bar is proportional to the standardized effect, Whereas the vertical line on the plot judges the effects that are statistically significant. Bars that extend beyond the line correspond to effects that are statistically significant at the 95% confidence level.

3.2. Injection volume: 10 μl

Statistically significant factors were the split flow for the heaviest PAHs and the splitless time for chrysene, benzo(*a*)anthracene and triphenylene. The factors with lower standardized effects for each compound were eliminated and second order interactions between the remaining variables were studied. We found that interaction between split flow and t1 was statistically significant. Fig. 1 shows an example of the standardized Pareto chart for chrysene and a second order interaction Pareto chart for phenanthrene.

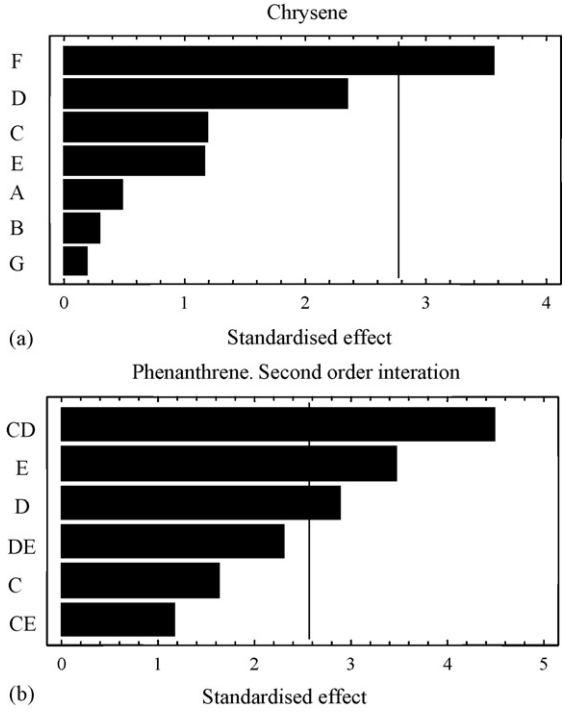

Fig. 1. (a) Standardized Pareto chart for chrysene and (b) second order interaction chart for phenanthrene obtained for an injection volume of 10 μl. Factors: (A) injector heating rate; (B) injection speed; (C) split flown; (D) t1; (E) oven isothermal time; (F) splitless time; (G) dummy.

Injector heating rate (A) and injection speed (B) were set at $1\,^{\circ}C\,s^{-1}$ and $5\,\mu l\,s^{-1}$ respectively and this according to practical chromatographic criteria, because they were no significant factors. The oven isothermal time had a positive influence on the response of some compounds and therefore a value of 3 min was selected for this variable.

The next step was the optimization of split flow (*C*), t1 (*D*) and splitless time (*F*). The optimization of these three factors was accomplished by an orthogonal central composite design (2^3 + star) that studied the effects of these factors in 16 randomized runs with 6 degrees of freedom. Low and high values for each factor were selected according to the positive or negative sign of the estimated effect in the Plackett–Burman design.

The results of the experiments were analyzed by the Main Effects plot. This plot shows the estimated response for each compound as a function of each experimental factor. In each plot, the factor is varied from its low level to its high level, while all other factors are held constant at their central values. Fig. 2 shows an example of a main effects plot obtained for acenaphthylene, Table 3 shows the optimum values for each factor and each compound. The splitless time was set at 4.3 min because this was the optimum value obtained for all the compounds.

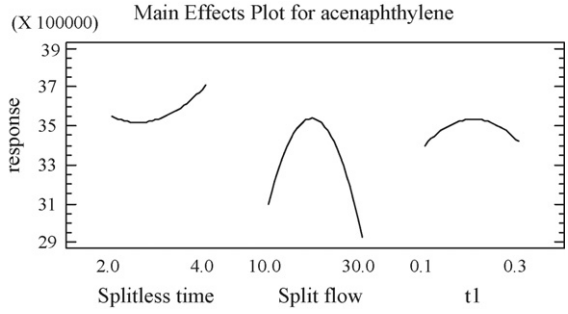

Fig. 2. Main effects plot obtained for acenaphthylene (10 μl injection volume).

Table 3
Optimum values obtained in the central composite design for 10 and 25 μl injection volume

Injection volume 10 μl				Injection volume 25 μl		
PAHs	Splitless time (min)	Split flow (ml min^{-1})	t1 (min)	PAHs	Splitless time (min)	t1 (min)
Naphthalene	4.3	17.6	0.32	Naphthalene	5.2	0.63
Dimethylnaphthalene	4.3	18.1	0.33	Acenaphthylene	5.2	0.69
Acenaphthylene	4.3	17.3	0.33	Acenaphtene	5.2	0.69
Fluorene	4.3	15.7	0.33	Fluorene	5.2	0.66
Dibenzothiophene	4.3	14.0	0.33	Dibenzothiophene	1.8	0.06
Phenanthrene	4.3	15.6	0.33	Phenanthrene	1.6	0.06
Pyrene	4.3	14.2	0.33	Pyrene	1.4	0.06
Benzo(*a*)anthracene	4.3	7.2	0.33	Chrysene	2.2	0.06
Chrysene	4.3	7.1	0.33	Dibenzo(*a*,*h*)anthracene	3.0	0.06
Benzo(*a*)pyrene	4.3	7.1	0.07	Benzo(*g*,*h*,*i*)perylene	3.0	0.06
Dibenzo(*a*,*h*)anthracene	4.3	7.1	0.31			
Benzo(*g*,*h*,*i*)perylene	4.3	7.1	0.10			

Two different behaviors were observed for split flow. For the most volatile compounds, the split flow optimum value ranged from 14 to 18 ml min^{-1}, whereas for the heaviest compounds (5–6 rings) it was 7 ml min^{-1}. Only for the heaviest compounds the split flow was a significant factor, so the value of this factor was set at a compromise value of 10 ml min^{-1}. For most compounds, the t1 optimum was 0.33 min, so this value was selected.

3.3. Injection volume: 25 μl

The Plackett–Burman matrix was the same as for 10 μl assay, but the high value selected for split flow was increased to 100 ml min^{-1}. The response in these experiments was measured as peak height in order to avoid deceptive results caused by the presence of broad and fronted peaks in some of the experiments.

The analysis of the Pareto charts shows two statistically significant factors: t1 (*D*) and splitless time (*F*). The values of the no significant factors were selected according to practical chromatographic criteria. The oven isothermal time was set at 3 min and the injector heating rate at 3 °C s^{-1}. A value of 5 μl s^{-1} was chosen for the injection speed, according to its influence on the peak shape. Since a higher response for volatile compounds and a lower response for heaviest PAHs is obtained when the split flow is low, in this case the chosen value was an intermediate value of 40 ml min^{-1}.

The statistically significant factors (t1 and splitless time) were optimized by an orthogonal central 2^2 + star design, resulting in ten randomized runs with 4 degrees of freedom. The experimental domain was 0.1–1 min for t1, and 0.5–5 min for splitless time.

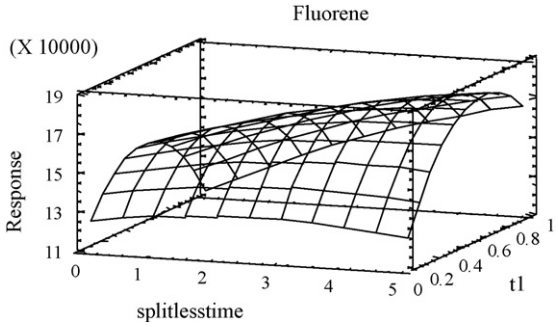

Fig. 3. Response surface obtained for fluorene (injection volume: 25 μl).

Finally, the results were analyzed by studying the response surfaces. For all PAHs, the response increased when the splitless time increased, as can be observed in Fig. 3 for fluorene. Table 3 shows the optimum values for this composite design. The optimum value obtained was 5 min for light compounds (2–3 rings) and 3 min for the heaviest compounds; thus an intermediate value of 4 min was chosen. We selected high values for t1 because broad and fronted peaks (Fig. 4) were obtained with short solvent elimination times. For this reason, the optimum value that was selected for t1 was 0.6 min.

A summary of the final conditions for each injection volume is presented in Table 4.

3.4. Figures of merit

After selecting the optimum value of each variable, the figures of merit were calculated using SIM mode for both injection

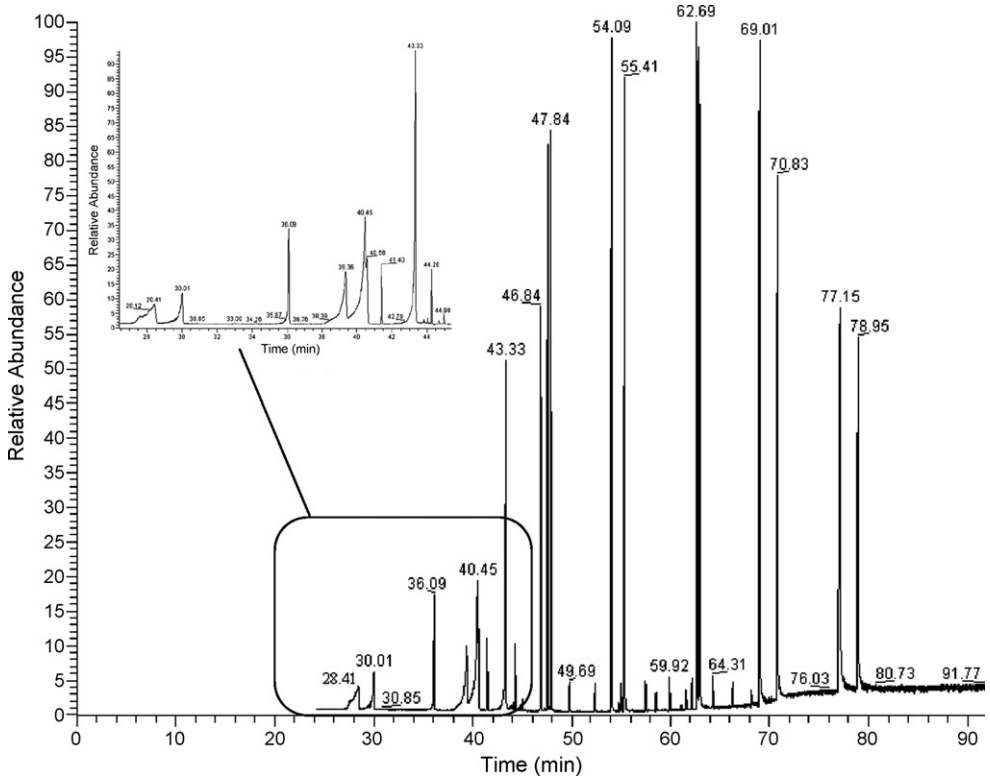

Fig. 4. PAHs chromatogram showing broad and fronted peaks obtained with low t1 values in 25 μl assay.

Table 4
Summary of the conditions selected for both injection volumes studied in PTV-GC–MS

Factor	Selected for 10 μl	Selected for 25 μl
Injector heating rate (°C s^{-1})	1	3
Injection speed (μl s^{-1})	5	5
Split flow (ml min^{-1})	10	40
t1 (min)	0.33	0.6
Isothermal oven time (min)	3	3
Splitless time (min)	4.3	4

volumes, 10 and 25 μl. Calibration curves were lineal from 0.01 μg ml^{-1} to 5 μg ml^{-1} for a 10 μl injection volume, and from 0.005 to 5 μg ml^{-1} for a 25 μl injection volume, with $r^2 = 0.9998$ as average for all the PAHs studied in both cases. The repeatability (ten consecutive replicates of the standard analyzed in the course of the same day) calculated for 0.25 μg ml^{-1} standard was satisfactory. The relative standard deviations ($n = 10$) ranged between 0.9 and 2.0% for the 10 μl injection volume and 0.8 and 1.6% for the 25 μl injection volume. Regarding intermediate precision (five replicates were analyzed in consecutive days by the same analyst), the relative standard deviations ($n = 5$) ranged between 1.4 and 2.8% for 10 μl, and 1.3 and 2.5% for 25 μl.

The instrumental detection and quantification limits were calculated as $X_b + 3S_b$ and $X_b + 10S_b$ respectively, where X_b is the average value and S_b the standard deviation of the background in a low concentration standard (0.005 μg ml^{-1}). These limits were calculated for both Full scan and SIM modes and were compared with those obtained with splitless injection in the conditions described in the Chromatographic Conditions section (Table 5).

Table 5
Instrumental detection (LOD) limits (μg l^{-1}) for splitless and PTV injection with 10 and 25 μl injected in GC–MS full scan and SIM mode

PAHs	Splitless		PTV 10 μl		PTV 25 μl	
	Full	SIM	Full	SIM	Full	SIM
Naphthalene	1.58	1.48	0.09	0.46	0.02	0.10
Methylnaphthalene	2.38	0.90	0.12	0.98	0.03	0.25
Acenaphthylene	1.04	1.09	0.17	0.84	0.05	0.29
Dimethylnaphthalene	1.64	2.47	0.51	0.46	0.07	0.20
Acenaphthene	1.42	0.88	0.20	0.59	0.06	0.32
Fluorene	0.67	0.80	0.21	0.69	0.05	0.05
Methylfluorene	0.89	2.17	0.68	0.40	0.19	0.13
Dibenzothiophene	0.69	0.68	0.04	0.19	0.01	0.07
Phenanthrene	1.22	1.34	0.07	0.25	0.02	0.06
Anthracene	1.40	1.78	0.08	0.32	0.02	0.08
Methylphenanthrene	3.52	1.53	0.11	0.38	0.03	0.25
Methylanthracene	2.91	1.02	0.12	0.29	0.03	0.19
Fluoranthene	2.13	0.89	0.04	0.18	0.01	0.06
Pyrene	2.61	0.94	0.04	0.21	0.01	0.06
Benzo(*b*)fluorene	9.26	3.31	0.05	0.39	0.01	0.11
Benzodiphenylenesulfure	7.30	2.25	0.04	0.27	0.01	0.09
Benzo(*a*)antraceno	11.0	6.47	0.08	0.53	0.02	0.17
Triphenylene	10.1	1.43	0.06	0.32	0.02	0.12
Chrysene	9.49	5.34	0.07	0.29	0.02	0.12
Benzo(*b*+*j*)fluoranthene	25.2	18.3	0.63	0.88	0.15	0.34
Benzo(*k*)fluoranthene	25.8	18.6	0.68	0.90	0.18	0.37
Benzo(*e*)pyrene	27.6	16.8	0.81	0.90	0.31	0.39
Benzo(*a*)pyrene	28.6	14.8	1.19	1.08	0.44	0.42
Dibenzo(*a*,*h*)anthracene	24.4	5.42	1.75	1.65	0.59	1.08
Benzo(*g*,*h*,*i*)perylene	19.2	14.6	1.08	0.90	0.40	0.83
Indeno(1,2,3-*cd*)pyrene	24.8	11.3	0.98	1.24	0.37	0.31

On average, the PTV limits improved those obtained for splitless injection with a factor 50 for 10 μl and a factor 100 for 25 μl, in Full scan mode, and with a factor of 7 for 10 μl and 20 for 25 μl, in SIM mode. In most cases, these instrumental limits were lower in Full scan mode than in SIM mode. In SIM mode, the mass spectrometer is only tuned to a few pre-selected ions, and complete mass spectra are not recorded during the GC–MS analysis. The gain in sensitivity for a specific ion over scanning the complete mass spectrum, is proportional to the ratio of the time the MS is tuned to that ion in SIM mode, to the time that the MS spends on the same ion when scanning to obtain a com-

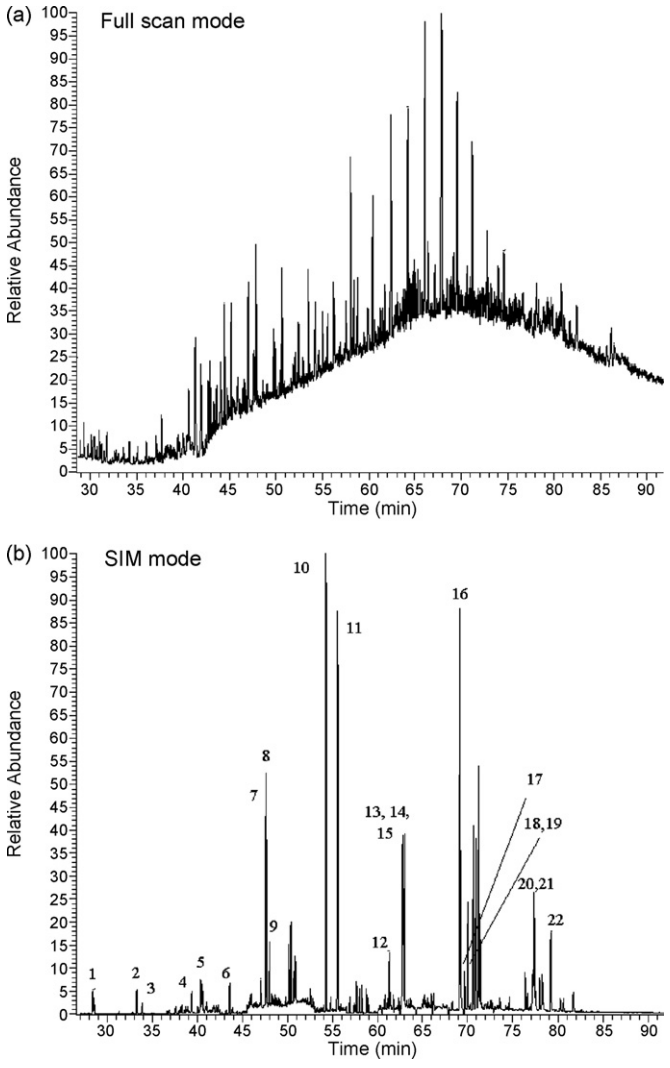

Fig. 5. Chromatograms of a marine sediment sample injected in full scan (a) and in SIM (b) mode. (1) Naphthalene; (2) methylnaphthalene; (3) dimethylnaphthalene; (4) acenaphthylene; (5) acenaphthene; (6) fluorene; (7) dibenzothiophene; (8) phenanthrene; (9) anthracene; (10) fluoranthene; (11) pyrene; (12) benzodiphenylenesulfure; (13) benzo(*a*)anthracene; (14) triphenylene; (15) crysene; (16) benzo(*b*+*j*)fluoranthene; (17) benzo(*k*)fluoranthene; (18) benzo(*e*)pyrene; (19) benzo(*a*)pyrene; (20) dibenzo(*a*,*h*)anthracene; (21) benzo(*g*,*h*,*i*)perylene; (22) indene(1,2,3-*cd*)pyrene.

Table 6
Detection limits ($\mu g\,kg^{-1}$) calculated with a real marine sediment sample PTV 25 μl

PAHs	Full	SIM	PAHs	Full	SIM
Naphthalene	0.11	0.03	Pyrene	0.56	0.20
Methylnaphthalene	0.11	0.06	Benzo(*b*)fluorene	0.41	0.05
Acenaphthylene	0.12	0.09	Benzodiphenylenesulfure	0.21	0.10
Dimethylnaphthalene	0.05	0.01	Benzo(*a*)anthracene	0.51	0.39
Acenaphthene	0.24	0.08	Triphenylene	0.61	0.42
Fluorene	0.54	0.04	Chrysene	0.55	0.42
Methylfluorene	0.18	0.13	Benzo(*b*+*j*)fluoranthene	0.24	0.19
Dibenzothiophene	0.25	0.23	Benzo(*k*)fluoranthene	0.31	0.21
Phenanthrene	0.60	0.39	Benzo(e)pyrene	0.54	0.40
Anthracene	0.68	0.45	Benzo(*a*)pyrene	0.58	0.49
Methylphenanthrene	0.18	0.14	Dibenzo(*a*,*h*)anthracene	1.33	0.10
Methylanthracene	0.26	0.20	Benzo(*g*,*h*,*i*)perylene	1.24	0.13
Fluoranthene	0.53	0.20	Indeno(1,2,3-*cd*)pyrene	1.05	0.12

plete mass spectrum. But ion trap mass spectrometry (IT-MS) has the ability to trap and to accumulate ions, hereby increasing the signal-to-noise ratio (S/N) of a measurement, and to scan the complete mass spectrum very rapidly. Therefore, when a standard solution is injected, the sensitivity for both modes is similar. This situation is entirely different when a sample is injected. GC–MS in SIM mode is unique in its ability to quantify trace levels of specific organic compounds in the presence of hundreds of other substances, some of which are present in higher concentrations than the analyte of interest. When a sample is analyzed, the background caused by the matrix has a great influence on the S/N when Full scan mode is selected. However, this influence is lower in SIM mode, as can be observed in Fig. 5(a) and (b) and Table 6, where the detection limits reached for a real sediment sample in full and SIM modes were calculated. As expected, the LOD calculated were lower in SIM mode.

The quantification limits were between 1.49 and 45.2 $\mu g\,l^{-1}$ for splitless injection, between 0.07 and 3.24 $\mu g\,l^{-1}$ for 10 μl, and between 0.02 and 1.09 $\mu g\,l^{-1}$ for 25 μl, all of them in full scan mode. For SIM mode, the quantification limits were between 1.32 and 36.3 $\mu g\,l^{-1}$ for splitless injection, between 0.40 and 3.03 $\mu g\,l^{-1}$ for 10 μl in PTV and between 0.11 and 2.24 $\mu g\,l^{-1}$ for 25 μl in PTV.

3.5. Application to the analysis of marine sediments

The proposed method with PTV injection of 25 μl was applied to the analysis of a reference material SRM 1941b *Organics in Marine Sediment* and to a real marine sediment sample in SIM mode (Fig. 5b). The sediments were extracted by microwave energy using hexane/acetone (1:1) as extracting solvent, according to the conditions mentioned in the Extraction Procedure section. The values obtained for SRM 1941b ($n=3$) were in good agreement with the certified values for all PAHs (Table 7). For the real marine sediment, some of the studied PAHs were detected in concentrations between 21 and 180 $\mu g\,kg^{-1}$ (Table 7). The peaks that appear in the full mode chromatogram of Fig. 5a show other hydrocarbonated compounds such as alkanes, ciclo-alkanes, and other wearing hydrocarbons that are commonly present in these kinds of samples. The hump up present in the chromatogram corresponds to the unresolved complex mixture (UCM) that consist of branched hydrocarbons from petrogenic inputs. The optimized method has demonstrated its suitability for the analysis of PAHs at trace levels in sediment samples.

Table 7
Certified concentrations of PAHs in SRM 1941b and concentrations obtained with the proposed method ($n=3$) and individual concentrations of PAHs found in a sediment sample ($n=3$)

PAHs	SRM 1941b ($\mu g\,kg^{-1}$) ± uncertainty[a]	Obtained ($\mu g\,kg^{-1}$) ± Standard deviation	Sediment sample ($\mu g\,kg^{-1}$) ± standard deviation
Naphthalene	848 ± 95	862 ± 54	70 ± 3
2-Methylnaphthalene[b]	276 ± 53	235 ± 11	
Acenaphthylene[b]	53.3 ± 6.4	56.4 ± 2	14 ± 1
Acenaphthene[b]	38.4 ± 5.2	34.6 ± 4	14 ± 2
Fluorene	85 ± 15	81 ± 6	28 ± 2
Phenanthrene	406 ± 44	417 ± 26	105 ± 2
Anthracene	184 ± 18	189 ± 14	16 ± 0.2
1-Methylphenanthrene	73.2 ± 5.9	68 ± 2	
2-Methylanthracene[b]	36 ± 15	29 ± 7	
Fluoranthene	651 ± 50	598 ± 40	140 ± 3
Pyrene	581 ± 39	510 ± 31	138 ± 2
Benzo(*a*)anthracene	335 ± 25	258 ± 35	42 ± 1
Chrysene	291 ± 31	311 ± 20	93 ± 4
Benzo(*b*+*j*)fluoranthene[b]	678 ± 21	590 ± 25	137 ± 5
Benzo(*k*)fluoranthene	225 ± 18	210 ± 10	47 ± 1
Benzo(*e*)pyrene	325 ± 25	331 ± 8	99 ± 5
Benzo(*a*)pyrene	358 ± 17	301 ± 19	51 ± 2
Dibenzo(*a*,*h*)anthracene	53 ± 10	56 ± 6	16 ± 1
Benzo(*g*,*h*,*i*)perylene	307 ± 45	350 ± 28	96 ± 2
Indeno(1,2,3-*cd*)pyrene	341 ± 57	357 ± 33	132 ± 3

[a] Expanded uncertainty about the mean with coverage factor 2 (95% of confidence).
[b] Reference concentrations.

4. Conclusions

A PTV injection method was optimized for the GC–MS analysis of 26 PAHs and alkylated PAHs by a multivariate approach. PTV injection offers the advantages of preventing losses of the most volatile compounds and the possibility of introducing large volumes of samples into the GC system, which improves the detection and quantification limits in various orders of magnitude with respect to those obtained by splitless injection. The use of experimental designs has reduced the number of experiments required to optimize all the variables and also the time consumed in the study. Two injection volumes were studied, 10 and 25 μl. Splitless time and t1 for 25 μl, and also split flow for 10 μl, were statistically significant. With the proposed PTV-GC–MS method, an improvement of 50- and 100-fold in the detection limits, for the 10 μl and 25 μl injection volumes respectively, was achieved for PAHs in comparison with splitless injection in Full scan mode. Small differences were observed between LODs in Full scan and SIM mode when a standard solution was injected in the PTV-GC–MS. When a sample was injected in SIM mode, the selectivity was improved and thus LODs were improved as well. The increase of injection volume, the high efficiency in solvent elimination, and the selectivity obtained in SIM mode notably improved the sensitivity of the proposed method, in comparison with traditional methods for the analysis of PAHs. The proposed PTV-GC–MS method with an injection volume of 25 μl in SIM mode was successfully applied to a reference material of marine sediment (SRM 1941b) and to a real marine sediment.

Acknowledgements

This study was supported by the Spanish Ministry of Science and Technology (project VEM 2003-20068-C05-05).

References

[1] G. Diletti, G. Scortichini, R. Scarpone, G. Gatti, L. Torreti, G. Migliorati, J. Chromatogr. A 1062 (2005) 247.
[2] European Union Health and Consumer Protection Directorate General, in http://europa.eu.int/comm/foof/fs/sc/scf/index_en.html, 2002.
[3] Z. Vecera, A. Bartosikova, J. Sklenska, P. Mikuska, Chromatographia 61 (2005) 197.
[4] S. Koning, M. Kurano, H.G. Janssen, U.A.T. Brinkman, J. Chromatogr. A 1023 (2004) 165.
[5] W. Vogt, K. Jacob, H.W. Obwexer, J. Chromatogr. 174 (1979) 437.
[6] E. Concha-Graña, I. Turnes-Carou, S. Muniategui-Lorenzo, P. López-Mahía, E. Fernández-Fernández, D. Prada-Rodriguez, Anal. Bioanal. Chem. 379 (2004) 1120.
[7] J. Teske, W. Engewald, Trends Anal. Chem. 21 (2002) 584.
[8] J.S. Lancaster, T.P. Lynch, P.G. McDowell, J. High Resolution Chromatogr. 23 (2000) 479.
[9] M. Godula, J. Hajslová, K. Mastouska, J. Krivánková, J. Sep. Sci. 24 (2001) 355.
[10] E.M. Kristenson, S. Angioi, R.J.J. Vreuls, M.C. Gennaro, U.A.T. Brinkman, J. Chromatogr. A 1058 (2004) 243.
[11] E. Concha Graña, M.I. Turnes Carou, S. Muniategui Lorenzo, P. López Mahía, E. Fernández Fernández, D. Prada Rodríguez, J. Chromatogr. A 958 (2002) 17.
[12] F.M. Norlock, J. Jang, Q. Zou, T.M. Schoonover, A. Li, J. Air Waste Manage. Assoc. 52 (2002) 19.
[13] V. Yusa, G. Quintas, O. Pardo, A. Pastor, M. de la Guardia, Talanta 69 (2006) 807.
[14] M. Hada, M. Takino, T. Yamagami, S. Daishima, K. Yamagushi, J. Chromatogr. 874 (2000) 81.
[15] P.L. Wylie. Trace level pesticide analysis by GC/MS using large-volumen injection. Application Note. Agilent Technologies, 1997.
[16] B.S. Crimmins, J.E. Baker, Atmos. Environ. 40 (2006) 6764.
[17] M. Miñones-Vázquez, M.E. Vázquez-Blanco, S. Muniategui-Lorenzo, P. López-Mahía, E. Fernández-Fernández, D. Prada-Rodríguez, J. Chromatogr. A 919 (2001) 363.

Available online at www.sciencedirect.com
ScienceDirect
Talanta 74 (2008) 1598–1602
Talanta
www.elsevier.com/locate/talanta

Quantification of residual nitrite and nitrate in ham by reverse-phase high performance liquid chromatography/diode array detector

I.M.P.L.V.O. Ferreira *, S. Silva

REQUIMTE- Serviço de Bromatologia, Faculdade de Farmácia da Universidade do Porto, Rua Anibal Cunha 164, 4099-030 Porto, Portugal

Received 14 May 2007; received in revised form 5 September 2007; accepted 3 October 2007
Available online 7 October 2007

Abstract

Nitrite and nitrate are used as additives in ham industry to provide colour, taste and protect against clostridia. The classical colorimetric methods widely used to determine nitrite and nitrate are laborious, suffer from matrix interferences and involve the use of toxic cadmium. The use of chromatography is potentially attractive since it is more rapid, sensitive, selective and provides reliable and accurate results. A rapid and cost-effective RP-HPLC method with diode array detector was optimized and validated for quantification of nitrites and nitrates in ham. The chromatographic separation was achieved using a HyPurity C18, 5 μm chromatographic column and gradient elution with 0.01 M *n*-octylamine and 5 mM tetrabutylammonium hydrogenosulphate to pH 6.5. The determinations were performed in the linear range of 0.0125–10.0 mg/L for nitrite and 0.0300–12.5 g/L for nitrate. The detection limits were 0.019 and 0.050 mg/kg, respectively. The reliability of the method in terms of precision and accuracy was evaluated. Coefficients of variation lower than 2.89% and 5.47% were obtained for nitrite and nitrate, respectively ($n = 6$). Recoveries of residual nitrite/nitrate ranged between 93.6% and 104.3%. Analysis of cooked and dried ham samples was performed, and the results obtained were in agreement with reference procedures.
© 2007 Elsevier B.V. All rights reserved.

Keywords: Nitrite; Nitrate; RP-HPLC; Ham; Validation

1. Introduction

Nitrite and nitrate salts of sodium and potassium (E_{249}, E_{250}, E_{251}, E_{252}) are permitted preservatives that may be added to cured meat products to protect these products against *Clostridium botulinum* and other *Clostridium* species [1]. Nitrite is a potent inhibitor of microorganisms, in particular clostridia. However, the contributions of nitrite to meat curing include not only antimicrobial effects but also characteristic colour development, oxidative stability of lipids, flavour production and texture improvement. The nitric oxide (NO) is the active specie and not its undissociated form. Nitrate is applied when a slow release of nitrite is wanted, nitrate diffuse in the product before it is reduced to nitrite [2,3].

Maximum levels of nitrate and nitrite that can be added to meat products and residual amounts are established in European Legislation [1]. The amount of nitrite necessary to inhibit *C. botulinum* differs from product to product, depending on the process, for example, for ham a maximum of 150 mg/kg of sodium nitrite can be added. Nitrite reacts with many components in the matrix and, for that reason, determination of nitrate and/or nitrite content does not reflect the amount of preservatives added. This particularly holds when ascorbic or erythorbic acid is added in order to enhance the release of nitric oxide from nitrite during heating. Most of the added nitrite is present as NO bound with myoglobin (5–15%), sulphydryl groups (5–15%), lipids (1–5%) and proteins (20–30%), partially is present as nitrate (<10%) and as nitrite (10–15%) [4,5]. Therefore, analytical methods usually determine the residual nitrite/nitrate.

The classic method for the determination of nitrite in food is based upon its ability to convert aromatic amines into diazonium ions, which, in turn, are coupled to another aromatic compound in order to produce an azo dye (the Griess-Romijn reaction) [6]. This is the base of many spectrophotometric methods. The most common arrangement utilizes sulphanilamide and *N*-(1-naphthyl)ethylenediamine as the target amine and coupler, respectively, with the product of the reaction detected at 540 nm. Nitrate is normally chemically reduced to nitrite and

* Corresponding author. Tel.: +351 2 22078929; fax: +351 2 22003977.
E-mail address: isabel.ferreira@ff.up.pt (I.M.P.L.V.O. Ferreira).

0039-9140/$ – see front matter © 2007 Elsevier B.V. All rights reserved.
doi:10.1016/j.talanta.2007.10.004

determined by the same type of reaction. A variety of reducing agents have been investigated to facilitate this conversion and include amalgamated cadmium [7], copperized cadmium [8] and zinc [9], and more recently, photo-induced reduction [10]. Other current methods for the determination of nitrite and nitrate rely on segmented-flow or flow-injection analysis variants of the traditional colorimetric Griess diazotisation procedure [11–14].

Alternative methods for nitrate and nitrite determination in foodstuffs have been developed more recently, including spectroscopic determination after enzymatic reduction [15], differential pulse voltammetry [16] and capillary electrophoresis [17]. The use of chromatography is potentially attractive since it is more rapid, sensitive and selective than methods based on reduction/colorimetry [3,18,19]. A study was performed to obtain an alternative chromatographic method to determine residual nitrite and nitrate in foods. Limits of detection of 1 and 10 mg/kg, respectively, for nitrite and nitrate are reported [3]. Columns containing a strong anion exchanger packing material, such as, polymethacrylate resin with a quarternary ammonium functional group are necessary for assuring reliability, the inconvenient is that this type of columns are expensive.

Ion-chromatographic methods have also been widely studied for the separation of nitrite and nitrate and other ions in several matrices [20–22]. Ion-pair HPLC methods offer, with respect to ion chromatography, advantages of relatively lower cost in instrumentation and columns and can be advantageously employed in laboratories where only conventional HPLC systems are available. Additionally, the theoretical column efficiency of ion-pair HPLC is better than that of an IC column, assuming that a suitable ion-pair reagent is chosen. However, little information is available on the analysis of residual nitrite and nitrate in food samples using ion-pair HPLC.

The simplest and easiest sample preparation methods namely dilution or filtration, are not suitable with some samples, some authors describe a solid-phase extraction clean-up step, but it is difficult to achieve reproducible recoveries of each analyte [23]. In the case of nitrite, sample manipulations need to be kept to a minimum, due to the instability of this ion that oxidizes to nitrous acid and/or nitrate.

The objectives of this study were to develop and validate a sensitive, selective and faster reverse-phase chromatographic method based on UV absorption (RP-HPLC/diode array) for quantification of residual nitrites and nitrates in ham.

2. Experimental

2.1. Chemicals and samples

All reagents used were of analytical grade purity. Solvents for HPLC were filtered through 0.22 μm NL 17 filters and degassed under vacuum for at least 15 min before use. Sodium nitrate, sodium nitrite, L-ascorbate and tetrabutylammonium hydrogenosulphate were supplied by Sigma Chemicals Co. (St. Louis, MO, USA), acetonitrile Licrosolv and activated charcoal were from Merk (Darmstradt, Germany) and *n*-octylamine was supplied by Fluka. Sep-pak cartridges were from Waters. Standard solutions of sodium nitrite (1000 mg/L) and sodium nitrate (1000 mg/L) were prepared from $NaNO_3$ and $NaNO_2$ previously dried in an oven (100 °C during 1 h). More diluted standard solutions, used in the calibration curves, and were obtained from the concentrated solutions by dilution. The solutions were treated with some chloroform drops to prevent the development of microorganisms and were stored in a refrigerator.

2.2. Instrumentation

The chromatographic analysis was carried out in an analytical HPLC unit (Jasco) equipped with one Jasco PU-2080 HPLC pump, a MD-2010 Plus Multiwavelength detector and a type 7125 Rheodyne Injector with a 20 μL loop. The column was a reversed-phase HyPurity C18 from Thermo Electron Corporation (5 μm; 150 mm length; 3 mm internal diameter). The Borwin PDA Controller Software (JMBS Developments, Le Fontanil, France) was also used.

Fungilab Ultrasonic cleaner and a METROHM 632 pH-Meter were used for eluent preparation. A vortex Heidolph REAX 2000 was used for sample preparation.

2.3. Sample preparation

Seven ham samples purchased from a local supermarket were pre-treated by homogenization in a triturator and stored at 4 °C during the study. These included four samples of cooked pork ham (samples 1–4), two samples of cooked turkey ham (samples 5–6) and one sample of dried ham (sample 7). All samples were from different brands.

Five different sample preparation procedures were tried. One set of samples was extracted with hot water (50–60 °C) and clarified by filter through filter paper and membrane filter. Two sets of samples were extracted with hot water (50–60 °C) and deproteinized, one with acetonitrile and the other with Carrez reagents and filtered. One set of samples was dried for 1 h in an oven, extracted with hot water (50–60 °C), added of 1 g activated charcoal, deproteinized with acetonitrile and filtered. Another set of samples was extracted with hot water (50–60 °C), deproteinized with acetonitrile and purified with sep-pak C18. A summarized description of the analytical methods assessed is presented in Table 1.

2.4. Method validation

Analyses were performed over a period of 2 weeks. Each batch consisted of replicate analyses of blanks (limit of detection), standard solutions (sensitivity and linear range) and both spiked and unspiked samples (recovery and precision).

2.4.1. Linearity and range

Linearity was addressed by preparing eight standard solutions of sodium nitrite and sodium nitrate ranging between 0.0125–10.0 and 0.025–15.0 mg/L. A linear regression analysis of analyte concentration versus peak response was performed.

Table 1
Summarized description of the analytical methods assessed

Method	Extraction	Clarification
1	10 g sample homogenized in 15 mL hot water (50–60°), placed in a water bath 15 min	Filter through filter paper and membrane filter
2	10 g sample homogenized in 10 mL hot water (50–60°), placed in a water bath 15 min	5 mL Carrez I and Carrez II. Filter through filter paper and membrane filter
3	10 g sample homogenized in 10 mL hot water (50–60°), placed in a water bath 15 min	5 mL of acetonitrile. Filter through filter paper and membrane filter
4	10 g sample homogenized and dried in an oven + 1 g activated charcoal in 20 mL hot water (50–60°), placed in a water bath 15 min	5 mL of acetonitrile. Filter through filter paper and membrane filter
5	10 g sample homogenized in 10 mL hot water (50–60°), placed in a water bath 15 min	5 mL of acetonitrile. purified with sep-pak C18 (2 mL methanol and 4 mL water, load 1 mL sample, wash with 3 mL × 1 mL water, elute with 2 mL 0.5 M NaCl solution

2.4.2. Detection limits

The detection limits were calculated as the concentration corresponding to three times the background noise of the blank.

2.4.3. Quantification limits

The quantification limits were calculated as the concentration corresponding to ten times the background noise of the blank.

2.4.4. Recoveries

The experimental recovery was obtained from difference between two measurements (sample and spiked samples), according to the following relationship:

$$\text{Recovery, \%} = (\text{total analyte found} - \text{analyte originally present}) \times \frac{100}{\text{analyte spike}}$$

The recovery ranges for nitrite and nitrate estimated immediately after sample preparation.

2.4.5. Precision

A total of three analyses were performed for one ham sample to evaluate the relative standard deviation (RSD%) of the method.

2.4.6. Reference methods

As no certified reference materials were available and in order to evaluate the accuracy of the results obtained by HPLC, the reference methods of the International Standards Organization ISO 3091–1975 and ISO 2919–1976 [24,25] were used for the determination of nitrite and nitrate levels, respectively in meat products.

3. Results and discussion

3.1. Method optimization

The optimization of the RP-HPLC/diode array procedure was focused on the chromatographic separation as well as on the sample preparation procedure. The stationary phase selected required the use of counter ions for peak separation. Different mobile phases and preparation procedures were assayed at a flow rate of 1 mL/min, with the aim of assess which mobile phase and sample preparation give better performance. An injection volume of 20 μL was chosen since it is usually described in literature [3].

3.1.1. Evaluation of mobile phase

A standard solution containing 1.25 mg/L of sodium nitrite and 2.50 mg/L of sodium nitrate was separated on a C18 column by using five different mobile phases: 0.01 M tetrabutylammonium hydrogenosulphate, pH 6.5; 0.01 M tetrabutylammonium hydrogenosulphate, pH 6.5 in 20% methanol; 0.01 M tetrabutylammonium hydrogenosulphate, pH 6.5 in 20% acetonitrile; 0.01 M *n*-octylamine, pH 4 and 0.01 M *n*-octylamine/5 mM tetrabutylammonium hydrogenosulphate, pH 6.5.

Isocratic elution with a mobile phase containing 0.01 M *n*-octylamine/5 mM tetrabutylammonium hydrogenosulphate, pH 6.5 enables nitrite and nitrate ion-pair chromatographic separation. The use of two different ion-pair compounds as eluents allows for adjustment of coeluting peaks and ensures appropriate peak resolution (Fig. 1). Additionally, the eluent should not give rise to high background UV absorbance.

Nitrite and nitrate spectrums were inserted in the software spectrum library. When studying the interference of L-ascorbate a usual ham additive, it reported a distinct retention time and spectrum.

3.1.2. Evaluation of sample extraction procedure

One of the problems in measuring nitrites and nitrates in food samples are the matrix interferences that may hamper the determination of the substances of interest, for example, the liquid chromatographic techniques generally utilized the inherent low-wavelength UV absorption of nitrate and nitrite anions (205–215 nm) and spectral interferences from closely eluting compounds can occur [26]. Thus, appropriate sample treatment is necessary.

The extraction of nitrite and nitrate from ham using only hot water (see Table 1, Method 1) was not appropriate, since interfering compounds were also extracted. Neither the deproteinization

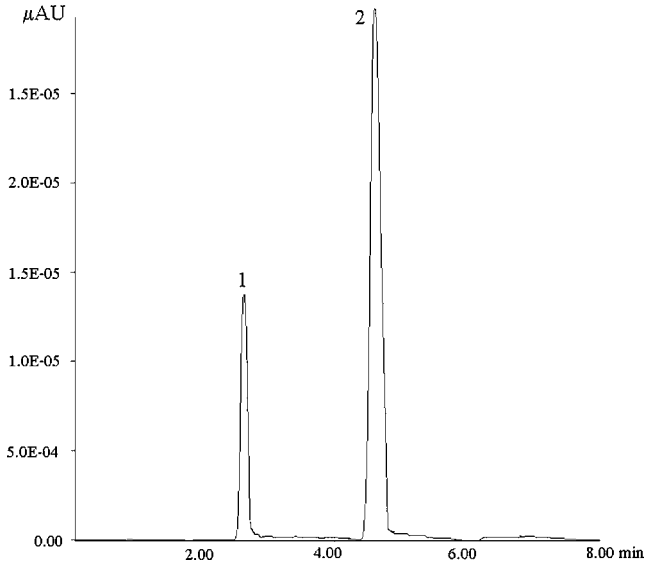

Fig. 1. Chromatogram obtained with the C18 column for an aqueous standard solution containing 1.25 mg/L of sodium nitrite and 2.50 mg/L of sodium nitrate.

with acetonitrile (Method 2) nor with Carrez reagents (Method 3) removed the interferences that co-elute with nitrite peak, and remain even after purification with Sep-Pak C18 (Method 5). Spectrum is a useful tool to determine peak purity and to establish correlations between the spectrum of sample and standard peaks with similar retention times using Borwin PDA controller software.

Ham samples extracted with hot water (50–60 °C), added of 1 g activated charcoal, deproteinized with acetonitrile (Method 4) and filtered gave a clean and interference-free baseline. Thus, this extraction procedure was chosen for further analyses. No peaks were observed in sample extracts after elution of nitrate peak, thus chromatographic analysis of 8 min could be performed (Fig. 2).

3.2. Method validation

Linearity within the concentration range of 0.0125–10.0 mg/L for nitrite and 0.0300–12.5 mg/L for nitrate was checked through the calibration curves, and obtained by linear regression of peak area versus concentration. The coefficients of determination (r^2) were 0.99981 and 0.99999, respectively. The detection limits of sodium nitrite and sodium nitrate were 0.0126 and 0.0318 mg/L, respectively. The quantification limits of sodium nitrite and sodium nitrate were 0.134 and 0.341 mg/L, respectively.

Three different extractions, as described above, were made for each ham sample and subsequently injected twice. The RSD ($n = 6$) reported for sample concentration was less than 2.89% and 5.47% for nitrite and nitrate, respectively.

The reliability of the method was confirmed by two recovery experiments. Two levels of nitrites (0.00075 mg and 0.0015 mg/kg) and nitrates (0.0008 and 0.0012 mg) were tested. Recoveries varied between 93.6% and 97% for nitrite and 99.5% and 104.3% for nitrate.

Similar qualitative chromatographic profiles were obtained for the three types of ham assayed (cooked pork ham, cooked turkey ham and dried pork ham), however, quantitative differences were obtained (Fig. 2). Table 2 presents results obtained from the analysis of seven ham samples. Nitrite and nitrate levels found in ham samples were in the same order of magnitude of those quantified in Portuguese ham (during its shelf-life) by automated flow injection analysis [27]. To confirm the reliability and accuracy of the method, part of the samples were analysed by the reference methods of the International Standards Organiza-

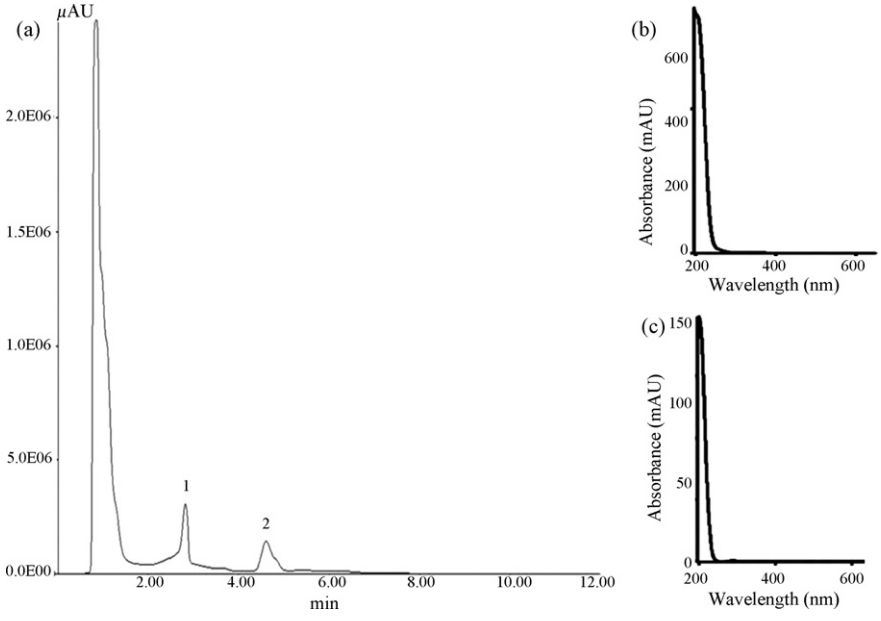

Fig. 2. (a) Chromatogram obtained for a ham sample extracted with hot water (50–60 °C), added of 1 g activated charcoal, deproteinized with acetonitrile and filtered. Peak 1 was identified as nitrite and peak 2 was identified as nitrate. (b) Spectrum of peak with a retention time of 2.6 min taken from 4a chromatogram. (c) Spectrum of peak with a retention time of 4.7 min taken from 4a chromatogram.

Table 2
Reported values of nitrite and nitrate in ham samples (cooked and dried) from the market, values expressed as mg of sodium nitrite/kg ham and sodium nitrate/kg ham

Sample	$NaNO_2$ (mg/kg)		$NaNO_3$ (mg/kg)	
	HPLC method	Reference	HPLC method	Reference
1	0.354 ± 0.012	–	0.810 ± 0.023	–
2	0.113 ± 0.006	–	0.663 ± 0.028	–
3	0.895 ± 0.022	–	0.791 ± 0.019	–
4	0.934 ± 0.022	0.986 ± 0.032	0.701 ± 0.020	0.789 ± 0.043
5	1.155 ± 0.024	1.201 ± 0.085	0.987 ± 0.019	1.003 ± 0.022
6	1.253 ± 0.021	1.307 ± 0.061	0.999 ± 0.041	1.121 ± 0.045
7	0.682 ± 0.022	0.701 ± 0.055	0.872 ± 0.031	0.901 ± 0.034

Part of the samples were analysed by the reference methods of the International Standards Organization ISO 3091-1975 and ISO 2919-1976 [24,25].

Table 3
Comparison between the optimized RP-HPLC method and NMKL method [3]

Methodologies	RP-HPLC/diode array		Method no. 165 2000 NMKL	
Parameters	NO_2^-	NO_3^-	NO_2^-	NO_3^-
Detection limit (mg/kg)	0.0189	0.0477	1	10
Correlation coefficient	0.9998	1.0000	0.9999	0.9997
Recovery (%)	93.7–97	99.5–104	96–108	96–107
Linearity (mg/L)	0.0126–10		0.5–20	
Running time (min)	8		≫8	

tion ISO 3091-1975 and ISO 2919-1976 [24,25]. No significant statistical difference between the two methods was observed, at the 1% significance level, from the analysis of variance, however, it should be pointed out that the reference method gave higher levels than the HPLC method. It is well known that classical colorimetric methods suffer from matrix interferences, caused primarily by added reducing compounds, such as ascorbate, that are not completely eliminated and will interfere with colour formation during the diazotisation method for nitrite analysis. A number of reviews have covered the effects of such interferences within food and environmental matrices [13,14] and justify our results.

Finally, comparison was performed between the results obtained by the validated methodology and the results described in the literature for NMKL Collaborative study [3] using a quaternary ammonium column and European standard ENV 12014-4. Weak anionic exchange chromatography with aminopropyl bonded-phase column and strong anionic exchange chromatography with two different eluents (5 mM K_2HPO_4) in 15% acetonitrile, pH 8.6 and buffer (boric acid, gluconic acid, lithium hydroxide and glycerol) in 12.5% acetonitrile, pH 6.5 were tested. The strong anionic exchange chromatography method with buffer in 12.5% acetonitrile as mobile was preferred and validated in a collaborative study. The authors, reported similar recoveries of nitrite and nitrate from meat products, and higher detection limits for nitrite and nitrate ions (Table 3). However, chromatographic column is much more expensive and eluent preparation much more laborious.

4. Conclusions

In conclusion, the described extraction procedure and RP-HPLC method seems to fulfil the criteria of selectivity, sensitivity, reproducibility and convenience for analysing the nitrite and nitrate content in ham. It is less laborious than reference procedures and strong anionic exchange chromatography. Thus, it is suitable for routine assays. HPLC analysis time is lower than 8 min and extraction procedure is rapid and cost effective. Chromatograms with a clean and interference-free baseline are obtained.

References

[1] Directive 2006/52/CE of the European Parliament and of the Council, Official Journal of the European Union (2006).
[2] H.R. Nordin, J. Technol. Aliment. 2 (1969) 79.
[3] L. Merino, U. Edberg, G. Fuchs, P. Aman, JAOAC Int. 83 (2000) 365.
[4] R.G. Cassens, G. Woolford, S.H. Lee, R. Goutefonge, Proceedings 2nd International Symposium of nitrite in meat Products, Zeist, Pudoc, Wageningen, The Netherlands, 1976, p. 95.
[5] W. Olsman, M. Cees, Z. Lebensm, Unters. Forsch. 164 (1977) 239.
[6] M.J. Moorcroft, J. Davis, R.G. Compton, Talanta 54 (2001) 785.
[7] Z. Marczenko, Spectrophotometric Determination of Elements, Ellis Horwood, Chichester, UK, 1976, pp 397–399.
[8] J.F. Van Staden, Anal. Chim. Acta 138 (1982) 403.
[9] M.A. Koupparis, K.M. Walczak, H.V. Malmstadt, Anal. Chim. Acta 142 (1982) 119.
[10] K. Takeda, K. Fijiwara, Anal. Chim. Acta 276 (1993) 25.
[11] I.M.P.L.V.O. Ferreira, J.L.F.C. Lima, M.C.B.S. Montenegro, R. Pérez-Olmos, A. Rios, Analyst 121 (1996) 1393.
[12] O. Pinho, I.M.P.L.V.O. Ferreira, M.B.P.P. Oliveira, M.A. Ferreira, Food Chem. 62 (1998) 359.
[13] J.B. Adams, Food Chem. 59 (1997) 401.
[14] J.C. Fanning, Coord. Chem. Rev. 199 (2000) 159.
[15] S. Girotti, E.N. Ferri, F. Fini, F. Ruffini, R. Budine, I. Moura, G. Almeida, C. Costa, J.J.G. Moura, G. Carrea, Anal. Lett. 32 (1999) 2217.
[16] S. Brunova, A. Mesarosova, Chem. Pap.-Chemicke Zvesti 52 (1998) 156.
[17] M. Jimidar, C. Hartmann, N. Cousement, D.L. Massart, J. Chromatogr. A 706 (1995) 479.
[18] V.D. Matteo, E. Esposito, J. Chromatogr. A 789 (1997) 213.
[19] G. Saccani, E. Tanzi, S. Cavalli, J. Rohrer, JAOAC Int. 89 (2006) 712.
[20] Y. Zuo, C. Wang, Van S T., Talanta 70 (2006) 281.
[21] Y. Zuo, H. Chen, Talanta 59 (2003) 867.
[22] C.R. Harrison, J.A. Sader, C.A. Lucy, J. Chromatogr. A 1113 (2006) 123.
[23] P. Reece, H. Hird, Food Addit. Contam. 17 (2000) 219.
[24] International Standards Organisation, Viandes et produits à base de viande. Détermination de la teneur en nitrites. Méthode de référence, ISO 2019, 1975.
[25] International Standards Organisation, Viandes et produits à base de viande. Détermination de la teneur en nitrates. Méthode de référence, ISO 3001, 1975.
[26] L.W. Gapper, B.Y. Fong, D.E. Otter, H.E. Indyk, D.C. Woollard, Int. Dairy J. 14 (2004) 881.
[27] I.M.P.L.V.O. Ferreira, N.S. Tavares, M.A. Ferreira, Cienc. Technol. Aliment. 2 (1999) 192.

Available online at www.sciencedirect.com
ScienceDirect
Talanta 74 (2008) 1085–1095
Talanta
www.elsevier.com/locate/talanta

Review

Elemental composition of seasoning products

A. Gonzálvez, S. Armenta, M.L. Cervera, M. de la Guardia *

Department of Analytical Chemistry, Research Building, University of Valencia, 50th Dr. Moliner Street, E-46100 Burjassot, Valencia, Spain

Received 25 May 2007; received in revised form 6 September 2007; accepted 28 September 2007
Available online 13 October 2007

Abstract

The elemental composition of seasoning products, like spices garlic and onion, has been reviewed paying special attention to methods proposed in the literature to determine specific elements or as much as possible components of these products which are widespread used in food preservation or food flavouring and can contribute to the intake of both, essential and toxic elements. Sample treatment and metal speciation aspects have been critically revised concerning onion, garlic and pepper (the most commonly studied products).
© 2007 Elsevier B.V. All rights reserved.

Keywords: Trace element; Onion; Garlic; Black pepper; Spices

Contents

1. Introduction 1085
2. Methods for the determination of trace elements 1089
   2.1. Absorption and fluorescence atomic spectrometry 1089
   2.2. Inductively coupled plasma techniques 1091
   2.3. Nuclear techniques 1091
   2.4. X-ray fluorescence spectrometry 1092
   2.5. Molecular fluorescence spectrometry 1092
   2.6. Voltammetry 1092
3. Sample treatment 1092
   3.1. Dry ashing 1093
   3.2. Wet digestion 1093
   3.3. Microwave-assisted treatment 1093
   3.4. Ultrasound-assisted extraction 1093
4. Speciation 1094
5. Conclusions 1095
   References 1095

1. Introduction

Since antiquity spices and herbs together with onion and garlic have been used throughout the world for flavouring and preserving food. In some cases, spices were even used to mask spoilage or off-flavour in products. Nowadays worldwide import of spices has continuously increased from 209,293 tonnes in 2000 to 226,910 tonnes in 2004, which correspond to a trade value of US$ 625 million [1].

During the last decade of the 20th century, food-borne infections and intoxications due to spices have increased in several European countries [2]. Moreover, in recent years the scientific community has evidenced a particular interest in the determination of trace and heavy metals in all food components including salt and spices.

* Corresponding author.
E-mail address: miguel.delaguardia@uv.es (M. de la Guardia).

0039-9140/$ – see front matter © 2007 Elsevier B.V. All rights reserved.
doi:10.1016/j.talanta.2007.09.039

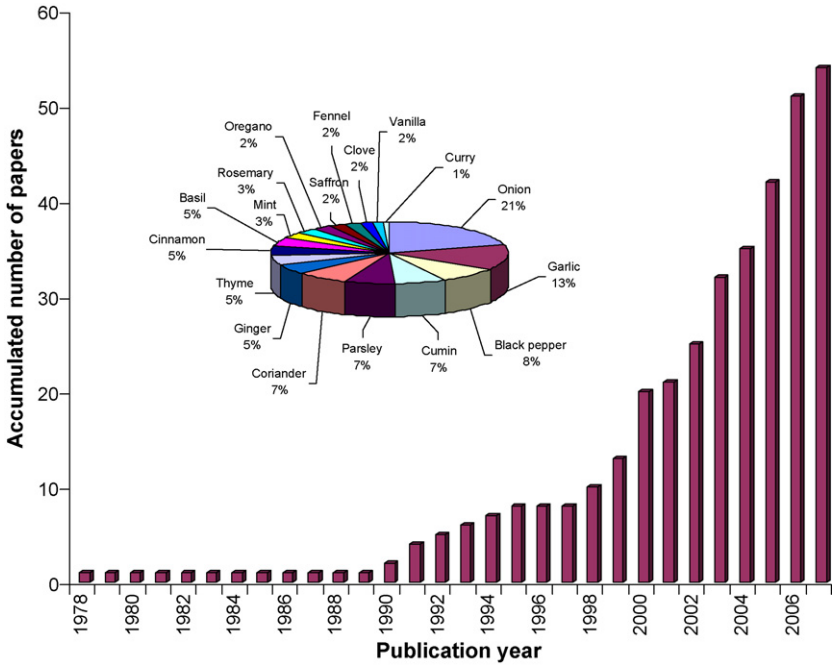

Fig. 1. Evolution of the literature about elemental composition of seasoning products.

The category of spices and herbs covers a number of different products. Regarding spices, we find, among others, vanilla, oregano, pepper, ginger, while some of the included herbal products are garlic and onion.

Trace elements include antimony, arsenic, bismuth, cadmium, cerium, chromium, cobalt, copper, gallium, gold, iron, lead, manganese, mercury, nickel, platinum, silver, tellurium, thallium, tin, uranium, vanadium, and zinc. In small concentration it seems that the main part of the aforementioned elements are nutritionally essential for a healthy life. Some of these elements like F, V, Cr, Mn, Fe, Co, Cu, Zn, Se, Mo and I belong to the category of micronutrients, which are needed by the human body in small quantities (generally less than 100 mg/day), as opposed to elements considered macronutrients, such as sodium, calcium, magnesium, potassium, chlorine, etc., which are required in larger quantities [3].

ISI Web of Science database from 1945 to 2007 has been used to look for the state of art in this field. The first precedent was published in 1978 [4], where cadmium, lead and zinc were determined in parsley, but the interest on the study of the elemental composition of seasoning products was not reflected in the scientific literature till 1990.

Fig. 1 depicts the evolution of the accumulated number of published papers devoted to the elemental composition of spices. It can be identified a clear change on the rate of the scientific literature production at the end of the 1990s, which varied from 0.5

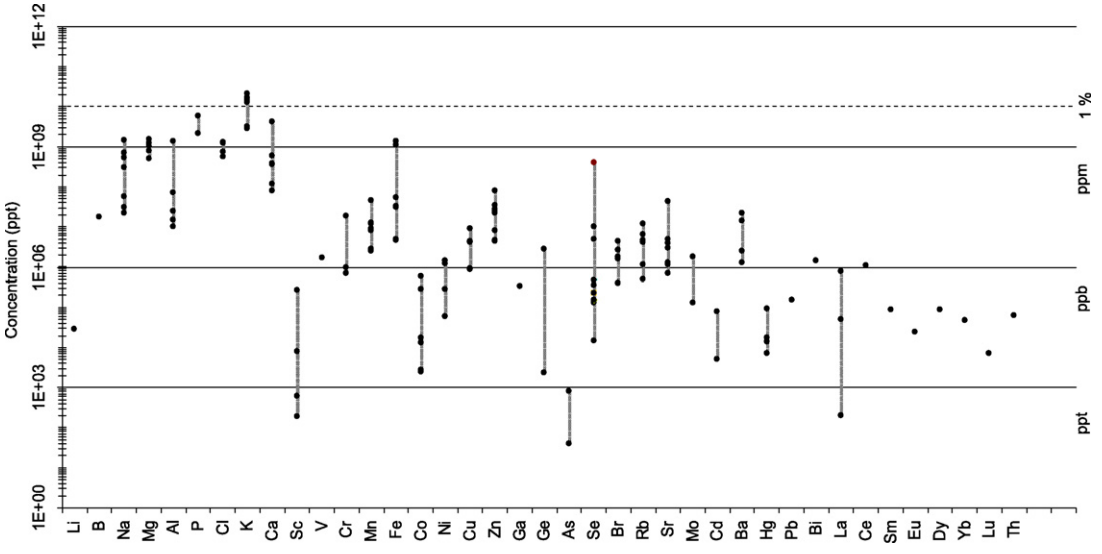

Fig. 2. Concentration ranges of elements determined in garlic from published studies.

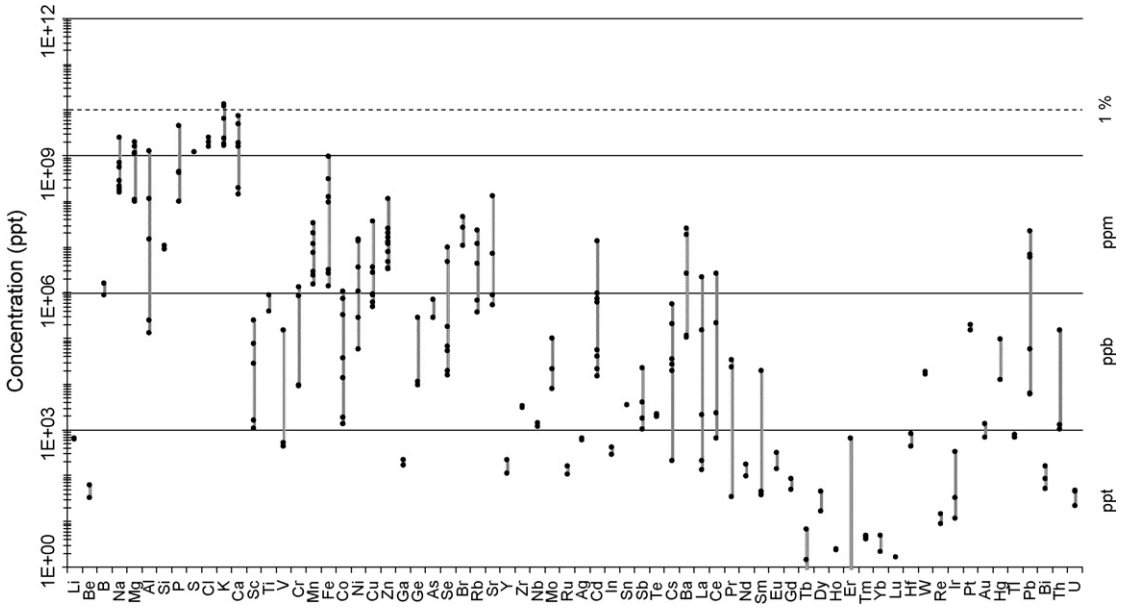

Fig. 3. Concentration ranges of elements determined in onion from published studies.

papers per year till the approximately 5 papers per year published from the beginning of the new century till today.

The dramatic change in the number of publications in this field could be associated to the introduction of powerful and reliable instruments based on the inductively coupled plasma (ICP) and the maturity of other instrumental methods suitable for elemental composition determination.

As it can be seen from the inset in Fig. 1, the major interest of the researchers concerns garlic, onion and black pepper analysis. So, this review has been mainly focused on the different analytical procedures developed for the determination of trace elements in the aforementioned products.

Regarding to the relative frequency of the elements determined in garlic, onion and black pepper the most studied elements were Ca, Mn, Fe, Cu, Zn considered as essentials for humans; Cd and Pb present also a relatively high-interest for the scientists because of their toxicity at concentrations beyond those necessaries for their biological functions and thus the aforementioned elements have been considered in 11–20 published papers. Na, Mg, Al, P, K, Ti, Cr, Co, Ni, Se, Rb, Sr and Sn have been evaluated in 6–10 papers and the rest of the considered elements were determined in only 1–5 studies. So, it can be concluded that in spite of the general use of garlic, onion and pepper in cooking and flavouring foods there is a lack of knowledge about the elemental contribution of these seasoning products to the presence of both, essential and toxic elements, in the human diet.

Figs. 2–4 show the concentration ranges of trace elements found in garlic, onion and black pepper, respectively. As it can be seen from these figures, potassium, ranging from 0.16 to 2.1%

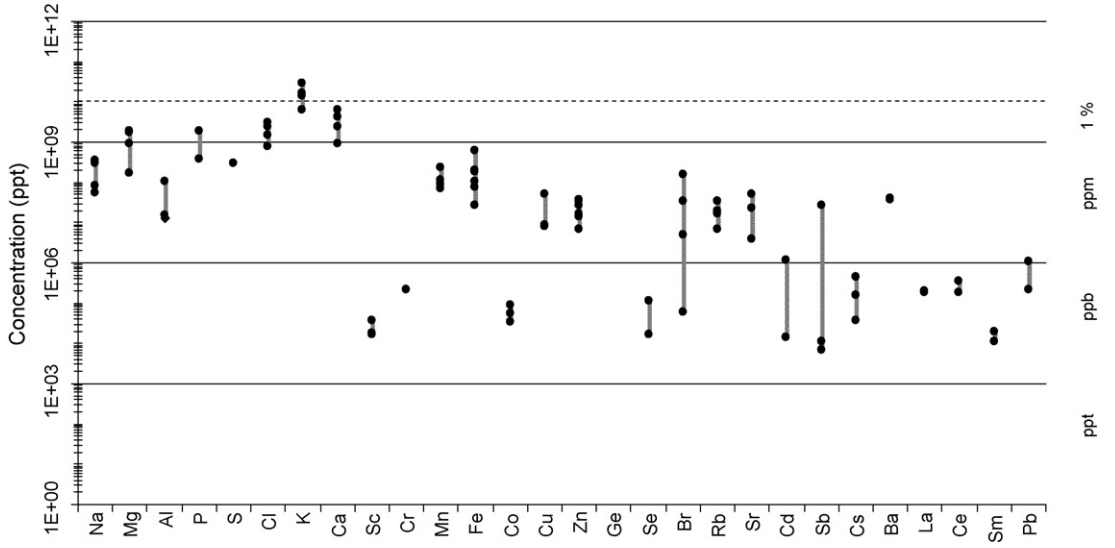

Fig. 4. Concentration ranges of elements determined in pepper from published studies.

Table 1
Methods proposed in the literature for the determination of trace elements in seasoning products

Methods	Materials	Elements	Reference
ETAAS	Onion	Pb, Cd	[7]
	Garlic, onion, black pepper, cinnamon, vanilla, mint, saffron, oregano, basil, parsley, thyme	Al	[8]
	Garlic, onion, black pepper, cinnamon, vanilla, mint, saffron, oregano, basil, parsley, thyme	Cr	[9]
	Garlic, onion, ginger	Ge	[10]
	Garlic	Se	[11]
	Thyme, coriander, rosemary	Cd, Pb	[12]
	Onion	Ca, Fe, Mg, Cd, Co, Cu, Mn, Ni, Pb, Zn	[13]
	Onion	15 elements	[14]
	Garlic, onion	Se	[15]
FAAS	Black pepper, cumin, parsley, basil, saffron, fennel	Pb, Cd, Cr, Ni, Sn, Zn, Mn, Cu, Fe	[5]
	50 spices	Pb, Cd	[16]
	Thyme, coriander, rosemary	Cu, Mn, Zn, Fe	[12]
	Onion	K, Na	[13]
	Fennel	Ca, Mg	[17]
	Basil, rosemary	Cu, Cd, Pb, Ni, Cr, Fe, Mn, Zn	[18]
	Onion	Na	[19]
	Black pepper, thyme, basil	Pb, Cd	[20]
	Garlic	Al, As, Ca, Cd, Cr, Cu, Fe, Hg, K, Mg, Mn, Na, Ni, P, Pb, S, Se, Se, Zn	[21]
	Garlic	15 elements	[14]
	Onion	Ca, K, Mn, Fe, Cu, Zn	[22]
	Onion, parsley	Pb, Ni	[23]
	Onion, pepper, garlic	Cu, Zn	[24]
	Garlic, onion, ginger	Fe, Ag, Pb, Hg, Cd, Cr, Ni	[25]
	Garlic, black pepper, cinnamon, cumin, rosemary, mint, oregano, basil, clove, parsley, thyme	Cu, Zn, Mn, Fe, Mg, Ca	[26]
CV-AAS	50 spices	Hg	[16]
AFS	Garlic	Al, As, Ca, Cd, Cr, Cu, Fe, Hg, K, Mg, Mn, Na, Ni, P, Pb, S, Se, Se, Zn	[21]
ICP-MS	Garlic	Se	[11]
	Onion	Co, Ni, Cu, Rb, Mo, Cd, Cs,	[19]
	Onion, garlic, mint, rosemary	Al, Ca, Cd, Ce, Cr, Cu, Fe, Mg, Mn, Ni, Pb, Si, Zn	[27]
	Onion	63 elements	[28]
	Onion	63 elements	[29]
	Garlic	Hg, Pd, Cd, As, U, Cr, V, Cu, Zn, Mo, Sb, Tl	[30]
	Garlic	Li, B, Na, Mg, P, S, Ca, Ti, Mn, Fe, Cu, Ni, Zn, Rb, Sr, Mo, Cd, Ba	[31]
	Onion, garlic, cumin	As, Cu, Ni, Mn, Zn, Se	[32]
	Onion, parsley	Pb, Cd	[33]
ICP-OES	Onion, garlic, mint, rosemary	Al, Ca, Cd, Ce, Cr, Cu, Fe, Mg, Mn, Ni, Pb, Si, Zn	[27]
	Onion	Na, Mg, P, Mn, Zn, Sr, Ba	[19]
	Black pepper, cumin, coriander	Fe, Mn, Zn, Cu, Co, Ni, Mo, Pb, Cr, Ca, Mg, Al, Si, P	[34]
	Onion, parsley	Cu, Cd, Ni, Pb, Zn	[35]
	Garlic	Al, As, Ca, Cd, Cr, Cu, Fe, Hg, K, Mg, Mn, Na, Ni, P, Pb, S, Se, Se, Zn	[21]
	Onion	Al, B, Ba, Cd, Cr, Cu, Fe, Mn, Ni, Sr, Zn	[36]
	Fennel	Al, Ba, Cd, Co, Cr, Cu, Fe, Mn, Ni, Pb, Sr, Zn	[17]
	Garlic	Al, B, Ba, Bi, Ca, Cd, Co, Cr, Cu, Fe, Ga, K, Li, Mg, Mn, Na, Ni, P, Pb, Sr, Zn	[37]
NAA	Onion	Na, Al, K, Ca, Sc, Ti, V, Cr, Mn, Fe, Co, Rb, Sb, Cs, La, Ce, Sm, Eu, Dy, Yb, Lu, Hf, Ta, Pa, U	[38]
	Onion	As, Pb, Cd	[39]
	Onion, garlic, black pepper, ginger, cinnamon, cumin, coriander, oregano, fennel	Br, Cl, Co, Cr, Cu, Fe, Hg, K, Mn, Mo, Na, P, Rb, Sb, Sc, Se, Sr, Th, Zn	[40]
	Garlic, onion	Se	[15]
	Ginger, coriander	18 elements	[41]
NAA, RNAA	Onion, garlic, black pepper, ginger, cinnamon, cumin, coriander, clove	Na, K, Rb, Cs, Mg, Ca, Sr, Ba, Cl, Br, Mn, Fe, Co, Zn, Sb, Al, Sc, La, Ce, Sm	[42]

Table 1 (*Continued*)

Methods	Materials	Elements	Reference
NAA	Onion, garlic, mint, rosemary	Al, Ca, Cd, Ce, Cr, Cu, Fe, Mg, Mn, Ni, Pb, Si, Zn	[27]
PIXE	Onion	Se	[43]
XRF	Black pepper, cumin, coriander	Mg, Al, Si, P, S, Cl, K, Ca, Ti, Mn, Fe, Cu, Zn	[44]
TXRF	Onion	Ca, K, Mn, Fe, Cu, Zn	[22]
Molecular fluorescence	Black pepper, coriander, cumin	Se	[45]
CSV	Garlic	Se	[46]
ADPV	Onion	Ni, Co	[47]
DPASV	Onion	As, Pb, Cd	[39]

ETAAS: electrothermal atomic absorption spectrometry, FAAS: flame atomic absorption spectrometry, ICP-MS: inductively coupled plasma mass spectrometry, ICP-OES: inductively coupled plasma optical emission spectrometry, NAA: instrumental neutron activation analysis, RNAA: radiochemical neutron activation analysis, PIXE: proton-induced X-ray emission, TXRF: total reflectance X-ray fluorescence, AFS: atomic fluorescence spectrometry, CSV: cathodic stripping voltammetry, ADPV: adsorption differential pulse voltammetry, and DPASV: differential pulse anodic stripping voltammetry.

(w/w), is the element with the highest concentration. S has not been analysed previously in garlic, however in onion and black pepper it is present at concentration levels ranging from 300 to 1000 ppm. P, Cl and Ca are also present at concentrations between 100 and 6000 ppm.

On the other hand Ga, Eu, Dy, Yb and Lu are at ppb level in garlic (see Fig. 2). However in the case of onion, they are present at ppt levels and they have not been analysed previously in black pepper.

For the main part of elements determined in onion, garlic and black pepper, there is a big fluctuation of their content which can vary from few ppb to 100 ppm, as a function of the origin and production conditions of samples considered. The relatively high-concentration of Pb and Cd found in onion and black pepper are certainly due to irrigation with contaminated water, as well as by the treatment of crops with some fertilizers and herbicides [5]. In addition, Pb contamination will depend on several factors, for example traffic densities and vicinity of industrial factories among others.

Additionally, it can be found in the literature several studies in which elemental composition of spices such as basil, cinnamon, clove, coriander, cumin, curry, fennel, ginger, mint, oregano, parsley, rosemary, saffron, thyme and vanilla was determined. As it can be seen in Fig. 5, K, Ca, Cl and Mg are in general at percentage levels. Moreover, Na, P and Fe present some fluctuations between spices varying their concentration levels from ppm to percentage. As for example, Na values observed in parsley and cinnamon were 5260 and 119.75 ppm, respectively and Fe values in mint and clove were 6580 and 131.3 ppm, respectively; thus evidencing the different nature of each spices. It is worth pointing out that elements such as Ba, Br, Rb, Cu and Ni show a similar tendency in all spices studied, being found at ppm levels. However, in the case of Al, a great fluctuation in its concentration is observed being reported, 5.2 ppm for parsley, 18.3 ppm for oregano, 117 ppm for cumin and 148 ppm for cinnamon. This variation is also observed in the case of Zn, being present at 14.8 ppm in clove and up to 103.7 ppm in parsley. Non-essential elements, like Pb and Cd, show low levels of concentration in all aforementioned spices, varying from 5 ppb to 5 ppm, except in parsley where Pb is higher than 5 ppm.

The World Health Organisation (WHO) prescribes limits for various plants of not more than 10 and 0.3 ppm for Pb and Cd, respectively [6]. Elements non-essential such as Sm, Cs, Ce and Co (except in cumin and parsley where it found in ppm level) were found at concentration levels of ppb. It is also highlighted that, it was not reported any of the 29 elements studied at ppt levels.

2. Methods for the determination of trace elements

Table 1 lists the papers published in the literature for trace elements determination in seasoning products, classified as a function of the different methods employed for their elemental analysis. Atomic absorption spectrometry techniques (AAS) using flame (FAAS), electrothermal atomic absorption spectrometry (ETAAS) or atomic fluorescence spectrometry (AFS) and inductively coupled plasma techniques (ICP) are the most commonly used by the greatest number of researchers. Other techniques, such as instrumental neutron activation analysis (INAA), proton-induced X-ray emission (PIXE), X-ray fluorescence spectrometry (X-ray), and voltammetry techniques including adsorption differential pulse voltammetry (ADPV), cathodic stripping voltammetry (CSV), and differential pulse anodic stripping voltammetry (DPASV) have been scarcely used in this field.

2.1. Absorption and fluorescence atomic spectrometry

AAS is a sensitive and highly selective spectrometric tool suitable for the determination of selected elements at trace and ultra-trace levels. The techniques commonly employed are graphite furnace atomic absorption spectrometry generally called ETAAS and additionally cold vapour atomic absorption, used for Hg determination and hydride generation atomic absorption, suitable to do the determination of covalent hydride forming elements.

The first precedent on the use of ETAAS for the elemental composition of seasoning products is that published in 1991 by Tahvonen et al. [7] in which Pb and Cd were analysed after wet digestion. The mean contents of Pb and Cd in onion from Finnish Market were 4 and 18 $\mu g\,kg^{-1}$, respectively.

Pb, Cd and Hg levels were analysed by flameless AAS and cold vapour atomic spectrometry reporting average concentrations of 0.470, 0.080 and 0.005 $mg\,kg^{-1}$ [16].

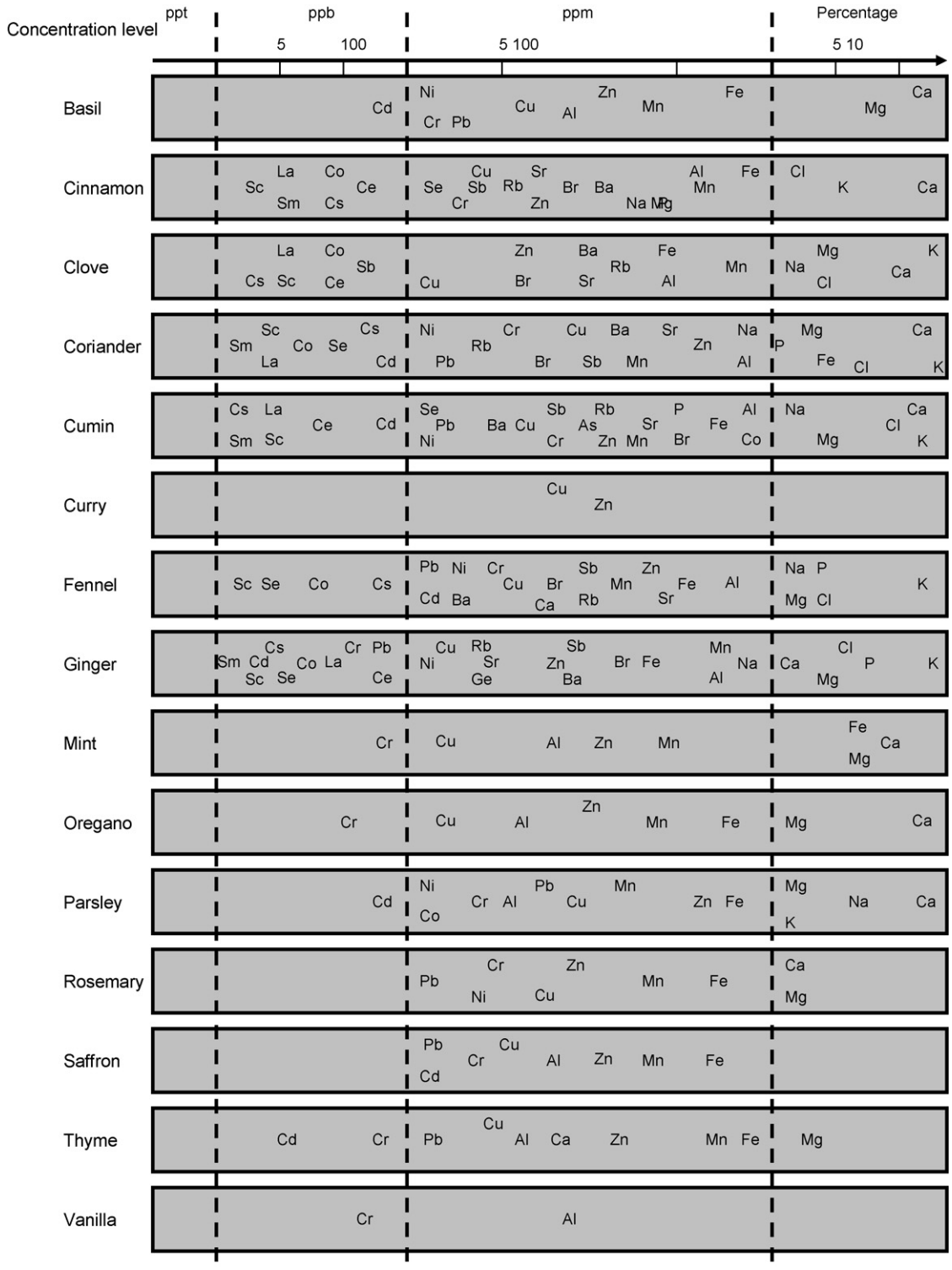

Fig. 5. Concentration values found for elements determined in different spices.

The levels of aluminium in onion, garlic and pepper have been determined using ETAAS. The accuracy and precision of the proposed method were verified against certified reference materials obtaining a range of precision from 1.10 to 4.07% [8]. The presence of Cr was also analysed in those three samples employing ETAAS. The proposed method is suitable to determine Cr in spices and is useful for routine control analyses of these kinds of products because of its sensitivity, versatility and speed. Detection limit (1 pg), analytical precision (5.0–5.2%) and accuracy (97.95%) obtained by this method were acceptable for the determination of Cr in foodstuff [9].

ETAAS has been also used for the determination of total germanium in foodstuff, such as garlic or onion [10]. It was found experimentally that Ca, Co, Cu, Mg, Ni, Pb and Zn do

not interfere Ge determination. The method was optimized with detection limits from 3.3 to 125 $\mu g\,L^{-1}$.

ETAAS has been used for the determination of the total concentration of Se in garlic samples from different geographical regions. The quantification was accomplished by using the standard addition technique. The influence of various modifiers was examined, and it was found that rhodium provided the best stabilization, enabling to apply the temperature even of 1200 °C during the pyrolysis step without any loss of Se. Spectral interferences were eliminated using Zeeman background correction. The analytical results have revealed differences in selenium content among garlic samples of various origins [11].

Cd and Pb have been determined by ETAAS and essential micronutrients, such as Cu, Mn, Fe and Zn were determined by FAAS using standard analytical conditions [12].

Both ETAAS and FAAS have been also employed to determine Ca, Cd, Co, Cu, Fe, Ni, Pb, K and Na in onion and parsley [13].

As it has been aforementioned, FAAS has been commonly used in the determination of elemental composition of several samples. In this sense, Ca and Mg were determined in herbs and infusions [17] and Cu, Fe, Ni, Cd, Mn, Pb, Cr and Zn were determined in spices and herbal plants from Turkey [18] obtaining R.S.D. values lower than 10%.

In other studies, Se was determined in onions to establish their geographical origin [19].

The limit of detection of FAAS for the determination of toxic elements like Cd, Hg, Pb and Tl was improved by using flame furnace AAS [20]. In this study, dissolved samples were introduced directly into a nickel tube located in the flame through a ceramic thermospray capillary. Parameters for the introduction of samples into the flame furnace using compressed air instead of a continuously flow were optimized.

Other interesting studies of elemental composition by ETAAS and FAAS published in the literature are listed in Table 1.

It is surprising that only a single precedent [21] was found for the use of atomic fluorescence spectrometry (AFS) in the determination of Hg, As and Se in spite of the high sensitivity and selectivity which can be found by AFS for elements such as Sb, Te or Bi.

2.2. Inductively coupled plasma techniques

The general trend observed worldwide is that the use of AAS for single-element analysis is being replaced by the use of ICP-OES and ICP-MS for the elemental analysis of samples concerning the determination of several elements per sample.

Inductively coupled plasma optical emission spectrometry (ICP-OES) is one of the most widely used techniques for multielement determinations. However, adequate pre-concentration and separation techniques are necessary before ICP-OES measurements because the analytical sensitivity of this technique is appropriate only at ppm levels.

Multi-elemental (Al, Ca, Cd, Ce, Cr, Cu, Fe, Mg, Mn, Ni, Pb, Si and Zn) analysis of onion and garlic were undertaken by ICP-OES and ICP-MS. For the elements listed the methodologies provide a good precision, with R.S.D. values between 1 and 10%. Exposure of crops to motor vehicle activities shows significant increase of Pb in spices by amount levels of 40–80% can be removed by washing plant surface [27].

ICP-OES was also used to determine mineral contents in garlic samples [37]. Several heavy metals like Fe, Mn, Zn, Cu, Co, Ni, Mo, Pb and Cr, alkaline earth metals like Ca and Mg, and other elements Al, Si and P were determined [34].

The elemental composition of different parts of the garlic plant was analysed by ICP-OES and alternatively by AAS and AFS after microwave oven sample pre-treatment. Al, As, B, Ca, Cd, Cr, Cu, Fe, Hg, K, Mg, Mn, Na, Ni, P, Pb, S, Se, Sr and Zn were determined. It was found that tender leaves and bulbs of garlic cumulate Cu, Fe, Mn, S, Se and Zn [21].

Geographical origin of onions can be determined based on their differences in mineral composition [19]. The objective of this study was to develop a method to determine seven elements (Na, Mg, P, Mn, Zn, Sr and Ba) by ICP-OES including an absolute calibration method and seven elements (Co, Ni, Cu, Rb, Mo, Cd and Cs) by ICP-MS including an internal standard method.

ICP-MS is one of the most sensitive analytical techniques for fast multielement determination of heavy metals at trace and ultra-trace concentrations in different sample matrices [34]. The use of ICP-MS has grown in the last decade as a simultaneous multielement detection method. This methodology presents excellent selectivity and it offers also a high sensitivity and the possibility of performing isotopic determinations.

ICP-MS methods were employed to determine 63 elements in onion samples [28] and onions and peas [29]. The isotopes analysed are chosen to obtain the best sensitivity and to avoid overlapping from polyatomic interferences. When polyatomic interferences could not be avoided, a high resolution was applied to solve the analyte peaks from the interfering polyatomic ones. However when a high resolution is applied, the ion transmissions is decreased significantly. On the other hand As and Se are two elements that suffer interferences with argon which cannot be resolved using high resolution [28].

An evaluation of metal composition in botanical supplements has been done by analysis of Pb, Hg, Cd, As, U, Cr, V, Cu, Zn, Mo, Pd, Sn, Sb, and Ta using ICP-MS. Before data acquisition the ICP-MS must be optimized with a standard solution of 10 $\mu g\,L^{-1}$ of Be, Co, In, Ce, Bi and U. Parameters such as torch position and gas flow rates were adjusted until the maximum and most stable signal was observed for a wide range of masses. The elements In and Bi were used as internal standards [30].

ICP-MS has been also used to determine the geographical origin of agricultural products based on its metal profile and as for example Li, B, Na, Mg, P, S, Ca, Ti, Mn, Fe, Cu, Ni, Zn, Rb, Sr, Mo, Cd and Ba were analysed in garlic samples [31].

2.3. Nuclear techniques

Instrumental neutron activation analysis (NAA) allows the simultaneous determination of trace elements giving sensitive and reliable results for seasoning product samples, in the range of very low concentrations. It does not require any dissolution

nor sample preparation and is not much affected by interferences if samples are properly measured, thus permitting, in some cases, the determination of elements difficult to be measured by other techniques. Nevertheless, it requires big facilities and laboratories with the adequate safety conditions to use a nuclear reactor.

NAA was firstly used to determine the concentration of 18 trace elements (essential, toxic and non-essential) in different spices consumed in the Rawalpindi in Islamabad area. The comparison of values obtained with Canadian and Egyptian data shows variation in trace element composition [41].

NAA and radiochemical neutron activation analysis (RNAA) were used to determine 26 trace elements in garlic, onion and black pepper. The concentration levels, their variation and the correlations between elements in these samples were investigated. High elemental correlations exist in some sets of elements, reflecting characteristics of chemical nature of elements and of their physiological functions [42].

The nutritive potential of black pepper, garlic and onion, in terms of trace element contents, has been evaluated using NAA. Samples were airlifted at different intervals (2 and 4 days, 2 and 4 weeks up to 3 months). Elemental concentrations from different irradiation periods or from different photo peaks of the same radionuclide were determined in short as well as long-term irradiations [40].

2.4. X-ray fluorescence spectrometry

X-ray fluorescence spectrometry (XRF) is a very convenient tool for the determination of major and minor components in solid samples. It has been used in the field of quality control procedures. Samples were irradiated under five different fixed conditions, namely: very light elements, solids, steels, medium elements and very heavy elements, under vacuum to achieve the best sensitivity and to cover all elements in the periodic table that are present in the samples [44].

XRF analysis was used for the in vivo determination of the distribution of total Se in roots and leaves of onion. Samples were irradiated with an X-ray beam of photons with energy in the 17.0–17.5 keV range. The arrangement of X-ray optical elements makes possible to visualize the distribution of constituents in arbitrarily selectable virtual cross sections. In this case, the self-absorption of the incident beam ($E = 17$ keV) and of the emitted fluorescent radiation ($E = 11.2$ keV) is assumed to be sufficiently small. During the in vivo experiment, onions were moisturized by wrapping them in sheets of wet filter paper and aluminium foil [53].

Unfortunately, there is a reduced sensitivity of the aforementioned methodology. Instrumental methods for improving the detection limits of XRF include the use of total reflectance XRF and polarized radiation-based XRF. The technique of TXRF was successfully applied for the simultaneous determination of Ca, K, Mn, Fe, Cu and Zn in onion samples. The excitation was performed with the Kα line of a molybdenum anode X-ray tube, operated at 40 kV and 20 mA. In comparison to atomic techniques, it has the advantage of the possibility of direct quantification of untreated samples [22].

Additionally, proton-induced X-ray emission (PIXE) technique has been employed for trace Se determination. It is a very selective methodology but it is necessary a pre-concentration step of Se by oxidation, reduction and co-precipitation with Te. The filtered probe material is dissolved, labelled with yttrium as an internal PIXE standard and deposited on a thin foil of polycarbonate by solvent drip evaporation. Se targets, isolated from samples of onions were irradiated by a 3 MeV proton beam of 70 nA beam current [43].

2.5. Molecular fluorescence spectrometry

The total selenium content of spices can be determined by fluorescence spectrometry. After a digestion process of samples, the different forms of selenium were reduced by boiling with diluted HCl and added EDTA solution being necessary to adjust the pH with ammonia using Cresol red as indicator. The Se in the sample was complexed with 2,3-diaminonaphthalene to give a fluorescent compound, which was extracted with cyclohexane and read on a spectrofluorometer at excitation and emission wavelengths of 378 and 518 nm, respectively [45].

2.6. Voltammetry

Selenium could be determined in species on hanging mercury drop electrode using cathodic stripping voltammetry (CSV). The effects of deposition potential, deposition time and sweep rate on Se peak were evaluated to determine the optimum experimental conditions. A deposition potential of −0.2 V was applied for 120 s while slurring the solution by passing nitrogen. The aforementioned method was used for the first time in 1999 for the determination of Se in garlic samples without any separation procedure or pre-concentration technique [46].

Differential pulse anodic stripping voltammetry (DPASV) was used for the determination of Cd and Pb in onions. The accuracy and precision of these analyses were checked against standard reference materials. Results obtained are in excellent agreement with certified values [39].

The simultaneous determination of Ni and Co at pH 9 after adsorption accumulation of their respective complexes with dimethylglyoxime at the mercury drop electrode was made by adsorption differential pulse voltammetry (ADPV) [47].

3. Sample treatment

Most analytical methods for trace element determination require homogeneous samples and solutions free, or almost free, from organic matter, which can interfere by interaction with both, metal ions and chemical reagents, used in the elemental determinations. Consequently, sample treatment is an important step in order to extract the analytes from the sample matrix, and to avoid interferences on the measurement step. Losses of volatile compounds caused by sample treatment are one of the major problems to be taken into account when a digestion system is selected.

For the preparation of vegetable or spice samples, dry ashing [54], wet digestion [14,13], microwave-assisted treatment [23]

or ultrasound-assisted extractions [22] are commonly used. In the case of nuclear techniques no sample treatment is required [39,42].

3.1. Dry ashing

Dry ashing methods present the disadvantage of possible losses of volatile elements, analyte reactions with the crucible material or combustion residues and also risks of sample contamination. However, several research groups have used this technique for the determination of many elements by ICP-OES. Samples digested in HNO_3 were ashed in a muffle furnace at 460 °C for 24 h [35] or by using a temperature gradient up to 550 °C and leaving this temperature during 10 h [24]. In fact it must be emphasized that dry ashing assures a complete elimination of the organic matter and provides high pre-concentration factors but they are tedious and prone to produce looses and contamination.

3.2. Wet digestion

Wet decomposition can be performed with a concentrated acid or mixture of acids in open or closed systems by the use of convective or microwave heating. In general, wet digestion procedures in open vessels usually require constant operator attention and are prone to systematic errors, such as contamination and loss of volatile elements.

The combination of HNO_3 at high-temperature (150 °C) during 1 h and addition of $HClO_4$ after cooling to 40 °C, and reheated to 80 °C was used as digestion process prior to elemental analysis of garlic, onion or ginger samples [25].

The use of a multiplace block digestion for sample mineralization has been proposed for chromium analysis in spices. In this case a portion of homogenized sample was treated with HNO_3 and V_2O_5 as a catalyst and heated at 120 °C for 90 min. The digestion procedure provides a rapid and complete sample mineralization, without analyte losses and or contamination. Moreover, mineralization of a large number of samples can be carried out at the same time with considerable reduction of reagents use and preparation time [9].

For the determination of Cu, Cd, Pb, Ni, Cr, Fe, Mn and Zn in basil and rosemary, purchased from farms of Turkey, samples were weighted (1.0 g) and dissolved with 8 mL of a mixture of HNO_3–$HClO_4$–H_2O_2 (2:1:1). Samples were heated at 170 °C for 3 h, cooled down, and then 2 mL of H_2SO_4 and 8 mL of acids mixture were added. The obtained solutions were centrifuged at 490 × *g* for 5 min and metals determined by atomic absorption spectrometry [18].

3.3. Microwave-assisted treatment

Microwave-assisted digestion has clear advantages over the traditional acid digestion using convective heating systems in terms of recovery, precision, time and looses of volatile elements. It reduces the possibility of cross contamination and the consumption of reagents. Nowadays it is the most widely used method for treatment of onion, garlic and spices before their elemental analysis by most of the available techniques.

Several digestion methods were attempted in closed vessels (low-pressure digestion 120 psi, medium-pressure 1200 psi and high-pressure 3000 psi). The three optimized methods were applied to the digestion of cinnamon samples. The main differences among the three digestion methods lie in the time required to complete the digestion and in safety aspects. Microwave digestion performed in low-pressure reactor with 5 mL of HNO_3 and 0.5 mL of HF had some advantages, it was the safest digestion procedure, it allowed the simultaneous dissolution of up to 12 samples and the digestion processes were developed in successive steps until completion [26].

Application of microwave-assisted extraction for the decomposition and dissolution of plant samples for trace metal determination by ICP-OES has been discussed earlier [36]. In this work water, EDTA and HCl were used as extractants. The influence of HCl concentration on the efficiency of the extraction process was studied. HCl was found to be very suitable for quantitative extraction of B, Ba, Cd, Cu, Mn, Ni, Pb, Sr and Zn. On the other hand, it was found that concentrations measured without extract digestion were higher for B, Cd, Mn and Zn with the exception of Cu and Pb. Extraction with EDTA led to much better results than those obtained with water.

The combination of different acids, sulphuric, nitric and hydrochloric is a very frequent method for preparing samples before their quantitative elemental analysis [32]. The mixture of some acids such as HNO_3 (10), HNO_3/HCl (10/5), HNO_3/H_2O_2 (10/2), $HNO_3/HClO_4$ (10/1) were investigated to select the optimal conditions for the digestion process. According to recovery results (garlic 44–48% and onion 71–78%) of digested sample with different acid combinations, HNO_3 plus H_2O_2 mixture was selected [15].

Microwave digestion process was employed for dried samples by adding concentrated HNO_3, $HClO_4$ and HCl. It seems that, for some elements, the microwave digestion provides higher recoveries that other procedure. Incomplete analyte recoveries may be caused by the presence of siliceous material in the samples. With the reagents used in this study, it is impossible to dissolve such material completely. Therefore, the recoveries of some elements that are associated with resistant fractions of the plant material strongly depend on digestion conditions [17].

3.4. Ultrasound-assisted extraction

Low-energy strategies, like the use of an ultrasound water bath, were assayed for the treatment of seasoning samples in order to do an acid extraction. Samples were homogenized with deionized water in a domestic homogenizer and different nitric acid concentrations (0, 5, 10 and 15%, v/v) were assayed. Samples, placed for 30 min in the ultrasound water bath were heated at 70 °C. It was found that the best results were found on using 5% (v/v) nitric acid and 5% of wet sample mass [22].

A major advantage of the use of soft digestion procedures, such as those based on the use of microwave-assisted digestion or ultrasound-assisted ones, are the possibilities offered to provide a quantitative dissolution of the elements to be determined,

without a complete matrix dissolution preserving the original chemical form of elements concerned and thus, opening a way for speciation of solid samples.

4. Speciation

The determination of the total concentration of trace elements is important but also the determination of the different chemical species of an element that are present in the samples is necessary in order to evaluate clearly their toxicity and or availability.

All analytical steps preceding speciation are extremely critical to assure the stability and quantitative recovery of chemical species present in natural samples. Sampling, sample preservation storage and sample treatment must be carefully controlled in order to not disturb the equilibrium established among the different species. Several elements can be speciated such as Sb, Fe, Te, Se, Pb, Cr, As, Hg as a function of their different oxidation states and specific chemical forms, but in the case of seasoning products only selenium speciation studies have been made on garlic and onion as it can be seen in Table 2.

The use of liquid chromatography hyphenated with ICP-MS offers an effective method for the speciation of Se; moreover, electrospray ionization-tandem mass spectrometry (ESI-MS–MS) is also effective for the identification of unknown seleno compounds because it provides the molecular information of the chromatographic peaks [50]. The same speciation techniques have been used for the determination of seleno compounds as selenite, selenate, Se-methylselenocysteine (MeSeCys) and γ-glutamyl-selenomethylselenocysteine (GluMeSeCys) [48]. In other cases it is also employed to determine Se-methionine and Se-cysteine/Se-cystine [51].

Anion and cation exchange chromatographies were applied for the separation of selenium species (Se(IV), SeMet) with mass spectrometric detection. Two different sample preparation methods: NaOH and enzymatic digestion were compared for the Se extraction [52].

An alternative, to the extraction of Se species is to use an ultrasound-assisted treatment. In this case, samples were homogenized through the action of ultrasounds applied through a titanium probe. The action of ultrasounds for longer than 3 min provided an important over heating of the mixture and therefore 3 min was selected as the best extraction time. The action of ultrasound probe is able to reduce dramatically the extraction time, which is of critical importance for speciation studies in order to guarantee species stability. However, in order to improve the suitability of the ultrasound-assisted extraction method, it is

Table 2
Speciation of Se through HPLC–ICP-MS and ESI-MS–MS in garlic and onion samples

Sample	Species	Concentration (ppm)	Reference
Garlic	Se(VI)	12.2	[48]
	Se-methylselenocysteine	2.2	
	GluMeSeCys	131.9	
Onion	Se(VI)	63.5	
	Se-methylselenocysteine	149.7	
	GluMeSeCys	12.2	
Garlic	Se-methylselenocysteine	–	[49]
	Se-methionine	–	
Garlic	γ-Glutamyl-Se-methylselenocysteine	78% total Se	[50]
Onion bulbs	Se(IV)	15.6	[51]
	Se(VI)	51.3	
Onion leaves	Se-methylselenocysteine Se(IV)	6.16	
	Se-methylselenocysteine Se(VI)	11.4	
	Se-methionine Se(IV)	0.5	
	Se-methionine Se(VI)	1.2	
	Se-cysteine/Se-cystine Se(IV)	0.8	
	Se-cysteine/Se-cystine Se(VI)	0.6	
Onion	Se(VI)	–	[36]
	Se(IV)	–	
	Se-methylselenocysteine	–	
	Se-methionine	–	
	L-Se-cysteine		
Onion bulbs	SeMet	10.9	[52]
	Se(IV)	14.4	
Onion leaves	SeMet	11.2	
	Se(IV)	11.8	

HPLC–ICP-MS: high performance liquid chromatography–inductively coupled plasma mass spectrometry, ESI-MS–MS: electrospray ionization-tandem mass spectrometry.

necessary to ensure species integrity during the whole extraction/separation/detection process [49].

In order to do Se speciation two different chromatographic mechanisms have been applied to the extracts: reversed phase ion pairing chromatography (RP-LP-HPLC) with heptafluorobutyric acid as ion pairing agent and an HPLC column combining size exclusion and ion exchange mechanisms. In all the experiments total Se extraction efficiencies ranged from 75 to 122% [49].

So, there is a lack of speciation studies of elements different than Se and, additionally there are no precedents on the use of non-chromatographic strategies to be applied to seasoning products.

5. Conclusions

The revision of the published papers has evidenced that ICP-MS is the most effective tool in profiling of single, multielement and speciation analysis of the different elements present in seasoning products, like spices, onion and garlic. Although atomic absorption spectrometric techniques, AAS, nuclear techniques and electrochemical method were also used, ICP-OES and ICP-MS were the unique techniques selected for determination of a big number of heavy metals in a same sample. The particular advantage of ICP-MS when compared to other techniques is its high sensitivity and the possibility to do isotope determination.

Acid treatment and microwave digestion have been the methods of choice for sample preparation. Microwave digestion has many advantages over the acid digestion in terms of better recovery of volatile elements and precision. However it is clear that additional research must be made to obtain accurate and reproducible data of the elemental composition of spices together with information about the main chemical forms of elements present in this kind of samples in order to evaluate the contribution of seasoning products to the daily intake of micronutrients and toxic elements.

References

[1] FAOS/TAT Food and Agriculture Organization of the United Nations, http://faostat.fao.org/.
[2] U. Schweiggert, R. Carle, A. Schieber, Trends Food Sci. Technol. 18 (2007) 260.
[3] C.G. Fraga, Mol. Aspects Med. 26 (2005) 235.
[4] J. Lag, I.H. Elsokkary, Acta Agric. Scand. 28 (1978) 76.
[5] A.A.K. Abou-Arab, M.A.J. Abou Donia, Agric. Food Chem. 48 (2000) 2300.
[6] WHO, WHO Monographs on Selected Medicinal Plants, vol. 1, World Health Organisation, Geneva, 1999.
[7] R. Tahvonen, J. Kumpulainen, J. Fresenius, Anal. Chem. 340 (4) (1991) 242–244.
[8] F. Lopez, C. Cabrera, M.L. Lorenzo, M.C. Lopez, Sci. Total Environ. 257 (2000) 191.
[9] E. Garcia, C. Cabrera, M.L. Lorenzo, M.C. López, Sci. Total Environ. 247 (2000) 51.
[10] M. Mc Mahon, F. Regan, H. Hughes, Food Chem. 97 (2006) 411.
[11] I.A. Wysocka, E. Bulska, K. Wrobel, K. Wrobel, Chem. Anal. Warsaw 48 (2003) 919.
[12] R. Chizzola, H. Michitsch, C. Franz, Eur. Food Res. Technol. 216 (2003) 407.
[13] A.E. Mohamed, M.N. Rashed, A. Mofty, Ecotoxicol. Environ. Saf. 55 (2003) 251.
[14] S.R. Sahito, T.G. Kazi, G.H. Kazi, M.A. Jakhrani, J. Chem. Soc., Pak. 24 (2002) 134.
[15] B. Izgi, S. Gucer, R. Jacimovic, Food Chem. 99 (2006) 630.
[16] B. Brunner, S. Stolle, Z. Ernahrungswiss. 34 (1995) 113.
[17] S. Basgel, S.B. Erdemoğlu, Sci. Total Environ. 359 (2006) 82.
[18] U. Divrikli, N. Horzum, M. Soylak, L. Elci, Int. J. Food Sci. Technol. 41 (2006) 712.
[19] K. Ariyama, Y. Aoyama, A. Mochizuki, Y. Homura, M. Kadokura, A. Yasui, J. Agric. Food Chem. 55 (2007) 347.
[20] H. Berndt, E. Pulvermarcher, Anal. Bioanal. Chem. 382 (2005) 1826.
[21] X.P. Wang, S.L. Xiang, Spectrosc. Spect. Anal. 26 (2006) 1907.
[22] J. Alvarez, L.M. Marco, J. Arroyo, E.D. Greaves, R. Rivas, Spectrochim. Acta B 58 (2003) 2183.
[23] S. Baytak, A.R. Turker, J. Hazard. Mater. 129 (2006) 130.
[24] P.C. Onianwa, A.O. Adeyemo, O.E. Idowu, E.E. Ogabiela, Food Chem. 72 (2001) 89.
[25] K. Masud, M. Jaffar, J. Chem. Soc., Pak. 20 (1998) 186.
[26] A. Lavilla, V. Filgueiras, C. Bendicho, J. Agric. Food Chem. 47 (1999) 5072.
[27] N.I. Ward, J.M. Savage, Sci. Total Environ. 147 (1994) 309.
[28] A. Bibak, A. Behrens, S. Sturup, L. Knudsen, V. Gundersen, J. Agric. Food Chem. 46 (1998) 3139.
[29] V. Gundersen, I.E. Bechmann, A. Behrens, S. Sturup, J. Agric. Food Chem. 48 (2000) 6094.
[30] P. Raman, L.C. Patino, M.G. Nair, J. Agric. Food Chem. 52 (2004) 7822.
[31] R.G. Smith, J. Agric. Food Chem. 53 (2005) 4041.
[32] T. Roychowdhury, H. Tokunaga, M. Ando, Sci. Total Environ. 308 (2003) 15.
[33] F. Capdevila, M. Nadal, M. Schuhmacher, J.L. Domingo, Trace Elem. Electrolytes 20 (2003) 256.
[34] K.K. Gupta, S. Bhattacharjee, S. Kar, S. Chakrabarty, P. Thakur, G. Bhattacharyya, S.C. Srivastava, Commun. Soil Sci. Plant 34 (2003) 681.
[35] D. Demirezen, A. Aksoy, J. Food Qual. 29 (2006) 252.
[36] J. Borkowska-Burnecka, Fresenius J. Anal. Chem. 368 (2000) 633.
[37] H. Hacıseferoğullarıa, M. Özcanb, F. Demira, S. Çalışıra, J. Food Eng. 68 (2005) 463.
[38] M.O.A. OIadipo, F. Rehman, Spectrosc. Lett. 24 (1991) 577.
[39] F. Queirolo, S. Stegen, M. Restovic, M. Paz, P. Ostapczuk, M.J. Schwuger, L. Munoz, Sci. Total Environ. 255 (2000) 75.
[40] V. Singh, A.N. Garg, Food Chem. 94 (2004) 81.
[41] I.H. Zaidi, I.H. Qureshi, M. Arif, I. Fatima, Int. J. Environ. Anal. Chem. 48 (1992) 33.
[42] Y. Miyamoto, A. Kajikawa, J.H. Zaidi, T. Nakanishi, K. Sakamoto, J. Radioanal. Nucl. Chem. 243 (1999) 747.
[43] A. Amokrane, M.E.A. Benamar, Nucl. Instrum. Methods A 480 (2002) 50.
[44] B.A. Al-Bataina, A.O. Maslat, M.M. Al-Kofahi, J. Trace Elem. Med. Bio. 17 (2003) 85.
[45] A. Kumar, K. Krishnaswamy, J. Agric. Food Chem. 45 (1997) 2565.
[46] R. Inam, G. Somer, Food Chem. 66 (1999) 381.
[47] S. Stegen, F. Queirolo, C. Carrasco, P. Ostapczuk, M.J. Schwuger, J. Chil. Chem. Soc. 47 (2002) 279.
[48] Y. Ogra, K. Ishiwata, Y. Iwashita, J. Chromatogr. A 1093 (2005) 118.
[49] M. Montes-Bayon, M. Molet, E. Gonzalez, A. Sanz-Medel, Talanta 68 (2006) 1287.
[50] S. Mc Sheehy, W.J. Yang, F. Pannier, J. Szpunar, R. Lobinski, J. Auger, M. Potin-Gautier, Anal. Chim. Acta 421 (2000) 147.
[51] W. Katarzyn, K. Wróbel, S.S. Kannamkumarath, J.A. Caruso, I.A. Wysock, E. Bulska, J. Witek, M. Wierzbicka, Food Chem. 86 (2004) 617.
[52] E. Kápolna, F. Péter, Microchem. J. 84 (2006) 56.
[53] E. Bulska, I.A. Wysocka, M.H. Wierzbicka, K. Proost, K. Janssens, G. Falkenberg, Anal. Chem. 78 (2006) 7616.
[54] M. Soylak, H. Colak, O. Turkoglu, Fresenius Environ. Bull. 15 (2006) 345.

Available online at www.sciencedirect.com
ScienceDirect
Talanta 74 (2008) 1371–1377
Talanta
www.elsevier.com/locate/talanta

On-line pretreatment and determination of parabens in cosmetic products by combination of flow injection analysis, solid-phase extraction and micellar electrokinetic chromatography

Fang Han, You-Zhao He *, Chang-Zhu Yu

Department of Chemistry, University of Science and Technology of China, Hefei, Anhui 230026, China

Received 2 July 2007; received in revised form 12 September 2007; accepted 13 September 2007
Available online 19 September 2007

Abstract

A convenient and automated method for on-line pretreatment and determination of three parabens (i.e. methyl, ethyl and propyl *p*-hydroxybenzoate) in cosmetic products is proposed by using flow injection analysis (FIA), solid-phase extraction (SPE) and micellar electrokinetic chromatography (MEKC). An improved split–flow interface is used to couple SPE on C_8-bonded silica with MEKC separation, which can avoid running buffer contamination and reduce buffer consumption, especially, containing expensive reagents. The analytes are loaded onto a C_8 column at 0.6 mL/min for 60 s and eluted with a mixed eluent of 40% (v/v) 10 mmol/L sodium tetraborate buffer (pH 9.3) and 60% (v/v) ethanol at 0.75 mL/min. The MEKC separation is accomplished with a running buffer of 20 mmol/L sodium tetraborate (pH 9.3) containing 100 mmol/L sodium dodecyl sulfate (SDS) at 15 kV. For butyl *p*-hydroxybenzoate did not be detected in the cosmetic products, it was used as an internal standard (IS) added into the real samples. This FIA–SPE–MEKC method using IS allows the sample separation within 12 min and the sample throughput of five samples per hour with the relative standard deviation (R.S.D.) less than 2.3% ($n = 5$). The limits of detection (LOD) are in the range from 0.07 to 0.1 μg/mL (S/N = 3 and $n = 11$). The proposed method has been used to determine three parabens in real cosmetic products satisfactorily.
© 2007 Elsevier B.V. All rights reserved.

Keywords: Flow injection analysis; Solid-phase extraction; Micellar electrokinetic chromatography; Split–flow interface; Parabens

1. Introduction

Parabens, viz., alkyl *p*-hydroxybenzoates, are widely used as preservatives in cosmetic products due to their broad spectrum of antimicrobial activity and ideal physicochemical properties [1–3]. Several animal and human studies on the safety of parabens appeared in recently published papers indicate that the exposure to parabens may modulate and disrupt the endocrine system, and may have harmful effects on human health [4,5]. Therefore, the highest concentration of single paraben allowed in a cosmetic product is 0.4% (w/w), and the highest total concentration for paraben mixtures is 0.8% (w/w) [6]. Consequently, the development of analytical methods of parabens in cosmetic products has practically demanded for consumer health.

For paraben separation and determination, a large number of chromatographic methods have been reported. High performance liquid chromatography (HPLC) is the most common method used for detecting these compounds, which often combines a pretreatment procedure to remove non-polar matrices and uses a gradient elution to improve the resolution typically [7–10]. In recent years, capillary electrophoresis (CE) including micellar electrokinetic chromatography (MEKC) was perceived to be an attractive separation technique in paraben analysis due to its high efficiency, low reagent consumption and high analysis speed [11–15]. In spite of its versatility, some limitations, such as discontinuous sample injection, limited analysis throughput, low sensitivity and large matrix effects, still call for the improvement of CE further. In addition, off-line sample pretreatment is time consuming and often requires considerable skill to maintain good precision. Flow injection analysis (FIA) has already been employed in paraben analysis during past 5 years [16–19]. The combination of FIA with CE has shown to be of great value and practical applicability as demonstrated by several papers

* Corresponding author. Tel.: +86 551 3607072; fax: +86 551 3603388.
E-mail address: yzhe@ustc.edu.cn (Y.-Z. He).

0039-9140/$ – see front matter © 2007 Elsevier B.V. All rights reserved.
doi:10.1016/j.talanta.2007.09.007

[20–28]. The advantages of FIA–CE system include outstanding reproducibility in peak response and retention time and enhanced sample throughout. These systems have been applied to on-line sample pretreatment, including sample filtration [26], dialysis [22], gas diffusion [24], ion exchange preconcentration [28], derivation [25] and solid-phase extraction [27], etc.

The sample pretreatment prior to CE separation for the determination of parabens in cosmetic products includes liquid–liquid extraction, ion exchange clean up, protein precipitation, etc. which are laborious, time consuming and insufficient for the removal of interference substances [29]. Solid-phase extraction (SPE) [30] can avoid or minimize the shortcomings of liquid–liquid extraction, particularly, for its large organic solvent consumption. To remove oil matrices in oil-based lotions and creams, and eliminate the interference in the paraben analysis, solid-phase extraction is used as the sample clean up and preconcentration procedure in this paper.

Focusing on the interface techniques in the combination of FIA with CE, several designs of on-line interfaces are reported [21,31,32]. In those systems, the sample solutions passed through the reservoir of running buffer, which was able to cause the buffer contamination and increase its consumption for injecting the sample solution and removing the polluted buffer. In this paper, an improved interface is adopted to protect the running buffer from contamination and reduce the buffer consumption, especially, containing expensive reagents, and is used for coupling continuous on-line SPE pretreatment with MEKC separation to determine three parabens in cosmetic products.

2. Experimental

2.1. Reagents and solutions

Methyl *p*-hydroxybenzoate (MP), ethyl *p*-hydroxybenzoate (EP), propyl *p*-hydroxybenzoate (PP), butyl *p*-hydroxybenzoate (BP), sodium tetraborate, sodium dodecyl sulfate (SDS), sodium hydroxide, hydrochloric acid, ethanol, methanol, acetonitrile (ACN), etc. were of analytical grade and obtained from Chemical Reagent Co. (Shanghai, China). Tri-distilled water was used to prepare solutions from an SZ-3 distilled water system (Huxi Anal. Instr. Factory, Shanghai, China).

Each paraben stock solution of 2.00 mg/mL was prepared in acetonitrile. The calibration solutions with different concentrations were prepared by diluting the stock solutions with 10 mmol/L sodium tetraborate buffer (pH 9.3) containing 20% acetonitrile (v/v). A 20 mmol/L sodium tetraborate (pH 9.3), the sodium tetraborate solution containing 100 mmol/L SDS and a mixed solution of 40% (v/v), 10 mmol/L sodium tetraborate buffer (pH 9.3) and 60% (v/v) ethanol were used as the carrier solution for FIA, the running buffer in MEKC and the eluent of SPE, respectively. BP did not be detected in the cosmetic samples, it was used as an internal standard (IS) added into each standard and real sample at a concentration of 50 μg/mL. All the solutions were degassed for 15 min by an S-2200 ultrasonic bath (120 W, 35 kHz, J&L Ltd., Shanghai, China) before use.

2.2. FIA–SPE–MEKC system

A 1229-HPCE Analyzer (Institute New Tech. Appl., Beijing, China) detecting at 254 nm and an N-2000 double-channel chromatography processor (Institute Info. Engineering, Zhejiang Univ., Zhejiang, China) were used throughout the MEKC separation. An uncoated fused silica capillary with 50 μm i.d., 70 cm total length and 40 cm effective length was purchased from Yongnian Chromatogr. Components Ltd. (Hebei, China). A power supply of negative high voltage was employed for the operation safety of the interface. An XW-80A vortex mixer (Jingke, Shanghai, China) was used for mixing sample solutions.

An FIA system (IFIS-C, Ruimai Electr. Tech. Ltd., Xi'an, China) equipped with two peristaltic pumps, one eight-way injection valve and one 90 μL sample loop was employed for the automated FIA operation. 0.5 mm i.d. PTFE tube and 1.2 mm i.d. Viton tubing (Cole-Parmer Instr. Co., USA) was used as the conduits and pump tubing of the FIA system, respectively.

A homemade split flow interface of the FIA–SPE–MEKC system is shown in Fig. 1. The schematic diagram of the system is illustrated in Fig. 2. The interface was prepared from a 1 mL plastic pipette, of which the upper part 25 mm and the lower part 3 mm from the pipette tip were cut off and the latter formed a hole of 1.6 mm diameter. To introduce the running buffer solution into the interface, a short silicone tube was connected with the side of the pipette through a 5 mm diameter hole. A Tee connector (TC) was used to joint a 0.5 mm i.d. and 1.5 mm o.d. PTFE tube, a separation capillary (SC) and a sample loop (SL), where the pretreated sample solution was filled and delivered by the pumps. The PTFE tube with a slope end and a grounded Pt electrode were fixed on the top of the pipette by a silicone rubber seal (SRS1), and the PTFE tube was inserted into the pipette tip connected with an injection valve (V) by a 1.2 mm i.d. Viton tubing (VT) to expel waste solutions from the interface. Before

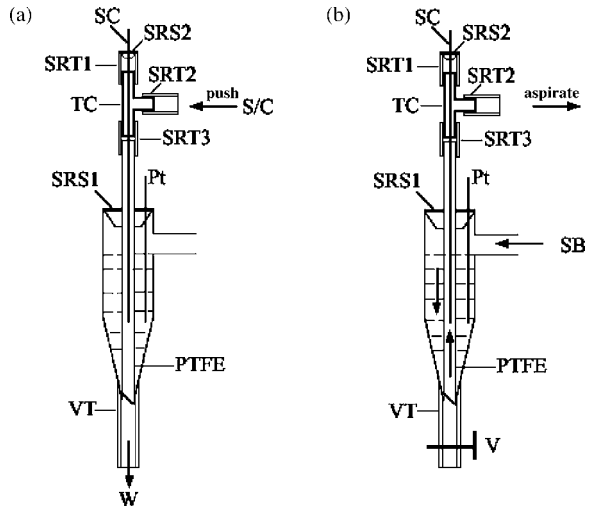

Fig. 1. Schematic diagram of split–flow interface: (a) injecting sample solution; (b) aspirating separation buffer. PTFE: polytetrafluoroethylene tube; Pt: platinum electrode; SB: separation buffer; SC: separation capillary; S/C: sample/carrier solution; SRS: silicone rubber seal; TC: Tee connector; VT: Viton tubing; SRT: silicone rubber tubing; V: injection valve; W: waste.

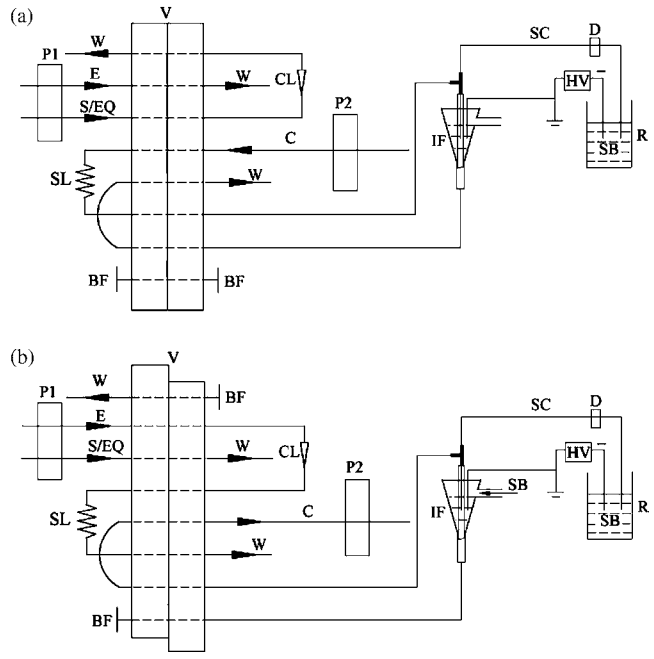

Fig. 2. Schematic diagram of FIA–SPE–MEKC system: (a) injection position; (b) fill position. P1 and P2: peristaltic pumps; V: injection valve; CL: microcolumn packed with C_8 sorbent; SC: separation capillary; HV: negative high voltage; IF: interface; R: buffer reservoir; D: detector; SL: sample loop; BF: blind fitting; C: carrier solution; S: sample solution; EQ: equilibrating solution; E: eluent; W: waste.

the sample analysis, the silicone rubber seal (SRS1) with the TC and PTFE tube was removed from the pipette and the running buffer solution was filled into the pipette until the liquid level reached the side hole of the pipette. Then the assembled part was replaced onto the pipette and the PTFE tube should be inserted into the pipette tip about 1.2 mm. With the interface, the running buffer in the pipette did not be polluted by the sample solution passed through, but the electric current was conducted between the running buffer and separation capillary inside the PTFE tube. On the other hand, the running buffer solution was able to be aspirated into the PTFE tube by P2 after injecting the sample solution into the separation capillary electrokinetically. It is beneficial to reduce the consumption of running buffer containing expensive reagents, such as chiral selection reagent or low conductivity electrolytes.

A homemade SPE microcolumn was prepared from a plastic pipette tip with two ends of 5 mm i.d. and 1.5 mm i.d and packed tightly with 50 mg C_8-bonded silica (50 μm particle size, Daisogel, Japan). A small amount of quartz wool was placed at both ends of the microcolumn to avoid loss of the silica particles. Each end of the column was connected with PTFE tubes by Viton tubing. To minimize dispersion, the column was arranged to introduce the sample stream from the narrow end, while to enter the eluent from the wider end [27,33].

2.3. Sample pretreatment

For water-based lotion, 1.00 g lotion was mixed with 2.0 mL, 50 mmol/L sodium tetraborate buffer and 2.0 mL acetonitrile, diluted to 10 mL with water, and then degassed by the ultrasonic bath for 5 min. For oil-based cream, gel and lotion samples, 1.00 g sample was stirred with 5.0 mL ethanol by the vortex mixer for 3 min, filtered through 0.45 μm nylon membrane, washed with a mixed solution of 12.5 mL, 20 mmol/L sodium tetraborate buffer and 5.0 mL acetonitrile, diluted to 25.0 mL with water, and then degassed by the ultrasonic bath for 5 min. The analytical recovery was examined by spiking the standard solutions of three parabens into real samples.

2.4. Analytical procedure

A daily start-up of FIA–SPE–MEKC was carried out by successively rinsing the separation capillary with 1.0 mol/L HCl (5 min), deioned water (1 min), 1.0 mol/L NaOH (10 min), deioned water (1 min) and the running buffer (10 min) via the capillary outlet by pressure, and washing the SPE column with 80% (v/v) acetonitrile by Pump 1 (P1) at a flow rate of 1.0 mL/min for 3 min.

The analytical processes of the FIA–SPE–MEKC system are listed in Table 1. Before sample loading, the SPE column packed with C_8-bonded silica should be equilibrated with the sample medium of 10 mmol/L sodium tetraborate buffer (pH 9.3) containing 20% (v/v) acetonitrile by Pump 1 (P1) at a flow rate

Table 1
Operation processes of on-line FIA–SPE–MEKC

Step	Figure	Duration (s)	Flow rate (mL/min)		Valve positon	Function
			Pump 1	Pump 2		
1	2(a)	60	1.0	1.0	Injection	Manifold washing and column equilibrating
2	2(a)	60	0.6	Off	Injection	Sample loading
3	2(b)	20	0.75	Off	Fill	Sample eluting
4	2(a)	10	Off	1.0	Injection	Sample transporting
5	2(a)	20	Off	Off	Injection	Sample injection
6	2(b)	10	Off	−1.0[a]	Fill	Buffer aspirating
7	2(b)	420[b]/540[c]	Off	Off	Fill	MEKC analysis

[a] The flow rate of Pump 2 reversed and the separation buffer was aspirated into the PTFE tube of the interface.
[b] Without using IS.
[c] With BP as IS.

of 1.0 mL/min for 60 s; meanwhile, the manifold was washed with the carrier solution, as shown in Fig. 2(a). During sample loading, the sample solution was introduced into the SPE column at a flow rate of 0.6 mL/min for 60 s by P1. In elution step, the valve was actuated to fill position, as shown in Fig. 2(b), and the retained analytes were eluted by the eluent of 10 mmol/L sodium tetraborate buffer (pH 9.3) containing 60% (v/v) ethanol at a flow rate of 0.75 mL/min for 20 s. In transporting step, the valve returned to injection position again and the eluted sample solution was transported from the sample loop (SL) to the PTFE tube inside the interface by the carrier stream with a flow rate of 1.0 mL/min for 10 s. With both the pumps stopped, a fraction of sample solution was electrokinetically injected into the separation capillary (SC) by its electroosmotic flow (EOF) at 6 kV for 20 s. Then the valve returned to fill position and Pump 2 (P2) reversed its flow direction to aspirate separation buffer containing SDS, which was supplied from the side hole of the pipette. Although SDS is not an expensive reagent, it is proved that the interface for saving reagent can be performed in this FIA–SPE–MEKC system. Subsequently, the MEKC analysis was carried out at 15 kV for 7 min without using IS or 9 min using IS. The next analysis cycle started from the first step for washing FIA conduit and equilibrating SPE column again.

3. Results and discussion

3.1. Selection of FIA–MEKC conditions

For simultaneous determination of MP, EP and PP by FIA–SPE–MEKC, the analytical conditions were investigated in the order of MEKC separation and SPE pretreatment. In this section, the separation conditions were optimized in accordance with the separation parameters, including peak area, migration time, separation efficiency and resolution.

3.1.1. Influence of separation buffer components

Four parabens could be separated with 20 mmol/L sodium tetraborate buffer (pH 9.3) by CZE. However, a baseline separation of MP and EP could not be achieved. Then FIA–MEKC was investigated for the analyte separation. By examining different sodium tetraborate concentration from 5 to 50 mmol/L (pH 9.3) containing 50 mmol/L SDS, 20 mmol/L sodium tetraborate was used to prepare the separation buffer, because the migration time of the analytes increased and the separation efficiency decreased with the sodium tetraborate concentration higher than 20 mmol/L, whereas the resolution decreased with the concentration lower than 20 mmol/L. The influence of buffer pH was examined from 8.5 to 10.0 with 20 mmol/L sodium tetraborate buffer containing 50 mmol/L SDS. It was found that the pH value of the separation buffer did not influence the paraben resolution obviously. However, the migration time increased with the pH value because the pK_a values of the parabens were around 8.4 and the hydroxy group of parabens dissociated higher than pH 8.4 [13]. By considering the migration time, the pH value of the separation buffer was chosen at 9.3.

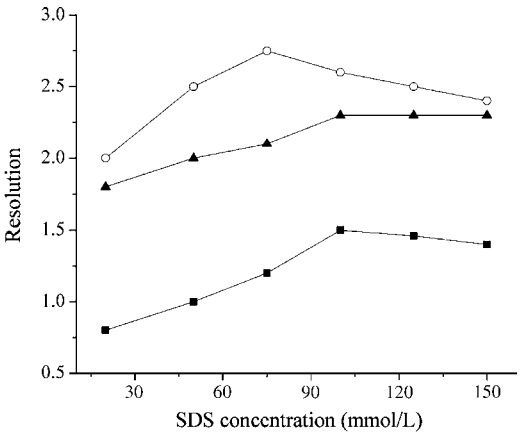

Fig. 3. Effect of SDS concentration on resolution of MP, EP, PP and BP. (■) Resolution of MP and EP, (◯) resolution of EP and PP and (▲) resolution of PP and BP. Standard solution: 100 μg/mL MP, EP, PP and 50 μg/mL BP in 10 mmol/L sodium tetraborate buffer (pH 9.3) containing 20% (v/v) ACN; running buffer: 20 mmol/L sodium tetraborate buffer (pH 9.3) containing different concentrations of SDS; carrier solution: 20 mmol/L sodium tetraborate buffer (pH 9.3); sample loop volume: 90 μL; working voltage: 15 kV; injection time: 20 s; detection wavelength: 254 nm.

SDS concentration had a strong effect on the resolution between MP and EP, which was examined from 20 to 150 mmol/L, as shown in Fig. 3. These two compounds could not be separated on baseline with the concentration lower than 100 mmol/L, and with the concentration higher than 100 mmol/L of the migration time and electric current increased, which could enhance the thermal effect and peak broadening. By compromising the resolution and thermal effect, a final concentration of 100 mmol/L SDS was chosen. So 20 mmol/L sodium tetraborate running buffer (pH 9.3) containing 100 mmol/L SDS was used in the paraben separation.

3.1.2. Influence of separation voltage

For the separation of the four parabens, the effect of the separation voltage was investigated in the range from 8 to 20 kV. As being expected, the migration time was reduced by increasing the separation voltage. However, the resolution decreased with the separation voltage higher than 15 kV owing to the increase of Joule heating. Moreover, the current increased to 86 μA and enhanced baseline noise with the separation voltage of 20 kV. For the concurrent consideration of migration time and resolution, the separation voltage was established at 15 kV in the separation.

3.1.3. Introduction of sample zone into separation capillary

To obtain optimal sensitivity and separation efficiency by the FIA–SPE–MEKC system, the sample loop volume and transporting flow rate were investigated. For transporting the pretreated sample to the PTFE tube in the interface and injecting into the separation capillary, sample loop volume and transporting flow rate determined the intercepted part of the eluted sample solution and the injecting position of the sample zone, which could influence the sample amount introduced into the separation capillary. First, the sample loop volume was examined in the range of 30–140 μL with an eluting flow rate of 0.8 mL/min

for 20 s. The peak area increased with the sample loop volume, meanwhile, the peak width was broadened and separation efficiency was reduced because of the sample zone dispersion. A sample loop of 90 μL was selected for compromising the sensitivity and separation efficiency.

The volume of connecting conduit between the sample loop and interface was about 30 μL. The transporting flow rate ranged from 0.6 to 1.4 mL/min with the operating time of 10 s was also investigated in this experiment. It was found that the peak areas of the parabens were reduced with the flow rate lower than 0.8 mL/min or higher than 1.0 mL/min. The transporting flow rate between 0.8 and 1.0 mL/min was the best to inject sample solution into the separation capillary. So a transporting flow rate of 1.0 mL/min was chosen finally.

3.2. Selection of SPE conditions

Before separating the parabens, the samples should be pretreated to remove the sample matrices and eliminate the analytical interference. In the proposed method, a pretreatment process of SPE was investigated for selecting an appropriate eluent of SPE elution and MEKC separation, concentrating the parabens and removing the sample matrices. C_8- and C_{18}-bonded silica was investigated as the SPE sorbent. The former was selected because C_{18}-bonded silica could result in a lot of bubbles during eluting process. With the sorbent of C_8-bonded silica in SPE, we expected that the parabens could be retained on the SPE column and eluted by an eluent containing organic solvent, whereas oil matrices were not retained on the C_8 column during sample loading. To achieve the effective pretreatment, the eluents containing three water-soluble solvents were investigated in the experiment, viz., 10 mmol/L sodium tetraborate buffer (pH 9.3) containing 50% (v/v) methanol, ethanol and acetonitrile, respectively. The elution was examined by using a mixed standard solution containing 50 μg/mL MP, EP, PP and BP, respectively, which passed through the SPE column at 0.6 ml/min for 60 s and were eluted with different eluent and volume from 50 to 500 μL at a flow rate of 0.6 mL/min. The eluted parabens were transported to the interface and separated by MEKC. It was found that the eluent containing ethanol was the best among three eluents for the parabens. The eluting results of the parabens were similar. Taking MP for example, the peak area was 1.2 and 1.7 times of those containing methanol and acetonitrile, respectively. The eluent volume lower than 150 μL could reduce the peak area due to the incomplete elution, whereas higher than 150 μL could result in the analyte dispersion. Therefore, 150 μL eluent volume was chosen in this work.

With 150 μL eluent, the influence of eluting flow rate on the peak area of three parabens was investigated. The peak areas of the parabens increased with the eluting flow rate from 0.3 to 0.75 mL/min and decreased rapidly higher than 0.75 mL/min. It manifested that different flow rate could influence the intercepted part of the eluted sample zone and high flow rate lead to an incomplete elution. In accordance with the experimental results mentioned above, 0.75 mL/min was selected as the eluting flow rate in this work.

The influence of different ethanol concentration on the peak area of the parabens was also investigated. When the ethanol concentration increased from 20 to 60% (v/v), the peak area of parabens was enhanced. However, when the concentration was higher than 60%, the peak area kept constant almost and the eluted solution became cloudy. So 20 mmol/L sodium tetraborate buffer (pH 9.3) containing 60% (v/v) ethanol was adopted as the eluent for the parabens in SPE pretreatment.

3.3. Analytical characteristics of FIA–SPE–MEKC

The detection limits, reproducibility, regressive equations, correlative coefficients and linear ranges were investigated for the proposed method. The calibration curves and corresponding regressive equations were obtained with five concentration levels of mixed standard solutions. Each point on the calibration curves corresponded to the mean value obtained from three times of individual measurement. The regressive equations, correlative coefficients and linear ranges for MP, EP and PP with and without using IS are compared in Table 2. The peak area R.S.D. and correlative coefficient using IS are better than those without using IS. The electropherogram of a mixed standard solution containing 50 μg/mL of each paraben is shown with three consecutive injections in Fig. 4(a). The R.S.D. ($n = 5$) of peak area for three parabens was <2.3% using IS and <2.8% without using IS. The day-to-day precision using IS was 3.1, 3.8 and 3.3% for MP, EP and PP, respectively. The analytical period using IS was 12 min by the FIA–SPE–MEKC method. The LODs were calculated with three times R.S.D. of baseline noises ($n = 11$). The breakthrough volume of the SPE column at a flow of 0.6 mL/min was found to be 2.0 mL with the three parabens solution of 50 μg/mL each. By loading the analyte solution at 0.6 mL/min for 3 min, the enrichment factors of 65,

Table 2
Analytical characteristics of FIA–SPE–MEKC

	MP[a]	EP[a]	PP[a]	MP[b]	EP[b]	PP[b]
LOD (S/N = 3) (μg/mL)	0.1	0.1	0.07	0.09	0.1	0.07
Peak area R.S.D. (%)	2.0	2.7	2.8	1.7	2.3	2.2
Regressive equations	$Y = 3.20X + 1.34$	$Y = 4.35X + 7.50$	$Y = 9.56X - 3.38$	$Y = 0.442X + 0.204$	$Y = 0.911X + 0.073$	$Y = 1.24X - 0.130$
Correlative coefficient	0.9991	0.9997	0.9974	0.9996	0.9998	0.9992
Linear range (μg/mL)	3–500	3–500	2–500	2–500	3–500	2–500

[a] Without using IS. Y, peak area (mV s); X, standard concentration (μg/mL).
[b] With BP as IS. Y, peak area ratio analyte/IS; X, concentration ratio analyte/IS.

Table 3
Concentrations of parabens determined in commercial cosmetic samples

Sample	Parabens	Detected concentration (μg/mL)[a]	Percentage (% w/w)[a]	Recovery (%)[a]	Detected concentration (μg/mL)[b]	Percentage (% w/w)[b]	Recovery (%)[b]
Cream a	MP	42	0.105	93.6	42	0.105	94.4
	PP	72	0.180	92.3	74	0.185	94.1
Cream b	PP	125	0.312	98.6	122	0.305	99.8
Cream c	MP	46	0.115	90.4	42	0.105	92.7
	PP	83	0.208	94.7	85	0.212	95.5
Water-based lotion a	PP	189	0.189	101	192	0.192	98.0
Water-based lotion b	PP	67	0.067	93.7	70	0.070	96.9
Oil-based lotion a	MP	112	0.280	91.3	111	0.278	93.2
	PP	31	0.076	98.2	33	0.082	101
Oil-based lotion b	PP	129	0.322	95.2	128	0.320	102
Gel a	MP	86	0.215	91.6	85	0.212	95.8
	EP	28	0.070	94.7	30	0.075	96.4
	PP	105	0.262	90.4	110	0.275	92.2
Gel b	MP	158	0.395	95.3	150	0.375	97.8

[a] Without using IS.
[b] With BP as IS.

68 and 72 for MP, EP and PP, can be obtained, respectively, compared with the FIA–MEKC without the SPE pretreatment. However, the sample loading time of 1 min was used because the amounts of parebens in cosmetic products could be detected even without the preconcentration. In this work, the SPE pretreatment was used for the clean up of the sample matrices and the enrichment factors of the parabens were only higher than 10.

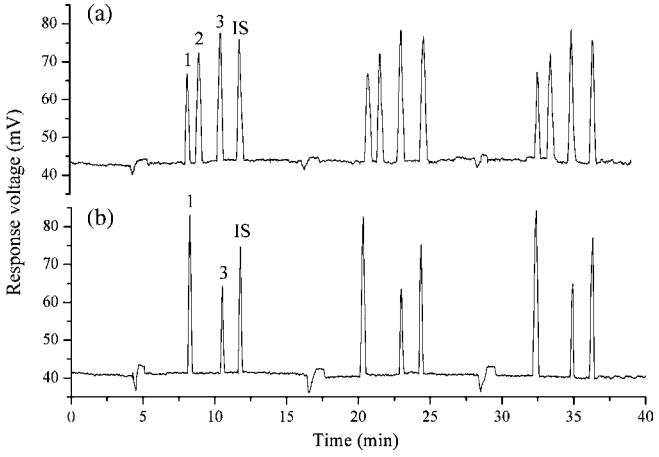

Fig. 4. Electrochromatograms of three consecutive injections with (a) a mixed standard solution of three parabens and (b) a sample of oil-based lotion using IS by FIA–SPE–MEKC. Peak identification: 1: MP; 2: EP; 3: PP; IS, PP. Standard solution: 50 μg/mL MP, EP and PP in 10 mmol/L sodium tetraborate buffer (pH 9.3) containing 20% ACN (v/v); running buffer: 20 mmol/L sodium tetraborate buffer (pH 9.3) containing 100 mmol/L SDS; carrier solution: 20 mmol/L sodium tetraborate buffer (pH 9.3); sample loading: 0.6 mL/min for 60 s; sample elution: 0.75 mL/min for 20 s with 10 mmol/L sodium tetraborate buffer (pH 9.3) containing 60% (v/v) ethanol; sample loop volume: 90 μL; working voltage: 15 kV; injection time: 20 s; detection wavelength: 254 nm. Fifty microgram per millilitre of BP was added as IS into the standard and real sample solutions.

3.4. Determination of parabens in cosmetic products

The proposed FIA–SPE–MEKC system was applied to determine three parabens in commercial cosmetic products, including water-based lotions and oil-based lotions, gels and creams. After off-line preliminary pretreatment described in Section 2.3, the sample solution was loaded on and eluted from the SPE column, and analyzed by MEKC. The peaks were identified by their relative retention time compared with IS. The analytical recovery of the proposed method, including extraction and separation procedure, was based on spiking experiments. The recovery with and without using IS are compared in Table 3, ranging from 92.2 to 102% using IS and 90.4 to 101% without using IS. The concentrations of three parabens found in nine cosmetic products are also listed in Table 3. The electropherograms of an oil-based lotion using BP as IS by three consecutive injections is shown in Fig. 4(b). It shows that the matrix interference was not observed owing to the high selectivity of the SPE pretreatment. The determination results of the three parabens were lower than the maximum addition levels established by China [6].

4. Conclusion

The on-line pretreatment and separation method with the FIA–SPE–MEKC system has been used to analyze three parabens of MP, EP and PP successfully. In the combination system of FIA–SPE–MEKC, the modified split–flow interface with low reagent consumption was introduced for coupling on-line sample pretreatment with MEKC separation. The throughput of five samples per hour was achieved for standard and sample solutions with the baseline separation of the parabens. With the proposed method, the analytical sensitivity and selectivity

were improved in the paraben determination and sample matrix removal.

Acknowledgements

The authors acknowledge the National Science Foundation of China (nos. 20675075 and 20275035) for financial support to carry out this work.

References

[1] M.C. Boyce, Electrophoresis 22 (2001) 1447.
[2] M.G. Soni, I.G. Carabin, G.A. Burdock, Food Chem. Toxicol. 43 (2005) 985.
[3] F.F. Cantwell, Anal. Chem. 48 (1976) 1854.
[4] P.W. Harvey, J. Appl. Toxicol. 23 (2003) 285.
[5] E.J. Routledge, J. Parker, J. Odum, J. Ashby, J.P. Sumpter, Toxicol. Appl. Pharmacol. 153 (1998) 12.
[6] Ministry of Health, Hygienic Standard for Cosmetics, Ministry of Health, PR China, 2007, p. 72.
[7] E. Marengo, V. Gianotti, S. Angioi, M.C. Gennaro, J. Chromatogr. A 1029 (2004) 57.
[8] E. Mikami, T. Goto, T. Ohno, H. Matsumoto, M. Nishida, J. Pharm. Biomed. Anal. 28 (2002) 261.
[9] E. Sottofattori, M. Anzaldi, A. Balbi, G. Tonello, J. Pharm. Biomed. Anal. 18 (1998) 213.
[10] M. Thomassin, E. Cavalli, Y. Guillaume, C. Guinchard, J. Pharm. Biomed. Anal. 15 (1997) 831.
[11] B. Baalbaki, M. Blanchin, H. Fabre, Anal. Chim. Acta 463 (2002) 15.
[12] P.E. Mahuzier, K.D. Altria, B.J. Clark, J. Chromatogr. A 924 (2001) 465.
[13] K.L. Kuo, Y.Z. Hsieh, J. Chromatogr. A 768 (1997) 334.
[14] H.Y. Huang, Y.C. Lai, C.W. Chiu, J.M. Yeh, J. Chromatogr. A 993 (2003) 153.
[15] S.H. He, Y.F. Zhao, Z.W. Zhu, H.W. Liu, M.X. Li, Y.H. Shao, Q.K. Zhuang, Talanta 69 (2006) 166.
[16] D. Šatínský, P. Solich, P. Chocholouš, R. Karlíček, Anal. Chim. Acta 499 (2003) 205.
[17] D. Šatínský, J. Huclová, P. Solich, R. Karlíček, J. Chromatogr. A 1015 (2003) 239.
[18] D. Šatínský, J. Huclová, R.L.C. Ferreira, M.C.B.S.M. Montenegro, P. Solich, J. Pharm. Biomed. Anal. 40 (2006) 287.
[19] A. Myint, Q.L. Zhang, L.J. Liu, H. Cui, Anal. Chim. Acta 517 (2004) 119.
[20] Y.Q. Cheng, H.L. Chen, Y.Q. Li, X.G. Chen, Z.D. Hu, Talanta 63 (2004) 491.
[21] Z.L. Fang, Z.S. Liu, Q. Shen, Anal. Chim. Acta 346 (1997) 135.
[22] P. Kuban, B. Karlberg, Anal. Chem. 69 (1997) 1169.
[23] L.H. Liu, X.G. Chen, Z.D. Hu, Talanta 71 (2007) 155.
[24] P. Kuban, B. Karlberg, Talanta 45 (1998) 477.
[25] H.L. Chen, K.T. Wang, Q.S. Pu, X.G. Chen, Z.D. Hu, Electrophoresis 23 (2002) 2865.
[26] H.W. Chen, Z.L. Fang, Anal. Chim. Acta 376 (1998) 209.
[27] H.W. Chen, Z.L. Fang, Anal. Chim. Acta 355 (1997) 135.
[28] L. Arce, P. Kuban, A. Ríos, M. Valcárcel, B. Karlberg, Anal. Chim. Acta 390 (1999) 39.
[29] L.A. Berrueta, B. Gallo, F. Vicente, Chromatographia 40 (1995) 474.
[30] Z.Q. Zhang, J. Ma, Y. Lei, Y.M. Lu, Talanta 71 (2007) 2056.
[31] P. Kuban, A. Engström, J.C. Olsson, G. Thorsén, R. Tryzell, B. Karlberg, Anal. Chim. Acta 337 (1997) 117.
[32] F.W.A. Tempels, J. Teeuwsen, I.K. Kyriakou, G. Theodoridis, J. Chromatogr. A 1053 (2004) 263.
[33] Y.Y. Hu, Y.Z. He, L.L. Qian, Anal. Chim. Acta 536 (2005) 251.

Available online at www.sciencedirect.com
ScienceDirect
Talanta 74 (2008) 1126–1131
Talanta
www.elsevier.com/locate/talanta

Molecularly imprinted silica prepared with immiscible ionic liquid as solvent and porogen for selective recognition of testosterone

Chiyang He [a,b], Yuanyuan Long [a], Junlan Pan [b], Kean Li [a], Feng Liu [a,*]

[a] *Beijing National Laboratory for Molecular Sciences, The Key Laboratory of Bioorganic Chemistry and Molecular Engineering, Ministry of Education, College of Chemistry, Peking University, Beijing 100871, PR China*
[b] *Department of Chemistry, Anqing Normal College, Anqing 246011, PR China*

Received 8 June 2007; received in revised form 12 August 2007; accepted 13 August 2007
Available online 17 August 2007

Abstract

1-Butyl-3-methylimidazolium tetrafluoroborate ([Bmim]BF_4), an ionic liquid (IL) immiscible with water, was used as a new type of solvent and porogen for the preparation of molecularly imprinted silica. The new imprinted silica was prepared by a sacrificial spacer molecular imprinting approach with testosterone as template molecule. The new covalent monomer-template complex used in the imprinting procedure was synthesized via the reaction of 3-(triethoxysilyl)propyl isocyanate with testosterone. The imprinted silica was characterized by FT-IR spectroscopy, N_2 gas adsorption–desorption isotherm and the high-resolution transmission electron microscopy. Moreover, the selective adsorption ability of the imprinted particles towards testosterone was investigated by the steady-state binding experiment with testosterone propionate as its structural analogue. Results showed that the imprinted silica obtained in this study had relatively homogenous structure with numerous mesopores, indicating that the IL used here is an excellent solvent and satisfactory porogen for the preparation of imprinted materials. Moreover, ILs are more environmentally friendly than traditional organic solvents due to their negligible vapor pressure. The imprinted silica possesses highly specific recognition property and high binding capacity towards testosterone, showing that the new imprinting technique is relatively successful.
© 2007 Elsevier B.V. All rights reserved.

Keywords: Ionic liquid; Sacrificial spacer method; Molecular imprinting; Silica; Testosterone; Recognition

1. Introduction

Molecular imprinting has become a powerful method for the preparation of robust materials that have the ability to recognize a specific chemical species [1–4]. The technique involves the synthesis of highly cross-linked polymers in the presence of template molecules. After the removal of template, the imprinted binding sites, which are complementary in size, shape, and chemical functionality to the template, are left within the polymer network. These binding sites can rebind template molecule in a highly selective manner. Compared with natural receptors, these synthetic materials have several advantages including the stability, ease of preparation, low cost and reusability, and therefore are widely applied in chromatographic separation [5,6], catalysis [7], chemical sensors [8–10], and solid-phase extraction [11,12]. However, the applications as real alternatives or complements to biomolecules are limited to some extent by their inherent shortcomings, such as the nonspecificity and low affinity of binding sites [13,14]. To overcome these problems, some new morphologies and manufacturing techniques have been developed [15–19]. However, there are few reports on the development of new solvents and porogen systems.

Ionic liquids (ILs) have been gaining great exposure recently for potential use as green solvents and possible replacements for traditional volatile organic solvents [20]. ILs are commonly defined as salts that are fluid at near-ambient temperature and consist of predominantly ionic species [21]. Besides having many properties of conventional organic solvents, such as excellent solvation qualities, a variable viscosity range and a wide temperature range, ILs have negligible vapor pressure and exhibit excellent chemical and thermal stabilities [22,23]. Furthermore, at least a million binary ionic liquids and 10^{18} ternary ionic liquids are potentially available [24], which enables them to be effectively designed for various applications. More recently, as a new type of solvent or template, ILs have been used to prepare mesoporous silica [25], microporous silica

* Corresponding author. Tel.: +86 10 62761187; fax: +86 10 62751708.
E-mail address: liufeng@pku.edu.cn (F. Liu).

0039-9140/$ – see front matter © 2007 Elsevier B.V. All rights reserved.
doi:10.1016/j.talanta.2007.08.009

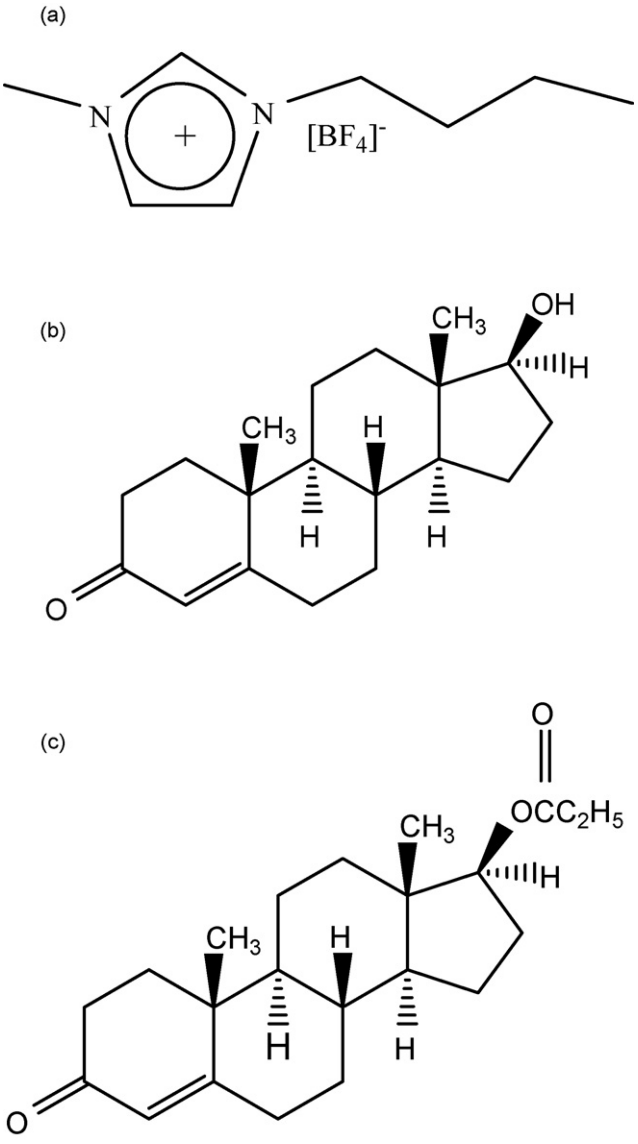

Fig. 1. Structures of: (a) [Bmim]BF_4; (b) testosterone; (c) testosterone propionate.

[26], microporous zeolite analogues [21], and polymers [27]. Moreover, ILs have also applied as solvent in the preparation of molecularly imprinted polymers by noncolvent imprinting technique [28,29]. However, to our knowledge, there is no report on the application of IL as solvent and porogen for the preparation of molecularly imprinted silica via covalent imprinting or sacrificial spacer imprinting technique.

In this study, 1-butyl-3-methylimidazolium tetrafluoroborate ([Bmim]BF_4, Fig. 1a), an IL immiscible with water, was used as a new type of solvent and porogen to prepare molecularly imprinted silica via sol–gel nanocasting and a sacrificial spacer molecular imprinting techniques. Testosterone (Fig. 1b), one of the endogenous anabolic androgenic steroids forbidden in sports since 1983 [30], was selected as template molecule in this study. The new covalent monomer-template complex synthesized for the preparation of imprinted silica was demonstrated by means of FT-IR spectroscopy, elemental analysis results, and ^{1}H NMR and ^{13}C NMR spectra. The imprinted silica was characterized by FT-IR spectroscopy, N_2 gas adsorption–desorption isotherm and the high-resolution transmission electron microscopy (HRTEM). Finally, selective adsorption ability of the imprinted particles towards testosterone was investigated by the steady-state binding experiment with testosterone propionate (Fig. 1c) as structural analogue.

2. Experimental

2.1. Reagents

3-(Triethoxysilyl)propyl isocyanate was purchased from Tokyo Kasei Kogyo Co. Ltd. (Tokyo, Japan). Testosterone was obtained from Acros (>99%, New Jersey, USA). Testosterone propionate was bought from Hangzhou Yumei Biological Health Care Co. Ltd. (≥98%, Hangzhou, China). Tetraethoxysilane (TEOS) was purchased from Aldrich (>98%, Steinheim, Germany). 3-Aminopropyltriethoxysilane was purchased from Acros (>99%). 1-Butyl-3-methylimidazolium tetrafluoroborate ([Bmim]BF_4) was obtained from Fluka (≥97%, Steinheim, Germany). Triethylamine obtained from Beijing Chemical Reagents Company (Beijing, China) was dried over calcium chloride overnight. Tetrahydrofuran (THF), chloroform, ethyl acetate and petroleum ether (boiling range 60–90 °C) were purified by standard method prior to use. *N*,*N*-Dimethylformamide (DMF) was purified by distillation under reduced pressure. Other chemicals were used as received without further purification.

2.2. Synthesis of TestSi

The monomer-template complex (TestSi) was synthesized as follows. Under nitrogen, testosterone (1.73 g, 6 mmol) was dissolved in a mixture of DMF (14 mL) and triethylamine (4.0 mL). To this solution, 3-(triethoxysilyl)propyl isocyanate (3.26 mL, 12 mmol) was added via syringe at room temperature over a period of 20 min. The reaction mixture was stirred for 48 h at 80 °C. After most of the solvent was evaporated, the product was isolated by column chromatography on silica gel (ethyl acetate:petroleum ether = 4:1). The yield was 81%. FT-IR (at resolution of 4 cm^{-1}): 2969/2937/2879 cm^{-1} (ν_{C-H}), 1720 cm^{-1} ($\nu_{HNC=O}$), 1668 cm^{-1} ($\nu_{HCC=O}$), 1547 cm^{-1} (δ_{N-H}), 1100–1000 cm^{-1} ($\nu_{Si-O-Si}$). Elemental analysis, calcd. for $C_{29}H_{49}NO_6Si$:C, 65.01%; H, 9.22%; N, 2.61%. Found: C, 64.43%; H, 9.10%; N, 2.52%. ^{1}H NMR (400 MHz, DMSO-d_6): δ (ppm) 6.98–7.01 (t, 1H, J = 5.7 Hz, NH), 5.63 (s, 1H, C=CH), 4.39–4.43 (t, 1H, J = 8.4 Hz, CHOC=O), 3.70–3.76 (q, 6H, ethoxy CH_2), 2.90–2.94 (q, 2H), 2.39–2.40 (m, 2H), 2.26 (m, 1H), 2.18 (m, 1H), 1.95–1.99 (m, 2H), 1.25–1.80 (bm, 11H), 1.13–1.16 (t, 9H, ethoxy CH_3), 1.15 (s, 3H), 1.13–0.80 (bm, 4H), 0.78 (s, 3H), 0.53–0.49 (m, 2H). ^{13}C NMR (400 MHz, DMSO-d_6): δ (ppm) 197.81, 170.22, 156.17, 123.14, 81.29, 57.62, 53.10, 49.54, 42.86, 41.93, 38.13, 36.27, 35.10, 34.73, 33.54, 31.87, 31.11, 27.31, 22.94, 22.87, 20.08, 18.13, 16.83, 14.02, 7.13.

2.3. Preparation of the imprinted silica

The imprinted silica was synthesized by a modified procedure of literature [25]. Typically, TestSi (0.112 mmol, 0.060 g)

was dissolved in the mixture of TEOS (2.24 mmol, 0.5 mL) and [Bmim]BF_4 (IL, 0.6 mL) under mild magnetic stirring. To the homogeneous solution, 0.25 mL of 0.01 mM HCl aqueous solution was added dropwise. The mixture solution was stirred at room temperature for 2 h, exposed under vacuum (1.0 kPa) at 60 °C for 1 h, and then set in an open flask at 60 °C for 48 h. After the complete gelation, the obtained silica monolith was ground into particles, and then those ranging from 20 to 30 μm were collected. The particles were Soxhlet extracted with acetonitrile for 48 h to remove the incorporated IL. The template molecules were removed from the silica following a literature procedure [31]. In a typical procedure, the IL-removed particles were treated with 70 mM $LiAlH_4$ for 24 h at 60 °C, and then sequentially rinsed with anhydrous THF, 0.1 M HCl, 0.1 M NH_3, water, and acetone over a period of 48 h. The obtained silica particles were dried in vacuum for 24 h at 120 °C for further characterization. The control silica particles were prepared in the almost same manner for the testosterone-imprinted particles except that 3-aminopropyltriethoxysilane was used in place of TestSi.

2.4. Characterization

Infrared spectra were recorded by a Nicolet Magna-IR 750 spectrometer (USA) with Nicolet NicPlan IR Microscope. The HRTEM graph was taken with a Hitachi H9000 NAR apparatus (Japan) operated at 300 kV. Nitrogen adsorption–desorption isotherm was measured using a Micromeritics ASAP-2010 apparatus (USA). The BET plot and the BJH method were used to determine the specific surface area, pore volume, and pore size distribution, respectively.

2.5. Steady-state binding experiment

Thirty milligrams of silica particles were added to the solutions of testosterone or testosterone propionate in 15 mL chloroform at various concentrations (0.5, 1.0, 1.5, and 2.0 mM). After incubating for 24 h at 30 °C, the silica particles were isolated by filtration. The filtrate was concentrated to dryness by the evaporation of solvent and then dissolved by acetonitrile. The amount of the analytes adsorbed by the silica particles were determined by measuring the residual analytes in the filtrate by HPLC method. The mean of three replicates was used as each adsorption value.

2.6. HPLC analysis

Chromatographic analyses were performed on an Agilent1100 HPLC system including a quaternary pump and a variable wavelength UV detector (Agilent, USA). The instrument control and data processing were carried out by an Agilent ChemStation software. An Agilent Zorbax Eclipse XDB-C8 (5 μm, 150 mm × 4.6 mm i.d.) analytical column was used for determination of analytes. The eluent was acetonitrile/H_2O (50/50, v/v) at a flow-rate of 1.0 mL min^{-1}. The injection volume was 20 μL, and the column effluent was monitored at 245 nm.

3. Results and discussion

3.1. Synthesis of the imprinted silica

To get specific imprinted sites, the testosterone-imprinted silica particles were prepared by a sacrificial spacer molecular imprinting technique as shown in Scheme 1. The new monomer-template complex (TestSi) was first synthesized by the reaction of 3-(triethoxysilyl)propyl isocyanate with testosterone in the presence of triethylamine. The reaction occurred between an isocyanato group of the monomer and a hydroxy moiety of testosterone. The obtained product was confirmed by FT-IR spectroscopy, elemental analysis results, and ^{1}H NMR and ^{13}C NMR spectra. Then, the imprinted silica monolith was

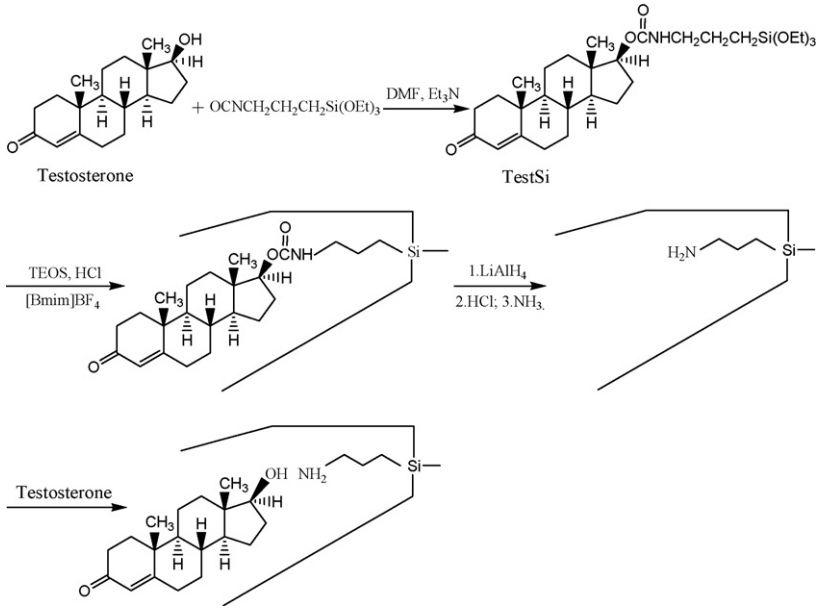

Scheme 1. Protocols for preparation of the molecularly imprinted silica and its recognition towards testosterone.

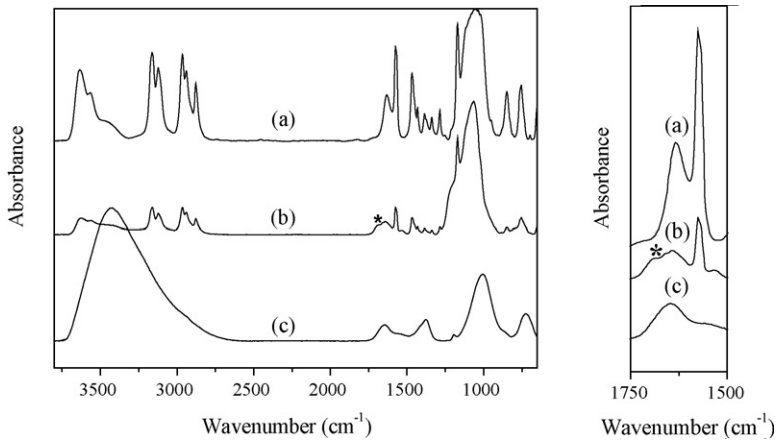

Fig. 2. FT-IR spectra of: (a) the neat IL; (b) the IL- and testosterone-incorporated silica; (c) the IL- and testosterone-removed silica. The right curves are the magnifications of the left spectra in the range of 1750–1500 cm^{-1}.

prepared by means of the gelation of TestSi with tetraethoxysilane (TEOS) in IL in the presence of aqueous HCl. The formation of the homogenous mixture solution in the procedure, which agreed well with a previous report [25], showed the excellent solvation quality of this IL. After gelation, the monolith silica was then ground into powder. The IL incorporated in silica was removed by Soxhlet extraction with acetonitrile, and the template molecules were removed by the reduction of $LiAlH_4$ and sequential treatments of HCl and NH_3 aqueous solutions [31].

From the comparison of the IR spectra of the neat IL, the IL- and testosterone-incorporated silica and the IL- and testosterone-removed silica (Fig. 2), the removals of IL and testosterone were confirmed by the disappearances of the ν_{C-H} of the imidazolium ring at 3200–3050 cm^{-1} and 1575 cm^{-1} and the $\nu_{C=O}$ of the urethane bond at 1691 cm^{-1} (marked by an asterisk in spectrum "b") in spectrum "c". The peak at 1375 cm^{-1} in spectrum "c" indicated the occurrence of CH_2–N band. Results showed that the new sacrificial spacer method used here is successful.

3.2. Characterization of the imprinted silica

Fig. 3 presents N_2 gas adsorption–desorption isotherm of the testosterone-imprinted silica. It is clear that the isotherm exhibits the typical IV curve with a hysteresis loop, which reflects the formation of a mesoporous structure. Some typical textural parameters of the imprinted silica are Brunauer–Emmett–Teller (BET) surface areas of 104 $m^2\,g^{-1}$, average pore diameter of 7.7 nm, and pore volume of 0.19 $cm^3\,g^{-1}$, which are similar to those of the molecularly imprinted polymers (MIPs) prepared in traditional organic solvents [32].

Fig. 4 shows the high-resolution transmission electron microscopy (HRTEM) images of the pore morphology and structure of the testosterone-imprinted silica, in which numerous mesopores are clearly noticeable. It was thought that such mesoporous structure would facilitate the mass transfer of substrate in binding experiment. Therefore, the IL used here is not only an excellent solvent, but also a satisfactory porogen for the preparation of imprinted materials.

3.3. Selectivity of the imprinted silica to testosterone

The recognition ability of the imprinted silica particles towards testosterone was investigated by a steady-state binding method. The tested concentrations of testosterone or testosterone propionate were 0.5, 1.0, 1.5, and 2.0 mM. As shown in Fig. 5, the testosterone-imprinted silica particles showed a high recognition ability and binding capacity for testosterone, while the control silica particles, prepared in almost the same manner except that 3-aminopropyltriethoxysilane was used in place of TestSi, had a much lower one. We also investigated the specific recognition ability of the silica particles for testosterone propionate, a structural analogue of testosterone, under the same conditions. Neither the imprinted silica nor the control silica show obvious recognition ability for testosterone propionate (Fig. 5c and d). Considering the structural difference between testosterone and testosterone propionate, we can conclude that the hydrogen bond interaction between –OH moiety in testosterone and $–NH_2$ group in imprinted silica might be crucial for template binding. Moreover, as shown in Fig. 5a,

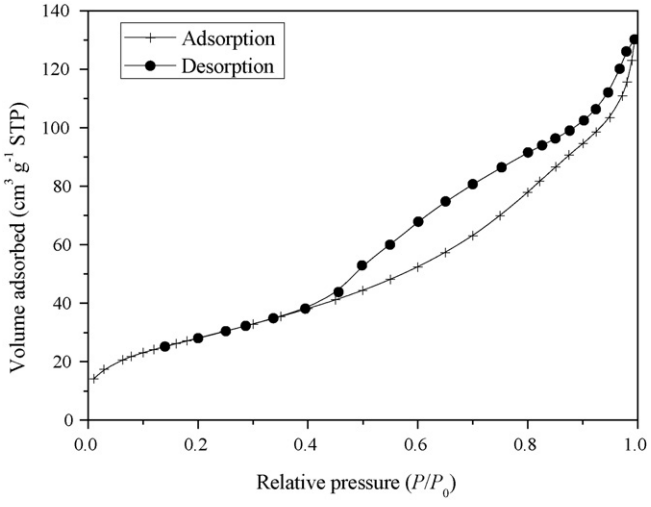

Fig. 3. Typical N_2 gas adsorption–desorption isotherm of the imprinted silica.

Table 1
Partition coefficients of analytes on silica and selectivity ratios of imprinted silica over control silica

Concentration of analytes (mM)	Testosterone			Testosterone propionate		
	K_{Imp}[a]	K_{Con}[a]	k[b]	K_{Imp}[a]	K_{Con}[a]	k[b]
0.0	–	–	–	–	–	–
0.5	0.424	0.150	2.83	0.067	–	–
1.0	1.137	0.091	12.49	0.032	0.008	4.00
1.5	0.625	0.045	13.89	0.020	0.003	6.66
2.0	0.354	0.034	10.41	0.016	0.010	1.60

[a] The K_{Imp} and K_{Con} are the partition coefficients of analytes on imprinted and control silica, respectiviely.
[b] The k is the selectivity ratio of imprinted silica towards analytes over control silica towards analytes.

with the increase of sample concentration, the bound testosterone by imprinted silica increases sharply at the beginning, while varies little when the sample concentration is larger than 1.5 mM, indicating that there is no significant contributions of coexisting nonspecific binding sites in the imprinted silica. This phenomenon could be attributed to the sacrificial spacer imprinting technique used in this study. To further assess the success of molecular imprinting, the partition coefficients (K) of analytes on imprinted or control silica were calculated through Eq. (1). In addition, a comparison between the imprinted and control silica was carried out by calculating a selectivity ratio (k) by following Eq. (2), where K_{Imp} and K_{Con} are the K values of analytes on imprinted and control silica, respectively.

$$K = \frac{\text{moles of analyte bound to silica/mass of silica}}{\text{moles of analyte remaining in solution/mass of solution}} \quad (1)$$

$$k = \frac{K_{Imp}}{K_{Con}} \quad (2)$$

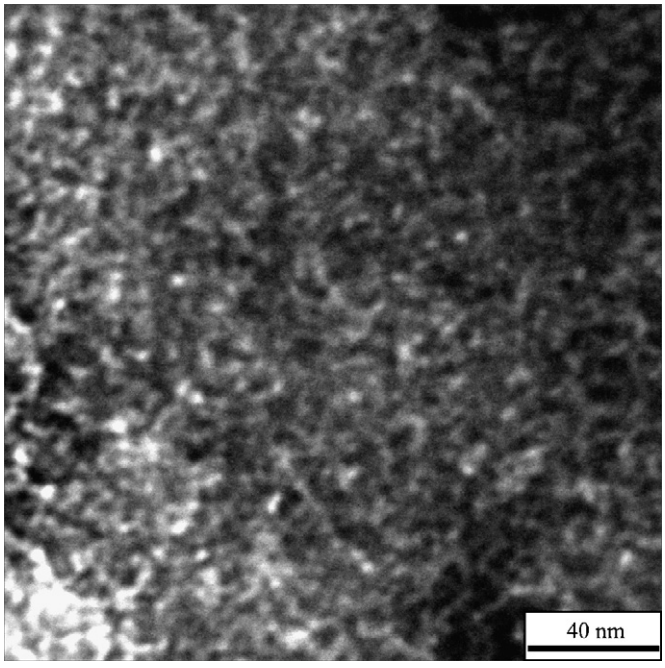

Fig. 4. HRTEM image of the pore morphology and structure of the testosterone-imprinted silica prepared with [Bmim]BF_4 as solvent and porogen via a sacrificial spacer molecular imprinting technique. The scale bar is 40 nm.

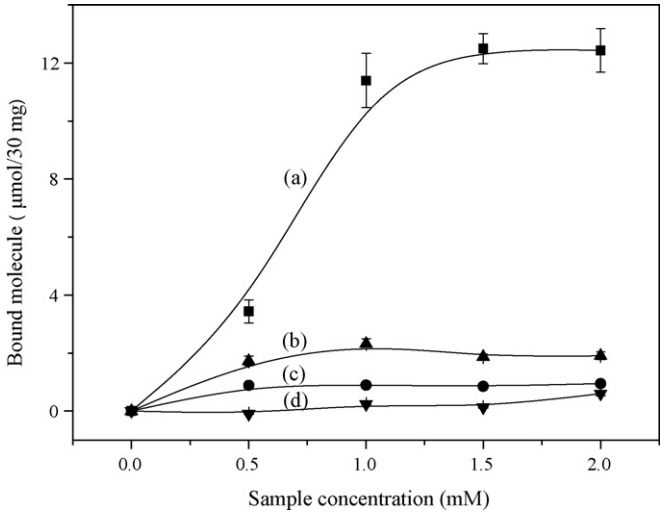

Fig. 5. Binding isotherms of: (a) the imprinted silica towards testosterone; (b) the control silica towards testosterone; (c) the imprinted silica towards testosterone propionate; (d) the control silica towards testosterone propionate. Thirty milligrams of the silica particles were added to 15 mL of the sample solutions in chloroform. The mean of three replicates was used as each adsorption value with error bar indicating the standard error.

The K and k values were listed in Table 1. Results showed that the K values of testosterone on imprinted silica are much larger than those on control silica correspondingly. Moreover, the k values of testosterone are also much higher than those of testosterone propionate. The results demonstrate that the molecular imprinting technique used here is successful.

4. Conclusions

[Bmim]BF_4, an ionic liquid immiscible with water, was used as a new type of solvent and porogen for the synthesis of molecularly imprinted silica via sol–gel nanocasting and a sacrificial spacer molecular imprinting techniques. [Bmim]BF_4 showed excellent solvation qualities and satisfactory porogen properties. Moreover, it is more environmentally friendly than traditional organic solvents because of its negligible vapor pressure. The imprinted silica thus prepared showed highly specific recognition property and high binding capacity towards testosterone. Furthermore, due to the designable structures of ILs, this new technique also opens up new opportunities in the preparation of the molecularly imprinted materials with tailored pore morphology and structure by using appropriate ILs.

Acknowledgement

This work was supported by the National Natural Science Foundation of China (Nos. 20675003, 20335010 and 20775003).

References

[1] G. Wulff, Angew. Chem. Int. Ed. Engl. 34 (1995) 1812.
[2] G. Vlatakis, L.I. Andersson, R. Müller, K. Mosbach, Nature 361 (1993) 645.
[3] K. Haupt, Anal. Chem. 75 (2003) 376A.
[4] P. Manesiotis, A.J. Hall, J. Courtois, K. Irgum, B. Sellergren, Angew. Chem. Int. Ed. 44 (2005) 3902.
[5] H. Kim, G. Guiochon, Anal. Chem. 77 (2005) 1708.
[6] J.J. Ou, X. Li, S. Feng, J. Dong, X.L. Dong, L. Kong, M.L. Ye, H.F. Zou, Anal. Chem. 79 (2007) 639.
[7] G. Wulff, Chem. Rev. 102 (2002) 1.
[8] K. Haupt, K. Mosbach, Chem. Rev. 100 (2000) 2495.
[9] D. Lakshmi, B.B. Prasad, P.S. Sharma, Talanta 70 (2006) 272.
[10] Z.H. Zhang, L.H. Nie, S.Z. Yao, Talanta 69 (2006) 435.
[11] X.J. Chang, N. Jiang, H. Zheng, Q. He, Z. Hu, Y.H. Zhai, Y.M. Cui, Talanta 71 (2007) 38.
[12] J.L. Urraca, M.A.C. Moreno-Bondi, A.J. Hall, B. Sellergren, Anal. Chem. 79 (2007) 695.
[13] K. Haupt, Chem. Commun. (2003) 171.
[14] S.C. Zimmerman, N.G. Lemcoff, Chem. Commun. (2004) 5.
[15] E. Yilmaz, K. Haupt, K. Mosbach, Angew. Chem. Int. Ed. 39 (2000) 2115.
[16] J.B. Beil, S.C. Zimmerman, Chem. Commun. (2004) 488.
[17] A. Katz, M.E. Davis, Nature 403 (2000) 286.
[18] H.H. Yang, S.Q. Zhang, W. Yang, X.L. Chen, Z.X. Zhuang, J.G. Xu, X.R. Wang, J. Am. Chem. Soc. 126 (2004) 4054.
[19] N. Perez, M.J. Whitcombe, E.N. Vulfson, Macromolecules 34 (2001) 830.
[20] M. Antonietti, D.B. Kuang, B. Smarsly, Y. Zhou, Angew. Chem. Int. Ed. 43 (2004) 4988.
[21] E.R. Cooper, C.D. Andrews, P.S. Wheatley, P.B. Webb, P. Wormald, R.E. Morris, Nature 430 (2004) 1012.
[22] J. Dupont, R.F. de Souza, P.A.Z. Suarez, Chem. Rev. 102 (2002) 3667.
[23] T. Fukushima, A. Kosaka, Y. Ishimura, T. Yamamoto, T. Takigawa, N. Ishii, T. Aida, Science 300 (2003) 2072.
[24] R.D. Rogers, K.R. Seddon, Science 302 (2003) 792.
[25] Y. Zhou, J.H. Schattka, M. Antonietti, Nano Lett. 4 (2004) 477.
[26] Y. Zhou, M. Antonietti, Adv. Mater. 15 (2003) 1452.
[27] P. Kubisa, Prog. Polym. Sci. 29 (2004) 3.
[28] K. Booker, M.C. Bowyer, C.I. Holdsworth, A. McCluskey, Chem. Commun. (2006) 1730.
[29] K. Booker, M.C. Bowyer, C.J. Lennard, C.I. Holdsworth, A. McCluskey, Aust. J. Chem. 60 (2007) 51.
[30] C.Y. He, S.H. Li, H.W. Liu, K.A. Li, F. Liu, J. Chromatogr. A 1082 (2005) 143.
[31] A.L. Graham, C.A. Carlson, P.L. Edmiston, Anal. Chem. 74 (2002) 458.
[32] M.L. Yang, Y.Z. Li, J. Mol. Recognit. 18 (2005) 103.

Available online at www.sciencedirect.com
ScienceDirect
Talanta 74 (2008) 1699
Talanta
www.elsevier.com/locate/talanta

Erratum

Erratum to "Simultaneous on-line preconcentration and determination of trace metals in environmental samples using a modified nanometer-sized alumina packed micro-column by flow injection combined with ICP-OES" [Talanta 71 (3) (2007) 1239–1245]

Chaozhang Huang, Bin Hu *, Zucheng Jiang, Nan Zhang

Department of Chemistry, Wuhan University, Wuhan 430072, PR China

Available online 17 July 2007

The publisher regrets that during the processing of the above paper an error occurred in one of the author's names. The author list is reproduced correctly above.

DOI of original article:10.1016/j.talanta.2006.06.033.
* Corresponding author. Tel.: +86 87218764; fax: +86 27 68754067.
E-mail address: binhu@whu.edu.cn (B. Hu).

0039-9140/$ – see front matter © 2007 Elsevier B.V. All rights reserved.
doi:10.1016/j.talanta.2007.06.002

Available online at www.sciencedirect.com
ScienceDirect
Talanta 74 (2008) 1435–1441
Talanta
www.elsevier.com/locate/talanta

Sensitive determination of phenylephrine and chlorprothixene at poly(4-aminobenzene sulfonic acid) modified glassy carbon electrode

Fei Huang, Guiying Jin, Yang Liu, Jilie Kong *

Department of Chemistry, Fudan University, Shanghai 200433, PR China

Received 18 July 2007; received in revised form 21 September 2007; accepted 22 September 2007
Available online 29 September 2007

Abstract

Phenylephrine (i.e. PHE) and chlorprothixene (i.e. CPT), two effective and important antipsychotic drugs with low redox activity, were found generating an irreversible anodic peak at about +0.89 V (vs. SCE) and +1.04 V in 0.05 M HAc–NaAc (pH 5.0) or NH_2CH_2COOH–HCl (pH 2.4) buffer solution at poly(4-aminobenzene sulfonic acid) modified glassy carbon electrode (i.e. poly(4-ABSA)/GC), respectively. Sensitive and quantitative measurement for them based on the anodic peaks was established under the optimum conditions. The anodic peak current was linear to PHE and CPT concentrations from 1×10^{-7} to 1.5×10^{-5} M and 2×10^{-6} to 4.5×10^{-5} M, the detection limits obtained were 1×10^{-8} and 1×10^{-7} M, separately. The modified electrode exhibited some excellent characteristics including easy regeneration, high stability, good reproducibility and selectivity. The method proposed was successfully applied to the determination of PHE and CPT in drug injections or tablets and proved to be reliable compared with ultraviolet spectrophotometry. The modified electrode was characterized by electrochemical methods.
© 2007 Elsevier B.V. All rights reserved.

Keywords: Phenylephrine; Chlorprothixene; Poly(4-amiinozenzene sulfonic acid); Determination; Excellent characteristics; Characterization

1. Introduction

As two effective and important antipsychotic drugs, phenylephrine (Scheme 1) and chlorprothixene (Scheme 2) are widely used in the treatment of hypertension and schizophrenia [1,2]. A variety of analytical methods have been applied to investigate their characteristics, such as spectrophotometry [3,4], spectrofluorimetry [5,6], high-performance liquid chromatography [7,8], capillary electrophoresis, etc. [9,10]. Nevertheless, owing to their low redox activity under normal conditions, there are few reports about them studied by means of electrochemical methods. Among the few examples, ion-selective electrodes [11,12], glassy carbon electrode [2], chemically modified carbon paste electrode [13], carbon nanotubes modified electrode [14], and self-assembled monolayer modified electrode [1] were used to study and determine them. However, their practical applications might be restricted to some extent due to some disadvantages including unsatisfactory detection limit, time-consuming preconcentration, complicated electrode preparation and difficult regeneration of electrode. Therefore, it is necessary to develop a new analytical method for them.

In the past decades, conducting polymer modified electrodes have received great attention due to their excellent characteristics, including high stability and selectivity, good reproducibility and conductivity, more active sites and good homogeneity [15]. They are widely applied in many areas, such as molecule or ion recognition [15], electrocatalysis [16], electron transfer [17]. Nevertheless, there is no report about electrochemical determination of PHE or CPT by using conducting polymer modified electrodes.

In this paper, the electrochemical behaviors of PHE and CPT at poly(4-ABSA)/GC modified electrode were investigated. Furthermore, a more sensitive and simpler determination method was proposed.

2. Experimental

2.1. Reagents

Phenylephrine hydrochloride ($C_9H_{13}NO_2$·HCl) and chlorprothixene ($C_{18}H_{18}ClNS$) were purchased from Sigma. Their stock solution (0.01 M) were prepared with twice distilled water

* Corresponding author. Tel.: +86 21 6564 2405; fax: +86 21 6564 1740.
E-mail address: jlkong@fudan.edu.cn (J. Kong).

0039-9140/$ – see front matter © 2007 Elsevier B.V. All rights reserved.
doi:10.1016/j.talanta.2007.09.018

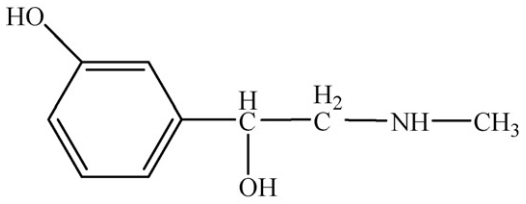

Scheme 1. Molecular structure of phenylephrine.

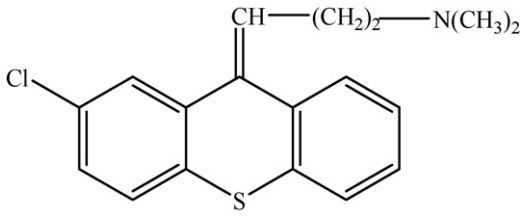

Scheme 2. Molecular structure of chlorprothixene.

or ethanol and stored at +4 °C in darkness. Buffer solution was a 0.05 M HAc–NaAc (pH 5.0) or NH_2CH_2COOH–HCl (pH 2.4) aqueous solution. 2×10^{-3} M 4-aminobenzene sulfonic acid (H_2N–C_6H_4–SO_3H, Aldrich) solution was prepared with 0.1 M NaH_2PO_4–Na_2HPO_4 (pH 7.0) buffer solution and also stored in refrigerator. The drug injections (PHE) and tablets (CPT) were obtained from Sine JiuFu Pharmaceutical Company (Shanghai, China). Prior to determination, the tablets were ground into powder, dissolved in ethanol, filtered into a container and diluted to certain volume, while the injections was directly diluted with water without further purification. Other reagents (Sigma or Aldrich) used were of analytical grade or chemical grade, and their solutions were prepared with twice distilled water or ethanol.

2.2. Apparatus

Electrochemical measurements were carried out on a CHI 440 electrochemical analytical instrument (ChenHua Instrument company, Shanghai, China). A three-electrode system was used, including a bare GC electrode ($\Phi = 3.0$ mm) or poly(4-ABSA)/GC modified electrode as working electrode, a saturated calomel electrode (SCE) as reference electrode and a platinum wire electrode as counter electrode. Electrochemical impedance spectroscopy (EIS) measurements were performed on an EG&G PAR Model 273 A bipotentiostat (Princeton, USA) in conjunction with a lock-in amplifier. A 5-mV amplitude sine wave was applied to the electrode under potentiostatic control and the frequency range was from 0.1 Hz to 100 KHz. Ultraviolet spectrophotometry (UV) measurements were performed on HP8453 ultraviolet-visible spectrophotometer (Agilent company, USA). Solution pH was measured with a Mettler-Toledo 320-s pH meter (Mettler-Toledo Instruments Limited Company, Shanghai, China). All experiments were carried out at about 25 °C.

2.3. Preparation of poly(4-ABSA)/GC modified electrode

The bare GC electrode was first polished to a mirror-like surface with 0.3 and 0.05 μm α-alumina slurry, then rinsed and ultrasonicated sequentially in water, acetone, diluted HNO_3 and water, then dried in air. The effective area of GC electrode could be calculated to be 0.0674 cm^2 according to literature [18]. The poly(4-ABSA)/GC modified electrode was prepared according to literature [15]. The cleaned bare GC electrode was immersed in 0.1 M NaH_2PO_4–Na_2HPO_4 (pH 7.0) buffer solution containing 2×10^{-3} M 4-ABSA and repetitively cycled between −1.5 and +2.5 V for 10 scans at a scan rate of 100 mV s^{-1}, then it was taken out. In order to get stable response, prior to measurements, the resulted modified electrode was also continuously cycled from +0.3 to +1.2 V in 0.05 M blank HAc–NaAc (pH 5.0) or NH_2CH_2COOH–HCl (pH 2.4) buffer solution for another 15 scans. Finally, the modified electrode was carefully rinsed with water, and stored in air for later use.

2.4. Procedure

The three-electrode system was immersed in a 10 mL cell containing proper amount of PHE or CPT and 0.05 M buffer solution. After accumulating for 60 s at open circuit under stirring and following quiet for 10 s, potential scan was initiated and cyclic voltammograms were recorded between +0.3 and +1.2 V at a scan rate of 100 mV s^{-1}. Before every test, the modified electrode needed easy regeneration in blank buffer solution. The determination was carried out using differential pulse voltammetry (DPV) within the same potential window. As to the chronocoulomertric experiment, the potential step was from +0.7 to +1.0 V for PHE and +0.8 to +1.15 V for CPT, respectively. Generally, voltammograms corresponding to the first cycle were recorded.

3. Results and discussion

3.1. Cyclic voltammograms of the electropolymerization and electrochemical characterization of the modified electrode

The electropolymerization of 4-ABSA on GC electrode surface was performed by means of repetitive cyclic voltammetry. As shown in Fig. 1, in the first scan, anodic peak A at about +1.5 V and cathodic peak B at about −0.7 V were observed. From the second cycle on, anodic peak C at about +0.2 V appeared. With the potential cycle repeating, the peaks increased and became larger, suggesting the continuous growth of the film. At the same time, it was also observed that film growth was faster for the first five cycles than other subsequent cycles. From the ninth cycle on, the film hardly grew, which indicated polymerization reached saturation. After electropolymerization, a uniform adherent blue polymer formed on the GC electrode surface. According to literature [15], it was the intermolecular $–NH_2$ functional group that took part in the polymerization reaction, while the $–SO_3H$ functional group did not.

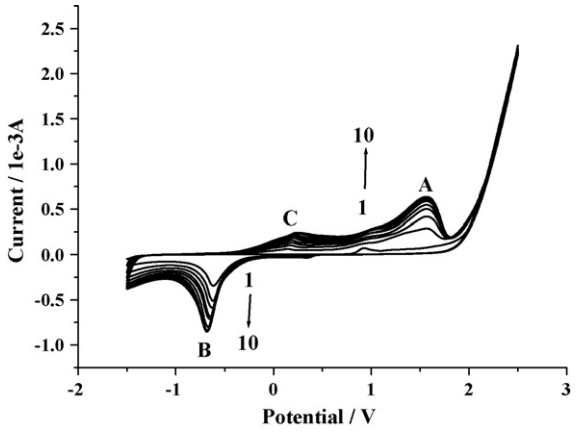

Fig. 1. Repetitive cyclic voltammograms (CVs) of 2 mM 4-ABSA at bare GC electrode. Scan rate: 100 mV s^{-1}; supporting electrolyte: 0.1 M phosphate (pH 7.0).

The poly(4-ABSA)/GC modified electrode was characterized by electrochemical methods. As shown in Fig. 2, $K_3Fe(CN)_6$ exhibited a pair of quite reversible redox peaks at bare GC electrode. The separation of peak potential ($\Delta E_p = E_{pa} - E_{pc}$) was about 68 mV and the formal potential ($E_F = (E_{pa} + E_{pc})/2$) was 256 mV. At the modified electrode, a pair of reversible redox peaks could still be observed. On one hand, compared with the former, the peak current decreased about 15%. This was related to the electrostatic interaction between polymer and probe. The pK_a of 4-ABSA was about 3.23 [19], so the sulfonic group of the polymer was negative charged due to the dissociation in neutral surroundings and repelled more $Fe(CN)_6^{3-}$ arriving at the electrode surface, which led to the decrease of current. On the other hand, the ΔE_p reduced to 56 mV and the E_F was 230 mV. The voltammetric response of $K_3Fe(CN)_6$ at poly(4-ABSA)/GC was affected by two factors. One was the surface charge of poly(4-ABSA)/GC, the other was the conductivity of poly(4-ABSA)/GC. Although the electrostatic repulsion between poly(4-ABSA)/GC and probe made the peak current decrease to some extent, the excellent conductivity of poly(4-ABSA)/GC was dominant, which accelerated the electron transfer of probe and resulted in the reduction of ΔE_p and E_F. This indicated the electrode process of probe became relatively reversible and easier in a way. In addition, the increase in background current also suggested the enhancement of conductivity. Fig. 3 shows the EIS spectra of the two electrodes in the given solution. Apparently, the resistor of modified electrode was much smaller than that of bare GC electrode, also indicating poly(4-ABSA)/GC had better conductivity.

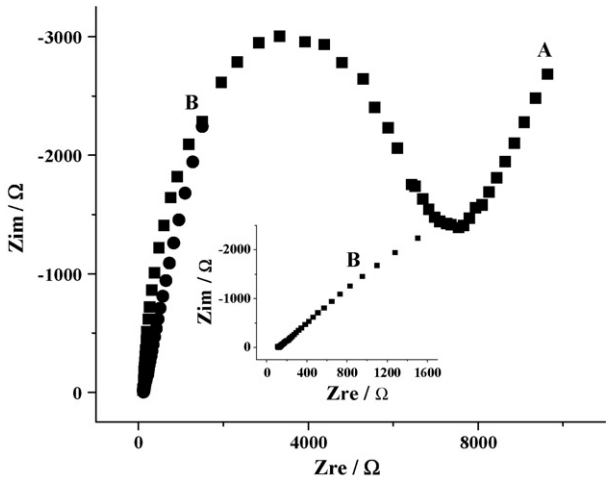

Fig. 3. EIS spectra of bare GC electrode (A) and poly(4-ABSA)/GC modified electrode (B). Frequency used: 0.1 Hz to 100 KHz; solution: 2 mM $K_3Fe(CN)_6/K_4Fe(CN)_6$ containing 0.1 M KNO_3. The insert was the amplification of (B).

3.2. Cyclic voltammograms of PHE and CPT at poly(4-ABSA)/GC modified electrode

In blank buffer solution, no obvious peaks were observed at both bare GC electrode and poly(4-ABSA)/GC modified electrode. As shown in Fig. 4, PHE generated a small anodic peak at about +0.9 V at bare GC electrode. However, at modified electrode, it produced a more sensitive anodic peak at about +0.89 V, the peak current was about ten times as high as that of bare GC

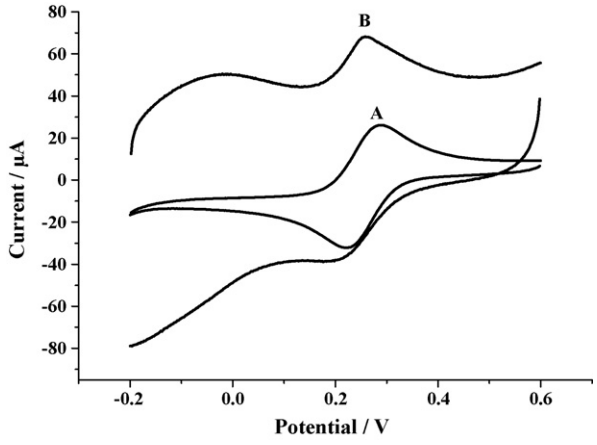

Fig. 2. CVs of 2 mM $K_3Fe(CN)_6$ at bare GC electrode (A) and poly(4-ABSA)/GC modified electrode (B). Scan rate: 100 mV s^{-1}; supporting electrolyte: 0.05 M KNO_3.

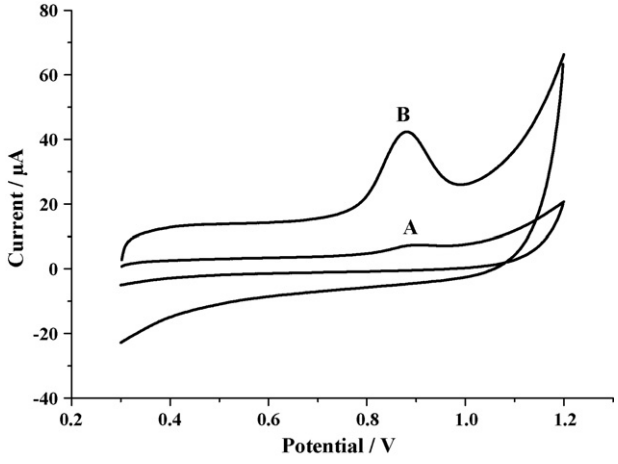

Fig. 4. CVs of 1×10^{-5} M PHE at bare GC electrode (A) and poly(4-ABSA)/GC modified electrode (B). Scan rate: 100 mV s^{-1}; supporting electrolyte: 0.05 M HAc–NaAc (pH 5.0); accumulation time: 60 s (at open circuit).

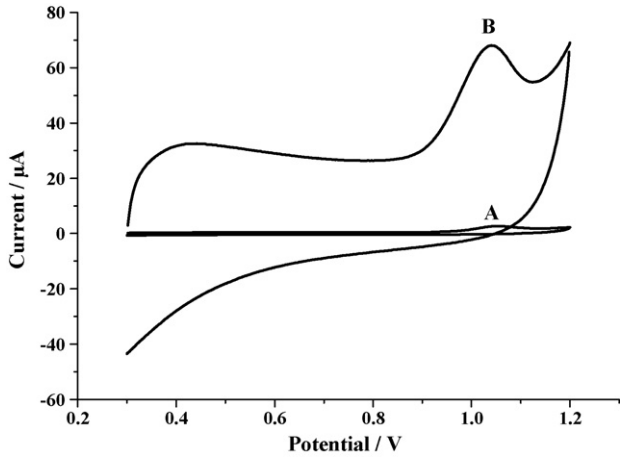

Fig. 5. CVs of 2×10^{-5} M CPT at bare GC electrode (A) and poly(4-ABSA)/GC modified electrode (B). Scan rate: 100 mV s^{-1}; supporting electrolyte: 0.05 M NH_2CH_2COOH–HCl (pH 2.4); accumulation time: 60 s (at open circuit).

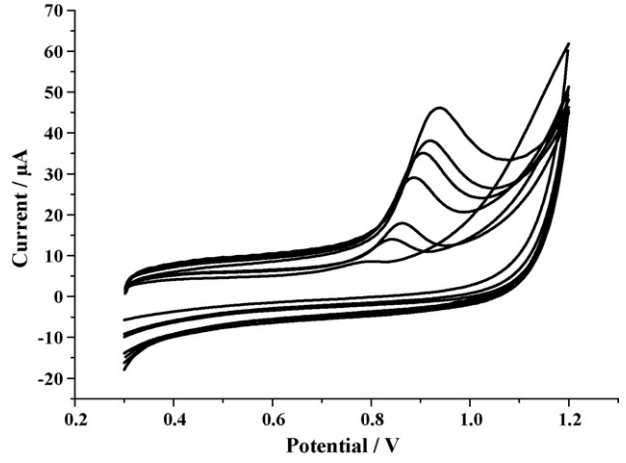

Fig. 6. Influence of scan rate on the anodic peak of 5×10^{-6} M PHE. Scan rate: 10, 30, 50, 100, 150, 200, 300 mV s^{-1} (from bottom to top). Other conditions as in Fig. 4.

electrode. This could be attributed to the good conductivity of the modified electrode. Meanwhile, the electrostatic interaction between polymer and PHE also contributed to the enhancement of sensitivity (described in the following section). For CPT, it produced a small anodic peak at about +1.06 V at bare GC electrode, and this anodic peak shifted negatively to +1.04 V with the current increasing about 17 times at the modified electrode (Fig. 5). This also suggested the modified electrode had better conductivity. Apparently, the poly(4-ABSA)/GC modified electrode could promote the electrochemical oxidation of PHE or CPT. In addition, no obvious cathodic peaks appeared at both bare GC electrode and modified electrode, which indicated the electrochemical oxidation of PHE or CPT was irreversible.

3.3. Effect of scan rate and chronocoulomertric investigation

For both PHE (Fig. 6) and CPT (Fig. 7), when scan rate increasing from 10 to 300 mV s^{-1}, the anodic peak grew. It was found that anodic peak current was linear to the square root of scan rate, the regression equations were: $I_p = -4.6 + 2.048v^{1/2}$ (I_p (μA), v (mV s^{-1}), $r = 0.999$) and $I_p = -3.088 + 3.809v^{1/2}$ ($r = 0.999$), respectively. This suggested the electrode process was diffusion-controlled. Additional, the anodic peak potential and the logarithm of scan rate showed a linear relationship, following the equation: $E_p = 0.701 + 0.0412 \ln v$ (E_p(V), $r = 0.998$) and $E_p = 0.722 + 0.0681 \ln v$ ($r = 0.998$), separately. According to the equation [20]: $E_p = E^{\Phi} + m[0.78 + \ln(D^{1/2}/k_s) - 0.51\,\text{nm}] + 0.5\,\text{mL}\,nv$ ($m = \text{RT}/(1-\alpha)nF$), the $n(1-\alpha)$ was calculated to be 0.312 (PHE) and 0.189 (CPT). For PHE, it was thought the oxidation occurred at the phenolic group, PHE turned into phenylephrinequinone and one electron was lost [14], thus $n = 1$ and the charge-transfer coefficient $\alpha = 0.688$. For CPT, according to literature [21], the oxidation occurred at the thioxanthene ring, the sulfur atom was oxidized to sulphoxide and two electrons were lost. Therefore, $n = 2$ and $\alpha = 0.906$.

The chronocoulomertric responses of PHE and CPT were investigated. After subtracting the background charge, the plots of charge (Q) against square root of time ($t^{1/2}$) were made. They were straight line and the regression equation were $Q = -8.316 + 52.97t^{1/2}$ (Q (μC), t (s), $r = 0.999$) and $Q = -17.326 + 94.467t^{1/2}$ ($r = 0.999$), separately. According to the integrated Cottrell equation [22]: $Q = 2n\text{FAD}^{1/2}\text{C}t^{1/2}/\pi^{1/2} + Q_{dl} + n\text{FA}\Gamma_0$, the diffusion coefficient (D) of PHE and CPT was calculated to be 5.20×10^{-7} and 1.03×10^{-7} cm^2 s^{-1}, respectively.

3.4. Optimization of the analytical conditions

3.4.1. Influence of electropolymerization conditions

The potential range, especially the positive potential, was very important for the preparation of the polymer. The results showed that if the positive potential was lower than +1.5 V or negative potential was higher than −0.8 V, no polymerization reaction occurred. When the positive potential reached +1.8 V, the electropolymerization happened. It was found that a better

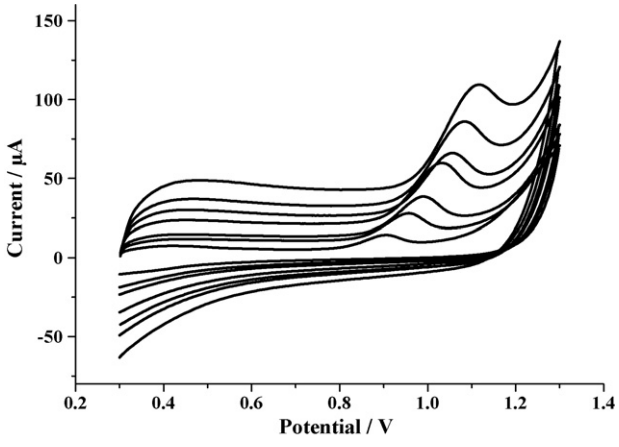

Fig. 7. Influence of scan rate on the anodic peak of 2×10^{-5} M CPT. Scan rate: 10, 30, 50, 100, 150, 200, 300 mV s^{-1} (from bottom to top). Other conditions as in Fig. 5.

conducting polymer could form within the potential range from −1.5 to +2.5 V, thus this potential window was selected.

Besides 0.1 M NaH_2PO_4–Na_2HPO_4 buffer solution (pH 7.0), 0.1 M H_2SO_4 (pH 0.7), 0.1 M HCOOH–HCOONa buffer solution (pH 3.5), 0.1 M HAc–NaAc buffer solution (pH 4.7) were tested as polymerization medium. The results showed that the responses of PHE and CPT at modified electrodes almost kept unchanged. This indicated the pH (0–7) and the medium had little effect on the electropolymerization. This was in accordance with literature [23]. In general, 0.1 M NaH_2PO_4–Na_2HPO_4 buffer solution (pH 7.0) was chosen as the polymerization medium for its mildness.

Additional, if the oxygen dissolved in the medium was removed before electropolymerization, the responses of PHE and CPT were not affected obviously. This suggested oxygen did not play a role in the electropolymerization, which was in compliance with the electropolymerization mechanism of 4-ABSA [15]. Generally, it was not necessary to remove oxygen before electropolymerization.

Furthermore, when the number of polymerization cycles was changed from 5 to 25 scans, it was found that the responses of PHE and CPT almost remained constant within 5–15 scans. If the scans increased further, the responses decreased obviously. This suggested the poly(4-ABSA)/GC modified electrode became insulated. In general, in order to get stable conducting polymer, 10 scans was selected as polymerization cycles.

3.4.2. Influence of pH and buffer solution

For PHE, within the range of pH 2.3–10.0, the peak potential shifted negatively with pH increasing, following the linear equation: $E_p = 1.153–0.0545$ pH (E_p (V), $r = 0.999$), meaning H^+ was involved in the oxidation. The slope 54.5 mV/pH suggested the number of protons was equal to that of electrons taking part in the oxidation. According to literature [14], one electron was lost during the oxidation, thus one proton played a role in the oxidation. At the same time, the peak current increased until it attained the maximum at pH 5.0, then it decreased. According to literature [13], the pK_a of PHE was 8.77 and 9.84, thus it was positive charged in acid and neutral surroundings. Generally, when the solution pH was lower than 3.23, the modified electrode was neutral charged, the electrostatic interaction between them was not strong, thus the response was not good; if the pH increased, the modified electrode was more negative charged, the electrostatic interaction strengthened, which resulted in the enhancement of response. At pH 5.0, the electrostatic interaction was the strongest, thus the response attained the maximum. However, with pH increasing further, in spite that the negative charge of the sulfonic group increased, the PHE cations decreased more, therefore, the weakness of the electrostatic interaction led to the decrease of response. Thus pH 5.0 was chosen as the optimum pH value for PHE. When pH was set at 5.0, several supporting electrolytes such as HAc–NaAc, NaH_2PO_4–Na_2HPO_4, HCOOH–HCOONa, $KHC_8H_4O_4$–NaOH were tested. It was found that the best response was obtained in HAc–NaAc buffer solution. Meanwhile, when the concentration of buffer changed from 0.02 to 0.2 M, the response remained almost unchanged. If the concentration increased further, the response decreased, which suggested high ion strength might reduce the electrostatic interaction between PHE and polymer [24]. Furthermore, pH 5.0 was near to the pK_a of HAc–NaAc (pK_a = 4.74 [25]) buffer solution, therefore, its buffer capacity was good and adequate. Hence, 0.05 M HAc–NaAc (pH 5.0) was chosen as the buffer solution for PHE.

For CPT, within the range pH 1.5–5.0, the peak potential also shifted negatively with pH increasing, following the linear equation: $E_p = 1.07–0.0122$ pH ($r = 0.998$), indicating H^+ took part in the oxidation. Meanwhile, the maximum response was obtained at pH 2.3. According to literature [21], the pK_a of CPT was about 9 and it was poorly soluble in neutral and basic solutions. If the solution pH was much lower, owing to the strong protonation, the oxidation might become difficult and response was lower; when pH was above 3.5 and increased further, its solubility decreased quickly and it became more hydrophobic due to the deprotonation, which resulted in the poor response. Therefore, pH 2.3 was selected as the optimum pH value for CPT. When pH was set at 2.3, several supporting electrolytes including H_3PO_4–NaH_2PO_4, $KHC_8H_4O_4$–HCl, NH_2CH_2COOH–HCl, HCOOH–HCOONa were tested, the best response was obtained in NH_2CH_2COOH–HCl buffer solution. And the variation in buffer concentration from 0.02 to 0.2 M had no obvious influence on the response. Furthermore, pH 2.3 was near to the pK_a of NH_2CH_2COOH–HCl (pK_a = 2.35 [25]) buffer solution, Therefore, 0.05 M NH_2CH_2COOH–HCl (pH 2.4) was chosen as the buffer solution for CPT.

3.4.3. Influence of accumulation time and potential

For a 1×10^{-5} M PHE or CPT solution, the anodic peak current remained almost constant with accumulation time increasing, indicating accumulation time had no effect and diffusion dominated the electrode process. However, when the concentration of PHE or CPT was much lower, the electrode process might exhibit adsorptive characteristics and suitable accumulation could contribute to the enhancement of sensitivity. Therefore, considering the need for the detection of lower concentration samples, 60 s was chosen as accumulation time. In addition, when accumulation potential changed from −0.8 to +0.6 V, the maximum responses were obtained at −0.4 V and −0.2 V, respectively. However, compared with at open circuit, the effect of accumulation potential was negligible. Hence, accumulation at open circuit was adopted.

3.5. Calibration curve

Under the optimum analytical conditions, the determination of PHE and CPT with different concentrations was performed. It was found that the anodic peak current was linear to concentration within the range from 1×10^{-7} to 1.5×10^{-5} M and 2×10^{-6} to 4.5×10^{-5} M, the detection limits obtained were 1×10^{-8} and 1×10^{-7} M ($S/N = 3$), respectively. The regression equations were: $I_p = 2.129 + 1.968c$ (I_p (μA), c (μM), $r = 0.997$) and $I_p = 1.192 + 1.431c$ ($r = 0.995$), separately.

Table 1
Measurement results of PHE injections and CPT tablets

	Add (μM)	Found (μM)	Recovery (%)
PHE (2.00 μM) No.			
1	2.00	3.92	96.0
2	4.00	5.85	96.3
3	6.00	8.02	100.3
4	8.00	10.26	103.3
CPT (3.96 μM) No.			
1	3.96	8.10	104.5
2	7.92	12.14	103.3
3	11.88	15.87	100.3
4	15.84	20.13	102.1

3.6. Regeneration, reproducibility, stability and selectivity of poly(4-ABSA)/GC modified electrode

The poly(4-ABSA)/GC modified electrode could be easily regenerated by repetitive cycling in a blank solution for several times. For eight parallel determinations of a 1×10^{-5} M PHE or CPT solution with the same electrode, the RSD of peak current was calculated to be 2.23% and 2.95%, respectively. This indicated the modified electrode had good reproducibility. After continuous use for 7 days, the modified electrode could retain 92% and 90% of its initial responses, separately, which suggested the modified electrode had high stability.

The influence of foreign compounds was tested. For PHE and CPT, it was found that several kinds of surfactants such as sodium dodecyl sulfate (SDS) did not interfere, while Tween-20, Triton X-100, cetylpyridiniumbromide (CPB), cetyltrimethylammoniumbromide (CTAB) made the peak decrease. 50-fold Cu^{2+}, Ag^{+}, Fe^{3+}, Pb^{2+}, Cd^{2+}, Zn^{2+}, riboflavine, folic acid, isoniazid, ascorbic acid, epinephrine, 100-fold thiamine, antipyrine, norfloxacin, propranolol, allopurinol, captopril, glucose, phenylanine did not interfere the determination. This suggested the modified electrode had good selectivity.

3.7. Applications

This method was applied to the detection of PHE or CPT in drug injections or tablets. The pretreatment and determination procedure were the same as described in Experimental. The analytical results were shown in Table 1, the recovery was 96.0–103.3% and 100.3–104.5%, respectively. According to Table 1, the PHE or CPT contents could be calculated, which was 9.9 mg/mL and 25.6 mg/tablet (their declared contents were 10 mg/mL and 25 mg/tablet), respectively. In order to examine the accuracy of this method, the drug samples were also measured by UV method proposed by Chinese Pharmacopoeia [26] and the analytical results were shown in Table 2. By means of *F*-test and *t*-test [27], the calculated *F*-value (2.30 and 3.22) and *t*-value (0.335 and 0.565) did not exceed the theoretical values (5.05 and 2.23, respectively, 95% confidence level). It suggested that the determination method proposed was reliable.

Table 2
Measurement results of parallel determinations of PHE injections and CPT tablets

	n					
	1	2	3	4	5	6
PHE (2.00 μM) Methods						
UV	1.97	2.00	2.04	2.04	2.06	2.08
EC	1.97	1.97	2.06	2.06	2.08	2.12
CPT (3.96 μM) Methods						
UV	3.95	4.00	4.03	4.03	4.05	4.07
EC	3.91	3.98	4.05	4.07	4.10	4.10

Statistical analysis results: $F_{exp} = 2.30$ and 3.22, smaller than the F_{crit} value (5.05, at the 5% probability level); $t_{exp} = 0.335$ and 0.565, smaller than the corresponding t_{crit} value (2.23, at the 95% confidence level).

4. Conclusions

The poly(4-ABSA)/GC modified electrode was fabricated and characterized by electrochemical methods. When potential was made to move, PHE and CPT could generate a sensitive and irreversible anodic peak at about +0.89 and +1.04 V at the modified electrode, respectively. Under the optimum analytical conditions, the anodic peak current was linear to PHE or CPT concentration over a certain range. The modified electrode exhibited some excellent characteristics, including easy regeneration, high stability, good reproducibility and selectivity. This method proposed could be successfully applied to the determination of PHE or CPT in practical drug samples and proved to be reliable.

Acknowledgements

This work was supported by the National Nature Science Foundation of China (Grant No: 20525519, 20475012) and Shanghai Leading Academic Discipline Project (B109).

References

[1] F. Huang, S. Qu, S. Zhang, B.H. Liu, J.L. Kong, Microchim. Acta 159 (2007) 157.
[2] T.Z. Peng, Z.P. Yang, H.P. Li, Analyst 116 (1991) 727.
[3] N.W. Beyene, J.F.V. Staden, Talanta 63 (2004) 599.
[4] W. Misiuk, Anal. Lett. 134 (2000) 23.
[5] A.J. Nepote, A.C. Ozden, Anal. Chim. Acta 439 (2001) 87.
[6] F. Belal, F. Ibrahim, S.M. Hassan, F.A. Aly, Anal. Chim. Acta 255 (1991) 103.
[7] K. Gumbhir, W.D. Mason, J. Pharm. Biomed. Anal. 14 (1996) 623.
[8] T. Sokoliess, U. Menyes, U. Roth, T. Jira, J. Chromatogr. A 948 (2002) 309.
[9] M.R. Gomez, R.A. Olsina, L.D. Martinez, M.F. Silva, J. Pharm. Biomed. Anal. 30 (2002) 791.
[10] T. Sokoliess, M. Gronau, U. Menyes, U. Roth, T. Jira, Electrophoresis 24 (2003) 1648.
[11] A.F. Shoukry, R. El-Sheikh, Y.M. Issa, M. Zareh, Microchim. Acta 99 (1989) 101.
[12] H. Hopkala, J. Drozd, S. Zareba, Pharmazie 52 (1997) 307.
[13] J.C. Perlado, A. Zapardiel, E. Bermejo, J.A. Perez, L. Hernandez, Anal. Chim. Acta 305 (1995) 83.
[14] Y.Z. Zhu, Z.L. Zhang, W. Zhao, D.W. Pang, Sens. Actuat. B 119 (2006) 308.

[15] G.Y. Jin, Y.Z. Zhang, W.X. Cheng, Sens. Actuat. B 107 (2006) 528.
[16] F. Xu, M.N. Gao, L. Wang, G.Y. Shi, W. Zhang, L.T. Jin, J.Y. Jin, Talanta 55 (2001) 329.
[17] J.H. Chen, J. Zhang, Q. Zhuang, S.B. Zhang, X.H. Lin, Talanta 72 (2007) 1805.
[18] B.Z. Zeng, F. Huang, Talanta 64 (2004) 380.
[19] Y.Y. Xia, Handbook of Chemical Laboratory, 1st ed., Chemical Industry Press, Beijing, 2004, p. 121.
[20] E. Laviron, J. Electroanal. Chem. 101 (1979) 19.
[21] F. Belal, M.M. Hefnawy, F.A. Aly, J. Pharm. Biomed. Anal. 16 (1997)369.
[22] A.J. Bard, L.R. Faulkner, Electrochemical Methods: Fundamentals and Applications, 1st ed., John Wiley & Sons, New York, 1980, p. 200.
[23] C.M.A. Brett, C. Thiemann, J. Electroanal. Chem. 538 (2002) 215.
[24] B.Z. Zeng, Y.X. Yang, F.Q. Zhao, Electroanalysis 15 (2003) 1054.
[25] Wuhan University, Analytical Chemistry, 4th ed., Higher Education Press, Beijing, 2000, p. 322.
[26] Chinese Pharmacopoeia Commission, Chinese Pharmacopoeia, 1st ed., Chemical Industry Press, Beijing, 2005, pp 469, 775.
[27] D. Harvey, Modern Analytical Chemistry, 1st ed., McGraw-Hill Higher Education, 2000, pp. 85, 726.

Available online at www.sciencedirect.com
ScienceDirect
Talanta 74 (2008) 1420–1427
Talanta
www.elsevier.com/locate/talanta

Design of two-dimensional biomimetic uranyl optrode and its application to the analysis of natural waters

D. James [a], J. Mary Gladis [a], A.K. Pandey [b], G.R.K. Naidu [c], T. Prasada Rao [a,*]

[a] *Inorganic and Polymer Materials, National Institute for Interdisciplinary Science and Technology (CSIR), Trivandrum 695019, India*
[b] *Radiochemistry Division, Bhabha Atomic Research Centre, Trombay, Mumbai 400085, India*
[c] *Department of Environmental Sciences, S.V. University, Tirupati 517502, India*

Received 24 July 2007; received in revised form 19 September 2007; accepted 20 September 2007
Available online 29 September 2007

Abstract

A two-dimensional biomimetic optrode for the detection and quantification of uranium in natural waters was fabricated. The sensing element was designed by the inclusion of uranyl ion imprinted polymer particles into polymethyl methacrylate followed by casting a thin film on a glass slide without any plasticizer. The ion imprinted polymer material was prepared via covalent immobilization of the newly synthesised ligand 4-vinyl phenylazo-2-naphthol by thermal polymerization. Operational parameters such as pH, response time and the amount of sensing material were optimized. The response characteristics of the imprinted and the corresponding non-imprinted polymer inclusion optrodes of uranium were compared under optimum conditions. The imprinted polymer inclusion optrode responds linearly to uranium in the concentration range 0–1.0 $\mu g\,mL^{-1}$ with a detection limit of 0.18 $\mu g\,mL^{-1}$, which is much better than the solution studies using 4-vinyl phenylazo-2-naphthol (1.5 $\mu g\,mL^{-1}$). Triplicate determinations of 100 μg of uranium(VI) present in 250 mL of solution gave a mean absorbance of 0.018 with a relative standard deviation of 8.33%. The superior sensitivity of imprinted polymer inclusion optrode is exemplified by lower detection limits and broader dynamic range over non-imprinted polymer inclusion optrode. The developed imprinted polymer inclusion optrode was found to give stable and precise response for 3 months and can be used without any loss in sensitivity. The applicability for analysing ground, lake and tap-water samples collected in the vicinity of uranium deposits was successfully demonstrated.
© 2007 Elsevier B.V. All rights reserved.

Keywords: Two-dimensional sensor; Optrode; Uranium; Determination; Solid phase extraction; Ion imprinted polymer

1. Introduction

Uranium is one of the emerging pollutants due to its high toxicity and radioactivity and most recently its persistence in environment. There is a possibility of contamination of ground water due to seeping in the areas close to uranium deposits or because of the uranium mining operations. Hence, there is a need to develop portable sensors that has the capability of analysing the concentration of toxin selectively. The WHO, Health Canada and Australian drinking water guidelines fixed the maximum uranium concentration in drinking waters to be less than 9, 20 and 20 $\mu g\,L^{-1}$ [1,2]. The inhalation of uranium compounds results in deposition of uranium in lungs and reaches kidneys through blood stream. The techniques which can be used for trace analysis generally have high sensitivity but are complex and costly, require skilled technicians and large laboratory-based instrumentation [3]. In addition, long analysis time, extensive sample handling with multiple washing steps and transportation and storage prior to detection and quantification are other limitations. The development of portable sensing probes in conjunction with more compact and low-cost instruments are highly desirable for facilitating the task of on-site monitoring and field studies. Of those, optical sensors that is selective toward a specific analyte, multiple interactions between host and guest in a complementary fashion have to be especially advantageous for field, in situ, and environmental applications [4]. Development of selective optical sensors can be a substitution of conventional analytical procedures in aqueous sample. In view of extremely low levels of uranium in a variety of environmental samples, the quantification requires a tedious and time consuming preconcentration step before determination. Here comes the role of

* Corresponding author. Tel.: +91 471 2515317/2490674; fax: +91 471 2491712/2490186.
E-mail address: tprasadarao@rediffmail.com (T. Prasada Rao).

0039-9140/$ – see front matter © 2007 Elsevier B.V. All rights reserved.
doi:10.1016/j.talanta.2007.09.019

two-dimensional sensors [5]. Two-dimensional sensor is based on the separation/preconcentrative separation of target analyte from the complex matrix of real sample and subsequent generation of signal proportional to the amount of analyte. This type of optrodes offer a unique possibility of simultaneous preconcentration and detection of the analyte and are well suited to this type of application as they may easily be incorporated into low-cost, easy-to-use kits. [6,7]. Optical sensors for uranyl ion was developed using Alizarin Red S–tetraoctyl ammonium bromide ion pair on a triacetyl cellulose membrane [9] and mesoporous thin films functionalized with silylated β-diketone compounds [8]. Eventhough optical sensors designed by immobilization techniques [8–11] are better in some of the aspects such as non-leaching of indicators and quick response, lacks in antibody-like selectivity. The selectivity, which is the bottleneck in most of the sensing devices with different transducers can be achieved by employing the plastic antibodies, i.e. molecularly/ion imprinted polymers [12–14]. Ion imprinted polymers (IIPs) are synthetic polymers with specific binding sites for a target metal ion. These ion imprinted polymers or plastic antibodies are much more stable to acids, bases and organic solvents and can withstand high temperatures and pressures unlike their biological counterparts. Moreover, the preparation of these materials is simple, cost effective and can be stored in dry state at room temperature for long periods of time [15,16]. Murray's group developed a lead ion imprinted fluoro-optrode for monitoring lead in streams to find the contamination. This optrode was prepared by binding 3% lead(II)-methyl-3,5-divinyl benzoate complex by in situ copolymerization on 400 μm optical fibre surface [17]. An optical flowthrough sensor was developed by Al-Kindy et al. using fluorescent Al(III)–morin complex by non-covalent imprinting [18]. The extensive literature survey revealed that there is no uranyl optrode based on imprinted polymer technology.

Hence, we now propose an optrode based on the use of IIP particles prepared via chemical immobilization after the formation of mixed ligand complex, uranium-4-vinyl phenylazo-2-naphthol (VPAN)–4-vinyl pyridine (VP) and then polymerization with matrix forming monomers. Furthermore the design of imprinted polymer inclusion (IPI) optrode by the inclusion of uranyl ion imprinted material in polymethyl methacrylate (PMMA) matrix is described and its possible application to natural waters is demonstrated.

2. Experimental

2.1. Instrumentation

A Shimadzu computer controlled UV–vis spectrophotometer UV-2401 PC (Shimadzu, Kyoto, Japan) was used during preconcentration studies. An AAnalyst Perkin-Elmer atomic absorption spectrometer (Perkin-Elmer, Shelton, CT, USA) was used for selectivity studies. pH measurements were carried out using LT-120 digital pH meter (Elico, Hyderabad, India). FT-IR spectra were recorded by KBr pellet method using Perkin-Elmer, Spectrum One FT-IR spectrometer. A 300 MHz Brucker NMR spectrophotometer was used for recording the NMR spectrum (Bruker Avance, Switzerland). Scanning electron microscopic (SEM) images were obtained using a JEOL JSM-5600 LV (SEM, Japan). Surface area and pore size analyser (ASAP 2020, Micromeritics, USA) was used to obtain the BET surface area and average pore dia by N_2 adsorption.

Mass spectrum was recorded using a JEOL JSM 600 fast atom bombardment (FAB) high-resolution mass spectrometer (HRMS) (JEOL, Tokyo, Japan). CHN analysis was carried out with a Perkin-Elmer series two elemental analyser 2400. Thickness of the film was measured by the use of Leica, DMRX optical microscope in Qwin software (Leica, Hurbrugg, Switzerland).

2.2. Materials

A stock solution of (1000 μg mL^{-1}) of uranium(VI) was prepared by dissolving uranyl nitrate, purchased from Aldrich (Milwaukee, WI, USA). Arsenazo III (Aldrich, USA) solution (0.01%) was prepared in 100 mL of deionised water. Polymethyl methacrylate (PMMA), 4-vinyl pyridine (VP), ethyleneglycoldimethacrylate (EGDMA), 2,2′-azobisisobutyronitrile (AIBN) was purchased from Aldrich. All other chemicals were of AR grade purchased from Merck, India.

2.3. Synthesis of polymerizable ligand

Eighteen millimoles (2.1 mL) of 4-vinyl aniline was dissolved in 1:1 HCl (15 mL). The solution was cooled until the temperature falls below 5 °C. The diazotisation of cold 4-vinyl aniline hydrochloride was carried out by adding 27 mmol (1.9 g) of $NaNO_2$ solution in small volume with stirring. Care has been taken in such a way that the reaction temperature should not rise above 10 °C to prevent the decomposition of diazonium compound.

Eighteen millimoles of 2-naphthol (2 g) was dissolved in NaOH solution and cooled. The diazotised compound was coupled with this 2-naphthol solution. The cold mixture was acidified with conc.HCl. The resulting product was filtered and washed with water until it is free from acid. The resulting residue was purified by column chromatography (see Fig. 1 for scheme).

The above-synthesised ligand, 4-vinyl phenylazo-2-naphthol was characterized by NMR, IR, MS and elemental analysis.

m.p: 110–115 °C, ^{1}H NMR (DMSO-d_6, TMS, ppm): 5.34(1H, *d*, CHH=CH), 5.85 (1H, *d*, CHH=CH), 6.81 (1H, *dd*, CHH=CH), 7.42 (2H, *d*, ArH), 7.59 (3H, *d*, ArH), 7.79 (5H, *d*, ArH), 8.59 (1H, OH). IR (KBr pellets, cm^{-1}):3377 (O–H), 1615 (C=C, vinyl), 1600 (C=C, ring), 1552 (Ar–H), 1507 (N=N), 1451 (C=CH) 1257 (C–OH). Mass spectrum (*m*/*z*): 274 (M^+). Elemental analysis (%): found: C (78.66), H (5.93), N (9.8); calculated: C (78.81), H (5.14), N (10.21).

2.4. Preparation of uranyl ion imprinted polymer (IIP) particles

Uranyl ion imprinted polymer materials were prepared by thermal polymerization method. The uranyl ion (1 mmol) was complexed with VPAN (2 mmol) and 4-vinyl pyridine (2 mmol) to form mixed ligand complex, which was then mixed with 8 mmol of VP (functional monomer), and 32 mmol of EGDMA

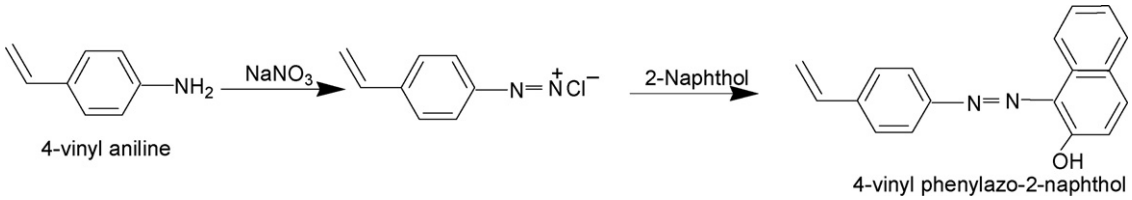

Fig. 1. Synthesis of 4-vinyl phenylazo-2-naphthol: a schematic representation.

(crosslinking monomer) to form the imprinted polymer. The above-prepared prepolymer mixture was polymerized using AIBN (0.05 g) as initiator at 80 °C under inert atmosphere. The IIP materials obtained were crushed and sieved to get uniform sized particles.

The uranyl imprint ion was leached using 5.0 mol L^{-1} HCl for 6 h. The resultant material can rebind uranium selectively from aqueous solutions. The synthesis of the corresponding non-imprinted polymeric materials was carried out by omitting uranyl ion under the same conditions as that of IIPs.

2.5. Solid phase extraction (SPE) studies

A solution containing 100 μg of uranium(VI) ion in 1 L of solution was subjected to preconcentration studies using 0.05 g of leached IIP and NIP particles at pH 7.0. The pH was adjusted after adding 10 mL of 1 M ammonia–ammonium chloride buffer and stirred for 30 min. The preconcentrated uranyl ions were eluted from the polymer particles using 15 mL of 1.0 M HCl by stirring for 30 min. The polymer particles were removed by filtration. The U(VI) ion content was determined spectrophotometrically using Arsenazo III method [19].

2.6. Retention capacity studies

The maximum amount of uranyl ion preconcentrated per gram of the material (IIP/NIP/Dowex/Chelex-100), viz., retention/binding capacity of materials was determined by saturating 0.02 g of material present in 25 mL of solution with 2.5 mg of uranyl ion under optimal conditions described in case of IIP solid phase extraction (SPE) procedure. The maximum amount of U(VI) thus preconcentrated was eluted with 1.0 M HCl and determined spectrophotometrically by using Arsenazo III procedure.

2.7. Spectrophotometric solution measurements

It was observed that VPAN is insoluble in water and soluble in DMSO. Hence 0.05% of VPAN in 25 mL of DMSO was prepared for solution measurements. To a series of U(VI) solutions containing 0–250 μg in 250 mL, add 5 mL of 1 M NH_3–NH_4Cl buffer solution and 2 mL of 0.05% VPAN. The pH was adjusted to 7.0 ± 1.5 using dil. HCl. The spectrum was recorded between 400 and 700 nm.

2.8. Sensor preparation and measurement

PMMA (20 mg) was dissolved in 0.5 mL of $CHCl_3$ and 5 mg of leached IIP/NIP particles were included into the polymeric matrix. The polymer particles were dispersed into the PMMA matrix using a cyclomixer to get homogeneous mixture. The mixed solution was uniformly coated onto a cleaned glass plate (5 cm × 1 cm). Prior to this, the glass plates were washed in conc. HNO_3 followed by ethanol, finally with distilled water and dried at 100 °C. The film thickness was measured using a Leica optical microscope for the films prepared at different batches and was found to be in the range ~68–70 μm. Design of uranyl ion imprinted polymer inclusion (IPI) optrode is given in the schematic diagram (Fig. 2).

The test solution (250 mL) containing 0–1.0 μg mL^{-1} of uranyl nitrate was adjusted to a pH of 7.0 ± 1.5 after adding 5 mL of 1.0 M NH_3–NH_4Cl buffer. The IPI optrode was exposed to the solution for 30 min with stirring. The response of the sensor was measured at a λ_{max} of 490 nm. The measurement was expressed as difference in absorbance between the optrode exposed to U(VI) and deionised water. NIPI films also cast in a similar manner and the response performance was tested.

2.9. Characterization studies

2.9.1. Scanning electron microscopy

The scanning electron micrograph of leached uranyl ion imprinted polymer materials prepared by bulk polymerization (Fig. 3a) showed an irregular shape with porous surface morphology. These IIP materials are encapsulated by PMMA on the surface of IPI optrode film (Fig. 3b). Also it is observed from the micrograph that the IIPs are almost uniformly dispersed in PMMA matrix which is responsible for the reproducible sensing of uranium from natural waters.

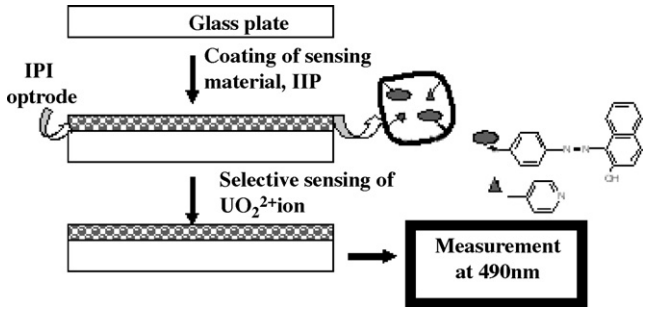

Fig. 2. Design of IPI optrode for the selective sensing of uranium.

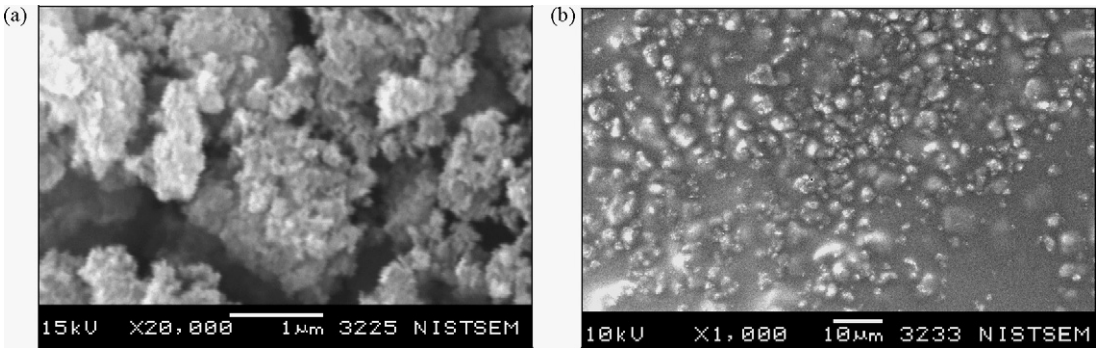

Fig. 3. SEM micrograph of (a) IIP particles and (b) surface of the IPI optrode film.

2.9.2. Surface area and pore size analysis

The surface area and pore size analysis of leached uranyl ion imprinted polymer materials has been carried out from the nitrogen gas adsorbed at the temperature of liquid nitrogen by BET method. The BET surface area of the IIP material was found to be 172.16 $m^2\ g^{-1}$ and the BJH average pore diameter during adsorption is 8–9 nm which confirms that the material is mesoporous in nature.

2.9.3. Analysis of real samples

Sample solution (250 mL) was adjusted to pH 7.0 using 5 mL of 1.0 M NH_3–NH_4Cl buffer (pH 7.0) and the U(VI) content was determined by standard addition method by adding 50 and 100 μg of uranyl ion. The response of the sensor was measured as described above.

3. Results and discussion

Covalent immobilization of ligand to the polymer matrix leads to operational stability of the sensor, since there is no leaching, crystallization or evaporation of components. Again, in the case of imprinted polymers, selective enrichment is its inherent property. Hence, a polymerizable ligand 4-vinyl phenylazo-2-naphthol (VPAN) was synthesised and is used for the preparation of sensing material, i.e. uranyl ion imprinted polymer. Similarly 4-vinyl pyridine (commercially available) was not only used for complex formation but also having the role in the formation of polymer matrix along with the crosslinking monomer (EGDMA). The formation of ternary mixed ligand complex was confirmed by UV–visible spectral studies. Fig. 4 shows the absorption spectra of 2-methoxy ethanol solutions of (a) U(VI), (b) 4-vinylpyridine (VP), (c) 4-vinyl phenylazo-2-naphthol (VPAN), (d) U(VI)–VP, (e) U(VI)–VPAN and (f) U(VI)–VPAN–VP against 2-methoxy ethanol. The absorption spectra of ternary mixed ligand complex shows hyperchromic shift compared to the corresponding binary complexes (U(VI)–VP and U(VI)–VPAN) and the ligands. This evidenced the formation of ternary complex in the prepolymer solution. Complex formation prior to imprinted polymer synthesis is advantageous because of the control of the structure and amount of species incorporated into the polymer and the possibility of regulating their microenvironment leading to predetermined selectivity.

3.1. SPE studies using NIP/IIP materials

The preconcentration of 100 μg of U(VI) ion in 1 L of solution was carried out with both ion imprinted and non-imprinted polymer materials to ascertain the imprinting effect as described in Section 2.5. The percent enrichment of uranyl ion is quantitative in the case of IIP (>99%) and it is only 57.4% for the corresponding NIP material. The imprinting effect is more pronounced compared to other uranyl IIP materials (except CAA–EGDMA) reported by several researchers including ours [20–25] which can be observed from the percent enrichment data compiled in Table 1. As seen from the table the imprinting efficiency of the IIP material under investigation is better than the reported uranyl IIPs or comparable (SA–VP) [25]. However, the material using chloroacrylic acid (CAA)–EGDMA possessing better imprinting efficiency. On the other hand, the amount of CAA–EGDMA material used for the enrichment study was very high (2.6 g) [21].

The maximum amount of uranyl ion preconcentrated per gram of the polymer particles (retention/binding capacity) was also determined by following the procedure described in Section

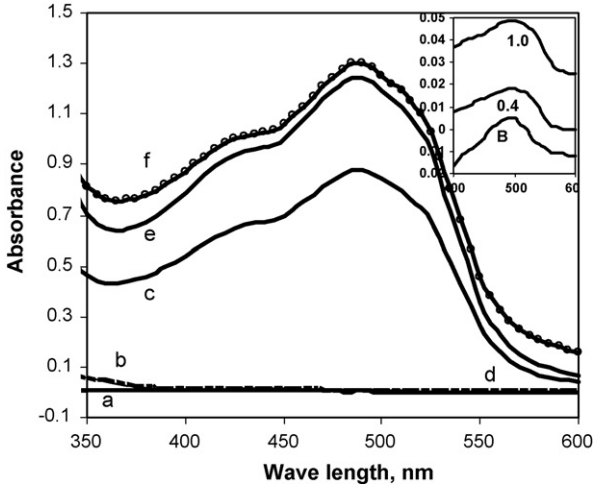

Fig. 4. UV–vis absorption spectra: (a) UO_2^{2+}, (b) VP, (c) VPAN, (d) UO_2^{2+}–VP, (e) UO_2^{2+}–VPAN and (f) UO_2^{2+}–VPAN –VP in 2-methoxy ethanol; (inset) differential absorbance of two dimensional IPI optrode after exposing to 0 μg mL^{-1} (B), 0.4 μg mL^{-1} and 1.0 μg mL^{-1} of U(VI) [volume of solution = 250 mL, pH 8.0; weight of sensing material = 5 mg per 20 mg of PMMA; equilibration/enrichment time = 30 min].

Table 1
Comparison of imprinting effect with various uranyl IIPs

S.No.	Functional group which interacts with UO_2^{2+}	Enrichment (%)		Ref.
		Non-imprinted	Imprinted	
1	Silica matrix	75.0	85.0	[20]
2	Vinyl benzoic acid–Styrene–DVB	Not dealt	>99	[22]
3	MAGA–EGDMA	Not dealt	96.0	[23]
4	VP–Styrene–DVB	41.7	78.8	[24]
5	DCQ–Styrene–DVB	30.6	40.0	[24]
6	Catechol–VP–HEMA–EGDMA	30.1	62.9	[25]
7	SALO–VP–HEMA–EGDMA	19.7	67.9	[25]
8	CAA–EGDMA	10.0	>98	[21]
9	DCQ-VP -Styrene-DVB	71.0 ± 0.7	>99	[24]
10	SA–VP–HEMA–EGDMA	58.2 ± 0.6	>99	[25]
11	VPAN–VP–EGDMA	57.4 ± 0.9	>99	Present work

CAA: chloroacrylic acid; EGDMA: ethylene glycol dimethacrylate; MAGA: methacryloylamidoglutamic acid; DVB: divinyl benzene; HEMA: 2-hydroxyethyl methacrylate; DCQ: 5,7-dichloroquinoline-8-ol; SA: succinic acid; SALO: salicylaldoxime.

2.6. The maximum amount of uranium preconcentrated onto the polymer materials was eluted using 15 mL of 1.0 M HCl and determined by Arsenazo III method. The retention/binding capacity of IIP and NIP materials are 126.0 and 60.0 μmol g^{-1} of the material, respectively. The higher retention capacity for IIPs than the corresponding NIPs can be attributed to the imprinting effect which is similar to the imprinting effect noticed during SPE studies carried out elsewhere using 5,7-quinoline-8-ol-VP as the ligands to form the mixed ligand complex with U(VI) [24,25]. The retention capacity of the IIP material in the present investigation is comparable to uranyl IIP particles prepared using DCQ–VP/SA–VP as ligands via trapping and better compared to other materials reported in the literature so far (Table 2). Again, the retention capacities of this IIP material (VPAN–VP) are of the same order as that of commercial Dowex 50wx-8, H^+ form and Chelex 100 ion exchangers.

Selectivity is a basic criterion for a successful optical sensor. Hence, the selectivity studies were carried out for the NIP and IIPs, which were used as the sensing material. 100 μg of each of individual inorganic species which are likely to coexist with U(VI) were equilibrated with 0.05 g of IIP and the enriched elements were determined by either spectrophotometry or flame atomic absorption spectrometry (FAAS). The percent extraction and the selectivity coefficients of uranyl ion using NIP and IIP materials with respect to other metal ions are listed in Table 3. It is clear from the table that the magnitudes of selectivity coefficients obtained with IIP materials in comparison with NIP materials are higher indicating once again the significant imprinting effect. Moreover, as seen from Table 3, selective enrichment was possible in the presence of Co(II), Ni(II) and Mn(II) ions. But the selectivity coefficients of uranium with respect to Th(IV), Fe(III), Cu(II) and Zn(II) are fairly good. From the above studies, the IIP material can selectively rebind the uranyl ion in the presence of other inorganic matrices. Hence, this material is used to design the optrode for the selective sensing of uranium.

Table 2
Comparison of retention capacities of uranyl IIPs

S.No.	Chelating moieties	Retention capacity (μmol g^{-1} of IIP)	Ref.
1	MAGA–EGDMA	~50	[23]
2	DCQ	13.2	[24]
3	VP	20.6	[24]
4	Catechol–VP	81.9	[24]
5	SALO–VP	79.4	[25]
6	SA–VP	115.3	[25]
7	DCQ–VP	137.0	[24]
8	VPAN–VP	126.0 ± 2.5	Present work
9	Chelex-100	194.5 ± 0.3	Present work
10	Dowex 50wx-8H^+	213.9 ± 1.8	Present work

3.2. Evaluation of sensing parameters

Polymer inclusion membranes (PIMs) are widely used in literature for the separation/preconcentration process due to its superior stability compared to other carrier-mediated membranes [26,27]. By amalgamating, the twin concepts of imprinted polymers (IPs) and PIM resulted in the preparation of ion imprinted polymer inclusion membranes (IPIMs) for potentiometric sensors [16,28]. In the present study, IIPs were used as a the sensing material for the development of IPI optrode due to the high selectivity and retention capacity compared to corresponding NIP material arising out of the "imprinting effect". The optrode film was cast onto a glass plate as given in Section 2.7 without the use of plasticizer. Compared to thick film, thin films are better to interact with the environment in a measurable way. PMMA, a commercially available polymer is used to cast the film by using IIPs as the sensing material. PMMA is a promising candidate for polymeric sensors due to its processability and mechanical stability [29]. VPAN on PMMA films were checked for sensing of uranyl ions. The values obtained were with less sensitivity compared to IPI optrode and no selectivity was observed.

The change in the absorbance depends on the concentration of analyte with which optrode was exposed. The analyte concentration was varied in the range of 0–1.0 μg mL^{-1}. The colour of

Table 3
The extraction (%), distribution ratio and selectivity coefficients of IIP and NIP polymer particles (0.05 g, pH 8, 1.0 L, 100 μg mL^{-1})

M^{n+}	Extraction[a] (%)		Selectivity coefficient, $S_{UO_2^{2+}/M^{n+}}$	
	NIP	IIP	NIP	IIP
U(VI)	57.40 ± 0.92	99.00	–	–
Th(IV)	82.40 ± 0.85	90.60 ± 0.78	0.28	10.3
Co(II)	19.30 ± 2.26	6.57 ± 0.22	5.54	1.40×10^3
Ni(II)	28.26 ± 3.07	7.27 ± 0.01	3.41	1.27×10^3
Mn(II)	14.46 ± 0.74	2.57 ± 0.06	7.82	3.80×10^3
Fe(III)	77.23 ± 0.78	64.50 ± 1.46	0.39	54.5
Cu(II)	14.07 ± 1.74	59.60 ± 0.75	8.31	66.9
Cr(VI)	12.14 ± 0.01	11.11 ± 0.23	9.50	790
Zn(II)	18.19 ± 1.46	11.55 ± 0.24	6.05	760

[a] Average of triplicate experiments of preconcentration and determination.

the optrode was intensified and a hyperchromic shift was noted with increase in analyte concentration (see inset of Fig. 4). The sensing of the optrode was tuned by proper selection of pH value. The effects of pH on the sensor response were investigated in the pH range 4–9 using 0.4 μg L^{-1} uranyl ion concentration in 250 mL of aqueous solution. The optimal pH range was found to be 5–8.5 (Fig. 5). The pH 7.0 was selected for further studies so that the absorbance for the complex was maximum. The ability of the imprinted polymer to bind uranyl ion at this elevated pH levels reflects the stability of the uranyl complex and the affinity of the interaction points in the imprinted cavity. The observed drift in absorbance at higher pH values (>8.5) could be due to the formation of hydroxyl complexes of uranyl ion in solution. No uranyl IIP material was reported which can be used to analyse the U(VI) in this pH range

Composition and nature of the film is important to improve the sensing characteristics of the optrode. Hence the amount of IIP materials included into the PMMA matrix was varied in the range of 2.5–20 mg. The film became brittle in the higher range. The sensing capability of optrode was very low when the amount of particles were <5 mg. Hence 5 mg of polymer particles were included into each film along with the 20 mg of PMMA in 0.5 mL of $CHCl_3$, but the concentration of complexing agent in the film

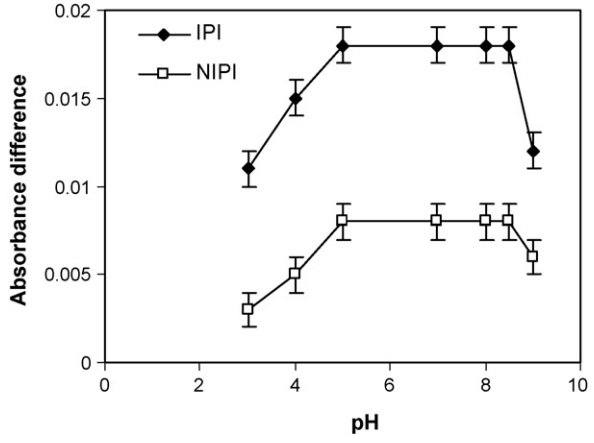

Fig. 5. Effect of pH on response of two-dimensional NIPI and IPI optrodes (uranium(VI): 0.4 μg mL^{-1}).

was very low compared to other membrane-based optical sensors [9,11]. The reproducibility in film casting was tested by measuring the thickness and magnitude of absorbance of film against glass plate at 490 nm (Table 4). The variation of thickness of the film in the range 68–70 μm and negligible change in the absorbance values proves the uniform coating of sensing material onto the glass plates. The response time of a two-dimensional sensor is mainly depends on the time required for the analyte to preconcentrate onto the sensing material. This was varied from 5 to 45 min. A minimum equilibration/enrichment time of 30 min was required to get an optimal absorbance of 0.018 for 100 μg in 250 mL of aqueous solution.

3.3. Mechanism of sensing

Direct analysis of traces uranium in environmental samples is difficult because of the complex nature of their matrices. Therefore pretreatment steps in analytical procedures such as preconcentration of the analyte before its determination will enhance the specificity of response and reduce false positive or negative responses [30]. The developed IPI optrode is based on the separation/preconcentration of target analyte by the sensing material and subsequent change in the microenvironment with predetermined selectivity leads to the generation of optical response signal, which is proportional to the amount of analyte. The IPI optrode responds linearly to uranium solutions of increasing concentrations by the formation of ternary mixed ligand complex with VPAN and VP on measuring the absorbance at 490 nm.

Table 4
Reproducibility in optrode preparation (0.005 g of IIP material, 0.02 g PMMA in 0.5 mL of $CHCl_3$)

No. of trials	Absorbance[a] (nm)	Thickness[a] (μm)
1	1.453	68
2	1.461	70
3	1.469	69
4	1.453	68
5	1.413	68

[a] Average of triplicate measurements.

3.4. Calibration and reproducibility

Under the optimum conditions described above, the calibration curve was linear over the concentration range 0–250 μg of U(VI) present in 250 mL of aqueous solution. The linear equation with regression is as follows:

$$A = 1.4 \times 10^{-3} + 7.5 \times 10^{-5}\, C \text{ (for NIPI optrode)}$$

$$A = 8.0 \times 10^{-4} + 1.6 \times 10^{-4}\, C \text{ (for IPI optrode)}$$

where correlation coefficients are 0.9966 and 0.9962, A is the absorbance and C is the concentration in microgram of U(VI) ion per 250 mL. The lowest concentration which can be analysed using the developed optrode was 0.18 μg mL^{-1}, calculated as the concentration of U(VI) which provided a signal equal to three times the standard deviation of the blank which is much better compared to the corresponding NIPI optrode (2 μg mL^{-1}) and U–VPAN solution studies (1.5 μg mL^{-1}). Thus, the lowering of detection limit with IPI compared to NIPI optrode is due to the chemical immobilization of ligands via polymerization and the concept of imprinting.

The reproducibility of the sensor was evaluated by analysing 0.4 μg mL^{-1} of U(VI) (three determinations each) using three films prepared at different timings. The relative standard deviation was found to be 8.33%.

3.5. Stability

The stability of the optrode film was established by measuring the signal at various interval of time, after exposing the film to test solution. There is no change in absorbance for more than 3 days. No loss in particles was observed when the film is exposed to aqueous solution (24 h). Also, no leakage of the ligand from the coated surface of the film was observed even after exposing the film to aqueous solution for 24 h with continuous stirring, since the ligand is chemically immobilized in the imprinted polymer during the process of polymerization. When the film was exposed to light, no drift in signal was observed. The IPI optrode was found to be stable for 3 months without loss in memory as confirmed by reproducibility of calibration range, detection limit and slope of calibration curve.

3.6. Analytical applications

The developed sensor was applied to the analysis of uranium in the natural water samples collected from locations in the vicinity of uranium [Cuddappa (1 and 2), India] and monazite sand deposits [Chavara (3) and Manavalakurichy (4), India]. The uranyl content of this samples were determined using IPI uranyl ion optrode by standard addition method as described in Section 2.8. The results obtained are shown in Table 5, from which it is clear that the uranyl ion recoveries obtained by spiking known amounts of uranium are quantitative, indicating the suitability of developed method for the routine monitoring or screening of natural waters for uranium.

3.7. Comparison with other uranyl optrodes

The developed IPI optrode with its selective binding sites in the polymer matrix offer lower detection limit (0.18 μg mL^{-1}) compared to the uranyl optrodes using Alizarin Red S (ARS)–tetraoctyl ammonium bromide ion pair on a triacetyl cellulose membrane (physical immobilization) [1.2 μg mL^{-1}] and mesoporous thin films functionalized (chemical) with silylated β-diketone compounds (1.0 μg mL^{-1}) reported by Safavi et al. [9] and Nicole et al. [8], respectively. The IPI optrode preparation is highly reproducible analogous to silica mesostructured optical sensors [8]. More significantly, this optrode can be used over a wider pH range (5.0–8.5) unlike the reported sensors such as optrode film with ARS (>5.5) [9] or mesostructured thin films [8]. Again, the previous reports applied to spiked river water samples [9] and this report addresses the analysis of real samples in the vicinity of uranium deposits which throw light in the environmental scenario of that locality.

Table 5
Analysis of real samples

S.No.	Description of the sample	Uranium (μg mL^{-1})		Recovery (%)
		Added	Found[a]	
1	Bore well water, Cuddapa	–	<0.18	
		0.2	0.201 ± 0.12	100.5
		0.4	0.402 ± 0.11	100.5
2	Lake water, Cuddapa	–	<0.18	
		0.2	0.202 ± 0.13	101
		0.4	0.404 ± 0.11	101
3	Pond water, Chavara	–	< 0.18	
		0.2	0.203 ± 0.09	101.5
		0.4	0.405 ± 0.14	101.3
4	Pond water, Manavalakurichy	–	<0.18	
		0.2	0.204 ± 0.14	102.0
		0.4	0.401 ± 0.13	100.3

[a] Average of three successive determinations.

4. Conclusions

The developed IPI optrode is selective for uranyl ion with multiple interactions towards the ligands in a complementary fashion. The predetermined selectivity, operational stability of the sensing material (IIP) is more advantageous compared to conventional optical sensors. The optrode developed was simple and its preparation was easy and reproducible and has flexibility in analytical variables such as pH. It can be used for the routine analysis of uranium down to 0.18 $\mu g\,mL^{-1}$ (which is one order lower than the two other optrodes reported previously [8,9]) in natural waters. Thus the developed optrode offer a possibility of simultaneous preconcentration and detection of the analyte especially from the complex environmental samples. Studies are in progress to develop rapid and reliable optrode with a better chromogenic reagent for naked eye detection and precise quantification of uranium in a variety of environmental samples.

Acknowledgements

The authors Dhanya J. would like to thank BRNS, Mumbai for the project fellowship and R.S. Praveen for the FAAS measurements. J.M. Gladis is grateful to CSIR, New Delhi for the RA research grant and Network project (NWP0023). G.R.K. and A.K.P are thankful to BRNS for sponsoring a project on MIP-based sensors.

References

[1] WHO, Guidelines for Drinking Water Quality, in: Health Criteria and Other Supporting Information, Addendum to vol. 2, 2nd ed., WHO/EOS/98.1, Geneva, 1998, p. 283.
[2] WHO, Guidelines for Drinking Water Quality, 3rd ed., WHO, 2003.
[3] T. Prasada Rao, P. Metilda, J.M. Gladis, Talanta 68 (2006) 1047.
[4] P.A. Lieberzeit, F.L. Dickert, Anal. Bioanal. Chem. 387 (2007) 237.
[5] H.H. Hill Jr., S.J. Martin, Pure Appl. Chem. 74 (2002) 2281.
[6] I. Oehme, O.S. Wolfbeis, Mikrochim. Acta 126 (1997) 177.
[7] G. Gauglitz, Anal. Bioanal. Chem. 381 (2005) 141.
[8] L. Nicole, C. Boissie‘re, D. Grosso, P. Hesemann, J. Moreaub, C. Sanchez, Chem. Commun. (2004) 2312.
[9] A. Safavi, M. Bagheri, Anal. Chim. Acta 530 (2005) 55.
[10] N. Malcik, O. Oktar, M.E. Ozser, P. Caglar, L. Bushby, A. Vaughan, B. Kuswandi, R. Narayanaswamy, Sens. Actuators B 53 (1998) 211.
[11] T.J. Sands, T.J. Cardwell, R.W. Cattrall, J.R. Farrell, P.J. Iles, S.D. Kolev, Sens. Actuators B 99 (2004) 608.
[12] K. Haupt, K. Mosbach, Chem. Rev. 100 (2000) 2495.
[13] G.M. Murray, O.M. Uy, Ionic sensors based on molecularly imprinted polymers, in: B. Sellergren (Ed.), Molecularly Imprinted Polymers, Elsevier Science, The Netherlands, 2001, p. 441.
[14] A.L. Hillberg, K.R. Brain, C.J. Allender, Adv. Drug Deliv. Rev. 57 (20051875).
[15] T. Prasada Rao, R. Kala, S. Daniel, Anal. Chim. Acta 578 (2006) 105.
[16] T. Prasada Rao, K. Prasad, R. Kala, J.M. Gladis, Crit. Rev. Anal. Chem. 37 (2007) 191.
[17] G.M. Murray, A.L. Jenkins, A. Bzhelyansky, O.M. Uy, Johns Hopkins APL Tech. Dig. 18 (1997) 464.
[18] Al-Kindy, R. Badia, M.E. Diaz-Garcia, Anal. Lett. 35 (2002) 1763.
[19] F.D. Snell, Photometric and Fluorimetric Methods of Analysis—Metals. Part 2, Wiley, New York, 1978.
[20] S. Dai, Y.S. Shin, C.E. Barnes, I.M. Toth, Chem. Mater. 9 (1997) 2521.
[21] G.D. Saunders, S.P. Foxon, P.H. Walton, M.J. Joyceb, S.N. Port, Chem. Commun. (2000) 273.
[22] S.Y. Bae, G.L. Southard, G.M. Murray, Anal. Chim. Acta 397 (1999) 173.
[23] R. Say, A. Ersoz, A. Denizli, Sep. Sci. Technol. 38 (2003) 3431.
[24] P. Metilda, J.M. Gladis, T. Prasada Rao, Anal. Chim. Acta 512 (2004) 63.
[25] P. Metilda, J.M. Gladis, G. Venkateswaran, T. Prasada Rao, Anal. Chim. Acta 587 (2007) 263.
[26] L.D. Nghiem, P. Mornane, I.D. Potter, J.M. Perera, R.W. Cattrall, S.D. Kolev, J. Membr. Sci. 281 (2006) 7.
[27] Y.M. Scindia, A.K. Pandey, A.V.R. Reddy, S.B. Manohar, Anal. Chem. 74 (2002) 4204.
[28] P. Metilda, K. Prasad, R. Kala, J.M. Gladis, T. Prasada Rao, G.R.K. Naidu, Anal. Chim. Acta 582 (2007) 147.
[29] P. Cywinski, M. Sadowska, A. Danel, W.J. Buma, A.M. Brouwer, B. Wandelt, J. Appl. Polym. Sci. 105 (2007) 229.
[30] A. Mizuike, Enrichment Techniques for Inorganic Trace Analysis, Springer, Berlin, 1983.

Available online at www.sciencedirect.com
ScienceDirect
Talanta 74 (2008) 1160–1165
Talanta
www.elsevier.com/locate/talanta

Dispersive liquid phase microextraction (DLPME) combined with graphite furnace atomic absorption spectrometry (GFAAS) for determination of trace Co and Ni in environmental water and rice samples

Hongmei Jiang, Yongchao Qin, Bin Hu *

Department of Chemistry, Wuhan University, Wuhan 430072, China

Received 26 June 2007; received in revised form 20 August 2007; accepted 21 August 2007
Available online 25 August 2007

Abstract

A new method of dispersive liquid phase microextraction (DLPME) combined with graphite furnace atomic absorption spectrometry (GFAAS) was proposed for the determination of trace Co and Ni using 1-(2-pyridylazo) 2-naphthol (PAN) as chelating reagent. Several factors influencing the microextraction efficiency of Co and Ni and their subsequent determinations, such as pH, extraction and disperser solvent type and their volume, concentration of the chelating agent, extraction time and ashing temperature and atomization temperature were studied, and the optimized experimental conditions were established. After extraction, the enrichment factors were 101 and 200 for Co and Ni, respectively. The detection limits of the method were 21 and 33 pg/mL for Co and Ni, and the relative standard deviations (R.S.Ds.) for five determinations of 0.5 ng/mL Co and Ni were 7.5% and 8.2%, respectively. The results for the determination of Co and Ni in East Lake water, Yangtse River water, Dongbei rice and spiked samples have demonstrated the accuracy, recovery and applicability of the proposed method. To validate the proposed method, two certified reference materials of Environment Water (GSBZ50009-88) and NIES No.10-b rice flour were analyzed, and the determined values were in good agreement with the certified values.
© 2007 Elsevier B.V. All rights reserved.

Keywords: Dispersive liquid phase microextraction; Graphite furnace atomic absorption spectrometry; Co and Ni; Environmental water; Rice

1. Introduction

Cobalt and nickel are known to be either essential or toxic at trace levels to human, animals and plants for metabolic processes depending on their concentration range [1–3]. It is clear that the determination of trace amounts of Co and Ni in environmental and food samples is of great significance from the public health and environmental point of view.

In recent years, continuous progress has been made in analytical instrumentation, however, direct determination of trace metal ions in environmental and food samples is difficult sometimes due to various factors, particularly their low concentrations and matrix effects. Under these circumstances, in order to determine trace levels of Co and Ni, a separation and enrichment step prior to their determinations could be a good choice. Several methods have been proposed for separation and preconcentration of trace Co and Ni including: solid phase extraction (SPE) [1,4], cloud point extraction (CPE) [2,3], liquid–liquid extraction (LLE) [5,6]. Among these separation and preconcentration methods, LLE is time consuming, tedious and multistage operation. And more importantly, it requires too much expensive and toxic organic solvent, which poses a health hazard and results in the production of hazardous waste. Compared with LLE, SPE offers simpler operation, higher enrichment factor and ease of automation, but the amounts of elution solvents are still relative large. As a preconcentration method, CPE is comparatively simple, cheap and less toxic [7]. However, there are several limitations associated with CPE: because of viscosity of the surfactant-rich phase, it cannot be injected directly to conventional analytical instruments and the surfactant bear chromophores which interferes with the UV detection by overlapping with the analyte signal [8].

Liquid phase microextraction (LPME), initially introduced by Cantwell in 1996 [9,10], has gained high popularity in organic analysis [11–13] because it incorporated sampling, extraction, concentration and sample introduction into a single virtually

* Corresponding author. Fax: +86 27 68754067.
E-mail address: binhu@whu.edu.cn (B. Hu).

0039-9140/$ – see front matter © 2007 Elsevier B.V. All rights reserved.
doi:10.1016/j.talanta.2007.08.022

solvent-free step, and moreover, it provided high sensitivity and eliminated the possibility of carry-over effects. With the development of LPME, its application has been extended to inorganic analytes. Our group first reported the application of LPME to inorganic trace analysis by combining LPME with electrothermal vaporization-inductively coupled plasma atomic emission spectrometry (ETV-ICP-AES) [14] and low temperature ETV-inductively coupled plasma mass spectrometry (ICP-MS) [15]. And in succession we also extended the method for the fractionation of Al in natural waters, coffee and tea using single drop microextraction (SDME) coupled with ETV-ICP-MS [16]. Mahmoud et al. [17] proposed a method for extraction and determination of arsenic in aqueous sample by Headspace (HS)-SDME combined with graphite furnace atomic absorption spectrometry (GFAAS). Sandra et al. [18–20] presented a HS-SDME technique for preconcentation of hydride-forming elements such as As, Sb and Se into a Pd(II)-containing aqueous drop prior to detection by GFAAS. Lately, direct SDME combined with GFAAS for the determination of trace Cd and Pb using dithizone (H_2DZ) as chelating reagent was reported by our group [21]. Although LPME has been proved to be a simple, inexpensive, fast and virtually solvent-free sample pretreatment technique with extensive application, in LPME, several microlitre organic solvent was suspended over the needle of syringe (single drop microextraction (SDME)) or protected by the fiber and then suspended over the needle (hollow fiber liquid phase microextraction (HF-LPME)) for microextraction, it requires careful and elaborate manual operations, given that problems of solvent dislodgment/instability have often been reported especially after faster stirring or longer extraction [22].

Recently, a new mode of LPME named dispersive liquid phase microextraction (DLPME) [23–26], which based on ternary component solvent system such as CPE and homogeneous liquid–liquid extraction (HLLE) [27] was proposed. In these methods the phase separation phenomenon from a homogeneous solution was used and the target solutes were extracted into a separated phase and then were determined. In DLPME, the appropriate mixture of the extraction and disperser solvents is rapidly injected into the aqueous samples containing analytes. Then, cloudy solution was formed and a drop of organic phase was sedimented in the bottom of the conical tube after centrifugation. DLPME has addressed some problems existing in HLLE, for example, HLLE is not compatible with some instrumental analysis and requires addition of some reagent such as acid, base, salt, etc., which leads to exothermic reaction during extraction. Compared with other LPME, DLPME offers simpler operation. And more importantly, it could be applied under batch conditions and extraction could be completed in several seconds thus resulting in faster extraction and shorter analytical time.

Several analytical techniques, such as flame-AAS [1,3,4,28], GFAAS [29,30], ICP-AES [31–34] and ICP-MS [35,36] have been applied to accurately determine trace Co and Ni in various samples. AAS is comparatively inexpensive, robust and easy to operate analytical technique that is readily available in most laboratories.

1-(2-Pyridylazo) 2-naphthol (PAN) is a kind of sensitive organic reagent used for the spectrometric determination of transition metals [37], so it was selected as chelating reagent in this work. The aim of this work is to develop a new method by combining DLPME with GFAAS for the determination of trace Co and Ni in environmental and food samples. The factors influencing the efficiency of microextraction and determination were systematically studied. The developed method was successfully applied to environmental water and rice sample with satisfactory results.

2. Experimental

2.1. Apparatus

The measurements were performed with a Hitachi 180-50 atomic absorption spectrometer (Japan) equipped with a heated graphite tube atomizer. A cobalt and nickel hollow cathode lamps operated at 10 mA were utilized as the radiation source. Measurements were carried out in the integrated absorbance (peak area) mode at 240.7 and 232.0 nm, using a spectral band width of 0.4 nm. The heating programs employed for cobalt and nickel determination were given as follows: the drying temperatures for Co and Ni were both 110 °C, ramp 10 s, hold 20 s; the ashing temperatures for Co and Ni were 1400 °C, ramp 10 s, hold 20 s and 1500 °C, ramp 10 s, hold 20 s, respectively; the atomizing temperatures for Co and Ni were both 2600 °C, 5 s; the clean temperatures for both Co and Ni were all 2800 °C, 3 s. Purge gas flow-rate inside the tube was 200 mL/min.

The pH values were controlled with a Mettler Toledo 320-S pH meter (Mettler Toledo Instruments (Shanghai) Co. Ltd.) supplied with a combined electrode. The phase separation was conducted with a centrifuge (Shanghai Scientific Instuments Co. Ltd., Shanghai, China).

2.2. Standard solution and reagents

The stock standard solution for Co and Ni (1000 mg L^{-1}) was separately prepared from analytical reagent grade $Co(NO_3)_2$ (AR, Shanghai Chemistry Reagent Company, Shanghai, China) and analytical reagent grade $Ni(NO_3)_2$ (AR, Shanghai Chemistry Reagent Company, Shanghai, China) by separately dissolving them in double deionized water. Standard solutions were prepared by appropriate dilution of the stock solutions daily. The solution of 1-(2-pyridylazo) 2-naphthol (PAN) was prepared by dissolving appropriate amount of PAN (AR, Shanghai Chemistry Reagent Company, Shanghai, China) in tetrachloride (AR, Shanghai Zhenxing Chemicals Reagent Co. Ltd., Shanghai, China). Analytical grade reagents were used unless otherwise specified. Doubly deionized water was used throughout this work. Plastic and glass containers and all other immersed laboratory materials that could come into contact with samples or standards were stored in 10% (v/v) nitric acid, and rinsed with double deionized water prior to use.

Ammonium chloride (0.01 M) buffer solution was prepared by dissolving an appropriate amount of ammonium chloride in double deionized water. And then hydrochloric acid (0.1 M) and ammonia (0.1 M) was used to adjust the desired pH.

2.3. Dispersive liquid phase microextraction procedure

First, 5 mL of aqueous sample solution containing Co and Ni was placed in a 10 mL screw cap glass test tube. Then, 1.00 mL of acetone (as disperser solvent) containing 15 μL of tetrachloride (as extraction solvent) and 0.25% (m/v) PAN (as chelating reagent) was rapidly injected into a sample solution by using 1.00 mL syringe. A cloudy solution was formed in a test tube and separation of the phases was achieved by centrifugation at 4000 rpm for 2 min. After this process, a small droplet of carbon tetrachloride was sedimented in the bottom of conical test tube. The 6.5 μL sedimented phase was withdrawn into the microsyringe and then injected into the GFAAS for analysis.

2.4. Sample preparation

Yangtse river water was collected from Yangtse River, Wuhan, China. Lake water sample collected from East Lake, Wuhan, China. Before use, all the water samples were filtered through a 0.45 μm membrane filter (Tianjin Jinteng Instrument Factory, Tianjin, China) and the pH value was adjusted to 9.2 with HCl and $NH_3{\cdot}H_2O$.

Certified Reference Material for Environment Water GSBZ50009-88 (Institute for Reference Materials of State Environmental Protection Administration, Beijing, China) was diluted by 100-fold and then adjusted to desired pH with HCl and $NH_3{\cdot}H_2O$.

The blank sample was prepared with the same procedure as water samples by using doubly deionized water.

Portions (0.200 g) of NIES No. 10-b rice flour (National Institute for Environmental Studies, Yatabe-machi, Tsukuba, Ibaraki, 305, Japan) were weighed into PTFE vessel. Then 5 mL of concentrated HNO_3 was added to each vessel. The vessels were then subjected to the following heating programs by microwave digestion procedure: 3 atm for 3 min, 8 atm for 5 min and then 10 atm for 5 min. After digestion, clear solution could be obtained. Then it was heated to very small volume by hot plate to remove the superfluous acid, the residue diluted to 25 mL with double deionized water in a calibrated flask. Dongbei rice was bought from market in Wuhan and then was homogenized in a blender and finally was prepared with the same procedure as NIES No 10-b rice flour. The blank sample without analytes but with the same amount of acid was prepared with the same procedure and subjected to digestion procedure.

3. Results and discussion

3.1. Effect of extraction solvent and its volume

The type of extraction solvent used in DLPME is an essential consideration for efficient extraction. Generally speaking, there are two requirements during selection of extraction solvent. First, it should have higher density than water. Second, it should have a low solubility in water and non-volatile to prevent solvent loss during extraction. For this purpose, three kinds of solvents: carbon tetrachloride (CCl_4), chlorobenzene (C_6H_5Cl) and bromobenzene (C_6H_5Br) were investigated. A series of sample solution were studied by using 1.0 mL acetone containing 0.01% (w/v) PAN and different volumes of the extraction solvent to achieve 5 μL volume of the sedimented phase. Because the solubility of extraction solvents in water is different, it is necessary to test the volume of extraction solvents to obtain 5 μL volume of the sedimented phase at the bottom of the test tube. According to the experimental results, 1.0 mL acetone including 13 μL of CCl_4, 12 μL C_6H_5Cl and 11 μL C_6H_5Br could give the same volume of the sedimented phase (5 μL), respectively. Fig. 1 was the effect of extraction solvent on the absorbance of Co and Ni. As could be seen, three kinds of extraction solvent gave almost the same analytical signal. Considering the solubility of PAN in extraction solvent, carbon tetrachloride was chosen for the following experiment due to the higher solubility of PAN in it.

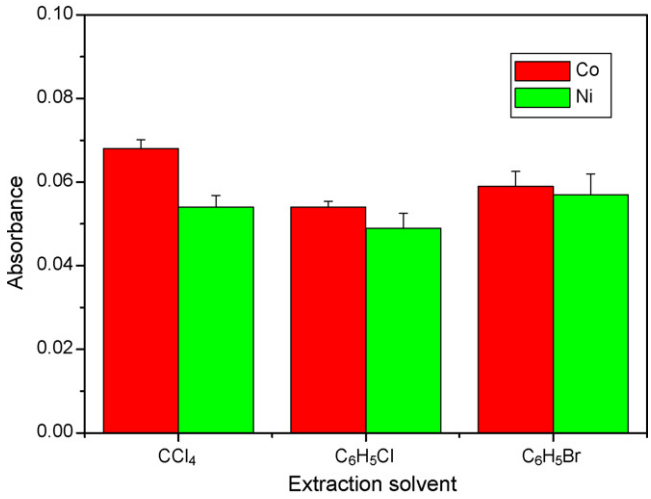

Fig. 1. Effect of extraction solvent on the absorbance of Co and Ni. Conditions: Co and Ni, 20 ng mL^{-1}; pH 9.2; PAN, 0.01% (w/v); aqueous sample volume, 5 mL; disperser solvent (acetone) volume, 1.00 mL; extraction solvent, CCl_4 (13 μL); C_6H_5Cl (12 μL); C_6H_5Br (11 μL).

To evaluate the influence of the extraction solvent volume, solutions with different volumes of CCl_4 were subjected to the same DLPME procedures. Through increasing the volume of CCl_4 in 1 mL acetone from 13 to 23 μL, the volume of the sedimented phase increases from 5 to 15 μL. It was found that by increasing the volume of CCl_4, analytical signal for Co increased with the increasing of extraction solvent volume in the first and then kept constant. With respect to Ni, analytical signal was constant during the range of all volume tested. However, using low volume of extraction solvent, high enrichment factor could be obtained. So, in further experiments, 15 μL of extraction solvent volume was selected.

3.2. Effect of disperser solvent and its volume

In DLPME, selecting an appropriate disperser solvent is important, since disperser solvent should be miscible with both extraction solvent and aqueous sample. For the sake of acquiring the most suitable disperser solvent, three kinds of disperser solvents: acetone, acetonitrile and methanol were studied. Fig. 2 showed the effect of the kind of disperser solvent on the

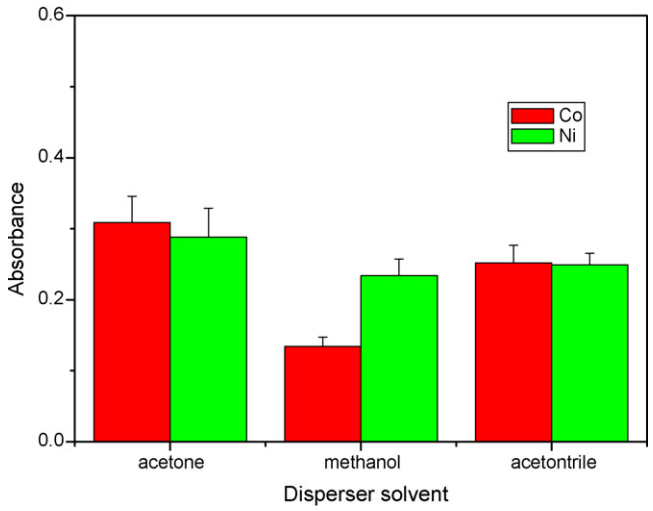

Fig. 2. Effect of disperser solvent kind on the absorbance of Co and Ni. Conditions: Co and Ni, 20 ng mL^{-1}; pH 9.2; PAN, 0.25% (w/v); aqueous sample volume, 5 mL; disperser solvent volume, 1.00 mL; extraction solvent (CCl_4) volume, 15 μL.

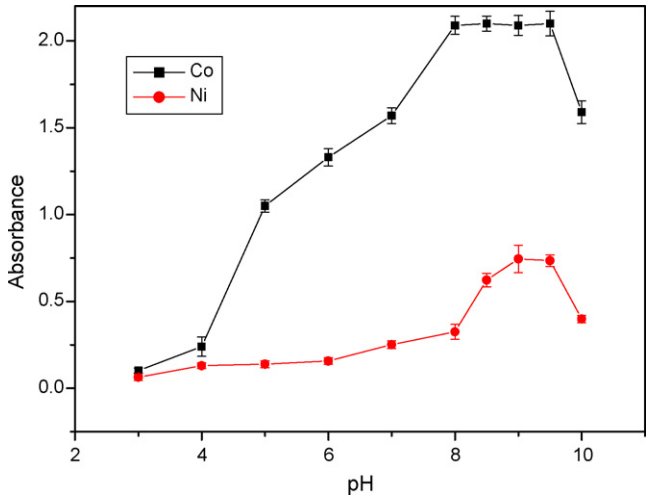

Fig. 3. Effect of pH on the absorbance of Co and Ni. Conditions: Co and Ni, 20 ng mL^{-1}; PAN, 0.25% (w/v); aqueous sample volume, 5 mL; disperser solvent (acetone) volume, 1.00 mL; extraction solvent (CCl_4) volume, 15 μL.

absorbance of Co and Ni. It could be seen that acetone was the most suitable disperser solvent as it could give the highest signal response of the target analyte and it is low toxic and low cost. So, acetone was selected as disperser solvent in the following experiment.

The influence of the volume of disperser solvent acetone on the absorbance of Co and Ni was also examined. Because different volume of acetone gave different volume of sedimented phase when the volume of extraction solvent CCl_4 was constant, in order to acquire the same volume of sedimented phase, the volume of disperser solvent and extraction solvent changed simultaneously. The experimental results indicated that analytical signal increased at the beginning and then decreased with increasing volume of acetone. It should be noted that the cloudy sedimented phase was not formed well when using low volume of acetone, so the extraction signal decreased. However, by increasing the volume of acetone, the solubility of complex in water increased also, thereby, analytical signal decreased. So, 1.0 mL acetone was chosen in the following work.

3.3. Influence of pH

It is well known that the pH of the sample solution was one of the important factors affecting the formation of complexes. Fig. 3 displayed the effect of pH on the signal intensity of Co and Ni. As can be seen, the signal intensity of Co improved with the increasing of pH from 3 to 8, and then remained constant. When pH was higher than 9.5, the signal of Co decreased with the increasing of pH. Similarly, the signal intensity of Ni was kept constant in comparatively narrow acid range (pH 9–9.5). Therefore, a pH 9.2 was selected for further study.

3.4. Influence of the amount of PAN

The influence of the amount of PAN was also evaluated and the results showed that the signals of Co and Ni were increased with the increase of PAN amount from 0.01 to 0.05% (m/v) and then kept constant up to the amount of 0.3% (m/v). In this study, a PAN amount of 0.25% (m/v) was employed.

3.5. Influence of extraction time

Extraction time is an important factor influencing the extraction efficiency. In DLPME, extraction time is defined as the time between injection mixture of disperser and extraction solvent, and starting to centrifuge. The effect of extraction time on signals was investigated with the time varying from 5 to 20 min and the results displayed that the extraction time has no significant influence on the signals of both analytes. This means that after formation of cloudy solution, the complex of metal ions and chelating reagent was formed instantly and then diffused into organic solvent quickly. Therefore, DLPME is a kind of fast equilibrium extraction and in the following experiment 5 s was selected as extraction time.

3.6. Interference effects

In order to demonstrate the selectivity of the developed method of DLPME for the determination of Co and Ni, the effect of alkali and alkaline earth metals (K^+, Na^+, Mg^{2+}, Ca^{2+}) and heave metals (Mn^{2+}, Fe^{3+}, Cu^{2+}, Zn^{2+}, Cd^{2+}, Al^{3+}, Pb^{2+}), which coexisting in environmental water and rice samples, on the measurement of 5 ng mL^{-1} Co and Ni was investigated. The results showed that Fe^{3+}, Zn^{2+} and Cd^{2+} could be tolerated up to 1 μg mL^{-1} for Co; Cu^{2+} and Mn^{2+} could be tolerated up to 0.8 μg mL^{-1} for Co while $Pb^{2+}$and Al^{3+} up to 4 and 3 μg mL^{-1}, respectively. And at least 1 mg mL^{-1} K^+, 0.6 mg mL^{-1} Na^+, 0.25 mg mL^{-1} Mg^{2+} and Ca^{2+} had no remarkable interferences with the determination of Co. For Ni, 0.8 mg mL^{-1} K^+, 0.6 mg mL^{-1} Na^+, 0.25 mg mL^{-1} Mg^{2+} and Ca^{2+}, 1 μg mL^{-1} Fe^{3+}, Mn^{2+} and Cd^{2+}, 0.8 μg mL^{-1} $Cu^{2+}$and Zn^{2+}, 4 μg mL^{-1} $Pb^{2+}$and 3 μg mL^{-1} Al^{3+} had no obvious interferences with the determination of Ni. The above results indicated that the

Table 1
Comparison of limits of detection (LODs) and enrichment factor

Method	LOD		Enrichment factor		Reference
	Co (pg mL^{-1})	Ni (pg mL^{-1})	Co	Ni	
DLPME-GFAAS	21	33	101	200	This work
CPE-FAAS	1090	1220	27	29	[3]
SPE-FAAS	–	300	–	72.66	[4]
SPE-FAAS	590	1290	23	25	[27]
SPE-GFAAS	5	–	190	–	[29]
CME-ICP-MS	0.33	1.5	10	10	[31]

DLPME-GFAAS: dispersive liquid phase microextraction-graphite furnace atomic absorption spectrometry; CPE-FAAS: cloud point extraction-flame atomic absorption spectrometry; SPE-FAAS: solid phase extraction-flame atomic absorption spectrometry; CME-ICP-MS: capillary microextraction-inductively plasma mass spectrometry.

developed method is applicable to the analysis of Co and Ni in environmental water and rice samples.

3.7. Effect of ashing and atomization temperature

Ashing and atomization temperature had an important effect on the determination of analytes. So both temperature effect on the signals of Co and Ni was investigated. It was found that the signals of both analytes were increased in the beginning and then remained constant and decreased in the last. Thereby, the ashing temperature of 1400 and 1500 °C was chosen for Co and Ni in this work. With regards to atomization temperature, the experimental results indicated that the signals of both analytes increased straightly during the all temperature range. But higher temperature could decrease the life of graphite tube. So atomization temperature evaluated was just up to 2600 °C and the same temperature was chosen for the following detection.

3.8. Limits of detection and precision

According to the definition of IUPAC, the limits of detection (LOD, 3σ) of this method were 21 and 33 pg mL^{-1} with an enrichment factor of 101 and 200 for Co and Ni, respectively. The enrichment factor was the slope ratio of the two calibration standard curve with microextraction and without microextraction. And the relative standard deviation (R.S.D.) was 7.5% and 8.2% ($C = 0.5$ ng mL^{-1}, $n = 5$) for Co and Ni, respectively. The regression equations for the calibration curves of Co and Ni after DLPME were $y = 0.29x + 0.15$ with a correlation coefficient (R^2) of 0.9990 and $y = 0.18x + 0.12$ with correlation coefficient (R^2) of 0.9970, respectively, where y is the absorbance value and x is the concentration of analytes in the extraction solvent. A comparison of LOD obtained by this method with that reported by several other approaches for the determination of Co and Ni by GFAAS is shown in Table 1. As could be seen, the presented method had relative low limits of detection and was suitable for trace analysis of Co and Ni in environmental and food samples.

3.9. Analysis application

The proposed method was applied to the determination of Co and Ni in East Lake water (Wuhan, China), Yangtse River water and Dongbei rice and the results along with the recovery for the spiked samples were given in Table 2. As could be seen, the recoveries for the three spiked water samples are in the range of 90–109%. In order to verify the accuracy of the proposed procedure, the method was then used to the determination of the content of Co and Ni in National Standard Reference Material for Environment Water (GSBZ50009-88) and certified reference material of NIES No. 10-b rice flour, and the results were given in Table 3. The Student t-test was applied to two certified reference materials of Environmental Water GSBZ50009-88 and NIES No. 10-b rice flour, and the $t_{0.05,2}$ values for Co and Ni in the two certified reference materials were also listed in Table 3. It could be seen that a good agreement between the determined values and the certified values were obtained.

Table 2
Determination of Co and Ni in environmental water samples and Dongbei rice (mean ± S.D., $n = 3$)

Sample	Co			Ni		
	Added	Found	Recovery (%)	Added	Found	Recovery (%)
East lake water (ng mL^{-1})	0	<LOQ	–	0	0.180 ± 0.014	–
	0.5	0.530 ± 0.060	106	0.5	0.610 ± 0.040	90
Yangtse Rive water (ng mL^{-1})	0	<LOQ	–	0	0.890 ± 0.040	–
	0.5	0.470 ± 0.030	94	0.5	1.380 ± 0.140	99
Dongbei rice (μg g^{-1})	0	0.031 ± 0.001	–	0	0.217 ± 0.018	–
	0.2	0.223 ± 0.020	97	0.2	0.458 ± 0.021	109

LOQ: limit of quantification.

Table 3
Analysis of certified reference materials (mean ± S.D., $n = 3$)

Sample	Found		Certified		t-Test[a]
	Co	Ni	Co	Ni	
GSBZ50009-88 ($\mu g\,mL^{-1}$)	<LOQ	0.927 ± 0.035	–[b]	0.886 ± 0.036	2.03
NIES No 10-b Rice flour ($\mu g\,g^{-1}$)	0.022 ± 0.020	0.384 ± 0.050	0.020[c]	0.390 ± 0.040	0.21(Ni), 0.17(Co)

LOQ: limit of quantification.
[a] $t_{0.05,2} = 4.30$.
[b] No certified value.
[c] Information value.

4. Conclusion

A new method of dispersive liquid phase microextraction combined with GFAAS has been described for the determination of Co and Ni in environmental water and food samples. The presented method had a lower limit of detection and higher enrichment factor over other methods reported in the references. Additional, compared with other modes of liquid phase microextraction, dispersive liquid phase microextraction is suitable bath experiment due to very fast extraction.

Acknowledgments

Financial supports from the Science Fund for Creative Research Groups of NSFC (No. 20621502), National Nature Science Foundation of China (No. 20575048, 20375030), MOE of China (NCET-04-0658) are gratefully acknowledged.

References

[1] A. Safavi, N. Iranpoor, N. Saghir, S. Momeni, Anal. Chim. Acta 569 (2006) 139.
[2] A. Safavi, H. Abdollahi, M.R.H. Nezhad, R. Kamali, Spectrochim. Acta 60A (2004) 2897.
[3] J.L. Manzoori, A. Bavili-Tabrizi, Microchim. Acta 141 (2003) 201.
[4] A. Ersöz, R. Say, A. Denizli, Anal. Chim. Acta 502 (2004) 91.
[5] B.R. Reddy, D.N. Priya, J. Power Sources 161 (2006) 1428.
[6] A. Oliva, Microchim. Acta 142 (2003) 129.
[7] C.D. Stalikas, Trends Anal. Chem. 21 (2002) 343.
[8] E.K. Paleologos, D.L. Giokas, M.L. Karayannis, Trends Anal. Chem. 24 (2005) 426.
[9] C.A. Lucy, F.F. Cantwell, Anal. Chem. 61 (1989) 101.
[10] C.A. Lucy, K.K.C. Yeung, Anal. Chem. 66 (1994) 2220.
[11] E. Psillakis, N. Kalogerakis, J. Chromatogr. A 907 (2001) 211.
[12] A. Tankeviciute, R. Kazlauskas, V. Vickackaite, Analyst 126 (2001) 1674.
[13] E. Psillakis, N. Kalogerakis, J. Chromatogr. A 999 (2003) 145.
[14] Y.L. Wu, Z.C. Jiang, B. Hu, Chem. J. Chin. Univ. 24 (2003) 1793.
[15] L.B. Xia, B. Hu, Z.C. Jiang, Y.L. Wu, Y. Liang, Anal. Chem. 76 (2004) 2910.
[16] L.B. Xia, B. Hu, Z.C. Jiang, Y.L. Wu, L. Li, R. Chen, J. Anal. At. Spectrom. 20 (2005) 1.
[17] M. Chamsaz, M. Arbab-Zavar, S. Nazari, J. Anal. At. Spectrom. 18 (2003) 1279.
[18] S. Fragueiro, I. Lavilla, C. Bendicho, Spectrochim. Acta 59B (2004) 851.
[19] S. Gil, S. Fragueiro, I. Lavilla, C. Bendicho, Spectrochim. Acta 60B (2005) 145.
[20] S. Fragueiro, I. Lavilla, C. Bendicho, Talanta 68 (2006) 1096.
[21] H.M. Jiang, B. Hu, Microchim. Acta, in press, doi:101007/s00604-007-0785-0.
[22] L. Xu, C. Basheer, H.K. Lee, J. Chromatogr. A 1152 (2007) 184.
[23] E.Z. Jahromi, A. Bidari, Y. Assadi, M.R.M. Hosseini, M.R. Jamali, Anal. Chim. Acta 585 (2007) 305.
[24] M. Rezaee, Y. Assadi, M.R.M. Hosseini, E. Aghaee, F. Ahmadi, S. Berijani, J. Chromatogr. A 1116 (2005) 1.
[25] S. Berijani, Y. Assadi, M. Anbia, M.R.M. Hosseini, E. Aghaee, J. Chromatogr. A 1123 (2006) 1.
[26] R. Rahnama Kozani, Y. Assadi, F. Shemirani, M.R.M. Hosseini, M.R. Jamali, Talanta 72 (2007) 387.
[27] S. Igarashi, A. Takahashi, Y. Ueki, H. Yamaguchi, Analyst 2000 (125) (2000) 797.
[28] V.A. Lemos, E.M. Gama, A. da, S. Lima, Microchim. Acta 153 (2006) 179.
[29] H. Matsumiya, T. Kageyama, M. Hiraide, Anal. Chim. Acta 507 (2004) 205.
[30] S. Cerutti, S. Moyano, J.A. Gasquez, J. Stripeikis, R.A. Olsina, L.D. Martinez, Spectrochim. Acta 58B (2003) 2015.
[31] S. Kagaya, Y. Araki, N. Hirai, K. Hasegawa, Talanta 67 (2005) 90.
[32] C.Z. Huang, Z.C. Jiang, B. Hu, Talanta 73 (2007) 274.
[33] A. Sabarudin, N. Lenghor, M. Oshima, L. Hakim, T. Takayanagi, Y.H. Gao, S. Motomizu, Talanta 72 (2007) 1609.
[34] B. Mikuła, B. Puzio, Talanta 71 (2007) 136.
[35] W.L. Hu, B. Hu, Z.C. Jiang, Anal. Chim. Acta 572 (2006) 55.
[36] D. Rahmi, Y.B. Zhu, T. Ei ji Fujimori, H. Umemura, Haraguchi, Talanta 72 (2007) 600.
[37] W. Thanasarakhan, S. Liawruangrath, S. Wangkarn, B. Liawruangrath, Talanta 71 (2007) 1849.

Available online at www.sciencedirect.com
ScienceDirect
Talanta 74 (2008) 1299–1312
Talanta
www.elsevier.com/locate/talanta

The effect of signal suppression and mobile phase composition on the simultaneous analysis of multiple classes of acidic/neutral pharmaceuticals and personal care products in surface water by solid-phase extraction and ultra performance liquid chromatography–negative electrospray tandem mass spectrometry

Barbara Kasprzyk-Hordern *, Richard M. Dinsdale, Alan J. Guwy

University of Glamorgan, Sustainable Environment Research Centre, Pontypridd CF37 1DL, UK

Received 31 May 2007; received in revised form 23 August 2007; accepted 30 August 2007
Available online 6 September 2007

Abstract

A new multi-residue method for the determination of 25 acidic/neutral pharmaceuticals (antibiotics, anti-inflammatory/analgesics, lipid regulating agents, diuretics, triazides, H2-receptor antagonists, cardiac glicozides and angiotensin II antagonists) and personal care products (sunscreen agents and preservatives) in surface water with the usage of a new technique: ultra performance liquid chromatography–negative electrospray tandem mass spectrometry (UPLC–MS/MS) was developed and validated. The novel UPLC system with 1.7 μm particle-packed column allowed for good resolution of analytes with the application of low mobile phase flow rates (0.05 mL min^{-1}) and short retention times (from 4.7 min to 13.3 min) delivering a fast and cost-effective multi-residue method. SPE with the usage of Oasis MCX strong cation-exchange mixed-mode polymeric sorbent was chosen for sample clean-up and concentration. The influence of mobile-phase composition, matrix assisted ion suppression and SPE recovery on the sensitivity of the method was identified and quantified. The instrumental limits of quantification varied from 0.2 μg L^{-1} to 30 μg L^{-1}. The method limits of quantification were at low nanogram per litre levels and ranged from 0.3 ng L^{-1} to 30 ng L^{-1}. The instrumental and method intra-day and inter-day repeatabilities were on average less than 5%. The method was successfully applied for the determination of PPCPs in River Taff. Thirteen compounds were determined in river water at levels ranging from a single to a few hundred nanograms per litre. Among them were ten pharmaceuticals (aspirin, salicylic acid, ketoprofen, naproxen, diclofenac, ibuprofen, mefenamic acid, furosemide, sulfasalazine and valsartan) and three personal care products (methyl- and ethylparaben and 4-benzophenone).
© 2007 Elsevier B.V. All rights reserved.

Keywords: Pharmaceuticals and personal care products; Ultra performance liquid chromatography–tandem mass spectrometry; Solid-phase extraction; Multi-residue method; Ion suppression; Mobile-phase additives

1. Introduction

Pharmaceuticals and personal care products (PPCPs) are a group of emerging, potentially hazardous contaminants, which have, to date, received limited attention, although interest in this area is increasing considerably and the need for further investigation in this field is continuously emphasised by different research groups [1–6]. PPCPs are found in surface water and wastewaters at levels of up to a few μg L^{-1} [1,2,6–30]. They enter the aquatic environment mainly through treated (or raw) sewage from domestic households and hospitals, waste effluents from manufacturing processes and runoff. Domestic animals are the main direct source of the environmental disposal of many PPCPs such as veterinary pharmaceuticals. The other direct route from which PPCPs enter the environment is recreational activities. Many PPCPs are ubiquitous and persistent in the environment. Some are capable of bioconcentration and many of those investi-

* Corresponding author. Tel.: +44 1443 483495; fax: +44 1443 482285.
E-mail addresses: bkasprzy@glam.ac.uk, B.Kasprzyk-Hordern@hotmail.co.uk (B. Kasprzyk-Hordern).

0039-9140/$ – see front matter © 2007 Elsevier B.V. All rights reserved.
doi:10.1016/j.talanta.2007.08.037

gated are biologically active compounds. Some are suspected, or are recognised to be, endocrine disruptors, which could potentially influence environmental and human health. Additionally, they are continuously introduced into the environment; therefore even compounds of a low persistence might cause adverse effects in human and aquatic life. The other issue is the synergic effect of different PPCPs on aquatic life, through their combined non-targeted action with many other biologically active compounds present in the environment [1,2]. A few pharmaceuticals and personal care products have been determined in drinking water, which poses a direct risk to humans [2] and raises the issue of contaminated water sources and especially water reuse.

Due to growing concern regarding the presence, fate and effects on the environment and humans, there is an obvious need for fast and sensitive multi-residue methods for the determination of low levels of PPCPs in the environment. Traditional gas chromatography is of limited value in the case of polar (non-volatile) compounds as it requires time consuming derivatization procedures. Liquid chromatography–mass spectrometry (LC/MS) using mainly ESI (electrospray ionisation) is the method of choice for the analysis of polar compounds in complex matrices. So far, a few multi-residue analytical methods for the determination of PPCPs in the aqueous environment have been established [31–36]. These methods utilise solid-phase extraction as a sample preparation method and almost exclusively liquid chromatography coupled with electrospray ionisation tandem mass spectrometry for separation and quantification of up to 30 compounds on C18 column with up to 50 min elution gradient time and average mobile phase flow rate of 0.2 mL min^{-1}.

Here a new fast and sensitive method for the determination of a broad range of pharmaceuticals and personal care products is presented. The method uses a single SPE method and single LC/MS/MS method utilising UPLC™ (ultra performance liquid chromatography) coupled with triple quadruple tandem mass spectrometry. UPLC is a novel technology providing significant improvements in resolution, speed and sensitivity due to the exploitation of a 1.7 μm particle-packed column.

This paper presents a novel method for the analysis of 25 acidic/neutral pharmaceuticals and personal care products in surface water with the utilisation of SPE/UPLC/ESI-(negative ionisation)-MS-MS and demonstrates its application in the Welsh environment. The group of PPCPs of interest have never previously been studied in the Welsh aqueous environment, to the best knowledge of the authors. A previous paper published by the authors [37], presented another novel multi-residue method for the analysis of a further 28 basic/neutral pharmaceuticals and illicit drugs in surface water by means of SPE/UPLC/ESI+(positive ionisation)-MS-MS. The overall methodology published in the form of the two papers allows for the analysis of almost 50 PPCPs in surface water. The rationale for the preparation of two separate methods for the analysis of all PPCPs resulted from their different structures and physico-chemical properties influencing both the composition of mobile phase used for analytes separation in LC and ionisation mode used in ESI-MS. Additionally, the paper identifies and quantifies the influence of matrix components on the performance of the analytical methods and presents possible ways to solve it.

2. Experimental

2.1. Chemicals and materials

Reference standards (>95% purity) were purchased from Sigma–Aldrich (Gillingham, UK) and Sequoia Products Research Limited (Pangbourne, UK). All solvents used as mobile phases and their additives were of LC/MS quality. Surrogate/internal standards (IS): clofibric-d4 acid (4-chlorophenyl-d4), 3,4-dichlorobenzoic (2,5,6-d3) acid, bisphenol A-d16 and 4-chlorophenol (2,3,5,6-d4) were purchased from QMX Laboratories Limited (Essex, UK). All standards used as both surrogate and internal standards were added to the samples before extraction and were also used for the quantification of the samples.

Stock solutions of PPCPs (0.5–1 g L^{-1}) were prepared in methanol and stored in the dark at 0 °C. Working solutions were prepared fresh daily by diluting stock solution with methanol stored at 0 °C. Ultrapure water was obtained using Neptune, Purite (MJ Patterson Scientific Ltd., UK). For method development and validation both HQ water (ultrapure water) and BB water (surface water collected from the source of the River Taff in Brecon Beacons National Park, which is not affected by PPCPs) were used. The average dissolved organic carbon of BB water was 4.5 mg DOC L^{-1}.

All glassware used was deactivated with 5% DMDCS (dimethylchlorosilane) in toluene to minimise sample loss through absorption of polar compounds onto –OH sites present on glass surfaces.

2.2. Sample preparation and solid-phase extraction

All samples were collected in 1 L silanized bottles with teflon faced phenolic caps (Wheaton, USA), acidified with 31% HCl to pH 2.0 and vacuum filtered through a 0.7 μm glass fibre filter GF/F (Whatman, UK).

The SPE method was optimised through several preliminary experiments involving the following variables: type of adsorbent, pH value of the sample, elution conditions and eluting agents. Out of all sorbents used (Oasis HLB, MCX, MAX, WCX and WAX (60 mg, Waters, UK), Chromabond C18ec (200 mg, Anachem, UK) and Isolute ENV+ and HCX (100 mg and 200 mg, respectively, Kinesis, UK)) Oasis MCX and HLB were found to give the best recoveries for most PPCPs and therefore they were used for further analysis.

SPE Gilson, Aspec XL4 (Anachem, UK) was utilised for solid-phase extraction. The SPE cartridges were conditioned with 2 mL of MeOH and equilibrated with 2 mL of water acidified with HCOOH (2% HCOOH; pH 2.1) at a rate of 3 mL min^{-1}. One litre of acidified and filtered water sample spiked with 200 ng of surrogate/internal standards was passed through the cartridge at a rate of 4 mL min^{-1}. The cartridges were subsequently washed with acidified water (2 mL 2% HCOOH/H_2O; flow rate, 3 mL min^{-1}). After drying, SPE cartridges were wrapped in aluminium foil and stored in a

freezer until eluted. PPCPs were extracted with 2 mL of MeOH and 1 mL of 5% NH_4OH in MeOH at a rate of 1 mL min^{-1}. The extracts were directly collected into a 6 mL collection tube and were evaporated to dryness with TurboVap evaporator (Caliper, UK; 40 °C, N_2, 5–15 psi) and finally reconstituted in 0.5 mL of HQ water modified with TrBA (tributylamine) and CH_3COOH (mobile phase, 100% A: 79.5% H_2O, 20% MeOH, 0.5% CH_3COOH and 10 mM TrBA). All reconstituted extracts were filtered through 0.2 μm PTFE filters (Whatman, Puradisc, 13 mm) and transferred to maximum recovery deactivated vials with PTFE septa (Waters, UK).

2.3. Ultra performance liquid chromatography–tandem mass spectrometry

Waters ACQUITY UPLC™ system (Waters, Manchester, UK) consisting of ACQUITY UPLC™ binary solvent manager, ACQUITY UPLC™ sample manager and ACQUITY UPLC BEH C18 column (1.7 μm; 1 mm × 100 mm) (Waters, UK) was used for the separation of analytes. Several mobile phases (H_2O, MeOH and acetonitrile) and their additives were studied for an improvement of compounds separation in LC and an improvement of ESI performance in negative ionisation mode. Among the mobile phase additives studied were basic additives: ammonia, ammonium formate and acetate, primary amines (methyl-, ethyl- and butylamine), secondary amines: (dimethyl-, diethyl- and dibutylamine), tertiary amines (trimethyl-, triethyl- and tributylamine) at concentrations in mobile phase ranging from 1 mM to 50 mM and/or acidic compounds: formic and acetic acid at concentrations ranging from 0.05% to 0.5%.

After initial analyses the following composition of mobile phases was chosen:

- mobile phase A (pH 3.9): 79.5% H_2O, 20% MeOH, 0.5% CH_3COOH, 10 mM TrBA;
- mobile phase B (pH 5.5): 5% H_2O, 94.5% MeOH, 0.5% CH_3COOH, 10 mM TrBA.

The gradient program was as follows:

$$100\%A \xrightarrow{0.1\ min} 100\%A \xrightarrow{3.4\ min} 50\%A \xrightarrow{1.5\ min} 50\%A \xrightarrow{5\ min} 20\%A \xrightarrow{2\ min} 0\%A \xrightarrow{2\ min} 0\%A \xrightarrow{2\ min} 100\%A \xrightarrow{4\ min} 100\%A$$

Ten microlitres of the sample was injected into the system. The column was kept at 22 °C and the temperature in the sample manager was kept at 6 °C. The flow rate of mobile phase was 0.05 mL min^{-1}, which gave an average initial pressure of 6500 psi.

A Quatro Micro triple-quadruple mass spectrometer (Micromass, Manchester, UK) equipped with an electrospray ionisation source was used for PPCPs identification and quantification. The analyses were performed in negative mode with a capillary voltage of 3 kV, a source temperature of 120 °C and a desolvation temperature of 350 °C. A cone gas flow of 20 L h^{-1} and desolvation gas flow of 400 L h^{-1} were used. Nitrogen, used as a nebulising and desolvation gas, was provided by a high purity nitrogen generator NM 30LA 230VOC (Peak Scientific Instrument Ltd., UK). Argon (99.999%) was used as a collision gas. The mobile phase at a flow rate of 0.05 mL min^{-1} was directly introduced into the ion source from LC, without splitting. MassLynx 4.1 (Waters, UK) software was used to collect and analyse the obtained data.

Mass spectrometry analyses were performed in the multiple reaction monitoring (MRM) mode, measuring the fragmentation of the deprotonated pseudo-molecular ions of each pharmaceutical and personal care product. A dwell time of 200 ms per ion pair was used. The choice of fragmentation products for each substance based on the most intense signal and the optimisation of cone voltages, energy collisions and other instrument parameters was done individually for each compound in a continuous-flow mode through a direct infusion of standard solutions at concentrations of 1 mg L^{-1} into the stream of the mobile phase. For optimisation of precursor ion/product ion transitions QuanOptimise software (Waters, UK) was used.

Signal suppression of analytes in ESI source was estimated for each PPCP as a percentage decrease in signal intensity in a sample matrix versus in deionised water using the following equation:

$$\text{Signal suppression}\,(\%) = \left(1 - \frac{I_{BB}}{I_{HQ}}\right) \times 100 \quad (1)$$

where I_{BB} was the PPCP peak area in BB water extract spiked after extraction with 500 μg L^{-1} of each PPCPs, and I_{HQ} was the PPCP peak area in HQ water extract spiked after extraction with 500 μg L^{-1} of each PPCP. No PPCPs were present in extracts of both HQ and BB water before their enrichment with PPCPs.

2.4. Quantification and method validation parameters

Quantification of PPCPs was carried out by means of MRM, using the highest characteristic precursor ion/product ion transitions and recording one to two transitions simultaneously. The following surrogate/internal standards (SS/IS) were used: clofibric-d4 acid (4-chlorophenyl-d4), 3,4-dichlorobenzoic (2,5,6-d3) acid, bisphenol A-d16 and 4-chlorophenol (2,3,5,6-d4) for the quantification of compounds analysed. The usage of only four internal standards is a limitation of the method due to the variability of chemical structure/properties between PPCPs studied and chosen internal standards. The choice of only four IS resulted from both the very high cost of isotope labelled compounds and difficulty with their purchase.

Detailed discussion concerning validation of the method is presented in authors' previous paper [37]. All instrumental validation parameters were determined for HQ water (containing 0.5% CH_3COOH, 20% MeOH and 10 mM TrBA) spiked with known concentrations of PPCPs. Method quantification and detection parameters were determined for BB water spiked with known concentrations of PPCPs before extraction.

Twelve-point multi-component internal standard calibration curves for the HQ water and BB water extract spiked with PPCPs before extraction (0–1200 ng L^{-1}) were applied for quantifica-

tion of PPCPs with the utilisation of QuanLynx software (Waters, UK).

Quantitation and detection limits were determined using both signal-to-noise approach and were calculated using Eq. (2). HQ water standard solutions were used for instrumental detection and instrumental quantification limits determinations ($IDL_{S/N}$ and $IQL_{S/N}$ respectively). BB water extract spiked with PPCPs before extraction were used for the determination of method detection and method quantification limits ($MDL_{S/N}$ and $MQL_{S/N}$ respectively). The quantitation limit ($QL_{S/N}$) was estimated for the concentration of compound that gave a signal-to-noise ratio of 10:1. The detection limit ($DL_{S/N}$) corresponded to the concentration that gave a signal-to-noise ratio of 3:1. For confirmation purposes method quantification limits (MQL_{calc}) were also calculated using the following equation [38]:

$$MQL_{calc} = \frac{IQL_{S/N} \times 100}{Rec \times CF} \quad (2)$$

where $IQL_{S/N}$ is the instrumental quantification limit (ng L^{-1}), Rec is the absolute recovery of the analyte (%) and CF is the concentration factor, which in this method denotes 2000.

Linearity and range of the analytical procedure were performed by serial dilution of a stock solution of PPCPs (10 mg L^{-1}). Accuracy of the method was evaluated as the percentage of deviation from the known added amount of analyte in the sample. Precision was evaluated as the relative standard deviation (R.S.D.) of replicate measurements. Instrumental intra-day precision and intra-day precision of the analytical method were verified under the same operating conditions over a short interval of time. Nine determinations covered respectively three concentrations (50 μg L^{-1}, 500 μg L^{-1} and 1000 μg L^{-1}) of acidified HQ standards and BB water extract spiked with PPCPs before extraction. Instrumental inter-day precision and inter-day precision of the analytical method were verified by determinations that covered three concentrations (50 μg L^{-1}, 500 μg L^{-1} and 1000 μg L^{-1}) of HQ standards solutions and BB water extract spiked with PPCPs before extraction, three replicates each undertaken on three different days.

3. Results and discussion

Seventeen pharmaceuticals and eight personal care products were the subject of the research (Table 1). The choice of pharmaceuticals was mainly based on the prescription data in Wales and England [39,40] and the metabolism routes of pharmaceuticals, mainly excretion as parent compounds and active main metabolites. The choice of PCPs was based on their high annual usage in wide range of household products and concern over their possible effect on human and aquatic organisms [41].

3.1. Liquid chromatography and mass spectrometry

3.1.1. Mobile phase and additives

Methanol and water were chosen as mobile phases for PPCPs separation. Ionic compounds are in general weakly retained in

Table 1
Chosen PPCPs and their properties

Group	Properties				
	Compound	CAS no.	Molecular formula	MW	pK_a
Pharmaceuticals					
Antibiotics	Sulfamethoxazole	723-46-6	$C_{10}H_{11}N_3O_3S$	253.28	5.8
	Chloramphenicol	56-75-7	$C_{11}H_{12}Cl_2N_2O_5$	323.13	11.0
Anti-inflammatory/analgesics	Ibuprofen	15687-27-1	$C_{13}H_{18}O_2$	206.28	4.9
	Diclofenac	15307-86-5	$C_{14}H_{11}Cl_2NO_2$	296.15	4.2
	Ketoprofen	22071-15-4	$C_{16}H_{14}O_3$	254.28	4.5
	Naproxen	22204-53-1	$C_{14}H_{14}O_3$	230.26	4.2
	Aspirin	50-78-2	$C_9H_8O_4$	180.16	3.5
	Salicylic acid (aspirin metabolite)	69-72-7	$C_7H_6O_3$	138.12	3.0
	Mefenamic acid	61-68-7	$C_{15}H_{15}NO_2$	241.29	4.2
Lipid regulating agents	Clofibric acid	882-09-7	$C_{10}H_{11}ClO_3$	214.65	–
	Bezafibrate	41859-67-0	$C_{19}H_{20}ClNO_4$	361.82	0
	Pravastain	81093-37-0	$C_{23}H_{36}O_7$	424.53	–
Diuretics	Furosemide	54-31-9	$C_{12}H_{11}ClN_2O_5S$	330.75	3.9
Triazides	Bendroflumethiazide	73-48-3	$C_{15}H_{14}F_3N_3O_4S_2$	421.42	8.5
H2-receptor antagonists	Sulfasalazine	599-79-1	$C_{18}H_{14}N_4O_5S$	398.39	–
Cardiac glicozides	Digoxin	20830-75-5	$C_{41}H_{64}O_{14}$	780.94	–
Angiotensin II antagonists	Valsartan	137862-53-4	$C_{24}H_{29}N_5O_3$	435.52	3.7
Personal care products					
Sunscreen agents	Benzophenone-1	131-56-6	$C_{13}H_{10}O_3$	214.22	–
	Benzophenone-2	131-55-5	$C_{13}H_{10}O_5$	246.22	–
	Benzophenone-3	131-57-7	$C_{14}H_{12}O_3$	228.24	–
	Benzophenone-4	4065-45-6	$C_{14}H_{12}O_6S$	308.31	–
Preservatives	Methylparaben	99-76-3	$C_8H_8O_3$	152.15	–
	Ethylparaben	120-47-8	$C_9H_{10}O_3$	166.17	8.3
	Propylparaben	94-13-3	$C_{10}H_{12}O_3$	180.20	–
	Butylparaben	94-26-8	$C_{11}H_{14}O_3$	194.23	8.5

reversed phase chromatography with aqueous-organic mobile phases. Basic additives were added to the mobile phase in order to increase retardation of acidic compounds through the formation of ion-pairs with charged groups of analytes, which resulted in subsequent suppression of their dissociation and allowed for an interaction of analytes with the hydrophobic stationary phase. Longer retention of analytes also allowed for the gradient elution to start with a higher content of organic solvent in the mobile phase, which is known to be beneficial for the ionisation of analytes in ESI-MS detector. Although non-volatile additives (e.g. tetraalkylammonium salts or phosphate buffer) generally provide better retention and subsequent separation, in this case only volatile additives were studied as this is a well known limitation of ESI-MS due to a possible deposition and contamination of ESI source with non-volatile salts. An additional issue concerns strong bases/acids used as additives. These additives (e.g. trifluoroacetic acid) can form strong ion pairs with analytes that cannot be broken and as a result they prevent ionisation of analytes. Ammonia and ammonium salts as well as alkylamines are a good compromise providing sufficient separation of analytes and sensitive ESI-MS detection.

Ammonium cation (in the form of ammonia), the weakest ion-pairing agent, and tributylamine (TrBA), a stronger, more hydrophobic basic additive, were found to be the most effective additives for the studied PPCPs. However, TrBA was chosen for this method as it provided higher sensitivity (with the exception of digoxin), better peak shapes and longer retention times resulting in better separation of all analytes (Fig. 1). On average a twice as high peak area of analytes (dissolved in HQ) was observed in the case of the method using TrBA as the mobile phase additive when compared to NH_4OH (e.g. salicylic acid, sulfasalazine and valsartan had respectively 3.5, 2.8 and 2.3 times higher signal intensity in the presence of TrBA than NH_4OH; see Fig. 1). Because high concentrations of mobile phase additives, despite good separation of analytes, may reduce, due to suppression effect, the sensitivity of ESI-MS detection, concentrations of mobile phase additives were kept to minimum: 10 mM TrBA or 5 mM NH_4OH. Acetic acid at the concentration of 0.5% was also added to mobile phases containing basic additives to lower the pH of mobile phase from above 10 to below 6. An increase of response of anions of acidic compounds containing carboxyl groups in the presence of alkylamines can be explained by a sodium displacement mechanism [42]. Alkylammonium cation displaces the sodium cation in the anionic groups of carboxylic analyte. The formed ion-pairs dissociate during the ionisation process taking place in ESI-/MS and as a result an increase of the signal of molecular anion of the acid, when compared to sodium adduct, is observed [42]. This theory explains an increase of ionisation of the following investigated compounds containing carboxyl groups: salicylic acid, furosemide, sulfasalazine, aspirin, pravastatin, ketoprofen, clofibric acid, naproxen, bezafibrate, valsartan, diclofenac, ibuprofen and mefenamic acid. The presence of TrBA also increased the ionisation of parabens and benzophenones and therefore these two groups of PPCPs were also analysed with the proposed method. It was, however, observed that the presence of matrix components extracted from BB water together with PPCPs causes higher suppression of some analytes, especially those characterised by short retention times (eluting with mobile phase of a high water to methanol ratio), when TrBA was used as a mobile phase additive when compared to NH_4OH (Fig. 1). Despite the higher suppression of some analytes caused by TrBA, this mobile phase additive was used in the analysis of acidic/neutral PPCPs as it resulted in an increase of retention of analytes in C18 column, an improvement of the shapes of the peaks, and their better separation, as is shown in Fig. 1.

3.1.2. *UPLC/MS/MS—the method*

Chromatograms of SPE extract of BB water spiked with PPCPs before extraction are presented in Fig. 2. Utilisation of

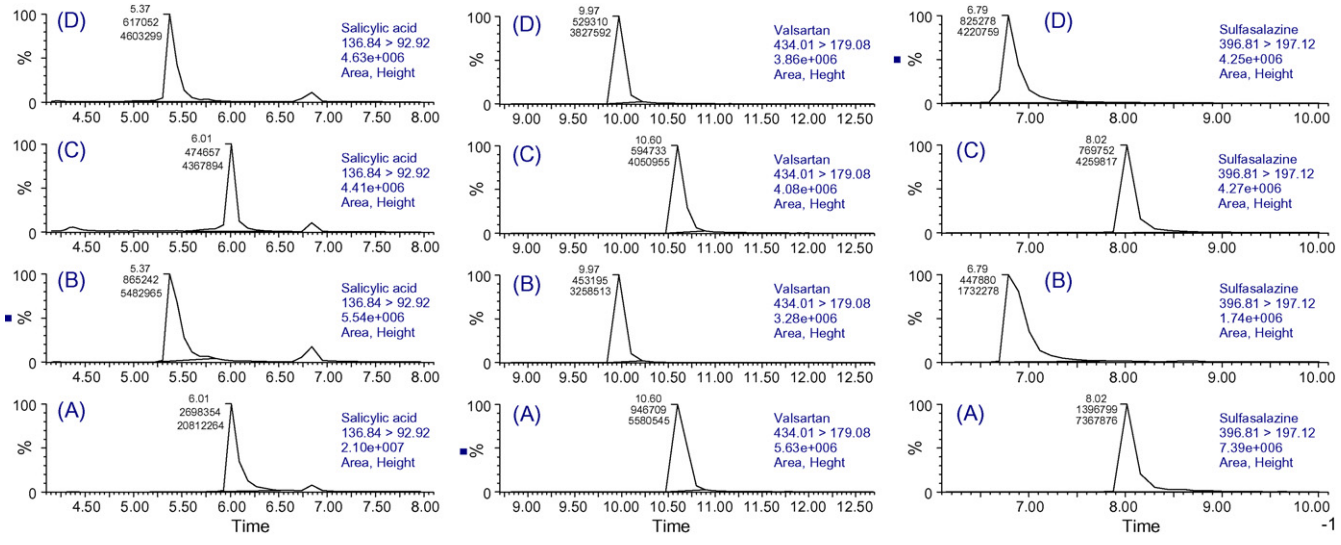

Fig. 1. UPLC/MS/MS separations for salicylic acid, sulfasalazine and valsartan (concentration of PPCPs, 500 $\mu g\,L^{-1}$; (A) PPCPs spiked into HQ water (mobile phase, 100%A) and analysed using TrBA as a mobile phase additive; (B) PPCPs spiked into HQ (mobile phase, 100%A) water and analysed using NH_4OH as a mobile phase additive; (C) PPCPs spiked into BB water extract and analysed using TrBA as a mobile phase additive; (D) PPCPs spiked into BB water extract and analysed using NH_4OH as a mobile phase additive).

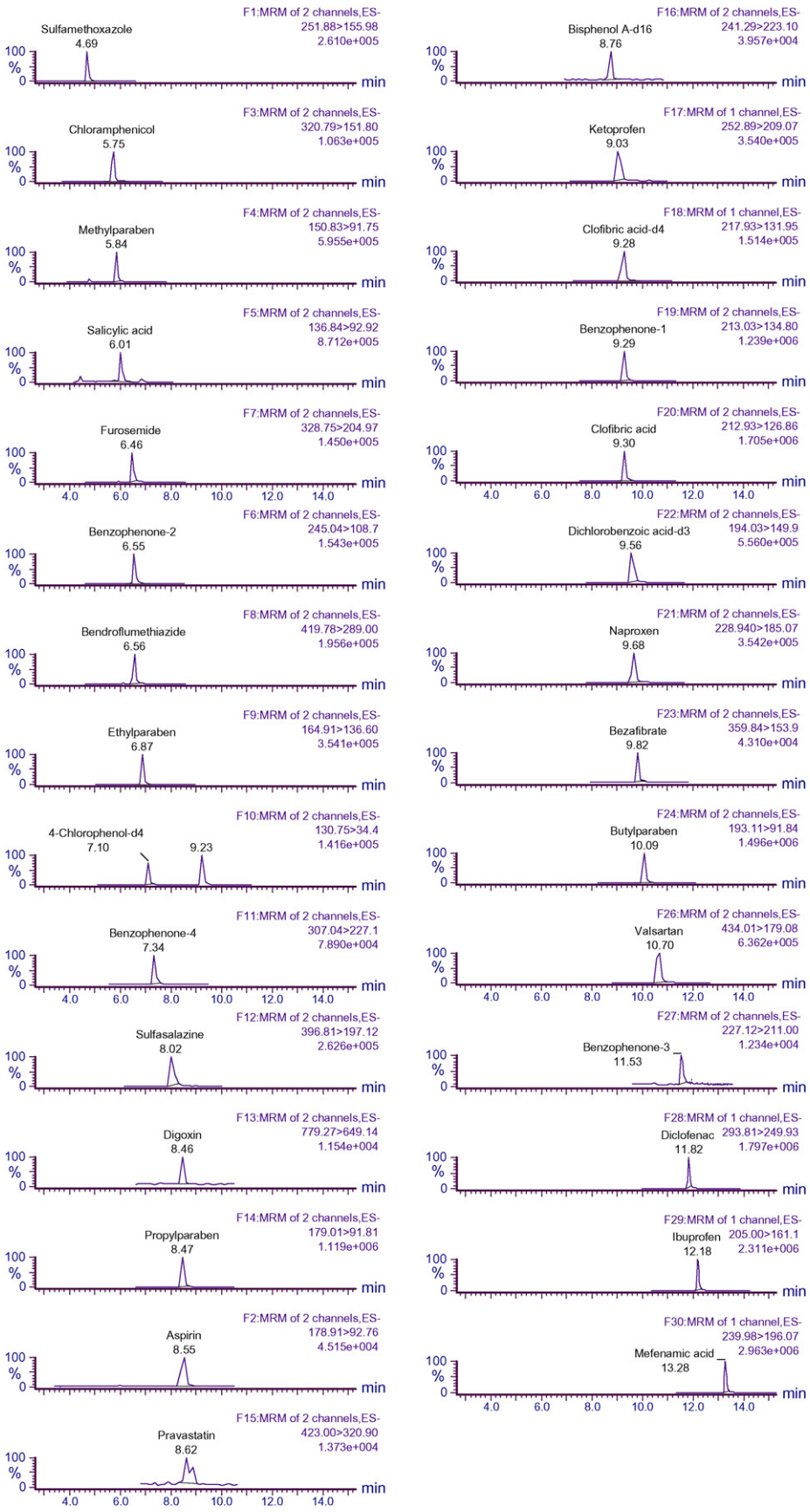

Fig. 2. UPLC/MS/MS separations for chosen PPCPs spiked into BB water and extracted by SPE (concentration of PPCPs, 100 ng L^{-1}; IS, 200 ng L^{-1}).

Table 2
Optimised MRM conditions for the analysis of chosen PPCPs by UPLC/MS/MS (CV: cone voltage (V); CE: collision energy (eV))

Compound	CV/CE	MRM1 (quantification)	CV/CE	MRM2 (confirmation)
Sulfamethoxazole	30/17	251.9 > 156.0	30/25	251.9 > 91.9
Chloramphenicol	27/15	320.8 > 151.8	27/15	320.8 > 256.0
Methylparaben	34/20	150.8 > 91.8	20/14	150.8 > 135.8
Salicylic acid	30/15	136.8 > 92.9	30/30	136.8 > 64.9
2-Benzophenone	26/20	245.0 > 108.7	26/15	245.0 > 135.1
Furosemide	30/20	328.8 > 205.0	30/15	328.8 > 284.9
Bendroflumethiazide	45/25	419.8 > 289.0	45/25	419.8 > 327.8
Ethylparaben	20/14	164.9 > 136.6	26/20	164.9 > 91.9
4-Benzophenone	44/24	307.0 > 227.1	42/35	307.0 > 211.1
Sulfasalazine	35/25	396.8 > 197.1	35/25	396.8 > 240.0
Digoxin	50/45	779.3 > 649.1	50/45	779.3 > 475.9
Propylparaben	34/25	179.0 > 91.8	20/16	179.0 > 136.0
Aspirin	12/20	178.9 > 92.8	12/6	178.9 > 136.9
Pravastatin	30/16	423.0 > 320.9	30/15	423.0 > 302.9
Ketoprofen	20/8	252.9 > 209.1	–	–
1-Benzophenone	36/20	213.0 > 134.8	34/25	213.0 > 90.8
Clofibric acid	20/15	212.9 > 126.9	20/10	212.9 > 84.9
Naproxen	15/8	228.9 > 185.1	15/15	228.9 > 170.1
Bezafibrate	30/19	359.8 > 153.9	30/30	359.8 > 273.9
Butylparaben	34/25	193.1 > 91.8	40/16	193.1 > 136.0
Valsartan	35/25	434.0 > 179.1	35/20	434.0 > 350.1
3-Benzophenone	30/20	227.1 > 211.0	34/24	227.1 > 183.9
Diclofenac	22/13	293.8 > 249.9	–	–
Ibuprofen	20/8	205.0 > 161.1	–	–
Mefenamic acid	30/15	240.0 > 196.1	–	–
Clofibric-d4 acid	18/15	217.9 > 132.0	–	–
3,4-Dichlorobenzoic-d3 acid	25/15	194.0 > 149.9	–	–
Bisphenol A-d16	40/18	241.3 > 223.1	–	–
4-Chlorophenol-d4	32/16	130.8 > 34.4	–	–

the novel ultra performance liquid chromatography system with 1.7 μm bridged ethylsiloxane/silica hybrid (BEH) particles and 1 mm internal diameter column allowed for the establishment of sufficient separation of 25 analytes using much lower mobile phase flow rates (0.05 mL min^{-1}) and shorter retention times (from 4.7 min to 13.3 min) when compared to methods established with the usage of conventional HPLC, where higher flow rates of 0.2 mL min^{-1} and longer method times of up to 50 min are applied to separate up to 30 compounds [31,34]. Additionally, a new column technology allowed for an application of very short column equilibration times (4 min). As a result, a sensitive, fast and cost-effective method was developed. Due to low column temperature (22 °C), which was optimal for the best separation of 25 analytes, a high initial pressure of 6500 psi was observed. This, however did not affect the performance of the method as a new technology implemented in the UPLC system is capable of pumping mobile phase at pressures up to 15,000 psi.

The mass spectrometry parameters are presented in Table 2. The most intensive product ion from each precursor ion was selected for quantification (MRM1). Retention time was the other primary criterion for identification of compound. A less sensitive secondary transition (MRM2) was used as the second criterion for confirmation purposes. In the case of ketoprofen, diclofenac, ibuprofen and mefenamic acid no secondary transition was observed. All of the compounds showed maximum sensitivity in the negative ionisation mode, although the degree of ionisation of PPCPs in ESI varied significantly and depended mainly on the functional groups present in the molecule. The highest response was observed for: salicylic, mefenamic and clofibric acids, diclofenac, ibuprofen and parabens. Digoxin and benzophenone-3 showed the lowest degree of ionisation, although it was sufficient enough to undertake environmental analysis (Fig. 2).

3.2. Solid-phase extraction and signal suppression

Out of eight different sorbents studied for the multi-residue analysis of investigated PPCPs (see Section 2), Oasis MCX and HLB were found to give the highest SPE recoveries for the studied PPCPs at acidic pH (pH 2.0). Oasis HLB is a hydrophilic–lipophilic water-wettable reversed-phase sorbent containing two monomers: hydrophilic *N*-vinylpyrrolidone and lipophilic divinylbenzene. It is a universal sorbent for acidic, neutral and basic compounds. Oasis MCX is a strong cation-exchange mixed-mode polymeric sorbent, which is capable of both ion-exchange and reversed-phase interactions. MCX sorbent is built upon HLB copolymer. The additional presence of sulfonic groups allows for cation-exchange interactions. Therefore, MCX adsorbent is designed for the extraction of basic and neutral compounds. Acidic pH of the solution is required in order to ionise basic compounds and neutralise acidic compounds.

The mean absolute and relative (relative to the recovery of surrogate/internal standard) recoveries PPCPs in both HQ and BB water are presented in Table 3. A maximum or close to

Table 3
SPE recovery for studied PPCPs (concentration, 500 ng L^{-1})

Compound	Sorbent	Recovery (%) ($n = 3$)			
		HQ water		BB water	
		Absolute	Relative[a]	Absolute	Relative[a]
Sulfamethoxazole	MCX	21.6 ± 0.5	25.6 ± 1.1[b]	18.1 ± 1.9	27.2 ± 4.5[b]
Chloramphenicol	MCX	93.8 ± 8.5	97.9 ± 4.9[d]	27.2 ± 1.3	69.5 ± 4.7[d]
			92.4 ± 4.7[b]		37.0 ± 1.4[b]
Methylparaben	MCX	127.8 ± 14.2	133.7 ± 8.4[d]	61.9 ± 8.4	163.8 ± 13.8[d]
			121.1 ± 1.4[e]		106.1 ± 2.4[e]
Salicylic acid	MCX	118.1 ± 14.2	122.9 ± 7.6[d]	28.1 ± 4.0	75.7 ± 5.1[d]
			116.6 ± 7.7[b]		39.9 ± 2.3[b]
2-Benzophenone	MCX	109.2 ± 8.2	114.4 ± 3.0[d]	32.7 ± 3.6	86.8 ± 10.4[d]
			111.1 ± 9.1[e]		56.4 ± 2.3[e]
Furosemide	MCX	88.0 ± 4.7	92.4 ± 1.3[d]	33.3 ± 2.9	89.0 ± 2.9[d]
			87.0 ± 1.0[b]		47.4 ± 2.3[b]
Bendroflumethiazide	MCX	78.3 ± 5.4	82.1 ± 2.4[d]	19.9 ± 1.7	52.7 ± 3.1[d]
			77.6 ± 3.0[b]		28.4 ± 0.6[b]
Ethylparaben	MCX	132.2 ± 11.5	138.4 ± 7.2[d]	48.1 ± 4.7	127.1 ± 6.1[d]
			134.4 ± 10.3[e]		82.5 ± 2.4[e]
4-Benzophenone	MCX	15.3 ± 4.1	16.0 ± 3.5[d]	6.6 ± 0.7	17.7 ± 3.1[d]
			15.6 ± 4.2[e]		11.7 ± 2.6[e]
	HLB	94.8 ± 10.1	109.5 ± 6.8[d]	11.9 ± 2.2	70.1 ± 6.5[d]
			120.4 ± 18.3[e]		37.2 ± 6.2[b]
Sulfasalazine	MCX	80.8 ± 6.3	84.5 ± 2.9[d]	33.2 ± 1.4	85.4 ± 3.4[d]
			79.8 ± 1.3[b]		47.4 ± 3.2[b]
Digoxin	MCX	45.7 ± 3.6	46.5 ± 3.7[e]	25.3 ± 3.5	46.5 ± 9.3[e]
			43.9 ± 3.3[b]		37.9 ± 5.3[b]
	HLB	76.7 ± 4.5	87.5 ± 4.8[e]	19.3 ± 5.3	113.2 ± 18.8[d]
			84.3 ± 4.7[b]		58.8 ± 10.3[b]
Propylparaben	MCX	124.8 ± 8.4	130.9 ± 3.1[d]	44.8 ± 4.1	119.3 ± 14.1[d]
			126.9 ± 8.4[e]		77.2 ± 3.7[e]
Aspirin	MCX	133.9 ± 1.7	138.7 ± 2.6[d]	63.5 ± 3.8	146.5 ± 3.7[d]
			132.6 ± 7.8[b]		90.4 ± 6.5[b]
Pravastatin	MCX	8.4 ± 2.4	8.6 ± 2.4[e]	5.5 ± 0.2	9.5 ± 1.3[e]
			8.3 ± 1.8[b]		7.8 ± 0.9[b]
	HLB	51.0 ± 1.0	64.7 ± 1.8[e]	9.9 ± 1.5	30.9 ± 1.3[e]
			56.9 ± 3.4[b]		30.5 ± 5.0[b]
Ketoprofen	MCX	114.1 ± 5.6	113.0 ± 4.8[b]	38.0 ± 1.8	54.3 ± 3.5[b]
			113.3 ± 3.5[b]		52.5 ± 4.6[c]
			117.8 ± 2.6[d]		98.1 ± 3.3[d]
			115.9 ± 3.7[e]		65.8 ± 4.6[e]
1-Benzophenone	MCX	104.6 ± 6.1	109.6 ± 1.0[d]	41.4 ± 2.9	109.9 ± 9.2[d]
Clofibric acid	MCX	100.0 ± 3.0	99.2 ± 4.1[b]	59.3 ± 2.9	84.7 ± 6.3[b]
Naproxen	MCX	107.0 ± 7.2	105.7 ± 0.9[b]	64.1 ± 4.6	91.4 ± 8.5[b]
Bezafibrate	MCX	107.4 ± 11.0	106.0 ± 2.0[c]	79.3 ± 6.1	104.8 ± 2.5[c]
			106.0 ± 4.5[b]		112.9 ± 4.0[b]
Butylparaben	MCX	112.1 ± 9.6	117.5 ± 4.3[d]	76.5 ± 4.7	203.3 ± 12.2[d]
			107.9 ± 0.9[e]		132.4 ± 8.5[e]
Valsartan	MCX	98.3 ± 8.5	99.8 ± 5.6[e]	54.2 ± 2.6	96.3 ± 2.2[e]
			97.1 ± 2.4[b]		77.4 ± 5.1[b]
3-Benzophenone	MCX	76.1 ± 9.0	79.7 ± 5.8[d]	46.6 ± 2.4	124.7 ± 14.4[d]
Diclofenac	MCX	104.0 ± 7.0	102.8 ± 1.1[b]	71.5 ± 2.3	102.1 ± 7.8[b]
Ibuprofen	MCX	82.8 ± 4.1	81.9 ± 1.2[b]	66.7 ± 1.8	95.4 ± 7.0[b]
Mefenamic acid	MCX	97.0 ± 3.5	96.0 ± 2.8[b]	101.7 ± 9.0	138.0 ± 10.5[b]
Clofibric-d4 acid	MCX	101.1 ± 6.5	–	70.3 ± 7.3	–
	HLB	89.6 ± 3.7	–	32.7 ± 3.4	–
3,4-Dichlorobenzoic-d3 acid	MCX	101.2 ± 9.1	–	77.2 ± 7.0	–
	HLB	83.6 ± 6.5	–	36.2 ± 5.2	–
Bisphenol A-d16	MCX	95.2 ± 4.6	–	39.2 ± 4.9	–
	HLB	86.4 ± 4.1	–	17.4 ± 4.8	–
4-Chlorophenol-d4	MCX	98.4 ± 4.0	–	58.0 ± 6.0	–
	HLB	79.2 ± 4.0	–	32.0 ± 3.7	–

[a] Recovery relative to surrogate/internal standard.
[b] Clofibric-d4 acid (4-chlorophenyl-d4).
[c] 3,4-Dichlorobenzoic (2,5,6-d3) acid.
[d] Bisphenol A-d16.
[e] 4-Chlorophenol (2,3,5,6-d4).

maximum recovery was observed for almost all PPCPs dissolved in HQ water both in the case of HLB and MCX adsorbents. MCX gave generally better recoveries than HLB with the exception of 4-benzophenone, digoxin and pravastatin. As can be observed from Table 3 the recoveries of 4-benzophenone, digoxin and pravastatin were respectively only 15.3, 45.7 and 8.4% in HQ water in the case of MCX and 94.8, 76.7 and 51.0% in the case of HLB sorbent. Therefore for these compounds the usage of HLB sorbent is strongly recommended.

A significant decrease of the absolute recovery of some PPCPs was observed in BB water due to the presence of the matrix components in the sample and is believed to result from both a reduction of sorption efficiency of SPE cartridges and also signal suppression in the electrospray interface due to the presence of matrix impurities. The second factor was found to be the dominant phenomenon affecting sensitivity of the method as it is discussed below. HLB sorbent, apart from giving lower PPCPs recovery than MCX sorbent in the case of HQ water, was also found to be much more affected by the presence of matrix components in BB water than MCX sorbent and therefore MCX adsorbent was chosen for final method development and validation purposes. It is suggested that HLB, because of its universal nature, is less selective than MCX sorbent and capable of sorption of many more matrix components, resulting in lower SPE recovery or more likely higher ion suppression in ESI source.

Signal suppression is the main disadvantage of electrospray mass spectrometry and results from the fact that ESI-MS is susceptible to organic and inorganic components that are present both in the sample together with analytes and in the mobile phase. In this paper signal suppression of analytes resulting from both matrix components (that were extracted together with analytes) and mobile phase additives was studied (see Section 3.1.1). Table 4 presents signal suppression observed for the analysed PPCPs dissolved in SPE extract of BB water. Chloramphenicol, salicylic acid, bendroflumethiazide, furosemide, methylparaben, ethylparaben, 2- and 4-benzophenone were found to be the most susceptible to matrix components. No or only a slight signal suppression was observed for diclofenac and ibuprofen. A low signal enhancement was observed in the case of mefenamic acid.

The results presented in Tables 3 and 4 lead to the conclusion that the effects of signal suppression and low SPE recovery, both resulting from the presence of matrix interferences, are the main factors affecting the sensitivity of the analytical method. Among the compounds characterised by the highest ion suppression in ESI source are chloramphenicol, salicylic acid, bendroflumethiazide, furosemide, methylparaben, ethylparaben and 2-benzophenone. Therefore, for these compounds, the lower absolute SPE recoveries (Table 3) are probably due to the suppression of the signal during electrospray ionisation (Table 4). It is evident that the presence of the higher percentage of H_2O in the mobile phase contributes to signal suppression of analytes, as the above compounds elute within the retention time of 5.7–7.3 and mobile phase gradient from 50 to 35% of mobile phase A containing 79.5% of H_2O.

The loss of method sensitivity for the majority of the PPCPs studied, which resulted both from low SPE recovery and signal suppression in ESI-MS, was in this work compensated by the usage of the appropriate surrogate/internal standards (Tables 3 and 4). It should be emphasised here that the choice of internal standard is crucial in terms of compensation for suppression effect, which is a common problem in MS-ESI. An influence of the type of IS/SS standard on relative recovery of ketoprofen is a good example (see Tables 3 and 4). The comparison of relative recoveries of ketoprofen (Table 3) clearly indicates that out of the four IS/SS standards studied only bisphenol-A-d16 compensates for suppression of ketoprofen because both compounds are similarly susceptible to suppression in ESI-MS (Table 4). Based on similarities in structures and susceptibility to suppression during ESI-MS analysis the following primary IS/SS were chosen for different groups of PPCPs:

(a) clofibric-d4 acid: sulfamethoxazole, clofibric acid, naproxen, diclofenac, ibuprofen and mefenamic acid,

Table 4
Signal suppression of PPCPs in BB water spiked after extraction (concentration, 500 $\mu g\,L^{-1}$)

Compound	Signal suppression (%)	
	Absolute	Relative[a]
Sulfamethoxazole	41.3 ± 1.9	11.1 ± 3.6[b]
Chloramphenicol	88.0 ± 0.5	73.7 ± 0.3[d]
Methylparaben	81.7 ± 0.4	59.8 ± 1.4[d]
Salicylic acid	80.7 ± 0.5	57.6 ± 1.6[d]
2-Benzophenone	72.1 ± 0.9	38.8 ± 0.2[d]
Furosemide	76.0 ± 0.8	47.4 ± 1.5[d]
Bendroflumethiazide	83.7 ± 0.5	64.1 ± 0.3[d]
Ethylparaben	79.3 ± 0.6	54.6 ± 0.5[d]
4-Benzophenone	75.0 ± 0.9	45.1 ± 1.5[d]
Sulfasalazine	41.3 ± 0.9	−29.1 ± 2.6[d]
Digoxin	67.2 ± 0.8	15.3 ± 1.8[e]
Propylparaben	62.4 ± 1.5	17.4 ± 3.4[d]
Aspirin	57.8 ± 2.1	−0.9 ± 4.6[d]
Pravastatin	62.1 ± 1.0	2.0 ± 3.9[e]
Ketoprofen	67.0 ± 2.1	50.1 ± 2.5[b]
		22.9 ± 4.2[c]
		14.8 ± 6.8[d]
		27.6 ± 3.2[e]
1-Benzophenone	61.6 ± 1.6	15.6 ± 2.0[d]
Clofibric acid	58.3 ± 1.3	37.0 ± 2.5[b]
Naproxen	45.4 ± 1.1	17.5 ± 1.6[b]
Bezafibrate	65.4 ± 1.7	30.8 ± 2.9[c]
Butylparaben	47.9 ± 1.5	−14.7 ± 6.4[d]
Valsartan	43.6 ± 3.0	2.0 ± 5.3[e]
3-Benzophenone	32.7 ± 0.7	−47.8 ± 6.4[d]
Diclofenac	17.6 ± 3.5	−24.7 ± 5.2[b]
Ibuprofen	10.9 ± 3.2	−34.7 ± 4.9[b]
Mefenamic acid	−16.0 ± 8.3	−76.2 ± 1.1[b]
Clofibric-d4 acid	34.2 ± 1.7	–
3,4-Dichlorobenzoic-d3 acid	57.3 ± 0.5	–
Bisphenol A-d16	54.5 ± 1.5	–
4-Chlorophenol-d4	61.2 ± 0.8	–

[a] Recovery relative to surrogate/internal standard.
[b] Clofibric-d4 acid (4-chlorophenyl-d4).
[c] 3,4-Dichlorobenzoic (2,5,6-d3) acid.
[d] Bisphenol A-d16.
[e] 4-Chlorophenol (2,3,5,6-d4).

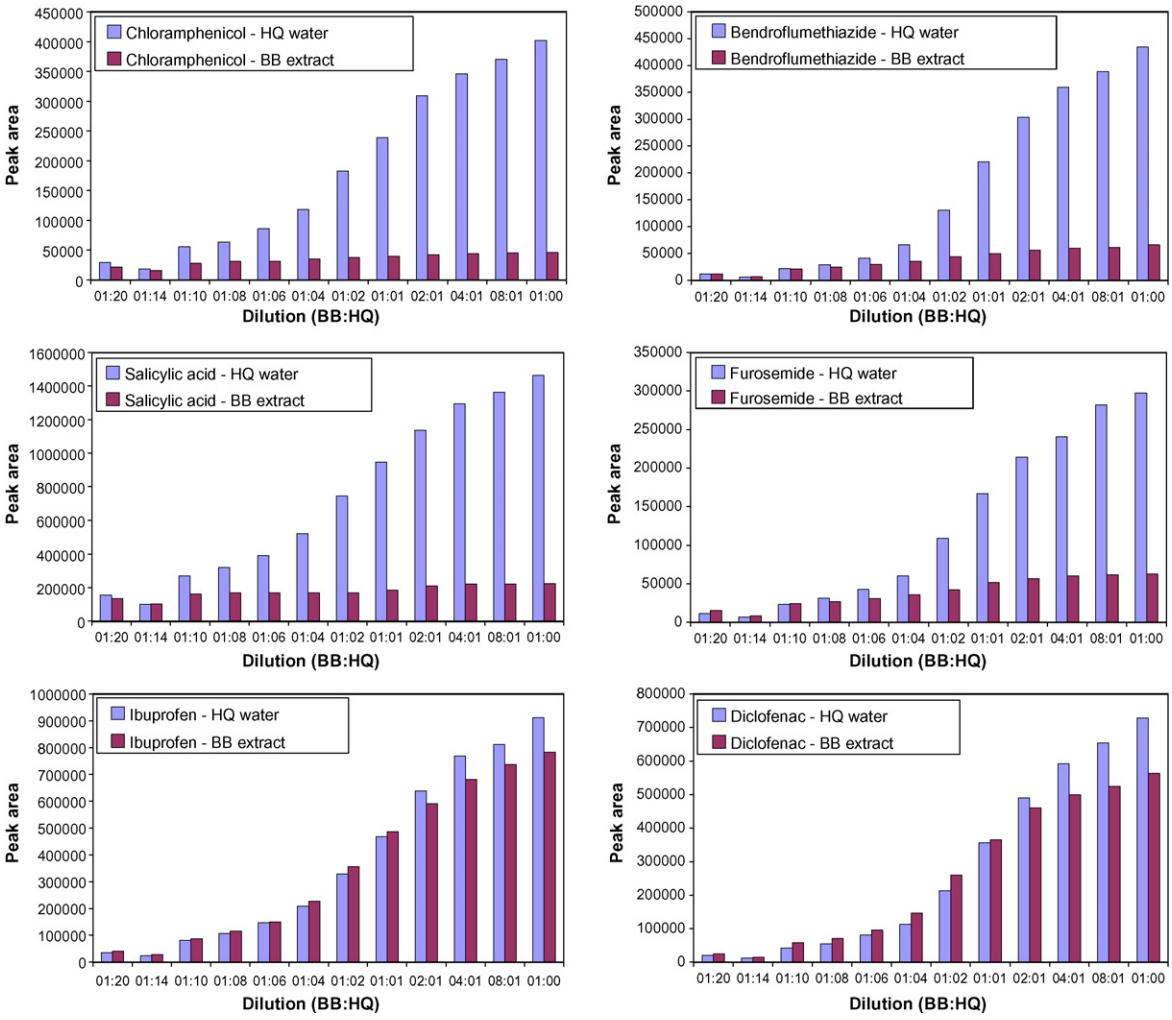

Fig. 3. Influence of BB extract dilution on the intensity of the signal of studied PPCPs (HQ water: mobile phase, 100%A spiked with 500 μg L^{-1} of PPCPs before dilution; BB extract: reconstituted with mobile phase, 100%A and spiked with 500 μg L^{-1} of PPCPs before dilution).

(b) 3,4-dichlorobenzoic-d3 acid: bezafibrate,
(c) bisphenol A-d16: aspirin, chloramphenicol, salicylic acid, furosemide, bendroflumethiazide, sulfasalazine, ketoprofen, parabens and benzophenones,
(d) 4-chlorophenol-d4: digoxin, pravastatin and valsartan.

A slight overestimation (>100%) was observed for the relative recoveries of these PPCPs, which were not significantly affected by matrix assisted signal suppression/low recovery (e.g. mefenamic acid). This phenomenon can be explained by the fact that signal suppression for the surrogate/internal standard is higher than for the analyte. In the case of the compounds that were characterised by good SPE recovery, but suffered high signal suppression (chloramphenicol, salicylic acid, furosemide and bendroflumethiazide) which was not compensated by the usage of IS/SS, two procedures can be undertaken. Firstly, the choice of a more suitable IS/SS, which is problematic, or the dilution of sample extracts as proposed by Gros et al. [34] and Gómez et al. [43]. It was observed that, on average a higher than 8-times dilution of BB extract with HQ water is necessary to avoid matrix assisted signal suppression for the studied PPCPs: chloramphenicol, salicylic acid, furosemide and bendroflumethiazide (Fig. 3). For comparison, a minor influence of dilution of sample extracts on the intensity of the signal of compounds which are not significantly susceptible to signal suppression (diclofenac and ibuprofen) is also presented in Fig. 3. It should be emphasised, however, that too high dilution can also lead to a considerable decrease in sensitivity and this has to be taken into consideration when applying this approach.

The above discussion indicates that there is an obvious need for the application of a higher number of surrogate/internal standards to more accurately compensate for matrix assisted signal suppression and the low SPE recovery of the different groups of PPCPs studied. This is, however, very often impossible due to the lack of suitable surrogate/internal standards or their high cost. The other possibilities that could eliminate matrix effect involve selective extraction/better sample clean-up, time consuming standard addition or dilution of sample extracts as proposed by Gros et al. [34] and Gómez et al. [43]. In summary, there are several approaches that can be undertaken concerning quantification issues. In this study internal standard calibration is considered to be the right approach for PPCPs determination

Table 5
Performance data for pharmaceuticals (instrumental/method limits of detection and quantification; linearity—R^2)

PPCPs	t_R (min)	Instrumental parameters[a]			Method parameters[b]			
		$IDL_{S/N}$ ($\mu g\,L^{-1}$)	$IQL_{S/N}$ ($\mu g\,L^{-1}$)	R^2	$MDL_{S/N}$ ($ng\,L^{-1}$)	$MQL_{S/N}$ ($ng\,L^{-1}$)	MQL_{calc} ($ng\,L^{-1}$)	R^2
Sulfamethoxazole	4.69	0.2	1.0	1.000	0.5	2.0	2.8	0.999
Chloramphenicol	5.75	0.05	0.2	0.999	0.5	2.0	0.4	0.999
Methylparaben	5.84	0.05	0.2	0.999	0.1	0.3	0.2	0.997
Salicylic acid	6.01	0.05	0.2	1.000	0.1	0.5	0.4	0.999
Furosemide	6.46	0.2	1.0	0.999	2.5	7.0	1.5	0.998
2-Benzophenone	6.55	0.1	0.4	0.997	0.1	0.5	0.6	1.000
Bendroflumethiazide	6.56	0.1	1.0	0.998	1.0	3.0	2.5	0.998
Ethylparaben	6.87	0.05	0.2	0.996	0.15	0.5	0.2	0.997
4-Benzophenone	7.34	0.05	0.2	0.997	1.5	5.0	1.5	1.000
Sulfasalazine	8.02	0.2	1.0	0.996	1.0	5.0	1.5	0.997
Digoxin	8.46	10.0	15	0.996	10.0	30.0	29.6	0.996
Propylparaben	8.47	0.1	0.4	0.997	0.1	0.3	0.5	1.000
Aspirin	8.55	0.2	1.0	0.999	0.1	0.5	0.8	1.000
Pravastatin	8.62	1.0	5.0	0.997	20.0	60.0	50.0	0.998
Ketoprofen	9.03	0.2	1.0	0.999	0.8	2.5	1.3	0.999
1-Benzophenone	9.29	0.05	0.2	0.997	0.1	0.3	0.2	1.000
Clofibric acid	9.30	0.1	0.4	0.994	0.1	0.5	0.4	0.997
Naproxen	9.68	0.2	0.6	0.997	0.5	1.5	0.9	1.000
Bezafibrate	9.82	2.0	10.0	0.996	2.5	10.0	6.3	1.000
Butylparaben	10.09	0.1	0.4	0.999	0.1	0.3	0.3	0.999
Valsartan	10.70	0.2	0.5	0.999	0.1	0.5	0.5	1.000
3-Benzophenone	11.53	10.0	30.0	0.996	10	30.0	32.2	0.999
Diclofenac	11.82	0.2	0.7	0.997	0.2	0.5	0.5	0.999
Ibuprofen	12.18	0.2	0.7	0.995	0.1	0.5	0.5	0.999
Mefenamic acid	13.28	0.3	1.0	0.997	0.1	0.5	0.5	0.999

[a] HQ standards spiked with pharmaceuticals; concentration, 0–1200 $\mu g\,L^{-1}$.
[b] BB water spiked with pharmaceuticals before extraction; concentration, 0–1200 $ng\,L^{-1}$.

in environmental samples. For the compounds that IS/SS did not compensate for ion suppression, dilution of samples should be undertaken. This approach was also proposed by Gómez et al. [43].

3.3. Quantification and method validation parameters

The instrumental and method limits of detection and quantification are presented in Table 5. The instrumental limits of quantification varied from 0.2 $\mu g\,L^{-1}$ for chloramphenicol, methyl-, ethyl- and butylparaben, salicylic acid, and 1-, 4-benzophenones to 30 $\mu g\,L^{-1}$ for 3-benzophenone. The method limits of quantification were at low nanogram per litre levels and ranged from 0.3 $ng\,L^{-1}$ for methyl-, propyl- and butylparaben and 1-benzophenone to 30 $ng\,L^{-1}$ for digoxin and 3-benzophenone, which makes the method useful for the determination of very low levels of PPCPs in the aqueous environment such as surface waters. The values of $MQL_{S/N}$ that were determined using a signal-to-noise approach were also confirmed with MQL_{calc} calculated using Eq. (2) (see Table 5).

The mean correlation coefficients (R^2) of the calibration curves, which are on average higher than 0.997 in both HQ water and BB surface water (Table 5), show good linearity of the method in the range of 0–1200 $ng\,L^{-1}$. The accuracy range was within the value of −30 to 20%. The instrumental intra- and inter-day repeatabilities as indicated by standard deviation calculated from the analysis of three replicates were below 5%. The method intra- and inter-day repeatabilities were on average less than 5% (Table 6).

3.4. Environmental application

The multi-residue method was successfully applied to verify the presence of PPCPs in River Taff in South Wales, a region of the UK which, according to the best knowledge of the authors, has never been studied for the analysis of the chosen PPCPs. Several sampling points were chosen along River Taff:

1. Brecon Beacons National Park, the source of River Taff.
2. Merthyr Tydfil—23.5 km downstream, just after Merthyr Tydfil (population, 55,000).
3. Abercynon—12 km downstream of Merthyr Tydfil, just after Abercynon, 1 km upstream of a WWTP.
4. Pontypridd—2 km downstream of a WWTP, just before Pontypridd (population, 33,000).
5. Trefforest Estate—7 km downstream of Pontypridd.
6. Cardiff—18 km downstream of Trefforest Estate, the bay area of Cardiff (population, 320,000), where the river enters the Bristol Channel.

The results are presented in Table 7. The research proved that River Taff at its source, which is in Brecon Beacons National Park, is not contaminated with PPCPs. The first signs of con-

Table 6
Performance data for pharmaceuticals (inter- and intra-day repeatability)

PPCPs	Method parameters[a], precision											
	Intra-day R.S.D.% ($n=3$)									Inter-day R.S.D.% ($n=3$)		
	50 (ng L^{-1})			500 (ng L^{-1})			1000 (ng L^{-1})			50 (ng L^{-1})	500 (ng L^{-1})	1000 (ng L^{-1})
	D1	D2	D3	D1	D2	D3	D1	D2	D3			
Sulfamethoxazole	1.3	1.1	0.4	1.0	0.2	2.1	1.6	1.0	1.5	3.9	4.8	5.4
Chloramphenicol	1.3	2.5	0.7	3.1	0.8	1.7	0.6	0.7	0.9	1.7	2.9	2.9
Methylparaben	3.1	2.6	0.8	3.8	1.2	1.1	1.0	1.5	2.2	4.6	6.4	5.5
Salicylic acid	0.9	1.4	0.4	3.3	1.0	1.4	2.2	1.6	1.0	3.3	3.3	5.4
Furosemide	1.0	1.5	0.5	1.5	1.6	1.0	1.4	1.7	0.5	4.6	4.9	3.2
2-Benzophenone	2.1	4.4	0.2	2.9	2.4	0.4	0.5	1.1	2.3	3.9	4.8	5.5
Bendroflumethiazide	2.7	2.1	0.8	1.0	2.0	1.6	3.0	1.2	1.1	1.8	2.7	5.1
Ethylparaben	2.3	3.9	1.2	1.0	1.8	1.8	4.8	0.2	1.4	2.5	5.6	4.0
4-Benzophenone	3.8	4.6	1.7	4.1	3.1	2.2	0.8	3.9	3.0	6.5	7.0	4.6
Sulfasalazine	2.7	1.6	0.6	3.3	0.7	1.3	0.6	0.8	0.5	2.0	1.8	2.9
Digoxin	13.7	1.9	3.9	4.2	3.8	6.6	4.7	0.6	3.4	8.3	8.1	8.9
Propylparaben	1.5	3.8	2.1	2.4	4.0	4.1	1.3	3.7	5.0	4.0	9.9	4.9
Aspirin	3.5	1.8	1.5	2.4	1.0	1.0	2.3	0.2	0.6	2.4	3.9	3.5
Pravastatin	–	–	–	4.1	3.7	1.0	1.0	0.3	4.4	–	7.9	5.0
Ketoprofen	2.2	1.4	1.2	2.5	1.2	1.0	4.2	1.1	0.6	2.8	2.9	3.0
1-Benzophenone	0.5	3.1	0.9	2.5	3.2	1.1	0.3	4.4	4.7	3.0	6.5	4.8
Clofibric acid	0.9	1.6	0.3	2.7	2.5	0.4	1.2	1.2	1.8	4.4	5.3	4.9
Naproxen	0.9	0.8	0.8	1.6	0.9	2.1	2.6	1.0	1.4	1.8	4.7	4.4
Bezafibrate	6.5	2.5	1.4	4.2	1.2	4.7	4.9	1.8	3.1	3.5	8.8	7.4
Butylparaben	0.4	2.6	1.6	1.3	1.4	2.8	1.5	2.6	1.2	2.2	5.2	4.7
Valsartan	4.5	2.2	1.2	4.8	2.4	2.3	1.6	0.7	0.4	4.3	4.7	3.2
3-Benzophenone	0.5	2.2	2.6	3.5	1.2	0.4	0.5	0.5	2.3	8.3	6.6	3.0
Diclofenac	1.5	0.5	0.5	1.0	0.6	1.0	2.1	0.8	0.7	2.6	3.2	3.6
Ibuprofen	1.7	0.6	1.0	1.3	1.4	1.2	2.2	1.0	1.4	3.2	4.8	4.4
Mefenamic acid	1.3	0.6	2.2	0.1	0.3	0.8	0.1	0.2	0.9	2.6	4.8	3.4

[a] BB water spiked with pharmaceuticals before extraction; concentration, 0–1200 ng L^{-1}.

Table 7
Concentration of PPCPs in River Taff (two replicate samples)

Compound	Concentration (ng L^{-1})				
	Merthyr Tydfil	Abercynon	Pontypridd	Trefforest Estate	Cardiff
Sulfamethoxazole	<MQL	<MQL	<MQL	<MQL	<MQL
Chloramphenicol	<MQL	<MQL	<MQL	<MQL	<MQL
Methylparaben	30 ± 5	48 ± 2	26 ± 2	17 ± 2	10 ± 10
Salicylic acid	21 ± 2	33 ± 4	18 ± 3	14 ± 1	14 ± 1
2-Benzophenone	<MQL	<MQL	<MQL	<MQL	<MQL
Furosemide	<MQL	<MQL	57 ± 8	40 ± 2	7 ± 1
Bendroflumethiazide	<MQL	<MQL	<MQL	<MQL	<MQL
Ethylparaben	4 ± 0.2	7 ± 1	8 ± 1	4 ± 1	4 ± 1
4-Benzophenone	<MQL	54 ± 9	220 ± 20	187 ± 22	128 ± 18
Sulfasalazine	7 ± 0.1	12 ± 0.4	30 ± 3	14 ± 0.4	20 ± 1
Digoxin	<MQL	<MQL	<MQL	<MQL	<MQL
Propylparaben	<MQL	<MQL	<MQL	<MQL	<MQL
Aspirin	3 ± 2	9 ± 2	7 ± 1	6 ± 1	7 ± 1
Pravastatin	<MQL	<MQL	<MQL	<MQL	<MQL
Ketoprofen	<MQL	<MQL	6 ± 1	4 ± 1	6 ± 2
1-Benzophenone	<MQL	<MQL	<MQL	<MQL	<MQL
Clofibric acid	<MQL	<MQL	<MQL	36 ± 1	21 ± 1
Naproxen	3 ± 0.2	9 ± 1	34 ± 2	29 ± 3	20 ± 2
Bezafibrate	<MQL	<MQL	<MQL	<MQL	<MQL
Butylparaben	<MQL	<MQL	<MQL	<MQL	<MQL
Valsartan	1 ± 0.1	7 ± 1	21 ± 2	19 ± 2	15 ± 0.2
3-Benzophenone	<MQL	<MQL	<MQL	<MQL	<MQL
Diclofenac	<MQL	1 ± 0.4	12 ± 2	8 ± 1	8 ± 1
Ibuprofen	0.6 ± 0.3	20 ± 2	25 ± 3	18 ± 2	37 ± 2
Mefenamic acid	<MQL	<MQL	9 ± 6	5 ± 4	<MQL

tamination are observed in Abercynon, which might be due to a run-off or an uncontrolled discharge of untreated sewage from surrounding housing estates. A significant increase of PPCPs concentration takes place in Pontypridd, which is after a wastewater treatment plant (WWTP Cilfynydd treating mainly communal wastewater). A slight decrease of PPCPs concentration is observed in Cardiff, but it still remains high when compared to the quality of river water upstream of the WWTP, at the first three sampling points.

PPCPs were identified at concentrations of a few ng L^{-1} to a few hundreds ng L^{-1}. The highest concentrations were observed in the case of pharmaceuticals for anti-inflammatory/analgesics such as salicylic acid, napoxen and ibuprofen and other pharmaceuticals such as: furosemide and valsartan. Among personal care products 4-benzophenone and methylparaben were found at the highest concentrations.

4. Conclusions

This paper concerns the development and validation of a novel, fast and cost-effective multi-residue method for environmental monitoring of 25 acidic/neutral pharmaceuticals (antibiotics, anti-inflammatory/analgesics, lipid regulating agents, diuretics, triazides, H2-receptor antagonists, cardiac glicozides and angiotensin II antagonists) and personal care products (susnscreen agents and preservatives) in the low nanogram per litre range. The method involved single solid-phase extraction with the usage of strong cation-exchange mixed-mode polymeric sorbent (Oasis MCX, 60 mg) and subsequent ultra performance liquid chromatography–negative electrospray ionisation tandem mass spectrometry. The usage of the novel ultra performance liquid chromatography system with 1.7 μm bridged ethylsiloxane/silica hybrid (BEH) particles and 1 mm internal diameter column allowed for good separation of analytes with the application of low mobile phase flow rates (0.05 mL min^{-1}) and short retention times (from 4.7 min to 13.3 min). High sensitivity, resolution and speed of analysis are some of the main advantages of the method when compared to other multi-residue methods using high-performance liquid chromatography combined with mass spectrometry.

The influence of mobile-phase composition, matrix assisted ion suppression and SPE recovery on the sensitivity of the method were evaluated. High recovery and reproducibility for MCX adsorbent was obtained for many of the pharmaceuticals studied. The effects of signal suppression and low SPE recovery, both resulting from the presence of matrix interferences, were found to be the main factors affecting the sensitivity of the established analytical method. Surrogate/internal standards were therefore added to the sample so as to compensate for losses of compounds during both the sample preparation procedure and resulting from matrix assisted suppression. For the compounds that IS/SS did not compensate for ion suppression, dilution of samples was undertaken.

The mean correlation coefficients (R^2) of the calibration curves, which are on average higher than 0.997 in both HQ water and BB surface water extract, showed good linearity of the method in the studied range of 0–1200 μg L^{-1} and 0–1200 ng L^{-1} respectively. The instrumental limits of quantification varied from 0.2 μg L^{-1} (chloramphenicol, salicylic acid, diclofenac, ibuprofen, methyl-, ethyl- and butylparaben, 1- and 4-benzophenone) to 30 μg L^{-1} (3-benzophenone). The method limits of quantification were at low nanogram per litre levels and ranged from 0.3 ng L^{-1} (methyl-, propyl-, butylparaben and 1-benzophenone) to 30 ng L^{-1} (dioxin and 3-benzophenone). The instrumental and method intra-day and inter-day repeatabilities were on average less than 5%.

The method was applied for the determination of PPCPs in River Taff. The results confirmed its applicability in environmental monitoring. Thirteen compounds were determined in river water at levels ranging from a single to a few hundred nanograms per litre. Among them were 10 pharmaceuticals (aspirin, salicylic acid, ketoprofen, naproxen, diclofenac, ibuprofen, mefenamic acid, furosemide, sulfasalazine, valsartan) and 3 personal care products (methyl- and ethylparaben and 4-benzophenone) The highest concentrations were determined in river water samples collected after wastewater plants, which confirms the hypothesis that wastewater effluents are the main source of water contamination with PPCPs.

Acknowledgment

This work was undertaken as a part of the EU Marie Curie Host Fellowship for the Transfer of Knowledge (contract number MTKD-CT-2004-509821).

References

[1] C.G. Daughton, T.A. Ternes, Environ. Health Perspect. 107 (1999) 907–942.
[2] K. Fent, A.A. Weston, D. Caminada, Aquat. Toxicol. 76 (2006) 122–159.
[3] C. Carlsson, A.-K. Johansson, G. Alvan, K. Bergman, T. Kühler, Sci. Total Environ. 364 (2006) 67–87.
[4] S.D. Costanzo, J. Murby, J. Bates, Mar. Pollut. Bull. 51 (2005) 218–223.
[5] J.B. Ellis, Environ. Pollut. 144 (2006) 184–189.
[6] S.D. Richardson, T.A. Thernes, Anal. Chem. 77 (2005) 3807–3838.
[7] T. Herberer, Toxicol. Lett. 131 (2002) 5–17.
[8] T.A. Ternes, Trends Anal. Chem. 20 (2001) 419–434.
[9] D. Calamari, E. Zuccato, S. Castiglioni, R. Bagnati, R. Fanelli, Environ. Sci. Technol. 37 (2003) 1241–1248.
[10] D. Bendz, N.A. Paxéus, T.R. Ginn, F.J. Loge, J. Hazard. Mater. 122 (2005) 195–204.
[11] D.W. Kolpin, M. Skopec, M.T. Meyer, E.T. Furlong, S.D. Zaugg, Sci. Total Environ. 328 (2004) 119–130.
[12] N.M. Vieno, T. Tuhkanen, L. Kronberg, Eviron. Sci. Technol. 39 (2005) 8220–8226.
[13] N. Lindqvist, T. Tuhkanen, L. Kronberg, Water Res. 39 (2005) 2219–2228.
[14] S.T. Glassmeyer, E.T. Furlong, D.W. Kolpin, J.D. Cahill, S.D. Zaugg, S.L. Werner, M.T. Meyer, D.D. Kryak, Environ. Sci. Technol. 39 (2005) 5157–5169.
[15] D.W. Kolpin, E.T. Furlong, M.T. Meyer, E.M. Thurman, S.D. Zaugg, L.B. Barber, H.T. Buxton, Environ. Sci. Technol. 36 (2002) 1202–1211.
[16] D. Ashton, M. Hilton, K.V. Thomas, Sci. Total Environ. 333 (2004) 167–184.
[17] P. Roberts, K.V. Thomas, Sci. Total Environ. 356 (2006) 143–153.
[18] M.D. Hernando, M. Mezcua, A.R. Férnandez-Alba, D. Barceló, Talanta 69 (2005) 334.
[19] Review of the State of Knowledge of Municipal Effluent Science and Research, Hydromantis Inc. Minnow Environmental Inc., University of Waterloo, Department of Civil Engineering, May 2005.

[20] A.M. Peck, K.C. Hornbuckle, Environ. Sci. Technol. 38 (2004) 367–372.
[21] M.E. Balmer, H.-R. Buser, M.D. Müller, T. Poiger, Environ. Sci. Technol. 39 (2005) 953–962.
[22] S.S. Verenitch, C.J. Lowe, A. Mazumder, J. Chromatogr. A 1116 (2006) 193–203.
[23] Z. Moldovan, Chemosphere 64 (2006) 1808–1817.
[24] D.A. Lambropoulou, D.L. Giokas, V.A. Sakkas, T.A. Albanis, M.I. Karayannis, J. Chromatogr. A 967 (2002) 243–253.
[25] D.L. Giokas, V.A. Sakkas, T.A. Albanis, J. Chromatogr. A 1026 (2004) 289–293.
[26] T. Poiger, H.-R. Buser, M.E. Balmer, P.-A. Bergqvist, M.D. Müller, Chemosphere 55 (2004) 951–963.
[27] H.-B. Lee, T.E. Peart, M.L. Svoboda, J. Chromatogr. A 1094 (2005) 122–129.
[28] J.L. Santos, I. Aparicio, E. Alonso, M. Callejón, Anal. Chim. Acta 550 (2005) 116–122.
[29] J.L. Santos, I. Aparicio, E. Alonso, Environ. Int. 33 (2007) 596–601.
[30] R. Hirsch, T. Ternes, K. Haberer, K.-L. Kratz, Sci. Total Environ. 225 (1999) 109–118.
[31] J.D. Cahill, E.T. Furlong, M.R. Burkhardt, D. Kolpin, L.G. Anderson, J. Chromatogr. A 1041 (2004) 171–180.
[32] S. Castiglioni, R. Bagnati, D. Calamari, R. Fanelli, E. Zuccato, J. Chromatogr. A 1092 (2005) 206–215.
[33] B.J. Vanderford, R.A. Pearson, D.J. Rexing, S.A. Snyder, Anal. Chem. 75 (2003) 6265–6274.
[34] M. Gross, M. Petrović, D. Barceló, Talanta 70 (2006) 678–690.
[35] M. Petrović, M. Gros, D. Barceló, J. Chromatogr. A 1124 (2006) 68–81.
[36] M. Petrović, M.D. Hernando, M.S. Díaz-Cruz, D. Barceló, J. Chromatogr. A 1067 (2005) 1–14.
[37] B. Kasprzyk-Hordern, R.M. Dinsdale, A.J. Guwy, J. Chromatogr. A 1161 (2007) 132–145.
[38] N.M. Vieno, T. Tuhkanen, L. Kronberg, J. Chromatogr. A 1134 (2006) 101–111.
[39] Prescription cost analysis, Wales, 2004, www.wales.nhs.uk.
[40] Prescription cost analysis, England, 2005, www.ic.nhs.uk.
[41] Household Products Database, United States National Library of Medicine, http://householdproducts.nlm.nih.gov/index.htm.
[42] J.B. Quintana, T. Reemtsma, Rapid Commun. Mass Spectrom. 18 (2004) 765–774.
[43] M.J. Gómez, M. Petrović, A.R. Fernández-Alba, D. Barceló, J. Chromatogr. A 1114 (2006) 224–233.

Available online at www.sciencedirect.com
ScienceDirect
Talanta 74 (2008) 1654–1658
Talanta
www.elsevier.com/locate/talanta

Diazo-coupled calix[4]arenes for qualitative analytical screening of metal ions

Tae Hyun Kim [a], Su Ho Kim [b], Le Van Tan [c], Yunyan Dong [a], Hasuck Kim [a,**], Jong Seung Kim [b,*]

[a] *Department of Chemistry, Seoul National University, Seoul 151-747, Republic of Korea*
[b] *Department of Chemistry, Korea University, Seoul 136-701, Republic of Korea*
[c] *Faculty of Chemical Engineering, Ho Chi Minh City University of Industry, Ho Chi Minh, Viet Nam*

Received 10 September 2007; received in revised form 12 October 2007; accepted 12 October 2007
Available online 26 October 2007

Abstract

New chromogenic diazophenylcalix[4]arenes **1** and **2** were synthesized in cone conformation. Compound **1** with the *ortho*-carboxyl groups in CH_3CN solution preferentially binds with alkaline earth and transition metal ions, whereas no significant changes in absorption spectra are observed in the presence of alkali metal ions. While **2** with the *ortho*-ester groups shows selective complexation properties towards transition metal ions over alkali and alkaline earth metal ions. The detection of metal ions gives rise to bathochromic shifts in the absorption spectra (from orange/yellow to red), which is clearly visible even to the naked eye. According to the selective color changes using both receptors upon cation complexation, one can set up a qualitative analytical routine to screen alkali, alkaline earth, and transition metal ions.
© 2007 Elsevier B.V. All rights reserved.

Keywords: Calix[4]arenes; Chromoionophores; Complexation; Metal ion

1. Introduction

Color reaction provides chemists a great deal of chemical information [1]. Color change is a direct indication of reaction taking place, and its intensity is a measure of the extent of its progress [1]. Chromoionophores are colored ionophores, which are composed of two different functional groups: an ionophore, recognizing specific ions, and a chromophore, transducing the chemical information produced by the ionophore–ion interaction into an optical signal [2]. Since cation binding is sensitive to the ligand environment, the binding equilibrium constant can be effectively controlled by employing a chromoionophore system where a supramolecule is bound intramolecularly to a signaling moiety which is responsive to an external stimuli [3]. A very interesting signaling moiety is the azophenol group because of its pronounced chromogenic behavior towards a variety of cations, and even chiral amines when coupled to crown ethers or calixarenes [4], which in most cases exhibited large bathochromic shifts in the UV–vis spectra upon complexation with ions. Among the azophenolic supramolecules, azocalix[4]arenes are especially attractive for their efficient ionophoric properties towards some of important guest ions such as Ca^{2+} or K^+ ion [5].

During the last two decades, calixarenes have attracted much interest because of their unique molecular structure, and have been extensively investigated as hosts for a wide range of metal ions [5,6]. Particularly, calixarene chromoionophores have long been studied as specific metal ion indicators since Shinkai and co-workers reported that calix[4]arene having one 4-(4-nitrophenyl)azophenol unit with three ethyl ester groups shows a Li^+ ion selectivity with respect to the UV–vis band shift [7]. The 4-(4-nitrophenyl)azo group has frequently been used in calixarene-based chromoionophores. Because azo group is usually considered to be only a chromogenic center and not a metal-chelating site; to enhance the metal-binding ability, a great number of attempts have been made at the modification of their lower rim (phenolic OH groups) in azocalix[4]arene [8]. However, azocalix[4]arenes without lower rim

* Corresponding author.
** Corresponding author.
E-mail addresses: hasuckim@snu.ac.kr (H. Kim), jongskim@korea.ac.kr (J.S. Kim).

0039-9140/$ – see front matter © 2007 Elsevier B.V. All rights reserved.
doi:10.1016/j.talanta.2007.10.033

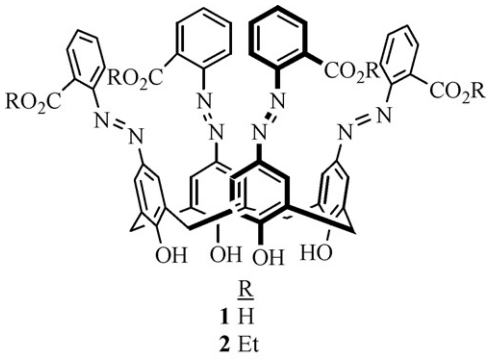

Fig. 1. Structures of azocalix[4]arene **1** and **2**.

modification are able to bind transition metal ions effectively [8,9].

Recently, we also reported that 5,11,17,23-tetra[(2-ethyl acetoethoxyphenyl)(azo)phenyl]calix[4]arene (**2**, Fig. 1) without lower rim modification binds transition metal ions selectively, which shows bathochromic shifts in the UV–vis spectra upon complexation with ions [10]. This may be because transition metal ion enhances the formation of hydrazone from azophenol to quinone–hydrazone tautomerization [8,9,11].

Our research group has been also interested in the designing selective coloring sensor (calixarene chromophores) towards specific metal cations [12–14]. In the end, we found an outstanding result that combinational use of the two molecules **1** and **2** is able to selectively discriminate alkali, alkaline earth, and transition metal ions (Fig. 1). Then we report now for the first time the discrimination system towards almost all metal ions, which can be pretty much useful in analytical chemistry.

2. Experimental

2.1. Synthesis and reagents

5,11,17,23-tetra[(2-ethyl acetoethoxyphenyl)(azo)phenyl] calix[4]arene (**1**) and 5,11,17,23-tetra[(2-benzoic acid) (azo)phenyl]calix[4]arene (**2**) were synthesized according to the procedure in the previous studies [10,15]. All reagents in the experiment were purchased from Aldrich and used without further purifications.

2.2. UV–vis spectrophotometry and titration

Absorption spectra were measured with a Sinco-S3130 UV–vis recording spectrophotometer (Korea). Stock solutions of iononphore (2×10^{-4} M, in CH_3CN) and metal perchlorate (2×10^{-2} M, in CH_3CN) were prepared. The metal solution was diluted 10 and 100 times to give 2×10^{-3} and 2×10^{-4} M solutions. Aliquots of metal solution were added to the ionophore solution, and the final concentration and composition of the solution were adjusted to the desired value by adding extra CH_3CN.

The stability constants (K_a) for complexation between ionophore and metal cations were determined on the basis of the nonlinear curve fitting procedure for a 1:1 complex:

$$r = \frac{A - A_f^0}{A_c - A_f^0} + \frac{A - A_f^0}{C_f^0 K_a (A_c^0 - A)} \quad (1)$$

where r is the added equivalents of cations, A_f^0, A and A_c^0 are absorbance of the free ligand, the ligand plus r equivalents of cations and the ligand plus large excess cation solutions. C_f^0 is the concentration of the free ligand and K_a is the stability constant [16].

3. Results and discussion

3.1. Chromogenic properties

The chromogenic ionophore properties of **1** and **2** were investigated by examining the UV–vis absorption behavior of the host in CH_3CN solution (Fig. 2). Many investigations indicated that azocalix[4]arenes may exist in two possible tautomeric forms, namely an azophenol form and quinone–hydrazone form [8,12,14,17]. The visible spectral properties and tautomeric equilibrium of the azocalix[4]arene derivatives change according to the substituents of azocalix[4]arene [17]. In the present case, **1** and **2** showed typical UV spectral behavior of azocalix[4]arene derivatives and their absorption maxima are located at 355 and 345 nm, respectively. However, **1** exhibited a weaker absorption band than that of **2** at 355 nm and a shoulder at around 480 nm, while absorption maxima of **2** are located at 345 and 487 nm corresponding to π–π* and n–π* transitions, respectively, which are in accordance with typical diazo spectra [8,12,14,17].

A pair of characteristic bands of **1** and **2** in the UV–vis absorption spectra indicated that **1** and **2** exist as a mixture of the two tautomeric forms in CH_3CN solution [11,17]. This can be explained by the assumption that an azophenol form of **1** or **2** gets stabilized through a six-membered hydrogen

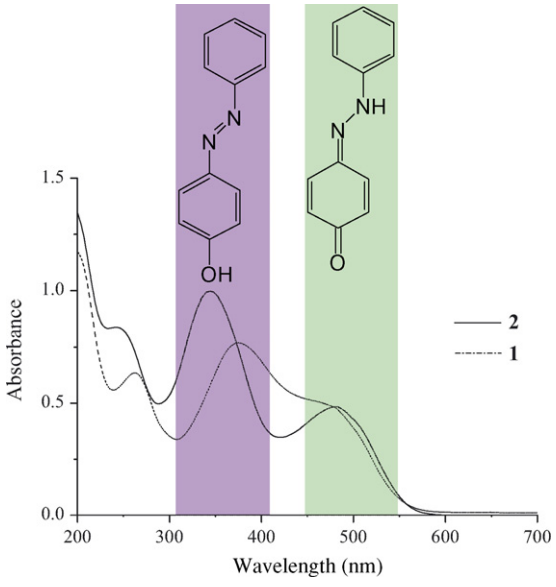

Fig. 2. Absorption spectra of **1** and **2** (2×10^{-5} M) in CH_3CN.

Table 1
Stability constants for the complexation of **1** and **2** with various metal ion perchlorates in CH_3CN at room temperature[a]

Metal ions	Stability constants (K_a)	
	Host **1**	Host **2**
Mg^{2+}	2.6×10^4	–
Ca^{2+}	6.0×10^4	–
Sr^{2+}	1.9×10^4	–
Ba^{2+}	1.6×10^4	–
Cr^{3+}	6.1×10^5	4.4×10^3
Fe^{2+}	2.8×10^3	1.4×10^3
Co^{2+}	6.8×10^3	–
Ni^{2+}	3.4×10^3	–
Cu^{2+}	6.2×10^4	2.1×10^4
Zn^{2+}	4.6×10^3	2.0×10^4
Pb^{2+}	3.5×10^3	5.5×10^3

'–' represents the spectral changes are too small to allow the calculation of the stability constants.
[a] Stability constants were determined by nonlinear fitting curve procedure from spectroscopic data.

bonded structure between nitrogen atom of azo unit and hydrogen atom of *o*-carboxyl group, or *o*-ester group represented by a quinone–hydrazone form [11].

3.2. Complexation behavior

We next investigated the affinity of **1** and **2** for a series of alkali, alkaline earth and transition metal ions. On the basis of UV band changes upon the addition of alkaline earth and transition metal ion to CH_3CN solution of **1** and **2**, their association constants were obtained and are listed in Table 1. Absorption spectra of 0.02 mM **1** and **2** in the presence of 1 equiv. of metal ions are shown in Figs. 3–5. Only minor changes in absorption spectra were seen when alkali metal ions were added to **1** (Fig. 3), whereas marked bathochromic shifts were observed for alkaline earth (Fig. 4) and transition metal ions (Fig. 5). In the case of **2**, alkali and alkaline earth metal ions did not show any significant absorption in the spectral range scanned, while

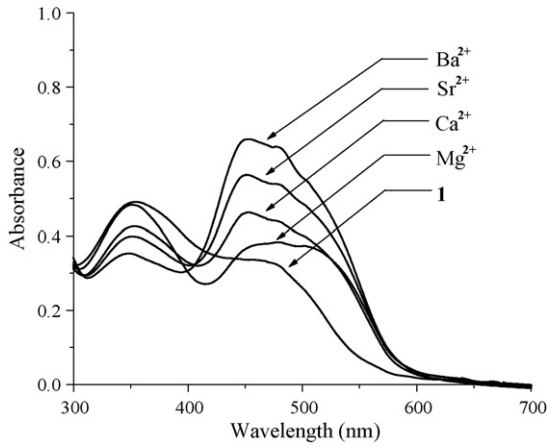

Fig. 4. Absorption spectra of **1** (2×10^{-5} M) with various alkaline earth metal ions (2×10^{-5} M) in CH_3CN.

addition of transition metal ions caused bathochromic shifts of absorption spectra [10].

Complexation of transition metal ions for compound **1** or **2** probably affects the equilibrium of tautomeric forms and there is a subtle balance between metal complexation-induced release of protons from the azophenols to the quinone–hydrazone tautomer [8,9]. Both the *o*-carboxyl and the *o*-ester groups of **1** and **2**, respectively, can stabilize the quinone–hydrazone form in azo calixarenes after adding transition metal ions.

In the case of azocalix[4]arenes with cone conformation, metal ion is able to interact with the phenol unit of the lower rim and azo group in the medium cavity. However, due to the intramolecular hydrogen bonding of lower rim, metal ions may be accommodated within the region of the medium cavity of the calixarene [9,18]. This arrangement could facilitate simultaneously π–π interactions between metal ions and the negative change center of **1** [9]. In the case of **1**, alkaline earth and transition metal ions can be bound more strongly to the polar cavity defined by the *o*-carboxylates and azo groups than monovalent alkali metal ions, whereas the binding of **2** with alkaline earth metal ions is weaker due to the lower polarity of *o*-ester group of **2**.

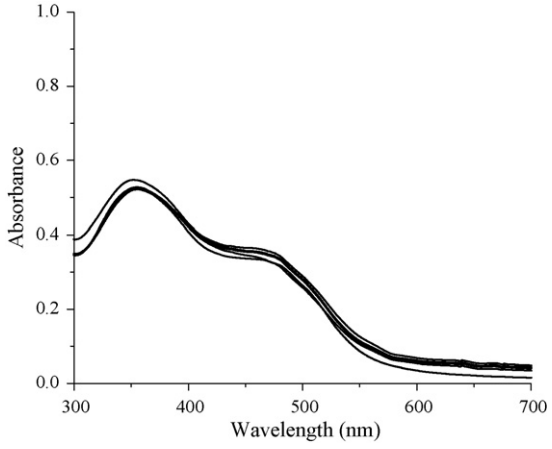

Fig. 3. Absorption spectra of **1** (2×10^{-5} M) with various alkali metal ions (2×10^{-5} M) in CH_3CN.

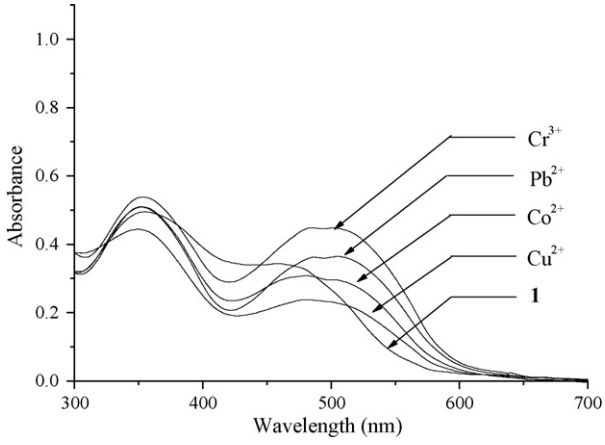

Fig. 5. Absorption spectra of **1** (2×10^{-5} M) with various transition metal ions (2×10^{-5} M) in CH_3CN.

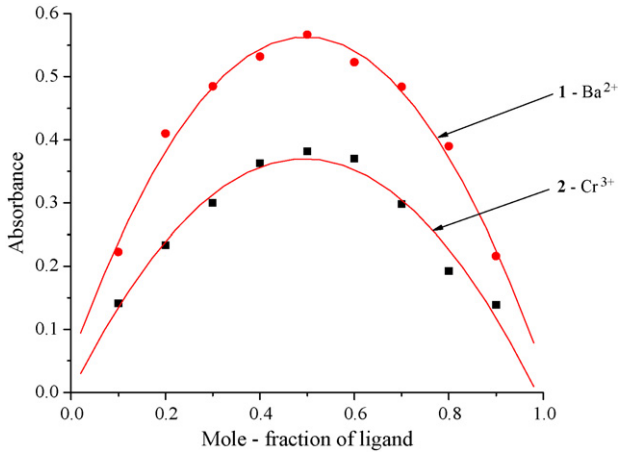

Fig. 6. Job's continuous variation plots for **1**-Br^{2+} at 505 nm and **2**-Cr^{3+} at 487 nm ([ligand] + [M^{n+}] = 2×10^{-5} mol L^{-1}).

For the stoichiometric ratio between host and metal ion, the Job's plot experiment was conducted by varying the concentration of both host and metal ion. Fig. 6 shows typical Job's plots of both host–metal complexations. Job's plot plotting experiment of **1**-Ba^{2+} was conducted at 481 nm where complex showed maximum intensity and Job's plot for **2**-Cr^{3+} was obtained at 487 nm. The maximum point at the mole fraction was about 0.5 which refers to a ligand–metal complex ratio of 1:1 as shown in Fig. 6.

In order to have a further insight into the chromogenic behavior of hosts, the absorption profile as a function of metal ion concentration was obtained. Fig. 7 shows characteristic absorption spectra in the spectrophotometric titration of both ligands with metal ions. A well-defined isosbestic point was observed in all cases. Fig. 7 shows UV band changes of **1** upon the addition of Ba^{2+}. The absorption peak at 355 nm shifts to 481 nm and grows largely at the expense of the oxidation peak at 355 nm as the concentration of the Ba^{2+} ion increases in the complexation of **1** with Ba^{2+}. Similarly, **2** exhibited a gradual increase in absorption intensity at the λ_{max} of 487 nm and a decrease at the λ_{max} of 345 nm upon the addition of incremental lead ions [10]. As a result, the plausible complexation mechanism based on the 1:1 complexation is proposed [10].

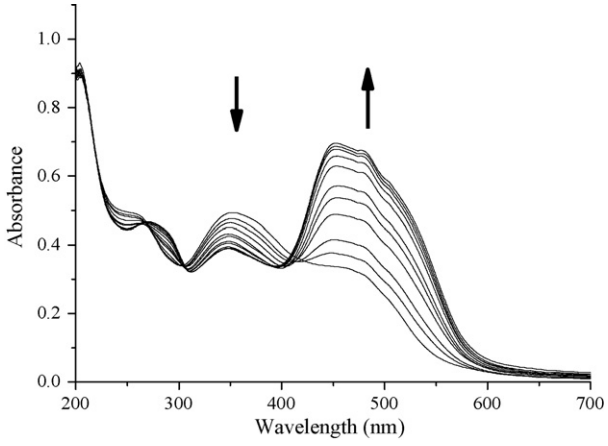

Fig. 7. Absorption spectra of **1** (2×10^{-5} M) with the increasing concentration of Ba^{2+} (10^{-6}–2.0×10^{-5} M).

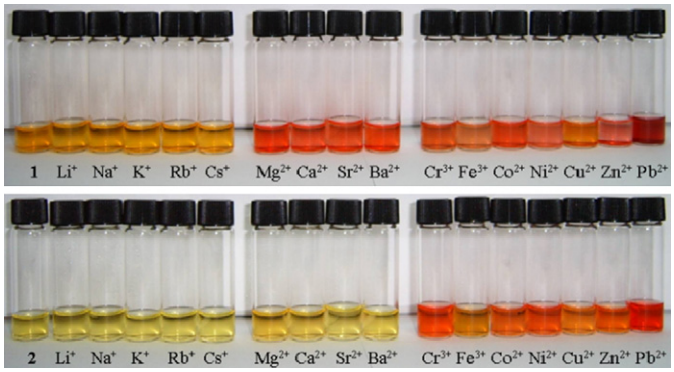

Fig. 8. Color changes of **1** and **2** (2×10^{-5} M) upon the addition of various metal ions (2×10^{-3} M) in CH_3CN.

3.3. Simple screening of metal ions with 'naked eye'

The visible color changes of **1** and **2** upon various metal cations were also observed and depicted in Fig. 8. The color of acetonitrile solution of **1** turned orange to red in the presence of alkaline earth and transition metal ions, and that of **2** turned yellow to deep orange in transition metal ions.

In this unique point of view with visual color changes, we can consequently demonstrate the screening process of the unknown metal ions with following two steps and its flow chart is given in Fig. 9.

(1) Add excess amount of unknown metal ion into a CH_3CN solution of **1**. If any visual change from orange to red is observed, the unknown metal ions must be either an alkaline earth metal ion or a transition metal ion, so the alkali metal ion is excluded. (2) Then add the unknown metal ion into acetonitrile solution of **2** again. It must be a transition metal ion if there is a color change from yellow to red. If not, it is an alkaline earth metal ion. In consequence, the use of a combination of **1** and **2** give us an informative clue to screen the metal ions (alkali, alkaline earth, or transition metal ion). This routine applies only to one group of ions, if the sample contains ions of different groups, prior separation steps are necessary.

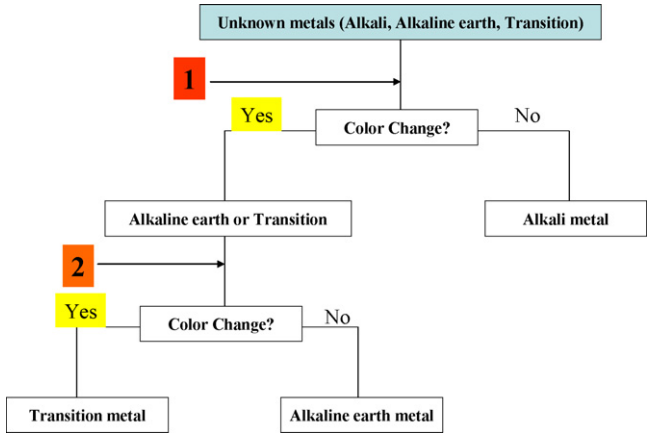

Fig. 9. Flow-chart for the determination of the metal ions.

4. Conclusions

We have developed simple qualitative analysis for screening of metal ions using the diazocalix[4]arenes based on the colormetry. In these diazocalix[4]arenes, **1** with the *ortho*-carboxyl groups in acetonitrile solution preferentially complexed alkaline earth and transition metal ions, whereas no significant changes in absorption spectra are observed in the presence of alkali metal ions. **2** with the *ortho*-ester groups showed selective complexation properties towards transition metal ions over alkali and alkaline earth metal ions. The detection of metal ions gives rise to bathochromic shifts in the absorption spectra (from orange/yellow to red), which is clearly visible to the naked eye. Complexation of metal ions probably affects the equilibrium of tautomeric forms and the polarity of *ortho*-substituents in azocalixarene derivatives may have an effect on binding strength of complexes. For the recognition of a specific metal ion, the detailed spectrophotometric and electrochemical studies of these novel structures in the various pH solutions are currently in progress.

Acknowledgements

This work was supported by the SRC program (JSK, R11-2005-008-02001-0(2007)) and Korea Research Foundation (no. 2005-C00101). Also HK acknowledges the financial support by the MOCIE through the Strategic National R&D Program on Nano Biochips in 2002 (M1-0213-05-0001) and the SRC program of MOST/KOSEF through the Center for Intelligent Nano-Bio Materials at Ewha Womans University (R11-2005-008-00000-0).

References

[1] Y. Inoue, G.W. Gokel, Cation Binding by Macrocycles: Complexation of Cationic Species by Crown Ethers, M. Dekker, New York, 1990.
[2] I.K. Lednev, M.C. Petty, J. Phys. Chem. 98 (1994) 9601.
[3] F.Y. Li, L.P. Jin, Y.Y. Huang, C.H. Huang, J. Zheng, J.Q. Guo, J. Mater. Chem. 11 (2001) 1783.
[4] J.L. Atwood, J.M. Lehn, Comprehensive Supramolecular Chemistry, 1st ed., Pergamon, Oxford, UK, 1996.
[5] Z. Asfari, Calixarenes 2001, Kluwer Academic Pub, Dordrecht, The Netherlands, 2001.
[6] C.D. Gutsche, Calixarenes Revisited, Royal Society of Chemistry, Cambridge, UK, 1998.
[7] H. Shimizu, K. Iwamoto, K. Fujimoto, S. Shinkai, Chem. Lett. (1991) 2147.
[8] I.T. Ho, G.H. Lee, W.S. Chung, J. Org. Chem. 72 (2007) 2434.
[9] T.L. Kao, C.C. Wang, Y.T. Pan, Y.J. Shiao, J.Y. Yen, C.M. Shu, G.H. Lee, S.M. Peng, W.S. Chung, J. Org. Chem. 70 (2005) 2912.
[10] T.H. Kim, S.H. Kim, L. Van Tan, Y.J. Seo, S.Y. Park, H. Kim, J.S. Kim, Talanta 71 (2007) 1294.
[11] H.M. Chawla, M. Nanda, Arkivoc (2003) 171.
[12] J.S. Kim, O.J. Shon, J.K. Lee, S.H. Lee, J.Y. Kim, K.M. Park, S.S. Lee, J. Org. Chem. 67 (2002) 1372.
[13] J.S. Kim, O.J. Shon, S.H. Yang, J.Y. Kim, M.J. Kim, J. Org. Chem. 67 (2002) 6514.
[14] J.Y. Kim, G. Kim, C.R. Kim, S.H. Lee, J.H. Lee, J.S. Kim, J. Org. Chem. 68 (2003) 1933.
[15] L.V. Tan, D.T. Quang, M.H. Lee, T.H. Kim, H. Kim, J.S. Kim, Bull. Korean Chem. Soc. 28 (2007) 791.
[16] C.D. Chriswell, A.A. Schilt, Anal. Chem. 47 (1975) 1623.
[17] F. Karci, I. Sener, H. Deligoz, Dyes Pigments 59 (2003) 53.
[18] T.C. Kram, I.S. Lurie, Forensic Sci. Int. 55 (1992) 131.

Available online at www.sciencedirect.com
ScienceDirect
Talanta 74 (2008) 1670–1674
Talanta
www.elsevier.com/locate/talanta

Short communication

Isotachophoretic separation of selected imidazolium ionic liquids

Przemysław Kosobucki, Bogusław Buszewski *

Department of Environmental Chemistry and Bioanalytics, Faculty of Chemistry, Nicolaus Copernicus University, 7 Gagarin Street, 87–100 Toruń, Poland

Received 25 October 2006; received in revised form 27 August 2007; accepted 30 August 2007
Available online 8 September 2007

Abstract

Results of determination of selected imidazolium ionic liquids by isotachophoresis (ITP) with conductometric detection was presented. The effects of the molar mass of different ionic liquids on electrophoretic mobility was observed. The presented method was validated and basic validation parameters were determined. Limit of detection (LOD) in a 10 and 25 ng/L for anions and cations, respectively, is very satisfied. Thanks to its low cost and high rate, the presented method can be used in qualitative routine analysis as an alternative technique to liquid chromatography.
© 2007 Elsevier B.V. All rights reserved.

Keywords: Imidazolium ionic liquids; Isotachophoresis; Ecoanalytics

1. Introduction

Room-temperature ionic liquids (RTIL), salts that are liquid at ambient temperature, are normally composed of relatively large organic cations and inorganic or organic anions. Unlike molecular liquids, ionic liquids, being polar solvents, are environmentally benign, nonvolatile, nonflammable; most of them have good solubility in water and are stable in air [1]. In addition, by varying the lengths and branching of alkyl chains of the anionic core and the cationic precursor, it is possible to design solvents for specific applications. Because of these characteristic properties, ionic liquids are widely used as new solvent media in heterogeneous catalysis, organic synthesis, electrochemistry, sensors, battery applications, analysis and separation [1,2]. Typical ionic liquids consist of an organic cation with delocalized charges and a small anion, most often weakly coordinating fluoroanions such as BF_4 or PF_6 [3]. Table 1 presents primary structures of the room-temperature ionic liquids. Millions of possible cation and anion combinations offer their widely tunable properties with regard to polarity, hydrophobicity and solvent miscibility behavior [3,4].

Currently, scientists are interested in the applications of ionic liquids in separation and analysis. Reports on ionic liquids used as a modifier of background electrolytes (BGEs) in capillary electrophoresis (CE) appeared frequently [5–7]. Other scientists systematically studied the stationary phase of gas chromatography based on ionic liquids. Ionic liquids were used as additives in eluents to separate in high performance liquid chromatography (HPLC) [1,4,8] and countercurrent chromatography (CCC) [9].

Ionic liquids are more toxic xenobiotics and probably can be rating to persistent organic pollutants (POPs) [10]. From this point of view, analyses of ionic liquids in different parts of ecosystem (water, soils, sediments) are important and necessary. Therefore, the development of new analytical methods for the rapid and reproducible separation and identification of ionic liquids is a prerequisite for future biological and environmental research into these substances. Additionally, ionic liquids can yield photodegradation or biodegradation and analytical control of secondary products of these processes is also necessary.

Ionic liquids are already associated with the term "green" and "green chemistry", but only because they have got no measurable vapour pressure, it means that they emit no volatile organic compounds (VOCs). Knowledge about their toxicological and ecotoxicological properties is deficient in spite of great importance from ecological point of view.

Isotachophoresis (ITP) with direct conductivity detection is useful and powerful method for high-sensitive determination of both anionic and cationic species in environmental analysis

* Corresponding author. Tel.: +48 56 6114308; fax: +48 56 6114837.
E-mail address: bbusz@chem.uni.torun.pl (B. Buszewski).

0039-9140/$ – see front matter © 2007 Elsevier B.V. All rights reserved.
doi:10.1016/j.talanta.2007.08.043

Table 1
Primary structures of the room-temperature ionic liquids

Quaternary ammonium salts $[RyNH_{4-y}]^+X^-$	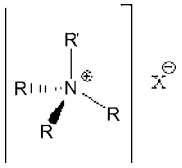
Imidazolium salts $[RR'IM]^+X^-$	
Pyrolidynium salts $[RR'Pyr]^+X^-$	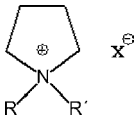
Phosphonium salts $[RyPH_{4-y}]^+X^-$	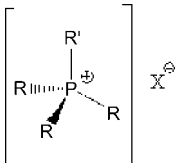
Pirydynium salts $[RPy]^+X^-$	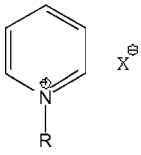

R,R′, alkyl substituent; X, anion (*e.g.* $AlCl_4^-$, BF_4^-, PF_6^-, Cl^-, Br^-, CH_3COO^-, CF_3COO^-); $y = 1, 2, 3, 4$.

of waters, wastewaters, sewage sludges and composts [11–20] and can be successfully used in ionic species (*eg.* ionic liquids) analysis.

The main aim of this study is to demonstrate the possibility of using a new isotachophoretic method to determination of selected room-temperature ionic liquids. The effects of the molar mass on different ionic liquids in the separation was observed. The methods quantitative analytical performance was satisfying and basic validation parameters were assigned.

2. Materials and methods

2.1. Instrumentation

An isotachophoretic analyzer EA 102 (Villa Labeco, Spisska Nova Ves, Slovakia) was used. This analyzer is provided with two FEP (fluoroethylenepropylene polymer) columns (a pre-separation one: 0.8 mm × 90 mm and an analytical one: 0.3 mm × 160 mm), two contact conductometric detectors, a sample loop 30 μL. Driving current in detection step was 50 μA in analytical column on both modes (anionic and cationic).

The isotachophoretic data were acquired and processed by an ITPPro 32 software (KasComp, Bratislava, Slovakia) installed on a Pentium computer.

2.2. Chemicals

Ammonium acetate was obtained from P.O.Ch. (Gliwice, Poland). Hydroxyethylcellulose, polyethylene glycol 600, tetrabutylammonium perchlorate were purchased from Sigma–Aldrich (Steinheim, Germany). All chemicals utilized for electrolytes, standard solutions, and sample preparation were pure per analysis (*p.p.a.)* class.

Deionised water was used from Milli-Q RG (Millipore, Molsheim, France).

The ionic liquids selected for these studies were obtained from the working group of Dr. Piotr Stepnowski (Faculty of Chemistry, Waste Management Laboratory, University of Gdańsk, Poland*).*

3. Results and discussion

Table 2 presents basic physicochemical properties of selected ionic liquids used in isotachophoretic experiments [21]. Five from them have got the same anion (BF_4) and different homologous imidazolium cations:

- PMIM (1-*n*-propyl-3-methyl-imidazolium cation),
- BMIM (1-butyl-3-methyl-imidazolium cation),
- AMIM (1-*n*-amyl-3-methyl-imidazolium cation),
- HMIM (1-*n*-hexyl-3-methyl-imidazolium cation),
- OMIM (1-*n*-octyl-3-methyl-imidazolium cation).

These abbreviations should be used in whole text.

Additionally, in experiments we used one ionic liquid with chloride anion.

Table 3 presents composition of leading (LE) and terminating (TE) electrolytes used to separate ionic liquids by isotachophoresis. Isotachophoresis worked in cationic and anionic analysis mode. Electrolytic systems were known earlier, but in this study we optimize driving current.

3.1. Cationic mode

Isotachophoresis working in cationic mode enables identification of cationic core of room-temperature ionic liquids. Fig. 1 shows results of identification of ionic liquids in model mixture using conductivity detection.

In Fig. 1, steps from all analytes are sharp and clear. Conductivity detection enables identification of [PMIM], [BMIM], [AMIM], [HMIM] and [OMIM], relative step heights (RSH) (parameter for qualitative analysis in isotachophoresis) of these cations are for [PMIM] 0.369, for [BMIM] 0.418, for [AMIM] 0.476, for [HMIM] 0.527 and for [OMIM] 0.626.

The advantage of conductivity detection is small error assign of RSH value. Standard deviation (S.D.) 0.023, 0.035, 0.03, 0.025 and 0.028 for [PMIM], [BMIM], [AMIM], [HMIM] and [OMIM], respectively, is admissible. Additionally, signal from conductivity detection is easy to interpretation.

In results of experiments we find interesting correlation between molar mass M_r of the RTIL and RSH value (Fig. 2).

Table 2
Physicochemical properties of selected ionic liquids [21]

No.	Chemical name	Chemical formula	Abbreviation	Structure	Molecular weight (g/mol)	λ_{max} (nm)
1	1-Butyl-3-methyl-imidazolium chloride	$C_8H_{15}N_2Cl$	[BMIM][Cl]	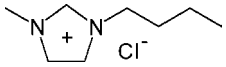	174	212
2	1-*n*-Propyl-3-methyl-imidazolium tetrafluoroborate	$C_7H_{13}N_2BF_4$	[PMIM][BF4]	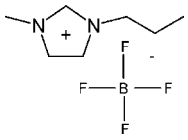	212	212
3	1-Butyl-3-methyl-imidazolium tetrafluoroborate	$C_8H_{15}N_2BF_4$	[BMIM][BF4]	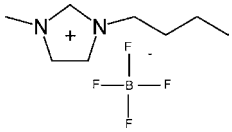	226	210
4	1-*n*-Amyl-3-methyl-imidazolium tetrafluoroborate	$C_9H_{17}N_2BF_4$	[AMIM][BF4]	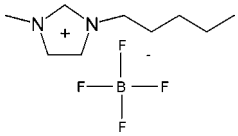	240	–
5	1-*n*-Hexyl-3-methyl-imidazolium tetrafluoroborate	$C_{10}H_{19}N_2BF_4$	[HMIM][BF4]	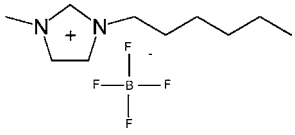	254	–
6	1-*n*-Octyl-3-methyl-imidazolium tetrafluoroborate	$C_{12}H_{25}N_2BF_4$	[OMIM][BF4]	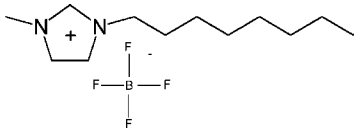	282	–

Probably this correlation enables to predict of identification of other homologues imidazolium cations in samples without standards (from the ethyl- to the decyl-imidazolium). Further investigations are necessary in this area, but the first results confirm data obtained by Markuszewski et al. [22] by capillary zone electrophoresis determination of ionic liquids. Markuszewski found linear correlation between migration time (t_m) and molar mass of 10 ionic liquids (from methyl- to *n*-decyl-imidazolium homologues) with $R^2 = 0.9966$ [22].

In isotachophoretic investigations we find a significant linear correlation of $R^2 = 0.9992$ between relative step height

Table 3
Operational systems for isotachophoretic separations of ionic liquids

Parameter	Cations		Anions	
	LE	TE	LE	TE
Ion	NH_4^+	TBA^+	Cl^-	CITR
Concentration (Mm)	10	5	8	2
Counter ion	CH_3COO^-	ClO_4^-	BALA	H^+
Co-counter ion	–	–	BTP	–
Concentrartion (Mm)	–	–	3 mM	–
pH	5.20	–	3.55	–
Additive	0.1% HEC	–	0.1% HEC	–

Where: LE, leading electrolyte; TE, terminating electrolyte; BALA, β-alanine; CITR, citric acid; BTP, 1,3-bis[tris(hydroxymethyl)-methylamino]propane; TBA^+, tetrabutylammonium cation; HEC, hydroxyethylcellulose.

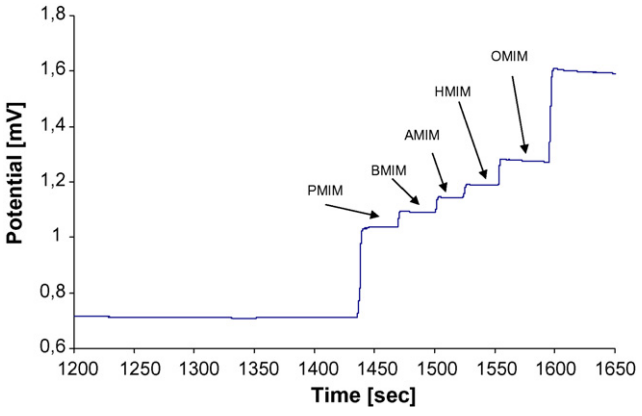

Fig. 1. Isotachophoregram of the standard mixture of ionic liquids of imidazolium cations obtained under optimum conditions. Running buffers – see Table 2, $I_2 = 50$ μA. Concentration of PMIM, BMIM, AMIM, HMIM and OMIM is 0.1, 0.1066, 0.1, 0.0874 and 0.0816 mmol/L, respectively.

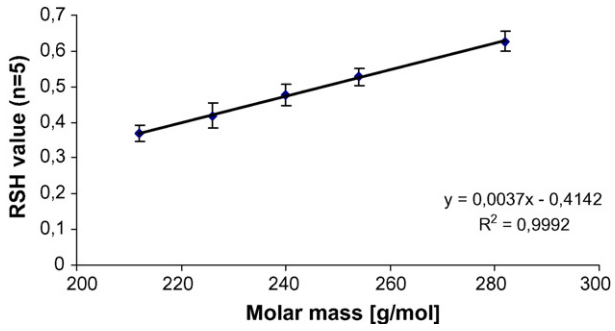

Fig. 2. Correlation between molar mass of RTIL and relative step height (RSH) value.

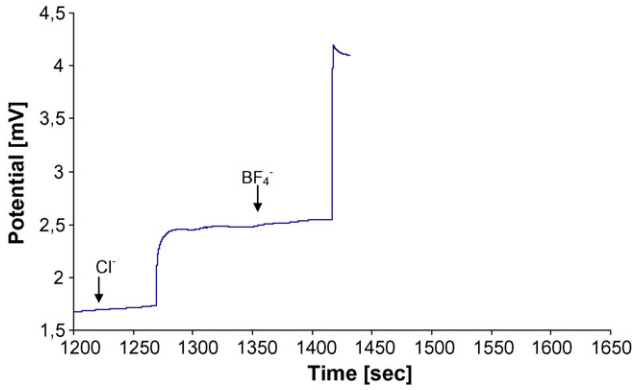

Fig. 3. Isotachophoregram of the standard mixture of ionic liquids of imidazolium anions obtained under optimum conditions. Running buffers – see Table 2, $I_2 = 50\,\mu A$. Concentration of BF_4^- and Cl^- is 0.369 and 0.1066 mmol/L, respectively.

and ionic liquids molar mass. Probably isotachophoretic procedure cannot separate cations with the same molar mass (with different cationic core, but the same molar mass). In experiments molar mass of examinated species were in narrow range (212–282 g/mol), but high value of R^2, allow to use this correlation below and above this range.

This study shows that isotachophoresis with direct conductivity detection is complementary technique to capillary zone electrophoresis (CZE) with UV detection. Similar data were obtained by Krivankova and Bocek [23]. Additionally, isotachophoresis in laboratory practice is cheaper techniques than CZE and finally the cost of single analysis is the lowest.

Total analysis time in cationic mode is about 20 min (using analytical column) and depends on complexity of mixtures (number of ionic liquids and its concentration).

3.2. Anionic mode

Isotachophoresis worked in anionic mode enables identification of anionic parts of room-temperature ionic liquids. Fig. 3 shows results of identification of ionic liquids in model mixture using conductivity detection.

In Fig. 3, we can see sharp and clear step of [BF_4]. RSH of this step is 0.346 ± 0.018 ($n = 5$). Chloride anion can be identified as lengthen of leading electrolyte signal. LE for anionic analysis contain Cl^- (Table 2), chloride from LE and from RTIL sum and finally we observe lengthen LE signal (this effect can be used in quantitative analysis as an internal standard method).

Total analysis time in anionic mode is about 20 min as for cationic one.

3.3. Quantitative analysis

Isotachophoretic method was validated. Precision, recovery and linearity were determined. Table 4 shows data obtained from validation and characteristics of qualitative and quantitative analyses. The presented method was characterized by wide range of linearity as well as by high precision that did not exceed 5%. The calibration curve method was used. Standards of examined species were injected (in duplicate) from water stock solutions at five levels (Table 4) utilizing sample valve with fixed volume (30 μL).

Under proposed isotachophoretic conditions (LE and TE electrolytes, current), all studied cations were analyzed in the analytical column in the 0.1–10.0 μg/L, chlorides 0.1–20.0 μg/L and tetrafluoroborate 0.1–12.0 μg/L. As repeatability of RSH is often a weak point of ITP analysis, these results demonstrate

Table 4
Method characteristics for the studied species

Characteristic	Units	Analytes						
		Anions		Cations				
		Cl^-	BF_4^-	PMIM	BMIM	AMIM	HMIM	OMIM
RSH		0.000 ± 0.000	0.346 ± 0.018	0.369 ± 0.023	0.418 ± 0.035	0.476 ± 0.030	0.527 ± 0.025	0.626 ± 0.028
Intra-assay[a]	%	1.9	2.8	4.1	4.5	4.4	4.3	4.8
Accuracy[b]	%	80.7 ± 8	91.4 ± 4	89.6 ± 4	88.2 ± 5	85.1 ± 7	82.3 ± 4	84.7 ± 8
Linearity[c]	μg/L	0.1–20.0	0.1–12.0	0.1–10.0	0.1–10.0	0.1–10.0	0.1–10.0	0.1–10.0
LOD[d]	ng/L	15	10	25	25	25	25	25
LOQ[e]	ng/L	45	30	75	75	75	75	75

Where: RSH—relative step height, parameter to isotachophoretic qualitative analysis.
[a] Repeated injection of the same sample, RSD, $n = 5$.
[b] Sample spiked with 2.5 mg/L analyte solution, $n = 3$.
[c] Correlation coefficient (min. 0.999).
[d] Based on the signal-to-noise ratio $n = 3$ (zones shorter than 0.1 s were treat as a noise).
[e] LOQ = 3LOD.

good performance of analytical conditions. The RSDs of zone length are also in reasonable good range from 1.9 to 2.8% for anions and from 4.1 to 4.8% for cations.

Limit of detection (LOD) on 10 ng/L for anions and 25 ng/L for cations is a more than satisfying and a few levels lower than CZE method (10 ppb for cations) [15] in comparable time. LOQ on 30–40 ng/L for anions and 75 ng/L for cations is very suffice and shows than ITP can be suitability in routine analysis.

4. Concluding remarks

The presented results allow to state that the isotachophoresis offers a very promising alternative to the chromatographic methods for analysis of the ionic liquids. Possibility of determination of cationic and anionic core of room-temperature ionic liquids in reasonable time (up to 20 min in cationic mode) is the main advantage of ITP in this type of analysis.

In water or wastewater samples no sample pre-treatment or only filtration is required before analysis. In analysis of solid samples (soils, sediments) before analysis extraction techniques are necessary.

Results clearly show that the method is suitable for the analysis of ionic liquids in standard solutions and probably in environmental samples.

Thanks to its low cost and high rate isotachophoresis could be useful in routine analysis. Resolution of all analytes in the presented study is more than sufficient.

Acknowledgements

This work was supported by a grant No. 3 T09D 035 29 and 2 P04G 083 29 from the Ministry of Education and Science (Warsaw, Poland).

The support of Dr. Piotr Stepnowski (University of Gdańsk, Poland) for this study is gratefully acknowledged, especially for samples of ionic liquids.

References

[1] X. Xiaohua, Z. Liang, X. Liu, S. Jiang, Anal. Chim. Acta 519 (2004) 207.
[2] P. Stepnowski, Anal. Bioanal. Chem. 381 (2005) 189.
[3] P. Stepnowski, A. Zaleska, J. Photochem. Photobiol. A 170 (2005) 45.
[4] B. Buszewski, S. Kowalska, P. Stepnowski, J. Sep. Sci. 29 (2006) 1116.
[5] M. Vaher, M. Koel, M. Kaljurand, J. Chromatogr. A 979 (2002) 27.
[6] T.F. Jiang, Y.L. Gu, B. Liang, J.B. Li, Y.P. Shi, Q.Y. Ou, Anal. Chim. Acta 479 (2003) 249.
[7] P.H. Shetty, P.J. Youngberg, B.R. Kersten, C.F. Poole, J. Chromatogr. 411 (1987) 61.
[8] P. Stepnowski, A. Muller, P. Behrend, J. Rauke, J. Hoffmann, B. Jastorf, J. Chromatogr. A 993 (2003) 173.
[9] A. Berthod, S. Carda-Broch, Anal. Bioanal. Chem. 380 (2004) 168.
[10] A. Latała, P. Stepnowski, M. Nędzi, W. Mrozik, Aquat. Toxicol. 73 (2005) 91.
[11] P. Blatny, F. Kvasnicka, E. Kenndler, J. Chromatogr. A 757 (1997) 297.
[12] R. Bodor, V. Madajova, D. Kaniansky, M. Masar, M. Johnck, B. Stanislawski, J. Chromatogr. A 916 (2001) 155.
[13] J. Polonsky, A. Horvathova, M. Panik, J. Chromatogr. 390 (1987) 141.
[14] P. Praus, Talanta 62 (2004) 977.
[15] F. Kvasnicka, V. Janda, D. Rousova, J. Manda, L. Kollerova, CEJC 3 (2005) 137.
[16] M. Hutta, E. Simunicova, D. Kaniansky, J. Tkacova, J. Brtko, J. Chromatogr. 470 (1989).
[17] P. Gebauer, P. Bocek, Electrophoresis 23 (2002) 3858.
[18] P. Kosobucki, B. Buszewski, Toxicol. Environ. Chem. 19 (2001) 109.
[19] P. Kosobucki, B. Buszewski, Chem. Anal. (Warsaw) 48 (2003) 555.
[20] P. Kosobucki, B. Buszewski, J. Liq. Chromatogr. Rel. Technol. 13 (2006) 1951.
[21] http://eckehaat.uft.uni-bremen.de/FB3/Ionische_Fluessigkeiten.
[22] M.J. Markuszewski, P. Stepnowski, M.P. Marszałł, Electrophoresis 25 (2004) 3450.
[23] L. Krivankova, P. Bocek, J. Chromatogr. B 689 (1997) 13.

Available online at www.sciencedirect.com
ScienceDirect
Talanta 74 (2008) 1455–1462
Talanta
www.elsevier.com/locate/talanta

Critical comparison of automated purge and trap and solid-phase microextraction for routine determination of volatile organic compounds in drinking waters by GC–MS

Azucena Lara-Gonzalo [a], José Enrique Sánchez-Uría [a], Eva Segovia-García [b], Alfredo Sanz-Medel [a,*]

[a] *Department of Physical and Analytical Chemistry, University of Oviedo, C/ Julian Clavería 8, 33006 Oviedo, Spain*
[b] *Laboratorio de Salud Pública del Principado de Asturias, C/ Camino de Rubin s/n, 33011 Oviedo, Spain*

Received 10 April 2007; received in revised form 7 September 2007; accepted 28 September 2007
Available online 2 October 2007

Abstract

The use of two automated sample preparation techniques, solid-phase microextraction (SPME) and purge and trap (P&T) systems are critically compared for the GC–MS determination of eight volatile organic compounds (VOCs), including trihalomethanes (THMs), in drinking water samples. Compounds chosen for the comparison are regulated by Spanish and European official guidelines for drinking waters. Experimental parameters investigated for the two sample preparation techniques included SPME type of fibers, SPME modality, P&T gas flow, extraction and desorption times and desorption temperatures. Thus, optimal experimental conditions have been worked out for the SPME and P&T techniques. Under such optimised conditions, detection limits, precision and accuracy were evaluated. Both methods fulfilled the values that the official guidelines establish. The P&T–GC–MS method offers LDs ranged from 0.004 to 0.2 ng mL^{-1}, repeatabilities below 6% and recoveries between 81 and 117%; while LDs ranging from 0.008 to 0.7 ng mL^{-1}, 1–12% R.S.D. and recoveries from 80 to 119% were achieved with the SPME–GC–MS method. Finally, we chose P&T–GC–MS method as the best for this determination and we validate this methodology by its application to the analysis of an Aquacheck Interlaboratory Exercise.
© 2007 Elsevier B.V. All rights reserved.

Keywords: P&T; DI-SPME; GC–MS; THMs; VOCs; Water samples

1. Introduction

Drinking water may be contaminated by volatile organic compounds (VOCs) as a consequence of disinfection processes using of chlorine or its derivatives in drinking water treatment plants, urban discharges or farming and industrial activities [1–3]. Trihalomethanes (THMs), the main class of VOCs present in waters, have the general formula CHX_3 where X may be Cl, Br or their combinations (i.e. chloroform, bromodichloromethane, dibromochloromethane and bromoform). Such compounds are produced by reactions of available chlorine reacting with organic matter (humic and fulvic acids) and bromide ions present in dinking waters [4].

VOCs have adverse effects on human health, even at very low concentrations, as they have toxic, carcinogenic or mutagenic properties [5,6]. Therefore analytical monitoring of VOCs in drinking water is a subject of concern and active research today. Regulatory values of some VOCs in drinking water were established by a European Directive of 1998 in the European Union [7] and more recently by a Real Decreto in Spain [8]. The maximum level permitted in dinking water for "total THMs" has been set at 150 μg L^{-1} (to be reduced to 100 μg L^{-1} on 31 December 2008). Also, both official guidelines recommend analytical control in waters of other four related compounds: trichloroethylene, tetrachloroethylene, benzene and 1,2-dichloroethane. In this vein, the sum of trichloroethylene and tetrachloroethylene levels must be lower than 10 μg L^{-1}, while for 1,2-dichloroethane the threshold limit is 3 μg L^{-1} and for benzene of 1 μg L^{-1} [7,8].

An appropriate technique for VOCs determination is capillary gas chromatography (GC) due to its unique features, including

* Corresponding author. Tel.: +34 98 5103474; fax: +34 98 5103125.
E-mail address: asm@uniovi.es (A. Sanz-Medel).

0039-9140/$ – see front matter © 2007 Elsevier B.V. All rights reserved.
doi:10.1016/j.talanta.2007.09.036

extremely high separation efficiency plus its ability to be directly coupled to mass spectrometry (GC–MS) for unambiguous identification and quantification. Unfortunately VOC concentration levels found in drinking and natural water samples are typically in the order of ppt (ng L^{-1}) to ppb (μg L^{-1}) [9] and these levels are generally too low for direct GC analysis. As a result, a preconcentration step is mandatory prior to such analysis.

Growing interest in the development and optimization of reliable and robust extraction, trapping and/or preconcentration techniques has resulted into intensive research [9]. The techniques used for sample preparation and preconcentration of VOCs from waters include liquid–liquid extraction (LLE) [5,10], head space (HS) [5,6,10], solid-phase microextraction (SPME) [1,11,12] and purge and trap (P&T) [1,3,4,13,14]. There is an increasing tendency for solid-phase microextraction-based preconcentration techniques [15]. SPME, developed by Pawliszyn et al. in 1989 [16,17], is based on the establishment of the analyte equilibrium between the sample and a polymeric coating on a fused silica fiber. The analytes retained in the coating are then desorbed by heating into a gas chromatograph (GC) injection port. This technique is simple, fast, inexpensive, portable and solvent-free and it can integrate sampling, extraction, preconcentration and sample introduction in one step [18]. In fate, SPME is applied today to the determination of many organic compounds including PAHs [19], pesticides [20], PCBs [21] in different sample types.

On the other hand, P&T is used to remove the volatile compounds from a liquid or solid matrix by an inert gas flow and has been applied in waters [2,6], snow [14], soils [22], body fluids [23], biological tissues [24] and beverages [4]. Later the volatile compounds are also introduced in a GC injection port. P&T is a solvent-free technique which became the technique of choice in the EPA [25] and standard [26] methods for the determination of VOCs. As in SPME, P&T integrates extraction, concentration and sample introduction in just one step using a solid trap [2–4] (although sometimes a cryogenic trap [14] can be used).

The aim of this work is to compare the analytical performance of both sample treatment methods (SPME and P&T) coupled to capillary gas chromatography–mass spectrometry (GC–MS) for simultaneous determination of eight VOCs (to be determined in waters to enforce European legislation) and the application of the selected P&T–GC–MS methodology to Spanish real drinking water samples.

2. Experimental

2.1. Chemicals, reagents and samples

The studied VOCs pure standards (>99.0%) were purchased from Supelco (Bellefonte, PA, USA). Stock standard solutions of each VOCs at a concentration of 1000 μg L^{-1} were prepared in methanol and stored at −20 °C. These solutions were used for the preparation of daily working standard mixtures of the eight VOCs in methanol and finally in water. Methanol for ultratrace analysis was obtained from Merck (Darmstadt, Germany) and ultrapure water was obtained from a Milli-Q water purification system (Millipore, Bedford, MA, USA). The optimization method standard mixtures were prepared at the following levels: 20 ng mL^{-1} for each one of THMs and 2 ng mL^{-1} for trichloroethylene, tetrachloroethylene, benzene and 1,2-dichloroethane. The calibration standard mixtures were between 2.5 and 100 ng mL^{-1} for the THMs and between 0.25 and 10 ng mL^{-1} for the rest of VOCs.

A commercial mineral water, which does not contain the VOCs in study, was purchased to prepare the spiked solutions used to work out the analytical characteristics. We have to point out that a very little contamination of chloroform were found in the blanks that were performed with the Milli-Q water, but this compound did not appear in the blanks performed with the commercial mineral water. No other VOC was detected in the blanks.

The Aquacheck Interlaboratory Exercise was supplied by Aquacheck Ltd. (Bury, UK). Samples were recollected in duplicate by specialized staff from different places in Asturias (north of Spain) directly in the P&T vials. This container should be filled up to avoid headspace. Then, the samples were cooled down to 4 °C till their analysis (carried out in the following week).

All glassware, equipped with silicone/PTFE caps or septums, were washed with an especial detergent for laboratory materials, rinsed with Milli-Q water and finally dried in a stove at 150 °C to eliminate any residue. One millilitre of sodium thiosulfate 0.3% from Merck (Darmstadt, Germany) was added to the P&T vials in order to remove the residual chlorine from previous samples. The caps and septum were kept in the stove just 1 h at 105 °C to avoid their degradation.

2.2. Chromatographic equipment and experimental conditions

A Varian (Walnut Creek, CA, USA) 3800 gas chromatograph equipped with an ion trap mass detector Varian Saturn 2200 mass spectrometer was used. Gas chromatography was carried out on a Factor Four VF-5 ms (5% polydiphenylsiloxane) 30 m × 0.25 mm i.d. × 0.25 μm film thickness (Walnut Creek, CA, USA) fused silica column. Helium (purity 99.999%) was employed as carrier gas with a constant column flow of 1 mL min^{-1}. The initial temperature was 35 °C, held for 3 min; ramped at 30 °C min^{-1} up to 125 °C, and held for 1 min; a second rate at 50 °C min^{-1} up to 270 °C and held for 5 min.

The mass spectrometer was operated in electron ionization mode (EI) at 70 eV. The mass range scanned from 40 to 350 *m/z* at 0.60 s/scan for full-scan mode. The trap, manifold and transfer line temperatures were maintained at 250, 50 and 280 °C, respectively. The elution order and quantification mass–charge relations (*m/z*) are shown in Table 1.

2.3. Solid-phase microextraction equipment

Initial studies, performed in an Agilent 6890 Network Gas Chromatograph equipped with a mass spectrometry detector Agilent 5973 Network MSD (Agilent Technologies, Waldbronn, Germany) operated in EI mode, showed that the 50/30 μm DVB/CAR/PDMS SPME fiber is to be preferred for the pur-

Table 1
The analytes elution order and quantification mass–charge ratios (*m*/*z*) for the selected GC–MS method

Compound	*m*/*z* quantification
$CHCl_3$	83, 85
$C_2H_4Cl_2$	49, 62, 64
C_6H_6	50, 78
C_2HCl_3	95, 130, 132
$CHCl_2Br$	83, 85
$CHClBr_2$	127, 129
C_2Cl_4	164, 166
$CHBr_3$	173

pose. The 100 μm PDMS, 85 μm PA, 85 μm CAR/PDMS and 50/30 μm DVB/CAR/PDMS were supplied by Supelco. All the fibers were conditioned by heating them in the injection port of the GC, following the manufacture's recommendations, prior to their use.

The SPME extraction was carried out as follows. 1.3 mL of the water sample was placed in a 2 mL SPME vial for a Varian CP-8200 SPME Autosampler and the experimental conditions were changed in a univariant mode to investigate optimum conditions. Three different series were carried out for each parameter. The fiber was exposed (DI-SPME) to the sample for 15 min at room temperature. During the extraction the liquid sample was stirred by the fiber vibration produced by the autosampler. After analytes extraction, the fiber was thermally desorbed at 260 °C for 2 min into the glass liner of the GC injection port. This liner had 0.8 mm of i.d., special for SPME. The injector port was operated in split–splitless mode, with a splitless time of 2 min. No carryover was observed.

2.4. Purge and trap equipment

The purge and trap system was a Velocity XPT Purge and Trap Sample Concentrador (Teledyne Instruments, Ohio, US) which has a VOCARB 3000 trap (10 cm Carbopack B, 6 cm Carboxen 1000 and 1 cm Carboxen 1001). This trap is better for the determination of VOCs than the EPA recommended one, Tenax/silica gel/charcoal, because of this one decompose in benzene (one of the analytes) and alkylbenzenes [27] at high temperatures. VOCARB 3000 trap is more stable thermally, so it allows high desorption temperatures and, in that way, we have narrower chromatographic peaks improving the resolution of the compounds.

Five millilitres of each sample were introduced in the P&T sparger by a Varian Archon Purge and Trap Autosampler and the conditions were changed one to one, maintaining constant the rest. Three different series were carried out for each parameter again. The analytes were purged at 40 mL min^{-1} for 11 min at room temperature and the inert gas used for the P&T process was the same helium used for the GC separation. Then, once preconcentrated in the trap, the temperature was raised to 250 °C during 1 min for desorption and determination in the GC instrument.

3. Results and discussion

3.1. SPME optimization

First, we proceeded to choose the appropriate fiber coating for the extraction of the eight VOCs. In initial studies developed using an Agilent GC–MS, we compared four types of SPME fiber: 100 μm PDMS, 85 μm PA, 85 μm CAR/PDMS and 50/30 μm DVB/CAR/PDMS. Two of them, 100 μm PDMS and 85 μm PA, were assayed at 50 ng mL^{-1} for each one of analytes, while 85 μm CAR/PDMS and 50/30 μm DVB/CAR/PDMS were assayed at 10 ng mL^{-1} for each one of analytes. In all cases, the solution was stirred magnetically during 2 min at room temperature for the extraction step and then the analytes in the fibers were desorbed in the injector port for 1.25 min. The injector temperature for the desorption step was different depending of the type of fiber: 250 °C was used for the PDMS and PA fibers, 260 °C for the CAR/PDMS fiber and 300 °C for the DVB/CAR/PDMS fiber. As shown in Fig. 1a, of the results observed, the CAR/PDMS and DVB/CAR/PDMS fibers offered better extraction efficiency. However, higher peak widths were also observed (Fig. 1b) for the CAR/PDMS fiber (up to 0.053 min). As the overlapping of two contiguous peaks could ruin the needed chromatographic selectivity the DVB/CAR/PDMS were selected eventually as the preferred

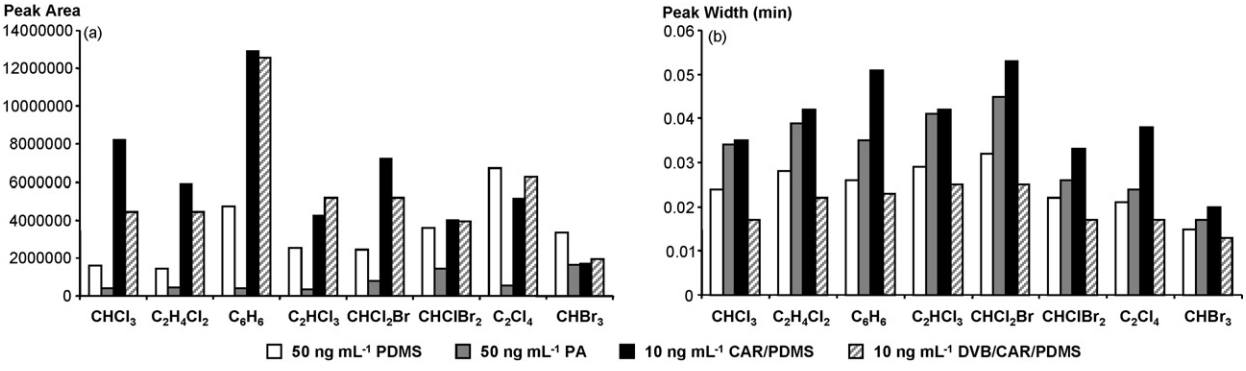

Fig. 1. Effect of the type of SPME coating on (a) the peak area and (b) the half peak width.

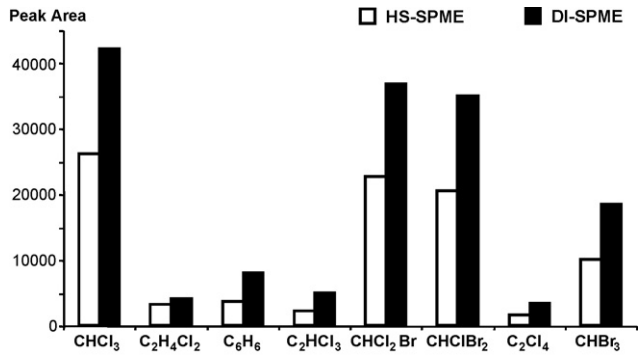

Fig. 2. Effect of the SPME modality on the peak area.

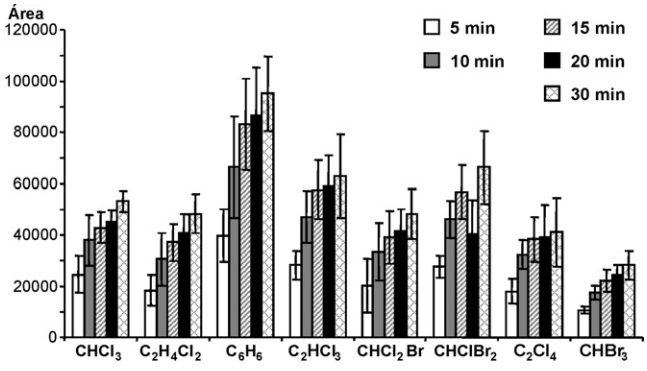

Fig. 3. Effect of the SPME extraction time on the peak area.

coating for the VOCs extraction from water (as it combined good extraction efficiency with narrow peak widths, less than 0.025 min, in the GC determinations).

Once the fiber coating was chosen, the best SPME mode was studied. By using the conditions referred to before, higher analytical signals were obtained using direct inmersion (DI-SPME) of the fiber (Fig. 2). These results differ from other reported in the bibliography recommending HS-SPME [1,11,12] (a plausible explanation is that our sample agitation system was quite different from those studies).

Then the effect of the extraction time was studied between 5 and 30 min. As shown by Fig. 3 the maximum signal was obtained for 30 min extraction time. For extracting the maximum amount of analyte, and therefore obtaining the maximum sensitivity, equilibrium should be reached. However, it is not needed just to carry out a quantitative analysis [28]. As a directly proportional relationship exists among the amount of analytes in the fiber and the initial concentration in the sample, the only condition is to use equal extraction times for calibration standards and for samples. Thus, in order to use a reasonable extraction time while obtaining a good compromise between sensitivity and time of analysis, 15 min were chosen. As our autosampler did not allow to vary the temperature of the sample solution, final extraction conditions selected were 15 min at room temperature.

Finally, we studied the influence of desorption parameters, including desorption temperature and heating time of the fiber into the GC injector. Considering the high volatility of the compounds under study, only temperatures between 100 and 270 °C were tested (higher temperatures are not recommended to avoid rapid fiber degradation). The time and temperature required to successfully desorb all VOCs from the selected fiber coating, with minimal carryover in the subsequent analysis, were established as 2 min at 260 °C.

3.2. SPME linearity, detection limits, precision and accuracy

In order to evaluate the developed SPME–GC–MS methodology, the analytical characteristics of detection limit, precision and accuracy were evaluated. Also the linearity was studied in the 2.5–100 ng mL^{-1} range for the THMs and to 0.25 from 10 ng mL^{-1} for the rest of VOCs (trichloroethylene, tetrachloroethylene, benzene and 1,2-dichloroethane). Their correlation coefficients (R^2), which can be observed in Table 2, were calculated as the average of three different calibration curves. All of them were lineal in the assayed range with $R^2 > 0.994$. The limits of detection (LDs) were calculated as three times the deviation of a batch of blank samples divided by the calibration slope (IUPAC). As shown in Table 2, the LDs varied between 0.02 and 0.7 ng THM/mL water for the THMs and between 0.008 and 0.1 ng analyte/mL water for the rest of VOCs. The precision and accuracy (expressed as repeatability and as the percent relative recovery, respectively) were determined by 10 replicates analysis of a commercial mineral water spiked with the standard mixture of the eight VOCs to give the concentration of the maximum levels permitted by the

Table 2
Observed analytical performance characteristics for the SPME–GC–MS methodology

	R^2	LD[a] (ng mL^{-1})	% R.S.D.[b]	% recovery[b]
$CHCl_3$	0.994 ± 0.002	0.7	2.4	119 ± 3
$C_2H_4Cl_2$	0.998 ± 0.001	0.008	5.7	104 ± 6
C_6H_6	0.9990 ± 0.0006	0.04	12.0	80 ± 15
C_2HCl_3	0.997 ± 0.003	0.02	4.6	107 ± 5
$CHCl_2Br$	0.995 ± 0.003	0.02	2.5	111 ± 3
$CHClBr_2$	0.999 ± 0.001	0.04	1.1	107 ± 1
C_2Cl_4	0.9986 ± 0.0006	0.1	4.0	113 ± 5
$CHBr_3$	0.9996 ± 0.0002	0.1	3.9	101 ± 4

[a] Number of blanks, $n = 20$.
[b] Number of replicates, $n = 10$. Concentrations: 25 ng mL^{-1} for each of the THMs, 5 ng mL^{-1} for trichloroethylene and for tetrachloroethylene, 3 ng mL^{-1} for benzene and 1 ng mL^{-1} for 1, 2-dichloroethane.

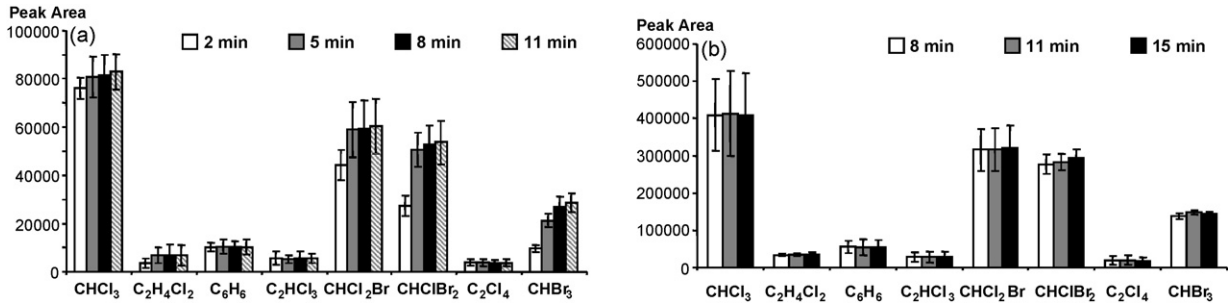

Fig. 4. Purge extraction time influence on the peak area using P&T technique: (a) a lower concentration (20 ng mL^{-1} for each one of THMs and 2 ng mL^{-1} for the rest of analytes) and (b) a five times higher concentration (100 ng mL^{-1} for each one of THMs and 10 ng mL^{-1} for the rest of analytes).

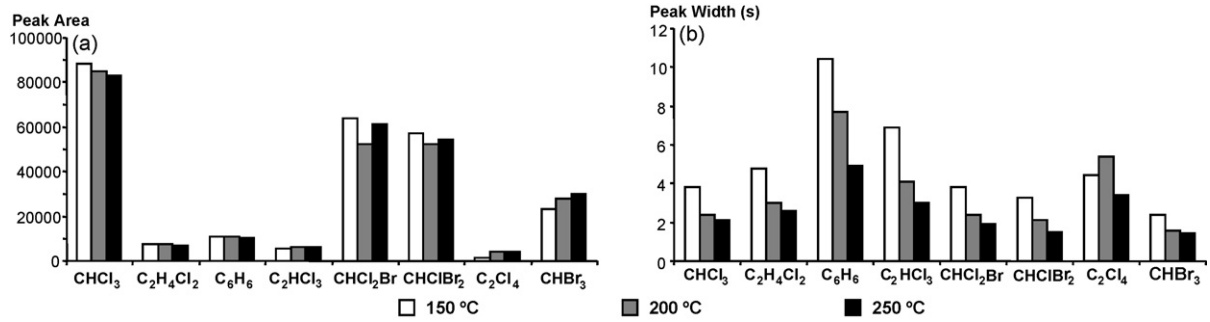

Fig. 5. Effect of the P&T desorption temperature on (a) the peak area and (b) the half peak width.

law. The % R.S.D. were between 1.1% ($CHClBr_2$) and 12% (C_6H_6) and the recoveries ranged from 80% (C_6H_6) to 119% ($CHCl_3$).

3.3. P&T optimization

The purge volume was set at 5 mL (this was the sparger tube volume) and was placed at room temperature. The optimum purge gas flow was determined by testing various flows. The gas flow to successfully blow all VOCs sougth from the water sample was finally set at 40 mL min^{-1}. The purge time was also assayed between 2 and 11 min. We found that at least 11 min were required to purge completely the analytes (see Fig. 4a) using 20 ng mL^{-1} for each one of THMs and 2 ng mL^{-1} for the rest of analytes. We also decided to test a higher concentration (five times) and higher purge times, in order to check that 11 min are enough to purge all analytes in case of having a sample with high levels of VOCs. Fig. 4b shows the observed results: between 8 and 15 min we did not observe significant differences. So, the purge was carried out at room temperature and at 40 mL min^{-1} during 11 min.

In order to optimise analyte desorption conditions, the desorption time was varied between 0.25 and 2 min and the desorption temperature between 150 and 250 °C. Results showed that 1 min was enough to get all assayed analytes desorbed. On the other hand, increasing the temperature from 150 to 250 °C did not change significantly the observed peak areas (Fig. 5a). However, a slight decrease of the retention times was observed while the peak widths decreased (see Fig. 5b) (better selectivity). Finally 250 °C was selected as desorption temperature (higher

Table 3
Observed analytical performance characteristics using the P&T–GC–MS methodology

	R^2	LD[a] (ng mL^{-1})	% R.S.D.[b]	% recovery[b]
$CHCl_3$	0.9995 ± 0.0003	0.2	2.5	100 ± 2
$C_2H_4Cl_2$	0.9993 ± 0.0002	0.004	2.9	117 ± 4
C_6H_6	0.9986 ± 0.0007	0.06	5.8	81 ± 5
C_2HCl_3	0.998 ± 0.001	0.03	4.2	103 ± 4
$CHCl_2Br$	0.9998 ± 0.0001	0.04	1.9	111 ± 2
$CHClBr_2$	0.9994 ± 0.0005	0.05	3.6	100 ± 3
C_2Cl_4	0.9996 ± 0.0004	0.02	2.7	95 ± 3
$CHBr_3$	0.9998 ± 0.0001	0.04	4.7	101 ± 4

[a] Number of blanks, $n = 20$.
[b] Number of replicates, $n = 10$. Concentrations of each analyte as in Table 2.

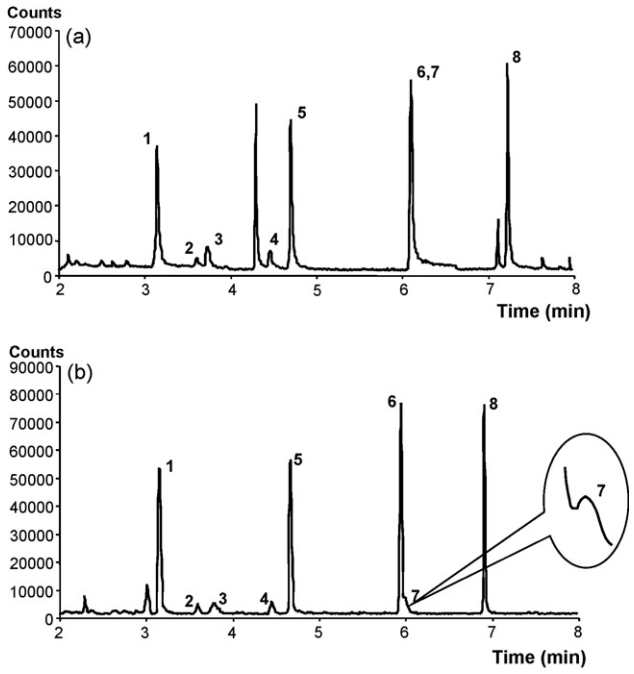

Fig. 6. GC–MS chromatograms for the eight VOCs studied by (a) SPME and (b) P&T. Peak assignment: 1, chloroform; 2, 1,2-dichloroethane; 3, benzene; 4, trichloroethylene; 5, bromodichloromethane; 6, dibromochloromethane; 7, tetrachloroethylene; 8, bromoform.

temperatures were not assayed to avoid progressive degradation of the trap).

3.4. P&T linearity, detection limits, precision and accuracy

As for the SPME technique, the analytical characteristics of the developed P&T–GC–MS method were evaluated and calculated in the same way as for the SPME–GC–MS in order to allow critical comparisons. Table 3 shows that R^2 was higher than 0.998, the LDs lied between 0.004 ng mL^{-1} ($C_2H_4Cl_4$) and 0.2 ng mL^{-1} ($CHCl_3$), the poorer repeatability observed was 5.8% while recoveries ranged from 81% (C_6H_6) to 117% ($C_2H_4Cl_2$).

3.5. A critical comparison of the two sample preparation methods

To start with it should be emphasised that both sample preparation approaches investigated are simple and do not require the use of organic solvents for sample preconcentration while, on the other hand, the required analysis time is also more or less the same (the P&T method took only 4 min less). However, Tables 2 and 3 critical comparison reveal that the P&T–GC–MS method offers superior analytical performance characteristics, because lower LDs and better precisions can be achieved (even if both methods provided similar recoveries).

Furthermore, as shown by comparing Fig. 6a and b, using the SPME–GC–MS method the peaks of bromodichloromethane and tetrachloroethylene appeared overlapped, while the P&T–GC–MS method provided better chromatographic resolution. This could be due to the fact that SPME produces a slightly higher broadening of the chromatographic peak. That fact forced us to determine the VOCs in two injections, one for the THMs and the other for determining the rest of VOCs if the SPME–GC–MS method is selected (so lengthening the time of analysis). Conversely, the P&T–GC–MS method allows the eight targeted determinations in a single chromatographic run. In brief, from our results it appears that P&T–GC–MS is the method of choice and so it was selected to analyze the real drinking water samples.

3.6. Validation of P&T–GC–MS method in the Aquacheck Interlaboratory Exercise

The ultimate way to validate the analytical method developed and guarantee the quality of environmental monitoring results is by participating in Interlaboratory Exercises followed by GC analysis [15]. So, to validate further the P&T–GC–MS selected methodology, the described procedure was applied in the analysis of an Aquacheck Interlaboratory Exercise (Distribution: 312, Group: 6A). This exercise consisted of analysing groundwater and a concentrated solution of eight VOCs (chloroform, bromodichloromethane, dibromochloromethane, bromoform, trichloroethylene, tetrachloroethylene, 1,2-dichloroethane and carbon tetrachloride instead of benzene). According to the instructions of the distributors (Aquacheck Ltd., Bury, UK), the analysis solutions must be prepared by dilution 1:10,000 of the concentrated solution in the groundwater supplied. Following instructions, the dilution was carried out in two steps: first 500 μL of the concentrated solution was diluted with 10 mL of methanol and next 1 mL of this solution was diluted 500 mL with the groundwater. Finally, that sample solution was distributed into P&T vials ($n = 10$) and was analyzed. Our results, as well as the number of participant laboratories, the mean of all labo-

Table 4
Results obtained for the Aquacheck Interlaboratory Exercise (Distribution: 312, Group: 6A)

	Found value (mean ± deviation) (ng mL^{-1})	Participant laboratories	Laboratory mean (ng mL^{-1})	Reference value (ng mL^{-1})	"Z score" value
$CHCl_3$	28.6 ± 0.2	30	35.1	34.3	−1.69
$C_2H_4Cl_2$	2.8 ± 0.1	18	3.06	3.00	−0.67
C_2HCl_3	2.48 ± 0.05	24	2.56	2.53	−0.06
$CHCl_2Br$	91 ± 1	29	105	104	−1.2
$CHClBr_2$	75 ± 3	29	86.1	87.5	−1.37
C_2Cl_4	7.5 ± 0.1	23	7.59	7.73	−0.23
$CHBr_3$	63 ± 2	30	64.5	62.6	0.14

Table 5
Concentration (ng mL^{-1}) of the VOCs in Asturian drinking waters

	Total number of samples	Number of samples		Concentration of total THMs (ng L^{-1})	
		THMs < LD	THMs > LD	Min.	Max.
East	50	12	38	0.4	31.7
Central	121	22	99	0.4	52.5
West	23	7	16	0.7	23.5
Total	194	41	153		

ratories, the reference value and the "*Z* score" values (if the "*Z* score" was lower than 2, the results would be acceptable and this would validate the developed methodology for the analysis of such analytes in real samples) are shown in Table 4.

As Table 4 shows our results were in good agreement with the reference values provided (except for benzene, absent in the Aquacheck solution). In brief, the P&T–GC–MS method proposed here can be used for the reliable determination of the assayed VOCs in real drinking waters.

3.7. Application of the P&T–GC–MS method to drinking waters

Once the trueness of the proposed method was validated, real drinking waters or Asturias (Spain) were analyzed for VOCs. So, 194 samples were taken in different places of Asturias and were analyzed by the P&T–GC–MS developed methodology. Of all studied VOCs, only THMs were detected in the samples. Table 5 shows the number of analyzed samples, the number of samples in which we did not detect any THMs and the number of samples in which we detected some THMs with the minimum and maximum found concentrations of the total THMs. All this information is classified according to the geographic places in that we divided Asturias: East, Central and West of Asturias. As we can see, fortunately the concentration of the VOCs in all drinking waters analyzed turned out to be lower than the maximum level permitted by the Spanish and European legislations (150 $\mu g\,L^{-1}$).

4. Conclusions

Aiming at selecting a sample preparation technique for the GC–MS determination of VOCs fulfilling the sensitivity requirements of the threshold levels of such compounds in European drinking waters legislation, two preconcentration techniques have been investigated. Results show that both techniques can be used to carry out simple and fast determinations of VOCs in drinking water samples by GC–MS. However, dibromochloromethane and tetrachloroethylene signals were overlapped when SPME was used as the extraction and preconcentration step. On the other hand, P&T–GC–MS offers better general analytical performance characteristics than SPME fulfilling the requirements of the official guidelines established. Thus, the developed P&T–GC–MS methodology was validated and then applied to the analysis of 194 drinking water samples and it has been successfully implemented in the Laboratorio de Salud Pública del Principado de Asturias for routine checking of VOCs contamination of drinking waters in Principado de Asturias.

Acknowledgement

Authors thank FYCIT (Asturias, Spain) for financial support under the frame of Project Ref. FC-04-PC-04-22.

References

[1] M.A. Stack, G. Fitzgerald, S. O'Connell, K.J. James, Chemosphere 41 (2000) 1821.
[2] E. Martínez, S. Lacorte, I. Llobet, P. Viana, D. Barceló, J. Chromatogr. A 959 (2002) 181.
[3] A.D. Nikolaou, S.K. Golfinopoulos, M.N. Kostopoulou, G.A. Kolokythas, T.D. Lekkas, Water Res. 36 (2002) 2883.
[4] N. Campillo, P. Viñas, I. López-García, N. Aguinaga, M. Hernández-Córdoba, J. Chromatogr. A 1035 (2004) 1.
[5] S.K. Golfinopoulos, T.D. Lekkas, A.D. Nikolaou, Chemosphere 45 (2001) 275.
[6] V.I. Safarova, S.V. Sapelnikova, E.V. Djazhenko, G.I. Teplova, G.F. Shajdulina, F.Kh. Kudasheva, J. Chromatogr. B 800 (2004) 325.
[7] European Directive 98/83/CE, 3 November, Published in Diario Oficial de las Comunidades Europeas (DOCE) L330, December 5 1998.
[8] Real Decreto 140/2003, 7 February, Published in Boletín Oficial del Estado (BOE) 45, February 21 2003.
[9] K. Demeestere, J. Dewulf, B. De Witte, H. Van Langenhove, J. Chromatogr. A 1153 (2007) 130.
[10] A.D. Nikolaou, T.D. Lekkas, S.K. Golfinopoulos, M.N. Kostopoulou, Talanta 56 (2002) 717.
[11] D.H. Cho, S.H. Kong, S.G. Oh, Water Res. 37 (2003) 402.
[12] S. Nakamura, S. Daishima, Anal. Chim. Acta 548 (2005) 79.
[13] M.N. Kostopoulou, S.K. Golfinopoulos, A.D. Nikolaou, N.K. Xilourgidis, T.D. Lekkas, Chemosphere 40 (2000) 527.
[14] L. Zoccolillo, L. Amendola, C. Cafaro, S. Insogna, J. Chromatogr. A 1077 (2005) 181.
[15] J. Dewulf, T. Huybrechts, H. Van Langenhove, Trends Anal. Chem. 25 (2006) 300.
[16] R.P. Belardi, J.B. Pawliszyn, Water Pollut. Res. J. Can. 24 (1989) 179.
[17] C.L. Arthur, J. Pawliszyn, Anal. Chem. 62 (1990) 2145.
[18] Z. Zhang, M.J. Yang, J. Pawliszyn, Anal. Chem. 66 (1994) 844A.
[19] A.J. King, J.W. Readman, J.L. Zhou, Anal. Chim. Acta 523 (2004) 259.
[20] N. Fidalgo-Used, G. Centineo, E. Blanco-González, A. Sanz-Medel, J. Chromatogr. A 1017 (2003) 35.
[21] F.E. Ahmed, Trends Anal. Chem. 22 (2003) 170.
[22] N. Campillo, P. Viñas, I. López-García, N. Aguinaga, M. Hernández-Córdoba, Talanta 64 (2004) 584.
[23] L. Dunemann, H. Hajimiragha, Anal. Chim. Acta 283 (1993) 199.
[24] P. Roose, U.A.Th. Brinkman, Analyst 123 (1998) 2167.

[25] Environmental Protection Agency, EPA, "Methods for the Determination of Organic Compounds in Drinking Water", EPA-600/4-88/039, December 1988, Internet web site: http://www.epa.gov.
[26] "Standard Methods for the Examination of Water and Wastewater", American Public Health Association (APHA), American Water Works Association (AWWA), Water Environment Federation (WEF), 19th ed., 1995.
[27] C. Cámara, P. Fernández, A. Martín-Esteban, C. Pérez-Conde, M. Vidal, Toma y tratamiento de muestras, Síntesis, Spain, 2002.
[28] H. Kataoka, H.L. Lord, J. Pawliszyn, J. Chromatogr. A 800 (2000) 35.

Available online at www.sciencedirect.com
ScienceDirect
Talanta 74 (2008) 1104–1112
Talanta
www.elsevier.com/locate/talanta

α-Cyclodextrin-modified infrared sensing system for rapidly determining the enantiomeric composition of chiral compounds

Chung-Jay Lee, Jyisy Yang *

Department of Chemistry, National Chung-Hsing University, Taichung 402, Taiwan

Received 13 July 2007; received in revised form 10 August 2007; accepted 10 August 2007
Available online 17 August 2007

Abstract

This paper describes a new infrared (IR) sensing method for rapidly determining the enantiomeric compositions of chiral compounds through the use of a chirality-selective compound immobilized on the surface of the evanescent-wave sensing elements. α-Cyclodextrin (α-CD) was selected as this agent and it was immobilized on a zinc selenide sensing element to allow different analytical signals to be generated for each compound of a pair of enantiomers. Theoretical working equations were developed to monitor the response of the ATR-IR spectroscopic sensor during this process. The difference between the formation constants of enantiomers was crucial to the sensitivity when determining the enantiomeric compositions. Control of the pH of the solution could be used to effectively increase the difference between these formation constants. Based on the static sensing system with optimal conditions, the ratio of the values of the signals of the two enantiomers was <0.4. A linear relationship between the analytical signals and the mole fraction of the enantiomers was obtained under conditions in which the concentration of the chiral compound was sufficiently low. Based on the detected time profiles, this sensing method had a fast response: the detection time could be <10 min. With a flow-cell configuration, the time to finish one determination can be shorter than 10 min with similar sensitivity and accuracy as in static sensing system.
© 2007 Elsevier B.V. All rights reserved.

Keywords: Infrared chemical sensor; Optical sensor; α-Cyclodextrin; Chiral compounds; Enantiomeric composition

1. Introduction

Determining the enantiomeric composition of a chiral compound is a challenging, but necessary, task in pharmacology because the enantiomeric forms of many compounds have different physiological and therapeutic effects [1–4]. A number of methods have been proposed for determining enantiomeric compositions, including separation [5–15], optical [16–21] and other [22–24] technologies. The separation technologies most commonly used are gas chromatography (GC) [5,6], high-performance liquid chromatography (HPLC) [7–10] and capillary electrophoresis (CE) [11–15]. The key to a successful determination of enantiomeric composition when using these separation techniques is that a suitable chiral recognition mechanism provides a sufficient difference between the interaction forces of the enantiomers. The formation of inclusion complexes, ligand exchange complexes and derivatization techniques are commonly utilized as chiral recognition mechanisms to enlarge the differences between the enantiomers' physical properties. Although separation-based methods have been applied successfully to determine a wide variety of chiral compounds, such analyses are generally time-consuming because of the separation and sample pre-treatment processes. Spectroscopic sensing methods also have been proposed as alternatives to simplify the analysis process. Such spectroscopic methods as circular dichroism [19], near-infrared spectroscopy [20] and nuclear magnetic resonance spectroscopy [21] have been applied successfully to determine enantiomeric compositions, but these methods are generally limited because of either low sensitivity or the necessity to use additional reagents.

A new optical sensing method based on Fourier transform infrared (FT-IR) spectroscopy that retains the advantages of the optical methods, but reduces the complexity of the sample pretreatment and instrumentation, is proposed in this work. In recent years, IR sensing methods have been applied widely to the detection of organic compounds in different matrices [25–27]. The direct extension of IR sensing methods to determining the chiralities of compounds has not been achievable to date because of

* Corresponding author. Tel.: +886 422840411x514; fax: +886 422862547.
E-mail address: jyisy@dragon.nchu.edu.tw (J. Yang).

0039-9140/$ – see front matter © 2007 Elsevier B.V. All rights reserved.
doi:10.1016/j.talanta.2007.08.010

the fact that the IR spectral features of a chiral compound are the same for both enantiomers. To overcome this weakness, a chiral recognition mechanism based on the use of cyclodextrins (CDs) has been applied to the IR sensing elements to create differences in the intensities of the detected IR signals when determining the enantiomeric compositions. CDs and their analogs exhibit unique physical and chemical properties and have been applied extensively in separation technologies; the large number of successful applications has been reported in the literature as can be seen in several review articles [28–31].

The attenuated total reflection effect was used to combine the chiral recognition ability of a CD with the IR sensing method. In this effect, the depth of penetration of the evanescent field can be estimated [32] as

$$dp = \lambda/\{2\pi n_1[\sin^2\theta - (n_2/n_1)^2]^{1/2}\} \quad (1)$$

where θ is the angle of incidence, λ the wavelength of the incident radiation, n_1 the refractive index of the internal reflection element (IRE) and n_2 is the refractive index of the surrounding medium. The variation of dp in the IR region occurs from a few tenths of a micron to a few microns. This small value of dp limits the sensitivity in this type of detection. To increase the sensitivity, a hydrophobic film is commonly applied to the surface of the IRE to attract analytes into the evanescent field to allow detection doe analytes in solution [33–36]. Similarly, the CD molecules should be fixed onto the surface of the IREs to attract the chiral compounds to the IRE surface. A two-layer modification method was used to immobilize the CD molecules onto the surface of the IREs. Basically, a hydrophobic film was pre-coated on the IREs to allow the further fixation of CD molecules upon it. If the hydrophobic film is thin enough, the analytes captured by the CD molecules can be sensed using IR radiation, as is depicted schematically in Fig. 1. Theoretical equations were developed to demonstrate that this new proposed method is applicable for determining chiral compounds (see below).

2. Theoretical aspects

As shown in Fig. 1, chiral compounds can be detected once they form inclusion complexes with immobilized CDs. Because a layer of CD molecules is immobilized on the IREs, the sensing behavior is believed to be similar to an adsorption process. Under conditions in which inclusion complexes of the R and S enantiomers are formed competitively in a mixture containing both forms, the two chemical equilibria can be written as

$$R + \mathrm{CD} \rightleftharpoons \mathrm{CDR} \quad (2)$$

$$S + \mathrm{CD} \rightleftharpoons \mathrm{CDS} \quad (3)$$

where CDR and CDS represent the inclusion complexes formed between the CD and the R and S enantiomers, respectively. In these equations, two formation constants can be defined as K_R and K_S. Assuming that the total number of CD molecules immobilized on the sensing element is N_{CD}, the original concentrations of the S and R enantiomers in the sample solution are C_S and C_R, respectively, the fraction of coverage by the R and S enantiomers at equilibrium condition can be calculated as

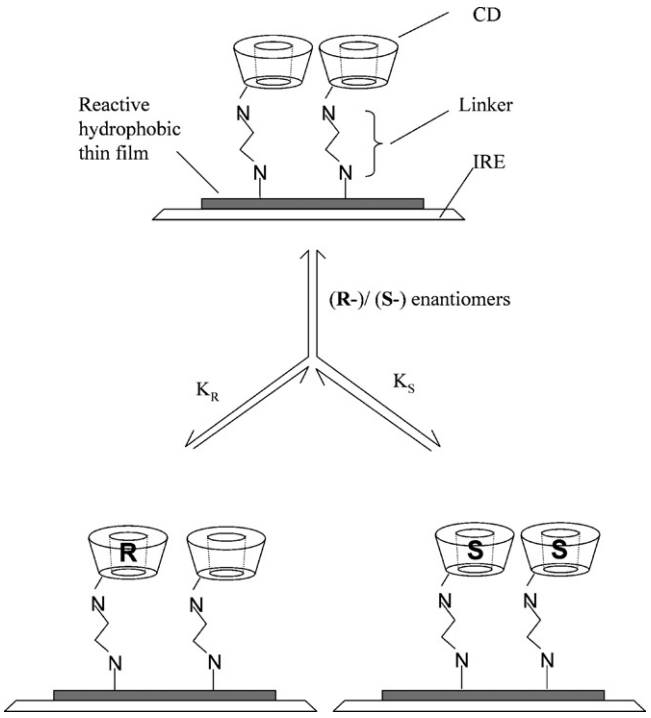

Fig. 1. Schematic diagram of the use of a CD-modified phase for the detection of compounds having different chiralities.

$$\alpha_{CDS} = N_{CDS}/N_{CD} = K_S \cdot C_S/(1 + K_S \cdot C_S + K_R \cdot C_R) \quad (4)$$

$$\alpha_{CDR} = N_{CDR}/N_{CD} = K_R \cdot C_R/(1 + K_S \cdot C_S + K_R \cdot C_R) \quad (5)$$

where N_{CDS} and N_{CDR} represent the number of immobilized CD molecules being occupied by S and R enantiomers and α_{CDS} and α_{CDR} represent the fractions of coverage by S and R enantiomers. The detected IR signals should be proportional to the sum of α_{CDS} and α_{CDR}:

$$S = k \cdot N_{CD} \cdot (\alpha_{CDS} + \alpha_{CDR}) = \varepsilon \cdot (K_S \cdot C_S + K_R \cdot C_R)/(1 + K_S \cdot C_S + K_R \cdot C_R) \quad (6)$$

where k is a proportionality constant that is related to the IR molar absorptivity of the analytes and ε equals $k{\cdot}N_{CD}$. Eq. (6) can be further simplified if the sum of $K_S{\cdot}C_S$ and $K_R{\cdot}C_R$ is much smaller than 1 as

$$S = \varepsilon \cdot (K_S \cdot C_S + K_R \cdot C_R) = \varepsilon \cdot C_T \cdot (K_S - K_R) \cdot \beta_S + \varepsilon \cdot C_T \cdot K_R \quad (7)$$

where β_S is mole fraction of the S enantiomer ($=C_S/C_T$) and C_T is the sum of C_S and C_R. From this equation, the mole fraction of the S enantiomer is linearly related to the IR signals when the sum of $K_S{\cdot}C_S$ and $K_R{\cdot}C_R$ is much smaller than 1. This equation suggests that it is feasible to utilize CD-modified IR sensors to determine the enantiomeric composition of a chiral compound.

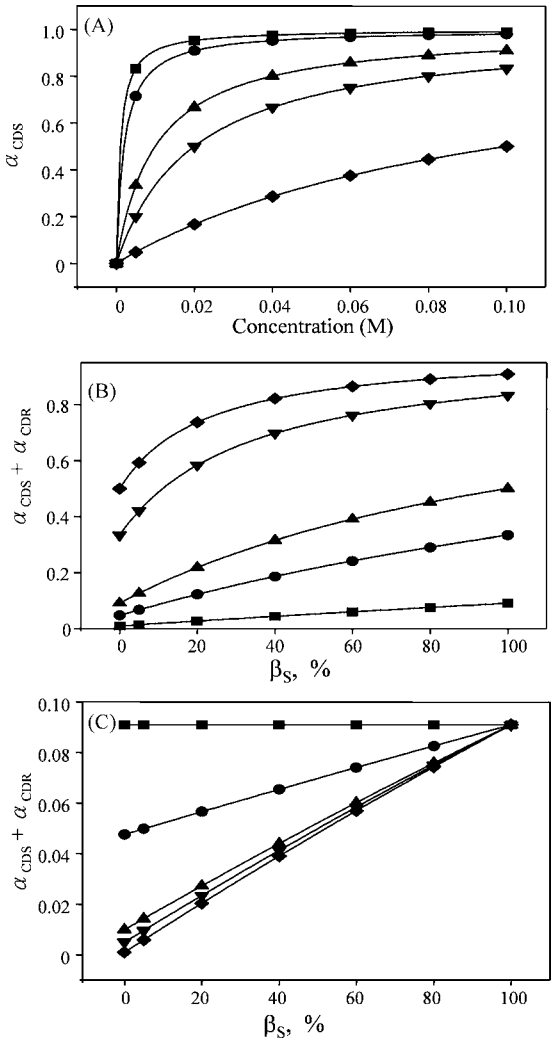

Fig. 2. (A) Theoretical plots of α_{CDS} vs. the concentration of the *S* enantiomer. The sample solutions were assumed to contain only the *S* enantiomer and the values of K_S were assumed to be 1000 M^{-1} (■), 500 M^{-1} (●), 100 M^{-1} (▲), 50 M^{-1} (▼) and 10 M^{-1} (♦). (B) Theoretical curves of the total coverage rates ($\alpha_{CDS} + \alpha_{CDR}$) for different compositions of a compound at fixed total concentrations of 0.1 mM (■), 0.5 mM (●), 1.0 mM (▲), 5.0 mM (▼) and 10.0 mM (♦). The formation constants K_R and K_S were assumed to be 100 and 1000 M^{-1}, respectively. (C) Theoretical curves of the total coverage rates ($\alpha_{CDS} + \alpha_{CDR}$) vs. the mole fraction of the *S* enantiomer for a solution containing both *R* and *S* enantiomers at a total concentration of 0.1 mM. The value of K_S was assumed to be 1000 M^{-1}; the values of K_R were assumed to be 10,000 M^{-1} (■), 500 M^{-1} (●), 1 M^{-1} (▲), 0.5 M^{-1} (▼) and 0.1 M^{-1} (♦).

Meanwhile, the IR signals are related to the difference between the formation constants of the *R* and *S* enantiomers, as indicated by Eq. (7). To examine the developed equations theoretically, the formation constants in Eqs. (2) and (3), and the concentrations of the sample solutions were varied and used to calculate the theoretical responses. Fig. 2A displays the values of α_{CDS} calculated from Eq. (4) for samples containing different concentrations of *S* enantiomer only; the value of K_S was varied from 10 to 1000 M^{-1}. As can be observed in this figure, the IR signals are strongly related to the formation constants: the higher of the formation constant, the lower the concentration required to saturate the analytical signals.

As stated above, the sum of $K_S \cdot C_S$ and $K_R \cdot C_R$ should be smaller than 1 in order to obtain the linear relationship in Eq. (7). To theoretically investigate the conditions for Eq. (7), the values of α_{CDS} and α_{CDR} were calculated individually from Eqs. (4) and (5). The sum of α_{CDS} and α_{CDR} was plotted in Fig. 2B by against the values of β_S with total concentrations (C_T) from 0.1, 0.5, 1.0, 5.0 to 10.0 mM. The formation constants K_S and K_R were assumed to be 1000 and 100 M^{-1}, respectively. A close-to-linear relationship is only observed when the C_T is lower than 0.5 mM. To further observe the effect that the difference between the formation constants of the *S* and *R* enantiomers has on the sum of the fraction of coverage, these calculations were simulated under the condition that the total concentration of the examined compound was 0.1 mM; the formation constant of the *S* enantiomer was fixed at 1000 M^{-1} and that of the *R* enantiomer was varied from 0.1 to 100 times the formation constant of the *S* enantiomer. The results are plotted in Fig. 2C; a difference in the analytical signals can be observed for the different compositions of the chiral compounds. This finding means that it is possible to determine the chirality of a compound based on the use of the CD-modified phase.

3. Experimental

3.1. Chemicals

α-Cyclodextrin (99%) was obtained from TCI (Tokyo, Japan). Tosyl chloride and 1,2-diaminoethane were obtained from Riedel-deHaen (Hannover, Germany). Pyridine 99.9% was obtained from TEDIA (Fairfield, Iowa, USA) and dried over solid NaOH before use. Poly(vinylbenzyl chloride) (PVBC) and polystyrene (PS), obtained from Aldrich Chemical (Milwaukee, WI), were used for the preparation of the hydrophobic film during surface modification. Sodium iodide was obtained from Shimakyu Chemicals (Osaka, Japan). (*S*)-mandelic acid (*S*-MA) and (*R*)-mandelic acid (*R*-MA) were obtained from ACROS (Milwaukee, Wisconsin, USA). (1*S*)-(+)-10-camphorsulfonic acid (*S*-CSA), (1*R*)-(−)-10-camphorsulfonic acid (*R*-CSA), *S*-acetyl mandelic acid (*S*-AMA) and *R*-acetyl mandelic acid (*R*-AMA) were obtained from Aldrich Chemical with a purity of 99%. All reagents were used as received and de-ionized Milli-Q water was used to prepare all of the aqueous samples.

3.2. Apparatus

A 45° trapezoidal (55 mm × 5 mm × 2 mm) zinc selenide was used as the internal reflection element. Compared the signals from transmission measurement, the number of internal reflection for this internal element is around 12. A static detection system and a flow-cell design were used in this work as shown in Fig. 3A and B, respectively. These devices were placed in the sample compartment of a Jasco 460 plus FT-IR spectrometer (Jasco Co., Tokyo, Japan) equipped with a mercury–cadmium–telluride (MCT) detector. For static detection system, the sample cell was constructed from stainless steel and had a sample volume of 10 mL. The IRE was placed in the center of the cell as indicated in Fig. 3A. For flow-cell device, the

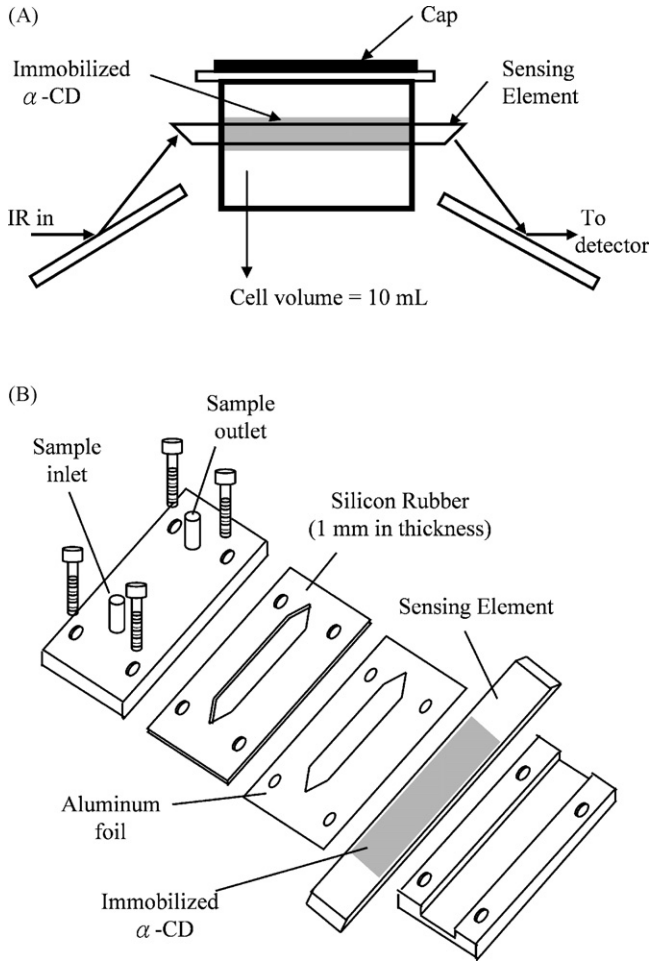

Fig. 3. (A) Schematic representation of the static sensing system used in this study. (B) Flow-cell design in dynamic sensing system.

ZnSe crystal was sandwiched in two acrylic plates as shown in Fig. 3B. A spacer of poly(tetrafluoroethylene) was placed on the top of the ZnSe crystal to form a flow channel. Jasco PU-1580 Intelligent HPLC Pump (Jasco Co.) equipped a flow selection switch was used to deliver sample and regeneration solutions. All spectra were detected from 64 scans at a resolution of 4 cm^{-1}.

3.3. Preparation of the α-cyclodextrin-modified phase

α-CD (1 g) and tosyl chloride (0.1 g) were dissolved in pyridine (18 mL). The solution was stirred at room temperature until both compounds had dissolved. 1,2-Ethylene diamine (30 μL) was added into the solution, which was then heated at 40 °C for 48 h. The color of the solution changed from clear to brown and the product, 6-deoxy-6-diamino-α-cyclodextrin, was obtained. A 1% (w/v) polymer solution of PVBC/PS (1:9, w/w) was prepared in toluene and 80 μL of this polymer solution was used for coating of the IRE. To increase the reactivity of the PVBC, the coated IRE was placed in an acetonitrile solution (200 mL) of containing NaI (4 g) and then it was heated at 60 °C for ca. 18 h. The chlorine atoms on the surface of PVBC were substituted by iodine atoms and the color of the polymer film changed from clear to light yellow. This prepared IRE was placed into the previous solution of 6-deoxy-6-diamino-α-cyclodextrin and heated at 60 °C for 6 h.

The stability of the synthesized α-CD phase in aqueous solution was examined to ensure that the prepared sensing phase is suitable for quantification purpose. To examine the water stability, the freshly prepared α-CD phase was first soaked in an aqueous solution to remove any unreacted α-CDs. After soaking in water for 30 min, the absorption band intensity of α-CD at 1100 cm^{-1} was used as an indication for the stability of the prepared sensing phase. Results indicate that the band intensities of α-CD sensing phase remain at certain level for a long period of time as no apparent variation of the band intensities within 20 days of observation.

4. Result and discussion

4.1. Preparation and characterization of the cyclodextrin-modified phase

In the synthesis of α-CD phase, a polymer solution of PS and PVBC in weight ratio of 9:1 was used. Because only PVBC is reactive to α-CD, PS is used to ensure that a thin and well-dispersed sensing phase can be obtained. Meanwhile, PS is dissolvable in the solvent of pyridine and should be removed in the final sensing phase. To verify the reaction products in each of preparation steps, both IR spectra and corresponding SEM photos were measured. Fig. 4 displays the typical spectra of neat PS, neat PVBC, neat α-CD, PS/PVBC, PS/PVBC after iodination (named PS/PVBI) and the final synthesized α-CD phase incorporating the ethylene diamine spacer. The spectral features of α-CD can be observed in the final synthesized phase, which

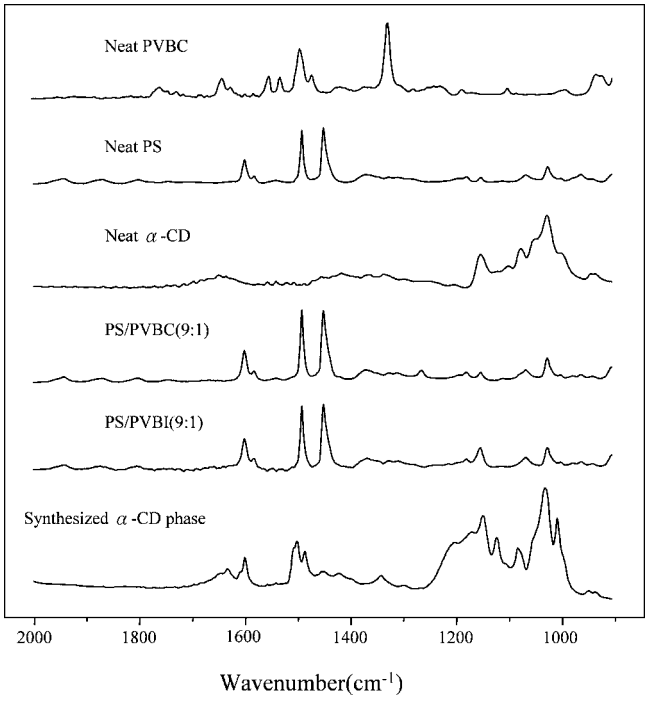

Fig. 4. IR spectra of neat PVBC, neat PS, neat α-CD, PS/PVBC (9:1), PS/PVBI (9:1) and final synthesized α-CD sensing phase.

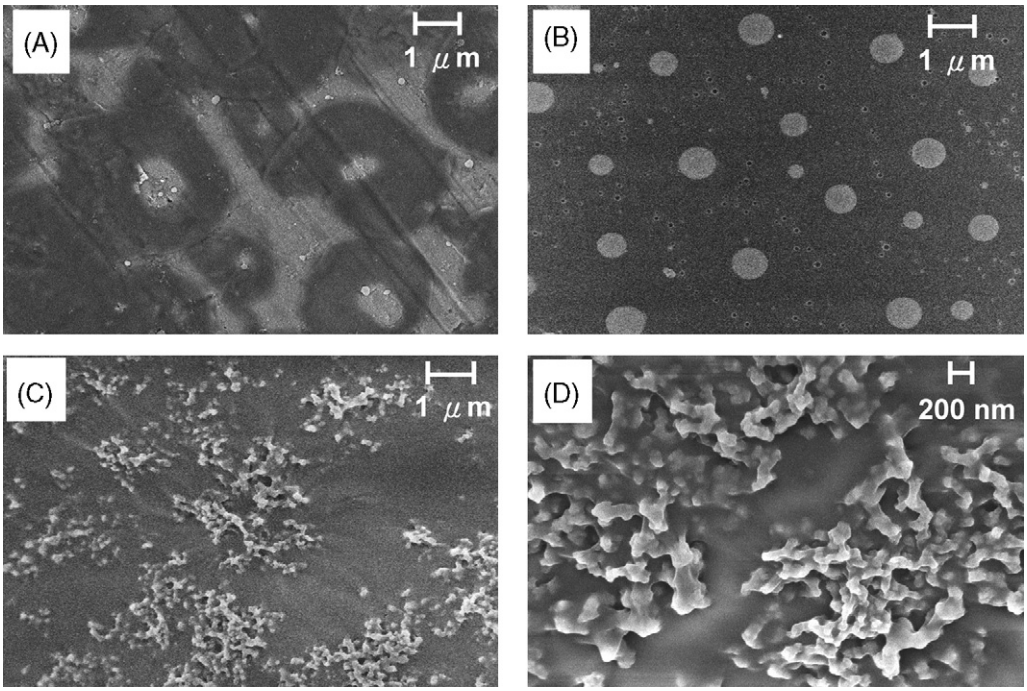

Fig. 5. SEM photos of PS/PVBC (A), PS/PVBI (B) and synthesized α-CD sensing phase (C and D).

reveals that the α-CD sensing phase was prepared successfully. Meanwhile, the disappearance of the spectral features of PS in the final synthesized phase indicated that PS was removed in the last step during immobilization of α-CDs. To observe the changes of the morphologies in each of the steps, SEM photos were taken as plotted in Fig. 5. As can be seen in Fig. 5, the formed thin film shows un-even distribution of the PVBC in PS matrix. After iodination, the PVBI tends to form droplets with diameters around 500 nm in the PS matrix as can be seen in Fig. 5B. After reaction in α-CD solution (pyridine as solvent), PS was dissolved as the characteristic absorption bands of PS disappeared. The SEM photos were also taken as shown in Fig. 5C and D (enlarged). As can be seen from these SEM photos, the droplets of PVBI were broken into a rough surface in the final sensing phase. Based on above results, α-CD sensing phase was successfully obtained.

4.2. *Effect of pH on the determination of enantiomeric compositions*

The success of the CD phase in determining the chirality of a compound is strongly dependent upon the difference between the detected signals of the *S* and *R* enantiomers of that compound. The pH of the solution was varied in an attempt to enlarge the difference between the detected signals. To examine the effect of pH on the IR spectral features for each form of a chiral compound, (*S*)- and (*R*)-mandelic acids (*S*-/*R*-MA) were selected and used as probe molecules. *S*- and *R*-MA contain carboxylic acid functional groups that have a value of pK_a of ca. 3.4. Sample solutions of *R*-MA and *S*-MA were each prepared at a concentration of 1 mM and the pH of the solution was adjusted to 3.4, 4.0, 5.0, 6.0 and 7.0 by adding dilute NaOH and HCl solutions. The typical detected spectra of *R*-MA and *S*-MA are plotted in Fig. 6. As can be observed in this figure, the adsorbed chemical forms of *R*-MA and *S*-MA are in the form of carboxylate as can be identified from the asymmetric and symmetric stretching absorp-

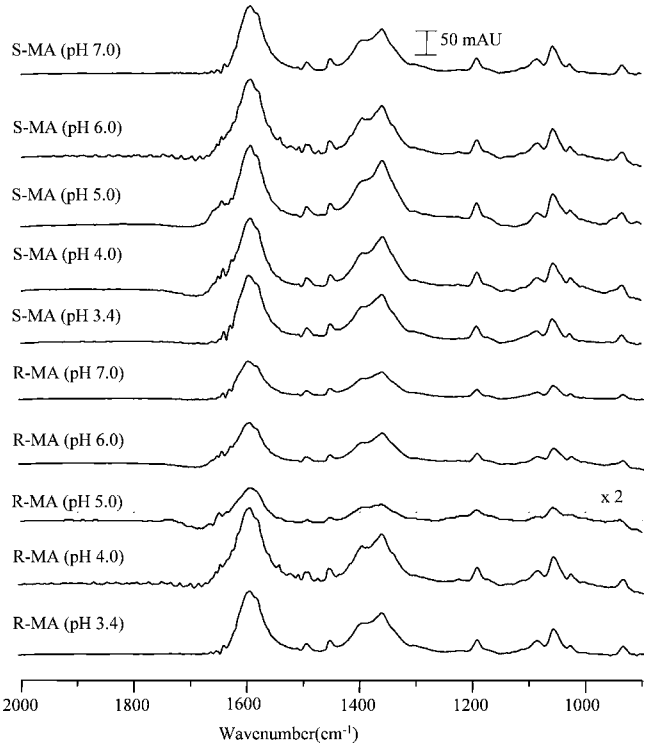

Fig. 6. Typical detected spectra of *S*-MA and *R*-MA at different pHs by α-CD-modified sensing phase. The concentrations of *S*-MA and *R*-MA were 1 mM and spectra were taken at a detection time of 30 min.

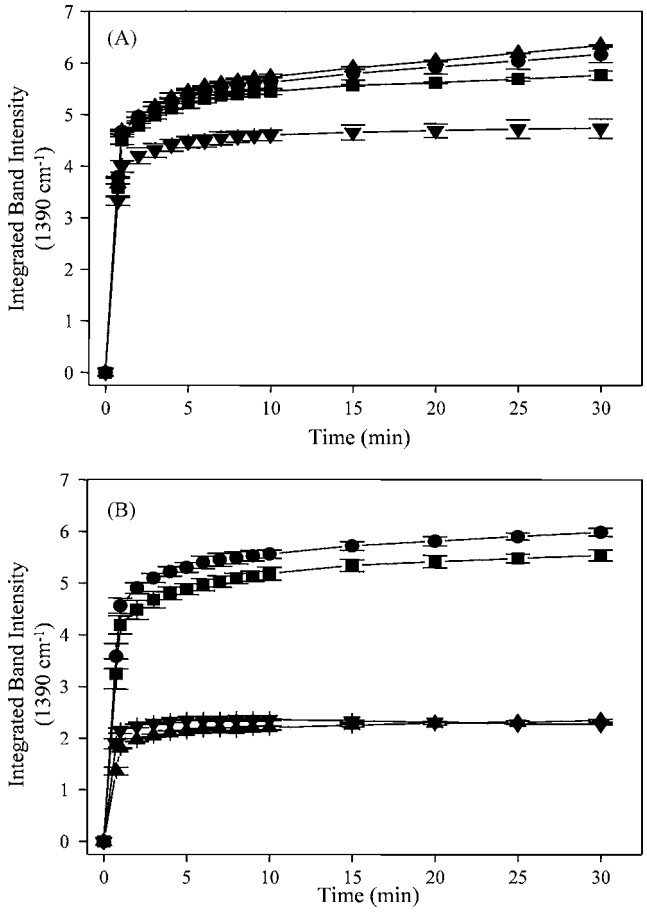

Fig. 7. Time profiles for the detection of (A) *S*-MA (1 mM) and (B) *R*-MA (1 mM). The values of pH of the solutions were adjusted to 4.0 (■), 4.5 (●), 5.0 (▲) and 7.0 (▼).

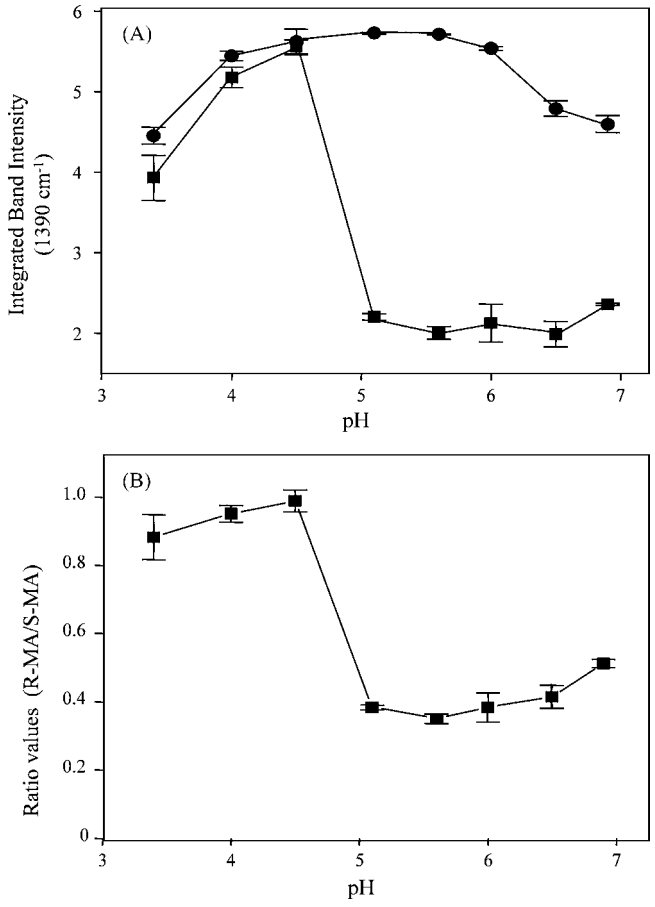

Fig. 8. (A) Plot of the IR signals of *R*-MA ((■; 1 mM) and *S*-MA ((●) 1 mM) vs. the values of pH of the sample solutions. The IR signals were measured after 10 min. (B) Values of the ratios of *R*-MA (1 mM) to *S*-MA (1 mM) at the different values of pH indicated in (A).

tion bands (ca. 1590 and 1390 cm^{-1}) of the carboxylate unit. In terms of formation of hydrogen bonding with the hydroxyl unit in the α-CD molecules, it is reasonable that the de-protonated *R*-MA or *S*-MA interacts stronger with α-CD than their protonated forms.

To further examine any influences of pH on the detection speed, the symmetric stretching band of carboxylate group of MA located at 1390 cm^{-1} was selected as an indication of the amount of the adsorbed analytes. This band was affected less by water absorption than was the other band (located at 1590 cm^{-1}). The typical detection time profiles for 1 mM *S*-MA and 1 mM *R*-MA examined at different values of pH are plotted in Fig. 7A and B, respectively. As can be observed in these detection time profiles, the response in the detection of either form of MA by the α-CD-modified IR sensors was fast; up to 90% of the maximum signal could be reached within 5 min. Comparing the equilibrium signals at different values of pH as plotted in Fig. 8A, the maximum signals for *R*-MA and *S*-MA occurred at ca. pH 4.5. Because differences in the IR signals are the major concern in determining the chirality of a compound, the IR signals obtained after 30 min were used to obtain the values of the ratios. The ratios of the detected IR signals for *R*-MA and *S*-MA are plotted in Fig. 8B as a function of pH. The value of the ratio was close to 1 at pH <4.5. For pH >4.5, the ratios decreased to a value of ca. 0.4. Thus, to maintain a large difference between the IR signals for *R*-MA and *S*-MA, the solutions for subsequent analyses were kept at pH >4.5.

4.3. Effect of temperature on the determination of enantiomeric compositions

To examine the effect of temperature on the formations of inclusion complexes, sample solutions of 1 mM *S*-MA and 1 mM *R*-MA were examined. The typical detection time profiles for *S*-MA and *R*-MA at different temperatures are plotted in Fig. 9A. Also, the ratios of the obtained signals after 30 min are plotted in Fig. 8B as a function of pH. As can be observed in Fig. 9A, the time to reach maximum signals for *R*-MA and *S*-MA were short and similar between different temperatures. The signals for *S*-MA were varied slightly when different temperature was used. However, an increase of the detected signal was observed for *R*-MA and the higher of the temperature, the higher of the detected signal. On the other hand, the values of the ratios were smaller at lower temperature. Thus, to maintain a large difference between the IR signals for *R*-MA and *S*-MA, the solutions for subsequent analyses were kept at 20 °C.

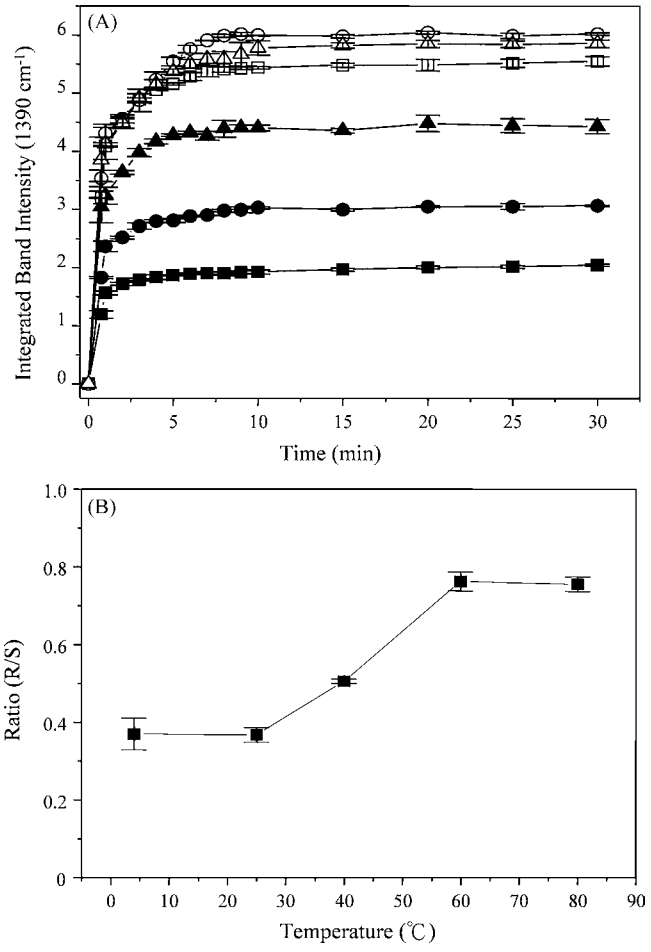

Fig. 9. (A) Time profiles for the detection of *R*-MA (1 mM) in temperatures of 20 °C (■), 40 °C (●) and 60 °C (▲). The corresponding time profiles for *S*-MA in temperatures of 20 °C (□), 40 °C (○) and 60 °C (△) are also plotted. (B) Values of the ratios of the detected signals of *R*-MA (1 mM) to *S*-MA (1 mM) at the different temperatures.

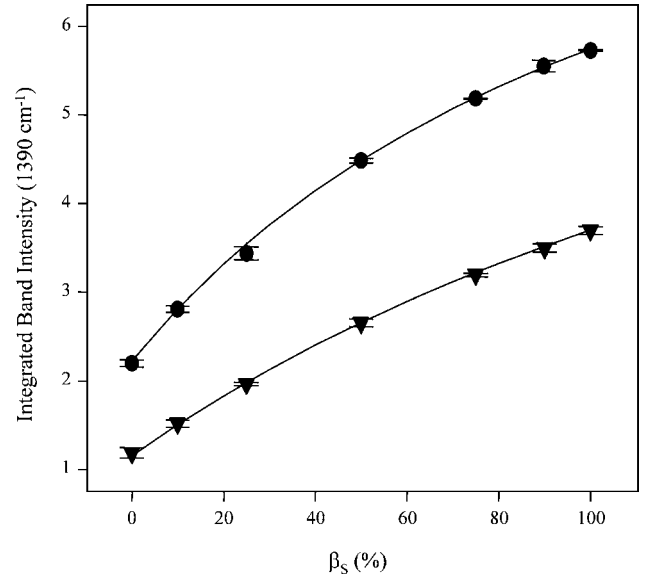

Fig. 10. The relationship between the percentage of *S*-MA and the detected IR signals recorded after 10 min. The pH of the solution was adjusted to 5.0 and the total concentration of MA ($C_S + C_R$) was maintained at either 1 mM (●) or 0.5 mM (▼) at pH 5.0. Fitted curves are also plotted (solid lines).

4.4. Performance of α-CD phase in determination of chirality

According to Eq. (7), a linear relationship can be obtained between the detected signals and the mole fractions of the *R* or *S* enantiomer if the concentration of the enantiomers is sufficiently low. To verify that the derived equation can be used to calculate the composition of a chiral compound at low concentration, *R*-MA and *S*-MA were prepared at total concentrations of 1 and 0.5 mM. The prepared solutions contained different compositions of *R*-MA and *S*-MA: the mole fractions of *S*-MA were varied from 100 to 0%. After detecting these mixtures using the α-CD-modified sensor, the obtained signals were plotted (Fig. 10) against the mole fraction of *S*-MA at total concentrations of 1.00 and 0.50 mM. As can be observed in Fig. 10A, a relationship exhibiting curvature occurred when the total concentration was 1 mM. When concentration was lower (i.e. 0.5 mM), a more linear relationship between the obtained signals and the mole fraction of *S*-MA could be obtained. The detected signals can be fitted with Eq. (6) very well; this fitted

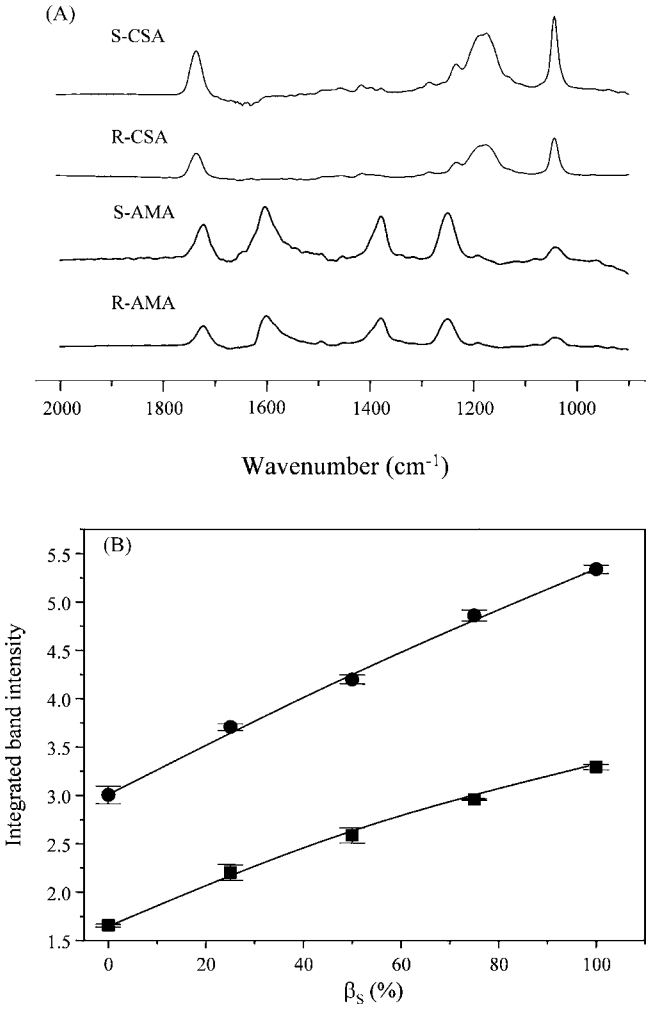

Fig. 11. (A) Typical detected spectra of AMA and CSA. (B) The relationship between the percentage of *S* enantiomer and the detected IR signals recorded after 10 min. AMA (■) and CSA (●) were examined at total concentrations ($C_S + C_R$) of 1 mM and at pH 5.0. Fitted curves are also plotted (solid lines).

curve is also plotted in Fig. 10 as solid lines. This finding suggests the prediction of the response for the mixture is suitable and that the equations shown in the Section 2 are feasible to describe the detection behaviors.

To further study the applicability of this proposed method in a general sense, two other chiral compounds were examined: acetylmandelic acid (AMA) and 10-camphorsulfonic acid, both as their *R* and *S* enantiomers. As can be observed at the bottom of Fig. 11A, the IR signals were intense, which reveals the sensitivity of the detection of these two compounds; in addition, based on the positions of the bands, the detected spectra of these two compounds were also similar to the corresponding spectra of the salt of MA. The detected IR signals were plotted (Fig. 11B) with respect to the mole fractions of the *S* enantiomers by preparing AMA and CSA solutions at total concentrations of 1 mM and varying the relative amounts of the *R* and *S* enantiomers at pH 5.0. The results indicated that the values of the ratios of the *R*- and *S* enantiomers of these two compounds – 0.52 (±0.03) and 0.56 (±0.03) for AMA and CSA, respectively – were close to that observed for MA at pH 5.0. These results reveal that this method may be applied to determine the enantiomeric composition of a range of organic compounds that form inclusion complexes with CDs.

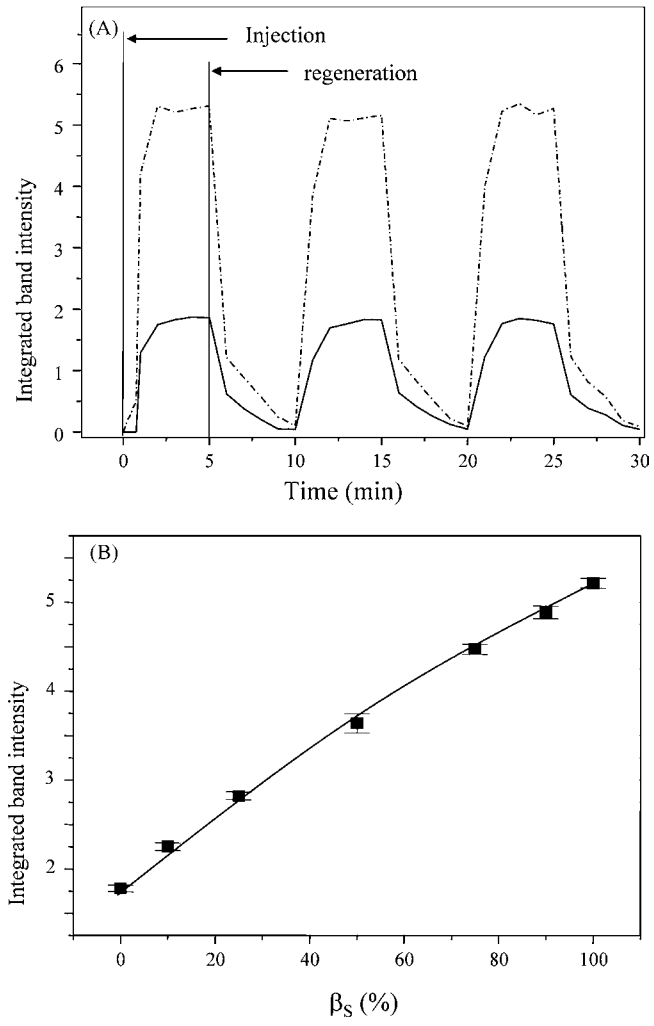

Fig. 12. (A) Detected signals for three consecutive runs based on flow-cell device. (B) The relationship between the percentage of *S*-MA and the detected IR signals. The pH of the solution was adjusted to 5.0 and the total concentration of MA ($C_S + C_R$) was maintained at 1 mM at pH 5.0.

4.5. Simplification of detection procedures by a flow-cell device

As can be seen in the response time profiles for static detection system, the response of α-CD sensing phase is fast. This reveals that the determination of enantiomeric composition is approachable in a configuration of flow-cell. To prove this, a flow-cell described in Section 3 was used to determine the enantiomeric composition of MA in a concentration of 1 mM. The pH was adjusted to 5.0 and the flow rate was kept 3 mL/min. A manual switch located in the pump head allows the switching between sample solutions and regeneration solutions. After pumping sample solution for 5 min, pump was switched to pump regeneration solution (pH 2.5 water) for another 5 min to regenerate the sensing phase. The obtained response profiles are plotted in Fig. 12A. By injection of series of MA solutions, the obtained IR signals (integrated band intensity) against the compositions of *S*-MA are plotted in Fig. 12B. By comparison to Fig. 10, it can be seen that the observed relationship is the same as static detection system. These data also proved that with a flow-cell device, the whole detection process for one run could be completed within 10 min.

5. Conclusion

An α-CD-modified sensing phase was applied to infrared sensing system for determining the composition of enantiomeric composition of chiral compounds. Theoretical equations were derived and their accuracy was proven by experimental data. Factors, such as pH and temperature of the solution, influenced the formation constants significantly. By manipulating these factors, the differences between the detected signals of enantiomers can be enlarged. Linear relationships were obtained theoretically and experimentally between the detected signals and the mole fractions of one enantiomeric form of the chiral compound under the condition that the concentration of the analytes is low enough. With a flow-cell design, this infrared sensing system can be further improved and one sample can be analyzed within 10 min.

Acknowledgement

The authors thank the National Science Council of the Republic of China for supporting this work financially under contract no. NSC96-2113-M-005-005.

References

[1] J. Bojarski, Chem. Anal. 42 (1997) 139.
[2] D.W. Armstrong, S.H. Han, CRC Crit. Rev. Anal. Chem. 19 (1988) 175.
[3] W.H. Hinze, Sep. Purif. Methods 10 (1981) 159.
[4] D.W. Armstrong, Anal. Chem. 59 (1987) 84A.

[5] R. Shellie, P.J. Marriott, Anal. Chem. 74 (2002) 5426.
[6] W. Liu, J.J. Gan, J. Agric. Food Chem. 52 (2004) 736.
[7] D.W. Armstrong, T.J. Ward, R.D. Armstrong, T.E. Beesley, Science 232 (1986) 1132.
[8] R.A. Menges, D.W. Armstrong, in: S. Ahuja (Ed.), ACS Symposium Series 471, American Chemical Society, Washington DC, 1991, p. 67.
[9] V. Schurig, H. Nowotny, Angew. Chem., Int. Ed. Engl. 29 (1990) 939.
[10] A. Glausch, J. Hahn, V. Schurig, Chemosphere 30 (1995) 2079.
[11] J.W. Jörgenson, K.D. Lukacs, J. Chromatogr. 218 (1981) 209.
[12] S.G. Penn, E.T. Bergstrom, D.M. Goddall, J.S. Loran, Anal. Chem. 66 (1994) 2866.
[13] J. Snopek, L. Jelinek, E. Smolkova', J. Chromatogr. A 609 (1992) 1.
[14] R. Kuhn, S. Hoffstetter-Kuhn, Chromatographia 34 (1992) 505.
[15] S. Terabe, K. Otsuka, H. Nishi, J. Chromatogr. A 666 (1994) 295.
[16] S. Eberhart, R. Rothchild, Appl. Spectrosc. 38 (1984) 74.
[17] M.G. Finn, Chirality 14 (2002) 534.
[18] R. Rothchild, Enantiomer 5 (2000) 457.
[19] J. Zukowski, Y. Tang, A. Berhod, D.W. Armstrong, Anal. Chim. Acta 258 (1992) 83.
[20] C.D. Tran, V.I. Grishko, D. Oliverira, Anal. Chem. 75 (2003) 6458.
[21] G. Hembury, M. Rekharsky, A. Nakamura, Y. Inoue, Org. Lett. 2 (2000) 3257.
[22] G. Grigorean, J. Ramirez, S.H. Ahn, B. Lebrilla, Anal. Chem. 72 (2000) 4275.
[23] W.A. Tao, R.G. Cooks, Anal. Chem. 75 (2003) 25A.
[24] L. Wu, E.C. Meurer, R.G. Cooks, Anal. Chem. 76 (2004) 663.
[25] J. Yang, W.C. Chen, Int. J. Environ. Anal. Chem. 79 (2001) 199.
[26] J. Yang, S.C. Chen, Appl. Spectrosc. 55 (2001) 399.
[27] J. Yang, C.P. Tsui, Anal. Chim. Acta 442 (2001) 267.
[28] S. Li, W.C. Purdy, Chem. Rev. 92 (1992) 1457.
[29] K.A. Connors, Chem. Rev. 97 (1997) 1325.
[30] J. Szejtli, Chem. Rev. 98 (1998) 1743.
[31] J. Snopek, E. Smolkova-Keulemansova, T. Cserhati, K.H. Gahm, A.A. Stalcup, in: J. Szejtli, T. Osa (Eds.), Comprehensive Supramolecular Chemistry, Pergamon Press, Oxford, 1996, p. 515.
[32] N.J. Harrick, Internal Reflection Spectroscopy, Wiley, New York, 1967.
[33] R. Krska, R. Kellner, U. Schiessel, M. Tacke, A. Katzir, Appl. Phys. Lett. 63 (1993) 1868.
[34] J. Heo, M. Rodrigues, S. Saggese, G.H. Sigel Jr., Appl. Opt. 30 (1991) 3944.
[35] M.C. Ertan-Lamontagne, S.R. Lowry, W.R. Seitz, S.A. Tomellini, Appl. Spectrosc. 49 (1995) 1170.
[36] R. Gobel, R. Krska, R. Kellner, W.R. Seitz, S.A. Tomellini, Appl. Spectrosc. 48 (1994) 678.

Available online at www.sciencedirect.com
ScienceDirect
Talanta 74 (2008) 1615–1620
Talanta
www.elsevier.com/locate/talanta

Separation and determination of polyethylene glycol fatty acid esters in cosmetics by a reversed-phase HPLC/ELSD

Yong Hwa Lee [a], Eun Sook Jeong [b], Hwang Eui Cho [b], Dong-Cheul Moon [b,*]

[a] *Analytical Laboratory, R&D Institute, LG Household and Health Care, Taejeon 305-343, Republic of Korea*
[b] *College of Pharmacy, CBITRC, Chungbuk National University 48, Gaeshin-Dong, Heungdukgu, Cheongju, Chungbuk 361-763, Republic of Korea*

Received 2 July 2007; received in revised form 5 October 2007; accepted 8 October 2007
Available online 18 October 2007

Abstract

A comprehensive analytical method was established for the separation of polyethylene glycol (PEG) stearates according to the distribution of ethylene oxide (EO) and subsequent determination of the surfactants in cosmetic samples by using a high-performance liquid chromatography–evaporative light scattering detection. Separation of the PEG stearates comprising approximately up to 82 EO adducts was performed on a reversed-phase YMC-Pack C_8 column using water–acetonitrile gradient elution. The PEG oligomers were separated in order of the increasing number of EO adducts. Quantitation of the PEG fatty acid esters, which was separated as single peak per each component, was performed by chromatography on a reversed-phase Wakosil 10 C_{18} column using water–methanol gradient elution. The standard curve to quantify the PEG stearates was constructed by the log–log plot, which showed good linearity with the correlation coefficients (R^2) 0.998 and more. Working range, repeatability, limit of detection and recovery were acceptable for analysis of the surfactants in cosmetic products. The analytical methods were applied to characterize the PEG stearates according to the EO distributions, then to quantify the surfactants in cosmetic products.
© 2007 Elsevier B.V. All rights reserved.

Keywords: HPLC; ELSD; EO units; Surfactants; Cosmetics; PEG stearate

1. Introduction

Non-ionic surfactants of the polyethylene glycol (PEG) fatty acid esters, alkylethoxylated alcohol and alkylphenol polyethoxylates, have extensively been used as emulsifiers, dispersing agents and defoamers in the fields of cosmetics, household goods and medicines [1,2]. The PEG stearates (Fig. 1) have been used as a typical emulsifier in the preparation of cosmetics. Industrial uses of PEG fatty acid esters are different according to their physicochemical properties, which depend on the number and distributions of ethylene oxide (EO) adducts. The PEG oligomers with more than 40 EO units are commonly used as the raw materials of cosmetics because they have better moisturizing effects, more safety and hydrophilic properties than those with less EO units. The EO distribution in individual oligomer depends on the reaction conditions and compositions of the reaction mixture. Therefore, analysis of the EO distributions of PEG oligomers and determination of each surfactant in complex formulations are essential for the quality control of cosmetic products.

Sample preparations, chromatography and detection methods for the analysis of non-ionic surfactants were reported in several papers [3–6]. Gas chromatography has been used widely, but it has some limitation from the necessity of volatile derivatization of high oligomers [7]. High-performance liquid chromatography (HPLC) has mostly been used for the analysis of the surfactants with high molecular weight because it is a popular analytical method for the distribution of ethoxymers, the average degrees of ethoxylation and the hydrophobic moieties in surfactants. Normally, separation of EO distribution was made by normal-phase HPLC [8–10], while analysis of the alkyl chains by reversed-phase HPLC on C_8 or C_{18} columns [11–14]. UV detection is not useful for the analyses of lacking chromophores. The use of refractive index (RI) detector has limitation from its low sensitivity and non-applicability of gradient elution [15,16]. Liquid chromatography–mass spectrometry (LC–MS) is a powerful tool in the analysis of the surfactants composed of EO oligomers and alkyl chains [17–19]. However, it requires too high cost

* Corresponding author. Tel.: +82 43 261 2819; fax: +82 43 275 6131.
E-mail address: dcmoon@chungbuk.ac.kr (D.-C. Moon).

0039-9140/$ – see front matter © 2007 Elsevier B.V. All rights reserved.
doi:10.1016/j.talanta.2007.10.020

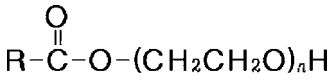

Fig. 1. Structure of PEG stearates.

and sophisticated technique to use the apparatus routinely in industrial fields. Evaporative light scattering detector (ELSD) has been used extensively for the analysis of non-ionic surfactants because it has high sensitivity of detection even for the surfactants without chromophores, as well, it has the capability for gradient elution. Recently, a few reports on the quantitative analysis of surfactants using HPLC–ELSD have appeared [20–23]. The HPLC methods reported up to present are only available for the analysis of non-ionic surfactants with less than 40 EO adducts [24].

Therefore, the aim of this work was to develop the successive analytical method to separate the PEG oligomers of high molecular weights in sequence of their EO units, and then to quantify the non-ionic surfactants in cosmetic products. This paper describes the HPLC separation of individual ethoxylated surfactants on a reversed-phase C_8 column according to their EO distribution, and then HPLC determination of the surfactants using a reversed-phase C_{18} column. The method to analyze the PEG stearates incorporating up to 82 EO units or more was successfully applied to the comprehensive analysis of cosmetic products.

2. Experimental

2.1. Reagents and chemicals

The PEG-25 and PEG-55 stearates (labeled as 99% pure) were obtained from Nikko Chemicals Co. Ltd. (Tokyo, Japan), and the PEG-40 stearate (labeled as 99% pure) from Uniqema (Gouda, The Netherlands). HPLC-grade methanol, acetonitrile and *n*-hexane were purchased from Burdick and Jackson Labs. (Muskegon, MI, USA). Sodium methoxide and sulfuric acid were purchased from Sigma–Aldrich (Saint Louis, USA). Deionized water (>18 MΩ cm^{-1}) was obtained by passing distilled water through Millipore Milli-RO4 and Milli-Q water purification systems (Bedford, MA, USA). The test samples of cosmetic products (lotion and cream) were provided by the LG Household & Health care Co. (Daejon, Korea).

2.2. Chromatographic conditions for HPLC analysis

The HPLC system consisted of an Agilent 1100 series (Agilent Technologies, Palo Alto, CA, USA) with a vacuum degasser, a quaternary pump and an autosampler with 100 μL injection loop (injection volume, 50 μL). Separation of EO distribution was performed on a YMC-Pack C_8 column (250 mm × 4.6 mm i.d., 5 μm) and quantitative analysis of PEG stearates was performed on a Wakosil 10 C_{18} column (250 mm × 4.6 mm i.d., 10 μm) with the column temperature set at 30 °C. The HPLC detector was an Alltech 3300 ELSD (Alltech Associates, USA) whose signal was integrated to a 35900E interface. The detector was warmed up for 30 min prior to each run, then operated at 45 °C with the optimum flow rate of the nebulizing gas (nitrogen, 99.99%) at 1.5 L/min. The gradient conditions for the separation of EO distribution and for quantitation are shown in Table 1.

Table 1
Gradient conditions for HPLC analysis of PEG stearates

Time (min)	Flow rate (mL/min)	H_2O (%)	Acetonitrile (%)
(A) Gradient condition for the EO separation on a C_8 column (stop time, 105 min; post-time (equilibration), 10 min)			
0	1.0	80.0	20.0
30	1.0	74.4	25.6
100	0.5	65.0	35.0
105	1.0	80.0	20.0
Time (min)	Flow rate (mL/min)	H_2O (%)	Methanol (%)
(B) Gradient condition for quantitative determination of the PEG stearates on C_{18} column (stop time, 45 min; post-time (equilibration), 10 min)			
0	1	60.0	40.0
10	2	20.0	80.0
30	2	20.0	80.0
45	1	60.0	40.0

2.3. Gas chromatography and LC–MS analysis

The gas chromatography which was used to analyze the alkyl chains of the PEG fatty acid esters was a HP 6890 series (Hewllet-Packard, Palo Alto, CA, USA) with FID detector and a capillary column, HP-FFAP (25 m × 0.320 mm, i.d., 0.5 μm). The injector and detector temperatures were set at 245 and 250 °C, respectively. One micro-liter aliquot of sample was injected through a split injection (1:30). The oven temperature was set at 80 °C (0 min) then, increased to 240 °C at 8 °C/min (hold for 20 min).

The molecular weights in a chromatogram showing the EO distribution of the PEG stearates were confirmed by a positive ion LC–ESI–MS analysis. The LC–MS system consisted of a PE-Sciex API-3000 triple quadrupole mass spectrometer (Applied Biosystems. MDS Sciex, Concord, Canada) coupled with an Agilent 1100 series HPLC system (Agilent Technologies, Palo Alto, CA, USA). The MS operating conditions using nitrogen as the nebulizing and curtain gas were as follows: the ion source voltage, 5.5 kV (temperature, 380 °C); nebulizing gas flow, 1.04 L/min; auxiliary gas flow, 6.1 L/min; curtain gas flow, 1.25 L/min; orifice voltage, 53 V; ring voltage, 400 V. A mass range of 120–1300 amu was scanned at a scan time of 2 s. Automated data acquisition and processing were carried out by using the software (PE-Sciex Analyst Version 1.1). LC separation of the column eluate (10-μL aliquots) was performed on a Gemini C_{18} column (Phenomenex, USA, 150 mm × 2.0 mm i.d., 5 μm) maintained at 40 °C. The gradient elution with the acetonitrile-20 mM ammonium acetate was used from 20:80 (v/v), 0 min to 35: 65(v/v), 80 min at 0.2 mL/min.

2.4. Preparation of standard and sample solutions

Stock solutions (5%, w/v) of the analytes were prepared in methanol. The working solutions were prepared by serially diluting the stock solutions with methanol. The concentration of calibration curve was 180.2, 305.8, 407.8, 543 and 725 μg/mL for PEG-40 stearate and 126.2, 250.1, 312.6, 390.7, 488.4, 610.5 and 763.1 μg/mL for PEG-55 stearate. The test samples (lotion and cream) were dissolved in methanol and centrifuged at 3500 rpm for 15 min at 25 °C, then the supernatant was filtered through a membrane filter (PTFE 0.45 μm) prior to HPLC analysis.

The fatty acid moieties of the PEG stearates were confirmed by the GC analysis of the HPLC eluates after methylation [25]. One-milliliter aliquots of the eluate were evaporated to dryness under nitrogen. The residue was refluxed for 20 min after addition of 0.2 M sodium methoxide in methanol (1.25 mL). To the reaction mixture, 4% sulfuric acid in methanol (1.5 mL) was added, then refluxed further for 40 min at 90 °C. After cooling the reaction mixture, the fatty acid methyl esters were extracted with *n*-hexane (2 mL), then 2-μL aliquots from the extracts were GC analyzed as described before.

3. Results and discussion

3.1. Chromatography

We separated and determined the highly ethoxylated fatty acid esters, PEG-25, PEG-40 and PEG-55 stearate by two reversed-phase HPLC methods. The ethoxylated oligomers of PEG stearates were eluted in order of increasing size of the oligomers from a C_8 column by the water–acetonitrile gradient elution, and exhibited the EO distribution for the PEG stearates (Fig. 2). The EO distributions were clearly resolved for PEG-25 (17–38 EO units), PEG-40 (27–52 EO units), and PEG-55 (37–68 EO units), respectively. Apparently, the PEG-55 stearate was highly ethoxylated even up to the 82 EO units or more. Therefore, this chromatographic method provided a mean of quality control for the non-ionic surfactants with high moles of EO adduct.

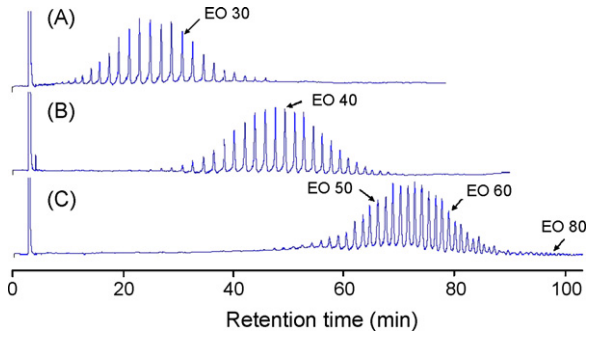

Fig. 2. HPLC chromatograms showing the EO separations of PEG stearates: (A) PEG-25 stearate, (B) PEG-40 stearate and (C) PEG-55 stearate. Upper trace in (C) is a magnified part near EO 80. HPLC conditions: YMC-Pack C8 (250 mm × 4.6 mm i.d., 5 μm) column; ELSD detection and gradient elution (Table 1A).

The EO chain length of the eluted peaks of PEG stearates were confirmed by comparing the corresponding mass spectra of EO adducts with the calculated mass of cluster ions

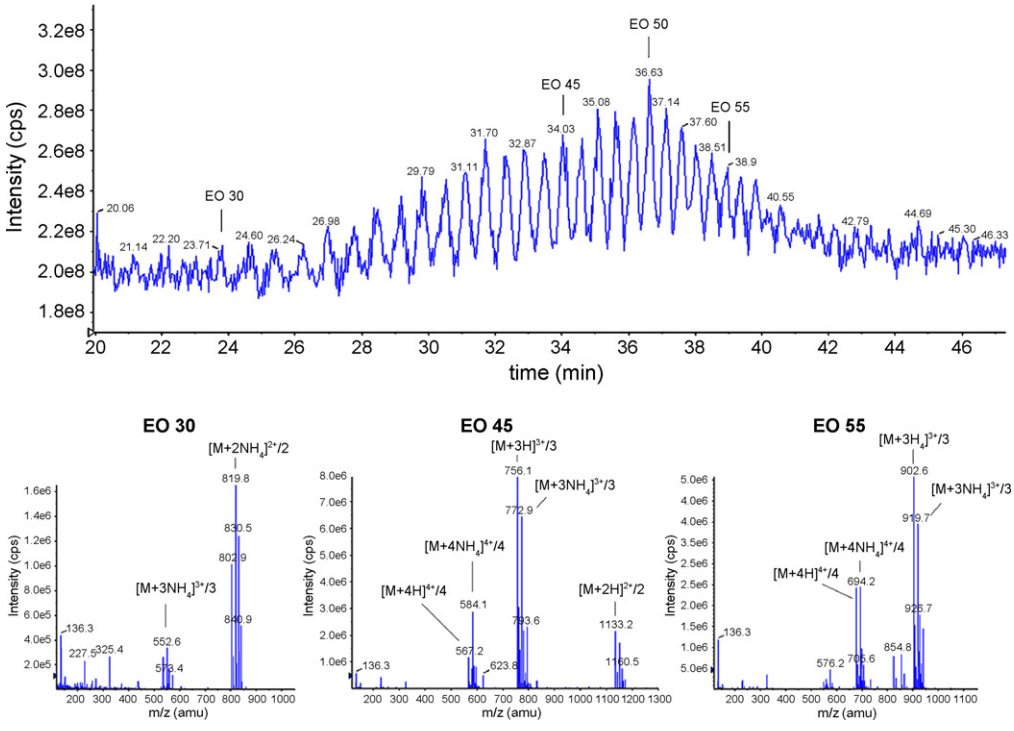

Fig. 3. LC–TIC–MS chromatogram of PEG-50 stearate (upper) and corresponding mass spectra (lower).

Table 2
Cluster ions (*m/z*) used for the identification of PEG stearates

PEG stearates	Nominal mass	Charge (+4)		Charge (+3)		Charge (+2)		Charge (+1)	
		H^+ adduct	NH_4^+ adduct	H^+ adduct	NH_4^+ adduct	H^+ adduct	NH_4^+ adduct	H^+ adduct	NH_4^+ adduct
$C_{17}H_{35}COO(CH_2CH_2O)_{23}H$	1296	325	342	433.0	450.0	649	666	1297	1314
$C_{17}H_{35}COO(CH_2CH_2O)_{24}H$	1340	336	353	447.7	464.7	671	688	1341	1358
$C_{17}H_{35}COO(CH_2CH_2O)_{25}H$	1384	347	364	462.3	479.3	693	710	1385	1402
$C_{17}H_{35}COO(CH_2CH_2O)_{26}H$	1428	358	375	477.0	494.0	715	732	1429	1446
$C_{17}H_{35}COO(CH_2CH_2O)_{27}H$	1472	369	386	491.7	508.7	737	754	1473	1490
$C_{17}H_{35}COO(CH_2CH_2O)_{38}H$	1956	490	507	653.0	670.0	979	996	1957	1974
$C_{17}H_{35}COO(CH_2CH_2O)_{39}H$	2000	501	518	667.7	684.7	1001	1018	2001	2018
$C_{17}H_{35}COO(CH_2CH_2O)_{40}H$	2044	512	529	682.3	699.3	1023	1040	2045	2062
$C_{17}H_{35}COO(CH_2CH_2O)_{41}H$	2088	523	540	697.0	714.0	1045	1062	2089	2106
$C_{17}H_{35}COO(CH_2CH_2O)_{42}H$	2132	534	551	711.7	728.7	1067	1084	2133	2150
$C_{17}H_{35}COO(CH_2CH_2O)_{48}H$	2396	600	617	799.7	816.7	1199	1216	2397	2414
$C_{17}H_{35}COO(CH_2CH_2O)_{49}H$	2440	611	628	814.3	831.3	1221	1238	2441	2458
$C_{17}H_{35}COO(CH_2CH_2O)_{50}H$	2484	622	639	829.0	846.0	1243	1260	2485	2502
$C_{17}H_{35}COO(CH_2CH_2O)_{51}H$	2528	633	650	843.7	860.7	1265	1282	2529	2546
$C_{17}H_{35}COO(CH_2CH_2O)_{52}H$	2572	644	661	858.3	875.3	1287	1304	2573	2590
$C_{17}H_{35}COO(CH_2CH_2O)_{53}H$	2616	655	672	873.0	890.0	1309	1326	2617	2634
$C_{17}H_{35}COO(CH_2CH_2O)_{54}H$	2660	666	683	887.7	904.7	1331	1348	2661	2678
$C_{17}H_{35}COO(CH_2CH_2O)_{55}H$	2704	677	694	902.3	919.3	1353	1370	2705	2722
$C_{17}H_{35}COO(CH_2CH_2O)_{56}H$	2748	688	705	917.0	934.0	1375	1392	2749	2766
$C_{17}H_{35}COO(CH_2CH_2O)_{57}H$	2792	699	716	931.7	948.7	1397	1414	2793	2810
$C_{17}H_{35}COO(CH_2CH_2O)_{58}H$	2836	710	727	946.3	963.3	1419	1436	2837	2854
$C_{17}H_{35}COO(CH_2CH_2O)_{59}H$	2880	721	738	961.0	978.0	1441	1458	2881	2898
$C_{17}H_{35}COO(CH_2CH_2O)_{60}H$	2924	732	749	975.7	992.7	1463	1480	2925	2942

concerning the EO adducts. Fig. 3 illustrates a LC–TIC–MS chromatogram of a PEG-50 stearate (upper trace) and the three mass spectra (lower trace). The measured mass of the multiple charged ions in mass spectra was in agreement with the calculated mass of the cluster ions of PEG stearates (Table 2). The mass differences (44 amu) between the homologous EO peaks was identified as well as the main cluster ions due to the pseudo molecular ions ($[M+n\mathrm{H}]^{n+}/n$ and $[M+n\mathrm{NH_4}]^{n+}/n$).

Another aim of the present work was to establish the optimized HPLC separation of the PEG stearates as single peak per each component in order to determine the PEG fatty acid esters in cosmetic products. Reversed-phase C_{18} column was appropriate for the separation of the PEG esters according to their hydrophobic characteristics. HPLC analysis was accomplished on a C_{18} column using water–methanol gradient elution (Fig. 4). The PEG-40 and PEG-55 stearate exhibited either two or three peaks that were attributed to alkyl homologous species of the PEG stearates.

GC analysis of the HPLC eluates after methylation showed that the PEG stearates included fatty acid homologs (C14, C16 and C18 carbon chains) with the composition such as C14, 0.4%; C16, 43.3%; C18, 55.3% for the PEG-40 stearate and C14, 3.3%; C16, 38.0%; C18, 58.7% for the PEG-55 stearate. Therefore, the fatty acid homologues of the PEG stearates were originated from the fatty acids (C16:0 and C18:0) contained in the raw materials (stearic acid or its esters) of the industrial grade prior to ethoxylation reactions.

3.2. Method validation

The working range, the limit of detection and repeatability for the analysis of PEG stearates is shown in Table 2. The linearity was determined by triplicate analyses of standard solutions. For calibration graphs, the log–log plots for the peak area versus concentration were drawn to obtain linearity [22] because of the nonlinearity of the detector response versus concentration. The limit of detection (LOD) for the PEG-40 and PEG-55 stearate was 50.2 and 55.5 μg/mL, respectively based on a signal-to-

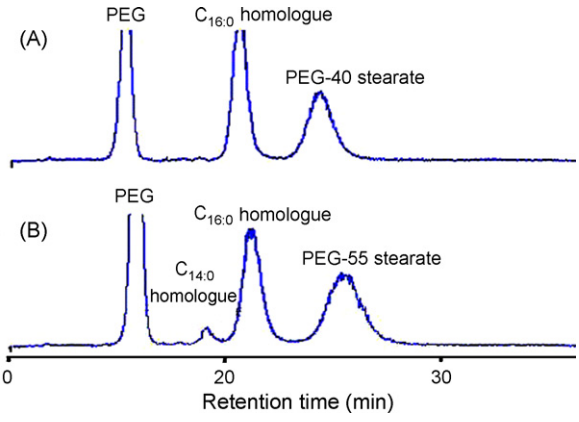

Fig. 4. Chromatograms of PEG stearates for quantitative determination by HPLC: (A) PEG-40 stearate and (B) PEG-55 stearate. HPLC conditions: Wakosil $10C_{18}$ column (250 mm × 4.6 mm i.d., 10 μm), ELSD detection, water–methanol gradient (Table 1B).

Table 3
Detection limits, working ranges, correction coefficients and repeatability

Surfactant	Detection limit (μg/mL)[a]	Working range (μg/mL)	Correlation coefficient	Repeatability (%)
PEG-40 stearate	50.2	180.2–725.0	0.998	0.9–3.6
PEG-55 stearate	55.5	126.2–763.1	0.999	0.6–3.7

[a] Detection limit: the measured concentrations of the analytes based on the three S/N values.

Table 4
Analytical results of two cosmetic products (±S.D., $n = 4$)

Cosmetic product	Surfactant	Concentration in sample (w/v, %)	Fortified concentration (w/v, %)	Concentration in fortified sample (w/v, %)
Lotion	PEG-40 stearate	1.0 ± 0.1	1.0	1.96 ± 0.1
Cream	PEG-55 stearate	1.5 ± 0.1	1.0	2.53 ± 0.1

noise ratio of 3. The repeatability of the measurements was better than R.S.D. at 3.7% for both surfactants (Table 3).

3.3. Application to real sample analysis

Fig. 5(A) represents the typical HPLC chromatograms of the EO separation of PEG stearates contained in real cosmetic samples (lotion and cream). The two EO chromatograms were clearly resolved with no interferences from other ingredients. Fig. 5(B) shows the HPLC chromatograms for determination of the non-ionic surfactants in the two cosmetic products. They showed adequate resolution with no interferences from other ingredients. The early eluting peaks were assumed some ingredients in the cosmetics and residual polyethylene glycols. As shown in Table 4, contents of the PEG stearates in the two cosmetic products were 1.0 and 1.5%, respectively. Recoveries calculated from standard addition method were in the range of 98–101%.

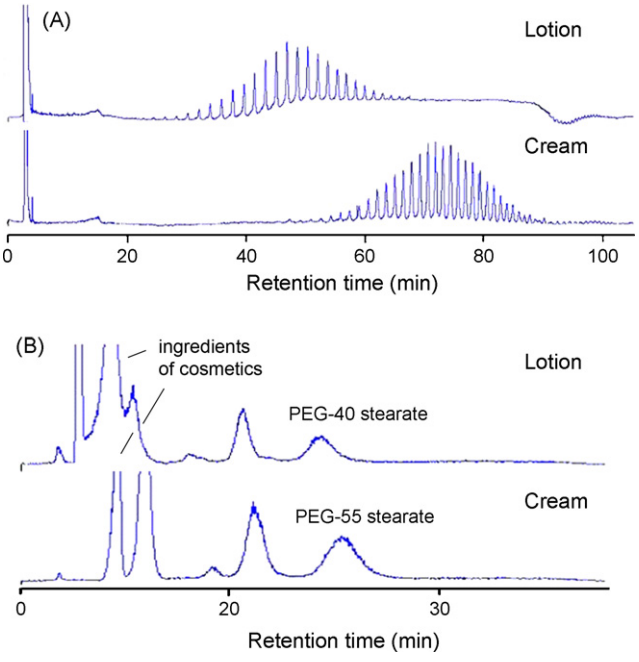

Fig. 5. HPLC chromatograms showing the EO separations of PEG stearates in cosmetic samples (lotion and cream) (A) and the HPLC chromatograms showing the separation of PEG fatty acid esters in the same cosmetic samples (B). The HPLC conditions of (A) and (B) are same as described in Figs. 2 and 4, respectively.

4. Conclusion

Two reversed-phase HPLC–ELSD detection methods were developed for the separation of the EO distribution of PEG stearates and the quantitation of the surfactants in cosmetic products. EO separation of the highly surfactant ethoxylated even up to 82 EO or more was performed on a C_8 stationary phase using water–acetonitrile gradient elution. Determination of the surfactants as single peak was performed on a C_{18} stationary phase with water–methanol gradient elution. The comprehensive analytical methods for the highly ethoxylated fatty acid esters would be useful as a practical mean for the quality control of cosmetic products.

Acknowledgements

This work was supported by the Regional Research Centers Program of the Ministry of Education & Human Resources Development in Korea, and partly by 2007 General subject support by Chungbuk National University, Republic of Korea.

References

[1] R. Kleber, Chemiefasern/Textilindustrie 38 (1988) E59.
[2] A. Schulberger, Chemiefasern/Textilindustrie 40 (1990) E27.
[3] C. Crescenzi, A. Di Corcia, R. Samperi, Anal. Chem. 67 (1995) 1797.
[4] M. Castillo, F. Ventura, D. Barceló, Waste Manage. 19 (1999) 101.
[5] K.A. Krogh, K.V. Vejrup, B.B. Mongensen, B. Halling-Sørensen, J. Chromatogr. A 957 (2002) 45.
[6] M. Takino, S. Daishima, K. Yamaguchi, J. Chromatogr. A 904 (2000) 65.
[7] A. Marcomini, M. Zanette, J. Chromatogr. A 733 (1996) 193.
[8] M. Ahel, W. Giger, Anal. Chem. 57 (1985) 2584.
[9] A.M. Rothman, J. Chromatogr. 253 (1982) 283.
[10] S. Cheng, M. Baird, H.A. Anderson, D.L. Brydon, J. Chromatogr. A 771 (1997) 145.
[11] R.E.A. Escott, M. Mortimer, J. Chromatogr. 553 (1991) 423.
[12] C.-Y. Cheng, W.-H. Ding, J. Chromatogr. A 968 (2002) 143.
[13] F.I. Portet, C. Treiner, P.L. Desbène, J. Chromatogr. A 878 (2000) 99.

[14] M. Balcan, Colloids Surf. A 221 (2003) 1.
[15] K. Rissler, J. Chromatogr. A 742 (1996) 1.
[16] P.L. Desbene, F.I. Portet, G.J. Goussot, J. Chromatogr. A 730 (1996) 209.
[17] M. Cantero, S. Rubio, D. Perez-Bendito, J. Chromatogr. A 1046 (2004) 147.
[18] C.J. Sparham, I.D. Bromilow, J.R. Dean, J. Chromatogr. A 1062 (2005) 39.
[19] B. Shao, J. Hu, M. Yang, J. Chromatogr. A 950 (2002) 167.
[20] G. Cretier, C. Podevin, J.-L. Rocca, J. Chromatogr. A 874 (2000) 305.
[21] L.M. Nair, N.V. Stephens, S. Vincent, N. Raghavan, P.J. Sand, J. Chromatogr. A 1012 (2003) 81.
[22] H.S. Park, H.R. Ryu, C.K. Rhee, Talanta 70 (2006) 481.
[23] H.S. Park, C.K. Rhee, J. Chromatogr. A 1046 (2004) 289.
[24] S. Cheng, M. Baird, H.A. Anderson, D.L. Brydon, J. Chromatogr. A 731 (1996) 161.
[25] IUPAC (Ed.), Standard Methods for the Analysis of Oils, Fats and Derivatives, 1st Supplement to the 7th Edition, International Union of Pure and Applied Chemistry, Pergamon Press, Oxford, 1992.

Available online at www.sciencedirect.com
ScienceDirect
Talanta 74 (2008) 1247–1255
Talanta
www.elsevier.com/locate/talanta

Molecularly imprinted polymer grafted on polysaccharide microsphere surface by the sol–gel process for protein recognition

Feng Li, Jing Li, ShuSheng Zhang *

Key Laboratory of Eco-chemical Engineering, Ministry of Education, College of Chemistry and Molecular Engineering, Qingdao University of Science and Technology, Qingdao 266042, PR China

Received 29 June 2007; received in revised form 28 August 2007; accepted 29 August 2007
Available online 5 September 2007

Abstract

An interfacial organic–inorganic hybridization concept was applied to the preparation of a new spherical imprinted material for protein recognition. The functional biopolymer chitosan (CS), shaped as microsphere and high-density cross-linked, constituted of the polysaccharide core for surface imprinting. After the model template protein, bovine serum albumin, was covalently immobilized by forming imine bonds with the functional amine groups of CS, two kinds of organic siloxane (3-aminopropyltrimethoxysiloxane: APTMS, and tetraethoxysiloxane: TEOS) assembled and polymerized on the polysaccharide–protein surface via sol–gel process in aqueous solution at room temperature. After template removal, the protein-imprinted sol–gel surface exhibited a prevalent preference for the template protein in adsorption experiments, as compared with four contrastive proteins. Bioinformatics methods were also employed to investigate the imprinting process and the recognition effect. The influence of siloxane type, pH, siloxane/water ratio on template removal and recognition selectivity was assessed. Under optimized imprinting conditions, a large quantity of well-distributed pores was observed on the immobilized-template imprinted surface. The surface-imprinted adsorbent offered a fast kinetics for template re-adsorption and could be reused. Compared with the imprinted material prepared with free-template, material prepared with immobilized-template possessed higher adsorption capacity towards template protein. Easy preparation of the described imprinted material, high affinity and good reusability make this approach attractive and broadly applicable in biotechnology for down-stream processing and biosensor.
© 2007 Elsevier B.V. All rights reserved.

Keywords: Surface imprinting; Organic–inorganic; Sol–gel; Polysaccharide; Protein recognition

1. Introduction

Synthetic materials specific for protein recognition are highly desirable in biotechnology for down-stream processing and biosensor. Selective recognition elements traditionally used within affinity materials have been molecules such as antibodies and cell receptors. Despite success achieved with those biomaterials, their limited stability and expensive production preclude the application in cheap and reusable affinity adsorbents, membranes, and sensors [1,2]. Recently, the use of relatively inert molecular imprinted polymers (MIPs) for protein recognition offers potential by introducing selective specificity into low-cost, stable and easily fabricated materials [1–5].

The preparation of MIPs using molecular imprinting technology lies in the template-mediated assembly of functional monomers. Despite applications target molecules with low molecular weight [1,6–8], MIPs have now proved success in mimicking natural receptors and biological macromolecules, e.g. whole cells, viruses, and especially proteins [1–4,9]. Due to the fragility and complexity of protein molecules, specific recognition is generally achieved by the introduction of a large number of weak complementary interactions between proteins and monomers, e.g. hydrogen bonds, Van der Waals forces, ionic bonds and hydrophobic interactions [1]. Such multiply interactions result in tailored binding pockets with distinct size, shape, and three-dimensional distribution of functional groups. Currently, novel protein-imprinted polymers have been conducted via different strategies. To overcome limitations associated with bulk imprinted materials, surface imprinting seems to be the most promising way in creating protein-imprinted polymers [10–12].

The majority of imprinting technology, demonstrated to date, involves the synthesis of MIPs in organic monomer-solvent systems. Moreover, most polymerization systems lack of true water

* Corresponding author. Fax: +86 532 84022750.
E-mail address: shushzhang@qust.edu.cn (S. Zhang).

0039-9140/$ – see front matter © 2007 Elsevier B.V. All rights reserved.
doi:10.1016/j.talanta.2007.08.032

compatibility. However, proteins are usually sparingly soluble and aggregate in common monomer-solvent systems. To tag MIPs with specificity for proteins, the synthesis of MIPs in aqueous environment is preferable for better selectivity and binding [10–13]. Acrylamide has often been applied as a monomer to perform surface imprinting in aqueous media [10–16]. Guo et al. prepared MIPs using free hemoglobin (Hb) as the template molecule, acrylamide as the functional monomer, chitosan (CS) beads or vinyl groups modified CS beads as supporting matrices [14–18]. Specific attention must be paid to improve weak mechanical strength and long-term stability [15,16]. For example, chemical modification of CS beads with maleic anhydride was performed to introduce vinyl groups, which took part in the copolymerization between acrylamide and the cross-linker, *N*,*N*′-methylenebisacrylamide. Such protocol resulted in the chemical interaction between the imprinted gel and CS matrix. However, template proteins are susceptible to the attack of free radicals in radical polymerization [19]. General synthesis of chemically and mechanically stable MIPs for protein recognition in aqueous media, therefore, remains a significant challenge.

With the development of sol–gel technique, molecularly imprinted sol–gel materials (MISGMs) have been extensively studied for the preparation of selective adsorbents [6,8,12,20]. Considering the easy preparation of sol–gels and their compatibility with proteins and polar environments, coating molecularly imprinted silica sol–gel polymer on a supporting matrix has considerable potential for creating novel materials specific for proteins. Results suggest that proteins could catalytically hydrolyze siloxane precursors and promote silica formation. Additionally, the overall stability of proteins embedded in the sol–gels has been broadly proven to enhance with regard to temperature, pH, and chemical denaturation [21–24]. Until now, preparation of MISGMs using protein-imprinted sol–gel process on silica-based matrix has been attempted in a number of works. Chou et al. combine sol–gel and self-assembly technology for the preparation of human serum albumin imprinted film on the surface of piezoelectric quartz crystal [25]. The imprinted film gives selective recognition to the template protein. Shiomia et al. prepare Hb imprinted sol–gel material on the surface of aminopropyl silica in aqueous media. The Hb recognition occurs through shape, hydrophobicity and surface charge [12].

The supporting matrix plays an important role in surface imprinting. Incorporation of the functional biopolymer, CS, into inorganic network via sol–gel process takes on increasing importance in developing affinity matrices for proteins [26]. The reason comes from three aspects. Firstly, unique properties of CS enable covalent assembly of biomolecules in a spatially selective manner. Those properties include reactivity of primary amine groups, hydrophilicity and biocompatibility [26–30]. Secondly, polysaccharide-manipulated sol–gel process has shown catalytic effect and acceleration on siloxane polymerization and potentially relates to the biomineralization processes [22]. Thirdly, silica materials containing covalently grafted gluconamide moieties provide biocompatible environment for the entrapped protein [31]. Very recently, we have reported direct preparation of porous functional matrix based on surface coating technique and CS incorporated sol–gel process [32–34]. The obtained organic–inorganic hybrid matrices show promising in metal ion removal and protein separation.

This work attempts to present a new strategy for the preparation of spherical imprinted polymer for protein recognition. High-density cross-linked CS microsphere, formed using emulsion cross-linking method, constituted of the supporting core. Bovine serum albumin (BSA) was used as the model template and covalently immobilized on CS core by forming imine bonds. In the presence of the immobilized BSA, surface grafting of imprinted polymer to the polysaccharide core was achieved through interfacial organic–inorganic hybridization via a sol–gel process in aqueous solution at room temperature. After template removal by breakage of imine bonds, the imprinted surface showed selective recognition towards template protein in adsorption experiments, as compared with four contrastive proteins. The preparation methodology, main characteristic features were described and discussed in detail.

2. Experimental

2.1. Chemicals

CS, with 98% deacetylation and an average molecular weight of 6×10^4 g mol^{-1} (Yuhuan Biomedical Corp., China) was used to prepare the polysaccharide microsphere. Liquid paraffin, span 80, and epichlorohydrin were purchased from Qingdao Chemical Co., China. Formaldehyde (25%) were from Shanghai Bioengineering Corp., China. The following siloxanes were used: 3-aminopropyltrimethoxysiloxane (APTMS, Alfa aesar), gamma-glycidoxypropyltrimethoxysiloxane (GPTMS, Alfa aesar), methyltrimethoxysiloxane (MTMOS, Sigma–Aldrich), tetraethoxysiloxane (TEOS, Alfa aesar). BSA (Sigma) was used as the template protein. Beta-amylase, cytochrome *C*, transferrin and lysozyme, all from Kejie Biomedical Corp., China, were used as contrastive proteins. All other chemicals used were in analytical grade. Doubly deionized water (DDW) was used throughout this work.

2.2. Preparation of CS microsphere

CS solution was prepared by dissolving in 1 mol l^{-1} acetic acid aqueous solution with a 4 wt% CS concentration. Fifty milliliters transparent CS solution was added to 100 ml liquid paraffin containing 3 ml surfactant, span 80, with vigorous stirring for 1 h. The aqueous droplets in the water-in-oil (w/o) emulsion were quickly harden by adding 8 ml formaldehyde and reacted for 30 min at 60 °C. Then, pH was adjusted to be 10–11 using sodium hydroxide and 15 ml epichlorohydrin was added. The cross-linking process was allowed for another 6 h at 60 °C. The formed microsphere with active epoxy groups was shaken in 0.5 mol l^{-1} ammonia solution at 60 °C for 4 h to recover some amino groups lost in cross-linking [35]. A soxhlet extraction with *n*-hexane was used to

remove un-reacted reagents and emulsifer involved in microsphere. The final product was washed with ethanol followed by DDW.

2.3. Preparation of immobilized-template imprinted composite microsphere (I-MIP)

To form free aldehyde ends, the terminal amino groups on CS microsphere reacted with bifunctional glutaraldehyde. One gram microsphere was added to 10 ml 2.5 wt% glutaraldehyde in borate buffer solution (pH 8.2) and incubated for 2 h at room temperature with shaking. Then, modified microsphere equilibrated with 10 ml template solution, 2 mg ml^{-1} BSA in borate buffer solution (0.2 mol l^{-1}, pH 8.2), for 4 h at room temperature. Protein in solution was measured by the Bradford method [36]. The amount of immobilized BSA was calculated by the following equation:

$$Q = \frac{(C_0 - C_e)V}{m} \quad (1)$$

C_0 and C_e represented initial and equilibration concentration of BSA, V was the volume of solution, and m was the weight of the microsphere.

After the template BSA was immobilized, the pH of the sol–gel process for the surface coating on the BSA-immobilized beads was optimized. One gram BSA-immobilized bead was respectively added to 10 ml of solution under different pH conditions. The pH of solution was adjusted using the following solutions: sodium acetate/hydrochloric acid for pH 2, sodium acetate/acetic acid for pH 4, sodium phosphate/phosphoric acid for pH 7, sodium carbonate/sodium biocarbonate for pH 9. All the solutions were controlled at 0.2 mol l^{-1}. Mixed binary siloxanes were then added and sol–gel process carried out for 12 h at room temperature with shaking. Afterwards, 10 ml of 0.5 mol l^{-1} oxalic acid was added to the obtained bead for template removal [12]. That was allowed for 8 h at room temperature with shaking and removed protein in the supernatant was measured. For the best performance, sol–gel process was finally set at pH 9. After thoroughly washed with DDW, the immobilized-template imprinted composite microsphere was obtained, which was designated as I-MIP.

For the preparation of control non-imprinted polymer, the same procedure was used only without addition of BSA. The obtained material was designated as NIP.

2.4. Preparation of free-template imprinted composite microsphere (F-MIP)

One gram initial CS microsphere was thoroughly mixed with 10 ml of 2 mg ml^{-1} BSA in sodium carbonate/sodium biocarbonate solution (pH 9). Then, mixed siloxanes were added and subsequent steps were performed in the same manner as described above. The final product, the free-template imprinted composite microsphere, was designated as F-MIP.

2.5. Characterization of the materials

The primary amino groups on CS microsphere were assayed by titration [15]. Water content of both CS microsphere and protein-imprinted composite microsphere in DDW was calculated as follows:

$$\text{water content} = \frac{W - W_d}{W} \quad (2)$$

After the microsphere was filtered, the weight of the wet sample (W) was determined after further removing the surface water by blotting with moistured filter paper. The weight of the dry sample (W_d) was determined after the microsphere was dried under vacuum.

To characterize surface morphology of the materials, scanning electron microscopy (SEM) images were obtained at 5.0 kV on a Hitachi S-4100 (Hitachi, Japan) field emission scanning electron microscope. X-ray energy dispersion spectroscopy (EDX) measurements were performed using a GENENIS 4000 energy dispersive X-ray micro analyzer (EDAX, USA) to investigate the transfer of elemental distribution on solid bead. The accelerating voltage used for the EDX analyses was 25 kV. The thermal and decomposition characteristics of the materials were determined using simultaneous thermogravimetry and differential scanning calorimeter (TG/DSC), conducted with a NETZSCH STA 409 thermogravimetric analyzer (Bruker, USA) in the temperature range of 30–800 °C at a heating rate of 20 °C min^{-1}, with air flushed at 200 ml min^{-1}. Nitrogen adsorption porosimetry measurement was performed on a Omnisorp 100CX (Coulter, USA) to provide data on surface area and pore diameter. Nitrogen isotherms were obtained in both adsorption and desorption modes. The surface areas of the supporting core and composite microsphere were determined by the BET method. Pore size distribution curves were established from the desorption branches of the isotherms using the BJH model.

2.6. Adsorption experiments

Binding kinetics of BSA to the I-MIP was performed by adding 200 μL BSA solution (100 mg ml^{-1}) to 1 g imprinted adsorbent immersed in 10 ml buffer solution. Taking a sample at regular interval to analyze BSA concentration in the supernatant until adsorption equilibrium was reached. Adsorption isotherm of BSA was determined to measure the adsorption capacity. One gram adsorbent was equilibrated with 10 ml solution of various BSA concentrations, ranged from 0.05 mg ml^{-1} to 2 mg ml^{-1}, for 60 min at room temperature. The BSA adsorptions to non-imprinted polymer (NIP), and free-template imprinted composite microsphere (F-MIP) were also determined. Molecular recognition selectivity was evaluated by differences in static equilibrium adsorption between BSA and contrastive proteins. One gram imprinted material was equilibrated with the solution containing 20 mg of the template BSA or contrastive protein for 90 min at room temperature.

In all above adsorption experiments, sodium phosphate/phosphoric acid at pH 7 was used. The protein adsorbed on

the adsorbent was determined by mass balance between liquid and solid phases, according to Eq. (1).

2.7. Desorption and reproducibility

Desorption studies were performed using 1% (v/v) acetic acid containing 5% (w/v) tween 20 to strip the re-adsorbed BSA, which was followed by thorough wash for regeneration. In test of adsorbent recycling, the imprinted material was used through four adsorption/regeneration cycles during 10 days.

3. Results and discussion

3.1. Preparation of immobilized-protein imprinted composite microsphere (I-MIP)

The surface imprinting strategy selected in present investigation relied on the use of a spherical core constituted by a polysaccharide, CS. The template protein was covalently immobilized on the supporting CS bead. Moreover, interfacial organic–inorganic hybridization via protein-imprinted sol–gel process was used for the surface coating. Schematic representation for synthesis of the protein-imprinted polymer on CS microsphere with immobilized protein template was illustrated in Fig. 1. The synthesis involved three steps. Firstly, template BSA was covalently immobilized on the polysaccharide core by forming imine bonds. The second step involved siloxanes polymerization on the polysaccharide–protein surface. It resulted in a polymeric network molded around the template. The template protein was removed in the third step. Cavities complementary to the template protein in shape, size, and functional group orientation were created.

In the developed affinity material, CS was used as integral component. Due to the reactivity of primary amine groups, CS has been exploited in many studies to covalently couple biomolecules. An analysis of the cross-linked CS microsphere gave 0.31 ± 0.01 mmol of amine content per gram wet beads (water content, $(55.4 \pm 2.1)\%$). A range of simple and standard methods could be used for coupling proteins to CS through amines. In our case, amino groups reacted with bifunctional glutaraldehyde to form aldehyde ends, which reacted spontaneously with free amino sites on protein by forming imine bonds (Schiff's bases) [37]. Without being reduced to secondary amines, imine bonds were fully reversible and could be readily broken for template removal. Shiomia et al. applied oxalic acid as an effective agent to remove the template protein, which was covalently immobilized using imine bonds [12]. In our experiments, washing with oxalic acid at 0.5 mol l^{-1} was also adopted as the template removing procedure.

Protein immobilization on aldehyde-modified surface involves amino sites exposed on protein surface, which were mainly located on the side-chain of lysine and arginine. To detect those two residues exposed on protein surface, the relative solvent accessibility to the amino acids sequence of BSA was predicted with AccPRO (http://www.igb.uci.edu/tools/scratch/) [38]. It was observed that no lysine and arginine were buried (accessibility no higher than 10%) inside the protein. Moreover, all 60 lysine and 20 arginine (76% of total 26 arginine residues) were exposed to the solvent with accessibility higher than 40%. Obviously, there were abundantly accessible amine groups on BSA surface, indicating the rational design of coupling by forming imine bonds. This circumstance also favored multipoint attachment between BSA and aldehyde-activated surface. That resulted in template protein assembling with stable spatial orientation and low-energy configuration [38]. Additionally, the "tumbling rate" and aggregation of template protein during the imprinting process were reduced. As a result, the functional groups possessed precise position around the template protein. The immobilized-protein imprinted materials possessed uniform binding sites and excellent recognition properties [16,39]. On average, 18 ± 0.42 mg of BSA was immobilized on 1 g of aldehyde-modified CS microsphere.

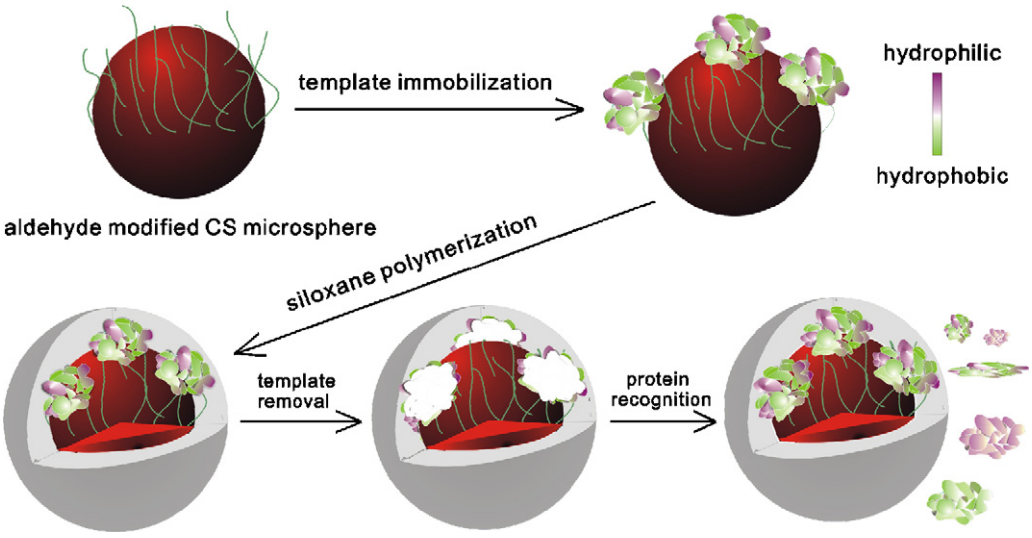

Fig. 1. Schematic representation for synthesis of the protein-imprinted polymer on CS microsphere using immobilized protein template.

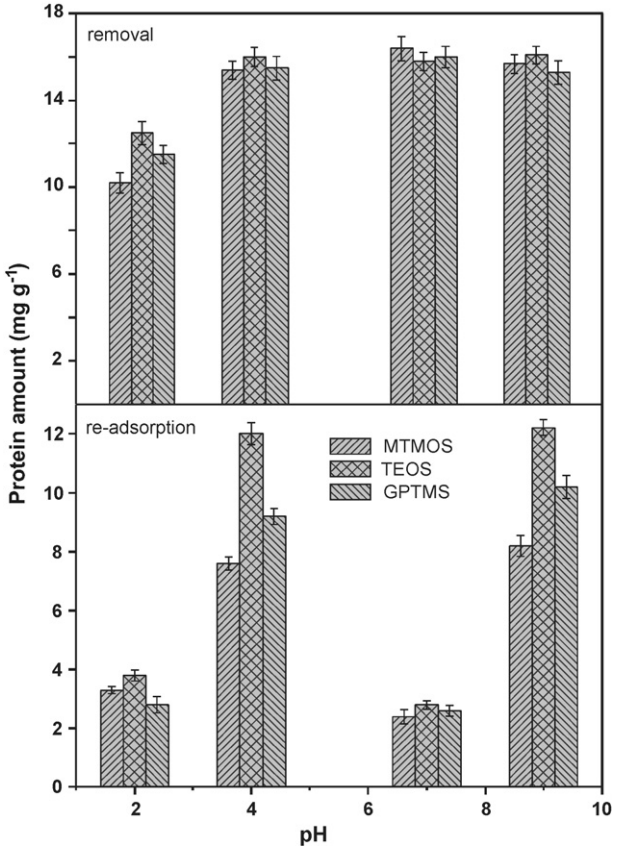

Fig. 2. Influences of siloxane type and pH of sol–gel process on removal and re-adsorption of template BSA Siloxane labeled in the figure showed the partnership of APTMS in three types of mixed binary siloxanes (mole ratio, 1:1). The siloxane/water ratio (v/v) was 1%.

3.2. Effect of starting siloxane type and pH of sol–gel process on characteristics of prepared I-MIP

Following immobilization of the template protein, siloxane monomers polymerized onto the BSA-CS surface through sol–gel process. The selectivity of imprinted sol–gel materials depended on various factors, including starting monomer type, siloxane to water ratio and pH of sol–gel process [20]. As suggested by Shiomia et al. APTMS could cover aldehyde groups [12]. In our procedure, APTMS was thus chosen as the universal monomer. Its partnership in three types of mixed binary siloxane was GPTMS, MTMOS, and TEOS, respectively. As a preliminary screening procedure to search for suitable monomers and pH, two siloxane monomers in three types of mixed binary siloxanes were all mixed at a fixed mole ratio of 1:1. The sol–gel reaction was acid (pH 2, pH 4), neutral (pH 7) or base (pH 9) catalysed, respectively (siloxane/water ratio (v/v), 1%). The influences on resulting characteristics of template removal and re-adsorption were evaluated. As seen from Fig. 2, both template removal and recognition capacity of the imprinted materials significantly depended on siloxane type, and pH of sol–gel coating process. Materials obtained using sol–gel process at pH 7 demonstrated high removal of immobilized template, whereas, re-adsorptions were lowest. As we know, siloxanes exhibited low gelation kinetics at neutral conditions.

Table 1
Characteristics of the template protein and contrast proteins

	Length[a]	MW[b]	p*I*	Number of predicted TMH[c]	Total prob. of N-in[d]
BSA	607	66	4.7	0	0.02293
Beta-amylase	546	57	6.5	1	0.99807
Cytochrome *C*	545	57	10.2	1	0.99021
Transferrin	706	76	5.9	0	0.00733
Lysozyme	211	14.6	10.8	1	0.45484

[a] The length of the protein sequence.
[b] The molecular weight (KDa) of the protein.
[c] The number of predicted transmembrane helices.
[d] The total probability that the N-term is on the cytoplasmic side of the membrane.

As a result, inefficient coating was obtained. Though immobilized template could be removed to a certain extent, materials prepared at pH 2 possessed low BSA re-adsorption capacities. It indicated inefficient template imprinting. In general, materials imprinted at pH 4 and pH 9 demonstrated easy template removal and considerable BSA re-adsorption. However, both template removal and BSA re-adsorption weakened in those six materials when MTMOS was used as the partnership of APTMS. This result suggested that MTMOS-derived sol–gel was inefficiently complementary to the template protein. Chou et al. used microcontact method for C-reactive protein (CRP) imprinting [25]. The affinity of the imprinted film towards template was found to be affected by hydrophilic/hydrophobic nature of the cover glass, which was used as a carrier for protein and functional monomer. In this regard, we also assumed that hydrophilic/hydrophobic characteristic played important role in complementary between siloxanes and proteins.

Transmembrane helices (TMHs) in BSA were predicted using TMHMM2.0 (http://www.cbs.dtu.dk/services) to evaluate hydrophobicity of the template protein [40]. It was noted that there were no predicted TMHs in BSA molecule. The total probability that the N-term was on the cytoplasmic side of the membrane (total prob. of N-in) was 0.02293 (Table 1). These results suggested that BSA was highly hydrophilic. When MTMOS was used as the co-precursor, the non-hydrolyzed hydrophobic group remained in the final sol–gel and endowed the sol–gel with a hydrophobic character. It was reported that TMOS-derived gel was fully hydrophobic when 20% MTMOS was used as co-precursor [41]. Due to the hydrophilic feature of the template, MTMOS-derived sol–gel was therefore not efficiently in template trapping and imprinting. In contrast to GPTMS, this trend was distinct considering the content of hydrophobic chain in siloxane molecule as well as the resulting sol–gel. Based on the above supposition, APTMS and TEOS were therefore chosen as the most appropriate co-precursors.

3.3. Effect of molar ratio of starting siloxane on characteristics of prepared I-MIP

The molar ratio of APTMS to TEOS was further scanned in sol–gel process at pH 4 and pH 9. Template removal and rebinding was used to evaluate the characteristics of the obtained

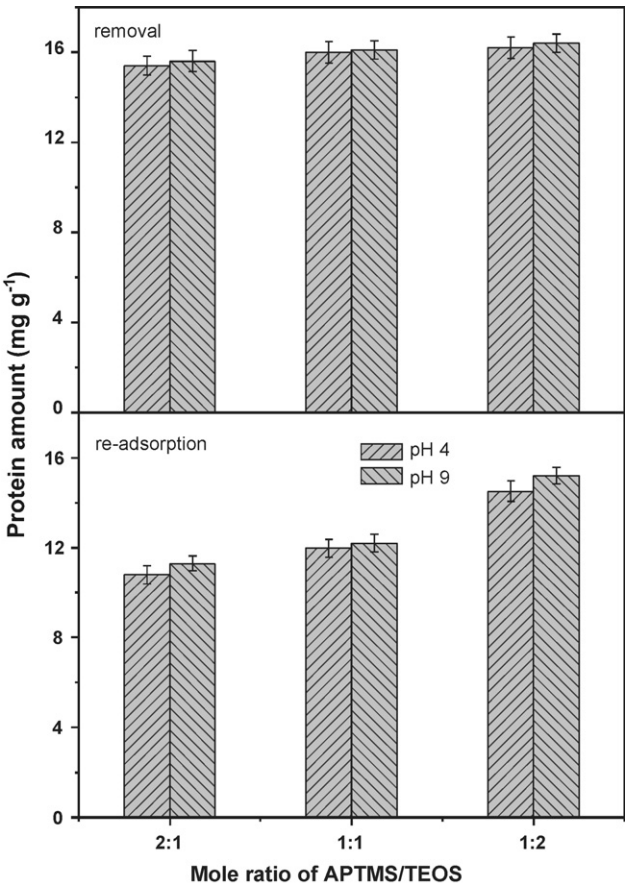

Fig. 3. Influence of the molar ratio of APTMS/TEOS on removal and re-adsorption of template BSA. Sol–gel process was performed at pH 4 and pH 9 using a siloxane/water ratio (v/v) of 1%.

materials. The molar ratios of APTMS to TEOS were 2:1, 1:1 and 1:2. The siloxane/water ratio (v/v) was fixed at 1%. As shown in Fig. 3, materials imprinted at alkaline condition demonstrated better performance than those obtained in acidic solution. It might attribute to the higher polymerization density in alkaline solution. As reported by Stancil et al. mismatched sites were less likely to form because the complementary pairs were less flexible in their motion when cross-linking density increased [42]. At a APTMS/TEOS ratio of 1:2, maximum template removal and re-adsorption capacity were observed. Therefore, sol–gel process was set at pH 9 using a APTMS/TEOS mole ratio of 1:2.

3.4. Effect of siloxane/water ratio on characteristics of prepared I-MIP

The influence of siloxane/water ratio on characteristics of template removal and re-adsorption was evaluated. The siloxane/water ratios (v/v), 0.5%, 1%, 1.5%, were scanned and result was shown in Fig. 4. High siloxane/water ratio (1.5%) led to rapid gelation in which the template BSA might be buried and thereby less removable. The remained template occupied binding sites and prevented the adsorption of other molecules. On the contrary, low siloxane/water ratio (0.5%) led to poor efficiency in coating. Though the template could be easily removed,

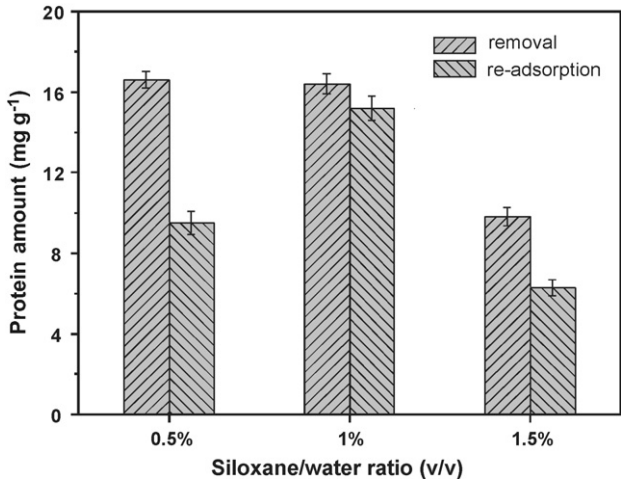

Fig. 4. Influence of siloxane/water ratio on removal and re-adsorption of template BSA. Sol–gel process was performed at pH 9 using a APTMS/TEOS mole ratio of 1:2.

re-adsorption capacity was low. At a moderate siloxane/water ratio of 1%, maximum template removal and re-adsorption capacity were observed. The transfer of elemental distribution on supporting CS microsphere and imprinted materials was investigated to validate surface grafting using X-ray energy dispersion spectroscopy (EDX). For CS microsphere, only C and O signals appeared. The appearance of Si signals in imprinted materials firmly established the existence of surface imprinting layer. Moreover, Si distribution increased as siloxane/water ratio increased, from a low value of 4.08% at low siloxane/water ratio (0.5%) to 11.15% at 1%, and the maximum of 18.17% at siloxane/water ratio of 1.5% (date not shown for brief). Finally, I-MIP prepared using polymerization between APTMS and TEOS (APTMS/TEOS mole ratio of 1:2, siloxane/water ratio (v/v) of 1%) at sodium carbonate/sodium biocarbonate solution (pH 9) was chosen for further investigation.

3.5. Characterization of the prepared I-MIP

The thermal stability of the prepared I-MIP was investigated by simultaneous thermogravimetry and differential scanning calorimetry (TG/DSC). Non-supported siloxane-condensed powder, which was prepared by casting mixed siloxanes on a clean glass plate, and the supporting CS microsphere were also tested for comparison. As shown in Fig. 5, thermogravimetric curves of CS microsphere (Fig. 5a) and non-supported siloxane-condensed powder (Fig. 5b) had two main degradation stages. The first weight loss occurred at about 100 °C, which resulted from the loss of adsorbed water. The second weight loss region might be caused by CS decomposition and structural reorganization of the polysiloxane, respectively. At the same time, those weight losses correlated with exothermic peaks in the DSC curve, indicating energy release. Due to synergic effects of CS and sol–gel layer, surface-grafted composite microsphere exhibited another two weight loss stages despite peak caused by loss of adsorbed water. As supported by previous observations, polymeric matrix formed by organic–inorganic hybridization usually

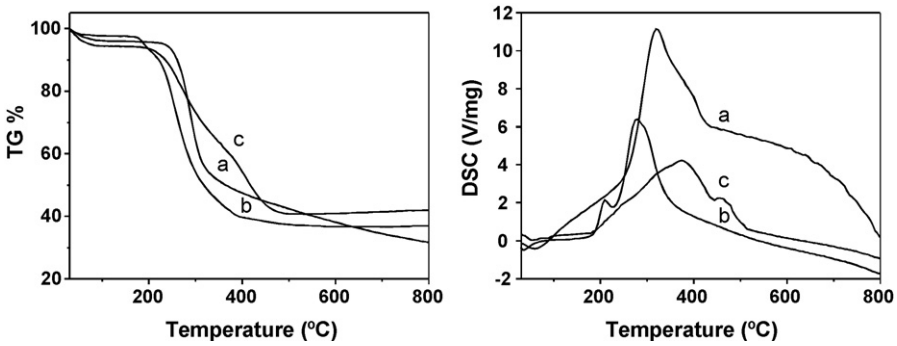

Fig. 5. The simultaneous thermogravimetry and differential scanning calorimetry analysis of CS microsphere (a), I-MIP (b) and non-supported siloxane-condensed powder (c).

showed improved thermal stability compared with single components [32,43]. In this regard, we attributed this observation to the hybrid effect between CS and polysiloxane at the core/shell interface.

Fig. 6 represented surface morphology of supporting CS microsphere and imprinted composite material. The supporting CS bead prepared via emulsion cross-linking was spherical with an average size of about 20 μm (Fig. 6a). The dense and slightly coarse microsphere possessed a porous structure. The BET surface area was 41.25 $m^2\ g^{-1}$ and average pore diameter was 8.7 nm, given by nitrogen adsorption porosimetry. The imprinted material demonstrated significantly different morphology (Fig. 6b). A large quantity of well-distributed pores was observed on the sphericial surface and they were netlike. The BET surface area was 48.65 $m^2\ g^{-1}$ and average pore diameter was 43.2 nm. The pores might possess geometrical distribution of ligands, increase specific surface area, and avoid problem of mass transfer [44].

3.6. Batch adsorption of template BSA to the prepared I-MIP

The surface-imprinted materials had good site accessibility for target protein molecules, because the protein-imprinted sites were located at, or close to, the surface. Consequently, restricted mobility associated with bulk imprinting materials was overcome. The general kinetic profile of template adsorption to I-MIP was investigated. As shown in Fig. 7, BSA possessed a fast adsorption profile in the initial step with significantly specific binding within 15 min. After about 60 min from the start, the adsorption process reached equilibrium. The adsorption of I-MIP was faster than that of F-MIP because 110 min must be

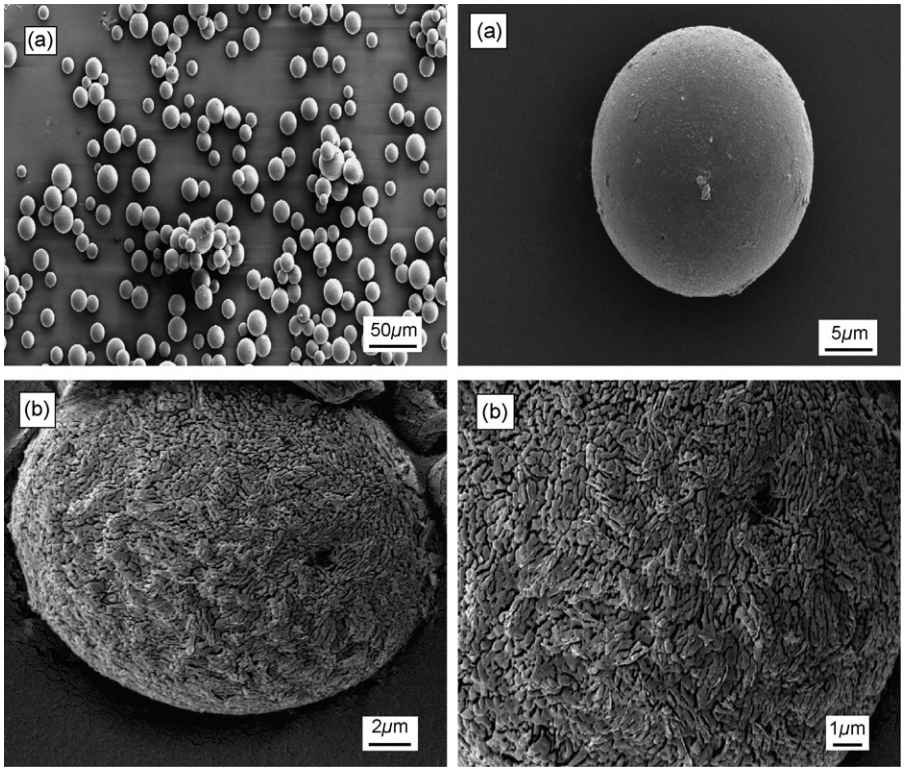

Fig. 6. SEM image (5.0 kV) of CS microsphere (a) and the immobilized-BSA imprinted material, I-MIP (b).

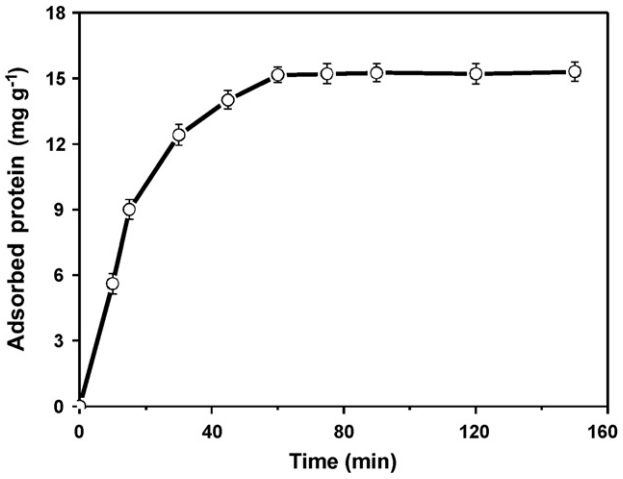

Fig. 7. Binding kinetics of BSA to the immobilized-BSA imprinted adsorbent (I-MIP).

required to reach adsorption equilibrium of F-MIP. Adsorption isotherm of BSA to I-MIP was similar to the Langmuir sorption isotherm. Data were well fitted to the linear form of the Langmuir equation expressed as following:

$$\frac{C_e}{Q} = 0.0063 + 0.0647C_e, \qquad \gamma^2 = 0.9903$$

C_e and Q represented equilibrium concentration of protein, and the amount of adsorbed protein on per gram of wet adsorbent respectively. The maximum protein adsorption, Q_{max}, was 15.5 mg g^{-1} wet bead (water content, (47.8 ± 1.9)%) and adsorption equilibrium constant (association constant) K was 1.03 L mol^{-1}.

3.7. Protein recognition selectivity of the prepared materials

Molecular recognition selectivity was evaluated by static distribution coefficient (K_D), and separation factor (α) being calculated according to static equilibrium adsorption of BSA and contrastive substrates, cytochrome C, transferrin, beta-amylase and lysozyme. Selective recognition of template and contrastive protein by immobilized-BSA imprinted (I-MIP), free-BSA imprinted (F-MIP) and non-imprinted (NIP) adsorbents were summarized in Table 2. The two template imprinted polymers, I-MIP and F-MIP, demonstrated selectivity towards template protein. However, the control non-imprinted material showed poor adsorption performance. In general, selective protein recognition was built on the assumption that molecularly imprinted polymer offered a three-dimensional microenvironment with shape-matching and complementary multiple-point interactions. In non-imprinting process, in contrast, groups were isolated from each other and distributed randomly in sol–gel network. So the multipoint interactions were much less, leading to reduced BSA adsorption (2.8 mg g^{-1} wet bead) and low selectivity [1]. Moreover, I-MIP possessed higher adsorption towards BSA (15.5 mg g^{-1} wet bead) than F-MIP did (12.6 mg g^{-1} wet bead). Compared with free-BSA imprinting process, template immobilization resulted in reduced "tumbling rate" and prevented aggregation. As a result, the uniform binding sites showed better accessibility and improved rebinding capacity.

Table 2
Selective recognition of template and contrastive proteins by BSA-imprinted (I-MIP, F-MIP) and non-imprinted adsorbent (NIP)

Adsorbent	Substrate	Q (mg g^{-1})	K_D[a]	α[b]
I-MIP	BSA	15.5	68.9	
	Transferrin	8.3	14.1	4.9
	Lysozyme	3.1	3.6	19.1
	Beta-amylase	2.1	2.3	30
	Cytochrome *C*	2.4	2.7	25.5
F-MIP	BSA	12.6	34.1	
NIP	BSA	2.8	3.3	

[a] K_D, Static distribution coefficient, K_D: C_p/C_s, where C_p and C_s represent the substrate concentration on the adsorbent and in the solution, respectively.
[b] α, Separation factor, α: K_D(BSA)/K_D(contrast protein). One gram imprinted or non-imprinted material was equilibrated with 20 ml of 1 mg ml^{-1} template BSA or contrastive protein for 90 min at room temperature. The buffer solution was sodium phosphate/phosphoric acid at pH 7.

For recognition of I-MIP, the level of selective discrimination naturally based the level of complementation between outer surface of protein and inner surface of "imprinting cavities". We speculated such complementation depended on shape-matching and multiple hydrogen bonding caused by matched hydrophilic/hydrophobic characteristics (Fig. 1). In our case, hydrophilic property of BSA made hydrophilic groups in the grafted layer spatially distribute at complementary positions. That leaded to the formation of a large quantity of hydrogen bonds between silanol groups of polysiloxane and surface polar residues of proteins [12]. The directional nature of hydrogen bond together with synergic action of multiple hydrogen bonds resulted in high degree of shape complementary. As shown in Table 2, hydrophobic proteins such as lysozyme (14.6 kDa, p*I* 10.8, 1 predicted TMH, total prob. of N-in: 0.45484), beta-amylase (57 kDa, p*I* 6.5, 1 predicted TMH, total prob of N-in: 0.99807) and cytochrome C (57 kDa, p*I* 10.2, 1 predicted TMH, total prob of N-in: 0.99021) could hardly bind to the imprinted adsorbent. Though beta-amylase and cytochrome *C* possessed similar hydrophobic property and molecular weight, however, isoelectric point was significantly different. In detail, beta-amylase was negatively charged while cytochrome *C* was positively charged in adsorption process (sodium phosphate/phosphoric acid at pH 7). However, the static distribution coefficients (K_D) for beta-amylase and cytochrome C were similar. Moreover, lysozyme and cytochrome C showed distinct K_D despite similar isoelectric point. Thus, recognition did not vitally depended on the electrostatic interaction. Transferrin (76 kDa, p*I* 5.9, 0 predicted TMH, total prob of N-in: 0.00733) had similar isoelectric point and hydrophilic property with BSA. Though it could be more efficiently adsorbed than the three hydrophobic proteins, K_D was much lower than BSA. The results might attribute to recognition based on shape-matching.

3.8. Desorption and reproducibility of the prepared I-MIP

Desorption and reproducibility properties of the prepared I-MIP were characterized. Re-adsorbed BSA could be stripped

by being washed with 1% (v/v) acetic acid containing 5% (w/v) tween 20, which was followed by regeneration through washing with DDW. In test of recycling, the imprinted adsorbent was used through four adsorption/regeneration cycles during 10 days. The capacity of I-MIP through four cycles was found to be $(91 \pm 3)\%$ of the fresh adsorbent. The sol–gel process endowed the adsorbent with physical robustness, mechanically durable network and stability in storage [42]. Additionally, the grafting of the imprinted layer through interfacial organic–inorganic hybridization also improved the stability of composite material.

4. Conclusions

The successful preparation of spherical imprinted material demonstrated the efficiency of interfacial organic–inorganic hybridization concept in surface imprinting. The imprinted polymer was conveniently grafted on polysaccharide core through immobilized-protein imprinted sol–gel process in aqueous solution at room temperature. The protein-imprinted surface possessed high affinity toward template protein. The complementation in hydrophilicity/hydrophobicity was a major factor affecting the imprinting formation and template recognition. The grafting of imprinted layer through interfacial organic–inorganic hybridization improved stability and reproducibility properties of the final material. Easy preparation of the I-MIP, its recognize ability and high stability make this methodological study and application attractive in biotechnology and biosensors.

Acknowledgements

This research was supported by the National Natural Science Foundation of China (No.20775038, 20775039), the Program for New Century Excellent Talents in Universities (No. NCET-04-0649) and the Special Project of Qingdao for Leadership of Science and Technology (No. 05-2-JC-80).

References

[1] B. Sellergren, Angew. Chem. Int. Ed. 39 (2000) 1031.
[2] K. Matsumoto, A. Torimaru, S. Ishitobi, T. Sakai, H. Ishikawa, K. Toko, N. Miura, T. Imato, Talanta 68 (2005) 305.
[3] A.H. Cui, A. Singh, D.L. Kaplan, Biomacromolecules 3 (2002) 1353.
[4] S.T. Wei, M. Jakusch, B. Mizaikoff, Anal. Chim. Acta 578 (2006) 50.
[5] Y. Li, H.H. Yang, Q.H. You, Z.X. Zhuang, X.R. Wang, Anal. Chem. 78 (2006) 317.
[6] Y.K. Lu, X.P. Yan, Anal. Chem. 76 (2004) 453.
[7] R. Suedee, W. Intakong, F.L. Dickert, Talanta 70 (2006) 194.
[8] G.Z. Fang, J. Tan, X.P. Yan, Anal. Chem. 77 (2005) 1734.
[9] D.M. Hawkins, D. Stevenson, S.M. Reddy, Anal. Chim. Acta 542 (2005) 61.
[10] K. Sreenivasan, Talanta 68 (2006) 1037.
[11] D. Lakshmi, B.B. Prasad, P.S. Sharma, Talanta 70 (2006) 272.
[12] T. Shiomi, M. Matsui, F. Mizukami, K. Sakaguchi, Biomaterials 26 (2005) 5564.
[13] S.A. Piletsky, H. Matuschewski, U. Schedler, A. Wilpert, E.V. Piletska, T.A. Thiele, M. Ulbricht, Macromolecules 33 (2000) 3092.
[14] S. Hjerten, J.L. Liao, K. Nakazato, Y. Wang, G. Zamaratskaia, H.X. Zhang, Chromatography 44 (1997) 227.
[15] T.Y. Guo, Y.Q. Xia, G.J. Hao, M.D. Song, B.H. Zhang, Biomaterials 25 (2004) 5905.
[16] T.Y. Guo, Y.Q. Xia, J. Wang, M.D. Song, B.H. Zhang, Biomaterials 26 (2005) 5737.
[17] G.Q. Fu, J.H. Zhao, H. Yu, L. Liu, B.L. He, React. Funct. Polym. 67 (2007) 442.
[18] T.Y. Guo, Y.Q. Xia, G.J. Hao, B.H. Zhang, G.Q. Fu, Z. Yuan, B.L. He, J.F. Kennedy, Carbohyd. Polym. 62 (2005) 214.
[19] S.H. Ou, M.C. Wu, T.C. Chou, C.C. Liu, Anal. Chim. Acta 504 (2004) 163.
[20] A.M. Siouffi, J. Chromatogr. A 1000 (2003) 801.
[21] J.E. Meegan, A. Aggeli, N. Boden, R. Brydson, A.P. Brown, L. Carrick, A.R. Brough, A. Hussain, R.J. Ansell, Adv. Funct. Mater. 14 (2004) 31.
[22] Y.A. Shchipunov, T.Y. Karpenko, Langmuir 20 (2004) 3882.
[23] A.M. Massari, I.J. Finkelstein, M.D. Fayer, J. Am. Chem. Soc. 128 (2006) 3990.
[24] A. Kumar, R.R. Pandey, B. Brantley, Talanta 69 (2006) 700.
[25] P.C. Chou, J. Rick, T.C. Chou, Anal. Chim. Acta 542 (2005) 20.
[26] J. Abdullah, M. Ahmad, L.Y. Heng, N. Karuppiah, H. Sidek, Talanta 70 (2006) 527.
[27] H. Yi, L.Q. Wu, R. Ghodssi, G.W. Rubloff, G.F. Payne, W.E. Bentley, Anal. Chem. 76 (2004) 365.
[28] Z.J. Wang, Y.H. Yang, J.S. Li, J.L. Gong, G.L. Shen, R.Q. Yu, Talanta 69 (2006) 686.
[29] H. Yi, L.Q. Wu, W.E. Bentley, R. Ghodssi, G.W. Rubloff, J.N. Culver, G.F. Payne, Biomacromolecules 6 (2005) 2882.
[30] L. Qian, X.R. Yang, Talanta 68 (2006) 721.
[31] J.A. Cruz-Aguado, Y. Chen, Z. Zhang, M.A. Brook, J.D. Brennan, Anal. Chem. 76 (2004) 4182.
[32] F. Li, X.M. Li, S.S. Zhang, J. Chromatogr. A 1129 (2006) 223.
[33] F. Li, H.Q. Jiang, S.S. Zhang, Talanta 71 (2007) 1487.
[34] F. Li, P. Du, W. Chen, S.S. Zhang, Anal. Chim. Acta 585 (2007) 211.
[35] L. Yang, W.W. Hsiao, P.J. Chen, Membr. Sci. 197 (2002) 185.
[36] M.M. Bradford, Anal. Biochem. 72 (1976) 248.
[37] M.G. Zhang, W. Gorski, J. Am. Chem. Soc. 127 (2005) 2058.
[38] M.M. El-Masry, A. De Maio, P.L. Martelli, R. Casadio, A.B. Moustafa, S. Rossi, D.G. Mita, J. Mol. Catal. B: Enzym. 16 (2001) 175.
[39] L. Betancor, A. Hidalgo, G. Fernández-Lorente, C. Mateo, R. Fernández-Lafuente, J.M. Guisan, Biotechnol. Prog. 19 (2003) 763.
[40] J. Ethier, J.M. Boyd, Mol. Microbiol. 38 (2000) 891.
[41] J.T. Huang, J.Q. Zhang, J. Zhang, S.H. Zheng, J. Appl. Polym. Sci. 95 (2005) 358.
[42] K.A. Stancil, M.S. Feld, M. Kardar, J. Phys. Chem. B 109 (2005) 6636.
[43] Y.L. Liu, Y.H. Su, J.Y. Lai, Polymer 45 (2004) 6831.
[44] J.H. Smått, S. Schunk, M. Lindén, Chem. Mater. 15 (2003) 2354.

Available online at www.sciencedirect.com
ScienceDirect
Talanta 74 (2008) 1476–1483
Talanta
www.elsevier.com/locate/talanta

Improvement of detection sensitivity of T-2 and HT-2 toxins using different fluorescent labeling reagents by high-performance liquid chromatography☆

Vincenzo Lippolis[a,*], Michelangelo Pascale[a], Chris M. Maragos[b], Angelo Visconti[a]

[a] *Institute of Sciences of Food Production (ISPA), National Research Council (CNR), Via G. Amendola 122/O, 70126 Bari, Italy*
[b] *Mycotoxin Research Unit, U.S. Department of Agriculture, Agricultural Research Service, National Center for Agricultural Utilization Research (USDA-ARS-NCAUR), 1815 North University Street, Peoria, IL 61604, USA*

Received 17 May 2007; received in revised form 27 September 2007; accepted 28 September 2007
Available online 2 October 2007

Abstract

T-2 and HT-2 toxins are *Fusarium* mycotoxins that can occur in cereals and cereal-based products. Three fluorescent labeling reagents, i.e. 1-naphthoyl chloride (1-NC), 2-naphthoyl chloride (2-NC) and pyrene-1-carbonyl cyanide (PCC), were used for the determination of T-2 and HT-2 toxins by high-performance liquid chromatography (HPLC) with fluorescence detection (FD). Pre-column derivatization of T-2 and HT-2 toxins was carried out under mild conditions (50 °C, 10 min) in toluene with 4-dimethylaminopyridine (DMAP) as catalyst. All fluorescent derivatives were identified and characterized by HPLC-tandem mass spectrometry (HPLC-MS/MS). Optimal stoichiometric ratios (toxin:derivatizing reagent:catalyst), linear range and repeatability of the reaction, stability and sensitivity of the derivatives were determined. A wide linear range (10–1000 ng of either derivatized T-2 or HT-2 toxin), good stability (up to 2 weeks at −20 °C or 5 days at room temperature) of the fluorescent derivatives and good repeatability of the reaction (RSD ≤ 8%) were observed. Detection limits (based on a signal-to-noise ratio of 3:1) were 10.0, 6.3 and 2.0 ng for derivatized T-2 toxin and 6.3, 2.3 and 2.8 ng for derivatized HT-2 toxin with 1-NC, 2-NC and PCC, respectively. In terms of sensitivity and repeatability, PCC and 2-NC reagents showed better performance than 1-anthroylnitrile (1-AN), a previously reported labeling reagent for T-2- and HT-2 toxins. Preliminary studies also showed the applicability of PCC and 2-NC as fluorescent labeling reagents for the simultaneous determination of T-2 and HT-2 toxins in cereal grains by HPLC/FD following immunoaffinity column clean-up.
© 2007 Elsevier B.V. All rights reserved.

Keywords: 1-Naphthoyl chloride; 2-Naphthoyl chloride; Pyrene-1-carbonyl cyanide; Fluorescent labeling reagents; T-2 and HT-2 toxins

1. Introduction

T-2 and HT-2 toxins are 'type-A' trichothecene mycotoxins produced by several *Fusarium* species, mainly *F. sporotrichioides*, *F. poae*, *F. equiseti* and *F. acuminatum*. These mycotoxins may contaminate a variety of cereal grains, such as wheat, maize, oats, barley and rice, especially in cold climate regions or during wet storage conditions. T-2 and HT-2 toxins can also be found in cereal-based products intended for direct human consumption [1–3]. A recent data collection, aiming to evaluate the risk of dietary exposure to *Fusarium* toxins by the population of EU member states, showed that T-2 and HT-2 toxins are quite common contaminants in cereals in the EU. In particular, the most frequently contaminated cereal samples were maize (28%), wheat (21%) and oats (21%) for T-2 toxin and oats (41%), maize (24%) and rye (17%) for HT-2 toxin [3].

T-2 toxin, the most toxic trichothecene, is a potent inhibitor of DNA, RNA and protein synthesis, and shows immunosuppressive and cytotoxic effects both *in vivo* and *in vitro* [1,4]. The acute toxicity of T-2 and HT-2 toxins are quite similar. *In vivo* animal experiments showed that T-2 toxin is rapidly metabolised to HT-2 toxin and, consequently, the toxicity of T-2 toxin *in vivo* might partly be attributed to HT-2 toxin [1]. Recently, the European Commission (EC) has established, with Regulations No. 856/2005 and No. 1881/2006, admissible levels of several *Fusarium* toxins in cereals and cereal-based products

☆ *Disclaimer*: Mention of trade names or commercial products in this article is solely for the purpose of providing specific information and does not imply recommendation or endorsement by the U.S. Department of Agriculture.

* Corresponding author. Tel.: +39 080 5929763; fax: +39 080 5929374.
E-mail address: vincenzo.lippolis@ispa.cnr.it (V. Lippolis).

0039-9140/$ – see front matter © 2007 Elsevier B.V. All rights reserved.
doi:10.1016/j.talanta.2007.09.024

which were effective from 1 July, 2006. Maximum admissible levels for T-2 and HT-2 toxins in unprocessed cereals and cereal products are currently under discussion [5,6].

There is a need to develop sensitive and accurate analytical methods for determining these mycotoxins in cereals and cereal-based products in order to properly assess the relevant risk of human exposure. Different chromatographic methods, including gas-chromatographic (GC) and liquid-chromatographic (LC) methods coupled with mass spectrometry (MS), for the analysis of 'type-A' trichothecenes (including T-2 and HT-2) have been reported by several authors [7–12], but problems of accuracy due to matrix effects were observed [9,11]. High-performance liquid chromatography (HPLC) with UV detection is generally not applicable to 'type-A' trichothecenes for sensitive detection due to the lack of a strong chromophore group within their structures. HPLC methods for T-2 and HT-2 toxins have been developed in which derivatizing reagents are used to allow detection by fluorescence. Currently, only coumarin-3-carbonyl chloride (not commercially available) and 1-anthroylnitrile (1-AN) have been used as fluorescent labeling reagents for some 'type-A' trichothecenes [13–17]. The latter has been applied for the simultaneous determination of T-2 and HT-2 toxins in wheat, maize and barley by HPLC with fluorescence detection (FD) following immunoaffinity column clean-up. The method allowed the determination of T-2 and HT-2 toxins at levels of 5 and 3 $\mu g\,kg^{-1}$ (LOD, limit of detection), respectively, with good accuracy and precision. Nevertheless, the method did not allow the determination of HT-2 toxin in oats because of interfering chromatographic peaks occurring at the retention time of the HT-2(1-AN) derivative [17].

Intake estimates indicate that the presence of T-2 and HT-2 toxins in the diet at low levels can be of some concern for human health. The Joint FAO/WHO Expert Committee on Food Additives (JECFA) established the PMTDI (provisional maximum tolerable daily intake) of T-2 and HT-2 toxins, alone or in combination, at 0.06 $\mu g\,kg^{-1}$ body weight per day. In addition, the Committee noted that data on T-2 and HT-2 toxins in food are quite limited and of low quality and the sensitivity of the analytical methods used was poor in many cases [1]. The aim of this work was to find new commercially available fluorescent labeling reagents to improve detection sensitivity for T-2 and HT-2 toxins by HPLC/FD analysis, so that they might be used for the monitoring/surveillance of these toxins in a variety of food matrices, including oats and processed cereal products.

2. Experimental

2.1. Chemicals and materials

Acetonitrile and methanol (both HPLC grade) and toluene (for organic residue analysis) were purchased from Mallinckrodt Baker (Milan, Italy). Ultrapure water was produced by a Millipore Milli-Q system (Millipore, Bedford, MA, USA). T-2 toxin, HT-2 toxin, 1-naphthoyl chloride (1-NC), 2-naphthoyl chloride (2-NC), 4-dimethylaminopyridine (DMAP) were purchased from Sigma–Aldrich (Milan, Italy). Pyrene-1-carbonyl cyanide (PCC) and 1-anthroyl cyanide (1-anthroylnitrile, 1-AN) were purchased from Wako (Neuss, Germany). T-2 immunoaffinity columns (T-2test^{TM} HPLC) were obtained from Vicam (Watertown, MA, USA), glass microfibre filters (Whatman GF/A) and paper filters (Whatman N. 4) from Whatman (Maidstone, UK).

2.2. Preparation of standard and reagent solutions

T-2 and HT-2 toxin stock solutions were prepared by dissolving the solid commercial toxins in acetonitrile (1.00 $\mu g\,\mu L^{-1}$). T-2 and HT-2 toxin standard solutions for HPLC calibration were prepared in acetonitrile/water (70:30, v/v) by dissolving adequate amounts of the stock solution, previously evaporated to dryness under nitrogen stream. T-2 and HT-2 toxin standard solutions for all other experiments were prepared in acetonitrile by diluting aliquots of the stock solution. DMAP solutions were prepared in toluene at concentrations of 0.16, 0.33, 0.63, 0.95 and 2.00 $\mu g\,\mu L^{-1}$. Derivatizing reagent solutions were prepared in toluene at concentrations of 0.12, 0.24, 0.49, 0.73 and 1.00 $\mu g\,\mu L^{-1}$ (1-NC and 2-NC), 0.16, 0.33, 0.66 and 1.00 $\mu g\,\mu L^{-1}$ (PCC) and 0.30 $\mu g\,\mu L^{-1}$ (1-AN).

2.3. Apparatus

HPLC analyses were carried out using a ProStar system (Varian Inc., Palo Alto, CA, USA) equipped with a Rheodyne (Cotati, CA, USA) model 7125 injection valve, a fluorometric detector and the Star data system version 6.20 (Varian Inc.). The analytical column was a Phenyl-Hexyl Luna® (150 mm × 4.6 mm, 5 μm) (Phenomenex, Torrance, CA, USA), preceded by a SecurityGuard^{TM} C_{18} cartridge (4 × 3 mm i.d., 5 μm) (Phenomenex). The flow rate of the mobile phase was 1.0 mL min^{-1}. A binary gradient was applied as follows: the initial composition of the mobile phase, 70% acetonitrile:30% water (v/v), was kept constant for 5 min, then the acetonitrile content was linearly increased to 85% in 10 min, and kept constant for 10 min. Finally, to clean the column the amount of acetonitrile was increased to 100% in 2 min and kept constant for 5 min.

2.4. Derivatization procedure

Due to its high efficiency for a variety of acylation reactions, the base DMAP was used as reaction catalyst. The derivatization procedure was performed as previously described by Visconti *et al.* [17], with minor modifications. In particular, a portion of T-2 and HT-2 toxin standard solutions (or purified cereal extract) was placed in a 4-mL screw-cap amber vial and evaporated under a stream of nitrogen gas at ca. 50 °C in a heater block. Fifty microliters of DMAP solution, followed by 50 μL of the fluorescent labeling reagent (1-AN, 1-NC, 2-NC or PCC), were added to the dried residue. The vial was closed and mixed by vortex for 1 min. After the cap was removed, the mixture was allowed to dry under a gentle stream of nitrogen for 10 min at ca. 50 °C and reconstituted with 1000 μL of a mixture acetonitrile/water (70:30, v/v). Twenty microliters of the solution were injected

into the chromatographic apparatus by a 'full loop' injection system.

2.5. Identification of T-2 and HT-2 derivatives

The identity of the new fluorescent derivatives [T-2(1-N); HT-2(1-N)$_2$; T-2(2-N); HT-2(2-N)$_2$; T-2(PC); HT-2(PC)$_2$] was confirmed by HPLC–MS/MS analysis (positive chemical ionisation mode) using a 1100 Series micro-LC chromatographic system (Agilent Technologies, Waldbronn, Germany) interfaced to a QTRAP® (Applied Biosystem/MSD Sciex, Foster City, CA, USA) equipped with a *TurboIonSpray®* interface. After derivatization with the labeling reagent (1-NC, 2-NC or PCC), a mixture containing 0.5 μg of each toxin, 20 μL of the reaction mixture were injected into the HPLC apparatus. Chromatographic conditions were as follows: analytical column, Phenyl-Hexyl Luna® (150 mm × 4.6 mm, 5 μm) (Phenomenex, Torrance, CA, USA); binary gradient, with the initial composition of the mobile phase, 70% acetonitrile:30% water containing 5 mM ammonium acetate, kept constant for 5 min, then the acetonitrile content was linearly increased to 85% in 10 min, and kept constant for 10 min; flow rate of the mobile phase, 1.0 mL min^{-1} and splitting was performed to allow 100 μL min^{-1} to enter the turbo-ionspray interface. Interface conditions were as follows: temperature, 300 °C; curtain gas (nitrogen), 20 psi; nebulizer gas (air), 10 psi; auxiliary gas (air), 30 psi; ionspray voltage, +4500 V.

Full scan experiments (Q1 scan mode, scan range 100–1000 amu) of the derivatization products were performed to analyze the presence of molecular ions or adducts with ammonium ion. HPLC-MS/MS analysis was carried out to find the characteristic fragment ions for each derivative.

2.6. Optimization of the excitation and emission wavelengths

Excitation and emission spectra of the new fluorescent derivatives were obtained with an Agilent 1100 Series HPLC system equipped with fluorescence detector (FD) (Agilent Technologies, Waldbronn, Germany). This programmable detector allowed the acquisition of fluorescence spectra during the chromatographic run and the determination of the optimum excitation and emission wavelengths of each chromatographic peak. After derivatization of a mixture containing 0.25 μg of each toxin with the labeling reagents (1-NC, 2-NC or PCC), 20 μL of the reaction mixture were injected twice into the HPLC/FD apparatus. The first injection was made to acquire excitation spectra (spectral ranges: λ = 230–350 nm for 1-NC and 2-NC, λ = 230–370 nm for PCC) in 2-nm steps by setting the emission wavelength at the maximum value of the labeling reagent (i.e. λ_{em} = 380 nm for 1-NC, λ_{em} = 370 nm for 2-NC and λ_{em} = 405 nm for PCC). The second injection allowed the acquisition of emission spectra (spectral ranges: λ = 280–650 nm for 1-NC and 2-NC, λ = 380–650 nm for PCC) in 2-nm steps by using the optimum excitation wavelength previously determined for each fluorescent derivative.

2.7. Optimization of stoichiometric ratios

Different stoichiometric ratios of toxin:derivatizing reagent:catalyst were tested for 1-NC and 2-NC (1:10:20; 1:20:40; 1:40:80; 1:60:120; 1:80:250; 1:160:250), and for PCC (1:10:20; 1:20:40; 1:40:80; 1:60:120; 1:60:250; 1:120:500, 1:250:1000) in order to optimize the reaction yield. A mixture containing 0.7 μg of T-2 and 0.7 μg HT-2 toxins (corresponding to the immunoaffinity column capacity) was derivatized with each of the three labeling reagents in triplicate experiments.

2.8. Sensitivity, linear response and stability of T-2 and HT-2 derivatives

In order to test the fluorescence intensities of T-2 and HT-2 derivatives obtained with 1-NC, 2-NC and PCC and to compare them to the previously reported 1-AN derivatives [17], mixtures containing 0.25 μg of T-2 and 0.25 μg HT-2 toxin, were evaporated to dryness under a nitrogen stream and derivatized with: (a) 50 μL of DMAP solution (0.63 μg μL^{-1}) and 50 μL of 1-NC or 2-NC solution (0.49 μg μL^{-1}); (b) 50 μL of DMAP solution (2.00 μg μL^{-1}) and 50 μL of PCC solution (1.00 μg μL^{-1}); (c) 50 μL of DMAP solution (0.33 μg μL^{-1}) and 50 μL of 1-AN solution (0.30 μg μL^{-1}). Experiments were carried out in triplicate.

To evaluate the linearity of the response for T-2 and HT-2 derivative-peak areas, equimolar amounts of the two toxins (equivalent to 10–1000 ng of each toxin) were placed in screw-cap amber vials and the solvent evaporated to dryness at about 50 °C under a stream of nitrogen before derivatization.

In order to establish the stability of the fluorescent derivatives, different amounts of T-2 and HT-2 toxins (from 0.1 to 0.7 μg) were derivatized with 1-NC, 2-NC and PCC. The reaction mixtures were reconstituted with acetonitrile/water (70:30, v/v) and stored at −20, +4 and +25 °C in amber vials ('dark') and at +25 °C in clear vials ('light') for up to two weeks (triplicate experiments). At selected time intervals, 20 μL of the reaction mixture were injected into the HPLC apparatus as described above.

2.9. Analysis of cereal samples

Naturally contaminated samples of wheat, maize, and spiked oats were analyzed for T-2 and HT-2 toxins by HPLC/FD using either PCC or 2-NC as the pre-column derivatization reagent. Sample preparation was performed according to the method described by Visconti *et al.* [17], with minor modifications. Fifty grams of cereal sample, finely ground with a Model MLI-204 Bühler (Milan, Italy), were weighed into a blender jar, added with 1 g NaCl, and extracted with 100 mL methanol/water (90:10, v/v) by blending at high speed for 2 min with a Sorvall Omnimixer (Dupont Instruments, Newtown, CT, USA). The extract was filtered through filter paper. Ten millilitres of filtrate were collected and mixed with 40 mL of distilled water. For oat samples it was necessary to adjust the pH of the diluted extract at 7.4 value with NaOH. This additional step eliminated the presence of colloidal species in the purified extract that otherwise

caused interfering peaks in the chromatogram at the retention times of the T-2 and HT-2 derivatives. The diluted extract was then filtered through a glass microfibre filter. Ten millilitres of filtrate (equivalent to 1.0 g sample) were passed through the immunoaffinity column at a flow rate of about one drop per second, followed by 10 mL of distilled water at a flow rate of one to two drops per second. T-2 and HT-2 toxins were then eluted with 1.5 mL methanol and collected in a 4-mL screw-cap amber vial. The eluted extract was evaporated under a stream of air at ca. 50 °C, and the dried residue was derivatized with PCC or 2-NC as reported above.

3. Results and discussion

Three commercially available fluorescent reagents for modifying alcohols, 1-naphthoyl chloride (1-NC), 2-naphthoyl chloride (2-NC) and pyrene-1-carbonyl cyanide (PCC), were tested for labeling T-2 and HT-2 toxins (Fig. 1). All labeling reagents reacted with T-2 and HT-2 toxins under mild conditions to form the corresponding fluorescent esters. With respect to the derivatization procedure used for 1-anthroylnitrile (1-AN) [17], the derivatization reaction was optimized. In particular, by performing the reaction while drying at 50 °C under a gentle stream of nitrogen in 10 min, instead of 15 min of reaction in solution at 50 °C followed by 10 min of cooling step in ice and solvent evaporation. Under these conditions the rate of reaction was increased by the effect of the increasing toxin concentration during the drying step and the cooling step, generally used to block similar esterification reaction, was avoided [13–15]. The dried mixture was directly reconstituted with acetonitrile/water (70:30, v/v) and injected in the HPLC/FD apparatus.

The identity of the T-2 and HT-2 esters [T-2(1-N); HT-2(1-N)$_2$; T-2(2-N); HT-2(2-N)$_2$; T-2(PC); HT-2(PC)$_2$] was confirmed by HPLC-MS and HPLC-MS/MS analysis (positive chemical ionization) of the reaction mixtures. In order to increase the sensitivity, 5 mM ammonium acetate was added to the mobile phase, allowing the detection of molecular ions as ammonium adducts $[M+NH_4]^+$. Full scan chromatogram of the reaction mixture with 1-NC revealed the presence of a molecular ion with *m/z* 638.3 at the T-2 derivative retention time, corresponding to the adduct $[T\text{-}2(1\text{-}N)+NH_4]^+$, and

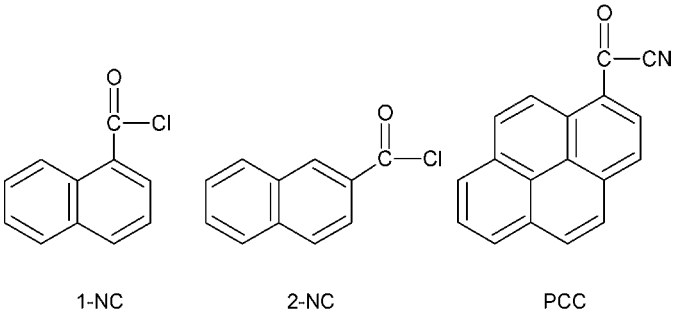

Fig. 1. Chemical structures of 1-naphthoyl chloride (1-NC), 2-naphthoyl chloride (2-NC) and pyrene 1-carbonyl cyanide (PCC).

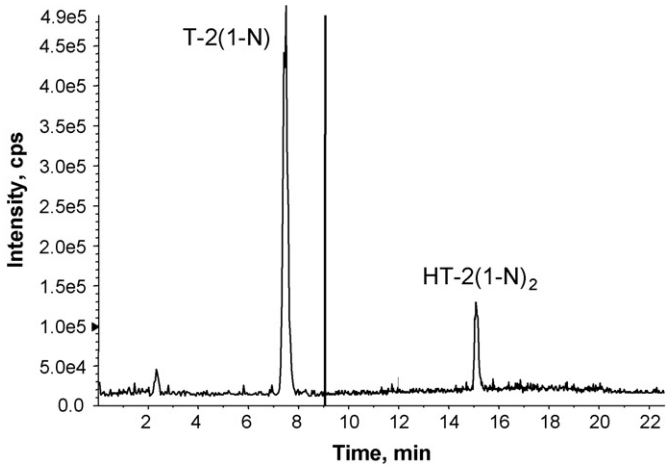

Fig. 2. HPLC-MS/MS chromatogram of T-2 and HT-2 toxins after reaction with 1-NC. Fragmented ions: *m/z* 638.3, $[T\text{-}2(1\text{-}N)+NH_4]^+$ (0–9 min); *m/z* 750.3, $[HT\text{-}2(1\text{-}N)_2+NH_4]^+$ (9–22 min).

a molecular ion with *m/z* 750.3 at the HT-2 derivative retention time, corresponding to the adduct $[HT\text{-}2(1\text{-}N)_2+NH_4]^+$. No peak relevant to the mono-derivatized product for HT-2 toxin was observed. The HPLC-MS/MS chromatogram relevant to $[T\text{-}2(1\text{-}N)+NH_4]^+$ and $[HT\text{-}2(1\text{-}N)_2+NH_4]^+$ is shown in Fig. 2. In order to confirm the identity of the 1-NC derivatives, HPLC-MS/MS spectra were performed and compared with those of T-2 and HT-2 standards. Both MS/MS spectra of the ions $[T\text{-}2(1\text{-}N)+NH_4]^+$ (*m/z* 638.3) and $[HT\text{-}2(1\text{-}N)_2+NH_4]^+$ (*m/z* 750.3) showed a main fragment due to 1-naphthoyl group (*m/z* 155.2), and additional fragments at *m/z* 245.3, 227.3, 215.3, 197.3 and 185.0, respectively, originating from the trichothecene moiety. Similar results were obtained with the 2-NC derivatives. Full scan chromatogram of the PCC reaction mixture revealed the presence of a molecular ion with *m/z* 712.3 at the T-2 derivative retention time, corresponding to the adduct $[T\text{-}2(PC)+NH_4]^+$, and a molecular ion with *m/z* 898.3 at the HT-2 derivative retention time, corresponding to the adduct $[HT\text{-}2(PC)_2+NH_4]^+$. Also in this case no peak relevant to the mono-derivatized product for HT-2 toxin was observed. Both MS/MS spectra of the ions $[T\text{-}2(PC)+NH_4]^+$ (*m/z* 712.3) and $[HT\text{-}2(PC)_2+NH_4]^+$ (*m/z* 898.3) showed a main fragment due to pyrene-carbonyl group (*m/z* 229.2), and the characteristic fragments of the T-2 and HT-2 toxin moiety (i.e. *m/z* 227.3, 215.3, 197.3 and 185.0). Fig. 3 shows the scheme of the derivatization reaction of T-2 and HT-2 toxins with the labeling reagents 1-NC, 2-NC and PCC.

In order to establish the optimum excitation and emission wavelengths of each T-2 and HT-2 toxin derivatives for the HPLC-FD analysis, excitation and emission spectra were recorded during the chromatographic run of each fluorescent derivative. Table 1 shows the optimum wavelengths of excitation (λ_{ex}) and emission (λ_{em}) selected for each fluorescent derivative to improve sensitivity and selectivity of the HPLC analysis.

Different stoichiometric ratios of toxin:derivatizing reagent:catalyst were tested in order to improve the reaction

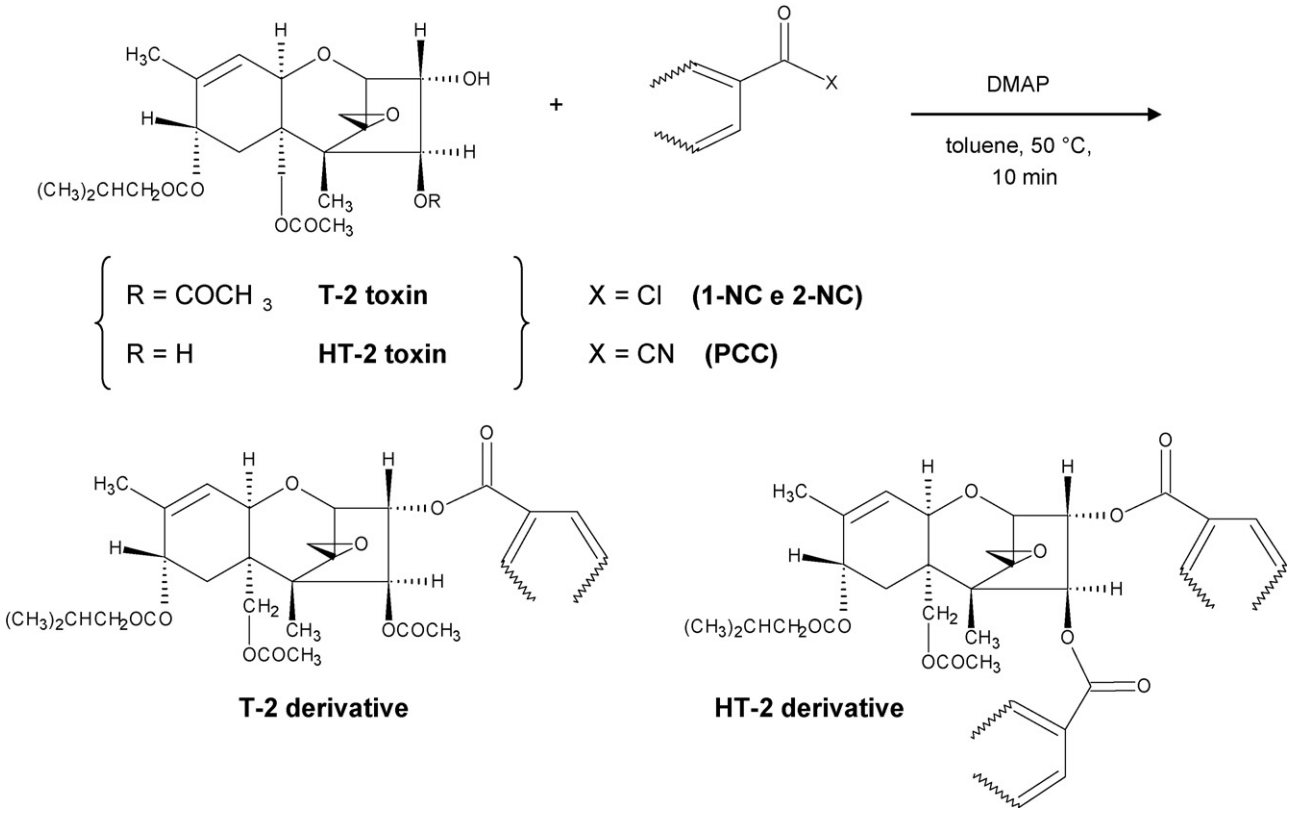

Fig. 3. Reaction of derivatization of T-2 and HT-2 toxins with 1-NC, 2-NC or PCC labeling reagents.

yields and to find the optimal conditions in terms of sensitivity and repeatability of the derivatization reaction for each labeling reagent. Fig. 4 shows fluorescence intensities of T-2 and HT-2 derivatives obtained at different stoichiometric ratios for 1-NC, 2-NC and PCC. No significant differences (ANOVA, test di Tukey, $p < 0.05$) were observed between peak areas obtained with ratios higher than 1:20:40 for HT-2(1-N)$_2$ and 1:40:80 for T-2(1-N), T-2(2-N), HT-2(2-N)$_2$ and T-2(PC). For HT-2(PC)$_2$ no significant difference ($p < 0.05$) was observed with ratios higher than 1:60:250. The PCC showed the highest reactivity towards both toxins, although the observed fluorescence intensity values of HT-2(PC)$_2$ derivative were unexpectedly lower than those of T-2(PC) at all tested stoichiometric ratios. Despite the apparent low reaction yield due to the low HT-2(PC)$_2$ signal, no peak corresponding to the unreacted HT-2 toxin was observed by HPLC-MS/MS analysis under the optimized stoichiometric ratio conditions. The low fluorescence signal intensity can be explained by the intramolecular excimer formation involving the two pyrene rings of HT-2(PC)$_2$ producing change in fluorescence spectral profile and lifetime [18]. The best compromise taking into account noise, peak intensity of reagents and sensitivity for both derivatized toxins was obtained by using stoichiometric ratios of 1:40:80 for 1-NC and 2-NC reagents, and 1:60:250 for PCC reagent.

Table 1
Optimum detection wavelengths of T-2 and HT-2 derivatives

Derivative	λ_{ex} (nm)	λ_{em} (nm)
T-2(1-N)	230	380
HT-2(1-N)$_2$	230	376
T-2(2-N)	237	370
HT-2(2-N)$_2$	237	365
T-2(PC)	355	403
HT-2(PC)$_2$	355	401

In order to evaluate the sensitivity of the new T-2 and HT-2 derivatives with respect to derivatives obtained by reaction with 1-AN [17], fluorescence intensities and signal-to-noise ratio values were determined by reacting the same amounts of toxins (250 ng of each toxin) under the optimized reaction conditions. Fig. 5 shows typical chromatographic profiles of derivatized T-2 and HT-2 toxins obtained by pre-column derivatization reaction with 1-NC, 2-NC and PCC. Detection limits (based on a signal-to-noise ratio of 3:1) were 10.0, 6.3 and 2.0 ng for derivatized T-2 toxin and 6.3, 2.3 and 2.8 ng for derivatized HT-2 toxin with 1-NC, 2-NC and PCC, respectively. As compared to detection limits of derivatized T-2 and HT-2 toxin with 1-AN (i.e. 5 and 3 ng, respectively), the sensitivity for both T-2 and HT-2 toxins was similar or better with 2-NC and PCC and worse with 1-NC.

A good linear response (peak area vs. injected amount) was observed, for all labeling reagents, in the range 10–1000 ng for either T-2 and HT-2 toxin, with coefficients of correlation (r) higher than 0.9995. Repeatability (relative standard devi-

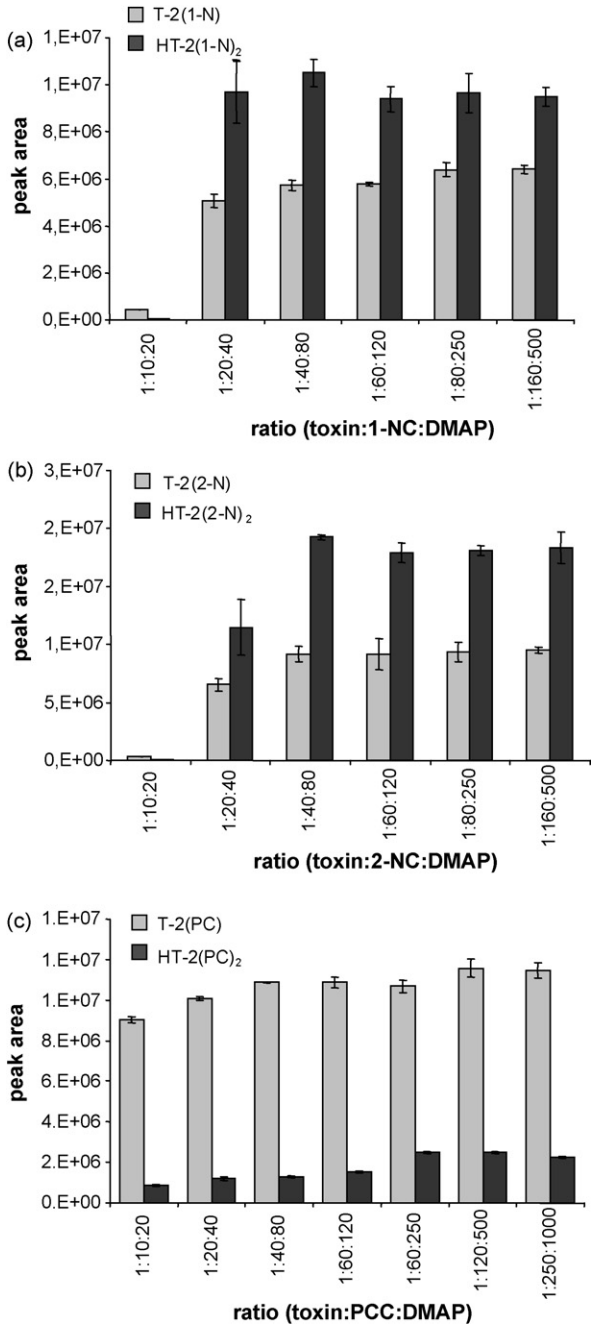

Fig. 4. Fluorescence intensities (peak areas) of T-2 and HT-2 derivatives obtained at different stoichiometric ratios of toxin:derivatizing reagent:catalyst for 1-NC (a), 2-NC (b) or PCC (c). Error bars represent relative standard deviations (triplicate experiments).

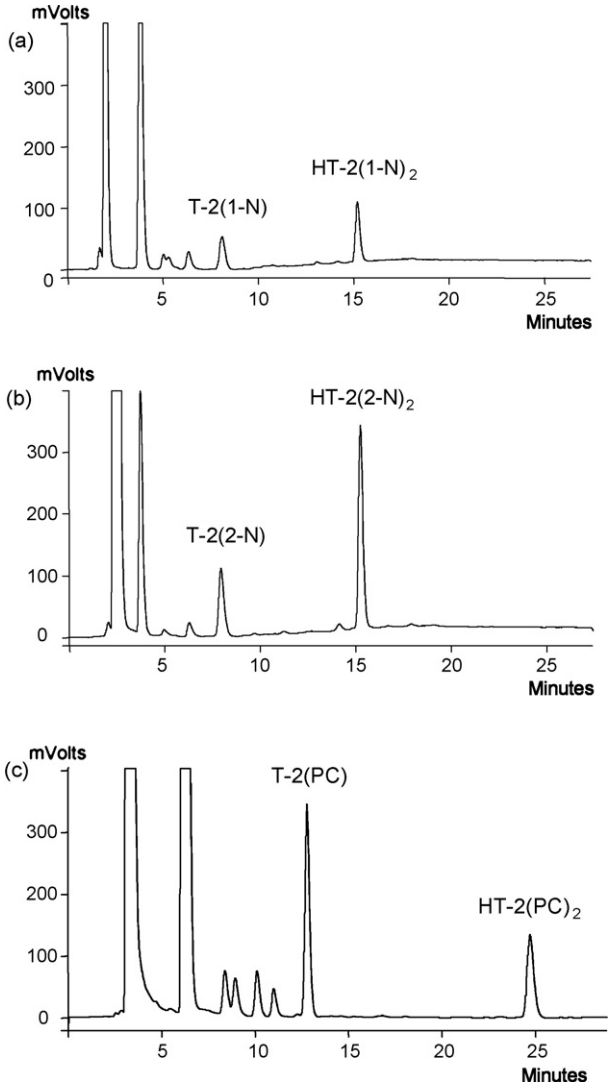

Fig. 5. Chromatograms of T-2 and HT-2 toxins (250 ng of each toxin,) derivatized with 1-NC (a), 2-NC (b) or PCC (c). Chromatographic conditions are reported in Section 2. All reaction mixtures were diluted (1:10, v/v) before HPLC injection to avoid off-scale peaks.

ations) of reactions was better than 8% for the derivatization of T-2 and HT-2 toxins over the whole concentration range tested.

Experiments to test the stability of the new T-2 and HT-2 fluorescent derivatives showed no significant difference of peak intensities up to 14 days after preparation of the solutions and storage at −20 °C in amber vials ('dark') and up to 5 days at +25 °C in clear vials ('light'), with the exception of T-2(PC) that showed highest stability under all the tested storage conditions. The high stability of the derivatives at room temperature would allow the use of an automatic sampler coupled with HPLC for the analysis of a large number of samples.

PCC and 2-NC reagents showed better performances in terms of the sensitivity of derivatives and the repeatability of reactions than 1-NC. In order to assess the applicability of the developed derivatization procedures with PCC and 2-NC for the simultaneous determination of T-2 and HT-2 toxins in cereals by HPLC/FD, preliminary experiments were carried out. Fig. 6 shows typical chromatograms of naturally contaminated wheat and maize extracts obtained by the procedure of Visconti *et al.* [17], and analyzed by HPLC/FD and pre-column derivatization with 2-NC and PCC. Fig. 7 shows chromatograms of a uncontaminated (blank) oat sample and the same oat sample spiked with T-2 and HT-2 toxin at levels of 30 and 15 ng g^{-1}, respectively, after immunoaffinity column clean-up of extracts and pre-column derivatization with 2-NC.

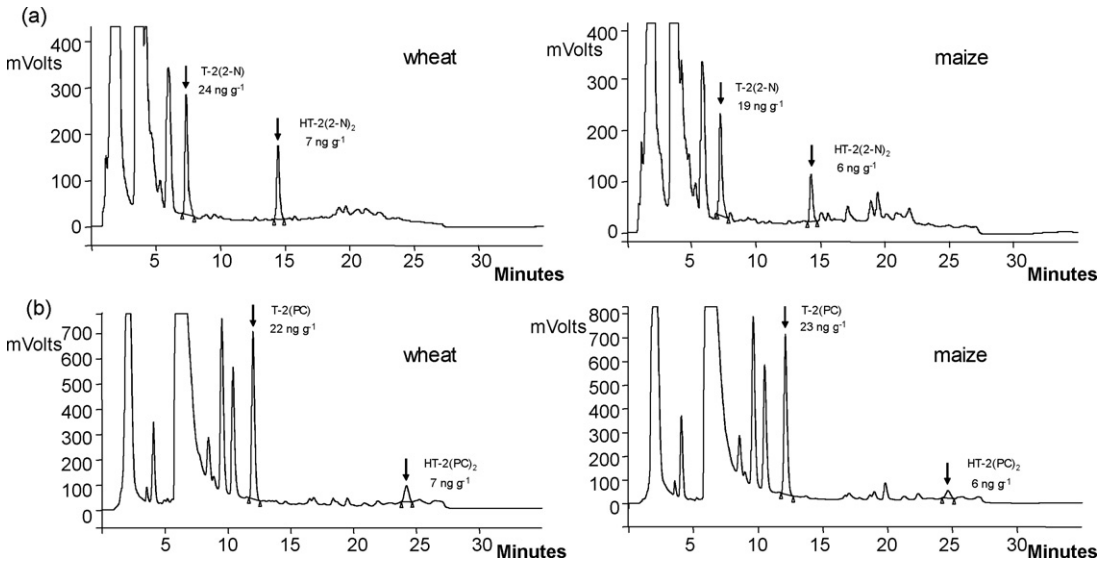

Fig. 6. Chromatograms of naturally contaminated wheat and maize samples after immunoaffinity column clean-up and pre-column derivatization with 2-NC (a) and PCC (b). Chromatographic conditions are reported in Section 2.

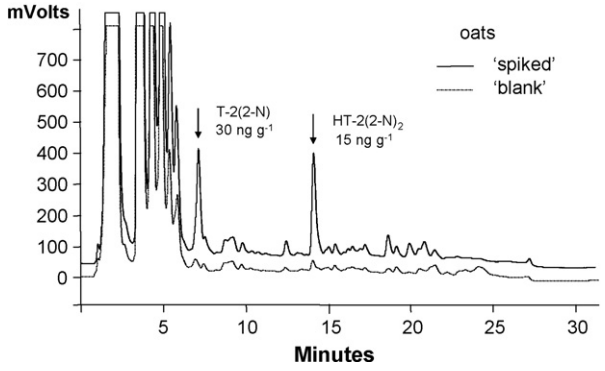

Fig. 7. Chromatograms of oat samples after immunoaffinity column clean-up and derivatization with 2-NC: (- · -) blank sample; (—) blank sample spiked with T-2 toxin (30 ng/g) and HT-2 toxin (15 ng/g). Chromatographic conditions are reported in Section 2.

4. Conclusions

1-NC, 2-NC and PCC, commercially available labeling reagents, reacted with T-2 and HT-2 toxins under mild conditions to give the corresponding fluorescent esters. The conditions of derivatization reactions were optimized in order to obtain good performance in term of rapidity, sensitivity, linearity, repeatability, and yield of reaction for each reagent. The use of 2-NC and PCC produced better performance, in term of sensitivity and selectivity, than 1-AN (a previously described labeling reagent for T-2 and HT-2 toxins) and 1-NC. Preliminary studies showed that derivatization reactions with 2-NC and PCC can be used for the simultaneous determination of T-2 and HT-2 toxins in raw cereals, including oats, by HPLC/FD after immunoaffinity column clean-up with good sensitivity. These novel fluorescent labeling reagents are useful tools to develop and validate sensitive and accurate analytical methods for determination of T-2 and HT-2 toxins in cereals and cereal-based products allowing a more correct evaluation of dietary exposure to these mycotoxins.

Acknowledgements

This work has been carried out within the project "Development of an improved method of analysis for the determination of T-2 and HT-2 toxins in foodstuffs" funded by the Food Standard Agency, UK. The authors would like to thank the National Research Council, Italy (Short-Term Mobility Program 2005) and V.M.T. Lattanzio (ISPA-CNR) for performing HPLC-MS analysis.

References

[1] R.A. Canady, R.D. Coker, S.K. Egan, R. Krska, M. Olsen, S. Resnik, J. Schlatter, T-2 and HT-2 toxins, in: WHO (Ed.), Safety Evaluation of Certain Mycotoxins in Food, FAO Food and Nutrition Paper 74, WHO Food Additives Series 47, Geneve, Switzerland, 2001, pp. 557–680.
[2] A. Visconti, C.J. Mirocha, A. Bottalico, J. Chelkowski, Mycotoxin Res. 1 (1985) 3.
[3] Reports on tasks for scientific cooperation, Task 3.2.10, Collection of occurrence data of *Fusarium* toxins in food and assessment of dietary intake by the population of EU Members States, http://europa.eu.int/comm./food/fs/scoop/task3210.pdf (pages consulted on 27th Sept., 2007).
[4] A. Visconti, Bull. Inst. Compr. Agr. Sci. Kinki Univ. 9 (2001) 39.
[5] Commission Regulation (EC) No 856/2005 of 6 June, 2005 amending Regulation (EC) No 466/2001 as regards *Fusarium* toxins, Off. J. Eur. Union L143 (2005) 3–8.
[6] Commission Regulation (EC) No 1881/2006 of 19 December, 2006 setting maximum levels for certain contaminants in foodstuffs. Off J. Eur. Union L364 (2006) 5–24.
[7] R. Krska, S. Baumgartner, R. Josephs, Fresenius' J. Anal. Chem. 371 (2001) 285.
[8] T. Yoshizawa, Chromatographic Method for Trichothecenes, in: M.W. Trucksess, A.E. Pohland (Eds.), Mycotoxin Protocols, Methods in Molecular Biology, vol. 157, Humana Press, Totowa, NJ, 2001, pp. 115–129 (Chapter 11).
[9] H. Petterson, W. Langseth, Intercomparison of trichothecene analysis and feasibility to produce certified calibrants and reference material, BCR Information, Project Reports EUR 20285/1 EN (Part I) and EUR 20285/2 EN (Part II), European Commission, Brussels, 2002.

[10] F. Berthiller, R. Schumacher, G. Buttinger, R. Krska, J. Chromatogr. A 1062 (2005) 209.
[11] V. M. T. Lattanzio, M. Solfrizzo, A.Visconti, Food Addit. Contam. (2007), in press., doi:10.1080/02652030701513792.
[12] V.M.T. Lattanzio, M. Solfrizzo, S. Powers, A. Visconti, Rapid Commun. Mass Spectrom. 21 (2007) 3253.
[13] H. Cohen, B. Boutin-Muma, J. Chromatogr. A 595 (1992) 143.
[14] M. Jiménez, J.J. Mateo, R. Mateo, J. Chromatogr. A 870 (2000) 473.
[15] M. Pascale, M. Haidukowski, A. Visconti, J. Chromatogr. A 989 (2003) 257.
[16] C. Dall'Asta, G. Galaverna, A. Biancardi, M. Gasparini, S. Sforza, A. Dossena, R. Marchelli, J. Chromatogr. A 1047 (2004) 241.
[17] A. Visconti, V.M.T. Lattanzio, M. Pascale, M. Haidukowski, J. Chromatogr. A 1075 (2005) 151.
[18] A.C. Benniston, A. Harriman, S.L. Howell, C.A. Sams, Y.-G. Zhi, Chem Eur. J. 13 (2007) 4665.

Available online at www.sciencedirect.com
ScienceDirect
Talanta 74 (2008) 1603–1607
Talanta
www.elsevier.com/locate/talanta

Pharmaceutical powders analysis using FT-Raman spectrometry: Simultaneous determination of sulfathiazole and sulfanilamide

Macarena López-Sánchez, María José Ruedas-Rama, Antonio Ruiz-Medina, Antonio Molina-Díaz, María José Ayora-Cañada *

Department of Physical and Analytical Chemistry, Faculty of Experimental Sciences, University of Jaén, 23071 Jaén, Spain

Received 20 June 2007; received in revised form 7 September 2007; accepted 3 October 2007
Available online 16 October 2007

Abstract

A procedure for rapid quantitative analysis of pharmaceutical powders is described. Powdered samples were measured in a rotating cell in order to avoid sub-sampling problems by increasing the irradiated area. Quantitative determination of sulfathiazole and sulfanilamide, using a simple univariate calibration model is proposed. Even though both antibacterials are of the same chemical family (sulfonamides), the richness of structural information contained in the Raman spectra allowed their determination using the area of two selected bands (1255 and 1629 cm^{-1} for sulfathiazole and sulfanilamide, respectively). Relative standard deviation (R.S.D.) values ($n = 10$) of 3.35% and 3.46% for sulfathiazole and sulfanilamide, respectively, demonstrate the good reproducibility of the measurement technique with the rotating cell. The method was successfully applied to the analysis of synthetic mixtures and commercial pharmaceutical powders. The procedure is suitable to be applied to pharmacopoeial uniformity of content testing of batches.
© 2007 Elsevier B.V. All rights reserved.

Keywords: Pharmaceuticals; Raman spectrometry; Solids; Powders; Quantitative determination; Sulfonamides; Sulfathiazole; Sulfanilamide

1. Introduction

Raman spectrometry is a rapid, non-destructive, non-invasive and reliable tool that is finding increasing application in the field of pharmaceutical analysis [1,2]. The richness of the vibrational spectroscopic information allows qualitative and quantitative analysis even of polymorphic crystal forms. Quantitative analysis can be performed either by manually selecting some of the bands due to each of the target compounds [3] or by using multivariate data analysis techniques [4,5] (i.e. partial least squares regression (PLS)). Raman spectroscopy is becoming an excellent analytical tool for both process control and finished product control in pharmaceutical production. The technique can be used to study solids, liquids, powders, gels, slurries and aqueous solutions without requiring any special sample preparation. It means that many studies may be performed in situ. Several approaches to direct active ingredient quantification in pharmaceuticals and audits on polymorphs have already been reported but there is still a lack of widespread acceptance of the technique in routine pharmaceutical analysis.

The major problem in the analysis of solid samples by Raman spectrometry appears because tablets or powders are heterogeneous on length scales greater than the size of a typical focused laser spot, which illuminates only a tiny area (50–500 μm) to collect spectral information. Two different approaches have been described to overcome this problem. One of them consists on measuring several spectra for each sample, with the position of the sample being changed randomly for each measurement. The average spectrum is then taken for the analysis [6]. A second useful approach to represent average sample composition is rotation of the sample during Raman collection to cover a wider surface area. It has been demonstrated that this procedure leads to improved calibration performance [7].

When dealing with powdered samples, the use of immersion probes with increased sampling area and continuous rotation of the sample in a vial have been demonstrated to provide good reproducibility [8,9]. Without the use of probes, the most common approach to rotate pharmaceutical powders and to measure them by means of Raman spectrometry involves grinding in a mortar for a few minutes and then preparing a pellet in a sim-

* Corresponding author. Fax: +34 953212940.
E-mail address: mjayora@ujaen.es (M.J. Ayora-Cañada).

0039-9140/$ – see front matter © 2007 Elsevier B.V. All rights reserved.
doi:10.1016/j.talanta.2007.10.015

ilar way to that used in IR spectroscopy [10–12]. This pellet can be then easily rotated. Another previously described procedure to increase sampling area consisted in placing the powders in a NMR-tube and rotating it with one motor while moving it up and down with a second motor [13]. In this work, a novel procedure for quantitative analysis of powders avoiding the time-consuming step of preparing pellets will be evaluated. It involves the use of a dedicated cell which facilitates the rotation of the powders achieving a large sampling area by using only one motor. Furthermore, the feasibility of quantifying closely related chemical substances on the basis of their distinct Raman spectral features using simple univariate calibration will be evaluated. Two sulfonamides (sulfathiazole and sulfanilamide), an important class of antibacterial agents used in medicine and veterinary practice, have been chosen as model analytes.

2. Experimental

2.1. Materials

Sulfathiazole and sulfanilamide were obtained from Aldrich (Madrid, Spain). Commercially available powder (Wilfe, containing g: 69.7 g sulfathiazole and 30.3 g sulfanilamide per 100 g *Ltd. Pérez Giménez*) was purchased in a local pharmacy.

2.2. Raman spectrometer and measurement cell

Raman spectra were recorded using a Bruker RFS (FT)-Raman Spectrometer fitted with a liquid nitrogen-cooled Ge detector. The excitation radiation was the 1064 nm line from a Nd–YAG laser (Coherent) with a laser power of 1.3 W using a non-focused laser beam. The Raman scattered radiation was collected at 180° geometry. All spectra were recorded with a resolution of 4 cm^{-1} and were averaged over 64 scans.

The measurements were made in a homemade cell (see Fig. 1). This consisted of a metallic washer over a glass window. The powdered sample was introduced into the washer hole, covered with an adhesive label and attached to a magnet. The cell was fixed to a synchronous motor mounted in the sample compartment by means of the magnet. The sample remained in the space between the magnet and the glass (20 mm inner diameter and 2 mm depth). The motor rotated the sample cell around the axis of the laser beam (5 r.p.m.) to yield an irradiation pattern of a circumference with a radius of 3 mm.

2.3. Procedure

To obtain the calibration curves, standards with suitable weight ratios of sulfathiazole and sulfanilamide were prepared by mixing accurately weighed amounts of both pure solids in a mortar and grinding for a few minutes to homogenise the powders properly. Powder samples of commercial formulations were also grinded in the mortar.

Approximately 300 mg of powder were placed into the homemade cell. Standards and samples were analysed by triplicate and calibration graphs were obtained by plotting selected band areas against the sulfonamides concentration expressed as a

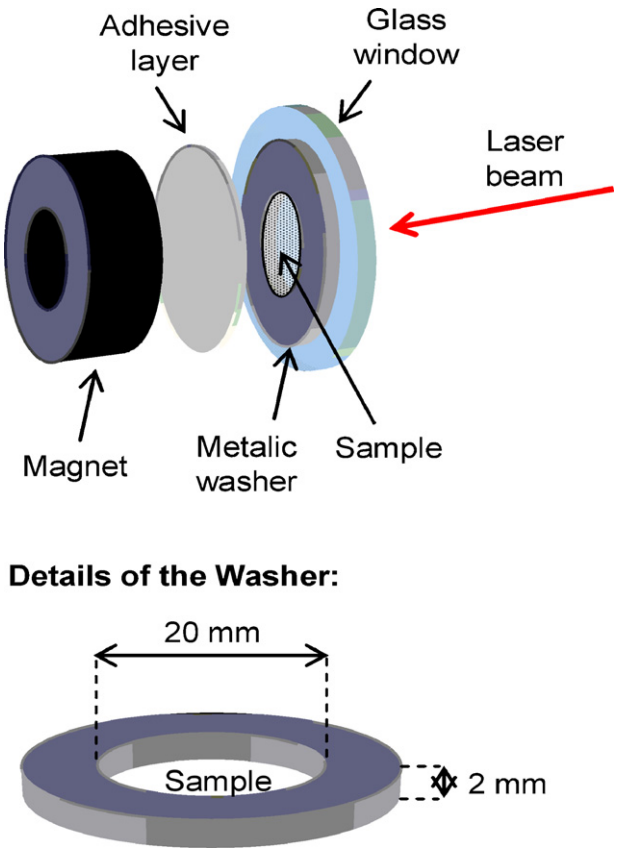

Fig. 1. Scheme of the measurement cell.

weight percent. Band areas were calculated employing one-point baseline correction. The range 1624–1636 cm^{-1} was used for sulfanilamide. A baseline point obtained averaging four points in the range 1650–1660 cm^{-1} was employed. Sulfathiazole was quantified using the band area between 1246 and 1276 cm^{-1} (baseline point average of four points between 1220 and 1230 cm^{-1}).

3. Results and discussion

3.1. Raman spectra of sulfathiazole and sulfanilamide

The FT-Raman spectra of sulfathiazole and sulfanilamide in solid state are presented in Fig. 2. The most intense spectral features, common to both sulfonamides, are located around 1595 and 1135 cm^{-1}. They can be assigned to the stretching of the benzene ring and the symmetric stretching of the SO_2 group, respectively [14]. In addition to these common bands, each sulfonamide showed spectral singularities. Thus, the S–N stretching is observed at 900 cm^{-1} in the spectrum of sulfanilamide [15] and characteristic bands of thiazole ring involving the C–S stretching mode are observed in sulfathiazole spectrum at 633 and 732 cm^{-1} [16]. Two bands, 1629 and 1255 cm^{-1} were selected for quantification of sulfanilamide and sulfathiazole, respectively. These bands are specific for each sulfonamide, without any contribution from the other one. The assignment of the band at 1255 cm^{-1} characteristic of sulfathiazole is dif-

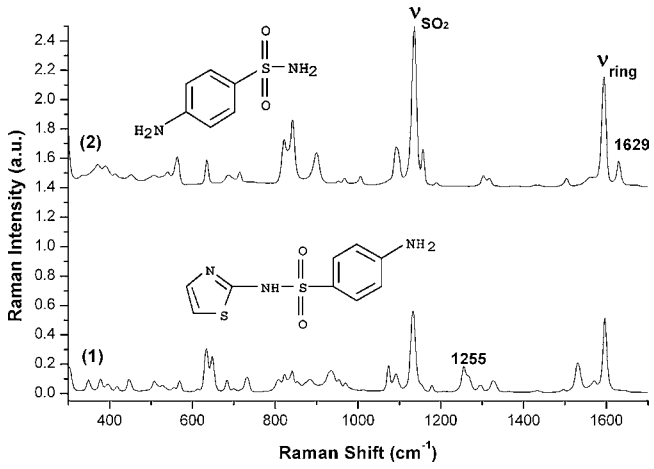

Fig. 2. FT-Raman spectra of sulfathiazole (1) and sulfanilamide (2) in solid state. Chemical structures of both sulfonamides are also shown.

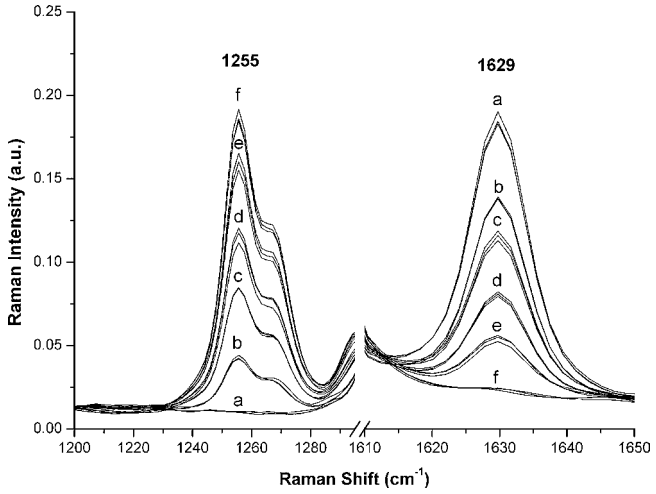

Fig. 3. FT-Raman spectra of the calibration standards showing the bands at 1255 cm^{-1} (sulfathiazole) and 1629 cm^{-1} (sulfanilamide). Standards containing sulfanilamide (%)/sulfathiazole (%): (a) 0/100, (b) 20/80, (c) 40/60, (d) 60/40, (e) 80/20 and (f) 100/0.

ficult due to the complexity of the spectrum. Probably, it has a contribution of the C–N stretch between the thiazole ring and the sulfonamide group [16] although other atoms of the thiazole ring are also involved. The band at 1629 cm^{-1}, which is absent in sulfathiazole spectrum, can be attributed to NH_2 in plane bending (scissoring) of the sulfonamide group in sulfanilamide.

3.2. Optimization of experimental parameters

Homogeneous sampling is a critical parameter that has to be considered when developing a solid-state quantitative method. Preliminary experiments were performed using commercially available windowless aluminium holders for measurement of solids. Single point measurements performed with these stationary holders were not reproducible enough to perform quantitative analysis. Relative standard deviations of band area for the same sample (measured after refilling the holder) ranged between 10% and 20%. This is due to both surface irregularities and the inaccurate compositional representation of the sample by the Raman spectrum because the laser illuminates only a tiny spot (about 0.5 mm diameter). The use of the above-described rotating cell (irradiating a circumference of 3 mm radius) increased the reproducibility. In this way R.S.D. values always lower than 4% were achieved without the need of preparing pellets or tablets. The powders were placed directly in the cell and measured. Furthermore, other experimental parameters like the optical arrangement, stability of laser power and collection optics were constant enough to guarantee reproducible measurements. Thus, the addition of an internal standard was not required.

3.3. Analytical parameters

Quantitative analysis was achieved by means of univariate calibration employing selected band areas as analytical readout. The spectra of the calibration standards in the selected spectral region are shown in Fig. 3. Band areas were calculated employing a one point baseline correction in the range 1246–1276 cm^{-1} for sulfathiazole and 1624–1636 cm^{-1} for sulfanilamide. To eliminate noise the baseline point was obtained by averaging the intensity of four points. These two calibration bands were chosen because they are characteristic of each sulfonamide and free of spectral interference from the other. The data were fitted by standard least-squares treatment. As can be seen in Table 1, where the figures of merit of the proposed method are summarized, calibration curves present excellent linearity.

The reproducibility was established by analysing 10 synthetic mixtures containing 70% and 30% of sulfathiazole and sulfanilamide, respectively. In both cases, relative standard deviation (R.S.D.) values were lower than 4% (3.35% for sulfanilamide and 3.46% for sulfathiazole).

3.4. Applications

In order to assess the utility of the proposed method and since these sulfonamides are commonly used in veterinary pharmaceuticals for topical use of the powders directly, three synthetic mixtures were prepared simulating some of these pharmaceuticals, with the two sulfonamides in different proportions (see Table 2). Results are in good agreement with the actual content: relative errors were below 3% for sulfanilamide, whereas for sulfathiazole relative errors were below 1% in all cases. The maximum R.S.D. value obtained ($n = 3$) was 2.2%.

Table 1
Analytical parameters

Parameter	Sulfathiazole A (1255 cm^{-1})	Sulfanilamide A (1629 cm^{-1})
Calibration graph		
Intercept	−0.2591	−0.1466
Slope	0.0341	0.0156
Correlation coefficient	0.9988	0.9979
R.S.D. (%) ($n = 10$)	3.35	3.46

S.D.: standard deviation (average of three determinations).

Table 2
Analysis of semi-synthetic mixtures

Semi-synthetic samples	Sulfanilamide mean ± S.D. (%)	Sulfathiazole mean ± S.D. (%)
Sample 1	29.4 ± 0.2	69.4 ± 0.9
Sample 2	34.0 ± 0.7	64.2 ± 0.3
Sample 3	25.5 ± 0.6	75.0 ± 0.3

Sample 1: 30/70, sample 2: 35/65 and sample 3: 25/75% of sulfanilamide/sulfathiazole, respectively.
S.D.: standard deviation (average of three determinations).

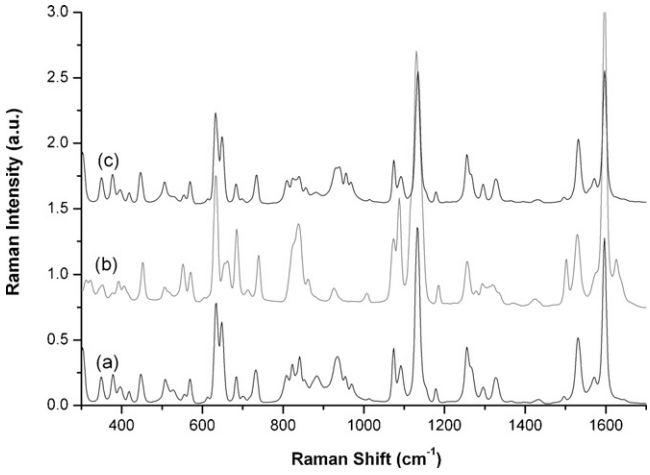

Fig. 4. Raman spectra of sulfathiazole from Aldrich (a) and two polymorphs obtained: (b) by heating commercial material at 180 °C for 15 min and (c) by dissolution in alkali followed by neutralization.

Finally, the method was also applied to the analysis of a commercial pharmaceutical preparation for humans, Wilfe (powder) which contained sulfathiazole and sulfanilamide. It is known that these substances exhibit polymorphism, which affect their peak positions and intensities in the Raman spectra [17]. Different polymorphs for sulfathiazole and sulfanilamide were prepared using literature techniques [18,19]. Their Raman spectra were different enough to be able to discern between them, as can be seen in Fig. 4 for some polymorphs for sulfathiazole.

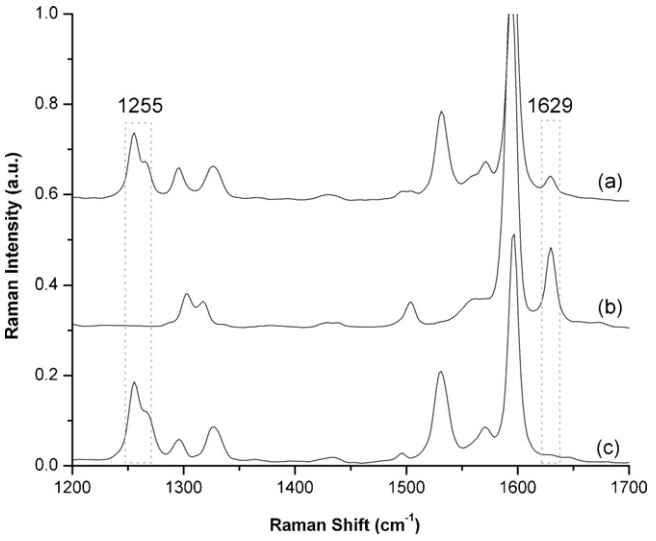

Fig. 5. FT-Raman spectra of a commercial formulation Wilfe (powder) containing sulfathiazole and sulfanilamide (a), sulfanilamide (b) and sulfathiazole (c) standards. Bands employed for calibration are remarked.

Having this into account, the polymorphic form of the pharmaceutical samples must be verified before performing quantitative analysis. In Fig. 5, the Raman spectrum of the sample (Wilfe) is compared with the spectra of the pure standards. From this figure, it is clear that band positions of the pharmaceutical correspond to those of the polymorphic forms employed as standards for sulfathiazole and sulfanilamide. Furthermore, bands employed for calibration are also highlighted in this figure to show how quantification of both sulfonamides can be easily achieved employing univariate calibration.

The fact that we measure Raman spectra of powders directly makes the method ideally suited to content uniformity testing [20,21]. The first step in the testing procedure requires the content of 10 different samples from a batch. To pass the uniformity content test (USP, United States Pharmacopoeia) [21], all 10 results must lie within 85–115% of the labelled value and the relative standard deviation must be less than 6%. When not more than one value exceeds ±15%, but less than ±25%, the batch

Table 3
Uniformity of content test

Wilfe powder (30.3% sulfanilamide, 69.7% sulfathiazole)	Sulfanilamide Concentration found (%) ± S.D.[a] (%)	Sulfathiazole Concentration found (%) ± S.D.[a] (%)
Bottle 1	31 ± 1	66 ± 2
Bottle 2	30 ± 2	69 ± 2
Bottle 3	30 ± 3	73 ± 3
Bottle 4	30.9 ± 0.5	70 ± 3
Bottle 5	32 ± 2	72 ± 2
Bottle 6	31 ± 4	77 ± 5
Bottle 7	32 ± 3	75 ± 2
Bottle 8	31 ± 2	68 ± 1
Bottle 9	32 ± 3	68 ± 1
Bottle 10	31 ± 1	68 ± 1.2
Mean (%)	31.2	71
Standard deviation (%)	0.8	3
Relative standard deviation (R.S.D.) (%)	2.48	4.95
Relative error (%)	2.87	1.20

[a] S.D.: standard deviation (average of three determinations).

may be retested by assaying a further 20 samples. If there is still only one sample in the range ±15–25% and R.S.D. for the 30 is less than 7.8%, the batch passes.

Table 3 shows the results obtained in the determination of sulfathiazole and sulfanilamide in ten different pharmaceutical bottles of Wilfe powder from the same batch (each measure corresponds to a different bottle, all of them owning to the same batch). Each sample was measured by triplicate.

In all cases, the results were in good agreement with the labelled amounts given by the fabricant, showing deviations from these values lower than 3% for both sulfonamides. The standard deviation for all the measurements was less than 3.5 for both. This indicated the utility of the proposed method for routine analytical control in pharmaceuticals. The presented results clearly demonstrate that Raman spectroscopy is adequate to be applied to uniformity of content testing.

4. Conclusions

The measurement of powdered samples in a rotating cell has allowed the quantification of two active sulfonamides with R.S.D. lower than 4% in pharmaceutical preparations. Many regulations are in place for pharmaceutical manufacture e.g., for in-process testing to demonstrate adequacy of mix and, specially, for the content uniformity of finished dosage forms. As demonstrated here, Raman spectroscopy is an excellent alternative for these analyses showing significant advantages over commonly employed methods such as HPLC analysis: (1) it is fast, reliable and precise; (2) there is no need of sample preparation; and (3) no solvents are required.

Acknowledgements

This work was financed by the research group FQM-323M of the Spanish Junta de Andalucía. M.L.S acknowledges the financial support from a predoctoral fellowship (Junta de Andalucía).

References

[1] T. Vankeirsbilck, A. Vercauteren, W. Baeyens, G. Van der Weken, F. Verpoort, G. Vergote, J.P. Remon, TrAC Trends Anal. Chem. 21 (2002) 869.
[2] C.J. Strachan, T. Rades, K. Gordon, J. Rantanen, J. Pharm. Pharmacol. 59 (2007) 179.
[3] S.G. Skoulika, C.A. Georgiou, Appl. Spectrosc. 57 (2003) 407.
[4] M. Kim, H. Chung, Y. Woo, M. Kemper, Anal. Chim. Acta 579 (2006) 209.
[5] R. Szostak, S. Mazurek, J. Mol. Struct. 704 (2004) 229.
[6] G.J. Vergote, C. Vervaet, J.P. Remon, T. Haemers, F. Verpoort, Eur. J. Pharm. Sci. 16 (2002) 63.
[7] J. Johansson, S. Pettersson, S. Folestad, J. Pharm. Biomed. Anal. 39 (2005) 510.
[8] J. Rantanen, H. Wikstrom, F.E. Rhea, L.S. Taylor, Appl. Spectrosc. 59 (2005) 942.
[9] M. Savolainen, K. Jouppila, O. Pajamo, L. Christiansen, M. Karjalainen, J. Rantanen, J. Pharm. Pharmacol. 59 (2007) 161.
[10] S. Mazurek, R. Szostak, J. Pharm. Biomed. Anal. 40 (2006) 1225.
[11] S.G. Skoulika, C.A. Georgiou, Appl. Spectrosc. 55 (2001) 1259.
[12] R. Szostak, S. Mazurek, Analyst 127 (2002) 144.
[13] F.W. Langkilde, J. Sjoblom, L. Tekenbergs-Hjelte, J. Mrak, J. Pharm. Biomed. Anal. 15 (1997) 687.
[14] C. Topacli, A. Topacli, J. Mol. Struct. 644 (2003) 145.
[15] H.T. Varghese, C.Y. Panicker, D. Philip, Spectrochim. Acta A: Mol. Biomol. Spectrosc. 65 (2006) 155.
[16] D. Lin-Vien, N.B. Colthup, W.G. Fateley, J.G. Grasselli, The Handbook of Infrared and Raman Characteristic Frequencies of Organic Molecules, Academic Press, INC, San Diego, 1991.
[17] J.E. Anderson, S. Moore, F. Tarczynski, D. Walker, Spectrochim. Acta A: Mol. Biomol. Spectrosc. 57 (2001) 1793.
[18] D.C. Apperley, R.A. Fletton, R.K. Harris, R.W. Lancaster, S. Tavener, T.L. Threlfall, J. Pharm. Sci. 88 (2007) 1275.
[19] A. Portieri, R.K. Harris, R.A. Fletton, R.W. Lancaster, T.L. Threlfall, Magn. Reson. Chem. 42 (2004) 313.
[20] European Pharmacopoeia, third ed., EDQM Publ., Strasbourg, Germany, 1997.
[21] United States Pharmacopoeia, 24th ed., The United States Pharmacopoeia Convention, Inc. 2000, Rockville, USA, 2000.

Available online at www.sciencedirect.com
ScienceDirect
Talanta 74 (2008) 1642–1648
Talanta
www.elsevier.com/locate/talanta

A new strategy for electrochemical immunoassay based on enzymatic silver deposition on agarose beads

Yan Luo, Xun Mao, Zhao-Feng Peng, Jian-Hui Jiang *, Guo-Li Shen, Ru-Qin Yu *

State Key Laboratory for Chemo/Biosensing and Chemometrics, College of Chemistry and Chemical Engineering, Hunan University, Changsha 410082, PR China

Received 18 July 2007; received in revised form 8 October 2007; accepted 12 October 2007
Available online 22 October 2007

Abstract

A novel, sensitive electrochemical immunoassay in a homogeneously dispersed medium is described herein based on the unique features of agarose beads and the special amplified properties of biometallization. The immunochemical recognition event between human immunoglobulin G (IgG) and goat anti-human IgG antibody is chosen as the model system to demonstrate the proposed immunoassay approach. Avidin-agarose beads rapidly react with the biotinylated goat anti-human IgG antibody to form agarose beads-goat anti-human IgG conjugate (agarose bead-Ab). Agarose bead-Ab, alkaline phosphatase conjugated goat anti-human IgG antibody (ALP-Ab) and the human IgG analyte are mixed to form sandwich-type immunocomplex followed by the addition of the enzymatic silver deposition solution to deposit silver onto the surface of proteins and agarose beads. The silver deposited are dissolved and quantified by anodic stripping voltammetry. The influence of relevant experimental variables was examined and optimized. The logarithm of the anodic stripping peak current depended linearly on the logarithm of the concentration of human IgG in the range from 1 to 1000 ng/ml. A detection limit as low as 0.5 ng/ml human IgG was attained by 3σ-rule. The R.S.D. of the approach is 9.65% for eight times determination of 10 ng/ml human IgG under same conditions. Optical microscope and TEM graphs were also utilized to characterize agarose beads and silver nanoparticles formed.
© 2007 Elsevier B.V. All rights reserved.

Keywords: Immunoassay; Enzymatic silver deposition; Agarose beads; Anodic stripping voltammetry

1. Introduction

Various kinds of micro-spheres, such as graphite particles, silica micro-spheres, magnetic beads and agarose beads, are useful as templates and separation tools in bio-assay systems. Micro-beads possess a high ratio of surface area to volume so that they can greatly improve the performance of biosensors. For example, Lee and Walt have adapted aptamers immobilized on the surface of silica micro-spheres to high-density fiber-optic arrays for detecting thrombin [1]. Functionalized magnetic beads are utilized as solid phase for immunoassay in order to improve the performances of the system [2], though the silica beads commonly bring a significant amount of non-specific protein binding in the immunoassays [1]. The magnetic particles might have problem associated with their toxicity in the biological systems, Dyal et al. reported that the specific activity of *Candida rugosa* lipase attached to the surface of magnetic nanoparticles was significantly decreased [3]. In contrast to the magnetic and silica beads, the agarose beads are more suitable for practical applications due to their excellent biocompatibility, nontoxicity and less non-specific protein binding. A variety of derivatized agarose beads have been applied to some isolation techniques such as electrophoresis [4] and affinity chromatography [5,6]. Furthermore, agarose beads have been used as solid phase and separation tools for DNA detections and immunoassays. In recent years, a chip-based on agarose micro-bead array (electronic taste chip) has been proven to be useful for rapid and specific detection of proteins and DNA by McDevitt's group [7–9]. However, the agarose beads as the capture probe containing sensing elements might not be able to effectively capture target analytes because they are usually nestled into the micromachined silicon wells. Because of the excellent biocompatibility, agarose beads have demonstrated their analytical

* Corresponding authors. Tel.: +86 731 8822577; fax: +86 731 8822782.
E-mail addresses: jianhuijiang@hnu.cn (J.-H. Jiang), rqyu@hnu.cn (R.-Q. Yu).

0039-9140/$ – see front matter © 2007 Elsevier B.V. All rights reserved.
doi:10.1016/j.talanta.2007.10.026

potential in detecting a variety of analyte classes in a homogeneously dispersed medium [10,11]. Gray and Bhunia used protein A-coated agarose beads (immunobeads) and Dynal magnetic beads to capture target bacteria from a sample suspension, they found that the immunoseparation using protein A-coated agarose beads (immunobeads) system was highly specific compared to immunomagnetic separation using Dynal magnetic beads system [12]. Agarose beads are potential immunoreaction carriers and immunoseparation tools in immunoassays owing to some of their unique features: agarose beads could provide a very flexible, cell membrane-like environment and a large outer surface on which target analytes can be attached in solution. In this way the use of agarose beads might provide improved efficiency of immunological reaction and amplified response signal compared to heterogeneous immunoassays.

Commonly, the precipitation of silver onto colloidal gold labels was utilized to enhance the sensitivity of electrochemical [13] and chemiluminescent [14] metalloimmunoassays. Recently, several biosensors have been reported using a process called 'biometallization', in which metallization is catalyzed by an enzyme. The electrochemical detection of DNA hybridization based on stripping voltammetry of enzymatically deposited silver showed that biometallization leads to a great enhancement in electrochemical signal, thus high sensitivity is accomplished by this approach [15]. A novel method for electrochemical amplification immunoassay has been proposed based on accumulation of silver metal by alkaline phosphatase (ALP)-catalyzed product of ascorbic acid, the subsequent anodic stripping voltammetry (ASV) provided an immunoassay with relatively good sensitivity [16]. Combining enzyme catalysis with metal deposition seems to be a promising strategy for sensitive immunoassay. To our knowledge, the solid phases of biosensors based on biometallization mostly are various electrodes or microtiter wells, the step-by-step immunoassay procedure is a slow and tedious process. Since agarose beads used as solid phase have large surface area per unit volume and excellent biocompatibility, they can provide not only higher reactive surface area but also short biochemical assay time compared to the continuous solid supports.

In this paper, we have developed a novel electrochemical immunoassay based on the unique features of agarose beads and the special amplified properties of biometallization in a homogeneously dispersed medium. The immunochemical recognition event between human immunoglobulin G (IgG) and goat anti-human IgG antibody is chosen as the model system to demonstrate the proposed immunoassay approach. Avidin-agarose beads rapidly react with the biotinylated goat anti-human IgG antibody to form agarose beads-goat anti-human IgG conjugate (agarose bead-Ab). Agarose bead-Ab, alkaline phosphatase conjugated goat anti-human IgG antibody (ALP-Ab) and the human IgG analyte are mixed in a small glass vessel to form sandwich-type immunocomplex followed by the deposition of silver onto the surface of proteins and agarose beads by the addition of the enzymatic silver deposition solution. The silver deposited are dissolved with concentrated HNO_3 solution and then quantified by ASV. In order to improve the performances of the system, functionalized agarose beads are used as solid phase for this immunoassay. Goat anti-human antibodies are immobilized on the surface of the agarose beads, which are able to effectively capture target human IgG analytes from a sample suspension. Furthermore, agarose beads also provide a large outer surface area for process of enzymatic silver deposition, the accumulation of metallic silver by a catalytically generated ALP product is further increased and electrochemical signal could be amplified. This new strategy is simple and rapid due to inducting the agarose beads as immunological reaction carriers in suspension, and a relatively high sensitivity could be achieved without other process of silver enhancement because of coupling the unique features of agarose beads and biometallization. Additionally, a comparison of analytical performances of immunosensors using avidin-agarose beads and avidin-modified magnetic nanoparticles is demonstrated. The immunosensor using avidin-agarose beads is more sensitive and specific than that of using avidin-modified magnetic nanoparticles.

2. Experimental

2.1. Materials and reagents

Avidin-agarose beads (1.5 mg avidin/ml) and carboxy-terminated magnetic nanoparticles (20 mg/ml) were purchased from Sigma. Avidin-agarose bead size ranged from 90 to 160 μm. Biotinylated goat anti-human IgG antibody, human IgG, biotin, avidin and bovine serum albumin (BSA) were products of Beijing Dingguo Biotechnology Development Center (Beijing, China). ALP-Ab (ZB-2312) was provided by Beijing Zhongshan Biotechnology Reagents. Ascorbic acid 2-phosphate (AA-p) was obtained from Express Technology Co. Ltd. (Japan). *N*-(3-Dimethylaminopropyl)-*N*′-ethylcarbodiimide hydrochloride (EDC) and *N*-hydroxysuccinimide (NHS) were purchased from Fluka. Triton X-100 was provided by Aldrich. Silver nitrate ($AgNO_3$) and potassium nitrate (KNO_3) were purchased from Shanghai Chemical Reagents (Shanghai, China). Buffer used in this study was phosphate-buffered saline (PBS: 2 mM NaH_2PO_4, 8 mM Na_2HPO_4 and 150 mM NaCl, pH 7.4). The enzymatic silver deposition solution was a glycine–NaOH buffer containing 1.5 mM AA-p and 1 mM $AgNO_3$ (pH 9.0). Other reagents were of analytical purity, and ultra pure water of specific resistance 18 MΩ was used throughout the experiments.

2.2. Apparatus

Electrochemical measurements were performed with a three-electrode system comprising a carbon paste electrode (CPE) with a diameter of 5 mm as working electrode, a platinum wire electrode as auxiliary electrode, and a saturated calomel electrode (SCE) as reference electrode. All of the electrochemical experiments were implemented on CHI 660 electrochemical workstation (Shanghai Chenhua Instruments, Shanghai, China).

Optical microscope graphs were performed on Leika optical microscope equipped with DMI 4000 B/DFC 480 camera attached with Leika IM 50 software. Transmission electron micrograph (TEM) was obtained by using JEM-3010 Electron

Microscope (JEOL, Japan) with Digitalgraph software at an accelerating voltage of 300 kV.

2.3. Procedure

2.3.1. Preparation of carbon paste electrode (CPE)

Carbon paste was prepared by thoroughly mixing 2 g of melted paraffin with 2 g of spectrally pure graphite powder, and then it was filled into a Teflon tube (5 mm inner diameter) to form the CPE with the surface polished on an ultrafine emery paper. For repeated use, the surface was renewed by turning the tube nut to extrude a 1 mm thick outer paste layer with subsequent polishing.

2.3.2. Preparation of the agarose bead-Ab conjugates and the magnetic bead-Ab conjugates

The avidin-agarose beads (1.5 mg avidin/ml, 100 μl) were first washed with PBS solution to remove the antifreeze of glycerol, and then the biotinylated goat anti-human IgG antibody (1 mg biotin/ml, 100 μl) was added to incubate at room temperature with ceaseless gentle stirring for 1 h, thus the agarose bead-Ab conjugates were formed. After gravity settling, the supernatant liquor was discarded and the precipitate was washed thoroughly with PBS solution. Next, 900 μl of 1% BSA and 100 μl of 1.25% biotin were injected followed by incubation at room temperature with stirring for 1.5 h to block active sites of the agarose beads. After washed with PBS solution, the agarose bead-Ab conjugates were dispersed in 500 μl PBS as stocking solution to be stored at 4 °C.

An aliquot of 30 μl of carboxy-terminated magnetic nanoparticles (20 mg/ml) was added to mixed solution containing 400 μl of EDC (0.2 M), 200 μl of NHS (0.1 M) and 500 μl of avidin (1.5 mg/ml) drop by drop at room temperature under stirring for 4 h. After magnetic separation and washing with PBS solution for several times, the avidin-modified magnetic nanoparticles were dispersed in 500 μl PBS solution. Next, 100 μl of primary avidin-modified magnetic nanoparticles and 100 μl of biotinylated goat anti-human IgG antibody (1 mg biotin/ml) were mixed followed by incubation with unceasing stirring for 1 h at room temperature. The resulting particles were isolated under external magnetic field, washed with PBS solution and separated by a permanent magnet. Following this step, 900 μl of 1% BSA and 100 μl of 1.25% biotin were injected followed by incubation at room temperature with stirring for 1.5 h to block active sites of the magnetic beads. After magnetic separation and washing with PBS solution, the magnetic bead-Ab conjugates were dispersed in 500 μl of 0.15 M NaCl PBS buffer solution containing 0.05% Triton X-100 and were stored at 4 °C for latter usage in parallel with agarose bead assays.

2.3.3. Immunoassay procedure

All of the experiments were performed at room temperature. In a small glass vessel, 30 μl of primary agarose bead-Ab or magnetic bead-Ab, 300 μl of PBS, 100 μl of diluted ALP-Ab (1:100) in PBS buffer, 50 μl of 10% BSA and 100 μl of the human IgG antigen analyte were mixed followed by incubation with unceasing stirring for 1.5 h. After gravity settling or magnetic separation, the supernatant liquor was discarded and the sediment was rinsed with ultra pure water five times followed by the addition of 100 μl of the enzymatic silver deposition solution to incubate for 30 min in the dark. The glass vessel was then washed with ultra pure water eight times. Finally, 100 μl of 5 M HNO_3 solution was injected to dissolve the deposited silver and then quantified by ASV as described in the following section.

2.3.4. Electrochemical measurement

After the silver nanoparticles deposited on the surface of proteins and agarose beads or magnetic beads were completely dissolved, the solution was transferred from the glass vessel into an electrolytic cell followed by the addition of appropriate amount of 0.1 M KNO_3 solution into the cell to arrive at a final volume of 5 ml. The aforementioned three-electrode system was used in the ASV. In contrast to the conventional three-electrode system, the reference electrode was separated from the electrolyte solution containing Ag(I) ions by a glass salt bridge of saturated KNO_3 solution in order to avoid determination interference caused by the continuous leaching of chloride anion that lead to AgCl precipitation. The released Ag(I) ions were then quantified by ASV under the following instrumental conditions: 5 min deposition at −0.5 V versus SCE reference and the potential scan from 0.1 to 0.7 V at a rate of 100 mV/s.

3. Results and discussion

The principle of the non-competitive electrochemical immunoassay based on the unique features of agarose beads and the special amplified properties of biometallization in a homogeneously dispersed medium is depicted in Fig. 1. First, avidin-agarose beads react with the biotinylated goat anti-human IgG antibody to form agarose bead-Ab conjugates owing to the special interaction of avidin and biotin. This type of interaction (association constant $K_a = 10^{15}\ M^{-1}$) belongs to the strongest known non-covalent, biological interaction between the protein and a ligand so that the reaction is rapid and unaffected by other denaturing agents [17]. After agarose bead-Ab conjugates are formed followed by stillness for a few minutes, the conjugates are facilely separated from the mixture due to the separation of agarose micro-spheres. Since the agarose beads are adopted as substrate for immobilization of probe molecules, the human IgG analyte and ALP-Ab could be added together in order to simplify the electrochemical immunoassay. The sandwich antigen–antibody assembles are separated and washed after the analyte antigen reacted with agarose bead-Ab and ALP-Ab in a homogeneously dispersed medium for several hours. The enzymatic silver deposition solution is then injected and incubated in the dark. AA-p is hydrolyzed into ascorbic acid under the enzymatic reaction of ALP. Silver nanoparticles are then deposited on the surface of proteins and agarose beads due to the reduction reaction between ascorbic acid with silver ions. The silver nanoparticles deposited are then completely dissolved in an acidic solution and the Ag(I) ions released in solution are quantitatively determined at CPE by ASV.

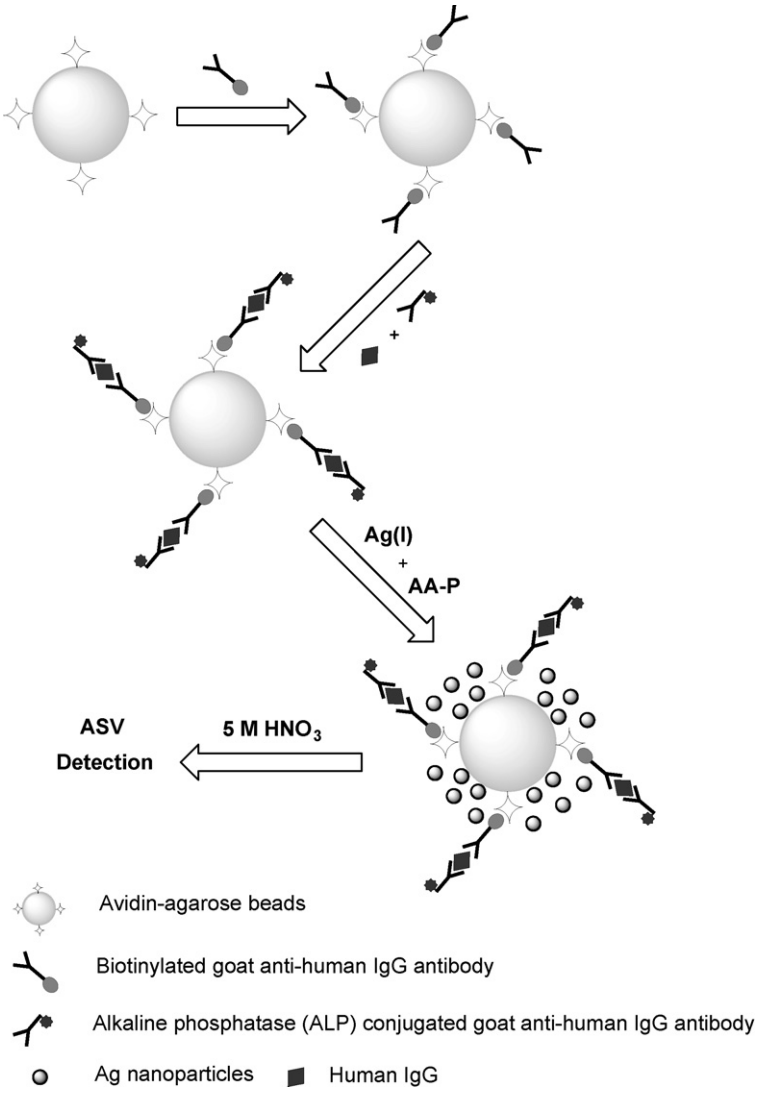

Fig. 1. The immunoassay protocol.

3.1. Optical microscope and TEM characterization

In this work, optical microscope and TEM graphs were applied to characterize the agarose micro-spheres before and after silver metal deposition. The optical microscope graphs of the agarose beads before and after silver metal deposition are shown in Fig. 2. One can see that the avidin-agarose beads used in this study are approximately 90–160 μm in diameter. Before silver metal deposition, the agarose beads are transparent (Fig. 2a). However, after silver metal deposition, the agarose beads are not evidently different from that of Fig. 2a except for the greyness (Fig. 2b). It can be assumed that a large amount of

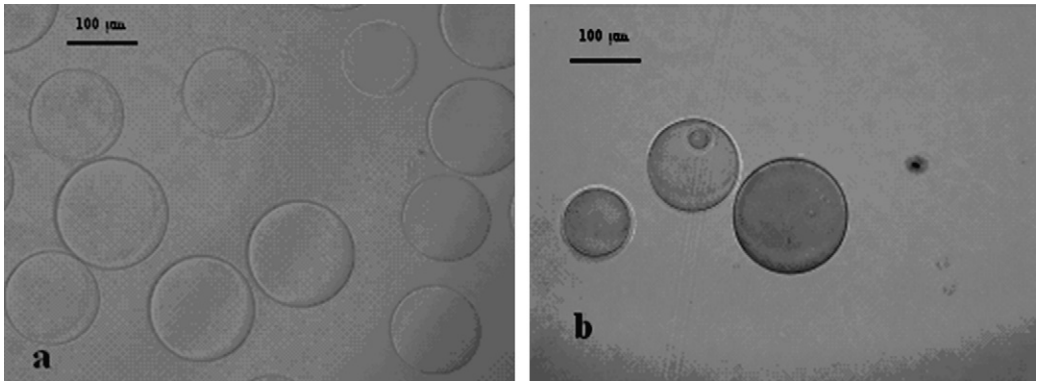

Fig. 2. Optical microscope graphs of the agarose beads, before (a) and after (b) enzymatic silver deposition (200×).

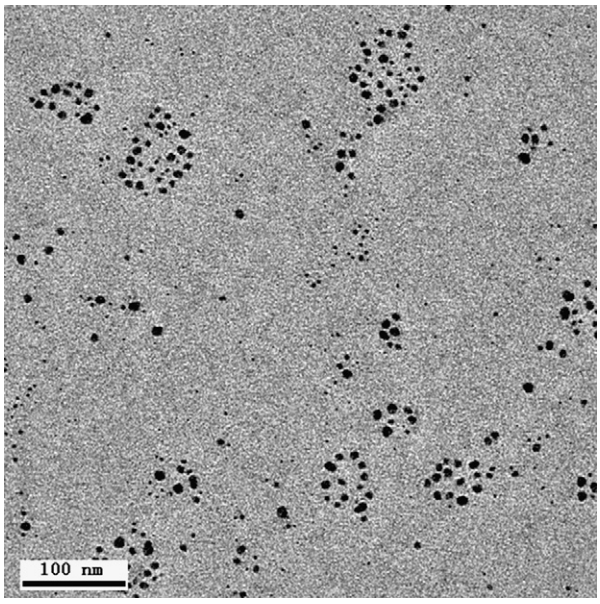

Fig. 3. Transmission electron micrograph of silver nanoparticles precipitated by enzymatic silver deposition.

silver nanoparticles would be precipitated to form a very thin metallic silver layer on the surface of the functionalized agarose beads in the process of enzymatic silver deposition that lead to the change of greyness of the agarose beads. This assumption was subsequently confirmed by the TEM characterization.

TEM was used for characterizing the silver particles deposited on the surface of agarose beads in that the silver particles are so small that cannot be observed through the optical microscope graphs. Fig. 3 is TEM micrograph of the silver nanoparticles deposited. A lot of small particles could be observed. It is obvious that the greyness of agarose beads seen from Fig. 2b were caused by the silver nanoparticles precipitated on the surface of the beads after the process of enzymatic silver deposition. The size of silver nanoparticles is approximately 10 ± 3 nm, some bigger particles on the micrograph are possibly caused by the aggregation of silver nanoparticles. The silver deposited is further confirmed by the electrochemical experiments in the following section.

3.2. Determination of Ag(I) ions at carbon paste electrode

During the step of enzymatic silver deposition, while the enzymatic silver deposition solution was added, the AA-P in this solution was converted to ascorbic acid hydrolyzed by the ALP enzyme immobilized on the surface of the agarose beads or magnetic beads; ascorbic acid is a reducing agent that reduces the silver ions in the enzymatic silver deposition solution, forming a metallic silver layer on the surface of agarose beads or magnetic beads. This process leads to a great enhancement in signal owing to the accumulation of metallic silver by a catalytically generated enzyme product as well as the high ratio of surface area to volume of the agarose beads or magnetic beads.

In order to quantify the silver nanoparticles deposited by ASV, the silver ions are released by adding concentrated HNO_3 solution. ASV is a very sensitive method for trace determination of metal ions. In this analytical technique, Ag(I) ions released are cathodically electrodeposited onto the surface of the carbon paste electrode during a preconcentration period. The electrodeposited silver are then stripped from the electrode by anodic oxidation. The electrochemical signal is directly proportional to the amount of human IgG analyte in the standard solution.

Several experimental parameters were investigated in order to obtain optimal conditions for quantification of Ag(I). A deposition potential of −0.5 V versus SCE and electrodeposition time of 300 s were selected for further studies. Fig. 4A shows the anodic stripping voltammograms of silver deposited on the surface of agarose beads in the presence and absence of 100 ng/ml human IgG when the immunoreaction time was 1.5 h, the incubation time of enzymatic silver deposition was 30 min. When carrying out an anodic scan from 0.1 to 0.7 V at 100 mV/s, an anodic peak at about 30 mV would be observed in the presence of certain quantity of human IgG. One notices that there is an evident anodic peak appeared in the presence of human IgG analyte,

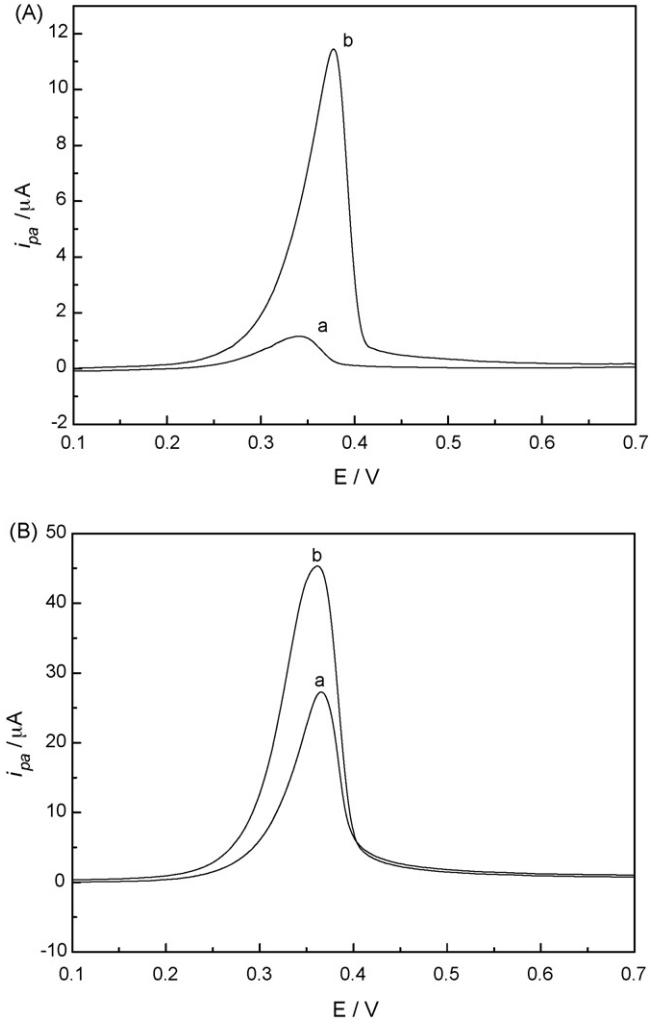

Fig. 4. Anodic stripping voltammograms of silver deposited on the surface of agarose beads (A) and magnetic beads (B). In the absence (a) and presence (b) of 100 ng/ml human IgG. The immunoreaction time was 1.5 h; the time of enzymatic silver deposition was 30 min.

and a relatively small anodic peak observed in the absence of human IgG analyte, thus it can be seen that the approach using agarose beads possesses relatively high signal-to-noise ratio by comparison of their anodic peak currents (i_{pa}). In contrast, the anodic stripping voltammograms of silver precipitated on the surface of magnetic beads under the same reaction conditions with Fig. 4A is displayed in Fig. 4B. It is demonstrated that the signal-to-noise ratio of immunosensor using avidin-modified magnetic beads is lower than that of using avidin-agarose beads. The larger background of the method using avidin-modified magnetic beads might attribute to the non-specific adsorption of proteins and the catalytic effect of magnetic nanoparticles as crystal nucleus on the deposition of metal silver. Though the non-specific adsorption of proteins or other biomolecules might be decreased due to the modification of the magnetic beads, the catalytic effect of magnetic nanoparticles as crystal nucleus on the deposition of metal silver could not be avoided because it would be rather difficult to make the modification layer of the magnetic nanoparticles completely compact and the surfaces of the pure magnetic nanoparticles would be partially exposed to solution phase. It is obvious that the analytical performances of immunosensors using avidin-agarose beads instead of avidin-modified magnetic nanoparticles are further improved.

3.3. Optimization of immunoassay conditions

The electrochemical immunoassay of human IgG was performed as demonstrated in Fig. 1 using the agarose beads-Ab conjugates in connection with the enzymatic silver deposition, and the detailed optimization of some steps was described below in detail.

Fig. 5 shows the effect of the immunoreaction time upon i_{pa}. The current i_{pa} increased with the immunoreaction time between 0 and 1.5 h and then leveled off above 1.5 h. This indicates that the interaction of antigen with antibody in a homogeneously dispersed medium has reached equilibrium after 1.5 h. Therefore, an immunoreaction time of 1.5 h was selected throughout the experiments.

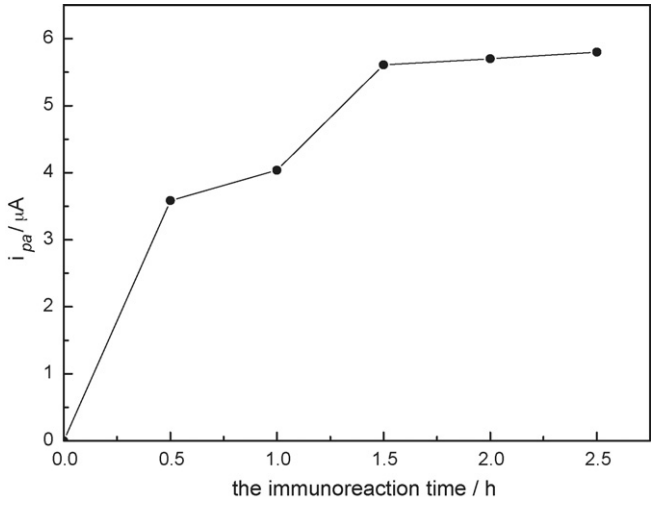

Fig. 5. Effect of the immunoreaction time. The time of enzymatic silver deposition was 30 min; 10 ng/ml human IgG was used.

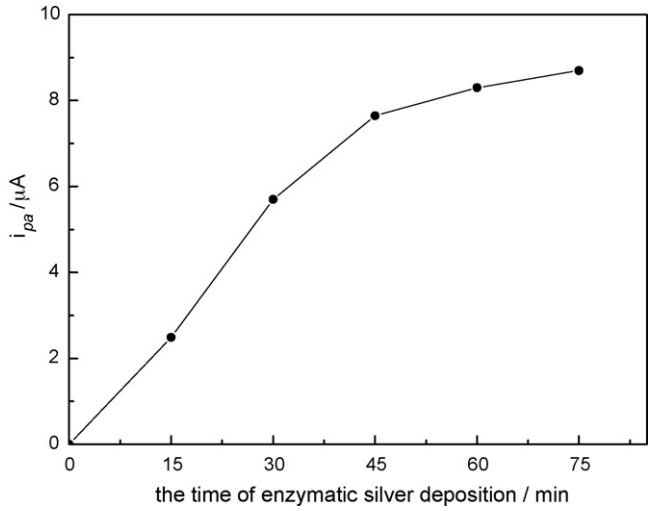

Fig. 6. Effect of the time of enzymatic silver deposition. The immunoreaction time was 1.5 h; 10 ng/ml human IgG was used.

Apparently, the amount of silver nanoparticles produced by enzymatic precipitation on the surface of proteins and agarose beads would be strongly affected by the time of enzymatic silver deposition as the concentration of silver ions in the enzymatic silver deposition solution is fixed. Indeed, it is clearly seen from Fig. 6 that the anodic peak current resulting from the oxidation of deposited silver sharply ascended with the increase of enzymatic silver deposition time before 45 min, and then inclined to be stable. It seems that the favorable electrochemical signal could be obtained through increasing the time of enzymatic silver deposition. However, the background response is also increased gradually. The relatively high stripping currents and low background currents are observed when the experiments were conducted with 30 min enzymatic silver deposition time. So, a time of enzymatic silver deposition of 30 min was accepted for further works.

3.4. Calibration curve for determination of human IgG

To our knowledge, ASV is a very sensitive method for detecting silver ions at CPE [18]. In our novel immunoassay protocol, ascorbic acid hydrolyzed by the relatively long time of enzymatic amplification reaction was utilized to realize deposition of silver nanoparticles. Thus relatively sensitive quantification of human IgG would be realized by ASV quantification of silver ions released. Fig. 7 displays the logarithm of the anodic peak current of silver are proportional to the logarithm of the concentration of human IgG in the range from 1 to 1000 ng/ml. The linear regression equation is $\lg i_{pa} = 0.2162 \lg C_{\text{Human IgG}} - 5.4626$, with a correlation coefficient of 0.9992. The detection limit as defined by 3σ-rule is 0.5 ng/ml. The R.S.D. of the approach is 9.65% for eight times determination of 10 ng/ml human IgG under the same conditions, reflecting that the method has a relatively good reproducibility.

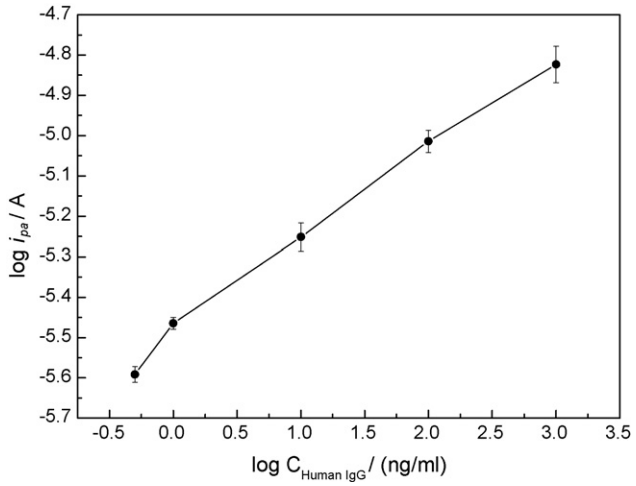

Fig. 7. Calibration curve for determination of human IgG. The immunoreaction time was 1.5 h; the time of enzymatic silver deposition was 30 min. Error bars represent S.D., $n = 4$.

4. Conclusion

We have developed a novel non-competitive electrochemical immunoassay protocol in a homogeneously dispersed medium, which coupled the unique features of agarose beads with the special amplified properties of biometallization for quantification of human IgG. Our assay in a homogeneously dispersed medium not only offers, in principle, faster target-binding kinetics than the planar substrate format owing to the homogeneous nature of the target-capture procedure but also cuts short some steps of biochemical assay in contrast to the heterogeneous immunoassays. So, compared to other heterogeneous electrochemical immunoassays [13,19,20], the new immunoassay possesses the attractive performance including speediness, simplicity, and relatively good sensitivity. Moreover, comparing the analytical performances of immunosensors using agarose beads and magnetic beads, we found that the signal-to-noise ratio of method using agarose beads (9.9) was approximately fivefold excess of that of using magnetic beads (1.7) under same reaction conditions. Advantages for agarose beads over magnetic beads as solid phases include that they would not interfere with the immunosensor and also could achieve better performances of the immunosensor in terms of sensitivity and specificity since they are nonmagnetic, excellently biocompatible and less non-specific protein binding. Furthermore, the combination of accumulation of metallic silver by a catalytically generated ALP product with anodic stripping voltammetry results in the relatively high sensitivity of this method without other process of silver enhancement. Accordingly, this strategy holds great promise for the extended application in a large variety of bioaffinity assays of analytes of pharmaceutical analysis, cellular studies, environmental monitoring and clinical diagnosis.

Acknowledgements

The work was financially supported by National Natural Science Foundation of China (grant nos. 20375012, 20435010, and 20205005) and Ministry of Education (NCET-04-0768).

References

[1] M. Lee, D.R. Walt, Anal. Biochem. 282 (2000) 142.
[2] S. Centi, et al., Talanta 73 (2007) 394.
[3] A. Dyal, K. Loos, M. Noto, S.W. Chang, C. Spagnoli, K.V.P.M. Shafi, A. Ulman, M. Cowman, R.A. Gross, J. Am. Chem. Soc. 125 (2003) 1684.
[4] C.M. Gooding, P.V. Choudary, J. Microbiol. Methods 34 (1998) 89.
[5] S. Punna, E. Kaltgrad, M.G. Finn, Bioconjugate Chem. 16 (2005) 1536.
[6] T. Tanaka, S. Tsukube, K. Izawa, M. Okochi, T.K. Lim, S. Watanabe, M. Harada, T. Matsunaga, Biosens. Bioelectron. 22 (2007) 2051.
[7] A. Goodey, J.J. Lavigne, S.M. Savoy, M.D. Rodriguez, T. Curey, A. Tsao, G. Simmons, J. Wright, S.J. Yoo, Y. Sohn, E.V. Anslyn, J.B. Shear, D.P. Neikirk, J.T. McDevitt, J. Am. Chem. Soc. 123 (2001) 2559.
[8] M.F. Ali, R. Kirby, A.P. Goodey, M.D. Rodriguez, A.D. Ellington, D.P. Neikirk, J.T. McDevitt, Anal. Chem. 75 (2003) 4732.
[9] R. Kirby, E.J. Cho, B. Gehrke, T. Bayer, Y.S. Park, D.P. Neikirk, J.T. McDevitt, A.D. Ellington, Anal. Chem. 76 (2004) 4066.
[10] D.J. Litman, T.M. Hanlon, E.F. Ullman, Anal. Biochem. 106 (1980) 223.
[11] K. Kim, M.Y. Han, D.Y. Yoon, B. Cho, M.J. Choi, I.S. Choe, T.W. Chung, Immunol. Lett. 31 (1992) 267.
[12] K.M. Gray, A.K. Bhunia, J. Microbiol. Methods 60 (2005) 259.
[13] X. Chu, X. Fu, K. Chen, G.L. Shen, R.Q. Yu, Biosens. Bioelectron. 20 (2005) 1805.
[14] Z.P. Li, C.H. Liu, Y.S. Fan, Y.C. Wang, X.R. Duan, Anal. Biochem. 359 (2006) 247.
[15] S. Hwang, E. Kim, J. Kwak, Anal. Chem. 77 (2005) 579.
[16] Z.P. Chen, J.H. Jiang, X.B. Zhang, G.L. Shen, R.Q. Yu, Talanta 71 (2007) 2029.
[17] S.J. Ding, B.W. Chang, C.C. Wu, M.F. Lai, H.C. Chang, Electrochim. Acta 50 (2005) 3660.
[18] E.S. Jacobs, Anal. Chem. 35 (1963) 2112.
[19] L. Alfonta, I. Willner, D.J. Throckmorton, A.K. Singh, Anal. Chem. 73 (2001) 5287.
[20] M. Dequaire, C. Degrand, B. Limoges, Anal. Chem. 72 (2000) 5521.

Available online at www.sciencedirect.com
ScienceDirect
Talanta 74 (2008) 1635–1641
Talanta
www.elsevier.com/locate/talanta

Diagnosis of copper ions in vascular tracts using a fluorine-doped carbon nanotube sensor

Suw Young Ly *

Biosensor Research Institute, Seoul National University of Technology, 172, Gongreung 2-dong Nowon-gu, Seoul 139-743, South Korea

Received 26 June 2007; received in revised form 9 October 2007; accepted 9 October 2007
Available online 16 October 2007

Abstract

The voltammetric assay of Cu(II) was investigated using a carbon nanotube electrode (CNE) and fluorine immobilized onto a carbon nanotube electrode (FCNE) in cyclic voltammetry (CV), square-wave (SW) stripping voltammetry, and chronoamperometry. Optimum SW conditions were attained at working ranges of 0.01–0.11 ng L^{-1} Cu(II) (11 points), and a relative standard deviation of 1.68% (RSD, $n = 15$) was observed at 10.0 μg L^{-1} Cu(II). Within a 200 s accumulation time, detection limit of 0.006 μg L^{-1} was attained. The life span of each electrode was more than 1 month. The sensor was applied to tap water, blood, and rat tail vascular (in vivo). It was found that the sensor could be used with an interface system in the assay of live cells and non-treated blood.
© 2007 Elsevier B.V. All rights reserved.

Keywords: Copper; Fluorine; Voltammetry; Vascular tract; Multi-walled carbon nanotubes (MWCNTs); Chemically modified electrodes (CMEs)

1. Introduction

Concentrated Cu(II) ions in human organs are associated with various diseases, such as Alzheimer's disease [1,2], prion disease [3], Wilson's disease [4], liver damage, and neuronal degeneration [5], ischemic heart disease [6], and amyotrophic lateral sclerosis (ALS) [7]. Trace Cu(II) ions and their complex assays are particularly important in vivo in live cells [8,9] and in blood [10]. Cu(II) ions are also present in drinking water [11] and in various food systems [12], but they are very rarely detected in human organs [13]. Therefore, disease assays require very low detection limits (DL), within nano-ranges. Various recent photometric analytical methods have been considered for this purpose, such as energy-dispersive X-ray fluorescence [14], laser ablation inductively coupled plasma mass spectrometry (LA-ICP-MS) (DL: 0.34 μg g^{-1}) [15], electrothermal vaporization inductively coupled plasma mass spectrometry (ETV-ICP-MS) (DL: 0.4 μg g^{-1}) [16], and ultrasonic nebulization and inductively coupled plasma optical-emission spectrometry (USN-ICP-OES) (23.0–28.0 μg L^{-1} working range) [17]. Some of these techniques attained low detection limits, but they are complicated and time-consuming, and they cannot be used in in vivo direct assay. Moreover, simple and sensitive voltammetric methods have already been developed, such as thiohydrazone-modified carbon paste electrode (DL: 0.5 g L^{-1}) [18], L-cysteine-modified gold electrode (DL: 5 μg L^{-1}) [19], tetraphenylporphyrin-coated glassy carbon electrode (DL: 12 μg L^{-1}) [20], selective PVC membrane electrodes (DL: 3.1×10^{-6} M) [21], *N*-phenylcinnamohydroxamic-acid-modified carbon paste electrode (5.00×1^{-10} M) [22], nontronite/cellulose-acetate-modified electrodes (DL: 1.73 μg L^{-1}) [23], and others [24–30]. Such methods, however, have high detection limits and cannot be used in in vivo assay. For this reason, to create a sufficiently sensitive implantable sensor of multi-walled carbon nanotubes (MWCNTs); and new type chemically modified electrodes (CMEs) of fluorine doped onto a carbon nanotube electrode was considered, as the properties of fluorinated –CF– include large electron capacities [31], hydrophilic or hydrophobic reaction [32], and strong charge depletion [33], which have been found useful in redox voltammetry. Moreover, the carbon nanotube structure is useful due to its bioelectronic [34], mechanical, electrocatalytic (its electrical conductivity is up to 1000 times greater than that of copper) [35], and electric capabilities [36]. Fluorination was combined with a carbon nanotube, which was made with the presence of HF solutions, using the covalent bond for $xC + (1/2)\ F_2 + yHF \rightarrow CxHF_2(HF)_{(y-1)} \rightarrow C_xF(HF)_y$ [37].

* Tel.: +82 2 970 6691; fax: +82 2 973 9149.
E-mail address: suwyoung@snut.ac.kr.

0039-9140/$ – see front matter © 2007 Elsevier B.V. All rights reserved.
doi:10.1016/j.talanta.2007.10.017

In this formula, the $–C_x–$ molecule was bonded with the hydrogen bonds [38] for $–C_x–(H—F)_n–$ so that it can react with the copper ions through the $–[C_x–(H—F)_n]^{n+}Cu^0 \leftrightarrow Cu^{2+}$ reaction [39]. The anodic voltammograms appeared to be very sensitive within the nano-level working ranges. There are techniques that can be attained to lower detection limit compared to that of the common analytical method [18–23]. The developed sensor was initially implanted into the vascular tracts and can be interfaced with an electrochemical workstation. The method was applied to blood vessel monitoring for in vivo diagnosis.

2. Experimental procedure

2.1. Systems, reagents, electrode preparation, and procedure

Measurement systems were performed using the CHI 660A electrochemical workstation from CH Instruments, Inc., Cordova. A Cu(II) standard solution (1000 mg L^{-1}) was obtained from Merck. The 1000 μg L^{-1} Cu(II) standard solution was prepared by diluting 0.1 mL of 1000 mg L^{-1} Cu(II) into 100 mL pure water. A 1000 ng L^{-1} standard solution was also prepared using the same method. All the chemicals that were used were of analytical-grade purity. Highly purified water was prepared through three-time distillation using 18 M Ω cm^{-1} of Milli-Q Ultra-Pure Water System (Millipore, Bedford, USA). The blood sample was obtained from the National Blood Research Center, TN. Multi-walled carbon nanotubes (by catalytic CVD; outside diameter: 15–40 nm; length: 30–50 nm; Nanotech Co., Ltd., Choongnam, South Korea, 330–816) were purified overnight prior to use, through magnetic stirring in a 2 M nitric-acid solution, then washed using triple-distilled pure water. The CNE sensor was prepared by mixing 80% carbon nanotube and 20% reagent-grade mineral oil (NJ, USA, 1-800-01, Acro) (8:2 weight ratio). FCNE was prepared by combining 40% carbon nanotube, 40% HF solution (standard), and 20% mineral oil (4:4:2 weight ratio). The mixed paste was inserted into a 2 mm-diameter × 50 mm-long capillary (inside paraffin coating) glass using a copper wire connected to the electric system. A 0.2 mm-diameter × 50 mm-long (63.05 mm^2) chloride-coated silver wire was used on the Ag/AgCl(s)/KCl(3 M) reference electrode, and a 0.2 mm-diameter × 50 mm-long (63.05 mm^2) platinum wire was used as the auxiliary electrode. The three-electrode system was immersed in a 10 mL 0.1 M $NH_4H_2PO_4$ solution. At this condition, HF immobilization was performed using a 10-cycle scan in a blank electrolyte solution, with a 1.0 V initial potential, a −1.0 V switching potential, and a 0.5 V s^{-1} scan rate, so that FCNE can be stabilized and then used in the optimization. All experiments were performed at room temperature, without removing oxygen.

Electrolyte solutions, composed of 0.1 M $NH_4H_2PO_4$ and with a pH of 3.06 FCNE and 7.35 CNE, was found to be the most suitable electrolyte solution. FCNE and CNE were compared for peak potential and cyclic voltammetric sensitivity. Composition phase was compared with field emission scanning electron microscope (FE-SEM), JSM-6700F JEOL LTD. Both pastes (0.5 g) were preheated at 750 °C for 12 h in anelectric furnace using 10 mL alumina crucible at closed condition. The phase structure was scanned using FE-SEM.

3. Results and discussion

3.1. FE-SEM, CV and chronoamperometric property

Fig. 1A, shows the FE-SEM scanning for FCNE and CNE, in the FCNE structure, $–C_x–(H—F)_n–$ phase is the height melting density and 750 °C preheated surface is a large pore. However CNE scan was observed for fiber type original phase. In this figure, FCNE and CNE were compared with CV effects using the 0.0–01.6 mg L^{-1} Cu(II) variation and 0.1 M $NH_4H_2PO_4$ electrolyte. The blank solution did not obtain any signal at both electrodes, the Cu(II) concentrations were further spiked within the range of 0.6–1.6, the FCNE currents rapidly increased from 6.63×10^{-8} to 32.91×10^{-8} A/mm^2, and the final peak appeared to be fivefold the CNE peak height. CNE peaks were obtained, however, only for 1.63×10^{-8} to 7.21×10^{-8} A/mm^2, in the 1.6 mg L^{-1} spike. The FCNE peak was much more sensitive than the CNE peak, in the CV condition, FCNE was set at 0.08 μg L^{-1} detection limit, 0 s accumulation time and 1.78% (RSD, $n = 5$), thus, the electrocatalytic reaction of $–[C_x–(H–F)_n]^{n+}Cu^0 \leftrightarrow Cu^{2+}$ was obtained [35,36]. The reverse scan shows that the sensor is very sensitive and can thus be used in in vivo analysis. Fig. 1B shows the results for the optimized chronoamperometry working range of 20–200 mg L^{-1} Cu(II): a sensitivity of $\Delta x/\Delta y = 1.4647$, a precision of $R^2 = 0.9924$, and a 6 mg L^{-1} detection limit, an environmentally useful high range for the Cu(II) assay. Lower working ranges were also examined, however, using stripping voltammetry.

3.2. SW Optimizations of FCNE and CNE

Variations of the SW amplitude were studied by maintaining the 3.0 mg L^{-1} Cu(II) spike, and the results that were obtained are shown in Fig. 2A. The FCNE peak current was shown to have increased very quickly and to have continued rising. The CNE peak, however, slowly increased from 0.05 to 0.03, then steadied. Subsequently, 0.4 V FCNE and 0.3 V CNE were chosen as the optimum SW amplitude. The FCNE peak high 2.187×10^{-5} A/mm^2 was four times that of the CNE 6.035×10^{-6} A/mm^2, at this condition. The SW accumulation potentials were examined, and the signal that was obtained is shown in Fig. 2B. An analysis of the influence of the varying pre-concentration potentials was carried out within the negative range of 0.0 to −1.4 V. The FCNE and CNE peak currents appeared to be very sharp, with a narrow half-width at 0.2 V. The FCNE current appeared to be linear at the potential range from 0.0 to −1.2 V, then decreased quickly, while the CNE peaks were at the maximum at −1.0 V, then decreased. Therefore, the optimum potential of −1.2 V FCNE 2.39×10^{-5} A/mm^2 and −1.0 V CNE 4.75×10^{-5} A/mm^2 was chosen for adsorptive stripping voltammetry. The SW accumulation times were examined at this condition. Fig. 2C shows the results of the tests

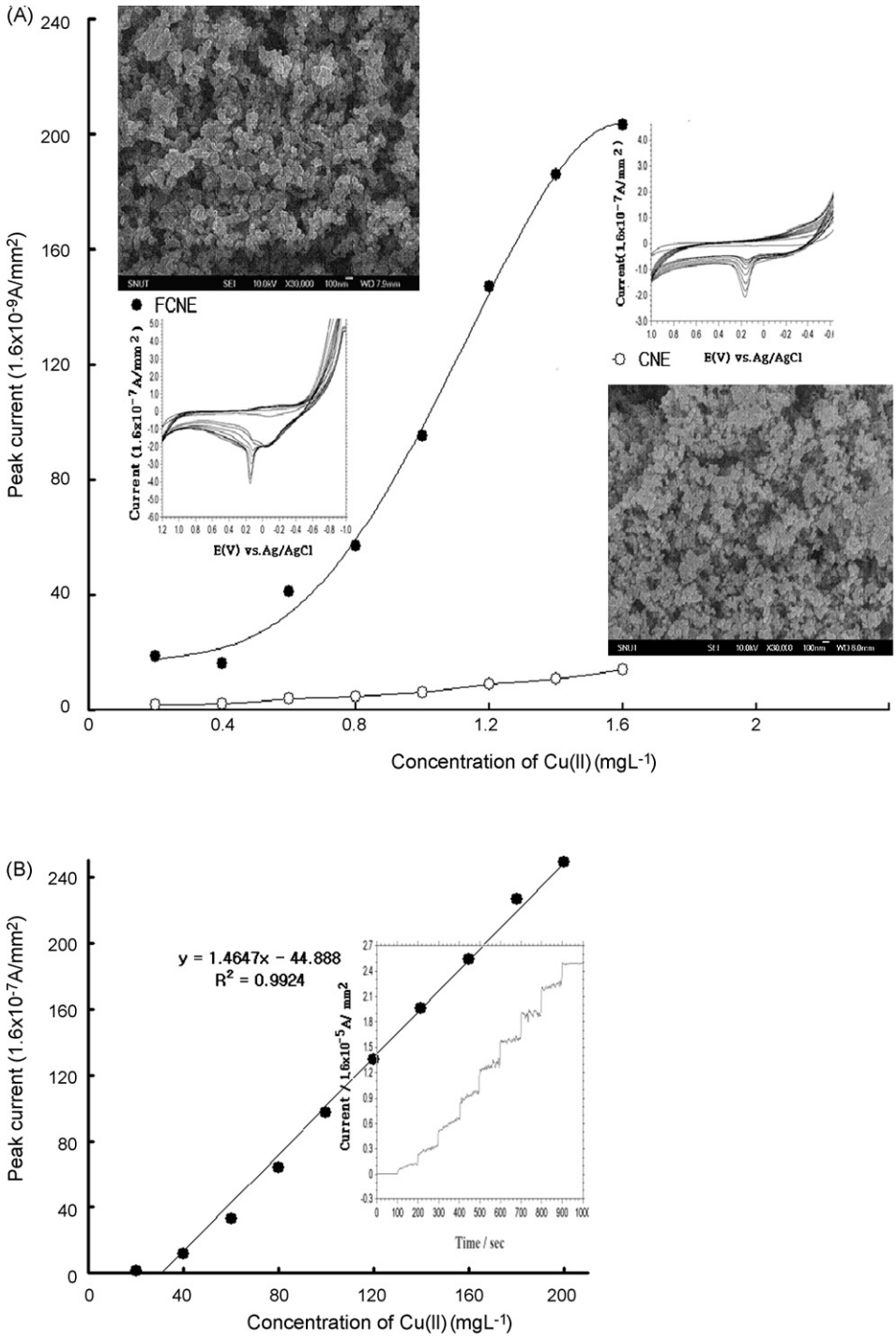

Fig. 1. (A) Insert FE-SEM micrograph is FCNE and CNE, 10.0 kV accelerating voltage, 300,000 magnification, secondary electron image and wide: 8.0 mm. And CV variations with blank, 0.2, 0.4, 0.6, 0.8, 1.0, 1.2, 1.4, and 1.6 mg L^{-1} Cu(II) spikes, in optimum conditions of −1.0 V initial potential, 1.2 V switching potential, and with a 0.5 V s^{-1} scan rate. (B) Chronoamperometric concentration effects of 20, 40, 60, 80, 100, 120, 140, 160, 180, and 200 mg L^{-1} Cu(II) spikes in the FCNE 0.1 M $NH_4H_2PO_4$ electrolyte solution.

that were conducted on various ranges, from 0 to 400 s, using nine points. The 200 s (FCNE) and 100 s (CNE) SW accumulation times showed good results 2.29×10^{-8} A/mm^2 for FCNE and 1.46×10^{-8} A/mm^2 for CNE. FCNE appeared to be more sensitive and responded quickly, and its peaks were sharp. At this condition, the other parameters of SW frequency and SW increment potentials were examined (data not shown), but they were determined to have had no influence. Finally, the optimum FCNE conditions were set at 0.4 V amplitude, 300 Hz frequency, 0.01 V increment potential, −1.2 V accumulation potential, 200 s accumulation time, and 3.06 pH, which appeared to be very sharp. Likewise, the optimum CNE conditions were obtained at 0.3 V amplitude, 200 Hz frequency, 0.01 V increment potential, −1.0 V accumulation potential, 100 s accumulation time, and

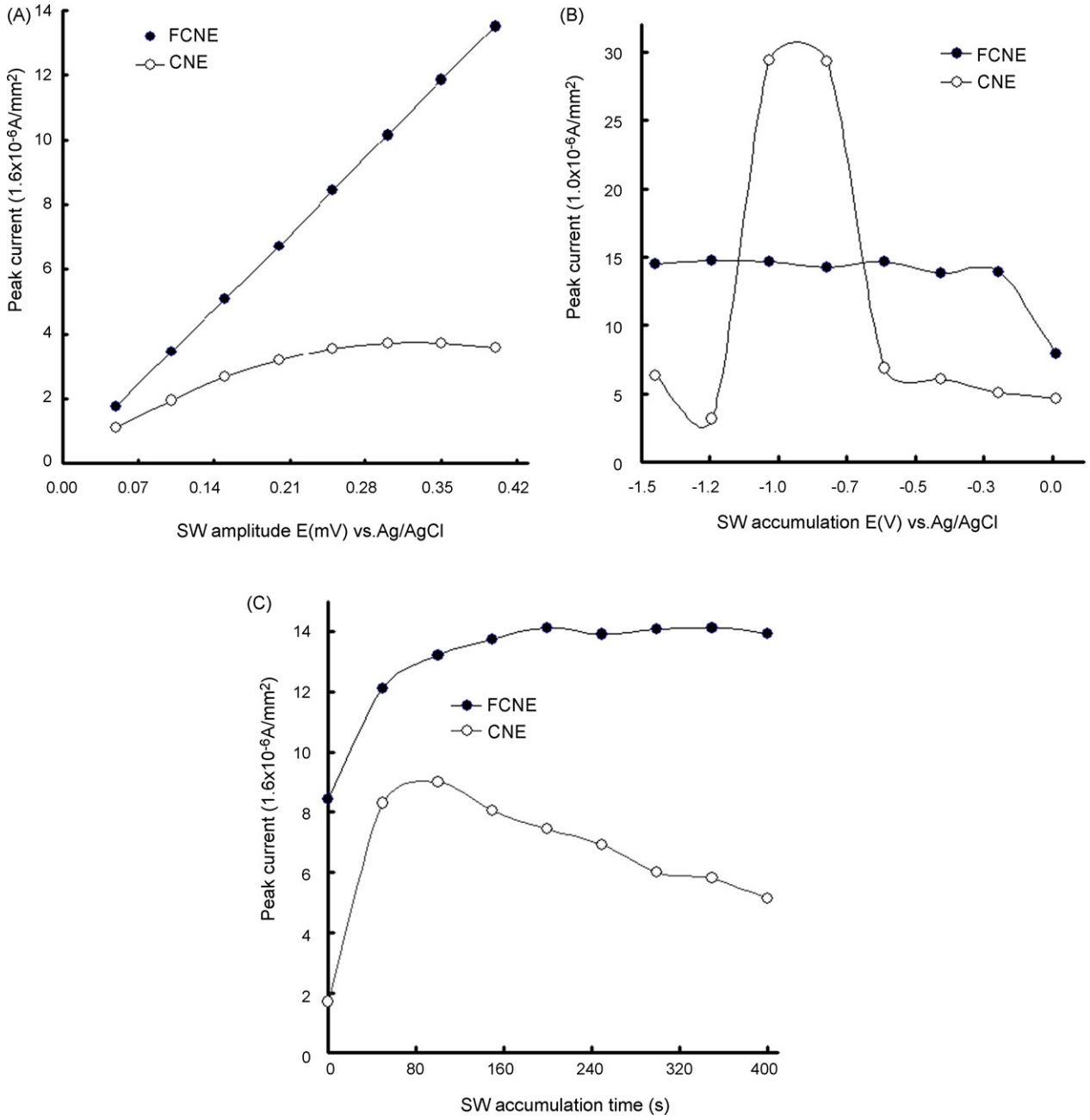

Fig. 2. (A) Variations of the SW amplitude range for 0.05, 0.1, 0.15, 0.2, 0.25, 0.3, 0.35, and 0.4 mV. (B) SW accumulation potential ranges of 0.0, −0.2, −0.4, −0.6, −0.8, −1.0, −1.2, and −1.4 V. (C) SW accumulation times of 0, 50, 100, 150, 200, 250, 300, 350, and 400 s. The 3.0 mg L^{-1} Cu(II) spike in the 0.1 M $NH_4H_2PO_4$ electrolyte solution. Other parameters were used for the following optimum conditions: pH 3.06, 0.4 V SW amplitude, 300 mV SW frequency, 0.01 V increment potential, −1.2 V accumulation potential, and 200 s accumulation time.

7.35 pH, which are broad. A wide peak width also appeared. Moreover, the analytical interference from metal and organic ions was examined using a 0.1 mg L^{-1} Cu(II) medium. Tenfold spiking was stripped for 1 mg L^{-1} cobalt, 1 mg L^{-1} barium(II), 1 mg L^{-1} bismuth, 1 mg L^{-1} germanium, 1 mg L^{-1} calcium(II), 1 mg L^{-1} iron, 1 mg L^{-1} chrome, 1 mg L^{-1} dopamine, 1 mg L^{-1} catechol, 1 mg L^{-1} epinephrine, and 1 mg L^{-1} glucose. The results showed changes of 32.4, 8.49, 8.11, −4.32, −7.47, 4.73, 7.71, 73.39, 133.01, −27.59, and 113.65%, respectively. The metal ions posed a weak interference, but glucose and catechol showed strong effects. Under these conditions, permselectivity of FCNE was examined using Cu(II) ion against organic interference ions. Table 1 shows the permeabibity of interferent ions, calculated using (i FCNE/i CNE × 100%) [41,42]. In organic interferent ions, glucose and dopamine ions strongly increased, while catechol and epinephrines exhibited only a slight increase. Thus, fluorine-doped FCNE is also desirable for in vivo live assay. Here, analytically usable working ranges and diagnostic application were examined using in vivo conditions.

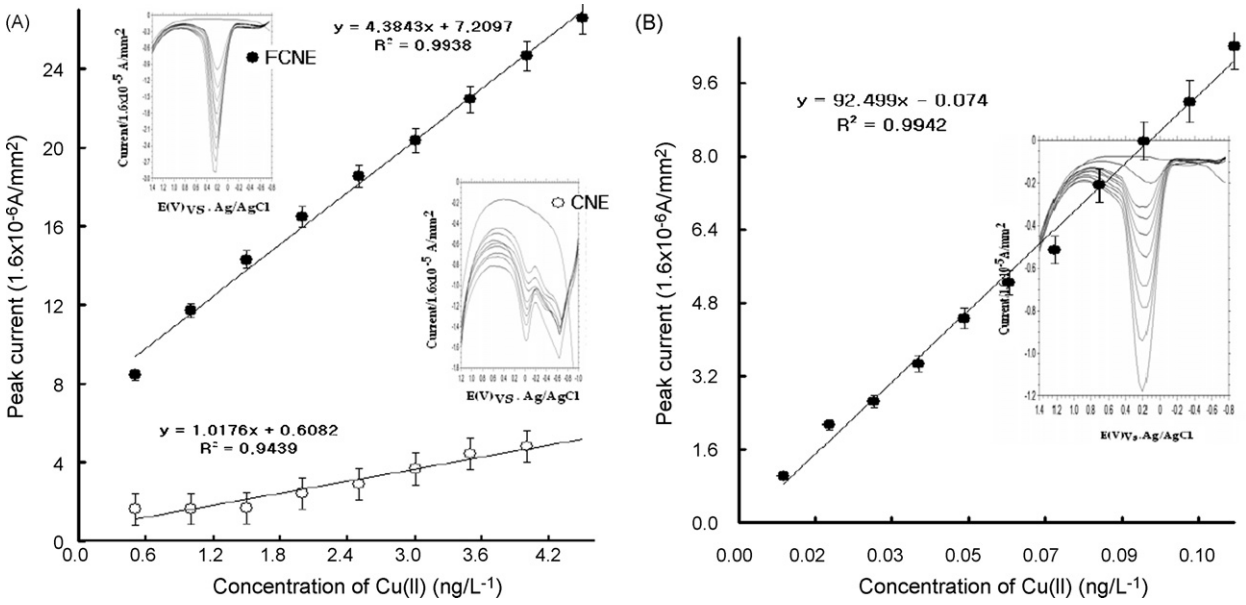

Fig. 3. (A) Analytical working ranges of 0.5, 1.0, 1.5, 2.0, 2.5, 3.0, 3.5, 4.0, and 4.5 ng L^{-1} Cu(II) spikes using FCNE and CNE. (B) FCNE working ranges of 0.01, 0.02, 0.03, 0.04, 0.05, 0.06, 0.07, 0.08, 0.09, 0.10, and 0.11 ng L^{-1} Cu(II) spikes in a 0.1 M $NH_4H_2PO_4$ electrolyte solution with a pH of 3.06, an SW amplitude of 0.4 V, an SW frequency of 300 mV, an increment potential of 0.01 V, an accumulation potential of −1.2 V, and an accumulation time of 200 s.

3.3. Working ranges and statistics

In optimized conditions, analytical working ranges were examined with two electrodes in the SW condition. Three usable ranges of FCNE were obtained (0.2–1.6 mg L^{-1}, 5–40 μg L^{-1}, and 10–80 ng L^{-1}), and two of CNE (5–40 μg L^{-1} and 10–140 ng L^{-1}) (data not shown). Fig. 3A shows the results for the varying concentration ranges of 0.5–4.0 ng L^{-1} Cu(II), both with a nine-point spike. The slope sensitivity was $\Delta x/\Delta y = 4.3843$ FCNE and $\Delta x/\Delta y = 1.0176$ CNE. FCNE appeared to be much more sensitive than CNE. In the 4.0 ng L^{-1} spike, a peak height of 3.99×10^{-5} A/mm^2 (FCNE) and 7.75×10^{-6} A/mm^2 (CNE) was obtained, and FCNE was shown to be five times more sensitive than CNE. Lower ranges were examined, however, using FCNE. Fig. 3B shows the results for the pico ranges: the peak width was very sensitive and sharp, and it was used for 200 s accumulation time. Since the sensitivity was $\Delta x/\Delta y = 92.499$ and the precision was $R^2 = 0.9942$ in the working condition, the methods were examined for their detection limits using kSb/m ($k = 3$, $n = 15$, $m = \Delta x/\Delta y$) and the detection limit of 0.006 μg L^{-1} (1.53×10^{-11} A/mm^2) (S/N = 3) SW was obtained, showing that they are much more sensitive than the other methods. Under such conditions, statistic precision was prepared with the replicated 15th determination of the 10.0 μg L^{-1} Cu(II) solution, from which 0.860% of RSD was obtained. These values are highly reproducible and sensitive, making them suitable for in vivo diagnosis. In blood and in vivo conditions, operational stability was examined using 2.0 μg L^{-1} Cu(II) standard injection, statistic peak currents were found for 5.06% RSD ($n = 5$), with the sensor used for 1 or 2 months.

3.4. In vivo and in vitro assay applications

The developed sensor was used to measure the Cu(II) content of tap water, human blood, and rat vascular tract. Spiked voltammograms for the standard and tap water are shown in Fig. 4A. In these curves, standard peaks closely appeared for the sample peak, yielding a defined copper current. The plot of peak height against copper was linear ($R^2 = 0.9991$, $n = 3$), and this water Cu(II) concentration was found to be 0.05 ± 0.004 μg L^{-1}. The values are lower than those indicated in other reports involving 0.6–2.55 μg L^{-1} [40]. For the in vivo assay, human blood was examined, and the results are shown in Fig. 4B (for the standard addition methods). The curve shows the blank electrolyte solution and the spiked human blood and standard addition. The sharp results of 0.13 ± 0.004 μg L^{-1} (RSD 4.05%) were obtained for raw blood, with a repeatability factor of five. The recovery values are shown in Table 2,

Table 1
Permselective of the FCNE to Cu(II) against organic ions

Interferent ion	Permselectivity
Dopamine	33
Catechol	18.28
Ephinephrine	16.57
Glucose	71.16

The data were obtained using permeability.

Table 2
Recovery value in real sample

	Tap water (μg L^{-1})	Human blood (μg L^{-1})	Electrolyte solution (μg L^{-1})
Initial value	0.05 ± 0.004	0.13 ± 0.004	0.2 ± 0.03
Standard addition	0.05	0.15	0.2
Recovery	0.108 ± 0.06	0.29 ± 0.07	0.41 ± 0.04
e (%)	7.4	3.4	2.4

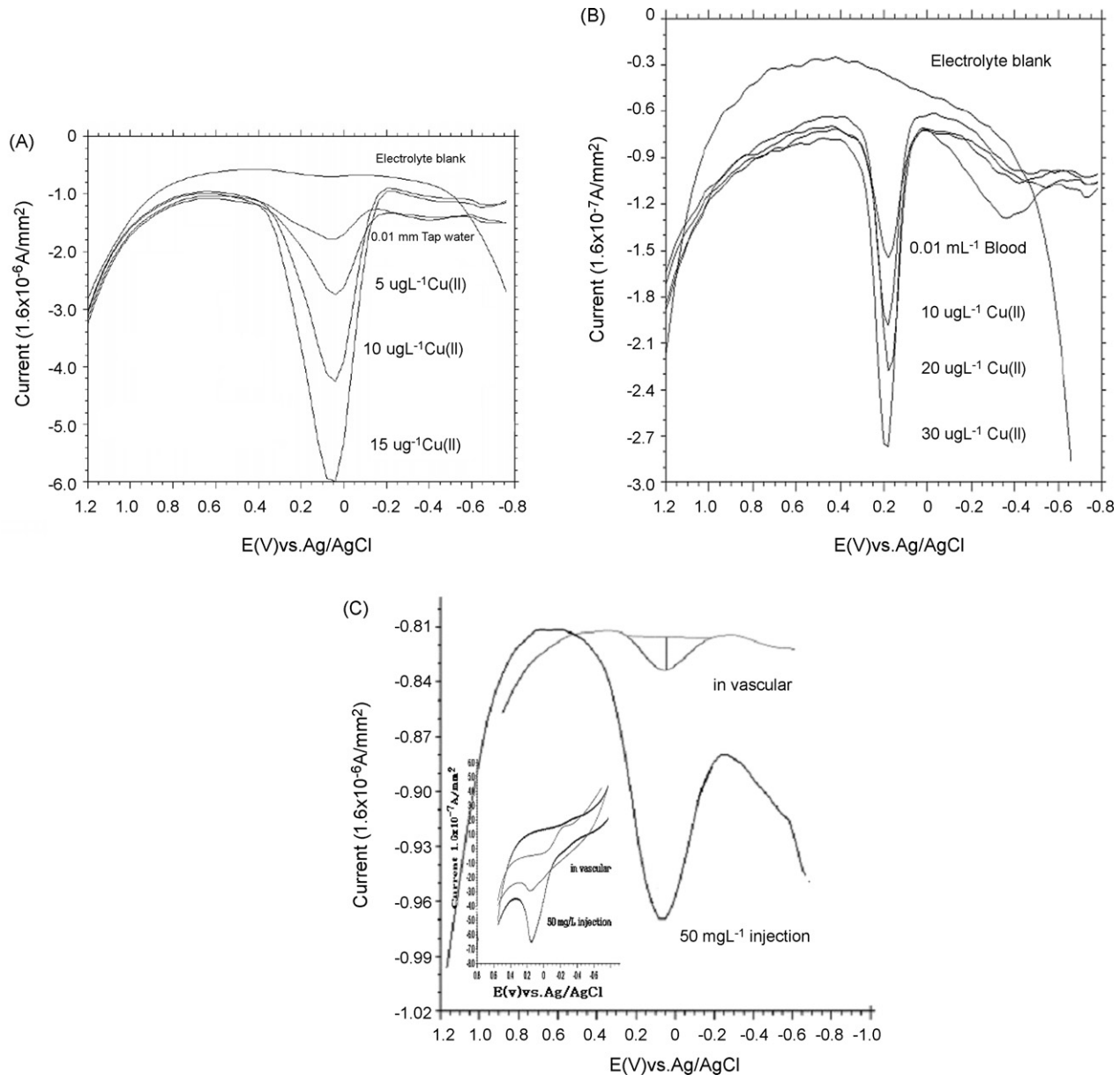

Fig. 4. Analytical applications: (A) the standard addition methods for the tap water, (B) human blood, and (C) inside the rat vascular tract by the implanted three-electrode cells. Other conditions are shown in Fig. 3.

indicating a level of precision that is useful in in vivo application.

A more advanced method can be used for the rat vascular tract. Under anesthetic conditions, the FCNE (0.5 mm in diameter, 5 mm in length, needle-type) was inserted deep (7 mm) into the rat tail vascular, then a 0.5 mm-diameter-wire-type platinum counter and Cl-coated 0.5 mm-diameter-silver-wire reference electrode were inserted into the tail muscle. The open tissue was closed using a dental adhesive binder. In the interfaced circuits, optimum SW voltammetry was performed. Fig. 4C shows the results of the vascular diagnosis, whose peak height was obtained for -2.88×10^{-8} A/mm^2, with a 0.1 V Cu(II) potential. A more accurate application was performed at this condition, with 50 mg L^{-1} standard copper injected into the vascular tract using a micro-syringe. The stripping current was then obtained for the -2.06×10^{-8} A/mm^2 peak height with the same potential. The inserted curves yielded the same results as the cyclic voltammetry in the vascular tract and the 50 mg L^{-1}-Cu(II)-injected conditions, and their peak potential also had the same results.

The methods developed herein can be applied to real-time assays in organs, and in the diagnosis of live subjects using an appropriate interface.

4. Conclusion

The novel FCNE sensor described herein is for the assay of trace Cu(II). The optimum conditions of pH 3.06, 0.4 V SW amplitude, 300 mV SW frequency, 0.01 V increment potential, −1.2 V accumulation potential, and 200 s accumu-

lation time were obtained at a lower DL of $0.006\,\mu g\,L^{-1}$ ($1.53 \times 10^{-8}\,A/mm^2$) (S/N = 3) SW, lower than that of the common voltammetric methods (DL: $1.73\,\mu g\,L^{-1}$ to $0.5\,g\,L^{-1}$ [18–23]). The implanted sensor was successfully applied to detect the amounts of trace copper in live vascular tracts and raw blood. It can also be applied in other fields requiring interfacial diagnosis in humans.

References

[1] H.H. Dieter, T.A. Bayer, G. Multhaup, Acta Hydrochim. Hydrobiol. 33 (2005) 72.
[2] J. Lu, Y.L. Zheng, D.M. Wu, D.X. Sun, Q. Shan, S.H. Fan, Letters 580 (2006) 6730.
[3] A. Becaria, D.K. Lahiri, S.C. Bondy, D. Chen, A. Hamadeh, H. Li, R. Taylor, A. Campbell, J Neuroimmunol. 176 (2006) 16.
[4] M. Senzolo, M. Loreno, S. Fagiuoli, G. Zanus, D. Canova, A. Masier, F.P. Russo, G.C. Sturniolo, P. Burra, Clin. Neurol. Neurosur. 109 (2007) 71.
[5] N. Fujiwara, H. Iso, N. Kitanaka, J. Kitanaka, H. Eguchi, T. Ookawara, K. Ozawa, S. Shimoda, D. Yoshihara, M. Takemura, K. Suzuki, Biochem. Biophys. Res. Commun. 349 (2006) 1079.
[6] F. Malek, E. Jiresova, A. Dohnalova, H. Koprivova, R. Spacek, Int. J. Cardiol. 113 (2006) e51.
[7] F. Haeffner, D.G. Smith, K.J. Barnham, A.I. Bush, J. Inorg. Biochem. 99 (2005) 2403.
[8] R.M. Tripathi, R. Raghunath, S. Mahapatra, S. Sadasivan, Sci. Total Environ. 277 (2001) 161.
[9] A. Safavi, N. Maleki, E. Shams, H.R. Shahbaazi, Electroanalysis 14 (2002) 929.
[10] D. Cruz, A. Cruz, M. Arteaga, L. Castillo, H. Tovalin, Contraception 72 (2005) 122.
[11] M. Etienne, J. Bessiere, A. Walcarius, Sens. Actuator B: Chem. B76 (2001) 531.
[12] J. Xu, L. Yang, Z. Wang, G. Dong, J. Huang, Y. Wang, Chemosphere 62 (2006) 602.
[13] M. Kuhbacher, G. Weseloh, A. Thomzig, H. Bertelsmann, G. Falkenberg, M. Radtke, H. Riesemeier, A. Kyriakopoulos, M. Beekes, D. Behne, X-ray Spectrom. 34 (2005) 112.
[14] L. Perring, D. Andrey, M.B. Dvorzak, D. Hammer, J. Food Compos. Anal. 18 (2005) 655.
[15] M.V. Zoriy, M. Dehnhardt, G. Reifenberger, K. Zilles, J.S. Becker, Int. J. Mass Spectrom. 257 (2006) 27.
[16] L.F. Diasa, G.R. Miranda, T.D. Saint'Pierre, S.M. Maia, V.L.A. Frescura, A.J. Curtius, Spectrochim. Acta B 60 (2005) 117.
[17] R. Lara, S. Cerutti, J.A. Salonia, R.A. Olsina, L.D. Martinez, Food Chem. Toxicol. 43 (2005) 293.
[18] J. Ruiperez, M.A. Mendiola, M.T. Sevilla, J.R. Procopio, L. Hernandez, Electroanalysis 14 (2002) 532.
[19] W. Yang, J.J. Gooding, D.B. Hibbert, J. Electroanal. Chem. 516 (2001) 10.
[20] H.H. Frey, C.J. McNeil, R.W. Keay, J.V. Bannister, Electroanalysis 10 (1998) 480.
[21] A.R. Fakhari, T.A. Raji, H. Naeimi, Sens. Actuator B: Chem. 104 (2005) 317.
[22] H. Alemu, B.S. Chandravanshi, Anal. Chim. Acta 368 (1998) 165.
[23] J.M. Zen, H.F. Wang, A.S. Kumar, H.H. Yang, V. Dharuman, Electroanalyis 14 (2002) 99.
[24] E. Canpolat, E. Sar, N.Y. Cos, K.H. Cankurtaran, Electroanalysis 19 (2007) 1109.
[25] C. Locatelli, J. Sci. Food Agric. 87 (2007) 305.
[26] A.S. Misiego, R.M.G.M. Carra, M.P.A. Carracedo, M.T.G. Sanchez-Simon, J. Agric. Food Chem. 52 (2004) 5316.
[27] M. Witt, S. Skrabal, R. Kieber, J. Willey, Atmos. Environ. 41 (2007) 3619.
[28] U. Celik, J. Oehlenschlager, Food Control 18 (2007) 258.
[29] A. Berduque, Y.H. Lanyon, V. Beni, G. Herzog, Y.E. Watson, K. Rodgers, F. Stam, J. Alderman, D.W.M. Arrigan, Talanta 71 (2007) 1022.
[30] R.M. Takeuchi, A.L. Santos, P.M. Padilha, N.R. Stradiotto, Talanta 71 (2007) 771.
[31] K. Matsumoto, J. Li, Y. Ohzawa, T. Nakajima, Z. Mazej, B. Zemva, J. Fluorine Chem. 127 (2006) 1383.
[32] S. Yonezawa, M. Yamasaki, M. Takashima, J. Fluorine Chem. 125 (2004) 1657.
[33] U.D. Weglikowska, V. Skakalova, J. Meyer, J. Cech, B.G. Mueller, S. Roth, Curr. Appl. Phys. 7 (2007) 42.
[34] J. Wang, M. Musameh, Anal. Chim. Acta 511 (2004) 33.
[35] E. Katz, I. Willner, Chem. Phys. Chem. 5 (2004) 1084.
[36] S.Y. Ly, Bioelectrochemistry 68 (2005) 232.
[37] T. Nakajima, V. Gupta, Y. Ohzawa, H. Groult, Z. Mazej, B. Žemva, J Power Sources 137 (2004) 80.
[38] O. Jeannin, M. Fourmigue, C. R. Chim. 9 (2006) 1287.
[39] Z. Mazej, P. Benkic, J. Fluorine Chem. 126 (2005) 803.
[40] O.A. Farghaly, Microchem. J. 75 (2003) 119.
[41] L.J. Murphy, Anal. Chem. 70 (1998) 2928.
[42] P. Sivaraman, J.G. Chavan, A.P. Thakur, V.R. Hande, A.B. Samui, Electrochim. Acta 52 (2007) 5046.

Available online at www.sciencedirect.com
ScienceDirect
Talanta 74 (2008) 1141–1147
Talanta
www.elsevier.com/locate/talanta

Development of formaldehyde sensing element using porous glass impregnated with β-diketone

Yasuko Yamada Maruo [a,*], Jiro Nakamura [a], Masahiro Uchiyama [b]

[a] NTT Energy & Environmental Labs, 3-1 Morinosato Wakamiya, Atsugi-shi, Kanagawa 243-0198, Japan
[b] National Institute of Environmental Studies, 16-2 Onogawa, Tsukuba-shi, Ibaraki 305-0053, Japan

Received 30 July 2007; accepted 17 August 2007
Available online 22 August 2007

Abstract

We have developed a sensor element for detecting formaldehyde. The sensor element is made of porous glass impregnated with both β-diketone and ammonium ions. We used three kinds of β-diketone; acetylacetone, 1-phenyl-1,3-butanedione, and 1,3-diphenyl-1,3-propanedione. The three kinds of sensor element, which are initially colorless, turn yellow after exposure to formaldehyde, and absorption with a peak wavelength of 407–424 nm appears. There is a linear relationship between the 407–424 nm absorbance of the sensor element after exposure to formaldehyde, and the formaldehyde concentration. The sensor element also works cumulatively, and the absorbance changes of the three kinds of sensor elements are acetylacetone > 1-phenyl-1,3-butanedione > 1,3-diphenyl-1,3-propanedione, when exposed to the same concentration of formaldehyde in the atmosphere. We also found that both the formation and decomposition reactions of lutidine derivative (yellow dye) occur on the acetylacetone element at 20 °C, and the kinetic constant of the former is 100,000 times larger than that of the latter. On the other hand, only the formation reaction occurs on the 1-phenyl-1,3-butanedione element at 20 °C. Therefore, the acetylacetone element would be suitable for short-term measurements and the 1-phenyl-1,3-butanedione would be suitable for long-term measurements.
© 2007 Elsevier B.V. All rights reserved.

Keywords: Formaldehyde; Acetylacetone; β-Diketone; Sensor; Porous glass

1. Introduction

Formaldehyde is an industrial chemical that is widely used to manufacture building materials and numerous household products, and a highly reactive compound released from several sources into the indoor environment [1–4]. Formaldehyde has a great impact on human health, because of its potentially carcinogenic and mutagenic properties and its ability to form intermediate and stable species of toxic and phytotoxic radicals [5–7]. The World Health Organization has set a standard for safe exposure of 0.08 ppm averaged over 30 min [8].

There are a large number of techniques for measuring gas-phase formaldehyde [9–14]. In this paper, we focus on sensors or samplers that are based on the solid state colorimetric method, because this method offers many advantages, for example portability, visualization, and ease of handling (does not include liquid). Nakano has reported a formaldehyde detection method called photoelectric spectrophotometry [15], which employs both hydroxylamine hydrochloride and methyl-yellow impregnated paper. Compton and Suzuki have reported a formaldehyde monitoring system [16,17] based on the colorimetric reagent, 4-amino-4-phenylbut-3-en-2-one. Also Kawamura has reported a formaldehyde-monitoring tablet based on the colorimetric reagent, 4-amino-3-hydrazino-5-mercapto-triazole [18]. Although formaldehyde can be detected using these three methods, the detection limit is slightly high at 50 ppb [15–18].

As regards the acetylacetone method, Nash reported that it could be used to analyze a formaldehyde solution [19]. With this method, a liquid state reaction and solution heating are needed. Compton and Suzuki reported a solid-state detection technique based on the acetylacetone method [16,17]. Although their approach does not use liquid, they have to use a special starting material, which is an intermediate product of the acetylacetone method, and a complex procedure is needed to

* Corresponding author. Fax: +81 462702320.
E-mail address: maruo@aecl.ntt.co.jp (Y.Y. Maruo).

0039-9140/$ – see front matter © 2007 Elsevier B.V. All rights reserved.
doi:10.1016/j.talanta.2007.08.017

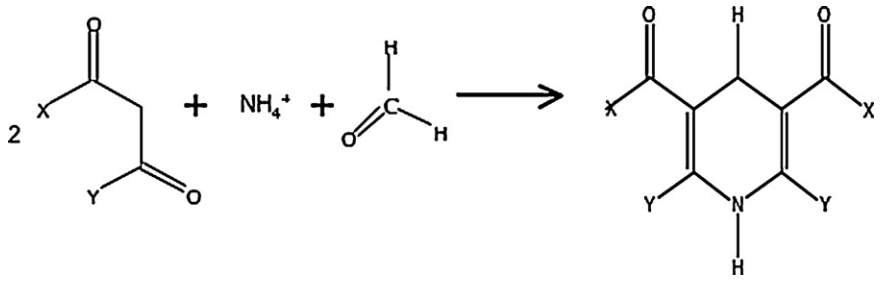

Fig. 1. Reaction formula between formaldehyde and diketone. Acetylacetone: X = CH_3, Y = CH_3; 1-phenyl-1,3-butanedione: X = C_6H_5, Y = CH_3; 1,3-diphenyl-1,3-propanedione: X = C_6H_5, Y = C_6H_5.

produce this material. Moreover, the detection limit is slightly high because they have to use a non-transparent substrate and the color change of the sensor element has to be measured by reflected absorption.

In our study, we developed a formaldehyde sensing element by incorporating both β-diketone and ammonium ions in a porous glass. We achieved a direct reaction between formaldehyde gas and β-diketone on the glass surface without the need to isolate an intermediate material, and realized a lower detection limit of 14 ppb for 24 h exposure.

2. Experiment

We used 1-mm thick Vycor 7930 glass sheets, with an average pore diameter of 4 nm, which we cut into 8 mm × 8 mm chips. Acetylacetone, 1-phenyl-1,3-butanedione, and 1,3-diphenyl-1,3-propanedione were obtained from the Kanto Chemical Co. Inc. (Japan). We prepared 50 ml of acetylacetone aqueous solution containing 0.1 ml of acetylacetone, 1 ml of acetic acid (Kanto Chemical Co. Inc. (Japan)), and 7.5 g of ammonium acetate (Kanto Chemical Co. Inc. (Japan)). The glass chips were immersed in a container filled with the solution containing the reagents for 2 h, and then dried in dry nitrogen gas for a further 24 h to remove the water.

A 60-ml mixture alcoholic (ethanol) solution containing 0.157 g of 1-phenyl-1,3-butanedione, 1 ml of acetic acid, 7.5 g of ammonium acetate, and 10 ml of water was also prepared for impregnation into the glass chips. The glass chips were immersed in a container filled with the solution containing the reagents for 2 h, and then dried in dry nitrogen gas for another 24 h to remove the water.

A 60-ml mixture alcoholic (ethanol) solution containing 0.253 g of 1,3-diphenyl-1,3-propanedione, 1 ml of acetic acid, 7.5 g of ammonium acetate, and 10 ml of water was also prepared for impregnation into the glass chips. The glass chips were immersed in a container filled with the solution containing the reagents for 2 h, and then dried in dry nitrogen gas for another 24 h to remove the water.

Fig. 1 shows the molecular formula of acetylacetone, 1-phenyl-1,3-butanedione, and 1,3-diphenyl-1,3-propanedione, and the reaction scheme for β-diketone and formaldehyde.

Fig. 2 shows the experimental setup we used to expose a chip to formaldehyde without a pump unit. We placed a formaldehyde transpiration source in a Tedlar bag (volume: 50 l) filled with ambient air. The formaldehyde transpiration source was

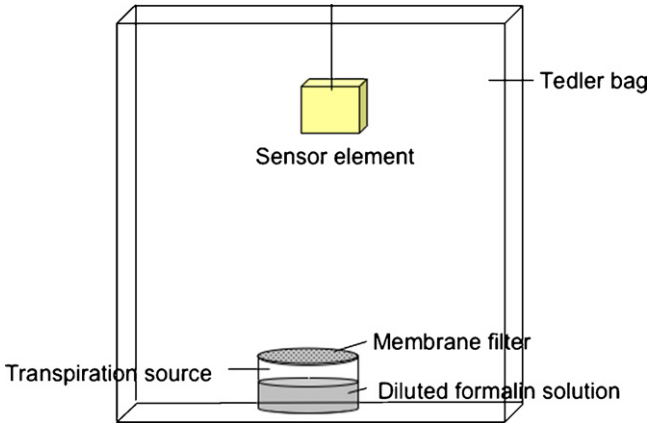

Fig. 2. Apparatus for formaldehyde exposure.

a bottle (volume: 100 ml) filled with diluted liquid formalin (Kanto Chemical Co. Inc. (Japan)), and its opening (diameter: 35 mm) was covered with an 80-μm thick Teflon membrane filter (Advantec Toyo (Japan): T020A) with a pore size of 0.2 μm. We made our formaldehyde transpiration source with reference to Yanagisawa's report [20], and we assumed that the transpiration rate would be close to the reported value (8.95 μg/(m^2 h)) [20].

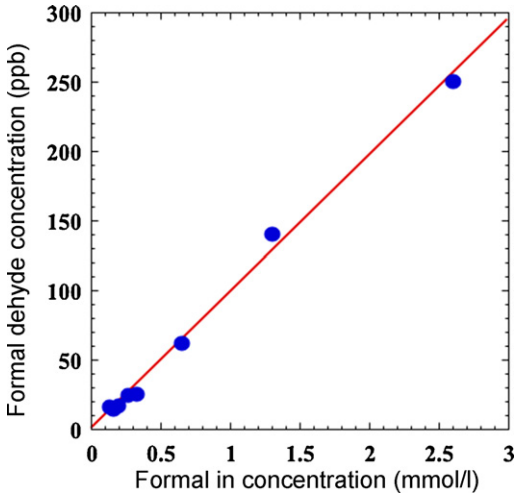

Fig. 3. Relationship between concentrations of formalin and equilibrated formaldehyde in air.

Fig. 3 shows the relationship between the diluted liquid formalin and equilibrium formaldehyde gas concentrations in the Tedlar bag after 24 h—still standing at 20 °C. The formaldehyde concentration was analyzed using the DNPH method [10]. Formaldehyde was collected as 2,4-dinitrophenylhydrazones, by drawing the air in the Tedlar bag at 1.0 l/min through Sep-Pak DNPH silica cartridges purchased from Waters (USA). The cartridges were extracted with 3 ml of HPLC grade acetonitrile, and the eluate was analyzed by HPLC. As shown in Fig. 3, we found that we could create a formaldehyde atmosphere with a concentration ranging from 14 to 250 ppb using the above method.

The impregnated chips were exposed to the gas by placing them in the Tedlar bag at 20 °C. The formaldehyde gas in the Tedlar bag would be balanced to formalin, which was in transpiration source, through the membrane filter, because it was 24 h after setting of transpiration source.

The transmission and absorption spectra of the samples were measured using a Hitachi U-3500 spectrometer.

The molecular structure of the chemicals and calculated UV–vis absorption spectra were obtained using the MOPAC program (Fujitsu-CaChe).

To investigate the stability and the reaction speed of the liquid, we prepared 50 ml of acetylacetone aqueous solution containing 0.1 ml of acetylacetone, 1 ml of acetic acid (Kanto Chemical Co. Inc. (Japan)), 7.5 g of ammonium acetate (Kanto Chemical Co. Inc. (Japan)), and 1 ml of 3.5×10^{-3}% formalin solution. We also prepared a 60-ml mixture alcoholic (ethanol) solution containing 0.172 g of 1-phenyl-1,3-butanedione, 1 ml of acetic acid, 7.5 g of ammonium acetate, 10 ml of water and 1 ml of 3.5×10^{-3}% formalin solution.

To investigate the stability and reaction speed of the glass element, we used a mini-pump unit with a pumping rate of 3 l/min.

3. Results and discussion

3.1. Reaction between formaldehyde and three kinds of β-diketone

We examined the color-changing reaction of formaldehyde gas and β-diketone coexisting with both acetic acid and ammonium ions in the pores of the glass by exposing the samples to several different concentrations of formaldehyde gas for 24 h at 20 °C. After exposure, the colorless sample became yellow. Fig. 4 shows the change in the absorbance spectra of the acetylacetone element. Before exposure, there is a specific absorption at wavelengths below 340 nm, which is the absorption of the conjugated electrons of acetylacetone.

After exposure, a specific absorption peak appeared at 407 nm and it was clear that the absorbance increased as the formaldehyde exposure concentration increased. This peak is clearly separated from the absorption peak of acetylacetone. The acetylacetone coexisting with both acetic acid and ammonium ions in the pores was stable and there was no peak at 407 nm after the sample had been placed in the Tedlar bag with a bottle filled with pure water as shown in Fig. 2. Then the appeared 407 nm

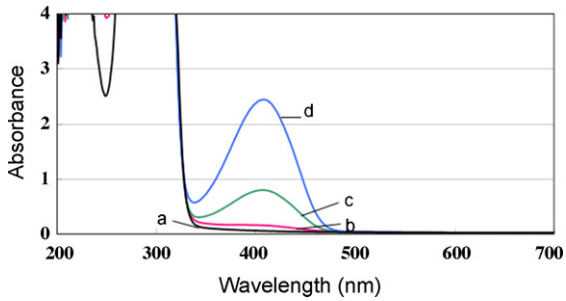

Fig. 4. Change in absorption spectra of acetylacetone impregnated sensor element by exposure to formaldehyde: (a) before exposure; (b) 14 ppb; (c) 90 ppb; (d) 250 ppb.

peak would be a product of reaction between acetylacetone and formaldehyde. It would be expected that if formaldehyde gas reacted directly with acetylacetone and ammonium ions in the glass pores then lutidine derivative, which has reported absorption at 400 nm in liquid [16], would be formed, and the glass would turn yellow. In other word, we realized direct reaction between acetylacetone and formaldehyde on the pore's surface without using intermediate product of the acetylacetone method. Also we could analyze 14 ppb of formaldehyde for 24 h exposure, without gas-adsorption acceleration method (ex. pump).

Fig. 5 shows the change in the absorbance spectra of the 1-phenyl-1,3-butanedione element. Before exposure, there is a specific absorption at wavelengths below 370 nm, which is the absorption of the conjugated electrons of 1-phenyl-1,3-butanedione.

After exposure, a specific absorption peak appeared at 414 nm and it was clear that the absorbance increased as the formaldehyde exposure concentration increased. The wavelength of this peak is separated from that of the absorption of 1-phenyl-1,3-butanedione. The 1-phenyl-1,3-butanedione coexisting with both acetic acid and ammonium ions in the pores was stable, and there was no peak at 414 nm after the sample had been placed in a Tedlar bag with a bottle filled with pure water as shown in Fig. 2. In the same of acetylacetone case, it would be expected that the formation of lutidine derivative (yellow dye). We realized direct reaction between 1-phenyl-1,3-butanedione and formaldehyde on the pore's surface without using inter-

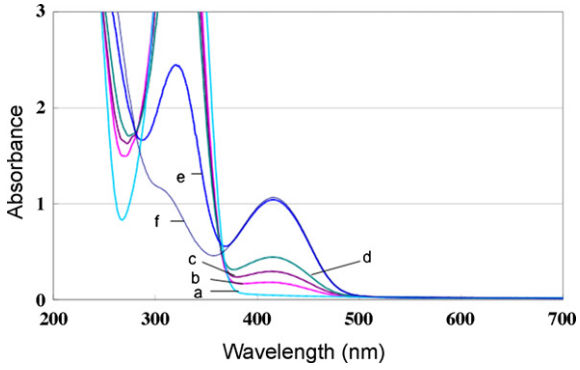

Fig. 5. Change in absorption spectra of 1-phenyl-1,3-butanedione impregnated sensor element by exposure to formaldehyde: (a) before exposure; (b) 14 ppb; (c) 24 ppb; (d) 62 ppb; (e) 110 ppb; (f) 250 ppb.

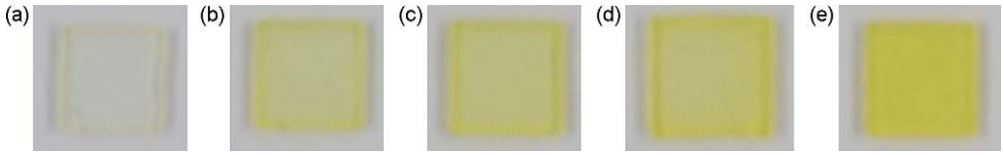

Fig. 6. Photographs of acetylacetone impregnated sensor element before and after exposure of formaldehyde: (a) before exposure; (b) 14 ppb; (c) 24 ppb; (d) 62 ppb; (e) 110 ppb. (For interpretation of the references to color in the text, the reader is referred to the web version of the article.)

mediate products of acetylacetone method. The wavelength of the peak is 7 nm longer than that of acetylacetone, because of the substituent effect of the one benzene ring that is included in 1-phenyl-1,3-butanedione. The absorption of the conjugated electrons of 1-phenyl-1,3-butanedione became small when the element was exposed to 140 ppb of formaldehyde for 24 h and the absorption disappeared when the element was exposed to 250 ppb of formaldehyde for 24 h. This indicates that there is no 1-phenyl-1,3-butanedione on the surface of the glass.

Fig. 6 shows the photographs of glasses before and after exposure to formaldehyde of 14, 24, 62, and 110 ppb, respectively. We can easily do visually checking down to 14 ppb because of clear color change.

Fig. 7 shows the change in the absorbance spectra of the 1,3-diphenyl-1,3-propanedione element at 20 °C. Before exposure, there is a specific absorption at wavelengths below 400 nm, which is the absorption of the conjugated electrons of 1,3-diphenyl-1,3-propanedione.

After exposure, a specific absorption peak appeared at 424 nm and it was clear that the absorbance increased as the formaldehyde exposure concentration increased. The wavelength of this peak is not separated from that of the absorption of 1,3-diphenyl-1,3-propanedione. The 1,3-diphenyl-1,3-propanedione coexisting with both acetic acid and ammonium ions in the pores was stable and there was no peak at 424 nm after the sample had been placed in a Tedlar bag with a bottle filled with pure water as shown in Fig. 2. In the same of acetylacetone case, it would be expected that the formation of lutidine derivative (yellow dye). We realized direct reaction between 1,3-biphenyl-1,3-propanedione and formaldehyde on the pore's surface. The wavelength of the peak is 17 nm longer than that of acetylacetone, because of the substituent effect of the two benzene rings including in 1,3-diphenyl-1,3-propanedione. The absorption of the conjugated electrons of 1,3-diphenyl-1,3-propanedione decreases slightly when the element is exposed to 140 ppb of formaldehyde for 24 h. This indicates that there is little 1,3-diphenyl-1,3-propanedione on the glass surface. A new absorption region from 340 to 400 nm appeared when the element was exposed to 250 ppb of formaldehyde for 24 h.

For three kinds of β-diketone, we realized direct reaction between β-diketone and formaldehyde on the glass pore's surface, especially the formation of the lutidine derivative (yellow dye) of 1,3-diphenyl-1,3-propanedione in liquids or on paper, have not reported anywhere yet. The formation of the lutidine derivative (yellow dye) of 1,3-diphenyl-1,3-propanedione succeeds only on the pore's surface. The mobility of molecules on the glass surface would be larger than that on the paper, because thin water layer exists on glass surface. The water layer was confirmed by the existence of absorption peaks at 1490 and 1900 nm, which were caused by water.

Adding that, the huge surface area and small diameter of pore would be an advantage factor for planer structure of lutidine derivative.

Fig. 8 shows the relationship between the formaldehyde exposure concentrations and absorbance change at 407, 414, and 424 nm for an exposure time of 24 h. The absorbance change increased with increasing formaldehyde concentration. A linear relationship was obtained between formaldehyde concentration and absorbance at 407 nm.

At 414 nm (1-phenyl-1,3-butanedione), we obtained a linear relationship up to a formaldehyde concentration of 140 ppb, and after that the absorbance was saturated. This is because, as indicated in Fig. 6, there is no 1-phenyl-1,3-butanedione on the glass surface. Therefore, we will be able to make a sensing element with a larger saturating concentration, if we can put more 1-phenyl-1,3-butanedione on the glass surface.

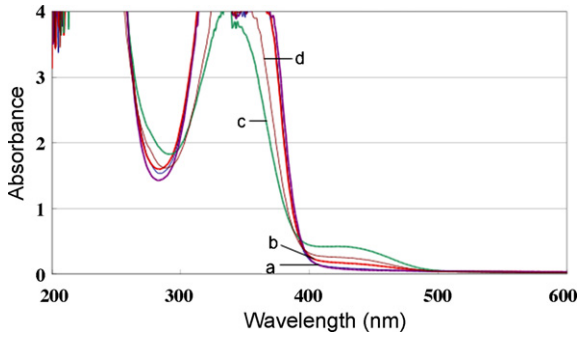

Fig. 7. Change in absorption spectra of 1,3-biphenyl-1,3-propanedione impregnated sensor element by exposure to formaldehyde: (a) before exposure; (b) 24 ppb; (c) 140 ppb; (d) 250 ppb.

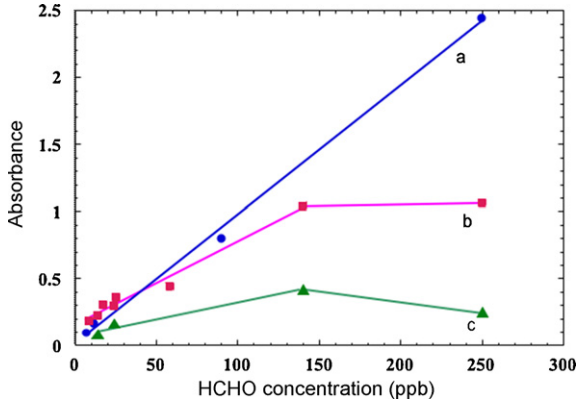

Fig. 8. Relationship between exposure concentration and peak absorbance of three sensors (exposure time = 24 h): (a) acetylacetone; (b) 1-phenyl-1,3-butanedione; (c) 1,3-biphenyl-1,3-propanedione.

At 424 nm (1,3-diphenyl-1,3-propanedione), a linear relationship was obtained up to a formaldehyde concentration of 140 ppb, and after that the absorbance decreased. As indicated in Fig. 7, there is a small amount of 1,3-diphenyl-1,3-propanedione on the glass surface after exposure to 140 ppb of formaldehyde, and if there were no 1,3-diphenyl-1,3-propanedione present during the 250 ppb exposure the absorbance would be saturated. However the experimental result showed a reduction in absorbance. Then we calculated the stabilized structure of 1,3-diphenyl-1,3-propanedione using the MOPA calculation program, and this indicated that the most stable 1,3-diphenyl-1,3-propanedione structure was not a plane and the calculated wavelength of the absorption peak of the most stable calculated structure was smaller than that of acetylacetone. When we exposed the sensing element to formaldehyde at 250 ppb, the absorption peak at 424 nm decreased and simultaneously absorption appeared from 340 to 400 nm (these wavelengths are smaller than the acetylacetone peak wavelength). We then assumed that the decrease in the absorption at 424 nm was caused by the structural change in the 1,3-diphenyl-1,3-propanedione; at first the 1,3-diphenyl-1,3-propanedione structure was quasi-planar and had an absorption wavelength longer than that of acetylacetone, later the structure changed from quasi-planar to a more stable one and had an absorption wavelength smaller than that of acetylacetone

3.2. Stability of liquid and elements and reaction speed of two kinds of β-diketone

First, we examined the stability and reaction speed of a liquid containing β-diketone, ammonium ions and formalin. We used acetylacetone or 1-phenyl-1,3-butanedione as β-diketone. Acetylacetone liquid changes from colorless to yellow, and absorption with a peak wavelength at 400 nm appears, and the color subsequently fades gradually. The color change of 1-phenyl-1,3-butanedione liquids are the same as that of acetylacetone liquid, except for the speed at which the color fades. Fig. 9 shows the change in absorbance at 410 nm for acetylacetone and at 414 nm for 1-phenyl-1,3-butanedione. The absorbance rapidly increases up to 24 h and then decreases. We assumed that lutidine derivative (yellow dye) compounds have a simple formation/decomposition reaction, as shown below:

$$2\beta\text{-diketone} + NH_4{}^+ + HCHO \xrightarrow{k_1} L \xrightarrow{k_2} D.C. \quad (1)$$

In Eq. (1), D.C. and L indicate the lutidine derivative (yellow dye) and the decomposition compound, respectively.

The concentration change of lutidine derivative (yellow dye) is described as follows:

$$\frac{d[\text{lutidine}]}{dt} = k_1[\beta\text{-diketone}]^2[NH_4{}^+][HCHO] - k_2[\text{lutidine}] \quad (2)$$

There are large amounts of β-diketone and ammonium ions in the liquid. The product of k_1, $[\beta\text{-diketone}]^2$ and $[NH_4{}^+]$ is constant, and we replace the product with k_1'. The change in formaldehyde is described as follows:

$$\frac{d[HCHO]}{dt} = -k_1'\,[HCHO] \quad (3)$$

Then [lutidine] is described as follows:

$$[\text{lutidine}] = \frac{k_1'}{k_2 - k_1'}[HCHO]_0(\exp(-k_1' \times t) - \exp(-k_2 \times t)) \quad (4)$$

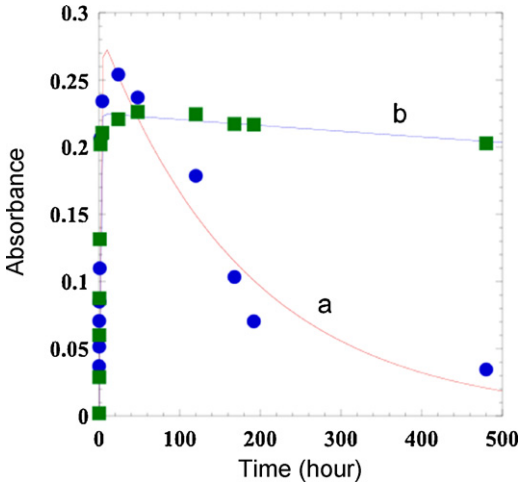

Fig. 9. Relationship between standing time and peak absorbance of β-diketone and formalin containing solution: (a) acetylacetone; (b) 1-phenyl-1,3-butanedione.

In Eq. (4), $[HCHO]_0$ indicates the initial molar concentration of formaldehyde.

We fitted the peaks of the absorbance change plots of the liquids to Eq. (4). The results are shown as solid lines in Fig. 9. The obtained values of k_1' and k_2 are 0.513 and 0.00571, respectively, for acetylacetone, and 0.957 and 0.000201, respectively, for 1-pheny-1,3-butanedione at 20 °C. The concentrations of the β-diketone and ammonium ions were 0.019 and 1.9 mol/l, respectively, and therefore their k_1 values are 748 and 1400, respectively.

In the next step, we examine the stability and reaction speed of sensor elements that contains β-diketone and ammonium ions and adsorbed formaldehyde gas. We use a pump unit to achieve the rapid adsorption of formaldehyde gas on the surface of pore. After the formaldehyde gas adsorption had finished, the glass was stored in a polyethylene bag and its spectrum measured at the intended intervals. With the acetylacetone element, the glass gradually became yellow and then colorless, on the other hand with the 1-phenyl-1,3-butanedione element, the color was stable and the absorbance was saturated.

Fig. 10 shows the change in absorbance of the acetylacetone element at 407 nm. The absorbance rapidly increased for 2 h and then decreased. We assumed a simple formation/decomposition reaction for the lutidine derivative (yellow dye) compounds as shown in Eq. (1). We fitted the peaks of the absorbance change plots of the acetylacetone element to Eq. (4). The results are shown as a solid line in Fig. 10. The obtained k_1' and k_2 values are 3.16 and 0.0200 at 20 °C, and these values are larger than

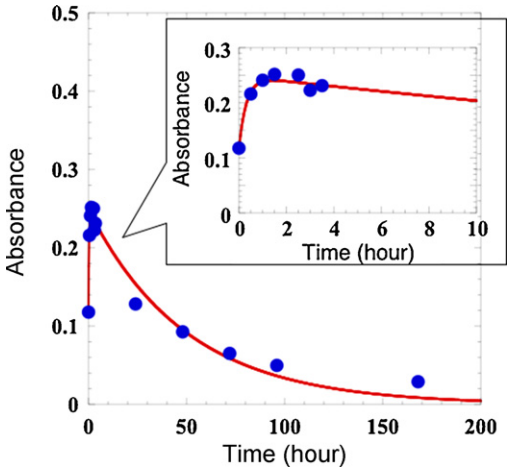

Fig. 10. Relationship between standing time and peak absorbance of acetylacetone impregnated sensor element after formaldehyde gas adsorption.

that for the liquid. The k_1' and k_2 values of porous glass are 6 and 3.5 times that of the liquid, respectively. The concentrations of the β-diketone and ammonium ions were 0.019 and 1.9 mol/l, respectively, and therefore k_1 was 4600.

Fig. 11 shows the change in absorbance at 414 nm for the 1-phenyl-1,3-butanedione element. The absorbance rapidly increased for 2 h and then saturated. We assumed a simple formation for the lutidine derivative (yellow dye) compounds as shown in Eq. (5):

$$2\beta\text{-diketone} + NH_4{}^+ + HCHO \xrightarrow{k_1} L \quad (5)$$

In Eq. (5), L indicates lutidine derivative (yellow dye).

The lutidine derivative concentration change is described as follows:

$$\frac{d[\text{lutidine}]}{dt} = k_1[\beta\text{-diketone}]^2[NH_4{}^+][HCHO] \quad (6)$$

There are large amounts of β-diketone and ammonium ions on the glass surface. The product of k_1, $[\beta\text{-diketone}]^2$ and $[NH_4{}^+]$ is constant, and we replace the product with k_1'. The change in the formaldehyde is described by Eq. (3).

Then [lutidine] is described as follows:

$$[\text{lutidine}] = [HCHO]_0(1 - \exp(-k_1' \times t)) \quad (7)$$

In Eq. (7), $[HCHO]_0$ indicates the initial molar concentration of formaldehyde.

We fitted the peaks of the absorbance change plots of the 1-phenyl-1,3-butanedione element to Eq. (7). The results are shown as a solid line in Fig. 11. We obtained a k_1' value of 1.01, and this value is almost the same as the liquid value. The concentrations of the β-diketone and ammonium ions were 0.019 and 1.9 mol/l, respectively, and therefore k_1 is 1470. The k_2 of porous glass is almost zero, and this is much smaller than the liquid value. This result indicates the good stability of the 1-phenyl-1,3-butanedione element.

Although the stability of the acetylacetone sensor element is not very good, its sensitivity is higher than that of the 1-phenyl-1,3-butanedione element, and the kinetic constant of the formation reaction is 100,000 times greater than that of the decomposition reaction. Therefore, we concluded that the acetylacetone sensor element is suitable for short-term measurements (e.g. less 8 h), and the 1-phenyl-1,3-butanedione sensor element is suitable for long-term measurements (e.g. more than 8 h).

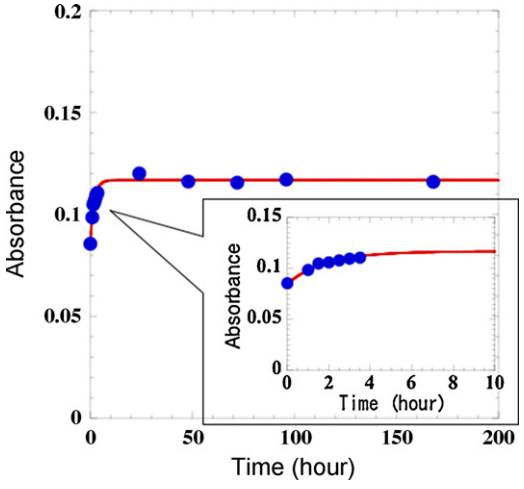

Fig. 11. Relationship between standing time and peak absorbance of 1-phenyl-1,3-butanedione impregnated sensor element after formaldehyde gas adsorption.

4. Conclusion

We developed a sensor element for formaldehyde. The sensor element was made of a porous glass that was impregnated with both β-diketone and acid and ammonium ions. We use three kinds of β-diketone; acetylacetone, 1-phenyl-1,3-butanedione, and 1,3-diphenyl-1,3-propanedione. The three kinds of sensor elements changed from colorless to yellow after exposure to formaldehyde, and absorption with a peak wavelength of 407–424 nm appeared. There was a linear relationship between the 407–424 nm absorbance of the sensor element after exposure to formaldehyde, and the exposed formaldehyde concentration. Also, the sensor element worked cumulatively, and the absorbance changes of the three kinds of sensor elements are acetylacetone > 1-phenyl-1,3-butanedione > 1,3-diphenyl-1,3-propanedione, when they were exposed to the same concentration of formaldehyde in the atmosphere. With the acetylacetone sensor element, we also found that both the formation and decomposition reactions occurred on the porous glass surfaces in the same way as in a liquid, and the reaction speed at 20 °C was higher than that of a liquid. On the other hand, with the 1-phenyl-1,3-butanedione-sensor element we also found that only the formation reaction is occurs on the porous glass surfaces. In addition, both the formation and decomposition reactions occur in a liquid, and the formation reaction speed at 20 °C is almost the same as that of the liquid. Although the stability of the acetylacetone sensor element is not very good, its sensitivity is higher than that of the 1-phenyl-1,3-butanedione element. Considering these results, we concluded that the acetylacetone sensor element is suitable for short-term measurements (e.g. less than 8 h), and the 1-phenyl-1,3-butanedione sensor ele-

ment is suitable for long-term measurements (e.g. more than 8 h).

References

[1] Formaldehyde, Chemical Week, June 12, 2002, pp. 32–33.
[2] S. Thorud, M. Gjolstad, D.G. Ellingsen, P. Molander, J. Environ. Monit. 7 (2005) 586–591.
[3] B. Hanoune, T. LeBris, L. Allou, C. Marchand, S. le Calve, Atmos. Environ. 40 (2006) 5768–5775.
[4] C.J. Weschler, A.T. Hodgson, J.D. Wooley, Environ. Sci. Technol. 26 (1992) 2371–2377.
[5] http://www.epa.gov/iaq/formalde.html.
[6] H. Tago, H. Kimura, K. Kozawa, K. Fujie, Water Air Soil Pollut. 163 (2005) 269–280.
[7] http://www.cancer.gov/cancertopics/factsheet/Risk/formaldehyde.
[8] http://www.euro.who.int/document/aiq/5_8formaldehyde.pdf.
[9] F. Vianello, A. Stefani, M.L. Di Paolo, A. Rigo, A. Lui, B. Margesin, M. Zen, M. Scarpa, G. Soncini, Sens. Actuat. B37 (1996) 49–54.
[10] R.W. Gillett, H. Kreibich, G.P. Ayers, Environ. Sci. Technol. 34 (2000) 2051–2056.
[11] J.A. Koziel, J. Noah, J. Pawliszyn, Environ. Sci. Technol. 35 (2001) 1481–1486.
[12] Y. Herschkovitz, I. Eshkenazi, C.E. Campbell, J. Rishpon, J. Electroanal. Chem. 491 (2000) 182–187.
[13] Y.I. Korpan, M.V. Gonchar, A.A. Sibirny, C. Martelet, A.V. El'skaya, T.D. Gibson, A.P. Soldatkin, Biosens. Bioelectron. 15 (2000) 77–83.
[14] J.A. Dirksen, K. Duval, T.A. Ring, Sens. Actuat. B80 (2001) 106–115.
[15] N. Nakano, M. Ishikawa, Y. Kobayashi, K. Nagashima, Anal. Sci. 10 (1994) 641–645.
[16] B.J. Compton, W.C. Purdy, Anal. Chim. Acta 119 (1980) 349–357.
[17] Y. Suzuki, N. Nakano, K. Suzuki, Environ. Sci. Technol. 37 (2003) 5695–5700.
[18] K. Kawamura, K. Kerman, M. Fujihara, N. Nagatani, T. Hashiba, E. Tamiya, Sens. Actuat. B 105 (2005) 495–501.
[19] C.N. Satterfield, R.E. Wilson, R.M. LeClair, R.C. Reid, Anal. Chem. 26 (11) (1954) 1792–1797.
[20] H. Shinohara, T. Uchi, S. Kitani, M. Fujii, Y. Kai, I. Kumagaya, M. Noguchi, Y. Yanagisawa, Knakyo no Kanri 52 (2004) 194–195 (in Japanese).

Available online at www.sciencedirect.com
ScienceDirect
Talanta 74 (2008) 1534–1538
Talanta
www.elsevier.com/locate/talanta

Spectrophotometric determination of chloride in waters using a multisyringe flow injection system

Fernando Maya, José Manuel Estela, Víctor Cerdà *

Department of Chemistry, Faculty of Sciences, University of the Balearic Islands, Carretera de Valldemossa km 7.5, E-07122 Palma de Mallorca, Illes Balears, Spain

Received 7 June 2007; received in revised form 31 August 2007; accepted 28 September 2007
Available online 2 October 2007

Abstract

A multisyringe flow injection system (MSFIA) with spectrophotometric detection is proposed as a fast, robust and low-reagent consumption system for the determination of chloride (Cl^-) in waters. The system is based in the classic reaction of Cl^- with Fe^{3+} and $Hg(SCN)_2$, but due to the hazardous properties of this last reagent, the proposed methodology has been developed with the aim to minimize the consumption of this one, consuming less than 0.05 mg of Hg for a Cl^- determination, being the system of this type with the lowest Hg consumption. The linear working range was between 1 and 40 mg L^{-1} Cl^- and the detection limit was 0.2 mg L^{-1} Cl^-. The repeatability (RSD) was 0.8% for a 10 mg L^{-1} Cl^- solution, and the injection throughput was 130 h^{-1}. The proposed system is compared with other chloride monitoring flow systems, this comparison is realized with a point of view of the equilibrium between the obtained analytical features and produced residues toxicity. The proposed system was applied to the determination of Cl^- in mineral, tap and well water.
© 2007 Elsevier B.V. All rights reserved.

Keywords: Multisyringe flow injection analysis (MSFIA); Chloride; Mercury-thiocyanate; Water samples

1. Introduction

Chloride (Cl^-) is one of the typical anions which its determination in waters has a great interest, overcoat in places with water salinity problems, being Cl^- one of the most widespread analysed anions in analytical laboratories. To obtain a maximum efficiency in a routinely analysis of Cl^- in a great number of water samples, a low-cost and automated analytical methodology is required. The principal route to obtain a simple and very fast, robust, sensitive, selective, completely automated and very high-autonomic system for Cl^- monitoring in waters is a flow injection system (FI) with spectrophotometric detection [1–6]. Usually these systems are based in the reaction between Cl^- and $Hg(SCN)_2$, being the liberated SCN^- quantity in previous reaction, proportional to the Cl^- concentration in the reaction medium. This free SCN^- reacts with Fe^{3+} [7], obtaining an intensely coloured coordination iron(III)-thiocyanate complex measured at 480 nm.

On the other hand, these advantages are eclipsed by the use of mercury in the form of $Hg(SCN)_2$, due to the high toxicity of this reagent, the proposed method does not seem to agree initially with the "Green Chemistry" analytical current trend. By this reason other spectrophotometric methods, in agreement with clean chemistry has been proposed [8–10], in these methods the measured property is usually the turbidity produced by the AgCl formation from the reaction between Cl^- and Ag^+. These turbidimetric methods have the advantage to produce less hazardous wastes than the $Hg(SCN)_2$-based methods for Cl^- monitoring, but also they have some disadvantages as the obtention of worse analytical features.

The Cl^-–$Hg(SCN)_2$–Fe^{3+} reaction system is also used actually in various commercial tests for Cl^- determination in waters (Merck, Macherey-Nagel), and for the sum parameter adsorbable organic halogens (AOX) determination in waters (Macherey-Nagel), prior preconcentration and digestion of the analyte.

The proposed method takes the advantages of working with MSFIA systems [11–14], in order to develop a direct colorimetric determination of Cl^- in waters, being this methodology similar to the used in first proposed FI systems [1,2], but with

* Corresponding author. Tel.: +34 971259576; fax: +34 971173426.
E-mail address: victor.cerda@uib.es (V. Cerdà).

0039-9140/$ – see front matter © 2007 Elsevier B.V. All rights reserved.
doi:10.1016/j.talanta.2007.09.031

a reduction of the produced waste until better levels than in the most recently proposed flow systems [5,6]. Then we intend with this work, show that MSFIA technique is adapted easily in a routinely analysis procedure, obtaining very good features in all points of view.

2. Experimental

2.1. Reagents and solutions

All reagents were of analytical grade and solutions were prepared with distilled water. Fe^{3+} stock solution was prepared dissolving 20.2 g $Fe(NO_3)_3{\cdot}9H_2O$ (Riedel-de Haën) in 0.1 L of a 1 mol L^{-1} HNO_3 solution. $Hg(SCN)_2$ working solution was prepared dissolving in a steam bath 0.12 g of $Hg(SCN)_2$ (Fluka) in 0.1 L of distilled water. Cl^- stock solution (1000 mg L^{-1}) was prepared dissolving 1.649 g of previously dried NaCl (Scharlau) in distilled water and filling to a final volume of 1 L. Working solutions were prepared by suitable dilutions from the stock solutions.

2.2. Flow system, optical detector and software

The correspondent manifold to the proposed method is shown in Fig. 1. A multisyringe piston pump (Crison, Barcelona, Spain) is used as a liquid driver, this system is characterized for having four syringes (S1–S4) which are moved by a single motor. In this work only three syringes (Hamilton, Switzerland) were used, S1 = 10 mL, S2 = 5 mL and S3 = 5 mL. Each syringe has a three-way solenoid valve (N-Research, Caldwell, NJ) at the head (E1–E4), these valves allow us the application of multicommutation schemes. The connection between the multisyringe module and the PC is a RS232C interface. Also, in our system, two additional solenoid valves (MTV-3-N 1/4 UKG, Takasago, Japan) were used (E5–E6).

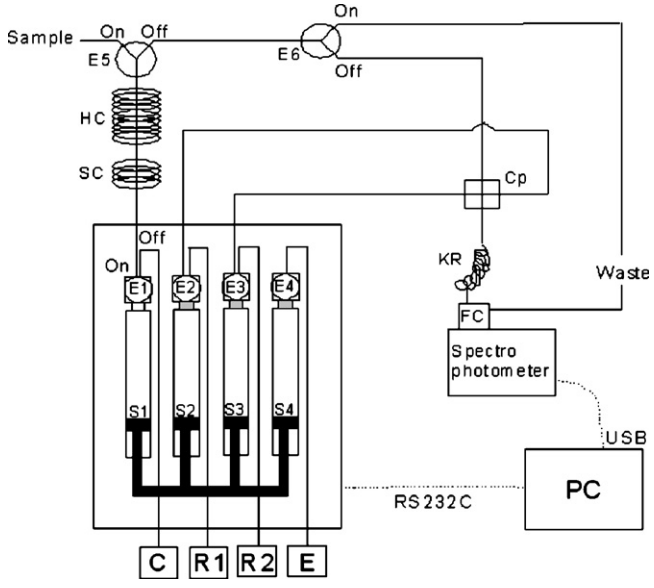

Fig. 1. Schematic representation of the MSFIA manifold for chloride determination. C: carrier (distilled water); R1: $Hg(SCN)_2$ reagent; R2: Fe^{3+} reagent; E: empty (not used); S1–S4: syringes; E1–E6: solenoid valves; On–Off: solenoid valves positions; SC: security coil; HC: holding coil; Cp: confluence point; KR: knotted reactor; FC: flow cell.

The E5 solenoid valve, let us the loading of the sample into the holding coil (HC), also the system has a security coil (SC) to prevent the introduction of the sample into the S1. The E6 solenoid valve has the function to prevent the carryover between two consecutive samples, and allow us to deposit the dead volume of the previous sample directly to the waste reservoir. All coils and connections were made from polytetrafluoroethylene (PTFE) 0.8 mm i.d. tubing.

The reaction coil (KR), was a knotted reactor made also from PTFE 0.8 mm i.d. With the use of these type reactors, we obtained a better mix between sample and reagents, and less dispersion than with a conventional reaction coil. The four-way confluence point (Cp) was made from polymethylmethacrylate (PMMA).

The detection system was composed by a light source (Sciware, Palma de Mallorca, Spain) with a wolfram lamp, a 18 μL inner volume and 1 cm optical path flow cell (FC) (Hellma, Müllheim, Germany), and a USB 2000 miniature spectrophotometer (Ocean Optics, Dunedin, FL, USA). Dual-wavelength spectrophotometry (480 and 720 nm) was used to minimize Schlieren effect.

Instrumental control and data acquisition were performed through the Autoanalysis 5.0 software package, developed by our research group, it allow us the automated implementation of MSFIA analytical methodologies. Autoanalysis 5.0 has a single protocol, and depending which are the instruments needed for a determined experiment, the correspondent dynamic link libraries (DLL's) are installed [15]. In the proposed experiment we need the suitable DLL's for the multisyringe module (it includes the four syringes and the two additional solenoid valves) and the spectrophotometer.

2.3. MSFIA procedure for chloride monitoring

The principal steps on the MSFIA used protocol are the following ones:

1. The syringes are filled everyone with their correspondent solution; all valves E1–E6 are in Off position. *Note*: the depicted flow rates and volumes are referred to S1, being the flow rates and volumes of S2–S3 the half than the S1 ones.
2. A volume of 3.5 mL is dispensed at 15 mL min^{-1} with all valves in Off position.
3. Sample loading. A volume of 3.5 mL of sample is filled up at 8 mL min^{-1} with the valves E1 = E5 = On, with other valves in Off position.
4. Injection protocol. Multicommuted reaction procedure, which is depicted in Table 1. This procedure consists on the accomplishment of three injections of the sample from the volume loaded in the previous step and posterior cleaning of the possible sample excess. In all steps, the volumes depicted are dispensed into the system almost continuously, with little intervals of 50 ms, the enough time for valves commutation.

Table 1
Multicommuted dispensing protocol for sample reaction

Step	Valves			Injected volume (mL)		Flow rate (mL min^{-1})	
	E1	E2	E3	S1	Total	S1	Total
1	On	Off	Off	0.90	0.90	6	6
2	On	On	On	0.12	0.24	3	6
3	On	Off	Off	0.90	0.90	6	6
4	On	On	On	0.12	0.24	3	6
5	On	Off	Off	0.90	0.90	6	6
6	On	On	On	0.12	0.24	3	6
7	On	Off	Off	2.50	2.50	6	6

Valves E5 and E6 are in Off position in all steps, valve E4 is not used.

The total flow rate remains constant in all the sub-steps. Then we can consider this step as a unique emptying movement of the syringes, but depending on the time, sample and reagents are mixed obtaining a signal (E1 = E2 = E3 = On), or only is dispensed the sample (E1 = On, E2 = E3 = Off), cleaning the FC.

5. The syringes are filled again with their correspondent solutions at 15 mL min^{-1}, with all valves in Off position, remaining prepared for next injection.

3. Results and discussion

3.1. Investigation of chemical variables

The concentrations of $Hg(SCN)_2$ and Fe^{3+} reagents were studied (Fig. 2), to obtain good conditions for the coloured reaction product development.

Fe^{3+} concentration was studied in a 4×10^{-3} to 5×10^{-1} mol L^{-1} range. The selected concentration was 10^{-1} mol L^{-1}.

$Hg(SCN)_2$ concentration was studied in a 8×10^{-3} to 2×10^{-5} mol L^{-1} range. The selected concentration was 3×10^{-3} mol L^{-1}.

Lower reagent concentrations than the selected ones, causes a signal decrease. Higher reagent concentration does not cause a significant net absorbance increase, due to the blank signal increasing.

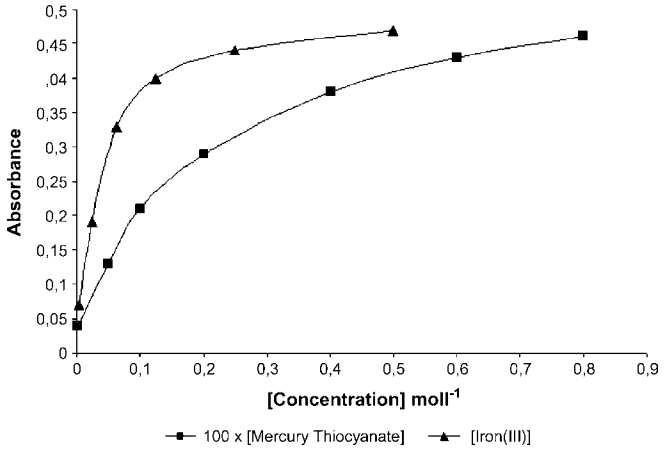

Fig. 2. Influence of reagent concentrations on the absorbance (analytical signal peak height–blank peak height), obtained analyzing a 30 mg L^{-1} Cl^- solution.

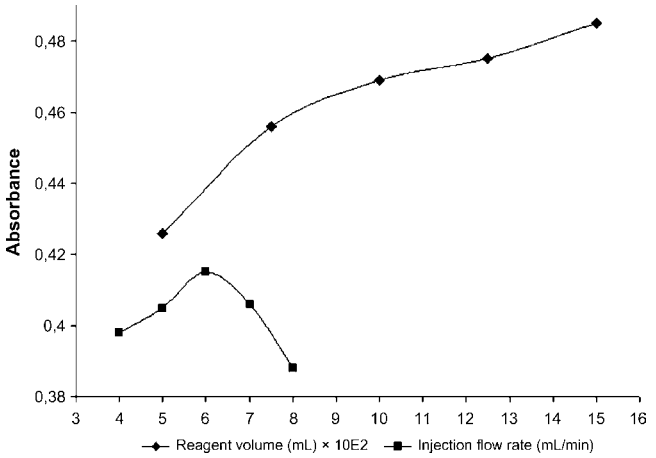

Fig. 3. Influence of injected reagent volumes and reaction plug injection flow rate on the absorbance (analytical signal peak height–blank peak height), obtained analyzing a 30 mg L^{-1} Cl^- solution.

3.2. Investigation of MSFIA parameters

In this work, the investigated parameters were injection flow rate; multicommutation procedure injected reagent volumes, sample volume and knotted reaction coil length.

As is shown in Fig. 3, reaction plug injection flow rate was studied between 4 and 8 mL min^{-1}, being the best signal height obtained with a 6 mL min^{-1} flow rate.

In the multicommutation injection step, the injected volumes of Fe^{3+} and $Hg(SCN)_2$ reagents were studied in the range between 0.05 and 0.15 mL, obtaining the best relation between net absorbance peak height and the lowest amount of spent $Hg(SCN)_2$, with the injection of 0.06 mL of each reagent solution. Increasing these reagent volumes the net absorbance does not increase significantly (Fig. 3).

Also was studied sample volume needed between two consecutive injections to obtain two completely separated signal peaks, this volume was studied in a range between 0.5 and 1.5 mL, and the selected volume was 0.9 mL.

The total sample volume loaded in the holding coil for the consecutive three injections were studied in a range between 3 and 4 mL, the selected volume was 3.5 mL. Lower volumes produce a height decrease of the third analytical peak.

The knotted reaction coil length was studied in a range between 20 and 150 cm. A 40 cm knotted reaction coil is enough to obtain the maximum analytical peak height. Reactors of less than 40 cm did not allow a good sample–reagents mixing, and longer reactors caused an increase of the reaction plug dispersion.

3.3. Interference studies

In order to investigate the selectivity of the proposed method, the effect produced by diverse anions usually presented in water samples, were studied. The tested anions were: HCO_3^-, CO_3^{2-}, NO_2^-, NO_3^-, PO_4^{3-} and SO_4^{2-}.

The effect of each interferences was examined by measuring the net absorbance obtained from 10 mg L^{-1} Cl^- solutions

Table 2
Analytical performance of the MSFIA proposed system for chloride monitoring, and the FI method with immobilized $Hg(SCN)_2$ [6]

Analytical parameter	MSFIA	FIA [6]
Detection limit ($mg\,L^{-1}$)	0.2	0.5
Linear dynamic range ($mg\,L^{-1}$)	1–40	2–8
Repeatability (%) (10 $mg\,L^{-1}$) ($n = 10$)	0.8	2.2
Injection frequency (h^{-1})	130	100

containing one of the previously stated potential interferences. Later, the previous study was repeated, but increasing 10 times the added amount of the potential interfering anions. An error in the analytical signal lower than a ±5% was obtained in all cases.

3.4. Analytical features of the proposed system

The analytical figures of merit of the proposed MSFIA system are reported in Table 2. Furthermore the proposed system is also compared with another low-reagent consumption spectrophotometric FI system for Cl^- monitoring, which is also based in the Cl^-–$Hg(SCN)_2$–Fe^{3+} reaction system [6], obtaining a moderate improvement of these figures using the MSFIA system.

The obtained linear working range was similar to the obtained with other flow systems based in the same reaction [1–6], furthermore $0.0132 \pm 0.0005\,L\,mg^{-1}$ sensitivity and a 0.9973 ± 0.0009 regression coefficient were obtained. The detection limit [16] was calculated as three times the standard deviation of the absorbance for 10 injections of the blank (distilled water), following the MSFIA procedure for Cl^- monitoring proposed in point 2.3. The peak height repeatability is reported as the RSD (%) from 10 consecutive injections of a 10 $mg\,L^{-1}$ Cl^- standard solution.

3.5. Comparison of the proposed system with other chloride monitoring systems

Nowadays, several FI systems for Cl^- determination had been proposed.

On one hand, various spectrophotometric Cl^- monitoring flow systems based in colorimetric reactions had been reported. These methods are based in the Cl^-–$Hg(SCN)_2$–Fe^{3+} reaction system, being very simple, direct, fast and robust methods [1–6], but with the disadvantage of a waste generation which contains high amounts of Hg. A comparison between these methods was made in [6], reporting in it the $Hg(SCN)_2$ consumption of each system.

Actually the lowest $Hg(SCN)_2$ consumption in a FI system for Cl^- monitoring is 0.12 mg of Hg(II) for a Cl^- determination [6], and it is due to the immobilization of the reagent in a solid phase reactor (SPR), being the autonomy of this system limited to 1000 Cl^- determinations. The proposed MSFIA system only requires 0.045 mg of Hg(II) per Cl^- determination, and does not require the use of a SPR, obtaining with only 1 g of $Hg(SCN)_2$ the realization of approximately 15,000 Cl^- determinations. Then we can affirm that the proposed system has a higher autonomy level, combined with the lowest reagent consumption.

On the other hand, can not be discussed that the spectrophotometric FI systems focused to the Cl^- determination, which are based in the turbidimetry produced by AgCl [8–10], are cleaner systems than the $Hg(SCN)_2$-based ones. Zenki and Iwadou [8] proposed a closed-loop FIA system with repetitive Cl^- determination, while Mesquita et al. [9] proposed a SIA system-based in the same reaction, which are simple, direct and environmentally friendly systems. In counterpoint, these systems have worse analytical features (i.e. higher detection limits) than the previously commented colorimetric systems.

These analytical features has been improved recently by Bonifácio et al. [10], exploiting the immobilization of silver chloranilate in a SPR, in this SPR the Cl^- ions are retained producing AgCl, and releasing free chloranilate ions which are measured spectrophotometrically at 530 nm, obtaining good analytical features due to the use of a 100 cm pathlength spectrophotometer, being the robustness of the system determined by the limited duration of this SPR.

Nowadays exist another MSFIA system for Cl^- monitoring, but with potentiometric detection [17], we agree that it works with a more environmentally friendly methodology, but the proposed spectrophotometric MSFIA system has other better analytical features, as a higher sample throughput or a lower detection limit. Then depending of a concrete application, potentiometric or spectrophotometric MSFIA systems will be the most adapted system in each case, or also would be feasible the development of a potentiometric/spectrophotometric multidetection FI system as the recent FIA system developed by Nascimento Moreira et al. [18].

Several commercialised tests for to the routine analysis of Cl^- in water samples, are based in the same reaction than the proposed methodology, but due to the automation of the MSFIA technique, we obtain apart of a higher sample throughput, a more than 100-fold decrease in used $Hg(SCN)_2$ amount [19].

3.6. Analytical application

Once adopted the final system configuration, it was applied to the determination of Cl^- in real samples. Mineral water, tap water and well water samples were analyzed with the proposed MSFIA method, and compared with the official APHA–AWWA–WPFC method [20]. The samples were previously diluted if it was necessary. The obtained results were

Table 3
Determination of chloride in environmental samples using the MSFIA proposed method, and the official APHA–AWWA–WPFC [20] method, three repetitions per sample were realized

Sample	Chloride ($mg\,L^{-1}$)		Relative error[a] (%)
	MSFIA method	Official method	
Mineral water	41.6 ± 0.3	41.1 ± 0.3	1
Tap water	51.1 ± 0.1	49.5 ± 0.2	3
Well water	102.4 ± 0.1	99.4 ± 0.2	3

[a] Relative error between MSFIA method and official method value.

compared applying *t*-test for paired data, obtaining no significant differences at a 95% confidence level. The results are presented in Table 3.

4. Conclusions

In the present work, a direct MSFIA system with spectrophotometric detection for Cl^- monitoring has been proposed. The developed system has a high robustness and the absence of elements with a determined limited duration, as solid phase reactors, unstable reagents, or the previously manual preparation of complex reagents. Then, the obtained system has a high autonomy degree and the absence of fragile parts, and in consequence of this, the system can run for a very long time with only a small quantity of reagents.

The analytical performance of the proposed methodology has not significant differences when is compared to other similar proposed systems [1–6], but with the advantage to work with a very autonomous system, with the lowest reagent consumption and a very high sample throughput.

In conclusion, we encourage the use of multisyringe flow injection technique not only as a useful tool in the development of new analytical methodologies, but also in the automation of standard methods of analysis, which are used generally following a manual methodology. Obtaining with this change a long list of advantages, with the unique requirement of basic laboratory automation knowledge acquisition on the part of the analyst.

Acknowledgements

The authors acknowledge the financial support of the Ministry of Education and Science (Spain) through the projects CTQ2007-64331 and CTQ2004-03256. F.M. also thanks the support of the Conselleria dĭEconomia, Hisenda i Innovació of the Balearic Islands Government through a PhD fellowship.

References

[1] J. Ruzicka, J.W.B. Stewart, E.A.G. Zagatto, Anal. Chim. Acta 81 (1976) 387.
[2] F.J. Krug, L.C.R. Pessenda, E.A.G. Zagatto, A.O. Jacinto, B.F. Reis, Anal. Chim. Acta 130 (1981) 409.
[3] A.M. Almuaibed, A. Townshend, Anal. Chim. Acta 245 (1991) 115.
[4] M. Cheregi, A.F. Danet, Anal. Lett. 30 (1997) 2847.
[5] S.T. Chalk, J.F. Tyson, Anal. Chim. Acta 366 (1998) 147.
[6] C.R. Silva, H.J. Vieira, L.S. Canaes, J.A. Nóbrega, O. Fatibello-Filho, Talanta 65 (2005) 965.
[7] D.M. Zall, D. Fisher, M.Q. Garner, Anal. Chem. 28 (1956) 1665.
[8] M. Zenki, Y. Iwadou, Talanta 58 (2002) 1055.
[9] R.B.R. Mesquita, S.M.V. Fernandes, A.O.S.S. Rangel, J. Environ. Monit. 4 (2002) 458.
[10] V.G. Bonifácio, L.C. Figueiredo-Filho, L.H. Marcolino Jr., O. Fatibello-Filho, Talanta 72 (2007) 663.
[11] V. Cerdà, J.M. Estela, R. Forteza, A. Cladera, E. Becerra, P. Altimira, P. Sitjar, Talanta 50 (1999) 695.
[12] F. Albertús, B. Horstkotte, A. Cladera, V. Cerdà, Analyst 124 (1999) 1373.
[13] B. Horstkotte, O. Elsholz, V. Cerdà, J. Flow Inject. Anal. 22 (2005) 99.
[14] M. Miró, V. Cerdà, J.M. Estela, Trends Anal. Chem. 21 (2002) 199.
[15] E. Becerra, A. Cladera, V. Cerdà, Lab. Robotics Automat. 11 (1999) 131.
[16] G.L. Long, J.D. Winefordner, Anal. Chem. 55 (1983) 712A.
[17] A. Andrade-Eiroa, J.A. Erustes, R. Forteza, V. Cerdà, J.L.F.C. Lima, Anal. Chim. Acta 467 (2002) 25.
[18] L. Nascimento Moreira, L.A. Ramos, C.R.T. Tarley, P.O. Luccas, J. Flow Inject. Anal. 24 (1) (2007) 13.
[19] Macherey-Nagel GmbH & Co. KG, Art. no. 91820 (2007).
[20] A.D. Eaton, L.S. Clesceri, A.E. Greenberg, American Public Health Association, American Water Works Association and Water Pollution Control Federation (APHA–AWWA–WPFC), 20th ed., Standard Methods for The Examination of Water and Wastewater, Washington, DC, 1998.

Available online at www.sciencedirect.com
ScienceDirect
Talanta 74 (2008) 1184–1190
Talanta
www.elsevier.com/locate/talanta

Method development for the determination of selected pesticides on tobacco by high-performance liquid chromatography–electrospray ionisation-tandem mass spectrometry

Bernhard Mayer-Helm *, Ludwig Hofbauer, Jutta Müller

Gallaher Group Plc, R & D, Hasnerstraße 127, 1160 Vienna, Austria

Received 6 April 2007; received in revised form 22 August 2007; accepted 24 August 2007
Available online 2 September 2007

Abstract

A method was developed for the quantitative determination of alachlor, benalaxyl, clomazone, diflubenzuron, dimethomorph, diphenamid, ethofumesate, metalaxyl, methoprene, metobromuron and piperonyl butoxide on tobacco. The pesticides were extracted with water and methanol from five different types of tobacco. The extracts were purified by partition on an extraction cartridge containing diatomaceous earth. The purified extracts were analysed by reversed-phase high-performance liquid chromatography connected to an atmospheric pressure ionisation–electrospray-triple quadrupole mass spectrometer operating in the positive ion mode. Two different transitions and their relative intensities were monitored for unambiguous identification. All pesticides presented overall recovery rates between 35% and 110%. The trueness is near 100% and the interday precision is below 15%. The limits of quantifications are equal or below the guidance residue levels proposed by the Agrochemical Advisory Committee of CORESTA, an association of organisations having scientific research relative to tobacco.
© 2007 Elsevier B.V. All rights reserved.

Keywords: Pesticides; Tobacco; Liquid chromatography; Tandem mass spectrometry

1. Introduction

Above 800 pesticides have been widely used throughout the world since the middle of the 20th century. They are used during farming and storage of agricultural products. Pesticides belong to more than 100 substance classes and their chemical and physical properties may differ considerably. This diversity causes serious problems in the development of a universal residue analytical method. However, such multiresidue methods are urgently needed, as the use of pesticides is regulated extensively. Maximum residue levels or tolerances have been established for pesticides in foodstuffs and drinking water in most countries to avoid any adverse impact on public health. To regulate the use of pesticides in tobacco cultivation, the Agrochemical Advisory Committee of CORESTA (Cooperation Centre for Scientific Research Relative to Tobacco) has recently defined guidance residue levels (GRLs) for 99 pesticides plus several metabolites on tobacco and tobacco products [1]. These GRLs have been developed to provide guidance to the tobacco industry interested in agrochemical application and implementation of good agricultural practice in tobacco production. GRLs do not replace requirements to comply with regulations.

In recent years liquid chromatography–atmospheric pressure ionisation-tandem mass spectrometry (LC–API-MS/MS) has been widely used for multiresidue analysis [2]. The soft ionisation techniques atmospheric pressure chemical ionisation (APCI) and electrospray ionisation (ESI) in combination with tandem mass spectrometry are universal and sensitive techniques for the determination of pesticides with a wide range of properties. Up to 100 of pesticides were analysed in foodstuff and drinking water by LC–API-MS/MS. For this study eight pesticides with GRLs on tobacco were selected for which no multiresidue methods are readily available, see Table 1. Three further pesticides with high priority were also included.

Some of the selected pesticides have already been analysed by multiresidue methods using LC–API-MS/MS, mainly in water, fruits and vegetables, and rarely in other food commodities,

* Corresponding author. Tel.: +43 1 31342 2253; fax: +43 1 31342 2430.
E-mail address: bernhard.mayer-helm@gallahergroup.com (B. Mayer-Helm).

0039-9140/$ – see front matter © 2007 Elsevier B.V. All rights reserved.
doi:10.1016/j.talanta.2007.08.033

Table 1
Guidance residue levels (GRLs) of 11 pesticides on tobacco and their corresponding factor ×GRL

Pesticide	GRL ($\mu g\,g^{-1}$) [1]	$1 \times$ GRL ($\mu g\,g^{-1}$)
Metobromuron	Not listed[a]	1.0
Metalaxyl	2.0	2.0
Diphenamid	0.5	0.5
Clomazone	Not listed	1.0
Ethofumesate	Not listed	1.0
Dimethomorph (sum of isomers)	2.0	2.0
Diflubenzuron	0.1	0.1
Alachlor	0.1	0.1
Benalaxyl	2.0	2.0
Piperonyl butoxide	0.1	0.1
Methoprene	1.0	1.0

[a] Recommended maximum amount 5.0 $\mu g\,g^{-1}$ [24].

such as cereals. Metalaxyl and dimethomorph were monitored in fruits and vegetables by LC–ESI-MS/MS after injection of raw extracts [3]. Metalaxyl was analysed in fruits and vegetables by LC–ESI-MS/MS [4]. Metalaxyl and diflubenzuron were analysed in crops after Chem Elut purification by LC–MS/MS [5]. Diflubenzuron was analysed in fruits in the negative ion mode by ESI [6,7] and APCI [8], but also in the positive ion mode by ESI [9–11]. Dimethomorph was analysed in fruits and vegetables by LC–ESI-MS/MS after injection of concentrated raw extracts [9] and after a solid phase extraction (SPE) purification step [10]. Metobromuron were determined in water and soil by LC–ESI-MS [11] and in water by LC–thermospray-MS [12]. Metalaxyl, metobromuron, dimethomorph and piperonyl butoxide were analysed in soya grain without any clean-up by LC–MS/MS [7]. Alachlor was determined in water by LC–thermospray-MS/MS [13], LC–API-MS/MS [14] and high-resolution LC–ESI-MS/MS [15]. Ethofumesate was determined in water by LC–ESI-MS after enrichment via SPE [16]. Piperonyl butoxide was determined in fruits and vegetables by LC–single quadrupole MS [17,18]. Methoprene is rather non-polar and lacks sensitivity necessary for trace analysis due to its insufficient ionisation efficiency in the ESI process. Therefore, derivatisation was required to improve sensitivity for its determination in water by LC–ESI-MS/MS [19].

Several of these methods are restricted to aqueous samples, where high enrichment is readily feasible via SPE. Furthermore, some of the selected pesticides were rarely analysed by LC–MS. Especially clomazone and diphenamid were determined the first time in plant material by LC–MS, although they are registered for use in several countries and used for control of grasses and weeds in numerous plants. So far, none of the selected pesticides has been analysed in tobacco by LC–MS. Benalaxyl and ethofumesate were measured in tobacco after two consecutive SPE steps by GC–MS/MS [20]. A target method for the determination of methoprene in tobacco is based on direct analysis of extracts by HPLC-UV [21]. Furthermore, diphenamid was determined in tobacco after gel permeation chromatographic clean up followed by HPLC-UV [22].

A previous study on tobacco showed that the injection of highly diluted extracts is a simple and fast approach to reduce matrix effects during LC–ESI-MS/MS [23]. In the course of method development it turned out that a stricter sample purification protocol is required to obtain improved sensitivity. A quick and robust solid supported liquid–liquid extraction step was established to be able to inject higher matrix-loaded samples.

2. Experimental

2.1. Reference pesticides

Analytical standards were purchased from Dr. Ehrenstorfer GmbH (Augsburg, Germany), except alachlor was from Riedel-de Haën (St. Louis, MO, USA) and methoprene was from Zoecon Corp. (Palo Alto, CA, USA). Their purity was higher than 90%. Stock solutions of individual pesticides at 1 mg ml^{-1}were prepared by dissolution in methanol, except dimethomorph was dissolved in acetonitrile and diflubenzuron was dissolved in acetone. Mixtures of all 11 pesticides were prepared by dilution with methanol. These standard working solutions were stored at −20 °C prior to use. The mixture was stable for more than 1 year at −20 °C (data not shown).

To ease comparison of pesticides with very different GRLs, a factor ×GRL was defined, see Table 1. This factor represents a multiple of the GRL. For example, $0.1 \times$ GRL corresponds to a concentration of 0.01 $\mu g\,g^{-1}$ of a pesticide with a GRL of 0.1 $\mu g\,g^{-1}$. A concentration of 1 $\mu g\,g^{-1}$ was fixed as $1 \times$ GRL for pesticides without a defined GRL on tobacco.

2.2. Sample extraction and purification

All solvents were used in HPLC grade quality, except for methanol, which had LC–MS quality (LC–MS grade; Riedel-de Haën, Buchs, Switzerland). One gram of ground tobacco (spiked or unspiked) was soaked with 12.5 ml water (for HPLC; LCG Promochem, Wesel, Germany) for 5 min before the pesticides were extracted with 25 ml methanol under ultrasound and shaking for 5 min, respectively. After centrifugation 4 ml of the supernatant were diluted with 1.33 ml 20% (w/w) aqueous sodium chloride. Five millilitre of this solution was applied to a Chem Elut cartridge (maximum sample volume 5 ml, Varian, Inc., Palo Alto, CA, USA) containing diatomaceous earth. After 5 min equilibration, the pesticides were eluted with two 8-ml aliquots of cyclohexane/toluene (85/15, v/v). The solvent was evaporated at 30 °C under a flow of nitrogen and the residue was reconstituted in 400 μl methanol and 400 μl 10 mM aqueous ammonium acetate. After filtration through a filter with a 0.45 μm PTFE membrane (Millex-LCR, Millipore Corp., Bedford, MA, USA), 10 μl of the extracts were injected onto the HPLC column. The analysis of filtered versus unfiltered pesticide solutions showed that no losses occurred during filtration (data not shown). The solutions ready for injection were stable for at least 3 days at 8 °C (data not shown).

2.3. HPLC analysis

The extracts were separated by reversed-phase high-performance liquid chromatography (HPLC) in the gradient

mode under similar conditions as previously reported [23]. The HPLC instrument consisted of an Alliance 2695 separation module and column oven, equipped with a built-in online degasser (Waters, Milford, MA, USA). Separation was achieved with a Synergi 4 μm Hydro-RP, 150 mm × 2.0 mm (Phenomenex, Torrance, CA, USA), thermostated at 35 °C. The analytical column was protected by a 10 μm Aqua guard column 4.0 mm × 2.0 mm (Phenomenex). The samples were cooled in the autosampler tray to 8 °C. Mobile phase A was 5 mM ammonium acetate in 90% water/10% methanol and mobile phase B was 5 mM ammonium acetate in 10% water/90% methanol. The flow rate was set to 0.2 ml min^{-1}. A simple binary HPLC gradient from 18% to 90% organic solvent was used to separate the mixture. The initial conditions of the binary gradient were 90% mobile phase A and 10% mobile phase B. The mobile phase composition was changed from 10% to 100% mobile phase B within 15 min. After maintaining the system for 8 min at 100% mobile phase B it was set to the initial conditions and equilibrated resulting in an overall run time of 30 min. A built-in valve was used to divert the effluent to waste between 0 and 13.9 min and between 29 and 30 min to reduce contamination of the interface.

2.4. Tandem mass spectrometry

The pesticides were detected with an atmospheric pressure ionisation quadrupole mass spectrometer Quattro Micro (Waters) operating in the positive ion electrospray mode. The triple quadrupole was operated in the multiple reaction monitoring (MRM) mode. Both HPLC and MS/MS were controlled by MassLynx 4.0 (Waters). Time-scheduled transitions were used to detect the pesticides. The capillary voltage was adjusted to 1.25 kV. The ionisation source was heated to 120 °C and the desolvation temperature was set to 450 °C. The nitrogen flow rate and the cone gas flow were set to 600 and 50 l h^{-1}, respectively. The mass spectrometric parameters for the 11 pesticides are summarised in Table 2. Manual optimisation of these parameters was performed by direct infusion of each compound in the respective mobile phase composition. The interscan delay was set to 0.03 s and the span was set to 0.2 Da. The dwell times were adjusted between 0.2 and 2 s depending on the sensitivity needed and the number of simultaneous transitions. To obtain maximum sensitivity, high dwell times were used for transitions, where only few transitions were monitored within a time window. To obtain enough data points for accurate integration, lower dwell times had to be used for several transitions within the same time window whereas sensitivity was sacrificed.

2.5. Quantitation and method validation

The method was validated for three different types of tobacco (Burley, Oriental, Virginia) and two tobacco products (Scandinavian oral snuff [25] and a full flavour American blend cigarette). External calibration with matrix-matched standards was used for quantification. Calibration curves were set up with concentration versus peak areas by spiking 1 g tobacco with 100 μl of standard working solutions resulting in 2 × GRL, 0.5 × GRL and 0.2 × GRL. The trueness of the method was determined by

Table 2
Mass spectrometric parameters for the quantification and confirmation of 11 pesticides in the multiple reaction monitoring (MRM) mode

Pesticide	Retention time (min)	Quantification transition				Confirmation transition				Dwell time (s)	Relative ion intensity (%)[a]
		Precursor ion	Product ion	Cone voltage (V)	Collision energy (eV)	Precursor ion	Product ion	Cone voltage (V)	Collision energy (eV)		
Metobromuron	17.2	259.0	170.0	24	16	261.0	172.0	24	16	0.5	105 (3)
Metalaxyl	17.3	280.2	220.1	20	14	280.2	192.0	20	18	0.2	72 (1)
Diphenamid	17.9	240.1	134.1	26	18	240.1	167.1	26	22	0.2	22 (1)
Clomazone	18.4	240.1	125.0	22	20	242.1	127.0	22	20	0.25	34 (1)
Ethofumesate	18.4	287.1	259.1	24	8	287.1	121.0	24	16	0.25	205 (9)
Dimethomorph	18.6 + 19.0[b]	388.1	301.1	34	18	301.1	165.0	52	18	0.25	130 (6)
Diflubenzuron	20.1	311.0	158.1	22	12	158.1	141.0	34	18	0.75	86 (5)
Alachlor	20.1	238.1	90.0	30	18	238.1	162.1	30	16	0.5	199 (17)
Benalaxyl	20.8	326.2	294.1	16	10	326.2	148.0	16	26	0.2	170 (4)
Piperonyl butoxide	23.0	356.2	177.1	17	12	177.1	119.0	34	14	0.5	46 (3)
Methoprene	27.4	279.2	191.2	14	6	279.2	237.1	16	9	2.0	22 (1)

[a] Mean values of all five tobacco matrices, standard deviations in brackets.
[b] Two isomers.

analysing spiked pesticide-free tobaccos at three different concentration levels (1.5 × GRL, 0.75 × GRL and 0.25 × GRL) on three different days [26]. The overall recovery was calculated from the percentage of the true concentration of a substance recovered during the analytical procedure. The recovery (in %) is 100 × measured content/fortification level [27]. The recovery was determined by spiking pesticide-free tobacco at four concentration levels, i.e., 0.25 × GRL, 0.5 × GRL, 0.75 × GRL and 1.5 × GRL. For recovery calculation, quantification was performed by external standard calibration curves.

2.6. Confirmation of positive results

The European Union has proposed criteria for unambiguous identification of organic residues [27]. For example, the minimum requirements for unambiguous analyte identification by LC–MS/MS are one precursor ion and two product ions, their relative intensities within maximum permitted tolerances, and retention times within a margin of 5% [27,28]. In this method, two different transitions of each pesticide were monitored in two consecutive HPLC runs to earn four (one precursor ion and two product ions) or even five (two precursor ions and two product ions) identification points. The most sensitive transition was used as quantification transition. The limit of quantification (LOQ) was given as determined by a signal-to-noise ratio of 10 [26]. The relative ion intensity of the confirmation transition was expressed as a percentage of the intensity of the quantification transition [27,28]. The mean values of the relative ion intensities and their standard deviation of all five tobacco matrices investigated are listed in Table 2.

3. Results and discussion

3.1. Method development

The HPLC separation provided narrow peaks without any peak tailing (Fig. 1). Five millimolar ammonium acetate was added to both mobile phases to support ionisation. Most of the precursor ions were $[M+H]^+$ ions. Only for piperonyl butoxide the $[M+NH_4]^+$ ion, and for alachlor and methoprene the $[M+H–CH_3O]^+$ ions were used as precursor ions. In the case of dimethomorph, diflubenzuron and piperonyl butoxide, abundant precursor ions were generated by increasing the cone voltage, which were used for the confirmation transitions, see Table 2. These precursor ions were $[M$-morpholine $+H]^+$ for dimethomorph, $[M–CONH–C_6H_4Cl+H]^+$ for diflubenzuron, and $[M–C_4H_9O(C_2H_4O)_2+H]^+$ for piperonyl butoxide. As the pesticides are from different classes and have different functional groups, their MS responses are very different. Surprisingly, even rather nonpolar pesticides are successfully ionised, although ESI is known to offer only low ionisation efficiency towards nonpolar compounds. In the case of methoprene even a derivatisation reaction was suggested to improve sensitivity [19].

The direct injection of methanolic tobacco extracts [23] turned out to offer too less sensitivity because highly diluted extracts are required to reduce matrix effects. Therefore, enrichment and purification is mandatory for pesticides, where GRLs below 0.5 μg g^{-1} are defined. Solid supported liquid–liquid extraction was successfully applied for sample pretreatment for the analysis of 100 pesticides in crops [5]. The method used dichloromethane to elute the pesticides from a Chem Elut extraction cartridge. However, this approach failed for the purification of tobacco extracts. Although almost all pesticides were recovered quantitatively, coeluting tobacco compounds partly disturbed the baseline of the chromatograms resulting in worse sensitivity. In the course of the ongoing study, several solvents and solvent combinations were assessed as eluents for the pesticides from the extraction cartridge. Diethyl ether and ethyl acetate provided similar to dichloromethane also high recovery of the pesticides, but some pesticides coeluted with tobacco compounds which can be seen in the MRM chromatogram giving worse sensitivity. Cyclohexane and *n*-hexane provided high recoveries of nonpolar pesticides and low background noise, but polar and medium polar pesticides were completely lost or not fully recovered. Cyclohexane provided higher recovery rates than *n*-hexane and additionally fewer compounds were coeluted. Mixtures of dichloromethane and cyclohexane failed to increase the recovery of medium polar pesticides, but increased the background noise of some nonpolar pesticides. Finally, mixtures of cyclohexane and toluene were investigated to improve the recovery of some pesticides with low recovery when eluted with 100% cyclohexane, see Fig. 2. Finally, a mixture of 85/15 (%, v/v) cyclohexane/toluene turned out to be able to improve the recovery of some pesticides. Simultaneously, the background noise remained acceptable low. Only in the case of ethofumesate signals from the tobacco matrix interfere with the pesticide leading to decreased sensitivity, see chromatogram of #5 in Fig. 1 and LOQ in Table 5.

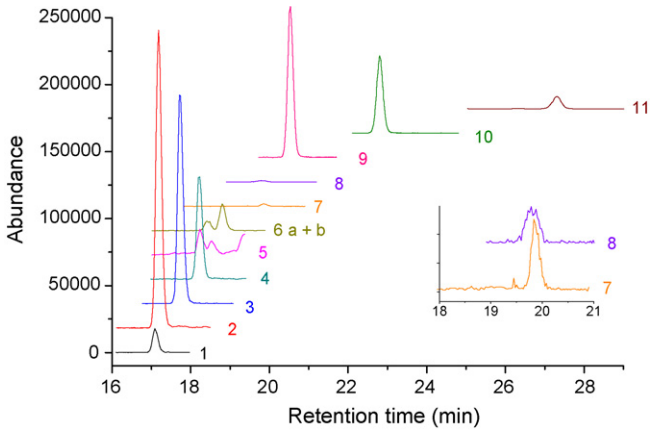

Fig. 1. Overlay of HPLC–ESI$^+$-MS/MS MRM chromatograms (quantitation transitions, Table 2) of spiked Burley tobacco at a concentration of 0.25 × GRL. The sample was purified as described under subsection 2.2. The insert displays magnified chromatograms. Peak assignment: 1, metobromuron; 2, metalaxyl; 3, diphenamid; 4, clomazone; 5, ethofumesate; 6 dimethomorph; 7 diflubenzuron; 8, alachlor; 9, benalaxyl; 10, piperonyl butoxide; 11, methoprene.

After the Chem Elut elution the solvent has to be evaporated. This step is unproblematic, as the eluent could be evaporated at 30 °C under a flow of nitrogen within 20 min despite the relatively high boiling point of toluene. However, care must be

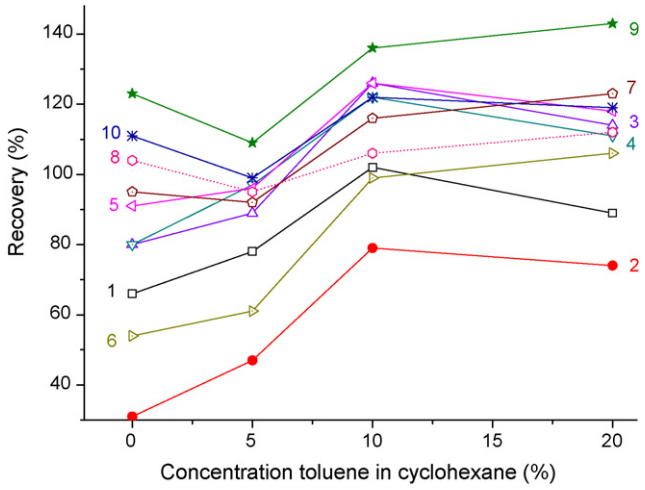

Fig. 2. Recovery of Chem Elut extraction with cyclohexane/toluene mixtures. Reference pesticides were extracted from methanol/water = 2/1 (v/v). Pesticide numbers see Fig. 1. Methoprene was not monitored in this experiment.

taken to keep evaporation as gentle as possible to reduce losses of methoprene.

As a rather nonpolar elution solvent is used, polar pesticides cannot be eluted from the extraction cartridge and exhibit low recovery rates. We failed to elute quantitatively more polar pesticides such as oxadixyl, carbendazim, and imidacloprid. Therefore, this elution step is limited to medium polar and nonpolar analytes. However, sample enrichment to 125 mg tobacco per ml is enabled. This is a 10-fold enrichment to a previously published method, where extracts with only 12.5 mg tobacco per ml were analysed after direct injection of the extracts [23].

3.2. Overall recovery

The overall recovery is a measure for the losses during sample preparation, chromatographic separation and detection. To calculate it, pesticide-free tobacco samples were spiked at four concentration levels and were analysed on three different days. Almost all overall recovery rates range between 70% and 110% which is in agreement with the EU criteria [27,28]. Only few recoveries are below 70%, see Table 3. However, recovery rates below 70% are very consistent and, therefore, acceptable [28]. These values clearly reveal that the use of matrix-matches calibration curves is mandatory for the analysis of tobaccos, as the recoveries are not equal in all tobacco types. Especially, Oriental tobacco exhibits lower recovery rates than the other tobacco types. These losses have to be attributed to losses during the Chem Elut extraction step and/or to signal suppression. The standard deviations of the overall recovery are low, indicating that the sample preparation step and subsequent LC–MS analysis are very reproducible.

Table 3
Overall recovery rates (%) of 11 pesticides in five tobacco types

Pesticide	Burley	Orient	Virginia	Snuff	Cigarette
Metobromuron	91 (4)	74 (2)	94 (4)	90 (4)	92 (1)
Metalaxyl	87 (4)	82 (1)	85 (5)	82 (4)	85 (1)
Diphenamid	105 (7)	83 (3)	109 (7)	105 (4)	108 (5)
Clomazone	89 (4)	57 (2)	96 (6)	91 (6)	89 (5)
Ethofumesate	94 (7)	54 (5)	100 (5)	94 (3)	93 (6)
Dimethomorph	93 (3)	79 (3)	93 (5)	90 (1)	95 (4)
Diflubenzuron	81 (11)	54 (3)	98 (3)	98 (2)	91 (7)
Alachlor	63 (6)	37 (3)	83 (3)	82 (3)	74 (2)
Benalaxyl	96 (5)	64 (3)	112 (6)	105 (5)	107 (7)
Piperonyl butoxide	92 (9)	52 (2)	99 (3)	91 (3)	85 (4)
Methoprene	98 (5)	88 (4)	91 (6)	99 (3)	92 (4)

Mean values of three determinations on three different days, standard deviations in brackets.

3.3. Confirmation of positive results

To meet the current requirement for unambiguous identification of organic residues [27], we used two different transitions in two consecutive HPLC runs to earn enough identification points. The relative ion intensities of the pesticides in the five tobacco matrices are presented as mean values in Table 2. Their low standard deviations reveal that the relative intensities are very similar in the five tobacco matrices. Theses values correspond also to those of reference standard solutions. Therefore, these mean values can be used as basis for the calculation of the maximum permitted tolerances [27,28] for confirmation of residues in all tobacco matrices investigated.

3.4. Trueness and precision

As no certified reference material was available, the trueness of the method recovery was determined by using two different approaches: first, the recovery was determined by experiments using fortified blank tobaccos [27]. The interday accuracy of the method was determined by analysing pesticide-free tobacco samples spiked at three different concentration levels (1.5 × GRL, 0.75 × GRL and 0.25 × GRL) on three different days. The calibration curves of all pesticide are linear from 0.2 × GRL to 2 × GRL with a coefficient of correlation >0.999 in all tobacco matrices investigated. Typical accuracy data of 11 pesticides spiked into pesticide-free Oriental tobacco are presented in Table 4. Although Oriental tobacco is the most

Table 4
The interday accuracy of the method (in %) for the determination of 11 pesticides in Oriental tobacco on at three concentration levels on three different days

Pesticide	Spike level (×GRL)		
	1.5	0.75	0.25
Metobromuron	109 (6)	106 (3)	101 (5)
Metalaxyl	112 (17)	112 (8)	104 (5)
Diphenamid	107 (4)	103 (4)	105 (2)
Clomazone	106 (6)	100 (6)	102 (5)
Ethofumesate	101 (5)	95 (2)	105 (11)
Dimethomorph	109 (9)	106 (6)	107 (1)
Diflubenzuron	105 (3)	98 (2)	102 (11)
Alachlor	107 (9)	104 (4)	111 (6)
Benalaxyl	107 (4)	102 (3)	106 (3)
Piperonyl butoxide	105 (7)	102 (5)	105 (0)
Methoprene	109 (9)	104 (10)	104 (3)

Precision as standard deviation in brackets.

Table 5
Limits of quantification (LOQ in $\mu g\,g^{-1}$) of the method for 11 pesticides in five tobacco types

Pesticide	Burley	Orient	Virginia	Snuff	Cigarette
Metobromuron	0.025	0.05	0.025	0.025	0.025
Metalaxyl	0.04	0.04	0.02	0.02	0.04
Diphenamid	0.013	0.025	0.025	0.025	0.013
Clomazone	0.025	0.05	0.025	0.025	0.02
Ethofumesate	0.75	1.0	0.2	0.1	0.5
Dimethomorph	0.1	0.2	0.05	0.05	0.1
Diflubenzuron	0.02	0.075	0.02	0.02	0.05
Alachlor	0.05	0.1	0.02	0.02	0.05
Benalaxyl	0.02	0.04	0.02	0.02	0.04
Piperonyl butoxide	0.02	0.1	0.01	0.02	0.02
Methoprene	0.05	0.2	0.1	0.1	0.1

problematic matrix regarding overall recovery and LOQs in comparison to the other tobaccos (see Tables 3 and 5), very accurate data were obtained. The interday trueness and precision data of the other tobacco matrices were in the same range as of Oriental tobacco presented in Table 4. Obviously, the use of matrix-matched standards provided very accurate data. Although some spike concentrations are below the LOQ of the method (see Table 5), accurate quantitation is possible for all pesticides, as the quantitation transition is frequently more sensitive than the confirmation transition. However, confirmation of the identity might not be carried out at those concentration levels.

A tobacco sample from a proficiency test was analysed as a second approach for the determination of the trueness of this method. Virginia tobacco was spiked with 12 unknown pesticides by FAPAS (Central Science Laboratory, Sand Hutton, UK) and was sent to 29 participating laboratories of the CORESTA Sub-group on Pesticide Residues. We found only metalaxyl in that sample, see chromatograms in Fig. 3. A 100-fold magnified abundance is presented for a better visual inspection of all MRM transitions. A concentration of $0.93\,\mu g\,g^{-1}$ was found for metalaxyl, which is very close to the spiking level

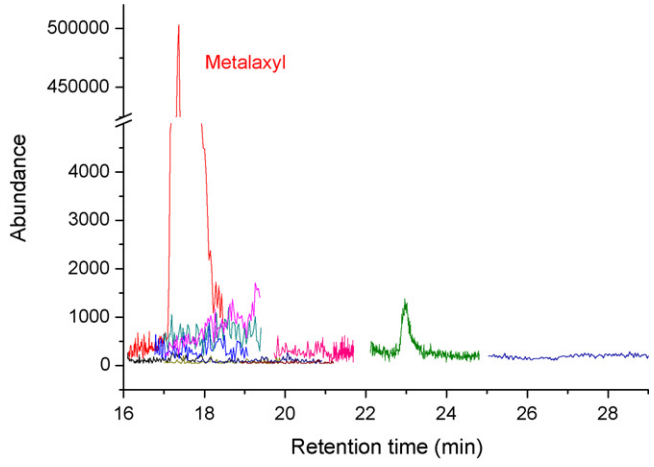

Fig. 3. Overlay of HPLC–ESI$^+$-MS/MS MRM chromatograms (quantitation transitions, Table 2) of tobacco spiked with 12 pesticides from a proficiency test.

of $1.0\,\mu g\,g^{-1}$ demonstrating the trueness of the method. The relative ion intensity of metalaxyl was 61% in the sample and 72% in spiked tobacco samples (see Table 2). This deviation is within the maximum permitted tolerances [27,28] confirming the identity of metalaxyl. FAPAS spiked that sample also with chlorothalonil, cypermethrin, deltamethrin, alpha- and beta-endosulfan, endosulfan sulfate, flumetralin, imidacloprid, methamidophos, metalaxyl, pendimethalin and profenofos at concentrations between 0.2 and $2.0\,\mu g\,g^{-1}$. Those pesticides were not detected by our method indicating that no false positive results were obtained.

3.5. Limit of quantification (LOQ)

The LOQ is given as determined by a signal-to-noise ratio of 10. It was estimated by analysing spiked pesticide-free tobacco samples at concentrations of 0.2 × GRL, 0.05 × GRL and 0.01 × GRL. The LOQ of the method is the LOQ of the confirmation transition, which is frequently much more insensitive than the quantification transition, especially for piperonyl butoxide. The method provides LOQs for all pesticides which are at or below the GRL [1], see Table 5. The most problematic matrix is Oriental tobacco where coeluting matrix compounds deteriorate the LOQs of the confirmation transitions of ethofumesate and piperonyl butoxide.

4. Conclusions

A stringent sample purification step was used to eliminate matrix effects in LC–MS. Partition of methanolic extracts of tobacco on Chem Elut extraction cartridges and subsequent selective elution with a nonpolar solvent mixture (cyclohexane/toluene) provide clean elutes. The purification step is very fast enabling high throughput analysis. All 11 pesticides can be quantified at or below the GRL defined by the CORESTA [1]. The overall recoveries range between 35% and 110%, whereas recoveries below 70% are very consistent and, therefore, acceptable [28]. The accuracy of the method ranges between 80% and 110% when using matrix-matched calibration. The calibration curves are linear in the range from 0.2 × GRL to 2 × GRL with a correlation coefficient >0.999. The method meets the current requirements for unambiguous identification of organic residues proposed by the European Community by monitoring two transitions and their relative ion intensity within maximum permitted tolerances [27]. In ongoing studies, the Chem Elut extraction step will be evaluated for the purification of other pesticides on tobacco, mainly the less polar organophosphorus pesticides.

References

[1] Cooperation Centre for Scientific Research Relative to Tobacco, Guide No. 1: The concept and implementation of agrochemical guidance residue levels, 2003. http://www.coresta.org/Guides/Guide-No1-GRLs.pdf.
[2] L. Alder, K. Greulich, G. Kempe, B. Vieth, Mass Spectrom. Rev. 25 (2006) 838.
[3] D. Ortelli, P. Edder, C. Corvi, Anal. Chim. Acta 520 (2004) 33.
[4] C.L. Hetherton, M.D. Sykes, R.J. Fussell, D.M. Goodall, Rapid Commun. Mass Spectrom. 18 (2004) 2443.

[5] J. Klein, L. Alder, J. AOAC Int. 86 (2003) 1015.
[6] J. Zrostlíková, J. Hajšlová, T. Kovalczuk, R. Štěpán, J. Poustka, J. AOAC Int. 86 (2003) 612.
[7] I.R. Pizzutti, A. de Kok, R. Zanella, M.B. Adaime, M. Hiemstra, C. Wickert, O.D. Prestes, J. Chromatogr. A 1142 (2007) 123.
[8] K.A. Barnes, R.J. Fussell, J.R. Startin, M.K. Pegg, S.A. Thorpe, S.L. Reynolds, Rapid Commun. Mass Spectrom. 11 (1997) 117.
[9] A. Garrido Frenich, J.L. Martínez Vidal, T. López López, S. Cortés Aguado, I. Martínez Salvador, J. Chromatogr. A 1048 (2004) 199.
[10] F. Hernández, O.J. Pozo, J.V. Sancho, L. Bijlsma, M. Barreda, E. Pitarch, J. Chromatogr. A 1109 (2006) 242.
[11] A. Belmonte Vega, A. Garrido Frenich, J.L. Martínez Vidal, Anal. Chim. Acta 538 (2005) 117.
[12] H. Bagheri, E.R. Brouwer, R.T. Ghijsen, U.A.T. Brinkman, J. Chromatogr. 647 (1993) 121.
[13] P.G.M. Kienhuis, J. Chromatogr. 647 (1993) 39.
[14] J. Slobodník, A.C. Hogenboom, J.J. Vreuls, J.A. Rontree, B.L.M. van Baar, W.M.A. Niessen, U.A.T. Brinkman, J. Chromatogr. A 741 (1996) 59.
[15] M. Mezcua, A. Agüera, J.L. Lliberia, M.A. Cortés, B. Bagó, A.R. Fernández-Alba, J. Chromatogr. A 1109 (2006) 222.
[16] C. Molina, P. Grasso, E. Benfenati, D. Barceló, Int. J. Environ. Anal. Chem. 65 (1996) 69.
[17] L.V. Podhorniak, F.J. Schenck, A. Krynitsky, F. Griffith Jr., J. AOAC Int. 87 (2004) 1237.
[18] P. Caboni, G. Sarais, A. Angioni, V.L. Garau, P. Cabras, J. Agric. Food Chem. 53 (2005) 8644.
[19] P.A. Aronov, K. Dettmer, J.A. Christiansen, A.J. Cornel, B.D. Hammock, J. Agric. Food Chem. 53 (2005) 3306.
[20] J. Haib, I. Hofer, J.M. Renaud, J. Chromatogr. A 1020 (2003) 173.
[21] S.S. Yang, Chromatographia 33 (1992) 309.
[22] H. Liu, Y. Dang, S. Zhang, H. Liu, L. Qu, X. Liao, Y. Zhao, Y. Wu, Ann. Chim. 95 (2005) 369.
[23] B. Mayer-Helm, L. Hofbauer, J. Müller, Rapid Commun. Mass Spectrom. 20 (2006) 529.
[24] W. Wittekindt, Beitr. Tabakforsch. Int. 13 (1986) 271.
[25] I. Wahlberg, T. Ringberger, in: D.L. Davis, M.T. Nielsen (Eds.), Tobacco Production, Chemistry and Technology, Blackwell Science, Oxford, 1999, pp. 452–460.
[26] J.M. Green, Anal. Chem. 68 (1996) 305A.
[27] European Communities, Commission decision 2002/657/EC, Off. J. Eur. Comm. L221 (2002) 8.
[28] European Commission, Quality control procedures for pesticide residues analysis, Document No. SANCO/10232/2006, Brussels, 2006.

Available online at www.sciencedirect.com
ScienceDirect
Talanta 74 (2008) 1527–1533
Talanta
www.elsevier.com/locate/talanta

Soil and sediment sample analysis for the sequential determination of natural and anthropogenic radionuclides

H. Michel *, D. Levent, V. Barci, G. Barci-Funel, C. Hurel

Laboratoire de Radiochimie, Sciences Analytiques et Environnement (LRSAE), Université de Nice Sophia-Antipolis, 06108 Nice Cedex, France

Received 7 June 2007; received in revised form 11 September 2007; accepted 28 September 2007
Available online 2 October 2007

Abstract

A new sequential method for the determination of both natural (U, Th) and anthropogenic (Sr, Cs, Pu, Am) radionuclides has been developed for application to soil and sediment samples. The procedure was optimised using a reference sediment (IAEA-368) and reference soils (IAEA-375 and IAEA-326). Reference materials were first digested using acids (leaching), 'total' acids on hot plate, and acids in microwave in order to compare the different digestion technique. Then, the separation and purification were made by anion exchange resin and selective extraction chromatography: transuranic (TRU) and strontium (SR) resins. Natural and anthropogenic alpha radionuclides were separated by uranium and tetravalent actinide (UTEVA) resin, considering different acid elution medium. Finally, alpha and gamma semiconductor spectrometer and liquid scintillation spectrometer were used to measure radionuclide activities. The results obtained for strontium-90, cesium-137, thorium-232, uranium-238, plutonium-239+240 and americium-241 isotopes by the proposed method for the reference materials provided excellent agreement with the recommended values and good chemical recoveries. Plutonium isotopes in alpha spectrometry planchet deposits could be also analysed by ICPMS.
© 2007 Elsevier B.V. All rights reserved.

Keywords: Natural radionuclides; Anthropogenic radionuclides; Soil; Sediment; Sequential radiochemical procedure; Microwave dissolution

1. Introduction

In environment sciences, radioelements are generally described on the basis of their natural (uranium and thorium) or anthropogenic origin (strontium, cesium, plutonium and americium).

Uranium and thorium are mainly considered in geochemistry (sediment chronology, sedimentation rate, erosion coefficient), whereas plutonium, americium, cesium and strontium are studied in radioecology to understand, and model their migrations and transfers in different ecosystems. In general, environmental sampling like sediments or soils is difficult and expensive and only a very small quantity of material is obtained. For this reason, it is very interesting to analyse as many radionuclides as possible from a single sample. In that way, numerous methods have been proposed for the determination of uranium, thorium, plutonium, americium, cesium and strontium in environmental samples [1–16] but few methods devoted to the simultaneous analysis of all these elements exist [17–21]. In previous works, the Laboratoire de Radiochimie, Sciences Analytiques et Environnement (LRSAE) has elaborated methods to analyse respectively (i) natural elements [2] and (ii) anthropogenic elements [1] from soil and sediment samples. The aim of this paper is to propose a highly efficient sequential method able to separate, from one same sample, both natural and anthropogenic radionuclides especially americium, plutonium, cesium, strontium, thorium and uranium. For this, ion exchange resin and extraction chromatography resins from EiChroM Inc. were used. The uranium and tetravalent actinide (UTEVA) resin was particularly studied to separate the americium–plutonium fraction to the uranium–thorium fraction. This resin has the specificity to fix actinides with oxidation states ≥IV and to have a low affinity for actinides and elements with oxidation states ≤III. Then, by changing the oxidation state of some radionuclides, one could expect that the chemical separation by UTEVA, at the beginning of the new procedure, allows the simultaneous extraction of natural and anthropogenic radionuclides. Three reference materials (two soils and one sediment) from the International Atomic Energy Agency (IAEA) were considered in this study to elaborate the extraction protocol. Before using the UTEVA resin, the

* Corresponding author. Tel.: +33 4 92 07 63 65; fax: +33 4 92 07 63 64.
E-mail address: hmichel@unice.fr (H. Michel).

0039-9140/$ – see front matter © 2007 Elsevier B.V. All rights reserved.
doi:10.1016/j.talanta.2007.09.030

reference samples were mineralised following three different protocols in order to check the solubilisation efficiency.

2. Experimental

2.1. Reference materials

Three representative IAEA reference materials were chosen for this study [22].

IAEA-368 is Pacific Ocean sediment. It was obtained from the Service Mixte de Sécurité Radiologique of the Commissariat à l'Energie Atomique (France) and was collected in the Pacific Ocean at Mururoa Atoll, a former French nuclear weapons testing site. The sediment was mainly composed of a mixture of carbonates species.

IAEA-375 is a soil (top soil to a depth of 20 cm) obtained from the "Staryi Viskov" collective farm in Novozybkov, Brjansk, Russia in July 1990. The material was air dried and milled to give a grain size less than 0.3 mm by the Brjansk Centre for Agricultural Radiology and Chemistry and dispatched for further processing to the Agency's Laboratories at Seibersdorf in November 1990.

IEAE-326 is a black soil collected from the Kursk region of Russia. The sample is originated from the surface layer with a depth ranging from 0 to 20 cm and was collected and processed on behalf of the Agency by the Khlopin Radium Institute, St. Petersburg, Russia in 1994.

These materials were γ-sterilised to ensure long-term stability of the material by inhibiting microbial action.

2.2. Reagents

All reagents were ACS grade: 65% HNO_3, 37% HCl, 45% HF, H_3BO_3, 25% NH_3.

Dilutions were made with deionised water.

2.3. Dissolution of the solid sample

A suitable mass of a dry solid sample was weighed into a porcelain crucible and ignited at 600 °C in an electric furnace during 24 h. Known amounts of radiochemical yield determinants: ^{242}Pu, ^{243}Am, ^{232}U, ^{229}Th and stable strontium carriers were added.

Three dissolution techniques were tested: acids (leaching), 'total' acids on hot plate and acids in microwave [17,23,24]. For each one, 5 g of soil or sediment samples was considered.

For the acids attack technique, the radionuclides were leached out from the matrices by a mixture of nitric and hydrochloric concentrate acids (1:1) under heating and stirring for 4 h. This step was repeated once and the two supernatants were combined.

For the 'total' acids attack, samples were digested and evaporated successively twice with 50 mL concentrate hydrofluoric acids, three times with 50 mL concentrate nitric acid and with 50 mL concentrate hydrochloric acid + 2g of boric acid.

For the microwave digestion system (Milestone Ethos Pro), samples were introduced in Teflon tube and treated in two consecutive steps. In the first step, the sample was treated with concentrated hydrofluoric acid (15 mL). In the second step, insoluble fluorides were dissolved with nitric acid (15 mL) saturated with boric acid. The temperature program of the microwave oven in the two steps is 10 min from ambient temperature to 250 °C and 20 min at 250 °C.

For the three methods, the solutions obtained were filtered through a 0.45 μm membrane before the pre-concentration of radionuclides by Ca-oxalate precipitation.

2.4. Procedures for separation

2.4.1. Gamma spectrometry sample preparation

^{137}Cs measurements were carried out by standard γ-spectrometry using methods described in Refs. [25–27]. The samples were oven-dried at 100 °C, homogenized and packed into plastic containers and counted on a coaxial HPGe detector (EG&G ORTEC) of 30% relative efficiency with an energy resolution full width at half maximum (FWHM) of 1.9 keV at 1.33 MeV. The efficiency of detector was determined using standard sources with the same geometrical configuration as the samples being measured. The detector is placed inside a 5 cm thick lead castle with a 2 mm thick copper lining reduced background radiation. The spectra were collected using a multichannel buffer analyzer (Spectrum Master ORTEC 919).

2.4.2. Pre-concentration of radionuclides by Ca-oxalate precipitation

Soils contain a high amount of natural iron. To normalize the procedure, iron was eliminated from the sample by using a Ca-oxalate precipitation. Aluminum, titanium, chromium, manganese, nickel and phosphate ions were also eliminated.

The Ca-oxalate precipitate was formed by adding calcium nitrate, oxalic acid and concentrate ammonia at pH 6. Americium, plutonium, strontium, uranium and thorium were coprecipitated with Ca-oxalate, while iron was complexed in solution with oxalate ions. The precipitate was finally dissolved with concentrate HNO_3.

2.4.3. Separation of strontium from actinide fractions [1]

The aim was to separate strontium from americium, plutonium, uranium and thorium.

A known amount of iron was added to the solution and iron hydroxide coprecipitation at pH 8 with concentrate ammoniac was obtained. The elements with oxidation state superior to III (Pu, Am, Th and U) were sorbed to the precipitate and element with oxidation states I and II (Sr) was left in solution.

2.4.4. Purification of strontium by Sr-spec® resin [1]

The pH of the supernatant was adjusted to 8 with ammonia and ammonium carbonate buffer. Strontium was precipitate (as Sr carbonate) by adding a saturated solution of Na_2CO_3. Monovalent stayed in the supernatant. The precipitate was dissolved with concentrate nitric acid, evaporated to dryness and dissolved in 3 M HNO_3. The solution was passed through Eichrom Sr-spec® resin pre-conditioned with 3 M HNO_3. Sr was fixed to the resin and Y and Ca were eliminated by 3 M HNO_3 washing solutions. It is very important to eliminate all Ca traces to have

a good quantitative gravimetric yield for the strontium separation at the end of the procedure. The strontium was eluted with deionised water. To estimate the Sr yield, an oxalic precipitation was made with concentrate ammonia (pH 9). The solid residue was weighted to determine the gravimetric yield of the strontium radiochemical separation. The precipitate was dissolved in 1 M nitric acid and scintillation cocktail (Packard Instagel) was added to determine the ^{90}Sr activity concentration by liquid scintillation spectrometer. The determination of the activity concentration of ^{90}Sr was performed using the double energetic windows method. The first energetic window (window A) includes the entire ^{90}Sr spectrum and the low energy region of ^{90}Y spectrum. The window B includes the high-energy region of ^{90}Y spectrum. Strontium-90 activity is determined by subtracting the contribution of ^{90}Y in region A from total counting rate in this region. The detection was made with liquid scintillation detector Packard 2000 CA.

2.4.5. Separation of americium and plutonium from uranium and thorium by UTEVA resin

The iron precipitate formed to separate strontium from actinide fraction was dissolved in 50 mL of 2.5 M nitric acid and 2–4 mL of 25% hydrazinium hydroxide were added. The solution was passed through the UTEVA resin (10 mm diameter and 80 mm long) pre-conditioned with 50 mL of 2.5 M HNO_3. The column was washed with 100 mL of 2.5 M HNO_3, plutonium and americium pass through the column while uranium and thorium are fixed on the resin. The effluents were kept for americium and plutonium separation. Hundred millilitre of 1 M HCl was passed to elute uranium and thorium and this solution was kept for uranium and thorium separation.

2.4.6. Separation of plutonium from americium by anion exchange resin [1]

The Pu–Am fraction is evaporated and the residue is diluted in 8 M HNO_3 and $NaNO_2$. Column is prepared from Bio Rad AG® 1-X8 (mesh 100–200) resin in the chloride form (inner diameter: 10 mm, resin bed length: 100 mm) pre-conditioned with 8 M HNO_3. Sample solution is loaded into the column followed by washing with 8 M HNO_3. Am passed through the column and Pu is fixed. The combined effluent is used for the purification of Am. Column is washed with 10 M HCl to desorb trace of Th and Pu is stripped with 0.1 M NH_4I–10 M HCl solution. It is possible also to elute neptunium at this step with 4.5 M HCl–0.1 M HF solution. The Pu strip solution is evaporated to dryness with 65% HNO_3 and some drops of H_2O_2 destroys ammonium iodide.

2.4.7. Purification of americium [1]

The combined effluent from the anion exchange column is evaporated to dryness and dissolved in 1 M HNO_3 with Ca and oxalic acid to coprecipitate Am at pH 6 with ammonia. The oxalate precipitate is destroyed with 65% HNO_3. The solution is converted in chloride with 10 M HCl. A mixed anion–cation exchange columns are prepared from Bio Rad AG® 1-X8 (mesh 100–200) resin and Bio Rad AG® 50w-X8 (mesh 100–200) resin pre-conditioned with 10 M HCl. Sample solutions are loaded into the column followed by washes with 10 M HCl. The effluents are evaporated to dryness and taken up in 65% HNO_3, then in 2 M HNO_3. The next column is prepared from TRU-Spec® resin and pre-conditioned with 2 M HNO_3. Samples are loaded to the column followed by washes with 2 M HNO_3, 9 M HCl + 25% $NaNO_2$ and 9 M HCl. Finally, Am is stripped with 4 M HCl solution. The Am solution is evaporated to dryness and converted to nitrate with 65% HNO_3. The residue is taken up with 1 M HNO_3–93% CH_3OH and passed on Bio Rad AG® 1 × 4 (mesh 100–200) resin pre-conditioned with 1 M HNO_3–93% methanol. The column is washed with 1 M HNO_3–93% methanol, 0.1 M HCl–0.5 M NH_4SCN–80% methanol and 1% HNO_3–93% methanol. Americium is stripped with 1.5 M HCl–86% methanol solution.

2.4.8. Separation of thorium from uranium by anion exchange resin [2]

The U–Th fraction is evaporated and the residue is diluted in 8 M HCl and $NaNO_2$. Column is prepared from Bio Rad AG® 1-X8 (mesh 100–200) resin in the chloride form (inner diameter: 10 mm, resin bed length: 100 mm) pre-conditioned with 8 M HCl. Sample solution is loaded into the column followed by washing with 8 M HCl. Th passed through the column and U is fixed. U is stripped with 1 M HCl solution.

2.4.9. Purification of thorium [2]

The solution was evaporated to dryness and dissolved in 8 M HNO_3. Column is prepared from Bio Rad AG® 1-X8 (mesh 100–200) resin in the chloride form (inner diameter: 10 mm, resin bed length: 100 mm) pre-conditioned with 8 M HNO_3. Sample solution is loaded into the column followed by washing with 8 M HNO_3. Alkaline metals and rare earths trace passed through the column and Th is fixed. Ten molar HCl solution strip Th from the column.

2.4.10. Purification of uranium [2]

The solution was evaporated to dryness and the residue was re-dissolved in 8 M HCl. The aqueous solution was stirred in a separatory funnel with di-isopropylether to extract iron trace. After two or three extractions the aqueous phase containing uranium was evaporated to dryness with 65% HNO_3.

2.4.11. Source preparation for alpha-spectrometry [1,2]

Americium, plutonium, uranium and thorium are analysed by alpha spectrometry. After the separation step, the solution is evaporated to dryness after addition of 5% $NaHSO_4$ and evaporating three times with 65% HNO_3. Three hundred microlitres of H_2SO_4, 4 mL deionised water and four drops of thymol blue are added to the solution. The pH is adjusted to 2.1–2.5 with ammonia. The solution is transferred into the electrodeposition cell and the radioelement electroplated with a current of 1 A on a stainless steel disc during 1 h. Before the end of the electrodeposition, 1 mL ammonia is added. After removal the disc is washed with 1% ammonia and acetone, and gently dries before alpha counting.

Alpha emissions from discs were analysed with Dual Alpha Spectrometers EG&G Ortec 576A equipped with boron implanted silicon detectors of active area: 450 mm^2 and alpha

Table 1
^{238}U and ^{232}Th activities (Bq kg^{-1}) obtained after three dissolution methods and IAEA reference values (Bq kg^{-1})

		IAEA reference values	Acids	'Total' acids	Acids in microwave
IAEA 368	^{238}U (Bq kg^{-1})	31	14	23	29
	^{232}Th (Bq kg^{-1})	–	–	–	–
IAEA 375	^{238}U (Bq kg^{-1})	24.4	12.1	19.5	21.9
	^{232}Th (Bq kg^{-1})	20.5	9.5	15.9	19.4
IAEA 326	^{238}U (Bq kg^{-1})	29.4	13.8	22.1	27.6
	^{232}Th (Bq kg^{-1})	39.4	18.9	31.1	36.6

resolution (FWHM) 20 keV at 5.47 MeV. Pulses were analysed with a multichannel buffer analyzer (Spectrum Master Ortec 919).

3. Results and discussion

This section reports the comparison results obtained for the three dissolution methods tested. The new separation step with UTEVA resin is described and ^{90}Sr, ^{137}Cs, ^{232}Th, ^{238}U, $^{239+240}Pu$ and ^{241}Am activities obtained with the sequential procedure, in the IAEA reference materials, and chemical recovery are presented and discussed. An additional analysis by ICPMS for plutonium isotopes is presented to show the complementarities of the alpha and mass spectrometry.

3.1. Comparison of microwave dissolution method with traditional total attack and leaching method

For the anthropogenic radionuclides (Pu, Am and Sr) the three methods give the same results and the activity concentrations are in good agreement with the reference values. The recoveries for this step were between 94% and 98%. The simple acids method (leaching) for anthropogenic radionuclide determination has been adopted by a number of laboratories [28].

However acids method is not suitable for naturally occurring uranium and thorium. Table 1 shows that acids in microwave dissolution is the best procedure to solubilise the radionuclides. The chemical yields for U and Th for acids, 'total' acids on hot plate and acids in microwave are 45–50%, 75–80% and 90–95%, respectively.

The best method to extract anthropogenic and natural radionuclides from the matrices tested is the microwave digestion because the elements are totally leached into solution and this method reduces preparation time and the volume of the acids used.

3.2. UTEVA resin used in Am, Pu and U, Th separation step

This step aims at separating anthropogenic radioelements from natural radioelements (Figs. 1 and 2). In the environment, these two categories of radioelements frequently show concentration activities very different according to the type of sample material (uranium-bearing or not uranium-bearing) and to the soil or sediment depth. Moreover the LRSAE could use the anthropogenic separation method and the natural separation method already developed by the laboratory.

For this new separation step, UTEVA resin was selected. Figs. 3 and 4 present the UTEVA partition coefficient in HCl and HNO_3 medium for actinides.

This resin has the specificity to fix actinides with oxidation states ≥IV and to have a low affinity for actinides and elements with oxidation states ≤III. The idea is to reduce plutonium in oxidation state III. Thus Pu should not be retained on the resin as well as americium, while uranium and thorium were strongly fixed. The plutonium reduction is made by monohydrate hydrazine in nitric acid.

The nitric acid concentration chosen to load the sample on UTEVA column is 2.5 M HNO_3. This concentration is the result of a compromise: when the HNO_3 concentration increases, the uranium and thorium Kd increases; but hydrazine is sensitive to oxidizing mediums like concentrated HNO_3. Pu, Am, U and Th solution in 2.5 M HNO_3 with hydrazine loaded on UTEVA resin should allowed U and Th sorption. Am and Pu should pass through the column. One molar HCl solution strip U and Th. $NaNO_2$ acid solution oxidizes Pu(III) in Pu(IV).

3.3. Comparison of sequential procedure results with the IAEA reference materials values

Table 2 presents the strontium-90, cesium-137, thorium-232, uranium238, plutonium-239+240 and americium-241 specific activities obtained in the three IAEA reference materials after the sequential procedure performed. The results obtained are all

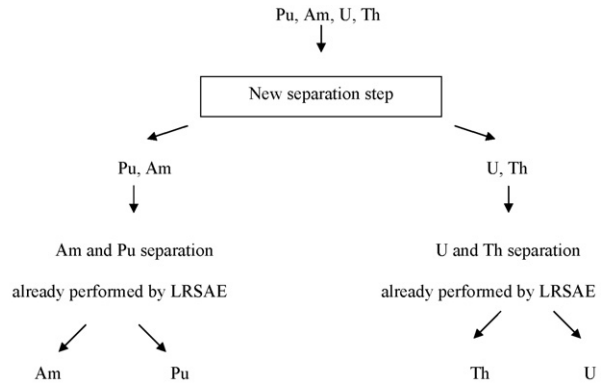

Fig. 1. Strategic scheme for the Am, Pu and U, Th separation step.

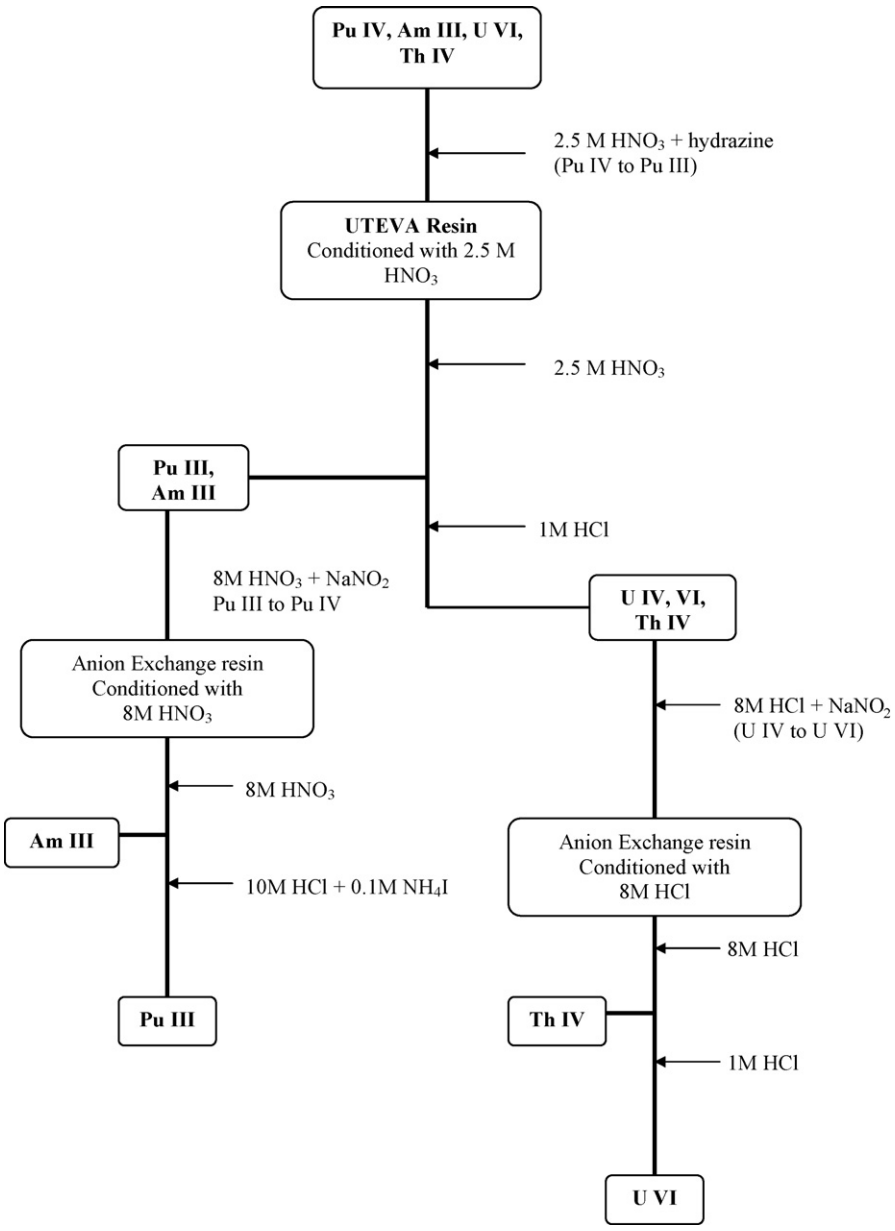

Fig. 2. Synoptic scheme for the radiochemical separation of Am, Pu, U and Th.

Table 2
^{90}Sr, ^{137}Cs, ^{232}Th, ^{238}U, $^{239+240}$Pu and ^{241}Am specific activities (Bq kg^{-1}) and chemical recovery (%) obtained with the sequential radiochemical procedure in the IAEA reference materials

IAEA reference materials	^{90}Sr	^{137}Cs	^{232}Th	^{238}U	$^{239+240}$Pu	^{241}Am
IAEA-368	4.8 ± 0.6	0.32 ± 0.04	–	28 ± 2	32 ± 2	1.3 ± 0.1
Bq kg^{-1}	0.45–6.90[a]	0.20–0.44[a]		25.0–33.0[a]	29.0–34.0[a]	1.2–1.5[a]
IAEA-375	103 ± 9	5250 ± 200	22 ± 1	19 ± 1	0.32 ± 0.02	0.12 ± 0.01
Bq kg^{-1}	101–114[a]	5200–5360[a]	19.2–21.9[a]	19.0–29.8[a]	0.26–0.34[a]	0.11–0.15[a]
IAEA-326	10 ± 1	–	39 ± 3	31 ± 2	0.51 ± 0.04	0.21 ± 0.02
Bq kg^{-1}	9.7–10.7[a]		37.6–41.2[a]	28.1–30.7[a]	0.48–0.52[a]	0.16–0.22[a]
Chemical recovery (%)	50–75	[b]	85–95	80–90	75–95	65–85

[a] Confidence interval given by IAEA.
[b] No chemical step.

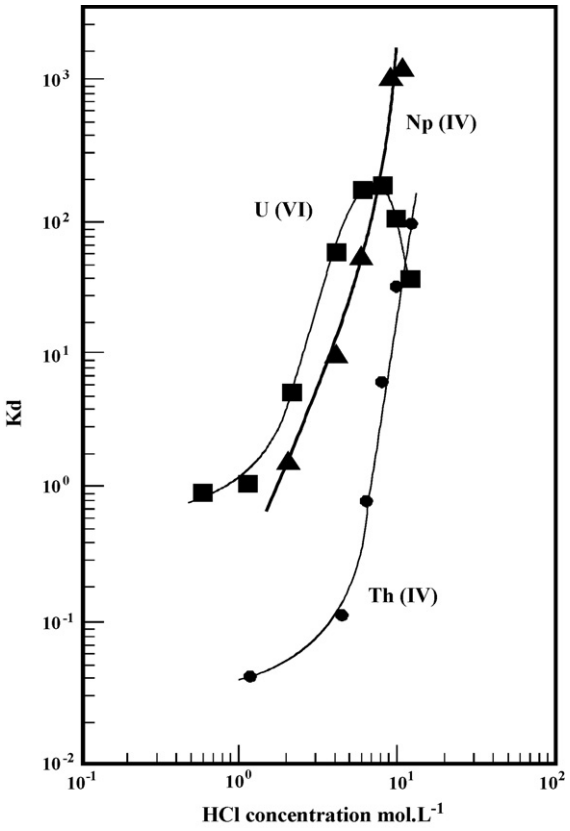

Fig. 3. UTEVA Kd vs. HCl concentration (mol L^{-1}) [29,30].

in good agreement with the IAEA confidence interval. No results are given by IAEA for ^{232}Th in the reference material 368 and ^{137}Cs in the reference material 326.

Chemical recovery are for ^{90}Sr, ^{137}Cs, ^{232}Th, ^{238}U, $^{239+240}$Pu and ^{241}Am, respectively 50–75, 100, 85–95, 80–90, 75–95 and 65–85%. For ^{137}Cs, the result is obtained by gamma spectrometry and no chemical preparation is necessary, so a chemical recovery of 100% could be assumed. The lower recoveries are obtained for strontium and americium because our determination needs chemical purification step which generated additional losses. Moreover the strontium chemical recovery is obtained by a gravimetric method less powerful than traditional radiochemical yield determination.

The alpha spectra of thorium-232, uranium-238, plutonium-239+240 and americium-241 isotopes obtained have shown clear peaks and give a proof of the good selectivity to the procedure. For strontium-90 beta spectrum, the vial with scintillation cocktail is counted by gamma spectrometry to control any contamination.

3.4. Possibility of additional analyses by ICPMS for plutonium isotopes [31]

The activity ratio ^{238}Pu/$^{239+240}$Pu and the atom ratio ^{240}Pu/^{239}Pu could be significantly different in samples from the general environment indicating the usefulness of these ratios for identification and apportionment of the plutonium contamination source.

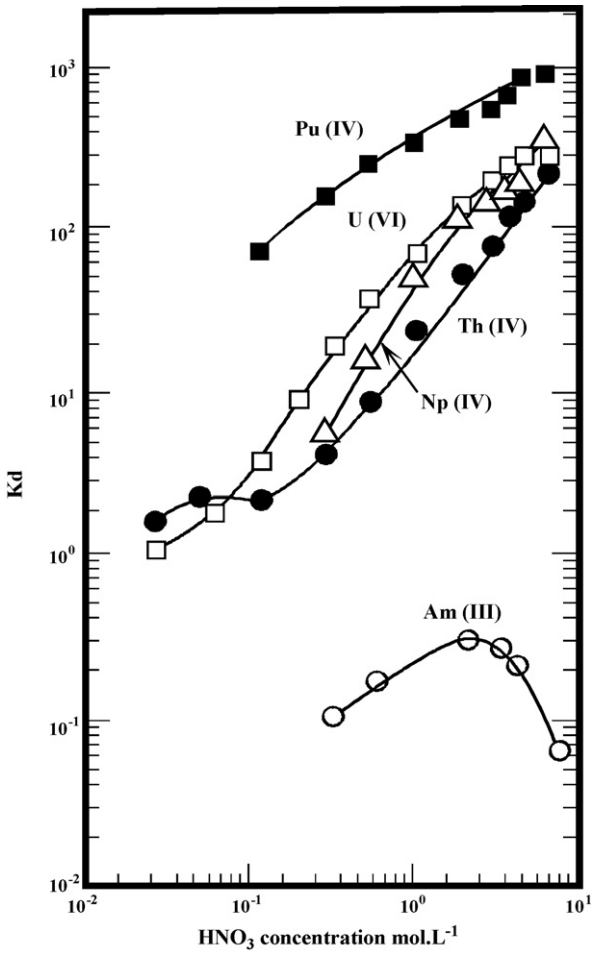

Fig. 4. UTEVA Kd vs. HNO_3 concentration (mol L^{-1}) [29,30].

^{239}Pu and ^{240}Pu cannot be readily distinguished since their α decay energies are unresolved. ICPMS can potentially provide rapid complementary determinations of $^{239+240}$Pu in α sources, with the added benefit of individual measurements of ^{239}Pu and ^{240}Pu. The methods are complementary; α spectrometry measures ^{238}Pu (inaccessible by ICPMS) and the activity ratio ^{238}Pu/$^{239+240}$Pu, and ICPMS measures the atom ratio ^{240}Pu/^{239}Pu.

The plutonium isotopes are dissolved from the deposit using 8 M HNO_3. In order to remove traces of ^{238}U from the planchet deposit solutions, a micro scale separation is performed using a commercially available plutonium selective resin (tetravalent actinide resin (TEVA) from EIChrom).

4. Conclusion

The worked out sequential radiochemical separation allows the simultaneous analysis by alpha, beta and gamma spectrometry of ^{137}Cs, ^{90}Sr, ^{232}Th, ^{238}U, $^{239+240}$Pu and ^{241}Am isotopes in soil and sediment samples. It is very interesting because generally the collected samples are in very small quantity, the time consuming by sample is long and the coast of chemical products is expensive.

Moreover this method will allow obtaining additional data for radioecological and geochemical studies. An additional measure by ICPMS of the plutonium isotopes can be made from alpha planchet deposits.

The measures made towards the reference values supplied by the IAEA are in good agreements and the chemical yields of the total separation for the different elements are superior to 50%. For the simultaneous measurement of the anthropogenic and natural radionuclides, this work confirms the literature to use a microwave total dissolution method.

References

[1] H. Michel, M. Schertz, G. Barci-Funel, G. Ardisson, J. Radioanal, Nucl. Chem. 258 (2003) 209.
[2] S. Rezzoug, G. Barci-Funel, J. Dalmasso, F. Fernex, H. Michel, G. Ardisson, J. Radioanal. Nucl. Chem. 256 (2003) 167.
[3] G.J. Ham, Sci. Total Environ. 173/174 (1995) 19.
[4] J. Moreno, N. Vajda, P.R. Danesi, J.J. Larosa, E. Zeiller, M. Sinojmeri, J. Radioanal, Nucl. Chem. 226 (1997) 279.
[5] E. Hrneceka, P. Steierb, A. Wallner, Appl. Radiat. Isot. 63 (2005) 633.
[6] J.J. La Rosa, J. Gastaud, L. Lagan, S.H. Lee, I. Levy-Palomo, P.P. Povinec, E. Wyse, J. Radioanal. Nucl. Chem. 263 (2005) 427.
[7] V.A. Ageyev, O. Odintsov, A.D. Sajeniouk, J. Radioanal. Nucl. Chem. 264 (2005) 337.
[8] H. Dulaiova, G. Kim, W.C. Burnett, E.P. Horwitz, Radioact. Radiochem. 12 (2001) 4.
[9] A.H. Thakkar, J. Radioanal. Nucl. Chem. 252 (2002) 215.
[10] J. Eikenberg, S. Bajo, I. Zumsteg, M. Ruethi, H. Beer, Radiat. Prot. Dosim. 97 (2001) 127.
[11] P. Spezzano, N. Silvestri, Stud. Environ. Sci. 34 (1988) 131.
[12] J.M. Godoy, D.C. Lauria, M. Luiza, D.P. Godoy, R.P. Cunha, J. Radioanal. Nucl. Chem. 182 (1994) 165.
[13] T. Prasada Rao, P. Metilda, J. Mary Gladis, Talanta 68 (2006) 1047.
[14] G. Kim, W.C. Burnett, E.P. Horwitz, Anal. Chem. 72 (2000) 4882.
[15] R.A. Boil, G.K. Schweitzer, R.W. Garber, J. Radioanal. Nucl. Chem. 220 (1997) 201.
[16] J.M. Oliveira, F.P. Carvalho, Czech. J. Phys. 56 (2006) 545.
[17] S.H. Lee, J.J. La Rosa, J. Gastaud, P.P. Povinec, J. Radioanal. Nucl. Chem. 263 (2005) 419.
[18] F. Sus, J. Krtil, Z. Malek, M. Beran, Nucleon 1 (1998) 13.
[19] W.C. Burnett, D.R. Corbett, M. Schultz, E.P. Horwitz, R. Chiarizia, M. Dietz, A. Thakkar, M. Fern, J. Radioanal. Nucl. Chem. 226 (1997) 121.
[20] S.H. Reboul, E.H. Borai, R.A. Fjeld, Bioanal. Chem. 374 (2002) 1096.
[21] E.P. Horwitz, M.L. Dietz, R. Chiarizia, H. Diamond, Anal. Chim. Acta 266 (1992) 25.
[22] Z. Radecki, IAEA Analytical Quality Control Services, Reference Materials Catalogue 2002–003, first ed., Seibersdorf, IAEA, Vienna, 2002, pp. 19–21.
[23] S.A. Mihai, J. Radioanal. Nucl. Chem. 266 (2005) 259.
[24] R. Garcia, B. Kahn, J. Radioanal. Nucl. Chem. 250 (2001) 85.
[25] G. Barci-Funel, J. Dalmasso, G. Ardisson, Sci. Total Environ. 70 (1988) 373.
[26] G. Barci-Funel, J. Dalmasso, G. Ardisson, J. Radioanal. Nucl. Chem. 156 (1992) 83.
[27] E. Holm, S. Ballestra, J.J. Lopez, A. Bulos, N.E. Whitehead, G. Barci-Funel, G. Ardisson, J. Radioanal. Nucl. Chem. 177 (1994) 51.
[28] M. Ristic, S. Degetto, T. Ast, C. Cantallupi, J. Environ. Radioact. 59 (2002) 179.
[29] E.P. Horwitz, R. Chiarizia, M.L. Dietz, H. Diamond, D.M. Nelson, Anal. Chim. Acta 266 (1992) 25.
[30] E.P. Horwitz, R. Chiarizia, M.L. Dietz, H. Diamond, D.M. Nelson, Anal. Chim. Acta 281 (1993) 361.
[31] H. Michel, M.E. Ketterer, G. Barci-Funel, J. Radioanal. Nucl. Chem. 273 (2007) 485.

Available online at www.sciencedirect.com
ScienceDirect
Talanta 74 (2008) 1608–1614
Talanta
www.elsevier.com/locate/talanta

A new simple sensitive differential pulse polarographic method for the determination of acrylamide in aqueous solution

Abdul Niaz [a,*], Sirajuddin [a], Afzal Shah [b], Muhammad Iqbal Bhanger [a], Munawar Saeed [a], Mohammad Khan Jamali [a], Mohammad Balal Arain [a]

[a] *National Center of Excellence in Analytical Chemistry, University of Sindh, Jamshoro, Sindh 76080, Pakistan*
[b] *Kohat University of Science and Technology, Kohat 26000, NWFP, Pakistan*

Received 13 August 2007; received in revised form 5 October 2007; accepted 5 October 2007
Available online 13 October 2007

Abstract

A new simple sensitive differential pulse polarographic (DPP) method was investigated for the determination of acrylamide (AA) directly in a neutral aqueous solution. The AA showed a well-defined and well-resolved peak in pure aqueous LiCl at −1.84 V in the potential range from −1.6 V to −1.97 V at nitrogen pressure of 0.5 kg cm^{-2}. Among the various electrolytes studied, the AA showed good DPP response in the presence of LiCl and tetra methyl ammonium iodide, while it showed poor response in the presence of tetra butyl ammonium hydroxide and tetra butyl ammonium bromide due to their strong adsorption on the surface of electrode which hindered its reduction. The effect of LiCl concentration, the cyclic voltammetric response and the drop time study showed that AA exhibited an irreversible adsorptive electrochemical behavior. The good electrochemical response in pure aqueous medium suggested that hydrogen bonding might be involved which may favor the electrode reaction. Under optimized conditions, the peak current was linear in the entire concentration range from 0.2 mg L^{-1} to 20 mg L^{-1} with the correlation coefficient of $R^2 = 0.9998$. The method showed good reproducible results with R.S.D. of 0.3% ($n = 16$). The detection limit (LOD) was 27 μg L^{-1}. The influence of various interfering agents was also studied. The method was applied successfully for the quantification of AA in water samples without any interference effect from alkali metals.
© 2007 Elsevier B.V. All rights reserved.

Keywords: Acrylamide; Differential pulse polarography; Aqueous solution; LiCl; Water samples

1. Introduction

Acrylamide is an important industrial organic compound which is used in a wide number of processes [1]. It is used in the production of polymers (polyacrylamide) and copolymers for various purposes. Polyacrylamide is mainly used for the purification of both drinking and waste water, where it acts as a flocculating agent. In paper industries it is used to enhance resistance to tearing. It has numerous applications in petroleum and textile industries. AA is also used as a grouting agent in concrete and in mineral processing [2,3].

It is used in the construction of dam foundations and tunnels. Besides its importance, it is also very much toxic and constitutes serious water pollution problems. Due to high solubility in water, AA is extremely mobile in aqueous environment. The main sources of water contamination result from the release of monomer residues from polyacrylamide used in water treatment, soil grouting and polymer industries, etc. It has been studied that heat, light and out-door environmental conditions promote deploymerization of polyacrylamide to AA [4]. The toxicity of AA have been stated already by the International Agency for Research on Cancer (IARC) that AA could be classified as "probably carcinogenic to humans" (group 2A) [5] and the World Health Organization (WHO) guideline value associated with a lifetime cancer risk in drinking water [6].

The US Environment Protection Agency (EPA) set the maximum contaminant level (MCL) for AA at zero and requires the water supplier to show that when AA is added to water, the

* Corresponding author: Tel.: +92 0221 771379; fax: +92 0221 771560.
E-mail addresses: niazchemist2k6@yahoo.com (A. Niaz), drsiraj03@hotmail.com (Sirajuddin), afzalnm@yahoo.com (A. Shah), dbhanger2000@yahoo.com (M.I. Bhanger), munwarsaeed@yahoo.com (M. Saeed), mkhanjamali@yahoo.com (M.K. Jamali), bilal_ku2004@yahoo.com (M.B. Arain).

0039-9140/$ – see front matter © 2007 Elsevier B.V. All rights reserved.
doi:10.1016/j.talanta.2007.10.010

amount of un-coagulated acrylamide is less than 0.5 $\mu g L^{-1}$ [7]. Due to its high toxic effects to humans and animals it is very much necessary to establish a simple, rapid, sensitive, highly selective analytical methodology for the direct quantification of AA in aqueous solution.

A variety of sensitive methods are available in the literature to analyze AA in aqueous solutions [8–14]. Most of these methods are based on the techniques such as HPLC–UV, GC–MS and LC–MS/MS. Derivatization of AA prior to analysis and large efforts involved in sample preparation come as disadvantages with the use of these techniques. The others major disadvantages of these methods are their high equipment costs and running costs. Recently, direct electrochemical detection following liquid chromatography has been proposed for the determination of AA in aqueous samples [15].

But in terms of simplicity, selectivity, relatively good sensitivity, without any derivatization, it carries very low running and equipments costs and is easily available in under developed areas, however, the electro analytical techniques, mainly DP polarography, are the most suitable techniques for the determination of AA in complicated matrices as compared to the other nonelectroanalytical techniques [16].

But unfortunately there is no sensitive polarograhic method available which could monitor AA directly at a trace level in aqueous solution [1], and till now. All the previously polarographic methods for the determination of AA in different matrices have been reported in nonaqueous or mix solvent system [17–25]. Among these methods the most efficient polarographic method till now has been reported by Betso and McLean to determine AA monomer in polyacrylamide containing 80/20 methanol/water [17]. They modified the polarographic method of McWilliams et al. [20] by using more advance instrumentation (differential pulse polarograph instead of the older direct-current instrument). By using this instrumentation the AA reduction peak became well-defined and well-resolved from the background. They lowered greatly the detection limit to less than 1 $mg L^{-1}$ (0.5) in relation to all previously reported polarographic methods for the determination of AA.

However, this method suffer from serious drawbacks for example this is not suitable to monitor AA directly in aqueous solution, less sensitive and at −2.0 V it suffer from major interferences mainly from the alkali metals cations. Therefore, a more sensitive and selective polarographic method is essential to determine AA directly in aqueous solution. To our best knowledge this is the first time that we have investigated a simple sensitive, selective polarographic method for the quantification of AA directly in aqueous solution.

2. Experimental

2.1. Reagents and solution

All reagents were of analytical grade. Acrylamide (electrophoresis grade) and LiCl were purchased from Merck Germany. Other reagents used in this study were also purchased from the same company. All solutions were prepared in double distilled water. A stock solution of 1000 $mg L^{-1}$ AA was prepared from which appropriate amount was taken for polarographic studies. Five molar LiCl solution was also prepared in a separate flask which was used as an electrolyte and carrier solution.

2.2. Apparatus

Polarographic experiments were performed by Metrohm polarographic analyzer (Switzerland) model 797 version 1.1 with a personal computer. A typical three electrode system equipped with a dropping mercury working electrode, a platinum counter electrode and Ag/AgCl/3 M KCl as a reference electrode. Nitrogen was used as an inert gas to purge the analyte solutions and to operate the mercury electrode. The optimum nitrogen gas pressure of 0.5 $kg cm^{-2}$ (0.49 bar) was used through out in this study. In the instrumental setup the voltage step time (drop time) automatically controlled the sweep rate. When the voltage time was made to increase the sweep rate decreased accordingly.

2.3. Procedures

2.3.1. Polarographic studies

A volume of 10 mL flask solution containing 5 $mg L^{-1}$ AA (50 $\mu g L^{-1}$ of 1000 $mg L^{-1}$ stock solution) in 0.5 M LiCl electrolyte (1 mL of 5 M LiCl) was transferred into a polarographic cell. After purging the solution with nitrogen for 5 min the polarograms were taken by scanning the potential from −1.6 V to −1.97 V at a voltage step time of 1.8 s, drop size 5, pulse amplitude of 0.05 V, pulse time of 0.04 s, voltage step of 0.006 V, sweep rate of 0.0033 V/s, peak potential of −1.84 V and nitrogen pressure of 0.5 $kg cm^{-2}$ (0.49 bar). The reversibility of the electrode reaction was tested by using cyclic voltammetry on the same instrument at a scan rate of 0.055 V/s. All the AA analyses and the linear calibration curves were carried out by using standard addition method. All the measurements were performed at room temperature (25 ± 5 °C).

2.3.2. Determination of acrylamide in water sample

For method validation a recovery tests were accomplished in local tape water for the quantification of AA in low, middle and high concentrations ranges using differential pulse polarography. A volume of 10 mL local tape water containing known amounts of AA in 0.5 M LiCl (1 mL of 5 M) were placed in a polarographic cell. Then for DPP measurements, the same conditions as mentioned previously, were performed and the amounts were calculated by using standard addition method. The concentrations of AA were also tested in the polymeric industrial discharge samples obtained from rubber and others petrochemical industries of Karachi, Pakistan.

The determinations of AA in these polymeric discharges were performed by employing the same polarographic procedure as described already. To test the matrix effect in these samples,

three successive additions of 0.001 μL of 1000 mg L^{-1} AA were spiked containing a known amount of 0.2 mg L^{-1} AA.

3. Results and discussion

To investigate the reduction of AA in various suitable supporting electrolytes, a broad differential pulse polarographic study was carried out in the potential range from −1.4 V to −2.4 V in aqueous solution. The peaks of AA were observed in the presence of some useful supporting electrolytes, but these peaks were found to be depressed completely due to high reduction current of the supporting electrolyte cations at about −2.0 V when broad potential range was employed.

Therefore, the study was performed by employing short potential range, i.e. from −1.4 V to −1.97 V instead of −1.4 V to −2.4 V broad potential range, in order to avoid the effect of high reduction current resulting from the supporting electrolyte cations at −2.0 V. By employing this short potential range, some well-defined and well-resolved peaks appeared to be observed and not depressed before the reduction of electrolyte cations, illustrated in Fig. 1. Thus in this study the selection of proper potential range from −1.4 V to −1.97 V was critical to investigate the peak current of AA in pure aqueous solution.

From Fig. 1 it can be seen that in the presence of tetra butyl ammonium bromide (TBAB) as a supporting electrolyte two polarographic peaks (A1 and A2) were obtained. The poorly defined peak (A1) at −1.90 V may be due to the reduction of AA and another relatively well-defined peak (A2) at −1.62 V may be due to the adsorption of electrolyte on the surface of electrode.

The adsorption peak (A2) attributed to TBAB at −1.62 V was further confirmed in the absence of AA. The broad and much poorly defined peak was obtained at −1.88 V in the case of TBAOH electrolyte, shown by curve (B). A relatively well-defined and well-resolved peak from the background at −1.86 V was obtained when tetra ethyl ammonium iodide (TEAI) was used which is shown by curve (C). The peak obtained at −1.87 V in lithium chloride was also well-defined and became increased, shown by curve (D). The maximum peak height at a peak potential of −1.86 V was obtained in TMAI, represented by curve (E).

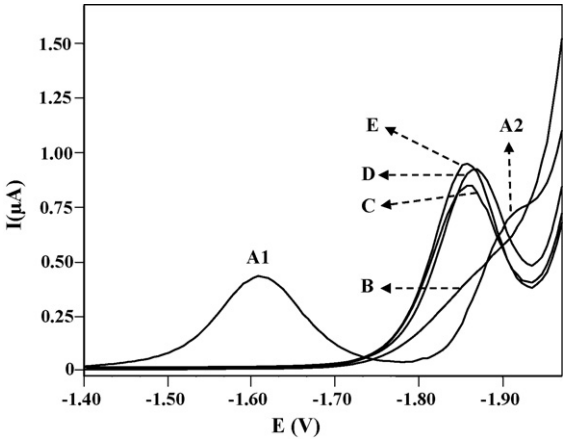

Fig. 1. Polarographic behavior of acrylamide in some useful supporting electrolytes in pure aqueous solution. (A) (A1 and A2) TBAB, (B) TBAOH, (C) tetra ethyl ammonium iodide (TBEI), (D) LiCl and (E) TMAI. The concentrations of all the supporting electrolytes used were 0.05 M. Potential range from −1.4 V to −1.97 V, drop size of 5, voltage step time of 1 s.

These results indicate that the type of supporting electrolyte cation has a considerable influence on the reduction of AA by changing the double layer structure of the electrode solution interface. By the addition of quaternary ammonium (R_4N^+) salts/hydroxide into the solution, the peak current became increased and the peak potential shifted toward more negative values as when the size of R-group (R_4N^+) was increased. This effect may probably attribute to the specific adsorption of R_4N^+ at the surface of electrode. The adsorbability of tetra alkyl ammonium ions (R_4N^+) increases in the order TMA < TEA < TBA [26,27]. The results reveal the obvious fact that the reduction of AA consumes protons from the surface of electrode and it was hindered by the adsorption of tetra butyl ammonium cations from TBAB and TBAOH electrolytes.

The size of the electrolyte cations has also shown a considerable influence on the rate of reduction of AA. The high reduction current at less negative potential was observed in the case of TMAI and then in LiCl as shown in Fig. 1. The effect of LiCl concentration on the reduction of AA was observed to be more pronounced as compared to TMAI because of its less adsorbability on the surface of electrode and its high solubility in aqueous medium.

The effect of LiCl concentration on the peak current and peak potential of AA was studied as shown in Fig. 2. The peak current increased gradually with the increasing concentration of LiCl from 0.005 mol L^{-1} to 0.5 mol L^{-1}, but at the same time the peak potential shifted towards less negative values. Then both the peak current and peak potential remained constant, while the peak width became broader after when the concentration of LiCl was increased from 0.5 mol L^{-1} to 1.75 mol L^{-1}. This showed that the reduction peak current of AA was strongly dependent on LiCl concentration thereby changing the double layer structure of the electrode solution interface. The effect of TMAI concentration on peak current of AA was also studied and the maximum peak current was obtained in 0.2 M without any shift of peak potential.

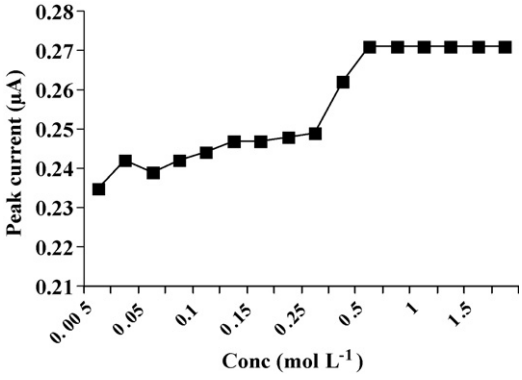

Fig. 2. Effect of LiCl concentration on the peak current of 5 mg L^{-1} acrylamide. Initial potential: −1.4 V; end potential: −1.97 V; voltage step time: 0.4 s; drop size: 4.

But the peak current obtained in TMAI was found to be low than the peak current obtained in LiCl.

This result also confirmed that replacing a cation in the supporting electrolyte by another more strongly absorbable one, e.g., (lithium by tetra methyl, tetra methyl by tetra ethyl and tetra ethyl by tetra butyl) caused the shifting of peak potential towards more negative value, whereas the peak current decreased or even absent, in the reduction of cationic AA. This result is consistent with the previous results [27,28], but in this case the electroactive species is cationic (AA) rather than anionic which displaced the peak potential towards more negative values due to electrostatic repulsion between cationic AA and tetra butyl ammonium cation adsorbed at the surface of electrode. The AA showed the highest sensitivity at less negative potential in the presence of LiCl because of its lowest adsobability at the surface of electrode due to small size. So LiCl of 0.5 M was chosen as a useful supporting electrolyte for the reduction of AA.

3.1. Cyclic voltammetric study

In order to check the reversibility of the electrode reaction, cyclic voltammogram (CV) of 10 mg L^{-1} AA in 0.5 M aqueous LiCl at a scan rate of 0.055 V/s was recorded. It can be seen from Fig. 3, that cathodic peak of AA appeared at about −1.85 V and there was no anodic peak appeared in the reverse scan, indicating the totally irreversible nature of the electrode reaction.

3.2. Effect of voltage step time (drop time) on the reduction current of AA

To elucidate the kind of electrode reaction the effect of voltage step time was studied. The peak current of AA increased gradually and the peak potential shifted towards less negative values with an increase in the voltage step time from 0.4 s to 2.6 s, while beyond this range it abruptly decreased in the form of distorted peak due to increased current oscillations.

The distortion of peak shape due to increased amplitude of current oscillations started after when the voltage step time was increased from 2.2 s to 3 s. The increase in peak current with an increase in voltage step time indicated that the limiting current was partly controlled by the rate of potential scan or drop time. This suggests an adsorptive chemical reaction involving a relatively slow step on the surface of electrode. Such type of reaction

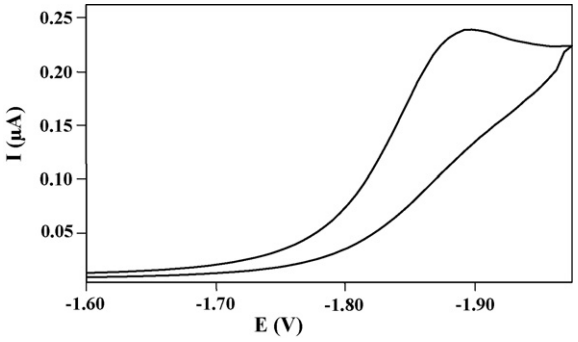

Fig. 3. Cyclic voltammogram of AA in pure aqueous solution of 0.5 M LiCl. Scan rate: 0.055 V/s.

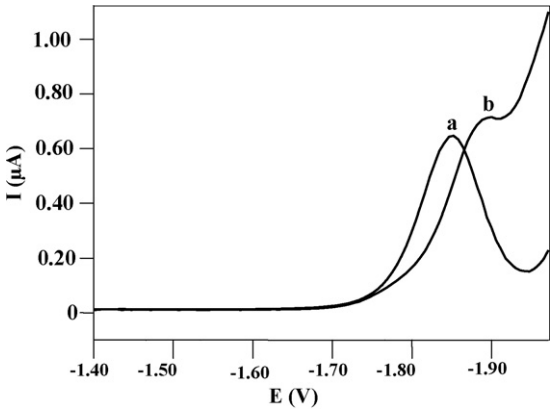

Fig. 4. Comparison of the reduction of AA (a) in pure aqueous solution and (b) in 80:20 methanol/water containing the same solution of 0.5 M LiCl in the potential range from −1.40 V to −1.97 V.

involving a slow step need not be observable further with dropping mercury electrode (DME) because there is a time limit for measurement and the rate of potential scan cannot be widely varied. The current oscillations may also result due to complete coverage of the reaction product at the electrode surface which inhibits the electrode reaction when using long voltage step time.

However, a voltage step time of 1.8 s at a sweep rate of 0.0033 m/s was selected for further study, because it completely avoided the deformation of peak attributed to the long voltage step time and also minimizing the time scale of measurement.

Fig. 4 shows the comparison between the peak current obtained in pure aqueous solution and the peak current obtained in 80% methanolic mixture containing the same solution of 0.5 M LiCl supporting electrolyte. A well-defined and well-resolved DPP peak was obtained at −1.84 V in pure aqueous solution (a), while a poorly defined DPP peak was obtained at −1.87 V in 80% methanolic mixture (b). This indicated that pure aqueous medium facilitates the reduction of AA in comparison to methanolic mixture.

The mechanism of the electrode reaction for AA as has been described already in neutral methanolic solutions of TMAI or LiCl [18]. It has been found that double bond becomes saturated by the addition of two protons and two electrons. Later on, it was suggested that neither the double bond nor the amide group would be reducible, and that the electronic conjugation of these two brings about a mesomeric electron shift towards the carbonyl oxygen, producing a keto–enol rearrangement allowing the reduction to propionamide.

In the reaction (Scheme 1) the equilibrium favors the keto form since the sum of its bond energies is higher than that of enol form. It has also been described that enolization is affected

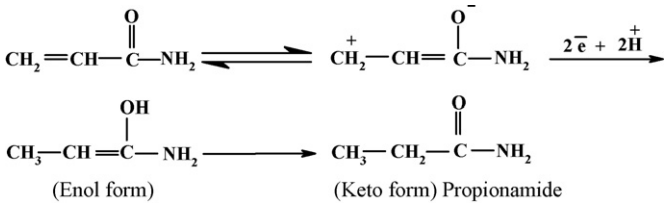

Scheme 1.

greatly by water which reduces the enol form by hydrogen bonding with the carbonyl thereby reducing the propensity for internal hydrogen bonding [29]. So from all these results it was concluded that in pure aqueous solution the electron proton transfer kinetics of AA takes place more easily by stabilizing greatly the electrode reaction product via hydrogen bonding.

Moreover, the nitrogen pressure also affected the peak current of AA. It was observed that by increasing the nitrogen pressure above from 0.5 kg cm^{-2} (0.49 bar) the noise level or current oscillations in the peak current became more pronounced as a result of distorted peak was found rather than well-resolved peak. Thus the nitrogen pressure was also found to be a significant factor to investigate the peak current of AA in aqueous solution.

Therefore the nitrogen pressure of 0.5 kg cm^{-2} was selected for further study because this showed best results in terms of peak shape and peak current. Moreover the drop size of 5 was optimized for further experiments because it showed relatively good sensitivity for AA.

After all the experiments, the conditions optimized for the determination of AA in aqueous solution were the use of dropping mercury electrode (DME) as a working electrode with DP mode, initial purge time of 300 s, drop size of 5, start potential of −1.6 V, end potential of −1.97 V, peak potential of −1.84 V, pulse amplitude of 0.05 V, pulse time of 0.04 s, voltage step of 0.006 V, voltage step time of 1.8 s, sweep rate of 0.0033 V/s and nitrogen pressure of 0.5 kg cm^{-2}.

3.3. Analytical performance of the method

3.3.1. Linear calibration curve

Calibration plot for AA was carried out under the optimized conditions using DPP in aqueous solution of 0.5 M LiCl. The reduction peak current for AA was linearly proportional to the AA concentration in the range from 0.2 mg L^{-1} to 20 mg L^{-1}

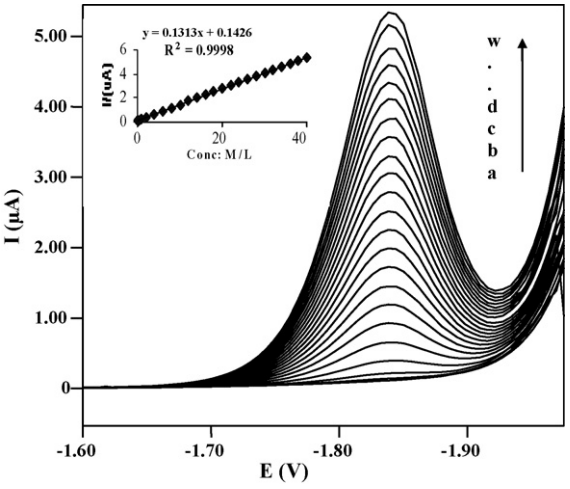

Fig. 5. DPP of AA in aqueous solution of 0.5 M LiCl containing: (a) 0, (b) 0.2, (c) 0.8, (d) 2, (e) 4, (f) 6, (g) 8, (h) 10, (i) 12, (j) 14, (k) 16, (l) 18, (m) 20, (n) 22, (o) 24, (p) 26, (q) 28, (r) 30, (s) 32, (t) 34, (u) 36, (v) 38 and (w) 40 mg L^{-1} AA. In the calibration curves after 0.8 mg L^{-1} (curve c), the same successive additions of 2 mg L^{-1} AA were carried out from curve (d) to curve (w).

with the correlation coefficient of $R^2 = 0.9998$. The calibration curve shown in Fig. 5, demonstrated good linear relationships between the concentrations and peak currents over the entire concentrations range. This indicated that the promoting reduction process did not block the surface of electrode even in this high concentrations range. This suggested that the method could be applied in the broad range of concentrations.

This result also indicated that the method could be sensitive for the quantification of AA in aqueous solution. The limit of detection (LOD) was calculated by using the equation:

$$\mathrm{LOD} = 3(s/S) \quad (1)$$

where "s" is the standard deviation of the response (blank) and "S" is the slope or sensitivity of the calibration curve at levels approaching the limit. The standard deviation "s" of the same solution of seven blank measurements was found to be 0.0012 μA and the slope value "S" of 0.1313 μA obtained from the calibration curve. By putting these values in Eq. (1), the detection limit of 27 μg L^{-1} was obtained and this is the concentration of AA that gave a signal three times the standard deviation of the background signal [30].

The reproducibility of the proposed method was evaluated by repeating 16 successive DPP measurements of the same solution of 5 mg L^{-1} AA in 0.5 M LiCl. The mean peak current value ($n = 16$) at a peak potential of −1.84 V was found to be 780 ± 2.4 nA with R.S.D. of 0.3%. This demonstrated the reproducibility and stability of the method.

3.3.2. Interference study

The influence of various likely interferences was tested by analyzing a standard solution of 5 mg L^{-1} AA in the presence of 0.5 M LiCl. These interferences were some carbonyl or unsaturated organic compounds and alkali metals cations. The interference effects of these agents in the presence of 5 mg L^{-1} AA in aqueous solution of 0.5 M LiCl are illustrated in Table 1.

The solutions containing different interferents to AA ratios in the range of 1:1–200:1, as given in Table 1, demonstrated that all the values obtained were within ±5%.

In this study the reduction of AA occurred at a peak potential of ca. −1.84 V before the reduction potentials of Ca^{++} (−2.22 V), K^+ (−2.10 V) and Na^+ (−2.07 V) by about 380 mV, 260 mV and 230 mV, respectively.

This showed that the difference between the peak potential of AA and the reduction potentials of alkali metals were suffi-

Table 1
Effect of interfering species on AA determination by using DPP

Interferent	Interferent to acrylamide ratio	Deviation (%) DPP
Formaldehyde	200:1	+4.2
Acetone	50:1	+4.8
Acrolein	1:1	−3.7
Acrylic acid	2:1	−4.1
Maleic acid	1:1	−2.6
Na^+	20:1	+5
K^+	25:1	+3.8
Ca^{++}	50:1	+2.7
NH_4^+	50:1	+4.9

Table 2
Determination results for acrylamide in local tape water

Sample no.	Acrylamide added ($\mu g\,mL^{-1}$)	Acrylamide found[a] ($\mu g\,mL^{-1}$)	Recovery (%)
1	0.5	0.49	98.1
2	5.0	4.97	99.4
3	10.0	10.2	102

[a] Average of five determinations.

ciently high which could allow the determination of AA in the presence of alkali metals cations. However, it was observed that at low concentration of AA in the presence of relatively high concentration of Na^+ and K^+, the peak became depressed without any change in peak current. This was due to the high final current rise of the background current resulting from these metals which started before the final background current of LiCl electrolyte.

The owns of the final background or residual current resulting in the presence of alkali metals cations depends on their reduction potentials which decreases in the order $-2.31\,V > -2.22\,V > -2.10\,V > -2.07\,V$ for Li^+, Ca^{++}, K^+ and Na^+, respectively. As the reduction potentials of Na^+ and K^+ are lower than others, so their final background currents started earlier than Li^+. Thus this was due to this reason that the peak became affected in the presence of these metals.

The effect was seen more in the determination of sufficiently low concentration of AA. In such a situation an accurate results were obtained by recording first the blank solution without analyte and then the solution containing analyte or using extrapolation method [31]. However, by the proposed method we could determine AA at a very low concentration in the presence of relatively high amount of Na^+ and K^+.

3.3.3. Sample analysis

In order to assess the possible applications of the proposed method for the determination of AA, the samples consisting of known amount of AA in local tape water was tested. When known amounts of AA added to the water control samples using standard addition method, quantitative recoveries of 98.1–102% were obtained as listed in Table 2. The values shown in Table 2 presented a relative error lower or equal to 2%. Thus the accuracy of the investigated method in pure aqueous solution was evident.

AA was also analyzed in polymeric industrial discharges samples collected from polymeric industries of Karach. But we could not find AA, as the concentration of AA in these discharged samples may be absent or low than the detection limit of the proposed method. In order to test the matrix affects in these polymeric discharges, a known amount of $0.2\,\mu g\,mL^{-1}$ AA was spiked using standard addition method. From this a quantitative recovery of 96% was obtained which showed a good selectivity of the proposed method.

4. Conclusion

After a long time, a new simple differential pulse polarographic method was investigated. The new proposed method offered rapidity, sensitivity and highly selectivity for the determination of AA directly in aqueous solution of LiCl. In this study the selection of proper potential range and applied nitrogen pressure to mercury electrode were important factors to investigate a well-resolved peak of AA in aqueous solution. The AA showed good response in the presence of LiCl or TBAI while it showed poor response in the presence of TBAOH and TBAB due to hindrance effects. The electrode reaction was found to be more favorable in pure aqueous solution which might be attributed to the hydrogen bonding thereby stabilizing greatly the reaction product. The sensitivity was greatly improved than the previously reported methods. Although the detection limit $27\,\mu g\,L^{-1}$ is not sufficient to verify the compliances with WHO guidelines and EPA recommended estimation of $0.5\,\mu g\,L^{-1}$ in drinking water and also not competable with the advance instrumental techniques. But however, the proposed method could open a new field of research for more sensitive investigations of AA in pure aqueous medium at this very simple, inexpensive technique which would be compatible to the advanced techniques.

Acknowledgements

We express our gratitude to Professor Michael Heyrovsky, Heyrovsky Institute of Physical Chemistry, Prague, Czech Republic for his valuable suggestions, and Professor Maher Kalaji, School of Chemistry, University of Wales, Bangor, Gwynedd, UK for updating our electrochemical approaches.

References

[1] C.G. Daughton, "Quantification of Acylamide (and Polyacrylamide)": Report No: CGD-O2/88, 1988.
[2] IPCS INCHEM, International Program on Chemical Safety Environmental Health Criteria, vol. 49, 1985, http://www.inchem.org/documents/ehc/ehc/ehc49.htm.
[3] M. Weideborg, T. Kallqvist, K.E. Odegrad, L.E. Sverdrup, E.A. Vik, Water Res. 35 (2001) 2645.
[4] E.A. Smith, S.L. Pruen, F.W. Oehme, Ecotoxicol. Environ. Saf. 35 (1996) 121.
[5] IARC, Monographs on the Evaluation of Carcinogenic Risks to Humans, vol. 60, International Agency for Research on Cancer (IARC), Lyon, 1994, pp. 389–433.
[6] World Health Organization (WHO), Recommendations, vol. 1, 2nd ed., WHO, Geneva, 1993, p. 72.
[7] Consumer Factsheet on Acrylamide, US Environmental Protection Agency, Cincinnati, OH, USA, http://www.epa.gov/safewater/contaminants/dwcontamfs/acrylami.html.
[8] S. Chu, C.D. Metcalfe, Anal. Chem. 79 (2007) 5093.
[9] S. Cavalli, S. Polesello, G. Saccani, J. Chromatogr. A 1039 (2004) 155.
[10] S. Cavalli, R. Maurer, F. Höfler, LC–GC Eur. 9 April 2003.
[11] Y. Zhang, G.Y. Zhang, Y. Zhang, J. Chromatogr. A 1075 (2005) 1.
[12] K. Kawata, T. Ibaraki, A. Tanabe, H. Yagoh, A. Shinoda, H. Suzuki, A. Yasuhara, J. Chromatogr. A 911 (2001) 75.

[13] US EPA, Acrylamide by Gas Chromatography; Method 8032A, US Environmental Protection Agency, Washington, DC, 1996.
[14] US EPA, Acrylamide, Acrylonitrile and Acrolein by High Performance Liquid Chromatography (HPLC), Method 8316, US Environmental Protection Agency, Washington, DC, 1994.
[15] I.G. Casella, M. Pierri, M. Contursi, J. Chromatogr. A 1107 (2006) 198.
[16] J. Barek, J. Cvacka, A. Muck, V. Quaiserova, J. Zima, Fresenius J. Anal Chem. 369 (2001) 556.
[17] S.R. Betso, J.D. McLean, Anal. Chem. 48 (1976) 766.
[18] F. Vajda, Acta Chim. Acad. Sci. Hung. 53 (1967) 241.
[19] F. Vajda, B. Kut, Lntez. Kozlem. 10 (1/2) (1965–1966) 221.
[20] D.C. McWilliams, D.C. Kaufman, E.F. Waling, Anal. Chem. 37 (1965) 1546.
[21] E.M. Skobets, G.S. Nestyuk, V.I. Shapoval, Ukr. Khim. Zh. 28 (1962) 72.
[22] E.M. Skobets, G.S. Nestyuk, Ukr. Khim. Zh. 28 (1962) 934.
[23] V.D. Bezuglyi, T.A. Alekseeva, I.P. Kruglyak, Ukr. Khim. Zh. 31 (5) (1965) 500.
[24] V.I. Shapoval, G.S. Shapoval, Uspechi Chimii 32 (1966) 244.
[25] L. Meites, Polarographic Techniques, 2nd ed., Interscience Publishers, John Wiley & Sons, New York, 1965, pp. 612–614.
[26] I.M. Kolthoff, K. Yamashita, Proc. Natl. Acad. Sci. 72 (1975) 2863.
[27] A.J. Bard, L.R. Faulkner, Electrochemical Methods, 2nd ed., John Wiley & Sons, New York, 2001, pp. 574–575.
[28] L. Meites, Polarographic Techniques, 2nd ed., Interscience Publishers, John Wiley & Sons, New York, 1965, p. 264.
[29] J. March, Advanced Organic Chemistry, Reactions Mechanisms and Structure, 4th ed., John Wiley & Sons, New York, 2004, p. 72.
[30] G.D. Christian, Analytical Chemistry, 6th ed., John Willey & Sons: Inc., New York, 2004, p. 113.
[31] L. Meites, Polarographic Techniques, 2nd ed., Interscience Publishers, John Wiley & Sons, New York, 1965, pp. 190–192.

Available online at www.sciencedirect.com
ScienceDirect
Talanta 74 (2008) 1242–1246
Talanta
www.elsevier.com/locate/talanta

Determination of fenfluramine based on potassium permanganate–calcein chemiluminescence system

Fei Nie [a,b], Jiuru Lu [a,*]

[a] School of Chemistry and Material Science, Shaanxi Normal University, Xi'an 710062, China
[b] Department of Chemistry and Chemical Engineering, Baoji University of Arts and Sciences, Baoji 721007, China

Received 18 June 2007; received in revised form 27 August 2007; accepted 29 August 2007
Available online 8 September 2007

Abstract

Calcein was found to be able to use as chemiluminescence reagent and post-chemiluminescence was observed when fenfluramine was injected into the mixture after the CL reaction of calcein–potassium permanganate. Based on this phenomenon, a flow injection CL method was established for the determination of fenfluramine. The possible CL mechanism was proposed. The CL intensity was correlated linearly with the concentration of fenfluramine over the range of 1.0×10^{-7} to 6.0×10^{-6} g mL^{-1} and the detection limit was 6×10^{-8} g mL^{-1}. The relative standard deviation was 2.2% for 5.0×10^{-7} g mL^{-1} fenfluramine ($n = 11$). This method was applied to the determination of fenfluramine in weight-reducing tonic successfully.
© 2007 Elsevier B.V. All rights reserved.

Keywords: Chemiluminescence; Fenfluramine; Calcein; Potassium permanganate

1. Introduction

Fenfluramine was widely prescribed as appetite suppressants for the treatment of obesity in conjunction to dietary restriction. However, it was withdrawn from the US market in September 1997 after many cases reported the development of serious side effects including valvular heart disease and primary pulmonary hypertension [1–3]. Yet, in spite of the withdrawal, fenfluramine is still being used by adding into weight-reducing tonic unlawfully. Therefore, it will be helpful to develop a method in monitoring its level in weight-reducing tonic.

Some methods have been developed for the determination of fenfluramine including HPLC [4–6] and CE [7,8]. LC–MS [9] and HNMR [10] methods are also developed recently. These methods need either expensive equipments or complex procedures for sample treatment. To our knowledge, no CL method for the determination of fenfluramine was reported.

Chemiluminescence analysis has many characteristics such as high sensitivity and simple instruments. CL reagent is often employed during CL analysis. CL reagent in common use can be divided into two types. One type of CL reagent is translated into luminant in the reaction and the luminant could absorb the energy of the reaction to produce CL. This type of CL reagents include luminol, lucigenin, tris(2,2′-bipyridyl)ruthenium(II), etc., which are used in the determination of oxidant, CL reagent or catalyzer [11–13]. The other type of CL reagent is peroxyoxalate. It can react with hydrogen peroxide to produce an active intermediate named dioxetanedione, which would decompose with some energy transferred into fluorescent molecule accompanied with CL. This type of CL reagent is often employed to determine some fluorescent substances and hydrogen peroxide [14,15]. It was found that calcein, a fluorescent reagent, could be used as a chemiluminescence reagent in potassium ferricyanide–calcein system, and it had been used to the CL analysis of some substances [16].

In our recent works, it was found when injecting some substances into reaction mixture after the finish of several CL reactions, such as potassium permanganate–fluorescein reaction and potassium permanganate–luminol reaction can cause a new chemiluminescence reaction. Such phenomenon is named as a post-chemiluminescence (PCL) phenomenon

* Corresponding author. Tel.: +86 29 85303911; fax: +86 29 85307774.
E-mail address: ljr@snnu.edu.cn (J. Lu).

0039-9140/$ – see front matter © 2007 Elsevier B.V. All rights reserved.
doi:10.1016/j.talanta.2007.08.042

and the corresponding chemiluminescence reaction as a post-chemiluminescence reaction [17,18].

In this work, it was found that calcein could also be used as a chemiluminescent reagent in potassium permanganate–calcein system and a PCL phenomenon was observed when fenfluramine was added into the mixture after the CL reaction of calcein and potassium permanganate. The CL intensity was strongly dependent on fenfluramine concentration. Based on this, a new, rapid and simple method is established for the determination of fenfluramine. The mechanism of the CL reaction is proposed. Furthermore, the method has been used for the determination of fenfluramine in weight-reducing tonic with satisfactory results.

2. Experimental

2.1. Apparatus

The IFFM-D flow injection CL analyzer (Xi'an Remex Electronic Instrument High-Tech Ltd., China) was equipped with an automatic injection system and a detection system. Polytetrafluoroethylene tube (0.8 mm i.d.) was used to connect all of the components in the flow system. The flow cell was a coil of glass tube that positioned in front of the detection window of the photomultiplier tube (PMT). The CL signal was treated with a personal computer.

The kinetic curve was measured with the static system of the IFFM-D CL analyzer (Xi'an Remex Electronic Instrument High-Tech Ltd., China). CL spectra were measured with the BPCL CL analyzer (Institute of Biophysics Chinese Academy of Science, China). Fluorescence spectra were obtained by a 970CRT spectrofluorometer (Shanghai Analysis Instrument Main Plant, China). UV absorption spectra were measured on a TU-1901 spectrophotometer (Beijing Currency Instrumental Ltd., China).

2.2. Reagents

Potassium permanganate was purchased from Xi'an Chemical Reagent Factory (Xi'an, China). Calcein was purchased from the No. 3 Beijing Chemical Reagent Factory (Beijing, China). Fenfluramine hydrochloride was purchased from National Institute for the Control of Pharmaceutical and Biological Products (Beijing, China).

The standard solution of fenfluramine hydrochloride (1.00×10^{-4} g mL^{-1}) was prepared by dissolving 0.0100 g fenfluramine hydrochloride with water and diluting to 100 mL with water. The 1.0×10^{-2} mol L^{-1} stock solution of potassium permanganate was prepared by dissolving 0.40 g of potassium permanganate with water and then diluting to 250 mL, and the working solution (5.0×10^{-5} mol L^{-1}) was prepared by diluting the stock solution with 0.05 mol L^{-1} of NaOH. The 1.0×10^{-4} mol L^{-1} working solution of calcein was prepared by dissolving 0.0340 g of calcein and then diluting to 500 mL with water.

All the reagents used were analytical reagent grades except for fenfluramine hydrochloride, which was a check sample. Doubly distilled water was used through out the whole experiment.

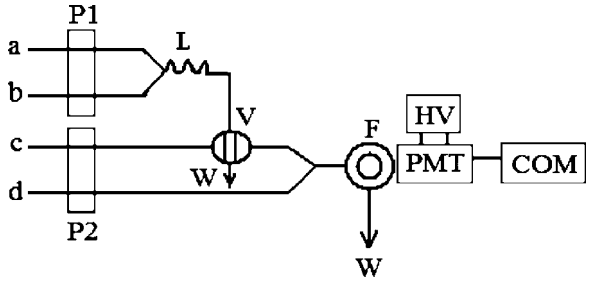

Fig. 1. Schematic diagram of CL flow system. (a) Potassium permanganate solution; (b) calcein solution; (c) water; (d) fenfluramine standard or sample solution. P: peristaltic pump; L: mixing tube; V: injection valve; W: waste; F: flow cell; HV: high-voltage; PMT: photomultiplier tube; PC: personal computer.

2.3. Procedure

Investigations of CL behaviors were performed using the system shown schematically in Fig. 1. Flow tubes (a–d) were connected with potassium permanganate solution, calcein solution, water and fenfluramine standard or sample solution, respectively. Calcein solution merged with potassium permanganate solution first with a Y-piece, and then was injected into water by a six-way injection valve. The reagent plug merged with fenfluramine standard solution or sample solution through a Y-piece to produce CL. The concentration of fenfluramine was quantified via the peak height (relative CL intensity), which was obtained by subtracting the blank CL intensity from that of the sample or fenfluramine standard solution.

3. Results and discussion

3.1. Kinetic characteristic of the PCL reactions

Kinetic characteristics of the CL reactions were examined. The CL intensity–time curve was shown in Fig. 2. When 5.0×10^{-5} mol L^{-1} of potassium permanganate solution (1.0 mL) was injected into 1.0×10^{-4} mol L^{-1} of calcein

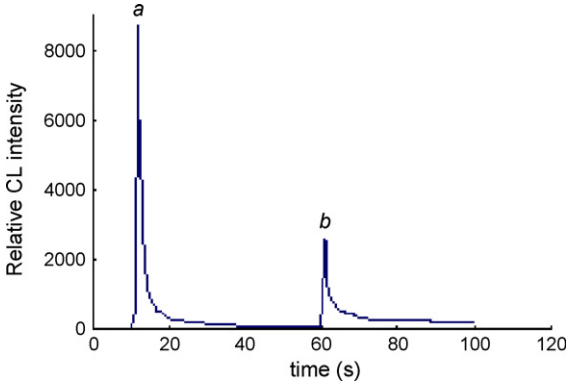

Fig. 2. The CL intensity–time curve. (a) 1.0×10^{-4} mol L^{-1} calcein solution (1.0 mL) was injected into 5.0×10^{-5} g mL^{-1} potassium permanganate solution (1.0 mL in 0.05 mol L^{-1} NaOH); (b) 1.0×10^{-6} mol L^{-1} fenfluramine solution (1.0 mL) was injected into the mixing solution of (a).

solution (1.0 mL), a CL signal was produced (peak a). After this CL reaction finished, a PCL reaction was initiated when 1.0×10^{-6} g mL^{-1} of fenfluramine (1.0 mL) was injected into the mixture of the above reaction (peak b). The maximum CL intensity was obtained within 1.5 s. After 60 s approximately, the CL signal declined to baseline.

CL signal was not detected by using the blank solution instead of the fenfluramine solution under the same condition, which indicated that the reaction initiated by fenfluramine in the potassium permanganate–calcein system was a PCL reaction.

3.2. Optimization of the reaction conditions

A series of experiments was conducted to select optimum analytical conditions using a 5.0×10^{-7} g mL^{-1} fenfluramine solution. The optimized conditions included flow system, flow rate, length of the mixing tube, reaction medium, calcein concentration and potassium permanganate concentration.

Several flow systems were designed in order to obtain the maximal PCL signal. When employing the system shown schematically in Fig. 1 and water as carrying stream, the reagent solution could mix adequately with sample solution as soon as they met and a strong CL signal with good repeatability was obtained. So, flow system in Fig. 1 was selected.

The flow rate is an important factor employing the system shown schematically in Fig. 1, which influences the analytical sensitivity. The effect of the flow rate of pump 2 on PCL intensity was examined in the range of 0.5–3 mL min^{-1}. The results showed that the PCL signal increased with the increasing of flow rate, because this CL reaction is rapid. So, a flow rate of 3 mL min^{-1} which was the maximal flow rate under present conditions was selected as optimum.

In order to make potassium permanganate and calcein react adequately before initiating the PCL reaction, a mixing tube was added in front of the six-way injection valve. The length of the mixing tube was examined in the range 15–50 cm when the flow rate was fixed at 3 mL min^{-1}. The results showed that the optimal length of mixing tube was 30 cm.

The PCL reaction was performed in alkaline condition. The alkalinity of reaction medium was adjusted by varying the concentration of sodium hydroxide in potassium permanganate solution. The effect of sodium hydroxide concentration on the PCL reaction was examined in the range 0.002–1 mol L^{-1}. The results showed that the suitable concentration of sodium hydroxide was 0.05 mol L^{-1} since a maximal PCL signal could be obtained under this alkalinity.

Calcein is the CL reagent. Its concentration had a great effect on the CL intensity. The effect of calcein concentration was studied in the range 5.0×10^{-6} to 5.0×10^{-3} mol L^{-1} and 1.0×10^{-4} mol L^{-1} of calcein was selected to get the maximal PCL signal finally.

Potassium permanganate is the oxidant in the CL reaction. Its concentration influences the CL signal. The effect of potassium permanganate concentration on the PCL reaction was examined in the range of 1.0×10^{-6} to 1.0×10^{-3} mol L^{-1}. The experiments showed the maximal PCL signal could be obtained when the concentration of potassium permanganate was 5.0×10^{-5} mol L^{-1}.

3.3. Analytical performance

When the concentration of calcein, potassium permanganate and sodium hydroxide were 1.0×10^{-4}, 5.0×10^{-5} and 0.05 mol L^{-1}, respectively, the analytical performance were obtained. The relative PCL intensity was linear to fenfluramine concentration over the range 1.0×10^{-7} to 6.0×10^{-6} g mL^{-1}. The determination limit was 6×10^{-8} g mL^{-1} (3σ). The relative standard deviation was 2.2% by 11 replicate determinations of 5.0×10^{-7} g mL^{-1} fenfluramine.

3.4. Interference studies

The influence of foreign species was studied by analyzing a standard solution of 5.0×10^{-7} g mL^{-1} fenfluramine to which increasing amounts of foreign species were added. A substance was considered no interference if the variation of the CL intensity was within ±5%. The influence of some inorganic ions and organic compounds were studied. The tolerable concentration ratios of foreign species to 5.0×10^{-7} g mL^{-1} of fenfluramine was over 1000-fold for fructose, glucose, starch, lactose, NO_3^-, Br^-, Cl^-, CO_3^{2-}, $C_2O_4^{2-}$, 500-fold for dextrin, PO_4^{3-}, 100-fold for Al^{3+}, Co^{2+}, 50-fold for Cu^{2+}, Ni^{2+}, Sr^{2+}, 10-fold for Ca^{2+}, Mg^{2+}, Fe^{3+}, Fe^{2+}, Cr^{3+}, Cd^{2+}, 5-fold for Pb^{2+}.

3.5. Application

In order to evaluate the applicability and reliability of the proposed method, fenfluramine in three samples including one kind of capsule and two kinds of anti-adipose tea was determined.

One bag of each kind of anti-adipose tea was steeped with 200 mL boiling water. After approximately 5 min, 0.05 mL of tea was transferred into a 50 mL volumetric flask and diluted to the graduation with water, respectively. These were regarded as the tea sample solutions. The powder of one capsule was dissolved in water and diluted into 50 mL, then filtered and the filtrate was used as the capsule sample solution. Both the tea sample solutions and the capsule sample solution were determined with the proposed CL method. The results showed that no fenfluramine was added in each sample and the coexisted substances in the samples did not interfere with the determination of fenfluramine. Therefore the recovery tests were performed to evaluate the accuracy of this method. The results of the determinations and the recovery tests were shown in Table 1. As can be seen from Table 1, the recoveries of added fenfluramine can be quantitative and *t*-test assumed that there is no significant difference between recovery efficiency and 100% at confidence level of 95%.

3.6. Possible mechanism

The fluorescence spectra of fenfluramine, calcein, the mixture of potassium permanganate–calcein, and the mixture of fenfluramine–potassium permanganate–calcein were measured

Table 1
Determination of fenfluramine in weight-reducing tonic

Samples	Found[a]	Added ($\times 10^{-7}$ g/mL)	Found[a] ($\times 10^{-7}$ g/mL)	Recovery (%)
Tea.1	0	2.00	2.11	105.5
		4.00	4.13	103.3
		6.00	5.87	97.8
Tea.2	0	2.00	2.08	104.0
		4.00	4.15	103.8
		6.00	6.11	101.8
Capsule	0	2.00	1.93	96.5
		4.00	3.94	98.5
		6.00	6.24	104.0

[a] Average of three measurements.

(Fig. 3). It was found in Fig. 3 that fenfluramine has no fluorescence and the maximal fluorescence wavelengths of b–d was not same. It was reported that the maximal fluorescence wavelength of calcein changes with pH and it shows a red shift with the increase of pH [19]. Therefore, in order to find out the actual forming reason of the difference of the maximal fluorescence wavelengths in Fig. 3, fluorescence spectra of the three kinds of solutions were measured in Na_2CO_3–$NaHCO_3$ buffer solution (pH 9.97) (Fig. 4). The maximal fluorescence wavelengths of c′ and d′ were identical with that of b′ in Fig. 4, which indicated that all the fluorescence emission was performed by calcein and the little difference of the maximal fluorescence wavelength was made by the change of the pH of the solution in Fig. 3.

The CL spectrum of fenfluramine–potassium permanganate–calcein CL reaction was measured (Fig. 5). Compared the CL spectrum with the fluorescence spectra of calcein in the mixture of fenfluramine–potassium permanganate–calcein, the luminant of the CL reaction was determined as calcein since its maximal fluorescence wavelength was identical with the maximal CL wavelength.

The UV–vis absorption spectra of calcein, potassium permanganate and potassium permanganate–calcein were measured (Fig. 6). Since the maximal absorption wavelength of calcein and potassium permanganate was adjacent, superfluous Mg^{2+} solution were added because it can combine with calcein and produced a blue shift in the visible portion of the spectrum of calcein [20]. It was found from Fig. 6 that calcein and

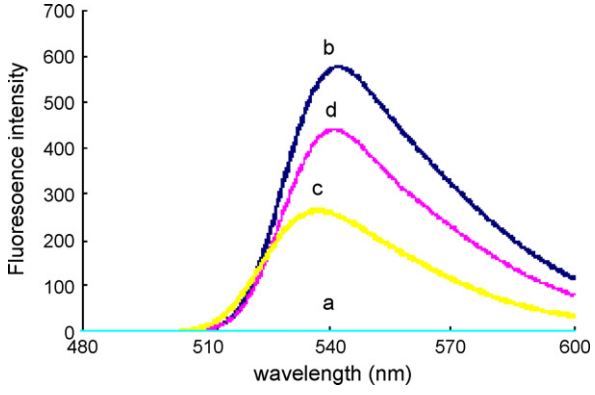

Fig. 3. Fluorescence spectra in 0.05 mol L^{-1} NaOH. (a) 1.0×10^{-5} g mL^{-1} fenfluramine; (b) 1.0×10^{-4} mol L^{-1} calcein; (c) 1.0×10^{-4} mol L^{-1} calcein + 5.0×10^{-5} mol L^{-1} potassium permanganate; (d) 1.0×10^{-4} mol L^{-1} calcein + 5.0×10^{-5} mol L^{-1} potassium permanganate + 1.0×10^{-5} g mL^{-1} fenfluramine (all the above solutions were prepared in 0.05 mol L^{-1} NaOH).

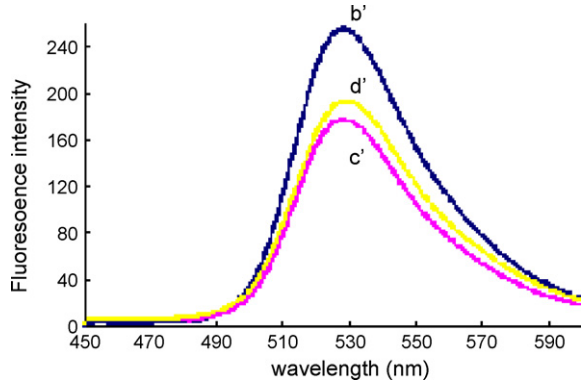

Fig. 4. Fluorescence spectra in buffer solution. (b′) 1.0×10^{-4} mol L^{-1} calcein; (c′) 1.0×10^{-4} mol L^{-1} calcein + 5.0×10^{-5} mol L^{-1} potassium permanganate; (d′) 1.0×10^{-4} mol L^{-1} calcein + 5.0×10^{-5} mol L^{-1} potassium permanganate + 1.0×10^{-5} g mL^{-1} fenfluramine (all the above solutions were prepared in Na_2CO_3–$NaHCO_3$ buffer solution, pH 9.97).

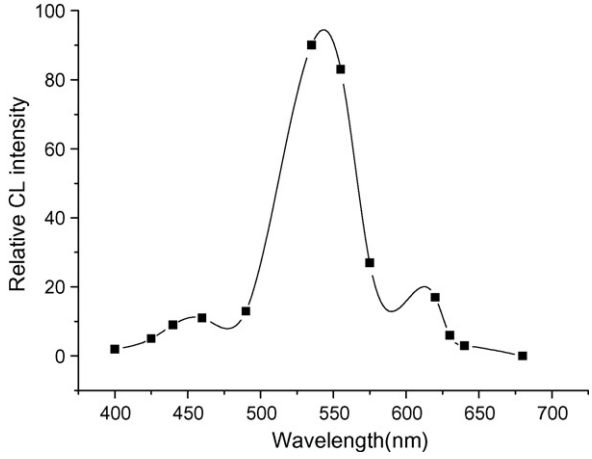

Fig. 5. CL spectrum of the PCL reaction 1.0×10^{-6} g mL^{-1} fenfluramine, 5.0×10^{-5} mol L^{-1} potassium permanganate (in 0.05 mol L^{-1} NaOH) and 1.0×10^{-4} mol L^{-1} calcein.

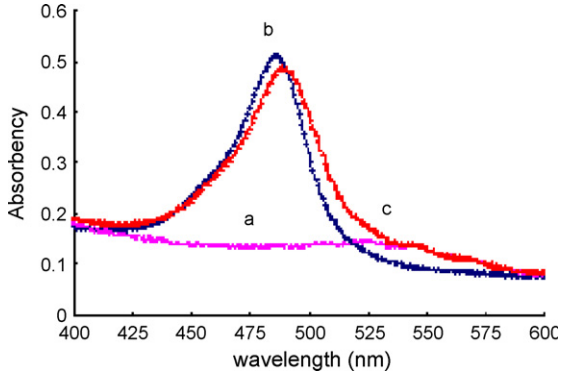

Fig. 6. UV–vis absorption spectra. (a) 5.0×10^{-5} mol L^{-1} potassium permanganate; (b) 1.0×10^{-4} mol L^{-1} calcein; (c) 1.0×10^{-4} mol L^{-1} calcein + 5.0×10^{-5} mol L^{-1} potassium permanganate (all the above solutions were prepared in 0.05 mol L^{-1} NaOH and 1.0×10^{-3} g mL^{-1} Mg^{2+} solution).

potassium permanganate were both present after the potassium permanganate–calcein CL reaction.

Based on the above experiments, the possible mechanism of fenfluramine–potassium permanganate–calcein PCL reaction was proposed as: potassium permanganate oxidized calcein accompanied with CL emission. When fenfluramine was injected into the mixture after the above CL reaction, the residual potassium permanganate reacted with fenfluramine and released energy. Calcein which was not reacted absorbed the energy and was excited to the excited state (calcein*). Calcein* came back to the ground state and brought the PCL.

The mechanism can be expressed simply as following:

$$\text{potassium permanganate} + \text{calcein} \rightarrow \text{products} + h\nu$$

$$\text{potassium permanganate} + \text{fenfluramine} \rightarrow \text{products} + \text{energy}\,(E)$$

$$\text{calcein} + E \rightarrow \text{calcein}*$$

$$\text{calcein}* \rightarrow \text{calcein} + h\nu$$

4. Conclusion

A novel PCL method for the determination of fenfluramine was established with calcein as the CL reagent and the method was satisfactorily applied to the determination of fenfluramine in weight-reducing tonics. The mechanism of the calcein–potassium permanganate–fenfluramine CL reaction was briefly discussed.

In this work, calcein, a common florescence reagent, was found to be able to use as CL reagent. It has an important meaning for widening the area of CL analysis, exploring the possibility of employing other florescence reagent as CL reagent and enriching the knowledge of people to CL reaction.

References

[1] M. Sachdev, W.C. Miller, T. Ryan, et al., Am. Heart J. 144 (2002) 1065.
[2] T. Tomita, Q. Zhao, Chest 121 (2002) 649.
[3] C. Blanpain, P.E. Le, J. Parma, et al., Cardiovasc. Res. 60 (2003) 518.
[4] A. Kaddoumi, M. Wada, M.N. Nakashima, et al., Forensic Sci. Int. 146 (2004) 39.
[5] A. Kaddoumi, M.N. Nakashima, K. Nakashima, J. Chromatogr. B 763 (2001) 79.
[6] A. Kaddoumi, M.N. Nakashima, M. Wada, et al., J. Liq. Chromatogr. Rel. Technol. 24 (2001) 54.
[7] R. Porra, S. Fanali, M.G. Quaglia, Chromatographia 41 (1995) 383.
[8] J.C. Reijenga, B.A. Ingelse, F.M. Everaerts, J. Chromatogr. A 772 (1997) 195.
[9] M.J. Bogusz, K.D. Kruger, R.D. Maier, J. Anal. Toxicol. 24 (2000) 77.
[10] J.S. Salsbury, P.K. Isbester, Magn. Reson. Chem. 43 (2005) 910.
[11] J. Pan, Y. Huang, W. Shu, et al., Talanta 71 (2007) 1861.
[12] J. Lin, A. Tsuji, M. Maeda, Anal. Chim. Acta 339 (1997) 139.
[13] C.A. Lindino, L.O.S. Bulhões, Talanta 72 (2007) 1746.
[14] W.H. Richardson, M.B. Yelvington, H.E. O'Neal, J. Am. Chem. Soc. 94 (1972) 1619.
[15] M. Katayama, H. Taniguchi, S. Akihama, et al., Anal. Chim. Acta 303 (1995) 333.
[16] F. Nie, J. Lu, Anal. Chim. Acta 592 (2007) 168.
[17] Y. Li, W. Niu, J. Lu, Talanta 71 (2007) 1124.
[18] J. Du, W. Liu, J. Lu, Acta Chim. Sin. 62 (2004) 1323.
[19] F.H.W. Donald, M.S. Douglas, S. Jon, et al., Anal. Chem. 31 (1959) 456.
[20] F. Donald, W. Hozelzl, L.S. Theodore, Anal. Chem. 35 (1963) 1085.

Available online at www.sciencedirect.com
ScienceDirect
Talanta 74 (2008) 1350–1354
Talanta
www.elsevier.com/locate/talanta

Micro-flow injection system for the urinary protein assay

Syouhei Nishihama [a,*], Hisano Imabayashi [b], Tomoko Matoba [b], Chika Toya [a], Kosuke Watanabe [a], Kazuharu Yoshizuka [a]

[a] *Department of Chemical Engineering, Faculty of Environmental Engineering, The University of Kitakyushu, Hibikino 1-1, Kitakyushu 808-0135, Japan*
[b] *Kitakyushu Foundation for the Advancement of Industry, Science and Technology, Hibikino 2-1, Kitakyushu 808-0135, Japan*

Received 17 July 2007; received in revised form 7 September 2007; accepted 7 September 2007
Available online 21 September 2007

Abstract

A urinary protein assay has been investigated, employing a micro-flow injection analysis (μFIA) combined with an adsorptive separation of protein from analyte. The adsorptive separation part of protein in the artificial urine with ceramic hydroxyapatite is integrated on the μFIA chip, since the interference of other components coexisting in urine occurs in the conventional FIA system. The typical FI peak can be obtained following the adsorption–elution process of the protein prior to the detection, and the protein concentration in artificial urine can be quantitatively determined.
© 2007 Elsevier B.V. All rights reserved.

Keywords: μTAS; Micro-flow injection analysis; Urinary protein assay

1. Introduction

The detection of components in human fluid is an indispensable test for the diagnosis and therapy. Recently, point of care testing (POCT), which is clinical test near the patient, has been developed. The blood and urine analyses at home such as glucose monitoring for diabetes sufferers, is also included to the POCT. The small and inexpensive monitoring instrument is therefore required for accomplishing the POCT. Considering the analytical instrument for the human fluid, the selectivity and sensitivity are also important, because the fluid usually contains a lot of components.

Miniaturization of flow-based assays is at present an actively pursued topic in analytical chemistry, along with progress in the precise machining techniques, and the micro-total analysis system (μTAS), based on a unit operations integrated micro-chip (lab-on-a chip), has been proposed [1]. Flow injection analysis (FIA) [2] and sequential injection analysis (SIA) [3,4], which is the second generation of FIA, are mostly applied as the template techniques for the μTAS. Since one of the present issues of μTAS is that the detector with high selectivity and/or high sensitivity is still large and expensive, another approach is necessary for applying μTAS to the analytical system for POCT. In our group, total urinary assay system for the POCT has been investigated, and the urinary glucose assay with micro-flow injection analysis (μFIA) was already reported [5]. In this system, the spectrophotometry was used as the detection method as an inexpensive assay system. However, the interference was progressed by other components, because the spectrophotometry has a disadvantage of poor selectivity for the analyte. When the separation part for the glucose from the urine was integrated on the μTAS chip, prior to the detection part, the glucose assay could be successfully achieved. In the urine, there are other components, except for glucose, of which the concentrations have to be determined for the health care testing, such as protein and blood.

Coomassie Brilliant Blue (CBB) is well-known dye binding with protein [6,7], and the CBB method has been applied for the protein assay in the human fluid [8,9]. Lott et al. reported, however, that there are positive or negative interferences for the urinary protein assay with the coexisting components [10]. In the present work, a μFIA system for the urinary protein assay without the interference with the coexisting components is investigated, based on the CBB method. The bovine serum albumin (BSA) was employed as a model protein, because the absorbance of the dye complex with CBB is hardly affected by kinds of proteins [6]. The separation part with ceramic hydroxyapatite adsorbent [11] for protein from other components in urine is

* Corresponding author. Tel.: +81 93 695 3283; fax: +81 93 695 3365.
E-mail address: nishihama@env.kitakyu-u.ac.jp (S. Nishihama).

0039-9140/$ – see front matter © 2007 Elsevier B.V. All rights reserved.
doi:10.1016/j.talanta.2007.09.014

Table 1
Components of the artificial urine used in the present study

Component	Concentration
NaCl	1.0 g/dL
Urea	1.0 g/dL
Creatinine	0.05 g/dL
Bovine serum albumin	30 mg/dL
Glucose	80 mg/dL
Acetone	160 mg/dL
Sodium nitrite	0.1 mg/dL
Human hemoglobin	30 μg/dL

integrated onto μFIA fabricated on the poly(methyl methacrylate) (PMMA) plate. The protocol for urinary protein assay is optimized to evaluate the potential of this μFIA system.

2. Experimental

2.1. Reagents

Bovine serum albumin (BSA) was supplied by MP Biomedicals to be used as a protein. Ceramic hydroxyapatite was supplied by Bio-Rad (Type I, 80 μm) as an adsorbent for BSA. Human hemoglobin was supplied by Sigma as a lyophilized powder. All other chemicals used were supplied by Wako Pure Chemical Industries, as analytical-grade reagents. Coomassie Brilliant Blue G-250 (CBB) was used as a reagent for the protein assay [6]. Artificial urine listed in Table 1 was prepared for investigating the interference of other components, since it is difficult to get the actual urine sample from the patients. All solutions were prepared with deionized water purified with a Milli-Q PLUS system (Millipore).

2.2. Fabrication of μFIA chip

The μFIA chips were made on PMMA plate using a table type NC micro-machining center (PMT Corporation Co. Ltd.). The micro-flow channel was designed with CAD software, and the channel was dug with a 0.5 mm square end mill. Two kinds of the μFIA chips both with and without protein separation part were fabricated. Fig. 1 shows the schematic diagrams of μFIA chips. In the case of μFIA chip without separation part, the micro-channel was made on the PMMA plate with 1 mm thickness. The channel was then adhered with another PMMA plate in the constant temperature oven at 120 °C. The optical fiber type spectrophotometer was attached to the PMMA plates at the fiber position of the micro-channel (Fig. 1a). In the case of μFIA chip with separation part, the micro-channel was made on PMMA plate with 5 mm thickness, and the part for fiber spectrophotometer ($\varphi = 1.8$ mm) was made with 10 mm thickness. The end point of the micro-channel was connected to the part for optical fiber type spectrophotometer. The adsorption part of 15 or 30 mm in length, 2 mm in width, and 1 mm in depth was made on the chip. The ceramic hydroxyapatite (0.0112 g for 15 mm and 0.0214 g for 30 mm) was filled together with glass beads. The two PMMA plates were then adhered in the constant temperature oven at 120 °C.

2.3. Procedures for the protein assay

The CBB method is well-known colorimetry method for protein quantification. The batchwise official protocol is that the absorbance of CBB complex is measured at 595 nm after incubation of a mixture of the sample solution (100 μL) and the reagent solution (5.0 mL) for more than 10 min. Actually, 30 min is necessary to achieve the maximum absorbance.

In the case of μFIA system, inlet of the μFIA chip and a programmable syringe pump (Harvard, MODEL 11 or MODEL 11-IW) were connected with polytetrafluoroethylene (PTFE) tubing of 0.50 mm i.d., via four-position valve (EYELA, VF-3420) in the case of the system without separation part, or six-position valve (Rheodyne Co., Model 9060) in the case of that with separation part, respectively. In the case of the system without separation part, the sample was directly injected into the reagent solution stream. In the case that with separation part, the carrier (10 mM potassium phosphate buffer, pH 6.5), sample, carrier, and elutant (100 mM potassium phosphate buffer, pH 6.5) were sequentially dispensed from inlet #1 into the μFIA chip, while the reagent solution was dispensed from inlet #2 simultaneously.

The absorbance was measured at 595 nm by using an Ocean Optics UV–vis spectrometer (USB2000, Ocean Optics Inc.). Fiber optic cables furnished with a stainless steel clad tip (400 μm i.d.) were used to connect the μFIA chip. Each analysis was repeated thrice, to obtain the calibration curves by plotting the average peak top values of the absorbance against reference

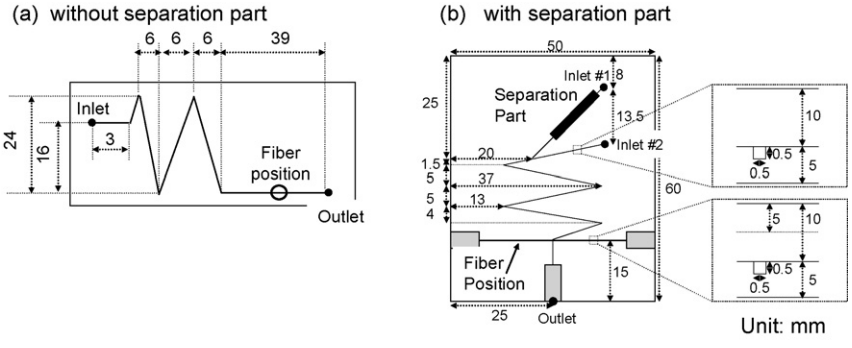

Fig. 1. Schematic diagram of μFIA system.

absorbance of carrier solution. A pH meter (F23, Horiba) was used to determine the pH of solutions.

2.4. Adsorption and elution behavior of protein with ceramic hydroxyapatite

The adsorption and elution behaviors of BSA with the ceramic hydroxyapatite were evaluated by both the conventional batchwise and column methods. In the case of batchwise method, potassium phosphate buffer of pH 5.5–9.0 containing 333.3 μg/mL of BSA was used as a feed solution. Two milliliters of feed solution was mixed with 0.05 g of ceramic hydroxyapatite, and shaken vigorously for 1 h at 25 °C. After centrifugal separation, the pH value and concentration of BSA were measured. In the case of column method, hollow column of 8 mm in length, 2 mm in width, and 2 mm in depth was made on PMMA plate, and 0.01 g of ceramic hydroxyapatite was packed in the column part (wet volume was 3.8 μL).

The 10 mM potassium phosphate buffer (pH 6.5) including 300 μg/mL BSA was fed into the column with 20 μL/min. After the adsorption, the column was washed once with 10 mM potassium phosphate buffer (pH 6.5) and then eluted with 100 mM potassium phosphate buffer (pH 6.5) at 20 μL/min. The effluent was collected at 45 s interval. The concentration of BSA was measured at the absorbance of 595 nm with a microplate reader (Model 680, Bio-Rad), followed by mixing the sample and CBB solutions at volume ratio of 1:50. Bed Volume was defined as the ratio of volume of effluent by wet volume of the adsorbent.

3. Results and discussion

3.1. μFIA system without separation part

Preliminary, the channel length of μFIA system was optimized for single protein assay with the μFIA chip without separation part. Considering the colorimetric reaction requires ca. 30 min, the longer flow channel is expected to give better results. However, the μFIA system with relatively short channel obtained wider calibration range. This is because the sample zone is dispersed too much during the traveling followed by worse FI peak, due to the small volume of the sample (mostly 3.33 μL). Therefore, the μFIA chip with shorter flow channel (Fig. 1a) was used in the present work. When 2 μL of sample was dispensed into the reagent solution stream, the linear relationship between the BSA concentration and absorbance at 595 nm (A_{595}) was widely obtained, with $Y = 5.80 \times 10^{-5}X + 3.58 \times 10^{-3}$ ($r^2 = 0.982$, 0–500 μg/mL).

Artificial urine was applied to detection of the urinary protein concentration with the μFIA chip without separation part. Although 300 μg/mL of BSA was originally contained in the artificial urine, lower concentration of BSA was detected as 166 μg/mL. Since this is due to the interference with other components containing in the artificial urine [9], the separation of protein from other components is necessary to detect the accurate concentration.

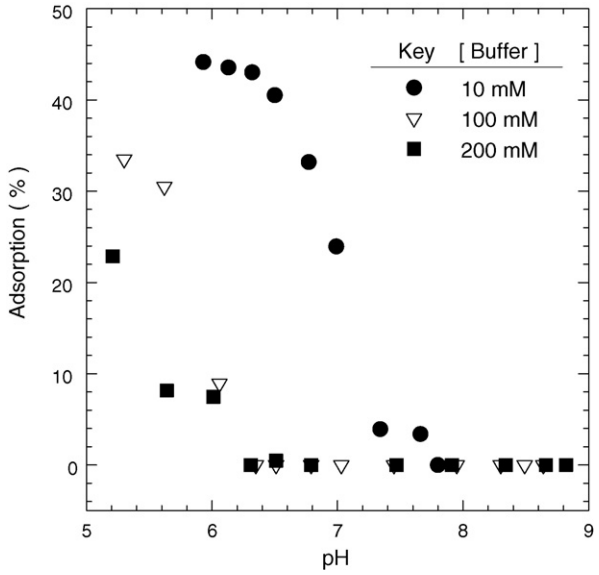

Fig. 2. Effect of pH values on the adsorption percentage of BSA on ceramic hydroxyapatite.

3.2. Adsorption behavior of protein on ceramic hydroxyapatite

The protein adsorption on the hydroxyapatite is based on the electrostatic interactions between carboxyl group of protein and calcium of hydroxyapatite as well as between amino groups of protein and phosphoric groups of hydroxyapatite. The adsorption of protein on the hydroxyapatite therefore depends on both pH value and ionic strength of the solution. Potassium phosphate buffer was used in the present work, because calcium was eluted from the hydroxyapatite in sodium phosphate buffer. Fig. 2 shows the effect of equilibrium pH on the adsorption percentage of BSA. The adsorption of BSA decreases with increase in the pH values in all cases. The adsorption in low pH range dramatically decreases with the ionic strength of the phosphate buffer. The effective adsorption could be achieved in pH < 6.5 of 10 mM phosphate buffer solution, while the elution could be carried out with 100 mM buffer solution of pH > 6.3. Fig. 3 shows the elution curve of BSA from the column with 100 mM potassium phosphate buffer solution (pH 6.5). The BSA was effectively eluted with 83.1% efficiency. When separation part is combined with the μFIA, the quantitative adsorption-elution of BSA in urine would be expected.

3.3. μFIA system combined with separation part

The adsorptive separation of protein on ceramic hydroxyapatite was combined with the μFIA. Two inlets were prepared for the sample solution and for the reagent solution, since the ceramic hydroxyapatite is dissolved by acidic reagent solution. The standard solution and artificial urine, dissolved in 10 mM potassium phosphate buffer, were preliminary fed to the μFIA chip. The sample solution of BSA in 10 mM phosphate buffer (3.33 μL), 10 mM phosphate buffer (30 μL), and 100 mM phosphate buffer (elutant, 80 μL) were sequentially dis-

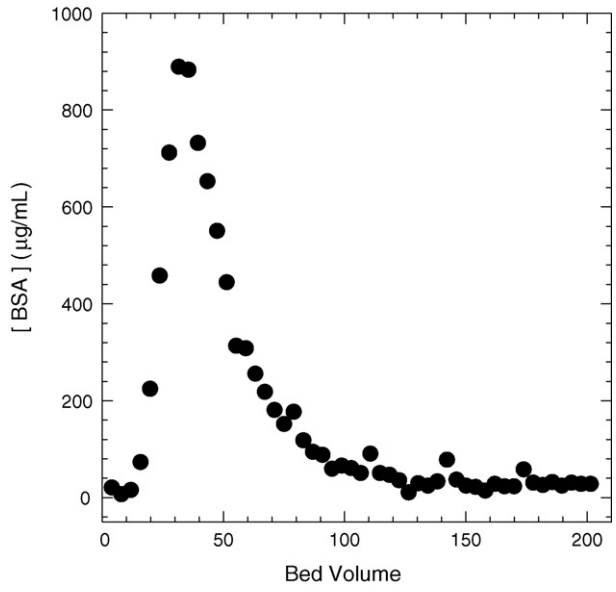

Fig. 3. Elution curve of BSA adsorbed on ceramic hydroxyapatite. Elutant is 100 mM potassium phosphate buffer (pH 6.5) and flow rate is 20 μL/min.

pensed from the inlet #1 with flow rate of 20 μL/min, while the reagent solution was dispensed from inlet #2 with flow rate of 30 μL/min. The FI peaks obtained and the calibration curve are shown in Fig. 4a and b, respectively. The ideal FI peaks were observed and the calibration curve with good linearity were obtained ($Y = 5.01 \times 10^{-4}X + 6.61 \times 10^{-2}$, $r^2 = 0.999$, 0–1000 μg/mL). The limit of detection (LOD) value, defined as the ratio of three times standard deviation of the background signal to the slope of the calibration curve, was obtained to be 15.8 μg/mL. The results indicate that the adsorbed BSA was successfully eluted from the separation part with the elutant. When the artificial urine, which includes 300 μg/mL of BSA and pH 6.44, was measured by the present protocol, the BSA concentration was obtained to be 324 μg/mL (R.S.D. = 2.07, $n = 3$). Since interference with other components in the artificial urine can be prevented, the BSA concentration can be detected quantitatively by using the proposed system, even in the multi component system like urine.

The determination of protein concentration should be achieved in wide pH range of the human urine. In this protocol of μFIA with separation part of the ceramic hydroxyapatite, however, the pH value of ca. 6.5 was required for the quantitative adsorption–desorption. Since the effect of pH of the sample on the calibration with the present system was investigated, there was no significant influence to the detection of BSA from pH 6.3 to 6.6. The preliminary tests revealed the pH values of the artificial urine, from 2 to 12, could be adjusted to 6.3–6.6 by 21 times dilution with 10 mM buffer (pH 6.5). The larger sample volume and correspondingly longer separation part are thus required to obtain the sufficient sensitivity. When the μFIA chip with the separation part of 30 mm in length was used, the sample solution of single BSA solution in 10 mM phosphate buffer (50 μL), 10 mM phosphate buffer (50 μL), and 100 mM phosphate buffer (elutant, 100 μL) were sequentially dispensed from the inlet #1 with flow rate of 20 μL/min, while the reagent solution was dispensed from inlet #2 with flow rate of 20 μL/min. The calibration curve, with a linear relationship of $Y = 1.14 \times 10^{-2}X + 1.46 \times 10^{-1}$ ($r^2 = 0.991$, 0–40 μg/mL), was obtained by using this protocol. The sensitivity was greatly improved by increasing the sample volume and lower LOD value of 1.59 μg/mL could be obtained. When the urinary protein containing 300 μg/mL of BSA was measured following 21 times dilution (the concentration of BSA was 14.3 μg/mL after dilution), the BSA concentration was obtained as 12.0 μg/mL (R.S.D. = 0.023, $n = 3$). These results indicate that by using the proposed μFIA system, the interference of other

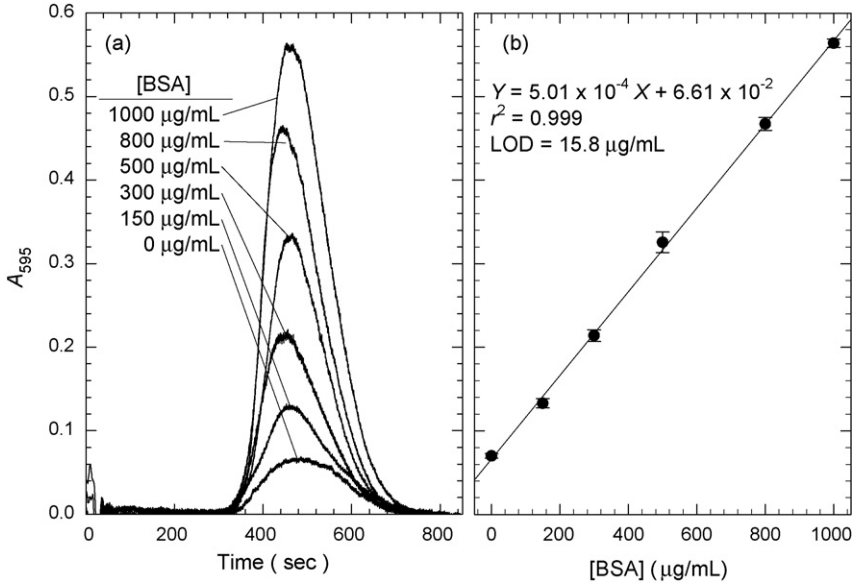

Fig. 4. (a) Actual FI peak and (b) calibration curve with the μFIA system with the separation part of 15 mm. Stacked zone of 3.33 μL of sample, 30.0 μL of 10 mM potassium phosphate buffer (pH 6.50, carrier), and 80.0 μL of 100 mM potassium phosphate buffer (pH 6.50, elutant) are dispensed from inlet #1, together with the reagent solution from inlet #2. The light pass is 5 mm, and the flow rate from the inlet #1 is 20 μL/min and that from the inlet #2 is 30 μL/min.

components and pH of the artificial urine could be prevented significantly.

When the total urine assay system for the POCT is to be developed, three components, glucose, protein, and blood, are at least required to be determined sequentially or simultaneously. The design of reagent cartridge, sample input unit, stream switching unit and the optimization of the protocol will be necessary for establishing the total urine instrument.

4. Conclusion

A μFIA system combined with the separation part has been investigated for the urinary protein assay, with the following results. The μFIA system with the separation part with ceramic hydroxyapatite was fabricated on the PMMA plate. The quantitative adsorption and desorption of protein can be achieved by just feeding the sample and elutant solutions, to obtain the typical FI peak. The concentration of protein in artificial urine containing other seven components can be quantitatively detected by using the μFIA system with the separation part. This μFIA approach combining with separation technique improves the quantitative urinary protein assay, with only pre-dilution of urines.

Acknowledgement

This work was supported by fund from the MEXT via Kitakyushu innovative cluster project.

References

[1] H. Manz, Becker (Eds.), Microsystem Technology in Chemistry and Life Sciences, Springer-Verlag, Berlin, 1999.
[2] J. Ruzicka, E.H. Hansen, Flow Injection Analysis, John Wiley & Sons, USA, 1988.
[3] J. Ruzicka, G.D. Marshall, Anal. Chim. Acta 237 (1990) 329.
[4] S. Nishihama, L. Scampavia, J. Ruzicka, J. Flow Injection Anal. 19 (2002) 19.
[5] Q. Jia, T. Matoba, S. Nishihama, K. Yoshizuka, Anal. Sci. 22 (2006) 99.
[6] M.M. Bradford, Anal. Biochem. 72 (1976) 248.
[7] J.J. Sedmak, S.E. Grossberg, Anal. Biochem. 79 (1977) 544.
[8] J.A. Johnson, J.A. Lott, Clin. Chem. 24 (1978) 1931.
[9] H.M.C. Heick, N. Begin-Heick, C. Acharya, A. Mohammed, Clin. Biochem. 13 (1980) 81.
[10] J.A. Lott, V.A. Stephan, K.A. Pritchard Jr., Clin. Chem. 29 (1983) 1946.
[11] L. Cummings, T. Ogawa, P. Tunon, Spec. Publ. Roy. Soc. Chem. 158 (1994) 134.

Available online at www.sciencedirect.com
ScienceDirect
Talanta 74 (2008) 1442–1449
Talanta
www.elsevier.com/locate/talanta

Fluorimetric determination of cyclofenil using photochemical derivatization

Wagner F. Pacheco, João A.L. Batalha, Cláudia C. de Oliveira, Ricardo Q. Aucelio *

Chemistry Department, Pontifícia Universidade Católica do Rio de Janeiro (PUC-RJ), Rio de Janeiro, RJ 22453-900, Brazil

Received 15 May 2007; received in revised form 26 September 2007; accepted 26 September 2007
Available online 2 October 2007

Abstract

In this work, a fluorimetric approach for the determination of cyclofenil, 4-4′-(cyclohexylidenemethylene)bis(phenylacetate), is presented. The method was based on the intense fluorescence (250/410 nm) observed after a UV photochemical treatment of cyclofenil. The influence of the pH and solvent system and UV exposure time on the fluorescence magnitude was studied. Optimization of parameters was made using experimental design (factorial design and central composite design). Limit of detection ($3S_b/m$) were estimated to be 1.1×10^{-8} mol L^{-1} with the linear dynamic range extending up to 8×10^{-5} mol L^{-1}. This analytical approach was tested through the analysis of a commercial pharmaceutical formulation. In this case, tests enabled an average recovery of $98.3 \pm 3.9\%$ (for $n = 9$) using the analytical curve. The identification of the fluorescent derivative is proposed based on results achieved from GC-MS.
© 2007 Elsevier B.V. All rights reserved.

Keywords: Cyclofenil; Spectrofluorimetry; Photochemical derivatization; Experimental design

1. Introduction

Cyclofenil is a drug with useful clinical applications. It is the active ingredient of pharmaceutical formulations employed for the stimulation of the ovaries and for the minimization of the symptoms related to female menopause [1–3]. Cyclofenil has also been used for the treatment of scleroderma, a disease characterized by the hardening of the skin [4–6]. Scleroderma or more properly termed "systemic sclerosis" is a complex disturbance of connective tissue, the vasculature, and the immune system. Such disease has always been difficult to treat and the survival rates are traditionally low. Nevertheless, a better understanding of the pathogenesis and the development of new therapies have enabled successful treatments [7]. Cyclofenil is one of the several agents have been tried to treat scleroderma, although controlled studies did not answer whether cyclofenil treatment over longer periods will exert a clinically significant effect [5].

Cyclofenil acts as an estrogen receptor blocker, allowing natural estrogens to be free in the organism therefore, this drug has been extensively used as illicit means of enhancing the performance of male athletes. For this reason, cyclofenil is an anti-estrogenic substance included in the World Anti-Doping Agency prohibited list [8].

There are only few analytical methods described in the literature for the detection and quantification of cyclofenil. Flame ionization gas chromatography has been used to determine cyclofenil after its extraction from bovine muscle tissue [9]. Analyte recovery of 95% has been reported with detection power estimated to be 0.02 μg g^{-1}. A spectrophotometric method was used for quantification of cyclofenil at 272 nm after analyte acid derivatization [10]. The derivatization was necessary because cyclofenil is not stable in aqueous solution. This method was used to analyze pharmaceutical formulations with recoveries of $101.6 \pm 0.8\%$. Although the limit of detection was not reported, this value has been estimated to be in the range of 10^{-6} mol L^{-1}. Gas chromatography coupled to mass spectrometry and chemical ionization tandem mass spectrometry coupled with high performance liquid chromatography have been employed only to detect the presence of cyclofenil and two of its metabolites [11]. The performance of this procedure for quantification of cyclofenil cannot be evaluated since this capability was not reported. Recently, square-wave adsorptive voltammetry was applied to enable the determination of cyclofenil at ultra-trace levels [12]. In this case, a stable and electrochemical active analyte photoderivative (peak potential at −1280 mV) was used

* Corresponding author. Fax: +55 21 3114 1637.
E-mail address: aucelior@rdc.puc-rio.br (R.Q. Aucelio).

0039-9140/$ – see front matter © 2007 Elsevier B.V. All rights reserved.
doi:10.1016/j.talanta.2007.09.022

for quantification after pre-concentration on the hanging mercury drop electrode. Limit of detection of 1.5×10^{-8} mol L^{-1} was achieved but with a relatively narrow linear dynamic range (about two orders of magnitude). Recovery tests enabled results from 93.6% to 106.5%. In the literature, there is no report of analytical methods based on the luminescence from cyclofenil.

In this paper, a sensitive spectrofluorimetric method is proposed. The method is based on the measurement of highly fluorescent cyclofenil derivative obtained through photochemical treatment with UV radiation. Several factors that influence the sensitivity of such determination were optimized using multivariate experimental design. The fluorimetric method is at least two orders of magnitude more sensitive than the reported spectrophotometric method and comes as an alternative to the sensitive voltammetric method which is based on the use of toxic mercury-based electrodes. This new analytical approach was tested through the analysis of one cyclofenil-based pharmaceutical formulation.

2. Experimental

2.1. Instrumentation

Fluorescence measurements were made on a Perkin-Elmer LS-45 luminescence spectrophotometer. Fluorescence spectra were acquired on a PC using the FLWinlab® software. A 10 nm spectral bandpass and a 600 nm mm^{-1} scan velocity were used. Quartz cuvetes (1 cm optical pathlength) were used to accommodate samples and blanks. A laboratory made photochemical reactor was used for the treatment of samples and standards. The photochemical reactor was constructed using an oven unit cabinet that was adapted by covering its internal part with aluminum foil and placing four 6 W mercury vapor sterilization lamps (with most intense UV lines at 253 nm and in the 296–313 nm range) on the top of the internal cavity. During operation, the internal temperature of the reactor did not surpass 30 °C. Solutions were placed in quartz test tubes during the photochemical treatment. A pH meter (MS Tecnopon, model MPA-210, Brazil) was employed.

GC-MS studies were made in a Hewlett Packard gas chromatograph model 5890 series II Plus with a mass detector model 5972 MSD (ion monitoring mode) and a capillary type column (30 cm length and 0.25 internal diameter) HP5MS, Splitless type sample injection was made with a injector kept at 300 °C. He (1 mL min^{-1}) was used as carrier gas. Laser desorption ionization (LDI) experiments were carried out in a laboratory-made two stage ion source linear modern laser desorption time-of-flight (TOF) mass spectrometer equipped with a delayed extraction system. The 337 nm radiation from a nitrogen laser (VSL-337-ND-S), Laser Science Inc., Franklin, MA, was brought into focus on the target with a 30° incidence angle after passing through a variable density neutral attenuator from Oriel, Stratford, CT.

2.2. Reagents

All chemical reagents were of analytical grade. De-ionized water (18.2 MΩ cm), from a water ultra purifier Master System 1000 (Gehaka, Brazil), was used to prepare all aqueous solutions. Cyclofenil was from Sigma, USA and the pharmaceutical formulation (Menopax® from Aché laboratories), containing 200 mg of cyclofenil per tablet, was obtained from local drugstores. Methanol, sulfuric acid, boric acid, phosphoric acid, acetic acid, sodium hydroxide was obtained from Merck (Darmstadt, Germany).

2.3. Procedures

2.3.1. Preparation of standard solutions

The cyclofenil stock solution (1.0×10^{-3} mol L^{-1}) was prepared by dissolving a specific mass of cyclofenil in methanol. Standard solutions with lower concentrations were made by further dilution of the stock solution with methanol. Britton–Robinson buffer (0.04 mol L^{-1}) was prepared by mixing acetic acid, boric acid and phosphoric acid aqueous solutions. The pH of the buffer was adjusted by adding concentrated sodium hydroxide solution.

2.3.2. Sample photochemical treatment

The optimized procedure to produce the photochemical derivative from samples and standards is described as follows: cyclofenil solution prepared in methanol was transferred to quartz test tubes (1.9 cm diameter and 13.7 cm high) and UV irradiated for 120 min. Then, 1 mL of the irradiated solution was mixed with 1 mL Britton–Robinson buffer (pH 10.5). The final volume (10 mL) was then adjusted by the addition of methanol. These solutions were stored until measurement since they were found to be stable under ambient light. Quartz cuvettes were washed with 1 mol L^{-1} nitric acid solution and deionized water before each fluorescence measurement.

2.3.3. Pharmaceutical sample preparation

The commercial pharmaceutical sample was prepared by pulverizing ten tablets of Menopax® with a pestle and a mortar. Three portions of the pulverized mass were separated, each one containing an amount of cyclofenil equivalent to 4 mg (according to the medicine instructions), and used to prepare three solutions. These three portions of pulverized material were mixed with methanol forming suspensions. These suspensions were vacuum filtered using a Buchner funnel and a piece of quantitative filter paper. The filter paper was washed several times with small volumes of methanol. Solutions were then prepared according procedure described in Section 2.3.2.

3. Results and discussion

3.1. Photochemical-induced fluorescence of cyclofenil

Photochemical reactions have been used to enhance luminescence from several substances of clinical–biological interest such as antihypertensives [13,14], antimicrobials [15], antidepressants [16], and anti-inflammatories [17–19]. This procedure may generate derivative species with higher fluorescence quantum efficiency from the original analyte molecule, improving the analytical signal and therefore the sensitivity of determinations.

Photochemical derivatization is an easy way to obtain fluorescent derivatives without the use of expensive and toxic chemical derivatization agents.

When dissolved in methanol, cyclofenil displays a weak natural fluorescence characterized by two excitation bands with maximum wavelength (λ_{exc}) at 306 and 381 nm and an emission band with maximum wavelength (λ_{em}) at 409 nm. Fluorescence from cyclofenil does not increase by its dissolution in organized aqueous media containing sodium dodecyl sulfate. Photometric studies have indicated that changes in cyclofenil structure are caused by the incidence of UV radiation since a bathochromic shift of 26 nm on the absorption band maximum was observed followed by absorbance increase of almost two times after only 15 min of UV exposure [12]. In terms of fluorescence, 60 min of UV exposure caused significant amplification (10 times) of the cyclofenil excitation band with λ_{exc} at 306 nm. In such a case, its emission band had a λ_{em} at 400 nm and a shoulder with maximum at 420 nm. Such a result indicates the formation of a fluorescent derivative with a higher fluorescence quantum yield than the one of the original analyte molecule. Variations in spectral characteristics of the cyclofenil photoproduct were very dependent upon composition of the solvent system and on the pH, which indicated three important factors to be studied: UV irradiation time, solvent system and pH.

3.2. Optimization of experimental parameters

In order to optimize the UV derivatization of cyclofenil, a univariate study of parameters was employed since no previous information was known about such chemical behavior of the system. Then, based on these univariate studies, factorial design was employed in order to establish the hierarchy of the importance of the main effects (principal experimental factors) and the interaction effects among these factors, and to achieve the final adjustment of the best conditions for the derivatization method.

3.2.1. Univariate studies

A first evaluation of the influence of the UV exposition time was made using cyclofenil dissolved only in methanol. The increasing of fluorescence (306/400 nm) occurred in two steps characterized by two signal plateaus, the first one between 25 and 75 min and the second one from 150 min of UV exposure (Fig. 1) where fluorescence remained constant up to 200 min. Such behavior indicated that photochemical derivatization may occur in two steps. Fluorescence (measured as peak height) from cyclofenil solutions irradiated for 150 min was about 50 times more intense than the one observed from non-irradiated cyclofenil, therefore, for the following univariate studies, 150 min UV treatment was used.

Fluorescence from the UV irradiated cyclofenil was evaluated in solutions containing different methanol/water proportions (90/10; 80/20; 50/50; 20/80 and 10/90%, v/v) at three different pH values (4, 8 and 10) adjusted using Britton–Robinson buffer. Methanol was used as the organic solvent because of the easy dissolution of cyclofenil. The reason in performing such study can be found in two previous works. The first one reported the non-stability of cyclofenil in aqueous solutions [10] while a second study, involving voltammetry, indicated the non-stability of cyclofenil in aqueous solutions while stable current signal and redox potential were observed from its UV photoderivative even in aqueous solution [12].

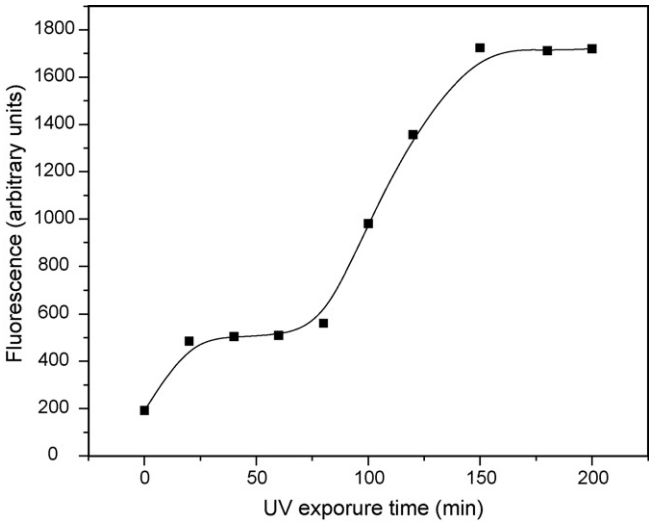

Fig. 1. Fluorescence signal from cyclofenil (1×10^{-4} mol L^{-1}) in function of UV exposure time.

When compared to the signal observed in solutions containing only methanol as solvent, the presence of water has shifted the λ_{em} to about 420 nm. The general trend was the observation of best signals in solutions containing higher quantities of methanol, in special, at higher pH values of the Britton–Robinson buffer added as part of the aqueous phase of the mixture (Fig. 2A). The effect of the hidrogenionic concentration was studied in more detail by measuring fluorescence from UV treated cyclofenil solutions containing lower content of water (10% and 20% in volume) using Britton–Robinson buffer at pH values between 2 and 12 (Fig. 2B). The best results were obtained for solutions containing buffer at pH 10, where significant differences in the $\lambda_{exc}/\lambda_{em}$ (250/410 nm) were observed in contrast to the $\lambda_{exc}/\lambda_{em}$ values found in the neutral-acid range.

3.2.2. Multivariate studies

Experimental design was used to get a final adjustment of experimental conditions, evaluate the hierarchy of the principal effects and identify any antagonic or synergic interaction among the main experimental factors. The amplitude for each of the parameters was chosen based on the results achieved from the univariate studies. The 3^3 factorial design was used and the chosen factors were: UV exposure time, pH and volume of buffer. For UV irradiation time, the lower level (−1) was 120 and 180 min was the higher level (+1), therefore, the intermediate point (0) was 150 min. The pH values chosen were pH 6 (−1), pH 8 (0) and pH 10 (+1). The final factor to be evaluated was the proportion of the aqueous phase in the solvent system, added as buffer solution. For 10 mL final sample volume, the amplitude of aqueous buffer was set from 1 mL (+) to 3 mL (−), with the intermediate point of 2 mL (0). The experiment was made using two authentic replicates for each experiment.

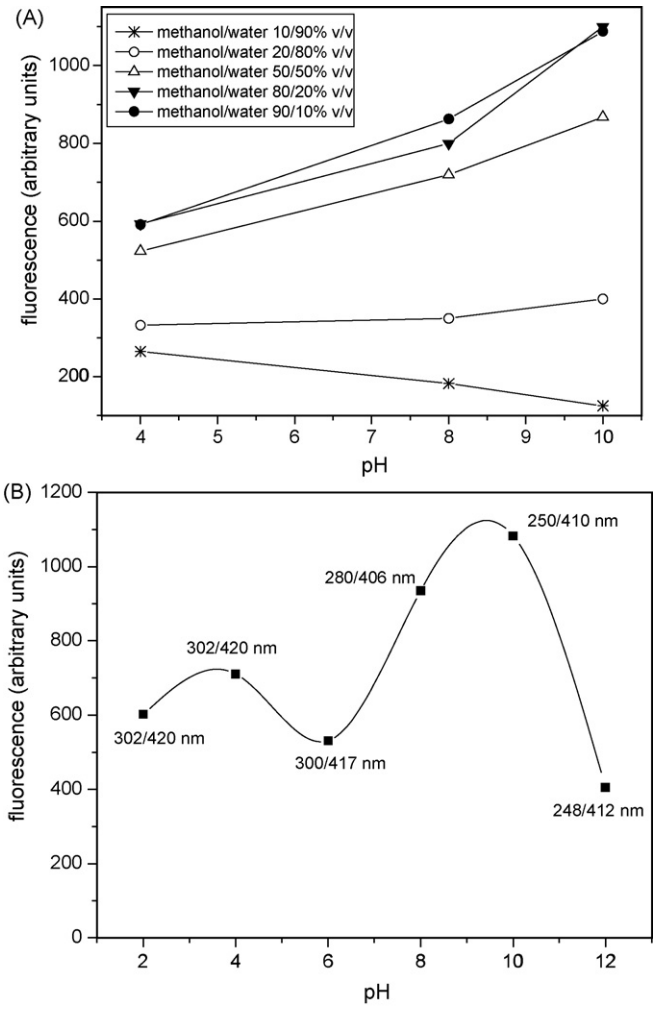

Fig. 2. Fluorescence from UV irradiated cyclofenil (5×10^{-5} mol L^{-1}) in function of pH (A) in different methanol/water proportions and (B) in methanol/water 90/10% (v/v).

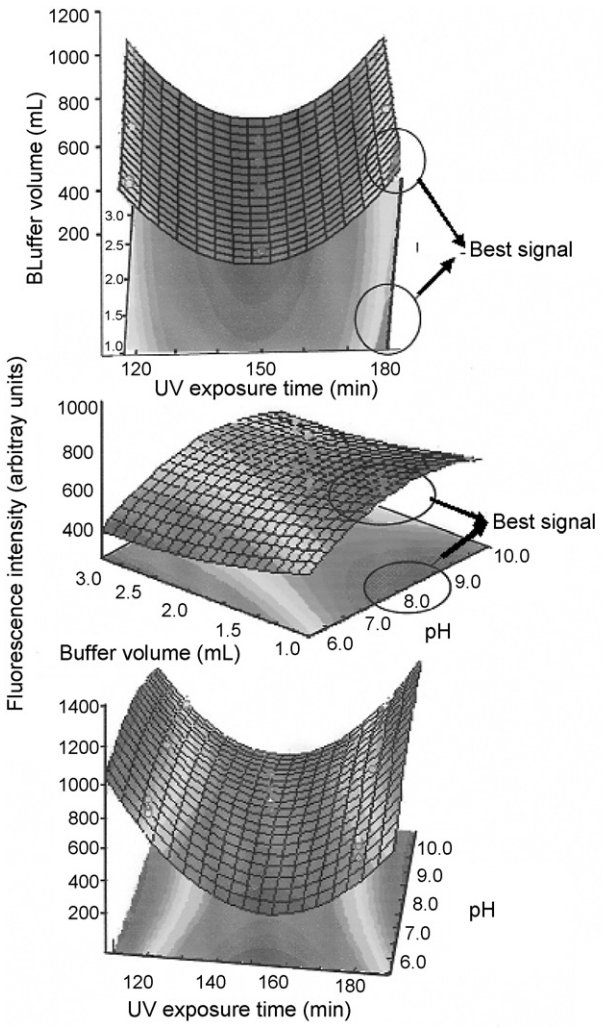

Fig. 4. Response surfaces from the third-level factorial design of the photoderivatization of cyclofenil.

The Pareto's chart (Fig. 3) obtained from these experiments indicated that for the chosen range of parameters, the UV irradiation time is the most relevant effect and has a quadratic contribution. Still significant but lower in hierarchy of the principal effects are the linear contribution of the volume of buffer and the pH. A relevant interaction between UV irradiation time and pH was also detected. Other interactions were statistically insignificant. The chart also indicated that maximum response is obtained by lowering the volume of the aqueous buffer, with response surfaces (Fig. 4) showing that best results are achieved by using 1 mL buffer volume and pH between 7 and 9. Up to this point, the results for UV exposure time were inconclusive in terms of selecting the optimum value since it indicated a quadratic behavior in function of the pH of the buffer solution (confirming what was indicated by the Pareto's chart) and a maximum value seemed to be outside the studied range.

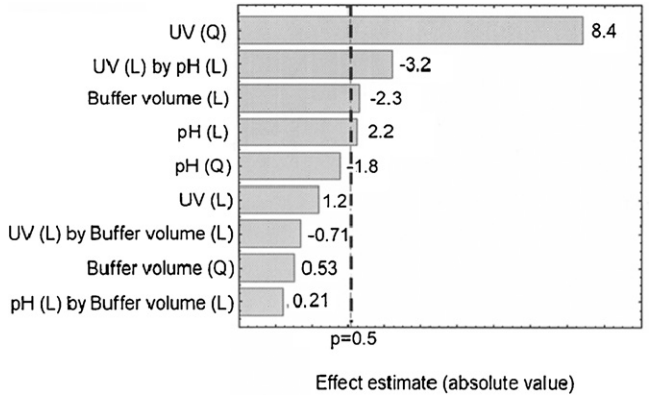

Fig. 3. Pareto's chart from the third-level factorial design of the photoderivatization of cyclofenil.

In order to establish the best experimental conditions, a central composite design was made using only two of the factors: UV exposure time and pH, since the best results were clearly achieved at lower buffer volume (1 mL). The chosen levels (*level*): *pH and UV exposure time*, established were ($\sqrt{2}$): pH 10.8 and 204.8 min; (+1): pH 10 and 180 min; (0): pH 8 and 120 min; (−1): pH 6 and 60 min; ($-\sqrt{2}$): pH 5.2 and 35.2 min. Replicates ($n = 3$) was made only at the central point (0). Fig. 5 displays the resultant response surface which has the following equation model (using codified coefficients) for the best

fluorescence signal (I):

$$I = 806.4 + 98.3(\mathrm{UV}) - 210(\mathrm{UV})^2 + 148.5(\mathrm{pH}) - 52.3(\mathrm{pH})^2 - 57.1(\mathrm{UV})(\mathrm{pH})$$

The resolution of the equation indicated that the best values for UV exposure time and pH were, respectively, 122.6 min and 10.8. The pH value indicated by the model is at the limit of the studied range, which could require the performing of a new design covering a pH range that includes higher values. However, since Pareto's chart (Fig. 5) for the experiment indicated that the final adjustment would be achieved by a small decreasing of pH ($t = -2.9$) and the univariate experiment using the methanol/water 10/90% (v/v) showed a fluorescence decreasing when pH changed from 10 to 12, only a robustness test was performed to verify the correct choice of pH. The robustness involved the measurement of fluorescence for irradiated cyclofenil solutions set at pH 10.5, 10.8 and 11.0. The study indicated that statistically similar results were observed ($n = 3$, 95%). Similarly, a robustness study was made using variations on the UV irradiation time around the value indicated by the equation of the model. The results indicated that fluorescence intensities were statisticaly the same ($n = 3$, 95%) from cyclofenil solutions irradiated during 115, 120 and 125 min. Optimized experimental values for the critical parameters are indicated in Table 1, and under such conditions, the fluorescence from the UV irradiated cyclofenil is shown in Fig. 6.

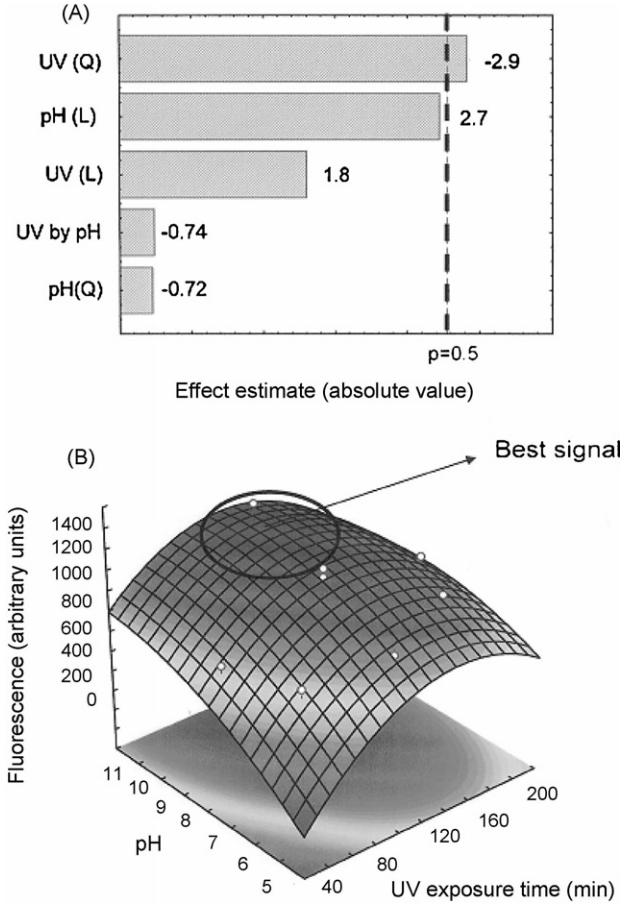

Fig. 5. Central composite design for the UV derivatization of cyclofenil: (A) Pareto's chart and (B) response surface.

Table 1
Optimized experimental conditions for photoderivatization

Experimental parameter	Optimized value
UV exposure time	115–125 min.
pH	10.5–11.0
Britton–Robinson buffer 0.04 mol L^{-1}	10% in volume

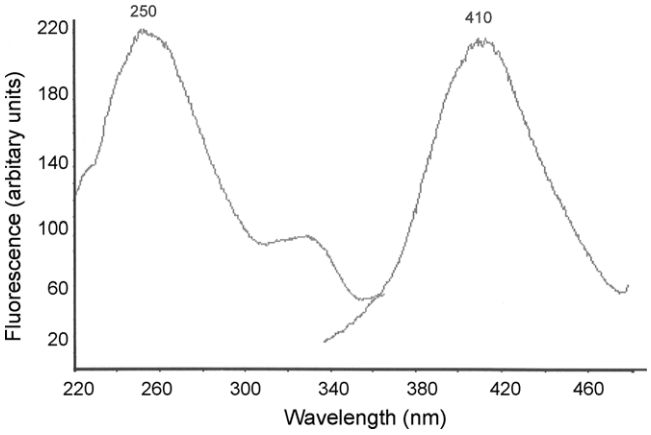

Fig. 6. Fluorescence spectrum of cyclofenil after photoderivatization.

3.3. Analytical performance of the method

3.3.1. Analytical figures of merit

Three analytical curves for cyclofenil using the photochemical derivatization approach were constructed. The maximum concentration of cyclofenil used was 8×10^{-5} mol L^{-1} in order to guarantee total solubilization of the analyte in the solvent system. A linear response with a homoskedastic behavior was found. The average analytical curve equation (confidence limit of 95%) is described by $Y = (2.65 \pm 0.08) \times 10^7 X + (49.7 \pm 25.6)$ with a coefficient of determination (r^2) of 0.9951. Limit of detection ($3S_b/m$) was estimated to be 1.1×10^{-8} mol L^{-1} while the limit of quantification was 3.7×10^{-7} mol L^{-1}. Repeatability studies were performed by consecutive fluorescence measurements from 10 cyclofenil solutions (5×10^{-7} and 1×10^{-5} mol L^{-1}). For both concentration levels, relative standard deviations (R.S.D) were below 4%. The comparison of the results achieved by two different analysts did not indicate any impact on the R.S.D. value indicated above.

3.3.2. Pharmaceutical formulation analysis

In order to test the method, the analytical determination of cyclofenil was performed using one available commercial formulation containing cyclofenil (Menopax, Aché®). This formulation contained 200 mg of cyclofenil and 100 mg of other non-fluorescent components (corn starch, microcrystaline cellulose, magnesium stearate, polvidone and manitol). A significant part of these substances was separated from cyclofenil during extraction with methanol. Of the concomitant substances,

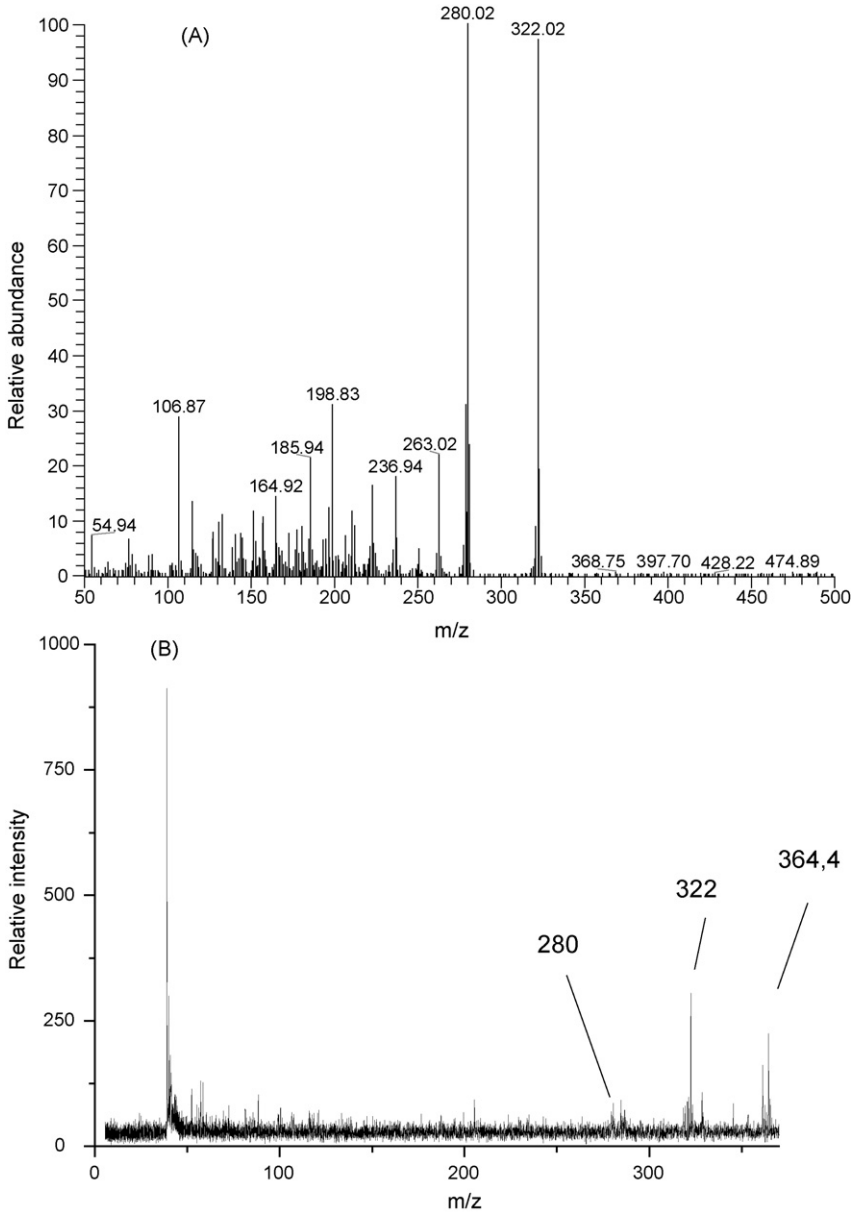

Fig. 7. GC-MS spectra of the UV irradiated cyclofenil solution (A) and LDI spectra from cyclofenil (B).

manitol is the most soluble in methanol, for this reason, the interference test was performed with this substance. Results indicated that no significant interference was observed when manitol was present in solutions at concentrations up to 100 times higher than the concentration of cyclofenil. Since there are no associations of cyclofenil with other active drugs in pharmaceutical formulations, no further interference studies were performed.

Three samples were chosen, each one was prepared from a pool of tablets from a different medicine box. Each sample was divided in three different portions and each one of them was analyzed separately in order to evaluate the day-to-day repeatability and reproducibility of the overall procedure. The results displayed in Table 2 indicated adequate precision (R.S.D. of recoveries below 5%, considering the independent samples) and overall standard deviation of 3.9% considering all recovery tests (three portions for each of the three samples, $n = 9$). Overall recovery of $98.3 \pm 3.9\%$ (values between 93.2% and 103.2%) was achieved. Variance analysis indicated that average recoveries achieved for each sample were statistically similar at the 95% confidence limit.

Table 2
Recoveries from the analysis of pharmaceutical formulation containing cyclofenil

Replicate (sample portion)	Recoveries			
Sample	Portion 1 (%)	Portion 2 (%)	Portion 3 (%)	Average result (%)
1	102.4	94.1	99.3	98.6 ± 4.2
2	94.2	93.2	102.4	96.6 ± 5.0
3	103.2	97.4	98.2	99.6 ± 3.1

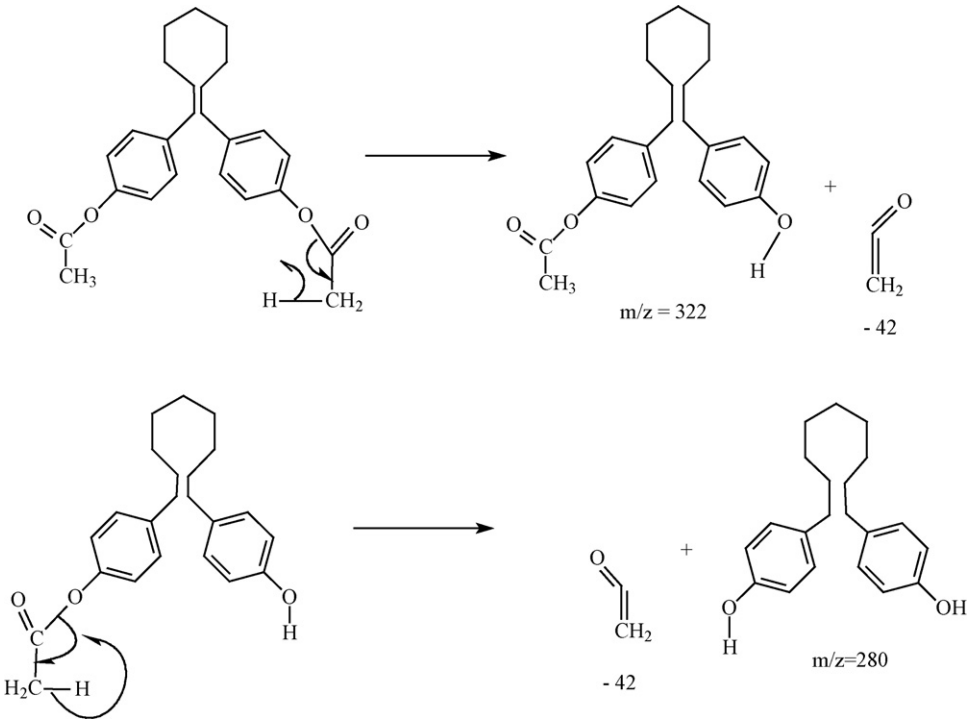

Fig. 8. Cyclofefil and its potential fluorescent photoderivatives.

3.3.3. Stability of the photoderivative

Stability tests were performed by monitoring fluorescence from the photochemical derivative of cyclofenil. The fluorescence was measured right after derivatization and after 6, 12, 24, 48, and 72 h as well as 1 week after derivatization. During storage, the sample was placed inside a refrigerator. The fluorescence intensity has shown variation less than 5% during the period of testing.

3.4. Proposed mechanism for the formation of photoproduct

Attempts to identify the fluorescent photoproduct produced by the UV treatment of cyclofenil were made. GC-MS experiments were performed using cyclofenil solutions (1×10^{-3} mol L^{-1}) before and after UV irradiation. By evaluating the mass spectra, the cyclofenil peak (*m/z* = 364.02 Da) and its fragmentation sequence was obtained at the retention time of 34.08 min. At 33.15 min, the peaks of the species with *m/z* at 322 and 280 Da and their fragmentation sequence (Fig. 6) are observed. The intensity of these two species (*m/z* of 322 and 288 Da) increased significantly (around four times) for the UV irradiated sample, indicating that the UV treatment favored their production (Fig. 7A). This behavior are in agreement with the two step profile for the increasing of fluorescence in function of the UV irradiation time (Fig. 1). This suggests that the photochemical process occurs in two steps. The LDI experiments have also indicated the production of two species (*m/z* = 322 and 288 Da) from the interaction of the UV laser beam with cyclofenil (Fig. 7B). The suggested structures for these chemical species and for the mechanism of photoderivatization are indicated in Fig. 8 with the 4-4′-(cyclohexylidenemethylene)bis(phenylhydroxi) being one of the derivatization products (288 Da).

4. Conclusion

A sensitive determination of cyclofenil is proposed using the fluorescent properties of its photochemical derivative. Fluorescence was found to be very dependent upon pH and the amount of water in the solvent system, however, the irradiation time was found to be the most important factor. The photochemical derivatization procedure is simple and clean, requiring no toxic or expensive reagents. Under optimized experimental conditions, fluorescence enabled high sensitivity (LD at the 10^{-8} mol L^{-1} level) and a wider linear dynamic range. These characteristics show a clear advantage over other previously proposed methods. The cyclofenil photoderivative was found to be very stable resulting in good precision of results. The performance of the method was found to be satisfactory when tested by the analysis of commercial pharmaceutical tablets. The method has the potential to be automated, however, in this case, the time required for derivatization must be reduced.

Acknowledgements

The authors thank CNPq and FINEP for financial support. R.Q. Aucélio, W.F. Pacheco and J.A.L Batalha thank scholarship from the Brazilian agencies CNPq and CAPES. The authors thank Dr A.L. Scofield (LABMAN-PUC-Rio) and Dr C.R. Ponciano, respectively, for the GC-MS and LDI data.

References

[1] S. Goto, K. Takakura, K. Nakanishi, T. Yokoi, Y. Noda, Fertil. Steril. 76 (2001) 409.
[2] U. Acharya, D.S. Irvine, M.P. Hamilton, A.A. Templeton, Hum. Reprod. 8 (1993) 437.
[3] S. Friedman, Reproduction 2 (1975) 324.
[4] A. Akesson, B. Blombulow, A. Scheja, P. Wollmer, S. Valind, F.A. Wollheim, Scand. J. Rheumatol. 21 (1992) 238.
[5] T. Gibson, R. Grahame, Brit. J. Rheumatol. 22 (1983) 218.
[6] T. Gibson, R. Grahame, Ann. Rheum. Dis. 40 (1981) 627.
[7] J. Korn, Clev. Clin. J. Med. 70 (2003) 954.
[8] The 2005 Prohibited List, World Anti-Doping Agency, Montreal, 2005.
[9] R.J. Crucs, J. Assoc. Off. Anal. Chem. 55 (1972) 643.
[10] E. Hassam, E.F. Elsayedma, S.T.P. Khamis, Pharm. Sci. 4 (1994) 305.
[11] S. Myung, H. Min, D. Kim, M. Kim, S. Cha, E. Yoo, Y. Yim, Rapid Commun. Mass Spectrom. 16 (2002) 761.
[12] W.F. Pacheco, P.A.M. Farias, R.Q. Aucelio, Anal. Chim. Acta 549 (2005) 67.
[13] J.M. Catalayud, C.G. Benito, Anal. Chim. Acta 245 (1991) 101.
[14] R.Q. Aucelio, Anal. Sci. 17 (2001) 865.
[15] C.G. De Lima, E.M. Nicola, Anal. Chem. 50 (1978) 1658.
[16] M.B.B. Nair, J.J. Aaron, P. Prognan, G. Mahuzier, Analyst 123 (1998) 2267.
[17] L. Bettaieb, J.J. Aaron, Turk. J. Chem. 25 (2001) 165.
[18] A.L. Coelho, R.Q. Aucélio, Anal. Lett. 39 (2006) 619.
[19] C.E. Cardoso, R.O.R. Martins, C.A.S. Telles, R.Q. Aucélio, Microchim. Acta 146 (2004) 79.

Available online at www.sciencedirect.com
ScienceDirect
Talanta 74 (2008) 1556–1561
Talanta
www.elsevier.com/locate/talanta

Kinetic method for the determination of traces of thyroxine by its catalytic effect on the Mn(III) metaphosphate–As(III) reaction

Ferenc T. Pastor*, Gordana A. Milovanović, Marija Todorović

Faculty of Chemistry, University of Belgrade, P.O. Box 158, 11001 Belgrade, Studentski trg 12-16, Serbia

Received 23 July 2007; received in revised form 27 September 2007; accepted 28 September 2007
Available online 2 October 2007

Abstract

A new, highly sensitive and simple kinetic method for the determination of thyroxine was proposed. The method was based on the catalytic effect of thyroxine on the oxidation of As(III) by Mn(III) metaphosphate. The kinetics of the reaction was studied in the presence of orthophosphoric acid. The reaction rate was followed spectrophotometrically at 516 nm. It was established that orthophosphoric acid increased the reaction rate and that the extent of the non-catalytic reaction was extremely small. A kinetic equation was postulated and the apparent rate constant was calculated. The dependence of the reaction rate on temperature was investigated and the energy of activation and other kinetic parameters were determined.

Thyroxine was determined under the optimal experimental conditions in the range 7.0×10^{-9} to 3.0×10^{-8} mol L^{-1} with a relative standard deviation up to 6.7% and a detection limit of 2.7×10^{-9} mol L^{-1}. In the presence of 0.08 mol L^{-1} chloride, the detection limit decreased to 6.6×10^{-10} mol L^{-1}. The proposed method was applied for the determination of thyroxine in tablets. The accuracy of the method was evaluated by comparison with the HPLC method.
© 2007 Elsevier B.V. All rights reserved.

Keywords: Thyroxine; Kinetic catalytic determination of thyroxine; Manganese(III) metaphosphate–arsenic(III) reaction in orthophosphoric acid

1. Introduction

The reduction of manganese(III) metaphosphate with arsenic(III), in the presence of orthophosphoric acid as indicator reaction was applied for trace determination of iodide [1]. We found that this reaction is catalyzed by thyroxine too.

Thyroxine is a thyroid hormone which regulates the rate of cellular oxidative processes in the human body. The thyroid gland is responsible for its synthesis and release. Thyroid hormones are general metabolic stimulants affecting almost all tissues of the body. A deficient or excessive production of thyroid hormones results in clinical disorders in the thyroid function in man, hypothyroidism and hyperthyroidism. In the case of hypothyroidism, thyroxine preparations are favoured for therapeutic use, thus the great need for sensitive analytical methods for the trace determination of thyroxine.

Several kinetic methods for the determination of thyroxine in the submicrogram range were described [2–4]. All of these methods were based on the catalytic effect of thyroxine on the reduction of Ce(IV) by As(III). There are also stopped-flow and flow-injection [5–8], electrochemical [9,10], colorimetric [11], spectrophotometric [12], fluorimetric [13] and chromatographic [14–16] methods. Sensitive and specific, but long-lasting, radio and enzyme-immunoassay methods [17–21] and isotope-dilution methods [22–24] have also been described.

In order to propose a sensitive, simple and inexpensive method for the determination of thyroxine traces, we studied the kinetics of the thyroxine-catalyzed manganese(III) metaphosphate–arsenic(III) reaction in the presence of orthophosphoric acid.

2. Experimental

2.1. Apparatus

Absorbance measurements were performed on a Specol 20 MA-9508 spectrophotometer (Carl Zeiss and Iskra) in a 1 cm cuvette. Absorption spectra were recorded on a GBC Cintra 6 UV–vis spectrophotometer, in a 1 cm quartz cuvette. The temperature was kept constant by means of an NBE ultrathermostat

* Corresponding author. Tel: +381 11 3336 744; fax: +381 11 2184 330.
E-mail address: fpastor@chem.bg.ac.yu (F.T. Pastor).

0039-9140/$ – see front matter © 2007 Elsevier B.V. All rights reserved.
doi:10.1016/j.talanta.2007.09.033

(VEB Prüfgeräte-Werk, Medingen). A Hanna HI 9321 pH-meter fitted with a combined glass–Ag/AgCl electrode HI 1131 was used. The HPLC apparatus (Waters, USA) consisted of a 1525 binary pump, a Rheodyne injector 7725i with a 20 μL loop, a spherisorb 5 μm ODS 2 4.6 mm × 250 mm analytical column and a 2487 absorbance detector.

2.2. Reagents

Analytical reagent grade chemicals (Merck) and redistilled water were used for the preparation of all solutions. The concentrations of the stock solutions were the following (mol L^{-1}): potassium permanganate, 2.03×10^{-1}; Mn(II) sulphate, 1.00; potassium nitrate, 2.5; and orthophosphoric acid, 6.0. Mn(III) solution (0.1 mol L^{-1}) in 3.1 mol L^{-1} metaphosphoric acid was prepared as in our previous paper [1]. For the preparation of the stock solution (1.00×10^{-3} mol L^{-1}) L-thyroxine Sigma T2376 (≥98%, HPLC) was dried for 7 days in a desiccator over phosphorus(V) oxide. The required amount was dissolved in 0.020 mol L^{-1} HCl in ethanol, and kept in refrigerator. The 0.2 mol L^{-1} As(III) stock solution was prepared by dissolving the required amount of As_2O_3 in hot 0.5 mol L^{-1} NaOH solution. After cooling to room temperature, the solution was neutralized with 2 mol L^{-1} H_2SO_4.

2.3. Preparation of the sample solutions

Ten tablets of each drug (Tivoral, Galenika a.d., Belgrade and Letrox 150, Berlin-Chemie AG, Berlin) were dried for 7 days in a desiccator over phosphorus(V) oxide, weighed, finely pulverized and left in the desiccator for 5 days. An accurately weighed amounts of the powders, equivalent to 7.5×10^{-8} mol of L-thyroxine sodium salt, were transferred into a glass cuvette and extracted with 8 mL of 0.020 mol L^{-1} HCl in ethanol. The suspensions were sonicated for 15 min, centrifuged at 4500 rpm for 10 min and the supernatants collected in a 50 mL volumetric flasks. The extraction procedure was repeated four more times.

The extraction method for determination of thyroxine assay in levothyroxine Tablets from British Pharmacopoeia 2004 [25] was used for the HPLC reference method. As the original procedure is adjusted to content tolerance of ±10%, instead of once we repeated extraction procedure four times.

Dried powders of tablets containing the equivalents of 50 μg of anhydrous levothyroxine sodium were accurately measured in to the microtubes. To each microtube were added 1 mL of solution of methanol and 0.1 mol L^{-1} sodium hydroxide 1:1 (V/V). After manual homogenisation microtubes were ultrasonicated for 5 min and shook for 3 min. After centrifugation during 10 min at 13,400 rpm, clear supernatants were collected in 5 mL volumetric flasks.

2.4. Procedure

The reaction was carried out in a special three-compartment vessel (Fig. 1) [26]. The solution of Mn(III) metaphosphate and orthophosphoric acid was placed in the first, thyroxine solution in the second, and As(III) and water, to a total volume of 12 mL, in the third compartment of the vessel. After the vessel was thermostated to 25 ± 0.1 °C, the reaction was started by mixing the reactants. The absorbance of the solution was then measured at 516 nm every 15 s for the first 5 min of the reaction. When the common excipients and chloride interfering with the reaction were investigated, they were weighed out in the second compartment of the reaction vessel. All measurements were performed at constant ionic strength $I = 1$ (KNO_3). All the vessels were washed before use with 6 mol L^{-1} hydrochloric acid and then rinsed several times with tap water, as well as distilled and redistilled water.

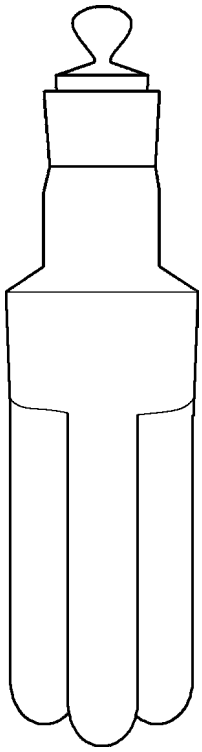

Fig. 1. Reaction-mixture vessel made by L.I. Budarin [26].

HPLC method used for accuracy evaluation. As the standard method for determination of content of levothyroxine sodium in tablets [25] allow the error up to ±10% and use relatively non-standard CN column we applied HPLC method from Gika et al. [27].

3. Results and discussion

In order to find the optimum experimental conditions for the determination of thyroxine (T_4) we studied the kinetics of the indicator reaction proposed.

3.1. Effects of acids

The rate of the catalytic reaction increased with increasing concentration of the orthophosphoric acid from 0.1 to 2.5 mol L^{-1}, while the rate of the non-catalytic reaction

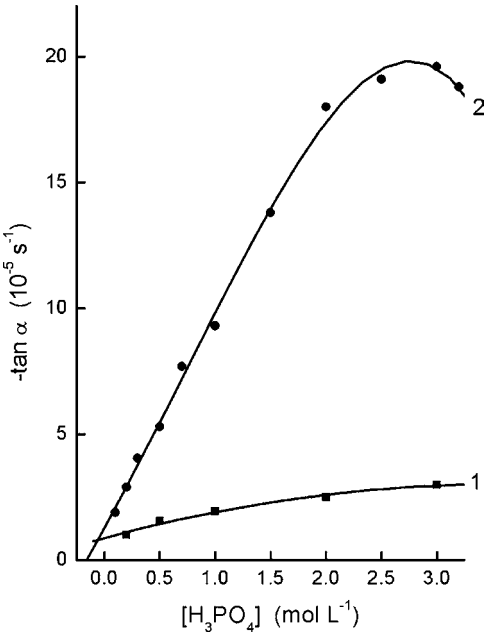

Fig. 2. Dependence of $-\tan\alpha$ on the H_3PO_4 concentration. (1) Non-catalytic reaction and (2) catalytic reaction.

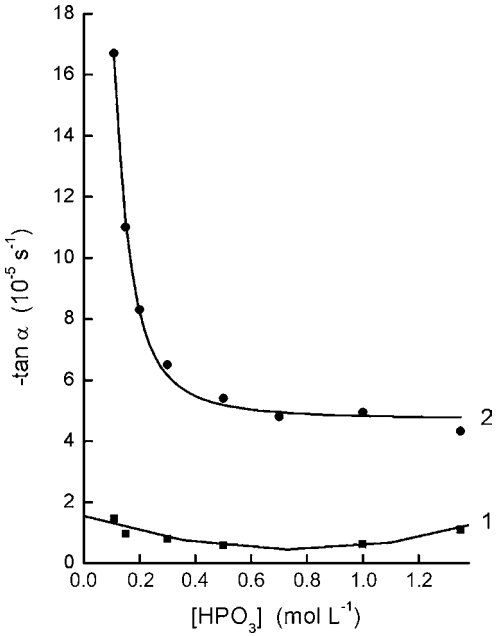

Fig. 3. Dependence of $-\tan\alpha$ on the HPO_3 concentration. (1) Non-catalytic reaction and (2) catalytic reaction.

increased only slightly, Fig. 2. The initial reagent concentrations used were (mol L^{-1}): Mn(III) metaphosphate, 7.0×10^{-3}; As(III), 3.5×10^{-2}; HPO_3, 0.22; T_4, 2.0×10^{-8}. The concentration of 2.0 mol L^{-1} orthophosphoric acid was found to be optimal for further investigations.

The effect of hydrogen ions was investigated by using nitric acid (from 0.01 to 0.6 mol L^{-1}) as it was found that KNO_3 used for maintaining constant ionic strength did not affect the reaction rate in concentrations lower than 0.8 mol L^{-1}. It was established that the reaction rate increased with increasing concentration of hydrogen ions.

Direct investigation of the effect of phosphate ions was not possible because the reaction rate was too small in the presence of a phosphate buffer ($[H_3PO_4]$:$[NaH_2PO_4]$ = 1:1) ranging from 0.5 to 4.0 mol L^{-1} (pH 1.4–1.2). A buffer of the component concentration ratio 4:1, in which the reaction rate was satisfactory, did not maintain the constant pH value in the mentioned phosphate concentration range.

In the investigated concentration range of orthophosphoric acid (0.1–3.2 mol L^{-1}), in which the hydrogen ion activity increases from 0.05 to 0.4, the reaction order with respect to the activity of hydrogen ions is 1.3. The change of hydrogen ion activity in the range 0.1–0.4 can be obtained by the variation of nitric acid concentration between 0.05 and 0.6 mol L^{-1} in the solution where the starting concentrations of the other reactants are (mol L^{-1}): Mn(III) metaphosphate, 7.0×10^{-3}; As(III), 2.5×10^{-2}; H_3PO_4, 0.3; HPO_3, 0.22; T_4, 2.0×10^{-8}. In that case, the reaction order with respect to the hydrogen ion activity is 0.9. It may be concluded that the rate of the thyroxine-catalyzed reaction increases with increasing orthophosphoric acid concentration due to an increase of the solution acidity, as well as an increase of the phosphate concentration.

The effect of metaphosphoric acid on the reaction rate was investigated by following initial reagent concentrations (mol L^{-1}): Mn(III) metaphosphate, 3.5×10^{-3}; As(III), 1.75×10^{-2}; T_4, 2.0×10^{-8}. It may be seen (Fig. 3) that the rate of the catalytic reaction decreased with increasing concentration of metaphosphoric acid. The effect of sulphate ions on the reaction rate was also investigated as they are present in the reagent solutions ($MnSO_4$ and As(III) solution). It was found that a sulphate concentration between 8.5×10^{-3} and 1.0×10^{-1} mol L^{-1} did not affect the reaction rate.

3.2. *Effects of components and products of indicator reaction*

Fig. 4 shows that the reaction rate increases with increasing concentration of Mn(III) from 1.0×10^{-3} to 1.5×10^{-2} mol L^{-1}. The experiment was carried out using the following initial reagent concentrations: 6.0×10^{-4} mol L^{-1} Mn(II); 2.5×10^{-2} mol L^{-1} As(III); 2.0×10^{-8} mol L^{-1} T_4. As the absorbance becomes too high at higher Mn(III) concentrations, we chose 7.0×10^{-3} mol L^{-1} as the optimal concentration. Mn(II) did not affect the reaction rate. It may be seen in Fig. 5 that the reaction rate increased with increasing concentration of As(III) up to 2.5×10^{-2} mol L^{-1}. As(V) did not affect the reaction rate.

3.3. *The results of kinetic investigations and kinetic equation*

The results of all the kinetic investigations are given in Table 1. The kinetic equation of the thyroxine-catalyzed Mn(III)

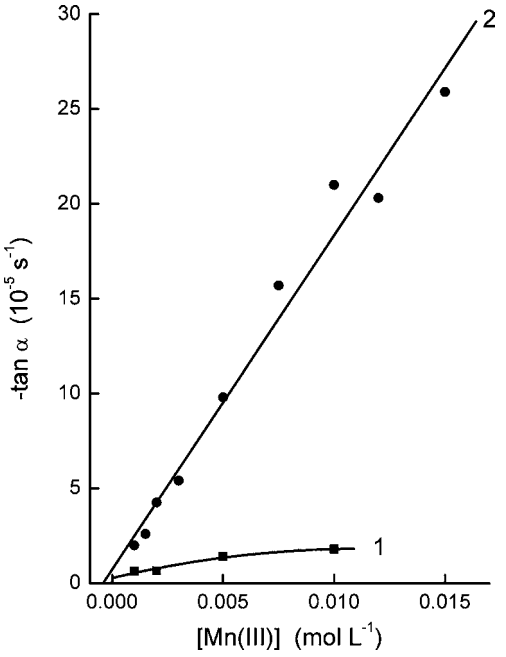

Fig. 4. Dependence of $-\tan\alpha$ on the Mn(III) concentration. (1) Non-catalytic reaction and (2) catalytic reaction.

metaphosphate–As(III) reaction in the presence of orthophosphoric acid was postulated and the apparent rate constant determined:

$$-\frac{dx}{dt} = k[\text{Mn(III)}]^{1.2}[\text{As(III)}]^{0.35}[\text{HPO}_3]^{-1}[\text{H}_3\text{PO}_4]^{0.8}[\text{T}_4]$$

$$k = (1.84 \pm 0.17) \times 10^4\ \text{L}^4\ \text{mol}^{-4/3}\ \text{s}^{-1}$$

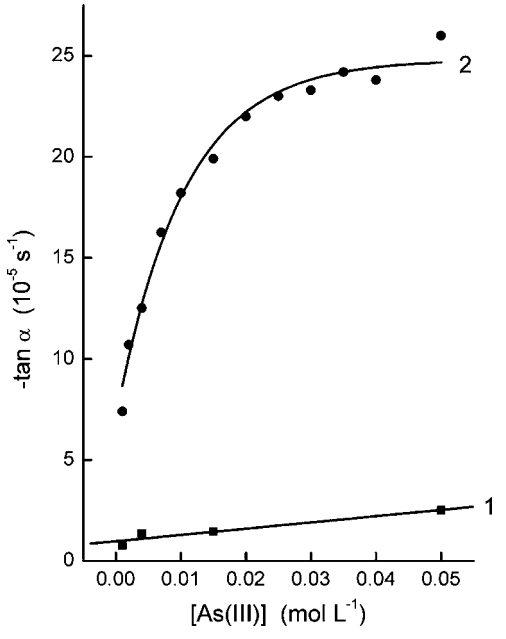

Fig. 5. Dependence of $-\tan\alpha$ on the As(III) concentration. (1) Non-catalytic reaction and (2) catalytic reaction.

Table 1
Summary of the kinetic data for the Mn(III) metaphosphate–As(III) reaction in orthophosphoric acid solution, in the presence of thyroxine

Variable	Concentration range (mol L^{-1})	Partial order
As(III)	1.0×10^{-3} to 2.5×10^{-2}	0.35
As(V)	0–1.0×10^{-2}	0.0
Mn(II)	1.7×10^{-4} to 2.0×10^{-3}	0.0
Mn(III)	1.0×10^{-3} to 1.5×10^{-2}	1.2
H_3PO_4	0.10–2.0	0.80
HPO_3	0.11–0.50	−1.0
HPO_3	0.50–1.35	−0.26
SO_4^{2-}	0.085–0.20	0.0
Thyroxine	0–1.0×10^{-7}	1.0
H_3O^+	0.05–0.80	0.48

3.4. Effect of temperature and kinetic parameters

The influence of temperature on the proposed reaction was investigated by the measurement of the reaction rate at 284.5, 288.5, 293, 298, 303, 308, 313 and 318 K, using the following initial reagent concentrations (mol L^{-1}): Mn(III) metaphosphate, 7.0×10^{-3}; As(III), 2.5×10^{-2}; T_4, 2.0×10^{-8}; H_3PO_4, 2.0. It was found that the reaction rate increased with increasing temperature. The dependence of $\log k$ on $1/T$ is presented in Fig. 6. The activation energy and other kinetic parameters were calculated and the following results obtained: $E = 24.63$ kJ/mol, $\Delta H^{\#} = 22.15$ kJ/mol, $\Delta S^{\#} = -91.65$ J/K mol, $\Delta G^{\#} = 49.48$ kJ/mol, $pK^{\#} = 8.68$.

3.5. Calibration graph, detection and determination limits

The optimum reagents concentrations found were: Mn(III) metaphosphate, 7.0×10^{-3} mol L^{-1}; As(III), 2.5×10^{-2} mol L^{-1}; orthophosphoric acid, 2.0 mol L^{-1}. Under that conditions a linear relationship was established

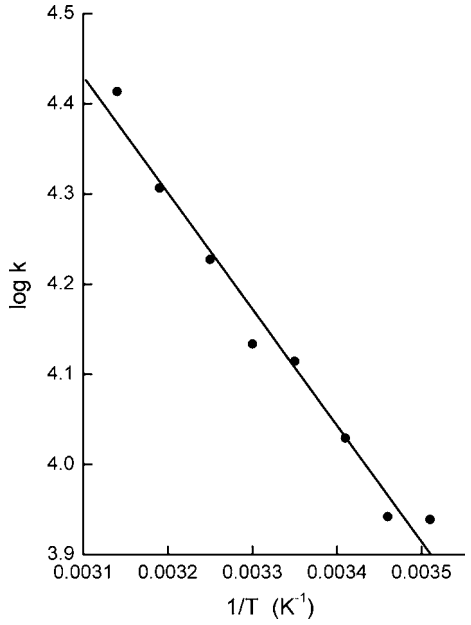

Fig. 6. Dependence of $\log k$ on $1/T$.

Table 2
Kinetic determination of thyroxine

Taken (mol dm^{-3})	Found[a] (mol dm^{-3})	R.S.D. (%)
0.70 ± 10^{-8}	$(0.68 \pm 0.03) \times 10^{-8}$	4.6
1.50×10^{-8}	$(1.54 \pm 0.10) \times 10^{-8}$	6.7
3.00×10^{-8}	$(3.06 \pm 0.08) \times 10^{-8}$	2.7

[a] Mean and standard deviation of seven determinations.

Table 3
Tolerance limits of common excipients

Molecule added	Tolerance level ($C_{Foreign}/C_{Thyroxine}$)
Fructose	1000
Lactose	1000
Sucrose	1000
Glucose	1000
Starch	600[a]
Gum acacia	200[a]

[a] ($W_{Foreign}/W_{Thyroxine}$).

between the reaction rate of the reduction of Mn(III) metaphosphate with As(III), in the presence of orthophosphoric acid, and the thyroxine concentration in the range from 0 to 1.0×10^{-7} mol L^{-1}: $\tan\alpha = -5.27 \times 10^{3}\ [T_4] + 6.6 \times 10^{-6}$, ($r = -0.9985$). Tan α represents the slope of the initial straight part on the graph of the Mn(III) absorbance as a function of time. The 3 S detection limit (the concentration of T_4 resulting in absorbance which exceed the mean blank response for a three times blank standard deviation) was 2.7×10^{-9} mol L^{-1} and the 10 S limit of the determination was 4.3×10^{-9} mol L^{-1} [28].

In order to test the sensitivity of the reaction studied, thyroxine was determined using the tangent method [29] under the optimal conditions. In the concentration range 7.0×10^{-9} to 3.0×10^{-8} mol L^{-1} a relative standard deviation was up to 6.7% (Table 2).

In order to test the applicability of the method, the effect of common excipients used in pharmaceutical preparations on the determination of 2.0×10^{-8} mol L^{-1} of thyroxine was investigated. The tolerance limit for foreign substances was estimated as the concentration of the substance that gives up to a 5% relative error in the determination of thyroxine. The maximum investigated concentration ratio was 1000:1. The results are summarized in Table 3.

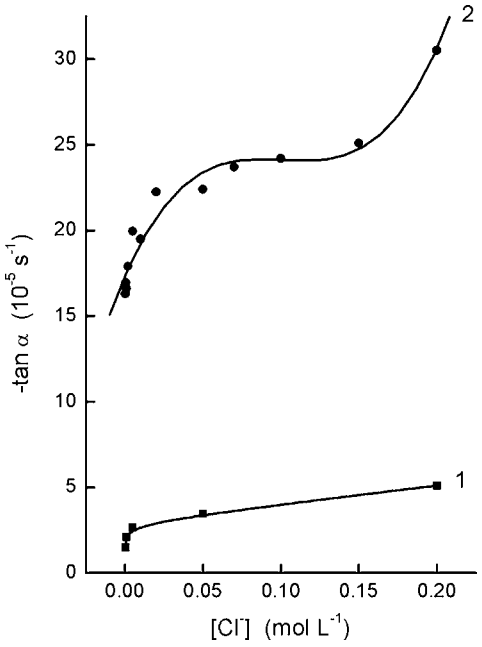

Fig. 7. Effect of chloride on the $-\tan\alpha$ in the concentration range: 4.0×10^{-4} to 2.0×10^{-1} mol L^{-1}. (1) Non-catalytic reaction and (2) catalytic reaction.

Investigation of the effect of chloride ions on the reaction rate shows that the catalyzed reaction rate increases with increasing chloride concentration (Fig. 7). That increase of the reaction rate is the highest at lower chloride concentrations. As there is only small change in the reaction rate when the chloride concentration ranges from 0.08 to 0.12 mol L^{-1} we recorded the calibration graph in 0.08 mol L^{-1} sodium chloride. Then the detection limit decreases to 6.6×10^{-10} mol L^{-1} and the limit of the determi-

Table 4
Determination of thyroxine in commercial tablets

Proposed method

Tablets	Expected concentration[a] ($\times 10^{-8}$ mol L^{-1})	Found concentration[b] ($\times 10^{-8}$ mol L^{-1})	Found ± R.S.D. (%)
Tivoral	1.669	1.672 ± 0.041	100.2 ± 2.5
Letrox 150	2.274	1.822 ± 0.157	80.1 ± 6.9

HPLC reference method

Tablets	Expected concentration[a] ($\times 10^{-5}$ mol L^{-1})	Found concentration ($\times 10^{-5}$ mol L^{-1})	Found ± R.S.D. (%)
Tivoral	1.272	1.274	98.9[b] ± 1.5
Tivoral	1.235	1.232	
Tivoral	1.261	$1.237^{c} \pm 0.018$	
Letrox 150	1.263	1.067	
Letrox 150	1.289	1.035	82.8[c] ± 2.2
Letrox 150	1.286	1.075	

[a] According to labelled tablets content.
[b] Mean of five determinations.
[c] Mean of three determinations.

Table 5
Results and critical values for comparison of standard deviations and means of proposed and reference method

Tablets	Calculated value of F	Critical value of F ($P=0.05$)	Calculated value of t	Critical value of t for:	
				$P=0.05$	$P=0.10$
Tivoral	2.84	6.39	1.44	2.31	1.86
Letrox 150	9.78	19.2	0.64	2.45	1.94

nation to 3.0×10^{-9} mol L^{-1} with a linear dependence of the reaction rate on the thyroxine concentration in the investigated range 0–5.0×10^{-8} mol L^{-1} ($r = -0.9992$).

3.6. Applications

In order to check the proposed method, we determined thyroxine in tablets. The results obtained by the use of proposed and reference HPLC method are presented in Table 4. The authors of HPLC method used find that the detection limit for the standard solution was 2.57×10^{-8} mol L^{-1} while the limit of determination was 1.29×10^{-7} mol L^{-1} [27]. In addition, the results obtained were compared statistically by variance ratio F-test and Student's t-test (Table 5). The experimental values were below the theoretical values in either test, indicating that there was no significant difference between the compared methods.

4. Conclusion

It may be concluded that the proposed method is simple, inexpensive and one of the most sensitive methods for the determination of thyroxine. From the obtained results it can be seen that the proposed method was successfully applied for the determination of thyroxine in pharmaceutical preparations without prior separation. The obtained results are in good accordance with reference method.

Acknowledgements

This work has been supported by the Ministry of Science of the Republic of Serbia (Project 142037). We would like to thank Prof. Živoslav Tešić for allowing access to GBC Cintra 6 UV–vis spectrophotometer and Waters HPLC system and Dr. Nenad Milosavić for technical assistance.

References

[1] G.A. Milovanović, F.T. Pastor, G.M. Petković, M. Todorović, Microchim. Acta 144 (2004) 51.
[2] M. Timotheou-Potamia, E.G. Sarantonis, A.C. Calokerinos, T.P. Hadjiioannou, Anal. Chim. Acta 171 (1985) 363.
[3] J.C. Arcq, A. Arcq, Clin. Chim. Acta 48 (1973) 287.
[4] K. Mueller, H. Skrube, H. Spitzy, Microchim. Acta (1962) 1081.
[5] M. Toledano, C.M. Gutierrez, A. Gomez-Hens, D. Perez-Bendito, Analyst 114 (1989) 211.
[6] A. Waseem, M. Yaqoob, A. Nabi, Luminiscence 21 (2006) 174.
[7] A. Waseem, M. Yaqoob, A. Nabi, Anal. Sci. 22 (2006) 1095.
[8] A. Waseem, M. Yaqoob, A. Nabi, Talanta 71 (2007) 56.
[9] Q. He, X. Dang, C. Hu, S. Hu, Colloids Surf. B 35 (2004) 93.
[10] L. Hernandez, P. Hernandez, O. Nieto, Analyst 119 (1994) 1579.
[11] M.W.I. Nassar, Egypt. J. Biomed. Sci. 12 (2003) 209.
[12] S.Z. Qureshi, M.I. Helaleh, N. Rahman, R.M.A.Q. Jamhour, Chem. Anal. (Wars.) 42 (1997) 65.
[13] E. Goek, S. Ates, J. Fluoresc. 13 (2003) 221.
[14] L. Bhavana, V.J. Ajimon, S.L. Radhika, M. Sindhu, C.S.P. Iyer, J. Chromatogr. B 803 (2004) 363.
[15] R. Wang, J.-W. Xie, Z.-P. Jia, X.-L. Hu, H. Xie, Y.-M. Li, L.-R. Chen, Sepu 19 (2001) 523.
[16] Wako Pure Chemical Industries, Ltd., Japan, Bunseki Kiki 15 (1977) 466.
[17] T. Tuuminen, Screening 2 (1993) 149.
[18] K. Horn, M.J. Castineiras, J. Ortola, R. Kock, F.C. Perriard, S. Bittner, J.V. Pairet, P. Ers, J. Boulanger, et al., Eur. J. Clin. Chem. Clin. Biochem. 29 (1991) 697.
[19] M. Matsumoto, A. Kawachi, H. Takei, M. Kambara, K. Sawada, M. Murata, Y. Chiba, Horumon To Rinsho 33 (1985) 375.
[20] W.F. Riesen, B. Muacevic, M.J. Jaggi, Clin. Chem. Clin. Biochem. 16 (1978) 387.
[21] A.J. Ozinskas, H. Malak, J. Joshi, H. Szmacinski, J. Britz, R.B. Thompson, P.A. Koen, J.R. Lakowicz, Anal. Biochem. 213 (1993) 264.
[22] J. Lesny, Z. Korenova, J.J. Klas, Radioanal. Nucl. Chem. 155 (1991) 155.
[23] J.K. Whitehead, D. Beale, Clin. Chim. Acta 4 (1959) 710.
[24] V.I. De Brabandere, P. Hou, D. Stockl, L.M. Thienpont, A.P. De Leenheer, Rapid Commun. Mass Spectrom.: RCM 12 (1998) 1099.
[25] British pharmacopoeia BP 2004, Ph. Eur. monograph 0401, The Stationery Office, London, 2004.
[26] (a) K.B. Yatsimirskii, Kinetic Methods of Analysis, Pergamon Press, Oxford, 1966, pp. 29–30;
(b) L.I. Budarin, K.E. Prik, Zavodskaya laboratoriya 26 (1960) 1018.
[27] H.G. Gika, V.F. Samanidou, I.N. Papadoyannis, J. Chromatogr. B 814 (2005) 163.
[28] D. Perez-Bendito, M. Silva, Kinetic Methods in Analytical Chemistry, Ellis Horwood Ltd., Chichester, 1988, pp. 252–253.
[29] K.B. Yatsimirskii, Kinetic Methods of Analysis, Pergamon Press, Oxford, 1966, p. 39.

Available online at www.sciencedirect.com
ScienceDirect
Talanta 74 (2008) 1271–1280
Talanta
www.elsevier.com/locate/talanta

Characterization of cobalt pigments found in traditional Valencian ceramics by means of laser ablation-inductively coupled plasma mass spectrometry and portable X-ray fluorescence spectrometry

J. Pérez-Arantegui [a], M. Resano [a,*], E. García-Ruiz [a], F. Vanhaecke [b], C. Roldán [c], J. Ferrero [c], J. Coll [d]

[a] *Departamento de Química Analítica, Universidad de Zaragoza, Pedro Cerbuna 12, E-50009 Zaragoza, Spain*
[b] *Department of Analytical Chemistry, Ghent University, Krijgslaan 281-S12, B-9000 Ghent, Belgium*
[c] *Instituto de Ciencia de los Materiales, Universidad de Valencia, P.O. Box 22085, E-46071 Valencia, Spain*
[d] *Museo Nacional de Cerámica y Artes Suntuarias "González Martí", C/ Poeta Querol 2, E-46002 Valencia, Spain*

Received 13 April 2007; received in revised form 25 August 2007; accepted 30 August 2007
Available online 8 September 2007

Abstract

In this work, a comparison of the performances of laser ablation-inductively coupled plasma mass spectrometry (LA-ICPMS) and portable X-ray fluorescence (XRF) spectrometry for the characterization of cobalt blue pigments used in the decoration of Valencian ceramics is presented. Qualitative data on the elemental composition of the blue pigments obtained using both techniques show a good agreement. Moreover, the results clearly illustrate that potters utilized different kinds of cobalt pigments in different historical periods.

While both techniques seem suitable for the proposed task, they show different strengths and weaknesses. Portable X-ray fluorescence spectrometry is a cheaper and totally non-destructive technique, capable of providing fast and reliable results at the mg g^{-1} level. LA-ICPMS, on the other hand, offers a much higher detection power and better spatial resolution, but its use results in some sample damage (sample consumption at the μg level), while it is a more expensive and non-portable technique.
© 2007 Elsevier B.V. All rights reserved.

Keywords: LA-ICPMS; XRF; Solid samples; Glaze; Cobalt pigments; Ceramic

1. Introduction

Natural pigments have been used since ancient times for coloring materials. Among these, cobalt pigments were already known in the Near and Middle Eastern Late Bronze Age [1–4] for the intense blue color they can induce in glass. Nevertheless, it seems they have been extensively used in glazes only since the Middle Ages [5]. Cobalt pigments were prepared from cobalt-rich minerals, such as cobaltite (CoAsS), erythrite ($Co_3(AsO_4)_2{\cdot}8H_2O$)), skutterudite ((Co, Ni)As_{3-x}) or asbolane ((Co, Ni)$_{1-y}(MnO_2)_{2-x}(OH)_{2-2y+2x}{\cdot}nH_2O$), or even cobaltiferous alum (a hydrated double sulfate that contains aluminum with or without another alkali, alkaline earth or transition metal). The latter was used to produce blue glass in New Kingdom Egypt [6–8].

Valencian ceramic workshops have manufactured blue-decorated glazed pottery since the 14th century AD in the areas of Paterna and Manises. The production of this type of ceramic continued until the 18th and 19th centuries, co-existing with the manufacturing of polychrome decorations [9]. Other colors, like green, brown or even metallic luster, were also used on Valencian ceramic. However, the likely local origin of the raw copper and manganese pigments, as well as their abundance in the Iberian Peninsula, make these pigments less suitable for the identification of different kinds of Valencian ceramic.

The chromatic characteristic of these decorated ceramics is an intense blue color, obtained by the application of the pigment (only cobalt compounds) over or under a white opacified glaze, mainly composed of tin oxide, lead oxide and silica. In general, traditional blue pigments fall into two distinct groups. The first group comprises the naturally occurring blue minerals, whilst the second group includes the blue compounds produced artificially from compounds usually having no obvious blue

* Corresponding author. Tel.: +34 976761634; fax: +34 976761292.
E-mail address: mresano@unizar.es (M. Resano).

0039-9140/$ – see front matter © 2007 Elsevier B.V. All rights reserved.
doi:10.1016/j.talanta.2007.08.044

characteristics in their raw unprocessed state in nature. Cobalt blue compounds occur only in the second group [10]. Thus, the elemental composition of the pigments is expected to depend both on the raw materials used and the workshop recipes, and it is important to establish the origin of the pigments as well as to investigate the temporal evolution of materials and techniques, although it is not always easy to discriminate between both sources of variation. The study of the pigment application technique [11], as well as the possible compositional differences between cobalt products used from the 14th to the 19th centuries, can bring about new insights on the technology and trade routes of raw materials related to Valencian ceramic production [12].

Trace element analysis can be particularly useful for the fingerprinting of art objects. Many analytical techniques can be used to reveal the trace chemical composition of archaeological samples. In the particular case of vitreous materials, the use of those techniques that provide information directly from the solid sample is recommended, taking into consideration the difficulties in dissolving this kind of sample and also having in mind the requirement of minimal sample damage. Among the different solid sampling techniques available, both X-ray fluorescence (XRF) spectrometry and laser ablation-inductively coupled plasma mass spectrometry (LA-ICPMS) can be particularly suitable to determine the elemental composition of glass and glazed ceramics [13–21]. Preliminary studies using both techniques [12,22] have demonstrated the presence of some characteristic elements in the blue pigments. These elements comprise arsenic, cobalt, copper, manganese and zinc. They might have been formerly present in the mineral ores used or were incorporated during the production of the ceramics. In any case, their presence can permit the classification of ceramic fragments according to period or workshop.

LA-ICPMS fulfills all the requirements (sufficient detection power, wide linear dynamic range and capabilities for spatially resolved analysis) demanded for these studies, providing multielemental results with no sample preparation, minimal sample damage and acceptable reproducibility and sample throughput. Applications of LA-ICPMS to investigate glazed ceramics are still scarce, but this approach is constantly gaining ground [22–27], mainly due to the availability of deep-UV laser systems that permit a more efficient ablation of this kind of samples [28,29]. On the other hand, energy dispersive X-ray fluorescence spectrometry (EDXRF) provides a non-destructive analytical technique and is widely applied for material analysis in Cultural Heritage investigations because of the possibility of in situ analysis by means of portable instrumentation and its high sample throughput (the analysis of a large number of objects or a high number of points in a object can be performed in a short time). EDXRF is a multi-element technique, allowing the fluorescence radiation of all of the elements with atomic number above $Z = 11$ (sodium) that are present in the object to be detected simultaneously, and it has already been used for a long time as an analytical tool to perform chemical analysis to determine major, minor and trace elements of historical objects [30]. In the field of glazed ceramic characterization, EDXRF analysis has permitted differentiation between two different types of decoration techniques: underglaze (where the pigment is applied on the fired clay body before the glaze application, whereafter clay body, pigment and glaze are subjected to a second firing process) and overglaze (where the raw glaze cover is applied on the previously fired clay body and then the pigment is applied directly on the top of the raw glaze cover, which vitrifies after a second firing process) [11]. Furthermore, this technique has allowed the identification of the chemical elements found in the compounds used in the production of the clay body, glaze and pigment decoration [12,31].

Also other solid sampling techniques, such as proton-induced X-ray emission spectrometry (PIXE), can provide useful analytical results on the elemental composition of this type of materials [16,32–35]. PIXE has been shown to be suitable for characterizing the elemental composition of different matrices, and some advantages of PIXE compared with other X-ray techniques are the higher sensitivity, the potential for spatially resolved analysis and the favorable excitation of light elements. Moreover, it is possible to implement this technique in the external beam mode (that is in air or in a helium atmosphere), enabling the analysis of large samples or of materials containing volatile compounds that would not stand vacuum conditions. [36]. But PIXE requires a particle accelerator and considerable operator skills. These prerequisites lead to high-operating expenses, making this technique unsuitable for most routine labs. For this reason, this work will focus on the comparison between two more widespread solid sampling techniques, EDXRF and LA-ICPMS, only. The possibilities of both techniques for the characterization of cobalt pigments found in Valencian ceramics dating from different periods will be discussed in detail and the results obtained with these techniques compared, with the aim of establishing consistent compositional differences that could allow the samples to be discriminated chronologically.

2. Experimental

2.1. Apparatus

EDXRF analyses were performed by means a portable spectrometer (see Fig. 1) with a palladium X-ray tube (EIS, Italy), working up to 38 kV–0.3 mA (the maximum values for the potential and current of the X-ray tube, respectively), and a 500 μm thick Si-PIN detector (XR-100 CR, AMPTEK Inc., USA), thermoelectrically cooled, with an energy resolution of 170–180 eV at 5.9 keV and an entrance beryllium window of 12.5 μm thickness. A multi-channel AMPTEK MCA Pocket was used to control data acquisition.

Direct analysis of ceramic fragments was also accomplished by using laser ablation (LA) for sample introduction. In the GeoLas ArF excimer-based LA system (MicroLas, Germany) used, the 193 nm UV-laser beam coming from the Compex102 laser unit (LambdaPhysik, Germany) undergoes homogenization [37], enabling flat-bottomed and straight-walled craters to be obtained. The ablation cell was coupled to the ICP torch of the ICPMS unit by means of a 3 mm internal diameter Tygon tubing and Ar was used as the carrier gas. All measurements were carried out using a Perkin-Elmer Sciex

Fig. 1. The portable EDXRF spectrometer used in this work.

DRC*plus* quadrupole-based ICP-mass spectrometer (Canada). Despite the availability of the dynamic reaction cell to overcome spectral interferences, all measurements were made in vented mode.

A JEOL (USA) JSM 6400 scanning electron microscope (SEM) was used for evaluation of the craters produced and for the quantitative determination of those elements (aluminum, lead, potassium, sodium, silicon and tin) present at higher levels (% level). The results obtained for these elements proved to be of little use for fingerprinting purposes. The SEM was equipped with a system for energy dispersive X-ray analysis, EDXA (Oxford Instruments, INCAx-sight), with ZAF correction.

2.2. Procedure for the characterization of the blue pigments by EDXRF

The EDXRF spectrometer used in this work has a light weight (10 kg including X-ray tube, X-ray detector, electronic modules and base tripod) and it is compact and easy-to-handle and hence, very well-suited for in situ and non-destructive analysis. The X-ray source is able to provide a collimated beam with a small diameter to analyze small areas or details on large objects, and the energy-dispersive detector system has an acceptable energy resolution (170–180 eV at 5.9 keV) for discriminating between adjacent X-ray fluorescence peaks. In this particular work, the X-ray beam was collimated down to 3 mm using aluminum pinholes. The ceramic samples were placed at the front of the measurement head with a 45° angle between the incident beam and the sample-detector, located at a distance of about 2 cm. EDXRF analyses were carried out, while operating the X-ray tube at a potential of 35 kV, a current intensity of 0.1 mA and an acquisition time of 300 s. With these parameters, fluorescence lines could be observed within a wide energy range and the EDXRF spectra were obtained with acceptable statistics. Prior to XRF analysis, the surface of the samples was cleaned with ethanol. Subsequently, XRF spectra were collected from three sampling points in colored zones and three sampling points in non-colored zones, to determine the composition of both the glaze and the pigment.

2.3. Procedure for the characterization of the blue pigments by LA-ICPMS

The parameters used during the analysis of the ceramics are presented in Table 1. Prior to analysis, the surface of the fragments was cleaned with diluted (0.14 M) HNO_3. In order to obtain representative values, for every ceramic fragment, fives sampling positions were selected across the glazed surface, ensuring focusing on the blue-colored (Co-enriched) areas, and each ablation consisted of 300 laser pulses. At every spot, the surface was first cleaned using 10 laser pulses of the same spot size to prevent the possible influence of any surface contamination or alteration. The analysis time per sample is approximately 5 min. The treatment of the transient signals generated was carried out as described elsewhere [38]. The signals for every nuclide were

Table 1
Instrumental operating conditions and data acquisition parameters for the LA-ICPMS measurements

GeoLas Laser ablation system	
Energy density	15.0 J cm^{-2}
Repetition rate	20 Hz
Spot size	120 μm
Number of cleaning pulses	10
Number of pulses for analysis	300 (15 s duration)
Cell volume	≈30 cm^3
ICP-mass spectrometer	
rf power	1200 W
Plasma argon flow rate	17 L min^{-1}
Auxiliary argon flow rate	1.2 L min^{-1}
Carrier argon flow rate	1.3 L min^{-1}
Sampling cone and skimmer	Platinum
Lens voltage	6.25 V
Data acquisition	
Scanning mode	Peak hopping
Dwell time per acquisition point	20 ms
Signals monitored[a]	$^{55}Mn^+$, $^{57}Fe^+$, $^{58}Ni^+$, $^{59}Co^+$, $^{65}Cu^+$, $^{68}Zn^+$, $^{75}As^+$, $^{209}Bi^+$ ($^{23}Na^+$), ($^{34}S^+$), ($^{35}Cl^+$)
Detector mode	Dual (pulse counting and analogue)

[a] Nuclides between parentheses were monitored only to assess the possible effect of interferences.

normalized to the signal of $^{59}Co^{+}$. In this way, five normalized signals were finally obtained for every element in every sample. The median of these five signals was taken as the representative value instead of the mean in order to minimize the possible influence of outliers [39–41]. This procedure was repeated on two different days for every sample to ensure consistency of the results.

3. Results and discussion

3.1. EDXRF measurements

Direct analysis of solid samples using a portable EDXRF spectrometer is very simple, because one just has to face the spectrometer to the surface of the object to be analyzed, and in a few minutes, the corresponding spectrum is obtained. However, the interpretation of the spectra is usually harder, due to the complexity of the sample composition. The main characteristics of this technique are summarized in Table 2, enabling comparison with those of LA-ICPMS.

The operating conditions chosen for EDXRF analysis (see Section 2.2.) provided detection limits of approximately 300 μg g^{-1} for those elements found in the periodic table between manganese ($Z=25$) and arsenic ($Z=33$) and of 1000 μg g^{-1} for elements between silver ($Z=47$) and tin ($Z=50$).

EDXRF analysis is generally based on an area of several mm^2 and a thickness between a few μm and a few mm, depending on the material under study and the surface conditions. In this case, the beam scans an area of 7 mm^2 and penetrates up to a depth of 100–200 μm under the superficial layer. The penetration depth of the X-ray beam was evaluated from the estimated total attenuation coefficient of the glaze cover for an exciting X-ray beam with an energy in the 5–20 keV interval and considering the typical average composition of tin-opacified lead glazes used in Spanish ceramics [42]. In glazed ceramic studies, the sample cross-section consists of a glazed external layer containing the pigment on top on a clay body; therefore, an EDXRF spectrum comprises information coming from these different layers due to the deep penetration of the X-rays in the sample. Discrimination between the characteristic elements of the pigment can be achieved by subtracting the EDXRF spectrum of a zone comprising glaze, pigment and ceramic body and the EDXRF spectrum of a zone comprising only glaze and ceramic body. From the net spectrum thus obtained, the characteristic elements of the pigments (arsenic, cobalt, copper, manganese and zinc) can be identified [12,43].

From the spectrum obtained for a blue pigment zone of about 7 mm^2, the net surface intensity of the Kα lines for the major elements cobalt, copper, manganese and zinc was calculated for each sample. For arsenic, on the other hand, the Kβ line was used instead, since its Kα line overlaps with the Pb Lα line. The calculation of the net peak intensities and the deconvolution of the fluorescence line pairs Mn Kβ/Fe Kα, Fe Kβ/Co Kα, Ni Kβ/Cu Kα and Cu Kβ/Zn Kα, were performed using the WinQXAS code [44]. Also other elements, such as iron and nickel, have been monitored, but these have not been included in the discussion, as they did not contribute significantly to the pigment discrimination. Lead has not been considered among the possible characteristic elements of the pigment because it is not possible to discriminate whether the fluorescence lines come from the pigment or from the glaze cover, in which it is very abundant due to its use as melting agent.

The use of certified standards or ceramic sherds of known composition for calibration could have been checked in order

Table 2
Comparison of the main characteristics of both solid sampling techniques discussed in this work

	LA-ICPMS	XRF
Types of samples	All Preparation of tablets for powders is required Decreasing the fragment size to fit into the ablation cell may be required	All Preparation of tablets for powders may be required
Usual working range	100 ng g^{-1} to wt%	100 μg g^{-1} to wt%
Precision	5–25%	1–5%
Selectivity	Medium–high[a]	Medium[b]
Calibration	Solid standards with an internal standard	Solid standard reference materials
Isotopic analysis	Yes	No
Multi-element potential	Yes	Yes
Sample throughput	2–5 min per sample	1–5 min per sample
Sample Consumption	100 ng–10 μg	None
Spatial resolution		
Lateral	Very good (μm)	Very poor (several mm^2)
In depth	Excellent (≈0.1 μm)	Poor (μm to mm)
Automation availability	No	No
Portability	No	Yes
Prices	From 250,000€[a]	From 30,000€[b]

[a] This aspect greatly depends on the type of mass analyzer used; with sector field instead of the more traditional quadrupole-based instrumentation the selectivity is greatly improved. On the other hand, the use of collision/reaction cells, located in-between the interface and the quadrupole mass analyzer can also bring about a significant improvement.

[b] Depends on the characteristics of the X-ray tube and the semi-conductor detector.

to obtain quantitative results. However, quantification was not attempted at, because obtaining reliable results is a difficult task due to both irregularities in the thickness of the analyzed surface layers and compositional heterogeneities. In fact, obtaining bulk information may even not be not very meaningful for fingerprinting purposes in this case, since the concentration of many elements may strongly depend on the amount of pigment added to the sample; even for one particular sample, the content may significantly vary in different sections depending on the coloration, as dark blue areas contain higher amounts of pigment that pale blue areas. Since all of the blue pigments used in the ceramic samples investigated in this work have been obtained from cobalt mineral ores, the signal for this element provides an indication of the amount of pigment added. Thus, the peak area ratios between the XRF lines of the detected elements (Mn Kα, Cu Kα, Zn Kα, As Kβ) and the line Co Kα might be considered as a guide to the source of the ore from which the colorant was derived and, thus, this parameter is more suitable to discriminate between different types of pigments.

3.2. LA-ICPMS measurements

The principle of the technique is based on the use of a short laser pulse (typically a few nanoseconds) that delivers a burst of energy to the sample surface. As a consequence, a small amount of material is ablated and the aerosol thus formed is transported by means of a gas (Ar in this work) flow into the ICPMS instrument for elemental and/or isotopic monitoring [28,29]. The main characteristics of this technique are summarized in Table 2.

This technique cannot be considered as entirely non-destructive, but the damage produced to the sample is very limited. Moreover, the technique allows spatial information to be obtained, both laterally and/or in depth. With the instrumentation used in this work, the laser beam diameter can be varied between 4 and 120 μm, giving rise to almost regular circular craters with radius ranging between 2 and 60 μm. The use of a large spot size results in more material ablated and thus, a higher sensitivity (which shows a linear dependence with the square of the radius), but also in more damage inflicted to the sample. In this work, a spot size of 120 μm was selected for maximizing the sensitivity. On the other hand, also the number of pulses used per sampling spot can be varied. Selecting a high number of pulses permits obtaining a more representative value, but it is necessary to ensure that only the upper layer containing the cobalt pigment is ablated since the main goal of the study is to investigate the characteristics of these cobalt pigments. This could be easily assured by monitoring the $^{59}Co^{+}$ signal (in addition to the final examination of the craters by SEM). An ablation time of 15 s (corresponding to 300 laser pulses) was finally chosen. This 300 laser-pulse ablation results in a crater depth of ≈25 μm (estimated using SEM), which represents approximately 1 μg of sample ablated per spot. This value can be further reduced if needed for other materials, but only at the cost of deteriorated LODs. For the samples investigated in the present work, these parameters are perfectly acceptable as the craters thus produced are hardly noticeable by visual observation.

Other important parameters for the ablation (repetition rate and the energy density), and some important ICPMS settings—the carrier gas flow rate that determines the transport efficiency from the ablation chamber to the ICPMS and the rf power that has an important influence on the sensitivity, were optimized aiming at maximum signal intensities for the target elements. The maximum repetition rate (20 Hz) available with the laser unit used was chosen. As to the energy output, no significant gain in sensitivity was obtained above ∼1.5 mJ (energy measured on the substrate, corresponding with an energy density of 13.3 J cm^{-2}). Finally, a value of 1.7 mJ (energy density 15.0 J cm^{-2}) was selected. All the settings finally used are summarized in Table 1.

The elements monitored in this study were selected based on the information available from a previous work, in which ceramic materials from a different Spanish region (Aragón) were investigated [22]. The conclusion of that work was that arsenic, copper, manganese and zinc provide the most relevant information for discriminating purposes. Other elements, such as iron, nickel and bismuth, were simultaneously monitored in order to check if more information could be obtained. Experiments were carried out to ensure that these elements could be monitored interference-free. The signal intensities observed for $^{35}Cl^{+}$ were practically irrelevant (glazed ceramics from this region are expected to show a low content of this element), therefore enabling the monitoring of $^{75}As^{+}$ with no risk of interference from $^{40}Ar^{35}Cl^{+}$. Due to the high-signal intensity encountered for $^{23}Na^{+}$ (which could be anticipated for a vitreous surface) on the other hand, the monitoring of the less abundant $^{65}Cu^{+}$ nuclide was preferred (overlap of the signals of $^{63}Cu^{+}$ and $^{40}Ar^{23}Na^{+}$). A less abundant isotope of zinc (^{68}Zn) was also selected to minimize the possible effect of sulfur-based polyatomic ions (overlap of the signals of $^{64}Zn^{+}$ and $^{66}Zn^{+}$ with those of $^{32}S^{16}O_2^{+}$ and/or $^{32}S^{32}S^{+}$ and $^{34}S^{16}O_2^{+}$ and/or $^{32}S^{34}S^{+}$, respectively). Table 1 shows the nuclides finally monitored for all the samples under investigation.

A typical signal profile obtained when ablating the same sample at five different locations and using the conditions summarized in Table 1 is presented in Fig. 2a. It appears that it is possible to achieve a controlled ablation of the sample, since the signals for all of the elements remain very stable (the R.S.D. ranged between 3 and 10%, values that can be further reduced to 2–5% when the respective signals are normalized to the $^{59}Co^{+}$ signal). Regular, flat-bottomed craters were observed by means of SEM in all cases, proving the suitability of the 193 nm ArF laser unit for efficient ablation of the vitreous surface of the ceramic samples, as can be appreciated in Fig. 2b.

The sensitivity of the technique permitted to obtain significant signals for all of the elements investigated in every sample. Limits of detection of 0.06 (arsenic), 0.02 (cobalt), 0.07 (copper), 0.06 (manganese) and 0.3 (zinc) μg g^{-1} were calculated (IUPAC 3s-criterion, using the gas blank). Even though it might be feasible to obtain quantitative information by means of calibration against a suitable standard (typically the NIST 610-617 series) and using the signal for an element of known concentration as internal reference (frequently an element present at a high level that can be determined using a less sensitive solid sam-

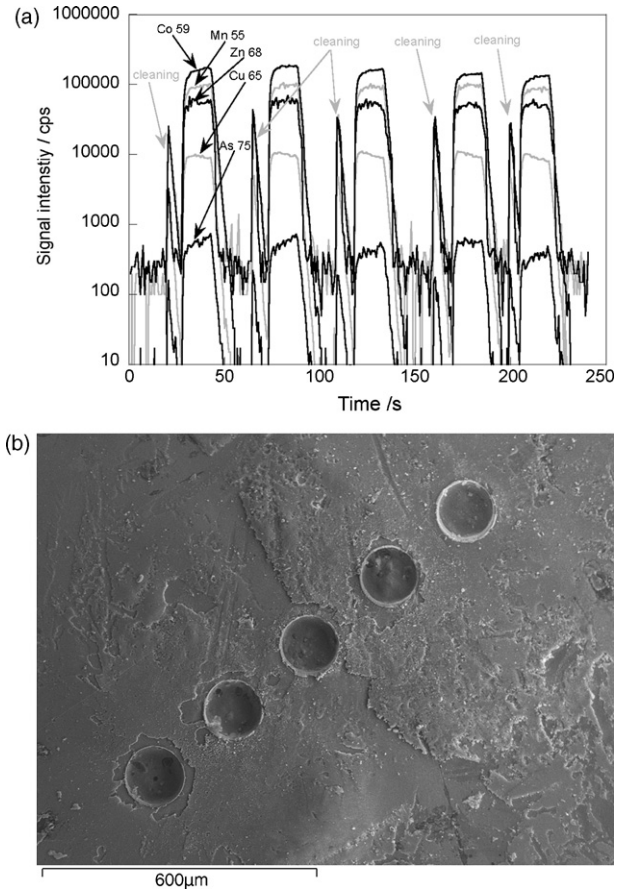

Fig. 2. (a) Signal intensity *vs*. time profiles obtained upon ablation of the glazed layer of a ceramic sample (GSM1). The cleaning period is not considered for quantification purposes. (b) Secondary electron image of the five craters produced by laser ablation.

pling technique, such as SEM), the goal of the study was not to obtain quantitative information, but rather enable discrimination between the different pigments used through the years. In fact, as already discussed in the previous section, since the amount of cobalt pigment that was added can differ very significantly from one sample to the other and even within one sample, bulk analysis of the glazed layers can hardly result in the establishment of any clear pattern. Instead, it was preferred to normalize the intensity values for all the nuclides monitored to the signal of $^{59}Co^{+}$, since this signal is directly related to the amount of pigment added. It was this parameter (the signal for every nuclide relative to the cobalt signal) that was finally used in order to look for possible differences among samples.

3.3. Characterization of the Valencian blue pigments

Ten ceramic fragments from the collection of the *Museo Nacional de Cerámica y Artes Suntuarias González Martí* (Valencia, Spain), with cobalt pigment decoration, were analyzed by EDXRF and LA-ICPMS. In Fig. 3, these samples are shown, while the corresponding caption offers a short description of the characteristics and the results of dating of the samples by experts using a traditional approach, based on stylistic and historical considerations.

Fig. 4 shows the ratio between the net intensities of the XRF lines of the selected elements (arsenic, manganese, copper, and zinc) and the net intensity of the Co Kα line. Cobalt was found in all the pigment samples analyzed. Copper and manganese were detected in the blue pigment of all of the ceramic samples in a relatively wide range of concentrations. Zinc was always detected, but was only found in a high concentration in the sample of the 14th century. This shows that, before the 15th century, the cobalt pigment was produced from cobalt ores probably extracted together with zinc blend [46]. The presence of arsenic was not detected in samples from the 14th and 15th century and in the samples Co29 (17th century) and GMS20 (19th century). This is an indication of the use of cobalt pigments with a very low-arsenic concentration ($<LOD_{XRF}$).

Fig. 5 shows the LA-ICPMS results of the more characteristic elements (arsenic, manganese, copper, and zinc), also expressed as normalized intensities, in order to distinguish chronological features. The results for other measured elements, like nickel, iron, or bismuth, have not been incorporated because they do not add any new discriminating information. Nickel and iron show a good correlation with the cobalt content ($r > 0.95$), and bismuth seems to be correlated with arsenic, so they do not significantly help to establish new differences among any group of samples. One of the advantages of the use of LA-ICPMS for this characterization is the better sensitivity attained, resulting in much improved limits of detections (see Section 3.2.), which can be particularly relevant for elements that are present at low levels in some of the samples, like arsenic. Owing to the very good spatial resolution (crater dimensions: 120 μm diameter and 25 μm depth), elements coming from the clay body do not affect the results obtained.

In general, the analytical results obtained by means of both techniques show a good agreement, leading to similar conclusions. It can be mentioned that it is not really meaningful to directly compare the signal intensity ratios obtained for every element with both techniques. Differences are expected owing to the different relative sensitivity of the analytes when using LA-ICPMS or XRF, particularly considering that the conditions selected are not always those corresponding to maximum signal intensity, but to a lower risk of interferences (e.g., when selecting the nuclides monitored or the emission lines). Moreover, the less homogeneous distribution of an element in one particular pigment may be the source for some discrepancies, owing to the very different amount of sample that is analyzed with these techniques. Furthermore, the reliability of the results obtained with XRF for samples with low-cobalt content (very pale blue samples, in which the cobalt signal might be close to the LOD) is lower and may give origin to some artificially high ratios (e.g., sample Co29). In spite of these considerations, what is relevant to stress is that very similar trends in the ratios were observed with both techniques, indicating that is possible to differentiate the Valencian samples chronologically because of the use of different cobalt pigments. The first noticeable pigment feature is higher arsenic contents from the 16th century up to the 18th century AD. Earlier samples (14th and 15th century) have very low proportions (see Fig. 4). This difference was already noted in previous papers [12,22] and also for other

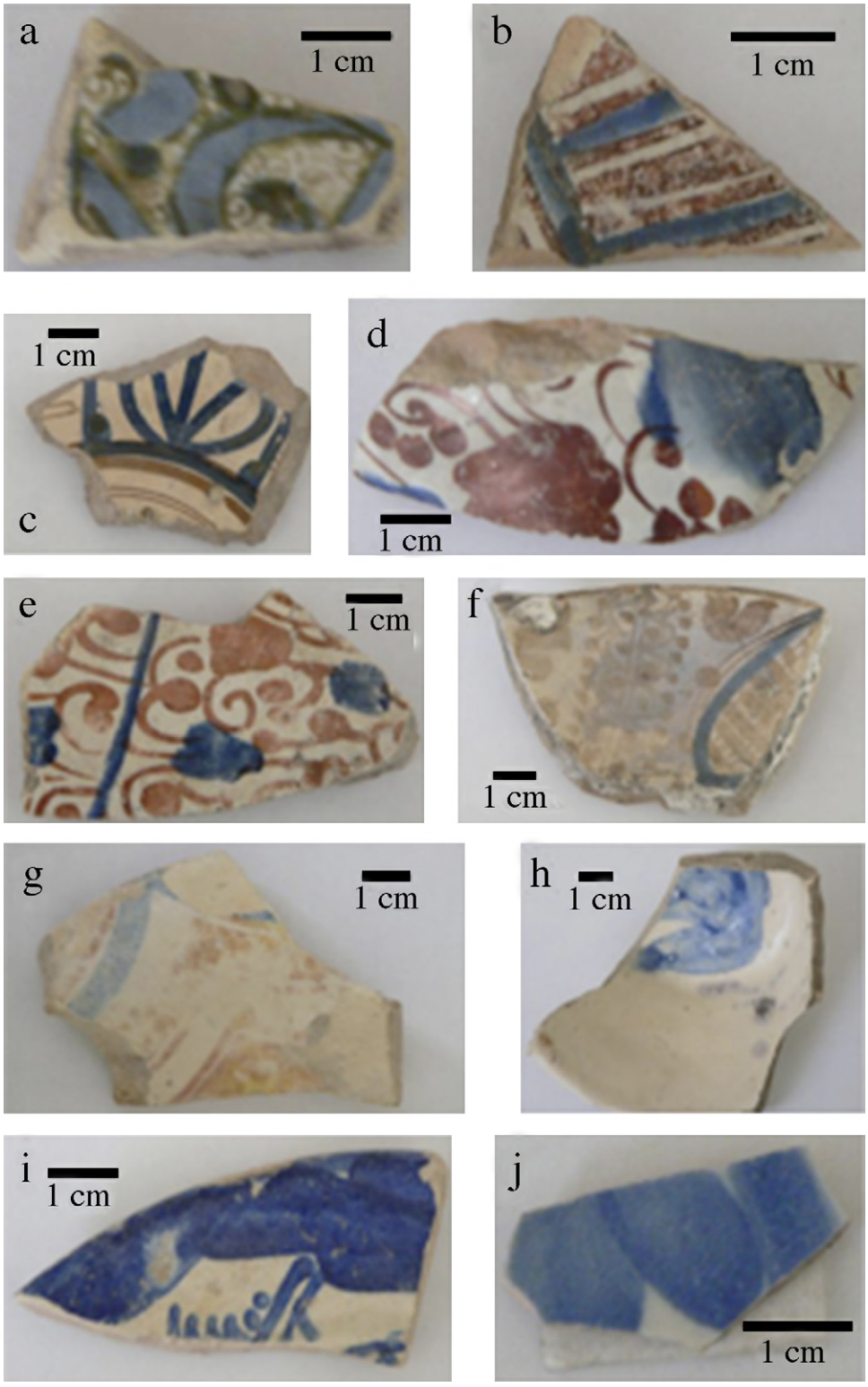

Fig. 3. (a) Sample GMS1, fragment of vase in Malaga style, century. 1330–1370. (b) Sample C124, fragment of bowl in Pula style with radial metopes, century 1380–1410. (c) Sample GMS6, fragment of bowl of the crown series, century 1410–1425. (d) Sample GMS9, fragment of "ivy leaf" vase, century 1450–1480. (e) Sample GMS10, fragment of "ivy leaf" vase, century 1475–1500. (f) Sample GMS11, fragment of bowl with scallop and lobed leaves, century 1580–1600. (g) Sample GMS12, fragment of dish edge with reserved elements, century 1600–1610. (h) Sample Co29, fragment of bowl with a blue fringed leaf, century 1650–1675. (i) Sample Co36, fragment of deep dish with decoration of hangings, century 1780. (j) Sample GMS20, a typical fragment of closed vessel, century 1850. All of the samples originate from Manises-Paterna workshops (Valencia, Spain). (For interpretation of the references to color in this figure legend, the reader is referred to the web version of the article.)

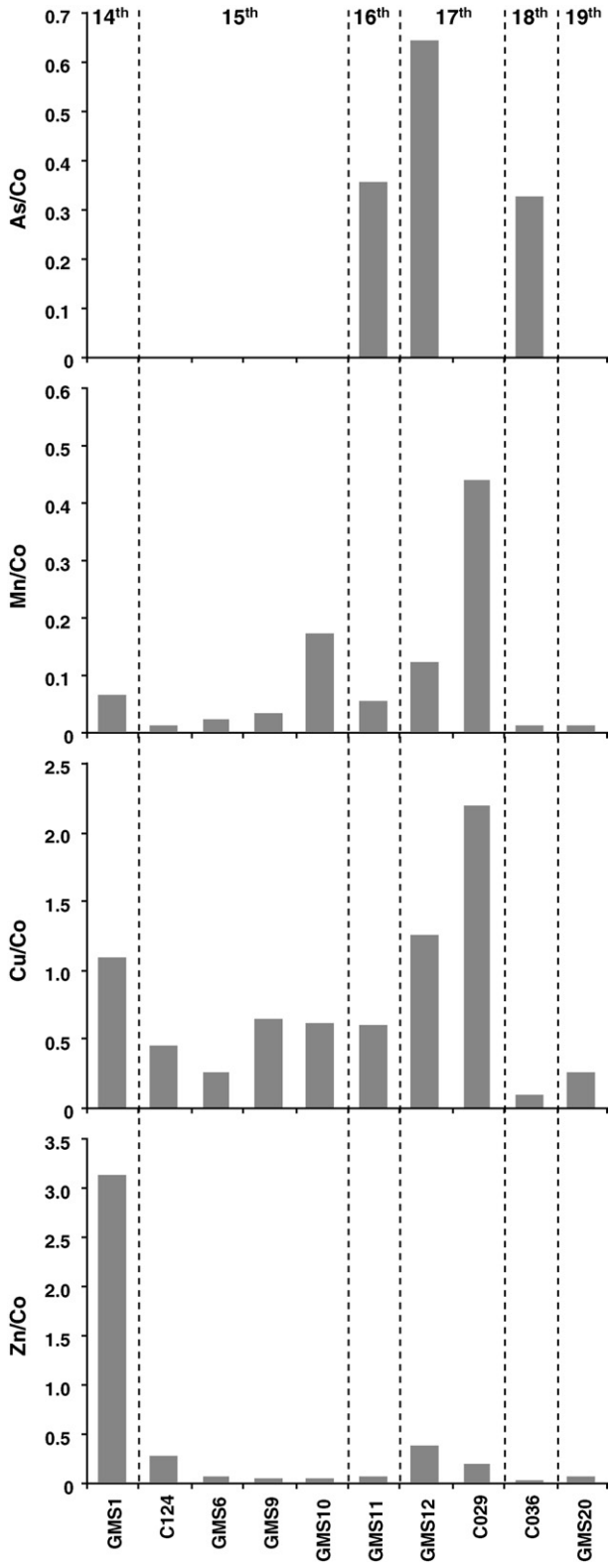

Fig. 4. Co-normalized intensities of the XRF lines of the selected elements detected in Valencian ceramic samples with cobalt-blue decoration. Histograms represent the ratios of the following signal intensities As Kβ/Co Kα, Mn Kα/Co Kα, Cu Kα/Co Kα and Zn Kα/Co Kα.

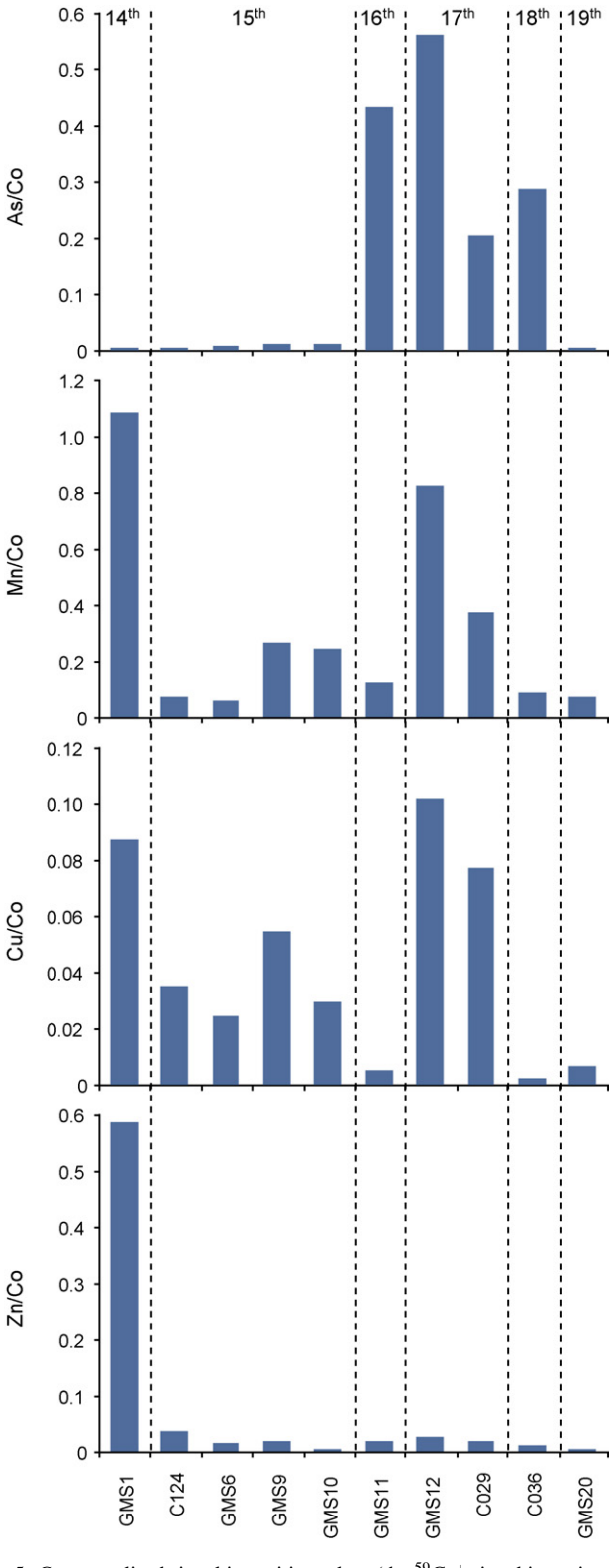

Fig. 5. Co-normalized signal intensities values (the $^{59}Co^{+}$ signal intensity was chosen as internal reference) for the elements of interest (^{75}As, ^{55}Mn, ^{65}Cu and ^{68}Zn) in blue decoration of Valencian ceramics, as obtained using LA-ICPMS.

blue-decorated ceramic materials [16,45]. Some authors even date this technological change more specifically between 1517 and 1520 [35]. Higher arsenic contents suggest that the pigment used in the samples could have been linked to minerals like cobaltite (CoAsS), erythrite ($[Co, Ni]_3[AsO_4]_2{\cdot}8H_2O$), smaltite ($[Co, Ni]As_{3-2}$) or skutterudite ($(Co, Ni)As_{3-x}$). The presence of arsenic in the blue pigments from the 16th century in glass and glazes from different regions (e.g., Italy, France and Spain) could be explained by the use of a new cobalt source or a different technology for obtaining cobalt from the mineral ores [35,45,46]. The fact that Spanish blue-decorated ceramics also show this change [12,22] would prove that there was a European technological event, not exclusive to some countries, in the use of cobalt pigments. The low arsenic proportions in the 19th century sample already suggest the more recent use of very pure cobalt pigments.

Two other characteristic elements are manganese and copper, with higher proportions in the 14th and the 17th century, and medium levels of copper in the 15th century. Zinc is only present in higher quantities in 14th century samples, as already noted in previous studies [12]. In this way, Valencian ceramics can be characterized by the use of different blue-pigment compositions during several periods: 14th century samples are characterized by an association of Co–Zn–Cu, 15th century samples by the combination of Co–Cu (with an increasing amount of manganese for samples corresponding to the late 15th century), 16th century samples by that of Co–As, 17th century samples by the combined presence of Co–As–Cu–Mn, 18th century samples by Co–As, and 19th century samples by the use of very pure cobalt. The latter purity could either suggest a change in pigment-supply or technological changes, but it also provides a most important chronological distinction.

4. Conclusions

The use of EDXRF and LA-ICPMS techniques has enabled to characterize the blue pigments of some selected Valencian ceramic fragments from the *Museo Nacional de Cerámica y Artes Suntuarias González Martí* (Valencia, Spain). EDXRF and LA-ICPMS results are in good agreement and similar conclusions can be extracted from the measurement data. Elemental information corresponding to arsenic, copper, manganese and zinc allow characteristic blue pigments from several periods to be distinguished from one another, proving that potters used different kinds of cobalt materials in several centuries and suggesting changes in pigment-supply or technological changes in the extraction of cobalt from the ore(s). Both techniques seem fit-for-purpose in this case, although they show different advantages and drawbacks: portable X-ray fluorescence spectrometry is an inexpensive and non-destructive technique, capable of providing results at the $mg\,g^{-1}$ level in a very fast way. LA-ICPMS, on the other hand, is a non-portable and more expensive technique that provides a superior detection power and a much better spatial resolution, both laterally and in depth, although its use results in some sample damage (μg level or lower).

Acknowledgements

This study was financially supported by CTPP03/2005 research project of the "Comunidad de Trabajo de los Pirineos" (Aragon-Catalonia-Aquitaine) and by the Diputación General de Aragón (DGA), Research Projects PM081/2006 and PM013/2007, and also by the Ministerio de Ciencia y Tecnología (projects Ref. BHA2003-05800 and CTQ2006-03649). Martín Resano acknowledges the Spanish Ministry of Science and Education (Secretaría de Estado de Universidades e Investigación, Programa Nacional de Ayudas para la Movilidad de Profesores de Universidad) and Esperanza García-Ruiz the 'Europa' program from CAI and DGA (CONSI + D; Grant reference CB13/05) for financially supporting their stay at Ghent University.

References

[1] A. Kaczmarczyk, R.E.M. Hedges, Ancient Egyptian Faience, Aris & Phillips, Warminster, 1983.
[2] C. Pulak, in: S. Swiny, R. Hohlfelder, H. Swiny (Eds.), Res Maritimae: Cyprus and the Eastern Mediterranean from Prehistory to Late Antiquity, Scholars Press, Atlanta, GA, 1997, pp. 233–262.
[3] T. Rehren, E.B. Pusch, J. Egypt. Archaeol. 83 (1997) 127–141.
[4] T. Rehren, Archaeometry 39 (1997) 355–368.
[5] Y. Porter, La céramique médiévale en Méditerranée, Actes du 6e congrès, Narration éditions, Aix-en-Provence, 1997 pp. 505–512.
[6] A. Kaczmarczyk, in: J.S. Olin, M.J. Blackman (Eds.), Proceedings of the 24th International Archaeometry Symposium, Smithsonian Institution Press, Washington, DC, 1986, pp. 369–376.
[7] A.J. Shortland, M.S. Tite, Archaeometry 42 (2000) 141–151.
[8] A.J. Shortland, M.S. Tite, I. Ewart, Archaeometry 48 (2006) 153–168.
[9] J. Coll, El azul en la loza de la Valencia medieval, Catálogo de la Exposición, Valencia, 1995.
[10] J.R. Taylor, Sci. Archaeol. 19 (1977).
[11] C. Roldán, J. Coll, J.L. Ferrero, D. Juanes, Xray Spectrom. 33 (2004) 28–32.
[12] C. Roldán, J. Coll, J. Ferrero, J. Cult. Herit. 7 (2006) 134–138.
[13] K.N. Yu, J.M. Miao, Xray Spectrom. 28 (1999) 19–23.
[14] Ph. Colomban, G. Sagon, L.Q. Huy, N.Q. Liem, L. Mazerolles, Archaeometry 46 (2004) 125–136.
[15] R. Padilla, O. Schalm, K. Janssens, R. Arrazcaeta, P. Van Espen, Anal. Chim. Acta 535 (2005) 201–211.
[16] G. Pappalardo, E. Costa, C. Marchetta, L. Pappalardo, F.P. Romano, A. Zucchiatti, P. Prati, P.A. Mandò, A. Migliori, L. Palombo, M.G. Vaccari, J. Cult. Herit. 5 (2004) 183–188.
[17] T. Trejos, J.R. Almirall, Talanta 67 (2002) 396–401.
[18] T. Trejos, J.R. Almirall, Talanta 67 (2002) 388–395.
[19] C. Latkoczy, S. Becker, M. Ducking, D. Gunther, J.A. Hoogewerff, J.R. Almirall, J. Buscaglia, A. Dobney, R.D. Koons, S. Montero, G.J.Q. van der Peijl, W.R.S. Stoecklein, T. Trejos, J.R. Watling, V.S. Zdanowicz, J. Forensic Sci. 50 (2005) 1327–1341.
[20] D.N. Papadopoulou, G.A. Zachariadis, A.N. Anthemidis, N.C. Tsirliganis, J.A. Stratis, Spectrochim. Acta B 59 (2004) 1877–1884.
[21] I. De Raedt, K. Janssens, J. Veeckman, L. Vincze, B. Vekemans, T.E. Jeffries, J. Anal. At. Spectrom. 16 (2001) 1012–1017.
[22] M. Resano, J. Pérez-Arantegui, E. García-Ruiz, F. Vanhaecke, J. Anal. At. Spectrom. 20 (2005) 508–514.
[23] H. Neff, J. Archaeol. Sci. 30 (2003) 21–35.
[24] R.J. Speakman, H. Neff, Am. Antiquity 62 (2002) 137–144.
[25] B. Gratuze, M. Blet-Lemarquand, J.N. Barrandon, J. Radioanal. Nucl. Chem. 247 (2001) 645–656.
[26] D.V. Hill, R.J. Speakman, M.D. Glascock, Archaeometry 46 (2004) 585–605.
[27] E.E. Cochrane, H. Neff, J. Archaeol. Sci. 33 (2006) 378–390.
[28] D. Günther, B. Hattendorf, Trends Anal. Chem. 24 (2005) 255–265.

[29] R.E. Russo, X. Mao, H. Liu, J. Gonzalez, S.S. Mao, Talanta 57 (2002) 425–451.
[30] E. Selin (Ed.), Special Millennium Issue on Cultural Heritage, X-ray Spectrom, vol. 29, 2000.
[31] K.N. Yu, in: D.C. Creagh, D.A. Bradley (Eds.), Radiation in Art and Archaeometry, Elsevier, 2000, pp. 317–346.
[32] A. Zucchiatti, A. Bouquillon, J. Salomon, J.R. Gaborit, Nucl. Instrum. Meth. Phys. Res. B 161–163 (2000) 699–703.
[33] A. Bouquillon, J. Castaing, E. Vartanian, A. Zink, A. Zucchiatti, in: J.R. Gaborit, M. Bormand (Eds.), Les della Robbia: Sculptures en Terre Cuite Émaillée de la Renaissance Italienne, Rèunion des Musées Nationaux, Paris, 2002, pp. 139–158.
[34] I. Biron, S. Beauchoux, Meas. Sci. Technol. 14 (2003) 1564–1578.
[35] A. Zucchiatti, A. Bouquillon, I. Katona, A. D'Alessandro, Archaeometry 48 (2006) 131–152.
[36] J.-C. Dran, T. Calligaro, J. Salomon, in: E. Ciliberto, G. Spoto (Eds.), Chemical Analysis Series, vol. 155, John Wiley Sons, 2000.
[37] D. Günther, R. Frischknecht, C.A. Heinrich, H.J. Kahlert, J. Anal. At. Spectrom. 12 (1997) 939–944.
[38] H.P. Longerich, S.E. Jackson, D. Günther, J. Anal. At. Spectrom. 11 (1996) 899–904.
[39] M.A. Belarra, M. Resano, J.R. Castillo, J. Anal. At. Spectrom. 14 (1999) 547–552.
[40] M. Resano, F. Vanhaecke, D. Hutsebaut, K. De Corte, L. Moens, J. Anal. At. Spectrom. 18 (2003) 1238–1242.
[41] F. Vanhaecke, M. Resano, E. Garcia-Ruiz, L. Balcaen, K.R. Koch, K. McIntosh, J. Anal. At. Spectrom. 19 (2004) 632–638.
[42] M. Vendrell, J. Molera, M.S. Tite, Archaeometry 42 (2000) 325–340.
[43] J. Molera, T. Pradell, M. Mesquida, M. Vendrell, in: M. Mesquida (Ed.), Las Ollerías de Paterna, Tecnología y Producción, Ayuntamiento de Paterna, 2001, pp. 235–261.
[44] R. Capote, E. López, E. Mainegra, WinQXAS Manual (Quantitative X-Ray Analysis System for Widows) Version 1.2, IAEA, 2000.
[45] B. Gratuze, I. Soulier, M. Blet, L. Vallauri, Revue d'Archéometrie 20 (1996) 77–94.
[46] J. Hartwig, Verre 7 (2001) 40–48.

Available online at www.sciencedirect.com
ScienceDirect
Talanta 74 (2008) 1231–1235
Talanta
www.elsevier.com/locate/talanta

Multi-elemental analysis of produced water by synchrotron radiation total reflection X-ray fluorescence

P.M. Pimentel [a,*], M.J. Anjos [b], D.M.A. Melo [a], M.A.F. Melo [a], L.M. Gonçalves Jr. [a], C.N. Silva Jr. [a], R.T. Lopes [b]

[a] *Federal University of Rio Grande do Norte, CCET, DQ, Environmental Technology Laboratory, P.O. Box 1662, 59072-970 Rio Grande do Norte, Brazil*
[b] *Federal University of Rio de Janeiro/COPPE, Nuclear Instrumentation Laboratory, P.O. Box 68509, 21945-970 Rio de Janeiro, Brazil*

Received 22 July 2007; received in revised form 25 August 2007; accepted 27 August 2007
Available online 1 September 2007

Abstract

The synchrotron radiation total reflection X-ray fluorescence (SRTXRF) technique was used for the analysis of heavy metals in produced water samples from oil field in Rio Grande do Norte, in order to determine potential sources of pollution. Since the inorganic components in produced water generally resembling sea water, pre-concentration procedures have been applied to increase the concentration of the analyte of interest and to minimize the salt matrix effects. This technique allows us to determine the contents of V, Cr, Mn, Fe, Co, Ni, Cu, Zn, Hg and Pb in 20 produced water samples. The great majority of the sampling points presented low elemental concentration value. However, in some sample, the Fe, Ni, Cu, Zn and Hg concentration were higher than the established limits by the Brazilian legislation.
© 2007 Elsevier B.V. All rights reserved.

Keywords: SRTXRF; Produced water; Heavy metals

1. Introduction

Produced water is wastewater that is brought to the surface during the natural gas and crude oil production at the oil fields. This water consists of formation water (the water naturally present in the reservoir); and floodwater previously injected into the formation. The salinity of the produced water can vary from almost fresh to saturated, depending upon the source geology and production process. On the surface, produced water is separated from the hydrocarbons, treated to remove as much oil as possible, and then either re-injected into the reservoir or discharged into the sea. Due to a complex chemical composition (oil, salt, heavy metals, radio nuclides and treating chemical) and the high water production volumes, these discharges are focused by the organizations responsible for environmental protection, which have established strict regulations on the maximum allowed contents of heavy metals in this water.

Total reflection X-ray fluorescence (TXRF) is a multi-elemental technique applied in several areas of the science and technology [1,2], and it has been used in the last year in environmental analysis (air, sediment, soil, plants and others) mainly in the water analysis [3,4].

The total reflection X-ray fluorescence technique using synchrotron radiation (SRTXRF) as an excitation source was applied, because of its advantageous features, namely multi-elemental capability, high sensitivity, precision and short time of analysis [5,6]. However, direct analysis of these elements in salty water is sometimes not feasible by SRTXRF due to the very low concentration of some trace metals and the high salt matrix. Therefore, a pre-concentration method has to be applied in order to improve the detection limit and to minimize the salt matrix effects [7–9].

The aim of this work was to determine the heavy metals concentration in the produced water of several oil fields in Rio Grande do Norte, Brazil using total reflection X-ray fluorescence by synchrotron radiation.

* Corresponding author at: Rua Itaúna, 2872 CJ Pirangi, Bairro Neópolis, CEP 59088-060 Natal, RN, Brazil. Tel.: +55 84 3211 9241; fax: +55 84 3211 9241.
E-mail addresses: patricia@materiais.ufrn.br, pimentelmp@yahoo.com (P.M. Pimentel).

0039-9140/$ – see front matter © 2007 Elsevier B.V. All rights reserved.
doi:10.1016/j.talanta.2007.08.028

2. Materials and methods

2.1. Sampling

The 20 samples of produced water were collected from oil fields in Rio Grande do Norte state in Brazil at different days and times, in order to determine potential sources of pollution. These samples were collected directly in pre-cleaned polyethylene bottle and kept frozen until analyzed.

2.2. Reagents

All reagents were of the highest analytical grade (Merck). The nitric acid used was ultra pure. For the complexation of different metals under investigation, 1% ammonium pyrrolidinedithiocarbamate (APDC) solution has been used [7]. The vermiculite used was supplied by the company União Brasileira de Mineração in Paraíba state, Brazil. To avoid contamination from the recipients and volumetric flasks used, they were washed with detergent, soaked in a 1 mol L^{-1} HNO_3 solution, rinsed with deionized water (Milli Q water), filled with 10 mol L^{-1} HNO_3, kept for at least one night and again rinsed with deionized water.

2.3. Sample preparation

Oil removal procedure was performed prior pre-concentration procedure. The oil content in produced water samples was removed by filtrating on hydrophobized vermiculite bed. A similar procedure was described in the literature [10].

In the pre-concentration method, 50 mL of produced water was poured into a volumetric flask and spiked with 75 μL of Se (internal standard). The pH of the solution was adjusted to about 3.0. Then, 2 mL APDC solution was added and the mixture was stirred for 20 min at room temperature. The carbamates were collected by filtration through a Millipore filter (0.45 μm pore size). Each filter was dried in infrared light and cut in three small disks (3 mm diameter). They were transferred to a Perspex reflector and digested with HNO_3. From each sample, three replicates were analyzed. Blanks and calibration standards were prepared using similar procedure.

2.4. Quantitative analysis by SRTXRF

Synchrotron radiation experiments (SRTXRF) were performed at the X-ray fluorescence beamline of the National Synchrotron Light Laboratory (LNLS), in Campinas, Brazil. Excitation was performed with a polychromatic beam with maximum energy of 20 keV. Characteristic radiation was detected by Si (Li) detector with a resolution of 165 eV at 5.9 keV. The samples were excited for 100 s and X-ray spectra obtained were evaluated by the software QXAS (Quantitative X-ray Analysis Software) in order to obtain the X-ray intensities [11]. All analyses were performed in air atmosphere.

In SRTXRF analysis, X-rays at an incidence angle below the critical angle strike on the optical flat surface (e.g. quartz or Perspex) and are totally reflected. Under these conditions, the scattering effects are minimized leading to a substantial reduction of the detection limits. The synchrotron radiation (SR) as a primary excitation source allows improving the overall sensitivity of TXRF [12]. Another characteristic of SRTXRF technique is the small volume required of liquid samples for analysis (microliters), then the samples can be considered as thin films so that absorption effects can be neglected [3]. The quantitative analysis can be calculated using the equation below:

$$I_i = S_i C_i$$

where I_i represents the intensity (counts/s) of the characteristic X-rays of the element i, C_i its concentration (μg mL^{-1}) and S_i is the system sensitivity for each element. The samples deposited on the Perspex support does not have regular geometry and therefore, the X-ray intensities depend on the position of the sample. This geometric effect can be corrected, by calculating the relative intensity for each element with respect to an internal standard added in the sample. Therefore, the equation above can be rewritten in the relative intensities form [4]:

$$I_{r,i} = S_{r,i} C_i$$

where $I_{r,i}$ represents the relative intensity for the element i and $S_{r,i}$ is the relative sensitivity. The relative sensitivity was determined by the measures of standards containing the elements: Al, Si, K, Ca, Ti, Cr, Fe, Ni, Zn, Se, Sr and Mo for the K-lines and Sr, Mo, Cd, Ba, Sb, Pt, Hg, Tl and Pb for the L-lines. A minimum detection limit (MDL) [13] is determined using the concentrations of the standards and the equation:

$$\mathrm{MDL}_i = 3\frac{C_{Se}}{S_{r,i} I_{Se}}\sqrt{\frac{I_{i,bg}}{t}}$$

where C_{Se} and I_{Se} correspond to the internal standard concentration and intensity, respectively. $I_{i,bg}$ represents the background intensity for element i and t is the measuring time.

3. Results and discussion

The relationship between the relative sensitivity of the system and the atomic number is shown in Fig. 1. The detection limits varied from 83 ng L^{-1} for Ti, 20 ng L^{-1} for Ni, 210 ng L^{-1} for Sr and 181 ng L^{-1} for Hg. These values are in agreement

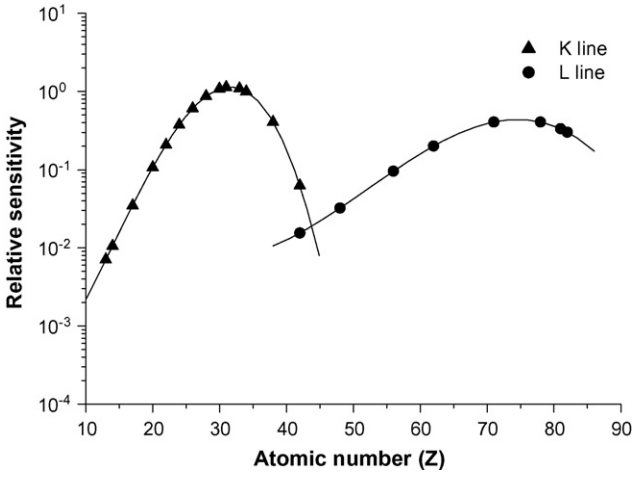

Fig. 1. Relative sensitivity curve for K- and L-lines.

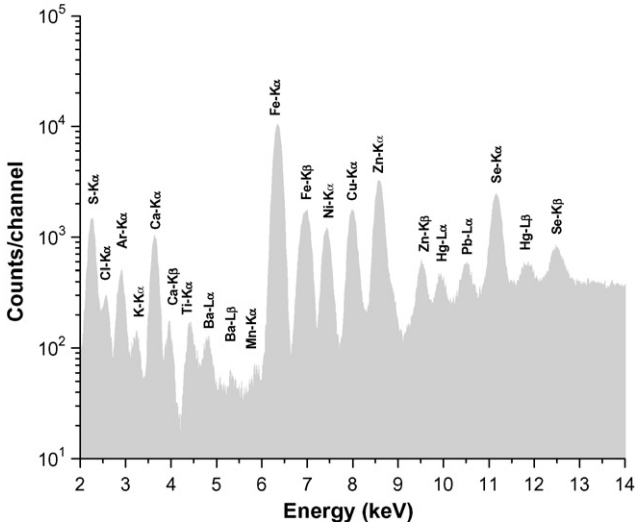

Fig. 2. Characteristic X-ray spectrum of produced water sample.

with the values present in literature [8]. Characteristic X-ray spectrum of produced water is shown in Fig. 2. Some elements such as Cl, K, Ca, Ba, Ar, Ti and S cannot be complexed by APDC. They are present in the spectrum due to their high concentration.

The obtained results for some heavy metal contents in produced water samples are displayed in Figs. 3–8

. The detection limits achieved for these elements are, at least, as good as those reported in the literature, which refer to SRTXRF measurements of residues of the precipitate dissolved in an organic solvent. It is observed that the relative concentrations of different metals in produced water vary widely from one sample to another. This can be explained by the fact that the composition of produced waters is strongly field-dependent, in other words, it results from the geological formation and chemical products added in the exploration and production of oil and/or gas. The great majority of the sampling points presented low elemental concentration values, however, in some sample, the Fe, Ni, Cu, Zn and Hg concentration were higher than the permitted limits by the Brazilian legislation. The element Fe presented

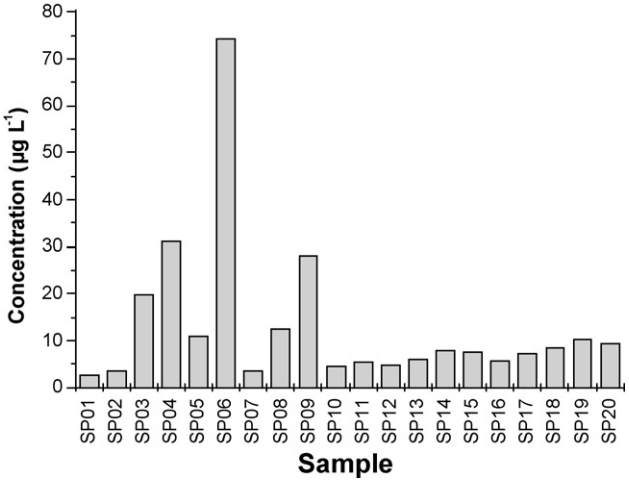

Fig. 3. Chromiun concentration ($\mu g\,mL^{-1}$) in produced water samples.

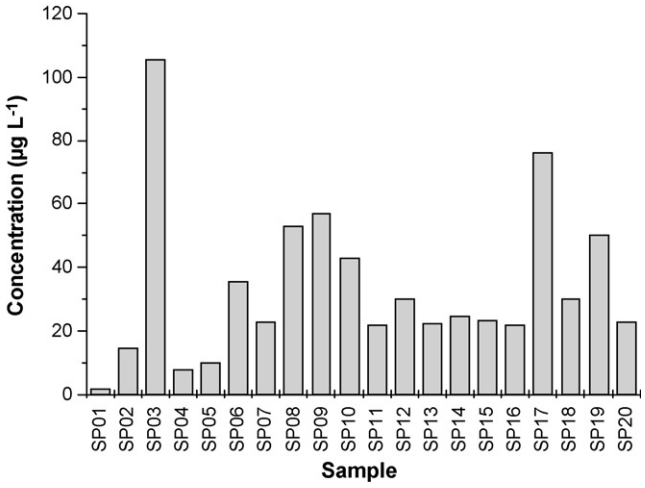

Fig. 4. Copper concentration ($\mu g\,mL^{-1}$) in produced water samples.

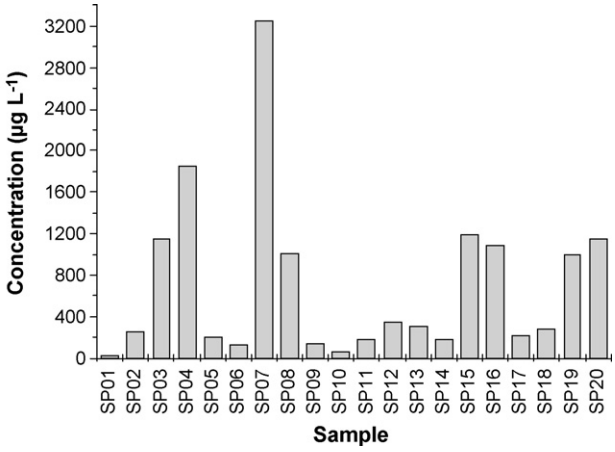

Fig. 5. Iron concentration ($\mu g\,mL^{-1}$) in produced water samples.

an anomalous content in some samples. These high values can be ascribed partly to geological characteristic of the reservoirs and other factors such as the corrosion of equipment could be a source of iron in produced water.

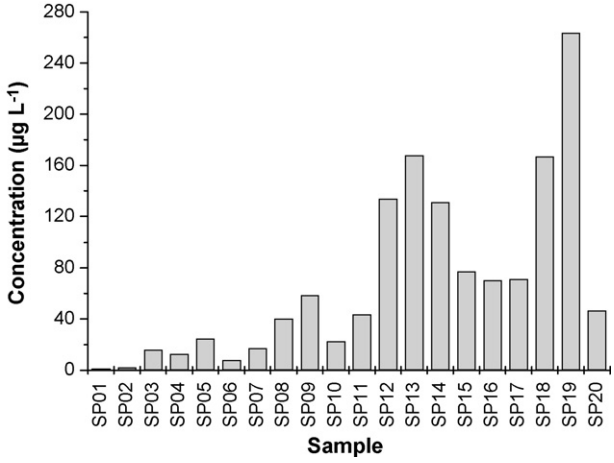

Fig. 6. Lead concentration ($\mu g\,mL^{-1}$) in produced water samples.

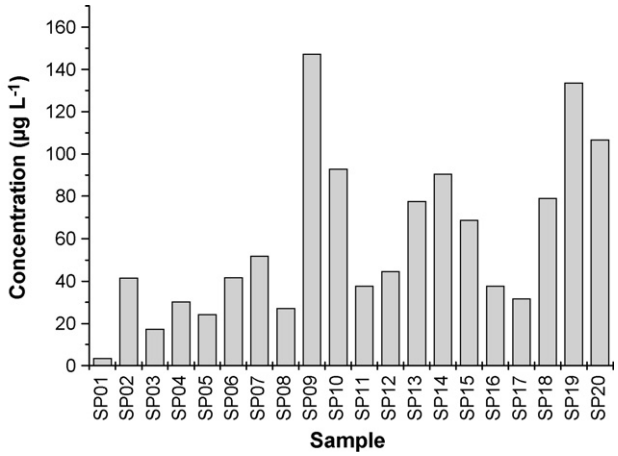

Fig. 7. Mercury concentration ($\mu g\,mL^{-1}$) in produced water samples.

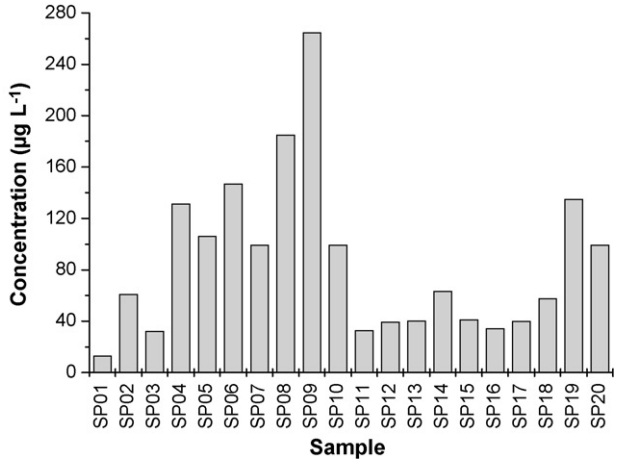

Fig. 8. Zinc concentration ($\mu g\,mL^{-1}$) in produced water samples.

Table 1 gives the maximum and minimum values for elemental concentration of 20 produced water samples. The results obtained, indicated both good standards deviation of the replicates for most elements. For elements Fe, Ni, Cu, Zn, Hg and Pb, it was possible to verify that in some samples the concentration were above the limit established by the Brazilian legislation (CONAMA 20/86) for the salt water. The concentrations of the elements Mn and V were lower than for other elements.

Table 1
Elements concentrations in produced water samples

Element	Concentration ($\mu g\,L^{-1}$)			
	Minimum	Maximum	S.D.[a]	Brazilian legislation[b]
V	0.01	37.90	2.90	100
Cr	2.80	74.40	1.00	Cr^{3+} 500, Cr^{6+} 50
Mn	1.00	41.00	0.20	100
Fe	22.6	3095	78.2	300
Co	22.0	88.20	0.90	200
Ni	33.8	102.0	1.00	250
Cu	2.00	107.0	2.70	500
Zn	13.1	264.8	1.40	180
Hg	3.70	147.3	6.80	0.20
Pb	1.60	263.8	3.50	30.0

[a] Standard deviation.
[b] CONAMA 20/86.

Table 2 compares the average values of the concentration of some elements found in produced water from oil fields in the North Sea, Gulf of Mexico, Bacia de Campos (Brazil) [14,15] and the values obtained in this research (oil fields from Rio Grande do Norte state). The quality of the data taken from the literature is not known due to the lack of information in the article about the analytical techniques used to obtain the concentrations. Then comparison among the fields should be made in the intention of having an estimate of the magnitude of the concentrations. Analyzing the table, it is verified that among the presented elements, the values obtained in this work are not too different from the one found in other regions, except in the content of the iron and chlorine, whose average values were significantly low. The higher concentrations of chlorine in the Bacia de Campos, perhaps be explained by the fact to

Table 2
Concentration of some elements in produced waters (average values)

Components	Concentration ($mg\,L^{-1}$)			
	North Sea [14]	Gulf of Mexico [15]	Bacia de Campos [15]	Rio Grande do Norte[a]
Chloride	–	–	45,380	2407
Barium	3.15	–	>0.2	4.890
Calcium	–	–	769.3	774.56
Chromium	0.100	0.186	>0.20	0.019
Copper	0.017	0.104	0.20	0.035
Iron	3.00	–	3.20	0.810
Lead	0.15	0.315	1.5	0.020
Mercury	0.006	0.192	0.003	0.048
Nickel	0.300	0.192	1.3	0.038
Zinc	1.700	0.170	0.4	0.114

[a] This research.

produce petroleum starting from reservoirs of salted waters, while in the Rio Grande do Norte are coming of less saline reservoirs.

4. Conclusions

The most important conclusion derived from this work is the suitability of SRTXRF for routine analysis of waters. The low detection limits of this technique enable us to detect low concentration values of heavy metals in produced water samples. High level of iron was found in this water. The results reveal us the possibility of environmental damage for areas very close to produced water discharge points and they are potentially useful to compose a database for heavy metal removal studies in these waters.

Acknowledgments

The authors thank LNLS (National Synchrotron Light Laboratory-project XRF-2044), where the analyses were performed. This research was financially supported by the National Petroleum Agency (ANP-Brazil).

References

[1] K. Baur, S. Brennan, D. Werho, L. Moro, P. Pianetta, Nucl. Instrum. Methods A 467 (2001) 1198.
[2] C. Calza, M.J. Anjos, C.R.F. Castro, R.C. Barroso, F.G. Araujo, R.T. Lopes, Radiat. Phys. Chem. 71 (2004) 787.
[3] S.M. Simabuco, E. Matsumoto, Spectrochim. Acta Part B 55 (2000) 1173.
[4] A.C.M. Costa, M.J. Anjos, S. Moreira, R.T. Lopes, E.F.O. Jesus, Spectrochim. Acta Part B 58 (2003) 2199.
[5] H. Aiginger, P. Wobrauschek, Nucl. Instrum. Methods 114 (1974) 157.
[6] A. Prange, H. Böddeker, K. Kramer, Spectrochim. Acta Part B 48 (1993) 207.
[7] M. Nagj, M. Jaksic, I. Orlic, V. Valkovic, Nucl. Instrum. Methods A 236 (1985) 563.
[8] A. Prange, A. Knochel, W. Michaelis, Anal. Chim. Acta 172 (1985) 79.
[9] R. Van Grieken, Anal. Chim. Acta 143 (1982) 3.
[10] U.G. Silva Jr., M.A.F. Melo, A.F. Silva, R.F. Farias, J. Colloid Interf. Sci. 260 (2003) 302.
[11] G. Bernasconi, A. Tajani, Quantitative X-ray Analysis System (QXAS), Software Package: Documentation Version 1.2, IAEA, Vienna, 1996.
[12] W. Maenhaut, Nucl. Instrum. Methods B 49 (1990) 518.
[13] V.F. Nascimento Filho, V.H. Poblete, P.S. Parreira, E. Matsumoto, S. Simabuco, E.P. Espinoza, A.A. Navarro, Biol. Trace Elem. Res. 71–72 (1999) 423.
[14] T.I.R Utvik, Chemosphere 39 (1999) 2593.
[15] E. Bessa, G.L. Sant'anna Jr., M. Dezotti, Appl. Catal. B: Environ. 29 (2001) 125.

Available online at www.sciencedirect.com
ScienceDirect
Talanta 74 (2008) 1463–1475
Talanta
www.elsevier.com/locate/talanta

Development and optimisation of a single extraction procedure for the LC/MS/MS analysis of two pharmaceutical classes residues in sewage treatment plant

Anne Piram, Arnaud Salvador*, Jean-Yves Gauvrit, Pierre Lanteri, René Faure

Université de Lyon, Lyon 1, UMR 5180, CNRS, Laboratoire des Sciences Analytiques, 43 Boulevard du 11 novembre 1918, 69622 Villeurbanne, France

Received 27 April 2007; received in revised form 5 September 2007; accepted 28 September 2007
Available online 9 October 2007

Abstract

A unique extraction procedure leading to the separation of 2 different pharmaceutical classes molecules has been developed and optimised by chemometric tools. From only one sampling, this analytical method allows the determination of 21 pharmaceuticals from corticosteroids and β-blockers classes. Performing the SPE on Oasis MCX (mixed-mode cation exchange), the sequential elution of each pharmaceutical class is achievable, allowing a high purity level of extracts as well as high recovery rates. Performing a unique sample preparation results in an important save of time. The extracts were then analysed by LC/MS/MS, using a Hibar Purospher Star column for β-blockers and an X-Bridge column for corticosteroids with formate buffer (pH 3.8)/AcN and water/AcN mobile phases, respectively. This work also includes a study of the chromatographic and mass spectrometric parameters in order to increase the analyte signal. The optimised SPE-LC/MS/MS method was then applied to environmental samples from sewage treatment plant (STP). β-Blockers and corticosteroids were detected, respectively, in concentrations up to 318 ng L^{-1} (sotalol) and 174 ng L^{-1} (cortisone), in STP influents. Moreover, both pharmaceutical classes have also been detected in STP effluents. As far as we know, this is the first paper reporting the detection of corticosteroids in environmental waters. The developed analytical method can be used in further studies to investigate the environmental contamination by these drugs.
© 2007 Elsevier B.V. All rights reserved.

Keywords: Pharmaceuticals; Water analysis; SPE; β-Blockers; Steroids; Liquid chromatography; Mass spectrometry

1. Introduction

Quantification of drugs in the environment is a matter of concern since they potentially represent an important environmental risk [1–4]. Indeed, these substances have been developed in order to perform a biological effect and are partially excreted unchanged by the body. Thus, they can affect non-targeted organisms and be harmful for the ecosystem.

Human medications reach the environment through sewage treatment plant (STP). Effectively it was recognised that STP efficiency is very low for this kind of micropollutants, allowing the passage of these compounds and their release into the environment. Several authors have reported the environmental occurrence of drugs in surface-, ground- and tap-water, as well as in STP influents and effluents [5–12]. Many studies report the quantification of large amounts of non-steroidal anti-inflammatory drugs (aspirin, paracetamol) [13–15], antidepressant (fluoxetine, paroxetine) [15], antibiotics (amoxicillin, sulfamethoxazole) [15–17], steroid sex hormones (estrone, estriol) [18–20] or cardiovascular drugs (atenolol, dilitiazem) [11,15,16,21]. β-Blockers (cardiovascular drugs) have been reported to contaminate both American and European waters in a large number of studies [13,21–25], with concentrations up to 2000 ng L^{-1}. The occurrence of steroids in environmental waters has been confined to the study of the estrogens subclass [18–20]. Few papers report the contamination by other steroid class molecules, such as cholestanes (cholesterol), progestagens (progesterone, levonorgestrel) or androgens (testosterone) [26–28]. However, no environmental measurements were done concerning corticosteroids although they are consumed in large quantities as anti-inflammatory or antiallergenic drugs. Moreover, this pharmaceutical class has been underlined as a potential

* Corresponding author. Tel.: +33 4 72 43 11 52; fax: +33 4 72 44 62 02.
E-mail address: arnaud.salvador@univ-lyon1.fr (A. Salvador).

0039-9140/$ – see front matter © 2007 Elsevier B.V. All rights reserved.
doi:10.1016/j.talanta.2007.09.038

environmental risk by a study of prioritisation based on a modelisation [29].

The aim of this study was to analyse simultaneously 2 pharmaceutical classes: β-blockers and corticosteroids whose structures are given in Tables 1 and 2 , respectively. These pharmaceutical classes were selected because of their high consumption (e.g. 35 t year^{-1} in France for propranolol β-blocker) and the information deficiency for the corticosteroids impact in the environment. Analytical method development for corticosteroid compounds analysis in environmental samples was necessary since so far no methods were proposed by the literature concerning this matrix (water).

The difficulty of tracking trace pollution of drugs in STP is linked with the complexity of environmental matrices. Indeed, they contain lots of other organic pollutants such as pesticides or personal care products. Moreover, there is an important dilution factor in the environment which results in expected environmental concentration in the ng L^{-1} range, as it has been found in both European and American waters [5–28]. Thus, it is necessary to concentrate and purify samples before analysis. In the literature, this sample preparation is mainly done by solid phase extraction (SPE) [5–28,30–33]. The development of multiresidue methods is important in environmental analysis of pharmaceuticals and continuous efforts have been made to design new analytical procedures able to quantify traces amounts of pharmaceuticals in environmental waters. These recently developed methods aim to improve the total analysis time and reduce the analysis cost. Then, it is useful to develop a unique extraction procedure, which allows the extraction of both pharmaceutical classes from only one sampling, on the same SPE sorbent, with a sequential final elution of each class.

The extracted sample analysis should be then carried out by means of sensitive and selective detection tools, such as the tandem mass spectrometers, which are widely used in environmental analysis. A liquid chromatographic device is coupled to the mass spectrometer as reported in literature [5–28,30–33]. This paper also presents a study for the LC/MS/MS parameters optimisation in order to improve the analyte response.

2. Experimental

2.1. Chemicals

Betamethasone (97.8%) (Be), budesonide (99.2%) (Bu), cortisol (98%) (Hy), cortisone (98.3%) (C), dexamethasone (98%) (D), flunisolide (98.6%) (Fs), fluocinolone acetonide (99.6%) (Fc), prednisolone (99%) (Pl), prednisone (99%) (P), triamcinolone (98.2%) (T), triamcinolone acetonide (99.3%) (TA), acebutolol hydrochloride (100%) (Ac), alprenolol hydrochloride (99%) (Al), atenolol (99%) (At), metoprolol tartrate salt (100%) (M), nadolol (100%) (N), propranolol hydrochloride (99%) (Pr), pindolol (99%) (Pi), sotalol hydrochloride (99%) (S), and timolol maleate salt (99.9%) (Ti) were provided by Sigma–Aldrich (Saint Quentin Fallavier, France). Bisoprolol fumarate (100%) (Bi) was provided by Sequoia research (Pangbourne, United Kingdom). Methanol HPLC grade (MeOH) was provided by SDS-Carlo-Erba (Peypin, France). Acetonitrile LC/MS grade (AcN), formic acid (85%) (FOA) and ammonium formate (99%) were obtained from Fisher Scientific (Val de Rueil, France). Ammonia solution RP Normapur (28%) was provided by Prolabo (Fontenay sous Bois, France). Ultra-pure water was generated by an Elgastat UHQ PS from Elga LabWater (High Wycombe Bucks, United Kingdom).

Each corticosteroid stock solution was prepared in AcN at 1000 mg L^{-1}, excepted for triamcinolone and triamcinolone acetonide (250 mg L^{-1}) which have a lower solubility. Each β-blocker stock solution was prepared in MeOH at 1000 mg L^{-1}. A first 50 mg L^{-1} standard working solution (WS_c) containing the 11 corticosteroids was prepared in AcN. A second 50 mg L^{-1} standard working solution (WSβ) containing the 10 β-blockers was prepared in MeOH. These solutions were stored at 4 °C, in the dark.

4, 2 and 1 mg L^{-1} working solutions were prepared by dilution of WS_c in water/AcN/FOA (75:25:0.1, v/v/v). Corticosteroids calibration standards were then prepared in water/AcN/FOA (75:25:0.1, v/v/v) by consecutive dilution of these solutions. A similar procedure has been performed for the preparation of β-blockers calibration standards from WSβ.

2.2. Sampling

Environmental matrices samples were collected from Pierre Benite STP (downstream from Lyon, France). This STP receives mainly urban and hospital wastewaters. For environmental analysis, 24 h average samples were collected, whereas direct samplings were used as matrix for method development. Both influent and effluent samples were filtered up to 0.45 μm on membrane filters provided by Millipore (Molsheim, France) and stored at 4 °C. Samples were extracted within a maximum of 3 days after the collect.

2.3. Sample preparation

Samples were extracted on Oasis MCX cartridges (60 mg, 3 cc) from Waters (Saint Quentin en Yvelines, France). The solid phase extraction was performed on an Aspec XL4 equipped with a 404 syringe pump and an 8 position valve mate from Gilson (Villiers le Sec, France), controlled by the 735 sampler Gilson software.

Each 400 mL environmental sample was acidified with 400 μL of FOA (85%), then spiked by the volume needed (<50 μL) of calibration standard for the standard addition method. The sample was then loaded at a flow rate of 15 mL min^{-1} using Aspec XL4 onto an Oasis MCX extraction cartridge preconditioned with 3 mL of MeOH and 3 mL of water acidified with 0.1% of FOA (85%). The cartridge was then rinsed with 1.5 mL of MeOH/water/FOA (10:90:0.1, v/v/v) mixture. Corticosteroids were eluted with 1 mL of MeOH/water/FOA (70:30:0.1, v/v/v). A second wash with 1 mL of MeOH/FOA (100:0.1, v/v) was performed. Finally, β-blockers were eluted with MeOH/ammonia solution (95:5, v/v). Consequently, 2 extracts were collected separately: the first one containing corticosteroids and the second one containing β-blockers. Each wash and elution step were performed at a flow rate of 0.3 mL min^{-1}.

Table 1
Structures and mass spectrometric parameters used for the analysis of corticosteroids

Molecule [CAS]	Structure	$[M+H]^+$ (*m*/*z*)	Product ion (*m*/*z*)	Orifice voltage (V)	Ring voltage (V)	Collision energy (eV)	Retention time (min)
Betamethasone (Be) [378-44-9]	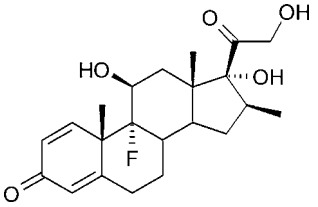	393.0	373.1	41	240	13	6.3
Budesonide (Bu) [51333-22-3]	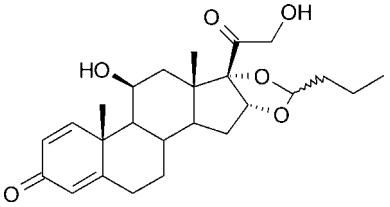	431.0	413.3	6	140	15	11.0
Hydrocortisone (Hy) [50-23-7]	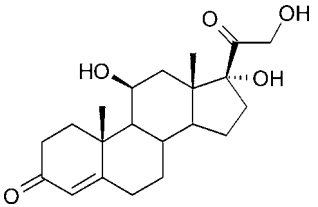	362.9	327.2	31	200	29	3.8
Cortisone (C) [53-06-5]	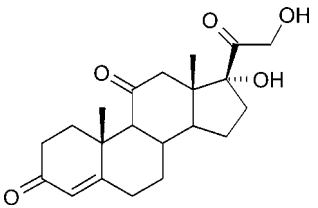	361.0	163.1	26	160	31	4.1
Dexamethasone (D) [50-02-2]	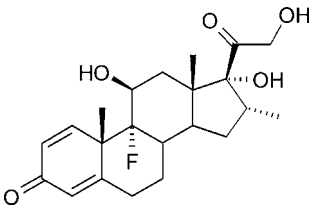	393.0	373.1	41	240	13	6.5

Flunisolide (Fs) [3385-03-3]	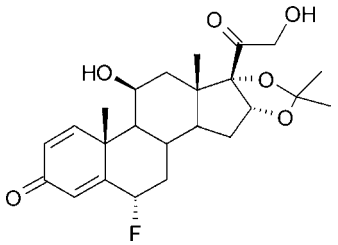	435.0	321.1	6	150	19	7.9
Fluocinolone acetonide (Fc) [67-73-2]	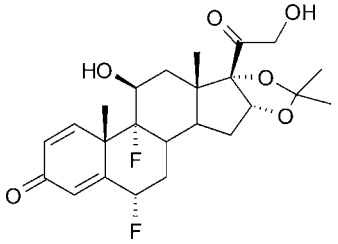	453.1	413.2	11	160	17	8.7
Prednisolone (Pl) [50-24-8]	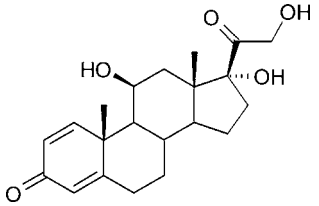	360.9	343.1	11	140	15	3.6
Prednisone (P) [50-03-2]	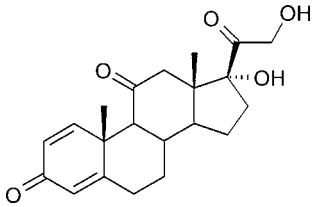	358.9	313.0	21	180	17	3.8
Triamcinolone (T) [124-94-7]	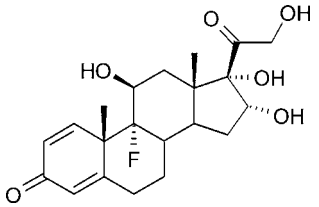	391.2	375.0	46	270	15	2.4
Triamcinolone acetonide (TA) [76-25-5]	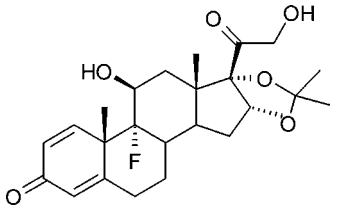	435.0	415.1	6	150	15	7.6

Table 2
Structures and mass spectrometric parameters used for the analysis of β-blockers

Molecule [CAS]	Structure	$[M+H]^+$ (*m/z*)	Product ion (*m/z*)	Orifice voltage (V)	Ring voltage (V)	Collision energy (eV)	Retention time (min)
Acebutolol (Ac) [37517-30-9]	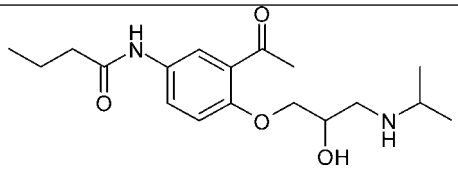	337.0	116.2	21	150	29	7.9
Alprenolol (Al) [13655-52-2]	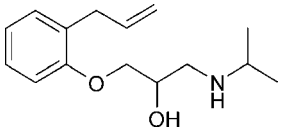	249.9	116.2	16	140	23	9.2
Atenolol (At) [29122-68-7]	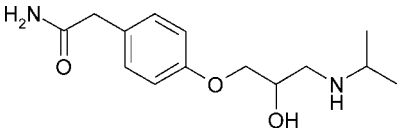	267.0	145.1	21	150	33	3.8
Bisoprolol (Bi) [66722-44-9]	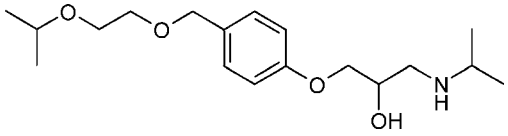	326.1	116.2	21	140	25	8.7
Metoprolol (M) [51384-51-1]	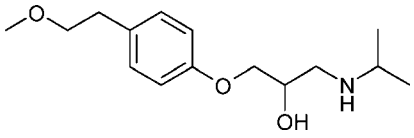	268.0	116.3	21	150	23	8.1
Nadolol (N) [42200-33-9]	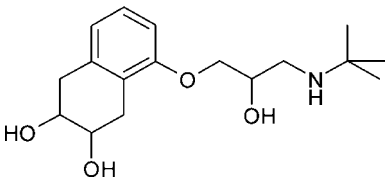	310.1	254.1	21	140	23	6.6
Pindolol (Pi) [13523-86-9]	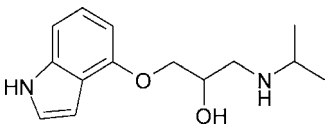	248.9	116.2	16	130	23	7.5
Propranolol (Pr) [525-66-6]	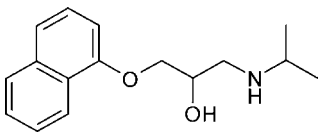	259.9	116.3	16	140	23	9.1
Sotalol (S) [3930-20-9]	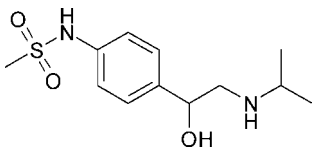	272.9	255.1	6	120	17	3.9
Timolol (Ti) [26-839-75-8]	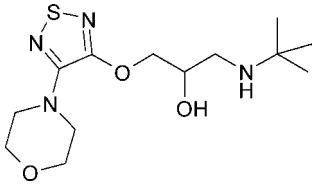	317.0	261.1	16	140	23	7.8

Both eluates were evaporated to dryness in a Speed Vac from Savant (Ramsey, Minnesota, USA). The dry residues were dissolved in 400 μL of a mixture AcN/water (25:75, v/v). An aliquot of 100 μL was then injected in the LC/MS/MS device.

2.4. Liquid chromatography–tandem mass spectrometry

The HPLC device consisted of Agilent 1100 series pump and autosampler (Massy, France). As corticosteroids and β-blockers possess very different physicochemical properties (regarding their hydrophobicity or chemical functions), they could not be analysed on a same chromatographic column. β-Blockers were chromatographied on a 5 μm Hibar Purospher Star column (250 mm × 4.6 mm I.D.) from Merck (Lyon, France), operating at 1 mL min^{-1}. A gradient elution was performed using two solvents: A1 was formate buffer (10 mM ammonium formate acidified to pH 3.8 with FOA) and solvent B was AcN (Table 3a). Corticosteroids were chromatographied on a 3.5 μm C_{18} X-Bridge column (150 mm × 2.1 mm I.D.) from Waters, operating at 0.3 mL min^{-1}. A gradient elution was performed using two solvents: A2 was ultra-pure water and solvent B was AcN (Table 3b). Both chromatographic separations were performed at room temperature.

The HPLC device was coupled to a Sciex API 300 triple quadrupole mass spectrometer from MDS Sciex (Toronto, Canada) equipped with a TurboIonspray Source (TIS) operating in positive ion mode. Instrument control, data analysis and processing were performed using the associated Analyst 1.4.1 software. The mass spectrometer was initially calibrated using polypropylene glycol as standard (Applied Biosystems, Foster city, USA), setting the resolution, as peak width at half height, in the range 0.7 ± 0.1 amu.

The nebulizer (zero air) and the curtain gas flow (nitrogen) were set at 10 arbitrary units. The TIS source was operating at 400 °C for corticosteroids and at 500 °C for β-blockers, with the auxiliary gas flow (zero air) set at 8 L min^{-1}. The TIS voltage was set at 5000 V. As both peak width and number of MRM transitions differed in these two analytical methods, dwell times were determined in order to define chromatographic peaks with about 20 points. Then, the dwell time was 100 and 50 ms for corticosteroids and β-blockers, respectively. Other mass spectrometric parameters are summarised in Table 1 for corticosteroids and Table 2 for β-blockers. These parameters were optimised using the autotune feature of the Analyst 1.4.1 software, by infusing each molecule separately. Product ions used for monitoring were selected based on their significance in the MS/MS spectra. For this study only one MRM (Multiple Reaction Monitoring) transition was used although a second transition is generally required to confirm the presence of an analyte by using the ratio MRM1/MRM2. As the mass spectrometer used in this study did not permit to work with large number of MRM transitions, it was not possible to analyse a large number of compounds with two MRM transitions. So we decided to use only one transition. During method development we noticed that when a peak was observed on STP sample extracts, at the required retention time, with the first MRM transition, the presence of the analyte was always confirmed by the second MRM transition. This methodology was considered as acceptable for method development. However, consecutive routine analysis will require an organisation of MRM transitions by retention time windows, in order to increase the number of followed MRM transitions up to two transitions per analyte, as lauded by the European directive 96/23/EC.

3. Results and discussion

3.1. Liquid chromatography–tandem mass spectrometry analysis

Tandem mass spectrometry is the best detection tool for environmental analysis because of its high sensitivity and selectivity, especially in the MRM mode. Moreover, operating the mass spectrometer in the MRM mode allows a shorter chromatography race since a perfect separation of all the compounds is not required using this acquisition mode. Nevertheless, some important aspects have to be considered in multiresidue method development and in some cases, chromatographic separation may be still required: (1) compounds measured at the same MRM transition (e.g. betamethasone and dexamethasone corticosteroids which are diastereroisomers and have the same precursor/product ion transition); (2) compounds which produce similar (overlapping) product ions upon fragmentation; (3) compounds that are measured using the same product ion but with different precursor ions, in order to avoid the risk of a cross talk phenomenon, which is the case of most β-blockers with a *m/z* 116 product ion (acebutolol, alprenolol, bisoprolol, metoprolol, pindolol and propranolol) and some corticosteroids (prednisolone/cortisone and budesonide/fluocinolone

Table 3
HPLC solvent gradient for the separation of (a) β-blockers and (b) corticosteroids

(a)				(b)			
Total time (min)	Flow rate (mL min^{-1})	%A1[a]	%B[b]	Total time (min)	Flow rate (mL min^{-1})	%A2[c]	%B[b]
0	1	85	15	0	0.3	70	30
2	1	85	15	6	0.3	60	40
5	1	55	45	9	0.3	0	100
10	1	55	45	20	0.3	0	100

[a] A1 = formate buffer.
[b] B = can.
[c] A2 = ultra-pure water.

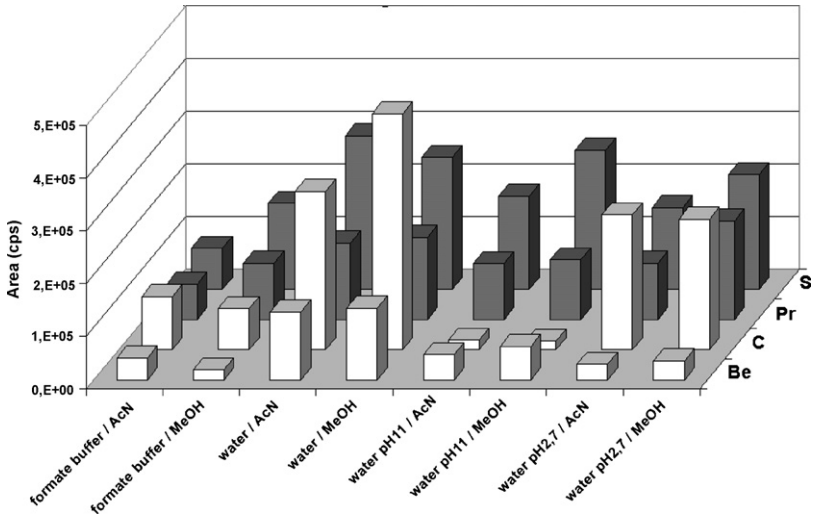

Fig. 1. Mass spectrometric responses of 2 representatives corticosteroids: betamethasone (Be) and cortisone (C), and 2 representatives β-blockers: propranolol (Pr) and sotalol (S).

acetonide have a similar product ion at *m/z* 343 and 413, respectively).

The couples of molecules quoted above have to reach the mass spectrometer separately, and to be previously separated by chromatography.

Thus, it is important to develop a chromatographic separation capable of separating these critical pairs. Although an enrichment factor of 1000 can be expected from the sample preparation, each parameter susceptible to lower the quantification limits is important to consider, such as mobile phase composition. Then, it is also interesting to improve the mass spectrometric sensitivity by using chromatographic mobile phases able to increase the analyte ionization in the mass spectrometer ion source. Indeed, the organic solvent or the added salts are susceptible to interfere with the ionization process in the source of the mass spectrometer and affect the analytical method sensitivity. So the quantification limits were lowered by studying the influence of the mobile phase composition on the analytes mass spectrometric response and it is possible to detect environmental concentration in the ng L^{-1} range, as it was reported in literature [5–28,30–33].

Chromatographic mobile phases were then chosen in order to facilitate the analyte ionization in the source of the mass spectrometer. Each compound was analysed in Flow Injection Analysis mode (FIA) by testing different combinations of hydro-organics mixtures. MeOH and AcN were tested with different aqueous phases: ultra-pure water, acidified water with 0.1% of FOA, formate buffer (10 mM ammonium formate acidified with FOA to pH 3.8) and basified water (ammonia solution addition up to pH 11). The analyte responses of 4 representative compounds of both families are presented in Fig. 1. (2 corticosteroids: betamethasone and cortisone, in white; and 2 β-blockers: propranolol and sotalol, in grey.)

For corticosteroids the best responses were observed with mixtures of unmodified water with MeOH or unmodified water with AcN. Therefore, the chromatographic gradient separation was performed with water/AcN mixtures (Table 3b). The resulting chromatogram is shown in Fig. 2. The critical analyte couples were separated within less than 12 min, excepted betamethasone and dexamethasone. Indeed it was not possible to achieve a satisfactory resolution for these two compounds since their chemical structures are very narrow (diastereoisomers), which results in similar interactions with the chromatographic stationary phase. These molecules will subsequently be quantified together. The chromatography of budesonide resulted in two chromatographic peaks, due to the presence of two epimers.

In the case of β-blockers, the use of MeOH as organic solvent gave better responses. However, this solvent did not fit with chromatographic separation criteria. Indeed, MeOH generated important peak tailing whatever the chromatographic column tested. Thus, AcN should be used as organic constituent. Although unmodified water gave the best results, it has not been chosen because of the risk of poor robustness of the chromatographic separation. Finally, the best compromise between a good chromatographic separation and a satisfactory analyte response was to use a mixture of formate buffer and AcN or acidified water (0.1% FOA) and AcN. A formate buffer/AcN gradient (Table 3a) was selected. This mobile phase composition allowed a satisfactory separation in less than 10 min as shown in Fig. 3.

3.2. Solid phase extraction

Solid phase extraction efficiency (purification and enrichment factor) is linked to a large number of parameters such as flow rates, composition, and elution solvent volumes used in each step of the procedure. Studying each parameter separately results in a high number of experiments, which should be time consuming. Therefore, evaluating simultaneously the influence of several parameters is interesting for method development and optimisation. Here is the advantage of chemometrics, which allow the evaluation of several parameters by a restricted number of experiments. This approach first requires a small knowledge about the retention of target molecules on the SPE support. This information can be obtained from a preliminary study.

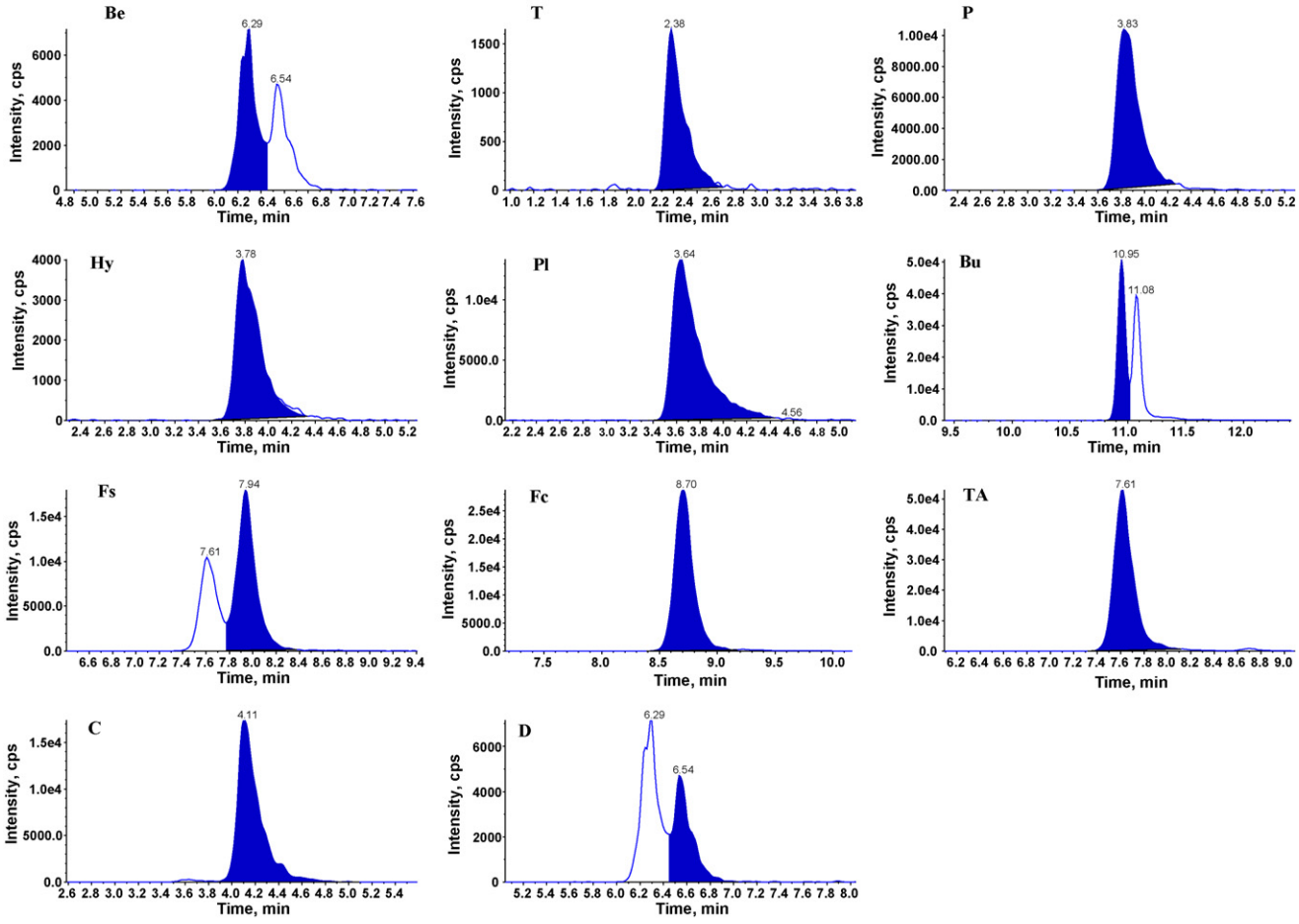

Fig. 2. LC/MS/MS chromatogram of a 5 ng injected corticosteroids solution (see abbreviations in Table 1).

Corticosteroids are non-polar molecules whereas β-blockers are basic molecules with pK_as around 9. According to these properties, in order to have a single sample preparation, a polymeric mixed-mode cation exchange reverse phase sorbent was selected: Oasis MCX. Indeed, with apolar interactions MCX sorbent is able to retain apolar molecules (such as corticosteroids) and with ionic interactions they can retain cations (such as β-blockers when protonated).

The evolution of the extraction yield of target analyte with the composition of the eluant mixture was evaluated. The volume of elution solvent used was fixed to 1 mL. In acidified MeOH/water mixtures, corticosteroids extraction yield varied with the polarity of the molecules. It has been concluded that (1) the composition of the eluant mixture should be less than 20% MeOH in order to rinse the cartridge without eluting triamcinolone, the less retained corticosteroid and (2) the percentage of MeOH used to elute corticosteroids has to be higher than 60% in order to have a satisfactory elution of budesonide, the most retained corticosteroid. Moreover, no elution of β-blockers was observed in acidified mixtures. These results were interesting as it allowed a second wash of the cartridge with 100% of acidified MeOH. Indeed, acidic pH condition maintains these molecules under their acidic structures, thus, they keep fixed on ion exchange sites, whereas in basic media, β-blockers become neutral and are only subjected to apolar interactions. To remove all β-blockers from the cartridge, 95% of basified MeOH was necessary as pindolol was not eluted with lower MeOH percentages.

These preliminary experiments showed that corticosteroids and β-blockers could be extracted from environmental samples with a unique solid phase procedure. Indeed, from the same sample loading on the cartridge, corticosteroids fraction is firstly purified then eluted. And secondly, β-blockers fraction was washed then eluted on this same cartridge.

Previous results can be strongly improved. Indeed, it does not take care of important parameters such as the influence of the volume loaded into the cartridge, nor evaluate the purification efficiency, which could be evaluated by measuring matrix effect. An improvement of the method on environmental samples was then required.

To improve the SPE protocol, all the experiments were performed on Pierre Benite STP influents in order to cover the worst scenario since untreated STP waters are expected to be the dirtiest matrix found in the environment and consequently the most problematic.

The nine following parameters were firstly studied: the flow rate used to percolate the sample on the cartridge, the sample vol-

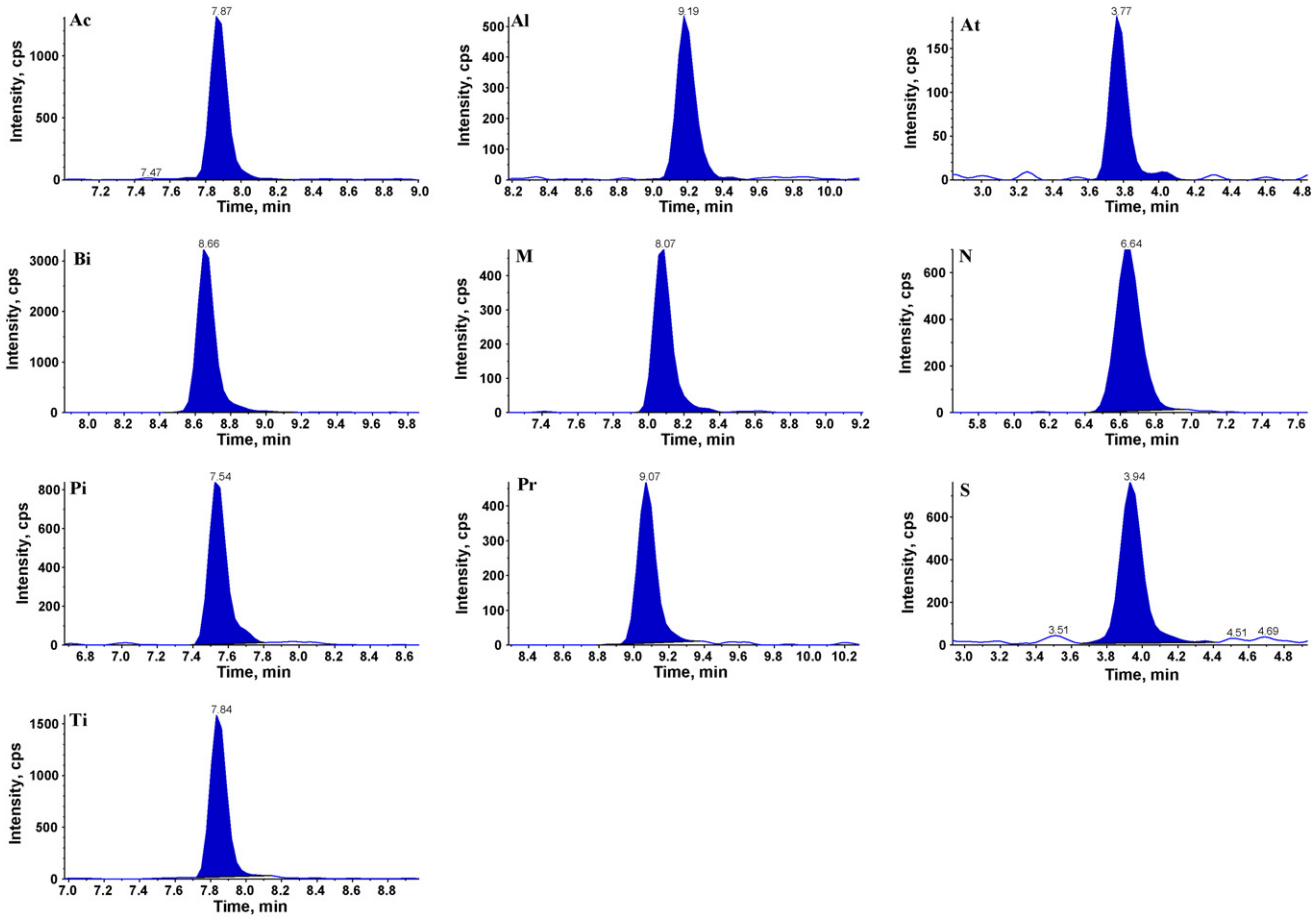

Fig. 3. LC/MS/MS chromatogram of a 100 pg β-blocker solution (see abbreviations in Table 2).

ume loaded, the eluant volume and methanol percentage for the corticosteroids wash step, the eluant volume and methanol percentage for the corticosteroids elution step, the acidified MeOH volume used to wash the β-blockers fraction, the eluant volume used to eluate β-blockers and its percentage of ammonia. This study, which would not be detailed in this paper, allowed to fix 5 critical parameters. The flow rate for loading (from 5 to 15 mL min^{-1}) did not influence neither the retention of target analytes nor interferences and was then fixed to 15 mL min^{-1} in order to shorter the sample preparation time. The sample volume percolated was studied from 100 to 1000 mL and did not affect the extraction yield of target molecules. It was then fixed to 400 mL (leading to a 400 μL extract) in order to perform until 4 chromatographic injections per sample. The increase of the volume percolated to clean up the β-blockers fraction (1–5 mL) did not increase the purification, and subsequently it was maintained to 1 mL of MeOH acidified with 0.1% FOA. This wash permits to eluate the remaining apolar interferents from the cartridge, allowing to achieve a high purification status for β-blockers extracts. The best extraction yields for β-blockers were obtained by eluting with 1.5 mL MeOH/ammonia solution 28% (95:5, v/v), when 0.5–1.5 mL of MeOH/ammonia solutions (98:2–95:5, v/v) were tested. These conditions gave satisfactory purifications.

The 4 remaining parameters were studied more precisely, thanks to a screening design (as shown in Table 4). The eluant volume for the corticosteroids wash step (called X_1) varied between 0.5 mL (level −1) and 1.5 mL (level +1); its composition (called X_2) was 10% MeOH (level −1) or 15% MeOH (level +1). The eluant mixture volume used to elute corticosteroids (called X_3) varied between 0.5 mL (level −1) and 1.5 mL (level +1); its composition (called X_4) was 65% MeOH (level −1) or 70% MeOH (level +1).

Table 4
2^2 factorial design of the experiment

Exp.	Step			
	1st wash		1st elution	
	V (mL)	%MeOH	V (mL)	%MeOH
1	0.5	10	0.5	65
2	1.5	10	1.5	65
3	0.5	15	1.5	65
4	1.5	15	0.5	65
5	0.5	10	1.5	70
6	1.5	10	0.5	70
7	0.5	15	0.5	70
8	1.5	15	1.5	70

Table 5
Corticosteroids extraction yields measured for the design of experiments (%)

Exp.	Pl	T	Fc	Be-D	C	P	Hy	Bu	Fs	TA
1	6	5	5	3	13	7	8	2	8	6
2	82	70	70	66	84	74	82	38	52	59
3	16	13	8	15	23	16	19	10	10	14
4	1	1	1	1	7	1	1	6	3	4
5	79	75	91	81	79	86	92	129	81	92
6	74	69	86	73	84	77	73	52	90	90
7	7	5	12	6	10	6	8	18	7	5
8	61	44	72	75	65	61	104	19	48	57

For each analyte 2 responses were considered. Firstly the extraction yield was calculated following equation:

$$\text{Yield}\,(\%) = \frac{\text{Area}_A}{\text{Area}_B} \times 100 \quad (1)$$

where Area_A is the analyte chromatographic area measured when a spiked matrix was extracted and Area_B is the analyte chromatographic area measured when an unspiked matrix was extracted then its eluate was spiked.

Secondly, the matrix effect was measured following equation:

$$\text{Matrix effect}\,(\%) = \left(\frac{\text{Area}_B}{\text{Area}_C} - 1\right) \times 100 \quad (2)$$

where Area_C represents the analyte chromatographic area in pure solvents.

Certainly the presence of matrix components in the extract, when compared to standard solution in pure solvent, can cause many errors, which can lead to inaccurate results. These matrix components can promote either ion suppression or improvement of the analyte ionization in the electrospray interface [34], and should be removed whenever possible.

The extraction yield was headlined and matrix effect was secondarily considered. The extraction yields obtained for each run of experimental design are shown in Table 5. Part of the experiments has been duplicated. The experiments were reproducible, except those which gave very poor extraction yields (under 5%) but this cannot misshape the interpretation. In Fig. 4, the effects of the screening model (yield $= b_1X_1 + b_2X_2 + b_3X_3 + b_4X_4$) are presented. The higher the absolute value of the effect (b_1, b_2, b_3, b_4), the higher the influence of the corresponding parameter on the response. As showed in Fig. 4, each tested parameter has a strong influence on the extraction yield, since the output effects values are meaningful. The signal of the measured response (− or +) is directly linked with the sign (− or +) of the experimental design parameter tested. b_1, b_3 and b_4 are positive for most analyte, thus the levels "+1" of the parameters X_1, X_3 and X_4 increase the response. b_2 is negative, thus the parameter X_2 should be fixed to the level "−1" in order to increase the response. In other words, washing with 1.5 mL ($X_1 = +1$) with an acidified 10% MeOH mixture ($X_2 = -1$) and eluting with 1.5 mL ($X_3 = +1$) of an acidified 70% MeOH mixture ($X_4 = +1$) resulted in increased extraction yields.

In order to decrease the eluant mixture volume, a final improvement was performed by using the optimisation module of Modde v.7 software (from Umetrics, Umeä, Sweden). This study shows that it is possible to obtain a satisfactory elution of all corticosteroids with "$X_3 = 0$", i.e. by eluting with only 1 mL of MeOH/water/FOA (70:30:0.1, v/v/v).

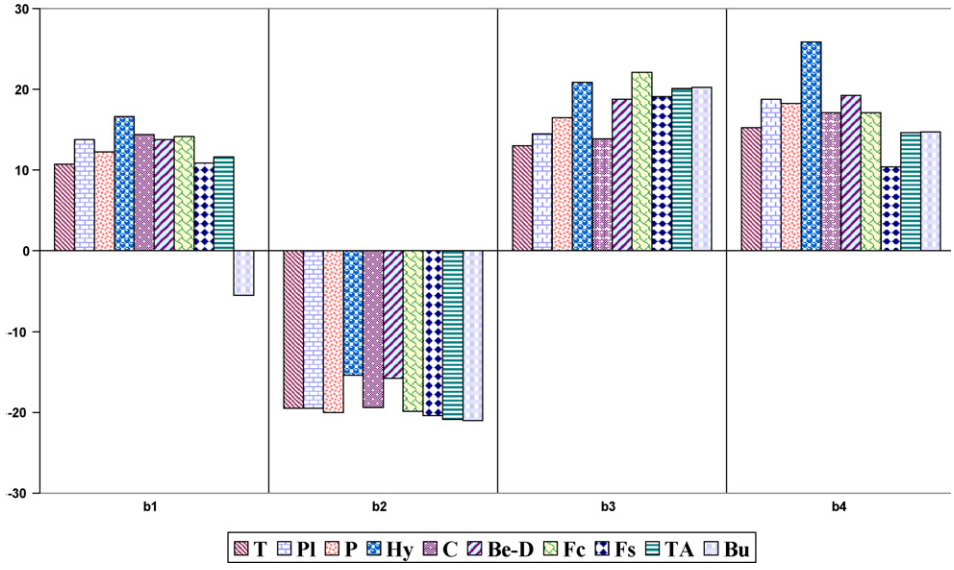

Fig. 4. Influence of the tested parameter on the extraction yield. b_1: volume used for the first wash; b_2: % MeOH used for the first wash; b_3: volume used for the first elution; b_4: % MeOH used for the first elution.

Table 6
Linearity range and IDL for the LC/MS/MS analysis

Molecule	Linearity range ($\mu g\,L^{-1}$)	Correlation coefficient	IDL (pg)
Corticosteroids			
Betamethasone + dexamethasone	1–400	0.999	32.0
Budesonide	1–100	0.999	0.7
Cortisol	4–400	0.993	7.7
Cortisone	1–400	0.998	1.3
Flunisolide	1–100	0.999	2.5
Fluocinolone acetonide	1–100	0.999	0.6
Prednisolone	1–400	0.992	9.1
Prednisone	1–400	1.000	6.7
Triamcinolone	1–100	0.996	77.3
Triamcinolone acetonide	1–100	0.998	0.5
β-Blockers			
Acebutolol	0.1–400	0.992	0.3
Alprenolol	0.1–100	0.995	1.0
Atenolol	0.1–400	0.993	0.4
Bisoprolol	0.1–100	0.985	0.1
Metoprolol	0.1–400	0.990	0.5
Nadolol	0.1–400	0.991	0.3
Pindolol	0.1–400	0.992	0.3
Propranolol	0.1–100	0.990	0.2
Sotalol	0.1–400	0.991	2.0
Timolol	0.1–400	0.989	0.9

The final protocol was described in detail in Section 2.

Moreover, we noticed that each experiment resulted in important matrix effects, except those that gave extraction yields under 10%. To avoid matrix effect higher purification would have to be reached; unfortunately we have shown that it could not be done without strongly decreasing the extraction yield. Another method consists in compensate matrix effect by working with deuterated compounds for each analyte. In this case the isotopic molecule undergoes the same matrix effect than the natural compounds, thus the chromatographic area ratio analyte/deuterated compound results unchanged and is independent of matrix effect. However, this method is very expensive, and moreover most studied deuterated molecules are not commercially available. As matrix effect could not be completely eliminated, it was necessary to quantify unknown samples by the standard addition method.

3.3. Method performance evaluation

Calibration plots were obtained by standard solution analysis at eight concentrations for each analyte. The linearity of the method was evaluated between 1 and 400 $\mu g\,L^{-1}$. To determine the best weighting factor, concentrations were back-calculated and the residual plot examined. The model with the lowest bias and the most constant variance across the concentration range was considered the best suited. A linear regression ($1/x^2$ weighted for β-blockers and $1/x$ for corticosteroids) gave the best fit for the concentration/detector response with R^2 values above 0.99 and residues less than 15% for each analyte in the concentration range tested (Table 6). As no blank matrix was found out within the tested samples, it was not possible to evaluate the method sensibility on environmental samples. Instrumental detection limits (IDL) were thus calculated as the minimum injected mass giving a signal to noise ratio 3. The IDLs ranged 0.1 and 77.3 pg analyte injected, as shown in Table 6.

Instrumental precision was assessed by replicate injection ($n=5$) of the calibration solution in the same day. The intra-day variance, expressed as relative standard deviation (R.S.D.%) for each analyte peak area was usually below 15%. The accuracy of the method was determined by recovery studies conducted on spiked environmental samples (STP influents) at 500 $ng\,L^{-1}$. Extraction yields and their R.S.D. are presented in Table 7.

The analytical protocol was not fully validated since the aim of this work was to develop an extraction procedure and test it on environmental samples, in order to investigate if target molecules were found in the environment.

3.4. Environmental analysis

Influent samples from Pierre Benite STP have been extracted and analysed as described above, by the standard addition method. With this protocol, the environmental sample is divided in 4 aliquots of 400 mL. Each aliquot was spiked with a relevant quantity of standard (up to twice the suspected environmental concentration). The linearity of standard addition was verified and allowed a reliable environmental quantitation. The quantities measured are reported in Table 8. The studied β-blockers have been detected with concentrations up to 318 $ng\,L^{-1}$ for

Table 7
Extraction yields and relative standard deviation in this study, on STP influents ($n=5$)

Corticosteroid	Yield (%)	R.S.D. (%)	β-Blocker	Yield (%)	R.S.D. (%)
Betamethasone	67	10	Acebutolol	68	4
Budesonide	86	12	Alprenolol	61	6
Cortisone	71	10	Atenolol	68	24
Cortisol	70	22	Bisoprolol	60	7
Dexamethasone	75	11	Metoprolol	62	7
Flunisolide	54	19	Nadolol	60	9
Fluocinolone acetonide	84	24	Pindolol	10	24
Prednisolone	62	16	Propranolol	66	7
Prednisone	55	13	Sotalol	68	9
Triamcinolone	63	11	Timolol	62	9
Triamcinolone acetonide	70	10			

Table 8
Measured concentration in Pierre Benite influents/effluents STP

Compound	Influents (ng L^{-1})	Effluents (ng L^{-1})
Corticosteroids		
Betamethasone + dexamethasone	15	7
Budesonide	n.d.	3
Cortisone	174	229
Cortisol	53	63
Flunisolide	7	5
Fluocinolone acetonide	0.3	11
Triamcinolone	31	30
Triamcinolone acetonide	40	3
β-Blockers		
Acebutolol	66	0.4
Atenolol	170	1.8
Bisoprolol	73	1
Metoprolol	111	1
Nadolol	10	0.1
Pindolol	2	0.4
Propranolol	92	2
Sotalol	318	65
Timolol	32	58

sotalol. The measured β-blockers concentrations are in accordance with the amounts reported in literature [13,21–25]. All the studied corticosteroids were detected, excepted budesonide. Concentrations reach 174 ng L^{-1} for cortisone. Cortisone and cortisol which are not only prescription drugs but also endogenous steroids are continuously discharged in sewages. So it is not surprising these 2 compounds were present to higher concentrations than other corticosteroids.

Then, the developed protocol was applied, to Pierre Benite STP effluent samples (results shown in Table 8). Our aim was to have a first estimation on the quantities discharged by STP effluents in environmental waters, i.e. to know if the treatment was able to totally remove corticosteroids from water. All the target compounds have been detected, including budesonide which had not been detected in influent samples. This can be due to the hydrolysis of budesonide conjugates during the STP treatment. This study demonstrates that corticosteroids reach STPs and are continuously discharged by them in environmental waters.

To our knowledge, this is the first study that demonstrates contamination of environmental waters by corticosteroids.

4. Conclusions

A quantitative analytical procedure has been developed to study 11 corticosteroids and 10 β-blockers in environmental waters. The use of mixed-mode MCX cartridges allows a single and specific sample preparation. As far as we know, this is the first procedure proposed for the environmental quantification of corticosteroids. Furthermore, it gives a high purification of β-blockers, compared to existing methods. Indeed a 100% MeOH wash is allowed for these compounds with no loss of analytes.

This method was applied on environmental samples and the β-blockers concentrations were in accordance with reported concentrations in Europe or America [5–28]. It also permitted the detection of corticosteroids in STP influents and effluents. This demonstrates that these molecules are a matter of concern in an environmental context and should be part of monitoring studies.

As both corticosteroids and β-blockers were detected on tested environmental samples, further work will include a full procedure validation and its application on a large number of samples.

Acknowledgements

The authors acknowledge the Region Rhône-Alpes for its financial support and Grand Lyon for assistance on sampling. The authors thank also Sanofi-Aventis for its materials help.

References

[1] M. Cleuvers, Ecotoxicol. Environ. Saf. 59 (2004) 309.
[2] M. Cleuvers, Toxicol. Lett. 142 (2003) 185.
[3] M. Cleuvers, Chemosphere 59 (2005) 199.
[4] K. Fent, A.A. Weston, D. Caminada, Aquat. Toxicol. 76 (2006) 122.
[5] D. Ashton, M. Hilton, K.V. Thomas, Sci. Total Environ. 333 (2004) 167.
[6] A.C. Berlfroid, A. Van der Host, A.D. Vehtaak, A.J. Schäfer, G.B.J. Rijs, J. Wegener, W.P. Cofino, Sci. Total Environ. 225 (1999) 101.
[7] J.D. Cahill, E.T. Furlong, M.R. Burkhardt, D. Kolpin, L.G. Anderson, J. Chromatogr. A 1041 (2004) 171.
[8] J.G.M. Derksen, G.B.J. Rijs, R.H. Jongbloed, Water Sci. Technol. 49 (2004) 213.
[9] T. Heberer, J. Hydrol. 166 (2002) 175.
[10] T. Heberer, Toxicol. Lett. 131 (2002) 5.
[11] K.V. Thomas, M.J. Hilton, Mar. Pollut. Bull. 49 (2004) 213.
[12] E. Zuccato, S. Castiglioni, R. Fanelli, J. Hazard. Mater. 122 (2005) 205.
[13] M.J. Hilton, K.V. Thomas, J. Chromatogr. A 1015 (2003) 129.
[14] O.A.H. Jones, N. Voulvoulis, J.N. Lester, Water Res. 36 (2002) 5013.
[15] S. Castiglioni, R. Bagnati, D. Calamari, R. Fanelli, E. Zuccato, J. Chromatogr. A 1092 (2005) 206.
[16] D. Bendz, N.A. Paxeus, T.R. Ginn, F.J. Loge, J. Hazard. Mater. 122 (2005) 195.
[17] P.E. Stackelberg, E.T. Furlong, M.T. Meyer, S.D. Zaugg, A.K. Hendersen, D.B. Reissmen, Sci. Total Environ. 329 (2004) 99.
[18] D.W. Kolpin, E.T. Furlong, M.T. Meyer, S.D. Zaugg, L.B. Barber, H.T. Buxton, Environ. Sci. Technol. 36 (2002) 1202.
[19] M.J. López de Alda, D. Barceló, J. Chromatogr. A 892 (2000) 391.
[20] A. Salvador, C. Moretton, A. Piram, R. Faure, J. Chromatogr. A 1145 (2007) 102–109.
[21] D.B. Huggett, I.A. Khan, C.M. Foran, D. Schlenk, Environ. Pollut. 121 (2003) 199.
[22] R. Andreozzi, M. Raffaele, P. Nicklas, Chemosphere 50 (2003) 1319.
[23] T.A. Ternes, Water Res. 32 (1998) 3245.
[24] D. Calamari, E. Zuccato, S. Castiglioni, R. Bagnati, R. Fanelli, Environ. Sci. Technol. 37 (2003) 1241.
[25] C. Miège, M. Favier, C. Brosse, J.P. Canler, M. Coquery, Talanta 70 (2006) 739.
[26] M. Petrovic, E. Eljarrat, M.J. López de Alda, D. Barceló, J. Chromatogr. A 974 (2002) 23.
[27] E.P. Kolodziej, T. Hareter, D.L. Sedlak, Environ. Sci. Technol. 38 (2004) 6377.
[28] K.V. Thomas, M.R. Hurst, P. Matthiessen, M. McHugh, A. Smith, M.J. Waldock, Environ. Toxicol. Chem. 21 (2002) 1456.

[29] H. Sanderson, D.J. Johnson, T. Reitsma, R.A. Brain, C.J. Wilson, K.R. Solomon, Regul. Toxicol. Pharmacol. 39 (2004) 158.
[30] T.A. Ternes, TrAC 20 (2001) 419.
[31] D. Bendz, N.A. Paxéus, T.R. Ginn, F.J. Loge, J. Hazard. Mater. 122 (2005) 195.
[32] H. Budzinski, A. Togola, Spectra Analyse 33 (2004) 1.
[33] L. Amendola, F. Molaioni, F. Botrè, J. Pharm. Biomed. Anal. 23 (2000) 211.
[34] W.A. Kormacher (Ed.), Using Mass Spectrometry for Drug Metabolism Studies, CRC press, Boca Raton, FL, 2005, p. 103.

Available online at www.sciencedirect.com
ScienceDirect
Talanta 74 (2008) 1539–1546
Talanta
www.elsevier.com/locate/talanta

Simultaneous stopped-flow determination of morphine and naloxone by time-resolved chemiluminescence

José A. Murillo Pulgarín *, Luisa F. García Bermejo, José M. Lemus Gallego, M. Nieves Sánchez García

Department of Analytical Chemistry and Foods Technology, University of Castilla-La Mancha, 13071 Ciudad Real, Spain

Received 27 June 2007; received in revised form 7 September 2007; accepted 28 September 2007
Available online 2 October 2007

Abstract

The first application of the flow analysis coupled with chemiluminescence detection and based on stopped-flow chemistry to the simultaneous determination of two components, using a two equation system, is described. The proposed method to determine simultaneously morphine and naloxone is based on the chemiluminescence oxidation of these compounds by their reaction with potassium permanganate in an acidic medium. The main feature of the system used is that the recording of the whole chemiluminescence intensity-versus-time profiles can be obtained, using the stopped-flow technique in a continuous-flow system. Then, the chemiluminescent signals obtained at two times of these profiles can be used to determine the concentration of both opiate narcotics. The effect of common emission enhancers on the chemiluminescence emission of these compounds in different acidic media, using the above-mentioned technique, was studied, in order to achieve the best conditions in which, the CL profiles of both compounds should be additive. The parameters selected were sulphuric acid 1.0 mol L^{-1}, permanganate 0.2 mmol L^{-1} and formaldehyde 0.8 mol L^{-1}. Taken in account the different profiles of the transient CL signal obtained with each compounds, using the selected chemical conditions, two measurement times (1.4 and 4.8 s) of these responses curves were considered with the purpose to establish a simple 2×2 matrix calculation. Using the chemiluminiscent signals obtained at these times, a linear calibration graph was obtained for each one of the compounds between 0.01 and 1.00 mg L^{-1} for morphine and 0.10–1.50 mg L^{-1} for naloxone. The present chemiluminescence procedure was applied to the determination of both compounds in mixtures and was found to be satisfactory.
© 2007 Elsevier B.V. All rights reserved.

Keywords: Time-resolved chemiluminescence; Stopped-flow; Morphine; Naloxone

1. Introduction

Opiate narcotics, typified by morphine and its derivatives, are of principal therapeutic use in the relief or abolition of pain. It is assumed that their electronic structure plays an important role in the attempt to rationalize their pharmacological activity [1]. Morphine is the most important alkaloid of opium and is extracted from Papaver somniferum. This substance is widely used for treating severe pain in cancer patients and for relieving pain following surgical procedures. However, the administration of this drug must be strictly controlled because excessive doses may have major side effects, whereas inadequate doses fail to alleviate pain. The determination of morphine is also of interest in order to confirm overdosing in addicts or doping in sporting events [2,3]. Naloxone, is a derivative of morphine and an specific opioid antagonist. In fact, this opioid antagonist reverses the action of many narcotic drugs including heroin, morphine, methadone and codeine [4].

In the bibliography, there are a great variety of papers in which, morphine and naloxone have been investigated individually by different methods, due to its high medical significance. Within these methods, the chemiluminescent behaviour of morphine has been used for its determination. In this sense, same works have been reported by capillary electrophoresis [5,6] or high-performance liquid chromatography [7,8], which used chemiluminescence (CL) detection. The coupling of flow injection with CL has made this technique more popular with wider applications. So, Abbott et al. [9] proposed a method based

* Corresponding author. Fax: +34 926 295318.
E-mail address: joseantonio.murillo@uclm.es (J.A.M. Pulgarín).

0039-9140/$ – see front matter © 2007 Elsevier B.V. All rights reserved.
doi:10.1016/j.talanta.2007.09.032

on the reaction of morphine and $KMnO_4$ in the presence of tetraphosphoric acid. Subsequently, this was modified to obtain the chemiluminescence–time profiles [10]. In addition, flow injection technique has been described for the determination of this opiate narcotic using the classical oxidation-reaction of luminol by hydrogen peroxide into a basic medium [11]. Other flow techniques such as pulsed flow chemistry analysis [12] or sequential-injection analysis [13], both coupled with CL detection, have been applied successfully. Another proposed chemiluminescent determination is based in the reaction between morphine and a novel oxidant such as Mn (IV) [14]. On the other hand, taken in account the ease with which naloxone can be oxidised, liquid chromatography with electrochemical detection is one of the most frequent choices for the determination of this opioid antagonist [15–20]. HPLC–mass spectrometry has also been applied for naloxone determination with a high sensitivity and selectivity, but it requires more expensive instruments than other techniques [21,22]. However, only a work has been described for the chemiluminescent determination of this drug [23]. In that work, a novel technique using kinetic parameters, as rate of the light-development reaction and rate of the light-decay reaction, was proposed and it was applied to the determination of naloxone in pharmaceutical preparations.

The CL phenomenon is relatively uncommon because, in most chemical reactions, excited molecules lose their excitation energy via non-radioactive pathways. Then, CL is an attractive detection method for analytical determination due their high sensitivities together with the wide linear working range that can be achieved and low cost of instrumental equipment, which is suitable to both batch and flow analytical techniques. One key aspect of CL techniques is the transient signal that results from the underlying spectroscopic, chemical and physical kinetics. This is primarily the result of the spectroscopic phenomenon (i.e., the emission of light by a molecule in an excited electronic state on return to its ground state) being intrinsically kinetic in nature. Because excited CL states are produced by a chemical reaction, chemical kinetics is also involved in the process. The way the ingredients of a CL reaction are mixed in an aqueous medium also influences the CL signal, particularly its initial portion.

In consequence, the typical profile of a CL transient signal (a plot of CL intensity versus time) is a kinetic response curve that corresponds to a first-order sequence of two consecutive steps, namely: generation of the light-emitting product by mixing of the chemical ingredients (the substrate and oxidant), and formation of the end product. The rate at which each step takes place depends on the formation and decay rate constant, which correspond to the rising and falling portion, respectively, of the transient signal. Various sample-reagent mixing modes have been used in combination with a detector to record the chemiluminescence signal, such as the continuous-addition-of-reagent technique [24], which is based on the continuous addition, at low pressure and constant rate, of one reaction ingredient (usually the reagent) over a vessel containing the analyte and the other reaction ingredients, and a stopped-flow mixing module coupled to a CL detector [25].

In the present work, time-resolved chemiluminescence is proposed as a novel analytical methodology to resolve simultaneously mixtures of two components; concretely, this is applied to the simultaneous determination of morphine and naloxone Fig. 1. The methodology used is based on the different chemiluminescent behaviours of these compounds when they react with potassium permanganate in an acidic medium. The recording of the whole chemiluminescence intensity-versus-time profiles, which were obtained using the stopped-flow technique, allows obtaining the chemiluminescence signals at two times of these profiles. Then, a 2×2 matrix calculation can be established using these measurements times. Even though, time-resolved methodology has been applied to the individual determination of different analytes [23,26–28], this working paper shows its first application to the simultaneous determination of two components in a mixture.

2. Experimental

2.1. Reagents

All solutions and chemicals were performed with analytical-reagent grade chemicals and water filtered through a Milli-Q system

A standard solution containing 50 mg L^{-1} of morphine (morphine sulphate pentahydrate, Sigma–Aldrich; St. Louis, MO, USA) and a standard solution containing 50 mg L^{-1} of naloxone (hydrochloride dihydrate, ICN Pharmaceuticals Inc.; Costa Mesa CA, USA) were prepared by dissolving both compounds in water. These stock solutions were stored protected from light and below 4 °C.

Solution of potassium permanganate (0.20 mmol L^{-1}) was prepared daily by dissolving 15.8 mg of potassium permanganate (Panreac, Barcelona, Spain) in 500 mL of water. It was protected from light.

Sulphuric acid was obtained from Panreac (Barcelona, Spain) and diluted solutions of 1.0 mol L^{-1} were prepared. Formaldehyde was obtained from Sigma–Aldrich (St. Louis, MO, USA) and diluted solutions of 0.8 mol L^{-1} were prepared by dissolving 16.23 mL of concentrated formaldehyde in 250 mL of water.

Other cofactors tested, such as acetaldehyde, glycolaldehyde and glutaraldehyde, were obtained from Sigma–Aldrich (St. Louis, MO, USA), and formic acid from Panreac (Barcelona, Spain). All cofactors were prepared at 0.25 mol L^{-1} concentration. Rhodamine 6G chlorhydrate, fluoresceine, rhodamine B and quinine were supplied by Sigma–Aldrich (St. Louis, MO, USA). These sensitizers were all prepared at 5×10^{-4} mol L^{-1} concentration.

2.2. Manifold

A simplified scheme of the continuous-flow manifold used to get the stopped-flow system is depicted in Fig. 2. The reaction reagents were pumped through the four-line manifold by a peristaltic pump (Gilson, Minipuls 3), which was controlled by a microcomputer. The flow rate of the reagents was 18 mL min^{-1} and the reagents went through poly(tetrafluoroethylene) (PTFE)

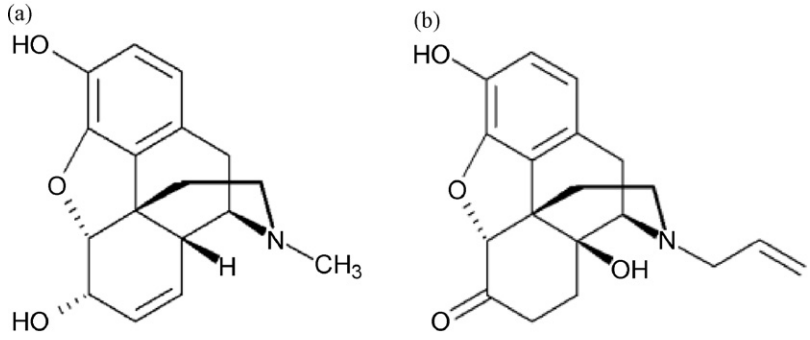

Fig. 1. Chemical structure of morphine (a) and naloxone (b).

flow tubes (Tygon, 0.8 mm i.d., resistant to acid). As can be seen in the scheme showed in Fig. 2, the potassium permanganate was carried out directly to the flow cell, located in front of the photomultiplier tube (PMT), to allow the total oxidation reaction took place in the detector cell when the flow was stopped. The chemiluminiscence–time data pairs were acquired using a Camspec chemiluminescence detector CL-2 (photosensor module Hamamatsu 45773-20; spectral response from 300 to 900 nm; spiral-type flow cell, volume 120 μL; Sawston, Cambridge). The detector was connected to a computer by a digital analogical converter; data were taken by Chromatography Station for Windows CSW32 software (Data Apex Ltd., Prague, The Czech Republic) and processed through a software developed by us [23].

2.3. General procedure for mixtures

The continuous-flow manifold used to get the stopped-flow system is outlined in Fig. 2. The first reaction components, sulphuric acid 1.0 mol L^{-1} and formaldehyde 0.8 mol L^{-1}, were transported through channels to the point where they were mixed. Then, the resultant mixed solution was added to the analyte (morphine, naloxone or a mixture) sample solution channel. The emergent solution and the potassium permanganate, 0.2 mmol L^{-1}, were then mixed in a merging point, which is a planar coiled quartz flow cell, located in front of the photomultiplier tube, in a flow-through Camspec Chemiluminescence Detector CL-2. The flow-through system was stopped for 30 s. In this way, the reaction took place in the flow cell and the detector, which was interfaced to a computer via an A/D converter, continuously monitored the CL transient signal to obtain a plot of CL intensity versus time. Finally, the pump was restarted to operate for at least 30 s before the flow was stopped again. All these measurement registers were acquired using the Chromatography Station for Windows CSW32 software and these were made in triplicate. The resulting throughput was 45 measurements/h.

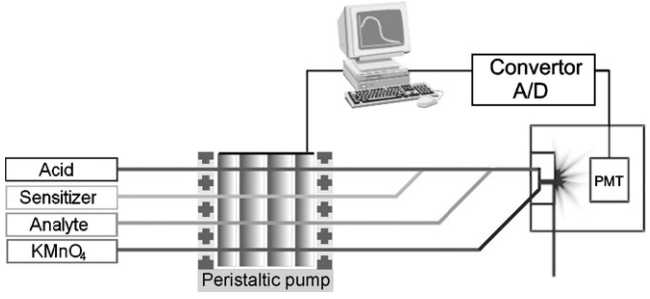

Fig. 2. Schematic diagram of the continuous-flow manifold, using $KMnO_4$–H_2SO_4 as oxidant and formaldehyde as emission enhancer; the analytes are aqueous solutions of morphine and naloxone.

In 25 mL calibrated flasks, standard solutions containing 0.01–1.00 mg L^{-1} of morphine or 0.10–1.50 mg L^{-1} of naloxone were prepared. With the optimum chemical conditions above displayed in the flow system, the whole chemiluminescence intensity-versus-time profile was recording for each one of them. Four calibration graphs, measuring the CL intensity on the profiles registered at two different times, were obtained. Concretely, two calibration graphs for morphine samples using the CL intensity measured at 1.4 s (t_1), where this compound shows maximum emission intensity, and at 4.8 s (t_2), which is the time where naloxone presents the CL maximum intensity. At the same times, chemiluminescent intensity measurements were realised for all samples of naloxone, and these were used to construct other two calibration graphs. These calibrations permitted to calculate the constants $K_{t1(\text{morphine})}$, $K_{t1(\text{naloxone})}$, $K_{t2(\text{morphine})}$ and $K_{t2(\text{naloxone})}$, which will be used to resolve simultaneously mixtures of the two narcotic compounds.

Subsequently, the chemiluminescence intensity-versus-time profile of a binary mixture of both analytes, which was treated the same as the individual compounds, was recording and CL intensity signals at the two times before mentioned, that is, 1.4 and 4.8 s, were measured. Using a simple 2 × 2 matrix calculation next showed, both analytes in the mixture could be directly determined.

$$\begin{vmatrix} K_{t1(\text{morphine})} & K_{t1(\text{naloxone})} \\ K_{t2(\text{morphine})} & K_{t2(\text{naloxone})} \end{vmatrix} \cdot \begin{vmatrix} C_{(\text{morphine})} \\ C_{(\text{naloxone})} \end{vmatrix} = \begin{vmatrix} I_{t1(\text{mixture})} \\ I_{t2(\text{mixture})} \end{vmatrix}$$

$$\begin{vmatrix} C_{(\text{morphine})} \\ C_{(\text{naloxone})} \end{vmatrix} = \begin{vmatrix} K_{t1(\text{morphine})} & K_{t1(\text{naloxone})} \\ K_{t2(\text{morphine})} & K_{t2(\text{naloxone})} \end{vmatrix}^{-1} \cdot \begin{vmatrix} I_{t1(\text{mixture})} \\ I_{t2(\text{mixture})} \end{vmatrix}$$

3. Results and discussion

Using the previously described system, the whole chemiluminescence intensity-versus-time profiles of morphine (1.00 mg L^{-1}), naloxone (3.00 mg L^{-1}) and their corresponding mixture were obtained with different chemical conditions.

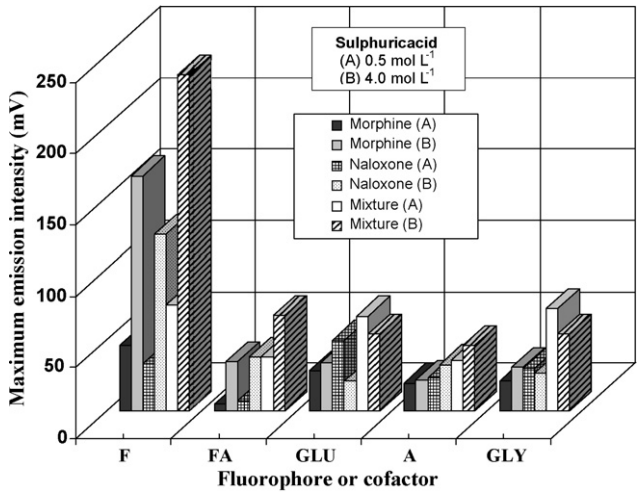

Fig. 3. Effect of emission enhancers on the maximum emission intensity in sulphuric acid at two concentrations levels: (A) 0.5 mol L^{-1} and (B) 4.0 mol L^{-1}. [Morphine] = 1.0 mg L^{-1}; [naloxone] = 3.0 mg L^{-1}; [$KMnO_4$] = 0.15 mmol L^{-1}; [glycolaldehyde, GLY] = [acetaldehyde, A] = [glutaraldehyde, GLU] = [formic acid, FA] = [formaldehyde, F] = 0.25 mol L^{-1}.

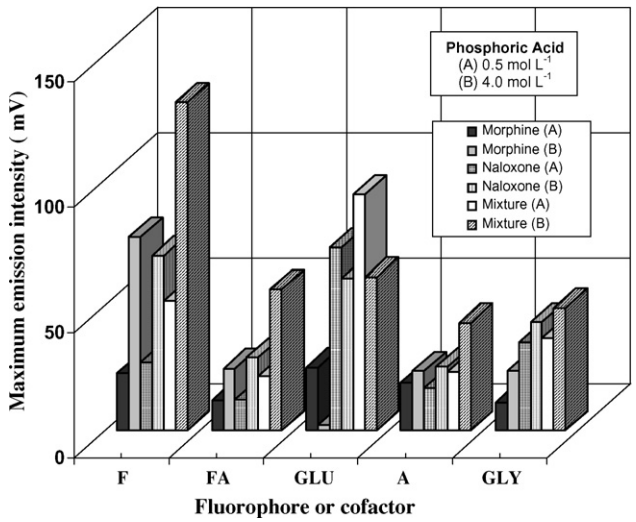

Fig. 4. Effect of emission enhancers on the maximum emission intensity in phosphoric acid at two concentrations levels: (A) 0.5 mol L^{-1} and (B) 4.0 mol L^{-1}. [Morphine] = 1.0 mg L^{-1}; [naloxone] = 3.0 mg L^{-1}; [$KMnO_4$] = 0.15 mmol L^{-1}; [glycolaldehyde, GLY] = [acetaldehyde, A] = [glutaraldehyde, GLU] = [formic acid, FA] = [formaldehyde, F] = 0.25 mol L^{-1}.

Besides, the mathematical summa of the individual CL profiles from each analyte was made and the resulting CL profile was represented (mixture theoretical profile). These four plots could provide to demonstrate if the theoretical profiles and the experimental profiles of the corresponding mixtures were similar, that is, to probe the mutual independence of the analytical signals of morphine and naloxone. Then, the chemical conditions of the chemiluminescence emission reaction of each analyte with permanganate in acidic medium were submitted to an exhaustive chemiluminescent study in order to obtain those working conditions in which there was not any interference between the narcotic drugs in study and, consequently, those conditions in which the mixture could be resolved.

3.1. Influence of emission enhancers and the acid medium

Even though morphine and naloxone, both react with acidified $KMnO_4$ eliciting light, the intensity is not enough for analytical purposes. In this aspect, the presence of sensitizers or co-factors in the CL reaction at different acid media was studied. The purpose of this investigation was double, firstly to obtain the greatest CL intensity with both compounds and next to get CL intensity-versus-time profiles for each drug the most separated as possible in the time.

In this regard, four sensitizers, rhodamine 6G, rhodamine B, quinine and fluoresceine, at concentration of 0.5 mmol L^{-1}, have been assayed. On the other hand, formic acid, glutaraldehyde, formaldehyde, glycolaldehyde and acetaldehyde, at 0.25 mol L^{-1} concentration, were selected and examined, as possible enhancers on present CL reaction. This study was approached together with the influence of two different acidic media, which were sulphuric acid and phosphoric acid both at two concentration levels, 0.5 and 4.0 mol L^{-1}. In Figs. 3 and 4 are located some results related with the CL emission intensity obtained for sulphuric acid and phosphoric acid, respectively. The highest values of maximum emission intensity were obtained using phosphoric acid, at high concentration, and rhodamine 6G as emission sensitizer. However, in order to resolve the mixture of the two drugs, we must take into account the whole CL profiles for selecting the best acid and CL emission enhancer. Some profiles obtained in this study are shown in Fig. 5. A similar situation to that showed in Fig. 5(c) using rhodamine 6G was obtained with all sensitizers in the CL reactions studied and then these were not useful in our simultaneous determination. Considering all these results, the presence of a co-factor was selected as emission enhancer; concretely, formaldehyde in a sulphuric acid medium was the optimum to resolve the mixture of morphine and naloxone. As can be seen in Fig. 5(b), the individual profiles are less overlapped, being its emission maxima more separated in the time using formaldehyde. Beside, this emission enhancer lead to typical profiles of CL transient signals, which correspond to a first-order sequence of two consecutive steps, namely: the generation of the light-emitting product by mixing of the chemical ingredients (the substrate and oxidant), and the formation of the end product [29]. So formaldehyde and sulphuric acid were selected for subsequent studies.

3.2. Influence of sulphuric acid concentration

In order to select the appropriate sulphuric acid concentration, the influence on the whole CL emission of both compounds using different acid solutions over the range 0.5–4.0 mol L^{-1} was evaluated. With reference to the emission intensity maxima, we could observed that, this increased with increasing H_2SO_4 concentration, being found the highest intensity value for a concentration of 4.0 mol L^{-1}. However, this concentra-

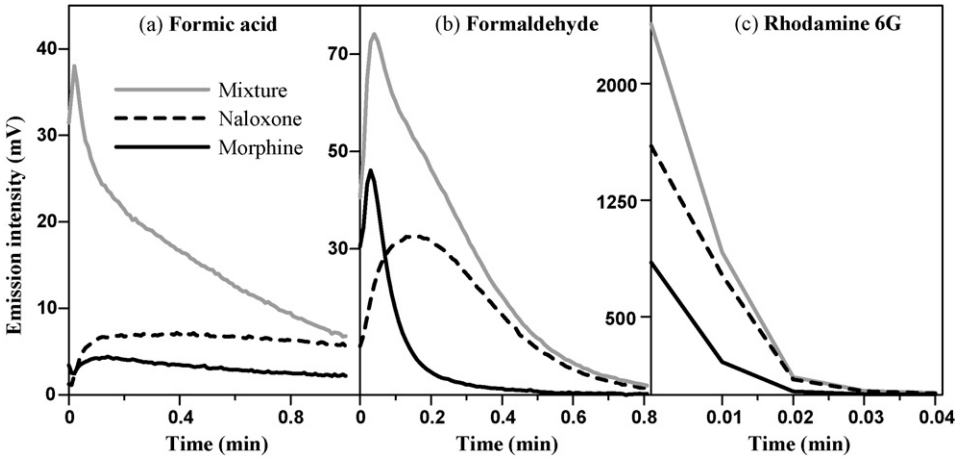

Fig. 5. Time courses of the CL reactions of morphine, naloxone and its mixture using formic acid (a), formaldehyde (b) and rhodamine 6G (c). [Morphine] = 1.0 mg L^{-1}; [naloxone] = 3.0 mg L^{-1}; [H_2SO_4] = 0.5 mol L^{-1} (a and b); [H_3PO_4] = 0.5 mol L^{-1} (c); [$KMnO_4$] = 0.15 mmol L^{-1}; [formic acid] = [formaldehyde] = 0.25 mol L^{-1}, [rhodamine 6G] = 0.5 mmol L^{-1}.

tion level was not selected since the individual profiles obtained for both drugs were highly overlapped at the time. In addition, there were more differences in the profiles resulting of the CL reaction of the experimental mixture and that one obtained from the curve corresponding to the theoretical summa of the individual CL development, which was a drawback for the simultaneous determination. A 1.0 mol L^{-1} H_2SO_4 concentration was selected for subsequent investigations, with which the best conditions to resolve the mixture were achieved, on the one hand not-overlapped individual profiles and on the other CL developments for experimental and theoretical mixtures more similar at the time.

3.3. Influence of the potassium permanganate concentration

The influence of $KMnO_4$ concentration over the range 0.03–1.0 mmol L^{-1} on the whole CL emission of both drugs was examined. The CL intensity increased sharply when the oxidant concentration was rising, up to 0.2 mmol L^{-1} and then, the intensity values were constants from this value to 1.0 mmol L^{-1}. Beside, it was noticed that the profiles obtained for both morphine and naloxone came near in the time when $KMnO_4$ concentration increased, resulting curves greatly overlapped. A concentration of 0.2 mmol L^{-1} was selected as optimum for application of the proposed method to the simultaneous chemiluminometric determination of both narcotic drugs.

3.4. Influence of the formaldehyde concentration

The variation of the chemiluminescent emission with the formaldehyde concentration in the range 0.05–1.0 mol L^{-1} was studied. The maximum emission intensity increased gently with the concentration of formaldehyde up to 0.4 mol L^{-1} and then this parameter was practically constant for values higher than that value. Taking into account the same consideration realised in the preceding studies, a concentration of 0.8 mol L^{-1} was selected as optimum.

3.5. Influence of the flow rate

The flow rate was the following experimental variable that was optimised. This parameter has a high influence upon the collection of the emitted light into the flow cell [28]. Too low or too high flow rates result in a decrease or even absence of CL in the flow cell. Taken into account the characteristics that the CL profiles of the two compounds should to be to resolve the mixture, the optimum flow rate of 18 mL min^{-1} was selected.

3.6. Influence of the temperature

Finally, the influence of the temperature on the whole CL developments of both drugs was studied. The temperature was assayed in the range between 4 and 40 °C. No important differences between the CL profiles obtained for both compounds were observed with an increase of the temperature up to 25 °C. However, when temperatures higher than 25 °C were used, a rise in intensity was resulted, but the individual CL signals were not additive, that is there were differences between the chemiluminescent profiles corresponding to experimental mixture and theoretical summa of the individual CL profiles. The room temperature, 20 °C, was selected to resolve the mixture proposed.

3.7. Calibration graphs and analytical parameters

Under the conditions selected, and using the above-described manifold, a method to determine simultaneously morphine and naloxone by direct measurements of CL transient signal, using the intensity obtained in the maximum of emission of each compound, was proposed. Fig. 6 shows the time courses of the CL reaction of morphine, naloxone and their mixture. As can be

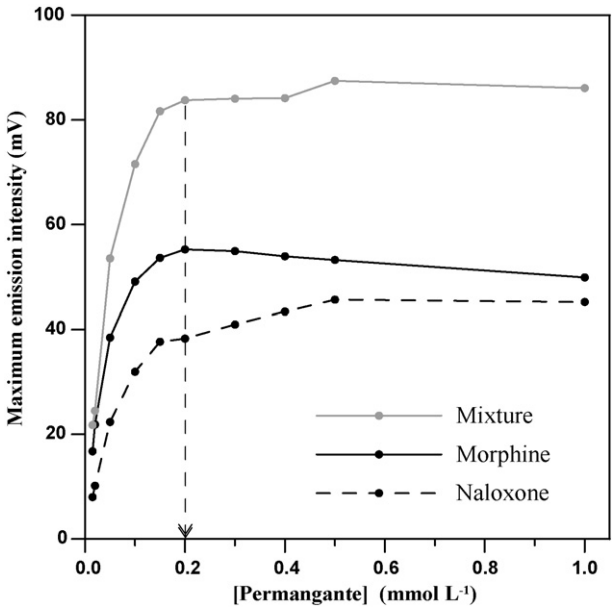

Fig. 6. Time course of the CL reaction of morphine, naloxone and their mixture. [Morphine] = 1.00 mg L^{-1}; [naloxone] = 3.00 mg L^{-1}; [H_2SO_4] = 1.0 mol L^{-1}; [$KMnO_4$] = 0.2 mmol L^{-1}; [formaldehyde] = 0.8 mol L^{-1}; flow rate 18 mL min^{-1}.

seen, the maximum emission intensity of morphine appears at 1.4 s (t_1) and this maximum emission occurs at 4.8 s (t_2) in the case of naloxone.

In order to test the mutual independence of the analytical signals of morphine and naloxone measured at 1.4 and 4.8 s, respectively, the following experiments were performed. Three calibration graphs were obtained from the CL transient signals by measuring the emission intensity at 1.4 s (t_1) for standard samples containing between 0.01 and 1.00 mg L^{-1} of morphine, in the absence of naloxone and in the presence of 0.40 and 1.00 mg L^{-1} of naloxone. Similarly, three calibration graphs were prepared from the CL transient signals by measuring at 4.8 s (t_2) for standard samples containing between 0.10 and 1.50 mg L^{-1} of naloxone, in the absence of morphine and in the presence of 0.30 and 0.80 mg L^{-1} of morphine.

Table 2
Precision of estimates and detection limits (LOD)

	Morphine	Naloxone
Relative standard error (R.S.E., %)	1.4	1.5
Relative standard deviation (R.S.D., %)	1.9	1.4
LOD (mg L^{-1}, IUPAC) [31]	0.003	0.003
LOD (mg L^{-1}, Long and Winefordner) [32]	0.004	0.029
LOD (mg L^{-1}, Clayton et al.) [33]	0.007	0.058

Each individual calibration was evaluated by statistical analysis of experimental data that were fitted to a $y = a + bx$ mathematical model using least-squares regression (LS). Table 1 shows the results of this statistical analysis. The CL signal measured at 1.4 s corresponding to a naloxone concentration of 0.40 or 1.00 mg L^{-1} was subtracted from the intensities resulting of the calibration of morphine in which that naloxone concentration was present. The same procedure was used with the calibration of naloxone containing morphine at two different concentration levels, in which the signal measured at 4.8 s corresponding to a constant morphine concentration of 0.3 or 0.80 mg L^{-1} was subtracted. The similarity among LS slopes can lead to conclude that the LS lines for individual calibrations are no different from a global LS line. The intercept on the y-axis were negligible throughout the concentration range studied and the determination coefficients were very close unity.

In order to check whether the times selected for measurements in the CL developments can be use to obtain the analytical signal for the individual analytes in a mixture of both, variance analysis was used to compare the three calibration lines for each analyte [30]. Two different F statistics were calculated. Thus, F_1 compares the total deviations from the overall linear region with respect to the deviations within each calibration in order to test the suitability of the single overall regression line. If the experimental F_1 value was less than its theoretical value, then

Table 1
Statistical analysis of calibration graphs in the determination of morphine and naloxone

Other narcotic present	Calibration graphs of morphine (t_1 = 1.4 s) (0.01–1.00 mg L^{-1})			Calibration graphs of naloxone (t_2 = 4.8 s) (0.10–1.50 mg L^{-1})		
		Naloxone			Morphine	
		0.40 (mg L^{-1})	1.00 (mg L^{-1})		0.30 (mg L^{-1})	0.80 (mg L^{-1})
Slope	77.21	74.53	75.33	23.44	22.20	23.36
Intercept	−0.17	−0.64	−1.02	−0.05	−0.18	−0.53
Determination coefficient (r^2)	0.9981	0.9983	0.9956	0.9977	0.9995	0.9985
F_1						
Experimental		1.02			2.69	
Theoretical (α = 0.05)		2.93			2.84	
F_2						
Experimental		0.99			2.26	
Theoretical (α = 0.05)		3.55			3.47	

Analysis of variance (95% level of confidence).

Table 3
Recoveries obtained in the determinations of morphine and naloxone in synthetic mixtures by the proposed CL method

Mixture sample	[Morphine]			[Naloxone]		
	Theoretical (mg L^{-1})	Found ± S.D.[a] (mg L^{-1})	Recovery (%)	Theoretical (mg L^{-1})	Found ± S.D.[a] (mg L^{-1})	Recovery (%)
1	0.05	0.04 ± 0.01	88.0	0.40	0.40 ± 0.01	100.3
2	0.20	0.19 ± 0.04	93.0	1.00	0.99 ± 0.03	99.2
3	0.30	0.30 ± 0.01	98.7	0.60	0.56 ± 0.60	93.5
4	0.30	0.28 ± 0.03	92.7	1.20	1.13 ± 0.04	94.4
5	0.80	0.81 ± 0.02	101.5	0.20	0.18 ± 0.02	89.0

[a] Mean ± S.D. for three replicates.

departure of the individual sets from the overall regression line was not significant. F_2 compares the slope of the overall regression line with respect to the slopes of the three regression lines for each analyte. If the experimental F_2 value was less than the theoretical one, then there are no significant differences between the individual slopes and the overall regression slope could be taken as representative one. In all cases, the validity of the overall regression lines was proven by the values of experimental F_1 and F_2 values (Table 1) which resulted less than the theoretical ones at 95% confidence level. In this way, the mutual independence of the CL signals of morphine and naloxone was demonstrated.

The precision of the method achieved with each analyte was assessed by preparing two series of 10 solutions, one containing 0.5 mg L^{-1} of morphine and other one 0.8 mg mL^{-1} of naloxone, and recording the time courses of the CL reaction of each analyte with 0.2 mmol L^{-1} $KMnO_4$, 1.0 mol L^{-1} H_2SO_4 and 0.8 mol L^{-1} formaldehyde on the same day, using the above-described manifold. By use of the theory of error propagation, the relative standard errors and the relative standard deviations for replicate samples were calculated. The results obtained at this study are summarized in Table 2.

The detection limits of the two analytes were calculated by applying the different definitions and the results are shown in Table 2. Detection limits were calculated in accordance with IUPAC's definition, which considers the standard deviation of the blank only [31]. If the theory of error propagation is considered, then the values of detection limits are consistent with the reliability of the blank measurements, and for the signal measurements of the standards. Table 2 shows the results obtained by calculating the detection limits according to Long and Winefordner [32] and to Clayton et al. [33] with provision for false positive and negative values.

3.8. Applications

In order to study the validity of the proposed method, and because there are no commercially available medicines containing simultaneously both of the narcotic drugs tested, the proposed method was applied to the determination of morphine and naloxone in binary synthetic mixtures. The assay was carried out as described under the general procedure for mixtures. The constants $K_{t1(\text{morphine})}$, $K_{t1(\text{naloxone})}$, $K_{t2(\text{morphine})}$ and $K_{t2(\text{naloxone})}$, which were calculated from the slopes of the calibration graphs of morphine and naloxone measuring the intensities at 1.4 s (t_1) and 4.8 s (t_2) were 75.50 and 13.93 for morphine and naloxone, respectively, at the time 1.4 s, and 20.33 and 22.57 for morphine and naloxone, respectively, at the time 4.8 s. Then, the 2×2 matrix calculation used to resolve directly a mixture of both narcotic compounds is showed.

$$\begin{vmatrix} 75.50 & 13.93 \\ 20.33 & 22.57 \end{vmatrix} \cdot \begin{vmatrix} C_{(\text{morphine})} \\ C_{(\text{naloxone})} \end{vmatrix} = \begin{vmatrix} I_{t1(\text{mixture})} \\ I_{t2(\text{mixture})} \end{vmatrix}$$

The previous matrix calculation was applied at samples prepared in the laboratory at different concentration levels of morphine and naloxone. The results are shown in Table 3. Satisfactory results were obtained for the recovery of both compounds, indicating that the method is effective for the simultaneous determination of morphine and naloxone.

To study the effect of the excipients on the whole CL signal and because there are no commercially available medicines containing simultaneously both of the narcotic drugs tested, several common excipients were added in binary synthetic mixtures of both analytes. Excipients such as lactose, saccharose, sodium chloride and methylparaben were studied. The procedure consisted of preparing different synthetic solutions with each one of these excipients in different amounts up to a concentration 40 mg L^{-1} and containing morphine and naloxone at 0.30 mg L^{-1} and 0.60 mg L^{-1}, respectively. Later, the whole CL signal of these solutions was measured, using the conditions previously established. No interferences were observed from each one of these excipients beside none alteration of the additive signal behaviour was found, obtaining recoveries values closed to 100%.

4. Conclusions

The study shown in this work proves the efficiency of time-resolved chemiluminescence for the simultaneous direct determination of compounds with very similar structures.

Experimental conditions, where the CL developments of the analytes are additive, could be achieved; only a partial separation of the chemiluminescence intensity-versus-time profiles is necessary to approach the resolution of mixtures, without any previous separation step. The CL emission intensity at two different times of these profiles will be considered with the purpose to establish a matrix calculation to determine the concentration of both compounds. The best analytical conditions of the proposed method can be obtained if the times selected coincide with

those times in which maximum emission intensity is reached with each one of the compounds.

The proposed methodology has been applied to solve mixtures of morphine and one of its very important antagonist, naloxone. Satisfactory results were obtained when the analytical signals were measured at 1.4 and 4.8 s for morphine and naloxone, respectively. Limits of detection were similar than the obtained in other methods of their individual determinations. The precision was agreed with that obtained using measurements of the flow for both analytes separated.

Acknowledgement

The authors gratefully acknowledge financial support from the "Consejería de Ciencia y Tecnología de la Junta de Comunidades de Castilla-La Mancha" (Project no. PBI-02-005)

References

[1] J. Kaufman, E. Kerman, W.S. Koski, Int. J. Quantum Chem. Quantum Biol. Symp. 1 (1974) 289.
[2] A.C. Moffat (Ed.), Clarke's Isolcliste, Reaction and Identification of Drugs, Pharmaceutical Press, London, 1986.
[3] Le Monde Cycliste, Report on the UCI Medical Commission Meeting of 28 January 1990, April 1990.
[4] S.J. Heishman, M.L. Stitzer, G.E. Bigelow, I.A. Liebson, J. Pharmacol. Exp. Ther. 248 (1989) 127.
[5] Z.L. Gong, H. Zhang, Y. Zhang, J.K. Cheng, J. Chromatogr. A 855 (1) (1999) 329.
[6] N.W. Barnett, B.J. Hindson, S.W. Lewis, Analyst 125 (1) (2000) 91.
[7] R.W. Abbott, A. Townshend, Analyst 112 (1987) 397.
[8] E. Amito, A.R.J. Andrews, J. Liq. Chromatogr. Relat. Technol. 20 (2) (1997) 311.
[9] R.W. Abbott, A. Townshend, R. Gill, Analyst 111 (6) (1986) 635.
[10] N.W. Barnett, D.G. Rolfe, T.A. Bowser, T.W. Paton, Anal. Chim. Acta 282 (3) (1993) 551.
[11] J.G. Li, J.R. Lu, Fénix-Shiyanshi 16 (3) (1997) 41.
[12] S.W. Lewis, P.S. Francis, K.F. Lim, G.E. Jenkins, X.D. Wang, Analyst 125 (10) (2000) 1869.
[13] N.W. Barnett, S.W. Lewis, D.J. Tucker, Fresenius J. Anal. Chem. 355 (5/6) (1996) 591.
[14] N.W. Barnett, B.J. Hindson, S.W. Lewis, P. Jones, P.J. Worsfold, Analyst 126 (10) (2001) 1636.
[15] T.D. Wilson, J. Chromatogr. 298 (1984) 131.
[16] H. Derendorf, A.E.A. El-Koussi, E.R. Garrett, J. Pharm. Sci. 73 (1984) 621.
[17] H. Albeck, S. Woodfield, M.J. Kreek, J. Chromatogr. Biomed. Appl. 80 (1989) 435 (2 (J. Chromatogr. 488)).
[18] E.F. O'Connor, S.W.T. Cheng, W.G. North, J. Chromatogr. Biomed. Appl. 83 (1989) 240 (1 (J. Chromatogr. 491)).
[19] H. Li, Z.H. Ge, N. Wang, Yaowu-Fenxi-Zazhy 16 (1996) 18.
[20] M. Franklin, J. Odontiadis, J. Chromatogr. B 679 (1996) 199.
[21] E. Razzazi-Fazeli, R.W. Schmid, Rapid Commun. Mass Spectrom. 12 (1998) 1859.
[22] D.E. Moody, M.H. Slawson, E.C. Strain, J.D. Laycock, A.C. Spanbauer, R.L. Foltz, Anal. Biochem. 306 (2002) 31.
[23] J.A. Murillo Pulgarín, L.F. García Bermejo, J.A. Rubio Aranda, Anal. Chim. Acta 517 (1/2) (2004) 111.
[24] M. Cobo, M. Silva, D. Pérez Bendito, Anal. Chim. Acta 356 (1997) 51.
[25] D. González Robledo, M. Silva, D. Pérez Bendito, Anal. Chim. Acta 217 (1989) 239.
[26] J.A. Murillo Pulgarín, A. Alañón Molina, G. Pérez-Olivares Nieto, Anal. Chim. Acta 518 (2004) 37.
[27] J.A. Murillo Pulgarín, L.F. García Bermejo, P. Fernández López, Anal. Chim. Acta 546 (2005) 60.
[28] J.A. Murillo Pulgarín, L.F. García Bermejo, J.A. Rubio Aranda, J. Agric. Food Chem. 53 (2005) 6609.
[29] D. Pérez-Bendito, M. Silva, in: A.M. García-Campaña, W.R.G. Baeyens (Eds.), Chemiluminescence in Analytical Chemistry, Marcel Dekker, Inc., New York, 2001 (Chapter 8).
[30] D.L. Massart, B.G.M. Vandeginste, L. Kaufman (Eds.), Chemometrics: A Textbook, first ed., Oxford University Press, Oxford, 1988.
[31] Nomenclature, symbols, units and their usage in spectrochemical analysis, Part II, Spectrochim. Acta (Part B) 33 (1978) 242.
[32] G.L. Long, J.D. Winefordner, Anal. Chem. 55 (1983) 712.
[33] C.A. Clayton, J.W. Hines, P.D. Elkins, Anal. Chem. 59 (1987) 2506.

Available online at www.sciencedirect.com
ScienceDirect
Talanta 74 (2008) 1649–1653
Talanta
www.elsevier.com/locate/talanta

Dendrimer films as matrices for electrochemical fabrication of novel gold/palladium bimetallic nanostructures

Lei Qian [a,b], Xiurong Yang [a,*]

[a] State Key Laboratory of Electroanalytical Chemistry, Changchun Institute of Applied Chemistry, Chinese Academy of Sciences, Changchun 130022, Jilin, China
[b] Graduate School of the Chinese Academy of Sciences, Beijing 100039, China

Received 29 July 2007; received in revised form 3 October 2007; accepted 12 October 2007
Available online 1 November 2007

Abstract

Electrodeposition of novel Au/Pd bimetallic nanostructures with dendrimer films as matrices has been reported. The dendrimers exhibited highly open structures arising from protonation of amines and this made them have good penetrability for solvent molecules. The unique properties of dendrimers obviously affected the morphologies and compositions of deposited bimetallic nanostructures compared with those from unmodified surfaces. Field-emitted scanning electron microscopy, energy dispersive spectroscopy, X-ray photoelectron spectroscopy and UV–vis spectroscopy were used to characterize these nanostructures. The results showed that these bimetallic nanostructures were consisted of many small nanoparticles. Effects of ratios of $KAuCl_4$ and K_2PdCl_6, electrodeposition time and layer number of assembled dendrimers were thoroughly investigated. At last, electrochemical properties of the bimetallic nanostructures were also studied.
© 2007 Elsevier B.V. All rights reserved.

Keywords: PAMAM; Au/Pd; Bimetallic; Electrodeposition

1. Introduction

Preparation of nanomaterials with different structures and morphologies is very necessary and has attracted considerable interest over the past decade. Their physical and chemical properties are related to the surface structures. Many metallic nanostructures have been reported and exhibited potential applications in electronics, catalysis and bioanalysis [1–5]. Among these nanomaterials, bimetallic nanoparticles are important materials due to their unique properties completely different from monometallic nanoparticles. Many methods including alcohol reduction, sonochemical method, microwave synthesis and electrolysis have been reported for preparation of bimetallic nanostructures [6–8].

Electrodeposition also is a widely used method for fabrication of nanomaterials and it provides remarkably fine-tuning and fast response of the system on the changes of deposition conditions. Both metal and semiconductor nanostructures can be deposited onto surfaces by corresponding electrochemical techniques [9–15]. Nanopyramidal, nanorod-like and spherical gold nanostructures have been prepared via electrochemical overpotential deposition [9,10]. Shape-controlled ZnO nanostructures also have been obtained by electrodeposition [11–14]. At the same time, electrodeposition has been processed on modified surfaces and many novel nanostructures have been constructed. Two-dimensional palladium nanostructures have been electrochemically fabricated onto the substrates modified by polypyrrole, which can be used for surface enhance Raman scattering [16]. Metallic aggregates also have been obtained on the polyelectrolytes-modified surfaces [17,18].

Dendrimers have been used as stabilizers for synthesis of nanoparticles with small sizes, which was developed by Crooks groups [19–23]. These nanoparticles have been used in many fields for special structures and properties of dendrimers. Gold/palladium bimetallic nanostructures have special catalytic properties and these nanostructures with core–shell and cluster shapes have been synthesized. However, there are few reports about electrodeposition of bimetallic nanostructures with dendrimers as matrices [24]. We reported that electrochemical fabrication of novel Au/Pd bimetallic nanostructures

* Corresponding author. Tel.: +86 431 85689711; fax: +86 431 85689711.
E-mail address: xryang@ciac.jl.cn (X. Yang).

0039-9140/$ – see front matter © 2007 Elsevier B.V. All rights reserved.
doi:10.1016/j.talanta.2007.10.042

with amine-terminated generation 4 dendrimers as matrices. It was found that the assembled dendrimer films obviously affected morphologies and compositions of bimetallic nanostructures relative to those from unmodified surfaces. These nanostructures were characterized by field-emitted scanning electron microscopy (FE-SEM), energy dispersive spectroscopy (EDS), X-ray photoelectron spectroscopy (XPS) and UV–vis spectroscopy. These experimental results demonstrated that the novel nanostructures were actually "nanoclusters" consisted of many small nanoparticles. Moreover, they tended to the growth of dendritic structures with decrease of the amount of $KAuCl_4$. The multilayer films of dendrimers resulted in formation of multilayer bimetallic nanostructures. Electrochemical behaviors of these bimetallic nanostructures were also studied.

2. Experimental

2.1. Chemical and reagents

Potassium tetrachloroaurate ($KAuCl_4$), potassium hexachloropalladate (K_2PdCl_6), poly(diallymethylammonium) chloride (20 wt.%, PDDA) and amino-terminated generation 4 PAMAM dendrimer (G_4-NH_2, 10 wt.% in methanol) were obtained from Aldrich. Poly(sodium-*p*-styrensulfonate) (PSS, Mw 70,000) was from ACROS. Hydrazine sulfate ($N_2H_4SO_4$) was purchased from Shanghai Sangon Biological Engineering Technology & Services Co. All aqueous solutions were made with double-distilled water.

2.2. Characterization and procedures

Indium tin oxide (ITO) glass (Changchun Institute of Optical and Mechanics, China) was carefully cleaned according to the reported method [24]. After dried in nitrogen, it was dipped into 1% PDDA solution and 1% PSS solution, respectively for 20 min. At last, the ITO glass was immersed into G_4-NH_2 solution for 40 min and the dendrimers-modified ITO glass was obtained. The multilayer film of dendrimers was assembled onto the ITO surface followed the same process. Au/Pd bimetallic nanostructures were electrodeposited by potentiostatic method in 0.1 M H_2SO_4 solutions containing $KAuCl_4$ and K_2PdCl_6 at −0.2 V. Electrochemical experiments were performed on a CHI630B electrochemical workstation (Shanghai, China). A conventional three-electrode system was employed with the ITO glass as the working electrode. The reference electrode was an Ag/AgCl (saturated potassium chloride), and the counter electrode was a platinum foil. Morphologies of bimetallic nanostructures were observed by FE-SEM (Philips XL-30 ESEM), and EDS was obtained from an EDAX system. XPS was conduced with an ESLAB 250 spectrometer (VG Co., UK). UV–vis absorbance spectra were collected from a Cary 50 UV–vis spectrometer (Varian, USA).

3. Results and discussion

Morphologies of deposited metallic nanostructures were characterized by FE-SEM. Au/Pd bimetallic nanostructures were electrodeposited from 0.1 M H_2SO_4 containing different amount of $KAuCl_4$ and K_2PdCl_6 in order to examine the effect of ratios of them. Fig. 1a–d gives the corresponding images of deposited nanostructures. The surfaces were coated by these nanostructures and they were well dispersed on surfaces. In addition, these nanostructures were all consisted of many small nanoparticles (inset of Fig. 1b). The corresponding EDS spectrum of deposited nanostructures is shown in Fig. 1f. Bimetallic nanostructures were also electrodeposited onto the bare ITO surface (Fig. 1e) for comparison. It was found that morphologies of nanostructures were different from those obtained on the dendrimers-modified surface. These results showed that dendrimers could obviously affect the seed nucleation and growth, and they induced the formation of novel nanostructures. As shown in Fig. 1a–d, morphologies of bimetallic nanoclusters could be controlled by the $KAuCl_4$:K_2PdCl_6 ratios. In the presence of high-$KAuCl_4$ concentration, irregular nanoclusters were observed. However, these nanoclusters tended to the growth of dendritic structures with decrease in the amount of $KAuCl_4$. Gold dendritic structures have been obtained on the polyelectrolytes-modified ITO surfaces [18]. But the ITO surfaces must be modified by at least six polyelectrolyte bilayers for preparation of gold clusters. In our experiments, dendritic bimetallic nanostructures were conveniently obtained with the monolayer dendrimer film as a matrix. It was reported that PAMAM dendrimers exhibited unique pH-response properties arising from protonation of terminated amines and tertiary amines inside them [25–27]. At low pH, all amines were protonated and these PAMAM dendrimers exhibited highly open structures for electrostatic repulsion between protonated amines [25]. Large amounts of solvent molecules could penetrate inside the dendrimers, so $AuCl_4^-$ and $PdCl_6^{2-}$ ions easily diffused into the dendrimer films via the electrostatic interaction between negatively ions and positively protonated amines. During the electrodeposited process, the protonated amines were in favor of seed nucleation and this resulted in the continuous formation of new nuclei. So bimetallic "nanoclusters" consisted of many small nanoparticles were obtained on surfaces. Au:Pd atomic ratios of these bimetallic nanostructures were investigated by EDS analysis. The corresponding results are given in Table 1. The experimentally obtained Au:Pd atomic ratios were different from the calculated values. It was found that the obtained Au:Pd ratios were high, indicating that $AuCl_4^-$ ions were more easily reduced on the electrode surface. However, the Au:Pd atomic ratio was about 1:8.38 from the unmodified ITO surface, which was similar to the calculated value. Thus it also indicated that compo-

Table 1
EDS analysis of Au/Pd bimetallic nanostructures

$KAuCl_4/K_2PdCl_6$	Au%	Pd%	Au/Pd
3:1	80.96	19.04	4.25:1
1:1	60.69	39.31	1.54:1
1:3	41.61	58.31	1:1.40
1:9	17.03	82.97	1:4.87
1:9[a]	10.66	89.34	1:8.38

[a] Bimetallic nanostructures obtained from the unmodified ITO surface.

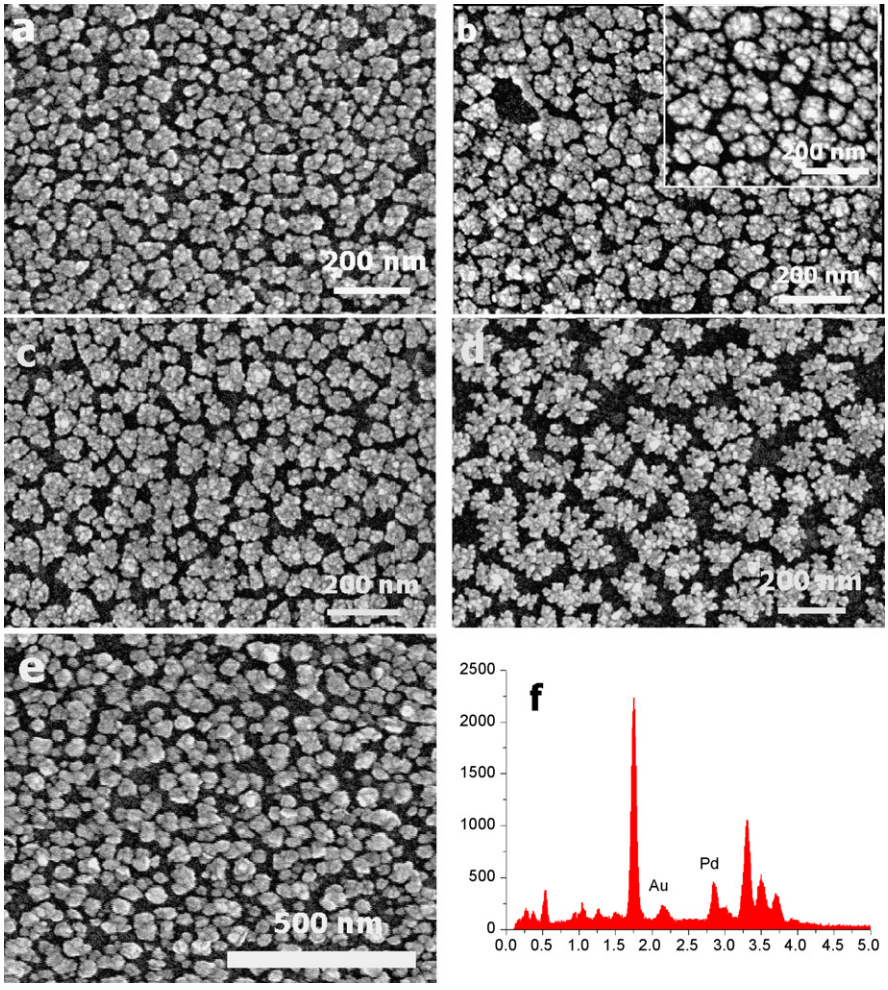

Fig. 1. FE-SEM images of Au/Pd bimetallic nanostructures on the dendrimers-modified ITO surfaces in 0.1 M H_2SO_4 containing 1.5 mM $KAuCl_4$ and 0.5 mM K_2PdCl_6 (a), 1 mM $KAuCl_4$ and 1 mM K_2PdCl_6 (b), 0.5 mM $KAuCl_4$ and 1.5 mM K_2PdCl_6 (c), and 0.2 mM $KAuCl_4$ and 1.8 mM K_2PdCl_6 (d). (e) FE-SEM image of bimetallic nanostructures from the unmodified ITO surface in 0.1 M H_2SO_4 with 0.2 mM $KAuCl_4$, 1.8 mM K_2PdCl_6. (f) EDS of the Au/Pd bimetallic nanostructures corresponding to (d). Electrodeposition conditions: −0.2 V; 200 s.

sitions of bimetallic nanostructures also were affected by dendrimers.

Bimetallic nanostructures obtained from the different deposited time were also investigated. Both sizes and density of nanostructures increased with time extending from 20, 60 to 800 s. The whole surface was coated by bimetallic dendritic nanostructures with the deposition time of 800 s. We also studied that effect of the layer number of dendrimers on morphologies of bimetallic nanostructures. Six and twelve layers of dendrimers were used as matrices for electrodeposition of bimetallic nanostructures and the corresponding FE-SEM images are given in Fig. 2. It was found that these deposited nanostructures did not grow into the similar structures with those from monolayer dendrimer-modified surfaces (Fig. 1d). Compared with the dendritic nanostructures, they tended to grow into multilayer bimetallic nanoclusters with increase in the modified layer number of dendrimers. Moreover, the density of nanostructures on the surfaces was high.

The spectral properties were also studied and the UV–vis absorbance spectra are given in Fig. 3A. Curves a and b corresponded to the absorbance spectra of the deposited pure gold and palladium nanostructures. The maximum peak at about 500 nm, resulting from the surface resonance plasmon band of Pd nanostructures, was observed for palladium nanostructures (curve b), indicating the sizes of nanostructures were large [16,28]. With increase in the amount of $KAuCl_4$, the absorbance peak of deposited bimetallic nanostructures positively shifted to the absorbance region of gold nanostructures (curves c and d). XPS experiments were carried out to confirm the chemical state of the bimetallic nanostructures. XPS spectra of Pd (3d) and Au (4f) are shown in Fig. 3B and C. It was found that Pd ($3d_{5/2}$) and Pd ($3d_{3/2}$) peaks at 334.9 and 340.2 eV appeared in the Pd (3d) binding region, which indicated the presence of Pd (0). The binding energy of Au (4f) was also similar to that reported for metallic gold nanoparticles. These results showed that nanostructures indeed were consisted of bimetallic nanoparticles.

It is well-known that metallic nanostructures exhibit highly catalytic properties for many substrates, especially for Pt and Pd nanoparticles. These unique properties make them be used as promising materials in fields of fuel cells, electrocatalysis. Here we also investigated the electrocatalytic properties of Au/Pd bimetallic nanostructures for oxygen and

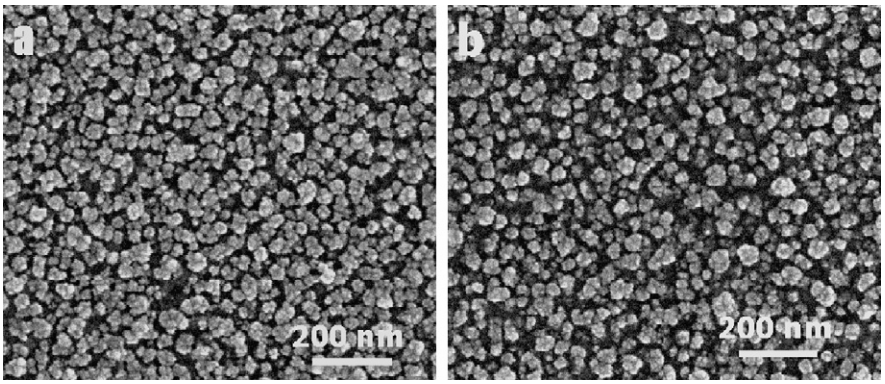

Fig. 2. FE-SEM images of Au/Pd bimetallic nanostructures on six (a) and twelve (b) layers of dendrimer films. Electrodeposition conditions: 0.1 M H_2SO_4 containing 0.2 mM $KAuCl_4$ and 1.8 mM K_2PdCl_6; −0.2 V; 200 s.

hydrazine sulfate [29,30]. Fig. 4A shows cyclic voltammograms of the Au–Pd/dendrimers/ITO, Au–Pd/ITO, dendrimers/ITO, Au/ITO and ITO electrodes in oxygen-saturated 0.1 M H_2SO_4 at a scan rate of 50 mV s^{-1}. The ITO and dendrimers/ITO electrodes (curves A and B) did not give electrocatalytic response for oxygen. For the Au–Pd/dendrimers/ITO electrode (curve C), two reductive peaks at about 0.22 and 0.06 V were observed corresponding to the two-step reduction of oxygen [31], indicating that the Au–Pd/dendrimers/ITO electrode showed catalytic activity for oxygen reduction. However, the Au–Pd/ITO electrode (curve D) showed reductive peak potential at 0.30 and 0.11 V, which positively shifted relative to the Au–Pd/dendrimers/ITO electrode. The electrocatalytic oxidation of hydrazine sulfate was also carefully investigated. Fig. 4B shows the cyclic voltammograms of the Au–Pd/dendrimers/ITO, Au–Pd/ITO, dendrimers/ITO, Au/ITO and ITO electrodes in 0.1 M Na_2SO_4 with 1 mM $N_2H_4SO_4$ at a scan rate of 100 mV s^{-1}. The ITO and dendrimers/ITO elec-

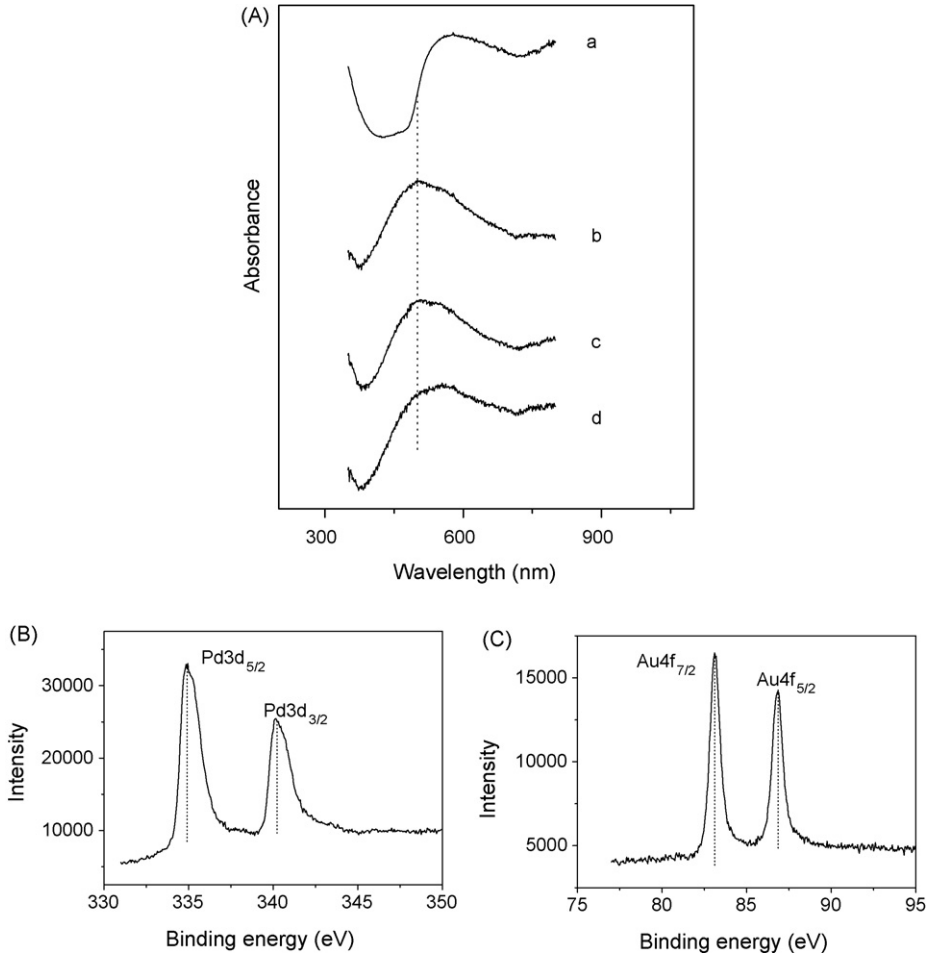

Fig. 3. (A) UV–vis spectra of the deposited bimetallic nanostructures from 0.1 H_2SO_4 solutions with 2 mM $KAuCl_4$ (a), 2 mM K_2PdCl_6 (b), 1 mM $KAuCl_4$ and 1 mM K_2PdCl_6 (c), and 1.5 mM $KAuCl_4$ and 0.5 mM K_2PdCl_6 (d) for 200 s at −0.2 V. (B and C) XPS of Pd (3d) and Au (4f) of the bimetallic nanostructures.

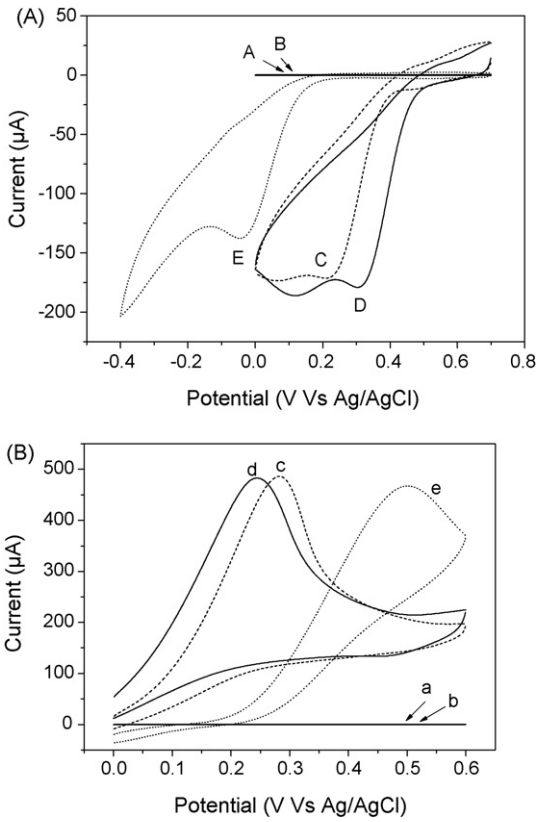

Fig. 4. (A) Cyclic voltammograms of the ITO (A), dendrimers/ITO (B), Au–Pd/dendrimers/ITO (C), Au–Pd/ITO (D) and Au/ITO (E) electrodes in oxygen-saturated 0.1 M H_2SO_4 at a scan rate of 50 mV s^{-1}. (B) Cyclic voltammograms of the ITO (a), dendrimers/ITO (b), Au–Pd/dendrimers/ITO (c), Au–Pd/ITO (d) and Au/ITO (e) electrodes in 0.1 M Na_2SO_4 with 1 mM $N_2H_4SO_4$ at a scan rate of 100 mV s^{-1}.

trodes (curves a and b) did not show electrocatalytic activity for $N_2H_4SO_4$. Oxidative peak potential from the Au–Pd/ITO electrode (0.24 V, curve d) was more negative than that from the Au–Pd/dendrimers/ITO electrode (0.28 V, curve c). In addition, the Au/ITO electrode exhibited weak catalytic activity towards oxygen (curve E) and $N_2H_4SO_4$ (curve e), and the peak potential was −0.04 and 0.5 V, respectively. This showed that Pd element had an important effect on electrocatalytic activity of bimetallic nanostructures. These electrochemical results indicated that the Au–Pd/ITO electrode exhibited slightly better electrocatalytic activity for oxygen and hydrazine sulfate compared with the Au–Pd/dendrimers/ITO electrode. This could be explained by the fact that lower atomic ratio of Pd and Au (Table 1), and interaction between metallic nanoparticles and dendrimers for the Au–Pd/dendrimers/ITO electrode [32].

4. Conclusion

In summary, novel Au/Pd bimetallic nanostructures were electrochemical fabricated with dendrimer films as matrices. Highly open structures of dendrimers at low pH were in favor of penetration of solvent molecules. This made $AuCl_4^-$ and $PdCl_6^{2-}$ ions easily diffuse into dendrimer interior. Seed nucleation and growth were largely affected by dendrimers and this resulted in the formation of novel nanostructures. Different ratios of $KAuCl_4$ and K_2PdCl_6 obviously controlled morphologies of bimetallic nanostructures, and multilayer bimetallic nanostructures could be obtained with multilayer films of dendrimers as matrices for electrodeposition. The electrocatalytic properties of novel bimetallic nanostructures were also investigated. It was found that they exhibited catalytic properties towards O_2 and $N_2H_4SO_4$. This method provides a new route for fabrication novel nanostructures via dendrimers as matrices for electrodeposition. Dendrimers will exhibit promising applications in the fields of electrodeposition based on their unique properties and structures.

Acknowledgement

This work was supported by the National Nature Science Foundation of China with the Grant (No. 90713022) and the Project of Chinese Academy of Sciences (No. KJCX2. Y W. H09, No. KJCX2-YW-H11).

References

[1] Y.G. Sun, Y.N. Xia, Science 298 (2002) 2176.
[2] T.K. Sau, C.J. Murphy, J. Am. Chem. Soc. 126 (2004) 8648.
[3] S. Link, M.A. El-Sayed, J. Phys. Chem. B 103 (1999) 8410.
[4] Z.L. Wang, J. Phys. Chem. B 104 (2000) 1153.
[5] J.S. Bradley, B. Tesche, W. Busser, M. Maase, M.T. Reetz, J. Am. Chem. Soc. 122 (2000) 4631.
[6] Y. Mizukoshi, T. Fujimoto, Y. Nagata, R. Oshima, Y. Maeda, J. Phys. Chem. B 104 (2000) 6028.
[7] N. Toshima, Y. Wang, Langmuir 10 (1994) 4574.
[8] W. Harpeness, A. Gedanken, Langmuir 20 (2004) 3431.
[9] Y. Tian, H. Liu, Z. Deng, Chem. Mater. 18 (2006) 5820.
[10] Y. Tian, H. Liu, G. Zhao, T. Tatsuma, J. Phys. Chem. B 110 (2006) 23478.
[11] M. Izaki, T. Omi, Appl. Phys. Lett. 68 (1996) 2439.
[12] L.F. Xu, Y. Guo, Q. Liao, J.P. Zhang, D.S. Xu, J. Phys. Chem. B 109 (2005) 13519.
[13] B. Cao, Y. Li, G. Duan, W. Cai, Cryst. Growth Des. 6 (2006) 1091.
[14] F. Xu, Z.-Y. Yuan1, G.-H. Du, T.-Z. Ren, C. Bouvy, M. Halasa1, B.-L. Su, Nanotechnology 17 (2006) 588.
[15] L. Qian, X. Yang, Talanta 69 (2006) 957.
[16] Y. Li, G. Lu, X. Wu, G. Shi, J. Phys. Chem. B 110 (2006) 24585.
[17] N. Zhao, F. Shi, Z. Wang, X. Zhang, Langmuir 21 (2005) 4713.
[18] X. Zhang, F. Shi, X. Yu, H. Liu, Y. Fu, Z. Wang, L. Jiang, X. Li, J. Am. Chem. Soc. 126 (2004) 3064.
[19] J.C. Garcia-Martinez, R. Lezutekong, R.M. Crooks, J. Am. Chem. Soc. 127 (2005) 5097.
[20] H. Ye, R.M. Crooks, J. Am. Chem. Soc. 127 (2005) 4930.
[21] R.W.J. Scott, A.K. Datye, R.M. Crooks, J. Am. Chem. Soc. 125 (2003) 3708.
[22] Y.-G. Kim, S.-K. Oh, R.M. Crooks, Chem. Mater. 16 (2004) 167.
[23] C. Zhang, S. O'Brien, L. Balogh, J. Phys. Chem. B 106 (2002) 10316.
[24] L. Qian, X. Yang, J. Phys. Chem. B 110 (2006) 16672.
[25] P.K. Maiti, W.A. Goddard, J. Phys. Chem. B 110 (2006) 25628.
[26] S.T. Lin, P.K. Maiti, W.A. Goddard, J. Phys. Chem. B 109 (2005) 8663.
[27] Y. Liu, M. Zhao, D.E. Bergbreiter, R.M. Crooks, J. Am. Chem. Soc. 119 (1997) 8720.
[28] G. Chang, M. Oyama, K. Hirao, J. Phys. Chem. B 110 (2006) 20362.
[29] D.-J. Guo, H.-L. Li, J. Colloids Interf. Sci. 286 (2005) 274.
[30] D.-J. Guo, H.-L. Li, Electrochem. Commun. 6 (2004) 999.
[31] B. Kumar, C.R. Raj, Langmuir 23 (2007) 4064.
[32] R.W.J. Scott, O.M. Wilson, R.M. Crooks, J. Phys. Chem. B 109 (2005) 692.

Available online at www.sciencedirect.com
ScienceDirect
Talanta 74 (2008) 1484–1491
Talanta
www.elsevier.com/locate/talanta

Spectrofluorimetric determination of irinotecan in the presence of oxidant agents and metal ions

M.I. Rodríguez Cáceres [a,*], I. Durán-Merás [a], Nancy E. Ornelas Soto [b], P.L. López de Alba [b], L. López Martínez [b]

[a] *Department of Analytical Chemistry, University of Extremadura, Badajoz, Spain*
[b] *Instituto de Investigaciones Cientificas, University of Guanajuato, Guanajuato, Mexico*

Received 27 May 2007; received in revised form 17 September 2007; accepted 28 September 2007
Available online 2 October 2007

Abstract

In this work four spectrofluorimetric methods for the determination of irinotecan (CPT-11) in human urine and pharmaceuticals have been developed. Initially, the fluorescent characteristics of irinotecan (CPT-11) have been studied in both acidic and basic media. Later, the fluorescence emission generated by the oxidation of CPT-11 with several agents was studied. A quenching of fluorescence could be observed in the presence of Ce(IV) and I_2/I^-. Also, the reaction between several divalent and trivalent metal ions with CPT-11 was studied, and one method in presence of Fe^{3+} was developed since it was the only metal ion that changes the fluorescence of the analyte. The proposed methods present limit of detection comprises between 0.46 and 2.57 ng mL^{-1}. The spectrofluorimetric methods were applied to human urine. No pre-treatment of the sample was necessary, only a dilution 1:20 with water was made. No interference of the matrix was observed in the conditions used. Recoveries were comprises between 100.0 and 104.3%. Also, pharmaceuticals preparations were analyzed with recoveries between 106.7 and 119.7%. The proposed spectrofluorimetric methods were validated by RP-HPLC, obtaining that the oxidation with iodine is the best method to analyze urine samples, while than, the fluorimetric method developed at acidic pH value is the best for the analysis of pharmaceuticals.
© 2007 Elsevier B.V. All rights reserved.

Keywords: Irinotecan; CPT-11; Fluorescence; Cerium; Iodine; Metals

1. Introduction

Irinotecan (CPT-11 or 7-ethyl-10-[4-(1-piperidino)-1-piperidino]-carbonyloxy-camptothecin) (Scheme 1) is a water soluble camptothecin derivative. It is a pro-drug, converted *in vivo* to its active metabolite, SN-38 (7-ethyl-10-hydroxy-camptothecin). CPT-11 interfere with mammalian DNA topoisomerase I and cancer cells death appears to result from DNA strand breaks caused by the formation of cleavable complexes [1].

In 1998, it received full FDA approval for treatment of metastatic colorectal carcinoma that has recurred or progressed after standard chemotherapy. Recently, CPT-11 has been approved in association with fluorouracil (FU) and leucovorin (LV) as first line treatment of metastatic colorectal cancer [2]. Also, as a single agent or in combined modality regimens has been investigated in gastric cancer [3], non-mall cells lung cancer [4], advancer solid malignancy tumor [5] and others. The major dose-limiting toxicity after administration of CPT-11 is severering diarrhea that is often unresponsive to common antidiarrheal agents [6].

The pharmacokinetics and metabolism of CPT-11 are extremely complex and has been the subject of intensive investigation in recent years. It is well known that CPT-11 presents an active lactone form that can be converted into the carboxylate inactive form as a function of pH, with a mean half-life of 9.5 min [7]. Several studies have shown that hepatic metabolism and biliary secretion are major pathways of CPT-11 elimination [8]. Several studies have examined the excretion of CPT-11 in bile, faeces and urine. In humans, only 52% of the given dose has been recovered [9]. CPT-11 is excreted for about 10–22% of the administered dose in urine, however, its active metabolite; SN-38 contributes only with a percentage comprises between 0.18 and 0.43% in the first 24 h [10].

* Corresponding author. Tel.: +34 924289375; fax: +34 924289375.
E-mail address: maribelro@unex.es (M.I. Rodríguez Cáceres).

0039-9140/$ – see front matter © 2007 Elsevier B.V. All rights reserved.
doi:10.1016/j.talanta.2007.09.025

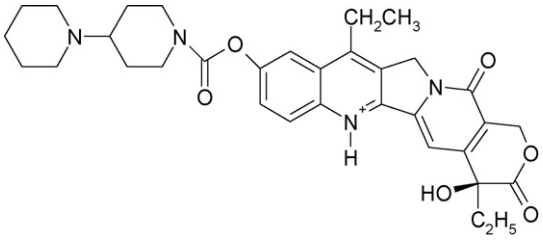

Scheme 1.

A survey of the literature reveals that most of the methods for the analysis of CPT-11 are chromatographic. A 70% of the methods found used fluorescence detection [11–16] while only a few used photometric [17] or mass detection [18,19]. The samples analysed were principally plasma [12–16,18,19]. Also, other samples were analysed, such as pharmaceuticals [11], saliva [12], urine and faeces [14] and tissues [18].

No references have been found about the fluorescence characteristics of CPT-11, as far as our knowledge. However, some references appeared about the parent compound camptothecin [20–23]. Thus, Warner et al. [20] studied the effect of pH in the absorbance and fluorescence spectra of camptothecin (CAM) in aqueous solution. Also, the fluorescence behaviour of CAM in different organic solvents has been studied. The quenching of both, the lactone and carboxylate form of CAM in the presence of iodine in aqueous media was studied. They concluded that the quenching is dynamic by use of Stern–Volmer equation [21].

The kinetic of hydrolysis of lactone ring of CAM has been followed by fluorescence [22]. Effect of the substitutes, pH and polarity of solvent were studied. Posokhov et al. [23] used theoretic approximations to calculate the dipolar moment of CAM in excited state. Also, they probated that fluorescence of CAM is quenched by Co^{2+} ions. Recently, spectroscopic studies of Fe(III)-CAM system has been carried out in DMSO when CAM was UV irradiated at 365 nm [24].

In this paper, the fluorescence characteristics of CPT-11 have been established, and interactions of CPT-11 with metal ions (Fe^{3+}) and oxidant agents, such as, cerium(IV) and iodine in acidic media has been studied by spectrofluorimetry. As far as our knowledge, no spectrofluorimetric method has been proposed for the determination of CPT-11 until date. The goal of this work is to propose several spectrofluorimetric methods for first time. Also, the aim of this work is to compare the sensitivity of the determination of CPT-11 by spectrofluorimetry working in acidic media in both the presence and the absence of oxidant agents or metal ions.

2. Experimental

2.1. Reagents

All experiments were performed with analytical reagent grade chemicals. CPT-11 was prepared by dissolving 0.0100 g of irinotecan·HCl (Sigma–Aldrich, Germany) in 100 mL of methanol. Appropriate CPT-11 solutions of different concentrations were prepared by dilution in EtOH:H_2O (50:50, v/v).

A 10^{-2} M Ce(IV) solution was prepared by dissolving 0.100 g of $Ce(SO_4)_2{\cdot}4H_2O$ (Merck) in 25.0 mL of 1.0 M H_2SO_4. Iodine solution was prepared by dissolving iodine (1%, w/v) and potassium iodide (2%, w/v) in ultrapure water.

Solutions of metallic ions were prepared by dissolution of the metal nitrates in ultrapure water (1 g L^{-1}). Ultrapure water from a Milli-Q system (Millipore, Bedford, MA, USA) was used.

2.2. Apparatus

Acquisition of fluorescence data were performed using a Fluorescence Spectrophotometer Varian Model Cary Eclipse, equipped with a Xenon flash lamp. The emission and excitation spectra were registered with $\lambda_{exc} = 368$ nm and $\lambda_{em} = 426$ nm, respectively. All measurements were recorded in a 10-mm quartz cell at 20 °C by use of a thermostatic cell holder and a Selecta Unitronic 320 OR thermostatic water-bath. A Crison MicropH 501 meter was used for pH measurements.

2.3. Procedures for the fluorimetric determination of CPT-11

2.3.1. General procedure in acidic media

An aliquot of CPT-11 stock solution was placed in a 5-mL volumetric flask in order to obtain the desired concentration. One milliliter of 0.5 M acetate buffer (pH 4.0) was added and the solution was dilute to volume with ultrapure water to the mark. The fluorescence intensity was measured at 426 nm ($\lambda_{exc} = 368$ nm), maintaining the temperature at 20 °C.

2.3.2. General procedure in presence of oxidant agents

2.3.2.1. Oxidation of CPT-11 by cerium(IV). An aliquot of CPT-11 was placed in a 5-mL volumetric flask in order to obtain the desired concentration. Next, 150 μL of Ce(IV) 10^{-3} M, prepared in 1.0 M H_2SO_4 were added and ultrapure water until the mark. The volumetric flask was shaken vigorously and immediately the excitation and emission spectra were recorder at 368 and 426 nm, respectively. The temperature was maintained constant at 20 °C.

2.3.2.2. Oxidation of CPT-11 by I_2/I^- solution. An aliquot of CPT-11 was placed in a 5-mL volumetric flask in order to obtain the desired concentration. Next, aliquots of HCl 0.5 M and iodine solution [1% (w/v) iodine in 2% (w/v) potassium iodide] were added until reach the optimum concentration, and ultrapure water was added until the mark. The volumetric flask was shaken vigorously and immediately the excitation and emission spectra were recorder at 368 and 426 nm, respectively. The temperature was maintained constant at 20 °C.

2.3.3. General procedure in presence of metal ions

An aliquot of CPT-11 was placed in a 5-mL volumetric flask in order to obtain the desired concentration. Next, add the optimum volume in order to obtain 0.5–4 mM solutions of several metallic ions and 0.5 mL of 0.5 M chloracetic buffer (2.8) and ultrapure water until the mark. The volumetric flask was shaken

vigorously and immediately the excitation and emission spectra were recorder at 368 and 426 nm, respectively. The temperature was maintained constant at 20 °C.

2.4. Analysis of CPT-11 in human urine

Two hundred microliters of urine sample spiked with appropriate amount of CPT-11 (in the range that can be found in urine) were placed in a 5-mL volumetric flask or a 3-mL quartz cell and the procedures described in Section 2.3 were followed.

2.5. Analysis of CPT in pharmaceutical preparations

An aliquot of pharmaceutical preparation of CPT-11 (CAMPTO of Aventis-Pharma) solution was placed in a 5-mL volumetric flask in order to obtain the desired concentration and was prepared as mentioned in Section 2.3. For each proposed method three replicates were made.

2.6. Validation of the proposed methods

The proposed spectrofluorimetric methods were validated by RP-HPLC using the method proposed by Scoriaza et al. [25]. An analytical column Nucleosil C18 (250 mm × 4 mm, 5 μm) was used at room temperature. The fluorescence detector excitation wavelength was set at 228 nm and the emission wavelength at 450 nm.

The chromatographic studies were performed on a Hewlett-Packard Model 1100 LC instrument equipped with degasser, quaternary pump, manual six-way injection valve, containing a 20 μL loop, rapid scan fluorescence spectrophotometer detector and the Chemstation software package to control the instrument, data acquisition and data analysis. The mobile phase was formed by 0.1 M potassium dihydrogenphosphate (adjusted to pH 4.2 with 1 M HCl)–acetonitrile (77:33, v/v), with a flow rate of 1 mL/min.

Samples were prepared in acetonitrile–citric acid 0.01 M, pH 3 (50:50, v/v) to be sure that CPT-11 is in the lactone form. External standard method was used with peak area as analytical signal.

3. Results and discussion

3.1. Spectral characteristic of CPT-11

CPT-11 presents native fluorescence with slight differences, in both, acidic and basic media. In Fig. 1, the excitation and emission spectra at pH 4.5 (1, 1′) and pH 9.0 (2, 2′) are shown. The pH 4.5 was fixed with acetate buffer (0.1 M) in aqueous: ethanol media (50:50, v/v). As can be seen in the figure, the excitation spectrum has two maxima located at 255 and 368 nm, whereas the emission spectrum has only a maximum located 426 nm. To register the spectra at basic pH, a Tris buffer was used and the solution of CPT-11 was prepared en H_2O:EtOH (50:50, v/v). In this case, a decrease in the fluorescence intensity has been observed, also, a third maximum appears at 222 nm in the excitation spectrum and a slight red shift of 4 nm in the emission maximum can be observed.

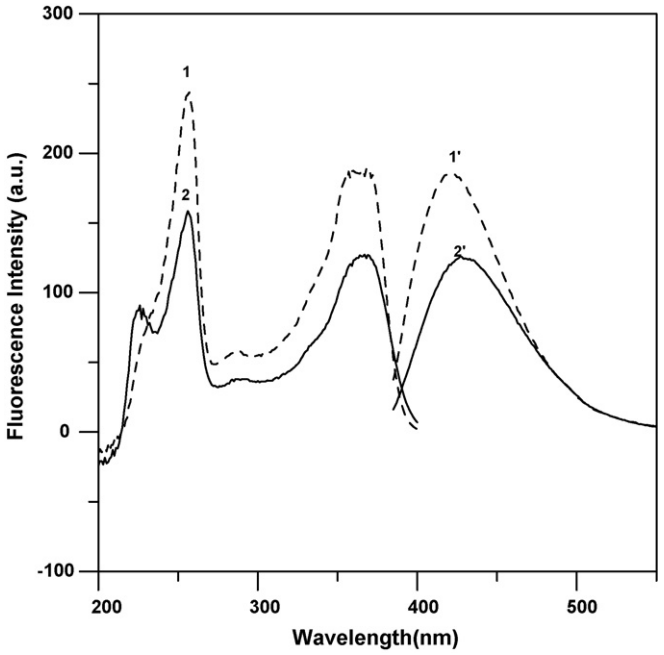

Fig. 1. Excitation and emission spectra of CPT-11 at pH 4.5 (0.1 M acetate buffer) (1, 1′) and pH 9.0 (0.2 M Tris buffer) (2, 2′) in aqueous: ethanolic medium (50:50, v/v). [CPT-11] = 500 ng mL^{-1}.

3.2. Influence of experimental variables

3.2.1. Influence of pH

The influence of the acidity on the fluorescence of CPT-11 has been studied. For that, a solution was prepared containing 500 ng mL^{-1} of CPT-11 and KCl 0.5 M, in order to maintain constant the ionic strength. The pH was modified with slightly additions of HCl or NaOH. The solution was keeping stirring all the time. The excitation and emission spectra obtained at different pH values are shown in Fig. 2A for acidic pH values and in Fig. 2B for basic pH values. It could be seen an isoelectric point at 495 nm in acidic media. A hypochromic shift was observed in this isoelectric point centred at 447 nm at pH values higher than 6.0. Besides, it is worth noting that when the pH decreases at pH values lower than 2, the maximum located at 426 nm disappears and a new maximum appears at 495 nm.

The variation of the emission fluorescence intensity at 426 nm (λ_{exc} = 368 nm) *versus* pH is shown in Fig. 3. The fluorescence intensity increases with the pH until it reaches a maximum between pH 3 and 7. At higher values the fluorescence intensity decreases and it completely disappears at pH strongly basic (pH 13). Starting from pH 10, CPT-11 begins with the hydrolysis process until complete destruction.

The ionization constants of CPT-11 were calculated using the changes in the fluorescence intensity produced by the variation of the pH. Wilson and Lester method [26] was used. Two ionization constants could be found and the values were pK_{a1} = 2.08 and pK_{a2} = 8.93.

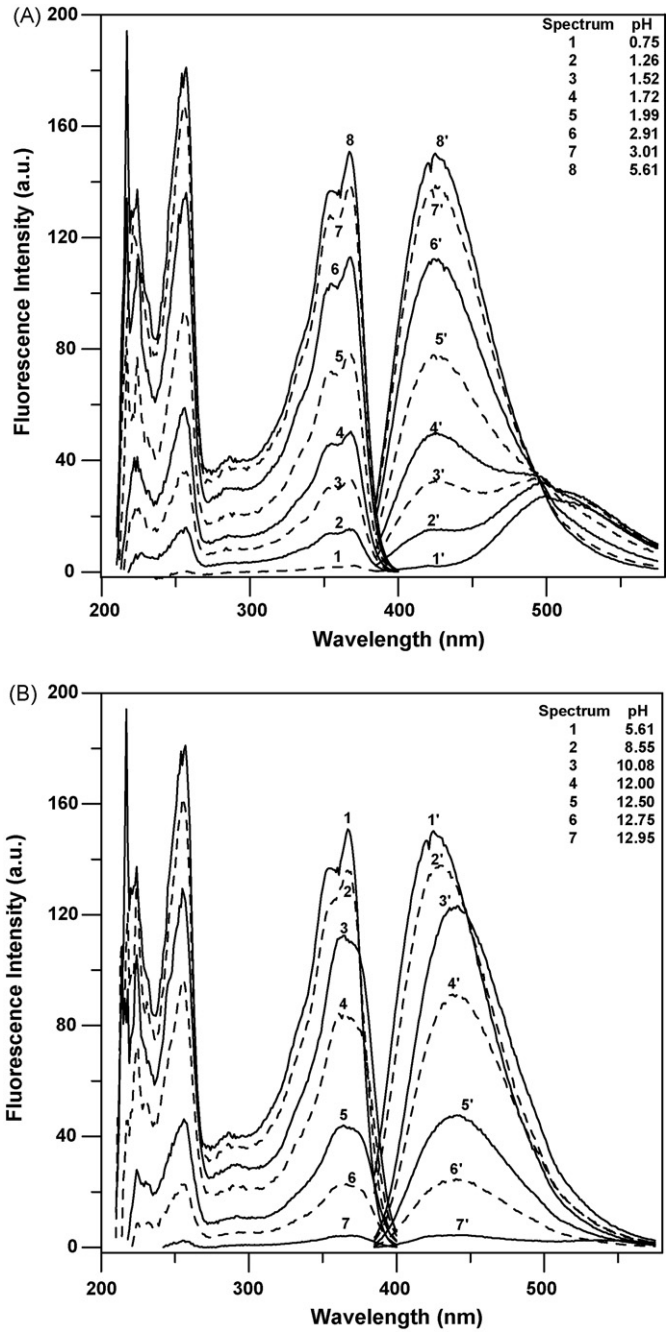

Fig. 2. (A) Excitation and emission spectra of CPT-11 in acidic medium and (B) in basic medium. [CPT-11] = 500 ng mL^{-1}.

3.2.2. Influence of solvents

Excitation and emission spectra of CPT-11 in different solvents at acidic pH were recorded. It could be observed that acetonitrile had no influence on the fluorescence intensity, whereas methanol or ethanol increased the signal. For this reason, different percentages of ethanol were tested and the results showed that the fluorescence intensity increased when the percentage of ethanol increases until reach a maximum at 50%. For that reason, H_2O:EtOH (50:50, v/v) was chosen as solvent for further experiences.

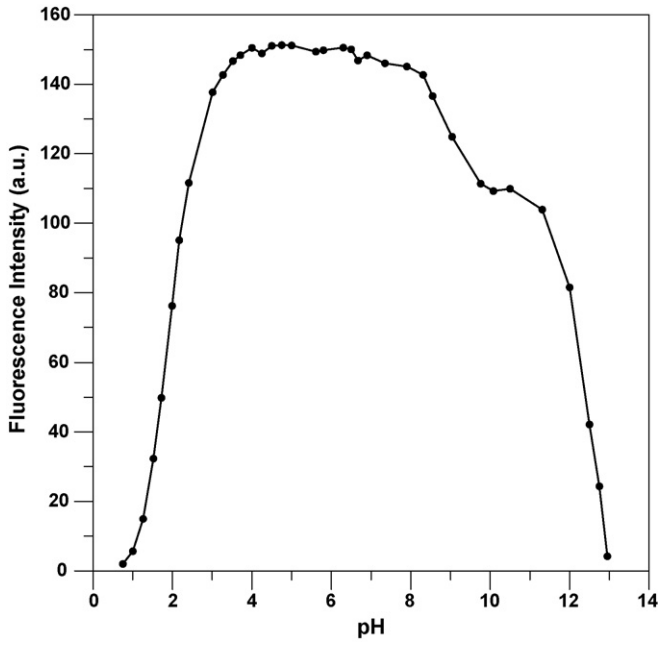

Fig. 3. Variation of the emission fluorescence intensity at 426 nm of CPT-11 with the pH in aqueous medium. [CPT-11] = 500 ng mL^{-1}; λ_{exc} = 368 nm.

3.2.3. Influence of buffer and temperature

To regulate the pH, different buffers at pH 4.0 were tested. Acetic/acetate buffer was chosen. Later, the influence of the concentration was studied and 0.1 M of acetic/acetate buffer was selected as optimum.

The influence of the temperature was studied between 10 and 40 °C. It could be observed that the fluorescence intensity decreased when the temperature increased. For that reason, 20 °C was chosen for further experiences.

3.2.4. Calibration curve and analytical parameters

Under the optimum physicochemical conditions, the fluorescence intensity was measured at λ_{exc} = 368 nm and λ_{em} = 426 nm. The calibration curve was obtained for different standard samples containing between 0.25 and 2.5 μg mL^{-1} of CPT-11. For each standard sample, three replicates were made. The calibration graph, I_F *versus* [CPT-11], was lineal for the CPT-11 concentration tested. Statistical parameters and analytical characteristics for the determination of CPT-11 with the proposed method at acidic medium are summarized in Table 1.

3.3. Fluorimetric study of CPT-11 in the presence of oxidant agents

Several oxidant agents, such as permanganate, hydrogen peroxide, iodine and cerium(IV) were tested, in order to investigate the behaviour of CPT-11 in its presence. Preliminary studies showed that no reaction happened between CPT-11 and hydrogen peroxide. However, a quenching of the fluorescence intensity could be observed in the presence of permanganate, iodine and cerium(IV) at acidic pH values.

Table 1
Statistical parameters for the spectrofluorimetric determination of CPT-11 in the presence of different oxidant agents and Fe(III)

	Acidic media	Oxidation with iodine	Oxidation with Ce(IV)	Reaction with Fe^{3+}
Equation	$I_F = 77.10$ [CPT-11] + 2.57	$\Delta I_F = 377.67$ [CPT-11] + 4.00	$\Delta I_F = 264.81$ [CPT-11] − 15.63	$\Delta I_F = 245.40$ [CPT-11] − 5.46
Range ($\mu g\,mL^{-1}$)	0.50–2.50	0.25–2.50	0.25–2.50	0.20–2.00
Linearity (%)	97.92	99.19	97.12	99.07
σ_{slope}	1.61	3.06	7.63	2.27
$\sigma_{intercept}$	2.15	4.10	12.30	2.51
Correlation coefficient	0.9974	0.9996	0.9942	0.9981
R.S.D. (1 $\mu g\,mL^{-1}$, $n = 11$)	2.55	1.35	1.67	1.50
L_D, $ng\,mL^{-1}$ (IUPAC)	2.05	0.46	2.57	1.96
L_D, $\mu g\,mL^{-1}$ (Long–Winefordner)	0.084	0.058	0.248	0.031
L_D, $\mu g\,mL^{-1}$ (Clayton)	0.1479	0.0326	0.1394	0.062

3.3.1. Iodine oxidation

At acidic media, the oxidation of CPT-11 by I_2/I^- was studied by spectrofluorimetry. A quenching of the fluorescence intensity could be observed. The oxidized compound, formed as a consequence of the oxidation of CPT-11 with iodine, does not present variations in the position of excitation and emission maxima. However, a difference in the excitation spectrum could be observed due to the disappearance of the maximum located at 222 nm (see Fig. 4).

The acidity was fixed with HCl and the influence of the concentration of HCl in the fluorescence intensity was studied. For that experience, different volumes of HCl 0.5 M, comprises between 10 and 100 μL were added to the CPT-11 solution. It could be observed that the fluorescence intensity decreased when the concentration of HCl increased. A volume of 40 μL of HCl 0.5 M was chosen for further experiences (4 mM).

The effect of the temperature was examined between 10 and 40 °C, and a decrease of the fluorescence could be observed with the increase of the temperature. Twenty degree Celsius was selected as optimum value.

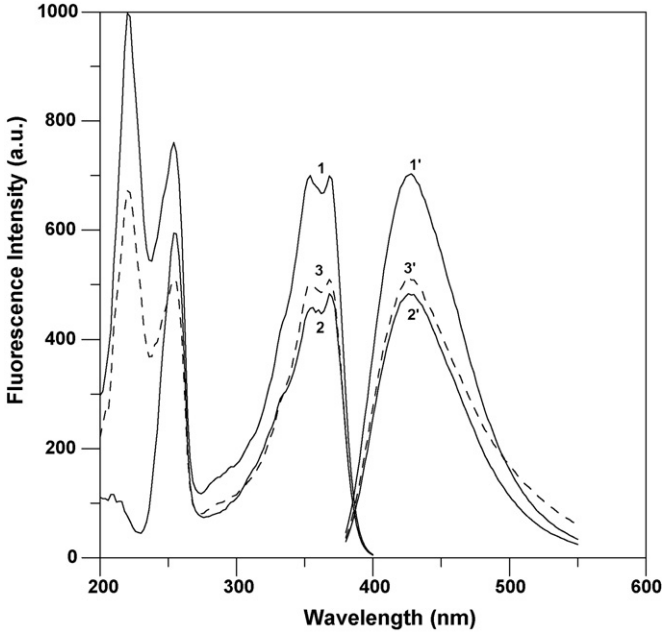

Fig. 4. Excitation and emission spectra of CPT-11 in absence of oxidant agents (1, 1′) and in the presence of I_2/I^- (2, 2′) and Ce(IV) (3, 3′).

Finally, the influence of I_2/I^- concentration was studied in the range between 0.05/0.10 and 0.53/1.05 mM of I_2/I^-, respectively. In this case, $\Delta I_F = F_o - F$, where F_o is the fluorescence in absence of iodine and F the fluorescence when iodine is present, was used as analytical signal. It could be observed that ΔI_F increased when increased the I_2/I^- concentration, thus, 0.26/0.53 mM of I_2/I^- was chosen as optimum.

Under the optimum physicochemical conditions, the calibration curve was obtained for different standard samples containing between 0.25 and 2.5 $\mu g\,mL^{-1}$ of CPT-11. For each standard sample, three replicates were made. The calibration graph, ΔI_F *versus* [CPT-11], was lineal for the CPT-11 concentration range tested. Statistical parameters and analytical characteristics for the determination of CPT-11 with the proposed method are summarized in Table 1.

3.3.2. Cerium(IV) oxidation

Similar studies were performed for the oxidation of CPT-11 with Ce(IV). As can be seen in Fig. 4, the presence of Ce(IV) gives a quenching of fluorescence (spectra 3 and 3′). Firstly, the concentration of Ce(IV) was optimized and 4×10^{-2} mM of Ce(IV) gave the best analytical signal (ΔI_F). The influence of acidity was not studied since it is controlled by the amount of Ce(IV) added, due that Ce(IV) is dissolved in sulphuric acid.

The influence of temperature was studied as well, showing no significant influence. Room temperature was selected.

Under the optimum physicochemical conditions, the calibration curve was obtained for different standard samples containing between 0.25 and 2.5 $\mu g\,mL^{-1}$ of CPT-11. For each standard sample, three replicates were made. The calibration graph (ΔI_F *versus* [CPT-11]) was lineal for the CPT-11 concentration range tested. Statistical parameters and analytical characteristics for the determination of CPT-11 with the proposed method are summarized in Table 1.

3.4. Fluorimetric study of CPT-11 in the presence of metal ions

The behaviour of CPT-11 in presence of several divalent and trivalent metal ions, such as Zn^{2+}, Cu^{2+}, Co^{2+}, Sr^{2+}, Ca^{2+}, Mg^{2+},

Fe^{3+} and Al^{3+} was tested. Preliminary studies showed that CPT-11 does not show changes in its fluorescence intensity with the presence of any metal (no interaction happened between CPT-11 and metal ions), except with Fe^{3+}, where a quenching of the fluorescence intensity could be observed in the presence of this metal at acidic pH values.

At acidic media, the complex formed between CPT-11 and Fe^{3+} ion was studied by spectrofluorimetry. Again, ΔI_F was used as analytical signal. The complex formed does no present variations in the position of excitation and emission maxima.

The change in the fluorescence of CPT-11:Fe^{3+} as a function of pH was studied. For that, a solution was prepared containing 500 ng mL^{-1} of CPT-11, 1.0 mM of Fe^{3+} and KCl 0.5 M, in order to maintain constant the ionic strength. The pH was modified with slightly additions of HCl or NaOH. The solution was keeping stirring all time. It could be seen that when pH increases, the fluorescence signal of the complex also increases until reach a maximum at pH 2.8. At higher pH values there is a quenching of the fluorescence signal, probably due to the formation of the corresponding hydroxide.

The influence of Fe^{3+} concentration was studied in the range between 0.5 and 3.0 mM. There is a quenching of fluorescence intensity of CPT-11 when concentration of Fe^{3+} increases. A concentration of 2.5 mM of Fe^{3+} was chosen as optimum.

The acidity was maintained with 0.1 M of chloracetic buffer (pH 2.8). For that experience, different concentrations of chloracetic buffer comprises between 0.05 and 0.20 M were tested. It could be observed that the fluorescence intensity decreased when the concentration of chloroacetic buffer increased.

The effect of the temperature was examined between 10 and 40 °C and no significant influence was observed, thus, 20 °C was selected as optimum. Addition order was studied and no influence was observed. However, CPT-11 + Fe^{3+} + buffer were chosen to perform the experiments.

Under the optimum physicochemical conditions, the calibration curve was obtained for different standard samples containing between 0.20 and 2.0 μg mL^{-1} of CPT-11. For each standard sample, three replicates were made. The calibration graph, ΔI_F *versus* [CPT-11] was lineal for the CPT-11 concentration range tested. Statistical parameters and analytical characteristics for the determination of CPT-11 with the proposed method are summarized in Table 1.

3.5. Application to human urine samples

Due to the difficulty to obtain real urine samples, the four proposed methods have been applied to the analysis of human urine samples spiked whit CPT-11. A survey of the literature [10] allows us choose the range in which CPT-11 is present in urine. The administered dose of CPT-11 varies between 100 and 350 mg/m^2, this take us to conclude that to know which the optimal dose of a patient is; it is necessary to know the body surface area (BSA), expressed in square meters (m^2). For this calculation, a nomogram was used.

A nomogram [27] is a table o three columns that correlates a person's height and weight. The patient's height is located in the left column, the weight is found in the right column, and a ruler is used to draw a line between the two. The point at which the line intersects the middle column represents the patient's BSA.

For example, if a patient has a weight of 80 kg and a height of 1.76 m, its BSA is 2 m^2. For this patient, the administered dose would be

$$\text{dose} = 100\text{–}350\,\text{mg/m}^2 \times 2\,\text{m}^2 = 200\text{–}700\,\text{mg of CPT-11}$$

Taking into account that 10–22% of this dose is excreted in the urine in the first 24 h, the concentration range of CPT-11 studied was comprises between 0.5 and 1.5 μg mL^{-1}. Only a dilution 1:20 of urine samples was assayed and after the application of the four methods proposed above, satisfactory recoveries for CPT-11 were obtained, comprises between 100.0 and 104.3% (Table 2). No interference of the matrix sample in these conditions was observed.

An analysis of the recoveries leads us to the conclusion that for the analysis of the assayed concentrations the four spectrofluorimetric methods are adequate. However, it is convenient to indicate that the most sensitive and reproducible method is the oxidation with iodine, for that, this one would be the most indicate for the analysis of traces of CPT-11 in urine samples.

Table 2
Recoveries obtained with the proposed spectrofluorimetric methods in urine samples

[CPT-11] added	Fluorimetric method		Oxidation with iodine		Oxidation with Ce(IV)		Reaction with Fe^{3+}	
	[CPT-11] found	% *R* (R.S.D.)	[CPT-11] found	% *R* (R.S.D.)	[CPT-11] found	% *R* (R.S.D.)	[CPT-11] found	% *R* (R.S.D.)
	0.495	100.7 (1.5)	0.514	102.3 (0.6)	0.499	100.0 (1.0)	0.529	104.3 (1.5)
0.500	0.505		0.511		0.502		0.517	
	0.509		0.510		0.500		0.518	
	1.007	100.0 (1.0)	1.007	101.3 (0.6)	1.027	103.3 (0.6)	1.023	100.7 (2.3)
1.000	0.995		1.018		1.032		0.985	
	1.002		1.015		1.037		1.020	
	1.512	101.0 (1.0)	1.519	100.7 (0.6)	1.516	101.7 (0.6)	1.468	102.3 (4.0)
1.500	1.513		1.506		1.526		1.587	
	1.514		1.513		1.526		1.540	
Recoveries media (S.D.)		100.6 (2.1)		101.4 (1.0)		101.7 (1.3)		102.4 (4.9)

Concentration in μg mL^{-1}. By RP-HPLC validation method, the recoveries found were 104.0 ± 2.0.

Table 3
Recoveries obtained with the proposed spectrofluorimetric methods in the analysis of the pharmaceutical formulation CAMPTO

	Fluorimetric method	Oxidation with iodine	Oxidation with Ce(IV)	Reaction with Fe^{3+}
[CPT-11] found	1.197 1.213 1.197	1.141 1.139 1.138	1.082 1.118 1.087	1.061 1.057 1.068
% *R* (R.S.D.)	119.7 (1.2)	114 (1.0)	109.7 (2.1)	106.7 (2.5)

[CPT-11] = 1.0 μg mL^{-1}. By RP-HPLC validation method, the recoveries found were 119.7 ± 2.5.

The methods were validated, using the RP-HPLC method mentioned in Section 2.6, in order to establish which one was the best. Determination of analyte by HPLC methodology was performed three times and each solution of them was injected three times into the system. The recoveries media obtained was 104.0 ± 2.0, which is in agreement with the conclusion obtained above.

3.6. Application to pharmaceutical formulations

The proposed methods have been applied to the pharmaceutical formulation of CPT-11 (CAMPTO of Aventis-Pharma). Samples with appropriate concentration (1 μg mL^{-1}) of CAMPTO were compared with samples of CPT-11 standard of the same concentration. All samples were prepared by triplicate as mentioned in Section 2.3. After the application of the four methods proposed above, the recovery values obtained for CAMPTO samples were comprises between 106.7 and 119.7%, as can be seen in Table 3.

Also, the methods were validated, by RP-HPLC, for the analysis of the pharmaceutical formulation CAMPTO, obtaining in this case, a recoveries media of 119.7 ± 2.5. This led us to the conclusion that the fluorimetric method is the most adequate for the analysis of pharmaceutical formulations, although the oxidation with iodine could be used too.

4. Conclusions

In this paper four spectrofluorimetric methods for the determination of CPT-11 are proposed. All of them present several advantages, such as, rapid preparation of the samples because it is not necessary a pre-treatment and short time of analysis, all the measurements can be made just after preparation.

The fluorescence characteristics of CPT-11 have been established in acidic and basic media. Due to the active form of CPT-11 is the lactone one and this only can be found in acidic media, one method has been proposed in this media for its characterization. CPT-11 can be oxidized by the presence of Ce(IV) and iodine. The conditions for the oxidation have been optimized. Also, several metal ions have been tested. Only Fe^{3+} reacted with CPT-11 producing a quenching of the fluorescence.

When the statistical parameters of the four methods were compared, they showed very good linearity in all cases. A comparison of slopes shows that the oxidation with iodine give the highest sensitivity, this is confirmed with the limit of detection, the reaction with iodine shows the lowest limit, concretely, 0.46 ng mL^{-1}. The highest limit of detection is 2.57 ng mL^{-1}, obtained when CPT-11 is oxidized with Ce(IV).

The proposed methods were applied to human urine and pharmaceutical preparations. For the human urine only a dilution with water was necessary and recoveries around 100% were obtained. No interference of the matrix sample was observed. When the pharmaceutical preparation was analyzed higher recoveries were obtained, comprises between 106.7 and 119.7%. In order to validate the obtained results a RP-HPLC method was used. It could be concluded that the four spectrofluorimetric methods were adequate for the analysis of urine samples, being the oxidation with iodine the one which give lower standard deviation values. However, for the analysis of the pharmaceutical preparation is the method based on the direct measurement of the fluorescence intensity at acidic pH the one that is in agreement with the results obtained by RP-HPLC.

In conclusion, four simple and sensitive methods have been proposed for the determination of CPT-11 in human urine and pharmaceutical preparations.

Acknowledgements

The authors are grateful to MEC of Spain (Project CTQ2004-02142) and CONACyT of México.

References

[1] G.C. Chabot, Clin. Pharmacokinet. 33 (1997) 245–259.
[2] A. Alimonti, A. Gelibter, I. Pavese, F. Satta, F. Cognetti, G. Ferretti, D. Rasio, A. Vecchione, M. Di Palma, Cancer Treat. Rev. 30 (2004) 555–562.
[3] H. Wilke, O. Bouché, P. Rougier, C.H. Köhne, EJC Suppl. 7 (2004) 48–51.
[4] M.H. Jagasia, C.J. Langer, D.H. Johnson, F. Yunus, J.S. Rodgers, L.L. Schlabach, A.G. Cohen, Y. Shyr, D.P. Carbone, R.F. DeVore, Clin. Cancer Res. 7 (2001) 68–73.
[5] H.C. Pilot, R.M. Goldberg, J.M. Reid, J.A. Sloan, P. Atherton Skaff, C. Erlichman, J. Rubin, P.A. Burch, A.A. Adjei, S.A. Alberts, L.J. Schaaf, G. Elfring, L.L. Miller, Clin. Cancer Res. 6 (2000) 2236–2244.
[6] D. Abigerges, J.P. Armand, G.G. Chabot, L. Da Costa, E. Fadel, C. Cote, P. Herait, D. Gandia, J. Natl. Cancer Inst. 86 (1994) 446–449.
[7] L.P. Rivory, E. Chanelut, P. Canal, A. Mathieu-Boue, J. Robert, Cancer Res. 54 (1994) 6330–6333.
[8] T. Itoh, I. Takemoto, S. Itagakli, K. Sasaki, T. Hirano, K. Iseki, J. Pharm. Pharmaceut. Sci. 7 (2004) 13–18.
[9] F. Lokiec, P. Canal, C. Gay, E. Chatelut, J.P. Armand, H. Roche, R. Bugat, E. Gaoncalves, A. Matieu-Boue, Cancer Chemother. Pharmacol. 36 (1995) 79–82.
[10] R.H.J. Mathijssen, T.J. van Alphen, J. Verweij, W.J. Loos, K. Nooter, G. Stoter, A. Sparreboom, Clin. Cancer Res. 7 (2001) 2182–2194.
[11] E. Gravel, P. Bourget, L. Mercier, A. Paci, J. Pharm. Biomed. Anal. 39 (2005) 581–586.

[12] S. Poujol, F. Pinguet, F. Malosse, C. Astre, M. Ychou, S. Culine, F. Bressolle, Clin. Chem. 49 (2003) 1900–1908.
[13] T.S. Owens, H. Dodds, K. Fricke, S.K. Hanna, K.R. Crews, J. Chormatogr. B: Anal. Thechnol. Biomed. Life Sci. 788 (2003) 65–74.
[14] A. Sparreboom, P. de-Brujin, M.J.A. de-Jonge, W.J. Loos, G. Stoter, J. Verweij, K. Nooter, J. Chromatogr. B: Biomed. Appl. 712 (1998) 225–235.
[15] D.F. Chollet, L. Goumaz, A. Renard, G. Montay, L. Vernillet, V. Arnera, D.J. Mazzo, J. Chromatogr. B: Biomed. Appl. 718 (1998) 163–175.
[16] V.M.M. Herben, D. Mazee, D.M. va-Gortel-vanZomeren, S. Zeedijk, H. Rosing, J.H.M. Schellens, W.W. ten-Bokkel-Huinink, J.H. Beijnen, J. Liq. Chromatogr. Relat. Technol. 21 (1998) 1541–1558.
[17] B. Di, F. Fang, Y.Y. Li, L.J. Yu, H.L. Song, Z.X. Zhang, Yaowu-Fenxi-Zazhi 19 (1999) 293–296.
[18] S. Bardin, W. Guo, J.L. Johnson, S. Khan, A. Ahmad, J.X. Duggan, J. Ayoub, I. Ahmad, J. Chromatogr. A 1073 (2005) 249–255.
[19] S. Ragot, P. Marquet, F. Lachatre, A. Rousseau, E. Lacassie, J.M. Gaulier, J.L. Dupuy, G. Lachatre, J. Chromatogr. B: Biomed. Appl. 736 (1999) 175–184.
[20] J. Dey, I.M. Warner, J. Photochem. Photobiol. A: Chem. 101 (1996) 21–27.
[21] J. Dey, I.M. Warner, J. Luminiscence 71 (1997) 105–114.
[22] I. Chourpa, J.M. Millot, G.D. Sockalingum, J.F. Riou, M. Manfait, Biochem. Biophys. Acta 1379 (1998) 353–366.
[23] Y. Posokhov, H. Biner, S. Içli, J. Photochem. Photobiol. A: Chem. 158 (2003) 13–20.
[24] D. Dvoranová, V. Brezová, M. Valko, A. Stasko, J. Photochem. Photobiol. A: Chem. 185 (2007) 172–180.
[25] J. Escoriaza, A. Aldaz, C. Castellanos, E. Calvo, J. Giráldez, J. Chromatogr. B 740 (2000) 159–168.
[26] R.F. Wilson, G.W. Lester, Talanta 10 (1963) 319–322.
[27] D.C. Baquiran, Cancer Chemotherapy Handbook, second ed., Lippincott, 2001.

Available online at www.sciencedirect.com
ScienceDirect
Talanta 74 (2008) 1236–1241
Talanta
www.elsevier.com/locate/talanta

Reverse flow injection spectrophotometric determination of iron(III) using chlortetracycline reagent

Wirat Ruengsitagoon *

Department of Pharmaceutical Chemistry, Faculty of Pharmaceutical Sciences, Khon Kaen University, Khon Kaen 40002, Thailand

Received 16 July 2007; received in revised form 28 August 2007; accepted 28 August 2007
Available online 2 September 2007

Abstract

A simple reversed flow injection colourimetric procedure for determining iron(III) was proposed. It is based on the reaction between iron(III) with chlortetracycline, resulting in an intense yellow complex with a suitable absorption at 435 nm. A 200 μl chlortetracycline reagent solution was injected into the phosphate buffer stream (flow rate 2.0 ml min^{-1}) which was then merged with iron(III) standard or sample in dilute nitric acid stream (flow rate 1.5 ml min^{-1}). Optimum conditions for determining iron(III) were investigated by univariate method. Under the optimum conditions, a linear calibration graph was obtained over the range 0.5–20.0 μg ml^{-1}. The detection limit (3σ) and the quantification limit (10σ) were 0.10 and 0.82 μg ml^{-1}, respectively. The relatives standard deviation of the proposed method calculated from 12 replicate injections of 2.0 and 10.0 μg ml^{-1} iron(III) were 0.43 and 0.59%, respectively. The sample throughput was 60 h^{-1}. The proposed method has been satisfactorily applied to the determination of iron(III) in natural waters.
© 2007 Elsevier B.V. All rights reserved.

Keywords: Flow injection; Reverse flow injection; Chlortetracycline; Iron(III)

1. Introduction

Iron is the fourth most abundant element in the earth's crust. The main source of iron in natural waters is from the weathering and leaching of rocks and soils. It is present as iron(II) and iron(III) states in natural waters, but it is usually present in the iron(III) state, and its salts are readily hydrolysed to insoluble forms, so the concentration of iron in natural waters is generally low [1].

Several methods for the determination of iron(III) using chelating agents have been reported. Some of these methods, reagents such as *o*-phenylenediamine with hydrogen peroxide [2], *p*-anisidine with *N*,*N*-dimethylaniline [3], ammonium thiocyanate [4–8], tiron [9], 3,3′,5,5′-tetramethylbenzidine [10], salicylate [11] and norfloxacin [12] have been used for the selective determination of iron(III). Other methods used Cd-Hg reductor column [13] or ferrozine [14], and coupled with reduction of iron(III) to iron(II), for a total iron determination, and a portable colourimeter using a red–green–blue light-emitting diode as a light source has been developed [15].

Iron(III) has been determined spectrophotometrically through complexation with tetracycline in acidic solution and subsequent measurement of the yellow complex formed at 423 nm [16]. However, a report of reverse flow injection method for the determination of iron(III) in natural waters using chlortetracycline as the complexing agent has not been yet available in the literature.

Chlortetracycline is an antibiotic, which is derived from *Streptomyces aureofaciens*. It has broad-spectrum activity against many gram-positive and gram-negative bacteria. In the present work, a new reverse flow injection (rFI) spectrophotometric method is proposed for the determination of total iron(III) in natural waters using chlortetracycline as the chromogenic agent. The normal FIA technique involves injection of a small volume of standard or sample into a stream of reagent flowing through the FIA system [17,18]. In the reverse flow injection, it is the reagent that is injected into the flowing system which is made up of the sample and some other solution [19]. Reverse flow injection mode has advantageous features such as high

* Tel.: +66 43 202378; fax: +66 43 202379.
E-mail address: wirat_ru@kku.ac.th.

0039-9140/$ – see front matter © 2007 Elsevier B.V. All rights reserved.
doi:10.1016/j.talanta.2007.08.031

sensitivity, selectivity, simple sample preparation and very low consumption of reagent.

This paper studies a rapid, sensitive and cost-effective reverse flow injection method for determination of iron(III) based on the spectrophotometric detection of the yellow complex formed by the reaction between iron(III) ions and chlortetracycline reagent. The resulting yellow complex is measured at 435 nm. The proposed method was successfully applied to the determination of total iron(III) in natural waters.

2. Experimental

2.1. Reagents

All chemicals were of analytical reagent grade and were used without further purifications. All solutions were prepared with distilled deionized water.

A stock solution of 100 μg ml^{-1} iron(III) was prepared by dissolving 8.6340 g of ammonium ferric sulfate dodecahydrate (Fluka) in 5.0×10^{-3} mol l^{-1} nitric acid (Merck) and diluting to 1000 ml in a volumetric flask. Solutions of iron(III) standards were obtained by appropriate, accurate dilutions of this solution with 5.0×10^{-3} mol l^{-1} nitric acid. The hydrochloride of chlortetracycline (CTC) was purchased from Fluka. Its stock reagent solution (1000 μg ml^{-1}) was prepared by dissolving 0.1000 g of this reagent in water and diluting to 100 ml. Phosphate buffer solution (pH 8.0) was prepared by dissolving of 2.8 g disodium hydrogen phosphate (BDH) and 14.0 g potassium dihydrogen phosphate (BDH) in 700 ml water. The solution was then adjusted to pH 8.0 with 0.1 mol l^{-1} sodium hydroxide or 0.1 mol l^{-1} phosphoric acid, and then diluted to 1000 ml.

2.2. Apparatus

The reverse flow injection manifold consisted of a peristaltic pump (Eyela® MP3A, Tokyo Rikakikai Co. Ltd., Japan), with the chlortetracycline reagent solution injected via a four way PTFE rotary valve with a 200 μl sample loop (Rheodyne® model 5041, Cotati, CA). PVC tubing (Elkay®, Galway, Ireland) with 0.8 mm i.d. was used as a flow line for iron(III) standard solutions, and phosphate buffer solution, and a Y-shaped connector was used for merging the reagent streams. A mixing coil used was made from PTFE tubing, 0.8 mm i.d. and 75 cm in length for the recommended configuration. The rFI peaks were acquired by using a UV–vis detector (Thermo Separation Product®, TSP UV-2000, USA), coupled with a chart recorder (Kipp & Zonen® BD50, The Netherlands).

2.3. Recommended procedure

Using the experimental setup as shown in Fig. 1, a 200 μl reagent solution containing chlortetracycline was injected into a stream of phosphate buffer solution at the optimum flow rate of 2.0 ml min^{-1} which was then merged with the iron(III) standard or sample solution in 5.0×10^{-3} mol l^{-1} nitric acid (HNO_3) with an optimum flow rate of 1.5 ml min^{-1}. Subsequently, the sample zone flowed through the 75 cm in length of reaction coil, where

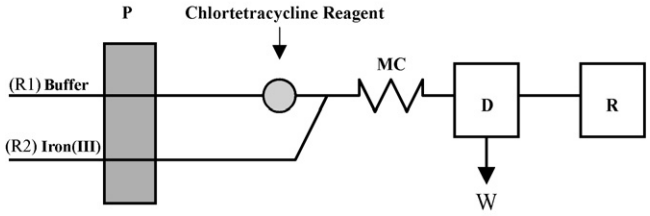

Fig. 1. Proposed FI manifold: R1, buffer solution; R2, acidic iron(III) standard/sample solution; P, pump; MC, mixing coil; D, detector; R, recorder; W, waste.

the complexation occurred. The absorption was monitored at 435 nm and the rFI signal was recorded using a chart recorder.

2.4. Sample preparation

The water samples were collected in 1000 ml polyethylene bottles from natural pond within Khon Kaen University, Khon Kaen Province without treatment with concentrated nitric acid, and analysed immediately after sample digestion. The water samples were filtered through No 41 Whatman filter paper then 100.00 ml of each filtered water sample was accurately transferred into a 250 ml round bottom flask, and 10.00 ml of a mixture consisting of HNO_3 and H_2O_2 (1:9, v/v) were added. These samples were digested by heating under reflux for 1.5 h. The cooled samples were transferred into each of 100 ml volumetric flask and made up to the mark with deionized distilled water, mixed well, then subsequently analyzed by the proposed rFI method and FAAS.

3. Results and discussion

3.1. Optimisation of the reverse flow injection system

The proposed flow system was investigated for development of an rFI procedure for iron(III) determination based on the complexation between iron(III) ions and chlortetracycline [7-chloro-4-(dimethylamino)-1,4,4a,5,5a,6,11,12a-octahydro-3,6,10,12,12a-pentahydroxy-6-methyl-1,11-dioxo-2-naphthacenecarboxamide monohydrochloride] resulting in yellow soluble complex having an absorption maximum at 435 nm. This is an adaptation of that reported for a batchwise method [16]. The metal-to-ligand ratio was determined by the mole ratio and continuous variation method, and was found to be 1:2 (Fig. 2). The variable by variable method was applied to select the optimum conditions for the reverse flow injection spectrophotometic determination of iron(III).

3.1.1. Effect of absorption spectra

The absorption spectra of the coloured complex obtained by complexation reaction between iron(III) ions and chlortetracycline and the reagent blank were measured over the range of 350–500 nm using a spectrophotometer. The absorption maximum of the complex was 435 nm. In order to achieve the greatest sensitivity, measurements were made at 435 nm in further studies.

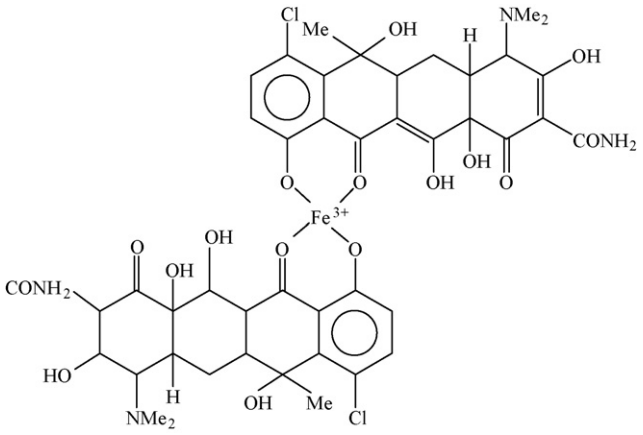

Fig. 2. Complexation between iron(III) ions and chlortetracycline.

3.1.2. Effect of chlortetracycline reagent concentration

The effect of varying concentrations of chlortetracycline reagent solution between 100 and 900 μg ml^{-1} was examined. The highest peak height was obtained when the concentration of chlortetracycline reagent was 500 μg ml^{-1}, so this concentration was chosen as the optimum concentration in order to obtain the greatest sensitivity. Above 500 μg ml^{-1}, further increase in the chlortetracycline reagent concentration to 900 μg ml^{-1} resulted in slight increase in peak height (Fig. 3).

3.1.3. Effect of mineral acids

The effect of 5.0×10^{-3} mol l^{-1} HNO_3, $HClO_4$, HCl, H_2SO_4 and H_3PO_4 in iron(III) standard solution was studied. The relative peak height were 100.0, 88.44, 64.16, 56.20 and 37.25%, respectively. The presence of HNO_3 gave the highest peak height, so was chosen for subsequent studies (Fig. 4).

The concentration of HNO_3 in iron(III) standard solutions was optimised. Various concentrations over the range 5.0×10^{-5} to 5.0×10^{-1} mol l^{-1} were investigated, and the HNO_3 concentration chosen for further studies was 5.0×10^{-3} mol l^{-1} because this concentration gave a maximum peak height (Fig. 5).

3.1.4. Effect of pH

The complex formed by the reaction between 10 μg ml^{-1} iron(III) standard solution and chlortetracycline reagent was studied at various pH value (pH 5.0–12.0). The results were shown in Fig. 6. It was seen that when the pH of the phosphate buffer stream was adjusted to 8.0, the greatest peak height was obtained. The results obtained by the present experiments were in good agreement with those reported by Pena et al. [20] and Liawruangrath et al. [21]. The stability of chlortetracycline was poor under strong acidic and alkaline conditions along with a reversible formation of epimers at position C4 to 4-epichlortetracycline in weak acid and anhydrochlortetracycline under strong acidic conditions [22]. Further increasing to pH 12.0 the peak height were slightly increased. Hence, pH 8.0 was chosen as optimum.

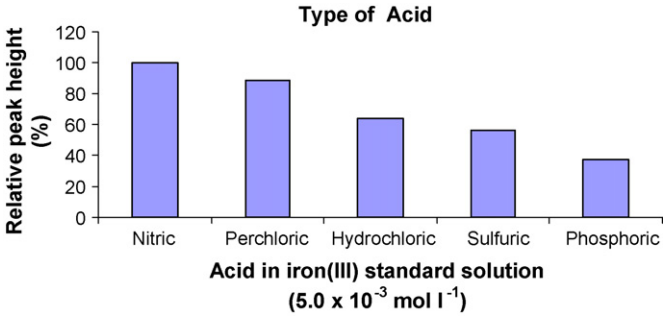

Fig. 4. Effect of type of acid on the mean peak height ($n = 5$) of 10 μg ml^{-1} iron(III) standard solution.

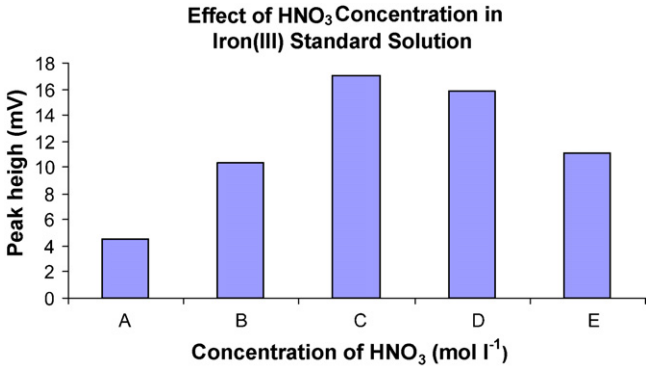

Fig. 5. Effect of HNO_3 concentration on the mean peak height ($n = 5$) of 10 μg ml^{-1} iron(III) standard solution ((A) 5.0×10^{-1}; (B) 5.0×10^{-2}; (C) 5.0×10^{-3}; (D) 5.0×10^{-4} and (E) 5.0×10^{-5} mol l^{-1} of HNO_3).

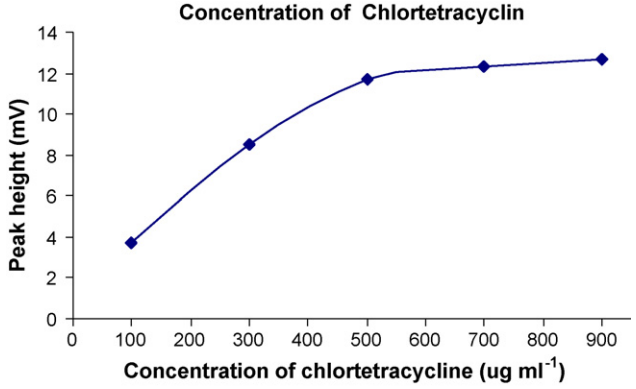

Fig. 3. Effect of chlortetracycline concentration on the mean peak height ($n = 5$) of 10 μg ml^{-1} iron(III) standard solution.

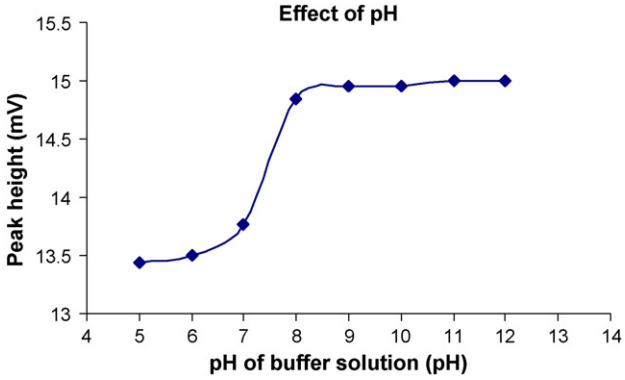

Fig. 6. Effect pH of buffer solution on the mean peak height ($n = 5$) of 10 μg ml^{-1} iron(III) standard solution.

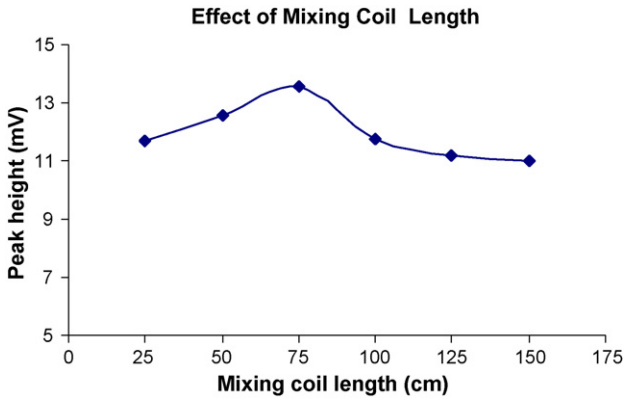

Fig. 7. Effect of mixing coil length on the mean peak height ($n = 5$) of 10 μg ml^{-1} iron(III) standard solution.

3.1.5. Effect of mixing coil length and injection loop volume

This study was carried out at various mixing coil lengths between 25 and 150 cm, and injection loop volumes between 50 and 300 μl on the complexation produced were investigated. It was found that the peak height increased with the mixing coil length up to 75 cm, and the mixing coil lengths of 25, 50, 75, 100, 125 and 150 cm provided the peak height of 11.66, 12.56, 13.58, 11.78, 11.22 and 11.00 mV, respectively (Fig. 7).

The influence of the reagent volume on the absorbance was investigated by injecting volumes in the range 50–300 μl of 500 μg ml^{-1} chlortetracycline reagent solution. It was seen that peak height increased from 7.77 to 15.69 mV on increasing the injection volume from 50 to 300 μl. It was found that the peak height increased with the injection volume up to 200 cm, and the injection volume of 50, 100, 150, 200, 250 and 300 μl produced the peak height of 7.77, 9.41, 13.45, 15.03, 15.24 and 15.69 mV, respectively. The appropriate peak height was reached at 200 μl. The most suitable mixing coil length and injection loop volume values for further use were 75 cm and 200 μl, respectively (Fig. 8).

3.1.6. Effect of reagent flow rate

The effect of flow rate of phosphate buffer solution (pH 8.0) and iron(III) standard solution (10 μg ml^{-1}) were investigated over the range 0.5–3.5 ml min^{-1} for both streams. Maximal peak

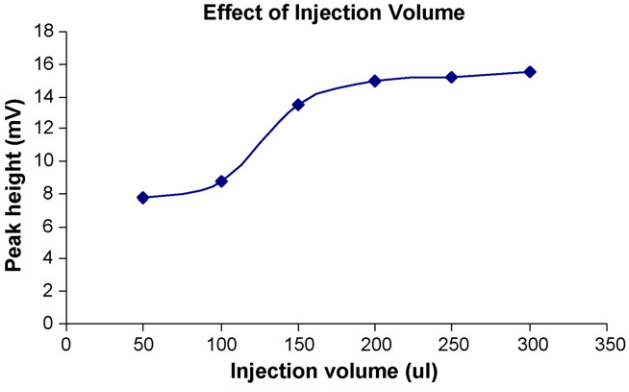

Fig. 8. Effect of injection volume on the mean peak height ($n = 5$) of 10 μg ml^{-1} iron(III) standard solution.

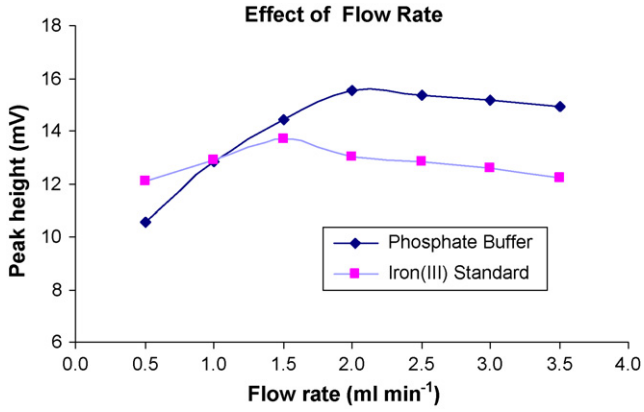

Fig. 9. Effect of flow rate on the mean peak height ($n = 5$) of 10 μg ml^{-1} iron(III) standard solution.

heights were obtained at 2.0 and 1.5 ml min^{-1} for phosphate buffer solution and iron(III) standard solution, respectively. Thus, 2.0 ml min^{-1} phosphate buffer solution and 1.5 ml min^{-1} iron(III) standard solution were regarded as the optimum flow rates (Fig. 9).

3.2. Analytical characteristics

Table 1 summarizes the optimum values of all the parameters studied in the proposed rFI method for the determination of iron(III).

3.2.1. Calibration curve

Using the proposed rFI manifold for iron(III) determination under the optimum conditions, the linear calibration curve over the range of 0.5–20.0 μg ml^{-1} iron(III) was established which can be expressed by the regression equation $y = 1.3613x + 0.0207$ ($r^2 = 0.997$) where y represents the peak height in mV and x is iron(III) concentration in μg ml^{-1} after subtraction of blank. The

Table 1
Variables range studied and optimum conditions for determination of iron(III)

Parameters studied	Range	Optimum
Wavelength (nm)	350–500	435
Chlortetracycline reagent concentration (μg ml^{-1})	100–900	500
Type of acid	HNO_3, HCl, H_2SO_4, H_3PO_4, $HClO_4$	HNO_3
HNO_3 concentration (mol l^{-1})	5.0×10^{-1} to 5.0×10^{-5}	5.0×10^{-3}
pH of buffer solution	5.0–12.0	8.0
Mixing coil length (cm)	25–150	75
Sample injection volume (μl)	50–300	200
Flow rate of iron(III) (ml min^{-1})	0.5–3.5	1.5
Flow rate of phosphate buffer (ml min^{-1})	0.5–3.5	2.0
Detector: UV–vis detection unit		
Rise time (s)	–	1.0
Display	–	AU
Range (AUFS)	–	0.20
Temperature	–	Room temperature

detection limit was defined as the concentration of analyte that gave the signal that was different from the blank by an amount equal to three times the standard deviation of the blank signal (3σ). It was found to be 0.10 μg ml^{-1} iron(III). The quantification limit is defined as the analyte producing a signal that is at least 10 times the standard deviation of the blank signal (10σ), and was found to be 0.82 μg ml^{-1} iron(III).

3.2.2. Reproducibility and accuracy

The relative standard deviation of the proposed method (peak height in mV) calculated from 12 replicate injections of 2.0 and 10.0 μg ml^{-1} of iron(III) was 0.43 and 0.59%, respectively. The accuracy expressed in term of percentage recovery was studied by spiking various amounts of iron(III) standard solution (2.0, 5.0 and 10.0 μg ml^{-1}) into the water samples. The percentage recoveries of 2.0, 5.0 and 10.0 μg ml^{-1} ($n = 7$) of iron(III) were found to be 98.86, 99.06 and 99.17%, respectively. It can be proved that the proposed method provides accurate results.

3.2.3. Interferences

Effects of some possible interfering ions on the determination of iron(III) were investigated with a maximum w/w ratio of interfering ions to iron(III) up to 50:1. Synthetic sample solutions containing 5.0 μg ml^{-1} of iron(III) and different concentrations of some metal ions at 50 and 250 μg ml^{-1} were tested, and peak heights were measured. All cations and anions tested caused interference <±10% for determining the analyte of interest. However, the most serious interference from tin(II) ions was observed (Table 2). The possible masking reagent for reducing the effect of tin(II) was trisodium citrate [23].

Table 2
Effect of some ions on the peak height of 5.0 μg ml^{-1} iron(III) standard solution ($n = 5$)

Interferences (μg ml^{-1})	Relative percentage of peak height (%)
None	100.00
Ca^{2+} (50)	102.99
Ca^{2+} (250)	108.74
Zn^{2+} (50)	102.35
Zn^{2+} (250)	103.35
Mg^{2+} (50)	98.08
Mg^{2+} (250)	96.70
Sn^{2+} (50)	28.25
Sn^{2+} (250)	22.39
Pb^{2+} (50)	93.50
Pb^{2+} (250)	90.24
Mn^{2+} (50)	104.16
Mn^{2+} (250)	108.77
Cu^{2+} (50)	101.12
Cu^{2+} (250)	105.27
NO_3^- (50)	98.96
NO_3^- (250)	92.75
SO_4^{2-} (50)	97.62
SO_4^{2-} (250)	90.13

Table 3
Accuracy of propose rFI method compared with FAAS method for determination of iron(III)

Samples[a]	Iron(III) found (μg ml^{-1})		
	rFI[b]	FAAS[c]	*t*-test
1	0.83	0.98	
2	1.08	1.05	
3	1.32	1.40	
4	3.51	3.48	
5	1.76	1.72	
6	1.12	0.95	
7	0.97	1.07	
8	2.67	2.45	
9	1.75	1.58	
10	2.28	2.09	
			$D = 0.04$
			S.D. = 0.0065
			$t = 1.95$
			t-Distribution (95%) = 2.23

[a] Average from five determinations.
[b] Reverse flow injection.
[c] Flame atomic absorption spectrophotometry.

3.2.4. Analysis of total iron in natural water samples

The method developed above was applied to the determination of total iron in natural waters after digesting the water sample with HNO_3:H_2O_2 (1:9, v/v) and heating under reflux for 1.5 h. The results obtained were compared favorably with those obtained by FAAS (Table 3). The accuracy was verified by the Student's *t*-test [24] with calculated Student's *t*-test value (1.95) less than the theoretical value (2.23, $n = 10$) at a confidence level of 95% (P value of 0.05). Reasonable agreement between rFI and FAAS methods was found.

The study also investigated to find out the use of cheap chlortetracycline reagent obtained from chlortetracycline capsules (commercially available in drug stores in Thailand) instead of the commercial standard one. This is a less expensive source of chlortetracycline than purum grade (>97%) of chlortetracycline. It was found that the relative peak heights from chlortetracycline reagent and chlortetracycline capsule were 100.00 and 105.34% ($n = 5$), respectively. It might be possible to use chlortetracycline capsules as a cheap and easily available alternative for the determination of iron(III) using this rFI method.

4. Conclusion

The proposed rFI spectrophotometric method has proved to be simple and cost-effective for determination iron(III) in water samples. This rFI method is based on complexation between iron(III) and chlortetracycline has been developed in which a small volume of chlortetracycline was injected into an iron(III) standard or sample stream and the resulting 1:2 complex of iron(III)—chlortetracycline monitored at 435 nm. The linearity of the calibration graph is in the useful range for quantitation of iron(III) in natural waters, with detection limit of 0.10 μg ml^{-1}. This method is fast and reasonably economic, providing a good sample frequency of 60 h^{-1}, and should be useful for routine analysis of iron(III) in natural waters.

Acknowledgements

The authors gratefully acknowledge Khon Kaen University for financial support. The special thanks are also expressed to the Pharmaceutical Chemistry Department, Faculty of Pharmaceutical Sciences, for their partial support of the research.

References

[1] J.R. Dojlido, G.A. Best, Chemistry of Water and Water Pollution, Ellis Horwood Limited, Chichester, 1993.
[2] S. Kawakubo, Y. Okazaki, M. Iwatsuki, Anal. Sci. 19 (2003) 373.
[3] S. Ohno, M. Tanaka, N. Teshima, T. Sakai, Anal. Sci. 20 (2004) 171.
[4] A.C.L. Conceição, M.T. Tena, M.M.C. Santos, M.L.S. Gonçalves, M.D.L. Castro, Anal. Chim. Acta 343 (1997) 191.
[5] H. Bagheri, A. Gholami, A. Najafi, Anal. Chim. Acta 424 (2000) 233.
[6] K. Oguma, O. Yoshioka, Talanta 58 (2002) 1077.
[7] C. Pons, R. Forteza, V. Cerdà, Anal. Chim. Acta 524 (2004) 79.
[8] C. Pons, R. Forteza, V. Cerdà, Talanta 66 (2005) 210.
[9] J.F. Staden, H. Plessis, R.E. Taljaard, Anal. Chim. Acta 357 (1997) 141.
[10] A. Tsuji, N. Teshima, M. Kurihara, S. Nakano, T. Kawashima, Talanta 52 (2000) 161.
[11] Y. Udnan, J. Jakmunee, S. Jayasavati, G.D. Christian, R.E. Synovec, K. Grudpan, Talanta 64 (2004) 1237.
[12] T. Pojanagaroon, S. Watanesk, V. Rattanaphani, S. Liawruangrath, Talanta 58 (2002) 1293.
[13] A.A. Ensafi, M.A. Chamjangali, H.R. Mansour, Anal. Sci. 20 (2004) 645.
[14] M.I.P. Pascual-Reguera, I. Ortega-Carmona, A. Molina-Díaz, Talanta 44 (1997) 1793.
[15] Y. Suzuki, T. Aruga, H. Kuwahara, M. Kitamura, T. Kuwabara, S. Kawakubo, M. Iwatsuki, Anal. Sci. 20 (2004) 975.
[16] S.M. Sultan, F.O. Suliman, S.O. Duffuaa, I.I. Abu-Abdoun, Analyst 117 (1992) 1179.
[17] J. Ruzicka, E.H. Hansen, Anal. Chim. Acta 78 (1975) 145.
[18] J. Ruzicka, E.H. Hansen, Flow Injection Analysis, second ed., Wiley, New York, 1988.
[19] K.S. Johnson, R.L. Petty, Anal. Chem. 54 (1982) 1185.
[20] A. Pena, A. Carmona, A. Barbosa, C. Lino, I. Silveira, B. Castillo, J. Pharm. Biomed. Anal. 18 (1998) 839.
[21] S. Liawruangrath, B. Liawruangrath, S. Watanesk, W. Ruengsitagoon, Anal. Sci. 22 (2006) 15.
[22] H. Oka, H. Nakazawa, K.-I. Harada, J.D. MacNeil, in: AOAC Int. (Eds.), Chemical Analysis for Antibiotics Used in Agriculture, AOAC Int., Arlington, 1995.
[23] E. Rothery, Analytical Methods for Graphite Tube Atomizers, Varian Australia Pty Ltd., Victoria, 1988.
[24] J.C. Miller, J.N. Miller, Statistics for Analytical Chemistry, third ed., Ellis Horwood Limited, Chichester, 1993.

Available online at www.sciencedirect.com
ScienceDirect
Talanta 74 (2008) 1211–1217
Talanta
www.elsevier.com/locate/talanta

Determination of organochlorine pesticides in sewage sludge by matrix solid-phase dispersion and gas chromatography–mass spectrometry

Consuelo Sánchez-Brunete, Esther Miguel, José L. Tadeo *

Departamento de Medio Ambiente, INIA, Ctra de la Coruña 7, 28040 Madrid, Spain

Received 18 April 2007; received in revised form 22 August 2007; accepted 24 August 2007
Available online 30 August 2007

Abstract

A method based on matrix solid-phase dispersion (MSPD) has been developed for the determination of 16 organochlorine pesticides (OCs) in sludge from municipal sewage plants. Samples of lyophilized sludge were blended with alumina, placed in small columns and OCs extracted with dichloromethane assisted by sonication. Purification of the extracts was accomplished by solid-phase extraction on C_{18} columns and OCs were eluted with acetonitrile. Analyses were performed by gas chromatography with electron impact mass spectrometric detection in the selected ion monitoring mode (GC–MS-SIM) using deuterated OCs as internal standards. The limits of detection were between 0.03 ng/g for 4,4′-DDE and 0.7 ng/g for endrin aldehyde.

Levels of OCs were determined in sewage sludge collected from 19 water treatment plants located in the province of Madrid (Spain). In all of the analyzed samples, aldrin was the compound most often found with a mean concentration of 76 ng/g. Endosulfan-I, α-BHC, 4,4′-DDE and 4,4′-DDT were also present at high concentrations, with average values ranging from 32.3 to 74.3 ng/g. OCs were detected in all of the samples, with a total concentration ranging from 52 to 528 ng/g dry weight.
© 2007 Elsevier B.V. All rights reserved.

Keywords: Sludge; OCs; GC–MS; Levels; MSPD

1. Introduction

Sewage sludge contains nutrients and organic matter that can provide soil benefits and it is often applied in agriculture to improve soil fertility, although it may also contain contaminants that have to be controlled. Organochlorine pesticides (OCs) used for the control of disease vectors and agricultural pests are highly lipophilic and tend to adsorb to solid particles of sewage sludge in wastewater treatment plants (WWTPs). Compounds such as aldrin, dieldrin and DDT are now restricted or banned in many countries because of their high persistence and potential effects on wildlife, although they are still found in monitoring studies.

Whereas many analytical methods have been developed for the determination of OCs in environment samples [1–3] only a few methods for pesticide residues in sludge have been reported in the literature. Traditional methods, such as Soxhlet extraction [4–7] and mechanical shaking [8], were initially used for the extraction of OCs in sludge, however these methods are time consuming and require large amounts of solvent. Therefore, more recently, some alternative techniques have been developed to minimize waste solvents and to shorten the extraction time. These techniques, such as ultrasonic assisted extraction [9], supercritical fluid extraction (SFE) [10,11] and pressurized liquid extraction (PLE) [12] have shown clear advantages because they require a relatively short time and solvent consumption, although some of them use expensive instrumental equipment. Matrix solid-phase dispersion (MSPD) can also be used with that aim because the simultaneous disruption and dispersion of sample together with a reduced solvent and time consumption greatly decrease costs. Although MSPD has been frequently used for the extraction of contaminants in food and other matrices [13–18], it has not been applied, to the best of our knowledge, to the determination of OCs in sewage sludge.

Numerous methods for the quantitative and qualitative determination of OCs have been reported using gas chromatography with electron capture detector (ECD) [6,7,9,19]. ECD is very sensitive for the detection of halogenated compounds but has

* Corresponding author. Tel.: +34 91 347 6821; fax: +34 91 357 2293.
E-mail address: tadeo@inia.es (J.L. Tadeo).

0039-9140/$ – see front matter © 2007 Elsevier B.V. All rights reserved.
doi:10.1016/j.talanta.2007.08.025

several disadvantages like not being very selective (interferences from sample matrix are difficult to avoid) and having a narrow linearity range. Gas chromatography with mass spectrometric detection is a selective technique with high sensitivity for the determination of halogenated pesticides, which allows the confirmation of residues [4,5,8,10,11,20].

This paper presents a new rapid and sensitive analytical method for the determination of the 16 organochlorine insecticides listed by the US Environmental Protection Agency (US EPA) in sewage sludge. The proposed method is based on the use of a MSPD procedure for sample preparation, with the aim of minimizing solvent usage, and OCs are determined by gas chromatography–mass spectrometry with selected ion monitoring (GC–MS-SIM). The method was validated and applied to the analysis of sewage sludge samples collected from 19 different wastewater treatment plants (WWTPs) located in the province of Madrid (Spain). There is no data on the levels of OCs in Spanish sewage sludge samples and this work will provide information about OC levels in sludge from municipal plants located in various zones, urban, industrial or rural.

2. Experimental

2.1. Materials

2.1.1. Standards

Aldrin, α-BHC, β-BHC, γ-BHC (lindane), δ-BHC, dieldrin, endosulfan-I (α), endosulfan-II (α), endosulfan sulfate, endrin, endrin aldehyde, heptachlor, heptachlor epoxide, 4,4′-DDD, 4,4′-DDE and 4,4′-DDT were analyzed in this study. The standard solution of the 16 OCs (2000 μg/ml each in hexane:toluene, 50:50), purity 99%, was supplied by Supelco (Bellefonte, USA). The deuterated internal standards (100 μg/ml in nonane, purity higher than 98%) lindane-d_6, $13C_6$ 4,4′-DDD-d_8 and endosulfan-I-d_4 were supplied by Cambridge Isotope Laboratories (Andover, MA, USA). Calibration solutions were prepared by dilution of the stock solution with nonane. The final concentration of the deuterated internal standards in the calibration solutions was 1 μg/ml.

2.1.2. Reagents

Aluminium oxide 90 standardized from Merck (Darmstadt, Germany) was activated at 180 °C for 24 h and deactivated with deionized water (3%, w/w) before use. Anhydrous sodium sulfate, from Merck (Darmstadt, Germany), was heated for 24 h at 180 °C before use. Acetonitrile, dichloromethane, ethyl acetate, hexane and isooctane residue analysis grade, and silica Bondesil-C_{18}, particle diameter of 40 μm, were purchased from Scharlab (Barcelona, Spain). A Milli-Q water purification system from Millipore (Bedford, MA, USA) was used to provide deionized water in this study. Copper was supplied by Panreac (Barcelona, Spain) and shortly before use was activated with 30% hydrochloric acid for 1 min to remove copper oxide from the surface, subsequently washed with deionized water, cleaned with acetone and hexane and dried under a stream of nitrogen. A 3 g of copper was added to each sample in the MSPD step to remove interferences from elemental sulphur.

2.2. Sample collection

Sludge samples were collected from 19 WWTPs located in urban, industrial or rural areas of the province of Madrid (Spain) during 2006. Sludge samples were transferred to the laboratory at 4 °C and frozen at −80 °C before being lyophilized. Prior to OCs extraction, sludge samples were homogenized and stored at −20 °C until analysis.

2.3. Sample preparation and purification

Alumina deactivated with water at 3% (3 g) and 3 g activated copper powder were mixed with lyophilized sludge finely ground (2 g dry weight) and placed in a glass mortar. For recovery studies, sewage samples were previously fortified with a mixture of the different pesticides to reach final concentrations of 50, 100 and 200 μg/kg and left at room temperature to allow solvent evaporation. Then, the mixture was gently blended with a glass pestle with circular motion to yield a homogeneous material. A 5 ml glass column (5 cm × 10 mm i.d., from Becton-Dickinson, Madrid, Spain) with a Teflon frit (1 cm diameter and 20 μm pore, Supelco, Madrid, Spain) at the end was filled with 2 g of anhydrous sodium sulfate. The blended sample was then transferred to the column, mortar and pestle were rinsed with 3 ml of dichloromethane that were also transferred to the column and an additional volume (3 ml) of dichloromethane was added. The corresponding columns for the different sludge samples were placed in an ultrasonic water bath (Raypa, Spain) at room temperature and extracted during 10 min. After extraction, the columns were placed on a multiport vacuum manifold where the solvent was filtered and collected in graduated tubes. The extraction step was repeated with 6 ml of dichloromethane. The combined extracts were concentrated with a gentle stream of air at ambient temperature in a fume hood to ∼0.5 ml and diluted to 2 ml with acetonitrile.

2.3.1. Purification of the extracts

C_{18} (2 g) was placed in 5 ml glass column and preconditioned by passing 3 ml of acetonitrile and 5 ml of distilled water. The sample extract (2 ml) was transferred to the column and the graduated tube was washed with acetonitrile (3 ml) that was also transferred to the column. The column was placed in a multiport vacuum manifold and OCs eluted with acetonitrile (10 ml), which was collected in a graduated tube and concentrated with a gentle stream of air at ambient temperature in a fume hood to ∼0.1 ml volume. Deuterated OCs (lindane-d_6, endosulfan-I-d_4 and 4,4′-DDD-d_8) (200 μl, 2 μg/ml) were added, the solution reconstituted to 2 ml with hexane:ethyl acetate (90:10, v/v) and a small amount of anhydrous sodium sulfate added to dry the concentrated extract, which was stored at 4 °C until analyzed by GC–MS-SIM.

2.4. GC–MS analysis

An Agilent 6890 (Waldbronn, Germany) gas chromatograph equipped with an automatic injector, Model HP 7683, and an inert mass spectrometric detector (MSD), Model HP 5973N,

equipped with an inert ion source was used in GC–MS analyses. A fused silica capillary column ZB-5MS, 5% phenyl polysiloxane as nonpolar stationary phase (30 m × 0.25 mm i.d. and 0.25 μm film thickness), from Phenomenex (Torrance, CA), was employed. Operating conditions were as follows: injector port temperature 250 °C; helium as carrier gas at a flow-rate of 1.0 ml/min and pulsed splitless mode (pulsed pressure 45 psi = 310 kPa for 1.5 min). The column temperature was maintained at 100 °C for 3 min, then programmed at 20 °C/min to 200 °C for 1 min; increased to 250 °C at a rate of 4 °C/min, followed by a final ramp to 280 °C at a rate of 8 °C/min and held for 1 min. The total analysis time was 26.25 min and the equilibration time 2 min. A 2 μl volume was injected splitless, with the split valve closed for 1.5 min.

The mass spectrometric detector (MSD) was operated in electron impact ionisation mode with an ionising energy of 70 eV, scanning from *m/z* 60 to 500 at 3.62 s per scan, an ion source temperature of 300 °C and a quadrupole temperature of 150 °C. The electron multiplier voltage (EM voltage) was maintained 100 V above autotune with a solvent delay of 5 min.

The OCs pesticides and the internal standards (surrogates), their retention times, target ions for quantitation and qualifier ions for confirmation are listed in Table 1. The SIM program used to determine and confirm OCs in sludge is indicated in Table 2. OCs were confirmed by their retention times, the identification of target and qualifier ions and the determination of qualifier to target ratios. The quality criteria used were the following: retention times must be within ±0.3 min of the expected time and qualifier-to-target ratios within a 20% range for positive confirmation. The quantification of the OCs were accomplished by calibration with internal deuterated standards calibration. A calibration solution was prepared with the OCs standards and 0.1 μg/ml of the internal deuterated standards. The linear range was established by a eight point calibration curve in the range 25–800 μg/l.

2.5. Assessment of matrix effect

In order to state if there was a matrix enhancement response effect and in that case to obtain a correction function for each pesticide, calibration solutions prepared in solvent and the corresponding calibration solutions prepared using blank matrix extracts, instead of pure solvent, were prepared. The analyte concentrations were the same in both cases: 25, 50, 100, 200, 300, 400, 600 and 800 μg/l. These calibration solutions were prepared by dilution with pure isooctane in the case of pure solvent and matrix matched in the case of blank matrix extracts. The internal standards (lindane-d_6, endosulfan-I-d_4 and 4,4′-DDD-d_8) were added to both calibration solutions.

Table 1
Retention times, limits of detection and quantification (LOD, LOQ; ng/g) and selected ions of the studied OCs

	OCs	t_R	LOD	LOQ	*m/z*[a]
1	α-BHC	9.432	0.10	0.3	219, 181, 183
2	β-BHC	9.969	0.10	0.3	219, 181, 183
3	Lindane-d_6[b]	9.976	–	–	230, 228, 191
4	Lindane	10.048	0.10	0.3	219, 181, 183
5	δ-BHC	10.687	0.15	0.5	219, 181, 183
6	Heptachlor	11.569	0.08	0.3	272, 274, 237
7	Aldrin	12.458	0.50	1.7	263, 265, 293
8	Heptachlor epoxide	13.529	0.09	0.3	353, 355, 357
9	Endosulfan-1-d_4[b]	14.628	–	–	237, 279, 343
10	Endosulfan-1 (α)	14.630	0.20	0.7	241, 237, 207, 339
11	4,4′-DDE	15.325	0.03	0.1	246, 318, 248
12	Dieldrin	15.479	0.60	2.0	263, 265, 277
13	Endrin	16.180	0.50	1.7	317, 263, 345
14	Endosulfan-II (β)	16.597	0.20	0.7	195, 237, 339
15	4,4′-DDD-d_8[b]	16.713	–	–	243, 245, 173
16	4,4′-DDD	16.786	0.05	0.17	235, 237, 165
17	Endrin aldehyde	17.107	0.70	2.3	345, 250, 347
18	Endosulfan sulfate	17.957	0.50	1.7	272, 274, 387
19	4,4′-DDT	18.115	0.40	1.3	235, 237, 165

[a] Target ions are underlined.
[b] Internal standards.

3. Results and discussion

3.1. Extraction and clean-up

The optimisation of MSPD procedure for the extraction of OCs from sludge samples was studied. Florisil and alumina were assayed using ethyl acetate as extraction solvent and cleaner extracts were obtained with alumina, which was selected as adsorbent. However, in both cases, for some compounds, such as aldrin and dieldrin, low recoveries were obtained. Alumina was then deactivated with deionized water (3%, w/w) before use and the recovery of these compounds was improved. In addition, dif-

Table 2
SIM program used to analyze OCs in sludge

Group	Time (min)	OCs	*m/z*	Dwell time (ms)	Scan rate (cycles/s)
1	5.00	α-BHC, β-BHC, γ-BHC, δ-BHC, lindane-d_8	181, 183, 219, 230	100	2.36
2	11.00	Heptachlor	237, 272, 274	100	3.11
3	12.00	Aldrin	263, 265, 293	100	3.11
4	13.00	Heptachlor epoxide	353, 355	100	4.53
5	14.00	Endosulfan-I, endosulfan-I-d_4	207, 237, 241, 339	100	2.36
6	15.10	4,4′-DDE, dieldrin	246, 263, 265, 277, 318	100	1.91
7	15.80	Endrin	263, 265, 317	100	3.10
8	16.40	Endosulfan-II, 4,4′-DDD, 4,4′-DDD-d_8, endrin aldehyde	195, 235, 237, 241, 243, 250, 345, 347	100	1.21
9	17.50	Endosulfan sulfate, 4,4′-DDT	235, 237, 272, 274, 387	100	1.91

ferent amounts of alumina (3 and 4 g) were tried in order to optimise the adsorbent-sample ratio but similar results were found.

Therefore, alumina (3 g), deactivated with 3% of water, was the adsorbent selected. The influence of the extracting solvent was then studied and solvents of different polarity, such as dichloromethane, hexane and ethyl acetate [4,8,10,19], or mixture of solvents, like dichloromethane-hexane (2:1, v/v) [5], were assayed. Low recoveries of some OCs were obtained when hexane and ethyl acetate were employed (data not shown). Good recoveries and clean extracts were achieved with dichloromethane, which was selected as the extracting solvent.

Some authors have reported an improvement in the recoveries and reproducibility using sonication in the extraction step [9]. In our case, the recovery increased in the range of 13–28% for the different OCs when sonication was used, therefore, the extraction assisted with sonication was employed in the analysis of sludge samples. In addition, copper powder was added in the MSPD step and the samples left at room temperature for 1 h to completely remove the chromatographic interferences of sulphur [5,10].

One of the usually employed techniques to remove co-extracted materials prior to the final chromatographic determination is solid-phase extraction (SPE), being octadecyl silica (C_{18}), among other sorbents, frequently employed [11,21]. Considering the matrix complexity of the WWTPs sludge, due to their high content of organic matter, and the low polarity of OCs a clean up procedure using C_{18} can be considered a suitable option. As OCs pesticides are readily soluble in acetonitrile, the elution efficiency of this solvent in SPE-C18 was tested. Recoveries equal or higher than 92% were obtained for all OCs with acetonitrile and extracts were clean enough to allow determination of OCs by GC–MS.

3.2. GC–MS analysis

OCs were analyzed by GC–MS-SIM. The SIM program used to determine and confirm OCs in sludge is indicated in Table 2 and Fig. 1 shows representative GC–MS-SIM chromatograms of a standard mixture solution containing 100 μg/l and a recovery sample fortified at 50 μg/kg.

3.2.1. Assessment of matrix effect

Sample cleanup is necessary for the determination of analytes free from interferences and to minimize the matrix effect. This effect may reduce or increase the intensity of analyte response and affect the reproducibility and accuracy of the assay. Elimination of the enhancement effect is essential for quantification of pollutants in complex environmental matrices, such as sludge, at trace levels. In some types of samples, the concentration of interfering components may be several orders of magnitude higher than the target compounds [22,23] and particularly GC–MS was found to be more sensitive to matrix enhancement than other detectors [22]. Matrix effect occurring in the GC analysis of some pesticides in extracts from real samples has a negative impact on the accuracy of generated results and the use of matrix matched standards represents a way of reliably correcting for response enhancement.

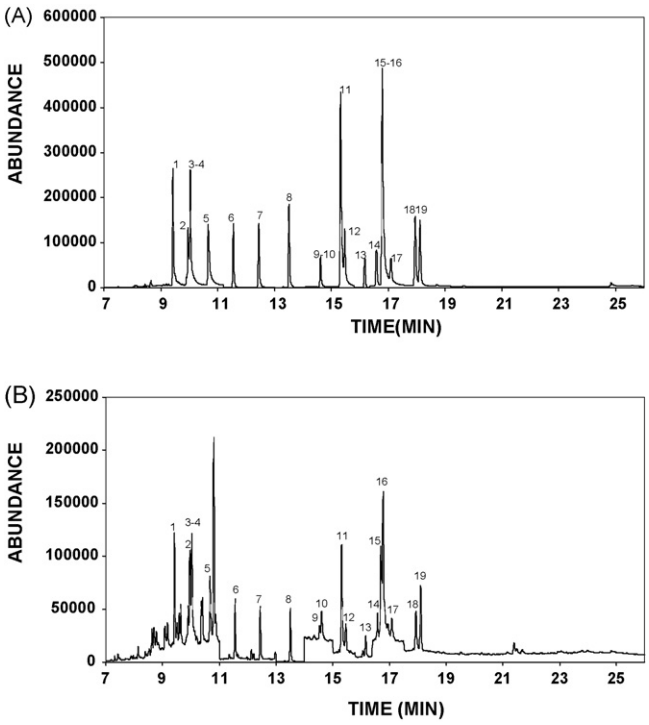

Fig. 1. (A) GC–MS-SIM chromatogram of a 16 OCs standard solution containing 100 μg/l. (B) GC–MS-SIM chromatogram of a recovery sample fortified at 50 μg/kg. See Table 1 for peak identification.

In this work, we evaluated the matrix enhancement effect on the OCs pesticides studied and this effect is in the range from 9% for β-BHC to 107% for 4,4′-DDT. To compensate for detector response enhancement, calibration should be carried out using matrix matched standards.

Nevertheless, this approach is more laborious than conventional calibration using standards prepared in neat solvents. On the other hand, some regulatory agencies, like the Environmental Protection Agency (EPA) and the Food and Drug Administration (FDA), in the USA do not permit matrix-matched standardization for enforcement purposes.

In the present work, we studied the use of isotope labeled internal standard to overcome the matrix effect problem and to improve reproducibility and accuracy.

Two multipoint calibration curves [matrix-free calibration curve (SC) and matrix-matched calibration curve (MC)] with eight standard solutions of different concentration levels, in the range of 25–800 μg/l, appropriate to the levels expected in our samples, were obtained. The deuterated internal standards at a concentration of 100 μg/l were added to the standard solutions prior to injection. In both cases, a good linearity of the calibrations curves was obtained in the range 25–800 μg/l. The correlation coefficient were 0.995 or higher for most of the OCs analyzed, Table 3. Plots of calibration curves for α-BHC (low matrix effect) and 4,4′-DDT (high matrix effect) in neat solvent (SC) and matrix-matched (MC) sludge extract are shown in Fig. 2A and B, respectively. Analysis of OCs pesticides in neat solvent produced calibration curves with lower slopes for most compounds, as compared with matrix matched standards. This is a typical manifestation of the matrix induced enhancement

Table 3
Calibration data and repeatability[a] of the studied OCs

OCs	Calibration data	Repeatability (R.S.D., %)[b]		
	Equation	r	Peak area	t_R
α-BHC	$y = 2.65 \times 10^{-1}x + 2.03 \times 10^{-3}$	0.995	4.7	0.01
β-BHC	$y = 3.28 \times 10^{-1}x + 1.21 \times 10^{-1}$	0.997	3.4	0.01
Lindane	$y = 2.19 \times 10^{-1}x - 5.08 \times 10^{-2}$	0.999	8.9	0.02
δ-BHC	$y = 2.64 \times 10^{-1}x + 7.51 \times 10^{-3}$	0.997	5.1	0.02
Heptachlor	$y = 2.94 \times 10^{-1}x - 3.09 \times 10^{-2}$	0.998	5.6	0.01
Aldrin	$y = 2.98 \times 10^{-1}x + 3.86 \times 10^{-2}$	0.998	4.4	0.01
Heptachlor epoxide	$y = 3.24 \times 10^{-1}x + 2.51 \times 10^{-2}$	0.998	4.3	0.01
Endosulfan-I (α)	$y = 1.13 \times 10^{-1}x + 9.97 \times 10^{-3}$	0.997	4.6	0.01
4,4′-DDE	$y = 8.19 \times 10^{-1}x + 7.15 \times 10^{-2}$	0.996	5.8	0.02
Dieldrin	$y = 1.62 \times 10^{-1}x + 2.12 \times 10^{-2}$	0.998	5.1	0.01
Endrin	$y = 1.26 \times 10^{-1}x - 8.84 \times 10^{-3}$	0.999	4.6	0.01
Endosulfan-II (β)	$y = 7.63 \times 10^{-2}x - 5.03 \times 10^{-3}$	0.998	5.2	0.02
4,4′-DDD	$y = 8.13 \times 10^{-1}x + 1.03 \times 10^{-1}$	0.997	7.2	0.01
Endrin aldehyde	$y = 1.05 \times 10^{-1}x - 1.38 \times 10^{-2}$	0.999	4.2	0.01
Endosulfan sulfate	$y = 2.18 \times 10^{-1}x + 1.95 \times 10^{-3}$	0.998	5.9	0.01
4,4′-DDT	$y = 5.18 \times 10^{-1}x - 1.50 \times 10^{-1}$	0.998	8.5	0.02

[a] Repeatability of the chromatographic method.
[b] R.S.D. of retention times and peak areas ($n = 10$).

effect, which would lead to overestimations of the calculated concentrations in the samples.

Stable surrogate pesticides (isotopically labeled or deuterated pesticides) are suitable internal standards for pesticide residue analysis when using mass spectrometric detection and can be used to correct the matrix-induced enhancement because there is no difference in physicochemical behaviour from the corresponding pesticide. In the absence of an isotope effect in the processes affecting the transfer of analytes from the injector to the separation column, the isotopically labeled or deuterated standards and analytes should be affected in the same way by matrix-induced enhancement. The concentration difference between the pesticide and surrogate (deuterated pesticide) should be small to represent a similar analyte/matrix concentration ratio. Fig. 3 shows calibration curves of α-BHC and 4,4′-DDT with surrogate deuterated standards. The addition of deuterated standards practically eliminated differences between calibrations obtained in matrix extracts versus matrix free solutions as shown in Fig. 3. Therefore, with the use of surrogate standards is possible to overcome the problems related to the matrix enhancement effect.

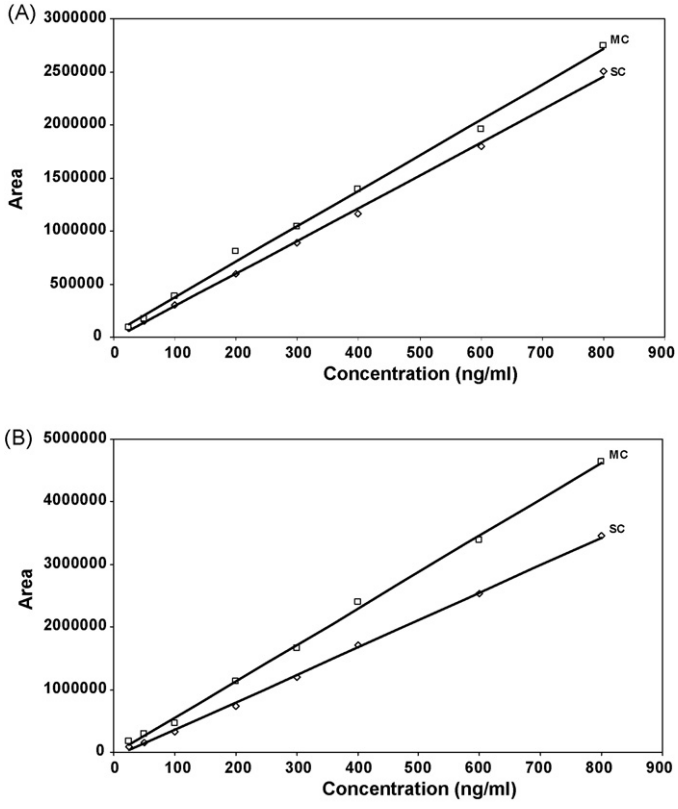

Fig. 2. Comparison of calibration curves of (A) α-BHC and (B) 4,4′-DDT, obtained by injection of standards in neat solvent (SC, ◊) and spiked sewage sludge extracts (MC, □) standards.

3.2.2. Chromatographic repeatability

The repeatability of the chromatographic determination was determined by injecting 10 times a standard solution of 0.4 μg/ml with an automatic injector. The relative standard deviations (R.S.D.) obtained for the retention times ranged from 0.01 to 0.02%, whereas for peak areas those values ranged from 3.4 to 8.9% (Table 3). Within-laboratory reproducibility of the chromatographic determination was evaluated during different days during two consecutive weeks and was found to be lower than 13%, expressed as R.S.D., for all OCs.

3.2.3. Recovery

To asses method accuracy and repeatability, extractions were carried out at three fortification levels, 50, 100 and 200 ng/g. Sludge samples were fortified with the target OCs in isooctane solution and left at room temperature to allow solvent evaporation. Unspiked "blank" samples were previously analyzed to determine the possible presence of OCs and the contribution of each OC in the "blank" sample was subtracted from the corre-

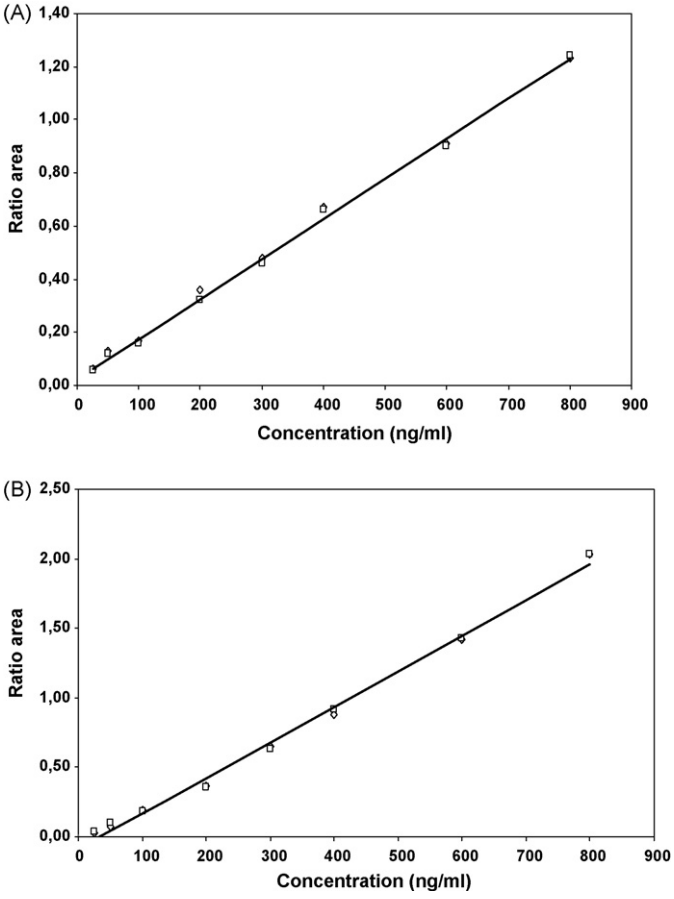

Fig. 3. Comparison of calibration curves of (A) α-BHC and (B) 4,4′-DDT, obtained by injection of standards in neat solvent (◊) and spiked sewage sludge extracts (□) with internal labeled standards.

sponding value obtained in each spiked sample to calculated the recovery values. Results are shown in Table 4. In all the fortification levels, recoveries were in the range of 84.5–104.1%, whereas R.S.D. values ranged from 1.1 to 7.7%, thus fulfilling the requirements of the European Union Guideline [24]. The obtained values are similar to the recoveries reported by other authors using supercritical fluid extraction [11], pressurized liquid extraction [5] or Soxhlet extraction [6,7] for the analysis of OCs in sewage sludge.

Table 4
Recoveries[a] of the studied OCs in sewage sludge

OCs	50	100	200
Fortification levels (ng/g)			
α-BHC	90.9 ± 4.3	96.5 ± 6.4	89.3 ± 7.3
β-BHC	88.2 ± 3.3	91.5 ± 2.3	102.3 ± 3.5
Lindane	96.7 ± 5.4	98.5 ± 2.8	99.3 ± 4.9
δ-BHC	92.6 ± 2.4	94.1 ± 5.9	96.8 ± 6.4
Heptachlor	88.5 ± 2.8	97.9 ± 6.2	94.3 ± 2.1
Aldrin	84.5 ± 6.8	86.5 ± 7.7	86.3 ± 5.7
Heptachlor epoxide	89.4 ± 3.0	90.2 ± 1.8	89.7 ± 4.0
Endosulfan-I (α)	102.3 ± 2.3	103.8 ± 2.6	101.7 ± 4.0
4,4′-DDE	103.0 ± 3.4	104.1 ± 2.0	102.3 ± 4.7
Dieldrin	87.9 ± 1.4	88.5 ± 2.4	86.5 ± 2.5
Endrin	90.7 ± 1.1	95.7 ± 2.9	99.3 ± 7.5
Endosulfan-II (β)	93.0 ± 3.1	102.5 ± 1.8	98.7 ± 5.5
4,4′-DDD	90.4 ± 4.5	95.4 ± 1.1	91.5 ± 1.4
Endrin aldehyde	91.8 ± 2.8	99.5 ± 2.3	95.5 ± 2.8
Endosulfan sulfate	89.8 ± 1.8	96.3 ± 2.5	92.8 ± 3.5
4,4′-DDT	93.1 ± 1.5	103.8 ± 1.8	101.7 ± 5.7

[a] Results are the mean of four replicates ± standard deviation.

3.2.4. Limits of detection (LOD) and quantification (LOQ)

Limits of detection (LODs) and quantification (LOQs) considered as the minimum amount of target analyte that produces a chromatogram peak with a signal-to-noise ratio of three and ten times the background chromatographic noise, respectively, were determined using extracts from blank samples. Low limits were obtained due to the selectivity of the analytical procedure and the high sensitivity of GC–MS-SIM, allowing the determination of OCs at the levels found in sludge samples. The LODs and LOQs corresponding to the different OCs are shown in Table 1. These values range from 0.03 to 0.7 ng/g for LODs and from 0.1 to 2.3 ng/g for LOQs and are in the lower end of those reported by other authors [5,6,8,9].

3.3. Levels of OCs in sewage sludge samples

Sludge samples collected from municipal wastewater treatment plants in the province of Madrid, located in industrial, urban or rural sites, were analyzed using the developed method. There is no data available on the concentration of chlorinated pesticides in sewage sludge from WWTPs of Spain. The levels of OCs found in sludge samples, expressed as ng/g dry weight, are given in Table 5. The identity of these compounds was confirmed using the quality criteria indicated above regarding the acceptable ranges of retention times and ratios of qualifier to target ions. The highest concentration of OCs, expressed as the sum of the 16 compounds, was found in urban and industrial WWTPs, 528 and 523 ng/g, respectively, and the lowest concentration in rural WWTPs, 52 ng/g. Total OCs concentrations are very close to the OCs values reported by other researchers [5,21]. Similar values in urban and industrial sludge were obtained, which is in agreement with data found in the literature [11,21]. In our study, the most frequent compounds found were aldrin (18 out of 19 samples, 18/19), DDE (16/19), DDD (11/19), DDT (14/19), α-BHC (14/19) and endosulfan-I (11/19), Table 5. However, other organochlorine pesticides (including β-BHC, δ-BHC, heptachlor, heptachlor epoxide, dieldrin, endrin, endosulfan-II, endrin aldehyde and endosulfan sulfate) were not detectable. These results are consistent with those of related studies on sewage sludge [5,9]. The highest concentrations were found for α-BHC, ranging from 34 to 160 ng/g, and aldrin in the range of 21–153 ng/g. DDT, DDE and DDD were detected in concentrations ranging from 6 to 128 ng/g. In contrast, lindane was only detected in four samples, with concentrations from 58 to 274 ng/g. Comparing our data with other reported levels, one study reported values of 39 ng/g for lindane, 35 ng/g for HCB and 70 ng/g for DDT and metabolites [21]. Usage of organochlorine pesticides has been falling for many years, because their use is restricted or banned in many countries, including Spain. Therefore, their presence in the environment may be explained by the atmospheric transport from areas of the world where they

Table 5
Concentration[a] of OCs (ng/g) in sewage sludge collected from municipal wastewater treatment plants located in the province of Madrid

OC	Waste water treatment plants																		
	1	2	3	4	5	6	7	8	9	10	11	12	13	14	15	16	17	18	19
α-BHC	n.d.	99	98	67	43	125	34	n.d.	89	89	n.d.	158	n.d.	124	100	115	160	n.d.	112
β-BHC	n.d.	n.d.	n.d.	n.d.	n.d.	n.d.	n.d.	n.d.	n.d.	n.d.	n.d.	n.d.	n.d.	n.d.	n.d.	n.d.	n.d.	n.d.	n.d.
Lindane	n.d.	n.d.	58	n.d.	105	274	132	n.d.	n.d.	n.d.	n.d.	n.d.	n.d.	n.d.	n.d.	n.d.	n.d.	n.d.	n.d.
δ-BHC	n.d.	n.d.	n.d.	n.d.	n.d.	n.d.	n.d.	n.d.	n.d.	n.d.	n.d.	n.d.	n.d.	n.d.	n.d.	n.d.	n.d.	n.d.	n.d.
Heptachlor	n.d.	n.d.	n.d.	n.d.	n.d.	n.d.	n.d.	n.d.	n.d.	n.d.	n.d.	n.d.	n.d.	n.d.	n.d.	n.d.	n.d.	n.d.	n.d.
Aldrin	58	142	121	153	61	93	51	75	90	60	n.d.	55	45	62	21	90	100	77	102
Heptachlor epoxide	n.d.	n.d.	n.d.	n.d.	n.d.	n.d.	n.d.	n.d.	n.d.	n.d.	n.d.	n.d.	n.d.	n.d.	n.d.	n.d.	n.d.	n.d.	n.d.
Endosulfan-I	n.d.	51	n.d.	n.d.	n.d.	n.d.	n.d.	98	n.d	49	40	62	87	99	92	90	145	n.d.	68
4,4′-DDE	28	128	71	n.d.	n.d.	n.d.	33	18	69	17	12	27	23	21	28	31	30	19	59
Dieldrin	n.d.	n.d.	n.d.	n.d.	n.d.	n.d.	n.d.	n.d.	n.d.	n.d.	n.d.	n.d.	n.d.	n.d.	n.d.	n.d.	n.d.	n.d.	n.d.
Endrin	n.d.	n.d.	n.d.	n.d.	n.d.	n.d.	n.d.	n.d.	n.d.	n.d.	n.d.	n.d.	n.d.	n.d.	n.d.	n.d.	n.d.	n.d.	n.d.
Endosulfan-II	n.d.	n.d.	n.d.	n.d.	n.d.	n.d.	n.d.	n.d.	n.d.	n.d.	n.d.	n.d.	n.d.	n.d.	n.d.	n.d.	n.d.	n.d.	n.d.
4,4′-DDD	11	10	11	n.d	n.d	n.d	n.d	n.d	8	6	n.d	n.d	8	8	8	13	10	n.d	16
Endrin aldehyde	n.d.	n.d.	n.d.	n.d.	n.d.	n.d.	n.d.	n.d.	n.d.	n.d.	n.d.	n.d.	n.d.	n.d.	n.d.	n.d.	n.d.	n.d.	n.d.
Endosulfan sulfate	n.d.	n.d.	n.d.	n.d.	n.d.	n.d.	n.d.	n.d.	n.d.	n.d.	n.d.	n.d.	n.d.	n.d.	n.d.	n.d.	n.d.	n.d.	n.d.
4,4′-DDT	61	98	n.d.	n.d.	100	n.d.	n.d.	79	97	67	n.d.	82	48	78	33	64	78	39	70
∑16 OCs	158	528	359	220	309	492	250	270	353	288	52	384	211	392	282	403	523	135	427

[a] Results are the mean of two samplings, expressed in ng/g; n.d.: <method detection limit.

are still used, or by their presence as impurities in other products. In comparison with OCs values found in the literature, the concentrations found in municipal sewage from the province of Madrid were in the same range than those found in other countries [6,11,22,25].

4. Conclusion

This work presents a rapid and simple analytical method for the reliable determination of 16 OCs in sludge samples. The proposed method is based on the MSPD extraction of pesticides, assisted by sonication, and their determination by gas chromatography–mass spectrometry. The addition of labeled standards was effective to compensate the matrix effect observed and improved the method reproducibility and accuracy. In addition, the proposed method requires a short extraction time and a low consumption of organic solvents. Sludge samples collected from municipal WWTPs located in the province of Madrid were analyzed by the developed method. In most of the samples, aldrin and α-BHC were main compounds found, followed by DDT and its metabolites. Levels of OCs found in sewage sludge were similar to the values reported by other authors.

Acknowledgments

This study was financed by the Ministry of Education and Science-National Institute for Agricultural and Food Research and Technology, INIA, Project number RTA 2005-00090. Authors wish to acknowledge Canal Isabel II for their helpful assistance.

References

[1] K.K. Chee, M.K. Wong, H.K. Lee, J. Chromatogr. A 736 (1996) 211.
[2] A.I. Gomez-Gutierrez, E. Jover, L. Bodineau, J. Albages, J.M. Bayona, Chemosphere 65 (2006) 224.
[3] J. Castro, C. Sánchez-Brunete, J.L. Tadeo, J. Chromatogr. A 918 (2001) 371.
[4] J.L. Stevens, G.L. Northcott, G.A. Stern, G.T. Tomy, K.C. Jones, Environ. Sci. Technol. 37 (2003) 462.
[5] M.I.H. Helaleh, A. Al-Omair, N. Hamed, B. Gevao, Anal. Bioanal. Chem. 382 (2005) 1127.
[6] U.K. Ahmad, Z. Ujang, C.H. Woon, S. Indran, M.N. Mian, Water Sci. Technol. 50 (2004) 137.
[7] E. Mangas, M.T. Vaquero, L. Comellas, F. Broto-Puig, Chemosphere 36 (1998) 61.
[8] A. Garrido Frenich, M.J. Gonzalez Rodríguez, J.L. Martinez Vidal, F.J. Arrebola, M.E. Hernández Torrres, Pest. Manage. Sci. 61 (2005) 458.
[9] A. Katsoyiannis, C. Samara, Water Res. 38 (2004) 2685.
[10] R.J. Trigg, G.A. Keenan, D. Mcmullan, A.I. Conner, Int. J. Anal. Chem. 70 (1998) 47.
[11] J.D. Berset, R. Holzer, J. Chromatogr. A 852 (1999) 545.
[12] J. Kohli, H.-B. Lee, T.E. Peart, Water Qual. Res. J. Canada 41 (2006) 47.
[13] B. Albero, C. Sánchez-Brunete, A. Donoso, J.L. Tadeo, J. Chromatogr. A 1043 (2004) 127.
[14] S.A. Baker, A.R. Long, A.R. Long, M.E. Hines II, J. Chromatogr. 629 (1993) 23.
[15] A. Di Municio, P. Pelosi, I. Camoni, D.A. Barbini, R. Dommarco, T. Generali, A. Ausili, J. Chromatogr. A 754 (1996) 497.
[16] B. Albero, C. Sánchez-Brunete, J.L. Tadeo, J. AOAC Int. 86 (2003) 576.
[17] C. Sánchez-Brunete, B. Albero, E. Miguel, J.L. Tadeo, J. AOAC Int. 85 (2002) 128.
[18] C. Sánchez-Brunete, E. Miguel, J.L. Tadeo, J. Chromatogr. A 1148 (2007) 219.
[19] A. Katsoyiannis, C. Samara, Environ. Res. 97 (2005) 245.
[20] A.C. Petrasek, I.J. Kugelman, B.M. Austern, T.A. Pressley, L.A. Wilnslow, R.H. Wise, J. WPCF 55 (1983) 1286.
[21] P. Frost, R. Camenzid, A. Mager, R. Bonjour, G. Karlaganis, J. Chromatogr. A 643 (1993) 379.
[22] F.J. Schenck, S.J. Lehotay, J. Chromatogr. A 868 (2000) 51.
[23] C. Sánchez-Brunete, B. Albero, G. Martín, J.L. Tadeo, Anal. Sci. 21 (2005) 1291.
[24] Document SANCO/10232/2006, European Union, Brussels, 2006.
[25] J. Falandysz, B. Strandberg, Pol. J. Environ. Stud. 13 (2004) 133.

Available online at www.sciencedirect.com
ScienceDirect
Talanta 74 (2008) 1592–1597
Talanta
www.elsevier.com/locate/talanta

Analytical and mineralogical studies of ore and impurities from a chromite mineral using X-ray analysis, electrochemical and microscopy techniques

S. Sánchez-Ramos [a,b], A. Doménech-Carbó [a], J.V. Gimeno-Adelantado [a,*], J. Peris-Vicente [a]

[a] *Department of Analytical Chemistry, Faculty of Chemistry, University of Valencia, C/Doctor Moliner 50, 46100 Burjassot, Valencia, Spain*
[b] *Escuela Superior de Cerámica, C/Ceramista A. Blat 22, 46940 Manises, Valencia, Spain*

Received 28 May 2007; received in revised form 19 September 2007; accepted 2 October 2007
Available online 7 October 2007

Abstract

A wide analytical study of South African chromite ore, material with high interest in ceramic industry, has been carried out. With this purpose, an accurate chemical identification and mineralogical characterization of the mineral and the gangue have been performed using X-ray fluorescence (XRF), voltammetry, X-ray diffraction (XRD), light microscopy (LM), and scanning electron microscopy (SEM/EDX). The elemental composition of the sample (ore and gangue) has been obtained by XRF. The voltammetric analysis has allowed to demonstrate that iron in the sample was as Fe(II). The main compound of the chromite ore was a spinel (magnesiochromite ferroan), identified by XRD from the sample, which constitutes the chromite ore. This technique has also been useful to characterize some silicates as impurities in the chromite ore sample. Light microscopy has allowed the detection of the spinel and the identification of a silicate impurity (chrome chlorite), by means of their colouration. On the other hand, the other silicate impurity was identified as labradorite by means of X-ray microscopy by SEM/EDX. Finally, a strategy was developed to calculate the composition of each mineral in the unknown sample. The obtained results were: chromite spinel 82.89%, chlorite 12.79% and labradorite 4.32%.
© 2007 Elsevier B.V. All rights reserved.

Keywords: Chromite; X-ray analysis; Microscopy; Voltammetry; Ceramic industry

1. Introduction

Pure chromite has a spinel crystalline structure and the theoretical chemical composition $FeCr_2O_4$. The structure of natural chromites is described by the cubic spinel having a formula unit $(Mg,Fe^{2+})O\cdot(Cr,Al,Fe^{3+})_2\cdot O_3$, due to the natural substitution in several amounts of Fe(II) by Mg and Cr by Al and even by Fe(III) in lower proportion. This occurrence depends on the type of minerals which are usually found with the chromite, especially metha- and orthosilicates. Thereby, the presence of serpentines, chlorites, olivine and other minerals has been described [1].

The industrial use of different chromite minerals is essentially determined by their total amount of Cr_2O_3 and Cr/Fe ratio. A higher proportion of chromium increases the heat resistance of the mineral, but this can be modified by the type and relative amount of the impurities. These compounds have a significant influence in the properties of the finished product and their applications, varying the proportion and the distribution of the crystalline phases. The presence of silicates lessens the melting point, so liquid phases at lower temperatures can appear, provoking breakage and decomposition of the product, and have a strong influence over their possible applications. Thus, the identification and quantification of chromite ore impurities is considered of high interest [2].

Generally, considering their possible applications, chromite ores are classified by grades, according to their chromium content and Cr/Fe ratio, which can be summarized in three types:

* Corresponding author. Tel.: +34 963544533; fax: +34 963544436.
E-mail address: jose.v.gimeno@uv.es (J.V. Gimeno-Adelantado).

0039-9140/$ – see front matter © 2007 Elsevier B.V. All rights reserved.
doi:10.1016/j.talanta.2007.10.006

(i) metallurgical grade (Cr_2O_3 content above 46–48% and Cr/Fe ratio above 3; and 25% alumina and magnesia together); (ii) chemical grade (Cr_2O_3 content above 44% and Cr/Fe ratio above 1.5%); and (iii) refractory grade (Cr_2O_3 between 30 and 40% and Cr/Fe ratio between 2 and 2.5 and above 63% of Cr_2O_3 and Al_2O_3 together). The properties of the mineral are improved by the content of magnesia [3,4]. Other authors proposed the following composition for the mineral for its use as refractory material: Cr_2O_3 above 31%; Fe_2O_3 under 17%; Al_2O_3 above 20%; SiO_2 under 6% and CaO content less than 1% [5].

Nevertheless, several refractory chromites have been successfully used in industries to obtain materials in disagreement, in principle, with their composition, although differing in the indicated parameters. Thus, some achieved works which studied the viability of the use of chromites in covering steel chromium-diffusive are of the utmost interest. The introduction of chromium on the surface of steel takes place by the products resulting from prereduced chromites [6–10].

The oxidation state of iron in chromites was studied by means of solid-state electrochemistry. This methodology is based on the mechanical transference of solid microparticles to graphite electrodes in contact with a suitable electrolyte, thus extending electroanalytical methods to solid materials, as described in recent extensive reviews [11,12]. This approach has been applied recently to characterize iron oxides [13,14].

In this paper, a study in order to accurately characterize a chromite mineral and its impurities has been performed. With this purpose, several techniques have been applied, together with other used to confirm or anticipate the presence or nature of some of the minerals in the unknown sample, by means of this following sequence. After the elemental analysis by XRF, a voltammetric study has been applied in order to determine the oxidation state of iron in the mineral. Later, an examination by light microscopy in order to characterize several compounds based on the colouration of the particles. Afterwards, the mineralogical and chemical composition was determined by XRD and then SEM/EDX was used in order to characterize and/or corroborate these components. Finally, a strategy was proposed to deduce the relative amount of each compound in the mineral based on the obtained results.

2. Experimental

2.1. Instrumentation

Glass discs for the XRF analyses were made from samples using the following instrumentation: muffle furnace (GALLUR, max *T* 1300 °C with temperature ascent speed regulator, Valencia, Spain); Wolfram Carbide disk mill (Fritsch Pulverisette 9, Idar-Oberstein, Germany); crucible (5% Au/Pt ZGS); glass discs conformator (Pt/Rh 30-mm diameter). XRF analyses were performed in an X-ray fluorescence spectrometer (Phillips PW with rhodium anticathode controlled by SuperQ/Quantitative software version 1.1, Eindhoven, Netherlands).

Studies by XRD were carried out with X-ray diffractometer Siemens D500 controlled by DIFFRACT/AT version 3 software, Munich, Germany) with DIFFRACTplus Evaluation Package Release 2001 and Powder Diffraction File (PDF) Release 1999 Database, provided by International Centre for Diffraction Data (ICCD).

Table 1
SEM/EDX microanalysis: instrumental working conditions

Accelerating voltages	20 kV
Beam current	8×10^{-9} A
Filament current	60 μA
Working range	0–10.230 keV
Working distance	10 mm
Magnification	100×
Tilt	0°
Life time	300 s
Dead time	20%
Multi-channel analyzer	20 eV/channel
Time constant	1.5 μs
Count rate	2000 c s^{-1}

Photographs were taken at 144 magnifications with a light microscope SZX12 Olimpus (Milan, Italy) coupled to a digital camera Olympus 4.5 M.p. noise reduction system F 1.8.

Images and X-ray microanalysis were performed with a XL 30 ESEM scanning electron microscopy with secondary electron detector and sapphire EDAX detector computer-controlled with EDAX DX4 software 3.11 (Phillips, Eindhoven, Netherlands). Experimental conditions in microanalysis are shown in Table 1.

Square wave voltammograms (SQWVs) were obtained with a CH I420 equipment in a conventional three-electrode cell using well-deaerated HCl solutions at 298 K. A sample-modified composite electrode was used as working electrode, a Pt-wire auxiliary electrode and a AgCl (3 M NaCl)/Ag reference electrode completed the three-electrode cells after immersion of modified electrodes in well-deaerated solutions at 298 K. The potential scan was routinely initiated at +1.0 V in the negative direction.

2.2. Electrochemical procedure

Voltammetric experiments were performed in HCl (Panreac, Barcelona, Spain) solutions in nanopure water, total concentration 1.0 M. Paraffin-impregnated graphite electrodes (PIGEs) consist on cylindrical rods of 5 mm diameter of graphite impregnated under vacuum by paraffin. Preparation details are described by Scholz and co-workers. The sample (ca. 10–20 μg) were accurately powdered in an agate mortar and pestle and then placed on a glazed porcelain tile forming a spot of finely distributed material. Then the lower end of the PIGE was gently rubbed over that spot of sample and finally cleaned with a tissue paper to remove ill-adhered particles [12].

3. Results and discussion

3.1. Chemical composition by X-ray fluorescence and electroanalysis

The chemical analysis of the chromite sample was performed by XRF, by means of a method proposed by the authors using lithium tetraborate as flux and a sample dilution of 1/40 at

Table 2
Elemental composition (weight%) of the mineral sample, obtained by XRF analysis

Oxide							
Cr_2O_3	SiO_2	Al_2O_3	Fe_2O_3	CaO	MgO	Na_2O	Others (TiO_2, K_2O, MnO, ...)
42.34	6.45	15.16	23.31	0.47	12.6	0.16	0.68

1200 °C for 30 min [15]. The obtained results are shown in Table 2. The loss on ignition (LOI) at 1100 °C was −1.08% (negative value), indicating a rising of the sample weight. In order to justify this behaviour, some hypotheses were proposed about these effects taking place during the heating. Probably, the Fe(II) in the sample was oxidized to Fe(III), provoking an increase of the weight ($FeO \rightarrow Fe_2O_3$). Some authors have confirmed by studying pure chromite spinels that this process happens continuously from low temperatures (200 °C) to 900–1000 °C [16]. In the studied sample, hydrated and/or hydroxylated silicate can be as impurities. The evaporation of the crystallization water, which always takes place at minor temperatures [17], would provoke a reduction of the weight. Once the water eliminated, the oxidation of the Fe(II) to Fe(III) continues nearly to 1000 °C. Finally, the found LOI was the final outcome of these two opposed reactions.

As seen in the previous chemical analysis by XRF, the iron was considered as Fe_2O_3. However, a complete information about the real oxidation state of the iron was needed, because iron(III) is able to replace chromium(III) in the mineral. The determination of this parameter was performed by means of a voltammetric study. Fig. 1 shows the square wave voltammetric response of a graphite electrode modified with pristine chromite. A thorough examination of the voltammogram shows a peak at −0.75 V corresponding to Fe(II) reduction, whereas no peaks corresponding to higher oxidation states were found as judged by comparison of the above voltammetric response with that reported for iron minerals [14]. This can be considered an evidence to establish that almost all the iron in the mineral was Fe(II). For this reason, in order to identify accurately the unknown chromite ore sample, the amount of iron must be shown in the chemical analysis as FeO, obtaining a content of 20.98% (Table 2).

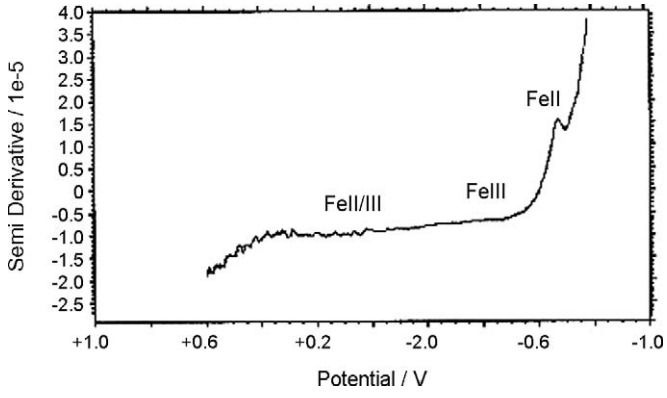

Fig. 1. Square wave voltammograms for chromite ore, attached to paraffin-impregnated graphite electrodes in contact with 1.0 M HCl. Potential scan initiated at +0.85 V in the negative direction. Potential step increment 4 mV; square wave amplitude 25 mV; frequency 5 Hz.

3.2. Mineralogical characterization by X-ray diffraction

In order to characterize the minerals in the original chromite ore, a diffractometric analysis of the sample, powdered, sieved and dried (for 1 h at 110 °C) was achieved. The obtained diffractogram is shown in Fig. 2.

The evaluation of the data based on the chemical composition allows to suggest that the peaks marked with a number correspond to a spinel. According to the database, the main compound was characterized as chromium chromite, and it matches to the generic magnesiochromite ferroan ($(Mg,Fe^{2+})(Cr,Al)_2O_4$, PDF Card 09-0353, crystal data 8.277 (CUBIC)), where almost all the iron is as Fe(II). Nevertheless, the presence of this spinel cannot explain the peak 10 in the diffractogram (Fig. 2), and the peaks 1 and 2 show higher intensity than in the diffractogram of the standard magnesiochromite ferroan.

A slight deviation between the values of the characteristic crystal structure distances of the standard chromite and the analyzed sample was observed. This occurrence has been also found by comparing the diffractogram sample with those obtained using other standard chromite [5,6]. These differences are due to the use as standard of a specific specimen from Cribou pitt, Coleraine Tp. Québec, Canada [18] with the following composition: 55.51% Cr_2O_3, 14.03% Al_2O_3, 3.79% Fe_2O_3, 11.35% FeO, 14.83% MgO and minor compounds of Si, Ti, Ca and Mn. This specimen has strong differences with the chromite sample studied in this work, for instance, its amount of Cr_2O_3 is higher, the content in iron is lower, and, above all, it has a significant amount of Fe(III).

In this standard, the oxidation state of the iron would be slightly higher than +2, and considering that only this oxidation state was found, the mineral has merely one phase, the chromite spinel, which corresponds to a standard obtained from a specimen with a chemical composition closer to the studied chromite ore sample (see previous paragraph).

Together to this spinel, some peaks, probably corresponding to silicates, were detected. This was in agreement with the high amount of SiO_2 found in the elemental analysis

Table 3
Semiquantitative elemental composition of the selected particle obtained by X-ray microanalysis and theoric amount corresponding to the chemical formula of the labradorite ($Na_{2.84}Ca_{4.16}Al_{12}Si_{20}O_{64}$)

Element	Analyzed sample weight%	Labradorite weight%
O K	51.67	47.85
Na K	2.59	3.05
Al K	15.01	15.14
Si K	22.40	26.17
Ca K	8.03	7.78

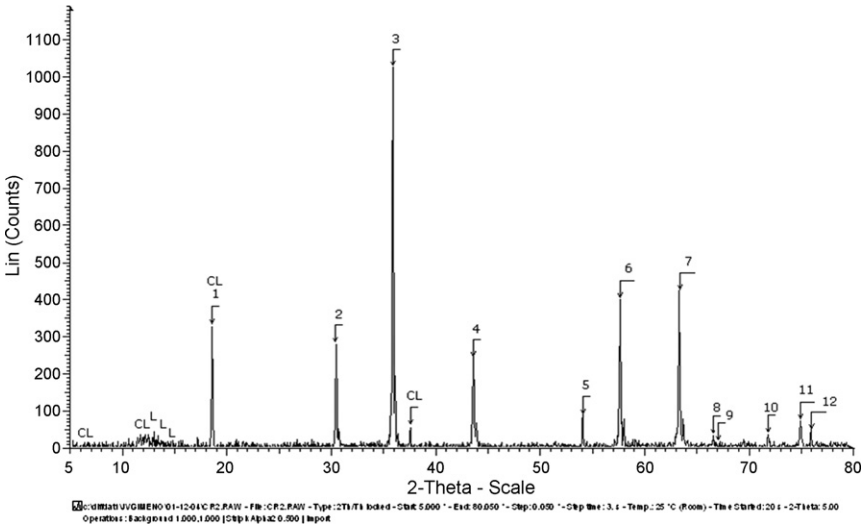

Fig. 2. Diffractogram of chromite ore. The peaks marked with numbers correspond to spinels and those indicated with letters CL and L correspond to chlorite and labradorite, respectively.

of the unknown chromite sample (6.45%). Some previous studies of other chromite ores with high amount of SiO_2, similar to the unknown sample analyzed in this work, point to these silicates could be hydroxylated aluminosilicates (with Mg and/or Al or Fe) antigorite or chlorite sort, or Fe-Mg chromite $(Mg,Fe)_6Si_{2-4}Al_{0-2}O_{10}(OH)_8$ chlorite sort [6].

The accurate mineralogical characterization of the impurities is of the utmost importance, so other analytical techniques, as light microscopy and SEM/EDX were used in order to complement and corroborate the results obtained by XRF, XRD and voltammetry.

3.3. Light microscopy study

In order to determine the chlorite type, the chromite ore sample was thinly powdered and sieved, and analyzed by light microscopy. The obtained photography is shown in Fig. 3.

In the microphotography, some particles with colouration typical of brown and mainly orange (distinctive of Fe(II)-rich minerals) spinels, which correspond in the image to several grey shades, were found. Between them, white and white-yellow spinels, indicating the presence of silica and silicates, can also be observed. However, the most important result was the detection of numerous inclusions of violet particles (marked with circles in Fig. 3), with marine blue interfering colours (depending on the luminosity), a typical colouration of chrome–chlorites. The presence of antigorites and Fe-Mg chlorite types was rejected, because of their green colouring.

Some authors have studied several chlorites, previous mineral purification [17,19,20]. Hey has proposed the term "chrome chlorite" for chlorites with less than 4% of Cr_2O_3 [20]. Lapham has given a brief historical account of the nomenclature of the chromium chlorites and has proposed a classification on the basis of cryslochemical study [17]. He concludes that the presence of Cr_2O_3 in higher amounts will not affect the crystal structure, and he restricts the term kaemerite to the former variety and kotschubeite to the latter.

A thorough comparison between the diffractogram peaks of the standards and the unknown chromite ore sample

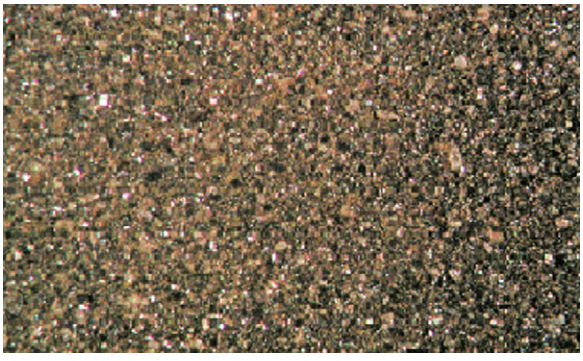

Fig. 3. Microphotography of the chromite ore obtained by light microscopy (144×, visible light).

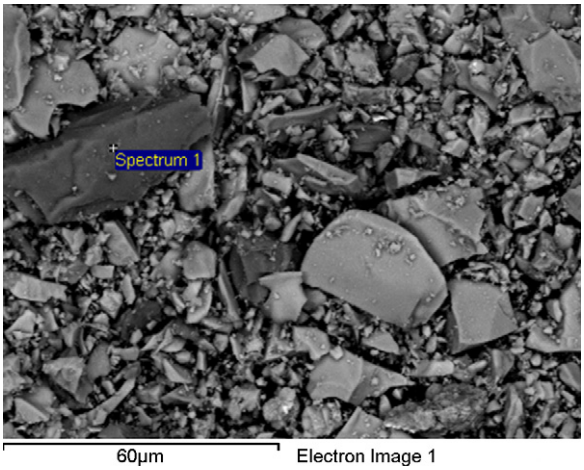

Fig. 4. SEM-image of the powdered chromite ore sample by detector secondary electron.

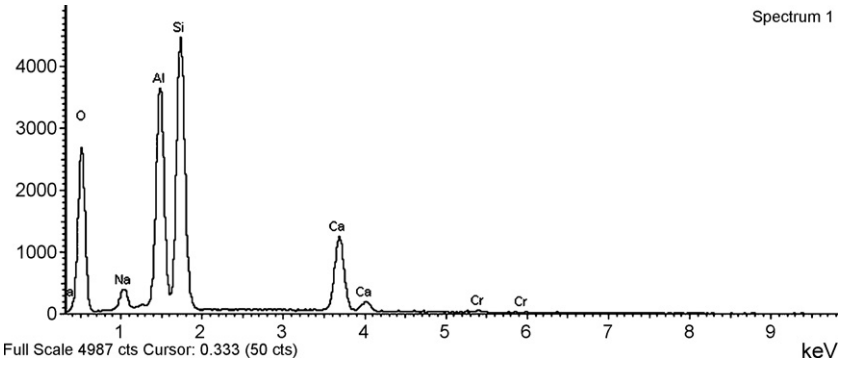

Fig. 5. Energy spectrum obtained by SEM/EDX of the analyzed phase found in the chromite ore sample (Fig. 4).

(Fig. 2) has allowed the characterization of the mineral as chlorite chromian (magnesium aluminium chromium silicate hydrate $Mg_{5.1}Al_{1.2}Si_3Cr_{0.7}O_{10}(OH)_8$), PDF Card 72-1385, whose peaks have been marked as CL in the diffractogram [21]. Specimen from Enzinca, Turkey). The presence of this chlorite also justifies the too high intensity of the peak 1 in the diffractogram (Fig. 2).

3.4. SEM/EDX analysis

The elemental analysis of the original sample shows the presence of calcium and sodium. However, these elements are not in the chemical formulas of the previously characterized minerals. In order to find the mineral which includes these minor elements in its composition, a thoroughly exploration of the powdered sample by SEM/EDX was carried out. A phase darker than the mineral easily distinguishable by SEM was observed (Fig. 4). X-ray microanalysis of a small area of this particle by SEM/EDX allowed the identification of the following elements: silicium, oxygen, calcium and sodium. The corresponding energy spectrum is shown in Fig. 5.

The chemical composition of the particle, provided by semiquantitative analysis, was found to be significantly similar to those obtained theoretically by the calculation from the elemental formula of the labradorite (Table 3). This information, together with the evaluation program of the diffractogram, allows to accurately determine the searched mineral, the Labradorite $Na_{2.84}Ca_{4.16}Al_{12}Si_{20}O_{64}$ PDF Card 85-0878, marked with L in the diffractogram (Fig. 2).

3.5. Mineral and impurities characterization

The analysis of the South African chromite ore sample reveals that the unknown mineral was made of a spinel, magnesiochromite ferroan. $(Mg,Fe^{2+})(Cr,Al)_2{\cdot}O_4$, PDF Card 09-0353.

The gangue would be mainly composed by chlorite chromian (magnesium aluminium chromium silicate hydrate $Mg_{5.1}Al_{1.2}Si_3Cr_{0.7}O_{10}(OH)_8$), PDF Card 72-1385 and by labradorite $Na_{2.84}Ca_{4.16}Al_{12}Si_{20}O_{64}$ PDF Card 85-0878. The presence of a small quantity of free silica was also envisaged (bright white points in Fig. 3).

3.6. Approximate mineralogical composition

The calculation of the quantitative mineralogical composition of the minerals in the ore was based on the relative amount of calcium oxide in the sample (0.47%), which was totally assigned to the labradorite, then the maximal proportion of this mineral was found to be 4.32%. From this result, the relative amount of Na_2O was calculated, obtaining a value of 0.18%. This value is in agreement with the theoretical proportion found from the chemical composition of the studied sample (Table 2). This corroborated that the calculation way and the obtained results were valid hypothesis. The relative amount of labraborite is then provided with high accuracy. By the same way, the relative amount of SiO_2 in the labradorite was 2.42%.

As the elemental analysis of the chromite ore sample provided a relative amount of SiO_2 was 6.45%, and considering all the SiO_2 is shared out only between labradorite and chlorite, the quantity of SiO_2 in the chlorite was 4.03%. Considering these entire hypotheses, the maximal amount of magnesium aluminium chromium silicate hydrate would be 12.79%. Then the total quantity of impurities in the sample was established to 17.11%. However, there probably was a small quantity of free silica, so the relative amount of impurities might be even lower.

Finally, the calculated total amount of spinels in the chromite ore sample was 82.89%. This value was calculated from the relative amount of impurities. This chromite spinel had the general formula $(Fe_xMg_{1-x})(Cr_yAl_{1-y})_2O_4$ and its oxide chemical composition was: 50.74% Cr_2O_3, 26.12% FeO, 15.06% Al_2O_3 and 8.08% MgO. These values were calculated by determining the content of each oxide in the impurities (chlorite and labradorite), and subtracting them from the general amount of each oxide in the whole ore sample (Table 2).

Alujas Diaz et al. have also analyzed a chromium compound with 3.40% of SiO_2 as chlorite and antigorite, finding, by means of a roentgenphasic study, that their relative amount was between 8 and 14%. This interval was considered too large and quite higher that found in this work [6].

4. Conclusions

The analysis of the South African chromite ore sample has allowed to establish that it was a mineral with a 42.43% of

Cr_2O_3 and a Cr_2O_3/FeO ratio of 2.02. According to this composition, the mineral was considered belonging to refractory grade for its possible applications. However, due to its high amount in Cr_2O_3 (above 40%) and SiO_2 (above 6%), which can provide some fragility to the mineral, and the average-proportion of Al_2O_3 (≈15.16%) and MgO (≈12.6%), it can be concluded that the studied mineral could also be considered as chemical grade.

Consequently, the mineral cannot be used to introduce chromium in alloys due to its high amount of silicate impurities. Therefore, their usual applications are as follows: the production of coloured pigments for porcelain and other ceramic materials, to produce a characteristic green colouration in the glass and even as pigment in enamels on metals. In these cases, the silica is not an inconvenience, and it might even be an advantage.

The mineralogical study by XRD and light microscopy allows to deduce that the chromite mineral was essentially made of chromite spinel (magnesiochromite ferroan), in which iron was mainly as Fe(II), under cubic system crystal. The impurities have been identified by XRD and SEM/EDX as silicates, mainly chlorite chromian (magnesium aluminium chromium silicate hydrate), labradorite in slighter proportion and a small quantity of free silica.

Acknowledgements

Financial support from the Spanish Ministry of Education and Science and the European Union (R + D + I Project CTQ2005-09339-CO3-02/BQU and E.R.D.F.) is gratefully acknowledged.

References

[1] S.M. Zubakov, E.N. Yusupova, Refract. Ind. Ceram. 3 (1962) 341.
[2] S.E. Swanson, Join Meeting of the Northeast Section (39th Annual) and Southeastern Section (53rd Annual) Geological Society of America, Abstract with Programs, vol. 36, Washington DC, USA, March, 2004, p. 135.
[3] M. Hock, G. Friedrich, W.L. Plüger, A. Wichowski, Miner. Deposita 21 (1986) 190.
[4] V.D. Tathavadkar, M.P. Anthony, A. Jha, Scand. J. Metall. 33 (2004) 65.
[5] C.A. Quintero, E. Delgado, Rev. Colomb. Quím. 27 (1998) 243.
[6] A. Alujas Diaz, Rev. Latin Am. Met. Mat. 23 (2003) 2.
[7] M. Cugat, Deformación Metálica 13 (1998) 197.
[8] Y.L. Ding, A.J. Merchant, Thermochim. Acta 292 (1997) 85.
[9] Y.L. Ding, N.A. Warner, The Proceedings of the 1996 I Chem E Research event/second European Conference for Young Research, University of Leeds, Leeds, 1996, pp. 506–509.
[10] Y.L. Ding, N.A. Warner, A.J. Merchant, Scand. J. Metall. 26 (1997) 55.
[11] F. Scholz, B. Meyer, in: A.J. Bard, I. Rubinstein (Eds.), Electroanalytical Chemistry, vol. 20, Marcel Dekker, New York, 1988, pp. 1–87.
[12] T. Grygar, F. Marken, U. Schröder, F. Scholz, Collect. Czech. Chem. Commun. 67 (2002) 163.
[13] T. Grygar, J. Electroanal. Chem. 405 (1996) 117.
[14] A. Doménech-Carbó, A. Doménech-Carbó, J.V. Gimeno-Adelantado, F. Bosch-Reig, M.C. Saurí-Peris, S. Sánchez-Ramos, Analyst 126 (2001) 1764.
[15] S. Sánchez Ramos, M.D. Jorge Cubillos, J.V. Gimeno Adelantado, D.J. Yusá-Marco, X-ray Spectrom. 35 (2006) 243.
[16] V.D. Tathavadkar, M.P. Anthony, A. Jha, Metall. Mater. Trans. B 36B (2005) 75.
[17] D.M. Lapham, Am. Miner. 43 (1958) 921.
[18] R. Thomtson, Mem. Geol. Soc. Am. 85 (1962) 195.
[19] K.T. Damodaran, B. Somasecar, Clays Clay Miner. 24 (1976) 31.
[20] M.H. Hey, Mineral. Mag. 30 (1954) 227.
[21] B.E. Brown, S.W. Bailey, Am. Miner. 48 (1963) 42.

Available online at www.sciencedirect.com
ScienceDirect
Talanta 74 (2008) 1659–1669
Talanta
www.elsevier.com/locate/talanta

Electroanalytical properties of cytochrome *c* by direct electrochemistry on multi-walled carbon nanotubes incorporated with DNA biocomposite film

Jan-Wei Shie, Umasankar Yogeswaran, Shen-Ming Chen *

Department of Chemical Engineering and Biotechnology, National Taipei University of Technology, No. 1, Section 3, Chung-Hsiao East Road, Taipei 106, Taiwan, ROC

Received 9 August 2007; received in revised form 14 October 2007; accepted 15 October 2007
Available online 26 October 2007

Abstract

A novel conductive biocomposite film (MWCNTs–DNA–cyt *c*) which contains multi-walled carbon nanotubes (MWCNTs) along with the incorporation of DNA and cytochrome *c* (cyt *c*) has been synthesized on glassy carbon electrode (GCE), gold (Au), indium tin oxide (ITO) and screen printed carbon electrode (SPCE) by potentiostatic methods. The presence of both MWCNTs and DNA in the biocomposite film enhances the surface coverage concentration (Γ), increases the electron transfer rate constant (K_s) up to 21% and decreases the degradation of cyt *c* during the cycling. The biocomposite film also exhibits a promising enhanced electrocatalytic activity towards the reduction of halogen oxyanions and oxidation of biochemical compounds such as ascorbic acid and L-cysteine. The cyclic voltammetry has been used for the measurement of electroanalytical properties of analytes by means of biocomposite film modified GCEs. The sensitivity of MWCNTs–DNA–cyt *c* modified GCE possess higher values than the values obtained for DNA–cyt *c* film modified GCE. Further, the reduction potentials of halogen oxyanions E_{pc}, clearly shows that the activity of the biocomposite is dependent on the electronegativity of halogen oxyanions. Electrochemical quartz crystal microbalance studies revealed the enhancements in the functional properties of MWCNTs, DNA and cyt *c*. We have studied the surface morphology of the biocomposite films using scanning electron microscopy and atomic force microscopy, which revealed that DNA and cyt *c* have been incorporated on MWCNTs. Finally, the flow injection analysis has been used for the amperometric detection of analytes at MWCNTs–DNA–cyt *c* film modified SPCE.
© 2007 Elsevier B.V. All rights reserved.

Keywords: Multi-walled carbon nanotubes; Composite film; Modified electrodes; Electrocatalysis; Halogen oxyanions; Vitamin c; L-Cysteine

1. Introduction

Cytochrome *c* protein (cyt *c*) has received considerable importance in recent years in the field of electroanalytical chemistry because of its unique binding property with other protein redox partners. The direct electron transfer of cyt *c* was first observed by Bowden et al. [1,2] but in that observation, the cyt *c* showed transient response and short-life on the metal surfaces. These shortcomings can be explained as; firstly the cyt *c* molecules form irreversible adsorption blocks on the electrode surface, secondly the poisoning and deactivation of protein molecules unfold and then the adsorption of these occur on the bare electrodes [3–5]. Studies were carried out previously to enhance the electron transfer rate of cyt *c* on the metal electrodes. But, these too showed an apparent deactivation by oligomer formation on the electrode surface [6–8]. After that, in the following decades, an idea of using an electrode surface that was modified with some species having specific adsorption interaction to improve the electron transfer rate of cyt *c* had been proposed [9–12]. Not limited to these sorts of ideas, numerous other studies were also carried out on cyt *c* using solid state electrodes, oligomer and some polymers as promoters [13–15]. However, the results showed that the interaction and binding of cyt *c* to all those electrodes were weak. Recently, charge–transfer interactions have also been reported between cyt *c* and deoxyribonucleic acid (DNA) [16]. DNA molecule contains three constituents as, phosphate acid groups, basic groups, and sugar units. The basic groups are adenine, guanine, cytosine and thymine. The structure of the DNA consists of two molecular chains, in which one chain is tightly bound to the other to

* Corresponding author. Tel.: +886 2270 17147; fax: +886 2270 25238.
E-mail address: smchen78@ms15.hinet.net (S.-M. Chen).

0039-9140/$ – see front matter © 2007 Elsevier B.V. All rights reserved.
doi:10.1016/j.talanta.2007.10.034

form a double helix and they are held together by many hydrogen bonds. Further, DNA is classified as natural polymer. The direct electron transfer of heme proteins and horseradish peroxidase immobilized on DNA modified electrodes were used for sensor applications [17]. The interaction of DNA with metal proteins in the analysis of electroactive metal proteins, especially cyt *c* was also reported [18].

On the other hand, a wide variety of applications of matrices made of carbon nanotubes (CNTs) for the detection of bioorganic and inorganic compounds such as insulin, ascorbic acid, etc. were also already reported [19–22]. The rolled-up graphene sheets of carbon, i.e., CNTs, exhibits a π-conjugative structure with a highly hydrophobic surface. This property of the CNTs allows them to interact with some organic aromatic compounds through π–π electronic and hydrophobic interactions [23–25]. These interactions are used for preparing composite sandwiched films for electrocatalytic studies [26] and in the designing of nanodevices with the help of non-covalent adsorption of enzyme and proteins on the side walls of CNTs. This has resulted in a novel CNTs based nanostructures which contain biochemical units in them [27]. Some attempts were also made to prepare hydrophilic surface CNTs to overcome the dispersion problems in aqueous medium for bio-electrochemical applications [28]. Electrodes modified with composite films are widely used in capacitors, battery, fuel cells, chemical sensors and biosensors [29–31]. Even though the electrocatalytic activity of the CNTs with protein matrices individually showed good results; some properties like mechanical stability, sensitivity for different techniques and electrocatalysis for multiple compound detections are found to be poor.

Interestingly, the direct electron transfer between the cyt *c* and DNA modified electrode from aqueous solution and its catalytic activity towards different compounds have already been reported [18]. Further, the literature survey reveals that there were no previous attempts for the synthesis of biocomposite film composed of CNTs, DNA and cyt *c* for use in sensor applications. In this paper, we report about a novel biocomposite film (MWCNTs–DNA–cyt *c*) made of multi-walled carbon nanotubes (MWCNTs) which has been incorporated with DNA and cyt *c*. Its characterization and enhancement in functional properties, stability, peak current and electrocatalytic activity have also been reported along with its application in electrocatalysis of halogen oxyanions, ascorbic acid (AA) and L-cysteine (LC). Among these, the halogen oxyanions catalytic reductions at MWCNTs–DNA–cyt *c* biocomposite film are dependent on their electronegativity. The film formation processing involves the modification of glassy carbon electrode (GCE) with uniformly well dispersed MWCNTs and which is then modified with DNA. The modified MWCNTs–DNA GCE is then electrodeposited with cyt *c* from the neutral aqueous solution.

2. Experimental

2.1. Apparatus

Cyclic voltammetry (CV) were performed in an analytical system model CHI-611, CHI-400 and CHI-1205A potentiostat. A conventional three-electrode cell assembly consisting of an Ag/AgCl reference electrode and a Pt wire counter electrode were used for the electrochemical measurements. The working electrode was either an unmodified GCE or a GCE modified with the DNA–cyt *c* or MWCNTs–DNA–cyt *c* biocomposite films. In these experiments, all the potentials have been reported versus the Ag/AgCl reference electrode. The working electrode used for the EQCM measurements was an 8 MHz AT-cut quartz crystal coated with gold electrode. The diameter of the quartz crystal was 13.7 mm; the gold electrode diameter was 5 mm. The flow injection analysis (FIA) of the analytes at screen printed carbon electrode (SPCE) was done using Alltech 426 HPLC pump containing an electrochemical cell. The morphological characterizations of the films were examined by means of SEM (Hitachi S-3000H) and atomic force microscopy (AFM) (Being Nano-Instruments CSPM4000). All the measurements were carried out at 25 °C ± 2.

2.2. Materials

Cytochrome *c* (cyt *c*), multi-walled carbon nanotubes (MWCNTs OD = 10–20 nm, ID = 2–10 nm and length = 0.5–200 μm), DNA, potassium hydroxide, L-cysteine and ascorbic acid were obtained from Aldrich and Sigma–Aldrich, KIO_3 and $KClO_3$ from Osaka and $KBrO_3$ from Nakarai were used as received. All other chemicals used were of analytical grade. The preparation of aqueous solution was done with twice distilled deionized water. Solutions were deoxygenated by purging with prepurified nitrogen gas. Buffer solutions were prepared from H_2SO_4 and 2-amino-2-hydroxymethyl-1,3-propanediol (0.1 M TRIS buffer) for the pH 1.0 and 8.4, respectively.

2.3. Preparation of MWCNTs and MWCNTs–DNA–cyt c modified electrodes

There was an important challenge in the preparation of MWCNTs. Because of its hydrophobic nature, it was difficult to disperse it in any aqueous solution to get a homogeneous mixture. Briefly, the hydrophobic nature of the MWCNTs was converted in to hydrophilic nature by following the previous studies [28]. This was done by weighing 10 mg of MWCNTs and 200 mg of potassium hydroxide in to a ruby mortar and grained together for 2 h at room temperature. Then the reaction mixture was dissolved in 10 ml of double distilled deionized water and it was precipitated many times in to methanol for the removal of potassium hydroxide. Thus obtained MWCNTs in 10 ml water was ultrasonicated for 6 h to get a uniform dispersion. This functionalization process of MWCNTs was done to get a hydrophilic nature by which, the MWCNTs can be homogeneously dispersed in water. This process not only converts MWCNTs to hydrophilic nature but this helps to breakdown larger bundles of MWCNTs in to smaller ones also. This process was confirmed using SEM, which is not shown in the figures. Then a homogenous 0.45 mg ml^{-1} concentration of DNA solution was prepared in double distilled deionized water.

Before starting each experiment, the GCEs were polished by a BAS polishing kit with 0.05 μm alumina slurry, rinsed and then

ultrasonicated in double distilled deionized water. The GCEs studied were uniformly coated with 5.8 μg cm^{-2} of MWCNTs then dried, and then coated with 4.4 μg cm^{-2} of DNA and again dried at 35 °C. The concentrations of homogeneously dispersed MWCNTs and DNA were exactly measured using micro-syringe. The electrochemical deposition of cyt *c* was performed from 2×10^{-4} M cyt *c* in pH 8.4 TRIS buffer aqueous solution by consecutive CV over a suitable potential region of −0.2 to 0.3 V. Then, the modified MWCNTs–DNA–cyt *c* electrode was carefully washed with double distilled deionized water. The concentrations of homogeneously dispersed MWCNTs and DNA were exactly measured using micro-syringe. For a detailed comparison of electrocatalysis reactions, we studied different types of modified electrodes such as DNA–cyt *c*, MWCNTs–cyt *c* and MWCNTs–DNA–cyt *c*. In all these studies, the electrodes were first modified by MWCNTs, DNA and then electrodeposited with cyt *c*. These characterization studies were done to reveal the obvious necessity for the presence of MWCNTs in the DNA–cyt *c* biocomposite film.

3. Results and discussions

3.1. Electrochemical synthesis of MWCNTs–DNA–cyt c biocomposite film and its characterization

The electrochemical deposition of cyt *c* (2×10^{-4} M) on MWCNTs–DNA modified GCE present in pH 8.4 TRIS buffer solution has been performed by consecutive CV for the preparation of MWCNTs–DNA–cyt *c* biocomposite film. The suitable potential range for cyt *c* deposition has been found to be −0.2 to 0.3 V (see ESI[1]). In the following experiments, each newly prepared biocomposite film on GCE has been washed carefully in deionized water to remove the loosely bounded cyt *c* on the modified GCE. It was then transferred to pH 8.4 of 0.1 M TRIS buffer or pH 1.0 aqueous solutions for the other electrochemical characterizations. These optimized pH solutions have been chosen to maintain the higher stability of the biocomposite film. Fig. 1(A) represents the electrochemical signal of cyt *c* at 20 mV s^{-1} on (a′) DNA modified GCE with a $Fe^{III/II}$ redox couple corresponding to the redox reaction of cyt *c* with the formal potential $E^{0\prime}$ = 8.95 mV versus Ag/AgCl in TRIS buffer solution, and no redox peak in (b′) show that there is no direct electron transfer of cyt *c* occurred at MWCNTs modified GCE, whereas in (c′) similar redox couple of cyt *c* show higher peak current at MWCNTs–DNA modified GCEs with the formal potential of $E^{0\prime}$ = −31.55 mV. When comparing with the formal potentials of cyt *c*, in both the cases (a′) and (c′), there is a shift in $E^{0\prime}$ towards lower positive potential of about 40.5 mV in the presence of MWCNTs. Also, there is a decrease in ΔE value of about 7.9 mV in the presence of MWCNTs. This is because of the high reversibility of cyt *c* in the presence of MWCNTs–DNA. The higher ΔE value for cyt *c* at DNA modified GCE could be the cause of an irreversible adsorption of cyt *c* on the modified electrode [18]. Further, comparing (b′) with the other two CVs (a′ and c′) in the same figure reveals the importance of DNA on the biocomposite film, where GCE modified with only MWCNTs has no active redox couple growth for cyt *c* (ESI see Footnote 1). The biocomposite film formation and the interactions between MWCNTs, DNA and cyt *c* can be cleaved in to two steps. The foremost step is the attachment of DNA on MWCNTs, this could happen in two ways, either by the attachment of amine groups present in DNA with that of carboxyl groups of modified MWCNTs or by the attachment of DNA on the sidewalls of MWCNTs by hydrophobic interactions [32]. The second step is the attachment of cyt *c* on the DNA. The immobilization of cyt *c* on DNA and the interaction between both of these compounds can be explained as the electrostatic attraction between the positively charged lysine (pK_a = 10.8) $-NH_3^+$ group or the other positively charged groups such as Fe^{2+} and Fe^{3+} in cyt *c* with that of the negatively charged phosphates of the DNA backbone [18,32]. Scheme 1 shows the possible interactions between MWCNTs, DNA and cyt *c*. From these CVs in Fig. 1(A), the surface cover-

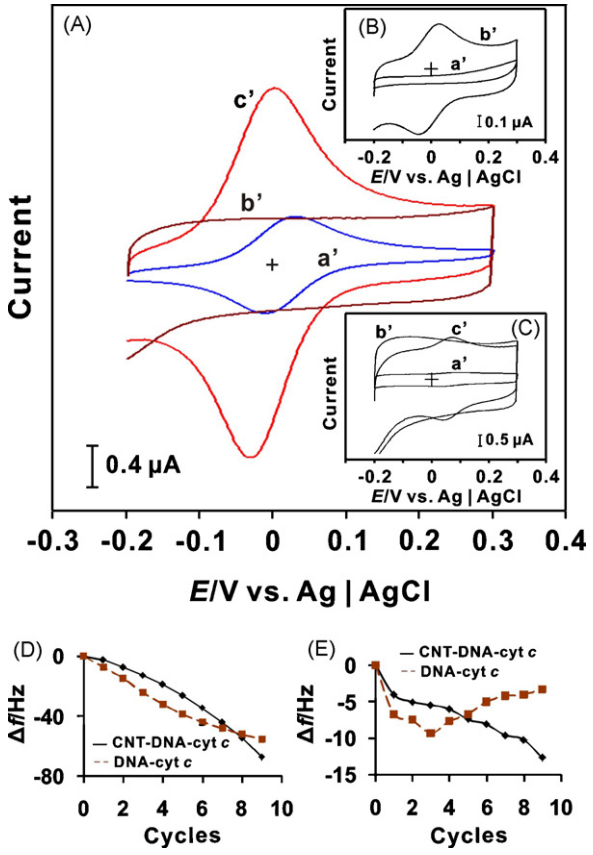

Fig. 1. (A) Comparison of CVs of (a′) DNA–cyt *c*, (b′) MWCNTs–cyt *c* and (c′) MWCNTs–DNA–cyt *c* biocomposite films at GCE in 0.1 M pH 8.4 TRIS buffer, scan rate at 20 mV s^{-1}, the redox couples in these CVs represents ($Fe^{III/II}$) reactions of cyt *c*. (B) CVs of Au modified from (a′) DNA–cyt *c* and (b′) MWCNTs–DNA–cyt *c* at similar conditions to that of GCE. (C) CVs of ITO modified from (a′) DNA–cyt *c*, (b′) MWCNTs–cyt *c* and (c′) MWCNTs–DNA–cyt *c* at similar conditions to that of GCE. From these CVs, the peak current and the calculated values (Table 1) reveals that the increase in Γ of cyt *c* has been taken place in presence of DNA and MWCNTs at all the electrodes. (C) Plot of frequency change in EQCM vs. scan cycles and (D) every cycle frequency change vs. scan cycles for both the films. These results show the biocomposite is a stabilized one and it is deposited homogeneously.

[1] Electronic Supplementary Information (ESI) available.

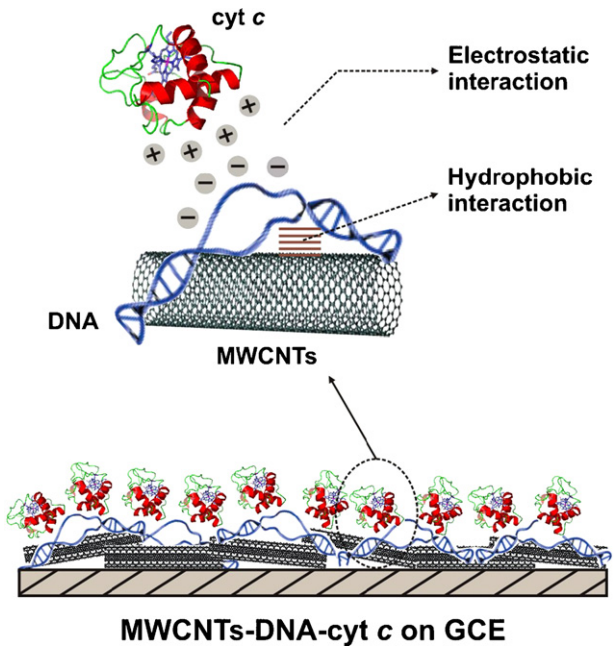

Scheme 1. Possible interaction between MWCNTs, DNA and cyt *c* for the formation of MWCNTs–DNA–cyt *c* biocomposite film modified electrodes.

age concentration (Γ) values have been calculated and are given in Table 1. In this calculation, the charge involved in the reaction (Q) has been obtained from CVs and it has been applied in the equation $\Gamma = Q/nFA$, where, the number of electron transfer involved in the cyt *c* redox reaction is assumed as two (one electron for each heme group) [18]. These values indicate that the presence of MWCNTs increased the surface area of the electrode, which in turn has increased the Γ of cyt *c*. For comparison, the Γ values at other modified electrodes from the literature have also been provided in the same table, and these values reveal that the MWCNTs–DNA at GCE enhances Γ of cyt *c* than the other modified electrodes.

Table 1
Surface coverage concentrations (Γ) of cyt *c* at different types of modified electrodes

Electrode type	Modified film	Γ (mol cm^{-2})
GCE[a]	DNA–cyt *c*	6.11×10^{-12}
	MWCNTs–DNA–cyt *c*	2.34×10^{-11}
Au[a]	DNA–cyt *c*	No peak
	MWCNTs–DNA–cyt *c*	6.72×10^{-12}
ITO[a]	DNA–cyt *c*	2.41×10^{-12}
	MWCNTs–cyt *c*	No peak
	MWCNTs–DNA–cyt *c*	1.50×10^{-11}
Mixed SAMs of MES/MEL[b] [42]		7.70×10^{-12}
SAMs of (T-COOH)/(T-NH$_2$)[c] [43]		9.20×10^{-12}
Fullerene [44]		1.70×10^{-11}
N-Butylpyridinium tetrafluoroborate [45]		1.57×10^{-11}
Sulfonated polyaniline nano-networks [46]		9.80×10^{-12}
Planar ITO [47]		9.50×10^{-12}
SAM of ω-carboxylalkanethiols [48]		1.19×10^{-12}

[a] Studied using CV technique in 0.1 M TRIS buffer aqueous solution (pH 8.4).
[b] MES/MEL is 2-mercaptoethanesulfonate/2-mercaptoethanol.
[c] (T-COOH)/(T-NH$_2$) is thioctic acid/thioctic amide.

Gold and ITO electrodes have also been used to characterize the biocomposite films in pH 8.4 TRIS buffer aqueous solution. Fig. 1(B) represents the redox peaks of cyt *c* on DNA modified Au electrodes in (a′) absence and (b′) presence of MWCNTs, where there is no peak for cyt *c* on DNA modified Au. This obviously shows that there is no occurrence of direct electron transfer on DNA modified Au as reported previously [18]. Similarly, Fig. 1(C) represents the redox peaks of cyt *c* on ITO modified electrodes in (a′) presence of DNA, (b′) presence of MWCNTs and (c′) presence of both DNA and MWCNTs. These results too reveal the importance of the presence of DNA and MWCNTs in the biocomposite films. This condition enhances the electron transfer on different electrodes which in turn widens their use in the sensor based applications. However, comparison of data in Table 1 shows that Γ of cyt *c* is lower on MWCNTs–DNA modified Au than that of MWCNTs–DNA modified GCE. The percentage of degraded Γ of cyt *c* on MWCNTs–DNA modified Au on comparing with GCE has been calculated as 249%. The electrochemical quartz crystal microbalance (EQCM) experiments have been carried out by modifying the gold in electrochemical quartz crystal with uniformly coated MWCNTs and DNA, which has been dried at 35 °C (ESI see Footnote 1). From the frequency change, the change in the mass of biocomposite film at the quartz crystal has been calculated by the Sauerbrey equation, however 1 Hz frequency change is equivalent to 1.4 ng of mass change [33,34]. The mass change during cyt *c* incorporation on the DNA modified and MWCNTs–DNA modified Au for total cycles has been found to be 77.85 and 93.92 ng cm^{-2}, respectively, which are consistent with that of the Γ of cyt *c* values. However, in both cases because of the poor direct electron transfer, the redox peak currents are very low. Fig. 1(C) indicates the variation of frequency change with the increase of scan cycles and Fig. 1(D) indicates every cycle frequency change with the increase of the scan cycles. From these plots, it is clear that there has an unstable deposition of cyt *c* on the DNA modified Au when compared with the MWCNTs–DNA modified Au. Up to six cycles the cyt *c* deposition rate is higher in DNA modified Au than that of MWCNTs–DNA modified Au, however in later stages the rate of deposition on DNA modified Au has been drastically reduced. This proves that the deposition of cyt *c* on MWCNTs–DNA biocomposite film is more stabilized and more homogeneous than on the other modified electrodes. Similar previous studies on CNTs biocomposite have also shown the necessity of the CNTs for improving the functional properties such as orientation, enhanced electron transport, high capacitance, etc. [35,36].

3.2. Electrochemical and morphological characterization of MWCNTs–DNA–cyt c biocomposite film

The CVs of MWCNTs–DNA–cyt *c* biocomposite film on GCE in pH 8.4 TRIS buffer solution at different scan rates (ESI see Footnote 1) demonstrated that the redox process is not controlled by diffusion up to 200 mV s^{-1}. Further investigation reveals that, the separation between anodic and cathodic peak currents for both the films increased as the scan rate

increased up to 2.0 V s^{-1} (CVs not shown). However, in Fig. 2(A) the separation between the anodic and cathodic peak of MWCNTs–DNA–cyt *c* is lower than DNA–cyt *c*, which shows MWCNTs–DNA–cyt *c* posses faster electron transfer rate than DNA–cyt *c* film. Also, the peak to peak potential separation ΔE_p for MWCNTs–DNA–cyt *c* is <200 mV below 1.52 V s^{-1} scan rate, but DNA–cyt *c* shows $\Delta E_p > 200$ mV even for 1.36 V s^{-1}. From the slope values in Fig. 2(B), by assuming the value of $\alpha \approx 0.5$, the electron transfer rate constant has been calculated based on Laviron theory [37] is $K_s \approx 0.89\ s^{-1}$ for MWCNTs–DNA–cyt *c* and 0.73 s^{-1} for DNA–cyt *c*. From these

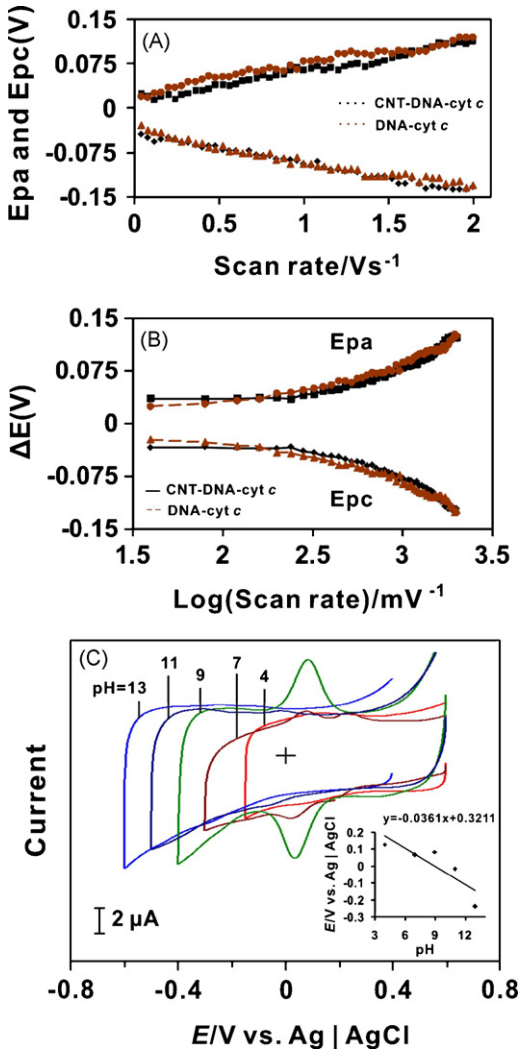

Fig. 2. (A) Shows the plot of E_{pa} and E_{pc} vs. different scan rate (0.02–2 V s^{-1}) for both DNA–cyt *c* and MWCNTs–DNA–cyt *c* biocomposite films present in 0.1 M pH 8.4 TRIS buffer. From this result, it is clear that the electron transfer rate is roughly higher for MWCNTs–DNA–cyt *c* biocomposite film when compared with DNA–cyt *c* film. (B) Shows a plot of ΔE vs. log of scan rate for both the films, from the slope values, α and K_s are calculated, which shows a higher K_s value for MWCNTs–DNA–cyt *c* biocomposite film when compared with DNA–cyt *c*. In all the curves the brown dotted line and the black continuous line represents DNA–cyt *c* and MWCNTs–DNA–cyt *c*, respectively. (C) CVs of the MWCNTs–DNA–cyt *c* biocomposite film synthesized at similar conditions and transferred to various pH solutions; scan rate: 100 mV s^{-1}. The inset in (C) shows the formal potential vs. pH (4–13), the slope −36 mV/pH is almost nearer to Nernstian equation for 2 electron and 1 proton transfer.

K_s values the increase in the ability of electron transfer between the electrode surface and the cyt *c* in presence of MWCNTs has been calculated and it is found to be ≈21%. These results too show that, there has been an enhancement in functional properties of the biocomposite film at lower scan rates in presence of both DNA and MWCNTs.

Fig. 2(C) shows the CVs of MWCNTs–DNA–cyt *c* on GCE at various pH aqueous buffers solutions in which the cyt *c* is absent. In these experiments, the GCE has been modified with cyt *c* using pH 8.4 TRIS buffer solution, and then it has been washed with deionized water and then transferred to various pH aqueous buffer solutions for CV measurements. These CV results show that the film is stable in the pH range between 7 and 11 and the E_{pa} and E_{pc} values depends on the pH value of the buffer solution. In other pH solutions, the $Fe^{III/II}$ redox couple of cyt *c* is not clearly visible. In detail, the CVs of the biocomposite film in pH 4, 7 and 9 shows that the cyt *c* is stable in these pH solutions. However at pH 11, the partial denaturation of cyt *c* reduces the peak current of $Fe^{III/II}$ redox couple. Further, it is obvious that the broad peak with low peak current of $Fe^{III/II}$ redox couple in pH 13 is because of the total denaturation of cyt *c*. The inset in Fig. 2(C) shows the formal potential of MWCNTs–DNA–cyt *c* plotted over a pH range of 4–13. The response shows a slope of −36 mV/pH, which is close to that given by the Nernstian equation for two electron one proton transfer [38]. The enhanced stability of the cyt *c* in presence of DNA and MWCNTs has been studied (ESI see Footnote 1) and the percentage of degradation [39] of MWCNTs–DNA–cyt *c* and DNA–cyt *c* is calculated. The amount of degradation after 120 min cycling for MWCNTs–DNA–cyt *c* and DNA–cyt *c* is less than 16.39% and 36.37%, respectively and the percentage of decrease in degradation of cyt *c* in presence of MWCNTs is about 19.99% for 120 min cycling. Similar enhancements in the biocomposite properties in presence of CNTs have been already reported in the literature [35,36].

Further, four different films; cyt *c*, DNA–cyt *c*, MWCNTs–cyt *c* and MWCNTs–DNA–cyt *c* have been prepared on the indium tin oxide (ITO) with similar conditions and similar potential as that of GCE and were characterized using SEM. From Fig. 3, it is significant that there are morphological differences between all these four films. All the four film images have been measured at the same resolution of about ×2 k. It is a well known fact that the prolonged exposure to the electron beam will damage the cyt *c* films, so an at most care was taken to measure these images. The top views of nanostructures Fig. 3(A) on the ITO electrode surface show white patches of cyt *c* deposited on this electrode. When comparing this with Fig. 3(B)–(D) shows that the deposition of cyt *c* has taken place on both DNA modified and MWCNTs modified ITOs, respectively. However as discussed earlier, there is no redox couples observed for MWCNTs–cyt *c*, which shows the importance of DNA, which enhances the electron transfer for $Fe^{III/II}$ redox reaction in cyt *c*. The MWCNTs–DNA–cyt *c* biocomposite film in Fig. 3(D) reveals that the DNA had covered the entire MWCNTs to form MWCNTs–DNA biocomposite and then the cyt *c* has been deposited on the MWCNTs–DNA modified ITO. The dotted

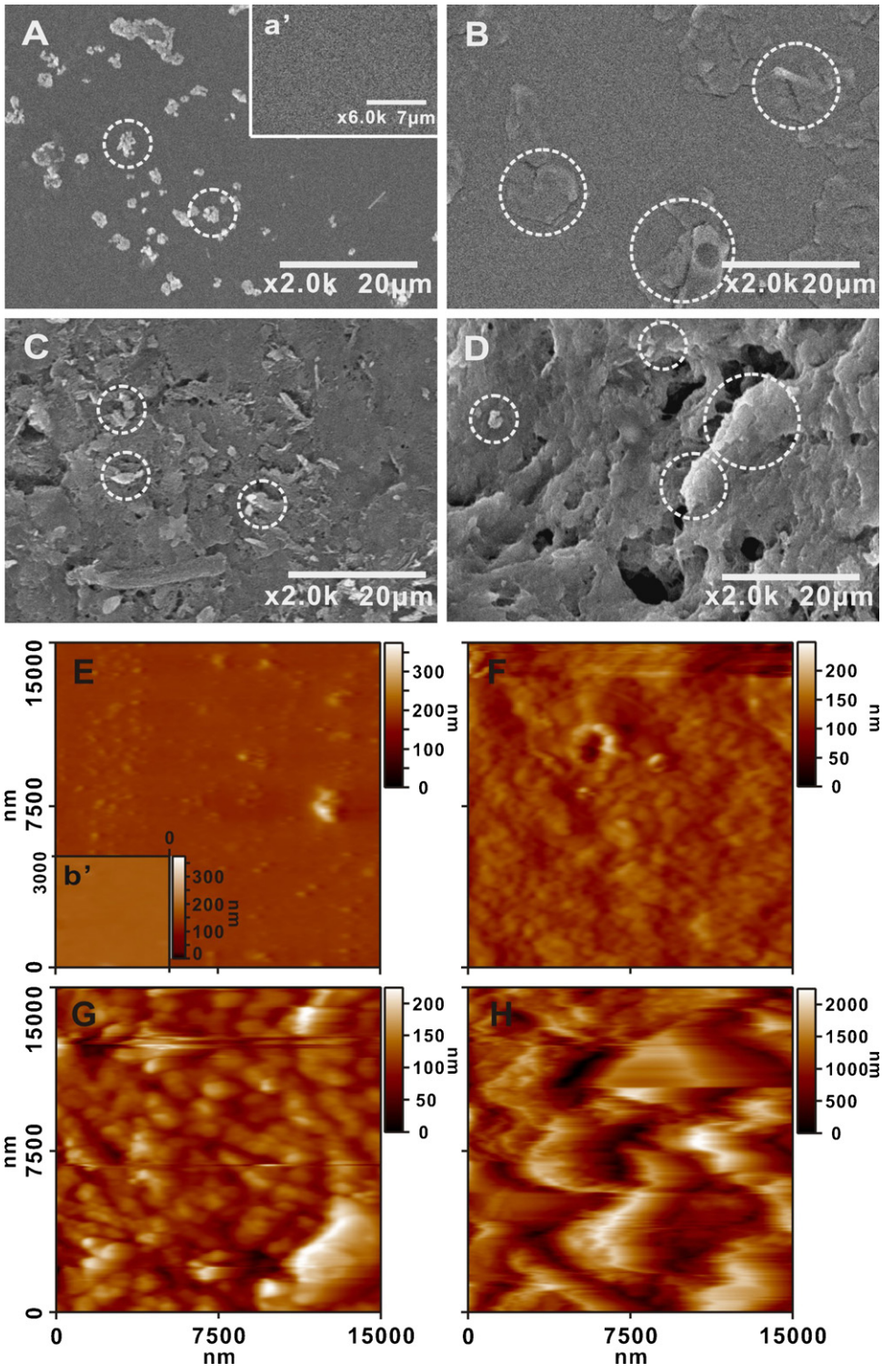

Fig. 3. SEM images of (A) cyt *c*, (B) DNA–cyt *c*, (C) MWCNTs–cyt *c* and (D) MWCNTs–DNA–cyt *c* biocomposite films. The white dotted circles represent the incorporation of cyt *c* on the unmodified and modified electrodes. AFM topography images of (E) cyt *c*, (F) DNA–cyt *c*, (G) MWCNTs–cyt *c* and (H) MWCNTs–DNA–cyt *c* biocomposite films. It is obvious that the observed morphological structure is similar to that of the structures obtained in SEM. (a′) and (b′) are the SEM and AFM images of bare ITO. Comparing all the figures it is obvious that the formation of biocomposite film in (D) and (H).

circles in all the four figures reveal that the deposition of cyt *c* occurred on the unmodified or modified ITOs. The same modified ITO electrodes have been used to measure the AFM topography images of (E) cyt *c*, (F) DNA–cyt *c*, (G) MWCNTs–cyt *c* and (H) MWCNTs–DNA–cyt *c*. In all these cases the observed morphological structure is similar to that of SEM. Further, for comparison, the SEM and AFM images of the bare ITO is shown in (a′) and (b′), respectively. These SEM and AFM results show the obvious formation of MWCNTs–DNA–cyt *c* biocomposite film.

3.3. Electroanalytical response of halogen oxyanions at MWCNTs–DNA–cyt c biocomposite film

The MWCNTs–DNA–cyt *c* biocomposite films have been synthesized on GCE at similar conditions as given in Section 2. Then, the modified biocomposite films have been washed carefully in deionized water and transferred to pH 1.0 H_2SO_4 aqueous solutions for studying the electrocatalysis of halogen oxyanions such as IO_3^-, BrO_3^- and ClO_3^-. This pH has been chosen as the most suitable one, as it is a well known fact that the reduction of halogen oxyanions is dependent on pH of the reaction medium [40]. All the CVs have been recorded at the constant time interval of 1 min with nitrogen purging before the start of each experiments. Generally in all the sections of Fig. 4, a′ represents bare GCE, b′ represents DNA–cyt *c* film and c′ represents MWCNTs–cyt *c* film modified GCEs. Fig. 4(A)–(C) shows the electrocatalytic reduction of IO_3^-, BrO_3^- and ClO_3^- at MWCNTs–DNA–cyt *c* biocomposite films, respectively at 20 mV s^{-1}. The CVs for MWCNTs–DNA–cyt *c* exhibit a reversible redox couple for cyt *c* ($Fe^{III/II}$) in the absence of the analytes, and upon addition of analytes, a new growth in the reduction peak of analytes appeared at $E_{pc} = -120$ mV for IO_3^-, $E_{pc} = -144$ mV for BrO_3^- and $E_{pc} = -163$ mV for ClO_3^-. These peak currents show that electrocatalytic reduction of all the three analytes took place at cyt *c* (Fe^{III}). Based on these results, the reaction between the analytes and the cyt *c* catalyst can be explained by the following Eqs. (1)–(3):

$$\text{cyt } c\,(Fe^{III}) + IO_3^- \rightarrow \text{cyt } c\,(Fe^{II}) + I^- \quad (1)$$

$$\text{cyt } c\,(Fe^{III}) + 2BrO_3^- \rightarrow \text{cyt } c\,(Fe^{II}) + Br_2 \quad (2)$$

$$\text{cyt } c\,(Fe^{III}) + 2ClO_3^- \rightarrow \text{cyt } c\,(Fe^{II}) + Cl_2 \quad (3)$$

An increase in concentration of analytes simultaneously produced a linear increase in the reduction peak currents of the analytes with good film stability as shown in the insets in Fig. 4(A)–(C). The cathodic peak currents are linear with the concentration of IO_3^- in the range of 5–15 μM. Similarly, for BrO_3^- and ClO_3^- it is in the range of 40–120 μM and 0.3–0.9 mM, respectively. It is obvious that the MWCNTs–DNA–cyt *c* shows higher electrocatalysis for IO_3^- and BrO_3^- when compared to all the other films. More specifically, the enhanced electrocatalysis of MWCNTs–DNA–cyt *c* can be explained in terms of higher peak current than that of MWCNTs–cyt *c*; and the both lower in overpotential and higher peak current than that of DNA–cyt *c*. Similarly, ClO_3^- shows higher electrocatalysis at MWCNTs–DNA–cyt *c* than all other films in terms of both lower in overpotential and higher peak current. These results can be observed from the I_{pa} and E_{pa} values in Table 2. Where, the increase in current and lower in overpotential, both are considered as the cause for the enhancement of electrocatalysis [41]. From the slopes of the linear calibration curves, the sensitivities of DNA–cyt *c* and MWCNTs–DNA–cyt *c* biocomposite modified GCEs and their correlation coefficient have been calculated and are given in Table 3. It is obvious that the sensitivity of MWCNTs–DNA–cyt *c* is high for all the three analytes when compared with DNA–cyt *c* modified GCEs. The shift towards negative potential in the E_{pa} values of IO_3^-, BrO_3^- and ClO_3^- clearly show that the electrocatalysis of halogen oxyanions at MWCNTs–DNA–cyt *c* biocomposite film is dependent on the analytes electronegativity. The overall view of these results, clearly reveal that MWCNTs–DNA–cyt *c* biocomposite film is efficient for halogen oxyanions detection.

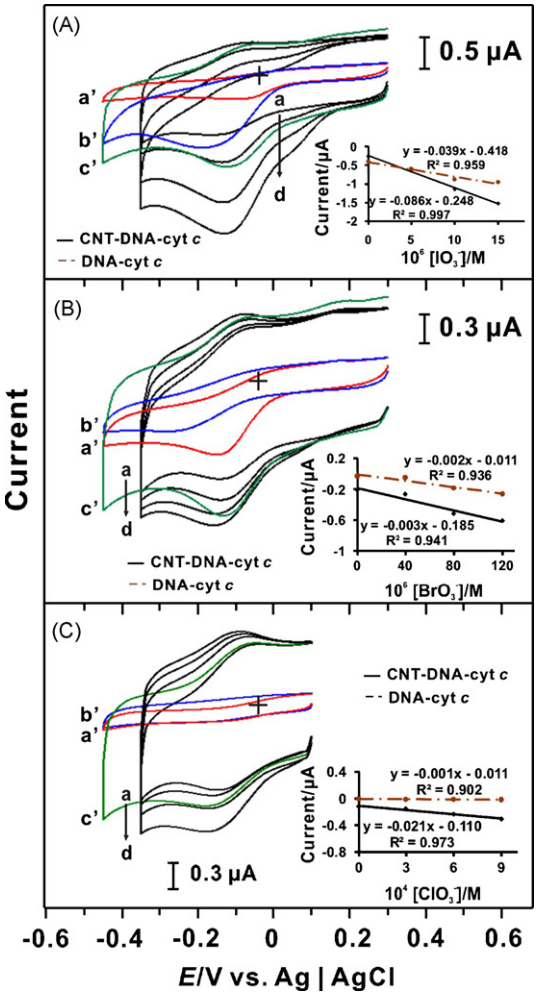

Fig. 4. (A) CVs of MWCNTs–DNA–cyt *c* biocomposite film in pH 1.0 H_2SO_4 aqueous solution with various concentrations of IO_3^- = (a) 0.0 M; (b) 5×10^{-6} M; (c) 1×10^{-5} M and (d) 1.5×10^{-5} M, where (a′), (b′) and (c′) in all the sections in figures represents bare, DNA–cyt *c* and MWCNTs–cyt *c* modified GCEs, respectively at the highest concentration of the analytes; scan rate: 20 mV s^{-1}. Similarly, (B) represents [BrO_3^-] = (a) 0.0 M; (b) 4×10^{-5} M; (c) 8×10^{-5} M and (d) 1.2×10^{-4} M. Similarly, (C) represents [ClO_3^-] = (a) 0.0 M; (b) 3×10^{-4} M; (c) 6×10^{-4} M and (d) 9×10^{-4} M. The insets in (A), (B) and (C) show the plot of current vs. different concentration of analytes, respectively at biocomposite films.

3.4. Electroanalytical response of ascorbic acid and L-cysteine at MWCNTs–DNA–cyt c biocomposite film

Fig. 5(A) and (B) shows the electrocatalytic oxidation of ascorbic acid (AA) and L-cysteine (LC), respectively. The electrolyte used for the electrocatalytic reactions was pH 8.4 TRIS aqueous buffer solution. In these studies, similar electrolyte has

Table 2
Comparison of E_{pa} and I_{pa} of analytes in electrocatalysis reactions using CV technique at different types of modified electrodes in pH 8.4 TRIS buffer solution

Analytes	Reaction type	pH	E_p (mV)			I_p (μA)		
			cyt c[a]	cyt c[b]	cyt c[c]	cyt c[a]	cyt c[b]	cyt c[c]
IO_3^-	Reduction	1.0	−190.0	−118.0	−120.0	−0.96	−0.58	−1.57
BrO_3^-	Reduction	1.0	−262.0	−125.0	−144.0	−0.33	−0.61	−0.76
ClO_3^-	Reduction	1.0	−181.1	−182.0	−163.0	−0.02	−0.29	−0.36
AA	Oxidation	8.4	79.0	−16.0	6.0	0.02	1.00	1.47
LC	Oxidation	8.4	61.0	70.0	58.0	0.01	0.32	0.89

[a] DNA modified GCE.
[b] MWCNTs modified GCE.
[c] MWCNTs–DNA modified GCE.

been used for both MWCNTs–DNA–cyt c biocomposite film preparation and the electrocatalytic studies. The CVs have been recorded at the constant time interval of 1 min with nitrogen purging before the start of each experiments. The scan rate used for electrocatalysis was 20 mV s^{-1}. In all the sections of Fig. 5, a′ represents bare GCE, b′ represents DNA–cyt c film and c′ represents MWCNTs–cyt c film modified GCEs. The CVs of the MWCNTs–DNA–cyt c in Fig. 5(A) and (B) exhibits a reversible redox couple for cyt c ($Fe^{III/II}$) in the absence of the analytes, upon addition of analytes, a new growth in the oxidation peak of analytes appeared at E_{pa} = 6 mV for AA and E_{pa} = 58 mV for LC. These peak currents show that electrocatalytic oxidation of both the analytes took place at cyt c (Fe^{II}). The interaction between the film and the analytes can be explained by the following equations, where (4) is for AA and (5) for LC [18]:

$$2\,\text{cyt}\,c\,(Fe^{II}) + \text{AA} \rightarrow 2\,\text{cyt}\,c\,(Fe^{III}) + \text{DHA} \quad (4)$$

$$\text{cyt}\,c\,(Fe^{II}) + 2\,CyS^- \rightarrow \text{cyt}\,c\,(Fe^{III}) + \text{CySSCy} \quad (5)$$

where DHA is dehydroascorbic acid (oxidized product of AA), CyS^- is L-cysteine and CySSCy is L-cysteine (L-cysteine's oxidized product). During the electrocatalysis experiments, an increase in concentration of analytes simultaneously produced a linear increase in the oxidation peak currents of the analytes with good film stability as shown in the insets in Fig. 5(A) and (B). The anodic peak currents are linear with the concentration of AA in the range of 0.1–0.4 mM. Similarly, for LC it is in the range of 0.6–2.1 mM. It is obvious that the MWCNTs–DNA–cyt c show higher electrocatalysis for both the analytes when compared to that of all other modified GECs, as we can observe it from the I_{pa} and E_{pa} values in Table 2. Further, the values in the same table reveal that there is no obvious peak for both the analytes at DNA–cyt c film. From the slopes of the linear calibration curves the sensitivity of the DNA–cyt c and MWCNTs–DNA–cyt c biocomposite modified GCEs and their correlation coefficient have been calculated and are given in Table 3. It is clear that, the sensitivity of MWCNTs–DNA–cyt c is higher for both the analytes and there is no electrocatalysis reaction at DNA–cyt c modified GCEs. These results clearly show that, the MWCNTs–DNA–cyt c biocomposite film can be efficiently used for the detection of AA and LC.

Table 3
Sensitivities and correlation coefficients of different modified electrodes for various analytes in CV technique

Analytes	Reaction type	Sensitivity (μA mM^{-1} cm^{-2}) [correlation coefficient]	
		DNA–cyt c	MWCNTs–DNA–cyt c
IO_3^-	Reduction	−37.6 [0.959]	−83.0 [0.997]
BrO_3^-	Reduction	−1.9 [0.936]	−2.9 [0.941]
ClO_3^-	Reduction	−1.0 [0.902]	−20.3 [0.973]
AA	Oxidation	−0.12 [0.952][a]	2.17 [0.988]
LC	Oxidation	−0.012 [0.673][a]	0.177 [0.875]

[a] The values indicate the instability and no electrocatalysis reaction at the film.

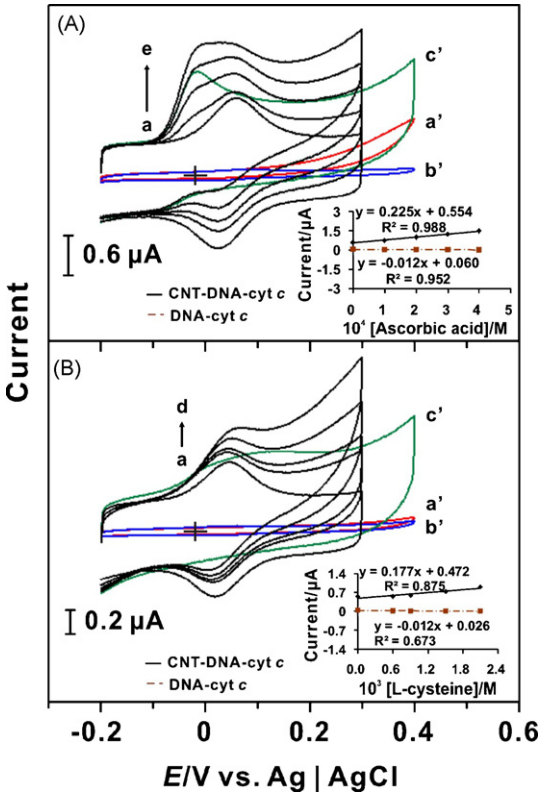

Fig. 5. (A) CVs of MWCNTs–DNA–cyt c biocomposite film in 0.1 M pH 8.4 TRIS buffer with five different concentrations of [AA] = (a) 0.0 M; (b) 1×10^{-4} M; (c) 2×10^{-4} M; (d) 3×10^{-4} M and (e) 4×10^{-4} M; scan rate: 20 mV s^{-1}. Similarly, (B) represents [LC] = (a) 0.0 M; (b) 6×10^{-4} M; (c) 9×10^{-4} M; (d) 1.5×10^{-3} M and (e) 2.1×10^{-3} M. The insets in (A) and (B) show the plot of current vs. different concentration of analytes, respectively at biocomposite films.

3.5. Flow injection analysis of the analytes at MWCNTs–DNA–cyt c biocomposite film

The MWCNTs–DNA–cyt *c* biocomposite films have been synthesized on SPCE at similar conditions to that of GCE. Then, the modified electrodes have been washed carefully in deionized water and used for the FIA of halogen oxyanions such as (A) IO_3^-, (B) BrO_3^- and (C) ClO_3^- as shown in Fig. 6. The carrier stream used was pH 1.0 H_2SO_4 aqueous solution with the flow rate of 0.03 ml s^{-1} and the volume of analytes injected at each cycle was 10 μl at the time interval of 50 s. All parts in Fig. 6 are the successive addition of analytes in the concentration range from 10 μM to 10 mM at the potential of −120.0 mV for IO_3^-, −144.0 mV for BrO_3^- and −163.0 mV for ClO_3^-, these are the optimized potentials obtained from CV studies. The rapid amperometric response of the MWCNTs–DNA–cyt *c* biocomposite film is proportional to the respective analytes concentration. After plotting these results, the slope obtained from the insets in Fig. 6

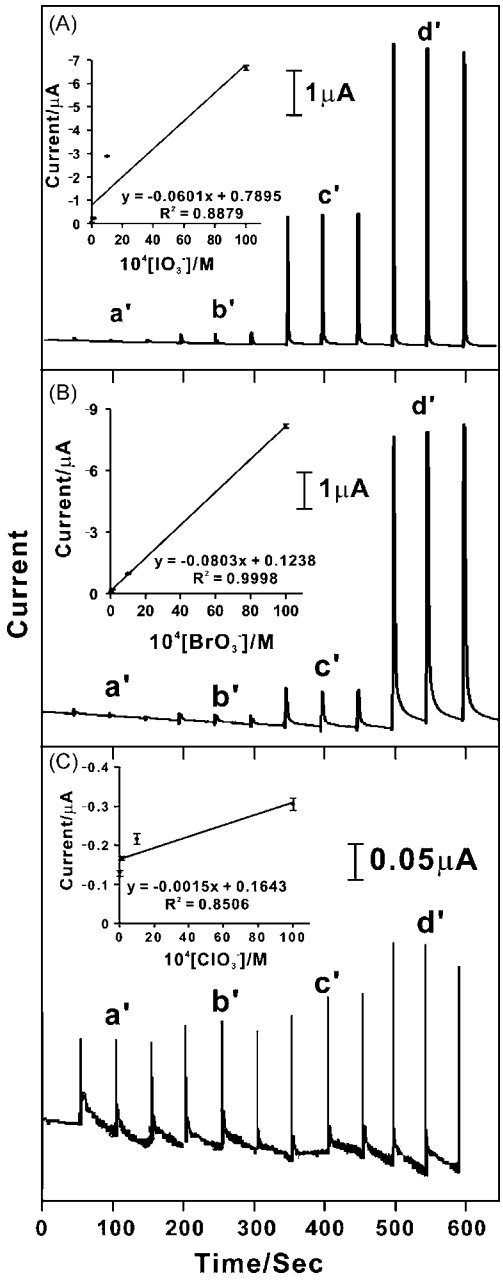

Fig. 6. (A) Flow-amperometric detection of halogen oxyanions at MWCNTs–DNA–cyt *c* biocomposite film present in pH 1.0 H_2SO_4 aqueous solution with four different concentrations of IO_3^- = (a′) 1×10^{-5} M; (b′) 1×10^{-4} M; (c′) 1×10^{-3} M and (d′) 1×10^{-2} M; potential = −120.0 mV. Similarly, (B) represents [BrO_3^-] = (a′) 1×10^{-5} M; (b′) 1×10^{-4} M; (c′) 1×10^{-3} M and (d′) 1×10^{-2} M; potential = −144.0 mV. Similarly, (C) represents [ClO_3^-] = (a′) 1×10^{-5} M; (b′) 1×10^{-4} M; (c′) 1×10^{-3} M and (d′) 1×10^{-2} M; potential = −163.0 mV. In all these three experiments the carrier stream used was pH 1.0 H_2SO_4 aqueous solution; flow rate = 0.03 ml s^{-1} and injected volume = 10 μl. The insets in (A), (B) and (C) show the plot of current vs. different concentration of analytes, respectively at MWCNTs–DNA–cyt *c* biocomposite films.

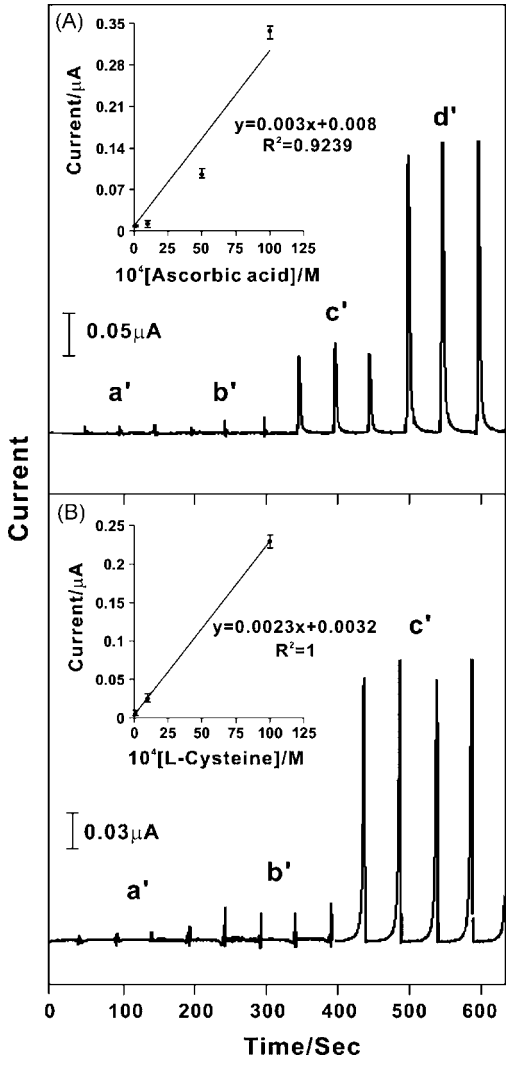

Fig. 7. (A) Flow-amperometric detection of AA and LC at MWCNTs–DNA–cyt *c* biocomposite film present in 0.1 M pH 8.4 TRIS buffer with four different concentrations of AA = (a′) 1×10^{-5} M; (b′) 1×10^{-4} M; (c′) 1×10^{-3} M and (d′) 1×10^{-2} M; potential = 6.0 mV. Similarly, (B) represents [LC] = (a′) 1×10^{-5} M; (b′) 1×10^{-4} M and (c′) 1×10^{-3} M; potential = 58.0 mV. In both of these experiments the carrier stream used was pH 8.4 TRIS aqueous buffer solution; flow rate = 0.03 ml s^{-1} and injected volume = 10 μl. The insets in (A) and (B) show the plot of current vs. different concentration of analytes, respectively at MWCNTs–DNA–cyt *c* biocomposite films.

is $-0.6\,\mu A\,mM^{-1}$ for IO_3^-, $-0.8\,\mu A\,mM^{-1}$ for BrO_3^- and $-0.01\,\mu A\,mM^{-1}$ for ClO_3^- with a correlation coefficient of 0.8879, 0.9998 and 0.8506, respectively, where $n = 4$. From these values, the sensitivity of the sensor has been calculated and it was -0.38, -0.51 and $-0.006\,\mu A\,mM^{-1}\,cm^{-2}$ for IO_3^-, BrO_3^- and ClO_3^-, respectively. Those insets also represent error bars, where each concentration of each analytes has been studied three times. These error bars showed that the MWCNTs–DNA–cyt *c* biocomposite films have good reproducibility for each analyte.

Similar MWCNTs–DNA–cyt *c* modified SPCEs have been prepared at similar conditions for the FIA of AA and LC. The experimental conditions have been similar to that of halogen oxyanions, however here, the pH 8.4 TRIS aqueous buffer solution was used as the carrier stream. Fig. 7(A) shows the successive addition of (A) AA and (B) LC in the concentration range from 0.1 to 10 mM at the potential of 6.0 mV for AA and 58.0 mV for LC, and these are the optimized potentials obtained from CV studies. The rapid amperometric response of the MWCNTs–DNA–cyt *c* biocomposite film is proportional to the respective analytes concentration. The insets show the slope obtained for AA is $0.03\,\mu A\,mM^{-1}$ and LC is $0.02\,\mu A\,mM^{-1}$ with a correlation coefficient of 0.9239 and 1.0, respectively, where $n = 4$ for AA and 3 for LC. From these values, the sensitivity of the sensor has been calculated and it was 0.02 and $0.01\,\mu A\,mM^{-1}\,cm^{-2}$ for AA and LC, respectively. These insets also represent error bars, similar to that of halogen oxyanions FIA, which showed that the MWCNTs–DNA–cyt *c* biocomposite films have good reproducibility for each analytes.

4. Conclusions

In conclusion, we have developed a novel biocomposite material with MWCNTs, DNA and cyt *c* (MWCNTs–DNA–cyt *c*) at the GCE, Au, ITO and SPCE electrode surfaces, which are more stable in aqueous solutions of pH 8.4 TRIS buffer and pH 1 H_2SO_4. The developed biocomposite film for the electrocatalysis, combines the advantages of ease of fabrication, high reproducibility and sufficient long-term stability. The EQCM results has confirmed the incorporation of cyt *c* on MWCNTs–DNA modified gold electrode, SEM and AFM results have shown the difference between cyt *c*, DNA–cyt *c*, MWCNTs–cyt *c* and MWCNTs–DNA–cyt *c* biocomposite films morphological data. The interactions between the MWCNTs, DNA and cyt *c* are presented with the scheme. Further, it has been found that the MWCNTs–DNA–cyt *c* biocomposite film has an excellent functional property along with good electrocatalytic activity on halogen oxyanions and biochemical compounds such as ascorbic acid and L-cysteine. The electrocatalytic reduction of halogen oxyanions such as IO_3^-, BrO_3^- and ClO_3^- and its electronegativity effect on electrocatalysis have also been studied in detail. The interactions between the analytes and the MWCNTs–DNA–cyt *c* biocomposite film have been given in equations with previous literature references. The experimental methods of CV and FIA with biocomposite film biosensor integrated into the GCE and SPCE which are presented in this paper, provide an opportunity for qualitative and quantitative characterization, even at physiologically relevant conditions. Therefore, this work establishes and illustrates, in principle and potential, a simple and novel approach for the development of a voltammetric and amperometric sensor which is based on the modified GCE, ITO, Au and SPCE electrodes.

Acknowledgement

This work was supported by the National Science Council of the Taiwan (ROC).

Appendix A. Supplementary data

Supplementary data associated with this article can be found, in the online version, at doi:10.1016/j.talanta.2007.10.034.

References

[1] E.F. Bowden, F.M. Hawkridge, H.N. Blount, J. Electroanal. Chem. 161 (1984) 355.
[2] H.A.O. Hill, N.I. Hunt, A.M. Bond, J. Electroanal. Chem. 436 (1997) 17.
[3] P. Yeh, T. Kuwana, Chem. Lett. (1977) 1145.
[4] M.J. Eddowes, H.A.O. Hill, J. Chem. Soc., Chem. Commun. 771 (1977) 364.
[5] A. Szucs, G.D. Hitchens, J.O.'M. Bockris, Electrochim. Acta 37 (1992) 403.
[6] G. Battistuzzi, M. Borsari, G. Rossi, M. Sola, Inorg. Chim. Acta 272 (1998) 168.
[7] A. Szues, M. Novak, J. Electroanal. Chem. 383 (1995) 75.
[8] Z.X. Huang, M. Feng, Y.H. Wang, J. Cui, D.S. Zou, J. Electroanal. Chem. 416 (1996) 31.
[9] M.J. Eddowes, H.A.O. Hill, J. Am. Chem. Soc. 101 (1979) 4461.
[10] F.A. Armstrong, H.A.O. Hill, N.J. Walton, Acc. Chem. Res. 21 (1988) 407.
[11] S. Dong, J. Li, Bioelectrochem. Bioenerg. 42 (1997) 7.
[12] Y. Zhou, T. Nagaoka, G. Zhu, Biophys. Chem. 79 (1999) 55.
[13] G. Niaura, A.K. Gaigalas, V.L. Viker, J. Electroanal. Chem. 416 (1996) 167.
[14] O. Ikeda, Y. Shirota, T. Sakurai, J. Electroanal. Chem. 287 (1990) 179.
[15] X. Qu, T. Lu, S. Dong, J. Mol. Catal. A: Chem. 102 (1995) 111.
[16] E.D.A. Stemp, J.K. Barton, Inorg. Chem. 39 (2000) 3868.
[17] A.E.F. Nassar, J.F. Rusling, J. Am. Chem. Soc. 118 (1996) 3043.
[18] S.M. Chen, S.V. Chen, Electrochim. Acta 48 (2003) 513.
[19] U. Yogeswaran, S.M. Chen, Electrochim. Acta 52 (2007) 5985.
[20] G. Wu, Y.S. Chen, B.Q. Xu, Electrochem. Commun. 7 (2005) 1237.
[21] J. Wang, M. Musameh, Anal. Chim. Acta 511 (2004) 33.
[22] J. Wang, M. Li, Z. Shi, N. Li, Z. Gu, Electrochim. Acta 47 (2001) 651.
[23] Q. Li, J. Zhang, H. Yan, M. He, Z. Liu, Carbon 42 (2004) 287.
[24] J. Zhang, J.K. Lee, Y. Wu, R.W. Murray, Nano Lett. 3 (2003) 403.
[25] A. Star, T.R. Han, J. Christophe, P. Gabriel, K. Bradley, G. Gruner, Nano Lett. 3 (2003) 1421.
[26] M. Zhang, K. Gong, H. Zhang, L. Mao, Biosens. Bioelectron. 20 (2005) 1270.
[27] R.J. Chen, Y. Zhang, D. Wang, H. Dai, J. Am. Chem. Soc. 123 (2001) 3838.
[28] Y. Yan, M. Zhang, K. Gong, L. Su, Z. Guo, L. Mao, Chem. Mater. 17 (2005) 3457.
[29] G. Han, J. Yuan, G. Shi, F. Wei, Thin Solid Films 474 (2005) 64.
[30] U. Yogeswaran, S. Thiagarajan, S.M. Chen, Anal. Biochem. 365 (2007) 122.
[31] E. Frackowiak, V. Khomenko, K. Jurewicz, K. Lota, F. Béguin, J. Power Sources 153 (2006) 413.
[32] S. Daniel, T.P. Rao, K.S. Rao, S.U. Rani, G.R.K. Naidu, H.Y. Lee, T. Kawai, Sens. Actuators B 122 (2007) 672.
[33] S.M. Chen, M.I. Liu, Electrochim. Acta 51 (2006) 4744.
[34] S.M. Chen, C.J. Liao, V.S. Vasantha, J. Electroanal. Chem. 589 (2006) 15.

[35] J. Wang, J. Dai, T. Yarlagadda, Langmuir 21 (2005) 9.
[36] M. Tahhan, V.T. Truong, G.M. Spinks, G.G. Wallace, Smart Mater. Struct. 12 (2003) 626.
[37] E. Laviron, J. Electroanal. Chem. 101 (1979) 19.
[38] T. Komura, G.Y. Niu, T. Yamaguchi, M. Asano, A. Matsuda, Electroanalysis 16 (2004) 1791.
[39] A. Mohadesi, M.A. Taher, Sens. Actuators B 123 (2007) 733.
[40] S.M. Chen, K.C. Lin, J. Electroanal. Chem. 511 (2001) 101.
[41] C.P. Andrieux, O. Haas, J.M. SavGant, J. Am. Chem. Soc. 108 (1986) 8175.
[42] S. Imabayashi, T. Mita, T. Kakiuchi, Langmuir 21 (2005) 1470.
[43] X. Ji, J. Ren, J. Jin, T. Nakamur, Biosens. Bioelectron. 23 (2007) 241.
[44] F. d'Souza, L.M. Rogers, E.S. O'Dell, A. Kochman, W. Kutner, Bioelectrochemistry 66 (2005) 35.
[45] S.F. Ding, W. Wei, G.C. Zhao, Electrochem. Commun. 9 (2007) 2202.
[46] L. Zhang, X. Jiang, L. Niu, S. Dong, Biosens. Bioelectron. 21 (2006) 1107.
[47] A.F. Runge, S.S. Saavedra, Langmuir 19 (2003) 9418.
[48] D.H. Murgida, P. Hildebrandt, J. Phys. Chem. B 105 (2001) 1578.

Available online at www.sciencedirect.com
ScienceDirect
Talanta 74 (2008) 1498–1504
Talanta
www.elsevier.com/locate/talanta

New approach on trace analysis of triclosan in personal care products, biological and environmental matrices

Ana Rita M. Silva [a], J.M.F. Nogueira [a,b,*]

[a] University of Lisbon, Faculty of Sciences, Chemistry and Biochemistry Department, Campo Grande Ed. C8, 1749-016 Lisbon, Portugal
[b] University of Lisbon, Faculty of Sciences, Center for Molecular Sciences and Materials, Campo Grande Ed. C8, 1749-016 Lisbon, Portugal

Received 30 May 2007; received in revised form 7 September 2007; accepted 28 September 2007
Available online 13 October 2007

Abstract

Stir bar sorptive extraction and liquid desorption followed by high performance liquid chromatography with diode array detection (SBSE-LD-LC-DAD) is proposed for the determination of triclosan in personal care products, biological and environmental matrices, which is included in the priority lists, set by several international regulatory organizations. Instrumental conditions and experimental parameters that affecting SBSE-LD efficiency are fully discussed. Throughout systematic assays on 25 mL water samples spiked at the 10.0 $\mu g\,L^{-1}$ level, it had been established that stir bars coated with 126 μL of polydimethylsiloxane, an equilibrium time of 1 h (1000 rpm) and acetonitrile under sonification (60 min) as back-extraction solvent, allowed the best analytical performance to determine triclosan in water matrices. From the data obtained, good recovery and remarkable repeatability were attained, providing experimental average yields (78.5 ± 2.2%), although slightly lower than the theoretical equilibrium (99.7%) described by the octanol–water partition coefficients ($K_{PDMS/W} < K_{O/W}$). The analytical performance proved suitable precision (<3.6%), convenient detection limits (0.1 $\mu g\,L^{-1}$) and excellent linear dynamic range ($r^2 > 0.9992$) from 0.4 to 108.0 $\mu g\,L^{-1}$. The application of the present method to determine triclosan in real matrices such as commercial toothpaste, saliva and urban wastewater samples, allowed appropriate selectivity, high sensitivity and accuracy using the standard addition methodology. The proposed method showed to be feasible and sensitive with a low-sample volume requirement to monitor triclosan in personal care products, biological and environmental matrices at the trace level, in compliance with international regulatory directives.
© 2007 Elsevier B.V. All rights reserved.

Keywords: Triclosan; Stir bar sorptive extraction; High performance liquid chromatography; Commercial toothpaste; Saliva; Wastewater

1. Introduction

Triclosan (2,4,4′-trichloro-2′-hydroxyphenyl ether) is a widely employed antimicrobial, antibacterial and preservative agent used in many personal care products, i.e. deodorants, soaps, handwashes, toothpastes, domestics and medical disinfectants, polymers and fibbers [1]. According to the European Union (EU) directive 76/768/CEE and subsequent amendments, its use in personal care products is allowed to a maximum concentration of 0.30% (w/w) [2]. Due to these applications and as a consequence of its lipophilic characteristics, this compound becomes a widespread contaminant in human body and environment. Evidences of the presence of triclosan have been also reported in consumer products [2], such as plasma [3], marine sediments [4], urban wastewaters [1,4,5], surface water [5], fish bile exposed to treated wastewater [6] and in human milk [3,6]. Triclosan has not shown yet toxicity to mammals but *in vitro* studies indicate that low levels may disturb metabolic systems and hormone homeostasis [3]. It was also reported as a bactericidal agent that modulates thyroid hormone-associated gene expression and disrupts postembryonic anuran development [7]. Furthermore, triclosan is toxic to aquatic living organisms such as fish, daphnia magna and in particular to algae, for which its presence in environment has serious implications on the resistance mechanisms of bacteria [6,8]. Attention has also been draw to this compound, due to its ability to form low chlorinated dioxins during the incineration process and under the sunlight radiation [8,9].

In the last years, several analytical methodologies have been proposed to monitor triclosan in environmental and biological matrices as well as in commercial formulations, which

* Corresponding author at: DQB/FCUL, Campo Grande Ed. C8, 1749-016 Lisbon, Portugal. Tel.: +351 217500899; fax: +351 217500088.
E-mail address: nogueira@fc.ul.pt (J.M.F. Nogueira).

0039-9140/$ – see front matter © 2007 Elsevier B.V. All rights reserved.
doi:10.1016/j.talanta.2007.09.040

includes an enrichment step prior to liquid chromatography with diode array (LC–DAD) [2,10] or mass spectrometry (LC–MS) [4,5] detection, but also gas chromatography coupled to mass spectrometry (GC–MS) [1,3,4,6,8,9]. Since GC–MS requires a previous derivatization step [5], i.e. methylation or silylation, LC has been accepted as an advantageous technique to monitor triclosan in several types of matrices, which is more rugged and versatile. In spite of liquid–liquid extraction or solid-phase extraction has been commonly employed as enrichment steps, these techniques are neither compatible with time consuming nor environmentally friendly. In the last decade, the solventless methods, e.g. solid-phase microextraction (SPME) has become very popular due to its simplicity of operation, great selectivity and high sensitivity [11], which had already been proposed for the analysis of triclosan in environmental matrices [1]. More recently, stir bar sorptive extraction (SBSE) has been introduced as a novel sample preparation technique based on the same principles of the SPME [12–27], where the analytes are extracted from an aqueous matrix towards to a polydimethylsiloxane (PDMS) polymer. The main difference between SPME and SBSE is the much larger amount of PDMS used in the latter, which results in higher recoveries, sample capacity and remarkable sensitivity at the sub-ppts level. In the SBSE theory [12], the partitioning efficiency of the analytes into the PDMS phase of the stir bar, at equilibrium, can be reliably predicted by the octanol–water partition coefficients ($K_{O/W}$), considering the approximation to the partitioning coefficients between PDMS and water ($K_{PDMS/W} \approx K_{O/W}$), as well as by the corresponding phase ratio $\beta = V_W/V_{SBSE}$, where V_W is the volume of the water sample and V_{SBSE} is the PDMS volume. The lower phase ratio between the sample and the extraction medium provides much higher recoveries.

The aim of the present work is the development of a new analytical approach by combining stir bar sorptive extraction and liquid desorption followed by high performance liquid chromatography with diode array detection (SBSE-LD-LC-DAD) for the determination of triclosan in commercially available health care products, biological and environmental matrices. The performance of the method was evaluated in terms of detection limits, linear dynamic range and accuracy, for which several systematic assays were carried out in order to determine the most important parameters that could affect the efficiency of the SBSE-LD process. Finally, the optimized method was applied to monitor real matrices, including commercial toothpaste, saliva and urban wastewater samples.

2. Materials and methods

2.1. Standards and reagents

HPLC-grade methanol (MeOH, 99.9%), acetonitrile (ACN, 99.9%) were supplied from Sigma–Aldrich (Steinheim, Germany). Sodium chloride (NaCl, 99.9%) was obtained from AnalaR (BDH Chemicals, Poole, UK). Ultra-pure water was obtained from Milli-Q water purification systems (Millipore, Bedford, MA, USA). Acid phosphoric (85%) was obtained from Riedel de Haën and triclosan (97%) was purchased from Aldrich. A stock standard solution of triclosan (136.0 mg L^{-1}) was used to prepare the working and calibration solutions in MeOH at the desired concentration and stored refrigerated at −20 °C. Wastewater samples were collected from influents and effluents of two urban treatment plants located in Cartaxo (Portugal) filtered and stored refrigerated at 4 °C until their analysis. A commercial toothpaste solution containing triclosan was prepared by weighting accurately 48.1 mg (Mettler Toledo AG135, Switzerland) and diluted to 100 mL following by re-dilution (1:125) with ultra-pure water. Saliva was obtained from a healthy woman that brushed her teeth with commercial toothpaste containing triclosan. The samples were collected without storage and analyzed immediately after the teeth were brushed and 12 h later on.

2.2. Experimental set-up

The stir bars (Twister; Gerstel, Müllheim a/d Ruhr; Germany) coated with 20 mm in length and 1.0 mm film thickness of PDMS (126 μL) were pre-conditioned before use by treating them with ACN for cleaning. In a typical assay, 25 mL of ultra-pure water (pH 7.0) spiked at the 10 μg L^{-1} concentrations was introduced into a glass vial (Macherey-Nagel, Düren, Germany), a stir bar was immersed and the vial closed with a seal using a hand crimper. For optimization studies, assays were performed in a fifteenth agitation point plate (Variomag H + P Labortechnik AG Multipoint 15, OberschleiBheim, Germany) at room temperature (25 °C) and each parameters such as extraction time (0.25, 0.5, 1, 2, 4, 6, 8 and 17 h), agitation speed (750, 1000 and 1250 rpm), ionic strength (NaCl; 5, 10 and 20%, w/v) and organic modifier (MeOH; 5, 10 and 15%, v/v) were systematically studied in triplicate and compared with suitable controls. To evaluate the best LD conditions, several assays using MeOH and ACN as back extraction solvents were performed in triplicate. For LD purposes, the stir bars were removed with clean tweezes, dried with a lint-free tissue, placed into a 2 mL amber vial (Chromacol, UK) containing 1.5 mL of the desorption solvent, ensuring their total immersion prior to ultrasonic treatment at a constant temperature (25 °C). The period of the ultrasonic treatment was also optimized (15, 30 and 60 min). After back extraction, the stir bars were removed by means of a magnetic rod, while the stripping solvent was evaporated to dryness under a gently stream of purified nitrogen (>99.5%). The dried residues were redissolved in 200 μL of MeOH and the vial was closed with a seal using a hand crimper and placed into the automatic liquid sampler tray for LC-DAD analysis. For validation purposes, triplicate assays and the corresponding controls were performed for triclosan under optimized experimental conditions. Blank assays were also performed using the same procedure as above, employing ultra-pure water samples without spiking. The standard addition methodology was used to quantify and suppress matrix effects on real matrices. For real sample assays, 25 mL of wastewater, toothpaste solution and 1 mL of saliva diluted to 25 mL with ultra-pure water were fortified at the desired concentration or directly analyzed in triplicate using the optimized procedure.

2.3. Instrumentation

LC-DAD analyses were carried out on an Agilent 1100 Series LC system (Agilent Technologies, Waldbronn, Germany), constituted by the following modules: vacuum degasser (G1322A), quaternary pump (G1311A), autosampler (G1313A), thermostatted column compartment (G1316A) and DAD (G1315B). The data acquisition and instrumental control were performed by the software LC3D ChemStation (version Rev.A.08.03[847], Agilent Technologies). Analyses were performed on a Tracer excel 120 ODS-A column, 150 mm × 4.0 mm, 5 μm particle size (Teknokroma, Spain). The mobile phase consists on a mixture of ACN and 0.1% phosphoric acid in ultra-pure water having a composition of 80/20%, respectively, and a flow of 1.0 mL min^{-1} (25 °C). The injection volume was 20 μL with a draw speed of 200 μL min^{-1} and the detector was set at 230 nm. For identification purposes, standard addition was used by spiking the samples with pure standards of triclosan, as well as by comparing the retention parameters and peak purity with the UV–vis spectral reference data. For recovery calculations, peak areas obtained from each assay were compared with peak areas of suitable controls used for spiking. For quantification purposes on real matrices, calibration plots using the standard addition methodology were performed.

3. Results and discussion

3.1. LC-DAD conditions

From the very beginning, the LC-DAD parameters were evaluated in order to attain appropriate instrumental conditions for triclosan analysis. Preliminary spectrophotometric studies on triclosan standard solutions showed that a wavelength (λ_{max}) at 230 nm providing enough sensitivity response for DAD and therefore, was selected in agreement with literature [2]. Subsequently, the best LC conditions were chosen to achieve suitable retention characteristics for triclosan analysis, according to previous works [2,10]. By using a conventional reversed phase column and a mobile phase constituted with ACN and 0.1% phosphoric acid in ultra-pure water (80/20%), very good analytical performance was obtained for triclosan, showing symmetrical peak shape with a convenient retention time (3.1 min), under the instrumental conditions used.

Instrumental calibration was performed using thirteen standard solutions with concentrations ranging from 0.2 to 136.0 mg L^{-1}. From the data obtained, excellent linear response was observed providing a correlation coefficient of 0.9995. The instrumental sensitivity was also checked through the limits of detection (LOD) and quantification (LOQ), obtained by the injection of diluted calibration standards and calculated with signal-to-noise ratio (S/N) of 3/1 and 10/1, respectively. The values obtained for triclosan were 18.0 μg L^{-1} for LOD and 60.0 μg L^{-1} for LOQ. Furthermore instrumental precision was evaluated through repeatability injections (0.2 and 10.0 mg L^{-1}), resulting in relative standard deviations (R.S.D.) lower than 3.2%. Throughout the present work, no instrumental carry-over was observed since the background was always below the LOD achieved.

3.2. Optimization of the SBSE-LD efficiency

During the experimental work, several parameters affecting the SBSE-LD efficiency yields were evaluated. Thereby, systematic assays were performed to optimize parameters that are known to influence this analytical process such as extraction time, agitation speed, matrix characteristics (polarity and ionic strength) and LD conditions [12,15,16,19–24]. During our experiments, stir bars coated with 126 μL of PDMS were chosen, since it had been proved to ensure higher sorptive capacity for sample volumes up to 50 mL.

3.2.1. Effect of the LD conditions

In a first approach, we start to evaluate the best LD conditions, which guarantee complete back extraction of triclosan from the stir bars. Therefore, solvents such as MeOH and ACN were studied in order to assess the LD performance, using experimental standard conditions, i.e. 1 h of extraction time (750 rpm) at room temperature and 15 min for desorption time under sonification treatment. Furthermore, solvents having non-polar characteristics were avoided which are known to swell of the PDMS polymer [18]. From the data obtained, ACN was chosen as back extraction solvent due to the slightly higher ability to desorbs triclosan from the stir bars. Since sonification treatment was implemented to accelerate the stripping efficiency of the analyte from the stir bars, a series of experiments were carried out by comparing several periods of time (15, 30 and 60 min) to achieve the best LD conditions. From the data obtained, the best chromatographic signal was observed for 60 min without further memory effects. Consequently, a period of 60 min was established for the back-extraction process under sonification treatment.

In the course of the LD optimization, it was also important to check for possible analyte losses during the evaporation step prior to LC-DAD analysis. Thus, standard methanolic solutions of triclosan at the 10.0 mg L^{-1} level were evaporated to dryness under a gentle stream of nitrogen and the residues were subsequently redissolved in MeOH and injected into the LC-DAD system. By comparing the data obtained with suitable standard controls, an average reconstitution of 94.8% with R.S.D. lower than 2.0% provided negligible losses of triclosan during the evaporation step.

3.2.2. Effect of the SBSE parameters

SBSE enrichment is an equilibrium technique and therefore, the analytical process is significantly influenced by the extraction time and agitation speed involved [12]. Starting with the stirring rate, this parameter can influence the mass transfer of the analytes towards to the PDMS phase during the equilibrium process. Throughout the presents work, three levels (750, 1000 and 1250 rpm) were performed to achieve the best stirring conditions. Fig. 1a depicts the data obtained, where it can be observed that 1000 rpm give slightly higher recovery yields for triclosan, under the experimental conditions used. An agitation

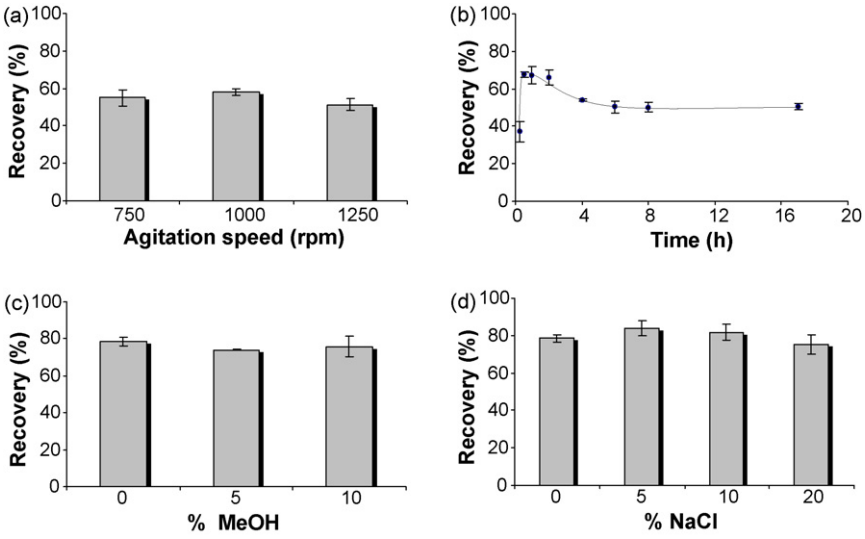

Fig. 1. Effect of the agitation speed (a), extraction time (b), MeOH percentage (c) and NaCl content (d) on the recovery yields of triclosan by SBSE-LD-LC-DAD. Conditions: see Experimental Section.

speed of 1250 rpm leads to lower recovery yields for triclosan since higher rates difficult to maintain the integrity of the stir bar, giving rise to instability that affects very much the efficiency of the extraction process for this compound in particular [22].

The effect of the equilibrium time on the extraction was also assessed by stirring the samples at different periods (0.25, 0.5, 1.0, 2.0, 4.0, 6.0, 8.0 and 17.0 h), for which the kinetic profile obtained are depicted in Fig. 1b. As can be observed, triclosan reached the equilibrium after an exposure time up to 2 h with recovery yields around 70%, while after that period decreases to lower efficiencies (50%). This observation seems to be explained by the "wall-effect" phenomena, i.e. after an initial period of time (2 h), the adsorption of triclosan onto the glass walls of the sampling flasks reaches a new equilibrium, which clearly influences the efficiency yields of the SBSE process. According to literature [18,27], MeOH addition onto sample matrix is frequently suggested as a solution to overcome this phenomenon in particularly for compounds that having non-polar characteristics. Consequently, the effect of MeOH onto aqueous matrix was also evaluated by using contents of 5, 10 and 15%. From the experiments performed (Fig. 1c), the progressive addition of MeOH slightly reduce the recovery yields of triclosan, showing in many cases disadvantages, because it turns the matrix less polar, helping the solubilization by reducing the affinity of this compounds on the PDMS phase of the stir bar. Consequently, further experiments were performed in the absence of MeOH in the aqueous matrices.

In accordance with previous works [15,16,18,22,23], we paid also some attention to the influence of the salting out effect on the recovery performance by adding NaCl (5, 10 and 20%) to the aqueous medium. As can be observed in Fig. 1d, the increment of the ionic strength has a negligible effect on triclosan recovery and therefore, the addition of NaCl was rejected for further experiments. Finally, several assays performed at different pH values proved a non-significant effect on the efficiency, according to some authors [1].

3.3. Validation of the SBSE-LD-LC-DAD method

In the SBSE theory [12], the distribution coefficients of the analytes between PDMS and the water matrix ($K_{PDMS/W}$) should be strongly correlated with the corresponding $K_{O/W}$. Thereby, the theoretical recovery for triclosan was estimated on the basis of sample volumes of 25 mL and stir bars with 126 μL of PDMS, where a β-value of 198.4 and a $\log K_{O/W}$ 4.8 provided an efficiency yield of 99.7%. Meanwhile, by using the optimized experimental conditions (SBSE: 1 h (1000 rpm), LD: ACN (60 min) with evaporation to dryness and reconstruction with MeOH), average recovery yields of $78.5 \pm 2.2\%$ were achieved for triclosan. When confronting theoretical with experimental recovery data, it can be observed a small but very acceptable deviation ($K_{PDMS/W} < K_{O/W}$), since $K_{O/W}$ is just a rough approximation of $K_{PDMS/W}$, according to previous works [12,18,20,23,24,27].

Subsequently, the linear dynamic range of the present methodology was also evaluated for triclosan under optimized experimental conditions, using eight calibration standards with concentrations ranging from 0.4 to 108.0 $\mu g\,L^{-1}$. From the data obtained, excellent linearity was attained with a remarkable correlation coefficient (0.9992). The precision of the present methodology by using convenient standards (1.0 $\mu g\,L^{-1}$) was evaluated through within- and between-day repeatability studies, calculated as R.S.D. on six replicates, giving rise to variations up to 3.6%. Furthermore, the sensitivity of the actual methodology was checked through the LOD and LOQ and calculated with S/N of 3/1 and 10/1, for which values of 0.1 and 0.4 $\mu g\,L^{-1}$ were respectively achieved for triclosan. Table 1 summarizes the log $K_{O/W}$, the theoretical and experimental recoveries attained, linear dynamic range and correlation coefficients, LOD, LOQ and repeatability data for triclosan in water samples by SBSE-LD-LC-DAD, under optimized experimental conditions.

Table 1
Log $K_{o/w}$, theoretical and experimental recoveries, linear dynamic range and correlation coefficients, LOD, LOQ and repeatability data achieved for triclosan in water samples by SBSE-LD-LC-DAD, under optimized experimental conditions

Log $K_{O/W}$[a]	4.8
Theoretical recovery[b] (%)	99.7
Experimental recovery[c] (% ± R.S.D.; $n=3$)	78.5 ± 2.2
Linear range[d] ($\mu g\,L^{-1}$)	0.4–108.0
r^2	0.9992
LOD ($\mu g\,L^{-1}$)	0.1
LOQ ($\mu g\,L^{-1}$)	0.4
Repeatability (% R.S.D.; $n=6$)[e]	3.6

[a] From Ref. [6].
[b] Phase ratio (β): 198.4, according to Ref. [12].
[c] Spiked at the 10 $\mu g\,L^{-1}$ level.
[d] Eight levels of concentration.
[e] Using a 1.0 $\mu g\,L^{-1}$ standard.

3.4. Application to real matrices

To evaluate the applicability of the present methodology on real matrices, assays were performed in commercial toothpaste, saliva and urban wastewater. In the course of triclosan studies on real samples, the standard addition methodology (SAM) was chosen to minimize for eventual matrix effects. Therefore, to guarantee a maximum control of the analytical methodology, the matrices were first and foremost fortified with four working standards to produce the corresponding spiking levels of triclosan and blank assays ("zero-point") were also performed without spiking [20,22,24,27]. Table 2 resumes the data obtained from the SAM assays performed on the matrices studied using the optimized experimental methodology, where the triclosan contents (C_0) achieved in each sample is also indicated. It is noteworthy the remarkable linearity ($r^2 > 0.9966$) obtained with

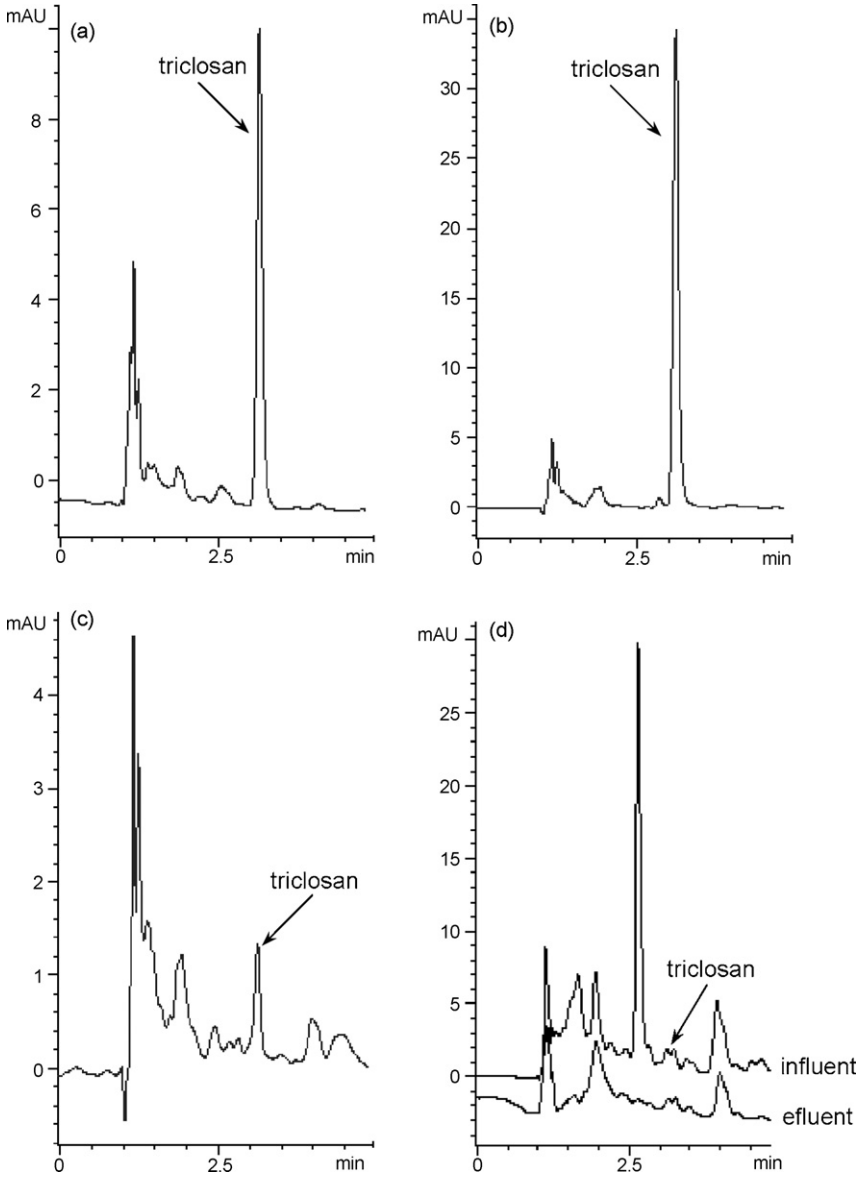

Fig. 2. Chromatograms obtained from assays performed on commercial toothpaste solutions (a) saliva immediately after brushing the teeth with commercial toothpaste (b), saliva 12 h later on (c) and urban wastewater matrices (d; plant #1) by SBSE-LD-LC-DAD, under optimized experimental conditions.

Table 2
Content (C_0) and regression parameters obtained from the standard addition method for triclosan determined on real matrices by SBSE-LD-LC-DAD, under optimized experimental conditions

Matrices	r^2	Slope	C_0 (μg L^{-1})	Remarks
Commercial toothpaste solutions	0.9997	5.8356	1284	0.27%[a]
Saliva	0.9966	3.2080	1570	0 h[b]
	0.9989	4.5729	26.5	12 h[c]
Urban wastewater				
Plant #1	0.9985	4.3996	<LOD	Influent
	0.9988	5.0930	<LOD	Effluent
Plant #2	0.9989	4.4203	<0.4	Influent
	0.9990	3.2996	<0.4	Effluent

[a] w/w.
[b] Immediately after brushing the teeth.
[c] 12 h later on brushing the teeth.

slopes presenting the same order of magnitude, which point out the absence of matrix effects. Fig. 2 exemplify chromatograms obtained from assays performed on commercial toothpaste solutions (a), saliva (b) and (c) and urban wastewater (d) matrices after the application of the present methodology.

In a first approach, it can be state that triclosan peak (3.1 min) is well resolved from other potential interferences coming from the matrices studied, under optimized experimental conditions, where the methodology presents good selectivity and enough sensitivity. Assays performed on commercial toothpaste solutions, as shown in the chromatogram of Fig. 2a, indicated levels of triclosan with an average concentration of 1284 μg L^{-1} (Table 2), which represent a content of 0.27% (w/w). As can be observed, the commercial toothpaste under study contains triclosan amounts in compliance with the EU directive (76/768/CEE), i.e. below 0.30%. On the other hand, it must be emphasize the very easy manipulation and sensitivity attained by the present methodology to determine triclosan in commercial toothpastes, when confronting with other dedicated analytical systems purposed for health care products [2]. Fig. 3 exemplifies the remarkable linearity attained from the SAM assays performed on aqueous solutions of commercial toothpaste for the determination of triclosan by the present methodology.

The present methodology also demonstrates the capability to detect and quantify triclosan in biological matrices, such as saliva samples. Thereby, triclosan contents in saliva were determined at two different periods of time, after brushing the teeth with the commercial toothpaste previously studied. Fig. 2b and c depicts chromatograms showing the occurrence of triclosan in saliva samples from a healthy woman just after brushing her teeth with commercial toothpaste and 12 h later on. It is noteworthy the remarkable performance attained with average concentrations of 1.6 mg L^{-1} and 26.5 μg L^{-1} (Table 2), respectively. As expected, the presence of triclosan in the human body decreases with time, but even after 12 h this compound is still present in the saliva matrix at the trace level. From the data obtained, it must be emphasized that the regular use of commercial toothpaste containing triclosan can leads to a continuous presence of this harmful compound in the mouth flora and consequently, influence negatively the overall human metabolism.

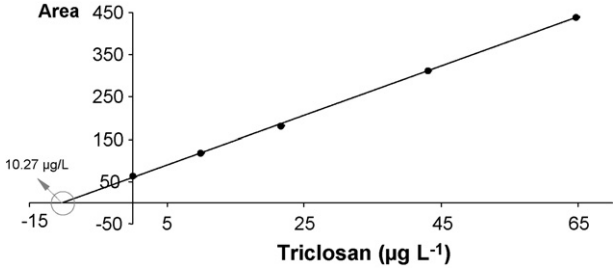

Fig. 3. Linear dynamic range obtained from the standard addition methodology performed on commercial toothpaste solutions by SBSE-LD-LC-DAD, under optimized experimental conditions.

At least, assays performed on environmental matrices were also carried out, particularly in influent and effluent samples coming from urban treatment plants (Table 2). As exemplified on the chromatogram depicted in Fig. 2d (plant #1), besides the greater complexity usually observed on those matrices, no contents of triclosan were detected (<LOD) in the samples studied.

In short and taking into consideration the high complexity usually associated to the matrices assessed in the present work, the methodology showed very good selectivity, enough sensitivity and accuracy to monitor triclosan at the trace level and a suitable alternative to replace the currently dedicated analytical systems.

4. Conclusions

The combination of stir bar sorptive extraction and liquid desorption followed by high performance liquid chromatography with diode array detection (SBSE-LD-LC-DAD) offers the opportunity of a new practical and reliable methodology for the determination of triclosan in aqueous media. Parameters affecting SBSE-LD processes were fully discussed. Under optimized experimental conditions a good analytical performance was attained, including suitable precision, excellent linear dynamic range and detection limits at the trace level. By using the standard addition methodology, the application of the present analytical approach to commercial toothpaste, saliva and urban wastewater matrices demonstrated remarkable selectivity, sensitivity and accuracy. Besides the present methodology has proved to be a convenient tool to monitor triclosan at the trace level, the analytical performance can be further improved by using LC–MS or LC–MS/MS systems.

Acknowledgments

The authors wish to thank Prof. Ana Paula Carvalho for supplying chemical reagents and Eng[a] Manuela Justino for her prompt availability to provide us the wastewater samples.

References

[1] P. Canosa, I. Rodriguez, E. Rubi, R. Cela, J. Chromatogr. A 1072 (2005) 107.
[2] A. Piccoli, J. Fiori, V. Andrisano, M. Orioli, Il Fármaco 57 (2002) 369.

[3] M. Allmyr, M. Adolfsson-Erici, M. McLachlan, G. Sandborgh-Englund, Sci. Tot. Environ. 372 (2006) 87.
[4] A. Agüera, A. Fernández-Alba, L. Piedra, M. Mézcua, M. Gómez, Anal. Chim. Acta 480 (2003) 193.
[5] W. Hua, E. Bennett, R. Letcher, Environ. Int. 31 (2005) 621.
[6] M. Adolfsson-Erici, M. Pettersson, J. Parkkonen, J. Sturve, Chemosphere 46 (2002) 1485.
[7] N. Veldhoen, R. Skirrow, H. Osachoff, H. Wigmore, D. Clapson, M. Gunderson, G. Aggelen, C. Helbing, Aquat. Toxicol. 80 (2006) 217.
[8] M. Mézcua, M. Gómez, I. Ferrer, A. Agüera, M. Hernando, A. Fernández-Alba, Anal. Chim. Acta 524 (2004) 241.
[9] L. Sanchez-Prado, M. Llompart, M. Lores, C. García-Jares, J. Bayona, R. Cela, Chemosphere 65 (2006) 1338.
[10] R.D. Thompson, J. AOAC Int. 84 (2001) 815.
[11] J. Pawliszyn, Solid Phase Microextraction—Theory and Practice, Wiley–VCH, New York, 1997.
[12] E. Baltussen, P. Sandra, F. David, C. Cramers, J. Microcolumn Sep. 11 (1999) 737.
[13] P. Popp, C. Bauer, L. Wennrich, Anal. Chim. Acta 436 (2001) 1.
[14] E. Baltussen, C.A. Cramers, P. Sandra, Anal. Bioanal. Chem. 373 (2002) 3.
[15] V. León, B. Alvarez, M. Cobollo, S. Muñoz, I. Valor, J. Chromatogr. A 999 (2003) 91.
[16] A. Peñalver, V. García, E. Pocurull, F. Borrull, R.M. Marcé, J. Chromatogr. A 1007 (2003) 1.
[17] P. Popp, C. Bauer, B. Hauser, P. Keil, L. Wennrich, J. Sep. Sci. 26 (2003) 961.
[18] P. Serôdio, J.M.F. Nogueira, Anal. Chim. Acta 517 (2004) 21.
[19] C. Blasco, M. Fernández, Y. Picó, G. Font, J. Chromatogr. A 1030 (2004) 77.
[20] P. Serôdio, J.M.F. Nogueira, Anal. Bioanal. Chem. 382 (2005) 1141.
[21] L. Brossa, R.M. Marce, F. Borrull, E. Pocurull, Chromatographia 61 (2005) 61.
[22] P. Serôdio, J.M.F. Nogueira, Water Res. 40 (2006) 2572.
[23] C. Almeida, J.M.F. Nogueira, J. Pharm. Biochem. Anal. 41 (2006) 1303.
[24] P. Rosário, J.M.F. Nogueira, Electrophoresis 27 (2006) 4694.
[25] R. Rodil, P. Popp, J. Chromatogr. A 1124 (2006) 82.
[26] M. Kawaguchi, R. Ito, K. Saito, H. Nakazawa, J. Pharm. Biochem. Anal. 40 (2006) 500.
[27] P. Serôdio, M.S. Cabral, J.M.F. Nogueira, J. Chromatogr. A 1141 (2007) 259.

Available online at www.sciencedirect.com
ScienceDirect
Talanta 74 (2008) 1265–1270
Talanta
www.elsevier.com/locate/talanta

Affinity-based elimination of aromatic VOCs by highly crystalline multi-walled carbon nanotubes

Hiroaki Sone [a], Bunshi Fugetsu [a,*], Takayuki Tsukada [b], Morinobu Endo [c,*]

[a] *Graduate School of Environmental Science, Hokkaido University, Sapporo 060-0810, Japan*
[b] *Nano Carbon Technologies Co. Ltd., 600 Tanaka-cho, Akishima, Tokyo, Japan*
[c] *Faculty of Engineering, Shinshu University, 4-17-1 Wakasato, Nagano-shi 380-8553, Japan*

Received 6 August 2007; received in revised form 29 August 2007; accepted 29 August 2007
Available online 7 September 2007

Abstract

Carbon nanotubes (CNTs) are capable of adsorbing pollutant chemicals. Their adsorptive capacities and adsorbing mechanisms, however, are not fully understood. As-grown CNTs often contain both crystalline and amorphous carbon, and the ratio of carbon types can affect adsorption. In this study, highly crystalline multi-walled carbon nanotubes (HC-MWCNTs) were used as the adsorbent for volatile organic compounds (VOCs) in contaminated air samples. Air containing 23 added VOCs (1,1-dichloroethylene, dichloromethane, *trans*-1,2-dichloroethylene, *cis*-1,2-dichloroethylene, chloroform, 1,1,1-trichloroethane, carbon tetrachloride, 1,2-dichloroethane, benzene, trichloroethylene, 1,2-dichloropropane, bromodichloromethane, *cis*-1,3-dichloropropene, toluene, *trans*-1,3-dichloropropene, 1,1,2-trichloroethane, tetrachloroethylene, dibromochloromethane, *m*-xylene, *p*-xylene, *o*-xylene, bromoform, and *p*-dichlorobenzene) was used for model samples. Adsorptive experiments were carried out by passing the air samples through a cartridge packed with HC-MWCNTs. Initial results showing high selectivity and high affinity for adsorbing aromatic VOCs (benzene, toluene, *m*-xylene, *p*-xylene, *o*-xylene, and *p*-dichlorobenzene) have provided new insight into the adsorption mechanisms. Data suggest that the HC-MWCNTs, unlike conventional carbon materials, adsorb aromatic compounds according to Fukui's frontier theory, which is based on the interactions between the HOMO and LUMO of the aromatic VOCs and those of the HC-MWCNTs.
© 2007 Elsevier B.V. All rights reserved.

Keywords: Highly crystalline multi-walled carbon nanotubes (HC-MWCNTs); Volatile organic compounds (VOCs); Affinity-based adsorption; LUMO–HOMO interaction

1. Introduction

Volatile organic compounds (VOCs) have received a great deal of attention in the field of environmental control for a number of reasons. First, VOCs are ubiquitous in the environment, workplace, and consumer products [1–4]. Humans can, therefore, be easily exposed to VOCs through skin contact, breathing, and eating. Second, VOCs are suspected to have primary and secondary harmful effects [5,6] due to prolonged exposure. These include eye and throat irritation, liver damage, and damage to the central nervous system. Third, VOCs can form photochemical smog, which contains ozone and other toxic byproducts, by reacting with other atmospheric chemicals such as nitrogen oxides [7]. Moreover, VOCs are emitted by landfill leachate and industrial effluent. Leakage into groundwater can cause serious contamination problems [8].

Among VOCs, the aromatic compounds, especially benzene, toluene, xylene and dichlorobenzene, are of particular interest. All of the aromatic VOCs are known or suspected to be carcinogenetic [9]. Furthermore, these compounds have no safety threshold dose for carcinogenic effects. Thus, even low-level exposure poses a finite risk. In fact, benzene, toluene, and xylenes, known as BTX, are the markers for human exposure to VOCs [10].

In the not-so-distant past, adsorptive treatment using activated carbon as the adsorbent was deployed for VOCs elimination [11–13]. However, the inability of activated carbon to selectively adsorb aromatic compounds results in an unpredictable lifespan for the carbon; the selectivity problem needs

* Corresponding authors.
E-mail addresses: hu@ees.hokudai.ac.jp (B. Fugetsu), endo@endomoribu.shinshu-u.ac.jp (M. Endo).

0039-9140/$ – see front matter © 2007 Elsevier B.V. All rights reserved.
doi:10.1016/j.talanta.2007.08.041

to be addressed. Over the last decade, growing effort has been devoted to developing and utilizing new carbon materials for VOCs elimination. The so-called carbon nanotubes (CNTs) are especially promising because of their unique properties. CNTs can be divided into multi-walled carbon nanotubes (MWCNTs) and single-walled carbon nanotubes (SWCNTs) based on the carbon atom layers in the walls of the tubes. MWCNTs have been known for more than 30 years [14] and SWCNTs for 14 years [15,16]. The hexagonal arrays of sp^2-like carbon atoms in the tubular graphene sheets on the surfaces of CNTs provide a favorable morphological structure for adsorbing aromatic compounds. Long and Yang [17] have used MWCNTs as an adsorbent for the removal of dioxin from model air samples. They found the adsorptive capability of CNTs to be much higher than that of conventional activated carbon, especially in the Henry's law region. Li et al. [18] employed MWCNTs as an adsorbent for solid-phase extraction of VOCs from model water samples. The MWCNTs exhibited excellent extraction capability and high recoverability [18,19]. These studies have provided experimental evidence that CNTs are capable of adsorbing pollutants. Nevertheless, none of these studies has explored the possibility of using CNTs as an adsorbent for separating aromatic VOCs from other types of VOCs.

This study presents the first data on the use of CNTs as an adsorbent for selectively eliminating aromatic VOCs. Model air samples containing six aromatic VOCs and 17 aliphatic VOCs were passed through a CNT-packed cartridge, and the amount of VOCs retained by the CNTs was quantitatively analyzed using GC–MS. The CNTs were found to be capable of selectively adsorbing the aromatic VOCs. This is also the first study to describe the possible mechanism for the adsorption of aromatic compounds by CNTs using an orbital framework (Fukui's frontier orbital theory).

2. Materials and methods

2.1. Preparation of the model air samples containing VOCs

A commercially available methanol solution (Wako Pure Chemicals) containing six aromatic VOCs (benzene, toluene, *m*-, *p*-, *o*-xylene, and *p*-dichlorobenzene) and 17 aliphatic VOCs (1,1-dichloroethylene, dichloromethane, *trans*-1,2-dichloroethylene, *cis*-1,2-dichloroethylene, chloroform, 1,1,1-trichloroethane, carbon tetrachloride, 1,2-dichloroethane, trichloroethylene, 1,2-dichloropropane, bromodichloromethane, *cis*-1,3-dichloropropene, *trans*-1,3-dichloropropene, 1,1,2-trichloroethane, tetrachloroethylene, dibromochloromethane and bromoform) was used for preparing the model air samples. Most compounds were present at a concentration of 1.0 mg/mL, except for *m*-xylene and *p*-xylene (*m*-xylene + *p*-xylene = 1.0 mg/mL). The model air samples were generated by using a syringe to inject 100 μL of the VOCs mixture into a 10-L tetra-bag that was previously filled with purified air under ambient pressure. The injection valve was immediately switched to the closed position and the tetra-bag was then heated at 80 °C in an oven for 1 h. Samples prepared in this manner were used for the adsorptive studies.

2.2. Highly crystallized multi-walled carbon nanotubes (HC-MWCNTs)

Highly crystalline multi-walled carbon nanotubes (HC-MWCNTs) were used as the adsorbent throughout this study. The HC-MWCNTs were produced using the floating reactant method [20–22]. Ferrocene was used as the catalyst precursor and toluene was used as the carbon feedstock, with hydrogen as the carrier gas. A toluene solution containing a specified amount of ferrocene was fed into a reactor with a temperature of approximately 1200 °C to produce the "as-grown" nanotubes. These nanotubes contain a substantial portion of amorphous carbon. The resultant nanotubes were further thermally annealed at 2600 °C for 30 min in a highly purified argon gas atmosphere to produce the HC-MWCNTs. MWCNTs and SWCNTs containing relatively large amounts of amorphous carbon were also prepared in the laboratory using the CVD method, and these "as-grown" CNTs were used as comparison adsorbents.

2.3. Laboratory-made CNT-packed cartridges

CNT-packed cartridges were made by dispersing carbon nanotubes in methanol using an ultrasonic generator (42 kHz) and then loading the CNTs into an empty cartridge (tubular shaped polypropylene: length, 16.5 mm; internal diameter, 10 mm) using a vacuum pump. The final mass of CNTs in each cartridge was approximately 80 mg. Polypropylene filters (10 μm) were placed at each end of the cartridges to hold the CNTs in place.

2.4. Adsorption and desorption of VOCs

The inlet end of the CNT-packed cartridge was connected to the sample bag. The other end was connected to a Sibata charcoal tube (Sibata, Tokyo, Japan), which is a glass tube filled with activated carbon and is used as the domestic standard cartridge for sampling VOCs in indoor air samples. In these experiments, the charcoal tube was used to trap any VOCs not retained by the CNT-packed cartridge. The outlet end of the tube was connected to a vacuum pump and the air samples were passed through the cartridges at an adjustable flow rate.

To measure the amounts of VOCs trapped by the charcoal, the tube was extracted with 5.0 mL CS_2. Analysis was performed with a Shimadzu GCMS-QP5050A system, using toluene D8 as the internal standard. The VOCs adsorbed by the CNT cartridge were estimated by subtraction of the VOCs retained by the charcoal from the initial quantities injected into the sample bag. Adsorptive and desorptive experiments were conducted in triplicate for each sample.

3. Results and discussion

3.1. Characteristics of the highly crystalline multi-walled carbon nanotubes (HC-MWNTs)

Fig. 1 shows typical SEM images of the HC-MWCNTs at low (upper photo) and high (lower photo) resolutions. Tubes with

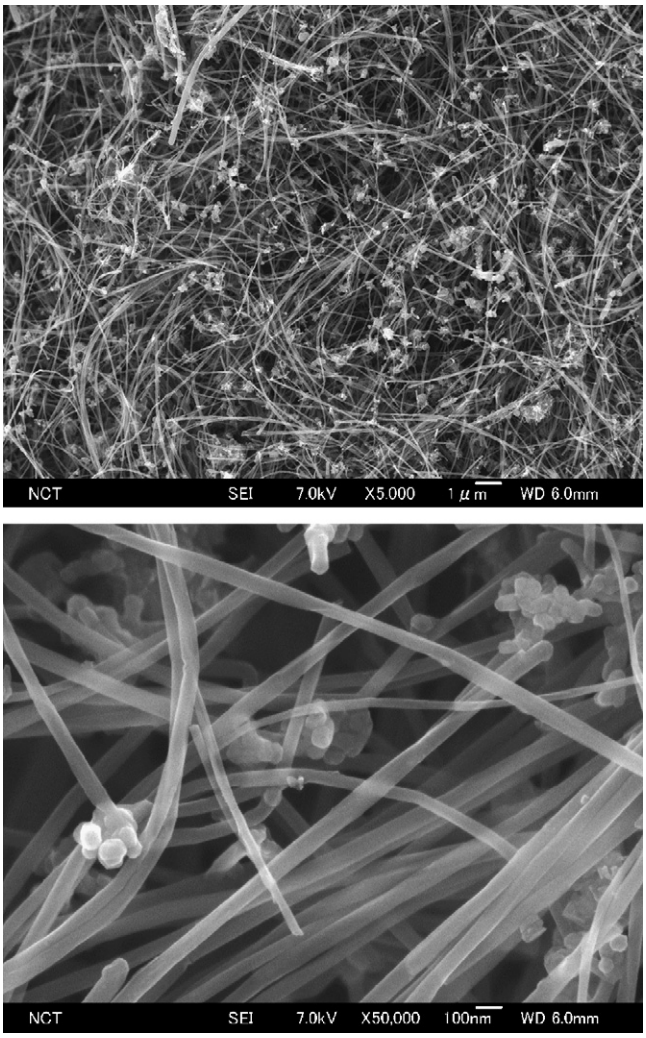

Fig. 1. SEM images of the HC-MWCNTs at low (upper photo) and high (lower photo) resolutions.

external diameters ranging from 40 to 90 nm were observed, together with a few carbon nano-particles. According to X-ray elemental analysis, the metallic impurity of the HC-MWCNTs was less than 450 ppm. The specific surface area (measured by N_2 adsorption based on the BET method) was 25 m^2/g.

Analysis using Raman spectroscopy (Fig. 2) revealed an extremely small *R*-value, which is the ratio of the intensity of the D band (1350 cm^{-1}) to that of the G band (1582 cm^{-1}). This indicates that the thermally annealed tubes were highly crystalline. Also, the G′ band, which corresponds to the overtone of 2D at 2700 cm^{-1}, was very intensive and symmetric for the HC-MWCNTs.

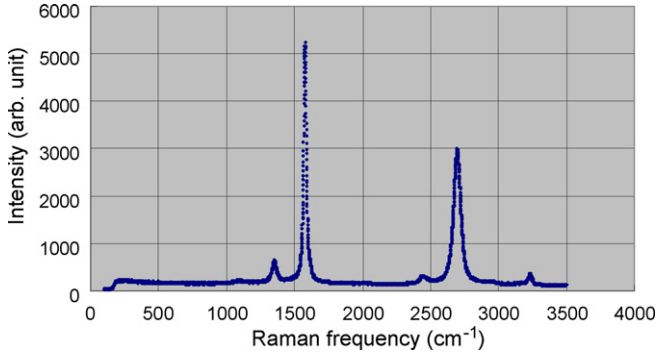

Fig. 2. Raman spectroscopy for the HC-MWCNTs.

Table 1
GC–MS conditions for quantitative VOCs determination

Chromatograph	
Column	DB-624, length: 60 m, ϕ: 0.25 mm, Film: 1.4 μm
Carrier gas	He
Total flow	50 mL/min
Split ratio	24
Injector temperature	200 °C
Detector temperature	230 °C
Oven temperature program	50 °C (2 min) to (10 °C/min) to 100 °C (5 °C/min) to 130 °C (10 °C/min) to 190 °C (5 min)
Mass spectrometer	
Interface temperature	230 °C
Electron multiplier voltage	1.0 kV
Scan mode	SIM

3.2. Adsorptive studies

In early experiments, only HC-MWCNT-packed cartridges were used as the adsorptive medium. However, difficulties were encountered in extracting VOCs from the cartridge. A small amount of the carbon nanotubes became entrained in the extraction solution and needed to be removed before the samples could be injected into the GC–MS system. Some of the extracted VOCs were lost during this extra step and recoveries were unsatisfactory. This difficulty was overcome by connecting a standard Sibata charcoal tube next to the HC-MWCNT-packed cartridge. The VOCs retained by the charcoal tube were extracted using CS_2 and the extraction solution was directly analyzed using GC–MS. Operating conditions for the GC–MS are summarized in Table 1.

Table 2 shows recoveries for four groups of standard samples processed using only the charcoal tube (no HC-MWCNT-packed cartridge). The samples were heated in an oven for 1 h at 50, 60, 70, and 80 °C, respectively. Recoveries were slightly dependent on the temperature (Table 2) and the best recoveries (from 93.9% to 106.3%) were obtained at 80 °C. Note that *m*-xylene and *p*-xylene were unable to be measured separately using this GC–MS system.

3.3. Affinity of HC-MWCNTs for aromatic VOCs

Average values for adsorption (μg VOCs/g HC-MWCNTs) are shown in Fig. 3. The HC-MWCNTs-packed cartridges demonstrated a high capacity for adsorbing *p*-dichlorobenzene, *o*-xylene, *m*-, *p*-xylene, toluene, and benzene (i.e., the aromatic VOCs). The adsorption capacity of the HC-MWCNTs for adsorbing *p*-dichlorobenzene was 1048.3 μg/g. For *o*-xylene, *m*,*p*-xylene, toluene, and benzene, adsorption capacities were

Table 2
VOCs recoveries (%) using the domestic standard cartridge (Sibata-charcoal) at the outlet

Recovery (%)	50 °C	60 °C	70 °C	80 °C
1,1-Dichloroethylene	96.65	104.08	88.64	96.51
trans-1,2-Dichloroethylene	99.83	101.27	87.73	93.90
cis-1,2-Dichloroethylene	100.29	102.37	90.04	95.44
Chloroform	104.47	106.36	94.32	100.56
1,1,1-Trichloroethane	107.17	106.63	95.16	100.32
Carbon tetrachloride	107.99	103.95	94.21	98.25
1,2-Dichloroethane	103.05	101.62	92.89	97.17
Benzene	104.16	101.77	93.49	95.27
Trichloroethylene	106.99	102.99	95.16	99.75
1,2-Dichloropropane	105.43	109.92	92.99	96.29
Bromodichloromethane	107.14	101.92	95.54	99.88
cis-1,3-Dichloropropene	101.47	105.25	94.92	96.78
Toluene	105.04	107.66	96.08	96.86
trans-1,3-Dichloropropene	102.30	106.16	95.76	96.92
1,1,2-Trichloroethane	104.99	108.63	97.41	99.44
Tetrachloroethylene	104.88	108.92	96.72	100.63
Dibromochloromethane	101.32	109.19	97.23	99.60
m,*p*-Xylene	104.11	104.93	97.20	95.88
o-Xylene	102.58	102.88	96.08	94.99
Bromoform	101.48	104.78	97.04	106.39
p-Dichlorobenzene	87.53	88.24	90.70	91.61

771.7, 740.3, 274.1 and 178.6 μg/g, respectively. The HC-MWCNTs thus showed an affinity order of *p*-dichlorobenzene > *o*-xylene > *m*,*p*-xylene > toluene > benzene ≫ the other aliphatic VOCs.

3.4. Effects of temperature on aromatic VOCs adsorption

The effect of temperature on adsorption was studied for four aromatic VOCs (*m*,*p*-xylene, *o*-xylene, and *p*-dichlorobenzene), chosen as representative compounds. Experiments were conducted at 25, 40, 50, 60, and 70 °C, and the adsorptive capacity (μg VOCs per g HC-MWCNTs) for each compound was plotted against temperature (K) (Fig. 4). The adsorptive capacities for these VOCs decreased as the temperature increased. Moreover, an adsorption hill was observed for all four compounds at approximately 333 K. This feature was also observed for toluene

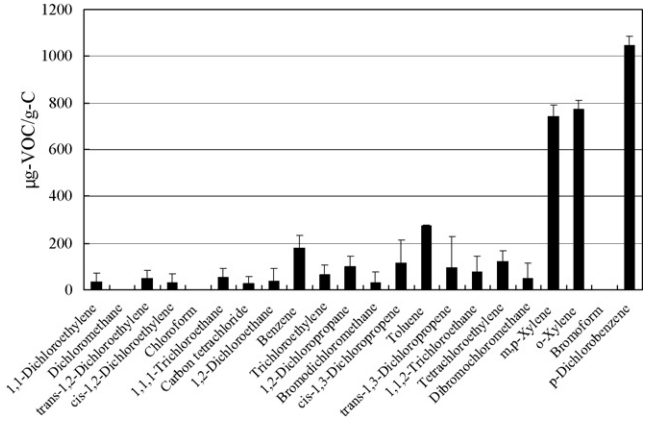

Fig. 3. Capacity of the HC-MWCNT-packed cartridges for adsorbing VOCs, expressed as micro-grams of VOCs per gram of HC-MWCNT.

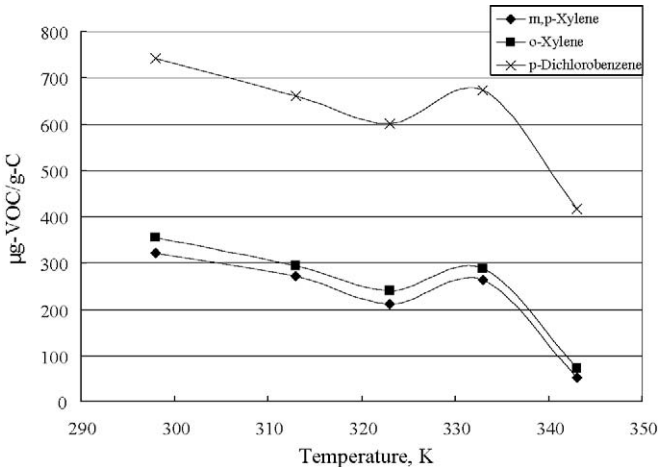

Fig. 4. Effects of adsorption temperature on the adsorptive capability of the HC-MWCNTs for VOCs.

and benzene, but was absent for the aliphatic VOCs (data not shown). The hills could be attributed to activated entry effects; *m*,*p*-xylene, *o*-xylene, and *p*-dichlorobenzene are disc-liked molecules [23]. Higher temperatures may facilitate diffusion of the aromatic VOCs, propelling the molecules through the tube/tube networks and enhancing the adsorptive capacity.

3.5. HOMO–LUMO interactions

The total energies of the highest occupied molecular orbital (HOMO) and the lowest unoccupied molecular orbital (LUMO) of the aromatic VOCs were calculated based on Fukui's frontier orbital theory [24,25] with a PM3 program. Table 3 summarizes the HOMO, LUMO, and LUMO–HOMO values. The *p*-dichlorobenzene had the highest HOMO energy (−9.459 eV), followed by *o*-xylene (−9.707 eV), *m*-xylene (−9.716 eV), toluene (−9.811 eV), and benzene (−10.945 eV). This sequence matches the order of the affinities of the aromatic VOCs for the HC-MWCNTs.

HOMO and LUMO electron densities for the aromatic VOCs were calculated using the MOPAC program (Fig. 5). The high frontier electron (HOMO) density points of the aromatic carbon atoms were C3 and C6 (0.3392, 0.3392) for *p*-dichlorobenzene, C1 and C6 (0.5080, 0.5082) for *o*-xylene, C3 and C6 (0.5663, 0.5663) for *p*-xylene, and C1 and C3 (0.4849, 0.5078) for *m*-xylene. The HOMO points for benzene were C1 and C4 (0.5429, 0.5429), and those for toluene were C3 and C6 (0.5960, 0.6118). The resulting HOMO electron density order was *p*-dichlorobenzene < *o*-xylene < *p*-xylene < benzene < toluene.

Table 3
HOMO, LUMO, and LUMO–HOMO energies of aromatic VOCs

VOCs	HOMO (eV)	LUMO (eV)	LUMO–HOMO (eV)
Benzene	−10.115	0.025	10.139
Toluene	−9.811	−0.069	9.742
m-Xylene	−9.716	−0.085	9.631
p-Xylene	−9.592	−0.105	9.487
o-Xylene	−9.707	−0.070	9.637
p-Dichlorobenzene	−9.459	−0.425	9.034

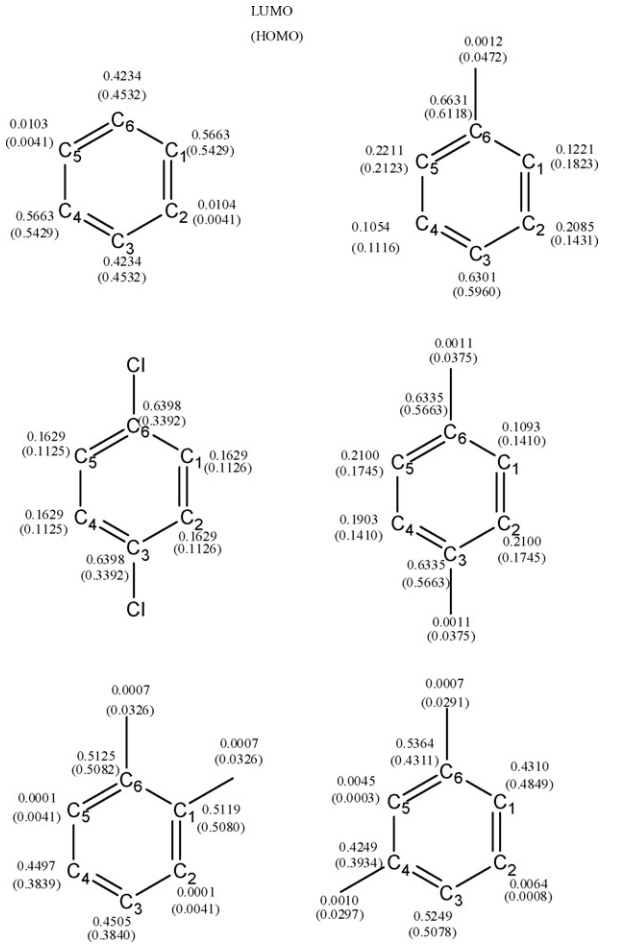

Fig. 5. Electron densities of HOMO and LUMO on the carbon atoms of the aromatic VOCs, calculated using the MOPAC program. Parentheses indicate HOMO values.

These calculations provide new insight into the mechanism of aromatic VOCs adsorption by HC-MWCNTs. The high degree of adsorption is due to the transfer of the π-electrons from the HOMO of the HC-MWCNTs to the LUMO of the aromatic VOCs. The *frontier* electrons (HOMO) of the aromatic VOCs, on the other hand, repel the π-electrons transferring to the LUMO. Therefore, a compound with a small HOMO–LUMO gap will have a higher affinity towards the HC-MWCNTs. For example, *p*-dichlorobenzene has the smallest HOMO–LUMO gap and was the most extensively adsorbed by the HC-MWCNTs. The order of the affinities of the aromatic VOCs for the HC-MWCNTs (*p*-dichlorobenzene > *o*-xylene > *m*,*p*-xylene > toluene > benzene) was identical to the order of the HOMO–LUMO gap values.

3.6. Comparison to "as-grown" CNTs

Fig. 6 shows the experimental data obtained using the as-grown MWCNTs and SWCNTs as adsorbents. The value of *R* (ratio of the intensity of the D band to that of G band) for the MWCNTs was 0.92. The specific surface area measured by N_2 adsorption (BET method) was 91 m^2/g. For the as-grown SWCNTs, $R = 1.86$ and the specific surface area was 254 m^2/g. The

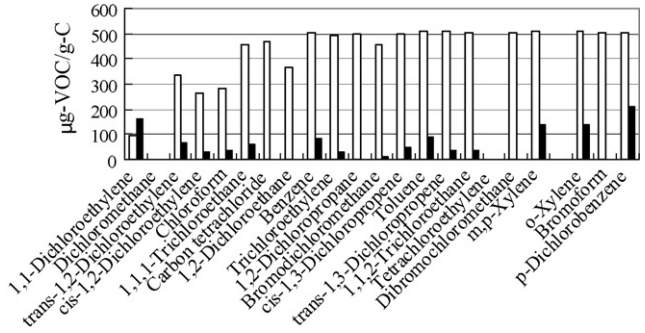

Fig. 6. Adsorptive studies carried out using the as-grown MWCNT-packed cartridge (white column) and the as-grown SWCNT-packed cartridge (black column) as the adsorbing media. Other experimental conditions were the same as for the HC-MWCNTs experiments.

selectivity/affinity for adsorbing the aromatic VOCs decreased and finally disappeared as the ratio of the crystalline to amorphous carbon decreased.

4. Conclusion

Carbon nanotubes with a highly crystalline structure have been demonstrated to be capable of selectively adsorbing aromatic VOCs. The affinity of a VOCs compound for MWCNTs was determined by both its LUMO and HOMO values. From the molecular orbital point of view, the adsorption of the aromatic VOCs by HC-MWCNTs can be considered a kind of "soft-chemical bonding" interaction. Research is ongoing on the use of MWCNT-based adsorbents for the elimination of aromatic VOCs from indoor air.

Acknowledgements

This work was supported by funding from Grants-in-Aid for Scientific Research from the Ministry of Education, Culture, Sports, Science and Technology of Japan (No. 18310049), by the Japan Science and Technology Agency (JST), and by the Ministry of Health, Labor, and Welfare (No. H18-Chem-Gen-006).

References

[1] S.K. Brown, M.R. Sim, M.J. Abramson, C.N. Gray, Indoor Air 4 (1994) 123.
[2] S.O. Baek, Y.S. Kim, R. Perry, Atmos. Environ. 31 (1997) 529.
[3] P.O. Fanger, Indoor Air 10 (2000) 68.
[4] P. Wolkoff, G.D. Nielsen, Atoms. Environ. 35 (2001) 4407.
[5] L.A. Wallace, E.D. Pellizzari, T.D. Hartwell, V. Davids, L.C. Michael, R.W. Whitmore, Environ. Res. 50 (1989) 37.
[6] L.A. Wallace, W. Nelson, R. Ziegenfus, E. Pellizzari, L. Michael, R. Whitmore, H. Zelon, T. Hartwell, R. Perritt, J. Expos. Anal. Environ. Epidemiol. 1 (1991) 157.
[7] D. Das, V. Graur, N. Verma, Carbon 42 (2004) 2949.
[8] M. Peng, L.M. Vane, S.X. Liu, J. Hazard. Mater. B98 (2003) 69.
[9] M.R. Tancerde, W.L. Zeise, E.A. Crouch, Atoms. Environ. 21 (1987) 2187.
[10] J. Begerow, E. Keles, T. Koch, L. Dunemann, J. Chromatogr. A 749 (1996) 181.
[11] M.J. Ruhl, Chem. Eng. Prog. 89 (1993) 37.

[12] M.A. Lillo-Rodenas, D. Cazorla-Amoros, A. Linares-Solano, Carbon 43 (2005) 1758.
[13] J.H. Byeon, J.H. Park, K.Y. Yoon, B.J. Ko, J.H. Ji, J. Hwang, Carbon 44 (2006) 2089.
[14] M.S. Dresselhaus, G. Dresselhans, P.C. Ekiund, Science of Fullerenes and Carbon Nanotubes, Academic Press, 1996.
[15] S. Iijima, Nature (Lond.) 354 (1991) 56.
[16] D.S. Bethune, C.H. Kiang, M.S. de Vries, G. Gorman, R. Savoy, J. Vasques, R. Breyers, Nature 363 (1993) 605.
[17] R.Q. Long, R.T. Yang, J. Am. Chem. Soc. 123 (2001) 2058.
[18] Q. Li, D. Yuan, Q. Lin, J. Chromatogr. A 1026 (2004) 283.
[19] E. Diaz, S. Ordonez, A. Vega, J. Colloid Interface Sci. 305 (2007) 7.
[20] M. Endo, M. Shikata, Jpn. J. Appl. Phys. 54 (1985) 507.
[21] M. Endo, Chem. Technol. 18 (1988) 568.
[22] Y.A. Kim, T. Hayashi, M. Endo, Y. Kaburagi, T. Tsukada, J. Shan, K. Osato, S. Tsuruoka, Carbon 43 (2005) 2243.
[23] Y. Chiang, P. Chiang, C. Huang, Carbon 39 (2001) 523.
[24] K. Fukui, T. Yonezawa, H. Shingu, J. Chem. Phys. 20 (1952) 722.
[25] K. Fukui, Acc. Chem. Res. 4 (1971) 57.

Available online at www.sciencedirect.com
ScienceDirect
Talanta 74 (2008) 1256–1264
Talanta
www.elsevier.com/locate/talanta

Enhancement of the chemiluminescence of penicillamine and ephedrine after derivatization with aldehydes using tris(bipyridyl)ruthenium(II) peroxydisulfate system and its analytical application

Fakhr Eldin O. Suliman *, Mohammed M. Al-Hinai, Salma M.Z. Al-Kindy, Salama B. Salama

Department of Chemistry, College of Science, Sultan Qaboos University, Box 36, Al-Khod 123, Oman

Received 1 July 2007; received in revised form 27 August 2007; accepted 29 August 2007
Available online 7 September 2007

Abstract

A novel sequential injection (SI) method was developed for the determination of penicillamine (PA) and ephedrine (EP) based on the reaction of these drugs with tris(bipyridyl)ruthenium(II) ($Ru(bpy)_3^{2+}$) and peroxydisulfate ($S_2O_8^{2-}$) in the presence of light. Derivatization of PA and EP with aldehydes has resulted in a significant enhancement of the chemiluminescence emission signal by at least 25 times for PA and 12 times for EP, leading to better sensitivities and lower detection limits for both drugs. The instrumental setup utilized a syringe pump and a multiposition valve to aspirate the reagents, ($Ru(bpy)_3^{2+}$ and $S_2O_8^{2-}$), and a peristaltic pump to propel the sample. The experimental conditions affecting the derivatization reaction and the chemiluminescence reaction were systematically optimized using the univariate approach. Under the optimum conditions linear calibration curves between 0.2–24 $\mu g\,mL^{-1}$ for PA and 0.2–20 $\mu g\,mL^{-1}$ for EP were obtained. The detection limits were 0.1 $\mu g\,mL^{-1}$ for PA and 0.03 $\mu g\,mL^{-1}$ for EP. The procedure was applied to the analysis of PA and EP in pharmaceutical products and was found to be free from interferences from concomitants usually present in these preparations.
© 2007 Elsevier B.V. All rights reserved.

Keywords: Chemiluminescence; Sequential injection; Tris(bipyridyl) ruthenium(II); Penicillamine; Ephedrine; Peroxydisulfate

1. Introduction

The use of chemiluminescence (CL) detection is growing rapidly owing to the attractive potentials it offers specially in miniature systems. CL is known to offer low detection limits, wide dynamic range yet with a relatively simple instrumental setup. Coupling this detection system to flow injection analysis (FIA), HPLC and capillary electrophoresis (CE) has enabled a large number of reports on the determination of various analytes to appear in the literature [1–5]. Tris(2,2′-bpyridyl)ruthenium (II) ($Ru(bpy)_3^{2+}$ is one of the most frequently utilized chemiluminogenic reagents and it has been used for the determination of different analytes such as amines, drugs, oxalates, amino acids and many more [6–11]. The most acceptable mechanism by which $Ru(bpy)_3^{2+}$ chemiluminescence is obtained is via oxidation of $Ru(bpy)_3^{2+}$ to the active $Ru(bpy)_3^{3+}$ either chemically or electrochemically [12]. Then presumably the emission of the ruthenium complex arises from the energetic electron transfer reaction between $Ru(bpy)_3^{3+}$ and a reducing agent. The electrochemiluminescent (ECL) generation of $Ru(bpy)_3^{3+}$ has received lots of interest due to the favourable characteristics of this species, such as excellent chemical stability, high emission quantum yield and long lifetime of the excited state [13–20]. The major limitations of ECL are those associated with electrodes, such as fouling, and the need for reconditioning of electrode surface to sustain a constant chemiluminescence signal. In addition electrochemical cells provide an additional complexity to the detection system. On the other hand the chemically generated $Ru(bpy)_3^{3+}$ avoids such complexity, however, it is characterized by instability of the reagent with respect to reduction. Two main

* Corresponding author. Fax: +968 24141469.
E-mail address: fsuliman@squ.edu.om (F.E.O. Suliman).

0039-9140/$ – see front matter © 2007 Elsevier B.V. All rights reserved.
doi:10.1016/j.talanta.2007.08.040

approaches have been employed in the literature (used) to overcome such an obstacle. The first one is through the mixing of $Ru(bpy)_3^{2+}$ with the analyte and then an oxidant such as Ce^{4+} is mixed downstream just before the detection cell. The second one involves recirculation of $Ru(bpy)_3^{2+}$ through a column containing an immobilized oxidant such as PbO_2 to generate $Ru(bpy)_3^{3+}$ which is then mixed with the analyte at a confluence point just before the detector. The protocol adopted in this paper depends on mixing of peroxydisulfate anions ($S_2O_8^{2-}$) with $Ru(bpy)_3^{2+}$, followed by passing the mixture through a photoreactor to produce $Ru(bpy)_3^{3+}$ which is finally mixed with the analyte just before the detection cell.

The chemiluminescence of $Ru(bpy)_3^{2+}$ was heavily used for the determination of many amine-containing compounds [7,20–25]. However, the detection limits of this method with respect to amines may be ordered tertiary < secondary < primary. It is known that only compounds with a tertiary or sometimes a secondary amine moiety give rise to strong chemiluminescence signal with $Ru(bpy)_3^{2+}$ systems. The selective determination of proline (a secondary amine) in the presence of many other amino acids (primary amines) using flow injection techniques has been recently reported [23]. Acquiring a strong and useful analytical signal by $Ru(bpy)_3^{3+}$ with primary amines clearly requires the transformation of primary amines to secondary or tertiary amines groups. Derivatization is the most attractive way of transforming primary amines to secondary and tertiary amines, however in most of the cases a separation step is required to eliminate the excess reagent which could also produce a significant CL signal. On the other hand, carbonyl compounds and specially aldehydes react with amines at room temperature at a reasonable rate to produce imine or enamine. Furthermore, aldehydes produce very weak chemiluminescence when reacted with ruthenium complexes. They, therefore, satisfy the requirement of an ideal derivatizing agent as they are generally stable, easy to obtain, and react with the analytes at a reasonable rate at room temperature using mild conditions.

In this work, two drugs penicillamine (PA) and ephedrine (EP) are investigated as primary and secondary amines, respectively. Penicillamine (2-amino-3-mercapto-3-methylbutanic acid) is a naturally occurring sulfur-containing amino acid that belongs to the amino-thiols family. It is the main product of the decomposition of penicillin antibiotics [26,27]. It is used for the treatment of many diseases such as rheumatoid arthritis, Wilson's cyctinura and heavy elements poisoning [28].

Various techniques for the assay of PA have been employed, including spectrophotometry and chromatography [29–33]. However, few chemiluminescence methods for the analysis of this drug have been reported in the literature. A method based on the inhibition by PA and cysteine of the chemiluminescence generated in the copper-catalyzed oxidation of luminol by hydrogen peroxide has been reported [34]. Another method utilized Ce(IV)-quinine system for the determination of PA [35].

Ephedrine, (1R, 2S)-2-(methylamino)-1-phenylpropan-1-ol is a secondary amine that is commonly used as a stimulant, decongestant and to treat hypotension associated with regional anaesthesia. Its principal mechanism of action relies on its indirect action on the adrenergic receptor system, which is part of the sympathetic nervous system (SNS) [36,37].

Many chemiluminescence methods have been proposed for the analysis of EP [15,38–40]. A self-assembly technique with the electrochemical polymerization method was developed where ephedrine was found to enhance luminol CL intensity at the electrode surface [15]. An on-line photodegradation with mercury lamp coupled to acidic potassium permanganate as an oxidant was used to determine EP [38]. These methods offer good detection limit, but lack simplicity, therefore new simple methods may be used to determine ephedrine and pseudoephedrine in pharmaceuticals preparations.

In this paper we report the enhancement of the CL of $Ru(bpy)_3^{2+}$–peroxydisulfate system with PA and EP through derivatization of these drugs with aldehydes. The enhancement of the emission signal forms the basis of the FI method proposed in this study for the analysis of PA and EP in pharmaceutical samples. The chemical and instrumental parameters that affect the derivatization and the CL reaction are systematically optimized. The method developed was successfully applied for the analysis of PA and EP in commercially available pharmaceutical samples.

2. Experimental

2.1. Reagents

All reagents were used without further purification. Acetaldehyde and formaldehyde were obtained from GCC (UK, London). Ammonium peroxodisulfate was purchased from Kanto Chemical CO. (Tokyo, Japan). Ruthenium(II) tris(2,2-bipyridine) chloride was purchased from Aldrich (UK, Gillingham). Penicillamine (PA) was from Sigma–Aldrich (Steinheim, Germany), and ephedrine was a gift from the National Pharmaceutical Company (Oman, Muscat). All other reagents are from BDH (UK, Pool).

Ultrapure water obtained from a Milli Q (Millipore Corporation) water system was used for the preparation of all solutions.

2.2. Standard drug solutions

A stock standard solution of 1000 μg mL^{-1} of PA or EP was prepared by dissolving 25 mg of the pure drug in 25 mL volumetric flask in deionzed water. The stock solutions were kept in cold dark place. Working solutions were daily prepared by appropriate dilutions.

2.3. Derivatization with aldehydes

The aldehyde derivatives were prepared by adding the appropriate volumes of PA or EP standard solutions to 1.5 mL of 0.2 mol L^{-1} phosphate buffer of pH 7 in 25.0 mL volumetric flasks. For the derivatization of PA, 1.25 mL of 0.5 mol L^{-1} acetaldehyde was added to the mixture. For EP, 1.0 mL of 1.5 mol L^{-1} formaldehyde was added to the drug buffer mixture. Finally, the flask was filled to the mark with 0.01 mol L^{-1} phosphate buffer of pH 8.

2.4. Sample preparation

Tablets were prepared by crushing 7–10 tablets priory weighed out and dissolving an amount of the powder equivalent to the mass of one tablet of the tested drug in water. The solutions were then mixed thoroughly by shaking for 30 min, and then centrifuged. Appropriate volumes were pipetted and transferred to a volumetric flask. The pH of the sample solution was adjusted to pH 7 using phosphate buffer. For capsules, the coating was first removed and the contents of capsules were emptied and weighed out individually. The average of one capsule mass was weighed and treated similar to tablets for further studies.

Nasal solutions were prepared by diluting a pipetted amount of the nasal solution into a calibrated flask with phosphate buffer system.

2.5. Apparatus

An Aminco Bowman Series 2 Luminescence Spectrofluorimeter (SLM instruments, NY, USA) was used to record emission spectra and to collect the CL emission. CL emission was obtained by setting the PMT voltage to 1275 V and slit width to 16 nm. The excitation slit was kept closed all the time. The flow cell is a coiled Teflon tube (3 cm in diameter), attached to an aluminium foil and placed in front of the emission slit. The wavelength was kept at 610 nm. The system is controlled by a computer using AB2 software. The data was collected in the time trace mode.

The pH of solutions was measured on Hanna HI8314 membrane pH meter (Romania).

2.6. Manifold and procedure

The flow system used for the determination and CL detection of PA and EP is shown schematically in Fig. 1. The SI analysis system, FIAlab-3000 (FIAlab Instruments, Medina, WA, USA) used in this study consists of the following components: 2.5 mL syringe pump driven by a stepper motor (24,000-step full stork), 200 cm holding coil (0.8 mm ID Teflon tubing, Upchurch Scientific, Oak Harber, USA), an eight port multiposition-valve (Valco, Houston, USA), 60 cm reaction coil (0.8 mm ID Teflon tubing, Upchurch Scientific), and a peristaltic pump (single speed) was used to drive the standard and the sample streams through the flow system. A home made flow cell, 3.0 cm in diameter (0.8 mm ID Teflon tubing, Upchurch Scientific), fixed to an aluminium foil, is placed in front of the detector. A home made tungsten-halogen lamp was used as the light source in the photoreactor. The fluids were controlled using FIAlab for Windows software (version 5.9.79).

Before the final manifold was selected and set up, three designs for producing suitable CL signals were considered. In the first one, the reagent $Ru(bpy)_3^{2+}$, the oxidant, $S_2O_8^{2-}$, and the standard drug solutions were aspirated by the multiposition-valve into the holding coil (HC). They are then pumped with the syringe pump through the reaction coil (photoreactor) before entering the flow cell. In the second one, the oxidant was pumped by the peristaltic pump through the photoreactor. The reagent ($Ru(bpy)_3^{2+}$) and the drug solutions were aspirated into the HC by the syringe pump then carried to mix with the oxidant (already passed through the photoreactor) at a confluence point, before passing through the flow cell. In the third design, both the reagent and the oxidant were aspirated into the HC and then pumped with the syringe pump through the photoreactor. In the same time the peristaltic pump was used to carry the standard or the sample drug solution to mix at the confluence point with $Ru(bpy)_3^{3+}$ generated in the reaction coil via photooxidation with peroxydisulfate before reaching the flow cell. The final design was found to produce the most intense signal; therefore it was selected for further investigations. The operation of the two pumps was synchronized by the FIAlab software. While the syringe pump is aspirating the reagents, the peristaltic pump is put off. When the syringe pump is programmed to dispense the reagents towards the detector, the peristaltic pump is put on to propel the sample which meets with the reagent mixture just before the flow through cell. This arrangement results in reducing the consumption of samples and reagents.

2.7. Method

100 μL of $Ru(bpy)_3^{2+}$ and 75 μL of $S_2O_8^{2-}$ were aspirated into the holding coil, and with a flow reversal were propelled

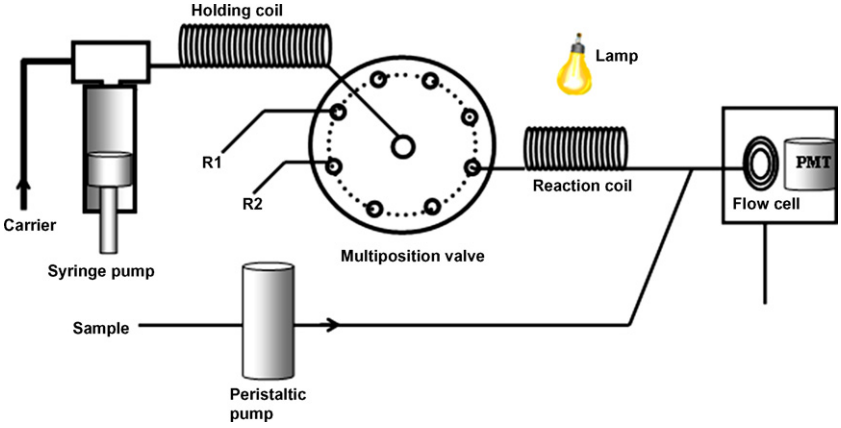

Fig. 1. Manifold used. R1, $Ru(bpy)_3^{2+}$; R2, $S_2O_8^{2-}$.

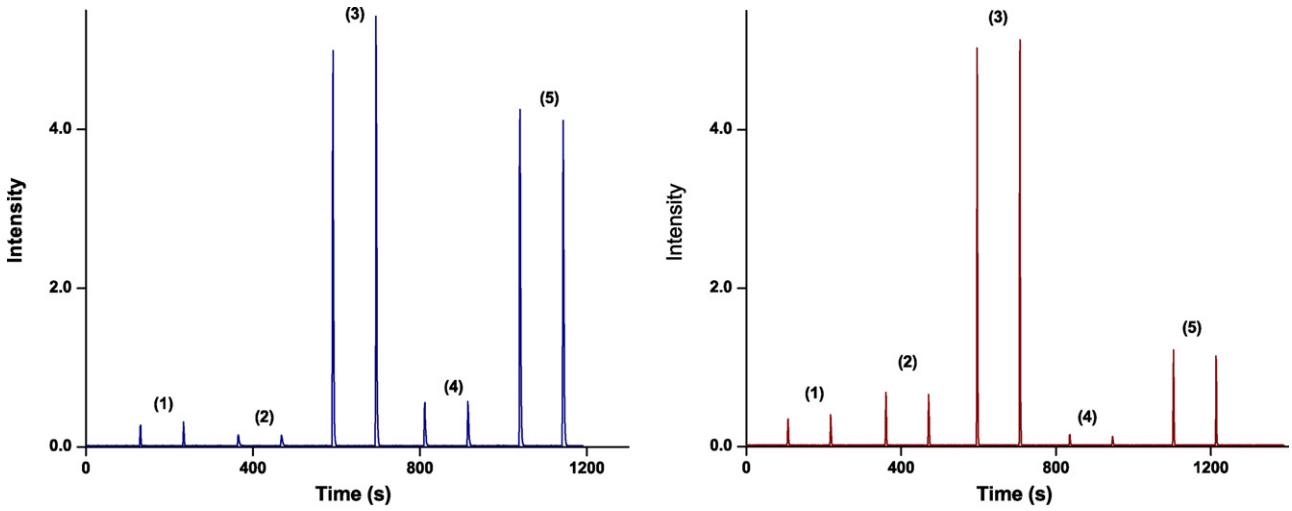

Fig. 2. (a) Fiagrams showing CL signals of the reaction of 100 μL of 2 mmol L^{-1} $Ru(bpy)_3^{2+}$ and 75 μL of 2 mmol L^{-1} $S_2O_8^{2-}$ with (1) PA, (2) acetaldehyde, (3) PA derivatized with acetaldehyde, (4) formaldehyde, (5) PA derivatized with formaldehyde. (b) Fiagrams showing CL signals of (1) EP, (2) formaldehyde, (3) EP derivatized with formaldehyde, (4) acetaldehyde, (5) EP derivatized with acetaldehyde. Conditions: PA, 20 μg mL^{-1}; EP, 10 μg mL^{-1}; acetaldehyde, 50 mmol L^{-1}; formaldehyde, 50 mmol L^{-1}.

through the photoreactor to convert $Ru(bpy)_3^{2+}$ to $Ru(bpy)_3^{3+}$. The mixture was then allowed to meet the sample or the standard stream at the confluence point just before entering the coiled flow cell. The emission signals were then collected by the detector in the time trace mode.

3. Results and discussion

3.1. Chemical system

When the mixture of $Ru(bpy)_3^{2+}$ and $S_2O_8^{2-}$ is passed through the photoreactor, $Ru(bpy)_3^{2+}$ is converted into $Ru(bpy)_3^{3+}$. Upon merging this stream with the solution of PA or EP, feeble chemiluminescence (CL) signals are observed as shown in Fig. 2. It is known that primary and secondary amines react with carbonyl compounds to produce secondary and tertiary amine derivatives, respectively [41,42]. To enhance the CL emission of PA with $Ru(bpy)_3^{3+}$ system, we reacted PA and EP with formaldehyde and acetaldehyde. As shown in Fig. 2a, derivatization of PA with acetaldehyde and formaldehyde resulted in a significant enhancement of its CL signal. It is clear from this figure that derivatization with acetaldehyde produces higher CL signals than derivatization with formaldehyde. Furthermore, it can be observed that both formaldehyde and acetaldehyde produce weak CL emission when reacted with $Ru(bpy)_3^{3+}$. However, a much weaker signal is obtained in the case of acetaldehyde. For EP a much stronger signal is observed in the presence of formaldehyde albeit its blank signals are higher than that of acetaldehyde as shown in Fig. 2b. In both cases the significant enhancement may be due to the formation of an intermediate secondary or tertiary amine.

The presence of acetaldehyde has increased the signal of PA 25 times more than that of PA alone, whereas formaldehyde enhanced the signal of EP by 12 times. Therefore, in this work acetaldehyde was used for the determination of PA and formaldehyde was used for the determination of EP.

3.2. Optimization

The optimization study was divided into two parts. The factors that influence the derivatization reaction were investigated first, by using constant concentrations of $Ru(bpy)_3^{2+}$, $S_2O_8^{2-}$ and PA of 2 mmol L^{-1}, 2 mmol L^{-1} and 20 μg mL^{-1}, respectively. For EP, the conditions were $Ru(bpy)_3^{2+}$ 1 mmol L^{-1}, $S_2O_8^{2-}$ 1 mmol L^{-1} and EP 10 μg mL^{-1}. The factors that are expected to influence the derivatization together with their investigated ranges are shown in Table 1. In the second part of the optimization study we investigated the factors that influence the CL system using the optimum derivatization conditions, these factors and their studied ranges are also listed in Table 1.

3.2.1. Optimization of PA derivatization conditions

The effect of pH on the derivatization of PA and EP with aldehydes was investigated in the range of 2–9. The derivtization of PA and EP with aldehydes is pH dependent as can be seen from Fig. 3. The CL intensity was found to increase as the pH

Table 1
Ranges of factors included in the optimization study and their optimum values

Variables	Range	Optimum	
		PA	EP
[Aldehyde] (mmol L^{-1})	0–100	25	60
Derivatization pH	2.0–9.0	7.0	7.0
[PBS] (mol L^{-1})	0.1–0.7	0.2	0.2
[$Ru(bpy)_3^{2+}$] (mmol L^{-1})	0.25–2.5	2.0	1.0
[$S_2O_8^{2-}$] (mmol L^{-1})	0.25–2.5	2.0	1.0
$Ru(bpy)_3^{2+}$ volume (μL)	25–125	100	100
$S_2O_8^{2-}$ volume (μL)	25–125	75	75
Flow rate (μL s^{-1})	20–100	60	60
Coil length (cm)	30–150	60	60
pH of sample	5–9	8	8
Carrier	H_2O/buffer	Deionized water	Deionized water

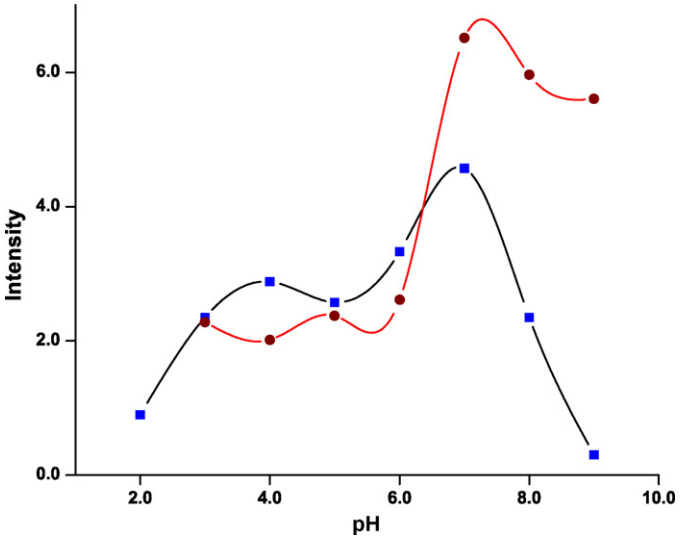

Fig. 3. Effect of phosphate buffer pH on the CL signals of the derivatization (■) PA (20 μg mL^{-1}) with acetaldehyde (25 mmol L^{-1}) and (●) EP (10 μg mL^{-1}) with formaldehyde (60 mmol L^{-1}) reacted with 100 μL of 2 mmol L^{-1} $Ru(bpy)_3^{2+}$ and 75 μL of 2 mmol L^{-1} $S_2O_8^{2-}$.

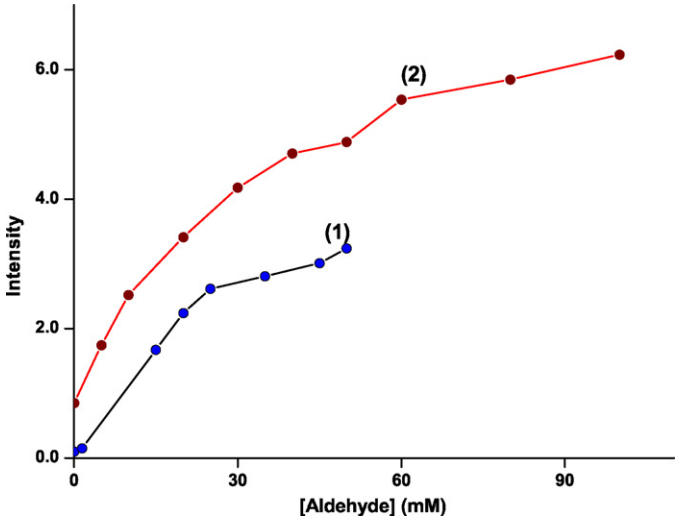

Fig. 4. Effect of the aldehyde concentration on the derivtization of (1) PA (20 μg mL^{-1}) with acetaldehyde and (2) EP (10 μg mL^{-1}) with formaldehyde in phosphate buffer pH 7. Other conditions are as in Fig. 3.

increases reaching a maximum at pH 7, above which a decrease in the CL intensity was observed. Thus, pH 7 was selected for derivatization of PA and EP with aldehydes.

The reaction of PA and EP with aldehydes starts by the nucleophilic addition of the amino group of PA or EP to the carbonyl group. Then, a proton transfer from nitrogen to the oxygen produces a neutral amino alcohol intermediate (hemiaminal). In a further step, the amino alcohol is protonated to convert the (–OH) into a better leaving group (–OH_2^+), which leave and the final product (imine or enamine) is formed.

At low pH the initial nucleophilic addition step by the amine lone pair of electrons on the aldehyde cannot occur because the amine nucleophile is totally protonated. With an increase in the pH, the amine becomes a more active nuclophile, therefore the CL intensity increases with pH up to 7. On the other hand, in basic media the rate of dehydration of the intermediate amino alcohol increases resulting in a decrease in the CL signal.

The concentration of the aldehyde was optimized by increasing acetaldehyde concentration from 1 to 50 mmol L^{-1} and that of formaldehyde from 1 to 100 mmol L^{-1}, respectively. As shown in Fig. 4 the chemiluminescence intensity increases as the concentration of acetaldehyde increases up to a concentration of 25 mmol L^{-1}, after which the CL signal increase became insignificant. Therefore, 25 mmol L^{-1} of acetaldehyde was selected as the optimum derivatization concentration for PA. For EP, the same trend was observed (Fig. 4), however the CL signal levelled off when the concentration of formaldehyde was 60 mmol L^{-1}. Therefore, for the derivatization of EP the concentration of formaldehyde was fixed at 60 mmol L^{-1}.

The influence of the buffer type and the buffer concentration on PA and EP derivatization was studied using acetate, phosphate and borate buffer systems. All buffers are kept at a constant pH of 7. The CL signals remained almost independent of the type of buffer used. The phosphate buffer, on the other hand was chosen for further studies as it exhibited the weakest signal with respect to the blank. Also it was found that the concentration of the buffer has no influence on the derivatization. Therefore, a phosphate buffer of 0.2 mol L^{-1} was used for the derivatization of PA and EP with aldehydes.

3.2.2. *Optimization of CL conditions*

The factors that influence the reaction of PA and EP aldehyde derivatives with $Ru(bpy)_3^{3+}$, resulted from photooxidation of $Ru(bpy)_3^{2+}$ with peroxydisulfate, are given in Table 1. The pH of the phosphate buffer used to dilute the sample (PA-acetaldehyde mixture or EP-formaldehyde mixture) was varied in the range 5–10. The signals-to-noise ratio was observed to increase with pH up to 8 after which the signals start to decrease due to consumption of $Ru(bpy)_3^{3+}$ by hydroxyl ions before reaching the detector. A 0.01 mol L^{-1} phosphate buffer with pH 8 was selected as the optimum. Both deionized water and 0.01 mol L^{-1} phosphate buffer were used as carrier and both gave the same results. Therefore, deionized water has been used as a carrier.

Common oxidants such as lead dioxide (PbO_2), cerium(IV) (Ce^{4+}), and potassium permanganate ($KMnO_4$) have been used to efficiently produce CL emission with $Ru(bpy)_3^{2+}$ [43]. In this study, six common oxidants were examined. Each of the oxidants (2.0 mmol L^{-1}) was prepared in 0.05 mol L^{-1} H_2SO_4. The oxidants studied were $KMnO_4$, $Ce(SO_4)_2$, $(NH_4)_2S_2O_8$, $KBrO_3$, KIO_3, and solid lead dioxide (5 mg). These oxidants were used with 2 mmol L^{-1} $Ru(bpy)_3^{2+}$ and 20 μg mL^{-1} PA. Fig. 5 shows the resultant CL signals. Obviously the highest CL signal was obtained in the presence of peroxydisulfate whereas Ce^{4+}, $KBrO_3$, and KIO_3 exhibited no CL emission. This behaviour is parallel to the oxidizing power of these reagents, where $S_2O_8^{2-}$ is the most powerful oxidizing agent amongst the reagents used and Ce^{4+}, $KBrO_3$, and KIO_3 are the weakest oxidizing agents. From these results $S_2O_8^{2-}$ was selected and used as the oxidant for this study.

The concentration of $Ru(bpy)_3^{2+}$ was varied from 0.5 to 2.5 mmol L^{-1}. The CL intensity continued to increase with

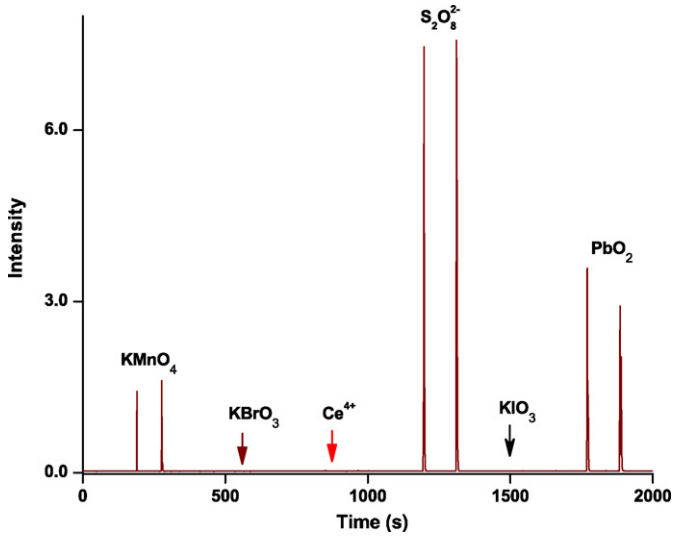

Fig. 5. Effect of oxidant type on the CL signals of (20 μg mL^{-1}) PA-acetaldehyde derivatives with 100 μL of 2.0 mmol L^{-1} $Ru(bpy)_3^{3+}$ at pH 8.0. All oxidant were prepared in 0.05 mol L^{-1} H_2SO_4 and their aspiration volumes were 100 μL.

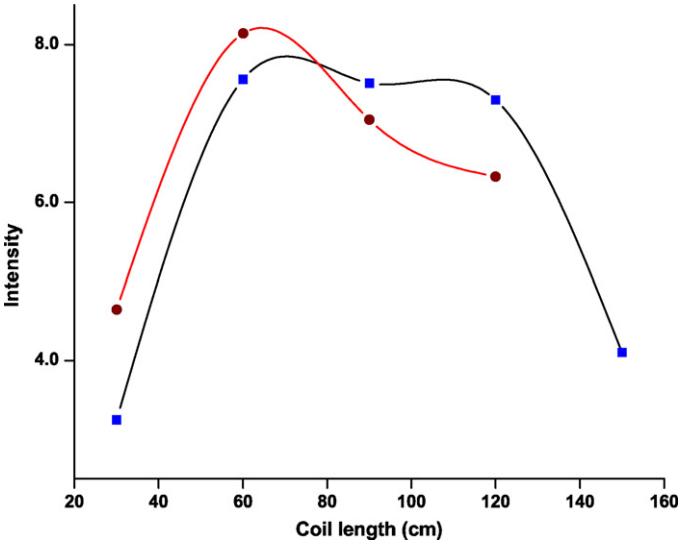

Fig. 6. Effect of coil length on CL signal of (●) PA-acetaldehyde derivatives and (■) EP-formaldehyde derivatives with 100 μL of 2.0 mmol L^{-1} $Ru(bpy)_3^{2+}$ and 75 μL of 2.0 mmol L^{-1} $S_2O_8^{2-}$.

the concentration of $Ru(bpy)_3^{2+}$ for both drugs. As a compromise a concentration of 2 mmol L^{-1} of the expensive reagent, $Ru(bpy)_3^{2+}$, was selected as the optimum concentration for PA and 1.0 mmol L^{-1} of $Ru(bpy)_3^{2+}$ was selected as the optimum concentration for the determination of EP.

In a similar way, the effect of $S_2O_8^{2-}$ concentration on the CL emission intensity was studied from 0.5 to 2.5 mmol L^{-1}. The CL intensity was found to increase with increasing the concentration of $S_2O_8^{2-}$ up to 2 mmol L^{-1} for PA, above which the CL intensity starts to decrease. The decrease in CL intensity at higher peroxydisulfate concentrations may be due to quenching of the excited state of the ruthenium complex by $SO_4^{\bullet -}$ radicals [44]. A 1.0 mmol L^{-1} of $S_2O_8^{2-}$ was found to be the optimum concentration for the assay of EP.

The volumes of reagents aspirated into the FI system should be sufficient when later mixed with the sample at the confluence point to permit effective CL reaction. The influence of the $Ru(bpy)_3^{2+}$ and $S_2O_8^{2-}$ volumes on the CL-signal was investigated by aspirating various volumes of the ruthenium complex solution (2 mmol L^{-1}) in the range 25–125 μL while the volume of $S_2O_8^{2-}$ (2 mmol L^{-1}) was kept constant at 100 μL. The emission intensity increases with an increase in the aspiration volume from 25 to 100 μL after which a further increase in the volume of the complex resulted in an insignificant increase in the CL signal. For $S_2O_8^{2-}$, the CL intensity increases with the aspiration volumes up to 75 μL, and then decreases as aspiration volumes are increased. The optimum aspiration volumes for $Ru(bpy)_3^{2+}$ and $S_2O_8^{2-}$ selected for further studies were 100 and 75 μL, respectively.

In this work, the oxidation of $Ru(bpy)_3^{2+}$ with $S_2O_8^{2-}$ was catalyzed by light. In the selected manifold both $Ru(bpy)_3^{2+}$ and $S_2O_8^{2-}$ are mixed in a Teflon tube (photoreactor) before meeting the derivative stream at the confluence point. Mixing coil lengths from 30 to 120 cm were used to study the effect of the coil length on the CL signals. From Fig. 6 it can be seen that the intensity increases with an increase in the coil length up to 60 cm, after which that it started to decrease. Therefore, 60 cm was chosen as the optimum mixing coil length in all measurements. The flow rate was investigated from 20–80 μL s^{-1}. The CL signals increase as the flow rate increases until 60 μL s^{-1}, beyond which a slight decrease in the signal was observed. Therefore, the flow rate was fixed at 60 μL s^{-1}. In the photoreactor, $Ru(bpy)_3^{2+}$ is converted to $Ru(bpy)_3^{3+}$ in the presence of $S_2O_8^{2-}$ and light. Increasing the coil length increases the residence time of the reagents, and as a result the efficiency of conversion of $Ru(bpy)_3^{2+}$ to $Ru(bpy)_3^{3+}$ is increased leading to higher CL signals. On the other hand, coil lengths higher than 60 cm causes further dilution of reagents and as a result a lower CL signal is obtained. Similar results are obtained for the flow rate. Clearly flow rates that allow faster reach of the CL mixture to the detector and at the same time maximizes the efficacy of production of $Ru(bpy)_3^{3+}$ are favoured.

3.3. Analytical appraisal

The analytical performance of the proposed method was investigated using the optimum conditions obtained above and summarized in Table 1. Calibration curves were generated by pumping series of standard solutions of PA or EP after offline derivatization with the appropriate aldehyde. Each standard was run in triplicate in order to assess the repeatability of the procedure. Linear calibration curves were obtained in the range 0.2–24 μg mL^{-1} with a correlation coefficient (R^2) of 0.996 for PA and in the range 0.2–20 μg mL^{-1} for EP (R^2, 0.991). Table 2 summarizes the analytical characteristics of the proposed method for both drugs.

The reproducibility of the proposed procedure was examined by preparing and analyzing nine solutions of two different standards. The relative standard deviations of nine runs of 1.0 and 18 μg mL^{-1} of PA were 0.45% and 1.3%, respectively. For EP,

Table 2
Analytical figures of merit obtained by the proposed method

Analytical figure of merit	Obtained value	
	PA	EP
Linear range ($\mu g\,mL^{-1}$)	0.3–24	0.04–20
Intercept (b)	0.12	0.08
Standard deviation of intercept (S.D.$_b$)	0.04	0.1
Slope (m)	0.265	0.43
Standard deviation of slope (S.D.$_m$)	0.006	0.01
Correlation coefficient (R^2)	0.996	0.991
Detection limit ($\mu g\,mL^{-1}$)[a]	0.1	0.03
Quantification limit ($\mu g\,mL^{-1}$)[b]	0.3	0.1
Relative standard deviation ($n=9$)	0.45%–1.3%	0.95%–4.3%

[a] 3 S.D.$_{bl}/m$.
[b] 10 S.D.$_{bl}/m$ (S.D.$_{bl}$, standard deviation of the blank).

the relative standard deviation was 0.95% and 4.3% for 1.0 and 18 $\mu g\,mL^{-1}$ of EP, respectively. This indicates that the method is characterized by a reasonable precision, making it suitable for routine analysis of these compounds.

The method developed here is sensitive, simple, and robust and covers a wide dynamic range. The proposed method confirms again the simplicity and accuracy of CL and its superiority in achieving both wide dynamic range and low detection limits. Also the method reported here utilized the merits of sequential injection analysis (SIA), where microliters of solutions are aspirated, using a multiposition valve, thus consumption of expensive reagents like $Ru(bpy)_3^{2+}$ is reduced. In addition the method is fast with a sampling frequency of $30\,h^{-1}$.

3.4. Analytical application

The proposed method was then applied to the determination of PA and EP in pharmaceutical formulations of various commercial dosage forms as shown in Table 3. The tablets, the capsules and the nasal solutions are prepared as described before, subjected to derivatization and then analyzed by the proposed procedure. The mean percent recoveries are shown in Table 3. Excellent recoveries were obtained for all samples analyzed indicating that the proposed method can be employed to the assay of PA and EP without interference from compounds usually present in these samples.

3.5. Interference study

The effect of some foreign compounds and ions on the assay of PA and EP was studied by analyzing synthetic sample solutions containing $1\,\mu g\,mL^{-1}$ of derivatized PA or EP together with various excess amounts of these compounds. A foreign species was considered not to interfere if it caused a relative error less than 5% during the determination of $1\,\mu g\,mL^{-1}$ PA or EP. No significant difference was observed between the results when the effect of interference was tested before and after the derivatization process. Most of the studied compounds exhibited no influence at the selected concentration.

Table 3
Determination of PA and EP in pharmaceutical samples by the proposed method ($n=9$)

Formulation	Claimed	Found	%Recovery (%) ± S.D.
PA tablets (mg)	125	126.8	101.4 ± 2.3
PA capsules (mg)	250	252.5	101.0 ± 2.9
EP tablets (mg)	120	120.8	100.7 ± 1.9
Nasal	0.1%	0.10%	100 ± 3.41

The tolerable concentration ratios of foreign species to PA were over 1000 for Na^+, K^+, NO_3^- and Cl^-; 500 for NH_4^+ and SO_4^{2-}; 100 for Br^-, sucrose and lactose; 10 for Mg^{2+}, Ca^{2+}, Cu^{2+}, Zn^{2+}, Fe^{2+}, Al^{3+} and Ag^+. However, Co^{2+} and Mn^{2+} were found to be strong interfering agents, both decreased the CL signals which reach only 10% of the original value at a 10:1 molar ratio of $[Mn^{2+}]$ or $[Co^{2+}]$:[PA].

Also in the case of EP determination, comparable results were obtained where the tolerable concentration ratio of foreign species to EP were over 1000 for Na^+, K^+, Mg^{2+}, NO_3^- and Cl^-; 500 for NH_4^+, Ca^{2+} and SO_4^{2-}; 100 for Br^-, Cu^{2+}, Zn^{2+}, sucrose and lactose; 10 for Fe^{2+}, Al^{3+} and Ag^+. Both cobalt and manganese exhibited the largest interference effects even at 1:1 molar ratio. Since EP is found in many of the commercially available forms of paracetamol, the effect of paracetamol was also studied. At a 1:1 EP: paracetamol molar ratio a significant interference is observed from paracetamol where a recovery of $73.0 \pm 3.0\%$ was obtained. This indicates that a separation step is required to apply this method to the analysis of EP in dosage forms containing paracetamol. Also several drugs in the market now-a-days contain mixtures of EP and chlorpheniramine. Chlorpheniramine is a tertiary amine and it produces a strong CL signal in the presence of $Ru(bpy)_3^{3+}$. We measured the CL signal of chlorpheniramine in the presence of ephedrine before and after derivatization. At a ratio of EP: chlorpheniramine of 1:1 the calculated recovery was $100.2 \pm 2.7\%$. This indicates that the simultaneous determination of both EP and chlorpheniramine is possible using this method.

3.6. Proposed reaction mechanism

Strong CL signals were detected only when the aldehyde derivatives of these drugs, $Ru(bpy)_3^{2+}$ and $S_2O_8^{2-}$ were present in the reaction system. However, no detectable signals were observed when the light of the photoreactor was put off even if all reagents were present or one of $Ru(bpy)_3^{2+}$ and $S_2O_8^{2-}$ is present with the derivatives.

Offline oxidation of $Ru(bpy)_3^{2+}$ by solid lead dioxide produced a reasonably strong CL emission with the drug-aldehyde derivatives. These results indicate that both $Ru(bpy)_3^{2+}$ and $S_2O_8^{2-}$ are indispensable to the CL reaction and the major role of light is to accelerate the formation of $SO_4^{\bullet -}$ which is a well-known powerful oxidizing agent, that oxidizes $Ru(bpy)_3^{2+}$ to $Ru(bpy)_3^{3+}$.

The satiability of the drug-aldehyde derivatives with time was investigated by allowing the mixture to stand for up to 2 h

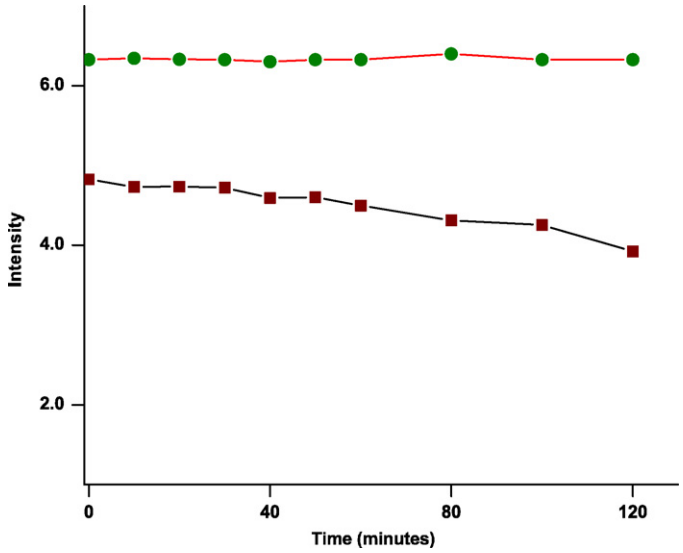

Fig. 7. Effect of time on the CL of (■) PA-acetaldehyde and (●) EP-formaldehyde derivatives, reacted with 100 μL of 2 mmol L^{-1} $Ru(bpy)_3^{2+}$ and 75 μL of 2 mmol L^{-1} $S_2O_8^{2-}$.

in room temperature. The CL emission was then obtained by analyzing aliquots of the derivatziation mixture every 10 min. The results for PA and EP are shown in Fig. 7. For PA the intensity remains almost constant during the first 30 min then the signal started to decrease slowly. At the end of 2 h the signal was found to decrease by 13% of its original value. For EP, the signal remains almost constant over 2 h as can be seen from the figure. The addition of PA to the acetaldehyde results initially in the formation of the *N*-substituted hemiaminal (intermediate amino alcohol). With time this intermediate is slowly converted into an imine. EP, on the other hand, when added to formaldehyde results in the formation of an *N*,*N*-disubstituted hemiaminal. Similar amino alcohol intermediates are reported to be very stable and can be isolated [41,42]. In the presence of an α-hydrogen they are converted slowly to enamine via loss of a water molecule. It has also been reported that the formation of an imine or enamine product could not produce favourable CL emission when oxidized by electrogenerated $Ru(bpy)_3^{3+}$ [9]. From these observations, it could be suggested that the amino alcohol intermediate is the species that reduces $Ru(bpy)_3^{3+}$ to $Ru(bpy)_3^{2+}$.

The oxidation of amines produces amine cation radicals which have been reported to possess short lifetime [45]. Therefore, these cation radicals lose a proton to produce the neutral amine radicals that have high enough energy. Upon reaction of these radicals with a second $Ru(bpy)_3^{3+}$ they produce the excited state $Ru(bpy)^*_3{}^{2+}$ which is the light emitting species. This species emits a strong orange light at a maximum wavelength of 610 nm upon its return to the ground state. Scheme 1 summarizes the steps of the mechanism of the CL reaction of PA and its acetaldehyde derivative with $Ru(bpy)_3^{2+}$.

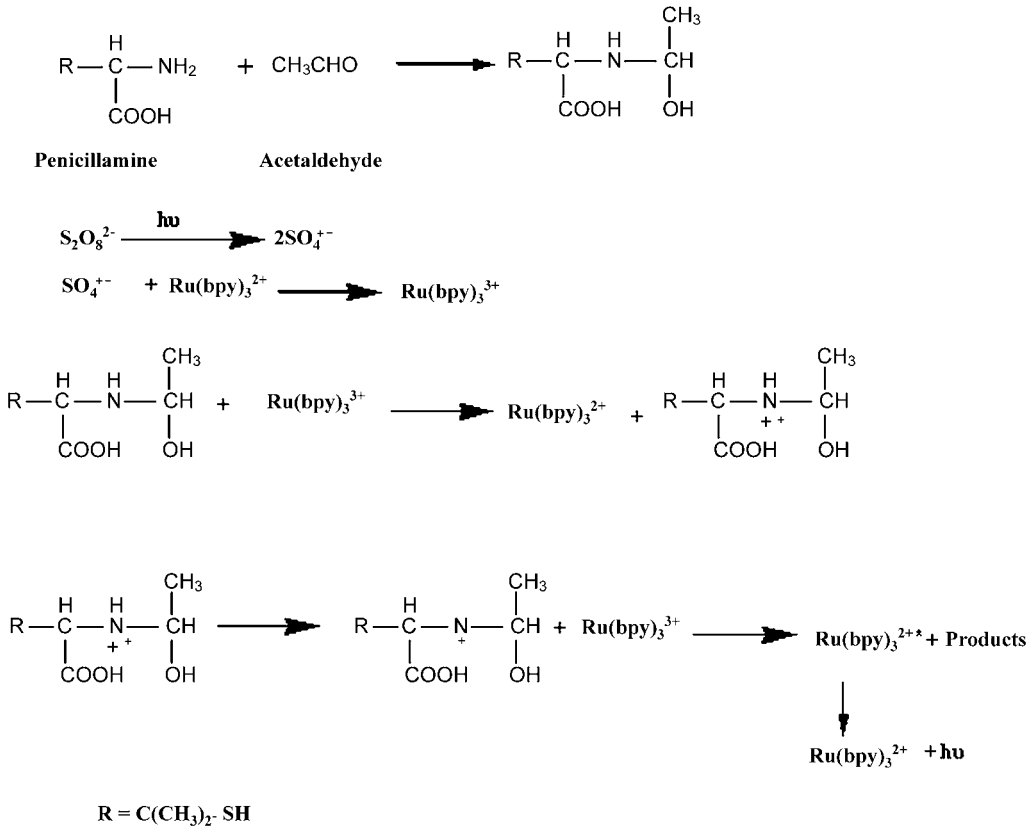

Scheme 1. The proposed mechanism for the CL reaction of PA with $Ru(bpy)_3^{2+}$.

4. Conclusion

A flow injection chemiluminescence method for the quantitative determination of PA and EP was successfully developed. The method is based on the CL emission generated when these drugs react with $Ru(bpy)_3^{3+}$ produced via photoxidation of $Ru(bpy)_3^{2+}$ by peroxydisulfate at pH 8. The CL emission for PA was significantly enhanced in the presence of acetaldehyde, whereas the largest enhancement in the CL emission of EP was observed in the presence of formaldehyde. The factors that influence both the derivatization reaction and the CL reaction were carefully investigated to obtain better sensitivity. The method developed is characterized by a wide dynamic range, a low detection limit and an excellent precision. Furthermore, the method is versatile with sampling frequencies of $30\,h^{-1}$. The method was applied to the analysis of PA and EP in commercially available dosage forms. No interference was observed from compounds usually added to these preparations. The method is also cost effective and environmentally friendly, as the expensive reagents are aspirated using a selection valve rather than continuously pumped as in conventional FI methods.

Acknowledgements

The financial support from SQU, grant #IG/SCI/CHEM/06/03, is gratefully acknowledged. M.M. AlHinai thanks the ministry of education for the MSc scholarship.

References

[1] Y. Mei, L. Ran, X. Ying, Z. Yuan, S. Xin, Biosens. Bioelectron. 22 (2007) 871.
[2] J. Du, L. Hao, Y. Li, J. Lu, Anal. Chim. Acta 582 (2007) 98.
[3] Y. Liu, W. Zhou, Anal. Sci. 22 (2006) 999.
[4] S. Zhao, H. Yuan, C. Xie, D. Xiao, J. Chromatogr. A 1107 (2006) 290.
[5] A. Waseem, M. Yaqoob, A. Nabi, Anal. Sci. 22 (2006) 1095.
[6] G.-H. Wan, H. Cui, Y.-L. Pan, P. Zheng, L.-J. Liu, J. Chromatogr. B: Analyt. Technol. Biomed. Life Sci. 843 (2006) 1.
[7] W. Ruengsitagoon, S. Liawruangrath, A. Townshend, Talanta 69 (2006) 976.
[8] Y. Zhuang, X. Cai, J. Yu, H. Ju, J. Photochem. Photobiol. A 162 (2004) 457.
[9] J. Liu, X. Yang, E. Wang, Electrophoresis 24 (2003) 3131.
[10] S.H. Lee, M. Li, J.K. Suh, Anal. Sci. 19 (2003) 903.
[11] N.W. Barnett, S.W. Lewis, S.D. Purcell, P. Jones, Anal. Chim. Acta 458 (2002) 291.
[12] R.D. Gerardi, N.W. Barnett, S.W. Lewis, Anal. Chim. Acta 378 (1999) 1.
[13] W. Pan, Y. Liu, Y. Huang, S. Yao, J. Chromatogr. B 831 (2006) 17.
[14] J. Li, Q. Yan, Y. Gao, H. Ju, Anal. Chem. 78 (2006) 2694.
[15] G. Li, X. Zheng, Z. Zhang, Microchim. Acta 154 (2006) 153.
[16] N.C. Han, Y.-K. Lyu, W.-Y. Lee, Electroanalysis 18 (2006) 275.
[17] Z. Chang, J. Zhou, K. Zhao, N. Zhu, P. He, Y. Fang, Electrochim. Acta 52 (2006) 575.
[18] S. Liu, Y. Liu, J. Li, M. Guo, W. Pan, S. Yao, Talanta 69 (2006) 154.
[19] L. Zhang, Z. Guo, Z. Xu, S. Dong, J. Electroanal. Chem. 592 (2006) 63.
[20] L. Zhang, S. Dong, Anal. Chem. 78 (2006) 5119.
[21] J.L. Adcock, N.W. Barnett, R.D. Gerardi, C.E. Lenehan, S.W. Lewis, Talanta 64 (2004) 534.
[22] N.A. Al-Arfaj, Talanta 62 (2004) 255.
[23] J.W. Costin, N.W. Barnett, S.W. Lewis, Talanta 64 (2004) 894.
[24] T. Ikehara, N. Habu, I. Nishino, H. Kamimori, Anal. Chim. Acta 536 (2005) 129.
[25] C. Thongpoon, B. Liawruangrath, S. Liawruangrath, R.A. Wheatley, A. Townshend, Anal. Chim. Acta 553 (2005) 123.
[26] J.M. Walshe, Mov. Disord. 18 (2003) 853.
[27] C.R. Chong, D.S. Auld, Biochemistry 39 (2000) 7580.
[28] S.R. Gooneratne, D.A. Christensen, Vet. J. 153 (1997) 171.
[29] B.G.-T. Corominas, J. Pferzschner, M.C. Icardo, L.L. Zamora, J.M. Calatayud, J. Pharm. Biomed. Anal. 39 (2005) 281.
[30] M.I. Walash, A.M. El-Brashy, M.S. Metwally, A.A. Abdelal, Bull. Korean Chem. Soc. 25 (2004) 517.
[31] F.O. Suliman, H.A.J. Al-Lawati, S.M.Z. Al-Kindy, Talanta 61 (2003) 221.
[32] K. Amarnath, V. Amarnath, K. Amarnath, H.L. Valentine, W.M. Valentine, Talanta 60 (2003) 1229.
[33] A.A. Al-Majed, Anal. Chim. Acta 408 (2000) 169.
[34] P. Vinas, I. Lopez Garcia, J.A. Martinez Gil, J. Pharm. Biomed. Anal. 11 (1993) 15.
[35] Z.D. Zhang, W.R.G. Baeyens, X.R. Zhang, G. Van Der Weken, Analyst 121 (1996) 1569.
[36] A. Lee, W.D. Ngan Kee, T. Gin, Anesth. Analg. 94 (2002) 920.
[37] T. Erkinaro, K. Makikallio, T. Kavasmaa, S. Alahuhta, J. Rasanen, Br. J. Anaesth. 93 (2004) 825.
[38] B. Gomez-Taylor, M. Palomeque, J.V. Garcia Mateo, J. Martinez Calatayud, J. Pharm. Biomed. Anal. 41 (2006) 347.
[39] M. Gil-Agusti, L. Monferrer-Pons, M.C. Garcia-Alvarez-Coque, J. Esteve-Romero, Talanta 54 (2001) 621.
[40] M.D. Paciolla, S.A. Jansen, S.A. Martellucci, A.A. Osei, J. Pharm. Biomed. Anal. 26 (2001) 143.
[41] J. March, Advanced Organic Chemistry: Reactions, Mechanisms, and Structure, fourth ed., Wiley, New York, 1992.
[42] J. McMurry, Organic Chemistry, Pacific Grova, New York, 2000.
[43] B.A.G. Barnett, P.S. Francis, Analyst 131 (2006) 616.
[44] S. Nishida, Y. Harima, K. Yamashita, Inorg. Chem. 28 (1989) 4073.
[45] J.B. Noffsinger, N.D. Danielson, Anal. Chem. 59 (1987) 865.

Available online at www.sciencedirect.com
ScienceDirect
Talanta 74 (2008) 1692–1698
Talanta
www.elsevier.com/locate/talanta

Letter to the Editor

Direct electron transfer and electrocatalysis of hemoglobin in layer-by-layer films assembled with Al-MSU-S particles

Zhiyu Sun [a], Youqin Li [a], Tianshu Zhou [b], Ye Liu [a], Guoyue Shi [a,*], Litong Jin [a,*]

[a] *Department of Chemistry, East China Normal University, Zhongshan Road (N), Shanghai 200062, PR China*
[b] *Department of Environmental Science, 3663 Zhongshan Road (N), Shanghai 200062, PR China*

Received 25 June 2007
Available online 13 October 2007

Abstract

In this paper, layer-by-layer (LBL) $\{MSU/Hb\}_n$/PDDA films assembled by alternate adsorption of positively charged hemoglobin (Hb) and negatively charged mesoporous molecular sieves of Al-MSU-S onto a glassy carbon electrode (GCE) were reported. Al-MSU-S was synthesized by the precursor of zeolite Y and ionic liquids 1-hexadecane-3-methylimidazolium bromide (CMIMB) as a template in basic medium. It exhibited larger pore diameter, pore volume and surface area. Direct electrochemical and electrocatalytic properties of Hb in these layer-by-layer films were investigated. A pair of well-defined nearly reversible cyclic voltammetric peaks was observed and the formal potential of the heme Fe^{III}/Fe^{II} redox couple was found to be −0.295 V (vs. SCE). The influences of layer's number and the pH of the external solution to the electron transfer behavior of Hb in $\{MSU/Hb\}_n$/PDDA films were also estimated by cyclic voltammetry and a set of optimized conditions for film fabrication was inferred. The hemoglobin in$\{MSU/Hb\}_n$/PDDA films displayed a good electrocatalytic activity to the reduction of hydrogen peroxide, which had linear current responses from 1.0×10^{-6} to 1.86×10^{-4} mol/L with the detection limit of 5.0×10^{-7} mol/L (S/N = 3). The apparent Michaeli–Menten constant (K_m^{app}) was 0.368 mmol/L. Thus, this methodology shows potential application of the preparation of third-generation biosensors.
© 2007 Elsevier B.V. All rights reserved.

Keywords: LBL assembled; $\{MSU/Hb\}_n$/PDDA; Hemoglobin; Hydrogen peroxide

1. Introduction

Hemoglobin (Hb) is a heme protein which contains two α and β polypeptide chains, each of which has one electroactive heme center. Hb functions physiologically in the storage and transport of molecular oxygen in mammalian blood. Although Hb does not function as an electron carrier in biological systems, it is believed to be an ideal model molecule for studying electron transfer of heme enzymes because of its commercial availability, moderate cost and a known and documented structure [1]. The investigation of direct electron transfer between proteins and underlying electrodes can establish a platform for fabricating new kinds of biosensors, bioreactors and biomedical devices without using mediators [2–4]. Nevertheless, the facilitation of electron transfer between the macromolecule Hb and the electrode is challenging. The inaccessibility of the heme buried in the large three-dimensional structure, and the subsequent electrode passivation due to protein adsorption make it generally difficult to establish direct electron transfer between hemoglobin and conventional electrodes [5]. Thus, the immobilization of redox protein on solid surfaces plays a key role and has aroused increasing interest among researchers [6,7].

The layer-by-layer (LBL) films assembled by alternative adsorption of positively and oppositely charged species from their solutions through electrostatic interactions have been reported as a new method for facilitating electron transfer [8–11], it has been wildly used in the investigation of direct electron transfer between proteins and underlying electrodes [12,13]. Recently, molecular sieves have been used as promising protein immobilization matrices because of their unique structural and catalytic properties. It can construct an electrochemical or electron transfer environment and resist the biodegradation of Hb [14,15]. Dai et al. investigated the direct electron transfer of cytochrome *c* immobilized on a NaY zeolite matrix and its application in biosensing [16]. Xie et al. assembled LBL films

* Corresponding authors. Tel.: +86 21 62237105; fax: +86 21 62232627.
E-mail address: gyshi@chem.ecnu.edu.cn (G. Shi).

0039-9140/$ – see front matter © 2007 Elsevier B.V. All rights reserved.
doi:10.1016/j.talanta.2007.10.009

by hemoglobin or myoglobin and zeolite particles [17]. Yu et al. studied the enzyme-immobilization ability and high sensitivity of the controlled nanozeolite-assembled electrode [18].

In this paper, mesoporous molecular sieves of Al-MSU-S (designated MSU in the following experiments) were used to immobilize the redox protein. Here, the Al-MSU-S was prepared from the precursor of zeolite Y using ionic liquids 1-hexadecane-3-methylimidazolium bromide (CMIMB) as a template in basic medium. As is known to us, ionic liquids are a new class of solvents and catalysts which have attracted considerable attention for their wide liquidus, negligible vapor pressure and thermal stability [19,20]. Herein, they are firstly used for the preparation of MSU and the prepared MSU exhibits larger pore diameter, pore volume and surface area than the MSU using cetyl trimethyl ammonium bromide (CTAB) as template. Especially, the pore volume is almost two times of that of the latter MSU [21].

In this work, we successfully constructed $\{MSU/Hb\}_n$/PDDA films modified GCE by alternately adsorbed positively charged hemoglobin and negatively charged MSU particles onto glassy carbon electrode. Transmission electron microscopy (TEM) was used to investigate the structure feature of the MSU particles and the $\{MSU/Hb\}_n$/PDDA films on electrodes. UV–vis spectrum showed that the Hb in the films still remained the biological activity as the native Hb. Electrochemical impedance spectroscopy (EIS) and cyclic voltammetry (CV) were utilized to monitor the layer-by-layer assembling procedure and the direct and reversible electrochemistry for the protein heme of Fe^{III}/Fe^{II} redox couple was characterized by cyclic voltammetry. The electrocatalytic reduction of hydrogen peroxide was also investigated and the apparent Michaeli–Menten constant (K_m^{app}) was evaluated in this work.

2. Experiment

2.1. Reagents

All chemical reagents were of analytical grade and were used without further purification. Bovine hemoglobin (Hb), poly(diallyldimethylammonium) (PDDA) and hydrogen peroxide (H_2O_2, 30%) were all obtained from Sigma (St. Louis, MO, USA) and used as received. 1.0×10^{-4} mol/L Hb solution was prepared in 0.02 mol/L phosphate buffer of pH 5.0 and stored at the temperature of 4 °C. Al-MSU-S was supplied by Shanghai Key Laboratory of Green Chemistry and Chemical Processes, East China Normal University. The H_2O_2 solutions with different concentrations were freshly prepared for each experiment. Phosphate buffer solutions with various pH values were prepared by mixed stock standard solutions of Na_2HPO_4 and KH_2PO_4, the pH was adjusted with 0.1 M H_3PO_4 or NaOH. All solutions were made from twice-distilled water.

2.2. Synthesis of the Al-MSU-S

The MSU used in this work was synthesized following the method which was reported [21]. In brief, 0.0088 mol of NaOH and 0.01 mol of $NaAlO_2$ were dissolved in 0.85 mol of H_2O. A solution containing 0.090 mol of $Na_2SiO_3 \cdot 9H_2O$ and 0.85 mol of H_2O was added slowly under vigorous stirring at room temperature and then heated at 100 °C for 10 h to obtain the precursor solution of zeolite Y. The precursor solution was added dropwise to an aqueous solution of ionic liquid containing 14 mol of H_2O and 0.02 mol of CMIMB at room temperature. The mixture was further stirred for 1 h and the pH of the gel was adjusted to 9.0–11.5 by adding dropwise a dilute solution of H_2SO_4 under stirring. Further stirred for more than 1 h and crystallized in Teflon-lined steel autoclave at 100 °C for 20 h, the as-synthesized sample was calcined in air at 540 °C for 7 h. The MSU prepared by CMIMB was synthesized. It was used for the fabrication of $\{MSU/Hb\}_n$/PDDA films in this paper.

For contrast, MSU sample prepared by cetyl trimethyl ammonium bromide (CTAB) was also synthesized in this work.

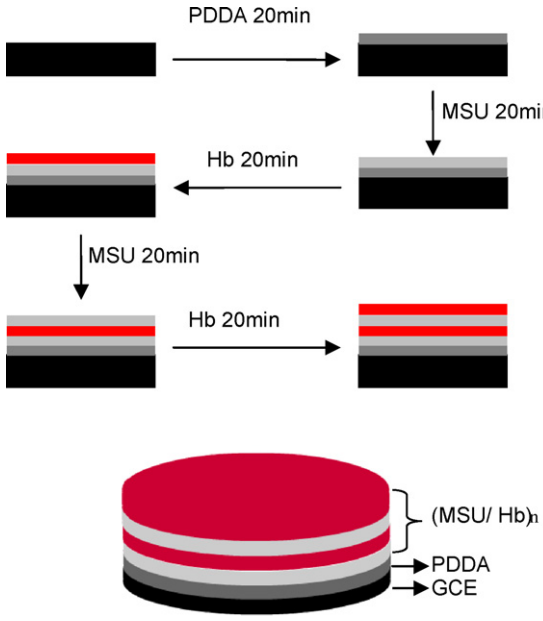

Scheme 1. Schematics of the self-assembly of $\{MSU/Hb\}_n$/PDDA films.

2.3. Electrode modification

The glassy carbon electrode was polished with 0.05 μm alumina slurry followed by thoroughly flushing with twice-distilled water, and then ultrasonically in 1:1 nitric acid, 1 M NaOH, acetone and twice-distilled water. At last, the electrode was dried in air.

$\{MSU/Hb\}_n$/PDDA films were deposited onto the clean, dry GCE following a layer-by-layer deposition strategy as Scheme 1. There were three main steps. Firstly, the clean GC electrode was immersed into the solution of PDDA (0.5%) for 20 min to adsorb a positively charged precursor layer of PDDA, and then the PDDA modified electrode was washed and dried under ambient conditions. Secondly, the electrode was immersed into the MSU solution (5×10^{-4} mol/L) for 20 min, the negative charged MSU was adsorbed on the positive charged PDDA on the surface of glassy carbon electrode. Thirdly, after the electrode was washed and dried, it was immersed into the hemoglobin solution (1×10^{-4} mol/L) of pH 5.0 for 20 min, in which Hb was positively charged [22]. The second and third steps can be repeated

several times to obtain desired $\{MSU/Hb\}_n$/PDDA electrode. When not in use, the electrode was kept at 4 °C in refrigerator.

2.4. Instrumentation and procedure

Electrochemical experiments were carried out on a CHI 660A electrochemical workstation (CH Instruments, USA) with a bared GCE (diameter 3 mm, BAS Co., Japan) or a $\{MSU/Hb\}_n$/PDDA modified GCE as the working electrode, a saturated calomel electrode (SCE) (Jiangsu Electroanalytical Instruments Factory, China) as the reference electrode and a platinum electrode as the auxiliary electrode. All electrochemical experiments were performed in 0.2 M potassium phosphate buffer solution (PBS) of pH 6.9. All solutions were deoxygenated by bubbling with highly pure nitrogen for at least 20 min and maintained under nitrogen atmosphere during the measurements.

Transmission electron microscopy (TEM) experiments were performed on a JEM-3010 electron microscope with an acceleration voltage of 300 kV. The UV–vis spectra of the Hb samples were measured at the wavelength ranging from 300 to 600 nm at room temperature using CARY 50 Conc UV–vis spectrophotometer.

3. Results and discussion

3.1. Morphologies of MSU and $\{MSU/Hb\}_5$ film

Fig. 1A is the transmission electron microscopy (TEM) of MSU prepared by the ionic liquid of CMIMB. From Fig. 1A, it can be seen that the sample has a nice one-dimensional ordered structure. The parallel curving lines that correspond to the mesoporous confirm their long-range-ordered continuity. XRD experiment (figure not shown) also showed that the as-synthesized sample exhibited well-defined (1 0 0), (1 1 0), (2 0 0) and (2 1 0) reflections associated with the *p6mm* hexagonal symmetry, suggesting the formation of the long-range-ordered MSU mesophase. So the data of TEM are consistent with that of XRD patterns. In addition, Table 1 shows that MSU-CMIMB exhibits larger pore diameter, pore volume and surface area than that of MSU-CTAB. It could be attributed to the larger and flatter polar head group of ionic liquid (CMIMB) compared with that of CTAB [23].

Meanwhile, the surface morphology of $\{Hb/MSU\}_5$ film was characterized by SEM. Fig. 1B shows a lot of globular particles with a mean diameter of ~0.5 μm scattering at the surface of the ITO electrode. In high resolution (inset in the figure), many white materials can be seen on the globular particles which are the hemoglobin molecules immobilized on the MSU particles, These observations suggest that Hb has been adsorbed around the MSU particles

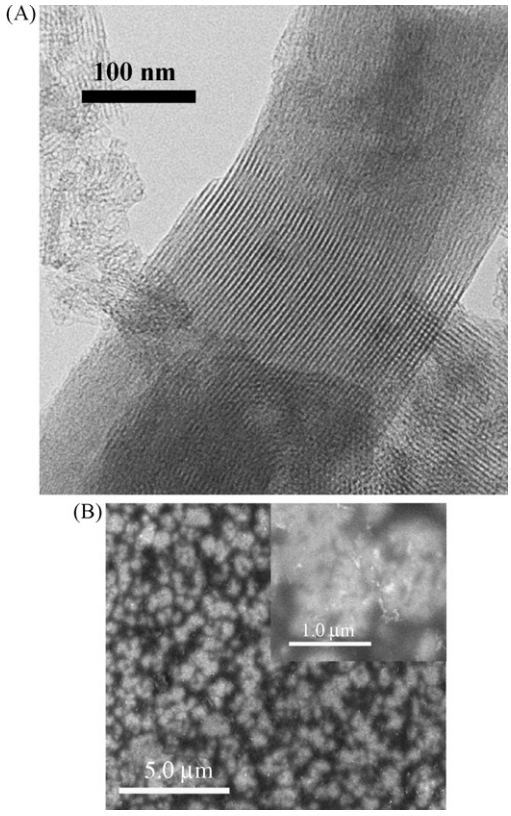

Fig. 1. (A) TEM of the mesoporous molecular sieves Al-MSU-S using ionic liquids as template, (B) SEM image of $\{Hb/MSU\}_5$ film on ITO electrode.

Table 1
Structural properties of MSU prepared by CMIMB and CTAB after calcinations at 540 °C

Sample	d_{100} (A)	a_0 (A)	S_{BET} (m^2/g)	φ_{BJH} (A)	Pore volume (cm^3/g)
MSU-CMIMB	38.7	44.6	996	29.5	1.15
MSU-CTAB	38.2	44.1	761	24.0	0.60
MSU-CTAB[a]	–	48.6	713	32.1	0.56

[a] CTAB-MY: data of reference [19].

3.2. UV–vis spectroscopic characterization

The position of the Soret absorption band of iron heme provides information about conformation of heme proteins [23,24]. The Soret band shifts or disappears when Hb is denatured [25]. In this work, UV–vis spectroscopy was used to investigate the possible denaturation of the hemoglobin in the $\{MSU/Hb\}_n$/PDDA film. The narrow Soret bands are observed in the UV–vis spectrum of pure Hb film and $\{MSU/Hb\}_n$/PDDA film (figure not showed). Both peaks are at 405 nm, revealing no significant denaturation of the Hb molecules occurred in the presence of MSU. So it can be concluded that MSU has good biocompatibility and is an excellent matrix to adsorb Hb.

3.3. Electrochemical impedance spectroscopy of $\{MSU/Hb\}_n$/PDDA film

Electrochemical impedance spectroscopy can provide useful information on the impedance changes of the electrode surface during the fabrication process. For the sake of simplicity, the equivalent electrical circuit (inset in Fig. 2A) is employed as

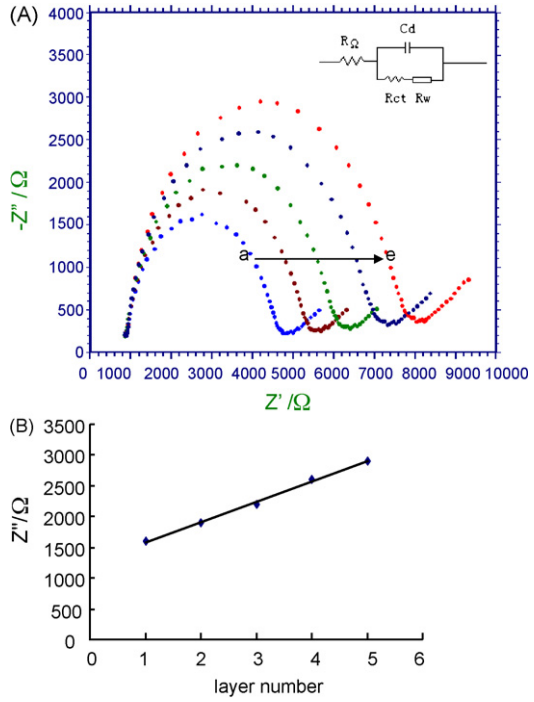

Fig. 2. (A) Electrochemical impedance spectroscopy (EIS) of different electrodes in 0.1 mol/L KCl solution containing 5.0 mmol/L $Fe(CN)_6^{3-}/Fe(CN)_6^{4-}$. (a) $\{MSU/Hb\}_1$/PDDA GCE, (b) $\{MSU/Hb\}_2$/PDDA GCE, (c) $\{MSU/Hb\}_3$/PDDA GCE,(d) $\{MSU/Hb\}_4$/PDDA GCE, (e) $\{MSU/Hb\}_5$/PDDA GCE. (B) The correlation between the layer thickness and the layer number.

a mode describing the electrical network of the electrochemical interface, in which R_Ω represents the electrolyte resistance between the working electrode and the reference electrode, C_d is the double-layer capacitance, R_{ct}, the charge transfer resistance, is related to the electron transfer kinetics of the redox probe ($Fe(CN)_6^{3-}/Fe(CN)_6^{4-}$) at the electrode interface and can be estimated from the diameter of the semicircular part (higher frequency) of the EIS curve, R_w, the mass transport resistance, can be estimated from the linear part (lower frequency) of the EIS curve represents [26,27].

Fig. 2A shows the results of impedance spectroscopy on modified electrodes with various MSU/Hb bilayer numbers in 0.1 mol/L KCl solution containing 5.0 mmol/L $Fe(CN)_6^{3-}/Fe(CN)_6^{4-}$, which are measured at the formal potential of −0.295 V. In Fig. 2A, significant differences in the impedance spectra are observed upon the stepwise formation of the multilayers. The impedance spectra presents a semicircle line that corresponds to the electron transfer limited process. Fig. 2B shows the correlation between the layer thickness and the layer number, after the adsorption of MSU/Hb multilayers, the diameters of the semicircle parts increase significantly as the number of layers increase, Z'' is 1600, 1900, 2200, 2600, 2900 Ω, respectively for different films of $\{MSU/Hb\}_n$/PDDA. This increase in diameter indicates that the charge-transfer rate of $[Fe(CN)_6]^{4-/3-}$ is reduced gradually which is attributed to the hindrance effect to the redox couples, caused by the deposition of MSU/Hb insulating multilayers on the electrode surface [28]. It is a confirmation of the successful immobilization of MSU/Hb

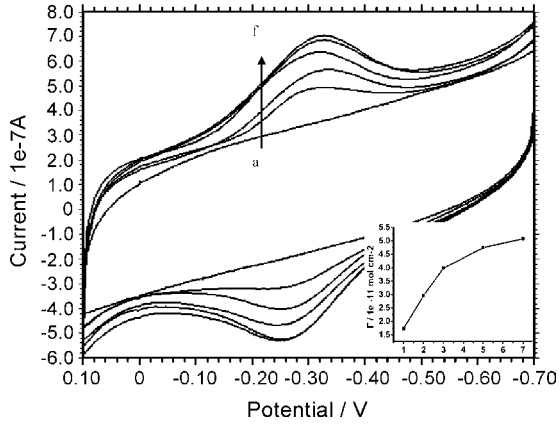

Fig. 3. Cyclic voltammograms of (a) bare GCE and GCE coated with (b) $\{MSU/Hb\}_1$/PDDA, (c) $\{MSU/Hb\}_2$/PDDA, (d) $\{MSU/Hb\}_3$/PDDA, (e) $\{MSU/Hb\}_5$/PDDA and (f) $\{MSU/Hb\}_7$/PDDA in PBS solution (pH 6.9) Inset: Influence of the number of bilayer (n) on average surface concentration of electroactive Hb (Γ, mol cm^{-2}).

bilayer on the surface of the electrode and it can also be seen that the amount of each bilayer adsorbed on the electrode is almost same.

3.4. Influences of layer's number

In order to examine the influence of the layers to the electron transfer of Hb, the optimal number of $\{MSU/Hb\}$ bilayer (n) on the electrochemistry was also investigated by the cyclic voltammograms (CV) in Fig. 3. A pair of well-defined nearly reversible redox peaks appear in each of the cyclic voltammograms at the electrodes with different films of $\{MSU/Hb\}_n$/PDDA on the surface of GCE. The peak currents of the cyclic voltammograms increase with the increment of the number of $\{MSU/Hb\}$ bilayers. Those voltammograms show that a good electronic communication is established between the Hb molecules and the surface of glassy carbon electrode in the presence of MSU. The redox peak is attributed to the protein heme Fe^{III}/Fe^{II} redox couple, revealing that the electron transfer process between Hb and the glassy carbon electrode is enhanced by the presence of MSU. At the scan rate of 100 mV/s of the $\{MSU/Hb\}_5$/PDDA GCE, the anodic peak potential ($E_{p,a}$) and the cathodic peak potential ($E_{p,c}$) of Hb are −0.258 and −0.332 V, respectively with a peak-to-peak separation (ΔE_p) of 74 mV. A formal potential (E°) of −0.295 V is calculated with $E^\circ = 1/2\ (E_{p,a} + E_{p,c})$. The small peak-to-peak separation indicates a fast electron transfer rate for $\{MSU/Hb\}_n$/PDDA GCE. In Fig. 3a, the voltammogram for the bare electrode contains only non-Faradaic current in the potential window of interest which indicates that the direct electron transfer is achieved through the entrapment of Hb in the MSU membrane.

Hb molecules in different $\{MSU/Hb\}$ bilayers assume different distance to the surface of GCE, and have different electron transfer rate constant. Therefore, even though each bilayer contains a constant number of Hb molecules, the bilayer that is closer to the electrode surface contains more electrochemically detectable Hb molecules. This behavior could be verified by cyclic coltammetry. The average surface concentration of elec-

troactive Hb (Γ, mol cm^{-2}) can be estimated from the charge integration of the reduction peak of the cyclic voltammogram of $\{MSU/Hb\}_n$/PDDA films, using the formula of $\Gamma = Q/nFA$, where Q is the charge (C), n is the number of transfer electron, F is faraday constant and A is geometric area of GC electrode (cm^{-2}). Inset in Fig. 3 plots the values of Γ (mol cm^{-2}) as a function of the number of the $\{MSU/Hb\}$ bilayers. The non-linear dependence of the Hb amount on the number of n is consistent with the hypothesis that the Hb molecules were immobilized layer-by-layer onto the GCE. As is shown in inset, a good communication between Hb molecules and the electrode surface is maintained even when n is as high as 7. In this work, five layers of $\{MSU/Hb\}$, designated as $\{MSU/Hb\}_5$ was chosen in most of the electrochemical and electrocatalytic experiments.

3.5. Influence of scan rate

Influence of scan rate at $\{MSU/Hb\}_5$/PDDA electrode is investigated in the phosphate buffer solution of pH 6.9 by cyclic voltammograms at different scan rates from 100 to 500 mV/s. Each voltammogram is symmetric and has a pair of well-defined redox peaks. The cathodic and anodic peak currents are linearly proportional to the scan rates in the range of 100–500 mV/s, which shows a characteristic of a surface-confined electrochemical process [29–31].

3.6. Influence of solution pH

The pH of the buffer solution affects the electrochemical behavior of Hb in $\{MSU/Hb\}_5$/PDDA film. As is shown in Fig. 4, the CVs with stable and well-defined peaks are observed from pH 3.6 to 8.5. However the voltammograms shift toward the negative direction with the increase of pH. Quantitative analysis shows that the formal potentials (E°) depend linearly on the buffer pH. In inset, the linear relationship of E° versus solution pH is obtained with the slope of −49.4 mV/pH (the correlative coefficient is 0.997) [32,33]. The value is close to the expected value of −58.0 mV/pH for the reaction of one proton transfer

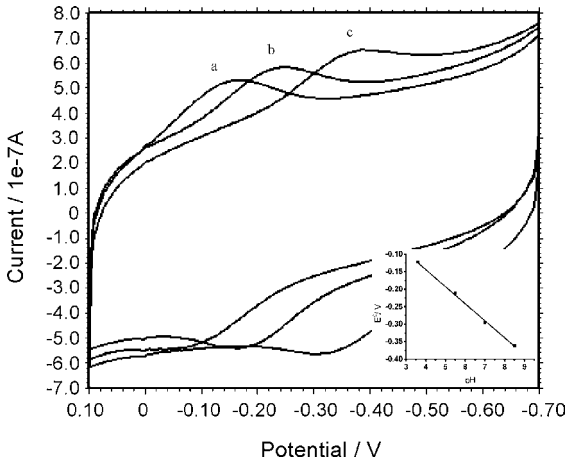

Fig. 4. CVs of $\{MSU/Hb\}_5$/PDDA/GCE electrode in 0.2 mol/L PBS with pH values (a) 3.6, (b) 5.5, (c) 8.5. Inset: plot of E° vs. solution pH.

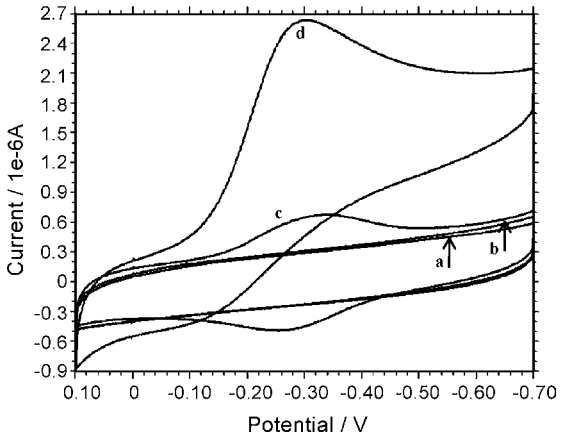

Fig. 5. Cyclic voltamograms at 100 mV/s for (a) bare GCE, (c) $\{MSU/Hb\}_5$/PDDA GCE in blank solution and (b) bare GCE, (d) $\{MSU/Hb\}_5$/PDDA GCE in 100 μM H_2O_2 solution.

coupled one electron transfer. It is written as [34–36]

$$HbFe(III) + H^+ + e^- \rightleftharpoons HbFe(III)$$

In addition, the voltammograms collected in a PBS of pH 3.6 before and after immersed in a PBS of pH 8.5 using the $\{MSU/Hb\}_5$/PDDA GCE were exactly the same.

3.7. Electrocatalytical activity of the $\{MSU/Hb\}_5$/PDDA electrode to H_2O_2

Electrocatalytic reductions of hydrogen peroxide were examined by CVs using the $\{MSU/Hb\}_5$/PDDA GCE. Fig. 5 shows the voltammograms of bare electrode and $\{MSU/Hb\}_5$/PDDA GCE in the absence or in the presence of H_2O_2. Only non-Faradaic signals are observed with bare electrode in blank solution and 1.0×10^{-4} M H_2O_2 solution (Fig. 5a and b). In contrast, when the $\{MSU/Hb\}_5$/PDDA GCE is used, there is a pair of well-defined peaks at about −0.3 V in the blank solution which can be attributed to the heme Fe^{III}/Fe^{II} redox couple. The addition of 1.0×10^{-4} mol/L hydrogen peroxide into a pH 6.9 buffer causes a large increase in CV reduction peak current, accompanied by the decrease of the oxidation peak, suggesting that an electocatalytic reduction of H_2O_2 is occurred with the $\{MSU/Hb\}_5$/PDDA electrode (Fig. 5c and d). No peaks were observed at MSU/GCE and Hb/GCE in the presence of H_2O_2 (figure not shown), indicating that the reduction of H_2O_2 was catalyzed by the Hb immobilized on the $\{MSU/Hb\}_5$/PDDA film.

Fig. 6 shows a typical amperometric responses of $\{MSU/Hb\}_5$/PDDA film with the successive additions of 10.0 μmol/L H_2O_2 at −300 mV. No response is observed at the MSU/PDDA electrode, but the reduction currents rise step by step at the $\{MSU/Hb\}_5$/PDDA GCE. The responses are linearly proportional to the H_2O_2 concentration from 1.0×10^{-6} to 1.86×10^{-4} mol/L with the detection limit of 1.0×10^{-7} mol/L (S/N = 3). At higher H_2O_2 concentration, the current response tends to level off, indicating a typical Michaeli–Menten process. The apparent Michaeli–Menten constant (K_m^{app}), which is an indication of enzyme–substrate kinetics, can be calculated

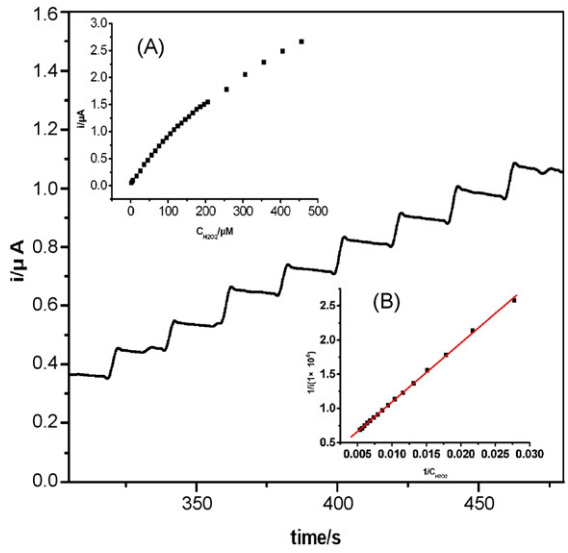

Fig. 6. Amperograms of H_2O_2 sensor with successive additions of 10 μmol/L at an operating potential of −300 mV. Inset A: plot of catalytic current vs. H_2O_2 concentration. Inset B: plot of $1/I_{cat}$ vs. $1/CH_2O_2$.

according to the Lineweaver–Burk equation:

$$\frac{1}{I_{cat}} = \frac{1}{I_{max}} + \frac{K_m^{app}}{I_{max}} C_{H_2O_2}$$

Here, I_{cat} is the electrocatalytic current, I_{max} is the maximum current under saturated substrate conditions and $C_{H_2O_2}$ is the bulk concentration of H_2O_2 [37]. In this work, K_m^{app} is about 0.368 mmol/L, which is smaller than that of Hb adsorbed onto electrodeposited mesoporous tungsten oxide (1.84 mmol/L) [38] and Hb entrapped in composite matrix based on chitosan and $CaCO_3$ nanoparticles (0.75 mmol/L)[39], indicating the higher catalytic activity of the $\{MSU/Hb\}_5$/PDDA film toward H_2O_2 (the smaller K_m^{app} shows the higher catalytic ability).

3.8. Stability and reproducibility of the $\{MSU/Hb\}_5$/PDDA electrode

The direct electrochemistry of $\{MSU/Hb\}_5$/PDDA film could retain constant current values upon continuous cyclic sweep over the potential range from −0.7 to 0.1 V at 100 mV/s. The immobilized $\{MSU/Hb\}_5$/PDDA film lost only 6.7% of its initial activity after 200 segments. The long-term stability of the biosensors was investigated over a 15-day period. When the modified electrode was stored in 0.2 mol/L pH 6.9 PBS and measured once every 2 days, the current response to 1.0×10^{-5} mol/L H_2O_2 decreased only 8.2%. In addition to good stability, the modified electrode also showed a good reproducibility. The fabrication of eight electrodes, made independently, showed an acceptable reproducibility with a variation coefficient of 4.7% for the determination of 1.0×10^{-5} mol/L H_2O_2. These results demonstrate that the MSU and the LBL method are very efficient for retaining the electrocatalytic activity of the hemoglobin and preventing it from leaking out of the electrode.

4. Conclusion

In this paper, we successfully constructed the $\{MSU/Hb\}_n$/PDDA LBL films modified electrode using mesoporous molecular sieves Al-MSU-S which exhibited larger pore diameter, pore volume, surface area and narrow pore diameter distribution. Electrochemical impedance spectroscopy (EIS) and cyclic voltammetry (CV) were utilized to monitor the layer-by-layer assembling procedure. UV-vis showed that the Hb in $\{Hb/MSU\}_n$/PDDA films still had a conformation nearly the same as the native Hb. The immobilized Hb displayed a direct electrochemistry and a good electrocatalytic behavior. The apparent Michaeli–Menten constant (K_m^{app}) was also evaluated and compared with other methods. This methodology shows potential application of the preparation of third-generation biosensors.

Acknowledgements

This work is supported by the National Natural Science Foundation of China (No. 20675032), the Project Sponsored by the Scientific Research Foundation of State Education Ministry for the Returned Overseas Chinese Scholars, the Natural Science Foundation of Shanghai (No. 05ZR14043) and Shanghai Rising-Star program (06QH14004).

References

[1] P.L. He, N.F. Hu, G. Zhou, Biomacromolecules 3 (2002) 139–146.
[2] F.A. Armstrong, G.S. Wilson, Electrochim. Acta 45 (2000) 2623–2645.
[3] I. Hamachi, A. Fujita, T. Kunitake, J. Am. Chem. Soc. 119 (1997) 9096–9102.
[4] F.A. Armstrong, H.A.O. Hill, N.J. Walton, Acc. Chem. Res. 21 (1988) 407–413.
[5] E. Stellwagen, Nature 275 (1978) 73–74.
[6] S. Conier, Biosens. Bioelectron. 14 (1999) 443–456.
[7] H.A. Heering, F.G.M. Wiertz, C. Dekker, S. de Vries, J. Am. Chem. Soc. 126 (2004) 11103.
[8] N.A. Kotov, I. Dékány, J.H. Fendler, J. Phys. Chem. 99 (1995) 13065–13069.
[9] N.A. Kotov, I. Dékány, J.H. Fendler, Adv. Mater. 8 (1996) 637–641.
[10] N.A. Kotov, T. Haraszti, L. Túri, G. Zavala, R.E. Geer, I. Dékány, J.H. Fendler, J. Am. Chem. Soc. 119 (1997) 6821–6832.
[11] I. Dékány, T. Haraszti, Colloids Surf. A 123–124 (1997) 391–401.
[12] G. Decher, Science 277 (1997) 1232–1237.
[13] Y. Lvov, B. Munge, O. iraldo, I. Ichinose, S.L. Suib, J.F. Rusling, Langmuir 16 (2000) 8850–8857.
[14] P. Rolison, Chem. Rev. 90 (1990) 867–878.
[15] Z.H. Dai, X.X. Xu, H.X. Ju, Anal. Biochem. 332 (2004) 23–31.
[16] Z.H. Dai, S.Q. Liu, H.X. Ju, Electrochim. Acta 49 (2004) 2139–2144.
[17] Y. Xie, H.Y. Liu, N.F. Hu, Bioelectrochemistry 71 (2006) 6–14.
[18] T. Yu, Y.H. Zhang, C.P. You, J.H. Zhuang, B. Wang, B.H. Liu, Y.J. Kang, Y. Tang, Chem. Eur. J. 12 (2006) 1137–1143.
[19] P. Wasserscheid, W. Keim, Angew. Chem. Int. Ed. 39 (2000) 3772–3789.
[20] J.R. Silkey, J.T. Yoke, J. Electrochem. Soc. 127 (1980) 1091–1095.
[21] X.Y. Yu, C.H. LIu, J.G. Yang, H.H. Wu, P. Wu, M.Y. He, Chin. J. Chem. 24 (2006) 1282–1284.
[22] J.B. Matthew, G.I.H. Hanania, F.R.N. Gurd, Biochemistry 18 (1979) 1919–1928.
[23] Y. Liu, W.Z. Zhang, T.J. Pinnavaia, J. Am. Chem. Soc. 122 (2000) 8791–8792.
[24] H. Theorell, A. Ehrenberg, Acta. Chem. Scand. 5 (1951) 823.

[25] A.E.F. Nassar, W.S. Willis, J.F. Rusling, Anal. Chem. 67 (1995) 2386–2392.
[26] A.H. Zhou, Q.J. Xie, Y.H. Wu, Y. Cai, L.H. Nie, S.Z. Yao, J. Colloids Interf. Sci. 229 (2000) 12–20.
[27] X.Y. He, L. Zhu, Electrochem. Commun. 8 (2006) 615–620.
[28] H. Zhang, H.Y. Lu, N.F. Hu, J. Phys. Chem. B 110 (2006) 2171–2179.
[29] H.C. Yoon, M.Y. Hong, H.S. Kim, Anal. Chem. 72 (2000) 4420–4427.
[30] A.J. Bard, L.R. Faulkner, Electrochemical Methods. Fundamentals and Applications, 2nd ed., Wiley, New York, 2001.
[31] Z.H. Dai, S.Q. Liu, H.X. Ju, H.Y. Chen, Biosens. Bioelectron. 19 (2004) 861–867.
[32] A.E. Nassar, Z. Zhang, N. Hu, J.F. Rusling, T.K. Kumosinski, J. Phys. Chem. 101 (1997) 2224–2231.
[33] J.J. Feng, G. Zhao, J.J. Xu, H.Y. Chen, Anal. Biochem. 342 (2005) 280–286.
[34] L. Meites, Polarographic Techniques, 2nd ed., Wiley, New York, 1965, pp. 282–284.
[35] H. Huang, P.L. He, N.F. Hu, Y.H. Zeng, Bioelectrochemistry 61 (2003) 29–38.
[36] H.H. Liu, Z.Q. Tian, Z.X. Lu, Z.L. Zhang, M. Zhang, D.W. Pang, Biosens. Bioelectron. 20 (2004) 294–304.
[37] R.A. Kamin, G.S. Wilson, Anal. Chem. 52 (1980) 1198–1205.
[38] J.J. Feng, J.J. Xu, H.Y. Chen, Electrochem. Commun. 8 (2006) 77–82.
[39] D. Shan, S.X. Wang, H.G. Xue, S. Cosnier, Electrochem. Commun. 9 (2007) 529–534.

Available online at www.sciencedirect.com
ScienceDirect
Talanta 74 (2008) 1224–1230
Talanta
www.elsevier.com/locate/talanta

Preconcentration and decomposition of perfluorinated carboxylic acids on an activated charcoal cartridge with sodium biphenyl reagent and its determination at μg L^{-1} level on the basis of flow injection-fluorimetric detection of fluoride ion

Toshio Takayanagi [a,*], Hiroki Yamashita [a], Shoji Motomizu [a], Jacek Musijowski [b], Marek Trojanowicz [b]

[a] *Graduate School of Natural Science and Technology, Okayama University, 3-1-1 Tsushimanaka, Okayama 700-8530, Japan*
[b] *Laboratory of Flow Analysis and Chromatography, Department of Chemistry, Warsaw University, Pasteura 1, 02-093 Warsaw, Poland*

Received 28 May 2007; received in revised form 23 August 2007; accepted 24 August 2007
Available online 30 August 2007

Abstract

Perfluorinated surfactants of heptafluorobutylate and pentadecafluorooctanoate ions were adsorbed on an activated charcoal cartridge and decomposed with sodium biphenyl (SBP) reagent to form inorganic fluoride ion. The fluoride ion thus formed was determined by flow injection analysis (FIA) using quercetin-Zr complex as a fluorimetric reagent, where λ_{ex} and λ_{em} were 422 and 491 nm, respectively. The limit of detection for fluoride ion by the FIA system was developed to 1.1×10^{-6} M (signal to noise ratio of three), when 50% (v/v) tetrahydrofuran (THF) was used as a dissolving solvent for quercetin. The perfluorinated surfactants in the sample solution were quantitatively adsorbed on the cartridge containing 100 mg of activated charcoal and were decomposed with 0.5 mL of sodium biphenyl reagent after drying thoroughly by flowing through dry nitrogen gas. The fluoride ion formed was recovered with 3 mL of purified water as an eluent, and it was determined by the fluorimetric flow injection system. The blank fluorescence signal accompanied during the adsorption/decomposition on the cartridge was reduced by washing the activated charcoal with acetone. The blank signal was also observed from dimethoxyethane, which was used in sodium biphenyl reagent. When 600 mL sample solution was used and 200 times enrichment was applied, the heptafluorobutylate and pentadecafluorooctanoate ions at the concentrations of 2.1 μg L^{-1} were quantitatively recovered as fluoride ion, and the limit of detections for the perfluorinated surfactants were 0.3 and 0.3 μg L^{-1} for the two perfluorinated surfactants, respectively (3 sigma of the blank signal).
© 2007 Elsevier B.V. All rights reserved.

Keywords: Perfluorinated surfactants; Sodium biphenyl reagent; Quercetin-Zr complex; Flow injection analysis; Activated charcoal cartridge; Solid-phase extraction/preconcentration

1. Introduction

Since a certain amount of perfluorooctane sulfonate (PFOS) was found in the human sera [1], concern about perfluorinated surfactants is rapidly growing [2,3]. Global survey in oceans [4] and biota [5] revealed that the perfluorinated surfactants, such as PFOS and perfluorooctanoate (or pentadecafluorooctanoate; PFOA), have been spreading all over the world, including the Arctic and Antarctic Oceans. The concentrations of the perfluorinated surfactants are trace as low as parts-per-trillion (ng L^{-1}) levels in the aqueous media and parts-per-billion (ng g^{-1}) levels in the biological samples [4,5].

Highly sensitive detection methods have been developed to determine the perfluorinated surfactants. Gas chromatography–mass spectrometry (GC–MS) is one of the promising methods; perfluorocarboxylates have been derivatized to methyl ester and determined at μg L^{-1} to sub-μg L^{-1} levels [6,7]. In addition to the solid-phase extraction with an anion exchanger [6] and of ion associate with tetrabutylammonium ion (TBA) to polydimethylsiloxane fiber [7], pressurized fluid extraction composed of 1:3 acetone–methanol was also proposed [8]. Derivatizing reagents of 2,4-difluoroaniline

* Corresponding author. Tel.: +81 86 251 7845; fax: +81 86 251 7853.
E-mail address: takayana@cc.okayama-u.ac.jp (T. Takayanagi).

0039-9140/$ – see front matter © 2007 Elsevier B.V. All rights reserved.
doi:10.1016/j.talanta.2007.08.026

and *N*,*N*-dicyclohexylcarbodiimide were also developed for GC–MS [9,10]. High performance liquid chromatography–mass spectrometry (HPLC–MS) and tandem mass spectrometry (HPLC–MS/MS) are promising alternatives, and the detection systems have been most commonly used for environmental water samples owing to the superior detection sensitivity [11]. The HPLC–MS and HPLC–MS/MS are usually combined with any preconcentration technique. One preconcentration technique is the liquid–liquid extraction, and the perfluorinated surfactants were extracted and concentrated into methyl *tert*-butyl ether (MTBE) as ion associate with TBA [12–15]. Solid-phase extraction is also used for the pretreatment and preconcentration of the perfluorinated surfactants; C18 cartridges [16–18] and anion exchanger [19] were used. On the comparison of the solid-sorbent cartridges, Oasis HLB cartridge was found to give smaller blank values [20]. Solid-sorbent cartridge was also utilized by placing it before the HPLC injector to remove the contamination from the instrumental components and to realize the determination of the perfluorinated surfactants at ng L^{-1} level [21]. The solid-phase extraction has been automated by incorporating the extraction cartridge in the HPLC line [22] or column switching [23,24].

The mass spectrometers are highly sensitive detectors for the anionic perfluorinated surfactants, and the surfactants can be detected at the concentration level of ng L^{-1}. However, the drawback of the mass spectrometer is its instrumental price and the running cost. Fluorimetric detection of the perfluorinated surfactants has been reported as a conventional method, at which 3-bromoacetyl-7-methoxycoumarin was used as a derivatizing reagent [25]. The detection limits for the perfluorinated carboxylic acids were 50 pmol/50 mg liver, which corresponded to sub-parts per million level. Ion chromatography coupled with conductivity detection was also reported; the limit of detection was yet mg L^{-1} level [26]. Electrophoretic method was also studied for the separation of seven kinds of perfluorocarboxylic acids by capillary electrophoresis coupled with direct and indirect detection [27], as well as zone electrophoresis on a chip coupled with conductivity detection [28]. Although the resolutions among the perfluorinated surfactants were excellent, the detection sensitivity was around mg L^{-1} level.

We aimed at developing conventional monitoring system for the perfluorinated surfactants at μg L^{-1} level in water samples, in which the detection system would be an important key. It would be noticed that the organic fluorine compounds including the perfluorinated surfactants can be adsorbed on the hydrophobic sorbents and that the organic fluorine compounds can be decomposed to inorganic fluoride ion by the cleavage of C–F bonds with commercially available sodium biphenyl (SBP) reagent [29]. The cleavage efficiency and the mild reaction conditions with SBP are very attractive for the generation of fluoride ion. Once fluoride ion is formed from the organic fluorine, it can be detected by a variety of analytical detection methods. We have proposed the determination of total organic fluorine by potentiometric and fluorimetric detections coupled with off-line defluorination with the SBP reagent [30]. The perfluorinated surfactants were adsorbed and concentrated on an activated charcoal cartridge by passing the solution through it. After the cartridge was completely dried with dry nitrogen gas, the perfluorinated surfactants was decomposed with sodium biphenyl reagent on the cartridge to give inorganic fluoride ion. The fluoride ion thus formed was recovered with purified water quantitatively, and it was determined by fluorimetric flow injection system applying quercetin-Zr complex as an on-line derivatizing reagent [31]. In this study, a conventional analytical system for the perfluorinated surfactants at μg L^{-1} level by applying preconcentration/enrichment is proposed on the basis of the fluorimetric detection of the fluoride ion. By using 600 mL sample solution and 3 mL purified water as an eluting solution including 200 times enrichment, heptafluorobutylate and pentadecafluorooctanoate ions at the concentrations of 2.1 μg L^{-1} were quantitatively adsorbed on an activated charcoal cartridge and converted to fluoride ion and detected. The limits of the detection for heptafluorobutylate and pentadecafluorooctanoate ions were estimated to be 0.3 and 0.3 μg L^{-1} (3S.D. of the blank signals), respectively.

2. Experimental

2.1. Apparatus

Schematic diagram of the flow injection analysis (FIA) system is shown in Fig. 1; the system was fundamentally proposed by Garrido et al. [31]. All PTFE tubing used for the construction of the system was of 0.5 mm i.d. Two dual plunger pumps (P_1 and P_2; Flom, Tokyo, Japan) and a DMX-2000 double plunger pump (P_3; Sanuki Kogyo, Tokyo, Japan) were used for propelling the carrier and the reagent solutions. Sample solutions and the standard solutions were introduced into the carrier stream via a six-way rotatory valve (Rheodyne LLC, California, USA). The fluorescence was monitored by an RF-550 spectrofluorometric detector (Shimadzu, Kyoto, Japan). A Hitachi D-2000 Chromato-Integrator was used for recording the fluorescence response.

A Hitachi (Tokyo, Japan) 650-10S Fluorescence Spectrophotometer equipped with a 1 cm quarts cell was used for the measurements of the fluorescence spectra. A TOA (Tokyo,

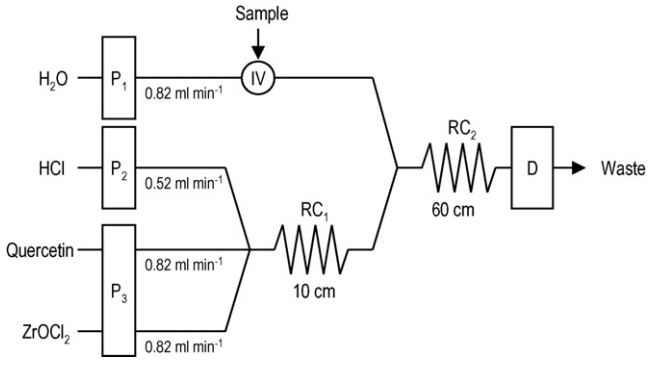

Fig. 1. Flow injection manifold for the fluorimetric detection of fluoride ion. P_1, P_2, P_3: Double plunger pumps; RC_1 and RC_2: reaction coils; D: spectrofluorimeter (λ_{ex}: 422 nm, λ_{em}: 491 nm); IV: six-way rotatory valve (injection volume: 150 μl). Reagent solutions: HCl, 1.75 M; quercetin, 0.3 mM in 50:50 H_2O–tetrahydrofuran; $ZrOCl_2$, 0.3 mM in 1.2 M H_2SO_4.

Japan) Flatbed Recorder FBR-251A was used for recording the spectrum.

2.2. Reagent

Fluorosurfactants of heptafluorobutylic acid (perfluorobutylic acid; PFBA) and PFOA were obtained from Tokyo Kasei Kogyo (Tokyo, Japan). A sodium biphenyl reagent was obtained from Kanto Kagaku (Tokyo, Japan) and used as received. Analytical grade of sodium fluoride (Yoneyama Chemical, Tokyo, Japan) was used to prepare the standard F^- solution at the concentration of 0.1 M; the solution was successively diluted with the purified water and used. Fluorimetric reagents of quercetin and $ZrOCl_2$ were from Wako Pure Chemical Industries (Osaka, Japan). The quercetin solution was prepared by dissolving a certain amount of quercetin in a certain organic solvent, and the solution was diluted with water at the volume ratio of 1:1. The Zr(IV) solution was prepared by dissolving a certain amount of $ZrOCl_2$ with a small amount of sulfuric acid. Hydrochloric acid, sulfuric acid, ethanol, methanol, acetone, acetonitrile, 1,4-dioxane, tetrahydrofuran (THF), and dimethoxyethane used were of reagent grade. Four types of activated charcoal were obtained from Wako Pure Chemical Industries and Kanto Kagaku. Water used was purified by ion exchange and distillation followed by Milli-Q Labo (Nippon Millipore, Tokyo, Japan) treatment.

2.3. Procedure for the off-line decomposition of the perfluorinated carboxylate

A 5 mL polypropylene syringe (12 mm Ø, 65 mm length; JMS, Hiroshima, Japan) was employed as an off-line treatment cartridge, and an aliquot of 100 mg activated charcoal was put in it sandwiched with glass wools on the both ends. The cartridge was used for the solid-phase extraction and preconcentration of the perfluorinated surfactants. The cartridge was prerinsed with 10 mL of methanol and 10 mL of the purified water, successively. An aliquot of sample solution (3–600 mL) containing the perfluorinated carboxylate was passed through the cartridge dropwisely. The cartridge was then dried thoroughly by flowing dry nitrogen gas through. After drying, an aliquot of 0.5 mL sodium biphenyl reagent was dropped to the cartridge by applying a reduced pressure, since the sodium biphenyl reagent is viscous. The cartridge was allowed to leave for 10 min to complete the decomposition. The fluoride ion thus generated was recovered with an aliquot of 3 mL purified water. The effluent solution was used for the FIA measurement.

2.4. Procedure for the flow injection analysis

In the FIA diagram shown in Fig. 1, an aliquot of 150 μL portion of the sample solution containing fluoride ion was introduced into the carrier stream (water) using the six-way rotatory valve. The fluorimetric reagent of quercetin-Zr was prepared *in situ* by merging the three reagent streams. The carrier stream and the reagent stream were then merged and mixed in a 60-cm tubing. The ternary complex of quercetin-Zr-F^- was monitored spectrofluorimetry at the excitation wavelength of 422 nm and the emission wavelength of 491 nm.

3. Results and discussion

3.1. Flow injection analysis of fluoride ion

Perfluorinated surfactants were decomposed to inorganic fluoride ion in this study, and therefore, sensitive detection of inorganic fluoride ion is a key technique to establish the sensitive detection of the fluorinated surfactants. Several detection methods have been reported for inorganic fluoride ion. Ternary complex of Zr-EDTA-pyrocatechol violet was decomposed with fluoride ion and the pyrocatechol violet was spectrophotometrically detected [32]. Fluorescence of ternary complex of Zr-EDTA-3-hydroxy-2′-sulfoflavone was quenched in the presence of fluoride ion [33]. Sapphyrin was used as a spectrophotometric and fluorimetric reagent for fluoride ion coupled with solvent extraction [34]. Alizarin Red S–Al(III) complex was used as a fluorimetric reagent for fluoride ion [35]. Catalytic oxidation of 2,4-diaminophenol with Fe–H_2O_2 was inhibited by F^- and fluoride ion was detected by spectrophotometric flow injection analysis [36,37]. Quercetin-Zr complex was also used as a fluorimetric reagent coupled with flow injection analysis [31]. Microdistillation coupled with spectrophotometric detection was also proposed [38]. Potentiometric detections have been also proposed coupled with preconcentration [39].

Among the determination methods proposed, fluorimetric one can detect the analyte fluoride ion sensitively, and flow-based analysis technique improves the sensitivity on the basis of the stable background. Therefore, we adopted quercetin-Zr complex as a fluorimetric reagent coupled with flow injection analysis proposed by Garrido et al. [31]. In the literature, the linear range was 0.1–3.0 $\mu g\,mL^{-1}$ of fluoride ion (5×10^{-6} to 1.5×10^{-4} M) with a limit of detection at 0.06 $\mu g\,mL^{-1}$ (3×10^{-6} M). When we set up the similar FIA system, linear calibration graph was reproduced in the concentration range of fluoride ion from 0.5×10^{-5} to 4.0×10^{-5} M with a limit of detection at 2.1×10^{-6} M in the previous study [30]; the performance was almost comparable with the reported one [31]. We aimed at improving the detection sensitivity, and a series of organic solvent to dissolve quercetin was investigated. As the solvent to dissolve quercetin, methanol, ethanol, acetonitrile, acetone, 1,4-dioxane, and tetrahydrofuran were chosen from the viewpoint of the mutual solubility with water. Calibration graphs for the standard fluoride ion were constructed at the concentration range from 0.5×10^{-5} to 4.0×10^{-5} M and the slope of the calibration graphs were compared with each other. The results are shown in Fig. 2; THF showed the largest slope among the solvents used, and the slope was plotted against the parameters of the solvents, such as specific inductive capacity, donor number, and acceptor number [40]. Fig. 3a shows the relationship between acceptor number of the solvent and the slope of the calibration graph. It can be read from Fig. 3a that such solvents possessing small acceptor number were found to give stronger fluorescence. The solvation of fluoride ion with

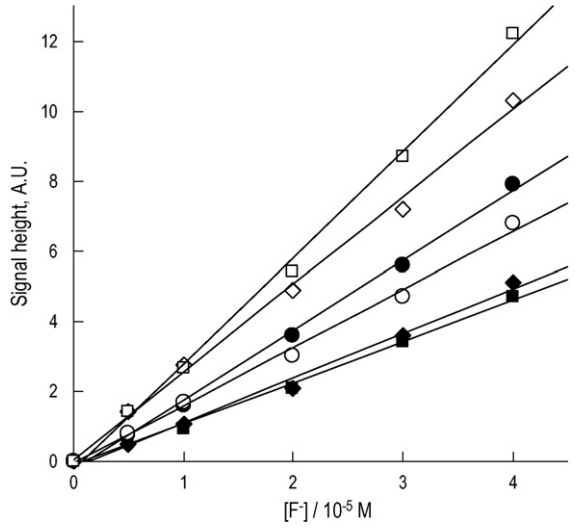

Fig. 2. Calibration graphs for fluoride ion with the different solvent used for the quercetin solution. Quercetin solution: 0.3 mM in 50:50 H_2O–organic solvent. Organic solvent: (■) methanol; (♦) ethanol; (◯) acetonitrile; (●) acetone; (◊) 1,4-dioxane; (□) tetrahydrofuran.

the solvent would be reduced, and fluoride ion would be much reactive with the quercetin-Zr complex. The slope of the signal was also plotted against the donor number and specific inductive capacity of the solvent (Fig. 3b); there is no dependence with the two parameters of the solvents. As a result, the sensitivity was preferably developed when THF was used as a quercetin solvent. The flow signals for the standard fluoride ion were linear at the concentration range of 0–4 × 10^{-5} M. The limit of detection for fluoride ion (signal to noise ratio of three) was 1.1 × 10^{-6} M (0.020 μg mL^{-1}) at these conditions. When the THF percentage in the quercetin solution was increased to 75% (v/v), the limit of detection was further developed at to 7.5 × 10^{-7} M (0.015 μg mL^{-1}). Conventionally, the concentration of THF at 50% (v/v) was used in this study for the quercetin solvent.

3.2. Collection and concentration of the perfluorinated surfactants and its decomposition to fluoride ion with the activated charcoal cartridge

It has been reported that the perfluorinated surfactants were adsorbed on activated carbon quantitatively [41]. Therefore, we used activated charcoals as adsorbent for the perfluorinated surfactant; an aliquot of 100 mg of the activated charcoal (Wako) was put in the syringe and the cartridge was used after conditioning with methanol and water. The adsorption behavior, the decomposition of PFBA or PFOA, and the elution with water were evaluated with the recovery percentages as fluoride ion. The off-line-decomposition procedure is fundamentally the same in Section 2.3. In a series of the experiments, an aliquot of 3 mL of the solution containing 2 × 10^{-5} M of the perfluorinated surfactant, as well as the blank solution, was used as sample solutions. Dry nitrogen gas was flown through for 10 min, and an aliquot of 1 mL of the SBP solution was used for the decomposition. On the FIA measurements, the effluent solution was diluted by 10 times on necessity. Magnification of the molar concentrations of the fluoride ion from that of the corresponding perfluorinated surfactant (7× for PFBA and 15× for PFOA) was considered on evaluating the recovery percentage.

In a series of the operation procedures, one of the most important processes was the drying of the activated charcoal cartridge after the adsorption of the perfluorinated surfactants. It took about 10 min at room temperature to obtain quantitative recovery of PFOA as fluoride ion. The drying time corresponded to the complete removal of the moisture with this cartridge. The incomplete recovery is attributed to the inactivation of the sodium biphenyl reagent with water. Advantage on using the syringe cartridge is that we can observe the drying status by seeing the cartridge with eyes.

The recovery percentage of the perfluorinated surfactant as fluoride ion was summarized in Table 1. The cartridge was repeatedly used for at least four times. It can be read from Table 1 that both PFBA and PFOA are adsorbed on the cartridge, decom-

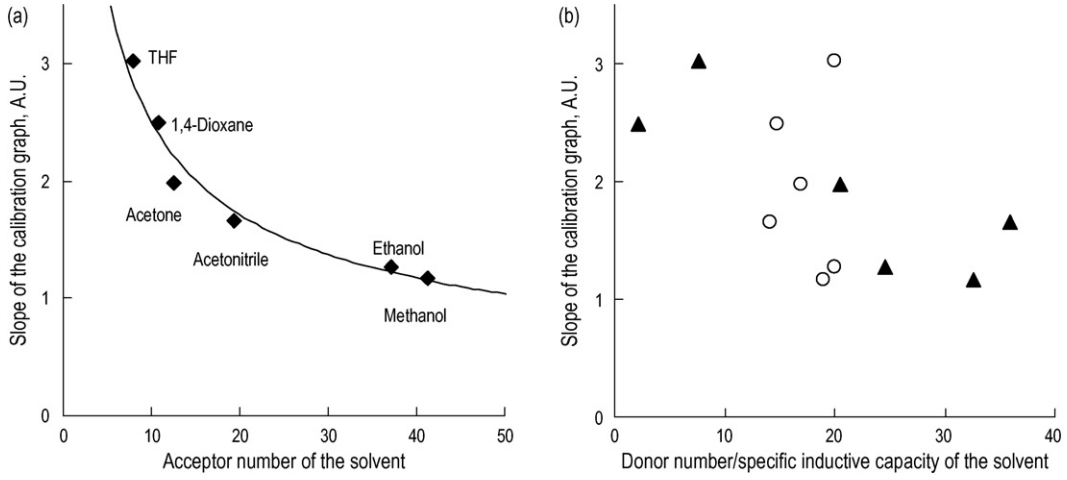

Fig. 3. Slope of the calibration graph representing the detection sensitivity vs. (a) acceptor number of the solvent and (b) donor number/specific inductive capacity of the solvent used for the quercetin solution. Range of the F^- concentrations: 0.5–4.0 × 10^{-5} M. Solvent property: (♦) acceptor number; (◯) donor number; (▲) specific inductive capacity.

Table 1
Repeatability of successive treatment of the perfluorinated surfactants with an activated charcoal cartridge

Run no.	Recovery (%)[a]	
	PFBA	PFOA
1	102	92
2	99	93
3	99	92
4	98	99
Mean	100 ± 2	94 ± 5

[a] Initial concentration of the perfluorinated surfactant: 2×10^{-5} M.

posed with SBP, and eluted with water, quantitatively. It can be also noticed that the cartridge can be used several times.

3.3. Reduction of the blank signal as fluoride ion occurring during the decomposition process

A large amount of sample solution was subjected to increase the enrichment factor and to develop the detection sensitivity for the perfluorinated surfactants; an aliquot of 600 mL solution was adopted considering the elution volume of 3 mL water. Consequently, the enrichment factor was 200 times. However, the high enrichment factor yielded undesirable results. Even when the blank solution of the perfluorinated surfactant was treated with the activated charcoal cartridge and with the SBP reagent, blank fluorescence signal was observed in the FIA chart (Fig. 4). The blank signal corresponded to 4.8×10^{-5} M fluoride ion. No signal was observed in the absence of treatment with the SBP reagent, and therefore, the activated charcoal would be free from inorganic fluoride ion. The inorganic fluoride ion would have been produced during the treatment with the SBP reagent. The blank signal interferes the development of the limit of detection, and we tried to reduce the blank signal.

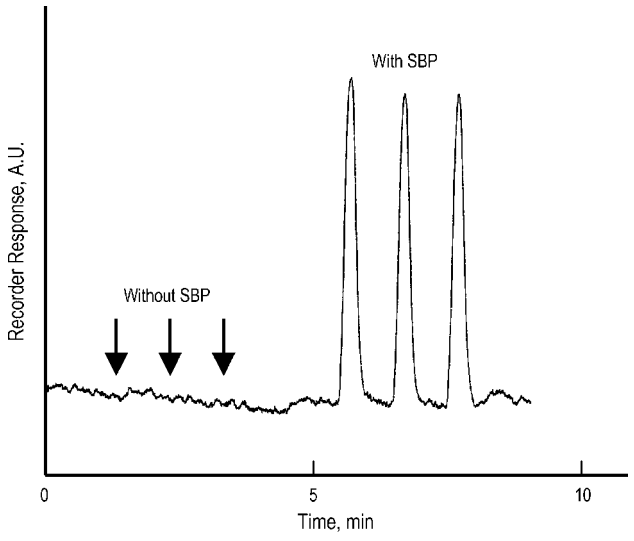

Fig. 4. Blank signal corresponding to F^- concentration observed with the thorough treatment of the blank solution of the perfluorinated surfactant. Sample solution: 600 mL purified water. The SBP reagent: 1 mL. Eluent: 3 mL purified water. Activated charcoal used was from Wako, 200 mg.

The preconditioned activated charcoal cartridge was repeatedly used for the thorough treatment of the blank solution of the perfluorinated surfactant with the SBP reagent. Activated charcoal from Wako was used throughout. The treatment was examined with different amounts of activated charcoal of 100 and 200 mg. The fluorescent signal tended to decrease with the treatment turn, and the blank signal was reduced to about one third from the fresh activated charcoal on third and more replicated treatments. Additionally, the amount of activated charcoal of 200 mg always showed higher blank responses than that of 100 mg. Therefore, any fluorescent substance and/or fluorinated carbons adsorbed on the activated charcoal would have been removed along with the thorough treatment. Treatment of the activated charcoal with 1 M nitric acid by passing 10 mL of the acid through the cartridge did not improve the blank signal; it was supposed that any organic substance might have been decomposed with SBP and eluted with the purified water. The activated charcoal was immersed in acetone for 24 h before the usage, and the blank signal was also evaluated with the charcoals treated; immersing the activated charcoal in acetone reduced the blank signal as low as one third from the fresh one; the blank signal as fluoride ion was reduced to 1.0×10^{-4} M. The grade of the acetone gave little difference.

Type of the activated charcoal was also compared with each supplier sources. Although the activated charcoals from Darco, Kanto, and Norit showed smaller blank signal than the one from Wako at the received status, the suction of the SBP reagent into the cartridge took quite long time (∼1 h) because of the small particle size of the charcoals and the viscosity of the SBP solution. Since the blank signal with the activated charcoal can be reduced by immersing it in acetone for 24 h, the activated charcoal from Wako was used after immersed in acetone. Most portion of the blank signal can be eliminated by the immersion.

Volume of the SBP solution put in the cartridge was also investigated at the amounts of 0.3, 0.5, and 1.0 mL. When smaller volume of the SBP solution was used, the blank signal was reduced. However, a certain amount of the SBP reagent was necessary to complete the decomposition reaction of the perfluorinated surfactants, and the volume of 0.5 mL was adopted for the cartridge with 100 mg of the activated charcoal. The SBP reagent itself would also have given the blank fluorescence signal, and the origin of the blank signal from the SBP reagent was investigated. Dimethoxyethane was used as a solvent of sodium biphenyl reagent, and the fluorescence from dimethoxyethane was examined. An aliquot of 0.5 mL portion of dimethoxyethane was diluted with water to give 3.0 mL total volume, and the mixed solution was injected into the FIA system. Blank signal corresponding to 2.9×10^{-5} M fluoride ion was obtained. The fluorescence spectrum of dimethoxyethane was also measured (Fig. 5); a significant fluorescence was observed at emission maximum at 473 nm with an excitation wavelength of 422 nm. Detection wavelength of fluoride ion with quercetin-Zr complex at 491 nm was affected by the fluorescence. Therefore, the SBP reagent was found to be also a source of the blank signal.

As the source of the blank fluorescence signal, it was concluded that any organic compounds adsorbed on the activated charcoal gave the contamination and that the dimethoxyethane

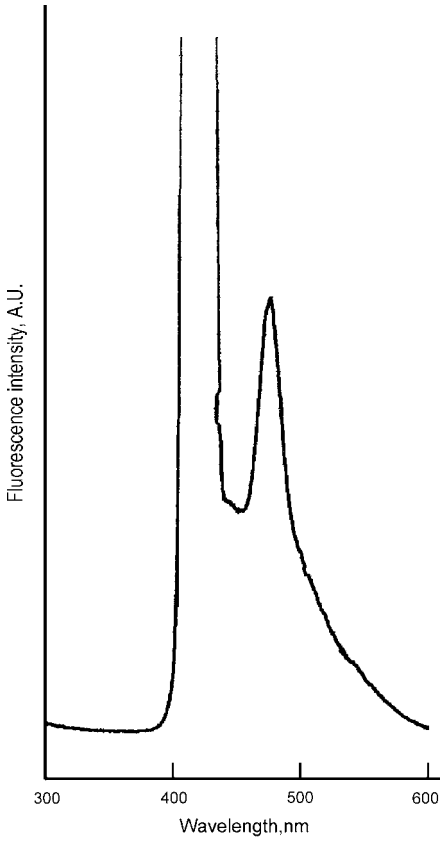

Fig. 5. Fluorescence spectrum of dimethoxyethane. Excitation wavelength: 422 nm.

used in the SBP reagent gave fluorescence signal. The former one can be reduced by immersing the activated charcoal in acetone, and the latter one can be suppressed by controlling the volume of the SBP reagent at 0.5 mL.

3.4. Determination of perfluorinated surfactants in water at $\mu g\,L^{-1}$ level

The proposed system including the solid-phase extraction on the activated charcoal cartridge, the decomposition with the SBP reagent, and the FIA monitoring of the fluoride ion was applied to the determination of trace level of perfluorinated surfactants. A sample volume of 600 mL aqueous solution containing 1×10^{-8} M ($2.1\,\mu g\,L^{-1}$) PFBA or 5×10^{-9} M ($2.1\,\mu g\,L^{-1}$) PFOA was passed through the activated charcoal cartridge, and the surfactant was recovered with 3 mL of water after the decomposition reaction with the SBP reagent. The eluate was subjected to the FIA determination of the fluoride ion. The results for PFBA are shown in Fig. 6. Blank signals are obtained as shown in signals a and b in Fig. 6; the signals correspond to 3.0×10^{-5} M fluoride ion. The limit of the detection for fluoride ion was calculated to be 2×10^{-6} M from the 3S.D. of the blank signal. The signals c–f in Fig. 6 are the results for the PFBA solutions. The signals e in Fig. 6 are the obvious failure that the SBP reagent have passed through the cartridge without retained; only the blank signals can be obtained. When the PFBA was quantitatively adsorbed on the cartridge, decomposed with the SBP

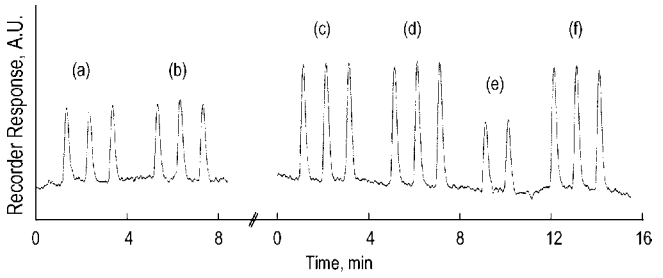

Fig. 6. Flow signals for the analysis of fluoride ion after the enrichment of PFBA on the activated charcoal and the treatment with SBP reagent. An FIA system shown in Fig. 1 was used for the determination of the fluoride ion. Concentration of PFBA: (a and b) none; (c–f) 1.0×10^{-8} M ($2.1\,\mu g\,L^{-1}$). Sample volume: 600 mL. Eluent: 3 mL of purified water. Amount of the activated charcoal in the cartridge: 100 mg. Volume of the SBP reagent: 0.5 mL.

reagent, and eluted with the purified water, the concentration of fluoride is calculated to be 1.4×10^{-5} M considering that seven fluoride ions are generated from one PFBA molecule and the concentration factor is 200 times. The recoveries as fluoride ion for c, d, and f in Fig. 6 were $97 \pm 3\%$ ($n = 3$), and the perfluorinated surfactant was quantitatively recovered and determined. The limit of detection for PFBA was calculated to be 1.5×10^{-9} M ($0.3\,\mu g\,L^{-1}$) from the limit of the detection for fluoride ion (2×10^{-6} M) and the signal intensity of the decomposed PFBA. The recovery and the limit of detection for PFOA were also examined in a same manner; they are $99 \pm 6\%$ ($n = 4$) and 0.8×10^{-9} M ($0.3\,\mu g\,L^{-1}$).

4. Conclusions

Perfluorinated surfactants of PFBA and PFOA were quantitatively adsorbed and preconcentrated on an activated charcoal cartridge, and they were decomposed with sodium biphenyl reagent. Fluoride ion thus formed by the decomposition was determined by the fluorimetric flow injection analysis, where quercetin-Zr reagent was used as an on-line derivatizing reagent. Detection sensitivity for fluoride ion was developed as low as 1.1×10^{-6} M, when THF was used as a dissolving solvent for quercetin. Blank signals were observed, when 200 times enrichment was made; the blank signal was suppressed by immersing the activated charcoal in acetone for 24 h and by reducing the amounts of the activated charcoal and the SBP solution. By using 600 mL sample solution, PFBA and PFOA at $2.1\,\mu g\,L^{-1}$ can be recovered and determined by the FIA system quantitatively after 200 times enrichment. The limit of detection of $0.3\,\mu g\,L^{-1}$ was obtained for PFBA and PFOA. The proposed method would be applied to the determination of the perfluorinated surfactants in environmental samples.

References

[1] G.W. Olsen, J.M. Burris, J.H. Mandel, L.R. Zobel, J. Occup. Environ. Med. 41 (1999) 799.
[2] R. Renner, Environ. Sci. Technol. 35 (2001) 154A.
[3] J.P. Giesy, K. Kannan, Environ. Sci. Technol. 36 (2002) 146A.
[4] N. Yamashita, K. Kannan, S. Taniyasu, Y. Horii, G. Petrick, T. Gamo, Mar. Pollut. Bull. 51 (2005) 658.

[5] M. Houde, J.W. Martin, R.J. Letcher, K.R. Solomon, D.C.G. Muir, Environ. Sci. Technol. 40 (2006) 3463.
[6] C.A. Moody, J.A. Field, Environ. Sci. Technol. 33 (1999) 2800.
[7] R. Alzaga, J.M. Bayona, J. Chromatogr. A 1042 (2004) 155.
[8] R. Alzaga, C. Salgado-Petinal, E. Jover, J.M. Bayona, J. Chromatogr. A 1083 (2005) 1.
[9] B.F. Scott, C.A. Moody, C. Spencer, J.M. Small, D.C.G. Muir, S.A. Mabury, Environ. Sci. Technol. 40 (2006) 6405.
[10] B.F. Scott, C. Spencer, S.A. Mabury, D.C.G. Muir, Environ. Sci. Technol. 40 (2006) 7167.
[11] S.D. Richardson, Anal. Chem. 78 (2006) 4021.
[12] K.J. Hansen, L.A. Clemen, M.E. Ellefson, H.O. Johnson, Environ. Sci. Technol. 35 (2001) 766.
[13] J.P. Giesy, K. Kannan, Environ. Sci. Technol. 35 (2001) 1339.
[14] C. Gonzalez-Barreiro, E. Martinez-Carballo, A. Sitka, S. Scharf, O. Gans, Anal. Bioanal. Chem. 386 (2006) 2123.
[15] L. Tao, K. Kannan, N. Kajiwara, M.M. Costa, G. Fillmann, S. Takahashi, S. Tanabe, Environ. Sci. Technol. 40 (2006) 7642.
[16] C.A. Moody, W.-C. Kwan, J.W. Martin, D.C.G. Muir, S.A. Mabury, Anal. Chem. 73 (2001) 2200.
[17] C.A. Moody, J.W. Martin, W.-C. Kwan, D.C.G. Muir, S.A. Mabury, Environ. Sci. Technol. 36 (2002) 545.
[18] C.-L. Tseng, L.-L. Liu, C.-M. Chen, W.-H. Ding, J. Chromatogr. A 1105 (2006) 119.
[19] C.A. Moody, G.N. Hebert, S.H. Strauss, J.A. Field, J. Environ. Monit. 5 (2003) 341.
[20] N. Yamashita, K. Kannan, S. Taniyasu, Y. Horii, T. Okazawa, G. Petrick, T. Gamo, Environ. Sci. Technol. 38 (2004) 5522.
[21] M. Stadalius, P. Connolly, K. L'Empereur, J.M. Flaherty, T. Isemura, M.A. Kaiser, W. Knaup, M. Noguchi, J. Chromatogr. A 1123 (2006) 10.
[22] Z. Kuklenyik, J.A. Reich, J.S. Tully, L.L. Needham, A.M. Calafat, Environ. Sci. Technol. 38 (2004) 3698.
[23] K. Inoue, F. Okada, R. Ito, M. Kawaguchi, N. Okanouchi, H. Nakazawa, J. Chromatogr. B 810 (2004) 49.
[24] Z. Kuklenyik, L.L. Needham, A.M. Calafat, Anal. Chem. 77 (2005) 6085.
[25] T. Ohya, N. Kudo, E. Suzuki, Y. Kawashima, J. Chromatogr. B 720 (1998) 1.
[26] H. Sanderson, T.M. Boudreau, S.A. Mabury, W.-J. Cheong, K.R. Solomon, Environ. Toxicol. Chem. 21 (2002) 1490.
[27] L. Wojcik, B. Szostek, W. Maruszak, M. Trojanowicz, Electrophoresis 26 (2005) 1080.
[28] M. Masar, L. Wojcik, D. Kaniansky, M. Trojanowicz, J. Sep. Sci. 28 (2005) 1271.
[29] P. Venkateswarlu, Anal. Chem. 54 (1982) 1132.
[30] J. Musijowski, M. Trojanowicz, B. Szostek, J.L.F.C. Lima, R. Lapa, H. Yamashita, T. Takayanagi, S. Motomizu, Anal. Chim. Acta, in press.
[31] M. Garrido, A.G. Lista, M. Palomeque, B.S. Fernandez Band, Talanta 58 (2002) 849.
[32] T. Balaji, H. Matsunaga, Anal. Sci. 21 (2005) 973.
[33] H. Matsunaga, C. Kanno, H. Yamada, Y. Takahashi, T.M. Suzuki, Talanta 68 (2006) 1000.
[34] J. Nishimoto, T. Yamada, M. Tabata, Anal. Chim. Acta 428 (2001) 201.
[35] R.S. Sathish, M.R. Kumar, G.N. Rao, K.A. Kumar, C. Janardhana, Spectrochim. Acta A 66 (2007) 457.
[36] D.G. Themelis, P.D. Tzanavaras, H.D. Tzanavaras, J. Pharm. Biomed. Anal. 25 (2001) 971.
[37] D.G. Themelis, P.D. Tzanavaras, Anal. Chim. Acta 429 (2001) 111.
[38] K. Shimada, T. Shimoda, H. Kokusen, S. Nakano, Talanta 66 (2005) 80.
[39] M. Fouskaki, S. Sotiropoulou, M. Koci, N.A. Chaniotakis, Anal. Chim. Acta 478 (2003) 77.
[40] The Chemical Society of Japan, Kagaku Binran, Handbook of Chemistry, Basic fifth ed., (2004) pp. I770–I777.
[41] M. Pabon, J.M. Corpart, J. Fluorine Chem. 114 (2002) 149.

Available online at www.sciencedirect.com
ScienceDirect
Talanta 74 (2008) 1492–1497
Talanta
www.elsevier.com/locate/talanta

Biosensing approach for glutathione detection using glutathione reductase and sulfhydryl oxidase bienzymatic system

Suna Timur*, Dilek Odaci, Ayse Dincer, Figen Zihnioglu, Azmi Telefoncu

Ege University, Faculty of Science, Biochemistry Department, 35100 Bornova, Izmir, Turkiye

Received 30 May 2007; received in revised form 18 September 2007; accepted 28 September 2007
Available online 2 October 2007

Abstract

Chitosan membrane with glutathione reductase and sulfhydryl oxidase (SOX) was subsequently integrated onto the surface of spectrographic graphite rods for obtaining a glutathione biosensor. The working principle was based on the monitoring of O_2 consumption that correlates the concentration of glutathione during the enzymatic reaction. A linear relationship between sensor response and concentration was obtained between 0.5 and 2.0 mM for oxidized glutathione (GSSG), and 0.2–1.0 mM for reduced glutathione (GSH) in the presence of 2 μM nicotinamide adenine dinucleotide phosphate (NADPH) under the optimum working conditions. Also, reduced/oxidized glutathione were separated by HPLC and utility of bienzymatic system was investigated as an electrochemical detector for the analysis of these compounds. All data were given as a comparison of two systems: biosensor and diode array detector (DAD).
© 2007 Elsevier B.V. All rights reserved.

Keywords: Glutathione reductase; Sulfhydryl oxidase; Reduced/oxidized glutathione; Electrochemical detection

1. Introduction

Thiolic compounds are characterized by the presence of sulfhydryl residues [1]. The biological thiols can by classified as high-molecular mass protein thiols and low-molecular mass free thiols. As well as disulfides, low-molecular weight thiols such as glutathione (GSH), cysteine (Cys), and homocysteine (HCys), have numerous roles in metabolism and homeostasis [2–4].

Glutathione is widely found in all forms of life and plays an essential role in the health of organisms, particularly aerobic organisms. In animals, including humans, and in plants, glutathione is the predominant non-protein thiol that functions as a redox buffer keeping with its own SH groups those of proteins in a reduced condition, among other antioxidant activities [5–8]. Reduced glutathione (GSH), a tripeptide (γ-glutamylcysteinylglycine) with a free thiol group, is a major antioxidant in human tissues. It provides reducing equivalents to the reactions of the glutathione peroxidase (GPx) catalyzed reduction of hydrogen peroxide and lipid hydroperoxides to water and the respective alcohol. During this process GSH becomes oxidized glutathione (GSSG). The GSSG is then recycled into GSH by glutathione reductase (GR) and nicotinamide adenine dinucleotide phosphate (NADPH) [9–11]. When mammalian cells are exposed to oxidative stress, the ratio of GSH/GSSG will reduce as a consequence of GSSG accumulation. Altered levels of glutathione in plasma have been implicated in a number of pathological conditions, including Alzheimer's, Parkinson's diseases, diabetes, mascular degeneration, and HIV disease [12–16]. Due to the importance and wide spread existence of glutathione and the possible use of its plasma levels as a biomarker of health status in many crucial biological functions, measurement of the GSSG level or determination of the GSH/GSSG ratio becomes a useful indicator of oxidative stress. Besides it can be used to monitor the effectiveness of antioxidant intervention strategies [17–19] and also its measurement is considered a primary goal in clinical chemistry [20].

A composite sulfhydryl oxidase (SOX) electrode was previously developed by our group and applied as an electrochemical biodetector for reduced thiolic compounds after HPLC separation [21]. In this work, an amperometric biosensor by co-immobilization of glutathione reductase (GR) and sulfhydryl oxidase by means of chitosan membrane was described. After

* Corresponding author.
E-mail address: sunatimur@yahoo.com (S. Timur).

0039-9140/$ – see front matter © 2007 Elsevier B.V. All rights reserved.
doi:10.1016/j.talanta.2007.09.026

optimization of the working conditions and examination of analytical characteristics, proposed system was applied for GSH and GSSG analysis in blood samples. The objective of this study was also to combine biocatalytic detection with HPLC separation for subsequent detection of reduced and oxidized forms of glutathione in the same matrices.

Glutathione reductase GR (EC 1.6.4.2, NADPH: oxidized glutathione oxidoreductase) is a ubiquitous enzyme, which catalyzes the reduction of oxidized glutathione (GSSG) to glutathione (GSH) [22]. Besides, SOX, an oxidoreductase with a cofactor of FAD, could oxidize thiols through the oxidization of sulfhydryl residue [23–26]. When two enzymes were co-immobilized, bienzymatic reaction that occurred in the bioactive layer was given below;

$$GSSG + NADPH + H^+ \xrightarrow{GR} 2GSH + NADP^+$$

$$G\text{–}SH + HS\text{–}G + O_2 \xrightarrow{SOX} R\text{–}S\text{–}S\text{–}R + H_2O_2$$

The proposed biosensor was based on the monitoring of consumed O_2 that correlates the concentration of glutathione as a result of the first enzymatic reaction which was shown above.

2. Experimental

2.1. Material

Sulfhydryl oxidase (SOX; EC 1.8.3.2, 2.0 U/ml, 0.4 mg protein/ml) was obtained X-Zyme GmbH (Düsseldorf, DE) and glutathione reductase (GR; Type II, EC1.6.4.2, 0.088 U/mg protein) from wheat germ, glutathione (GSH; reduced and GSSG; oxidized form), β-nicotinamide adenine dinucleotide phosphate, reduced form (β-NADPH), glutaraldehyde, chitosan, were purchased from Sigma (St. Louis, MO, USA). All other chemicals were analytical grade. All solutions were prepared with water purified with a Milli-Q (Millipore, Bedford, MA, USA) system.

1.0 wt.% chitosan solution was prepared by dissolving 1.0 g of chitosan flakes into 100 ml of 1.0% acetic acid and stirred for 3 h at room temperature until complete dissolution [27]. The chitosan solution was stored in refrigerator when not in use.

Blood samples were obtained from a local hospital and prior to use, samples were centrifuged. And then, buffy-coat was denaturized by adding 70% $HClO_4$. Finally, the obtained sample was diluted 10-fold and spiked with known amount of standard glutathione solution.

2.2. Apparatus

Chronoamperometric experiments were performed by a Radiometer electrochemical measurement system (VoltaLabPGP201) and bienzyme electrode was used as a working electrode. Ag|AgCl (with 3 M KCl with saturated AgCl as an internal solution, Radiometer Analytical, REF321) and Pt (Radiometer Analytical, M241PT) were used as reference and counter electrodes respectively. The electrodes were inserted into thermostatic reaction cell (25 ml).

High-performance liquid chromatography (HP1100) with a photodiode array detector (DAD) and controlled by a HP-Chemstation from Agilent (Karlsruhe, Germany).

2.3. Preparation of biosensors

For the construction of the bienzyme layer on the top of the graphite electrode, first the spectrographic graphite rods (Ringsdorff Werke GmbH, Bonn, Germany, 3.05 mm diameter and 13% porosity) were polished on wet emery to obtain a smooth surface, washed thoroughly with distilled water and sonicated for 2 min, and then rinsed again with water and dried in an oven at 105 °C [28].

Premixed solution composed of 20 μl chitosan solution, 10 μl GR (0.002 U) and 10 μl SOX (0.02 U) were placed on top of the polished end of the electrode and spread evenly. Bienzyme electrodes were kept at 4 °C overnight and treated with the glutaraldehyde solution (1.0% in phosphate buffer) for 30 min at 4 °C [29], then washed with distilled water.

2.4. Measurements

Measurements were carried out in phosphate buffer (50 mM, pH 6.5) medium containing coenzyme, NADPH, under the operating potential of −0.7 V by monitoring of consumed O_2 while the solution was stirred. The current changes were registered in terms of current density (nA/cm^2 or μA/cm^2) in 1 min of response time. After each measurement, the electrode was rinsed with distilled water and allowed to equilibrate in working buffer before another measurement. During the experiments, daily prepared electrodes were used.

In order to examine the non-enzymatic reaction of GSH, GSSG substrates as well as NADPH at the electrode surface, blank measurements were performed for each compounds and no interference was observed.

2.5. Chromatographic system and conditions

Separation was carried out by HPLC with DAD. The flow rate was 1.4 ml/min and detection wavelength was set at 220 nm. Reduced/oxidized glutathione were passed through a Waters Spherisorb ODS-2 C_{18} column (250 mm × 4.6 mm, 5 μm) and the column temperature was 37 °C. The mobile phase consisted of 3.0% acetonitrile, 0.1% TFA (v/v) using an isocratic elution [30].

When bienzyme electrodes were used as an electrochemical detector for GSH and GSSG separation, these compounds that passed through the C_{18} column were transferred by tubing system into the biosensor reaction cell containing working buffer solution as well as coenzyme afterwards, electrode responses at the working potential were registered as current densities. The retention times of both substrates (GSH, GSSG) were primarily estimated by DAD and then used to analyze the mixture of oxidized and reduced forms of glutathione by the proposed biosensing system.

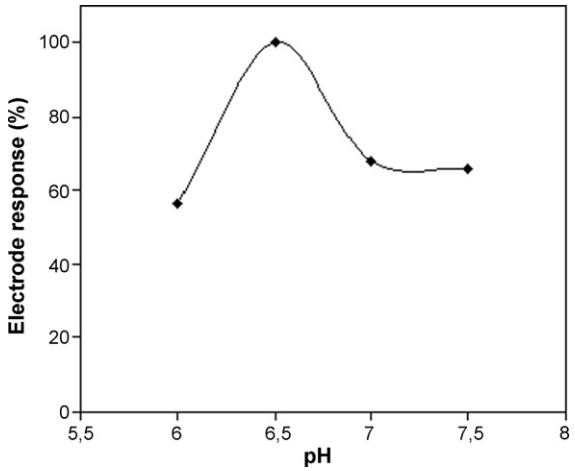

Fig. 1. Effect of pH on the electrode response for GSSG (in 50 mM phosphate buffers (pH 6.0–7.5) at 30 °C; −0.7 V; GSSG: 0.5 mM; NADPH: 2 μM).

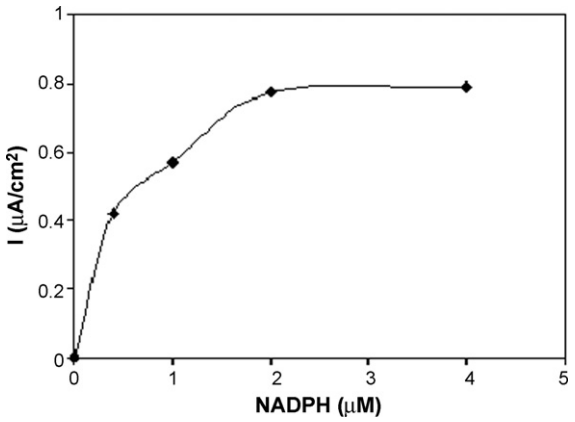

Fig. 2. Effect of NADPH on the electrode response for GSSG (in phosphate buffer; 50 mM at pH 6.5; 30 °C; −0.7 V; GSSG: 0.5 mM).

3. Results and Discussion

Glutathione measurement has always been proven to be difficult. Most of the methods are time consuming and either needs derivatization or they are lack of adequate sensitivity [31–36]. Compared to spectrophotometric methods, electroanalysis has the advantages of simplicity and high sensitivity and also the possibility of being used with colored samples without applying any pre-treatment. A less labor-intensive way for thiol measurement is the sensor method. A variety of amperometric systems for thiol detection has been previously described [37–42]. These systems generally do not require extensive sample preparation and have fast response [43,44].

The optimized and characterized biosensor was applied to online detection of reduced (GSH) and oxidized glutathione (GSSG) after HPLC separation. As mentioned before, when a composite electrode containing only SOX enzyme was used, only reduced thiolic compounds such as GSH could be analyzed [21]. Combination of GR and SOX enzyme enable us to detect GSSG as well as GSH in the same matrices.

3.1. Optimization of biosensor response

3.1.1. pH effect

The effect of pH on the bienzyme electrode was investigated by using phosphate buffer at 50 mM between pH 6.5 and 7.5 (Fig. 1). The response of the bienzyme electrode increases significantly from pH 6.0 to 6.5, and then a decrease is obtained at higher pH values. As a result pH 6.5 was chosen as optimum pH and used for further studies.

3.1.2. NADPH amount

To examine this effect, the responses of bienzyme electrodes were measured in the presence of different amounts of NADPH (0.5–4.0 μM) and plotted versus coenzyme concentration (Fig. 2). The best result was obtained with 2.0 μM of NADPH, higher concentrations caused the same response so further experiments were carried out by using this value.

3.2. Analytical characteristics

3.2.1. Linear range

Linearity was obtained in concentration range between 0.5 and 2.0 mM of GSSG in the presence of NADPH (2.0 μM). As well as GSSG, the response for GSH which is a substrate of SOX enzyme that takes place as a constituent of bienzyme layer was also investigated and found in the range of 0.2 and 1.0 mM, respectively. At higher concentrations, standard curve showed a deviation from linearity (Fig. 3).

Repeatability was tested by the subsequent measurements ($n = 5$) by bienzyme electrode standard deviation (S.D) as well as variation coefficient (c.v) were calculated as 1.082 ± 0.011 mM and 1.0% for 1 mM GSSG while these values were found as 0.422 ± 0.008 mM and 1.9% respectively for 0.4 mM GSH.

The stability of the biosensor was investigated at working conditions (30 °C in phosphate buffer) and 11% decrease in the activity was observed after 3 h. During this period approximately 20 measurements were made.

3.3. Chromatographic separation

GR has substrate specificity mainly to GSSG in contrast to the SOX enzyme which acts different thiolic compounds in reduced forms such as GSH [22]. It is well known that thiolic compounds were found together in different matrices particularly in physiological fluids, plant extracts as well. Chromatographic separation of these components is therefore a necessary requirement for an accurate analysis of each substrate. Especially, measurement of GSSG level or determination of the GSH/GSSG ratio is very important as a marker of oxidative stress [45], as mentioned before. It is known that the accurate measurement of GSSG levels is very difficult due to the low GSSG amount in tissues. In this study, the proposed bienzyme electrodes were initially, characterized and then combined with HPLC system as a post column electrochemical detector to analyze GSSG in the presence of GSH. At the beginning, as we have done in our previous work [21], DAD was utilized to obtain retention times of GSH and GSSG respectively. Additionally, the calibration graphs for both substrates were also drawn by using DAD. As a result, sim-

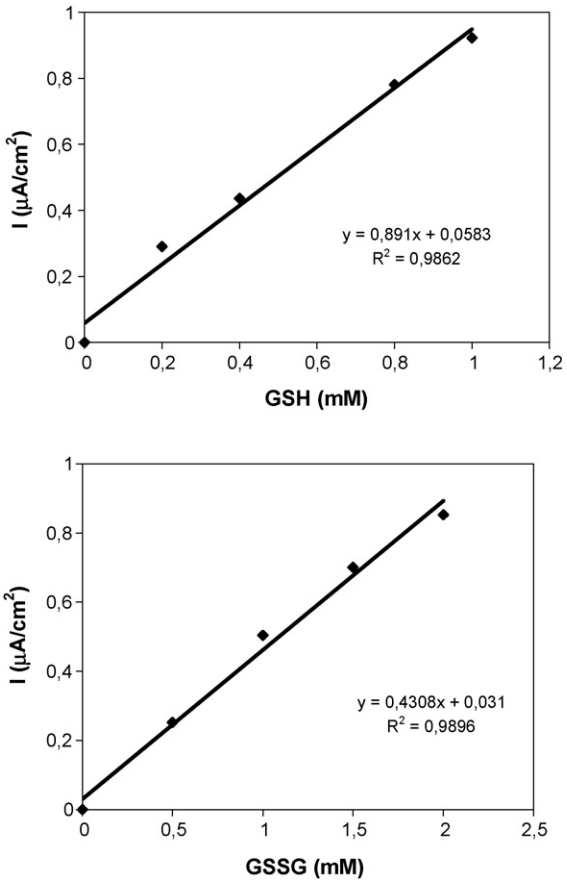

Fig. 3. Calibration graph for the GSH and GSSG determination (in phosphate buffer; 50 mM, pH 6.5, 30 °C, −0.7 V; NADPH: 2 μM).

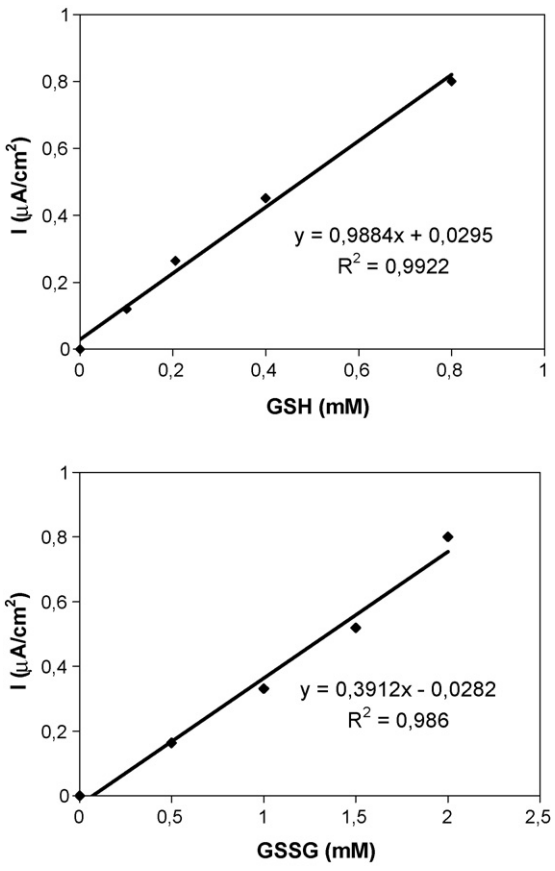

Fig. 4. Detection of GSH and GSSG after HPLC separation by GR-SOX biosensor as an electrochemical detector (−0.7 V; NADPH: 2 μM).

ilar data were obtained in terms of linearity (0.25 and 1.5 mM for GSSG and 0.125 and 1.5 mM for GSH, respectively) and the equation of linear graphs with Ref. [21]. These calibration graphs were used in sample application to estimate the glutathione amounts in blood sample as a reference method.

Furthermore, calibration graphs were obtained for GSSG and GSH that were applied to HPLC and analyzed by bienzyme biosensor as a biodetector. In this case linearity was obtained in concentration range between 0.1 and 0.8 mM for GSH and between 0.5 and 2.0 mM for GSSG (Fig. 4).

Chromatograms obtained by DAD resulting from injection of a GSH and GSSG mixture were presented in Fig. 5. The flow rate of the mobile phase was optimized to yield both good chromatographic resolution and electrode responses. Lower flow rates caused peak broadening. A flow rate of 1.4 ml/min caused quite acceptable results with better peak symmetry. Running the system at higher flow rates did not exhibit further advance. Hence, a flow rate of 1.4 ml/min was chosen as the optimal flow rate.

3.4. Sample application

In order to observe the sample matrix effects for glutathione analysis, standard addition method was used. Denaturized blood sample was prepared as described in Section 2 and used as stock solution. Initially, samples were applied to HPLC under the optimized conditions and analyzed by both DAD and biosensing system. DAD was used as a reference to evaluate these findings. In case of using biosensor system, when the samples passed through the column and reached to the reaction cell, changes in the response were recorded.

Finally, obtained signals from both DAD and biosensor systems were converted to the concentration values via GSH and GSSG calibration curves. Data for blank (non-spiked) and spiked samples were compared in terms of recoveries (Table 1). As shown in the table, recovery values were very similar to 100%. As a result, it can be concluded that the nature of sample does not affect the measurements. As a result developed

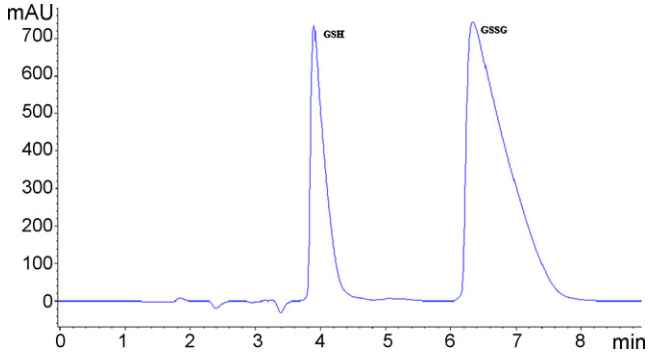

Fig. 5. Chromatogram of standard mixed reduced/oxidized glutathione [GSH and GSSG: 1.5 mM]. Chromatographic separation was performed according to the conditions described in Section 2.5.

Table 1
Application of glutathione biosensor to human blood sample after HPLC separation

	Amount of glutathione in sample (mM)[a] (C_0)	Added glutathione (mM)[a] (C_{add})	Detected glutathione (mM)[a] (C_{tot})	% Recovery $(C_{tot} - C_0)/C_{add}$
DAD[b]				
GSH	0.156	1.00	1.10 ± 0.06	94
GSSG	0.013	0.266	0.271 ± 0.0034	97
GR-SOX biosensor				
GSH	N.D	0.20	0.21 ± 0.014	105
GSSG	N.D	0.50	0.50 ± 0.0282	100

N.D: Not detected. All results are given as value ± S.D, $n = 3$ or 4.

[a] Glutathione concentration were calculated using the standard curves obtained for each substrate.

[b] For the detection by DAD system, calibration graphs with the following equations were used for GSH and GSSG analysis ($y = 6921.3x$ and $y = 25460x$, x and y shows substrate concentration, mM and peak area, mAus, respectively) [21].

biosensor shows promising results to be used in the analysis of glutathione in both oxidized and reduced forms without requiring any laborious derivatization steps.

4. Conclusion

An amperometric biosensor based on the immobilization of two enzymes is developed both for GSSG and GSH detection. Glutathione reductase and sulfhydryl oxidase were immobilized onto a graphite electrode and the change in current density due to the oxygen consumption was monitored. The obtained data confirm the most attractive property of the new system which is the possibility to detect subsequently two different substrates without application of any complex treatment procedure prior to the measuring step. Hence they proved that the proposed biosensor is a simple, practical and sensitive tool for GSSG and GSH analysis. Because of these attractive properties, developed bi-enzymatic electrode in combination with HPLC separation can be accepted as an alternative method for GSSG and GSH detection.

Acknowledgements

The Scientific and Technological Research Council of Turkey (TUBITAK; Project No: 104T453) and Ege University Research and Application Center of Science and Technology (EBILTEM) are acknowledged for the financial support. D. Odaci acknowledges the scholarship obtained from TUBITAK with the same project number.

References

[1] F. Ricci, F. Arduini, C.S. Tuta, U. Sozzo, D. Moscone, A. Amine, G. Palleschi, Anal. Chim. Acta 558 (2006) 164.
[2] R. Possari, R.F. Carvalhal, R.K. Mendes, L.T. Kubota, Anal. Chim. Acta 575 (2006) 172.
[3] Z.P. Li, X.R. Duan, C.H. Liu, B.A. Du, Anal. Biochem. 351 (2006) 18.
[4] D. Potesil, J. Petrlova, V. Adam, J. Vacek, B. Klejdus, J. Zehnalek, L. Trnkova, L. Havel, R. Kizek, J. Chromatogr. A 1084 (2005) 134.
[5] J.J. Haddad, Cell. Signal. 14 (2002) 799.
[6] K. Kino, S. Kuratsu, A. Noguchi, M. Kokubo, Y. Nakazawa, T. Arai, M. Yagasaki, K. Kirimura, Biochem. Biophys. Res. Commun. 352 (2007) 351.
[7] L. Rhazi, R. Cazalis, E. Lemelin, T. Aussenac, Plant Physiol. Biochem. 41 (2003) 895.
[8] G. Potters, L. De Gara, H. Asard, N. Horemans, Plant Physiol. Biochem. 40 (2002) 537.
[9] M. Erat, M. Ciftci, K. Gumustekin, M. Gul, Eur. J. Pharmacol. 554 (2007) 92.
[10] G.G. Yannarelli, A.J. Fernandez-Alvarez, D.M. Santa-Cruz, M.L. Tomaro, Phytochemistry 68 (2007) 505.
[11] L.K. Rogers, C.M. Bates, S.E. Welty, C.V. Smith, Toxicol. Appl. Pharmacol. 217 (2006) 289.
[12] R.M.L. Galera, J.C. Juárez Giménez, J.B. Montoro Ronsano, R.M. Segura Cardona, M.A. Arbós Via, C. Altisent Roca, J.M. Tusell Puigbert, Clin. Chim. Acta 254 (1) (1996) 63.
[13] R.L. Mosley, E.J. Benner, I. Kadiu, M. Thomas, M.D. Boska, K. Hasan, C. Laurie, H.E. Gendelman, Clin. Neurosci. Res. 6 (2006) 261.
[14] C.B. Pocernicha, R. Sultanaa, H. Mohmmad-Abdula, A. Nath, D.A. Butterfielda, Brain Res. Rev. 50 (2005) 14.
[15] Y. Zhua, P.M. Carveya, Z. Linga, Brain Res. 1090 (2006) 35.
[16] A. McCaddon, P. Hudson, D. Hill, J. Barber, A. Lloyd, G. Davies, B. Regland, Biol. Psychiatry 53 (2003) 254.
[17] M. Valko, D. Leibfritz, J. Moncol, M.T.D. Cronin, M. Mazur, J. Telser, Int. J. Biochem. Cell Biol. 39 (2007) 44.
[18] A. Pastore, G. Federici, E. Bertin, F. Piemonte, Clin. Chim. Acta 333 (2003) 19.
[19] W. Yang, S.E. Toffa, J.W.G. Lohn, A.M. Seifalian, M.C. Winslet, Gynecol. Oncol. 96 (2005) 430.
[20] P.M. Abuja, R. Albertini, Clin. Chim. Acta 306 (2001) 1.
[21] S. Timur, D. Odaci, A. Dincer, F. Zihnioglu, A. Telefoncu, L. Gorton, Sens. Actuators, B 125 (2007) 234.
[22] P.G. Winyard, C.J. Moody, C. Jacob, Trends Biochem. Sci. 30 (8) (2005) 453.
[23] S. Raje, N.M. Glynn, C. Thorpe, Anal. Biochem. 307 (2002) 266.
[24] S. Matsuba, Y. Suga, K. Ishidoh, Y. Hashimoto, K. Takamori, E. Kominami, B. Wilhelm, J. Seitz, H. Ogawa, J. Dermatol. Sci. 30 (2002) 50.
[25] H.E. Swaisgood, Trends Biochem. Sci. 23 (2005) 71.
[26] J.E. Lee, G. Hofhaus, T. Lisowsky, FEBS Lett. 477 (2000) 62.
[27] M. Yang, Y. Yang, B. Liu, G. Shen, R. Yu, Sens. Actuators B 101 (2004) 269.
[28] S. Timur, Y. Yigzaw, L. Gorton, Sens. Actuators B 113 (2006) 684.
[29] B. Krajewska, Enzyme Microb. Technol. 35 (2004) 126.
[30] B. Klejdus, J. Zehnálek, V. Adam, J. Petek, R. Kizek, J. Vacek, L. Trnková, R. Rozik, L. Havel, V. Kubá, Anal. Chim. Acta 520 (2004) 117.
[31] J. Vaceka, J. Petriek, R. Kizek, L. Havel, B. Klejdus, L. Trnkova, F. Jelen, Bioelectrochemistry 63 (2004) 347.
[32] H. Wang, W.S. Wang, H.S. Zhang, Spectrochim. Acta Part A 57 (2001) 2403.
[33] R. Kandar, P. Zakova, H. Lotkova, O. Ku¡cera, Z. Cervinkova, J. Pharmaceut. Biomed. 43 (2007) 1382.
[34] A.E. Katrusiak, P.G. Paterson, H. Kamencic, A. Shoker, A.W. Lyon, J. Chromatogr. B 758 (2001) 207.
[35] R. Rellán-Álvarez, L.E. Hernández, J. Abadía, A. Álvarez-Fernández, Anal. Biochem. 356 (2006) 254.

[36] E. Camera, M. Picardo, J. Chromatogr. B 781 (2002) 181.
[37] M.F.S. Teixeira, E.R. Dockal, E.T.G. Cavalheiro, Sens. Actuators B 106 (2005) 619.
[38] A. Salimi, S. Pourbeyram, Talanta 60 (2003) 205.
[39] P. Calvo-Marzal, K.Y. Chumbimuni-Torres, N.F. Höehr, L.T. Kubota, Clin. Chim. Acta 371 (2006) 152.
[40] A. Salimi, R. Hallaj, Talanta 66 (2005) 967.
[41] L. Rover Jr., L.T. Kubota, N.F. Hoehr, Clin. Chim. Acta 308 (2001) 55.
[42] W. Jin, Y. Wang, Anal. Chim. Acta 343 (1997) 23l.
[43] B. Filanovsky, Anal. Chim. Acta 394 (1999) 91.
[44] P. Calvo-Marzal, K.Y. Chumbimuni-Torres, N.F. Hoer, G. Oliveira Neto, L.T. Kubota, Sens. Actuators B 100 (2004) 337.
[45] M.A. Bayorh, A.A. Ganafa, R.R. Socci, N. Silvestrov, I.K. Abukhalaf, Am. J. Hypertens. 17 (2004) 31.

Available online at www.sciencedirect.com
ScienceDirect
Talanta 74 (2008) 1428–1434
Talanta
www.elsevier.com/locate/talanta

Simultaneous determination of bromide and nitrate in contaminated waters by ion chromatography using amperometry and absorbance detectors

K. Tirumalesh *

Isotope Applications Division, Bhabha Atomic Research Centre, Mumbai 400085, India

Received 28 June 2007; received in revised form 17 September 2007; accepted 21 September 2007
Available online 29 September 2007

Abstract

This study describes a new ion chromatography method using a low-capacity anion exchange column with amperometric and absorbance detection for rapid and simultaneous determination of Br^- and NO_3^- in contaminated waters where one of these ions is present in excess compared to other. The use of two detectors overcomes the problem of baseline separation for Br^- and NO_3^- for accurate quantification, which was commonly encountered when using a low-capacity anion exchange column and suppressed conductivity detection mode. The method achieved accurate quantification of these two ions without requirement of baseline separation. The accuracy of 2.8% for NO_3^- was determined using a quality control sample obtained from UN GEMS/Water PE Study No. 6. The detection limits for Br^- and NO_3^- were 20 and 6 $\mu g\,l^{-1}$ (25 μl sample), respectively. Linearity of these two ions was over three orders of magnitude with a correlation coefficient >0.998. The influence of potential interfering ions was also studied followed by the determination of Br^- and NO_3^- in seawater, unsaturated zone water, soil extract and groundwater.
© 2007 Elsevier B.V. All rights reserved.

Keywords: Ion chromatography; Bromide; Nitrate; Amperometry; UV absorbance detector

1. Introduction

Water quality has received considerable attention over the last few decades due to serious surface and groundwater contamination by anthropogenic and natural contaminants. Anthropogenic activities like agriculture, sewage and industrial effluents have elevated toxic contaminants in surface water and shallow groundwater. The indiscriminate exploitation of the groundwater in coastal aquifers has resulted in seawater intrusion or upconing of deep seated saline water resulting in the deterioration of water quality. Identification of contaminant source can help in the determination of the potential impact of contaminants on water supplies, the development of management practices to preserve water quality and its decontamination.

Bromide and nitrate can serve as indicators of seawater intrusion and agricultural activities, respectively. Determination of bromide is of importance as it is considered as a conservative tracer for identifying seawater intrusion into coastal aquifers [1,2]. In general, bromide in normal groundwater lie below 0.1 $mg\,l^{-1}$ but waters contaminated by seawater intrusion, evaporite dissolution or oil field brines show very high concentration of bromide [3,4]. Nitrate in potable water is found to be <0.1 to 10 $mg\,l^{-1}$. Presence of high nitrate content in water reflects pollution from organic matter or synthetic fertilizers or manures [5]. Fertilizers, animal husbandry, liquid and solid industrial wastes also increase soluble nitrogen compounds in water. Intense cultivation may lead to very high levels of nitrate in groundwater. Nitrate is also considered as one of the important substances to be determined in water as its consumption through water or food results in health related problems in human beings. The permissible limit for nitrate in drinking water is 50 $mg\,l^{-1}$ [6]. Hence determination of these ions in water will be helpful in finding the possible source of contamination.

Determination of these anions (Br^- and NO_3^-) from different matrices has been performed using ion chromatography (IC) by many investigators [7–10], which involves separation of ions on an ion exchange column followed by suppressor column and a conductivity detector. These methods require a resolution of $R = 1.5$ for accurate quantification of the analyte ions. In general it is observed that peak resolution is inadequate

* Correspondence address: Water Resource Development Section, Isotope Applications Division, Trombay, Mumbai 400085, India. Tel.: +91 22 25590177; fax: +91 22 25505151.
E-mail address: tirumal@barc.gov.in.

0039-9140/$ – see front matter © 2007 Elsevier B.V. All rights reserved.
doi:10.1016/j.talanta.2007.09.021

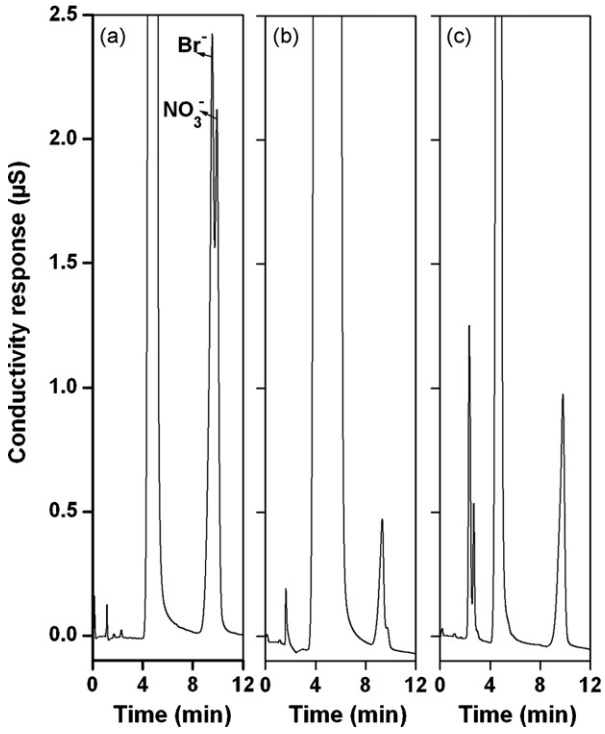

Fig. 1. Typical chromatograms of (a) lab standard (Cl^-, Br^- and NO_3^- are 50, 7.5 and 5 mg l^{-1}, respectively), (b) diluted seawater and (c) saline water samples in suppressed conductivity mode using 25 μl sample loop, 1 mM NaOH eluent and Dionex IonPac AG 11 + AS 11 analytical column. Br^- and NO_3^- peaks elute at about 10 min.

especially in the case of Br^- and NO_3^- using a low-capacity anion exchange column in suppressed conductivity detection mode [11–16] and it becomes difficult to determine these ion concentrations accurately in some contaminated water samples, where one of these ions is present in excess compared to other. Typical chromatograms of lab standard (a mixture of Cl^-, Br^- and NO_3^- in 50, 7.5 and 5 mg l^{-1} concentrations, respectively) and field samples (diluted seawater and saline groundwater) are shown in Fig. 1. Bromide and nitrate peaks are either merged or show poor resolution in the case of field samples. Since the resolution is insufficient in this type of contaminated samples (peaks close together or shoulder peaks, etc.) quantification is prone to error. Baseline separation is of great advantage from the quantitative point of view and it can be attained by adjusting the nature and strength of eluent composition. Though the eluent concentration strongly affects the retention behavior of ions, it has little effect on selectivity of ions of same charge and the selectivity modification works mainly with high-capacity columns [17]. It was observed that there is no considerable improvement in the baseline separation of Br^- and NO_3^- peaks by decreasing the eluent concentration, on the contrary, the sensitivity was severely affected. Large errors in quantification were observed especially when the difference between these ion concentrations is high. Even computer-assisted models fail to quantify the peaks in this case. Some researchers have used high-capacity anion ion exchanging columns and UV or conductivity detectors to determine anions in aqueous samples [18–22]. These methods were either applicable for fresh water samples [18,22] or suffer interference by high nitrate concentrations (>100 mg l^{-1}) [19] or involve chemical modification of the reverse phase columns [20].

None of the papers attempted the applicability of a combination of UV and amperometric detection methods for accurate determination of bromide and nitrate simultaneously using low-capacity anion exchange columns.

Several studies have reported the application of electrochemical detector (DC Amperometry) for determination of oxidizable species like Cl^-, Br^-, I^-, SCN^-, $S_2O_3^{2-}$ and S^{2-} in aqueous samples [23–27]. In DC amperometry, a constant voltage is applied to the working electrode and the resulting current due to ion oxidation or reduction is monitored. Analyte concentration is calculated from the predetermined calibration equation obtained from amperometric response and known analyte concentration. It is observed that bromide ion is detected at Ag-electrode with increased sensitivity at +0.3 V in amperometric cell, whereas nitrate ion produces no signal.

UV absorbance detectors, generally used for organic compounds, were not considered to be equally sensitive for the detection of several inorganic ions but studies by several authors [28,29] demonstrated that these detectors are also sensitive to inorganic and organic anions. Inorganic anions like Br^-, I^-, NO_3^-, NO_2^-, etc. have large extinction coefficients between 195 and 215 nm to make UV absorbance detection a useful analysis technique for these ions [30]. Both Br^- and NO_3^- exhibit useful UV absorbance at 210 nm and direct monitoring of UV absorbance is the most straightforward mode of detection for these ions [31,32].

This paper demonstrates the applicability of a low-capacity anion exchange column (Dionex AG11 + AS11) for the simultaneous determination of bromide and nitrate in contaminated waters. The developed method was applied for the determination of Br^- and NO_3^- in seawater (bromide ion dominated), unsaturated zone samples and soil extracts (nitrate ion dominated) and groundwaters from coastal aquifer (both nitrate and bromide ions are present).

2. Experimental setup

All the analyses were conducted on Dionex ion chromatography equipment (DX-500) consisting of a gradient pump (GP 40), Rheodyne injection port, anion trap column (ATC), anion guard column (AG 11, 4 mm), anion separating column (AS 11, 4 mm), anion self-regenerating suppressor unit (ASRS-ULTRA, 4 mm), electrochemical detector (ED 40), UV–vis absorbance detector (AD 20) and auto-sampler (AS 40). A Dionex Peaknet (version 5.01) chromatography workstation was used for system control and data collection. The experimental conditions used for the determination of Br^- and NO_3^- are given in Table 1.

2.1. Reagents

All the chemicals used were of analytical grade quality (Fluka and Merck). Standards were prepared daily by diluting 1000 mg l^{-1} ICP standard solutions. Mobile phase (3 mM NaOH) was prepared from 50% (w/w) sodium hydroxide aque-

Table 1
Experimental conditions for Br^- and NO_3^- determination in IC

Analytical separation	
Column	Dionex IonPac AG 11 + AS 11
Mobile phase	3 mM NaOH
Flow rate	1 ml min^{-1}
Injection volume	25 μl
Column backpressure	850 psi
Electrochemical detector	
Working electrode	Ag
Operating potential	+0.3 V
Reference electrode	pH electrode
Counter electrode	Titanium cell body
Detector scale	±500 nA
Background current	42 nA
Chemical suppression	
Regenerant	25 mM H_2SO_4
Flow rate	5–7 ml min^{-1}
UV–vis absorbance detector	
Wavelength	210 nm
Background absorbance	80 mAU

ous solution. The mobile phase and standard solutions were prepared using deionised water of 18.2 MΩ cm resistivity (Barnstead).

2.2. Sample preparation

All water samples were filtered through 0.45 μm Nylon-66 membrane filter, degassed under vacuum and stored in prewashed polyethylene bottles. Seawater was diluted by 50-folds in order to avoid column over loading. Soil extracts were prepared by placing 5 g of dried soil, collected from an agricultural site, in a 100 ml beaker with water added to 50 ml and were kept for overnight and filtered before injection. Unsaturated samples were collected from Lysimeters.

2.3. Procedure

The schematic representation of the ion chromatography setup comprising of the electrochemical detector, the chemical suppressor and the UV detector is shown in Fig. 2. The sample was loaded via an auto-sampler (AS 40) on a 25 μl sample loop. After injection, the separation of the analyte ions takes place on a low-capacity analytical separating column (AS 11) by running a hydroxide eluent (3 mM NaOH). The separated ions with the eluent pass through the amperometric detector where the current due to Br^- was recorded and the NO_3^- was not electroactive at this voltage. Then the ions with eluent flow through anion suppressor unit, where the hydroxide eluent converts to water and the analyte ions to corresponding acids. This leads to enhanced sensitivity of UV detection as the eluent is UV absorbing in its deprotonated state [17,31]. Since both Br^- and NO_3^- are UV active, the peak registered by the UV detector is the summation of the two ions.

3. Results and discussion

3.1. Optimization of mobile phase concentration

Different concentrations of the NaOH mobile phase were tried in order to achieve proper separation of bromide peak from chloride peak so that in the case of saline water samples high amounts of chloride does not overlap with bromide peak. A 3 mM NaOH was found to be appropriate for this purpose and at this strength bromide and nitrate ions co-elute after about 5 min from injection.

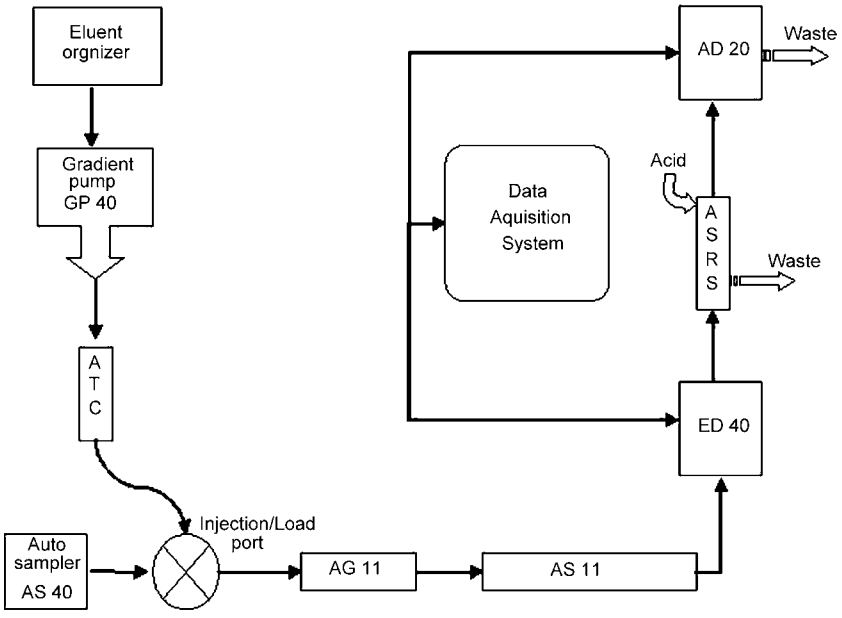

Fig. 2. Schematic representation of the ion chromatography setup used for simultaneous determination Br^- and NO_3^-.

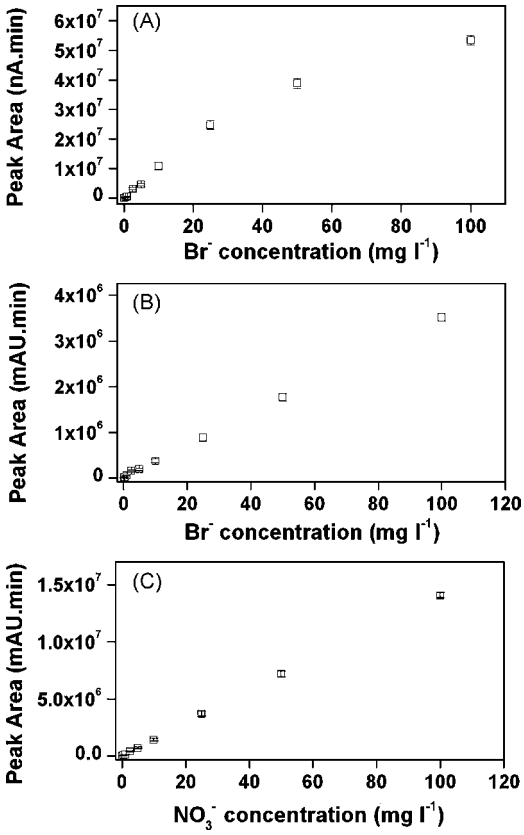

Fig. 3. Calibration plots of Br^- and $NO_3{}^-$ in amperometric and UV detectors. Error bars represent $\pm 2\sigma$ limits.

3.2. Calibration and detection limits

Calibrations were done for bromide and nitrate ions separately. Standard solutions of Br^- and $NO_3{}^-$ of different concentrations were analyzed using this method and the peak areas in amperometry and UV detectors were determined and corresponding response factors (R^f, slope of the calibration equation) were calculated for quantification purpose. It was found that bromide ion concentration above 30 mg l^{-1} shows saturation in the amperometry detector (Fig. 3a), hence the measurements were restricted only up to 25 mg l^{-1}. A linear calibration curve for standard Br^- solution in the range 0.1–25 mg l^{-1} was obtained. In the case of UV detection, linearity was observed up to 100 mg l^{-1} for both the Br^- and $NO_3{}^-$ (Fig. 3b and c). Linearity of these two ions was over three orders of magnitude with a correlation coefficient >0.998 in both the detectors. Detection limits for Br^- and $NO_3{}^-$ were calculated as the concentration corresponding to three times the peak height of the baseline noise, whereas quantification limits were set as 10 times the noise height. Table 2 shows the summary of the calibration data comprising calibration range, slope of calibration equation (R^f), correlation coefficient, detection and quantification limits.

3.3. Quantification of Br^- and $NO_3{}^-$ ions

As the peak area in amperometry detector corresponds to bromide concentration, it can be quantified simply by the following equation.

$$\mathrm{Br}^-_{\mathrm{conc}} = \frac{A_{\mathrm{Br,AMP}}}{R^{\mathrm{f}}_{\mathrm{Br,AMP}}} \tag{1}$$

where $\mathrm{Br}^-_{\mathrm{conc}}$ is the concentration of bromide ion in water sample, $R^{\mathrm{f}}_{\mathrm{Br,AMP}}$ is the response factor and $A_{\mathrm{Br,AMP}}$ is the peak area of Br^- in amperometry detector. Bromide ion peak area in UV detector is calculated using its response factor in UV detector and bromide ion concentration obtained from amperometry detector.

$$A_{\mathrm{Br,UV}} = R^{\mathrm{f}}_{\mathrm{Br,UV}} \times \mathrm{Br}^-_{\mathrm{conc}} \tag{2}$$

where $A_{\mathrm{Br,UV}}$ is peak area and $R^{\mathrm{f}}_{\mathrm{Br,UV}}$ is response factor of bromide in UV detector.

Since the peak area in UV detector is the summation of both Br^- and $NO_3{}^-$ peak areas, $NO_3{}^-$ peak area is calculated by subtraction of Br^- peak area from total peak area and corresponding $NO_3{}^-$ concentration is calculated from its response factor in UV detector.

$$A_{\mathrm{T,UV}} = A_{\mathrm{Br,UV}} + A_{\mathrm{NO_3,UV}} \tag{3}$$

$$A_{\mathrm{NO_3,UV}} = R^{\mathrm{f}}_{\mathrm{NO_3,UV}} \times \mathrm{NO_{3(conc)}}^- \tag{4}$$

where $A_{\mathrm{T,UV}}$ is the total peak area and $A_{\mathrm{NO_3,UV}}$, $R^{\mathrm{f}}_{\mathrm{NO_3,UV}}$ and $\mathrm{NO_{3(conc)}}^-$ are peak area, response factor and nitrate ion concentration in absorbance detector, respectively. From the above four equations, $NO_3{}^-$ concentration can be calculated using the following equation,

$$\mathrm{NO_{3(conc)}}^- = \frac{A_{\mathrm{T,UV}} - (R^{\mathrm{f}}_{\mathrm{Br,UV}} \times A_{\mathrm{Br,AMP}}/R^{\mathrm{f}}_{\mathrm{Br,AMP}})}{R^{\mathrm{f}}_{\mathrm{NO_3,UV}}} \tag{5}$$

Different concentrations of standard bromide solutions were analyzed using both UV and amperometry detectors to compare the results obtained from these detectors. Bromide concentrations were calculated using corresponding response factors

Table 2
Calibration parameters of Br^- and $NO_3{}^-$ in amperometric and UV detectors

Analyte	Detector	Calibration range (mg l^{-1})	Slope of calibration equation	Correlation coefficient (r^2)	Detection limit (mg l^{-1})	Quantification limit (mg l^{-1})
Bromide	Amperometry	0.1–25	999577[a]	0.998	0.030	0.10
Bromide	UV	0.1–100	35226[b]	0.999	0.020	0.08
Nitrate	UV	0.1–100	141679[b]	0.999	0.006	0.02

[a] nA min l mg^{-1}.
[b] mAU min l mg^{-1}.

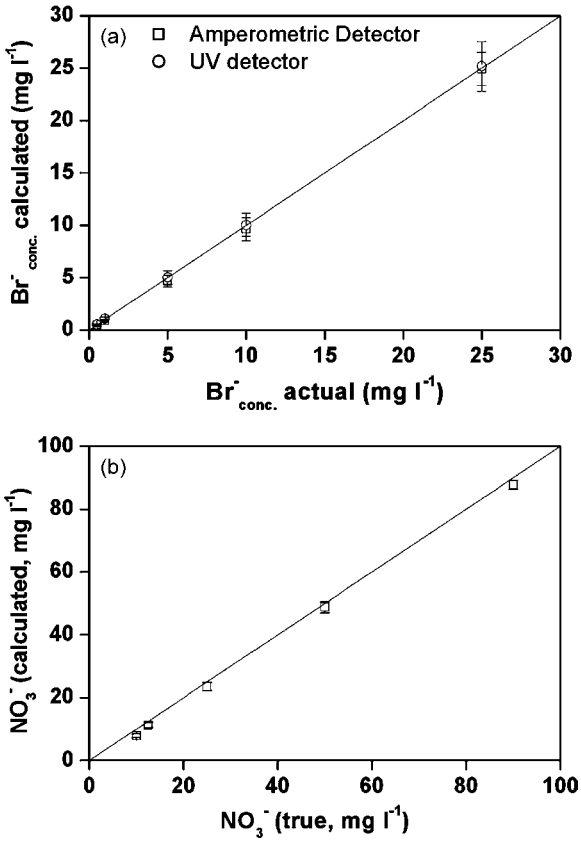

Fig. 4. (a) Plot of Br^- concentration observed in amperometric and UV detectors against its true concentration and (b) plot of NO_3^- concentration calculated vs. its true value. Solid line indicates line of slope one and error bars represent $\pm 2\sigma$ limits.

given in Table 2 and the results obtained from these two detectors match with the true values as shown in Fig. 4a. Similarly to check the validity of the Eq. (5), solutions containing various proportions of Br^- and NO_3^- were analyzed and the peak area in amperometry and UV detectors were noted. Using the response factors given in Table 2 and applying Eq. (5), nitrate ion concentrations were calculated. It was found that calculated nitrate concentrations match very well with that of actual nitrate concentrations (Fig. 4b). Nitrate results were also cross-checked by analyzing quality control (QC) sample obtained from UN GEMS/Water PE Study No. 6 (under IAEA inter-laboratory exercise, RAS/8/097). Average concentration of nitrate as nitrogen (N-NO_3) in QC sample of 10 determinations was 4.24 ± 0.15 as against certified values of 4.36 ± 0.00295. Here the uncertainty was expressed as two times the standard deviation (σ) divided by the square root of the number of determinations (i.e. $2\sigma/\sqrt{n}$).

3.4. Reproducibility and interferences

The relative standard deviations (R.S.D.) were calculated from the experimental data obtained over a period of 1 month. The R.S.D. ($n = 25$) of Br^- at 1 mg l^{-1} concentration is 4.1 and 4.6% in amperometry and UV detectors, respectively, whereas NO_3^- in UV detector showed a R.S.D. ($n = 25$) of 3.5% at

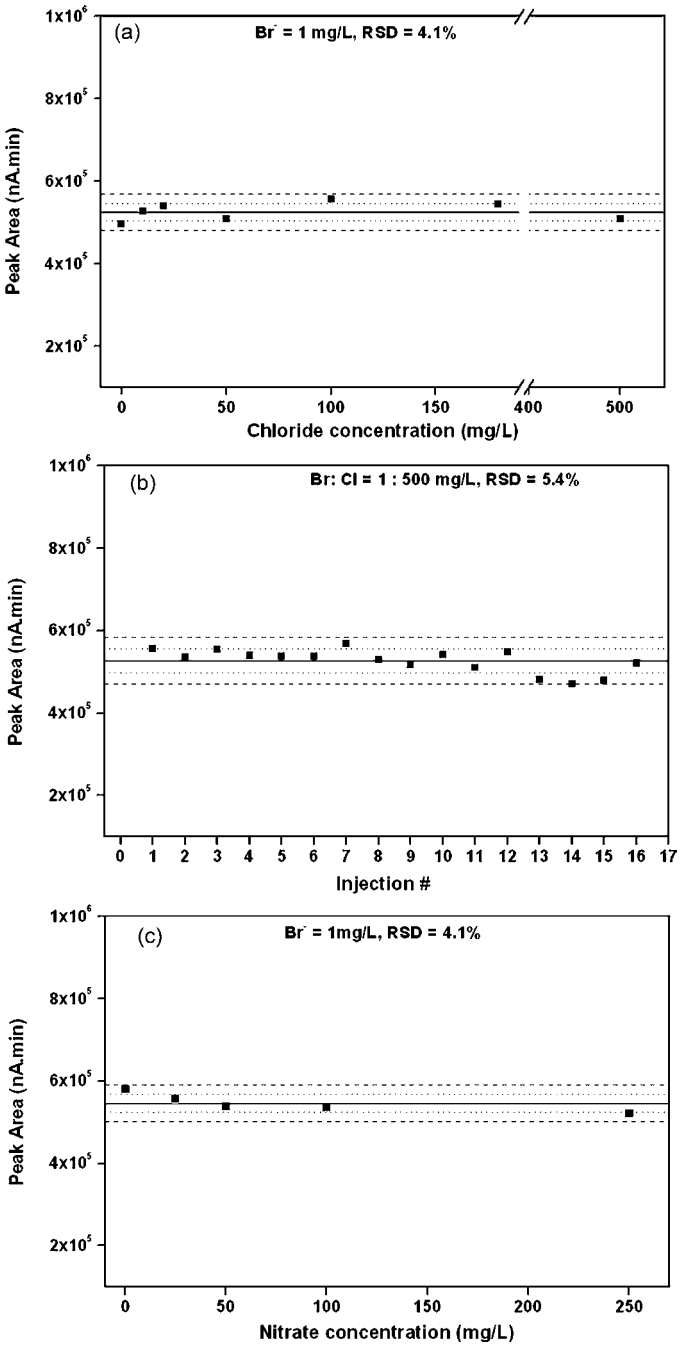

Fig. 5. (a and b) Effect of Cl^- and (c) NO_3^- concentrations on Br^- determination in amperometric detector. Solid line indicates average peak area whereas dotted and dashed lines show $\pm 1\sigma$ and $\pm 2\sigma$ confidence levels.

1 mg l^{-1} concentration. Interferences by chloride ion might be significant in the case of saline groundwaters as Ag-electrode in amperometry detector forms AgCl precipitate and deposits on the surface of the electrode, which can hamper the Br^- signal. To find out the effect of chloride interference on Br^- peak, varying amounts of chloride was added into a solution of fixed bromide concentration (1 mg l^{-1}) and peak area was noted. It is observed that bromide peak area data falls within $\pm 2\sigma$ confidence levels (Fig. 5a). Repetitive injections of a solution containing Br^- and Cl^- in the ratio 1:500 mg l^{-1} also showed that Br^- peak area data

fall within $\pm 2\sigma$ confidence levels (Fig. 5b). Interference due to nitrate concentration was also checked in similar manner. Even in this case Br^- peak area data fall within $\pm 2\sigma$ confidence levels (Fig. 5c). A close look at the data indicates a decreasing trend in Br^- peak area with increasing NO_3^- concentration. This is due to negative peak of nitrate ion which can be attributed to nitrate reduction at high concentration, however, NO_3^- concentration up to 250 mg l^{-1} does not affect the results significantly.

Bromide and nitrate concentrations can be determined accurately in water samples having Br^-/NO_3^- ratio of the order of 0.05–250.

3.5. Application to field sample and validation

In order to test the reliability of the proposed method, the method was applied to the determination of bromide and nitrate in a few field samples such as unsaturated zone sample, soil extract, diluted seawater and groundwaters from a coastal aquifer. The groundwater sample (GW-4) was diluted 10-folds in order to avoid column over loading by high chloride present in the sample. The results are tabulated in Table 3. From the results, it can be seen that groundwaters collected from a coastal aquifer are contaminated by both agricultural activities and seawater whereas unsaturated zone samples and soil extract show high nitrate levels. Typical chromatograms (amperometric and UV detectors) of some field samples are shown in Fig. 6. The recovery of Br^- and NO_3^- in the samples was checked by addition of standard Br^- and NO_3^- solutions separately into these samples (seawater sample was diluted by 50 times whereas all other samples were diluted by 10 times by deionised water) and the results were shown in Table 4. The Br^- and NO_3^- recoveries were ranging from 93 to 119% and 84 to 109%, respectively.

Table 3
Br^- and NO_3^- concentrations of some field samples

Sample description	Br^-	NO_3^-
DSW-1	1.0	0.13
DSW-2	0.9	0.04
DSW-3	0.8	0.05
UZW-1	1.5	103
UZW-2	1.0	85.8
UZW-3	2.0	85.8
SE-1	1.2	50.8
SE-2	0.8	42.6
SE-3	0.6	51.7
GW-1	12.0	36.7
GW-2	14.9	3.5
GW-3	10.5	1.0
GW-4	2.4	4.8

Note: All concentrations in mg l^{-1} with a R.S.D. of 5%. DSW, UZW, SE and GW refer to diluted seawater, unsaturated zone water, soil extract and groundwater, respectively. Seawater and GW-4 samples are diluted 50 times and 10 times, respectively.

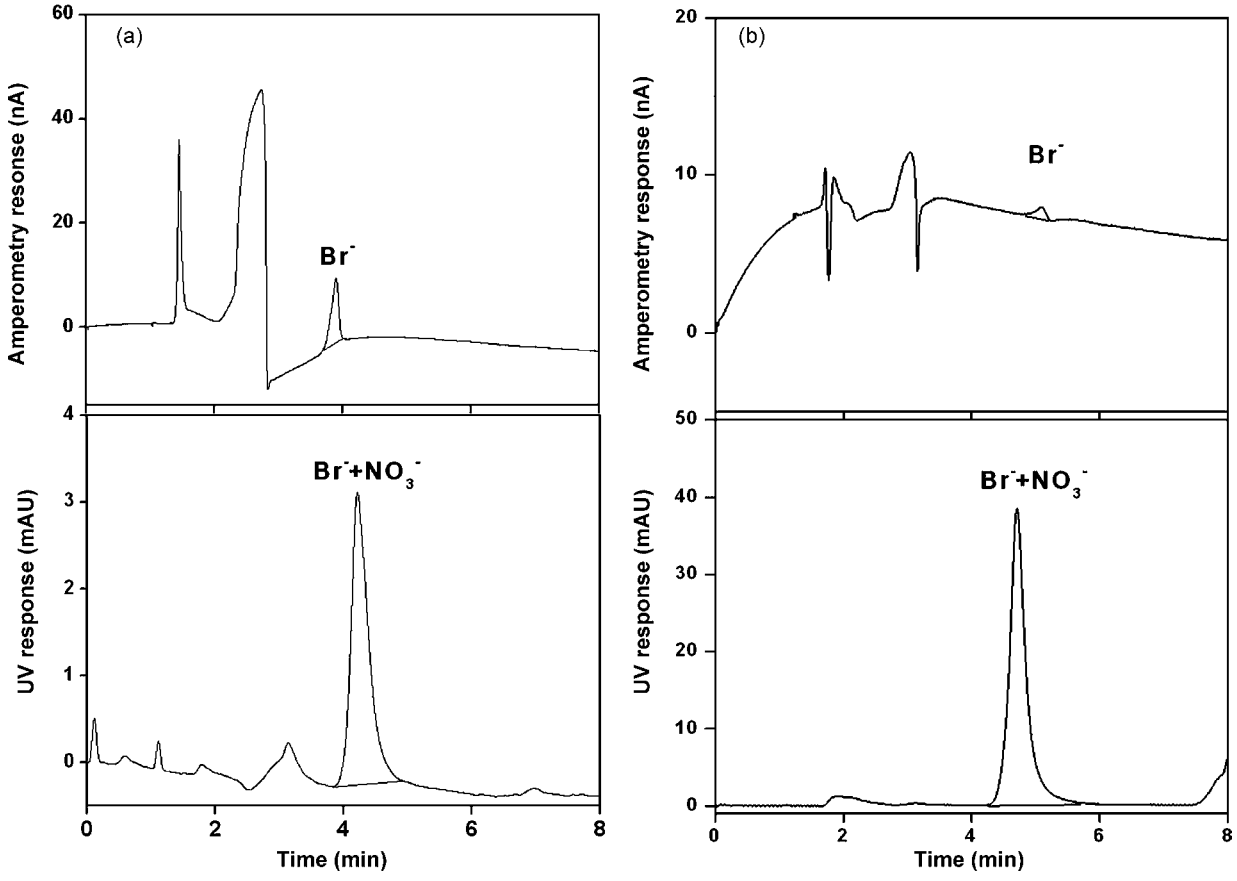

Fig. 6. Typical chromatograms (amperometry and UV detectors) of (a) diluted seawater and (b) soil extract samples.

Table 4
Recoveries of Br^- and NO_3^- concentrations in some field samples

S. No.	Sample	Bromide concentration ($mg\,l^{-1}$)			Nitrate concentration ($mg\,l^{-1}$)		
		Found mean $\pm\,\sigma$	Added	%Recovery	Found mean $\pm\,\sigma$	Added	%Recovery
1	Seawater	1.06 ± 0.06	1.00	119	0.13 ± 0.01	0.50	90
2	Unsaturated zone water	0.20 ± 0.02	0.50	97	8.58 ± 0.32	5.00	84
3	Soil extract	0.12 ± 0.01	0.50	98	5.08 ± 0.21	5.00	97
4	Groundwater	2.45 ± 0.15	5.00	93	4.80 ± 0.20	5.00	109

Concentrations expressed are mean of the 10 determinations. Seawater was diluted to 50-folds and other samples by 10-folds.

4. Conclusions

A new method is optimized using ion chromatography system on a low-capacity AS 11 column coupled with amperometry detector and UV absorbance detector which provides a simple, accurate, precise and sensitive approach for the determination of bromide and nitrate in water samples. The use of two detectors overcomes the problem of baseline separation for Br^- and NO_3^- for accurate quantification, which was commonly encountered when using AS 11 column and suppressed conductivity detection mode. This method is tested with synthetic samples and the range of linear relationships of these ions was found to be over three orders of magnitude of concentration and their correlation coefficients were >0.998. The detection limits of these ions were as low as $0.03\,mg\,l^{-1}$ (25 μl sample). No chloride and nitrate interferences were found at given concentrations. This method is further applied to the determination of Br^- and NO_3^- in some field samples. The results were precise and the recoveries were within acceptable range.

All the above results indicate that the proposed method is a useful approach with satisfactory sensitivity and stability for the simultaneous determination of Br^- and NO_3^- by ion chromatography using amperometry and UV absorbance detectors.

Acknowledgements

Author is grateful to Dr. K. Shivanna, Head, Water Resources Development Section and Dr. Gursharan Singh, Head, Isotope Applications Division for their co-operation and Dr. K.L. Ramakumar Head, Radioanalytical Chemistry Section for his valuable suggestions. Thanks are also due to Shri K. Sudarshan of Radiochemistry Division for helping in deriving the equations and Shri U.P Kulkarni of my section for proving soil and lysimeter samples.

References

[1] B.F. Jones, A. Vengosh, E. Rosenthal, Y. Yechilieli, Geochemical Investigations, in: J. Bear, A.H.-D. Cheng, S. Sorek, D. Ouazar, I. Herrera (Eds.), Seawater Intrusion in Coastal Aquifers—Concepts, Methods and Practices, vol. 14, Kluwer Academic Publishers, Netherlands, 1999, pp. 51–71.
[2] W.A. Hounslow, Water Quality Data-Analysis and Interpretation, Lewis Publishers, New York, 1995, p. 54.
[3] G. Matthess, The Properties of Groundwater, Wiley-Interscience publication, John Wiley & Sons, New York, 1982.
[4] B.K. Handa, J. Appl. Hydrol. II 1 (1989) 27.
[5] B. Hitchon, E.H. Perkins, W.D. Gunter, Introduction to Ground Water Geochemistry, Geoscience Publishing Ltd., Alberta, 1999.
[6] C.A.J. Appelo, D. Postma, Geochemistry, Groundwater and Pollution, A.A. Balkema, Netherlands, 1999.
[7] H. Small, T. Stevens, W. Bauman, Anal. Chem. 47 (1975) 1801.
[8] J.A. Morales, L.S. de Graterol, J. Mesa, J. Chromatogr. A 884 (2000) 185.
[9] P.E. Jackson, C. Weigert, C.A. Pohl, C. Saini, J. Chromatogr. A 884 (2000) 175.
[10] G. Schminke, A. Seubert, J. Chromatogr. A 890 (2000) 295.
[11] Dionex Corporation, Installation Instructions and Trouble Shooting Guide for the Ionpac AG 11 Guard Column and Ionpac AS 11 Analytical Column, Document No. 034791, Revision 04, 1998.
[12] Dionex Corporation, Installation Instructions and Trouble Shooting Guide for the Ionpac AG 12A Guard Column and Ionpac AS 12A Analytical Column, Document No. 034975, Revision 06, 2002.
[13] Dionex Corporation, Installation Instructions and Trouble Shooting Guide for the Ionpac AG 14 Guard Column and Ionpac AS 14 Analytical Column, Document No. 031199, Revision 06, 2003.
[14] Dionex Corporation, Installation Instructions and Trouble Shooting Guide for the Ionpac AG 17 Guard Column and Ionpac AS 17 Analytical Column, Document No. 031529, Revision 02, 2002.
[15] Metrohm, IC anion columns for analyses with chemical suppression, Phenomenex Star Ion A300 (6.1005.100), p. 19.
[16] Metrohm, IC anion columns for analyses with chemical suppression, Metrosep A Supp (6.1005.300), p. 21.
[17] C.A. Lucy, P. Hatsis, Ion Chromaography, in: E. Heftmann (Ed.), Chromatography, sixth ed., Fundamentals and Applications of Chromatography and Related Differential Migration Methods, Part A: fundamentals and techniques, J. chromatogr. Library, vol. 69A, Elsevier, 2004, pp. 171–211.
[18] E.N. Kapinus, I.A. Revelsky, V.O. Ulogov, Y.A. Lyalikov, J. Chromatogr. B 800 (2004) 321.
[19] E. Salhi, U. Gunten, Water Res. 33 (1999) 3239.
[20] W.Z. Hu, P.R. Haddad, K. Tanaka, S.J. Sato, M. Mori, Q. Xu, M. Ikedo, S. Tanaka, J. Chromatogr. A 1039 (2004) 59.
[21] S. Carrozzino, F. Righini, J. Chromatogr. 706 (1995) 277.
[22] Z.Q. Lu, Y. Liu, V. Barreto, C. Pohl, N. Avdalovic, R. Joyce, B. Newton, J. Chromatogr. A 956 (2002) 129.
[23] S. Seefeld, U. Baltensperger, Anal. Chim. Acta 283 (1993) 246.
[24] G. James Tarter, Anal. Chem. 56 (1984) 1264.
[25] K. Han, F.K. William, W.K. Pratt, Anal. Chem. 59 (1987) 731.
[26] C.Y. Wang, B.D. Scott, G. James Tarter, Anal. Chem. 55 (1983) 1617.
[27] R.D. Rocklin, L. Edward Johnson, Anal. Chem. 55 (1983) 4.
[28] J. Cortes Hernan, J. Chromatogr. A 234 (1982) 517.
[29] F.A.J. Armstrong, Anal. Chem. 35 (1963) 1292.
[30] J. Klaus Stetzenbach, M. Glenn Thompson, Ground Water 21 (1983) 36.
[31] J. Richard Williams, Anal. Chem. 55 (1983) 851.
[32] R.C. Hoather, R.F. Rackham, Analyst 84 (1959) 548.

Available online at www.sciencedirect.com
ScienceDirect
Talanta 74 (2008) 1191–1200
Talanta
www.elsevier.com/locate/talanta

Electroanalytical investigation and determination of pefloxacin in pharmaceuticals and serum at boron-doped diamond and glassy carbon electrodes

Bengi Uslu, Burcu Dogan Topal, Sibel A. Ozkan *

Ankara University, Faculty of Pharmacy, Department of Analytical Chemistry, 06100 Tandogan-Ankara, Turkey

Received 12 April 2007; received in revised form 9 August 2007; accepted 24 August 2007
Available online 30 August 2007

Abstract

The anodic behavior and determination of pefloxacin on boron-doped diamond and glassy carbon electrodes were investigated using cyclic, linear sweep, differential pulse and square wave voltammetric techniques. In cyclic voltammetry, pefloxacin shows one main irreversible oxidation peak and additional one irreversible ill-defined wave depending on pH values for both electrodes. The results indicate that the process of pefloxacin is irreversible and diffusion controlled on boron-doped diamond electrode and irreversible but adsorption controlled on glassy carbon electrode. The peak current is found to be linear over the range of concentration 2×10^{-6} to 2×10^{-4} M in 0.5 M H_2SO_4 at about +1.20 V (versus Ag/AgCl) for differential pulse and square wave voltammetric technique using boron-doped diamond electrode. The repeatability, reproducibility, precision and accuracy of the methods in all media were investigated. Selectivity, precision and accuracy of the developed methods were also checked by recovery studies. The procedures were successfully applied to the determination of the drug in pharmaceutical dosage forms and humans serum samples with good recovery results. No electroactive interferences from the excipients and endogenous substances were found in the pharmaceutical dosage forms and biological samples, respectively.
© 2007 Elsevier B.V. All rights reserved.

Keywords: Pefloxacin; Voltammetry; Boron-doped diamond electrode; Glassy carbon electrode; Pharmaceuticals; Serum samples

1. Introduction

Pefloxacin (PEF) is a medication belonging to the antibiotic group known as fluoroquinolones. The fluoroquinolones are a family of broad-spectrum antibiotics. PEF is the member of second generation of the quinolone group antibiotics. They are bactericidal drugs, actively killing bacteria or preventing their growth. Flouroquinolones such as pefloxacin possess excellent activity against gram-negative aerobic bacteria such as *Escherichia coli* and *Neisseria gonorrhoea* as well as gram-positive bacteria including *Streptococcus pneumoniae* and *Staphylococcus aureus*. This group of antibiotics inhibit the bacterial DNA gyrase or the topoisomeraze II enzyme, thereby inhibiting DNA replication and transcription. PEF should have a bactericidal effect [1,2]. PEF is given by mouth or by intravenous infusion in the treatment of susceptible infections. It is well absorbed by the oral route. Its bio-availability is 100% and it has a long plasma half-life. Peak plasma levels are reached in 1–1.5 h. Peak serum levels of 3.8–6.6 $\mu g\,mL^{-1}$ after a single dose of 400 mg. About 20–30% of PEF is bound to plasma proteins [2]. About 85–90% of PEF is metabolized into *N*-desmethyl pefloxacin in the liver. *N*-desmethyl pefloxacin (norfloxacin) which is the main and active metabolite of PEF, has a very similar structure like PEF. PEF is available as the mesylate salt [1,2] (Scheme 1).

PEF has been studied and determined by several procedures: HPLC for the determination of PEF in pharmaceutical dosage forms [3,4] and in milk [5], spectrophotometric [6–12] and spectrofluorimetric [13–17] analysis, flow injection analysis [18,19], capillary electrophoresis method [20]. All these reported methods are either not sufficiently sensitive or tedious and require highly sophisticated instrumentation.

The voltammetric techniques offered the possibility for the sensitive estimation of PEF. Reviewing the literature revealed that, up to the present time, electrochemical studies on the determination of PEF are scarce with cathodic stripping voltammetric

* Corresponding author. Fax: +90 312 223 82 43.
E-mail address: ozkan@pharmacy.ankara.edu.tr (S.A. Ozkan).

0039-9140/$ – see front matter © 2007 Elsevier B.V. All rights reserved.
doi:10.1016/j.talanta.2007.08.023

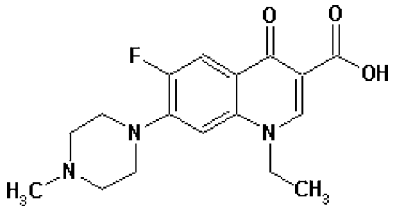

Scheme 1. The chemical structure of pefloxacin.

method using hanging mercury drop electrode [21] and voltammetric method using dsDNA modified electrode [9]. However, nothing has been published concerning the electrooxidative behavior of PEF at solid electrodes.

The widespread use of PEF and the need for clinical and pharmacological study require fast and sensitive analytical techniques to assay the presence of the drug in pharmaceutical dosage forms and biological samples. Already published methods show that there are no methods for the determination of PEF in biological samples on solid electrodes except spiked urine [9] and serum [21] sample applications.

To the best of our knowledge, no electrochemical oxidative assay has been performed on pefloxacin using boron-doped diamond electrode. Also, there have been no studies published related to the electrochemical oxidation details and voltammetric determination of PEF at diamond electrode neither from pharmaceutical dosage forms nor in biological samples.

In the last decades modern computer-based voltammetric techniques have been used to realize the determination of organic chemicals in diverse types of samples, especially pharmaceutical field [22–24]. The advance in experimental electrochemical techniques in the field of drug analysis is because of their simplicity, low cost, and relatively short analysis times no need for derivatizations or time-consuming extraction steps when compared with other techniques. Also electroanalytical methods are less sensitive to matrix effects than other analytical techniques [25,26]. Additional application of electrochemistry includes the determination of electrode mechanism. Redox properties of the drug molecules can give insights into their metabolic fate or their in vivo redox processes or pharmacological activity [23].

Boron-doped diamond electrodes (BDDE) are used as useful alternatives to other carbon-based electrodes. Glassy carbon electrodes are the most common carbon-based electrodes in current use. However, the use of diamond electrodes in electroanalytical chemistry is in its infancy, but the results obtained to date indicate a bright future for this advanced material. Diamond electrodes open up new opportunities for work under extreme conditions such as at extremely high anodic potentials, in chemically extremely aggressive media, e.g. strongly acidic media, and are now available commercially in polycrystalline boron-doped form. Because of its extraordinary chemical stability, diamond undoubtedly is a promising candidate as an electrode material. Compared to classical carbon electrodes and other metallic electrodes, boron-doped diamond electrodes differ by their excellent chemical inertness and chemical stability that enable their use in extreme chemical environments such as strongly acidic media [27].

The aim of this study was to establish the experimental conditions, to investigate the voltammetric behavior and possible oxidation mechanism of PEF on BDD using cyclic, linear sweep, square wave and differential pulse voltammetric techniques. In this study, the results of the boron-doped diamond electrode (BDDE) are compared with the results of the glassy carbon electrode. This work was also aimed to development of new, fully validated, rapid, selective and simple voltammetric methods for the direct determination of PEF in raw materials, pharmaceutical dosage forms and spiked human serum samples without any time-consuming extraction, separation, evaporation or adsorption steps prior to drug assay. The proposed methods might be alternatives to the LC techniques in therapeutic drug monitoring or the experimental data might be used for the development LC–EC method.

2. Experimental

2.1. Apparatus

Electrochemical measurements were carried out using a BAS 100 W (Bioanalytical system, USA) electrochemical analyzer. A conventional three-electrode cell with an Ag/AgCl (BAS; 3 M KCl) reference and a Pt wire counter, and a glassy carbon (BAS; Ø 3 mm, diameter) and boron-doped diamond (Windsor Scientific Ltd.; Ø 3 mm, diameter) working electrodes was used. A standard one-compartment three-electrode cell of 10 mL capacity was used in all experiments. Before each experiments the glassy carbon and BDD electrodes were polished manually with aqueous slurry of alumina powder (Ø 0.01 μm) on a damp smooth polishing cloth (BAS velvet polishing pad). All experiments were realized at room temperature.

The pH measurements were made using a Model 538, WTW pH-meter (Austria) with a combined electrode (glass-reference electrodes) with an accuracy of ±0.05 pH.

Operating conditions for DPV were: pulse amplitude, 50 mV; pulse width, 50 ms; scan rate, 20 mV s^{-1}; for SWV: pulse amplitude, 25 mV; frequency, 15 Hz; potential step, 4 mV.

2.2. Reagents

Pefloxacin mesylate (PEF) and its pharmaceutical dosage forms Peflacine® coated tablets and injectable forms containing PEF (400 mg per tablet and 400 mg (5 mL)$^{-1}$ for injectable preparations) were supplied from Eczacıbaşı Pharm. Comp. (Istanbul, Turkey).

All chemicals for preparation of buffers and supporting electrolytes, such as H_2SO_4, H_3PO_4, NaH_2PO_4, Na_2HPO_4, H_3BO_3, CH_3COOH, and NaOH were reagent grade (Merck or Sigma). Stock solutions of PEF (1×10^{-3} M) were prepared in distilled water and kept in the dark in refrigerator. Five different type of supporting electrolytes, were used in this study. Working solutions under, voltammetric investigation were prepared by the direct dilution of the stock solution with the selected supporting electrolytes just before use. H_2SO_4 (0.1 and 0.5 M), 0.2 M phosphate buffer at pH 2.0; 6.0; 8.0, 0.2 M acetate buffer at pH 3.60–5.70; 0.04 M Britton–Robinson buffer at pH 2.0–12.0 and

0.15 M borate buffer at pH 10.0 were used for supporting electrolyte. The calibration equation for DPV and SWV techniques was constructed by plotting the peak current against PEF concentration. The diluted solutions were prepared daily by accurate dilution with the selected supporting electrolyte before use and should be protect from light. All solutions were kept in the dark in a refrigerator and used within several hours to avoid hydrolysis. PEF solutions were stable and their concentration did not change with time. All measurements were carried out ambient temperature of the laboratory (23–27 °C).

The ruggedness and precision were checked at different days and results were given as repeatability (within day) and reproducibility (between days). Relative standard deviations were calculated to check the ruggedness and precision of the method [28–31].

2.3. Pharmaceutical dosage forms assay procedure

Ten tablets of Peflacine® (each tablet contains 400 mg pefloxacin mesylate) were weighed accurately and finely powdered by pestle in a mortar. An adequate amount of this powder, equivalent to a stock solution of concentration 1×10^{-3} M, was weighed, transferred into a 50-mL calibrated flask and completed to volume with bidistilled water. The content of the flask were sonicated for 10 min to affect complete dissolution. The non-dissolved excipients were waited for settle down. The sample from the clear supernatant liquor was withdrawn and quantitatively diluted with the selected supporting electrolyte. This solution was then transferred to a voltammetric cell and DP and SW voltammograms were recorded. The nominal content of the tablet amounts were calculated from the corresponding regression equations of previously plotted calibration plots.

In case of injectable ampoule dosage form, no sample preparation required for this dosage form. The necessary volume (accurately pipetted) of this dosage form, corresponding to a stock solution of concentration ca. 1×10^{-3} M was transferred to a 50-mL calibrated flask and complete to the volume with bidistilled water. Aliquots volume were taken from this stock solution and diluted with the selected supporting electrolyte injectable dosage form samples were then transferred to a voltammetric cell and voltammograms were recorded. The drug content (400 mg (5 mL)$^{-1}$) was determined referring to the related regression equations.

2.4. Recovery studies

Because other components of the matrix of the pharmaceutical dosage forms may interfere with the analysis or accurate quantitation of the analyte, potential effects from matrix components must be investigated. If no adequate placebo can be prepared, a known amount of drug substance can also be added to an authentic batch of drug product (standard addition). In this case, recovery experiments are performed in the presence of the real matrix [28–31]. To study the accuracy, reproducibility and to check the interference from the excipients used in the formulations of these techniques, recovery experiments were carried out using the standard addition method. In order to know whether the excipients show any interference with the analysis, known amounts of the PEF were added to the pre-analyzed tablet and injectable dosage forms. The mixtures were analyzed by the DP and SW voltammetric techniques. For both techniques, after five repeated experiments, the recovery results were obtained.

2.5. Analysis of spiked serum samples

Drug-free human blood, obtained from healthy volunteers (after obtaining their written consent), was centrifuged (5000 rpm) for 30 min at room temperature and separated serum samples were stored frozen until assay. An aliquot volume of serum sample was fortified with PEF dissolved in bidistilled water to achieve final concentration of 1×10^{-3} M. Acetonitrile removes serum proteins more effectively, as the addition of 1–1.5 volumes of serum is sufficient to remove the proteins. After vortexing for 45 s, the mixture was then centrifuged for 10 min at 5000 rpm for getting rid of serum protein residues and the supernatant was taken carefully. Appropriate volumes of this supernatant were transferred into the volumetric flask and diluted up to the volume with the selected supporting electrolyte. The concentration of PEF was varied in the range of 2×10^{-6} to 2×10^{-4} M in human serum samples. Quantifications were performed by means of the calibration curve method from the related calibration equations.

3. Results and discussion

PEF appears to be an electroactive drug for both directions. Specifically, PEF is capable to be both, oxidizable and reducible. The cathodic determination of PEF has been studied using hanging mercury drop electrode (HMDE) by Beltagi et al. [21]. However, no previous electrooxidative behavior was reported concerning the boron-doped diamond electrode of PEF. To demonstrate the usefulness of a solid electrode for determination of PEF, which may offer advantages for the use of such electrodes as sensors, the electrochemical behavior of PEF on a diamond and glassy carbon electrode were investigated in this research. As a first step PEF was subjected to a cyclic and linear sweep voltammetric studies with the aim of the detailed characterizing its electrochemical oxidation behavior, on the BDD and glassy carbon electrodes, and to a voltammetric study in the differential pulse and square wave modes. Therefore, the electrochemical behavior of PEF was studied over a wide pH range (1.0–12.0) at a BDD and glassy carbon disc electrodes in buffered aqueous media.

The cyclic voltammetric behavior of PEF yielded on well-defined peak in all media and all pH values and one ill-defined wave depending on the pH and supporting electrolyte nature for both electrodes (Fig. 1A and B). Cyclic voltammetric measurements showed an irreversible nature of the oxidation process for both electrodes. The scanning was started at −0.20 V in the positive direction in 0.5 M H_2SO_4 and at pH 5.65 acetate buffer, the anodic oxidation of PEF did not occur until about +1.20 and +0.85V for BDD and glassy carbon electrodes, respectively (Fig. 2a and b). By reversing at high potentials no reduction wave or peak corresponding to the anodic peak

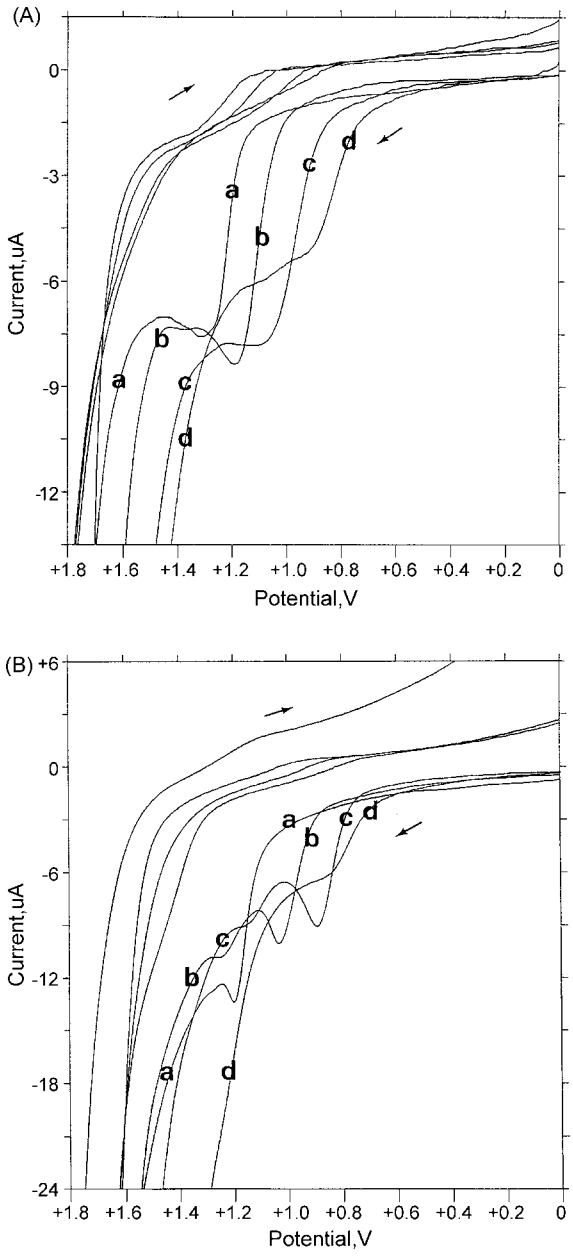

Fig. 1. Cyclic voltammograms of 8×10^{-5} M pefloxacin in 0.5 M H_2SO_4 (a), acetate buffer at pH 4.10 (b), phosphate buffer at pH 6.00 (c), Britton–Robinson buffer at pH 9.00 (d) obtained with glassy carbon electrode (A) and obtained with BDDE (B). Scan rate 100 mV s^{-1}.

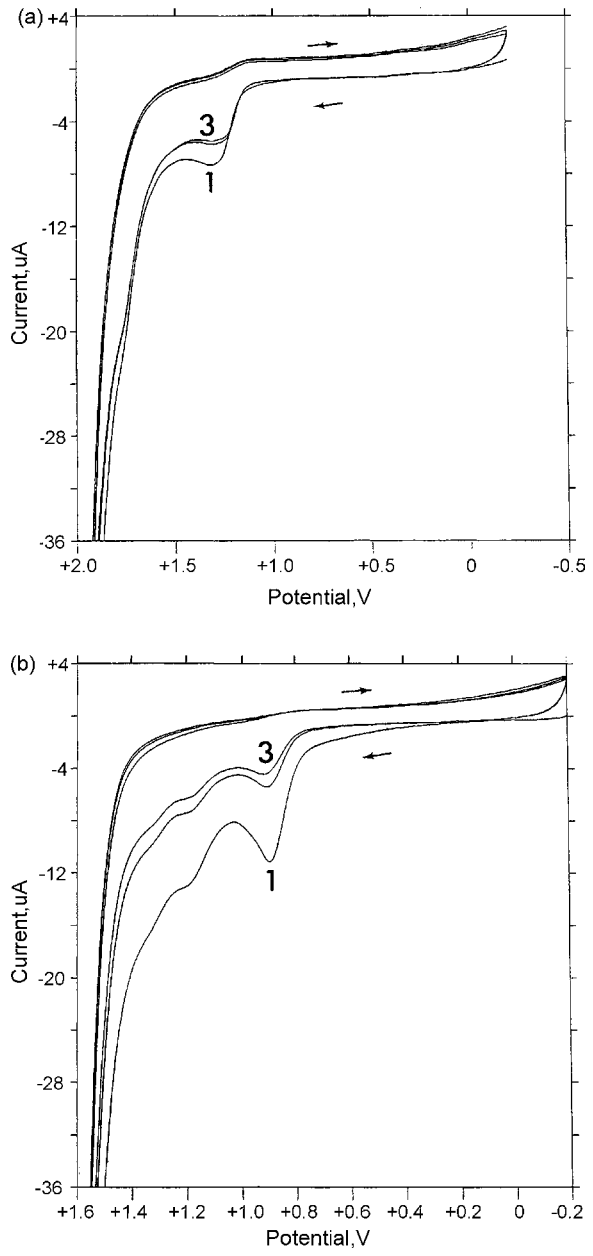

Fig. 2. Multisweep cyclic voltammograms of 8×10^{-5} M pefloxacin solutions in 0.5 M H_2SO_4 for BDDE (a), in acetate buffer at pH 5.65 for glassy carbon electrode (b). Scan rate 100 mV s^{-1}. The numbers indicate the number of scans.

was observed on the cathodic branch for both electrodes. It was observed that at the second and higher cycles the PEF peak and wave decreased (Fig. 2). This phenomenon may be partly attributed to the consumption of adsorbed PEF on the electrode surface.

The effect of pH on peak potential and peak intensity were studied using CV, DPV and SWV techniques for both electrodes, between pH 1.0 and 12.0. All obtained graphs from CV, DPV and SWV were found similar. For this reason, only CV results for the main oxidation step was given as E_p–pH and I_p–pH graph as Fig. 3a and b, and Fig. 4a and b for glassy carbon and BDD electrodes, respectively. In all instances and using all techniques, PEF undergoes one main irreversible oxidation process, which shifted towards less positive potentials as the pH was increased for both electrodes. It is a general rule that a conjugate base is oxidized at less positive potentials than the corresponding acid form. Thus the observed pH dependence indicates that the electroactive group which is corresponding to the PEF oxidation peak is in acid–base equilibrium with pK_a about 7.0. Above pH 7.0 the peak potential nearly becomes pH independent (Fig. 3a and 4a). This intersection point of the curves is close to the both pK_a values of PEF. The pK_{a1} and pK_{a2} values are 6.3 and 7.6, respectively [32]. It seems that the electroactive grouping responsible for the oxidation process is in acid–base equilibrium with pK_a of about 7.0. At pH > pK_a the conjugate base predominates in

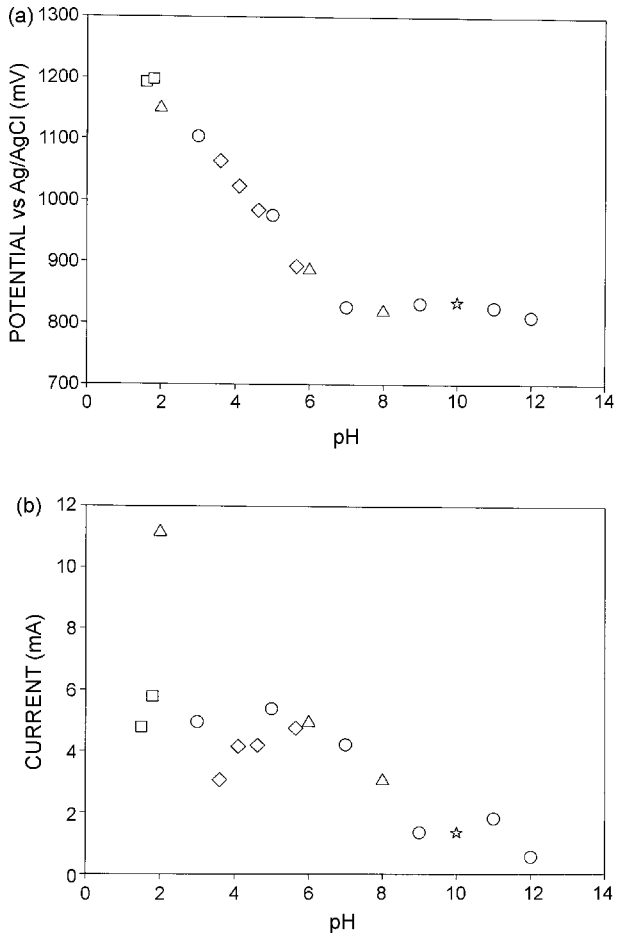

Fig. 3. Effects of pH on pefloxacin anodic peak potential (a) and peak current (b); pefloxacin concentration 8×10^{-5} M: 0.1 and 0.5 M H_2SO_4 (□), 0.04 M Britton–Robinson (◯), 0.2 M acetate (◊), 0.2 M phosphate (△), and borate (☆) buffers obtained with glassy carbon electrode.

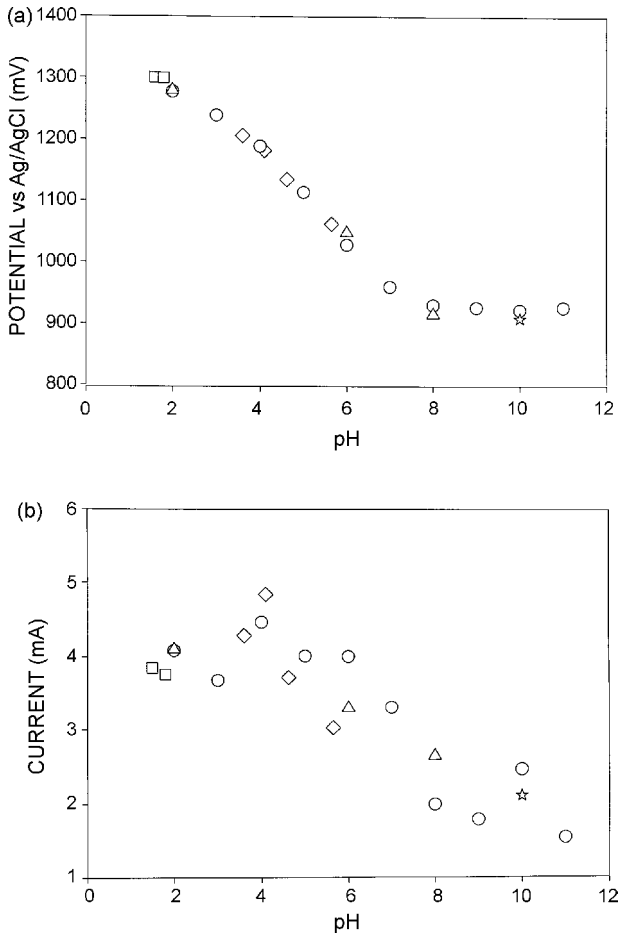

Fig. 4. Effects of pH on pefloxacin anodic peak potential (a) and peak current (b); pefloxacin concentration 8×10^{-5} M: 0.1 and 0.5 M H_2SO_4 (□), 0.04 M Britton–Robinson (◯), 0.2 M acetate (◊), 0.2 M phosphate (△), and borate (☆) buffers obtained with BDD electrode.

the supporting electrolyte. The pH-independent zone above pH 7 means that there are no proton transfer steps before the electron transfer rate-determining step. Since, no dissociation occurs before the electron transfer rate-determining step, the oxidation potential remains pH-independent for both electrodes. At $pH < pK_a$, the conjugate base must be formed by a rapid dissociation of the protonated form. Two linear regions intersect at about pH 7. The increase in the slope at pH <7 indicates the presence of an antecedent acid–base equilibrium with pK_a of about 7.0 which is supposed to correspond to the pK_a value of the piperazine moiety [33]. These results strongly prove that in PEF, the monoprotonated form of piperazine ring is oxidized. According to the Fig. 4a and 5a, the plot of the peak potential versus pH showed a straight line between pH 1.6 and 7.0 on glassy carbon and BDD electrodes, which can be expressed by the following equations:

$$E_p\ (\text{mV}) = 1308.72\text{–}69.82\text{pH}, \quad r = 0.996 \quad \text{(for glassy carbon electrode);}$$

$$E_p\ (\text{mV}) = 1418.62\text{–}62.69\text{pH}, \quad r = 0.991 \quad \text{(for BDD electrode)}$$

The linearity was observed in the pH range 1.6–7.0, giving a negative slope of approximately 65 mV per pH unit for both electrodes. The intersection observed in the plot between pH 1.6 and 7.0 can be explained by changes in protonation of the acid–base functions in the molecule.

The influence of pH on the PEF current at glassy carbon and BDD electrodes was also studied. The I_p versus pH plot shows that peak current is maximum in the acidic pH (Fig. 3b and 4b) for both electrodes. The experimental results showed that shapes of the curve and the maximum peak current were better in acetate buffer at 5.65 and 0.5 M H_2SO_4 for glassy carbon and acetate buffer at 4.10 and 0.5 M H_2SO_4 for BDDE (Fig. 3b and 4b). However, after detailed studies in 0.5 M H_2SO_4 and acetate buffer, the best medium was selected as 0.5 M H_2SO_4. In acetate buffer, the peak was split to two peaks with increasing concentrations. Therefore, we have not been able to obtain good linear responses in acetate buffer. At the end of all these experiments, 0.5 M H_2SO_4 was chosen with respect to sharp response and single and better peak shape for the calibration curve for quantitative determination in dosage forms and biological media.

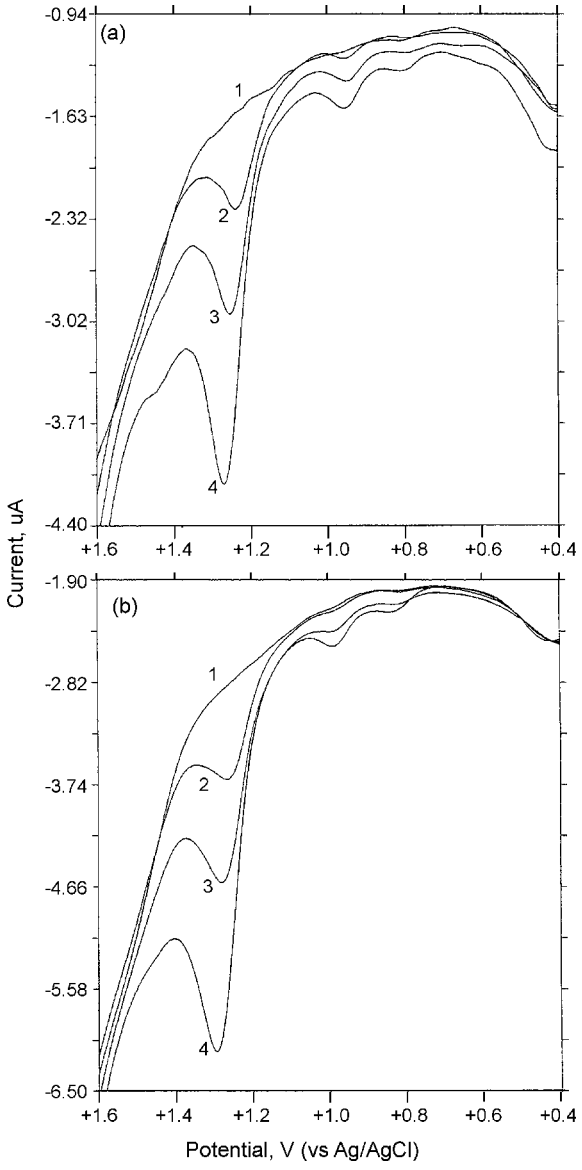

Fig. 5. Differential pulse (a) and square wave (b) voltammograms obtained for the determination in spiked serum (1) blank, (2) 2×10^{-5} M, (3) 4×10^{-5} M, (4) 8×10^{-5} M pefloxacin in 0.5 M H_2SO_4.

Scan rate studies were carried out to assess whether the processes at the glassy carbon electrode was under diffusion or adsorption control. The effect of the potential scan rate between 5 and 1000 mV s^{-1} on the peak current and potential of PEF were evaluated for both electrodes in different supporting electrolytes. The 77 and 110 mV positive shifts in the peak potential together with the absence at the cathodic wave in cyclic voltammetry confirmed the irreversibility of the oxidation process for glassy carbon and BDD electrodes, respectively. When the scan rate was varied from 5 to 1000 mV s^{-1} in 8×10^{-5} M PEF solution, a linear dependence of the peak current I_p (μA) upon the square root of the scan rate $v^{1/2}$ (mV s^{-1}) was found for BDDE, demonstrating a diffusional behavior. The equation is noted below in 0.5 M H_2SO_4:

$$I_p\ (\mu A) = 0.32 v^{1/2}\ (\text{mV s}^{-1}) + 0.0013, \quad r = 0.999 \quad (n = 10)$$

In contrast to this, in the same scan rate region and in 8×10^{-5} M PEF solution, a linear dependence was found for the peak current I_p (μA) upon the scan rate v (mV s^{-1}) was found for glassy carbon electrode, confirmed an adsorptional behavior. This equation is noted below in acetate buffer at pH 5.65:

$$I_p\ (\mu A) = 0.04 v\ (\text{mV s}^{-1}) + 0.6547, \quad r = 0.999 \quad (n = 10)$$

A plot of logarithm of peak current versus logarithm of scan rate gave a straight line with a slope of 0.49 for BDDE and 0.83 for glassy carbon electrode, close to the theoretical value of 0.5 and 1.0, respectively, which expressed for an ideal reaction the diffusion controlled electrode process for BDDE and for an ideal reaction the adsorption controlled electrode process for glassy carbon electrodes [34].

The equations obtained are:

$$\text{Log } I_p\ (\mu A) = 0.49 \log v\ (\text{mV s}^{-1}) - 0.47,$$

$r = 0.998$ $(n = 10)$ for boron-doped diamond electrode

and $\text{Log } I_p\ (\mu A) = 0.83 \log v\ (\text{mV s}^{-1}) - 0.95,$

$r = 0.997$ $(n = 10)$ for glassy carbon electrode

The Tafel plots (log I versus E) was obtained with a scan rate of 5 mV s^{-1} beginning from a steady-state potential in 0.5 M H_2SO_4 and acetate buffer at pH 5.65 for BDD and glassy carbon electrodes, respectively. The α_n value of anodic reaction from the slope of the linear part of the Tafel plot was found to be as 0.26 and 0.30 for boron-doped diamond and glassy carbon electrodes, respectively. The exchange current density (I_o) is 2.04×10^{-8} μA cm^{-2} and 2.69×10^{-7} μA cm^{-2} for BDD and glassy carbon electrodes. These values together with the absence of cathodic waves and positive shift in the peak potential with the scan rate indicated the irreversibility of the oxidation reaction on both electrodes. The effect of scan rate on peak potential was investigated in the sweep range 10–1000 and 5–1000 mV s^{-1} for glassy carbon and BDD electrodes, respectively. The relation between E_p and log v can be expressed by the equations:

$$E_p\ (\text{mV}) = 42.73 \log v + 813.95, \quad r = 0.990 \quad \text{(for glassy carbon electrode);}$$

$$E_p\ (\text{mV}) = 56.42 \log v + 1186.90, \quad r = 0.991 \quad \text{(for BDDE)}$$

The plot of E_p versus log v was linear with correlation coefficient of 0.990 and 0.991 for glassy carbon and BDD electrodes, respectively. This behavior of both electrodes is consistent with the EC nature of the reaction in which the electrode reaction is coupled with an irreversible follow-up chemical step [35,36].

To identify the grouping responsible for the oxidation process and to support the working hypothesis, the oxidation of PEF was compared to that of some model compounds. Nefazodone, vardenafil, piribedil, enoxacin, trazodone, and quatiapine are oxidized over most of pH range, producing one well defined, main irreversible oxidation peak by cyclic voltammetry strongly acidic media [34]. These drugs, which all include a piperazine

ring, were investigated by cyclic voltammetry at both electrodes as a function of pH in order to identify the oxidation behavior of PEF. The heights of the peak of these model compounds remain practically unchanged up to pH 7.0. So, again the monoprotonated form of piperazine ring generated from the dication is oxidized at pH <7.0. We may assume that when the aliphatic nitrogen of piperazine rings, distal to the benzene ring of the molecule, is protonated, oxidation occurs on the proximal nitrogen which represents a typical redox system with two electron oxidation processes [33] in acidic and basic media. This mechanism and all the obtained results are also in agreement with reported data concerning anodic voltammetry of the selected model compounds [33,37–39] and similarly structured fluoroquinolones [40–44] at glassy carbon and carbon paste electrodes.

3.1. Analytical parameters and validation of the developed methods

Pulse voltammetric techniques such as DPV, SWV, and adsorptive pulse are effective and rapid electroanalytical techniques with well-established advantages, including good discrimination against background current and low detection limits [23,26]. These techniques have been shown to be highly suitable for measuring organic drug compounds. The advantages of SWV are greater speed of analysis, lower consumption of electroactive species in relation to the other electroanalytical techniques and reduced problems with blocking of the electrode surface. In this study DPV was used as an alternative technique.

In this study, DPV and SWV techniques were used for the determination of PEF using BDDE because of diffusion controlled electrode process. Using glassy carbon electrode, the adsorptional behavior was obtained with PEF. However, different adsorptive stripping techniques (e.g. AdSDPV, AdSSWV) and parameters (e.g. stirring rate, accumulation time and potential effect, etc.) were tried for optimizing and determining PEF concentration using glassy carbon electrode. In spite of trying all variables and factors we could not obtained the linear response for PEF determination using glassy carbon electrode neither using adsorptive stripping techniques nor using direct DPV and SWV techniques. For this reason we continued the determination studies only with BDDE and using DPV and SWV techniques.

Diffusion of the analyte was confirmed by the results obtained with cyclic voltammetry. The plot of logarithm of peak current versus logarithm of scan rate has a slope of 0.49, close to the theoretical value of 0.5 which is expressed for an ideal reaction of the diffusion controlled electrode process for BDDE.

To develop rugged and suitable voltammetric method for the quantitative determination of PEF, various supporting electrolytes, buffer systems, ionic strength and pH were employed. Different supporting electrolytes, such as sulfuric acid, phosphate, acetate, borate and Britton–Robinson buffers were examined. Based on above study, the best conditions for analytical applications proved to be 0.5 M H_2SO_4. For analytical purposes, best response such as peak current sensitivity, single peak, peak morphology and reproducibility was obtained by working with 0.5 M H_2SO_4 using BDDE. This supporting electrolyte was chosen for the subsequent experiments.

The quantitative evaluation is based on the dependence of peak current on PEF concentration using BDDE. The peak currents increased linearly with increasing amounts of PEF by DPV and SWV techniques at BDDE. Using optimum conditions described in Section 2 and in 0.5 M H_2SO_4 supporting electrolyte, linear calibration curves were obtained for PEF in the range of 2×10^{-6} to 2×10^{-4} M for DPV and SWV methods, indicating that the response was diffusion controlled in this range. Above this concentration a loss of linearity was probably due to the adsorption of PEF on the electrode surface. The characteristics of the calibration lines and their related validation parameters are summarized in Table 1. The developed methods were validated according to the standard procedures [28–30]. Accuracy, precision, reproducibility and other parameters of the proposed methods were assessed by performing replicate analysis of the standard solutions in supporting electrolyte and spiked serum samples within calibration ranges, the selected concentrations were prepared in both media and assayed with related calibration curves to determine within day (repeatability) and between day (reproducibility) variability. Also the limits of

Table 1
Regression data of the calibration lines quantitative determination of pefloxacin by DPV and SWV in standard solution and human serum

	DPV		SWV	
	Standard solution	Serum	Standard solution	Serum
Measured potential (V)	1.20	1.26	1.24	1.29
Linearity range (M)	2×10^{-6} to 2×10^{-4}	2×10^{-6} to 2×10^{-4}	2×10^{-6} to 2×10^{-4}	2×10^{-6} to 2×10^{-4}
Slope ($\mu A\,M^{-1}$)	35,074	20115.2	36,325	25482.5
Intercept (μA)	−0.067	0.055	−0.005	0.030
Correlation coefficient	0.999	0.999	0.999	0.999
S.E. of slope ($\times 10^2$)	2.82	1.57	3.05	1.69
S.E. of intercept ($\times 10^{-2}$)	2.12	1.18	2.29	1.27
LOD ($\times 10^{-7}$ M)	4.12	4.65	1.54	5.78
LOQ (M)	1.37×10^{-6}	1.55×10^{-6}	5.12×10^{-7}	1.93×10^{-6}
Repeatability of peak current (R.S.D., %)	0.49	0.44	0.37	0.46
Repeatability of peak potential (R.S.D., %)	0.45	0.26	0.14	0.17
Reproducibility of peak current (R.S.D., %)	0.63	0.70	0.66	0.95
Reproducibility of peak potential (R.S.D., %)	0.24	0.26	0.42	0.17

detection (LOD) and limits of quantification (LOQ) were shown in Table 1.

Several approaches are given in the ICH guideline to determine the LOD and LOQ values. The LOD and LOQ were calculated on the peak current using following equations:

$$\mathrm{LOD} = 3s/m; \qquad \mathrm{LOQ} = 10s/m$$

where s is the standard deviation of the peak currents (three runs) and m is the slope of the related calibration equation. Both LOD and LOQ values confirmed the sensitivity of the proposed methods. The precision of the proposed methods was evaluated by repeating five experiments on the same day in the same solutions (repeatability) and over 6 days from different solutions (reproducibility) repeating the experiment for five times [28–30]. For realizing these experiments, 8×10^{-5} M PEF solutions were used in both media. The obtained results were given in Table 1. The within day (repeatability) and between day (reproducibility) precision and accuracy were determined as the R.S.D.% and mean value and the related results were shown in Table 1. These results demonstrate good precision, accuracy, reproducibility and sensitivity [28–30].

All solutions were freshly prepared to ensure stability of analyte in solutions. However, for stability indicating, standard sample solutions recorded after a week period and aged at +4 °C, in the dark after 2 weeks period, against a sample freshly prepared, did not show any appreciable change in assay values. The results demonstrated that the working reference solutions were stable for up to 2 weeks.

When working on standard solutions, and according to the obtained validation parameters, results encourage the use of the proposed methods described for the assay of PEF in pharmaceutical dosage forms and spiked serum samples.

3.2. Application to analysis of pharmaceuticals

The validity of the proposed DPV and SWV techniques at the BDDE for the determination of PEF in pharmaceutical dosage forms was investigated by assaying tablet and injectable (ampoule) dosage forms. On the basis of obtained results, both DPV and SWV methods were applied to the direct determination of PEF tablets and ampoules, using related calibration equations without any sample preparation, extraction, and filtration or evaporation steps other than an adequate dilution step. The results show that the optimized proposed DPV and SWV techniques at BDDE were successfully applied for the assay of PEF in its pharmaceutical dosage forms (Table 2). The mean results for five determinations of both techniques are very close to the declared value of 400.00 mg; the confidence limits were calculated for a significance level of 0.05. These results showed that the proposed methods could be applied with great success to PEF assay in tablet and injectable dosage forms without any interference.

Both of the proposed methods performance was checked using Student's t- and F-tests between each other. The F- and t-tests were carried out on the data and statistically examined the validity of the obtained results by DPV and SWV. At the 95% of the confidence level, the values of t- and F-tests (calculated from experiments) were less than that of theoretical t- and F-values showing that there are no significative differences between both of the proposed methods.

For checking the accuracy of the proposed methods and in order to know whether the excipients in pharmaceutical dosage forms show any interference with the analysis, the recovery studies were realized by its recovery during spiked experiments. Recovery studies were carried out after the addition of known amounts of pure PEF to various pre-analyzed formulation of PEF. Recovery experiments using the developed assay procedure further indicated the absence of interference from commonly encountered pharmaceutical excipients used in the selected formulations (Table 2). These results have also shown that both methods had adequate precision and accuracy and consequently cam be applied to the determination of PEF in pharmaceuticals without any interference from inactive ingredients.

3.3. Determination of PEF in spiked serum samples

In order to check, the possibility of applying the proposed techniques to the human serum samples, the calibration equa-

Table 2
Results obtained for the DPV and SWV determination and recovery experiments in tablets and ampoules

	Tablet (mg)		Ampoule (mg (5 mL)$^{-1}$)	
	DPV	SWV	DPV	SWV
Labeled claim	400.00	400.00	400.00	400.00
Amount found[a]	400.96	402.79	402.33	402.02
R.S.D. (%)	0.47	0.15	0.59	0.85
Bias%	−0.24	−0.70	−0.58	−0.50
95% confidence limit	398.62–403.30	401.98–403.68	399.37–405.28	397.76–406.27
t_{value}	$t_{theoretical}$: 2.31	$t_{calculated}$: 0.07	–	$t_{calculated}$: 0.87
F_{value}	$F_{theoretical}$: 2.60	$F_{calculated}$: 0.08	–	$F_{calculated}$: 0.50
Added (mg)	20.00	20.00	20.00	20.00
Found (mg)[a]	20.03	20.03	20.05	20.10
Average recovered (%)	100.13	100.15	100.26	100.48
R.S.D. (%) of recovery	0.32	0.22	0.35	0.19
Bias (%)	−0.13	−0.15	−0.26	−0.48

[a] Each value is the mean of five experiments.

Table 3
Results obtained for pefloxacin determination from spiked serum

	DPV	SWV
Added concentration ($\times 10^{-5}$ M)	8.000	8.000
Obtained concentration ($\times 10^{-5}$ M)	8.003	8.001
Number of experiments	5	5
Average recovered (%)	100.036	100.010
R.S.D. (%) of recovery	0.46	0.49
Bias (%)	−0.036	−0.010

tions were obtained in spiked human serum samples. The determination of PEF in spiked human serum could be achieved adopting the DPV and SWV modes in 0.5 M H_2SO_4 as supporting electrolyte. Acetonitrile and methanol were tried as the biological sample precipitating agents. Also different amount of acetonitrile and methanol were examined. The best results were obtained using 1 mL acetonitrile. The measurements of PEF in human serum samples were performed as described in Section 2. The applicability of the proposed methods to the human serum, the calibration equations were obtained in spiked human serum samples. Calibration equation parameters and necessary validation data were shown in Table 1. Obtained recovery results of spiked human serum samples were given in Table 3. Analysis of drugs from biological samples such as human serum usually requires extensive time-consuming sample preparation, use of organic solvents and other chemicals. In this study, the serum proteins and endogenous substances in serum samples as precipitated by the addition of acetonitrile, which is centrifuged at $5000 \times g$ and the supernatant was taken and diluted with the selected supporting electrolyte and directly analyzed. Typical DPV and SWV curves of PEF examined in serum samples are shown in Fig. 5a and b, respectively. Using both proposed techniques, no sample pretreatment was required, other than precipitation and dilution steps. The recovery results of PEF (Table 3) in human serum samples were calculated from the related linear regression equations, which are given in Table 1. As can be seen in Fig. 5, no oxidation compounds and no extra noise peaks present in biological material peak occurred in the potential range where the analytical peak appeared. Stability of the serum samples kept in refrigerator (+4 °C) was tested by making five consecutive analyses of the sample over a period of approximately 6 h. There were no significant changes in the peak currents and potentials between the first and last measurements.

4. Conclusions

Due to the high sensitivity and selectivity of electrochemical methods, the determination of fluoroquinolones has been a subject of considerable interest and time-consuming methods [9,21,40–44] have been developed for their determination. Stripping techniques are one of the best-known analytical methods that incorporate an electrolytic preconcentration step. These techniques couple the advantage of extremely low detection limits, and suitability for online and in situ measurements. Two major problems encountered in using such methods is the need for obtaining right accumulation parameters or the need for time-consuming accumulation procedures before each measurement. The amount of PEF varies between 200 and 800 mg (generally 400 mg) in tablet dosage forms. Hence, this kind of pharmaceutical analysis requires rapid, selective, sensitive, less expensive, and most importantly simple electroanalytical techniques such as square wave (SWV) and differential pulse (DPV) voltammetry. These techniques eliminate the long preconcentration process before each measurement onto the BDD electrode surface prior to the voltammetric analysis. Thus, no surface poisoning of the solid electrode occurs during the accumulation procedure. PEF showed diffusional behavior on BDD electrode.

This paper on the anodic behavior of PEF at BDD and glassy carbon electrodes has described how the compound is irreversibly oxidized at high positive potentials. BDDEs exhibit high stability because of their inertness with respect to the adsorption of chemical species and the easiness of cleansing of the surface compared to the glassy carbon electrodes. Another advantage of BDDE is that it enables to work with higher positive potentials than the glassy carbon electrodes which also provide a wider electrochemical range for BDDEs. A relatively low noise-to-signal and background-to-signal ratios and mechanical robustness [27] are the other desirable characteristics for BDDEs for electroanalytical applications.

This paper on the anodic behavior of PEF at BDD and glassy carbon electrodes has described how the compound is irreversibly oxidized at high positive potentials. The electrochemical behavior of PEF on electrodes was investigated for the first time on BDDE. The electroreduction method and voltammetric method using dsDNA modified electrode which are found in literature [9,21] related to the of PEF determination. Cyclic voltammetric measurements showed an irreversible oxidation at all pH values, and buffers investigated for both electrodes. PEF presents one main anodic peak and an additional one ill-defined wave depending on the pH value and using buffer. The electrochemical processes were attributed to the oxidation of the piperazine moiety on the molecule like other similarly structured fluoroquinolones [9,21,40–44]. The main and sharp oxidation step in 0.5 M H_2SO_4 was used for the determination of PEF in pharmaceutical dosage forms and spiked human serum samples. The proposed DPV and SWV methods for the determination of PEF in pharmaceutical dosage forms and human serum samples was found to be more simple, selective, fully validated and as sensitive as the reported methods [9,21]. Application of the DPV and SWV techniques to pharmaceuticals is possible after a simple dilution step with direct measurements. The principle advantage of the proposed methods, over the published procedures, is that the inactive ingredients of dosage forms and endogenous substances of biological samples do not interfere the analysis and the separation procedure is not necessary. The sample preparation procedure is very simple since there is no need to eliminate the excipients, thus it results an increase in sensitivity, selectivity, precision and accuracy. This paper is not intended to be a study of the pharmacodynamic properties of PEF, since only healthy volunteers were used for the sample collection and results may be of no significance. Norfloxacine which is the principal active metabolite of PEF is shown similar

oxidative behavior and has the same oxidation potentials with PEF. For this reason, their response may be obtained as total current in these proposed electroanalytical techniques.

This study only shows the possibility of monitoring this compound makes the method useful for pharmacokinetic and pharmacodynamic purposes. Also the proposed methods are rapid, requiring less than 4 min to run a sample and do not include time-consuming de-aeration procedure with pure nitrogen for each measurements [21]. Consequently, the above-presented techniques are a good analytical alternative determining PEF in dosage forms and biological samples.

Acknowledgements

This work was supported by the Ankara University Scientific Research Foundation (Grand nos.: 20030803037 and 20030803043). The authors also gratefully acknowledge Eczacıbaşı Pharm. Comp. for supplying pefloxacin mesylate standard sample and its pharmaceutical dosage form.

References

[1] Goodman and Gilman's The Pharmacological Basis of Therapeutics, 9th ed., Section V. CD ROM, Mc Graw-Hill Companies Inc., 1996.
[2] S.C. Sweetman (Ed.), Martindale: The Complete Drug Reference, 35th ed., Pharmaceutical Press, London, 2007, p. 280.
[3] M.I.R.M. Santoro, N.M. Kassab, A.K. Singh, E.R.M. Kedor-Hackmam, J. Pharm. Biomed. Anal. 40 (2006) 179.
[4] D. Kowalczuk, H. Hopkala, J. Planar Chromatogr. Modern TLC 15 (2002) 345.
[5] G.X. Yang, B.Y. Lin, Z.L. Zeng, Z.L. Chen, X.H. Huang, J. AOAC Int. 88 (2005) 1688.
[6] J.B. Chao, H.B. Tong, D.S. Liu, S.P. Huang, Spectrochim. Acta A 64 (2006) 166.
[7] A.C. Huet, C. Charlier, S.A. Tittlemier, G. Singh, S. Benrejeb, P. Delahaut, J. Agric. Food Chem. 54 (2006) 2822.
[8] I.A. Darwish, I.H. Refaat, H.F. Askal, M.A. Marzouq, J. AOAC Int. 89 (2006) 334.
[9] A. Radi, M.A. El Ries, S. Kandil, Anal. Bioanal. Chem. 381 (2005) 451.
[10] K. Basavaiah, H.C. Prameela, Indian J. Chem. Technol. 9 (2002) 428.
[11] S. Mostafa, M. El-Sadek, E.A. Alla, J. Pharm. Biomed. Anal. 28 (2002) 173.
[12] S. Mostafa, M. El-Sadek, E.A. Alla, J. Pharm. Biomed. Anal. 27 (2002) 133.
[13] L.M. Du, H.Y. Yao, M. Fu, Spectrochim. Acta A 61 (2005) 281.
[14] G.Z. Li, Y.M. Liu, G.Z. Li, Spectrosc. Spect. Anal. 24 (2004) 1086.
[15] L.M. Du, A.P. Lin, Y.Q. Yang, Anal. Lett. 37 (2004) 2175.
[16] L.R. Du, J.P. Wang, C.X. Wang, Spectrosc. Spect. Anal. 24 (2004) 855.
[17] M.E. El-Kommos, G.A. Saleh, S.M. El-Gizawi, A. Abou-Elwafa, Talanta 60 (2003) 1033.
[18] H.Y. Ma, X.W. Zheng, Z.J. Zhang, Luminescence 20 (2005) 303.
[19] Z.Q. Zhang, Y.C. Jiang, H.T. Yan, Atom. Spectrosc. 24 (2003) 27.
[20] S. Furlanetto, S. Orlandini, E. La Porta, S. Coran, S. Pinzauti, J. Pharm. Biomed. Anal. 28 (2002) 1161.
[21] A.M. Beltagi, J. Pharm. Biomed. Anal. 31 (2003) 1079.
[22] M.R. Smyth, J.G. Vos (Eds.), Analytical Voltammetry, Elsevier, Amsterdam, 1992.
[23] J. Wang (Ed.), Electroanalytical Techniques in Clinical Chemistry and Laboratory Medicine, VCH Publishers, New York, 1988.
[24] S.A. Ozkan, B. Uslu, H.Y. Aboul-Enein, Crit. Rev. Anal. Chem. 33 (2003) 155.
[25] J.M. Kaufmann, J.-C. Viré, Anal. Chim. Acta 273 (1993) 329.
[26] P.T. Kissenger, W.R. Heinemann (Eds.), Laboratory Techniques in Electroanalytical Chemistry, 2nd ed., Marcel Dekker, NY, 1996.
[27] B. Uslu, S.A. Ozkan, Anal. Lett. 40 (2007) 817.
[28] C.M. Riley, T.W. Rosanske (Eds.), Development and Validation of Analytical Methods, Elsevier Science Ltd., New York, 1996.
[29] M.E. Swartz, I.S. Krull (Eds.), Analytical method Development and Validation, Marcel Dekker, New York, 1997.
[30] J. Ermer, in: J.H.McB. Miller (Ed.), Method Validation in pharmaceutical Analysis, Wiley-VCH Publ., Weinheim, 2005.
[31] P. De Bievre, H. Günzler (Eds.), Validation in Chemical Measurements, Springer Publ., Berlin, 2005.
[32] F.M.E. Wagenlehner, K.G. Naber, Curr. Urol. Rep. 5 (2004) 309.
[33] J.-M. Kauffmann, J.-C. Viré, G.J. Patriarche, L.J. Nunez-Vergara, J.A. Squella, Electrochim. Acta 32 (1987) 1159.
[34] B. Uslu, S.A. Ozkan, Anal. Chim. Acta 462 (2002) 49.
[35] R.N. Goyal, V.K. Gupta, M. Oyama, N. Bachheti, Electrochem. Commun. 8 (2006) 65.
[36] R.N. Goyal, N. Jein, V. Gurnani, Monatsh. Chem. 13 (2001) 575.
[37] B. Uslu, B. Dogan, S.A. Ozkan, H.Y. Aboul-Enein, Anal. Chim. Acta 552 (2005) 127.
[38] S.A. Ozkan, B. Dogan, B. Uslu, Microchim. Acta 153 (2006) 27.
[39] B. Uslu, S.A. Ozkan, J. Pharm. Biomed. Anal. 31 (2003) 481.
[40] M. Warowna-Grzeskiewicz, J. Chodkowski, Z. Fijalek, Acta Poloniae Pharmaceutica-Drug Res. 52 (1995) 187.
[41] M.M. Ghoneim, A. Radi, A.M. Beltagi, J. Pharm. Biomed. Anal. 25 (2001) 205.
[42] M.A. El Ries, A.A. Wassel, N.T. Abdel Ghani, M.A. El-Shall, Anal. Sci. 21 (2005) 1249.
[43] K. Girish Kumar, P. Augustine, R. Poduval, S. John, Pharmazie 61 (2006) 291.
[44] S. Hanwen, X. Tao, L. Kaoqi, L. Shuxuan, Chem. J. Internet 8 (2006), art. no. 088054pe.

Available online at www.sciencedirect.com
ScienceDirect
Talanta 74 (2008) 1385–1391
Talanta
www.elsevier.com/locate/talanta

Determination of volatile and non-volatile nickel and vanadium compounds in crude oil using electrothermal atomic absorption spectrometry after oil fractionation into saturates, aromatics, resins and asphaltenes

Maria Goreti R. Vale [a,*], Márcia M. Silva [a], Isabel C.F. Damin [a], Pedro J. Sanches Filho [b], Bernhard Welz [c,d]

[a] *Instituto de Química, Universidade Federal do Rio Grande do Sul, Av. Bento Gonçalves 9500, 91501-970 Porto Alegre, RS, Brazil*
[b] *Centro Federal de Educação Tecnológica de Pelotas CEFET, RS, Brazil*
[c] *Instituto de Química, Departamento de Química Analítica, Universidade Federal da Bahia, 40170-290 Salvador, BA, Brazil*
[d] *Departamento de Química, Universidade Federal de Santa Catarina, 88040-900 Florianópolis, SC, Brazil*

Received 6 September 2007; received in revised form 13 September 2007; accepted 14 September 2007
Available online 19 September 2007

Abstract

In recent work, it has been shown that electrothermal atomic absorption spectrometry (ET AAS) can be used to differentiate between volatile and non-volatile nickel and vanadium compounds in crude oil. In the present work, the distribution of these two groups of compounds over different fractions of crude oil was investigated. For this purpose two crude oil samples were separated in two steps: firstly, the asphaltenes were precipitated with *n*-heptane, and secondly, the maltenes were loaded on a silica column and eluted with solvents of increasing polarity. The four fractions of maltenes eluted from silica column were: F1, saturated and light aromatics; F2, polyaromatics; F3, resins; and F4, polar compounds. Fractions F1 and F2 were further investigated using gas chromatography, and all fractions were characterized by CHN analysis, confirming the increase of aromatics in the fractions 2, 3, 4 and asphaltenes. For the determination of Ni and V by ET AAS, oil-in-water emulsions were prepared. The speciation analysis was carried out measuring without chemical modifier (stable compounds) and with 20 μg palladium (total Ni and V) and the volatile fraction was calculated by difference. The limits of detection were 0.02 μg g^{-1} and 0.06 μg g^{-1}, for Ni and V, respectively, based on an emulsion of 2 g of oil in 10 mL. The volatile species of Ni and V were associated with fractions F3 and F4, while only thermally stable Ni and V was precipitated in part together with the asphaltenes.
© 2007 Elsevier B.V. All rights reserved.

Keywords: Crude oil fractionation; Nickel and vanadium in crude oil fractions; Electrothermal atomic absorption spectrometry; Oil-in-water emulsion; Palladium modifier; Speciation analysis

1. Introduction

Crude oil, shale oil, and sand oil are sources of petroleum and contain hundreds of compounds, which can be grouped into four main classes: (i) saturates (alkanes and cycloparaffins), (ii) aromatics (mono-, di-, and polynuclear aromatic hydrocarbons (PAHs) with alkyl side chains), (iii) resins (aggregates with a multitude of building blocks such as sulfoxides, amides, thiophenes, pyridines, quinolines and carbazoles), and (iv) asphaltenes (aggregates of extended polyaromatics, naphthenic acids, sulfides, polyhydric phenols and fatty acids). The latter two classes contain many species that are not volatile and hence are difficult to analyze. Besides these organic compounds crude oil also contains a variety of trace metals at concentrations between a few μg kg^{-1} up to several hundreds of mg kg^{-1}. These metals are usually in combination with naphthenic acid as soaps or in the form of complex organometallic compounds such as metalloporphyrins [1].

Rudzinski and Aminabhavi [2] published a review discussing the important papers in the area of crude oil separation and

* Corresponding author. Tel.: +55 51 3308 6278; fax: +55 51 3308 7304.
E-mail address: mgrvale@iq.ufrgs.br (M.G.R. Vale).

0039-9140/$ – see front matter © 2007 Elsevier B.V. All rights reserved.
doi:10.1016/j.talanta.2007.09.009

identification of the products using conventional approaches as well as supercritical fluid technologies. The volatility and stability of the compounds determines whether they can be determined using standard gas chromatography/mass spectrometry (GC/MS) or if other fluid systems are required, such as liquid chromatography (LC), supercritical fluid extraction (SFE) and supercritical fluid chromatography (SFC).

Because of the complexity of crude oils, preliminary fractionation according to the chemical class usually precedes identification of individual components. Several such fractionation and isolation schemes have been proposed [2] depending on the type of crude oil under investigation. One of the most widely used separation schemes is the SARA method, which has its name from the fractions produced, namely saturates (S), aromatics (A), resins (R), and asphaltenes (A). The approach is based on the adsorption of the sample on either silica [3,4] or alumina followed by selective elution of the constituents using a series of increasingly polar solvents [5–7]. Mansfield et al. [8] have reviewed the literature on crude oil separation and identification methods including the SARA method. Two of the more recent advances in SARA characterization involve high-performance liquid chromatography (HPLC) [9] and infrared and near-infrared spectroscopy [10].

Asphaltenes comprise the most polar fraction of crude oil and consist of polyaromatic condensed rings with short aliphatic chains and heteroatoms such as nitrogen, oxygen, sulfur and various metals [11]. Asphaltenes can cause a series of problems along the whole production chain from the reservoir to the refinery. Reservoir damage and well-bore plugging in the oil production, pipeline and tank clogging in transportation lines adversely affect the petroleum industry [12]. Many methods have been described in the literature to separate asphaltenes [4,13] and it has been shown that the physicochemical properties of asphaltenes are sensitive to the separation techniques and solvents used. Moreover, fundamental understanding of asphaltene–metal interaction can provide insight into whether and how surface characteristics can influence asphaltene deposition [12]. Asphaltenes have been precipitated in solvent mixtures at various temperatures [14–17]. Analysis of asphaltene samples from eight different crude oils indicate that the fractionation technique may be a powerful tool for predicting the dissolution rate constant of an asphaltene and subsequently its difficulty of remediation. Ali and Abbas [1] reported in a recent review about methods for the demetallization of residual fuel oils and the various situations where the metal can be removed from the petroleum by solvents. The majority of the metal compounds may be precipitated along with the asphaltenes by hydrocarbon solvents; the removal of asphaltenes with *n*-alkanes might reduce the metal content of the oil by up to 95%.

Among the metals in crude oil the most abundant and undesirable ones are vanadium and nickel. Depending on the origin of crude oil, the concentration of vanadium may vary from less than 0.1 mg kg^{-1} to more than 1000 mg kg^{-1} [1,18], while that of nickel commonly varies from trace to 150 mg kg^{-1} [1]. Vanadium and nickel are known to occur in petroleum in two distinctly different classes of compounds: non-polar porphyrin complexes and polar non-porphyrins. Little is known about the nature of non-porphyrins. However, the porphyrins have been extensively studied not only because of their deleterious effects but also for their important role as geochemical markers [19].

The determination of nickel and vanadium in crude oil by electrothermal atomic absorption spectrometry (ET AAS) has been investigated in detail recently [20–22]. Using high-resolution continuum source AAS (HR-CS AAS) [23] it could be observed that up to 50% of the nickel and vanadium in crude oil, most likely the non-polar nickel and vanadyl porphyrins, were lost already at pyrolysis temperatures >400 °C, whereas the rest of the nickel and vanadium compounds in oil, as well as the calibration standards (polar organic salts) were thermally stable up to 1300 °C and 1600 °C, respectively. These losses could not be detected by conventional line source AAS, as the background absorption caused by the petroleum matrix made it impossible to carry out any measurements with pyrolysis temperatures <600 °C. Due to the far superior simultaneous background correction available with HR-CS ET AAS it was possible to determine the total content of nickel and vanadium in crude oil using a pyrolysis temperature of 400 °C [19,21]. The accuracy of this determination was also confirmed using palladium as a modifier to avoid losses of volatile compounds of both elements [20]. Using a pyrolysis temperature of 800–1000 °C it was possible to determine the content of 'thermally stable' nickel and vanadium [19,21], i.e., the non-porphyrin fraction; the content of volatile porphyrins could then be calculated by difference. This method for speciation analysis of nickel and vanadium compounds in crude oil has recently been extended using direct sampling ET AAS without any sample preparation [24]. This kind of speciation analysis is considered particularly important, as it is most likely the volatile porphyrin fraction of vanadium and nickel that is transported during the distillation process, causing problems with catalyst poisoning, etc.

The goal of this work was to investigate in more detail the distribution of the volatile porphyrin complexes and the non-porphyrin compounds of vanadium and nickel over the different fractions of crude oil samples with a minimum of sample preparation. The method included a two-step separation process of the crude oil, starting with precipitation of the asphaltenes in heptane, followed by chromatographic fractionation of the maltenes in a silica column according to the SARA method. The speciation analysis of volatile and non-volatile nickel and vanadium compounds in asphaltenes and in the maltene fractions of crude oil was realized measuring without chemical modifier (stable compounds) and by stabilization with 20 μg palladium (total Ni and V); the volatile fraction was calculated by difference. The work also included an investigation of the stability of volatile compounds of nickel and vanadium in petroleum samples.

2. Experimental

2.1. Instrumentation

All atomic absorption measurements were carried out using a model AAS 5EA atomic absorption spectrometer (Analytik Jena AG, Jena, Germany) with deuterium background correction, equipped with a transversely heated graphite tube atomizer.

Table 1
Graphite furnace temperature program for the determination of nickel and vanadium in crude oil with emulsification

Program stage	Temperature (°C)	Ramp (°C s^{-1})	Hold time (s)	Gas flow rate (L min^{-1})
Drying 1	90	5	50	2.0
Drying 2	270	5	20	2.0
Pyrolysis	1200[a] 1450[b]	100	20	2.0
Atomization	2400[a] 2600[b]	1500	5[a] 6[b]	0
Cleaning	2600	100	4	2.0

[a] Determination of Ni.
[b] Determination of V.

NARVA hollow cathode lamps for nickel and vanadium (GLE, Berlin, Germany) were used as the radiation sources, both with a current of 5.0 mA. The main analytical lines at 232.0 nm and 318.4 nm were used for all determinations with a spectral bandwidth of 0.2 nm and 0.7 nm for nickel and vanadium, respectively. The spectrometer was interfaced to an IBM PC/AT-compatible computer. All experiments were carried out using pyrolytically coated graphite tubes with an integrated PIN platform (Analytik Jena Part No. 407-A81.025). An MPE 5 furnace autosampler (Analytik Jena AG) was used for introduction of the emulsions. Argon with a purity of 99.996% (White Martins, São Paulo, Brazil) was used as the purge gas. Integrated absorbance (peak area) was used exclusively for signal evaluation and quantification. The optimized graphite furnace temperature program is given in Table 1.

The GC measurements were carried out using a Shimadzu QP5050A gas chromatograph (Shimadzu, Kyoto, Japan) with a DB 5 column, 30 m × 0.25 mm × 0.25 μm; the injector and interface temperature was 280 °C and the ionization energy was 70 eV. The fraction was solved with 250 μL of the dichloromethane and the injected volume was 1 μL in split mode (ratio 1:20). The furnace temperature was increased from 100 °C to 220 °C with a rate of 10 °C min^{-1} and from 220 °C to 280 °C with a rate of 5 °C min^{-1}.

The elemental analyses were carried out using a model 2400 elemental analyzer (Perkin Elmer, MA, USA).

A Unique-Thorton model USC-2850 ultrasonic bath (Thorton, São Paulo, Brazil) operated at a frequency of 37 ± 3 kHz, with temperature control up to 80 ± 5 °C, was used for preparation of the emulsions.

A centrifuge model Excelsa Baby I Fanem 206 (Fanem, São Paulo, Brazil) was used for separating the asphaltenes.

2.2. Reagents

Analytical grade reagents were used throughout. Distilled, and deionized water (DDW) with a specific resistivity of 18 MΩ cm, from a Milli-Q water purification system (Millipore, Bedford, MA, USA), was used for the preparation of the emulsions and standards. All containers and glassware were soaked in 3 mol L^{-1} nitric acid for at least 24 h and rinsed three times with DDW before use. Aqueous stock solutions of nickel and vanadium (1000 mg L^{-1}) were prepared from Titrisol concentrates (Merck). The working standards were prepared by serial dilution of the stock solutions with the addition of base mineral oil (BMOMS, High Purity Standards, Charleston, SC, USA) and emulsification, as described below, using Xylene (Merck, Germany) and Triton X-100 (Union Carbide). A palladium nitrate stock solution with 10 g L^{-1} Pd in 15% (v/v) nitric acid (Merck) was used as chemical modifier. *N*-Heptane and toluene (Merck) were used for precipitation and dissolution of asphaltenes, respectively. Silicagel, 70–230 mesh (Merck) was used to fill the chromatographic column (l = 50 cm, i.d. = 1.5 cm) and *n*-hexane, dichloromethane (DCM) and methanol (all from Merck) were used as eluents for fractionation of the maltenes.

2.3. Samples

The samples analyzed in this work were acquired from refineries of Petrobras in the state of Bahia, Brazil.

2.4. Emulsification

The composition and mode of preparation of the oil-in-water emulsion has been optimized in previous work using a multivariate approach [20]. Between 0.05 g and 2 g of oil sample, depending on the analyte concentration, were weighed into 10 mL borosilicate glass volumetric flasks and diluted with 1.0 mL of xylene. The flasks were closed, fitted into a polystyrene support and put into the ultrasonic bath at ambient temperature for 5 min. Then 100 μL of Triton X-100 was added with a micropipette and the volume was completed with DDW. The flasks were agitated manually for 2 min and then put in the ultrasonic bath at ambient temperature for another 5 min, and finally agitated manually again for 2 min. All samples and reference materials were weighed in triplicate directly into the flasks in order to reduce sampling errors due to the high viscosity and inhomogeneity of crude oil to a minimum. Blank and calibration solutions were prepared in the same way, using the base mineral oil instead of the sample with appropriate concentrations of aqueous standard solutions added to the aqueous phase to cover the calibration range. The homogeneity of the emulsions was maintained by manual agitation with a Pasteur pipette just before the sample emulsion was taken up by the autosampler capillary.

A volume of 5 μL of ethanol (Merck) was introduced into the graphite tube together with 10 μL of the emulsion to avoid foam formation. In case a modifier was used, 20 μL of the palladium solution was injected into the graphite tube and dried completely before the ethanol and the emulsion were introduced. The standard calibration technique was used throughout.

2.5. Oil fractionation

The fractionation of crude oil included two separation steps: (1) precipitation of asphaltenes with *n*-heptane and (2) fractionation of maltenes by chromatography. In order to avoid variations in the mass balance due to evaporation losses of light hydrocar-

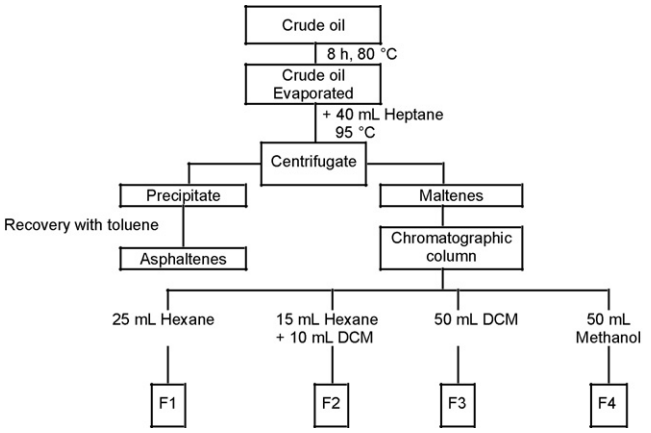

Fig. 1. Schematic presentation of the separation of the crude oil samples into asphaltenes and maltenes, and the chromatographic fractionation of the maltenes.

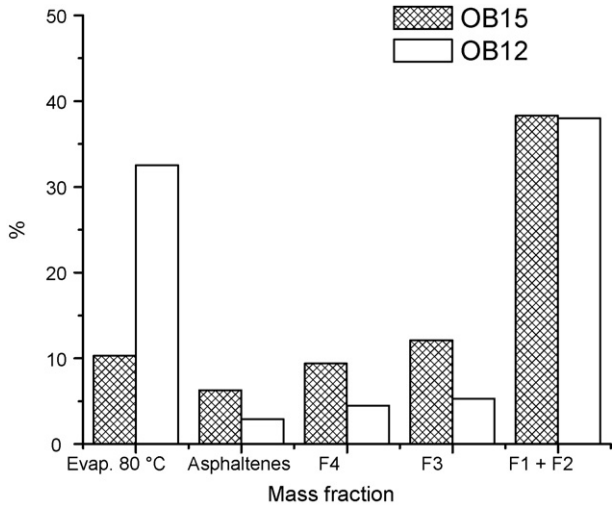

Fig. 2. Mass fraction of light hydrocarbons volatilized at 80 °C, asphaltenes and chromatographic fractions of the two crude oil samples, compared to their original mass.

bons, all oil samples (1 g) were heated overnight at 80 °C before further use. The samples (after evaporation) were mixed with 40 mL of *n*-heptane and maintained at 95 °C for 1 h [25,26]. The precipitated asphaltenes were separated by centrifugation and the precipitate was washed with hot heptane to remove the adsorbed resins from the asphaltenes, which were recovered with toluene. The solvent was evaporated under a flow of nitrogen until constant weight and the asphaltenes were stored in glass vials in the dark at 4 °C.

The maltene fraction (soluble in hot heptane) was separated using a chromatographic column filled with Silica gel, which was activated at 150 °C overnight. The elution of maltenes was carried out as shown in the Fig. 1. The elution of the column resulted in four fractions, according with increasing polarity of the solvent mixtures. Fraction 1 was predominantly composed of saturates and light aromatics; fraction 2 contained polyaromatic compounds; fraction 3, eluted with DCM contained all the resins (nitrogenated and oxigenated compounds). The polar compounds with high molecular weight were remained on the column and eluted with methanol in fraction 4. The fractions were evaporated under nitrogen flow to constant weight, and stored for further analysis under the same conditions as the asphaltenes. The validation included recovery data for nickel and vanadium as well as total mass balance (TMB) calculations for each element in crude oil and its fractions.

3. Results and discussion

3.1. Fractionation and characterization of the fractions

The mass fractions of the two crude oil samples that were evaporated during the treatment at 80 °C, precipitated with *n*-heptane (asphaltenes) and the fractions F1, F2, F3 and F4 of maltene loaded on a silica column are shown in Fig. 2. It is obvious that the sample OB 12 had a more than three times higher content of compounds that were volatile at temperatures ≤80 °C, whereas for the sample OB 15 the mass of asphaltenes and resins (fractions 3 and 4) was about twice that of OB 12. The mass fraction of the maltene fractions 1 + 2 was essentially identical for both crude oil samples. Comparison between the initial mass of the crude oil and the addition of the evaporated and recovered fractions resulted in recuperation values of 83% for the sample OB 12 and 76% for the sample OB 15. Such losses are normal; they occur during transferring processes of the fractions and due to irreversible retention in the chromatographic column.

The two lighter fractions F1 and F2 were further characterized using GC with a temperature increase from 100 °C to 220 °C with a rate of 10 °C min^{-1} and a further increase to 280 °C with a rate of 5 °C min^{-1}. Twenty-three peaks could be identified in F1, which could be ascribed to the complete series of alkanes from $C_{14}H_{30}$ to $C_{36}H_{74}$. In addition, a few cyclic hydrocarbons and alkenes could be identified as well. The absence of lighter components in this fraction is due to the preparation procedure, i.e., their evaporation for 8 h at 80 °C. Fraction F2 consisted mostly of aromatics, such as anthracenes, phenanthrenes, pyrenes and benzo-anthracene.

The original sample OB 15 as well as all its fractions has also been submitted to an elemental analysis, the results of which are presented in Table 2. The data confirm enrichment in N from fraction F2 to the asphaltenes, as well as an increase in the aromaticity of these fractions. The decreasing aromaticity in the direction from asphaltenes over resins (F3) to F2 is in agreement with literature data [27]. The C:H ratio for asphaltenes found in

Table 2
Elemental analysis (CHN) for OB 15 crude oil sample and its fractions

Fraction	C (w/w)	H (w/w)	N (w/w)	Total (w/w)	C/H
Crude oil[a]	84.5	11.5	0.65	96.7	0.61
Evaporate[b]	85.3	11.4	0.62	97.3	0.62
Asphaltene	81.3	7.9	1.47	90.7	0.85
F4	80.8	10.3	1.35	92.5	0.65
F3	89.3	10.3	1.15	101	0.73
F2	77.0	12.8	1.08	90.9	0.63
F1	85.4	14.5	0.25	100	0.49

[a] Original crude oil before evaporation.
[b] After heating to 80 °C for 8 h.

Table 3
Analytical results obtained for nickel and vanadium in two crude oil samples

Analyte	Sample	Total ($\mu g\,g^{-1}$)	Stable ($\mu g\,g^{-1}$)	Volatile ($\mu g\,g^{-1}$)
Ni	OB 12	10 ± 0.2	5.4 ± 0.1	4.6 ± 0.2
Ni	OB 15	16 ± 0.7	11 ± 0.6	5.0 ± 0.9
V	OB 12	12 ± 1.2	8.9 ± 0.8	3.1 ± 1.4
V	OB 15	31 ± 1.5	20 ± 1.2	11 ± 2.0

The total content was determined with the addition of 20 μg Pd as modifier and the thermally stable fraction without a modifier. The volatile analyte fraction was determined by difference.

this work shows a level of aromaticity similar to that reported by Nalwaya et al. [28].

The physical appearance of the most polar fraction (F4) and least polar fraction (F1) also differed dramatically. The F4 fraction had a dark black color and consisted of hard, shiny, dense, black particles, while the F1 fraction was transparent and the particles were soft, dull and of yellow color. This difference in physical appearance has also been observed in other work [11,28].

3.2. Analytical results

At first the content of 'total' and 'stable' nickel and vanadium was determined in the two original crude oil samples and the 'volatile' analyte fraction was calculated by difference. The analytical procedure adopted was the same as the one described in earlier work [20], i.e., the total analyte content was determined with the addition of palladium as a chemical modifier, and the content of thermally stable analyte was determined without the addition of a modifier. The results are shown in Table 3. The total concentration of nickel and vanadium in OB 15 is much higher than in OB 12 and the content of the thermally stable fraction of nickel and vanadium is about twice as high as compared to the volatile fraction in OB 15. This might be related to the results of the initial fractionation, which indicates that the sample OB 15 is much richer in polar compounds containing heteroatoms. It is known that the organic compounds of nickel and vanadium are typically associated with nitrogenated organic compounds, such as porphyrins and salts of naphthenic acids. The content of stable nickel in OB 12 is essentially the same as that of the volatile components; but the content of thermally stable vanadium in OB 12 is about three times higher than the content of volatile vanadium compounds.

However, the main goal of this work has been to investigate the distribution of the two analytes and their thermally stable and volatile species over the different fractions obtained by the SARA method. The results of this investigation are summarized in Table 4. Firstly, there was no detectable concentration of nickel or vanadium in fractions F1 and F2; hence these fractions are not shown in Table 4. Secondly, there was no statistical difference between the results for total and thermally stable nickel and vanadium in the asphaltene fractions of both crude oil samples, i.e., this fraction did not contain any volatile compounds or the content of volatile compounds could not be determined because the uncertainty of the results for the total and thermally stable concentration was greater than the difference between them. The same was actually the case for vanadium also in all the other fractions of OB 12, i.e., it was not possible to determine any volatile vanadium in the individual fractions of this crude oil sample due to the uncertainty of the individual values, although a value could be determined in the crude oil before the fractionation (Table 3). In OB 15, in contrast, it was possible to determine the content of volatile vanadium in fractions F3 and F4, and this content was higher than the content of thermally stable vanadium in both fractions. The content of volatile nickel could also not be determined in fraction F4 of both crude oil samples for the same reasons discussed for vanadium. However, the volatile content of nickel could be determined in fraction F3 of both crude oils, and this content was higher than that of the thermally stable form again in both crude oil samples.

From these results a number of conclusions might be drawn: (1) only thermally stable nickel and vanadium compounds have been found to be associated with the asphaltene fractions of the two crude oils, and no volatile compounds could be detected. (2) Only about 40–45% of the total nickel and about 55–70% of the total vanadium could be precipitated with the asphaltenes, which is a significantly smaller portion than that reported in the

Table 4
Analytical results obtained for nickel and vanadium in different fractions of two crude oil samples

Sample	Fraction	Ni ($\mu g\,g^{-1}$[a])			V ($\mu g\,g^{-1}$[a])		
		Total	Stable	Volatile	Total	Stable	Volatile
OB 12	Asphaltene	3.2 ± 0.8	3.1 ± 0.8	n.d.[b]	4.0 ± 1.8	3.9 ± 2.5	n.d.[b]
	F4	0.9 ± 0.4	0.7 ± 0.2	n.d.[b]	0.7 ± 0.4	0.6 ± 0.2	n.d.[b]
	F3	2.9 ± 0.1	0.9 ± 0.1	2.0 ± 1.3	1.0 ± 0.5	0.6 ± 0.3	(0.4)[b]
	Total	7.1 ± 1.8	4.8 ± 0.8	2.3 ± 1.3	5.7 ± 1.8	5.1 ± 2.5	n.d.[b]
OB 15	Asphaltene	4.8 ± 1.5	4.8 ± 1.3	n.d.[b]	13 ± 2.5	11 ± 2.7	n.d.[b]
	F4	2.7 ± 0.6	2.2 ± 0.5	(0.5)[b]	8.9 ± 1.4	3.7 ± 2.2	5.2 ± 2.6
	F3	4.7 ± 1.0	1.7 ± 1.4	3.0 ± 1.7	2.3 ± 0.7	0.9 ± 0.2	1.3 ± 0.7
	Total	12 ± 2.0	8.8 ± 2.0	3.5 ± 2.8	24 ± 2.9	16 ± 3.5	8.5 ± 4.6

The total content was determined with the addition of 20 μg Pd as a modifier and the thermally stable fraction without a modifier. The volatile analyte fraction was determined by difference.

[a] Mass in μg normalized for 1 g of original sample.

[b] n.d., cannot be determined as there is no statistical difference between the results for total and stable Ni or V according to the confidence interval.

Table 5
Recuperation of total, stable and volatile fractions of crude oil

Analyte	Sample	Recuperation (%)		
		Total	Stable	Volatile
Ni	OB 12	71	89	75
	OB 15	57	58	71
V	OB 12	47	57	n.d.[a]
	OB 15	77	80	77

[a] n.d., cannot be determined as there is no statistical difference between the results for total and stable Ni or V according to the confidence interval.

literature [1]. (3) Significant amounts of thermally stable nickel and vanadium compounds, i.e., polar, salt-like compounds could still be detected in fractions F4 and F3, i.e., associated with maltenes. (4) The predominance of volatile nickel and vanadium (vanadyl) compounds in fraction F3 is according to expectation as the metal porphyrin complexes are expected to elute with this fraction.

It is obvious from the comparison of the "Total" data in Tables 3 and 4 that the sum of the fractions in Table 4 is less than the total, stable and volatile content for each element in Table 3. This is a phenomenon very typical for chromatographic separations, as part of the analyte might always be retained irreversibly at the column. Recoveries were calculated for total, the thermally stable and the volatile fractions of both elements in both crude oil samples and are reported in Table 5. The results are acceptable for all elements and fractions except for volatile vanadium in OB 12, which could not be quantified in any of the fractions. No explanation could be found for this extremely low recovery rate, but it must be due to the retention of a vanadyl porphyrin complex at the chromatographic column.

3.3. Figures of merit

The linear regression equations, the correlation coefficient R and the characteristic mass obtained for nickel and vanadium using oil-in-water emulsions prepared with aqueous solutions for calibration, are given in Table 6. The characteristic mass values are in good agreement with literature values for both analytes [29]. The limits of detection (LOD) and quantification (LOQ), defined as the analyte concentration corresponding to an integrated absorbance signal equal to three times and nine times the standard deviation of the blank, were found to be 0.02 μg g^{-1} and 0.06 μg g^{-1}, respectively, for Ni, and 0.06 μg g^{-1} and 0.17 μg g^{-1}, respectively, for V in oil, based on an emulsion of 2 g of oil in 10 mL.

Table 6
Analytical figures of merit for the determination of Ni and V in oil using oil-in-water emulsions without and with the addition of 20 μg Pd as a modifier

Analyte	Modifier	Linear regression equation	R	m_0 (pg)
Ni	–	$A = 0.0167 + 0.2069m$	0.9999	20
Ni	Pd	$A = 0.0352 + 0.2179m$	0.9988	16
V	–	$A = 0.0279 + 0.1122m$	0.9996	37
V	Pd	$A = 0.0094 + 0.1301m$	0.9993	33

4. Conclusion

The present work is a continuation of our previous investigations about the separate determination of the total content and the thermally stable species of nickel and vanadium in crude oil, and calculation of the volatile fraction by difference. It has been speculated in previous work that it is particularly the volatile fraction that is transported in the refining process and that is causing catalyst poisoning and other detrimental problems in petroleum processing. By precipitating the asphaltenes and separating crude oil samples into saturate, polyaromatic, resin and polar fractions using the SARA method it was possible to study the association of nickel and vanadium species to specific crude oil fractions. Only thermally stable species of nickel and vanadium were precipitated with the asphaltenes, however not quantitatively. Some 35–45% of the thermally stable nickel and 25–30% of the thermally stable vanadium and all the volatile species of both elements appeared in the polar and resin fractions of the crude oil samples. This finding underlines the importance of a speciation analysis and a separate determination of the volatile fractions of these two elements. Obviously, a chromatographic separation does not necessarily reflect the processes that might occur during the thermal refining process; however, it is obvious that precipitation of the asphaltenes, a process that is also used to reduce the metal content of crude oils, does not remove the volatile fractions, i.e., the porphyrin complexes of nickel and vanadium.

Acknowledgements

The authors are grateful to Conselho Nacional de Desenvolvimento Científico e Tecnológico (CNPq), to Coordenação de Aperfeiçoamento de Pessoal de Nível Superior (CAPES), to Fundação de Amparo a Pesquisa do Rio Grande do Sul (FAPERGS) and to Fundação de Amparo à Pesquisa do Estado da Bahia (FAPESB) for financial support. M.G.R.V., M.M.S. and I.C.F.D have scholarships from CNPq and BW has a research scholarship from FAPESB. The authors are also grateful to CNPq-Programa de Ciências e Tecnologia do Petróleo (CTPetro Processo 479333/01-7) for financial support, and to Analytik Jena AG for the donation of an atomic absorption spectrometer.

References

[1] M.F. Ali, S. Abbas, Fuel Process. Technol. 87 (2006) 573.
[2] W.E. Rudzinski, T.M. Aminabhavi, Energy Fuels 14 (2000) 464.
[3] S.I. Andersen, A. Keul, E. Stenby, Pet. Sci. Technol. 15 (1997) 611.
[4] C.A. Islãs-Flores, E. Buenrostro-Gonzalez, C. Lira-Galeana, Energy Fuels 19 (2005) 2080.
[5] P.R. Seidl, E.C.A.N. Chrisman, C.C.V. Carvalho, K.Z. Leal, S.M.C. de Menezes, J. Dispersion Sci. Technol. 25 (2004) 349.
[6] B.K. Sharma, S.L.S. Sarowha, S.D. Bhagat, R.K. Tiwari, S.K. Gupta, O.S. Venkataramani, J. Anal. Chem. 360 (1998) 539.
[7] P.R. Seidl, E.C.A.N. Chrisman, R.C. Silva, S.M.C. de Menezes, M.A.G. Teixeira, Pet. Sci. Technol. 22 (2004) 961.
[8] C.T. Mansfield, B.N. Barman, J.V. Thomas, A.K. Mehrotra, J.M. McCann, Anal. Chem. 71 (1999) 81R.
[9] T.G. Fan, J.S. Buckley, Energy Fuels 16 (2002) 1571.
[10] N. Aske, H. Kallevik, J. Sjöblom, Energy Fuels 15 (2001) 1304.

[11] T.J. Kaminski, H.S. Fogler, N. Wolf, P. Wattana, A. Mairal, Energy Fuels 25 (2000) 25.
[12] K. Xie, K. Karan, Energy Fuels 19 (2005) 1252.
[13] A. Hannisdal, M.H. Ese, P.V. Hemmingsen, J. Sjoblom, Colloids Surf., A 276 (1–3) (2006) 45.
[14] A. Jada, A.A. Chaou, Fuel 81 (2002) 1669.
[15] M.D. Garcia, L. Carbognani, M. Orea, A. Urbina, J. Pet. Sci. Eng. 25 (2000) 99.
[16] S.I. Andersen, Pet. Sci. Technol. 15 (1997) 185.
[17] S.I. Andersen, E.H. Stenby, Fuel Sci. Technol. Int. 14 (1996) 261.
[18] F.A.C. Amorim, B. Welz, A.C.S. Costa, F.G. Lepri, M.G.R. Vale, S.L.C. Ferreira, Talanta 72 (2007) 349.
[19] M. Ali, H. Pernazowski, A. Haji, Energy Fuels 7 (1993) 179.
[20] M.G.R. Vale, I.C.F. Damin, A. Klassen, M.M. Silva, B. Welz, A.F. Silva, F.G. Lepri, D.L.G. Borges, U. Heitmann, Microchem. J. 77 (2004) 131.
[21] I.C.F. Damin, M.G.R. Vale, M.M. Silva, B. Welz, F.G. Lepri, W.N.L. dos Santos, S.L.C. Ferreira, J. Anal. At. Spectrom. 20 (2005) 1332.
[22] F.G. Lepri, B. Welz, D.L.G. Borges, A.F. Silva, M.G.R. Vale, U. Heitmann, Anal. Chim. Acta 558 (2006) 195.
[23] B. Welz, H. Becker-Ross, S. Florek, U. Heitmann, High-resolution Continuum Source AAS, Wiley-VCH, Weinheim, 2005.
[24] M.M. Silva, I.C.F. Damin, M.G.R. Vale, B. Welz, Talanta 71 (2007) 1877.
[25] C. Duyck, N. Miekeley, C.P. Silveira, P. Szatmari, Spectrochim. Acta, Part B 57 (2002) 1979.
[26] J.G. Speight, R.B. Long, T.D. Trowbridge, Fuel 63 (1984) 616.
[27] E.T. Premuzic, M.S.L.M. Bohenck, W.M. Zhou, Energy Fuels 297 (1999) 297.
[28] V. Nalwaya, V. Tantayakom, P. Piumsomboon, S. Fogler, Ind. Eng. Chem. Res. 38 (1999) 964.
[29] B. Welz, M. Sperling, Atomic Absorption Spectrometry, third ed., Wiley-VCH, Weinheim, New York, 1999, p. 531.

Available online at www.sciencedirect.com
ScienceDirect
Talanta 74 (2008) 1681–1685
Talanta
www.elsevier.com/locate/talanta

Short communication

Amperometric L-ascorbic acid biosensors equipped with enzyme micelle membrane

Xiuyun Wang [a,b], Hiroaki Watanabe [a], Shunichi Uchiyama [a,*]

[a] *Department of Materials & Science, Graduate School of Engineering, Saitama Institute of Technology, Fukaya, Saitama 369-0293, Japan*
[b] *School of Chemical Engineering, University of Science and Technology Liaoning, Anshan, Liaoning 114051, PR China*

Received 24 July 2007; received in revised form 14 September 2007; accepted 14 September 2007
Available online 19 September 2007

Abstract

Ascorbate oxidase (ASOD) bound to polymaleimidostyrene (PMS) forms stable ASOD micelle structure in polystyrene (PS) membrane. The oxygen permeable hydrophobic ASOD micelle membrane were coated on both aminated glassy carbon electrode (AGCE) and gold electrode (AuE) for the amperometric detections of L-ascorbic acid (AsA) based on the consumption of oxygen. These AsA sensors have good sensitivities with short response time (within 1 min.). A good linear relationship was observed in the concentration range of 5 μM to 0.4 mM when AGCE was used and the applied potential was −0.5 V vs. Ag/AgCl. Interferences from the reducing agents can be avoided because the detections were conducted at cathodic potential.
© 2007 Published by Elsevier B.V.

Keywords: L-Ascorbic acid biosensor; Aminated glassy carbon electrode; Ascorbate oxidase micelle; Polystyrene membrane; Polymaleimidostyrene

1. Introduction

L-Ascorbic acid (AsA) is a very important species in the processes of oxidation and reduction in living organisms. Various determination methods of AsA using chromatographic methods [1,2], spectrophotometric methods [3,4], electrochemical methods [5–9] have been reported. Electrochemical methods have long been used to detect AsA either directly or combined with other techniques. The enzymatic methods are known to be very sensitive, specific, simple and useful methods, in which the immobilizations of enzymes are generally used.

Polystyrene (PS) which has admirable properties such as excellent biocompatibility, no toxicity, strong adsorption ability, and the chemical inertness is one of the most popular supporting materials for protein immobilization in enzyme-linked immunosorbent assays (ELIA). Many scientists have immobilized enzymes [10–15], antigens or antibody [16] on the activated polystyrene surface to develop bioanalytical methods. However, the conventional approaches need multi-step procedures and are tedious and time consuming. If polystyrene membrane was directly used to immobilize enzyme, it is expected that a simple and mild procedure for immobilization of proteins can be realized. But polystyrene membrane is known to be strongly hydrophobic material and stable enzyme immobilization into PS membrane is very difficult, because hydrophilic enzyme must be separated from hydrophobic PS membrane and enzyme structure is damaged by adsorption to PS surface.

Recently, it has been found that polymaleimidostyrene (PMS) is very effective reagent to immobilize enzyme strongly via covalent bond, because high density of maleimide groups of PMS react with not only exposed SH groups but also buried SH groups of proteins [17] and PMS can preserve enzyme conformation [18,19]. In our previous study, we found enzyme micelle formed in PS membrane in the presence of PMS and uricase, and AuE coated by enzyme micelle membrane exhibited good response of oxygen [20]. Therefore, if ascorbate oxidase (ASOD) micelle membrane can be formed as well as uricase micelle membrane, an amperometric sensor of AsA based on the consumption of oxygen can be developed.

* Corresponding author. Tel.: +81 48 585 6839; fax: +81 48 585 6004.
E-mail address: uchiyama@sit.ac.jp (S. Uchiyama).

0039-9140/$ – see front matter © 2007 Published by Elsevier B.V.
doi:10.1016/j.talanta.2007.09.008

The amount of oxygen consumed by ASOD reaction can be measured by the reduction current of oxygen and both enzymatic and electrochemical reactions occur according to the following Eqs. (1) and (2).

$$\text{L-ascorbic acid} + \tfrac{1}{2}O_2 \xrightarrow{\text{ASOD}} \text{dehydroascorbic acid} + H_2O \quad (1)$$

$$O_2 + 4e^- + 4H^+ \rightarrow 2H_2O \quad (2)$$

AsA is well known to be strong reducing agent and many amperometric sensors using direct oxidations of AsA using GCE have been fabricated. To increase selectivity or electrocatalytic activity for AsA, many researches focused on the pretreatment or modification of GCE surface have been reported [21–25]. However, the direct electrode oxidation of AsA is interfered by the coexistence of many common reducing agents. On the other hand, if the reduction of oxygen is used as a detection principle, such interferences can be avoided because the detection was conducted at cathodic potential. However, the reduction of oxygen has not been used in AsA biosensor using GCE because the reduction rate of oxygen at GCE is very slow compared with that by gold electrode (AuE). Recently, we have reported that aminated GCE (AGCE) is fabricated by electrooxidation of GCE in ammonium carbamate solution [26] and we have found that oxygen reduction current was significantly amplified by amination of GCE [27]. In this study, AsA biosensor was developed by combining AGCE with ASOD micelle membrane, and it has been estimated that the response obtained by AsA biosensor using AGCE is superior to that obtained by AsA biosensor using AuE.

2. Experimental

2.1. Reagents and chemicals

All chemicals used were of analytical grade and were used without any further purifications. Ascorbate oxidase (ASOD, 162 U mg^{-1}) from cucumber was purchased from Oriental Yeast Co., Ltd. Polymaleimidostyrene (PMS) was supplied by Tsukuba Materials Information Laboratory (Japan). Polystyrene (PS) and L-ascorbic acid sodium salt (AsA) were purchased from Wako Pure Chemical Industries Ltd. Ammonium carbamate (Merck, Germany) was used to pre-electrolyze the glassy carbon electrode (GCE). Commercially available fruit juices were used as real samples of AsA.

2.2. Apparatus and procedure

Electrochemical analyzer (BAS 100B) was used to perform electrochemical measurements. A three-electrode cell consisted of a GCE (1.0 and 3.0 mm of diameters) or AuE (3.0 mm of diameter) as a working electrode, an Ag/AgCl reference electrode, and a platinum wire counter electrode. Constant potential amperometric measurements of AsA were conducted using enzyme-immobilized AGCE (or AuE) in phosphate buffer solutions (PBS, 0.1 M) saturated with oxygen at room temperature under stable stirring condition. A stirrer (SSR-112N, IWAKI) was used to coat polystyrene membrane onto AGCE or AuE surface.

A scanning electron microscope (SEM, JSM-5500LV) was employed to observe the surface morphologies of the PS membranes which were coated on the electrodes surfaces

2.3. Sensor preparation

GCE was prepared by polishing 6, 1 and 0.05 μm alumina powders on polishing pads. After rinsed with pure water, the GCE was pre-electrolyzed in 0.1 M of ammonium carbamate aqueous solution for 1 h at +1.1 V. Then it was placed on a stirrer with a rotation speed of 120 rpm.

ASOD micelle membrane was prepared as follows: 20 μL of chloroform, 10 μL of PS chloroform solution (30.0 mg mL^{-1}), 10 μL of PMS chloroform solution (5.0 mg mL^{-1}) and 0.5 mg of ASOD were mixed. The mixture was spread onto the rotating AGCE surface with a pipette to form a thin membrane. In order to make a good immobilization of enzyme, 10 μL of PS solution was spread onto the dried PS membrane surface and dried again (in 5 min). The AGCE coated with ASOD micelle membrane was used to conduct amperometric measurements.

AuE surface was coated with ASOD micelle membrane in a similar manner to AGCE by replacing AGCE by AuE.

3. Results and discussions

3.1. Morphologies of the enzyme micelle membranes

The thickness of the membrane was obtained to be about 7 μm that was calculated by presuming the PS density of 1.05 g cm^{-3}. The surface morphologies of PS membranes coated on GCE electrodes or gold electrodes were characterized by scanning electron microscopy (SEM). Fig. 1 displays the PS membrane structure containing ASOD micelle on GCE surface. There is no obvious difference between the surface morphologies of PS membrane containing ASOD micelle coated on the GCE surface and that on the AuE surface. The ASOD micelles in the PS membrane are roughly uniform with diameters of 0.8–1.0 μm.

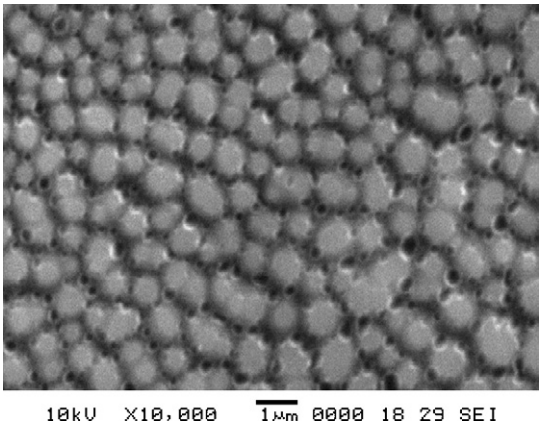

Fig. 1. SEM image of PS membrane containing ASOD micelle coated on GCE surface.

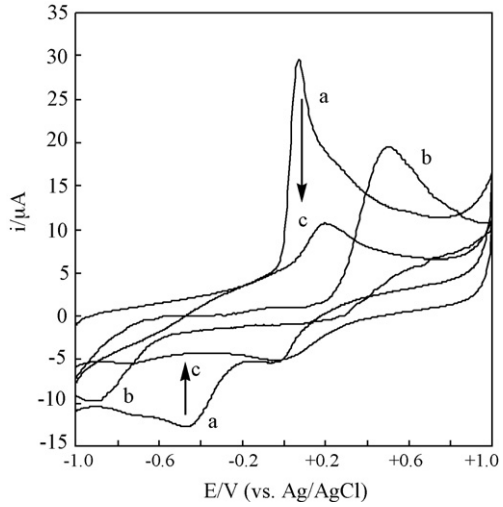

Fig. 2. Cyclic voltammetric response of 1 mM of AsA obtained at (a and c) aminated and (b) bare GCE in the presence (c) or absence (a and b) of 1 mg mL^{-1} of ASOD. Scan rate: 100 mV s^{-1}. PBS: 0.1 M pH 5.5.

3.2. Effect of amination of GCE on catalytic oxygen reduction

Fig. 2 shows the cyclic voltammograms of 1 mM of AsA at AGCE (Fig. 2a and c) and bare GCE (Fig. 2b) in PBS at a scan rate of 100 mM s^{-1}. The oxidation potential of AsA and the reduction potential of oxygen observed at AGCE shifted toward positive and negative directions, respectively, compared with those observed at bare GCE. Fig. 2c indicates the cyclic voltammogram obtained after enzymatic reaction of AsA proceeded for 30 s. It can be recognized that both AsA oxidation and oxygen reduction waves decreased indicating that the catalytic oxidation of AsA and catalytic reduction of oxygen can be realized at AGCE. It can be seen that the reduction current of oxygen begins to appear from approximately −0.1 V and reaches the maximum value at −0.42 V at AGCE, nevertheless the reduction current begins to appear from −0.5 V and reaches the maximum value at around −0.85 V at bare GCE. Until now, the amperometric sensors using GCE have not been popular because the reduction rate of oxygen is very slower than metal electrodes such as AuE. The reducing agents such as uric acid and catechol amines exhibited no responses, at such negative potential, however a low applied potential is desirable for the practical application of AsA sensor in real samples in which oxidizing agents such as hydrogen peroxide are contained. Then, highly selective amperometric determination of AsA using AGCE must be carried out if enzyme membrane is coated onto an AGCE.

3.3. Response characteristics of AsA

Fig. 3 shows the constant potential amperometric response curves of AsA at −0.5 V and −0.3 V in oxygen saturated PBS under stable stirring condition at room temperature. The results indicate that this sensor exhibited an excellent response for AsA with short response time (within 1 min). Good linear relationships were observed between AsA and constant potential amperometric current response in the concentration

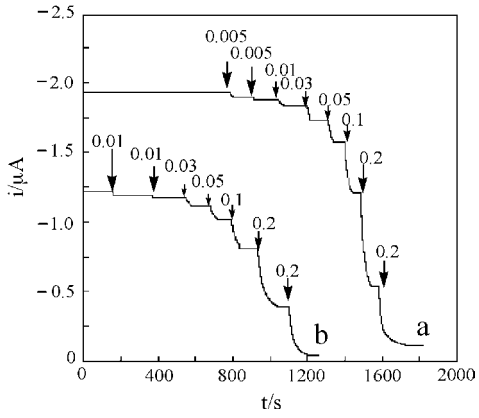

Fig. 3. Constant potential amperometric response curves of AsA at AGCE coated by ASOD micelle membrane at (a) −0.5 V and (b) −0.3 V in PBS (0.1 M, pH 5.50) under stirring condition at room temperature. Addition unit: mM.

range of 5 μM to 0.4 mM ($y = 3.4468x + 0.0196$, $r = 0.9999$) at −0.5 V while the linear range extended from 0.01 to 0.6 mM ($y = 1.9761x - 0.0057$, $r = 0.9995$) at −0.3 V. The detection limit is 2 μM and 4 μM, respectively. The relative standard deviation of 10 data was under 3.0% when AsA concentration was 0.1 mM.

The amperometric detections of AsA were also conducted at bare AuE coated with ASOD micelle membrane at −0.7 V in PBS. This sensor exhibited an amperometric response for AsA with short response time (Fig. 4 within 1 min). The good linear relationship of AsA and constant potential amperometric current response was observed in a concentration range from 0.01 to 0.6 mM. However, this sensor exhibited low response at −0.7 V compared with the sensor fabricated by AGCE at −0.5 V in the same method.

The cyclic voltammetric results of PBS saturated with oxygen at AGCE, AuE and GCE and amperometric results of AsA using at those electrodes modified with ASOD micelle membranes were summarized in Table 1. From these results, in a low potential range, the current responses of oxygen obtained by both AGCE and AuE were found to be significantly higher than the current response obtained by bare GCE. The cyclic voltam-

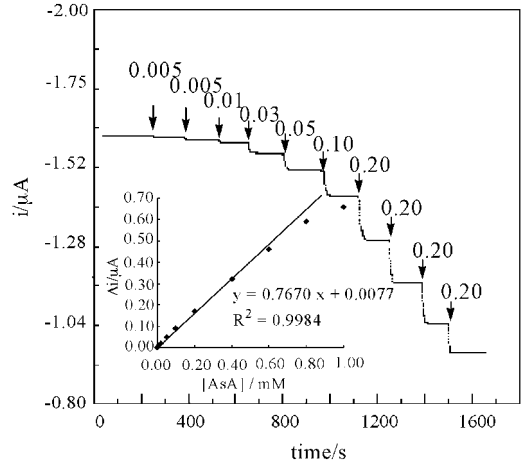

Fig. 4. Constant potential amperometric response curve of AsA at AuE coated by ASOD micelle membrane under stable stirring condition in PBS (0.1 M, pH 5.50) at −0.7 V (vs. Ag/AgCl). Addition unit: mM.

Table 1
Comparison of the cyclic voltammetric response of PBS saturated with oxygen at AGCE, AuE and GCE and amperometric results of AsA at those electrodes modified with ASOD micelle membranes

Electrode	Cyclic voltammetric responses of PBS saturated with oxygen at −0.3 V (μA)	Amperometry of AsA		
		Current response of 0.1 mM AsA (μA)		Detection limit of AsA at −0.3 V (μM)
		−0.3 V	−0.7 V	
AGCE	7.9	0.192	0.48	4
AuE	9.2	0.037	0.11	18
GCE	1.4	0.004	0.08	200

Table 2
Constant amperometric detection of AsA contents in fruit juices at −0.5 V vs. Ag/AgCl

Beverage (100 mL)	Declared content (mg)	Found content[a] (mg)	R.S.D.%	Recovery%
Lemon juice	400	403	0.79	100
Vitamin lemon juice	714	716	0.18	103
Orange juice	44	43.5	1.3	100
Fruit drink	50	50.8	1.7	101

[a] Mean value of five data.

metric response of oxygen at AuE exhibited better sensitivity than at AGCE, however the amperometric current response of AsA obtained by using AGCE modified with ASOD micelle membrane was more than four times as large as that obtained by AuE modified with ASOD micelle membrane. The affinity of PS membrane to GCE is much stronger than that to AuE, and the stability of the enzyme micelle membrane coated on glassy carbon is superior to that coated on AuE. It can be considered that the excellent affinity of enzyme micelle membrane to GCE may enhance the AsA responses, differing from AsA sensor using AuE.

3.4. Effect of pH and stability

Effect of pH on amperometric response currents was studied at −0.5 V at AGEC coated with ASOD micelle. And the optimum pH value was 5.50.

The long-term stabilities of the sensor responses of AsA sensors using AGCEs with diameters of 1.0 mm and 3.0 mm were studied as shown in Fig. 5. AsA sensor using AGCE with a diameter of 3.0 mm maintained its initial response for 6 days, and decreased to approximately 60% after being stored for 2 weeks. When ASOD micelle membrane was coated on an AGCE with a diameter of 1.0 mm, no loss of sensor response was observed for 2 weeks and 80% of activity still remained even after stored for 30 days. This result suggests that the major reason of the decrease of the sensor response is not due to the loss of enzyme activity and the good sensor stability of small AGCE surface was due to the strong affinity of PS membrane to the polyetheretherketone part of GCE surface because of its hydrophobic property and no smoothness. However, the AGCE surface (central part) has hydrophilic property and is very smooth, then, the smaller the AGCE surface is, the stable is the enzyme micelle membrane. The sensors were stored in 0.1 M, pH 7.0 PBS at 4 °C when not in use.

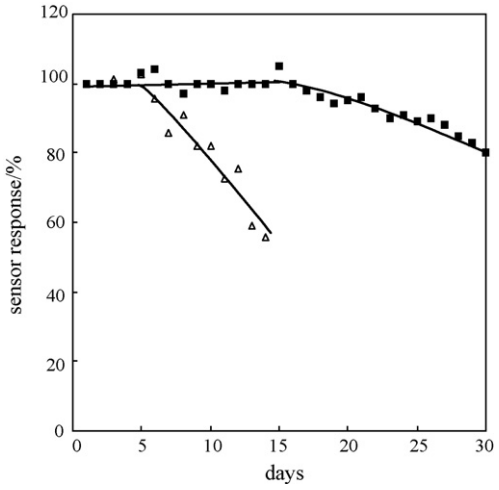

Fig. 5. Long-term stabilities of the responses of AsA sensors using AGCEs with diameters of 1.0 mm (■) and 3.0 mm (△).

3.5. Detection of vitamin C content in fruit juice

Both the AsA biosensor fabricated with AGCE and that fabricated with AuE exhibited good responses to the contents of AsA in real samples, however, the sensitivity of AsA sensor using AGCE was higher than that using AuE. Then, the contents of AsA in fruit juices detected by AsA biosensor using AGCE at −0.5 V are shown in Table 2. The AsA values detected were in good agreement with those of the declared content.

4. Conclusions

Inexpensive PS membrane was successfully employed as the support of ASOD micelles which were formed by binding ASOD with PMS. Oxygen penetrated the enzyme micelle membrane and was reduced at AGCE or AuE. The detection of AsA at

both AGCE and AuE exhibited good response of catalytic reduction current of oxygen with high sensitivity and were less time consuming. The successful immobilizations of other enzymes into PS membrane can be expected and the other biosensors based on enzyme micelle will be reported in the near future.

References

[1] P. Lopes, J. Drinkine, C. Sacier, Y. Glories, Anal. Chim. Acta 555 (2006) 242.
[2] Y. Hernandez, M.G. Lobo, M. Gonzalez, Food Chem. 96 (2006) 654.
[3] B. Tang, Y. Wang, M. Du, J. Ge, Z. Chen, J. Agric. Food Chem. 51 (2003) 4198.
[4] Y. Andreu, S.D. Marcos, J.R. Castillo, J. Galban, Talanta 65 (2005) 1045.
[5] V.S. Ijeri, P.V. Jaiswal, A.K. Srivastava, Anal. Chim. Acta 439 (2001) 291.
[6] Z. Bae, J. Park, S. Lee, H. Chang, J. Electroanal. Chem. 468 (1) (1999) 85.
[7] V.S. Ijeri, M. Algarra, A. Martins, Electroanalysis 16 (2004) 2082.
[8] S. Uchiyama, Y. Kobayashi, S. Suzuki, O. Hamamoto, Anal. Chem. 63 (1991) 2259.
[9] M.F.S. Teixeira, L.A. Ramos, O. Fatibello, E.T.G. Cavalheiro, Anal. Bioanal. Chem. 376 (2003) 214.
[10] Y. Kumada, Y. Tokunaga, H. Imanaka, K. Imamura, T. Sakiyama, S. Katoh, K. Nakanishi, Biotechnol. Prog. 22 (2006) 401.
[11] U. Bora, L. Chugh, P. Nahar, J. Immunol. Methods 268 (2002) 171.
[12] A. Sellborn, M. Andersson, J. Hedlund, J. Andersson, M. Berglin, H. Elwing, Mol. Immunol. 42 (2005) 569.
[13] P. Nahar, N.M. Wali, R.P. Gandhi, Anal. Biochem. 294 (2001) 148.
[14] J. Kaur, K.V. Singh, M. Raje, G.C. Varshney, C.R. Suri, Anal. Chim. Acta 506 (2004) 133.
[15] H. Sun, N. Hu, Analyst 130 (2005) 76.
[16] J.A.G. Aleixo, B. Swaminathan, S.A. Minnich, V.A. Wallshein, J. Immunoassay 6 (1985) 391.
[17] S. Uchiyama, R. Tomita, N. Sekioka, E. Imaizumi, H. Hamana, T. Hagiwara, Bioelectrochemistry 68 (2006) 119.
[18] R. Tomita, K. Kokubun, T. Hagiwara, S. Uchiyama, Anal. Lett. 40 (2007) 449.
[19] X. Wang, H. Watanabe, N. Sekioka, H. Hamana, S. Uchiyama, Electroanalysis 19 (12) (2007) 1300.
[20] X. Wang, T. Hagiwara, S. Uchiyama, Anal. Chim. Acta 587 (2007) 41.
[21] P. Janda, J. Weber, L. Dunsch, A.B.P. Lever, Anal. Chem. 68 (1996) 960.
[22] A. Domenech, H. Garcia, M.T. Domenech-carbo, M.S. Galletero, Anal. Chem. 74 (2002) 562.
[23] P.J. O'Connell, C. Gormally, M. Pravda, G.G. Guilbault, Anal. Chim. Acta 431 (2001) 239.
[24] T.R.L.C. Paixao, D. Lowinsohn, M. Bertotti, J. Agric. Food Chem. 54 (2006) 3072.
[25] R.P. Kalakodimi, M. Nookala, Anal. Chem. 74 (2002) 5531.
[26] S. Uchiyama, H. Watanabe, H. Yamazaki, A. Kanazawa, H. Hamana, Y. Okabe, J. Electrochem. Soc. 154 (2) (2007) F31.
[27] H. Watanabe, S. Uchiyama, Bunseki Kagaku 56 (2007) 433.

Available online at www.sciencedirect.com
ScienceDirect
Talanta 74 (2008) 1122–1125
Talanta
www.elsevier.com/locate/talanta

A phenylhydrazone-based indole receptor for sensing acetate

Yuehong Wang [a], Hai Lin [b], Jie Shao [a], Zun-Sheng Cai [a], Hua-Kuan Lin [a,*]

[a] *Department of Chemistry, Nankai University, Tianjin 300071, China*
[b] *State Key Laboratory of Functional Polymer Materials of Ministry of Education Nankai University, Tianjin 300071, China*

Received 8 June 2007; received in revised form 8 August 2007; accepted 13 August 2007
Available online 22 August 2007

Abstract

A novel phenylhydrazone-based indole anion receptor is synthesized by a simple method, and the receptor binds acetate anions with good selectivity in DMSO solution, which is related to the structure of the receptor matching with the anion. The binding properties of the host are examined by UV–vis changes. The color changes of the host upon the addition of a variety of structurally different anions were also utilized as nake-eyed recognization (from orange to purple, first figure), The hydrogen bonds between recognization sites (phenylhydrazone and indole N–H) and anions were determined on the basis of ^{1}H NMR experiments.
© 2007 Elsevier B.V. All rights reserved.

Keywords: Indole; Phenylhydrazone; Receptor; Nake-eyed recognization

1. Introduction

Anion recognition has attracted considerable attention due to their medicinal and environmental potential application [1–3]. Receptors [4] and sensors [5–7] having strong affinity and selectivity for specific anions arouses of great interest in supramolecular chemistry [8]. So, the design of anion receptors with high selectivity is challenging [9–11]. Synthetic receptors for anions are usually based on urea/thiourea [12,13], amides [14,15,25], macrocyclic ammonium/guanidinium [16,17], functionalized calixarenes [18,19], phenylhydrazone [20], indole [21] and –OH [26]. Take the phenylhydrazone for example, first, this kind of the receptor is neutral and the synthetic method is simple. Secondly, the reactant indoline-2,3-dione and 2,4-nitrophenylhydrazine could recognize anion by itself and had a nake-eyed color change. Of particular interest in this regard is the color of phenylhydrazone, which changed so obviously (from orange to purple) upon addition of AcO^- anion that we could use the nake-eyed detection without resorting to any spectroscopic instrumentation.

In the present work, we designed and synthesized the 3-(2′,4′-dinitrophenylhydrazone)indolin-2-one. It is provided with the merit, which we referred to. We believe that the receptor will have a better-applied foreground.

2. Experimental

2.1. Reagents

All anions, in the form of tetrabutylammonium salts, were purchased from Sigma–Aldrich Chemical Co., stored in a desiccator under vacuum containing self-indicating silica, and used without any further purification. Solvents were purified prior to use and stored under nitrogen. Dimethyl sulfoxide was dried with calcium hydride and distilled at reduced pressure. Unless stated otherwise, commercial grade chemicals were used without further purification.

2.2. Synthesis

3-(2′,4′-Dinitrophenylhydrazone)indolin-2-one. A solution of 2,3-dikedoine (isatin) (4 mmol) in ethanol (20 ml) was added dropwise to a solution of 2,4-nitrophenylhydrazine (4 mmol) in ethanol (60 ml) with stirring at reflux. After being stirred for 5 h, the solvent was removed by evaporation. Recrystallization (ethanol) yielded yellow crystals. δ_H (400 MHz, DMSO-d_6, Me_4Si): 11.73 (s, 1H, N–H), 10.91 (s, 1H, N–H), 8.92 (d, 1H, Ar–H, $J = 4$ Hz), 8.59 (d, 1H, Ar–H, $J = 8$ Hz), 8.16 (d, 1H,

* Corresponding author. Fax: +86 22 23502458.
E-mail address: hklin@nankai.edu.cn (H.-K. Lin).

0039-9140/$ – see front matter © 2007 Elsevier B.V. All rights reserved.
doi:10.1016/j.talanta.2007.08.015

Ar–H, $J = 8$ Hz), 7.89 (d, 1H, Ar–H, $J = 8$ Hz), 7.48 (t, 1H, Ar–H, $J = 12$ Hz), 7.21 (t, 1H, Ar–H, $J = 12$ Hz), 6.97 (d, 1H, Ar–H, $J = 8$ Hz). Anal. Calcd. for $C_{14}H_9N_5O_5$: C 51.38, H 2.77, N 21.40, Found C 51.54, H 2.38, N 21.55.

2.3. General methods

Unless otherwise specified, all of the experiments were carried out at 298 ± 1 K. The ^{1}H NMR spectra were recorded on a Varian UNITY-plus 400 MHz spectrometer using tetramethylsilane (TMS) as an internal standard. UV–vis spectra were recorded on a Shimadzu UV-2450 PC spectrophotometer.

2.4. Absorption titration studies

The binding ability of receptor for $CH_3CO_2^-$, $H_2PO_4^-$, and halide anions (as tetrabutylammonium salts) was investigated by UV–vis spectroscopy in DMSO solution using a constant host concentration (3.0×10^{-5} M) and increasing concentrations of anions. The change in absorbance at 561 nm for receptor was plotted against anion concentration and fitted by the equation as described by Connors [22].

2.5. ^{1}H NMR titrations

Receptor 1 (5.0×10^{-3} M in DMSO-d_6) was titrated against acetate anions (tetrabutylammonium salts) by addition of excess anion in DMSO-d_6.

3. Results and discussion

Here, we reported a remarkable selective indolehydrazone-based acetate chromo-chemosensor of a Schiff-base compound, 3-(2′,4′-dinitrophenylhydrazone)indolin-2-one. It contained an indolehydrazone group that could be transformed to phenol form in the presence of anions (Scheme 1) [23,24].

3.1. UV–vis experiments

In DMSO solution, the receptor could form hydrogen bond with AcO^-, F^- and $H_2PO_4^-$ anions, respectively, and the color of solution changed significantly (Fig. 1). The anion-binding properties were investegated by UV–vis titration of the recepror in DMSO solution using standard tetrabutylammonium salts of AcO^-, F^- and $H_2PO_4^-$. As shown in Fig. 2 , the titration of receptor ($c = 3.0 \times 10^{-5}$ M), exhibited a broad strong absorption band at 383 nm due to the nitrophenylhydrazone. The intensity

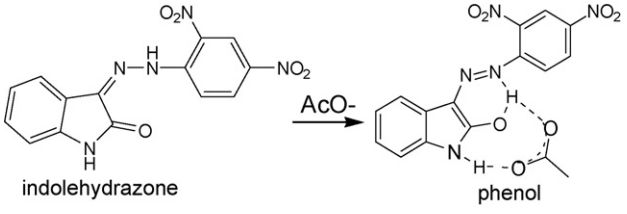

Scheme 1. Proposed mode of transformatin of the receptor upon binding anion.

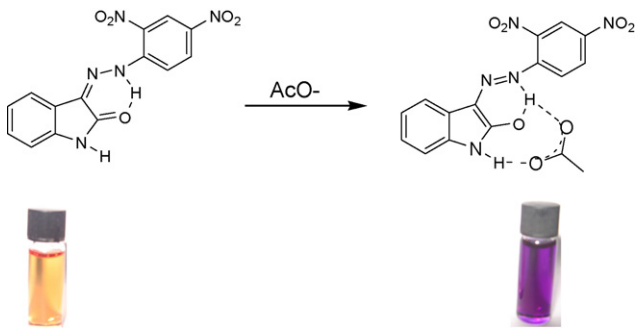

Fig. 1. Color changes from receptor (3×10^{-5} M) to receptor + AcO^- (3×10^{-4} M) in DMSO.

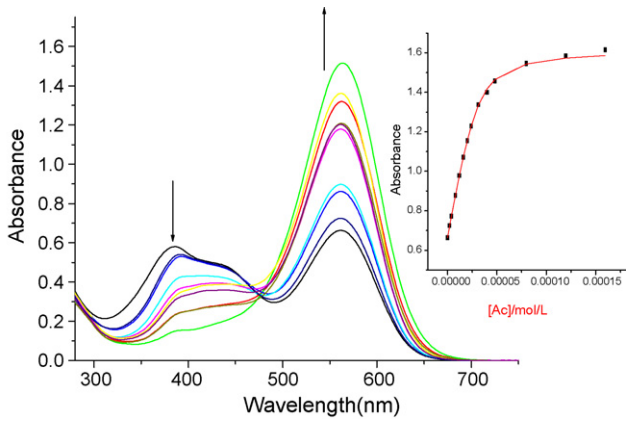

Fig. 2. The UV–vis spectra of receptor (3×10^{-5} M) in DMSO solution during the titration with tertrabutylammonium (TBA) acetate (0, 0.067, 0.133, 0.266, 0.5, 0.633, 0.67, 0.766, 1.2, 1.6, 1.8, 2.0, 4.2, 5.6 equiv.). Inset: titration plots observed binding profiles and corresponding nonlinear fit plots monitored by the absorption increase at 561 nm.

of the absorption peak at 383 nm was remarkably reduced with a simultaneous growth of the peak at 561 nm (Fig. 2) and meanwhile the solution color changed from orange to purple (Fig. 1). The presence of isobestic points during titration with acetate revealed the formation of 1:1 complexes (Fig. 3). No significant changes in absorption or a noticeable color changes were observed for other anions such as Cl^-, Br^-, I^-.

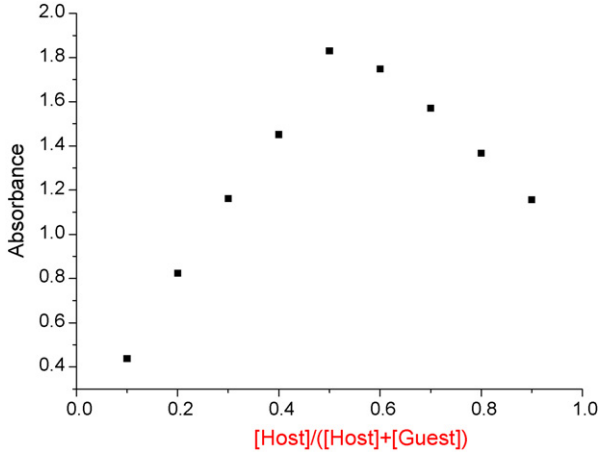

Fig. 3. A job plot of receptor with tetrabutylammonium acetate.

Table 1
Association constants K_{ass} of receptors 1 with anions in DMSO

Anion	AcO^-	F^-	$H_2PO_4^-$	Cl^-	Br^-	I^-
$K_{ass}(M^{-1})$	2.32×10^5	6.22×10^4	2.25×10^4	ND	ND	ND

The anions were added as their tetrabutylammonium salts. All errors are ±10%; ND: the spectra have too small change with adding anion so we cannot determine the affinity constant by the spectra.

Detail data was given in Table 1. The association constant K_{ass} was calculated by non-linear least square regression method [22]. For the receptor, the association constant for AcO^- was larger than that of F^- and $H_2PO_4^-$. The reason was probably that the selective recognition for acetate anion is related to the configuration of the acetate matching with the receptor (Fig. 1) and the alkalescence of the anion, as well as the basicity of receptor. Because acetate anion was a plane and triangular and the angle of O–C–O was about 120°, the distance of two oxygen atoms might be fit to the two hydrogen atoms on recognition sites of the receptor in the triangular configuration, Furthermore, the alkalescence of acetate anion was also stronger than the other anions (Cl^-, Br^-, I^-). So, the association constant K_{ass} for acetate was maximal. The angle of O–P–O is about 108° for $H_2PO_4^-$ (tetrahedral configuration) and the distance of two oxygen atoms of AcO^- was longer than that of $H_2PO_4^-$; so two oxygen atoms of $H_2PO_4^-$ could not match well with two hydrogen atoms in the receptor. As for F^-, it was global and had the smallest atom radius in halide atom, but the better alkalescence made itself have the higher association constant K_{ass} than $H_2PO_4^-$. Table 1 illustrated that the receptor can bind anions in the order $AcO^- > F^- > H_2PO_4^- > Cl^- \sim Br^- \sim I^-$.

3.2. ^1H NMR titrations

Further supports for the notion that the formation of hydrogen bonds between N–H groups and anions came from ^1H NMR spectroscopic analyses. These were carried out in DMSO-*d* under normal conditions of so-called NMR titration, with the spectra of the receptors being recorded in the presence of increasing concentrations of anions (Fig. 4). A notable feature of these titrations was that the resonances corresponding to the indole N–H proton, as well as the hydrazone N–H signal shift downfield over the course of the titration. However, the fact the N–H signals were observable throughout the titration was consistent with a hydrogen-binding process involving the receptor. In the specific case of receptor with acetate anion, the singlet peak of the indole N–H protons broadened and meanwhile shifted from 11.73 to 11.94 ppm upon addition of 0.8 equiv. of tetrabutylammonium acetate (Fig. 4). Addition of the second equivalent of acetate caused substantial broadening and downfield shift of all indole N–H protons, as well as all hydrazone N–H protons. Similarly, much broadening of the aromatic protons was observed in NMR titrations of all anions. These results clearly indicated that, in addition to the formation of hydrogen bonds between acetate and N–H groups. But some shifted slightly upfield, the others appeared slightly downfield for the aromatic protons, and two effects were responsible for the spectral changes of the aromatic protons upon NH-anion hydrogen bond formation (1) through-bond effects, which increased the electron density of the phenyl ring and promoted upfield shifts, and (2) through-space effects, which polarized the C–H bond in proximity to hydrogen bonds, created partial positive charge on the proton, and caused downfield shifts. As mentioned above, the proposed binding mode was shown in Scheme 1.

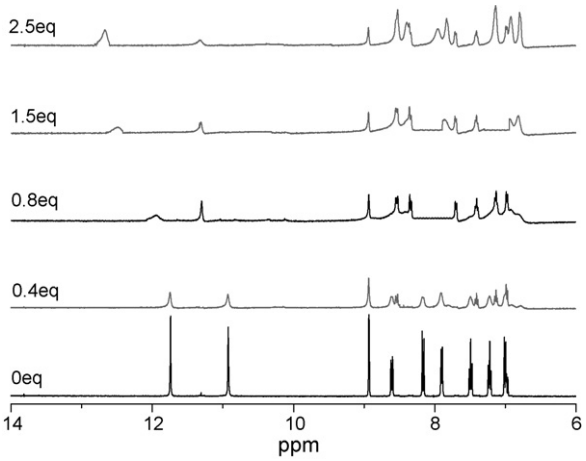

Fig. 4. 1H NMR titration of a DMSO-d_6 solution of receptor with AcO^-.

4. Analytical application

The phenylhydrazone-based indole receptor would have potential application in analytical chemistry, because the receptor was applied in the monitoring of binding ability with various anions (AcO^-, $H_2PO_4^-$, F^-, Cl^-, Br^-, and I^-), which existed widely in biological, industrial, and environmental processes; e.g., carboxylate anions (CH_3COO^-) played an important role in organic, environmental, biological processes, etc. The carboxylate functions of enzymes and antibodies ascribed to their specific biochemical behaviors. Moreover, they were critical components of numerous metabolic processes. So, the development of sensitive detection systems for their binding-ability was very important. In the paper, the selective recognization of the receptor for acetate anion was designed; synthesized and studied. In the first place, color changes of the receptor solution was tested in DMSO (3×10^{-5} M) and the solution color changed from orange to purple upon addition of 10 equiv. AcO^-, which was shown in the Fig. 1. In the next place; the binding ability of the host with different anions was investigated through UV–vis titration in DMSO. Obviously; AcO^- anion; whose association constant was maximal; could be recognized selectively from the other anions tested according to the affinity constants in the Table 1. Especially, the interactions between the receptor and anions accompanied the naked-eyed color changes (from orange

to purple), which were expected to be convenient and feasible application in the practical detection of anions. So; the receptor could be considered as a potential AcO^- anion sensor in many biological and analytical applications.

5. Conclusion

Examination of the binding patterns of chemosensors by UV–vis titrations with a series of structurally different anions (in solvents with strong polarity) provided very important information that the chemsensor preferred structure matching anion such as acetate. Such behavior is speculated to reflect the sizes of the binding sites of these chemosensors. The solution color of the receptor changed obviously (from orange to purple) with the addition of AcO^-, F^- and $H_2PO_4^-$, thus usefullness in distinguishing these anions. ^1H NMR Titrations indicated that the pattern of the receptor interaction with anion was hydrogen bond.

Acknowledgements

This work was supported by a project 20371028, 20671052 from the National Natural Science Foundation of China and a project 023605811 from the Natural Science Foundation of Tianjin.

References

[1] P.D. Beer, P.A. Gale, Angew. Chem. Int. Ed. 40 (2001) 486.
[2] P.A. Gale, Coord. Chem. Rev. 199 (2000) 181.
[3] A. Bianchi, K. Bowman-James, E. Garcia-Espana, Supramolecular Chemistry of Anions, Wiley–VCH, New York, 1997.
[4] F.P. Schmidtchen, M. Berger, Chem. Rev. 97 (1997) 1609–1646.
[5] R. Martinez-Manez, F. Sancenon, Chem. Rev. 103 (2003) 4419–4476.
[6] C. Suksai, T. Tuntulani, Chem. Soc. Rev. 32 (2003) 192–202.
[7] P.D. Beer, Acc. Chem. Res. 31 (1998) 71–80.
[8] J.L. Atwood, J.E.D. Davies, D.D. MacNicol, F. Vogtle, K.S. Suslick (Eds.), Comprehensive Supramolecular Chemistry, Pergamon, Oxford, 1996.
[9] Y. Kubo, M. Tsukahara, S. Ishihara, S. Tokita, Chem. Commun. (2000) 653.
[10] M.J. Deetz, M. Shang, B.D. Smith, J. Am. Chem. Soc. 122 (2000) 6201.
[11] K. Choi, A.D. Hamilton, J. Am. Chem. Soc. 123 (2001) 2456.
[12] B.H.M. Snellink-Ruel, M.G.M. Antonisse, J.F.J. Engbersen, P. Timmerman, D.N. Reinhoudt, Eur. J. Org. Chem. (2000) 165.
[13] E. Fan, S.A. Van Arman, S. Kincaid, A.D. Hamilton, J. Am. Chem. Soc. 115 (1993) 369.
[14] P.B. Beer, Chem. Commun. (1996) 689.
[15] S. Valiyaveettil, J.F.J. Engbersen, W. Verboom, D.D. Reinhoudt, Angew. Chem. Int. Ed. 32 (1993) 900.
[16] E. Kimura, S. Aoki, T. Koike, M. Shiro, J. Am. Chem. Soc. 119 (1997) 3068.
[17] K. Niikura, A. Metzger, E.V. Anslyn, J. Am. Chem. Soc. 120 (1998) 8533.
[18] Y. Morzherin, D.M. Rudkevich, W. Verboom, D.N. Reinhoudt, J. Org. Chem. 58 (1993) 7602.
[19] J. Schreeder, J.F.J. Engbersen, A. Casnati, R. Ungaro, D.N. Reinhoudt, J. Org. Chem. 60 (1995) 6448.
[20] Z.-H. Lin, S.-J. Ou, C.-Y. Duan, B.-G. Zhang, Z.-P. Bai, Chem. Commun. (2006) 624–626.
[21] V.M. Sharma, P. Prasanna, K.V.A. Seshu, B. Renuka, C.V.L. Rao, G.S. Kumar, C.P. Narasimhulu, P.A. Babu, R.C. Parank, D. Subramanyam, A. Venkateswarlu, S. Rajagopal, K.B.S. Kumar, C. Seshagiri Rao, N.V.S. Rao Mamidi, D.S. Deevi, R. Ajaykumar, R. Rajagopalan, Bioorg. Med. Chem. Lett. 12 (2002) 2303.
[22] K.A. Connors, Binding Constants, 1st ed., John Wiley & Sons, New York, 1987.
[23] B. Chiswell, F. Lions, M.L. Tomlinson, Inorg. Chem. 3 (1964) 492–499.
[24] H. Tong, G. Zhou, L. Wang, X. Jing, F. Wang, J. Zhang, Tetrahedron Lett. 44 (2003) 131–134.
[25] X.-F. Shang, H. Lin, Z.-Sh. Cai, H.-K. Lin, Talanta 73 (2007) 296–303.
[26] A.K. Jain, V.K. Gupta, L.P. Singh, P. Srivastava, J.R. Raisoni, Talanta 65 (2005) 716–721.

Available online at www.sciencedirect.com
ScienceDirect
Talanta 74 (2008) 1363–1370
Talanta
www.elsevier.com/locate/talanta

Nanodiamond MALDI support for enhancing the credibility of identifying proteins

Li-Ming Wei [a,b], Yan Xue [a,b], Xin-Wen Zhou [a], Hong Jin [a,b], Qian Shi [a], Hao-Jie Lu [a,b,*], Peng-Yuan Yang [a,b,*]

[a] *Institute of Biomedical Sciences, Fudan University, Shanghai, China*
[b] *Department of Chemistry, Fudan University, Shanghai, China*

Received 6 June 2007; received in revised form 11 September 2007; accepted 11 September 2007
Available online 29 September 2007

Abstract

Matrix-assisted laser desorption/ionization mass spectrometry (MALDI-MS) is a standard analytical tool for protein identification and peptide sequencing. High sensitivity and resolution are two critical parameters for recording good peptide mass fingerprinting (PMF) of low abundance proteins. Here, we report a novel nanodiamond (ND) (normal size 3–10 nm) support for MALDI-MS target, over which α-cyano-4-hydrocinnamic acid (CCA) crystallizes evenly. Good reproducibility of relative peak intensity (R.S.D. less than 11.8%) among sample spot (from ring to center) is achieved on ND support. Therefore, the search for "hot spots" during the analysis is not necessary, which is supporting for the automatic acquisition of data. Due to high absorbability of energy from the laser, the ND support improves ionization efficiency of samples. In general, the sensitivity of MS obtained on ND support can be enhanced three to four times compared to the conventional MALDI sample preparation technique. Sensitivity obtained on ND support ranges from 62.5 amol of Arg-vasopressin standard peptide to 1.0 fmol of myoglobin tryptic peptide mixture. Reduced spot size and increased sensitivity in MALDI-MS are also accomplished by ND support. With spot size reduced, the signal intensity of cytochrome *c* (Cyt *c*) tryptic peptide obtained on ND support is at least seven times greater than it acquired on stainless steel. And ND support has been found better tolerance for salt (up to 500 mM NaCl) to MALDI-MS analysis. All these properties make ND support a valuable tool for MALDI-MS identification of proteins.
© 2007 Published by Elsevier B.V.

Keywords: Matrix-assisted laser desorption/ionization (MALDI); Support; Nanodiamond; Sample preparation; Protein identification

1. Introduction

Matrix-assisted laser desorption/ionization time-of-flight mass spectrometry (MALDI-TOF-MS) is used frequently for the rapid identification of proteins in proteolytic digests of bands and spots from one- or two-dimensional gels [1,2]. Although MALDI-MS is very effective for screening high abundance proteins in complex samples, low abundance peptides often remain undetected. In this case, database searching becomes difficult and results may be incredible. These demands put stress on sample purification and sample preparation [3–5].

For sample purification and concentration, integration of small reversed-phase (RP) column at the outlet of pipette tip has been demonstrated to be efficient [6–8]. As an alternative to RP microcolumn, several permanently coated MALDI-MS targets have been developed to allow for more efficient sample concentration and on-target clean up [9–13].

For obtaining satisfactory mass spectra, sample preparation is also an important step [14–16]. Sample preparation in MALDI-MS requires samples and matrix form a "co-crystallite", which strongly influenced by electrolytes, detergents, and other additives [17,18]. And during the ionization step in MALDI-MS, shot-to-shot signal variations can be occurred, which caused mainly by non-homogeneous nature of samples in "co-crystallite" [19]. Much effort has been invested to form crystal as homogeneous as possible [20–22]. At the same time, there are some different materials as target material applied for MALDI-MS analysis. The aim of these experiments is to improve

* Corresponding author at: Institute of Biomedical Sciences, Fudan University, Shanghai 200032, China. Tel.: +86 21 54237416; fax: +86 21 54237961.
E-mail addresses: luhaojie@fudan.edu.cn (H.-J. Lu), pyyang@fudan.edu.cn, weiliming@fudan.edu.cn (P.-Y. Yang).

0039-9140/$ – see front matter © 2007 Published by Elsevier B.V.
doi:10.1016/j.talanta.2007.09.020

sensitivity and reproducibility, to render signal suppression less frequent, and to find materials for a matrix-free laser desorption technique [23–29]. It includes not only choosing material for the plate itself, but also making any surface modifications on the material. For example, there are specialty plates which have hydrophobic coatings or hydrophilic anchors bonded to the surface of plate [30–33]. The use of poly(tetrafluoroethylene) (PTFE) as sample support for MALDI-TOF-MS has been demonstrated to improve the crystallization and the salt tolerance of DNA samples and, thereby, to improve sensitivity [34]. An interesting approach using a removable 3 M product Scotchgard hydrophobic coating (3 M Canada, London, ON, Canada) for MALDI plates has been also reported. Spot size reduction and increased sensitivity in MALDI of small molecules have been demonstrated [35]. In addition to these approaches, Li et al. [36] have made the coated MALDI-MS targets with a silicone/graphite layer, an ideal technique for routine analysis in large-scale proteomic experiments.

Diamond, because of its chemical stability, biological compatibility, and the ability of being doped and deposited in very thin films on a variety of substrates, is gaining increasing attention in biosensor and biochip applications [37,38]. Furthermore, diamond is an exceptional platform for protein adsorption and immobilization [39,40]. Kong et al. [41] have shown nanoparticles could be embedded more firmly in the matrix crystals than microbeads, thereby reducing material loss during sample preparation and analysis. In this study, we applied ND as MALDI support to increase sensitivity and enhance the credibility of identifying protein. Over ND support, peptides are evenly distributed on sample surface, leading to better reproducible of MS detection within sample spot. The detection sensitivity obtained on ND support was improved as documented by mass spectra recorded from 62.5 amol of Arg-vasopressin standard peptide to 1.0 fmol of myoglobin tryptic peptide mixture. The improvement in salt tolerance was also shown on ND support. Likewise, on ND support, we obtained more satisfactory PMF maps and tandem mass spectra of silver-stained proteins separated by 2-DE. Based on these improved mass spectra, unknown proteins were successfully identified.

2. Experimental

2.1. Chemicals and materials

CCA, NH_4HCO_3, bovine serum albumin (BSA), horse heart cytochrome *c* (Cyt *c*), horse heart myoglobin (Myo) were from Sigma–Aldrich (Mississauga, ON, Canada). Citric acid ammonium salt (dibasic) was purchased from Amresco (Solon, OH, USA). Porcine trypsin was obtained from Promega (Madison, WI, USA). Trifluoroacetic acid (TFA) was purchased from Merck (Darm, Germany). Sodium dodecyl sulfate (SDS) and all reagents for gel electrophoresis were from Bio-Rad Laboratories (Hercules, CA, USA). Laminine B (CDPGYIGSR, Mr 966.43) and Arg-vasopressin (Mr 1084.25) were from Applied Biosystems (Framingham, MA, USA). ZipTip μ-C18 was from Millipore (Bedford, MA, USA). The water used for all the experiments was purified with a Milli-Q Plus systems (Millipore) with a resistivity ≥18.2 MΩ/CM.

2.2. Matrix solutions

The matrix solution consists of CCA and citrate in 0.001:1:2 (v/v) trifluoroacetic acid (TFA)-acetonitrile (ACN)-water with the concentration of 4 and 0.2 mg/mL.

2.3. Analyte solutions

2.3.1. Sample solutions

Digestion buffer (25 mM NH_4HCO_3, pH 8.0) containing 200 μg/mL modified trypsin (sequencing grade, Promega) was added to BSA, Cyt *c* and Myo in the proportion of 1:40, then which was incubated overnight at 37 °C. The concentration of BSA, Cyt *c*, and Myo was 3, 6 and 5 μM, respectively. All stock solutions were refrigerated at around 4 °C for further use. For optimizing the concentration of ND support, 30 nM of BSA tryptic peptide was used.

2.3.2. Standard peptide solutions

To evaluate the reproducibility of relative peak intensity of ND support among and within sample spot (from ring to center), 100 nM of laminine B was used. To determine whether ND support would enhance the sensitivity of MALDI-MS, the Arg-vasopressin standard peptide (130 nM) and Myo tryptic peptide (500 nM) were diluted to 125 pM and 2 nM, respectively.

2.3.3. Tryptic digests of gel-separated epithelial cell proteins

Gel pieces were excised from a large-format 2D gel of total cellular proteins from the epithelial cell and transferred to 96-well plate, respectively. They were distained in the mixture solution of 15 mM $K_3Fe(CN)_6$ and 50 mM $Na_2S_2O_3$, then were dried in ACN for 5 min, following which 6 μL of digestion buffer (25 mM NH_4HCO_3, pH 8.0) containing 10 ng/μL modified trypsin was added. After overnight incubation, 60 μL of extraction buffer was added and gel spots were extracted for 20 min. The extraction procedure was repeated once with additional 60 μL of extraction buffer. These operations mentioned above were all performed by the XCISE gel processor systems (Shimadazu Biotech, Shimadazu, Japan). For the corresponding control experiments, peptide solutions were separated evenly to two parts. Finally, peptide solutions were dried by solvent evaporation, except for three spots (11–13), which were concentrated and desalted by ZipTip μ-C18 with XCISE gel processor systems. One part of the concentrated peptide were dissolved by 1 μL of matrix solution and disposed directly on stainless steel. And the other parts were prepared on ND supports for MALDI-MS analysis.

2.4. The preparation of ND support

ND particles used in the experiment were a gift from Prof. Kang Xu, Lanzhou Institute of Chemical and Physics, Chinese

Academy of Sciences (Lanzhou, China). ND particles were in spherical or spherical-like shapes and had an average diameter of 3–10 nm obtained by explosive detonation, as shown in report [42]. ND particles were ultrasonically dispersed in 0.1% TFA at the concentration of 2, 4, 6, 8, 10, 12, 14, 16, 18 and 20 mg/mL. ND particles can suspend in aqueous solution at the concentration of 4 mg/mL with long-term stability, indicating that their surface are grossly hydrogen bonding with aqueous molecule. After being ultrasonic for two times, 0.5 μL of ND suspension was deposited on stainless steel and left in air at room temperature for 5–10 min to form a thin layer. Then 0.5 μL of sample was deposited on ND support, followed by 0.5 μL of matrix, air-dried for 5–10 min and then for further analyzed by MALDI-TOF-MS.

For the conventional sample preparation on stainless steel, matrix solution was coated on the sample spot as its volume reduced.

2.5. MALDI-TOF-MS analysis

An Applied Biosystems 4700 Proteomics Analyzer (TOF/TOF) (Framingham, MA, USA) was used for mass spectral analysis of sample preparation. The UV Nd:YAG laser was operated at a 200 Hz repetition rate with wavelength of 355 nm. The accelerated voltage was operated at 20 kV and batch mode acquisition control. A stainless steel sample plate with 192 spots was used. The analytical range of laser energy was adjusted to slightly above the threshold to obtain good resolution and signal-to-noise ratio (S/N). Reflector spectra were obtained over a mass of 700–3200 Da. All mass spectra shown were obtained in the positive-ion reflection mode with delayed extraction for 120 ns. External calibration was performed with proteolytic peptides of standard Myo with known molecular masses. All the spectra of the real samples were acquired using a default mode. The first five precursor ions with highest intensity were selected for fragmentation. The mass accuracy was about 100 ppm or better. Examination and processing of mass spectral data was performed by Data explorer 4.0 software supplied by Applied Biosystems.

MASCOT search engine (version 2.0; Matix Science, UK)) was used to search all of the tandem mass spectra. GPS explorer software (version 3.0; Applied Biosystems, USA) was used to create and search files with the MASCOT search engine for peptide and protein identifications. Swiss-Prot database (http://www.expasy.ch/sprot-top.html) was used for the search and was restricted to tryptic peptides. One missing cleavage was allowed. Precursor error tolerance was set to <100 ppm, and MS/MS fragment error tolerance was set to <0.5 Da. For unknown proteins, both MS and MS/MS data were submitted for the search. All identified proteins should have at least one MS/MS match with expect value <0.05, and it should be the best match.

To compare the characteristics of ND support and stainless steel, samples were prepared onto the same plate and analyzed by MALDI-TOF under the same experimental conditions.

3. Result and discussion

3.1. Optimization the concentration of ND support

To form different concentration ND support, 0.5 μL of ND suspension (ranged from 2 to 20 mg/mL) was deposited on stainless steel. Each concentration had repeated thrice. 0.5 μL of 30 nM BSA tryptic peptides was deposited on these ND supports, then with matrix solution for MALDI-MS analysis. There are no distinct changes in the resolution of ions, but show differences in the signal intensity. The signal intensity of BSA tryptic peptides was measured with respect to the different concentration of ND support. As illustrated in Fig. 1, the signal intensity of BSA tryptic peptides reached a maximum value at 4 mg/mL and decreased rapidly at 14 mg/mL. As the concentration of ND support is lower, ND support does not absorb enough energy from laser. As the concentration of ND support is higher, the energy absorbed by ND support cannot be transferred to matrix efficiently, and then the signal of peptide ions is decreased. Therefore, the concentration of ND suspension at 4 mg/mL was chosen for the preparation of ND support. Fig. 2 shows the spectra of BSA tryptic peptides obtained on ND support (Fig. 2a) and on stainless steel (Fig. 2b). Good spectra were acquired for 1500 laser shots. As can be clearly seen from the two spectra, the spectrum of BSA tryptic peptides obtained on ND support shows higher signal intensity than that obtained on stainless steel.

3.2. Reproducibility among and within sample spot

One concern we had was ND support would degrade the relative standard deviation (R.S.D.) of among sample spots and within sample spot. The R.S.D. value of peak intensity for laminine B among ten ND supports (prepared by 0.5 μL of 4 mg/mL ND suspension) is around 13.0%, while it is 9% obtained on stainless steel. The uneven magnitude of ND particles may explain the phenomenon. The R.S.D. value of peak intensity for laminine B within one sample spot (six spectra obtained from ring to center on stainless steel) is around 18.8%, while it is down to 11.8% obtained on ND support. With the evaporation of solvent, hydrophobic peptides were distributed on the ring of stainless steel. However, hydrophilic peptides were concentrated

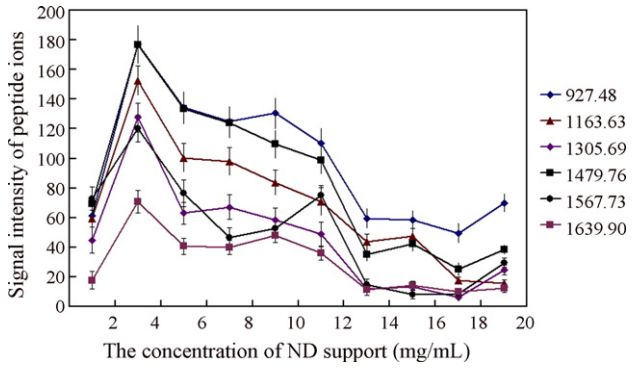

Fig. 1. The signal intensity of BSA tryptic peptide ions vs. the different concentration of ND support.

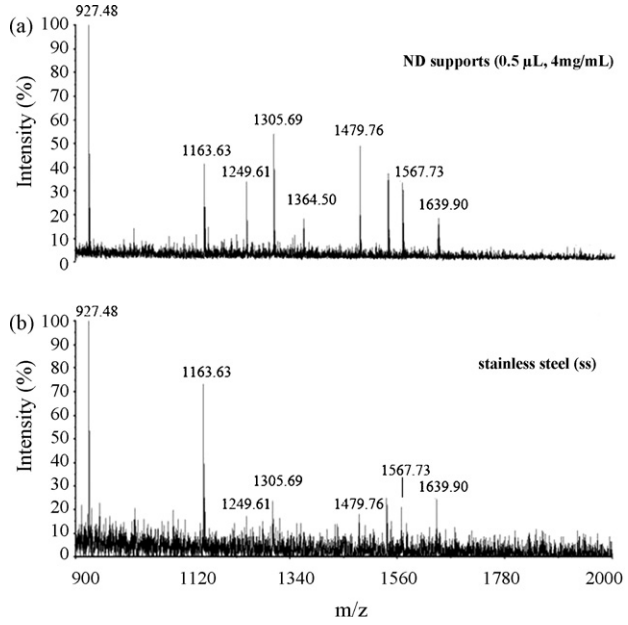

Fig. 2. MALDI-TOF-MS obtained from 0.5 μL of 30 nM BSA tryptic peptide. The sample was prepared on the ND support (0.5 μL, 4 mg/mL) (a) and on stainless steel (SS) (b), respectively. (a and b) Show the observed *m/z* of BSA fragments. The database search results were obtained with (a).

on the center of spot. The matrix-mixture method was reported that the generation of ions from the rim of the sample spot required twice the laser power than that used for generating ions from the center [43]. Over ND support, a homogeneous, evenly distributed layer was shown. ND particles absorbed peptides to its surface via hydrophobic interaction and other molecular interaction. The ND nucleation results in high retention of hydrogen (up to 20%) and different C–H bonding proved by Michaelson and Hoffman [44]. The peptides can be distributed on ND support evenly, which helps for the automatic analysis of targets without finding the "hot spots".

3.3. Decreasing spot size and increasing sensitivity

While MALDI sample preparation remains a complex and often mysterious task, the areas to MALDI-MS applied continue to expand due to its versatility. Spot size reduction is advantageous when using diluted matrix solutions to analyze samples obtainable only in low concentration [45,46]. In a series of experiments, the spot size was controlled by the volume of ND suspension (4 mg/mL) deposited on stainless steel. Fig. 3a–d shows photographs documenting crystals on spot. For the stainless steel CCA spot (Fig. 3a), no further shrinkage happened and the crystal was distributed on spot and centralized on center. While the CCA with peptide produced a homogeneous crystal layer on ND support in Fig. 3b–d and the area of crystal could be controlled by ND support.

To evaluate the advantages of spot size reduction, different volumes of ND suspension were used from 0.1 to 1.2 μL. And 0.5 μL of 60 nM Cyt *c* tryptic peptide was deposited directly on them. The MALDI-MS spectra were presented in Fig. 4a–c. Because Cyt *c* tryptic peptides were concentrated on small area ND support, the average S/N values for pep-

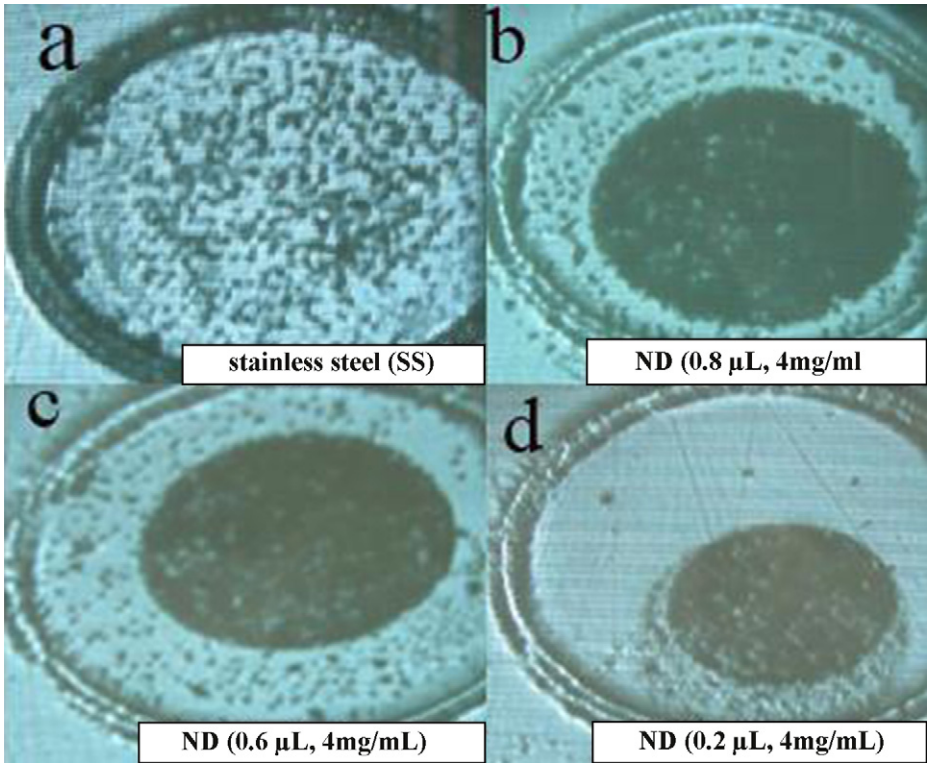

Fig. 3. Photographs of the crystals of CCA with peptide on stainless steel (SS) (a), ND support (0.8 μL, 4 mg/mL) (b), ND support (0.6 μL, 4 mg/mL) (c) and ND support (0.2 μL, 4 mg/mL) (d).

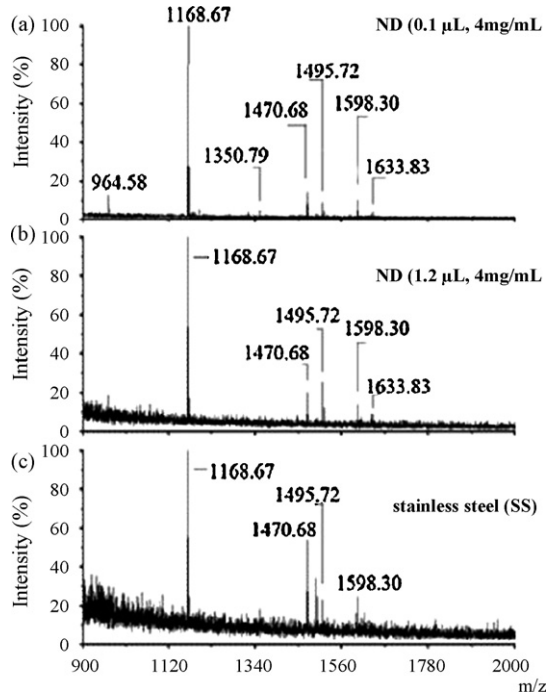

Fig. 4. MALDI-TOF-MS obtained from 0.5 μL of 60 nM Cyt *c* tryptic peptide. The sample was prepared on ND support (0.1 μL, 4 mg/mL) (a), ND support (1.2 μL, 4 mg/mL) (b) and on stainless steel (c). (a–c) Show the *m/z* of match-expected tryptic peptides to Cyt *c*.

tides was increased with the shrinkage of ND support. The S/N of peptide (Mr, 1168.74) was increased from 80.87 (obtained on stainless steel) to 573.28 (obtained on ND support (0.1 μL, 4 μg/μL)). Therefore, the signal intensity of peptides acquired on the ND support (0.1 μL, 4 μg/μL) was at least seven times greater than that obtained on stainless steel and three-fold greater than that obtained on the ND support (1.2 μL, 4 μg/μL) (Fig. 4b), respectively. Compared with the spectrum obtained on the ND support (0.1 μL, 4 μg/μL) (Fig. 4a), four tryptic peptides were not observed in it acquired on stainless steel (Fig. 4c). The evidence indicated that the enhancement of sensitivity was directly correlated with the reduction of spot size on ND support.

3.4. Detection sensitivity

To determine the sensitivity of MALDI-MS with ND support, a serial dilution experiment with test peptides was performed. The Arg-vasopressin stock solution and the Myo tryptic peptide were diluted to 125 pM and 2 nM, respectively. The relative abundance of analytes was recorded and the procedure repeated three times for each sample. The spectra obtained on ND support and on stainless steel from 62.5 amol Arg-vasopressin were shown in Fig. 5a–b. The S/N and resolution of Arg-vasopressin obtained on ND support were 46.00 and 13,009.18, respectively (Fig. 5a). However, it was difficult to obtain signal on stainless steel (Fig. 5b). The spectra from 7.5 fmol of Myo tryptic peptides obtained on ND support and on stainless steel were shown in Fig. 5c–d. The different of sensitivity between the MS

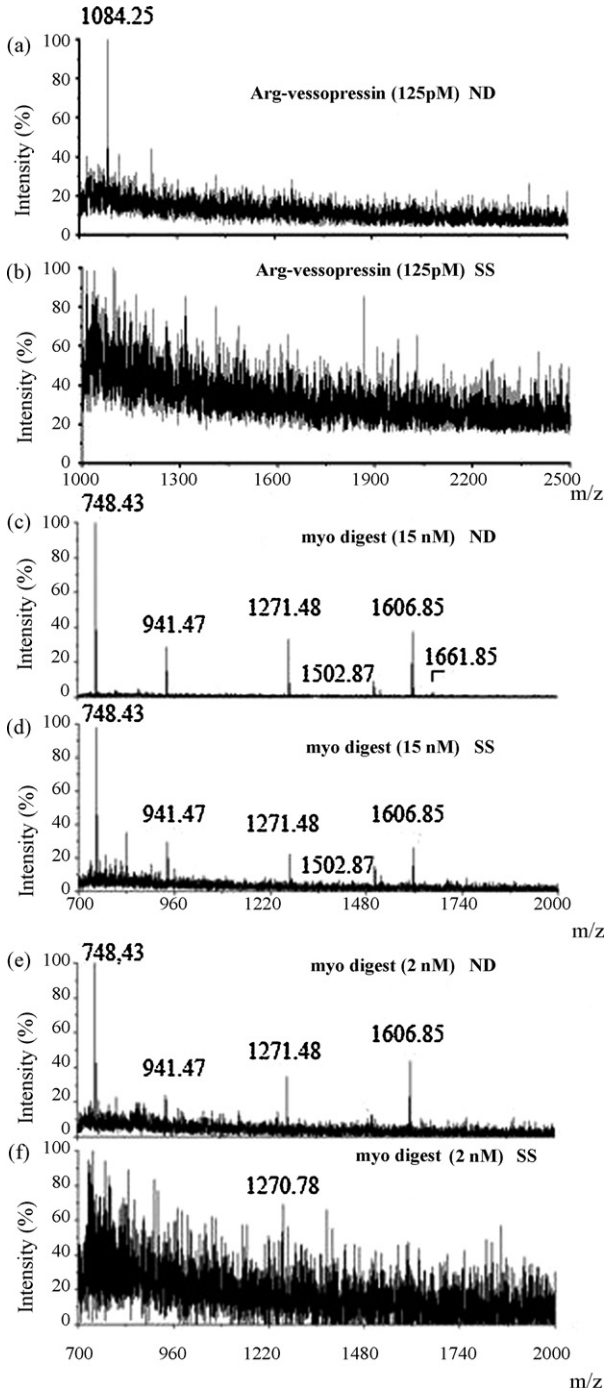

Fig. 5. MALDI-TOF-MS obtained from Arg-vasopressin standard peptide and Myo tryptic peptide mixture. 0.5 μL of Arg-vasopressin (125 pM) was prepared on ND support (0.6 μL, 4 mg/mL) (a) and on stainless steel (SS) (b). 0.5 μL of Myo tryptic peptide mixture (15 nM and 2 nM) were prepared on ND support (0.6 μL, 4 mg/mL) (c) and (e), respectively. And 0.5 μL of Myo tryptic peptide mixture (15 nM and 2 nM) were prepared on stainless steel (SS) (d) and (f), respectively.

spectrum obtained on ND support and on stainless steel was visible. The advantage of ND support becomes more obvious when the concentration drops to 2 nM (Fig. 5e–f). Compared with the spectrum obtained on ND support (Fig. 5e), there is no signal observed on stainless steel (Fig. 5f).

Table 1
Laminine B obtained on ND support (0.6 μL, 4 mg/mL) and on stainless steel with different concentration of NaCl and SDS solutions

Solvent	ND support			Stainless steel		
	Intensity	S/N	R.S.D. (%)	Intensity	S/N	R.S.D. (%)
25 mM NaCl	2564.3 ± 328.2	1984.3 ± 254.0	12.8	918.2 ± 85.4	905.7 ± 84.2	9.3
50mM NaCl	1082.2 ± 141.8	1150.7 ± 150.7	13.1	221.6 ± 21.9	227.2 ± 22.5	9.9
100 mM NaCl	983.5 ± 137.7	481.8 ± 67.4	14.0	134.2 ± 14.1	150.4 ± 15.8	10.5
200 mM NaCl	106.8 ± 15.3	131.6 ± 18.8	14.3	13.7 ± 1.5	16.1 ± 1.7	10.8
500 mM NaCl	27.6 ± 4.0	10.3 ± 1.5	14.8	–	–	–
0.1% SDS	364.5 ± 47.4	312.5 ± 40.6	13.0	294.8 ± 29.5	278.9 ± 27.9	10.0
0.2% SDS	–	–	–	–	–	–

'–' Indicates no signal was detected.

3.5. Salt tolerance of ND support

Normally, biologists employ non-volatile salts in preparing samples for several reasons, including maintenance of a non-toxic environment for cells, stabilization of solvated samples, and maintenance of enzymatic or other biological activity. The ionization efficiency of analytes was decreased in the presence of salts, which can hardly produce good mass spectrum.

Another feature of ND support is better tolerance of inorganic salt. To obtain 100 pM of laminine B, the stock solution was diluted by NaCl solution (from 25 mM to 2 M). With different amount of salt, mass spectra were obtained from 50 fmol of laminine B on ND support and on stainless steel, respectively. Table 1 shows the S/N and intensity of laminine B obtained on different sample support. Compared with the intensity of laminine B obtained on stainless steel, the ND support preparation technique yields high response with the presence of NaCl. When the concentration of NaCl reached 500 mM, no signal could be seen on stainless steel, but the signal intensity was 27.6 ± 4.0 obtained on ND support.

When sample solution stands for a period of time on ND support, peptides can be captured on ND particle surfaces by hydrophobic interaction and other molecular interaction. Then salt is embedded in the gap among ND particles. For its infusibility in water, CCA is also absorbed on ND particle surface and made crystal with peptides. Therefore, ND support shown better

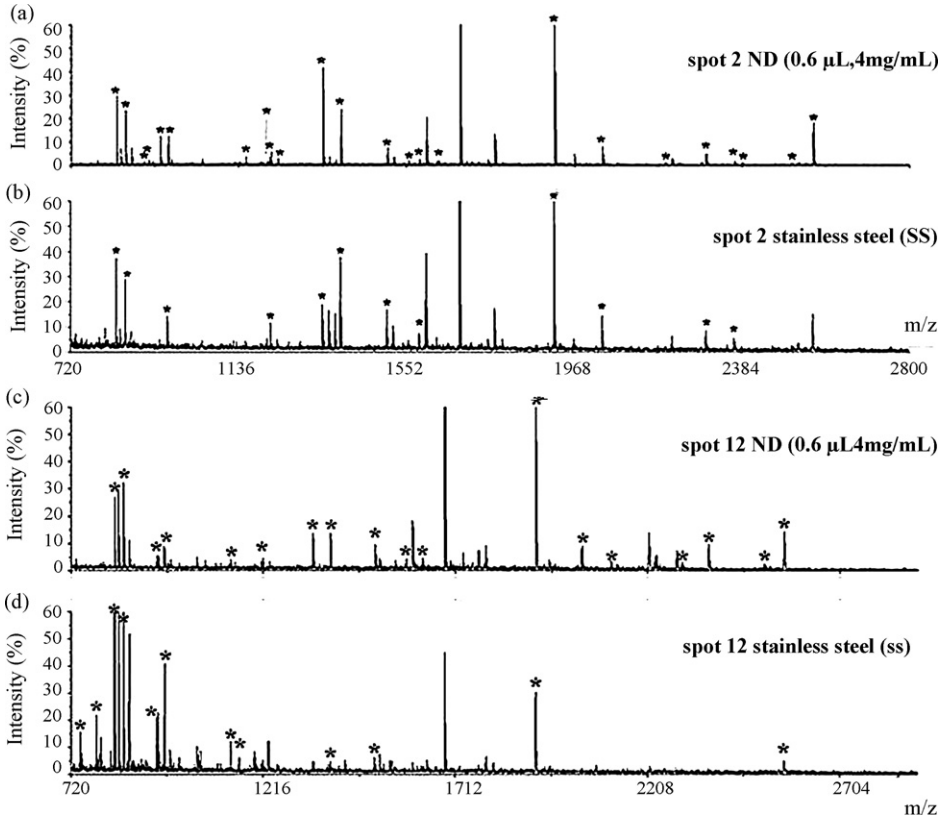

Fig. 6. ND support improves MALDI-MS peptide mapping. The tryptic digestion mixtures of spots 2 and 12 separated by 2-DE were analyzed on ND support (0.6 μL, 4 mg/mL) (a and c) and stainless steel (SS) (b and d), respectively. '*' Indicates the match-expected tryptic peptides to (P10809) 60 kDa heat shock protein, mitochondrialprecursor (Hsp60).

salt tolerance than stainless steel. This can be further demonstrated by SDS solution (Table 1). For example, if laminine B was diluted with 0.1% SDS solution, there was a little difference between the S/N of laminine B analyzed on ND support (312.5 ± 40.6) and obtained on stainless steel (278.9 ± 27.9). It is proposed hydrophobic actions between ND particles with SDS and it with peptides are similar. Besides peptides, ND particles captured SDS molecule simultaneously. So, ND support did not show better tolerance of SDS.

3.6. Application to the 2D gel spots

The proposed ND support has been proven to be effective in a real proteomic analysis. Two hundred and fifty micrograms of epithelial cell lysate was separated with Bio-Rad on a Protean II xi 2-DE system and 13 protein spots were analyzed after 2D electrophoresis separation (Fig. S1, Supplementary Material). Protein identification results by MALDI-MS recorded on stainless steel and on ND support were given in Table S1 (Supplementary Material). Compared with the desalt procedure by ZipTip μ-C18, ND support shows better result in the identification of protein. This may be due to the better salt tolerance and better desorption/ionization of ND support and the losing of peptide mixture in the purification procedure by ZipTip μ-C18. The spectra of tryptic digests of spots 2 and 12 obtained on ND support and on stainless steel are shown in Fig. 6a–d, respectively. These results clearly demonstrate the superiority of ND support coated on stainless steel in proteomic applications.

4. Conclusions

A novel nanodiamond support has been developed and is proven to be very effective and useful for MALDI-TOF-MS protein identification. It has superior qualities in comparison to stainless steel. During sample preparation, CCA crystallized homogeneously over ND support. Good reproducibility of relative peak intensity (R.S.D. less than 11.8%) within spot (from ring to center) was achieved using ND support, considerably reducing the data acquisition time for searching the "hot spot". As one type of UV absorbent assistant material, ND improved desorption and ionization of peptides. The sensitivity can be enhanced three to four times compared to the conventional MALDI sample preparation techniques. In a set of test experiments, they shown the increased detection sensitivity on ND support correlated well with the reduced spot size. ND support has been also found with salt tolerance in MALDI-MS analysis, even with 500 mM NaCl. For these observations, ND support provides a novel measure to improve the application of MALDI-MS into the identification of proteins, particularly for the low abundance proteins in proteomics researches.

Acknowledgements

This work is financially supported by National Science and Technology Key Project of China (2007CB914101 and 2006AA02Z134) and National Natural Science Foundation of China (20405003, 30672394 and 30530040), Shanghai Science and Technology Development Program (03DZ14024 and 04DZ14005) and Shanghai Rising-Star Program (06QA14004). Thanks Prof. Chun-Hui Deng for some advises to the manuscript.

Appendix A. Supplementary data

Supplementary data associated with this article can be found, in the online version, at doi:10.1016/j.talanta.2007.09.020.

References

[1] P. Lee, W. Chen, J.C. Gebler, Anal. Chem. 76 (2004) 4888.
[2] D.C. Delinsky, K.D. Greis, J. Proteome. Res. 1 (2002) 279.
[3] S. Ekström, J. Malmström, L. Wallman, M. Löfgren, J. Nilsson, T. Laurell, G. Marko-Varge, Proteomics 2 (2002) 413.
[4] G. Zhang, T.A. Neubert, Proteomics 6 (2006) 571.
[5] W. Morelle, K. Canis, F. Chirat, V. Faid, J. Michalski, Proteomics 6 (2006) 3993.
[6] F. Kiroekar, E. Nordhoff, L.K. Larsen, K. Kristiansen, P. Roepstorff, F. Hillenkamp, Nucleic Acids Res. 26 (1998) 2554.
[7] J. Gobom, E. Nordhoff, K. Ekaman, P. Roepstorff, J. Mass Spectrom. Ion Process. 169 (1997) 153.
[8] J. Gobom, E. Nordhoff, E. Mirgorodskyaya, P. Roepstorff, J. Mass Spectrom. 34 (1999) 105.
[9] A. Brockman, B.S. Dodd, R. Orlando, Anal. Chem. 69 (1997) 4716.
[10] L. Zhang, R. Orlando, Anal. Chem. 71 (1999) 4753.
[11] S.A. Trauger, E.P. Go, Z. Shen, J. Apon, B.J. Compton, E.S.P. Bouvier, M.G. Finn, G. Siuzdak, Anal. Chem. 76 (2004) 4484.
[12] J.A. Blakledge, A.J. Alexander, Anal. Chem. 67 (1995) 843.
[13] M. Schuerenberg, C. Luebbert, H. Eickhoff, M. Kalkum, H. Lehrach, E. Nordhoff, Anal. Chem. 72 (2000) 3436.
[14] J. Sunner, E. Dratz, Y. Chen, Anal. Chem. 67 (1995) 4335.
[15] L. Li, A.P.L. Wang, L.D. Coulson, Anal. Chem. 65 (1993) 493.
[16] K. Tanak, H. Waki, Y. Idao, S. Akita, Y. Yoshida, T. Yoshida, Rapid Commum. Mass Spectrom. 2 (1988) 151.
[17] N. Zhang, A. Doucette, L. Li, Anal. Chem. 73 (2001) 2968.
[18] Y. Xu, T. Waston, M. Bruening, Anal. Chem. 75 (2003) 185.
[19] Y. Dai, R.M. Whittal, L. Li, Anal. Chem. 68 (1996) 2494.
[20] J. Zheng, N. Li, M. Ridyard, H. Dai, S.M. Robbins, L. Li, J. Proteome. Res. 4 (2005) 1709.
[21] N. Li, A.R.E. Shaw, N. Zhang, A. Mak, L. Li, Proteomics 4 (2004) 3156.
[22] H. Liu, J. Stupak, J. Zheng, B.O. Keller, B.J. Brix, L. Fliegel, L. Li, Anal. Chem. 76 (2004) 4223.
[23] S. Ren, L. Zhang, Z. Cheng, Y. Guo, J. Am. Soc. Mass Spectrom. 16 (2005) 333.
[24] F.O. Ayorinde, K. Garvin, K. Saeed, Rapid Commum. Mass Spectrom. 14 (2000) 608.
[25] Y.C. Chen, J. Shiea, J. Sunner, Rapid Commum. Mass Spectrom. 14 (2000) 86.
[26] L. Michalak, K.J. Fisher, D.S. Alderdice, D.R. Jardine, G.D. Willett, Org. Mass Spectrom. 29 (1994) 512.
[27] S. Xu, Y. Li, H. Zou, J. Qiu, Z. Guo, B. Guo, Anal. Chem. 75 (2003) 6191.
[28] C. Black, C. Poile, J. Langley, J. Herniman, Rapid Commum. Mass Spectrom. 20 (2006) 1053.
[29] J. Wei, J.M. Buriak, G. Siuzdak, Nature 399 (1999) 243.
[30] S. Xu, M. Ye, D. Xu, X. Li, C. Pan, H. Zou, Anal. Chem. 78 (2006) 2593.
[31] M. Han, J. Sunner, J. Am. Soc. Mass Spectrom. 11 (2000) 644.
[32] C. Pan, S. Xu, L. Hu, X. Su, J. Ou, H. Zou, Z. Gou, Y. Zhang, S. Guo, J. Am. Soc. Mass Spectrom. 16 (2005) 883.
[33] T. Miliotis, G. Marko-Varga, J. Nilsson, T. Laurell, J. Neurosci. Meth. 109 (2001) 41.
[34] K.C. Hung, H. Ding, B. Guo, Anal. Chem. 71 (1999) 518.

[35] S.J. Owen, F. Meier, S. Brombacher, D.A. Volmer, Rapid Commum. Mass Spectrom. 17 (2003) 2439.
[36] X. Li, M. Wilm, T. Franz, Proteomics 5 (2005) 1460.
[37] W.C. Poh, K.P. Loh, W.D. Zhang, S. Triparthy, J. Ye, F. Sheu, Langmuir 20 (2004) 5484.
[38] T.G. Drummond, M.G. Hill, J.K. Barton, Nat. Biotechnol. 21 (2003) 1192.
[39] L.C.L. Huang, H.C. Chang, Langmuir 20 (2004) 5879.
[40] W.H. Chen, S. Lee, S. Sabu, H. Fang, S. Chung, C. Han, H. Chang, Anal. Chem. 78 (2006) 4228.
[41] X.L. Kong, C.L. Huang, C.M. Hsu, W.H. Chen, C.C. Han, H.C. Chang, Anal. Chem. 77 (2005) 259.
[42] T. Xu, K. Xu, J.Z. Zhao, Master. Sci. Eng. B 38 (1996) L1.
[43] S. Laugesen, P. Roepstorff, J. Am. Soc. Mass Spectrom. 14 (2003) 992.
[44] S. Michaelson, A. Hoffman, Diamond Related Mater. 14 (2005) 470.
[45] D.P. Little, T.J. Cornish, M.J. O'Donnel, A. Braun, R.J. Cotter, H. Köster, Anal. Chem. 69 (1997) 4540.
[46] J. Goborn, J. Mass Spectrom. 34 (1999) 105.

Available online at www.sciencedirect.com
ScienceDirect
Talanta 74 (2008) 1148–1153
Talanta
www.elsevier.com/locate/talanta

Highly sensitive and selective optical chemosensor for determination of Cu^{2+} in aqueous solution

Yu Xiang, Zifan Li, Xiaotong Chen, Aijun Tong *

The Key Laboratory of Bioorganic Phosphorus Chemistry & Chemical Biology, Department of Chemistry, Tsinghua University, Beijing 100084, China

Received 20 May 2007; received in revised form 15 August 2007; accepted 19 August 2007
Available online 23 August 2007

Abstract

A highly selective and sensitive rhodamine-based colorimetric chemosensor (**1**) for quantification of divalent copper in aqueous solution has been investigated in this work. It was designed using salicylaldehyde hydrazone and rhodamine 6G as copper-chelating and signal-reporting groups, respectively. In environmentally friendly media (50% (v/v) water/ethanol and 10 mM NaAc–HAc neutral buffer (pH 7.0)), the sensor exhibited selective absorbance enhancement to Cu^{2+} over other metal ions at 529 nm, with a dynamic working range of 0.05–5.00 μM and a detection limit of 10 nM Cu^{2+}, respectively. To achieve fluorometric determination of Cu^{2+}, the Cu^{2+}-induced absorbance enhancement of **1** was efficiently converted to fluorescence quenching by fluorescence inner filter effects using rhodamine B (RB) as a fluorophore. The selectivity and sensitivity of fluorescence analysis were similar to those of absorptiometric measurement. Both absorptiometric and fluorometric methods were successfully applied to the detection of Cu^{2+} in three water samples.
© 2007 Elsevier B.V. All rights reserved.

Keywords: Chemosensor; Cu^{2+}; Colorimetry; Fluorescence inner filter effects; Fluorometry

1. Introduction

The design of artificial chemosensors for selective and sensitive quantification of biologically and environmentally important ion species, especially transition-metal ions, has attracted wide-spread interests of chemists, biologists, clinical biochemists and environmentalists in recent years. Because of their advantages of simple instrumentation, high sensitivity and facile analysis, many efficient colorimetric/fluorescent sensors for transition-metal ions have been developed during the last two decades [1–6]. Generally, a typical synthesized probe of this type is constructed by covalent linkage of three parts: a chelating unit, a spacer and a reporting group, though there are some examples of spacer-free probes. Upon the binding of metal ions, these sensor molecules will display completely different absorption/fluorescence signals compared to free sensors in solution, enabling the quantitative determination of metal ions [7]. On the other hand, among the transition-metal ions of interest, divalent copper, Cu^{2+}, is particularly attractive, because it is not only an environmental pollutant at high concentrations [8,9], but also an essential trace element for many biological process and systems [10,11]. Therefore, many excellent works of Cu^{2+} sensing by synthesized colorimetric/fluorescent probes have been reported and investigated [12–17]. However, there is still an intense demand for new efficient Cu^{2+} optical chemosensors, especially those that can work in aqueous solution with high selectivity and sensitivity [18–20]. Works related to this area are of great challenge and increasing interest.

Rhodamines are classic dyes/fluorophores whose photochemical properties have already been well studied. Because of their low cost, long-wavelength (>500 nm) absorption/emission and high molar absorption coefficient and quantum yield, these dyes/fluorophores are usually utilized as reporting groups in routine optical analysis. Since the work of Dujols' on the development of a highly selective and sensitive Cu^{2+} chemodosimeter derived from rhodamine B [21], many rhodamine derivatives have been designed and applied as efficient chemosensors for transition-metal ions [22–24]. These rhodamine-based ionophores not only exhibit the advantages of rhodamine dyes,

* Corresponding author. Tel.: +86 10 62787682; fax: +86 10 62787682.
E-mail address: tongaj@mail.tsinghua.edu.cn (A. Tong).

0039-9140/$ – see front matter © 2007 Elsevier B.V. All rights reserved.
doi:10.1016/j.talanta.2007.08.018

but also display selective optical response to a specific metal ion after chemical modification. The metal ion sensing behavior of these rhodamine-based optical sensors is very interesting. Typically, in the absence of metal ions, the sensor molecules prefer their spirolactam ring-closed state [25], which shows little absorption or fluorescence in visible range (400–700 nm). However, upon the addition of specific metal ions, the chelating or reaction of metal ions with sensor molecules will simultaneously open the spirolactam ring and make the sensors converted into their ring-opened state [25], which is highly absorbent and fluorescent above 500 nm. Therefore, most of the reported rhodamine-based chemosensors for metal ions are of colorigenic or fluorogenic type. Nevertheless, there is still only a little study focused on the reversible detection of Cu^{2+} in aqueous solution using rhodamine derivatives [26].

Except for the direct introduction of fluorophores into sensor molecules, fluorometric detection can also be achieved by fluorescence inner filter effects (FIFEs) using a colorimetric chemosensor (nonfluorescent) and another fluorescent dye [27–31]. When the absorption spectrum of the former sensor has a complementary overlap region with the excitation or emission spectrum of the fluorescent dye, the fluorescence emission of the fluorophore will be modulated by the absorption change of the colorimetric sensor. Thus the absorption responses of the sensor to analyte will be efficiently converted to fluorescence signals, enabling fluorescence analysis of the analyte. The advantages of this approach are: (1) it does not need covalent linkage of a fluorophore to sensor molecules, so the design and synthesis of fluorescent sensors will be significantly simplified; (2) because the changes in the absorbance of sensors transform exponentially into fluorescence intensity changes, the sensitivity of the analysis may be further improved using fluorescence method compared to absorption analysis; (3) the measurement is more facile since no blank measurement is required for fluorescence analysis.

We have previously reported a mechanism study of a new copper-selective chemosensor based on rhodamine B hydrazone as a short communication [26]. In this work, a highly selective and sensitive colorimetric chemosensor (**1**, Scheme 1) for the quantification of Cu^{2+} in neutral aqueous solution was investigated and well applied for the analysis of real samples by both absorptiometric method and fluorescence inner filter effect. It was designed using rhodamine 6G and salicylaldehyde hydrazone as reporting and chelating parts, respectively. The advantages of the proposed chemosensor for Cu^{2+} determination are: (1) they were applicable in environmentally friendly and neutral aqueous media; (2) they were highly sensitive and selective for Cu^{2+}; (3) the analysis was performed above 500 nm; (4) the synthesis of **1** was facile and inexpensive.

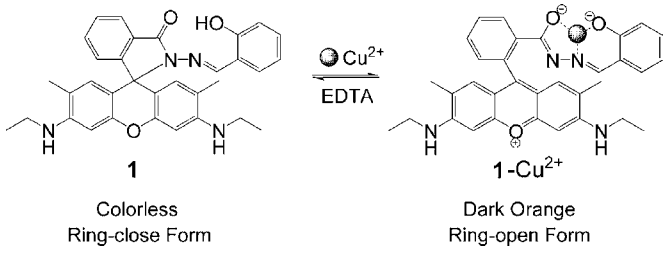

Scheme 1. Reversible binding of **1** and Cu^{2+}.

2. Experimental

2.1. Reagents

Absolute ethanol of analytical grade and deionized water (distilled) were used throughout the experiment as solvents. All the materials for synthesis were purchased from commercial suppliers and used without further purification. The solutions of metal ions were prepared from their nitrate salts of analytical grade, except for $FeCl_2$ and $MnCl_2$, and then subsequently diluted to prepare work solutions. The use of $Cu(NO_3)_2$ or $CuCl_2$ yielded nearly the same results. Tris–HCl and NaAc–HAc buffer solutions of different pH were prepared using proper amount of Tris, HCl, NaAc and HAc (all of analytical grade) under adjustment by a pH meter.

2.2. Apparatus

Absorption spectra were determined on a JASCO V-550 UV–vis spectrophotometer. Fluorescence spectra measurements were performed on a JASCO FP-6500 spectrofluorimeter equipped with a xenon discharge lamp, 1 cm quartz cells. All pH measurements were made with a Model pHS-3C pH meter (Shanghai, China). NMR spectra were recorded using a JOEL JNM-ECA300 spectrometer operated at 300 MHz. ESI-MS spectra were obtained on a HP 1100 LC–MS spectrometer without using the LC part. All of the measurements were operated at room temperature at about 298 K.

2.3. Synthesis of *1*

Rhodamine derivative **1** was synthesized by a similar procedure, which had been reported [26]:

(a) *Rhodamine 6G hydrazide*. Excess hydrazine hydrate (85%, 5 g, 85 mmol, caution: hydrazine is volatile and strongly poisonous) was added dropwise to a solution of rhodamine 6G (2.39 g, 5 mmol) in absolute ethanol (50 mL). After the addition, the resulting mixture was refluxed in an oil bath with stir for 10 h (pink precipitation could be observed soon after the mixture was heated). Then the precipitation was filtered, washed by ethanol (5 × 15 mL) and dried in vacuo to afford rhodamine 6G hydrazide (1.73 g, yield 81%) as light pink solid. ESI mass spectrometry: *m/z* 429.3 (88% $[M+H]^+$), 451.2 (12% $[M+Na]^+$); M^+ calculated 428.2. ^{1}H NMR ($CDCl_3$), δ (ppm): 1.29 (t, 6H, $NHCH_2CH_3$, $J=7.0$ Hz), 1.89 (s, 6H, xanthene–CH_3), 3.18 (q, 4H, $NHCH_2CH_3$, $J=7.0$ Hz), 3.45–3.65 (b, 4H, N–NH_2, $NHCH_2CH_3$), 6.24 (s, 2H, xanthene–H), 6.37 (s, 2H, xanthene–H), 7.04 (dd, 1H, Ar–H, $J_1=5.4$ Hz, $J_2=3.3$ Hz), 7.42 (dd, 2H, Ar–H, $J=3.3$ Hz), 7.93 (dd, 1H, Ar–H, $J_1=5.4$ Hz, $J_2=3.3$ Hz). ^{13}C NMR ($CDCl_3$) δ (ppm): 14.8, 16.8, 38.4, 66.1, 96.9,

105.0, 118.1, 123.1, 123.9, 127.8, 128.2, 130.0, 132.7, 147.6, 151.8, 152.3, 166.3.

(b) *Salicylaldehyde rhodamine 6G hydrazone* (***1***). To a solution of rhodamine 6G hydrazide (0.428 g, 1 mmol) in 1:2 (v/v) ethanol/dichloromethane (30 mL) was added 5 equiv. salicylaldehyde (0.611 g, 5 mmol). After the addition, the mixture was refluxed in an oil bath with stir for 12 h (if precipitation appeared, then added 5–10 mL dichloromethane). Then the solvent was removed in vacuo. The residue was washed by ethanol (6× 15 mL) and dried in vacuo to afford **1** (0.479 g, yield 90%) as pink solid. ESI mass spectrometry: *m/z* 533.3 (81% $[M+H]^+$), 555.2 (19% $[M+Na]^+$); M^+ calculated 532.2. ^{1}H NMR ($CDCl_3$), δ (ppm): 1.30 (t, 6H, $NHCH_2CH_3$, $J=7.0$ Hz), 1.87 (s, 6H, xanthene–CH_3), 3.20 (q, 4H, $NHCH_2CH_3$, $J=7.0$ Hz), 3.45–3.65 (b, 2H, $NHCH_2CH_3$), 6.31 (s, 2H, xanthene–H), 6.44 (s, 2H, xanthene–H), 6.75 (dd, 1H, Ben–H, $J=5.9$ Hz), 6.86 (d, 1H, Ben–H, $J=5.9$ Hz), 7.05 (d, 1H, Ben–H, $J=5.9$ Hz), 7.12 (1H, Ben–H), 7.15 (1H, Ar–H), 7.52 (2H, Ar–H), 8.00 (1H, Ar–H), 9.12 (s, 1H, N=*CH*), 10.91 (s, 1H, Ben–OH). ^{13}C NMR ($CDCl_3$) δ (ppm): 14.8, 16.9, 38.4, 66.5, 96.9, 105.7, 117.1, 118.2, 118.6, 119.0, 123.4, 124.2, 127.9, 128.7, 129.9, 131.3, 131.5, 133.7, 147.8, 151.3, 151.9, 152.3, 158.7, 164.4.

2.4. Absorption and fluorescence measurements

Absorption and fluorescence titrations were performed by addition of small aliquots of metal ion work solutions to a 3 mL solution of proper amount **1** in buffered water/ethanol with different pH and ethanol fractions in a 1 cm quartz cell. After well mixed, the solutions were allowed to stand at ambient condition for 5 min, and absorption or fluorescence spectra were recorded.

For the analysis of Cu^{2+} containing water samples, 1.50 mL of a certain sample water, 1.50 mL ethanol, 30 μL of 1.0 M NaAc–HAc buffer of pH 7.0, 30 μL 1 mM **1** in ethanol (30 μL 0.1 mM RB in water was added when using fluorometric method) were mixed in a 1 cm quartz cell for 5 min. Then the absorption measurement was performed at 529 nm (fluorescence measurement was performed at ex/em = 529/575 nm).

3. Results and discussion

3.1. Binding of *1* with divalent copper

Before the application of **1** in the detection of Cu^{2+}, the binding mechanism of **1** with Cu^{2+} was first studied by UV–vis absorption spectra. In aqueous media of 50% (v/v) water/ethanol buffered by 10 mM NaAc–HAc at pH 7.0, **1** (10 μM) displayed no absorbance above 400 nm in its absorption spectra in the absence of Cu^{2+}, suggesting the spirolactam ring of rhodamine 6G unit preferred its ring-closed state at this condition. However, upon the addition of Cu^{2+} as nitrate salt to the solution of **1**, a significant enhancement of absorbance in 450–575 nm range was simultaneously observed (Fig. 1). The absorption band appeared

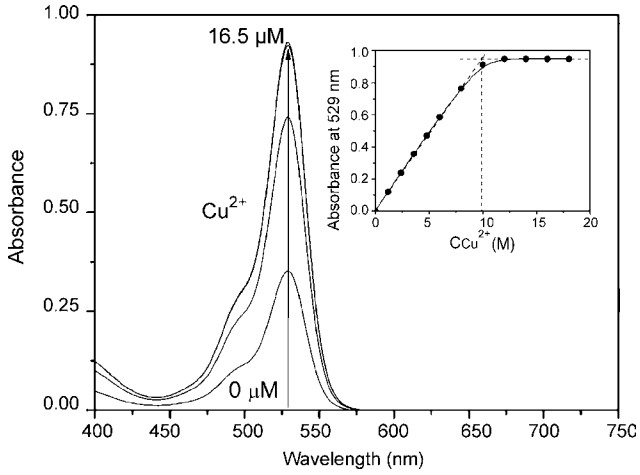

Fig. 1. Absorption spectra of **1** (10 μM) in the absence and presence of Cu^{2+} in 50% (v/v) water/ethanol buffered by 10 mM NaAc–HAc at pH 7.0. Inset: absorbance at 529 nm as a function of Cu^{2+} concentration.

was the characteristic absorption pattern of rhodmamine 6G. Thus it could be inferred that the interaction of **1** and Cu^{2+} opened the spirolactam ring of rhodamine 6G unit, because only ring-opened form of rhodamine 6G unit was absorbent above 450 nm.

To further investigate the binding mode and reversibility of **1** and Cu^{2+}, experiments of absorption spectra titration, Job's method, ESI-MS, and competitive binding with EDTA were carried out. As illustrated in Fig. 1, upon the addition of Cu^{2+} up to 1.65 equiv. into 10 μM **1** in 50% (v/v) water/ethanol buffered by 10 mM NaAc–HAc at pH 7.0, the absorbance of absorption band peaked at 529 nm increased linearly at first, and then reached its maximum when the amount of added Cu^{2+} was above 1.0 equiv. The nonlinear fit of the data revealed the binding of **1** and Cu^{2+} was most probably a 1:1 stoichiometry, with an association constant (K_a) about 10^6 M^{-1} [32]. The data of Job's method using a total concentration of 10 μM **1** and Cu^{2+} exhibited a maximum absorbance at 529 nm when the molecular fraction of **1** was close to 50%, which also suggested the 1:1 stoichiometry of **1**–Cu^{2+} complex [33].

A more direct evidence for the formation of this 1:1 complex was evaluated from the ESI-MS spectra of **1** in the absence and presence of 1.2 equiv. Cu^{2+} in 50% (v/v) water/ethanol [34–36]. There were only peaks at *m/z* = 533.3 ($[\mathbf{1}+H]^+$) and 555.2 ($[\mathbf{1}+Na]^+$) when **1** was alone. However, in the presence of excess Cu^{2+}, both of the above two peaks disappeared and a new unique peak at *m/z* = 594.2 ($[\mathbf{1}+Cu–H]^+$) appeared. The isotopic patterns of $[\mathbf{1}+Cu–H]^+$ cation were in agreement with calculated values.

Moreover, upon the addition of 50 μM EDTA to the solution of 10 μM **1** with Cu^{2+} (16.5 μM), the absorption band peaked at 529 nm would disappear due to the competitive binding of Cu^{2+} from **1** by EDTA, and further addition of 75 μM Cu^{2+} could recover the absorption band again. All these results indicated that the binding of **1** and Cu^{2+} (Scheme 1) was (1) through a 1:1 stoichiometry, (2) reversible, (3) and yield a very stable **1**–Cu^{2+} complex with K_a about 10^6 M^{-1}.

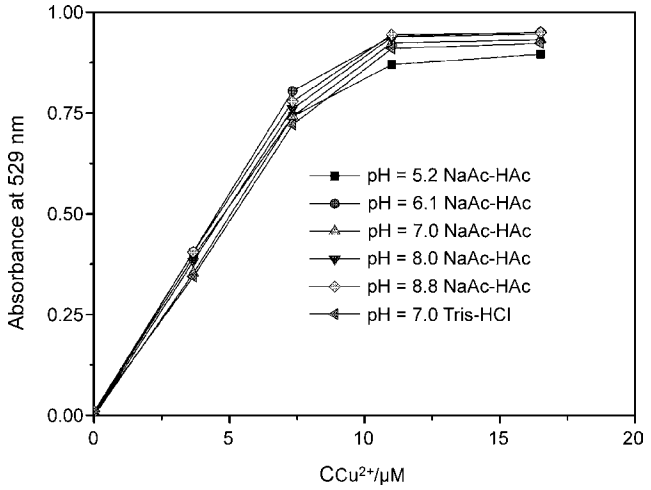

Fig. 2. Effect of pH and type of buffer on the absorbance at 529 nm of **1** upon the addition of Cu^{2+} using 10 μM **1** in 50% (v/v) water/ethanol. The concentration of buffer salts was 10 mM.

3.2. Selectivity of *1* to Cu^{2+} over other metal ions

The selectivity of **1** to Cu^{2+} over other metal ions was also investigated to evaluate whether **1** could serve as a Cu^{2+}-selective colorimetric chemosensor in aqueous condition. In the presence of 1.0 equiv. other metal ions such as Na^{+}, K^{+}, Mg^{2+}, Ca^{2+}, Mn^{2+}, Fe^{3+}, Fe^{2+}, Co^{2+}, Ni^{2+}, Zn^{2+}, Ag^{+}, Cd^{2+}, Hg^{2+} and Pb^{2+}, no significant enhancement of absorbance could be observed at 529 nm compared to that of Cu^{2+} at the same concentration. The ratio of absorbance enhancement at 529 nm for each metal ion compared to Cu^{2+} was listed in Table 1. It suggested that **1** was an excellent Cu^{2+}-selective chemosensor in aqueous condition.

3.3. Optimizing the condition for colorimetric quantification of Cu^{2+}

For better quantification of Cu^{2+} in aqueous conditions, the pH of buffer, ethanol fraction and sensor concentration used in the proposed absorptiometric method was investigated to evaluate the optimized condition for analysis. Because the binding of 10 μM Cu^{2+} to 10 μM **1** could complete within 5 min, all the absorption and fluorescence spectra were recorded after equilibration for 5 min.

3.3.1. Effect of buffer pH

To investigate the effect of pH on the response of **1** to Cu^{2+}, 10 mM NaAc–HAc solutions (50% water/ethanol) of pH 5.2, 6.1, 7.0, 8.0, 8.8 and 10 mM Tris–HCl (50% water/ethanol) of pH 7.0 were used as buffer media, respectively (Fig. 2). It could be observed that the absorbance of 10 μM **1** at 529 nm depended mostly on the concentration of Cu^{2+}, and the use of buffers of different pH or types only slightly varied the curves. Considering that most samples for Cu^{2+} analysis were neutral, and that NaAc–HAc buffers were more environmentally friendly than Tris–HCl, the media for Cu^{2+} quantification was then buffered by 10 mM NaAc–HAc at pH 7.0.

3.3.2. Effect of ethanol fraction

Ethanol was a clean and inexpensive solvent compared to many other organic solvents such as acetone, DMF, DMSO, methanol, tetrahydrofuran and acetonitrile. Thus it was chosen as a cosolvent for the proposed method. The fraction of ethanol used in aqueous media played an important role in the affinity of **1** to Cu^{2+}. Generally, because of the strong hydration of Cu^{2+} in water, high fraction of organic cosolvent was of benefit to the binding of **1** and Cu^{2+}. However, a solution of too much organic solvent might also cause the low solubility of inorganic salts and strong interaction between buffer anions and Cu^{2+}, which should be avoided for Cu^{2+} analysis. Therefore, 10 mM NaAc–HAc aqueous buffers containing different fractions of ethanol (10%, 30%, 50%, 70% and 90% (v/v) at pH 7.0 were used as media for Cu^{2+} determination by **1** (Fig. 3). The results suggested that 50% water/ethanol was already enough for efficient monitoring of Cu^{2+}, thus ethanol volume fraction of 50% was selected.

3.3.3. Effect of sensor concentration

The effect of sensor (**1**) concentration used for Cu^{2+} analysis was also investigated. It seemed that the concentration of **1** was proportional to the maximum absorbance upon the addition of excess Cu^{2+}. However, within dynamic range, the sensor concentration did not play a notable role in Cu^{2+} sensing. In the following tests, the concentration of **1** used was fixed to 10 μM.

According to the above results, the optimized condition for Cu^{2+} analysis was selected as: 10 μM **1**, 10 mM NaAc–HAc at pH 7.0 and 50% (v/v) water/ethanol.

3.4. Tolerance of other metal ions

For a solution of 10 μM **1** in the presence of 2.5 μM Cu^{2+} under optimized condition, the tolerance ratios of other metal ions (yielding error lower than 5%) compared to Cu^{2+} were also tested and listed in Table 1. Alkali and alkali earth metal ions showed little interference to the absorbance at 529 nm of **1**–Cu^{2+}, and could exist in 50-fold more than the concentration of Cu^{2+}. 25-Fold transition-metal ions of Mn^{2+}, Ni^{2+}, Pb^{2+}, Cd^{2+} and

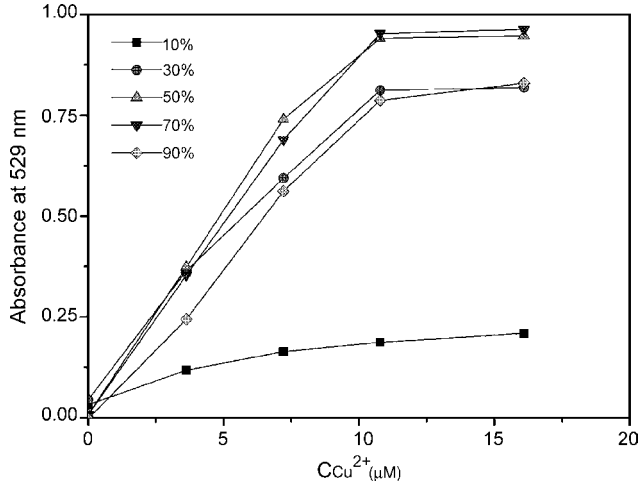

Fig. 3. Effect of ethanol volume fraction on the absorbance at 529 nm of **1** upon the addition of Cu^{2+} using 10 μM **1** buffered by 10 mM NaAc–HAc at pH 7.0.

Table 1
Absorbance enhancement ratio[a] and tolerance[b] of other metal ions compared to Cu^{2+}

Metal ion	Na^+, K^+, Ca^{2+}, Mg^{2+}	Mn^{2+}, Ni^{2+}, Pb^{2+}, Cd^{2+}, Ag^+	Zn^{2+}, Hg^{2+}, Co^{2+}	Fe^{3+}, Fe^{2+}
Response ratio (%)	<0.1	0.2	0.4	1
Tolerance (fold)	>50	25	15	5

[a] Absorbance enhancement ratio of 10 μM metal ions compared to 10 μM Cu^{2+}.
[b] With an interference within 5% to the absorbance of 10 μM **1** and 2.5 μM Cu^{2+}. Conditions: 10 μM **1** in 50% (v/v) water/ethanol buffered by 10 mM NaAc–HAc at pH 7.0.

Table 2
Determination of Cu^{2+} in water samples[a]

Sample	Cu^{2+} added (μM)	Cu^{2+} found (μM)	Recovery (%)	R.S.D.[b] (%)
Tap	0.00	0.00 (0.00)	–	–
water	0.25	0.24 (0.29)	96 (121)	4.5 (6.2)
River	0.00	0.12 (0.16)	–	4.2 (7.3)
water	0.25	0.36 (0.40)	97 (108)	3.5 (5.1)
Cu^{2+}-polluted water[c]	0.00	1.10 (1.14)	–	3.9 (4.6)
	1.00	2.18 (2.25)	104 (105)	3.3 (5.5)

[a] The data in parenthesis were obtained by fluorometric method, while others were evaluated from absorptiometric measurement.
[b] $n = 5$.
[c] Synthesized by: tap water, 1.00 μM Cu^{2+}, 1.00 μM Pb^{2+}, 1.00 μM Cd^{2+}, 2.00 μM Fe^{2+}, 2.00 μM Fe^{3+} and 10.0 μM Na^+, K^+, Mg^{2+} and Ca^{2+}. Conditions: 10 μM **1** (50 μM **1** and 1 μM RB for fluorometric method) in 50% (v/v) water/ethanol buffered by 10 mM NaAc–HAc at pH 7.0.

Ag^+ were also tolerant. The tolerance ratio of Zn^{2+}, Hg^{2+} and Co^{2+} was 15-fold. The major interference was Fe^{3+} and Fe^{2+}, and their concentration should be kept below fivefold of that of Cu^{2+}.

3.5. Analytical figures of merit

According to the proposed procedure, the calibration curve for the determination of Cu^{2+} by **1** was constructed under the optimized condition, which was: 10 μM **1**, 50% (v/v) ethanol, NaAc–HAc buffer (10 mM) at pH 7.0. The relationship between absorbance at 529 nm and Cu^{2+} concentration was: $A = 0.105C + 0.001$, where A was the absorbance at 529 nm and C was the concentration of Cu^{2+} in μM. The linear range of the method was found to be at least 0.05–5.00 μM Cu^{2+} with a correlation coefficient of $R^2 = 0.9993$ ($n = 25$). The detection limit, based on the definition by IUPAC ($C_{DL} = 3\,S_b/m$) [37], was found to be 10 nM from 10 blank solutions. The relative standard deviation (R.S.D.) for five repeated measurements of 0.5 μM Cu^{2+} was 3.0%.

3.6. Application of *1* in Cu^{2+} analysis in water samples

Under optimized condition of 10 μM **1** in 50% (v/v) water/ethanol buffered by 10 mM NaAc–HAc at pH 7.0, three water samples of drinking water, river water and Cu^{2+}-polluted water were analyzed by the proposed absorption method. The results were summarized in Table 2, which showed satisfactory recovery and R.S.D. values for all of the samples, suggesting the potential applications of real sample analysis by **1**.

3.7. Fluorescence detection of Cu^{2+} by *1* and rhodamine B (RB)

Although the addition of Cu^{2+} to **1** could cause a significant enhancement of absorbance above 500 nm, the fluorescence quantum yield of **1**–Cu^{2+} complex was too low for sensitive fluorescence analysis mainly because of the paramagnetic nature of divalent copper ion [38–40]. However, the absorption spectra of **1**–Cu^{2+} overlapped well with the fluorescence excitation spectra of rhodamine B (RB). Therefore, when using RB as a fluorophore, the absorbance enhancement of **1** upon the addition of Cu^{2+} could be successfully converted to fluorescence quenching by fluorescence inner filter effects (FIFEs) [41].

In addition, no interaction was found between Cu^{2+} and RB, and the optimized condition of absorptiometric method was also applicable for fluorometric detection. The fluorescence titrations of Cu^{2+} by **1** in the presence of RB were performed in 50% (v/v) water/ethanol buffered by 10 mM NaAc–HAc at pH 7.0 under excitation at 529 nm (Fig. 4), which was the peak wavelength of the absorption band of **1**–Cu^{2+}. Upon the addition of Cu^{2+}, the excitation light was partially absorbed by **1**–Cu^{2+} complex, thus the light for exciting RB was reduced. Because fluorescence intensity was proportional to the intensity of excitation light absorbed by the fluorophore [29], the fluorescence of RB was then observed to be quenched by the addition of Cu^{2+} to a mixture of **1** and RB. As illustrated in Fig. 5, the concentration of **1** used for Cu^{2+} measurement played a crucial role in the max-

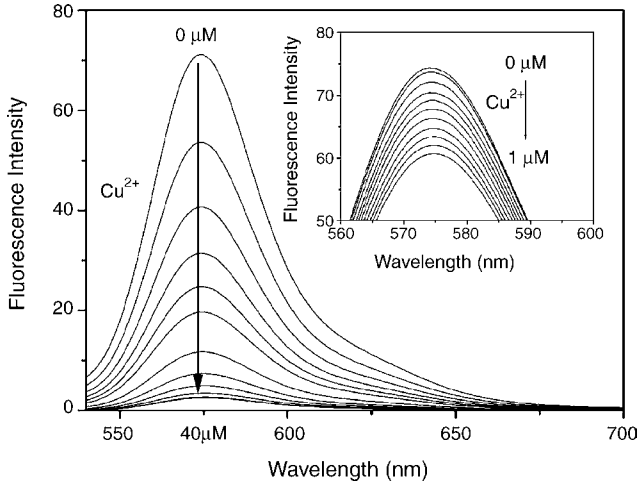

Fig. 4. Fluorescence emission spectra of 50 μM **1** in the presence of 1 μM RB upon the addition of Cu^{2+} in 50% (v/v) water/ethanol buffered by 10 mM NaAc–HAc at pH 7.0. Excitation was performed at 529 nm. Inset: fluorescence emission spectra of 10 μM **1** and 1 μM RB in the presence of 0–1 μM Cu^{2+}.

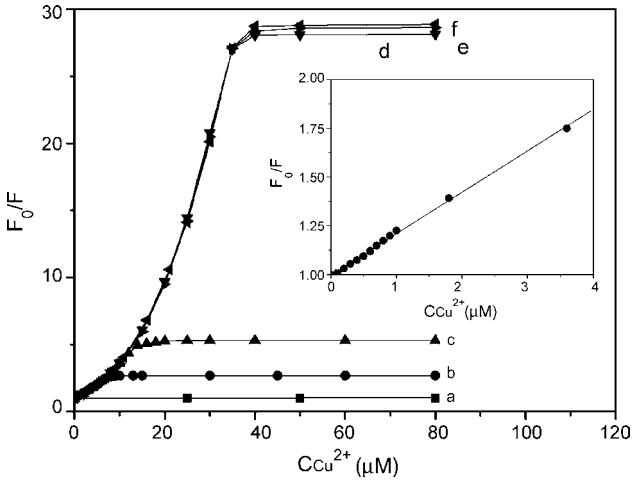

Fig. 5. Fluorescence quenching ratio (F_0/F) at 575 nm as a function of Cu^{2+} concentration for the mixtures of **1** and RB in 50% (v/v) water/ethanol buffered by 10 mM NaAc–HAc at pH 7.0. (a) 0 μM **1**, 1 μM RB; (b) 10 μM **1**, 1 μM RB; (c) 20 μM **1**, 1 μM RB; (d) 50 μM **1**, 0.5 μM RB; (e) 50 μM **1**, 1 μM RB; (f) 50 μM **1**, 3 μM RB. Inset: F_0/F at 575 nm as a function of Cu^{2+} concentration within 0–4 μM range using 50 μM **1**, 1 μM RB in 50% (v/v) water/ethanol buffered by 10 mM NaAc–HAc at pH 7.0. Excitation was performed at 529 nm.

imum fluorescence quenching ratio (F_0/F) when excess Cu^{2+} was added, although F_0/F was hardly affected by the amount of **1** when the concentration of **1** was higher than that of Cu^{2+}. For higher concentration of **1**, F_0/F was more significantly increased in the presence of excess Cu^{2+}, and the dynamic working range was broader. On the contrary, the concentration of RB added as fluorophore showed no obvious interference to the relationship between F_0/F and Cu^{2+} concentration. The fluorescence sensing of Cu^{2+} at submicromolar level by **1** and RB was still successful using 50 μM **1** and 1 μM RB in 50% (v/v) water/ethanol buffered by 10 mM NaAc–HAc at pH 7.0 (Fig. 5), with a linear range of 0.1–3.6 μM ($R^2 = 0.9981$, $n = 13$) and detection limit of 25 nM Cu^{2+}. The three water samples were also tested using this fluorescence quenching method, and the result was listed in Table 2.

4. Conclusion

In this paper, a rhodamine derivative **1** was applied to detect Cu^{2+} in aqueous media. Under optimized condition, the quantification of Cu^{2+} by **1** using absorptiometric method was satisfactory in a linear working range of 0.05–5.00 μM, with a detection limit of 10 nM Cu^{2+} and good tolerance of other metal ions. Fluorometric measurement of Cu^{2+} using **1** and rhodamine B was also successful, with a linear working range of 0.1–3.6 μM and detection limit of 25 nM Cu^{2+}. Both absorptiometric and fluorometric methods were applied for the detection of Cu^{2+} in three water samples, and the results were good.

Acknowledgement

We are very grateful for the financial support from the National Natural Science Foundation of China (NSFC, No. 20675043).

References

[1] A.P. de Silva, H.Q.N. Gunaratne, T. Gunnlaugsson, A.J.M. Huxley, C.P. McCoy, J.T. Rademacher, T.E. Rice, Chem. Rev. 97 (1997) 1515.
[2] L. Pu, Chem. Rev. 104 (2004) 1687.
[3] G.W. Gokel, W.M. Leevy, M.E. Weber, Chem. Rev. 104 (2004) 2723.
[4] P.D. Beer, P.A. Gale, Angew. Chem. Int. Ed. 40 (2001) 487.
[5] L. Prodi, F. Bolletta, M. Montalti, N. Zaccheroni, Coord. Chem. Rev. 205 (2000) 59.
[6] V. Amendola, L. Fabbrizzi, F. Forti, M. Licchelli, C. Mangano, P. Pallavicini, A. Poggi, D. Sacchi, A. Taglieti, Coord. Chem. Rev. 250 (2006) 273.
[7] B. Valeur, I. Leray, Coord. Chem. Rev. 205 (2000) 3.
[8] B. High, D. Bruce, M.M. Richter, Anal. Chim. Acta 449 (2001) 17.
[9] L. Tapia, M. Suazo, C. Hodar, V. Cambiazo, M. Gonzalez, Biometals 16 (2003) 169.
[10] H. Sigel (Ed.), Metal Ions in Biological Systems, Properties of Copper, vol. 12, Dekker, New York, 1981.
[11] D.J. Waggoner, T.B. Bartnikas, J.D. Gitlin, Neurobiol. Dis. 6 (1999) 221.
[12] R. Krämer, Angew. Chem. Int. Ed. 37 (1998) 772.
[13] P. Ghosh, P.K. Bharadwaj, S. Mandal, G. Sanjib, J. Am. Chem. Soc. 118 (1996) 1553.
[14] Y. Zheng, J. Orbulescu, X. Ji, F.M. Andreopoulos, S.M. Pham, R.M. Leblanc, J. Am. Chem. Soc. 125 (2003) 2680.
[15] M. Royzen, Z. Dai, J.W. Canary, J. Am. Chem. Soc. 127 (2005) 1612.
[16] J.P. Sumner, N.M. Westerberg, A.K. Stoddard, T.K. Hurst, M. Cramer, R.B. Thompson, C.A. Fierke, R. Kopelman, Biosens. Bioelectron. 21 (2006) 1302.
[17] H. Yang, Z.-Q. Liu, Z.-G. Zhou, E.-X. Shi, F.-Y. Li, Y.-K. Du, T. Yi, C.-H. Huang, Tetrahedron Lett. 47 (2006) 2911.
[18] Y. Zheng, X. Cao, J. Orbulescu, V. Konka, F.M. Andreopoulos, S.M. Pham, R.M. Leblanc, Anal. Chem. 75 (2003) 1706.
[19] A. Mokhir, R. Krämer, Chem. Commun. (2005) 2244.
[20] J. Kovács, T. Rödler, A. Mokhir, Angew. Chem. Int. Ed. 45 (2006) 7815.
[21] V. Dujols, F. Ford, A.W. Czarnik, J. Am. Chem. Soc. 119 (1997) 7386.
[22] Y.-K. Yang, K.-J. Yook, J.J. Tae, Am. Chem. Soc. 127 (2005) 16760.
[23] J.Y. Kwon, Y.J. Jang, Y.J.K.M. Lee, Kim, M.S. Seo, W. Nam, J. Yoon, J. Am. Chem. Soc. 127 (2005) 10107.
[24] Y. Xiang, L. Mei, N. Li, A. Tong, Anal. Chim. Acta 581 (2007) 132.
[25] T. Nguyen, M.B. Francis, Org. Lett. 5 (2003) 3245.
[26] Y. Xiang, A. Tong, P. Jin, Y. Ju, Org. Lett. 8 (2006) 2863.
[27] J.F. Holland, R.E. Teets, P.M. Kelly, A. Timnick, Anal. Chem. 49 (1977) 706.
[28] R. Leese, E.L. Wehry, Anal. Chem. 50 (1978) 1193.
[29] J.R. Lakowicz, Principles of Fluorescence Spectroscopy, Springer, 1999.
[30] P. Yuan, D.R. Walt, Anal. Chem. 59 (1987) 2391.
[31] G. Gabor, D.R. Walt, Anal. Chem. 63 (1991) 793.
[32] K.A. Connors, Binding Constants—The Measurement of Molecular Complex Stability, John Wiley & Sons, New York, 1987 (Chapter 4).
[33] W.C. Vosburgh, G.R. Cooper, J. Am. Chem. Soc. 63 (1941) 437.
[34] A.R.S. Ross, M.G. Ikonomou, J.A.J. Thompson, K.J. Orians, Anal. Chem. 70 (1998) 2225.
[35] A. Matsumoto, T. Fukumoto, H. Adachi, H. Watarai, Anal. Chim. Acta 390 (1999) 193.
[36] B.D. Di Marco, G.G. Bombi, M. Tubaro, P. Traldi, Rapid Commun. Mass Spectrom. 17 (2003) 2039.
[37] H.M.N.H. Irving, H. Freiser, T.S. West (Eds.), IUPAC Compendium of Analytical Nomenclature, Definitive Rules, Pergamon Press, Oxford, 1981.
[38] L. Fabrizzi, M. Licchelli, P. Pallavicini, A. Perotti, D. Sacchi, Angew. Chem. Int. Ed. 33 (1994) 1975.
[39] A. Torrado, G.K. Walkup, B. Imperiali, J. Am. Chem. Soc. 120 (1998) 609.
[40] Y. Li, C.M. Yang, Chem. Commun. (2003) 2884.
[41] N. Shao, Y. Zhang, S.M. Cheung, R.H. Yang, W.H. Chan, T. Mo, K.A. Li, F. Liu, Anal. Chem. 77 (2005) 7294.

Available online at www.sciencedirect.com
ScienceDirect
Talanta 74 (2008) 1621–1629
Talanta
www.elsevier.com/locate/talanta

Electrical impedance spectroscopy for detection of bacterial cells in suspensions using interdigitated microelectrodes

Liju Yang *

Biomanufacturing Research Institute & Technology Enterprise (BRITE), and Department of Pharmaceutical Sciences, North Carolina Central University, Durham, NC 27707, United States

Received 8 August 2007; received in revised form 6 October 2007; accepted 8 October 2007
Available online 18 October 2007

Abstract

In this study, we present a new, simple and rapid impedance method to detect bacterial cells by making use of the impedance properties of bacterial cell suspensions using interdigitated microelectrodes. It was found that bacterial cell suspensions in deionized (DI) water with different cell concentrations could generate different electrical impedance spectral responses, whereas cell suspensions in phosphate buffered saline (PBS) solution could not produce any significant differences in impedance spectra in response to different cell concentrations. In DI water suspensions, impedance at 1 kHz decreased with the increasing cell concentrations in the suspensions. The impedance of cell suspensions in DI water was discussed and found that it was resulted from the cell wall charges and the release of ions or other osmolytes from the cells. A linear relationship between the impedance and the logarithmic value of the cell concentration was found in the cell concentration range from 10^6 to 10^{10} cfu/ml, which can be expressed by a regression equation of $Z\,(\mathrm{k}\Omega) = -2.06 \log C\ (\text{cells}/20\ \mu\mathrm{l}) + 5.23$ with $R^2 = 0.98$. The detection limit was calculated to be 3.45×10^6 cfu/ml, which is comparable with many label-free immunosensors for detection of pathogenic bacteria reported in the literature. To achieve the selectivity of this method, we also demonstrated the feasibility of integrating magnetic separation to this impedance method. This study has demonstrated that bacterial cell concentration can be inferred by measuring the impedance of cell suspensions in DI water. This new detection mechanism could be an alternative to current impedance methods that have been reported for the detection of bacterial cells, e.g. impedance microbiology and electrical/electrochemical impedance biosensors.
Published by Elsevier B.V.

Keywords: Impedance spectroscopy; Bacterial detection; Bacterial suspension; *Salmonella*

1. Introduction

Impedance technique, as one of the principle electrical/electrochemical transductions, is becoming a fertile area for developing interdisciplinary methods for applications in a wide range of biological and biomedical detection. This is due to a number of facts including: (i) the electrical properties of the biological entities and/or biological reactions motivates attention to impedance techniques; (ii) impedance is one of the most promising techniques for developing label-free, real-time, and non-invasive methods for biological detection; (iii) impedance as an electronic detecting mechanism can easily interface with miniaturized devices, such as biosensors and biochips, to meet the growing need to offer an analytical foot print considerably smaller than laboratory-based instruments.

Detection and quantification of foodborne pathogenic bacteria remains a challenge and an important issue for ensuring food safety and security for our society. It is reported that foodborne disease causes approximately 76 million illnesses, accounting for 325,000 hospitalizations and more than 5000 deaths each year in the United States [1]. *Salmonella* is one of the major causes of worldwide foodborne disease. The US Centers for Disease Control and Prevention (CDC) estimates that 1.4 million people are infected and 1000 people die each year with salmonellosis in the US. These infections account for 1 billion dollars yearly in direct and indirect medical costs [1]. *Salmonella* Typhimurium is recognized as the second most common serotype (after *Salmonella enteritidis*) of *Salmonella* found in humans.

The impedance technique has been applied in the field of microbiology as a means to detect and/or quantify foodborne

* Tel.: +1 919 530 6704; fax: +1 919 530 6600.
E-mail address: lyang@nccu.edu.

0039-9140/$ – see front matter. Published by Elsevier B.V.
doi:10.1016/j.talanta.2007.10.018

pathogenic bacteria with a long history, and it has received increasing attention from researchers in different fields in recent years. The electrical nature of bacterial cells and their electrophysiology are fundamental for developing impedance methods for detection of bacterial cells. The same as all biological cells, bacterial cells consist of adjacent structures of materials that have very different electrical properties. The cell membrane consists of a lipid bilayer containing many proteins, where the lipid molecules are oriented with their polar groups facing outwards into the aqueous environment, and their hydrophobic hydrocarbon chains pointing inwards to form the membrane interior. The inside of a cell is complex and contains membrane-covered particulates, such as mitochondria, vacuoles, a nucleus, and many dissolved charged molecules. While the cell membrane is highly insulated, the interior of the cell is highly conductive. The conductivity of the cell membrane is around 10^{-7} S/m, whereas the conductivity of the interior of a cell can be as high as 1 S/m [2].

Based on electrophysiological and impedance properties of biological cells, there are three major mechanisms that have been reported for detection/quantification of bacterial cells using impedance measurements: (i) Making use of the metabolic activity of biological cells. This is represented by impedance microbiology, which is a technique based on the measurements of the change in electric impedance in a medium or a reactant solution resulting from the bacterial metabolism [3,4]. The impedance changes are mainly produced by the release of ionic metabolites from live cells that include mainly energy metabolism (catabolism) and maybe ion exchange through the cell membrane (such as K^+, Na^+ ion channels) [5]. For quantification of bacterial cells in a sample, detection time is defined as the time corresponding to the point where the decrease in impedance exceeds a threshold value or a certain percentage on a impedance growth curve. This detection time is the indication of a growth characteristic of a certain initial bacterial concentration, thus is the basis for quantifying the initial cell concentration in a sample. The applications of this detection mechanism for bacterial cell detection, from classic impedance microbiology to novel on-chip impedance microbiology, have been reviewed by Silley and Forsythe [3], Wawerla et al. [4], and Yang and Bashir [6]. (ii) Making use of the insulating properties of the cell membrane. Because of their highly insulated cell membrane, cells attached on an electrode surface effectively reduce the electrode area that the current reaches and hence increase the interface impedance. Most impedance biosensors for bacterial detection are based on this principle, in which antibodies that are specific for the target bacterial cells are immobilized on an electrode surface and serve to facilitate the attachment of cells to the electrode surface and provide selectivity to the sensor. Obviously, these impedance biosensors require the cell attachment/adherence onto electrode surfaces to reach a certain coverage for generating detectable impedance signals. To obtain impedance signals, these sensors may or may not use a redox probe (for example, $[Fe(CN)_6]^{3-/4-}$) in the detection systems [7–10]. More recently, relatively new techniques, such as microfluidics, nanoparticle-based magnetic separation, have been integrated with impedance biosensors with the purpose of improving detection efficacy [11–13]. These impedance biosensors have been developed for detection of various bacterial cells with detection limits varying from 10^2 to 10^6 cfu/ml with detection times from 30 min to several hours. (iii) Making use of the highly ionic cytoplasm of the cells. As mentioned above, the inside of a cell contains many dissolved charged molecules and is highly conductive (1 S/m). This provides a means to detect biological cells by impedance due to the lysis of cells or release of intracellular ions. To date, only a few papers have been published on this subject. Impedance detection of CD4+ T lymphocytes through cell lysates has been demonstrated in a microfluidic chip [14]. Intracellular ion release through electropermeabilization of *Escherichia coli* cells causes a conductance increase after cells are captured to the electrodes by dielectrophoresis. By this method, 10^2 cfu/ml of *E. coli* was detected [15].

In this study, beyond the above three mechanisms for impedance detection of bacterial cells, we present a new, simple and rapid impedance method to detect bacterial cells by making use of the impedance properties of bacterial cell suspensions using interdigitated microelectrodes. We found that electrical impedance spectroscopic responses of bacterial cell suspensions are very dependent on the buffers used in the detection systems. Conductivity of bacterial suspensions has been reported to study the electrical properties of bacterial cell surface and related cell surface interfacial physiology [16,17], but has not yet been reported to quantify the concentration of bacterial cells in the suspensions. In this study, *Salmonella* cell suspensions in deionzed (DI) water and phosphate buffered saline (PBS) solution were studied over a wide range of frequencies. It was found that bacterial cell suspensions in DI water with different cell concentrations can result in different electrical impedance spectral responses. In a certain frequency range, impedance of the cell suspension is related to the cell concentration in the suspension, which can provide an alternative way for quantifying bacterial cells in a label-free, inexpensive, and very simple approach. To achieve the selectivity of this method, we also investigated the integration of magnetic separation by using antibody coated Dynal beads to capture bacterial cells from samples prior to impedance detection.

2. Experimental

2.1. Chemicals

Phosphate buffered saline (PBS) (JAW PBS pack) was purchased from G Bioscience (St. Louis, MO). PBS solution, containing 0.1 M sodium phosphate and 0.15 sodium chloride, (pH 7.0), was made by dissolving 1 pack of PBS powder into 1 l DI water according to the instruction. The conductivity of the PBS solution is ~58 mS/cm, while the conductivity of DI water is ~3 μS/cm, as measured by a pH/conductivity meter (Mettler Toledo GmbH, Switzerland).

2.2. Bacteria culture and media

Salmonella Typhimurium culture was purchased from Carolina Biological Supply Company (Burlington, NC). The culture was grown in brain heart infusion (BHI) broth (TEKnova, Hol-

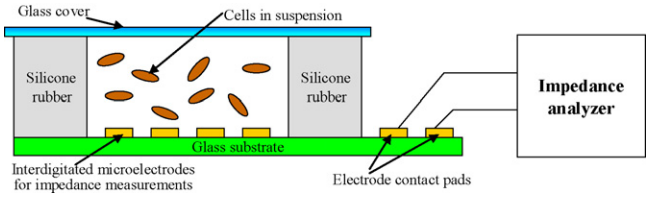

Fig. 1. A schematic diagram of the setup for electrical impedance spectroscopic measurements of bacterial cell suspensions in DI water or PBS. The chamber capacity is ~25 μl. The gold interdigitated microelectrode consists of 50 pair of finger electrodes with 15 μm of digit electrode width and 15 μm interdigit space.

lister, CA) at 37 °C for 16–18 h. The cells were pelleted by centrifuging (Eppendorf, Westbury, NY) at 6000 × *g* for 2 min and resuspended in sterilized DI water or PBS. The cells were washed 3 times in order to get rid of ionic residues from the growth medium, then they were serially (1:10) diluted with DI water or PBS to desirable concentrations for further experiments. The cell numbers were determined by surface plating 0.1 ml of appropriate dilutions onto XLT4 agar plates (Difco, Sparks, MD). Colonies were counted after incubation of the plates at 37 °C for 24 h. *E. coli* K12 culture was obtained from Carolina Biological Supply Company (Burlington, NC). The culture was grown in BHI broth at 37 °C for 16–18 h. The cells were prepared using the same procedure as we prepared *Salmonella* cells. The cell number was determined by surface plating of appropriate dilutions on BHI agar plates. The cell numbers in the cultures averaged about 10^9 colony forming units per milliliter (cfu/ml). Samples with mixed *Salmonella* and *E. coli* cells were prepared by diluting both types of cells in DI water to desired concentrations.

For fluorescent imaging, *S.* Typhimurium cells were stained with 3,3′-dihexyloxacarbocyanine iodide ($DiOC_6(3)$) dye (green) (Molecular Probes, Eugene, OR) for visualization purposes under fluorescence microscope. All stained bacteria cells were centrifuged and washed with DI water or PBS 3–4 times to remove excess dye molecules.

2.3. Electrical impedance spectroscopy (EIS) and devices

The device for electrical impedance measurements consists of an array of interdigitated microelectrode and a microchamber (~25 μl capacity) right above the electrode formed by silicone rubber, as shown in Fig. 1. The gold interdigitated microelectrode was fabricated on a flat glass substrate with a total of 50 pairs of finger electrodes. The finger electrodes are 15 μm of wide and 15 μm of space between finger electrodes (Abtech Scientific, Inc., Richmond, VA).

Impedance measurements were performed using an IM-6 impedance analyzer (Zahner-elektrik CMBH & Co. KG, Germany) with the IM-6/THALES software. For measurements, 20 μl of each sample was placed into the microchamber and covered with a glass cover. One of the two microband array electrodes was connected to the test and sense probes, and the other was connected to the reference and counter electrodes on the IM-6 impedance analyzer. EIS measurements were carried out in a frequency range from 1 Hz to 100 kHz. Bode (impedance and phase vs. frequency) diagrams were recorded. Impedance at fixed frequency was measured using the Capacitance-Potential (C/E) program at 1 kHz with an amplitude of ±50 mV. Impedance data were recorded at every minute. All tests were performed at room temperature.

Simulation was performed using the SIM program. Fifty points of data from each measured spectrum were automatically selected by the software as input to an equivalent circuit to generate a fitting spectrum.

2.4. Fluorescence imaging

The fluorescent images were taken on a Nikon ECLIPSE E600FN fluorescence microscope (Japan) with a Coolsnap HQ camera (Roper Scientific, Inc.—Photometric, Tucson, AZ) using a FITC (Fluorescin isothiocyanate) filter.

2.5. Magnetic separation

One millilitres of *Salmonella* suspension or the mixture of *Salmonella* and *E. coli* suspension was mixed with 20 μl anti-*Salmonella* antibody coated magnetic beads (2.8 μm in diameter, Dynal Biotech, Invitrogen, Carlsbad, CA) in a centrifuge tube (1.7 ml, VWR International, West Chester, PA). The mixture was kept rotating on a RKVSD 10101 mixer (ATR, Inc. Laurel, MD) at a speed of 20 rpm for 30 min at room temperature. After applying the magnetic field, the supernatant was removed. The beads were washed with 1 ml DI water 3 times, and resuspended with 50 μl DI water. Twenty microlitres of the suspension was introduced to the impedance detection chamber for impedance measurements.

3. Results and discussion

3.1. EIS of bacterial cell suspensions in DI water and PBS

Fig. 2 presents the Bode impedance spectra of *Salmonella* Typhimurium cell suspensions in DI water (A) and in PBS (B) along with their equivalent circuits and fitting spectra. For *Salmonella* cell suspension in DI water, the measured spectrum (Fig. 2A, blank dots) is a typical Bode plot for a system where the polarization is due to a combination of kinetic and diffusion processes. Based on the general electronic equivalent model of an electrochemical cell [18] and the behavior of the IME microelectrode [19], an equivalent circuit which consists of ohmic resistance (R_s) of the solution between two electrodes and double layer capacitance (C_{dl}), electron-transfer resistance (R_{et}) and Warburg impedance (Z_w) around each electrode, was considered for simulation of the measured spectra. Among these electrical elements, R_s and Z_w represent the properties of the bulk solution and the diffusion of the electrochemical active ions in the solution. The other two elements, C_{dl} and R_{et}, represent the dielectric and insulating features at the electrode/electrolyte interface. For simulation, 50 data points on the impedance measured spectrum were automatically selected by the software and used as input to the equivalent circuit, generating a fitting impedance spectrum (Fig. 2 solid line). The agreement between the mea-

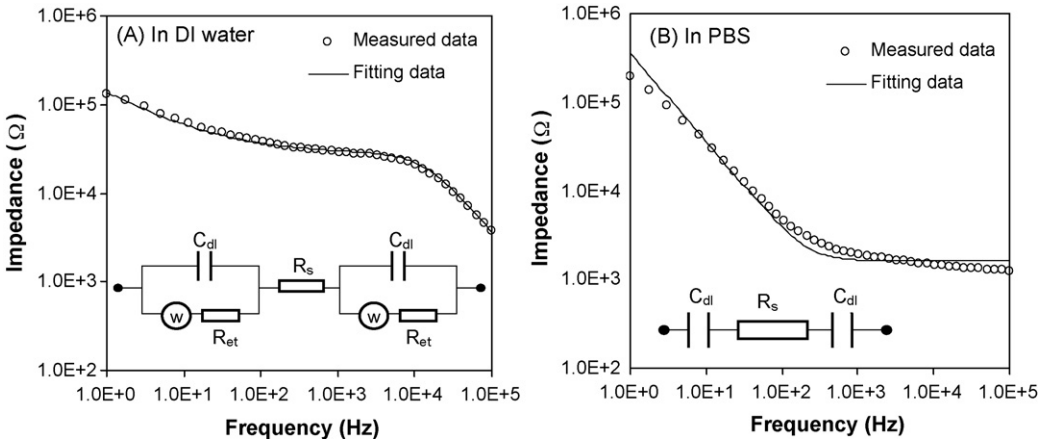

Fig. 2. Impedance spectra of *Salmonella* cell suspensions in (A) DI water and (B) in PBS together with their fitting spectra and the equivalent circuits. Frequency range: 1 Hz–100 kHz. Amplitude: ±50 mV. *Salmonella* concentration: 1.93×10^6 cfu/ml.

sured data and the fitting spectra indicated that the equivalent circuits provided a feasible, if not unique, model to describe the impedance characteristics of *Salmonella* suspensions in DI water. Using this simulation, the values of C_{dl}, Z_w, R_{et}, and R_s were 884.9 pF, 147.2 kΩ/s$^{1/2}$, 13.54 kΩ, and 491.2 Ω, respectively, with the mean error of modulus impedance of 0.6%.

For *Salmonella* suspensions in PBS, the impedance spectrum (Fig. 2B blank dots) shows two domains: a double layer region in low frequency range from 1 Hz to approximately 500 Hz and a resistive region in the frequency range from ∼500 Hz to 100 kHz. The electric impedance behavior of the cell suspension in PBS can be represented by the equivalent circuit of the IME system in aqueous solutions reported previously [19–22]. In this circuit model, two identical double layer capacitances (C_{dl}) of each set of the IME are connected to the medium resistance (R_s) in series. C_{dl} dominates the impedance in the low frequency range (double layer region), whereas R_s dominates the impedance in high frequency range (resistive region). By simulation, the values of C_{dl}, and R_s were 892.8 nF, 1.62 kΩ, respectively, with the mean error of modulus impedance of 3.0%.

Detailed reasons accounting for the difference in the impedance spectral behavior between the cell suspensions in DI water and PBS need to be discussed. The characteristics of the spectrum along with the equivalent circuit in Fig. 2A suggest that there are electrochemical reactions occurring on the IME electrodes in the cell suspension in DI water. The electron-transfer resistance (R_{et}) and Warburg impedance (Z_w) are the parameters indicating the electrochemical reactions and the diffusion of the electrochemical active species in the suspension. This implies that cells may release some electrochemical active composites to the DI water. However, in the cell suspension in PBS, the impedance spectrum does not show any characteristics related to electrochemical active parameters, which implies cells may not release active electrochemical species into PBS.

3.2. EIS of bacterial suspensions with different concentrations

Fig. 3 shows the Bode impedance spectra of *Salmonella* suspensions in DI water (A) and PBS solution (B) with different cell concentrations from 10^4 to 10^9 cfu/ml. It can be seen that the impedance spectra of *Salmonella* suspensions in DI water respond significantly different with cell concentrations in the frequency range from 100 Hz to 10 kHz, whereas impedance spectra of *Salmonella* suspensions in PBS show no significant difference at any frequency. For cell suspensions in DI water, it is obvious that in the frequency range from 100 Hz to 10 kHz,

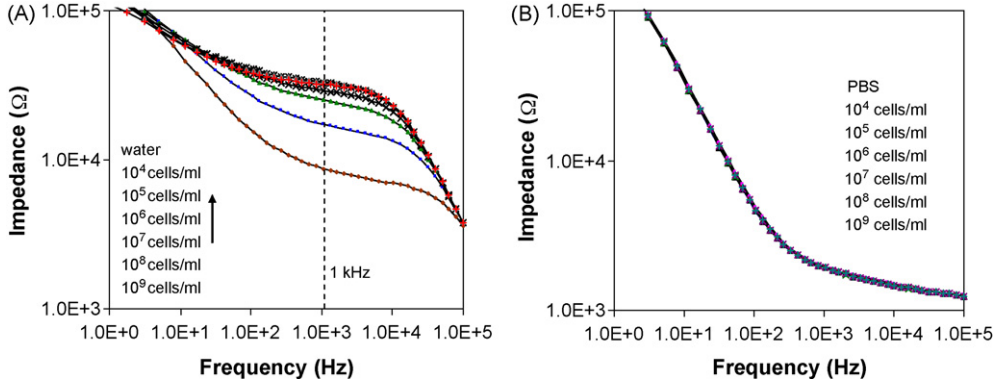

Fig. 3. Impedance spectra of *Salmonella* suspensions in (A) DI water and (B) PBS with the cell concentrations in the range of 10^4 to 10^9 cfu/ml, along with water and PBS as controls. Frequency range: 1 Hz–100 kHz. Amplitude: ±50 mV.

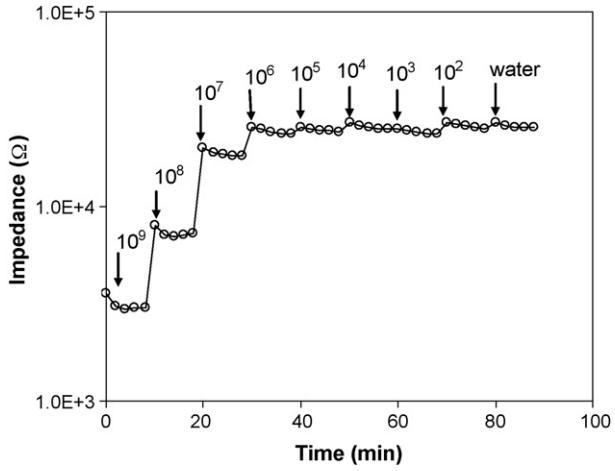

Fig. 4. Typical impedance responses to the samples with different concentrations of cells when the samples were measured sequentially in the impedance detection chamber. The arrows indicate the time when a sample was introduced into the detection microchamber. The numbers in the figure indicate the concentrations of *Salmonella* cells in the samples in units of cfu/ml.

impedance decreases with the increasing cell concentrations. This would allow us to estimate the cell concentration in the DI water suspension by using the impedance value at a fixed frequency. As a best representative frequency, we identified 1 kHz as the test frequency to investigate the relationship between impedance value and cell concentration in DI water suspensions. Fig. 4 shows typical impedance responses at 1 kHz to the samples containing different bacterial concentrations in impedance measurements. The impedance of each sample was measured after the cells were suspended in DI water for ~1 h. The impedance value at 1 kHz increased with the decreasing concentration of cells in the suspension. When bacterial concentration decreased from 10^9 cfu/ml to 10^8, 10^7, 10^6 cfu/ml, the impedance of the suspension significantly increased from 3.13 ± 0.26 kΩ to 7.29 ± 0.17, 18.7 ± 0.28, 24.4 ± 0.58 kΩ. When cell concentrations were lower than 10^6 cfu/ml, the impedance values of the suspensions were not significantly different from each other or from DI water.

By fitting the impedance spectra of cell suspensions in DI water in Fig. 3 to the equivalent circuit model in Fig. 2A, we found that the values of almost all electrical elements, Z_w, R_{et}, and R_s of the suspensions changed when the cell concentration changed, except that C_{dl} kept relatively stable. This simulation result is consistent with the spectra in Fig. 3. As reported in our previous studies, C_{dl} usually appears on the spectra in the double layer region which is always in the low frequency range (<10 Hz) and usually contributes to the impedance value in a frequency-dependent manner ($Z = -j/\sqrt{2\pi fC}$, f is frequency) that impedance in this region decreases with frequency. As seen in Fig. 3, impedances on the spectra in the low frequency range (<10 Hz) are not significantly different with different cell concentrations. Frequency ranges from 100 Hz to 10 kHz on these impedance spectra are resistive regions which reflect the impedance contributed by all resistive components in the detection system, which in this case include Z_w, R_{et}, and R_s. At 1 kHz, we believe that the impedance value reflects the combination of Z_w, R_{et}, and R_s components. These results indicate that alteration in cell concentration could alter the impedance of the suspension by changing the Z_w, R_{et}, and R_s components in the detection system. Therefore, the cell concentration in the DI water suspensions can be determined by measuring the total impedance of the suspensions at 1 kHz regardless whether the changes are from the Z_w, R_{et}, or R_s components. However, impedance of cell suspensions in PBS did not cause any difference at any tested frequency in response to different cell concentrations, and thus could not be used as an indicator for cell concentrations in PBS suspensions.

3.3. Discussion on the impedance properties of cell suspensions in DI water

The observation of decreases in impedance of the cell suspensions with increasing cell concentrations indicates that cell suspensions with high concentrations are more conductive than those with lower concentrations. This implies that bacterial cells contribute to conductive compositions to the suspension. We found that there are two possible sources for the bacterial cells to alter the impedance of DI water suspensions. One is the electrical nature of bacterial cell surfaces. The bacterial cell walls contain various acidic groups such as carboxyl, phosphate, and amino groups, which may be present in high concentrations [23]. Generally, they contain higher concentrations of anionic groups than of cationic groups, which results in a negative cell wall charge at neutral pH. This charge is compensated by counter-ions that penetrate into the porous cell well and to a minor extent by co-ions that are expelled from it, thereby conferring electrostatic charge to the cell periphery [16,17,24]. The charge density of bacterial cell wall can be as high as 0.5–1.0 C/m^2 [16]. In our experiments, the conductivity of the DI water is in a range from as low as about 1–2 μS/cm, to up to about 10–15 μS/cm. When *Salmonella* cells were suspended in such low conductive DI water and reached a sufficient concentration (in our experiments, 10^6 cfu/ml), they could alter the conductivity of the suspension because of their cell wall charges. Whereas in PBS solution, the bacterial cell wall charges are not sufficient to alter the conductivity of the bulk solution due to the high background conductivity of the PBS (~58 mS/cm). In some studies, the conductivity of the cell suspension was considered to vary linearly with the bacterial cell volume fraction [16]. Fig. 5 shows the images of the bacterial cell distribution in the test chamber at different concentrations, which are representative cell densities in the suspensions at the certain cell concentrations. Here, we can expect that the conductivity of the solution should vary proportionally to the number of the cells in the solution or the cell concentration when the total volume is fixed.

The other source of bacterial cells to alter the conductivity of DI water suspension is the ion release from bacterial cells. When bacterial cells were suspended a solution, phenomena, such as leakage of ions through the cytoplasmic membrane and negative adsorption of electrolyte or by ion uptake in the cytoplasm and specific adsorption of ions, may occur, which influence the conductivity of the bulk solution [16]. Fig. 6 shows the plot of impedance changes at 1 kHz as a function of time for the sample

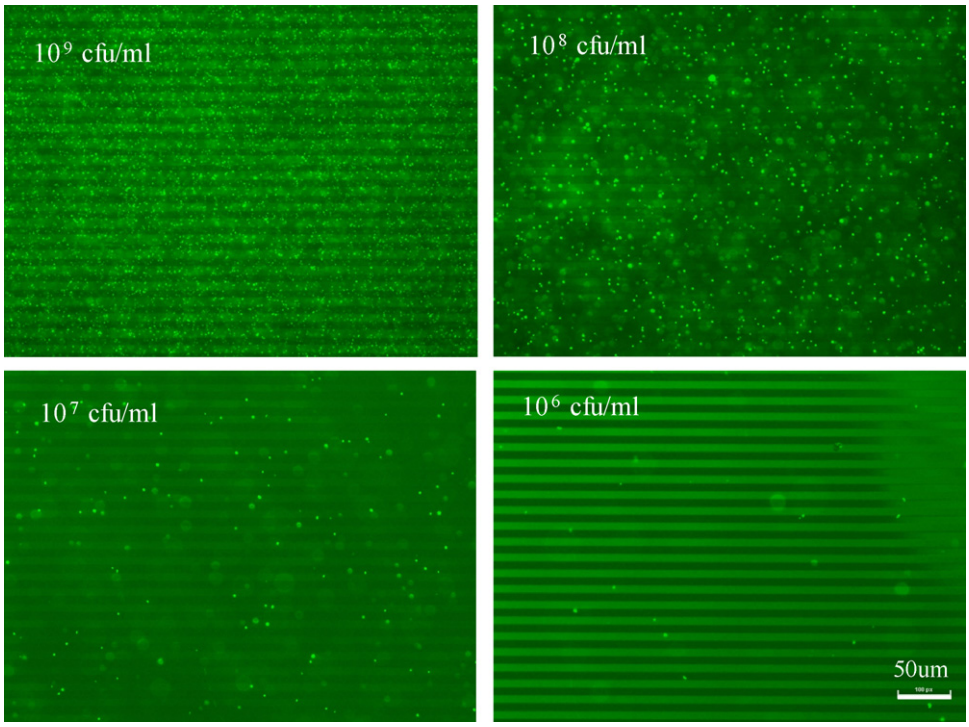

Fig. 5. Representative densities of the *Salmonella* cells in DI water with concentrations range from 10^9 to 10^6 cfu/ml in a thin layer right above the interdigitated microelectrodes. The green dots are the cells stained with $DiOC_6$ (3) dye. The thin layer of the solution is about 100 μm. All pictures were taken with focus on the surface of the electrodes. Green dots that are out of focus are the cells in the suspensions. The bacterial concentrations were 1.3×10^9, 1.3×10^8, 1.3×10^7, 1.3×10^6 cfu/ml. (For interpretation of the references to colour in this figure legend, the reader is referred to the web version of the article.)

of *Salmonella* suspensions in DI water and PBS and with water and PBS as control samples. The cell concentrations in the suspensions were at 1.9×10^9 cfu/ml. We observed a slight decrease trend in impedance values with time for the pure DI water. This may be due to the slight temperature change at the electrode locality. However, when the *Salmonella* suspension (10^9 cfu/ml) in DI water was tested, significant decreases in impedance with time were observed. Impedance decreased by 15% at the first 10 min, and decreased by 22.5% at 25 min. It became relatively stable after 1 h (not shown in Fig. 6). Decreases in impedance suggested that the solution became more conductive, which may due to the release of ions or other intracellular and/or extracellular materials from the cells into the solution. When *Salmonella* cells were suspended into DI water, it is obvious that there is a difference in ionic concentration between cell growth medium and the DI water, which may cause the cells to experience an osmotic shock. In response to the fluctuations in environmental osmolarity, cells adjust their intracellular solute concentrations in order to maintain a constant turgor pressure and ensure continuation of cellular activity. It is reported that yeast cells released glycerol upon hypo-osmotic shock, and possibly arabitol and erythritol as well depending on cell type [25]. Other studies reported that osmotic shock could cause the release of extracellular enzymes including invertase, a Co^{2+} activated 5′-nucleotidase, acid phosphatase, and alkaline pyrophosphatase from yeast cells [26], and decreases in the Na^+, and Cl^- levels in isolated axons of *Carcinus maenas* [27]. Other properties of cells such as cell size and buoyant density could also be altered in response to osmotic shock [28]. We therefore think that the combination of the release of ions and other various responses to the osmotic shock could account for the decrease in impedance with time as we observed in Fig. 6. It is reported that the responses of osmotic shock are rapid [25,26]. As we can see in Fig. 6, the impedance decreases rapidly at the beginning (first 10 min), and gradually slows down, and becomes relative stable after 1 h. However, for low cell concentrations (10^6 cfu/ml or lower), we were not able to observe the significant decrease trends in impedance during the first 25 min after the cells were

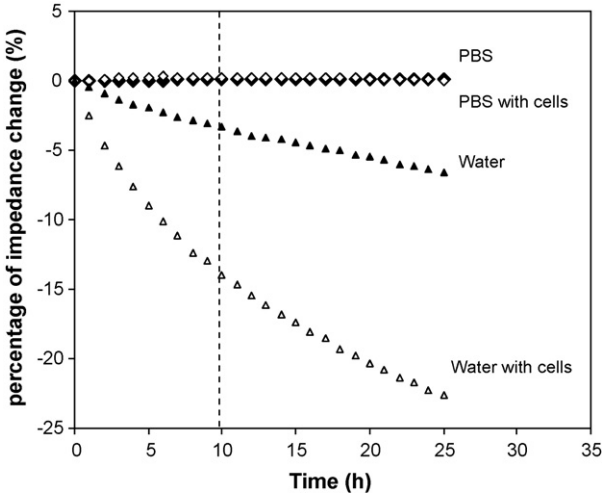

Fig. 6. The percentage of impedance change with time for bacterial cells in DI water and PBS suspensions. *Salmonella* concentration: 2.1×10^9 cfu/ml. Impedance was measured at 1 kHz with an amplitude of 50 mV.

suspended in DI water. This may be because ion release from the lower concentrations of cells could not generate a measurable impedance change in the solution. It should be noted that the cells were washed 3–4 times with DI water before the performance of impedance measurements in our experiments, hence we believe that ion release initiated during the wash steps. It is believed that the impedance of the cell suspension measured at 1 kHz (in Fig. 4) is contributed from both ion release from the cells and cell surface charges. In Fig. 6, the impedance values of both PBS and PBS with *Salmonella* cells are constant with time, indicating that bacterial cells at the concentration of 10^9 cfu/ml did not cause impedance change in the cell suspension in PBS. It is likely that bacterial cells in PBS solution did not experience osmotic shock and thus ion release did not occur (PBS is commonly used to provide biological cells a condition similar to their natural physiological condition).

3.4. Quantifying bacterial concentration in DI water suspension by impedance

Under the experimental conditions in this study, the plot of the impedance values as a function of the bacterial concentrations is shown in Fig. 7. We found that there is a linear relationship between the impedance and the logarithmic value of the cell concentration in the range from 10^4 to 10^8 cells/20 μl (10^6 to 10^{10} cfu/ml). Impedance decreases with increasing cell concentration. The linear regression equation is $Z\,(\mathrm{k}\Omega) = -2.06 \log C$ (cells/20 μl) + 5.23 with $R^2 = 0.98$. The detection limit was calculated to be 6.9×10^4 cells/20 μl (3.45×10^6 cfu/ml). These results indicated that the cell concentrations in DI water suspensions can be determined from the impedance of the bacterial suspensions. This can be an alternative impedance approach to quantify bacterial cells in suspensions other than impedance microbiology and impedance biosensors for bacteria detection. This method does not require any labels or amplification steps. The detection limit of this method is comparable with many other label-free immunosensors for detection of pathogenic bacteria using different transducer techniques, including QCM immunosensors for detection of *Salmonella* with detection limits of 3.2×10^6 cfu/ml and 9.9×10^5 cfu/ml [29,30], SPR immounosensors for detection of *Salmonella enteritidis* and *Listeria monocytogens* with detection limits of 10^6 cfu/ml [31], a SPR sensor for detection of *E. coli* O157:H7 with a detection limit of 10^7 cfu/ml [32], and an electrochemical impedance immunosensor for detection of *E. coli* O157:H7 with detection limit of 10^6 cfu/ml [8].

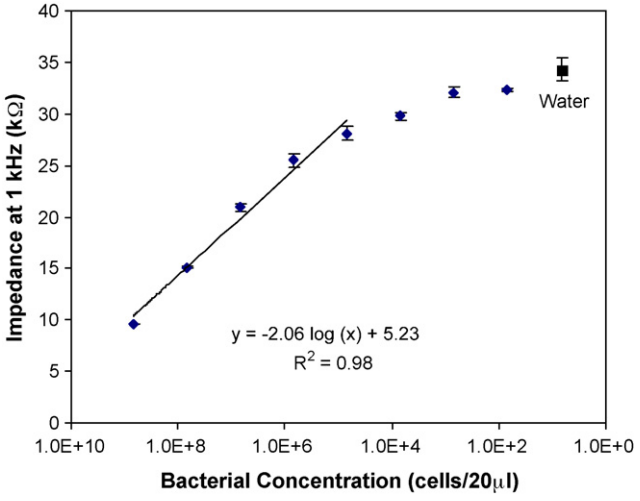

Fig. 7. The linear relationship between the logarithmic value of the concentration of *Salmonella* cells and the impedance measured at 1 kHz. Error bars are standard deviations of 3–5 measurements.

3.5. Coupling of magnetic separation

It is important that a detection method should be able to selectively detect the target analyte. Magnetic separation has been proven to be one of the best approaches to provide selectivity to an analytical method for bacterial detection by separating specific bacteria from food samples. Basically, antibody-coated magnetic beads are used to react with target cells in the samples to form bead–bacteria complexes. The bead–bacteria complexes are subsequently separated from the sample by using a magnetic field and can be detected by various methods. For example, magnetic separation has been coupled with a variety of analytical methods for bacterial detection, including conductance detection [33], immunoassays [34,35], flow cytometry [36], immunoelectrochemical detection [37], chemiluminescence biosensors [38], and impedance detection [12,39].

Here, we investigated the feasibility of coupling magnetic separation with our detection system. In the experiments, anti-*Salmonella* antibody coated Dynal beads (Invitrogen) were used to separate *Salmonella* from the samples. The bead–*Salmonella* complexes in DI water suspensions were measured by impedance. Fig. 8A shows the impedance spectra of the cell suspensions in DI water different concentrations (from 10^6 to 10^9 cfu/ml) after magnetic separation. These spectra show the same characteristics as in Fig. 3A, indicating that after bacterial cells are captured by magnetic beads and suspended in DI water, they behave the same as what they do when they are free in the suspensions. In other words, we can conclude that magnetic beads do not affect the measurement of impedance for these suspensions, meaning that they can be incorporated with this method and feasibly provide selectivity to this detection method. We also found that there is a linear relationship between the impedance and the log value of the cell concentration in the range from 10^9 to 10^7 cfu/ml. At our optimized experimental condition, the linear relation can be represented by the regression equation $Z\,(\mathrm{k}\Omega) = -5.02 \log C$ (cfu/ml) + 120.20, with $R^2 = 0.99$. The detection limit is 10^7 cfu/ml in the sample, which is slightly higher than that without magnetic separation. This is not surprising due to the efficiency of magnetic separation. As reported previously, the efficiency of magnetic separation of *Salmonella* Typhimurium using Dynal beads could be ~80% [39]. For example, the cell concentration of a sample containing 10^7 cfu/ml of *Salmonella* would reduce to an actual cell concentration of 10^6 cfu/ml after magnetic separation, because not all the cells would be captured by the beads.

The selectivity of the method is actually dependent on the quality of the anti-*Salmonella* antibody on the Dynal

beads. According the manufacturer's instruction, the antibodies on the beads are affinity purified antibodies against *Salmonella*, and they recognize *Salmonella* species. Several previous studies have proven that the selective separation of *Salmonella* in the presence of certain concentrations of *E. coli* and/or other bacteria (*Listeria*) can be achieved by using the anti-*Salmonella* coated beads with subsequent chemiluminescence detection [38], impedance detection of *Salmonella* growth [39], and fluorescence detection [40]. In this study, we used *E. coli* K12 as competing bacteria to demonstrate the feasibility of coupling magnetic separation in this detection system. Fig. 8B shows the impedance spectra of the suspensions containing *Salmonella* only (2.85×10^8 cfu/ml) or the mixture of *Salmonella* (2.85×10^8 cfu/ml) and *E. coli* (1.38×10^8 cfu/ml) with and without magnetic separation. As shown in Fig. 8B, without magnetic separation, the mixture of *Salmonella* (2.85×10^8 cfu/ml) and *E. coli* (1.38×10^8 cfu/ml) has lower impedance values in the frequency range from ~500 Hz to ~50 kHz when compared with those of the sample containing *Salmonella* only. It is believed that the ion release and cell surface charges from *E. coli* cells also contribute to the impedance of the mixture, resulting in lower impedances (~500 Hz to ~50 kHz) of the mixture compared with those of the suspension with *Salmonella* only. With magnetic separation, the mixture of *Salmonella and E. coli* and the sample with *Salmonella* only show similar impedance spectra in the tested frequency range. This indicates that magnetic separation by capturing only *Salmonella* cells from the mixed culture prior to impedance measurements can minimize the interference from *E. coli* cells in impedance measurements. In Fig. 8B, it can also be seen that the impedances of the samples with magnetic separation are higher than those without magnetic separation. It is understandable that there are lower concentrations of cells in the samples after magnetic separation compared with the samples without magnetic separation because not all the cells can be captured by the beads. Overall, these results indicate that incorporation of magnetic separation with this impedance method could provide a feasible detection method for the selective detection of bacterial cells in DI water suspensions.

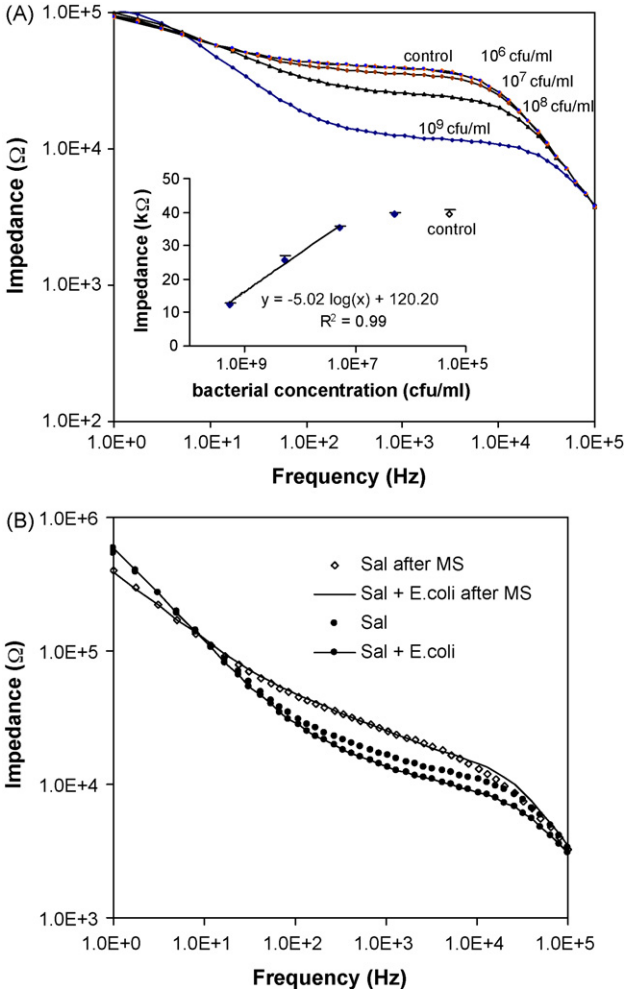

Fig. 8. (A) Impedance spectra of *Salmonella* suspensions in DI water along with water as control after magnetic separation. The cell concentrations in the range of 10^6 to 10^9 cfu/ml. The inset is the linear relationship between the logarithmic value of the concentration of *Salmonella* cells and the impedance measured at 1 kHz. Error bars are standard deviations of 3–5 measurements. (B) Impedance spectra of the suspensions containing *Salmonella* only (2.85×10^8 cfu/ml) and the mixture of *Salmonella* (2.85×10^8 cfu/ml) and *E. coli* (1.38×10^8 cfu/ml) with and without magnetic separation (MS). Frequency range: 1 Hz–100 kHz. Amplitude: ±50 mV.

4. Conclusions

In this study, we have demonstrated a new, simple and rapid impedance method to detect bacterial cells by making use of the impedance properties of bacterial cell suspensions using interdigitated microelectrodes, which is beyond the mechanisms currently used for impedance detection of bacterial cells. We found that bacterial cell suspensions in DI water with different cell concentrations can result in different electrical impedance spectral responses, whereas cell suspensions in PBS could not produce any significant differences in impedance spectra in response to different cell concentrations. The impedance value at a fixed frequency (1 kHz) of the cell suspension was examined to quantify the cell concentration in the cell suspensions in DI water. We found that impedance decreases with the increasing cell concentrations in the suspensions. The impedance of bacterial cell suspensions in DI water was discussed and found that it is resulted from the cell wall charges and the release of ions or other osmolytes from the cells. There is a linear relationship between the impedance and the log value of the cell concentration in the range from 10^4 to 10^8 cells/20 μl (10^6 to 10^{10} cfu/ml), which can be expressed by a regression equation of $Z\,(\mathrm{k\Omega}) = -2.06 \log C\ (\mathrm{cells/20\ \mu l}) + 5.23$ with $R^2 = 0.98$. The detection limit was calculated to be 6.9×10^4 cells/20 μl (3.45×10^6 cfu/ml). The detection limit of this method is comparable with many label-free immunosensors for detection of pathogenic bacteria reported in the literature, including QCM immunosensors [29,30], SPR immunosensors [31,32] and electrical/electrochemical impedance immunosensors [8]. To achieve the selectivity of the method, we also demonstrated the feasibility of integrating magnetic separation to this method to provide the selectivity to this impedance method. This study

has demonstrated that measurements of impedance of cell suspensions can provide an alternative method for quantifying bacterial cells in a label-free, inexpensive, rapid and very simple approach.

Advances in microfabrication have paved the way for miniaturization of many traditional detection platforms into microdevices/chips. To further improve the detection limit of this method, we believe that the use of microdevices which can concentrate low number of bacterial cells into an ultramicro-detection chamber would be very useful. The concentration step could effectively increase the cell concentration at the locality of the detection chamber such that they can generate a detectable impedance signal at the electrodes. Work is in progress to further improve this method by integrating dielectrophoresis to concentrate cells in a microfluidic detection chip. As mentioned above, the interior of the cell is highly conductive. Lyses of cells prior to impedance measurements may also help to enhance impedance signals of this method. Investigation on the use of other low conductivity buffers other than DI water is also in progress.

Acknowledgements

The author acknowledges the Funding from Golden LEAF Foundation and North Carolina State through the Biomanufacturing Research Institute & Technology Enterprise (BRITE) Center for Excellence at North Carolina Central University.

References

[1] P.S. Mead, L. Slutsker, V. Dietz, L.F. McCraig, S. Bresee, C. Shapiro, P.M. Griffin, R.V. Tauxe, Emerg. Infect. Dis. 5 (1999) 607–625.
[2] R. Pethig, G.H. Markx, TIBTECH 15 (1997) 426–432.
[3] P. Silley, S. Forsythe, J. Appl. Bacteriol. 80 (1996) 233–243.
[4] M. Wawerla, A. Stolle, B. Schalch, H. Eisgruber, J. Food Prot. 62 (1999) 1488–1496.
[5] J. Owicki, J. Parce, Biosens. Bioelectron. 7 (1992) 257–272.
[6] L. Yang, R. Bashir, Biotechnol. Adv. (2007) (in review).
[7] C. Ruan, L. Yang, Y. Li, Anal. Chem. 18 (2002) 4814–4820.
[8] L. Yang, Y. Li, G.F. Erf, Anal. Chem. 76 (2004) 1107–1113.
[9] S.M. Radke, E.C. Alocilja, Biosens. Bioelectron. 20 (2005) 1656–1661.
[10] J. Suehiro, A. Ohtsubo, T. Hatano, M. Hara, Sens. Actuator B: Chem. 119 (2006) 319–326.
[11] M. Varshney, Y. Li, Biosens. Bioelectron. 22 (2007) 2408–2414.
[12] M. Varshney, Y. Li, B. Srinivasan, S. Tung, Sens. Actuator B: Chem. 128 (2007) 99–107.
[13] D.A. Boehm, P.A. Gottlieb, S.Z. Hua, Sens. Actuator B: Chem. 126 (2007) 508–514.
[14] X. Cheng, Y. Liu, D. Irimia, U. Demirci, L. Yang, L. Zamir, W.R. Rodriguez, M. Toner, R. Bashir, Lab. Chip. 7 (2007) 755–764.
[15] J. Suehiro, T. Hatano, M. Shutou, M. Hara, Sens. Actuator B: Chem. 109 (2005) 209–215.
[16] A. Van Der Wal, M. Minor, W. Norde, A. Zehnder, J. Lyklema, J. Colloid Interface Sci. 186 (1997) 71–79.
[17] W.W. Wilson, M.M. Wade, S.C. Holman, F.R. Champlin, J. Microbiol. Methods 43 (2001) 153–164.
[18] A.J. Bard, L.R. Faulkner, Electrochemical Methods: Fundamentals and Applications, John Wiley & Sons, New York, 2001.
[19] P. Van Gerwen, W. Laureyn, W. Laureys, G. Huyberechts, M. Op De Beek, K. Baert, J. Suls, W. Sansen, P. Jacobs, L. Herman, R. Mertens, Sens. Actuator B: Chem. 49 (1998) 73–80.
[20] W. Laureyn, D. Nelis, P. Van Gerwen, K. Baert, L. Hermans, R. Magnee, J.J. Pireaux, G. Maes, Sens. Actuator B: Chem. 68 (2000) 360–370.
[21] L. Yang, Y. Li, C.L. Griffis, M.G. Johnson, Biosens. Bioelectron. 19 (2004) 1139–1147.
[22] Z. Zou, J. Kai, M.J. Rust, J. Han, C.H. Ahn, Sens. Actuator A: Phys. 136 (2007) 518–526.
[23] E.L. Carstensen, R.E. Marquis, Biophys. J. 8 (1968) 536–548.
[24] N. Mozes, P.G. Rouxhet, in: R.J. Doyle, M. Rosenberg (Eds.), Microbial Cell Surface Hydrophobicity, American Society for Microbiology, Washington, DC, USA, 1990, pp. 75–105.
[25] G. Kayingo, S.G. Kilian, B.A. Prior, Arch. Microbiol. 177 (1) (2001) 29–35.
[26] J. Schwencke, G. Farís, M. Rojas, J. Biochem. 21 (1) (1971) 137–143.
[27] C. Kevers, A. Péqueux, R. Gilles, J. Comp. Physiol. B: Biochem. Syst. Environ. Physiol. 129 (4) (1979) 365–371.
[28] W.W. Baldwin, M.J.T. Sheu, P.W. Bankston, C.L. Woldringh, J. Bacteriol. 170 (1) (1988) 452–455.
[29] I. Park, N. Kim, Biosens. Bioelectron. 13 (1998) 1091–1097.
[30] I. Park, W. Kim, N. Kim, Biosens. Bioelectron. 15 (2000) 167–172.
[31] V. Koubova, E. Brynda, L. Karasova, J. Skvor, J. Homola, J. Dostalek, P. Tobiska, J. Rosicky, Sens. Actuator B: Chem. 74 (2001) 100–105.
[32] P.M. Fratamico, T.P. Strobaugh, M.B. Medina, A.G. Gehring, Biotechnol. Tech. 12 (1998) 571–576.
[33] N. Parmar, M.C. Ester, S.J. Forsythe, Lett. Appl. Microbiol. 15 (1992) 175–178.
[34] A.R. Bennett, S. MacPhee, R.P. Betts, Lett. Appl. Microbiol. 22 (1996) 237–243.
[35] S. Tu, M. Golden, P. Andreotti, L.S.L. Tu, P. Irwin, J. Rapid Methods Automat. Microbiol. 9 (2001) 71–84.
[36] K.H. Seo, R.E. Brackett, J.F. Frank, S. Hilliard, J. Food. Prot. 61 (1998) 812–816.
[37] Y.H. Che, Z. Yang, Y. Li, D. Paul, M. Slavik, J. Rapid Methods Automat. Microbiol. 7 (1999) 47–59.
[38] M. Varshney, Y. Li, R. Nanapanneni, M. Johnson, C.L. Griffis, J. Rapid Methods Automat. Microbiol. 11 (2003) 111–131.
[39] L. Yang, Y. Li, J. Microbiol. Methods 64 (2006) 9–16.
[40] L. Yang, Y. Li, J. Food Prot. 68 (2005) 1241–1245.

Available online at www.sciencedirect.com
ScienceDirect
Talanta 74 (2008) 1408–1413
Talanta
www.elsevier.com/locate/talanta

Determination of 40 synthetic food colors in drinks and candies by high-performance liquid chromatography using a short column with photodiode array detection

N. Yoshioka *, K. Ichihashi

Hyogo Prefectural Institute of Public Health and Environmental Sciences, 2-1-29 Arata-cho, Hyogo-ku, Kobe 652-0032, Japan

Received 27 July 2007; received in revised form 18 September 2007; accepted 19 September 2007
Available online 26 September 2007

Abstract

Forty synthetic food colors were determined in drinks and candies by reversed-phase high-performance liquid chromatography with photodiode array detection. The following food colors were analyzed within 19 min using a short analytical column (50 mm × 4.6 mm i.d., 1.8 μm) at 50 °C with gradient elution: Ponceau 6R, Tartrazine, Fast yellow AB, Amaranth, Indigotine, Naphthol yellow S, Chrysoine, Ponceau 4R, Sunset yellow FCF, Red 10B, Orange G, Acid violet 7, Brilliant black PN, Allura red AC, Yellow 2G, Red 2G, Uranine, Fast red E, Green S, Ponceau 2R, Azorubine, Orange I, Quinoline yellow, Martius yellow, Ponceau SX, Ponceau 3R, Fast green FCF, Eosine, Brilliant blue FCF, Orange II, Orange RN, Acid blue 1, Erythrosine, Amido black 10B, Acid red 52, Patent blue V, Acid green 9, Phloxine B, Benzyl violet 4B, and Rose bengal. The recoveries of these compounds added to soft drinks and candies at 5 μg/g ranged from 76.6 to 115.0%, and relative standard deviations (R.S.D.s) were within 6.0%. The limits of detection and the limits of quantitation were 0.03 and 0.1 μg/g, respectively.
© 2007 Elsevier B.V. All rights reserved.

Keywords: Synthetic food colors; Drinks and candies; HPLC; Photodiode array detection; Short column

1. Introduction

Food colors are used for maintenance and improvement of color appearance in foods. In recent years, natural food colors have been increasingly used for the consumer preference. However, they are relatively unstable and the costs are higher than synthetic food colors. Therefore, synthetic food colors are still used instead of natural colors in many foods such as drinks, candies, and sweets.

The lists of permitted food colors vary from country to country. In Japan, there are some violation cases of food products containing non-permitted food colors such as Azorubine, Quinoline yellow, and Patent blue V [1]. These food colors are permitted and frequently used in EU countries, however, they are not permitted in other countries including Japan and USA.

All ingredients including food colors are required to be listed on the food labels. Some people are sensitive to particular food colors, so the colors in the food products must be the same as those on their labels. Thus, determination of synthetic food colors is required to ensure the food safety.

A large number of analytical methods for food colors have been proposed, such as thin layer chromatography (TLC) [2,3], voltammetry [4], polarography [5], spectrophotometry [6,7], capillary electrophoresis (CE) [8–10], ion chromatography [11], and high-performance liquid chromatography (HPLC) [12–17]. Voltammetry, polarography, and spectrophotometry are simple and rapid methods, however, they are not suitable for determining multiple food color mixtures in the food matrix. Capillary electrophoresis gives high resolution and short analysis time, but tailing or fronting peaks of some food colors are observed in the electropherograms. In HPLC methods, the followings were reported: determination of 38 food colors within 40 min [12], 14 food colors within 50 min [14], 10 food colors within 25 min [15], and 13 food colors within 29 min [17].

In this study, we analyzed 40 synthetic food colors within 19 min: 12 colors permitted in Japan (Tartrazine, Amaranth, Indigotine, Ponceau 4R, Sunset yellow FCF, Allura red AC, Fast green FCF, Brilliant blue FCF, Erythrosine, Acid red 52, Phloxine B, and Rose bengal), 6 colors permitted in EU and their analytical standards were commercially available in Japan

* Corresponding author. Fax: +81 78 531 7080.
E-mail address: Naoki_Yoshioka@pref.hyogo.lg.jp (N. Yoshioka).

0039-9140/$ – see front matter © 2007 Elsevier B.V. All rights reserved.
doi:10.1016/j.talanta.2007.09.015

(Brilliant black PN, Red 2G, Green S, Azorubine, Quinoline yellow, and Patent blue V), and 5 colors occasionally detected as illegal use at quarantine stations and public health centers in Japan (Red 10B, Fast red E, Orange II, Orange RN, and Amido black 10B) [1,18].

This paper describes an analytical method of 40 synthetic food colors in drinks and candies by HPLC equipped with a photodiode array detector using a short analytical column.

2. Experimental

2.1. Chemicals and reagents

Ponceau 6R (CI 16290), Chrysoine (CI 14270), Brilliant black PN (CI 28440), Yellow 2G (CI 18965), Fast red E (CI 16045), Green S (CI 44090), Azorubine (CI 14720), Martius yellow (CI 10315), Ponceau SX (CI 14700), Ponceau 3R (CI 16155), Eosine (CI 45380), Acid blue 1 (CI 42045), Amido black 10B (CI 20470), and Acid green 9 (CI 42100) were obtained from Tokyo Kasei Kogyo (Tokyo, Japan). Tartrazine (CI 19140), Amaranth (CI 16185), Indigotine (CI 73015), Ponceau 4R (CI 16255), Sunset yellow FCF (CI 15985), Allura red AC (CI 16035), Fast green FCF (CI 42053), Brilliant blue FCF (CI 42090), Erythrosine (CI 45430), Acid red 52 (CI 45100), Phloxine B (CI 45410), and Rose bengal (CI 45440) were purchased from Society of Japanese Pharmacopoeia (Tokyo, Japan). Naphthol yellow S (CI 10316), Red 10 B (CI 17200), Orange G (CI 16230), Uranine (CI 45350), Orange I (CI 14600), Orange II (CI 15510), and Benzyl violet 4B (CI 42640) were supplied by Wako Pure Chemical (Osaka, Japan). Acid violet 7 (CI 18055), Red 2G (CI 18050), Quinoline yellow (CI 47005), and Orange RN (CI 15970) were obtained from MP Biomedicals (Irvine, CA, USA). Ponceau 2R (CI 16150) was purchased from Waldeck (Münster, Germany). Fast yellow AB (CI 13015) was from Sigma–Aldrich (St. Louis, MO, USA), and Patent blue V (CI 42051) was from Fluka (Buchs, Switzerland). Sodium salts of the standards were used except Martius yellow and Acid blue 1. These food color standards were used as received. The purity was over 85% in the standards which had purity data on the labels or certificates of analysis. Other food color standards met or exceeded company standards of purity.

Ethanol and methanol (HPLC grade), polyamide (particle size 150–425 μm), acetic acid, ammonia solution, and ammonium acetate were obtained from Wako Pure Chemical. Syringe filter (PVDF, 0.45 μm, 13 mm) was purchased from Whatman (Clifton, NJ, USA).

Water was purified using Milli-Q water purification system (Millipore, Bedford, MA, USA).

All of the stock solutions (1000 μg/ml) except for Martius yellow were prepared in water. Martius yellow was dissolved in methanol. Working solutions (20 μg/ml) were prepared freshly by mixing the stock solutions and diluting with water.

Forty food colors were divided into 2 groups, groups A and B for working solutions.

Working solution A contains following food colors (group A): Ponceau 6R, Tartrazine, Amaranth, Indigotine, Chrysoine, Ponceau 4R, Sunset yellow FCF, Orange G, Acid violet 7, Allura red AC, Red 2G, Uranine, Green S, Azorubine, Quinoline yellow, Ponceau SX, Fast green FCF, Brilliant blue FCF, Orange II, Acid blue 1, Erythrosine, Acid red 52, Acid green 9, Phloxine B, and Rose bengal.

Working solution B contains following food colors (group B): Fast yellow AB, Naphthol yellow S, Red 10B, Brilliant black PN, Yellow 2G, Fast red E, Ponceau 2R, Orange I, Martius yellow, Ponceau 3R, Eosine, Orange RN, Amido black 10B, Patent blue V, and Benzyl violet 4B.

2.2. Liquid chromatography and separation conditions

The analyses were performed with a Shimadzu (Kyoto, Japan) LC-10 system equipped with LC-10AT pumps and a diode array detector SPD-M10AVP. Separations were done using a ZORBAX Eclipse XDB-C18 Rapid Resolution HT (50 mm × 4.6 mm i.d., 1.8 μm, Agilent Technologies, CA, USA). Solvent A was 0.1 mol/l of ammonium acetate aqueous solution (pH 6.7) and solvent B was methanol–acetonitrile (50:50, v/v). The flow rate was set at 1.5 ml/min and the injection volume was 5 μl. In gradient-elution analysis, the initial mobile phase was 3% of solvent B, increased linearly to 60% in 18 min, and held at 60% for 2 min. A return to the initial conditions was carried out in 10 min. The column was kept at 50 °C in the column oven.

The column eluate was monitored at 450, 490, 520, and 620 nm for the yellow, orange, red, and blue colors, respectively. The absorption spectra of the food colors were recorded between 200 and 700 nm. Peak identification was done by comparing the retention times and absorption spectra of the samples with food color standards.

2.3. Sample preparation

Sample preparation was performed as follows based on the modified Japanese official analytical method [19].

For drinks and syrups, a 10 g amount of the sample was weighed accurately in a beaker. If the sample was carbonated, it was degassed by ultrasonication for 5 min. In case of alcoholic beverages, ethanol in the sample was evaporated on a hot plate and the evaporated volume of water was added. Ten milliliters of water was added to the sample and mixed. The content was adjusted to approximately pH 3 with 6% acetic acid.

For candies, gelatin candies, and marshmallows, a 10 g amount of the crushed sample was weighed accurately in a beaker. Adding 50 ml of water, the sample was dissolved heating on a hot plate. The content was adjusted to approximately pH 3 with 6% acetic acid.

Polyamide column was prepared by making slurry of polyamide and packing it on to a column with a 10 mm i.d. The column was packed up to a height of ca. 5 cm.

The sample solution was applied to the column conditioned with 20 ml of 1% acetic acid, and then the column was washed with 20 ml of 1% acetic acid followed by 20 ml of water. The column was eluted with 15 ml of 1% ammonia solution/ethanol (1:1, v/v), and then the eluate was filtrated through a 0.45 μm syringe filter. The filtrate was neutralized with 6% acetic acid

and evaporated to dryness on a rotary evaporator at 40 °C. The residue was dissolved in 2 ml of methanol/water (1:1, v/v). For Quinoline yellow, Acid green 9, and Benzyl violet 4B, sum of the two major peak areas were used for quantitation.

2.4. Precision and accuracy

Method validation samples were prepared by fortifying 10 g of food samples (soft drinks and candies) with 2.5 ml of 20 μg/ml working solutions. Each fortification level was 5 μg/g to the sample. Recoveries were calculated comparing the peak areas of the fortifying samples with those of standard solutions.

Intra-day and inter-day reproducibility of the method were assessed by performing replicate analyses. Intra-day precision was determined by analyzing six fortified samples on the same day. Inter-day repeatability was determined by analyzing the fortified sample on six different days.

3. Results and discussion

3.1. Separation of mixed food colors by liquid chromatography

Simultaneous analysis of 40 different food colors by HPLC is difficult. As using ion-pair reagents, which increase the retention time and improve separation of charged analytes, is tedious and time-consuming for column equilibration [13,15], gradient elution without ion-pair reagent was adopted.

Ammonium acetate aqueous solution was used for solvent A. Ammonium acetate is often used as a mobile phase additive of LC/MS [20]. Addition of ammonium acetate promotes ionization of analytes and enhances the sensitivity. For the further confirmation analysis by LC/MS, we used ammonium acetate solution which can also be used for LC/MS.

For solvent B, the common reversed-phase solvents such as methanol, acetonitrile, and methanol–acetonitrile were compared. Methanol–acetonitrile (50:50, v/v) gave the best separation of the peaks.

The elution order of synthetic food colors mainly determined by their polarities, depending on the number of polar functional groups such as hydroxyl groups or sulfonate groups. Azo groups generally tended to elute earlier than triphenylmethane and xanthene groups.

By using the conventional analytical column (STR ODS-II, Shinwa Chemical, Kyoto, Japan, 150 mm × 4.6 mm i.d., 5 μm) at flow rate 1.0 ml/min, total analysis time of these 40 colors was 39 min. In order to shorten the analysis time, we tried to use a short analytical column. The column we used was a ZORBAX Eclipse XDB-C18 Rapid Resolution HT (50 mm × 4.6 mm i.d., 1.8 μm), whose maximum operating pressure and temperature are 60,000 kPa and 60 °C, respectively. The initial column pressure was 18,100 kPa at flow rate 1.5 ml/min. In spite of the small particle and high flow rate, the column pressure was low enough to be used for conventional HPLC system not for ultra-high-pressure or ultra-fast LC. Forty food colors were analyzed within 19 min by using this short column. This analytical method is more efficient than other methods [12,14,15,17] in terms of analysis time and the number of analytes.

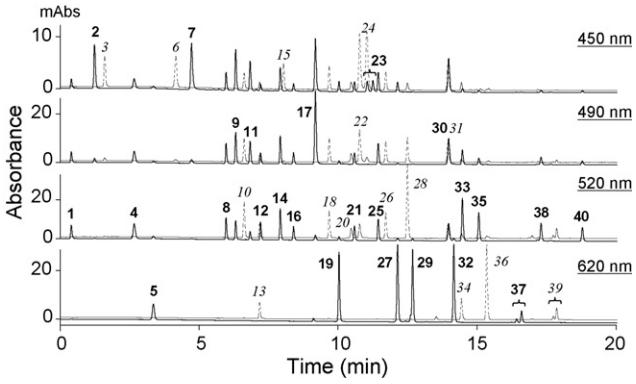

Fig. 1. HPLC chromatograms of mixed food color standard solutions (5 μg/ml). The solid lines with bold numbers indicate chromatograms of group A and the dotted lines with italic numbers indicate those of group B. Peak numbers correspond to food colors listed in Table 1.

Loading the mixed standard solution onto HPLC, some peaks in the chromatogram were partly overlapped and not separated completely. Therefore, 40 food colors were divided into 2 groups in order to avoid overlapping of peaks for the recovery test. HPLC chromatograms of mixed food color standard solutions are shown in Fig. 1.

Orange II in group A and Orange RN in group B are isomers, giving similar retention times. However, since the spectra around 410 nm were slightly different [21], they were distinguishable. Other food colors except Orange II and Orange RN were identified by their retention times.

As shown in Fig. 2, setting Column temperature at 40 °C, Orange II and Acid blue 1 had similar retention times. Increasing the column temperature to 45 °C, the peak had a shoulder and started to separate. At 50 °C they were separated (resolution, Rs = 1.67), and at 55 °C completely separated (Rs = 2.47). We chose the column temperature 50 °C in terms of the column lifetime. High temperature increased resolution and decreased the column pressure reducing viscosity of the solvent.

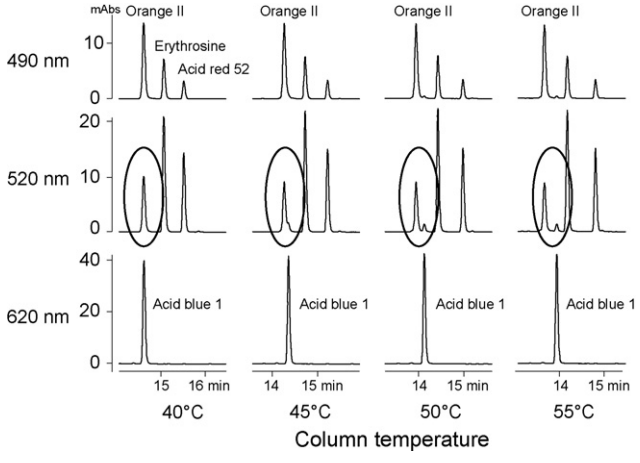

Fig. 2. Effect of column temperature in separating Orange II and Acid blue 1.

Table 1
Detection wavelengths and limits of detection (LODs) of the food color standard solution

Peak number	Compound	CI number	E number	Detection wavelength (nm)	LOD (μg/ml)
1	Ponceau 6R	16290		520	0.078
2	Tartrazine	19140	E102	450	0.040
3	Fast yellow AB	13015		450	0.060
4	Amaranth	16185	E123	520	0.053
5	Indigotine	73015	E132	620	0.039
6	Naphthol yellow S	10316		450	0.063
7	Chrysoine	14270		450	0.036
8	Ponceau 4R	16255	E124	520	0.050
9	Sunset yellow FCF	15985	E110	490	0.027
10	Red 10B	17200		520	0.011
11	Orange G	16230		490	0.038
12	Acid violet 7	18055		520	0.047
13	Brilliant black PN	28440	E151	620	0.047
14	Allura red AC	16035	E129	520	0.032
15	Yellow 2G	18965		450	0.058
16	Red 2G	18050	E128	520	0.060
17	Uranine	45350		490	0.014
18	Fast red E	16045		520	0.048
19	Green S	44090	E142	620	0.013
20	Ponceau 2R	16150		520	0.086
21	Azorubine	14720	E122	520	0.051
22	Orange I	14600		490	0.017
23	Quinoline yellow	47005	E104	450	0.084
24	Martius yellow	10315		450	0.040
25	Ponceau SX	14700		520	0.038
26	Ponceau 3R	16155		520	0.015
27	Fast green FCF	42053		620	0.005
28	Eosine	45380		520	0.006
29	Brilliant blue FCF	42090	E133	620	0.006
30	Orange II	15510		490	0.040
31	Orange RN	15970		490	0.039
32	Acid blue 1	42045		620	0.007
33	Erythrosine	45430	E127	520	0.011
34	Amido black 10B	20470		620	0.019
35	Acid red 52	45100		520	0.019
36	Patent blue V	42051	E131	620	0.009
37	Acid green 9	42100		620	0.075
38	Phloxine B	45410		520	0.012
39	Benzyl violet 4B	42640		620	0.125
40	Rose bengal	45440		520	0.059

3.2. Quantitation

Each food color has different wavelength of maximum absorption. We chose four typical wavelengths, 450, 490, 520, and 620 nm. The food colors were monitored at the wavelengths nearest to their own maximum absorption in the four wavelengths. They were monitored at 450, 490, 520, and 620 nm for the yellow, orange, red, and blue colors, respectively. The detection wavelengths of the food colors are presented in Table 1.

As Quinoline yellow, Acid green 9, and Benzyl violet 4B standards we used have two major peaks in the chromatograms, sum of the peak areas were used for quantitation.

Since Ponceau 6R has four sulfonate groups in a molecule, it was eluted very early (0.39 min). However, the peak shape was good and separated from other interference peaks detected at 520 nm.

The linearity for each compound was checked by analyzing mixed standard solutions of 7 different concentrations (0.01, 0.05, 0.1, 0.5, 1, 5, and 20 μg/ml). Calibration curves for the standard solutions except Benzyl violet 4B were linear ($r^2 = 0.999$) between 0.05 and 20 μg/ml (0.5–20 μg/ml for Benzyl violet 4B). The limit of detection (LOD) was defined as three times the peak-to-peak noise. LODs of standard solutions are presented in Table 1. The LODs ranged from 0.005 (Fast green FCF) to 0.125 (Benzyl violet 4B) μg/ml.

3.3. Extraction and purification

There are many sorbents for solid phase extraction (SPE) such as ODS [9,13,22], quaternary amine [23], NH_2 (aminopropyl) [24], polyamide [8,12] for clean-up of synthetic colors in foods. Polyamide adsorbs synthetic food colors more specifically than other sorbents, so we used polyamide column clean-up for the sample purification. The pH of the sample solution for the polyamide column clean-up was adjusted to approximately pH 3 by checking with pH indicator paper because synthetic food

Table 2
Recoveries of the food colors fortified to soft drinks and candies

Peak number	Compound	Intra-day recovery ($n=6$)				Inter-day recovery ($n=6$)			
		Soft drink		Candy		Soft drink		Candy	
		Mean (%)	R.S.D. (%)	Mean (%)	R.S.D. (%)	Mean (%)	R.S.D. (%)	Mean (%)	R.S.D. (%)
1	Ponceau 6R	89.9	1.9	91.3	5.7	85.1	3.6	88.9	3.1
2	Tartrazine	91.4	1.6	93.9	5.6	89.5	3.4	93.2	1.8
3	Fast yellow AB	90.9	2.1	92.2	1.5	88.3	4.3	87.6	2.8
4	Amaranth	90.6	2.1	92.8	5.4	89.1	3.2	93.0	2.2
5	Indigotine	86.3	2.0	82.9	4.3	86.5	3.3	80.0	3.8
6	Naphthol yellow S	90.1	2.2	93.2	2.3	88.0	4.1	87.8	2.7
7	Chrysoine	76.6	2.7	76.9	4.5	78.8	2.0	76.0	2.4
8	Ponceau 4R	91.5	1.5	93.6	5.7	89.9	3.4	94.4	1.9
9	Sunset yellow FCF	91.6	2.4	93.0	5.6	90.0	4.1	94.1	1.9
10	Red 10B	90.1	2.8	90.9	1.6	87.3	4.1	85.6	2.9
11	Orange G	91.9	1.9	93.7	5.9	90.0	3.7	94.0	1.9
12	Acid violet 7	90.7	1.4	93.0	5.4	89.5	3.3	94.2	2.8
13	Brilliant black PN	84.3	1.9	88.7	1.8	84.0	3.7	82.3	3.4
14	Allura red AC	91.7	1.7	93.3	5.6	90.2	3.5	94.9	2.3
15	Yellow 2G	91.7	2.2	93.7	1.7	89.3	4.6	88.1	3.1
16	Red 2G	91.5	1.8	93.9	5.8	90.0	3.9	93.3	2.4
17	Uranine	92.0	1.6	90.8	4.5	90.3	3.8	94.7	3.0
18	Fast red E	89.7	3.1	92.6	1.8	88.4	4.6	87.3	3.3
19	Green S	90.3	1.5	91.0	5.2	88.7	3.5	92.7	1.9
20	Ponceau 2R	90.2	3.6	92.7	6.0	88.1	4.1	88.5	3.9
21	Azorubine	90.5	1.7	91.6	5.5	88.8	3.2	92.8	2.0
22	Orange I	89.1	2.7	91.2	1.4	88.2	3.2	87.2	2.2
23	Quinoline yellow	88.6	2.3	87.3	4.6	88.3	1.9	92.7	3.0
24	Martius yellow	88.3	3.4	90.7	2.7	85.7	5.1	85.0	3.7
25	Ponceau SX	91.2	1.6	92.4	5.5	89.4	3.6	93.4	1.9
26	Ponceau 3R	91.7	2.3	93.1	1.6	88.8	4.5	88.2	2.9
27	Fast green FCF	92.3	1.4	92.4	5.4	90.2	3.6	94.1	2.0
28	Eosine	90.0	2.7	89.6	4.0	87.8	4.1	84.0	4.9
29	Brilliant blue FCF	92.2	1.5	92.6	5.5	90.3	3.7	94.3	2.2
30	Orange II	90.9	1.7	89.2	3.7	89.5	3.2	94.0	2.7
31	Orange RN	90.9	3.0	94.2	3.0	88.4	5.0	88.1	3.6
32	Acid blue 1	92.7	1.3	93.0	5.4	91.4	3.4	95.3	2.4
33	Erythrosine	88.3	2.1	85.1	3.6	87.0	3.1	88.5	1.8
34	Amido black 10B	83.4	2.5	87.0	2.6	83.0	4.4	80.2	4.1
35	Acid red 52	92.8	1.7	92.9	5.7	91.7	3.6	95.6	2.5
36	Patent blue V	93.2	2.0	94.8	1.7	90.6	4.4	89.7	3.1
37	Acid green 9	95.9	4.4	91.3	5.5	100.9	6.7	102.6	5.7
38	Phloxine B	89.4	1.8	85.9	4.2	88.9	2.8	87.6	1.5
39	Benzyl violet 4B	114.8	3.8	115.0	2.0	114.9	4.6	114.3	3.9
40	Rose bengal	92.3	3.1	83.9	3.7	93.8	3.2	90.1	2.3

Each food color was fortified to the food sample at 5 μg/g.

colors are adsorbed on polyamide most strongly under acidic conditions at pH 3–4.

After the column clean-up, small particles of polyamide were observed in the eluate. They adsorbed the food colors in the eluate under neutral and acidic conditions, causing low recoveries especially for Brilliant black PN, Erythrosine, Amido black 10B, and Rose bengal. Therefore, the eluate was filtrated through a 0.45 μm syringe filter and small particles were removed under basic condition before neutralization and evaporation.

3.4. Recoveries

Table 2 shows the intra-day and inter-day recoveries of 40 food colors from soft drinks and candies fortified at 5 μg/g. The intra-day recoveries ($n=6$) ranged from 76.6 to 115.0%, with relative standard deviations (R.S.D.s) ranging from 1.3 to 6.0%, while the inter-day recoveries over six working days ranged from 76.0 to 114.9%, with relative standard deviations (R.S.D.s) ranging from 1.5 to 6.7%. Both intra-day and inter-day accuracy and precision data showed good R.S.D.s and recovery values.

Typical HPLC chromatograms of soft drink samples are shown in Figs. 3. They were fortified with food colors at the level of 0.5 μg/g. LODs and limits of quantitation (LOQs) in real food samples depended on food matrix of the samples. LODs (S/N = 3) in soft drinks (soda) were 0.03 μg/g (0.2 μg/g for Ponceau 6R and Acid green 9), and LOQs (S/N = 10) were 0.1 μg/g (0.5 μg/g for Ponceau 6R and Acid green 9). These LOD and LOQ values were confirmed by analyzing fortified samples and calculating recoveries. Recoveries of samples fortified at LOQ levels were over 60%.

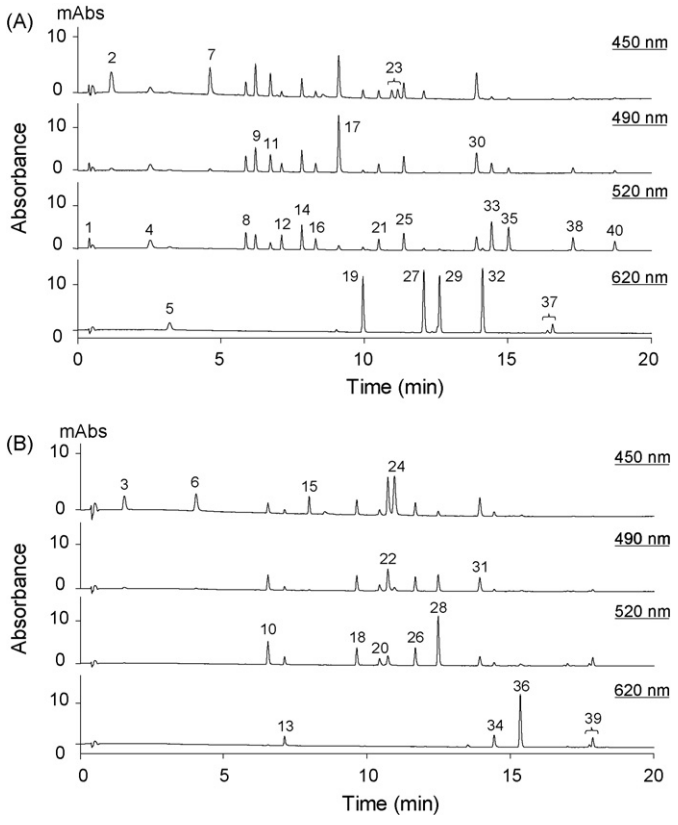

Fig. 3. Typical HPLC chromatograms of soft drink samples fortified with food colors at 0.5 μg/g. Peak numbers correspond to food colors listed in Table 1.

3.5. Application

Thirty imported commercial products (soft drinks, syrups, candies, gelatin candies, and marshmallows) colored with synthetic or natural food colors were analyzed by using this method. They were obtained from local markets at Hyogo prefecture in Japan. Quantitation was done by using calibration curves and confirmed by comparing absorption spectra of the samples with food color standards.

The food labels on 14 products out of 30 listed the names of the synthetic food colors. As their food labels, 14 food products contained some synthetic food colors: Tartrazine (1.3–21.8 μg/g, 7 samples), Amaranth (27.2 μg/g), Indigotine (trace−18.3 μg/g, 4 samples), Ponceau 4R (6.0 μg/g), Sunset yellow FCF (3.1–17.3 μg/g, 5 samples), Allura red AC (0.2–41.6 μg/g, 5 samples), and Brilliant blue FCF (0.9–5.9 μg/g, 3 samples). In addition, Fast red E which was not permitted in Japan was detected in grape-flavored soft drink at 0.7 μg/g.

Fast red E was one of the subsidiary colors in commercial Amaranth [25]. It was detected together with Amaranth (permitted in Japan), the ratio of Fast red E to Amaranth was 2.5%, which was lower than the maximum limit (3%) of total subsidiary colors regulated by JECFA [26]. It was considered to be a subsidiary color in Amaranth.

4. Conclusions

An analytical method was developed for quantitation of 40 synthetic food colors in drinks and candies by HPLC with photodiode array detection. Using a short analytical column, these food colors were analyzed within 19 min. This method gave reliable and reproducible results with satisfactory detection limits and short analysis time for the routine analysis of food colors.

References

[1] Office of Quarantine Station Administration, Policy Planning and Communication Division, Department of Food Safety, Pharmaceutical and Food Safety Bureau, Ministry of Health, Labour and Welfare, Food Sanit. Res. 56 (2006) 97.
[2] J.A. Steele, J. Assoc. Off. Anal. Chem. 67 (1984) 540.
[3] H. Oka, Y. Ikai, N. Kawamura, M. Yamada, H. Inoue, J. Chromatogr. 411 (1987) 437.
[4] Y. Ni, J. Bai, L. Jin, Anal. Chim. Acta 329 (1996) 65.
[5] S. Combeau, M. Chatelut, O. Vittori, Talanta 56 (2002) 115.
[6] J.J.B. Nevado, J.R. Flores, M.J.V. Llerena, N.R. Fariñas, Fresen. J. Anal. Chem. 365 (1999) 383.
[7] E.C. Vidotti, J.C. Cancino, C.C. Oliveira, M.D.C.E. Rollemberg, Anal. Sci. 21 (2005) 149.
[8] H.Y. Huang, Y.C. Shih, Y.C. Chen, J. Chromatogr. A 959 (2002) 317.
[9] F. Ishikawa, M. Oishi, K. Kimura, A. Yasui, K. Saito, J. Food Hyg. Soc. Jpn. 45 (2004) 150.
[10] M.A. Prado, L.F.V. Boas, M.R. Bronze, H.T. Godoy, J. Chromatogr. A 1136 (2006) 231.
[11] Q.C. Chen, S.F. Mou, X.P. Hou, J.M. Riviello, Z.M. Ni, J. Chromatogr. A 827 (1998) 73.
[12] K. Nakazawa, Y. Shimamura, K. Nakajima, Y. Kikuchi, K. Nakagome, Y. Tamura, Annu. Rep. Tokyo Metr. Res. Lab. P.H. 46 (1995) 108.
[13] F. Ishikawa, S. Shigeoka, M. Nagashima, M. Takahashi, H. Kamimura, K. Onishi, M. Nishijima, J. Food Hyg. Soc. Jpn. 41 (2000) 194.
[14] J. Kirschbaum, C. Krause, S. Pfalzgraf, H. Brückner, Chromatographia 57 (2003) S115.
[15] M.G. Kiseleva, V.V. Pimenova, K.I. Eller, J. Anal. Chem. 58 (2003) 685.
[16] M.S. García-Falcón, J. Simal-Gándara, Food Control 16 (2005) 293.
[17] K.S. Minioti, C.F. Sakellariou, N.S. Thomaidis, Anal. Chim. Acta 583 (2007) 103.
[18] T. Matsuda, H. Matsumoto, Y. Kasuya, M. Nakazato, K. Yasuda, Annu. Rep. Tokyo Metr. Res. Lab. P.H. 53 (2002) 157.
[19] Ministry of Health, Labour and Welfare, Japan, Standard Methods of Analysis in Food Safety Regulation, Japan Food Hygiene Association, Tokyo, 2003, pp. 169–177.
[20] S. Tsuji, K. Yoshii, Y. Tonogai, J. Chromatogr. A 1101 (2006) 214.
[21] E. Ueno, H. Nakashima, K. Takakura, K. Okazaki, H. Nagai, H. Oka, Y. Ikai, J. Hayakawa, N. Ishikawa, J. Food Hyg. Soc. Jpn. 37 (1996) 226.
[22] M.L. Young, J. Assoc. Off. Anal. Chem. 67 (1984) 1022.
[23] T. Hayashi, Y. Fukaya, H. Tanaka, M. Kunimatsu, I. Hotta, Y. Ikai, H. Oka, J. Hayakawa, R. Suzuki, J. Food Hyg. Soc. Jpn. 34 (1993) 398.
[24] S.M. Dugar, J.N. Leibowitz, R.H. Dyer, J. AOAC Int. 77 (1994) 1335.
[25] M. Yamada, Y. Kato, M. Nakamura, T. Yamada, T. Maitani, Y. Goda, Chem. Pharm. Bull. 46 (1998) 494.
[26] Joint and FAO/WHO Expert Committee on Food Additives (JECFA), Compendium of Food Additive Specifications, vols. 1 and 2, Food and Agriculture Organization of the United Nations, Rome, 1992.

Available online at www.sciencedirect.com
ScienceDirect
Talanta 74 (2008) 1586–1591
Talanta
www.elsevier.com/locate/talanta

Development of amperometric glucose biosensor through immobilizing enzyme in a Pt nanoparticles/mesoporous carbon matrix

Jingjing Yu, Donglei Yu, Tian Zhao, Baizhao Zeng *

Department of Chemistry, Wuhan University, Wuhan 430072, PR China

Received 5 July 2007; received in revised form 29 September 2007; accepted 1 October 2007
Available online 7 October 2007

Abstract

Pt nanoparticles were deposited on mesoporous carbon material CMK-3. Glucose oxidase (GOx) was immobilized in the resulting Pt nanoparticles/mesoporous carbon (Pt/CMK-3) matrix, and then the mixture was cast on a glassy carbon electrode (GCE) using gelatin as a binder. The glucose biosensor exhibited excellent current response to glucose after cross-linking with glutaraldehyde. At 0.6 V (*vs.* SCE) the response current was linear to glucose concentration in the range of 0.04–12.2 mM. The response time (time for achieving 95% of the maximum current) was 15 s and the detection limit (S/N = 3) was 1 μM. The Michaelis–Menten constant (K_m^{app}) and the maximum current density (i_{max}) were 10.8 mM and 908 μA cm^{-2}, respectively. The activation energy of the enzymatic reaction was estimated to be 22.54 kJ mol^{-1}. The biosensor showed good stability. It achieved the maximum response current at about 52 °C and retained 95.1% of its initial response current after being stored for 30 days. In addition, some fabrication and operation parameters for the biosensor were optimized in this work. The biosensor was used to monitor the glucose levels of serum samples after being covered with an extra Nafion film to improve its anti-interferent ability and satisfied results were obtained.
© 2007 Elsevier B.V. All rights reserved.

Keywords: Mesoporous carbon; Pt nanoparticles; Glucose oxidase; Glucose; Biosensor; Amperometry

1. Introduction

Nano-materials have been used widely in many fields in the past years [1–3]. One of their important functions is catalysis; especially noble metal nanoparticles present high catalytic activity for many chemical reactions. Because nano-materials also have good biocompatibility, they are used to immobilize biomolecules for the fabrication of biosensor, etc. Pt nanoparticles have been widely adopted to prepare biosensors due to their excellent catalytic action to the oxidation of H_2O_2 [4–6]. To construct a Pt nanoparticle-based biosensor, both Pt nanoparticles and enzyme should be loaded in an appropriate matrix. The matrix should be able to load many Pt nanoparticles and make them highly dispersed. Meantime, it can immobilize enzyme molecules effectively. Recently, various materials were tested for Pt nanoparticles loading and then were used for the fabrication of biosensors, such as carbon nanotubes [4–10], polyaniline [11], silicates [10,12] and so on. Among them carbon nanotubes attracted much attention. For example, Tang et al. developed an amperometric glucose biosensor based on the adsorption of glucose oxidase (GOx) at a platinum nanoparticles–carbon nanotubes modified glassy carbon electrode (GCE) [6]. The biosensor showed a large linear response range (0.1–13.5 mM glucose), short response time (within 5 s) and high stability. Besides, Zhou et al. reported a glucose biosensor, which was based on the immobilization of GOx on Pt nanoparticles dispersed in nano-fibrous polyaniline [11]. The biosensor exhibited linear response to glucose in the range from 2×10^{-3} to 12 mM and the response time was 7 s.

Mesoporous materials have well-ordered pore structure, high specific surface area and narrow pore size distribution [13,14]. Therefore, they are promising materials for the loading of nanoparticles and biomolecules. When nanoparticles are loaded on mesoporous materials, they are likely to be dispersed well and exhibit controlled size as they can be confined in the pores to some extent [15]. It was reported that Pt nanoparticles deposited on mesoporous carbon were highly dispersed and presented high

* Corresponding author. Tel.: +86 2787218704; fax: +86 2787647617.
E-mail addresses: bzzeng@whu.edu.cn, zengbz@chem.whu.edu.cn (B.Z. Zeng).

0039-9140/$ – see front matter © 2007 Elsevier B.V. All rights reserved.
doi:10.1016/j.talanta.2007.10.005

catalytic activity [16,17]. In addition, in the pores of mesoporous materials biomolecules generally display good stability due to some folding forces of pores [18,19]. For example, lysozyme [20], cytochrome *c* [21], and glucose oxidase [22] were immobilized on mesoporous carbon materials with large loading amounts and high stability.

Mesoporous carbon materials possess better electron conductivity and higher thermal, mechanical and water stability than other mesoporous materials [23–25]. Hence, mesoporous carbon materials have more potential in the construction of electrochemical biosensors. In this work, a glucose biosensor based on glucose oxidase immobilized on a Pt nanoparticles/mesoporous carbon CMK-3 (Pt/CMK-3) matrix has been fabricated. The biosensor displays good catalytic activity and rapid response to glucose, and it also shows high stability. When a Nafion film is covered on it, the resulting enzyme electrode can be used to monitor glucose level of human blood.

2. Experimental

2.1. Reagents

Glucose oxidase (GOx, 146,000 U g^{-1}) was purchased from Sigma. Gelatin and polyvinyl alcohol (PVA, average degree of polymerization, 1750 ± 50) came from Sinopharm Chemical Reagent Co. Ltd. (Shanghai, China). Glutaraldehyde (25%) was purchased from Jingyu Fine Chemicals Corporation (Tianjin, China). Other chemicals used were of analytical grade and the solutions were prepared with double-distilled water.

2.2. Synthesis of Pt/CMK-3

Mesoporous carbon material CMK-3 (Carbon Molecular Sieve Korean Advanced Institute of Science and Technology No. 3) was prepared according to literature [26]. Mesoporous silica material SBA-15 (Santa Barbara Material No. 15) was used as template and sucrose as carbon source. The mesoporous carbon material with high loading of Pt nanoparticles was prepared following literature [27]. In brief, H_2PtCl_6 was dissolved in water. CMK-3 was preheated at 110 °C in air and then poured into the H_2PtCl_6 solution. The weight ratio of Pt to C was controlled according to the target metal loaded. After ultrasonic agitating for 30 min, the suspension was heated until it became slurry. The slurry was left overnight, and then further dried at 110 °C in an oven. The resulting agglomerate was ground in an agate mortar, placed in a glazed ceramic boat and then heated at 120 °C for 2 h in a tube furnace with H_2 atmosphere. Finally, the powder was cooled to room temperature in argon atmosphere. In this work, a Pt/CMK-3 composite material with 20 wt% Pt nanoparticles was synthesized. The morphology of Pt/CMK-3 was characterized with transmission electron microscopy (TEM, JEM-2010FEF, Japan) using an accelerating voltage of 200 kV.

2.3. Preparation of modified electrodes

Before modification, the bare glassy carbon electrode was polished to mirror smooth with 0.05 μm Al_2O_3 slurry, rinsed with water, and then ultrasonicated in water bath. Pt/CMK-3 and GOx were added into 0.6% gelatin aqueous solution. Their final concentrations were 5 and 8 mg ml^{-1}, respectively. The mixture was stirred for 10 min to obtain homogenous suspension. Three microliters of the resulting suspension was transferred onto the GCE surface, and let it dry in air. Then the electrode was immersed in 2.5% glutaraldehyde solution for 10 min in order to induce chemical cross-linking. Before use, the enzyme electrode was rinsed with buffer solution for 10 min to remove the enzyme not firmly immobilized. The obtained enzyme electrode was noted as Pt/CMK-3-GOx-gelatin/GCE. For comparison, a CMK-3-GOx-gelatin/GCE was prepared through similar way. The enzyme electrodes were stored in pH 7.0 phosphate buffer solution (PBS) at 4 °C when they were not used.

In addition, to study the electrocatalytic behavior of CMK-3 and Pt/CMK-3 to H_2O_2, CMK-3 and Pt/CMK-3 films modified electrodes were prepared. In brief, CMK-3 or Pt/CMK-3 was dispersed in *N*,*N*-dimethylformamide to prepare 3 mg ml^{-1} suspension. Then, 20 μl suspension was mixed with 2 μl 3% PVA aqueous solution. Three microliters of the resulting colloid solution was transferred onto the cleaned GCE surface, and the solvent was evaporated in air. Then CMK-3-PVA/GCE and Pt/CMK-3-PVA/GCE were obtained. Here, PVA was chosen as binder, because the modified electrodes were unstable when gelatin was used.

2.4. Methods

All electrochemical experiments were performed on a CHI 660A electrochemical workstation (CH Instru. Co., Shanghai, China) at 25 °C (±2 °C). The working electrode was a modified GCE (2 mm in diameter). A saturated calomel electrode (SCE) served as the reference electrode, and a Pt wire served as the counter electrode. The amperometric response of the enzyme electrode to glucose was measured at an applied potential of 0.6 V (*vs.* SCE) under stirring. The supporting electrolyte was 0.1 M air-saturated PBS (pH 6.0). After the background current reached steady value, glucose solution was injected into the solution and the current was recorded.

3. Results and discussion

3.1. Characterization of Pt/CMK-3

The TEM image of the synthesized Pt/CMK-3 material is shown in Fig. 1. The CMK-3 displays well-ordered pore structure with pore size of about 4 nm. A large number of Pt nanoparticles are embedded in the pore channels. The Pt nanoparticles show narrow size distribution and the average diameter is about 2 nm. The Pt/CMK-3 material has large surface area, which is favorable to the immobilization of GOx. The high dispersion of Pt nanoparticles can make their electrocatalytic efficiency increase.

In addition, the electrochemical behavior of Pt/CMK-3 is also investigated. As can be seen in Fig. 2, the Pt/CMK-3-PVA/GCE shows sensitive response to H_2O_2, which is due to the electrochemical oxidation of H_2O_2 on the electrode surface at 0.6 V.

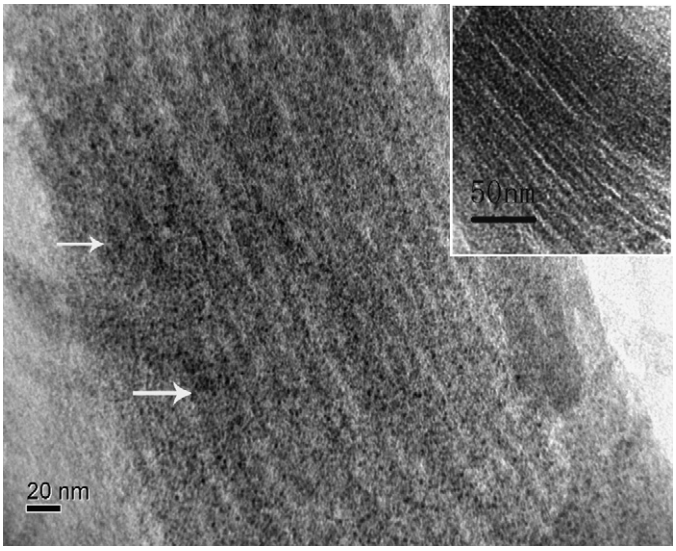

Fig. 1. TEM images of Pt/CMK-3 material taken along to the channel direction. Inset: TEM image with different magnification.

However, the current response caused by the CMK-3-PVA/GCE is quite small, which is only one-fifteenth as large as that of Pt/CMK-3-PVA/GCE. This indicates that the Pt nanoparticles deposited on mesoporous carbon have good catalytic activity to the oxidation of H_2O_2. The response to H_2O_2 covers a large concentration range, thus Pt/CMK-3 has great potential in constructing biosensor.

3.2. Amperometric responses of the enzyme electrodes to glucose

Fig. 3 shows the typical amperometric responses of different enzyme electrodes to glucose. The current response features step-like increase with successive addition of glucose, which is due to the enzyme catalytic oxidation of glucose. As for CMK-3-GOx-gelatin/GCE, the response current is rather small. Furthermore, the response decreases rapidly with glucose concentration rising. However, the Pt/CMK-3-GOx-gelatin/GCE displays sensitive and fast response to glucose, the response time ($t_{95\%}$) is less than 15 s. What is more, the response current is about 24 times as large as that of CMK-3-GOx-gelatin/GCE for 1 mM glucose. Hence, it can be proposed that Pt nanoparticles enhance the current response to glucose significantly. The response of glucose biosensor is related to the electrochemical oxidation of H_2O_2 produced in the enzymatic catalytic reaction. The reaction mechanism can be described as follows [4]:

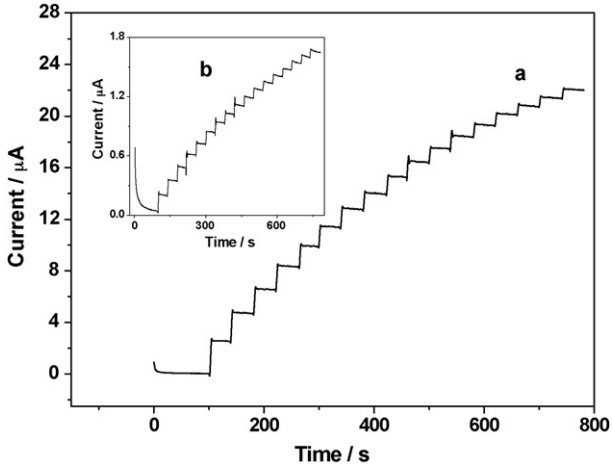

Fig. 2. Steady-state current response of Pt/CMK-3-PVA (a) and CMK-3-PVA (b) films coated GCEs to the addition of 0.975 mM H_2O_2 in the stirred PBS (pH 7.0). Applied potential: 0.6 V.

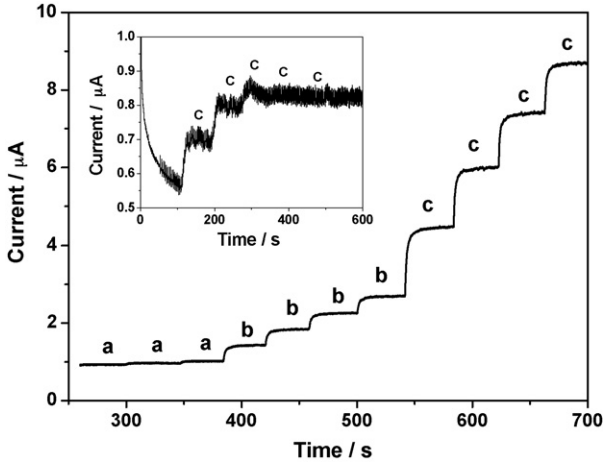

Fig. 3. Steady-state current response of Pt/CMK-3-GOx-gelatin/GCE to glucose in the stirred PBS (pH 6.0) at 0.6 V. Glucose concentrations: (a) 2×10^{-5} M, (b) 2×10^{-4} M, (c) 1×10^{-3} M; inset: the response of CMK-3-GOx-gelatin/GCE.

$$\text{Glucose} + \text{GOx}_{ox} \rightarrow \text{Gluconic acid} + \text{GOx}_{red} \quad (1)$$

$$\text{GOx}_{red} + O_2 \rightarrow \text{GOx}_{ox} + H_2O_2 \quad (2)$$

$$H_2O_2 \rightarrow O_2 + H_2O + 2e \quad (3)$$

In this case, the Pt nanoparticles deposited on CMK-3 can catalyze the oxidation of H_2O_2 markedly because they are highly dispersed and the loading amount is quite large. As a consequence, the Pt/CMK-3-GOx-gelatin/GCE shows sensitive current response to glucose.

3.3. Optimization of experimental conditions

3.3.1. Effects of fabrication parameters

The concentrations of GOx and gelatin influence current response significantly as shown in Fig. 4. When the concentration of Pt/CMK-3 is 5 mg ml^{-1}, with the concentration of GOx increasing, the response current increases until it reaches the maximum at 8 mg ml^{-1}, and then decreases slightly. When the concentration of GOx is high enough, the amount of GOx may exceed the maximum immobilization-amount of the Pt/CMK-3-gelatin matrix. Thus the response current stops increasing, even decreases. As for gelatin, it acts as binder. When gelatin concentration changes from 0.2 to 1 wt%, a maximum current response is observed at 0.6 wt%. When its concentration is too low or too high, GOx and Pt/CMK-3 cannot be immobilized effectively on the electrode surface or the current response becomes small due to the insulated property of gelatin. Accordingly, 8 mg ml^{-1}

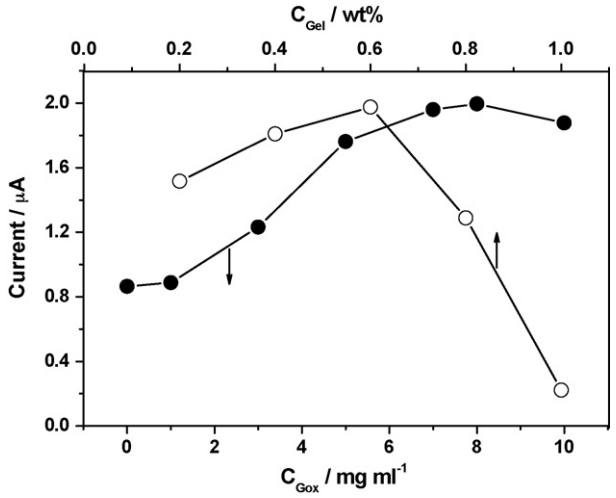

Fig. 4. Effects of the concentrations of GOx and gelatin on the response current of the Pt/CMK-3-GOx-gelatin/GCE. Steady-state currents are measured at 0.6 V in the stirred PBS (pH 6.0) with 1 mM glucose.

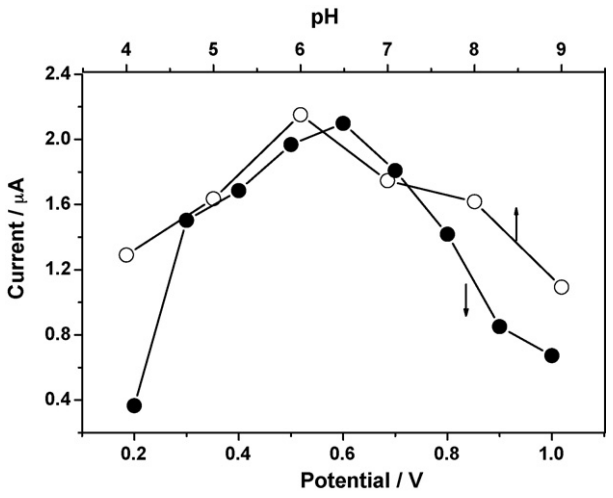

Fig. 5. Effects of the solution pH and applied potential on the response current of Pt/CMK-3-GOx-gelatin/GCE. Other conditions are the same as those in Fig. 4.

GOx and 0.6 wt% gelatin are chosen to fabricate the enzyme electrode.

To avoid the loss of GOx chemical cross-linking with glutaraldehyde is introduced. Without covalent cross-linking, the biosensor does not exhibit sharp step-like response and the current signal is small. With increasing cross-linking time, the response time decreases. But when it exceeds 10 min, the response time almost stops changing. Glutaraldehyde can react with amino groups of GOx and gelatin to generate the intramolecular or intermolecular covalent linkages [28], leading to the formation of a three-dimensional net structure. The reason for the improvement of current response after covalent cross-linking is probably related to the netlike structure as it benefits mass transfer. In addition, the three-dimensional net structure can improve the stability of the biosensor. When gelatin is replaced by PVA, no such effect is observed because PVA cannot react with glutaraldehyde.

3.3.2. *Effects of operation parameters*

The effects of applied potential and solution pH on the response current of Pt/CMK-3-GOx-gelatin/GCE are also studied (Fig. 5). The response current increases rapidly when the applied potential changes from 0 to 0.6 V. But when the potential is higher than 0.6 V, the response current falls down. This is related to the electrochemical oxidation of H_2O_2. The effect of potential on electrocatalytic oxidation of H_2O_2 at platinum electrodes was studied intensively by Hall et al. [29]. When a sufficiently positive potential is applied (e.g. +0.6 V *vs.* Ag/AgCl), the rate limiting reaction is: $Pt(OH)_2{\cdot}H_2O_2 \rightarrow Pt + 2H_2O + O_2$.The response current depends on the surface coverage of $Pt(OH)_2{\cdot}H_2O_2$, while $Pt(OH)_2{\cdot}O_2$ and $Pt(OH)_2{\cdot}H_2O_2{\cdot}H^+$ can inhibit this reaction. In this work, the Pt nanoparticles are imbedded in the pore channels; the diffusion of the O_2 is more difficult. At higher potential more O_2 is produced. These contribute to the formation of $Pt(OH)_2{\cdot}O_2$. In addition, the acidic condition (i.e. pH 6.0 PBS) benefits the formation of $Pt(OH)_2{\cdot}H_2O_2{\cdot}H^+$. When the two inhibiting species increase, the surface coverage of $Pt(OH)_2{\cdot}H_2O_2$ decreases. So the response current decreases when the potential is too higher.

The effect of solution pH on response current is studied between pH 4.0 and 9.0. The maximum response current is obtained at pH 6.0 (Fig. 5). Similar results were reported in literatures [6,11]. According to literature [30], good response for free enzyme occurred in the pH range of 4.0–7.0. Therefore, it can be concluded that the GOx immobilized in the Pt/CMK-3-gelatin matrix has higher bioactivity at about pH 6.0.

The effect of temperature on the response current is presented in Fig. 6. The response current increases when it changes from 2 to 52 °C, resulting from the increase of enzyme reaction rate. But the response current lowers when the temperature is over 52 °C because of the denaturation of GOx. The response current reaches the maximum at 52 °C. This temperature is higher than those observed for GOx entrapped in zeolite matrix [31] (i.e. 45 °C) and Pt nanoparticles/nano-fibrous [11] (i.e. 45 °C). It indicates that the Pt/CMK-3-GOx-gelatin/GCE can handle a

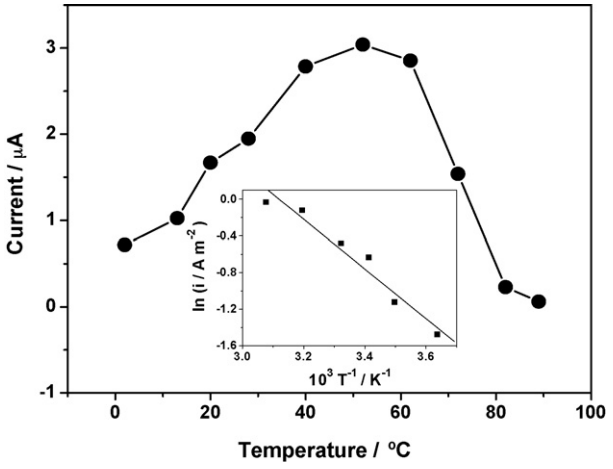

Fig. 6. Effect of temperature on the response current of Pt/CMK-3-GOx-gelatin/GCE. Inset: plot of the ln *i* *vs.* T^{-1}; other conditions are the same as those in Fig. 4.

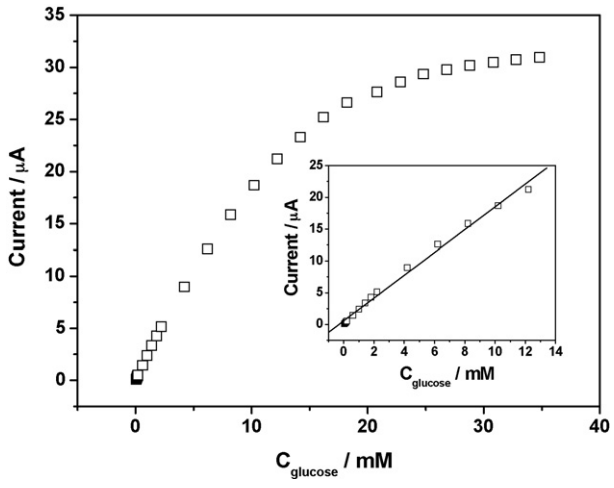

Fig. 7. Variation of response current with glucose concentration. Inset: the linear plot of response current *vs.* the concentration of glucose; other conditions are the same as those in Fig. 4.

wider temperature range, which can be attributed to the protection effect of mesoporous carbon matrix. The dependence of response current on temperature in the range of 2–52 °C can be expressed through the Arrhenius relationship [32,33]. The activation energy can be calculated according to the slope of the plot of logarithm of current density (ln *i*) *versus* reciprocal of temperature (T^{-1}) (Fig. 6). It is 22.54 kJ mol^{-1}, which is quite different from that reported for the free enzyme, namely 14.63 kJ mol^{-1} [34], but is in good accordance with those reported for immobilized GOx (i.e. 22.4–50 kJ mol^{-1}) [33].

3.4. Calibration curve, reproducibility and stability

Fig. 7 shows the calibration curve of glucose. The response current increases with the glucose concentration rising. When it is enough high, the current tends to stable, showing the characteristic of Michaelis–Menten kinetics. The response current is linear to the concentration of glucose over the range from 0.04 to 12.2 mM. The regression equation is $I = 5.53 \times 10^{-7} c_{\text{glucose}} + 1.79 \times 10^{-3}$ (A, M, $R = 0.996$, $n = 10$). The detection limit is 1 μM (S/N = 3). According to the Lineweaver–Burk equation [35], the apparent Michaelis–Menten constant (K_m^{app}) and the maximum current density (i_{max}) of the enzyme reaction at the Pt/CMK-3-GOx-gelatin/GCE can be calculated. In this case they are 10.8 mM and 908 μA cm^{-2}, respectively. These values are close to the reported values for free enzyme [6].

The reproducibility of the Pt/CMK-3-GOx-gelatin/GCE has been evaluated by comparing the response currents of 10 enzyme electrodes prepared. The relative standard deviation (RSD) was 8.1% when 1 mM glucose was determined. The operational stability was examined too. An enzyme electrode was used to determine 1 mM glucose for 10 times continuously, and the RSD of the response current was 4.2%. To test the long-time stability of the enzyme electrode under storage condition (pH 7.0 PBS, 4 °C), an enzyme electrode was used to determine 1 mM glucose solution one time everyday. Up to 30 days the response current retained 95.1% of the initial value. Compared with those glucose biosensors based on enzyme immobilized on Pt nanoparticles and carbon nanotubes matrixes [6,10], the Pt/CMK-3-GOx-gelatin/GCE has better storage stability. This indicates that the mesoporous carbon-gelatin film after covalent cross-linking is very stable and the matrix can prevent enzyme from leaking, contamination and biodegradation.

Table 1
The determination of glucose levels in serum samples

Samples	Provided by the local hospital (mM)	Determined by current method (mM)	Relative error (%)
1	4.95	4.80	−3.03
2	5.57	5.53	−0.72
3	4.51	4.73	4.88
4	4.44	4.76	7.21

3.5. Interference and serum sample analysis

The interference of some electroactive compounds to the glucose response was examined. When the glucose concentration was 5.6 mM, the deviation of response was calculated according to $(I_i - I_g)/I_g$, where I_i and I_g were the steady-state current recorded for solutions containing glucose and interferent or glucose alone. At Pt/CMK-3-GOx-gelatin/GCE, the deviations caused by ascorbic acid (0.1 mM), *p*-acetaminophenol (0.05 mM) and uric acid (0.5 mM) were 0.44%, 4.69% and 13.2%, respectively. This indicates that the biosensor suffers some influence from the coexistents in serum samples. Therefore, 1 μl 1 wt% Nafion was cast on the surface of Pt/CMK-3-GOx-gelatin/GCE to prevent the interference. And then, at Nafion/Pt/CMK-3-GOx-gelatin/GCE, the deviations were in the acceptable range (±10%). The current response of the resulting biosensor was linear to the concentration of glucose from 0.02 to 16.9 mM ($R = 0.993$). However, for 1 mM glucose the response current decreased by 21% in comparison with that of Pt/CMK-3-GOx-gelatin/GCE. The detection range is sufficient for monitoring glucose level of human blood, which is generally 4.4–6.6 mM [36].

The determination of glucose in human serum samples was performed with the Nafion/Pt/CMK-3-GOx-gelatin/GCE. The serum samples were assayed by the glucose oxidase method on a Hitachi 7080 biochemical automatic analyzer in local hospital at the same time. For current method, 50 μl serum was added into the stirred 5 ml PBS (pH 6.0), and amperometric response was recorded at 0.6 V. The results were shown in Table 1. The recoveries for the electrochemical assays of 1–3 mM glucose were between 94.4% and 98.3%. The glucose levels determined in this work were close to the values declared by hospital, indicating that the fabricated glucose biosensor has practical potential.

4. Conclusions

A glucose biosensor has been fabricated based on GOx immobilized in Pt/CMK-3 matrix. Pt nanoparticles loaded have strong electrocatalysis to the oxidation of H_2O_2. The glucose biosensor shows sensitive and rapid response to glucose. With an extra

Nafion film to eliminate the interferents, the resulting biosensor could be used to determine the glucose levels of serum samples. Owing to the protection effect of mesoporous material to GOx, the biosensor has high thermal stability and long-time stability. Therefore, the Pt nanoparticles/mesoporous carbon CMK-3 system is promising in biosensor construction.

Acknowledgement

The authors appreciate the support from the National Nature Science Foundation of China (Grant No. 20173040).

References

[1] H.C. Choi, M. Shim, S. Bangsaruntip, H. Dai, J. Am. Chem. Soc. 124 (2002) 9058.
[2] C.Y. Tsai, A.L. Shiau, P.C. Cheng, D.B. Shieh, D.H. Chou, C.S. Yeh, C.L. Wu, Nano Lett. 4 (2004) 1209.
[3] T. Uemura, S. Kitagawa, J. Am. Chem. Soc. 125 (2003) 7814.
[4] J.N. Xie, S.Y. Wang, L. Aryasomayajula, V.K. Varadan, Nanotechnology 18 (2007) 1.
[5] X. Chu, D.X. Duan, G.L. Shen, R.Q. Yu, Talanta 71 (2007) 2040.
[6] H. Tang, J.H. Chen, S.Z. Yao, L.H. Nie, G.H. Deng, Y.F. Kuang, Anal. Biochem. 331 (2004) 89.
[7] S. Hrapovic, Y.L. Liu, K.B. Male, J.H.T. Luong, Anal. Chem. 76 (2004) 1083.
[8] H.Y. Zhu, Y.H. Zhu, X.L. Yang, C.Z. Li, Chem. Lett. 35 (2006) 326.
[9] L.H. Xu, Y.H. Zhu, L.H. Tang, X.L. Yang, C.Z. Li, Electroanalysis 19 (2007) 717.
[10] M.H. Yang, Y.H. Yang, Y.L. Liu, G.L. Shen, R.Q. Yu, Biosens. Bioelectron. 21 (2006) 1125.
[11] H.H. Zhou, H. Chen, S.L. Luo, J.H. Chen, W.Z. Wei, Y.F. Kuang, Biosens. Bioelectron. 20 (2005) 1305.
[12] S. Bharathi, N. Fishelson, O. Lev, Langmuir 15 (1999) 1929.
[13] P. Schmidt-Winkel, W.W. Lukens Jr., D.Y. Zhao, P.D. Yang, B.F. Chmelka, G.D. Stucky, J. Am. Chem. Soc. 121 (1999) 254.
[14] D.Y. Zhao, J.L. Feng, Q.S. Huo, N. Melosh, G.H. Fredrickson, B.F. Chmelka, G.D. Stucky, Science 279 (1998) 548.
[15] T. Asefa, R.B. Lennox, Chem. Mater. 17 (2005) 2481.
[16] J. Ding, K.Y. Chan, J.W. Ren, F.S. Xiao, Electrochim. Acta 50 (2005) 3131.
[17] J.B. Joo, P. Kim, W. Kim, J. Yi, J. Electroceram. 17 (2006) 713.
[18] C. Lei, Y. Shin, J.K. Magnuson, G. Fryxell, L.L. Lasure, D.C. Elliott, J. Liu, E.J. Ackerman, Nanotechnology 17 (2006) 5531.
[19] J.F. Diaz, K.J. Balkus, J. Mol. Catal. B: Enzymol. 2 (1996) 115.
[20] A. Vinu, M. Miyahara, K. Ariga, J. Phys. Chem. B 109 (2005) 6436.
[21] A. Vinu, C. Streb, V. Murugesan, M. Hartmann, J. Phys. Chem. B 107 (2003) 8297.
[22] D. Lee, J. Lee, J. Kim, J. Kim, H.B. Na, B. Kim, C. Shin, J.H. Kwak, A. Dohnalkova, J.W. Grate, T. Hyeon, H. Kim, Adv. Mater. 17 (2005) 2828.
[23] J.J. Feng, J.J. Xu, H.Y. Chen, Biosens. Bioelectron. 22 (2007) 1618.
[24] A.B. Fuertes, F. Pico, J.M. Rojo, J. Power Sources 133 (2004) 329.
[25] M. Zhou, L.P. Guo, F.Y. Lin, H.X. Liu, Anal. Chim. Acta 587 (2007) 124.
[26] S. Jun, S.H. Joo, R. Ryoo, M. Kruk, M. Jaroniec, Z. Liu, T. Ohsuna, O. Terasaki, J. Am. Chem. Soc. 122 (2000) 10712.
[27] B. Yang, Q.Y. Lu, Y. Wang, L. Zhuang, J.T. Lu, P.F. Liu, Chem. Mater. 15 (2003) 3552.
[28] D. Hopwood, Histochemie 24 (1970) 50.
[29] S.B. Hall, E.A. Khudaish, A.L. Hart, Electrochim. Acta 43 (1998) 2015.
[30] J.Z. Zhu, Z.Q. Zhu, Z.S. Lai, R. Wang, X.M. Guo, X.Q. Wu, G.X. Zhang, Z.R. Zhang, Y.T. Wang, Z.Y. Chen, Sensors 2 (2002) 127.
[31] B. Liu, R. Hu, J. Deng, Anal. Chem. 69 (1997) 2343.
[32] S. Cosnier, S. Szunerits, R.S. Marks, A. Novoa, L. Puech, E. Perez, I. Rico-Lattes, Talanta 55 (2001) 889.
[33] D. Shan, M. Zhu, H. Xue, S. Cosnier, Biosens. Bioelectron. 22 (2007) 1612.
[34] L. Coche-Guérente, A. Deronzier, P. Mailley, J. Moutet, Anal. Chim. Acta 289 (1994) 143.
[35] R.A. Kamin, G.S. Wilson, Anal. Chem. 52 (1980) 1198.
[36] G. Reach, G.S. Wilson, Anal. Chem. 64 (1992) 381.

Available online at www.sciencedirect.com
ScienceDirect
Talanta 74 (2008) 1568–1578
Talanta
www.elsevier.com/locate/talanta

Quantification of target components in complex mixtures using alternative moving window factor analysis and two-step iterative constraint method

Zhong-Da Zeng [a,b], Yi-Zeng Liang [a,*], Zhi-Hong Jiang [c], Foo-Tim Chau [b], Jing-Rong Wang [c]

[a] *College of Chemistry and Chemical Engineering, Research Center of Modernization of Chinese Medicines, Central South University, Changsha 410083, PR China*
[b] *Department of Applied Biology and Chemical Technology, The Hong Kong Polytechnic University, Hung Hom, Kowloon, Hong Kong*
[c] *School of Chinese Medicines, The Hong Kong Baptist University, Kowloon Tong, Hong Kong*

Received 10 May 2007; received in revised form 23 September 2007; accepted 1 October 2007
Available online 10 October 2007

Abstract

Alternative moving window factor analysis (AMWFA) has shown the powerfulness for comprehensive comparison and individual identification of chemical components among different but related mixture systems. However, quantification of these components can only be attained after extraction of all spectra of pure components in samples with least square technique. In this study, a novel two-step iterative constraint method (TICM) is developed for independent quantification of the interested target analytes. The pure chromatographic profiles of the components can be mined out from mixtures with high complexity using a two-step iterative operation and stepwise purification of the targets from interferers. Some effective constraints of chromatographic profiles, such as non-negative and single-peaked properties, as well as zero-concentration outside of elution windows of components, are employed to further improve the efficiency of the method. One of the strong advantages of TICM is simplification of complex mixtures to several sub-systems for processing easily with the help of AMWFA, as well as bi-linear property of data sets obtained from coupled chromatographic instruments. It meets the urgent requirements and challenges of qualitative and quantitative analysis of complicated systems with multi-component in the investigation of herbal medicines (HMs), metabonomics and systems biology. From the results of simulated LC–DAD data, GC–MS data of volatile chemical components in three kinds of ginseng with different growth conditions, and four different medicinal parts of the same herb, good performance of the proposed method is achieved.
© 2007 Elsevier B.V. All rights reserved.

Keywords: Alternative moving window factor analysis (AMWFA); Two-step iterative constraint method (TICM); Quantification; GC–MS; Ginseng; Chemometrics

1. Introduction

Qualitative and quantitative analyses of multi-component in mixture samples with high complexity are challenges to analytical chemists. It is not easy to get the accurate information buried in complicated systems, just like a herbal medicine (HM) or metabolite profiling with hundreds or more ingredients [1], if only the conventional techniques of chemical separation and extraction are employed in experiments. In order to attain the goals, chromatographic techniques like GC, LC and CE have been the preferred tools in the study of the above fields because of the high separation ability and efficiency [2,3]. Especially, hyphenated chromatographic instruments with the power to get the spectra of pure components, such as GC–MS, GC–TOF-MS, LC–DAD, CE–DAD, LC–MS–MS, and others, are widely used in identification and quantification of environment pollutants, bioactive components, metabolites and biomarkers from the complex samples like serum, metabolite profiling, urine and plasma [4–6]. In the last decades, mountainous of works with these techniques were reported for qualification and quantification of multi-component embedded in HMs, plants, foods, environment, and so on [4–6].

However, the chromatographic peak clusters with overlapping components can always be found because of the high

* Corresponding author. Tel.: +86 731 882 2841; fax: +86 731 882 5637.
E-mail address: yizeng_liang@263.net (Y.-Z. Liang).

0039-9140/$ – see front matter © 2007 Elsevier B.V. All rights reserved.
doi:10.1016/j.talanta.2007.10.008

complexity of mixture systems and limited separation ability of instruments. Then, many chemometric resolution methods, such as EFA [7,8], WFA [9,10], HELP [11–13], SFA [14,15], OPR [16], and SIMPLISMA [17–19], were developed to find the qualitative and quantitative information of pure components with strong mathematical supports [20–22]. These methods can be divided into three types following the different principles and theories, including employment of selective information and pure variables of target components, and iterative optimization procedures, respectively [23]. Among these methods, some of them can extract the pure chromatographic and spectral profiles of target components simultaneously [11–13,19–21]. But most of them can only attain one goal at one time [7–10,14–16]. Chemometric resolution methods have been widely used to resolve the problems arising from the hot research subjects described above. For instance, Yi et al. and Li et al. studied the chemical components of HMs with the help of chemometric methods [24–26]. Wang et al. found the relationship of bioactive ingredients existing in the HMs of *Angelica sinensis*, Dangguibuxue decoction, and rabbit plasma after oral administration with the medicines [27,28]. Chemometric multivariate methods also extended the use of conventional techniques and tools [29]. Li et al. further compared the performance of some widely used resolution methods in deconvolving the multi-component of complicated peak clusters [30].

But all these conventional methods were constructed on the basis of only one bi-linear data matrix (called matrix **X** commonly). They cannot make full use of the additional information provided by new data matrix (called **Y** for comparison) acquired at different but related mixture samples, if exist. This type of samples is the same mixture analyzed under different chromatographic columns, instruments, and other experimental conditions, or different medical parts, collection seasons, storage conditions of the same herb, even metabolite profilings with and without disease. The additional information of new data sets cannot be employed to solve the difficult problems using the conventional methods. The three-way resolution methods of this kind such as Tucker 3 [31] and PARAFAC [32] can utilize two or more related data matrices for analysis. But the strong assumption of tri-linear data set makes it difficult to treat the data with shifts of retention times, and so on.

The newly developed method, alternative moving window factor analysis (AMWFA), just meets the requirement for data comparison and analysis of mixture samples [33]. The selective information of chemical components both in data sets **X** and **Y** can be alternatively used for identification of the interested components, which is also one of the main advantages of this method. But quantification of target components using AMWFA method only can be attained after getting all the pure spectra of the components included with least square method. In this work, a two-step iterative constraints method (TICM) is proposed based on AMWFA method. The main idea is stepwise purification of chromatographic profiles of the target analytes from the interferers with the spectral results obtained from AMWFA. The operation is stopped until the errors between two neighboring iterative steps attain a presetting value, and the residue is lower than experimental noise. Also, several effective constraints of chromatographic peaks, especially, the zero-concentration property of the target components outside of elution windows, are further utilized to optimize the results. The employment of AMWFA and TICM methods is interactional and interdependent. The former helps to get the spectrum of pure components and the latter then helps to improve the ability of AMWFA in deconvolution of complicated mixtures.

Ginseng is a well-known natural medicine. It is one of the earliest marketable herbs used in many countries and areas, especially in North America and Asia. Its pharmacological activities include improving psychological and immune functions, lowering blood sugar and cholesterol levels, protecting against stress, enhancing strength and promote relaxation [34,35]. The planting conditions are one of the very important factors for formation of the small molecular metabolites in ginseng. Different growth conditions will lead to different formation and contents of the bioactive components. From the results of analysis of simulated LC–DAD data, volatile chemical components in cultivated, wildly cultivated and wild ginseng, and different medicinal parts of the same herb including head, taproot, side and fibre root, the combination of AMWFA and TICM methods will be a promising tool in the analysis of complex samples of HMs, metobonomics, systems biology, and others.

2. Theory

In terms of the statements in Ref. [33], data matrices **X** and **Y** used in this study are titled the original and compared data sets, respectively. AMWFA method can be summarized to five steps as follows. (1) Data pretreatment including background deduction, signal smoothing, and estimation of the numbers of chemical rank in data sets **X** and **Y**; (2) multi-component spectral correlative chromatography (MSCC) and inverse projection MSCC methods used to get the integrated relationships of components of **X** and **Y**; (3a) fixed-size moving window evolving factor analysis (FSMWEFA) was used to find the possible selective information of components in the two data sets; (3b) obtainments of the base and target matrices proposed in AMWFA with the results from FSMWEFA; (3c) singular value decomposition (SVD) operation on the two data sets to get the orthogonal bases matrices **E** and **F** for AMWFA analysis; (4) common rank analysis (CRA) proposed to acquire the number of common components; (5) identification of common components with the help of the two techniques, common rank maps (CRM) and spectral auto-correlative curve (SACC), respectively. The moving window search technique used on both the above two strategies was developed to extract the spectra of pure target components. With the pure target spectrum ($\mathbf{s}_t$) obtained from AMWFA at hand, how to extract the pure chromatographic profiles for quantitative analysis without more prior knowledge is concern of the next step. If this goal can be achieved, the complex mixture samples can be simplified to some subsystems for processing in terms of the additivity of bi-linear data sets. This will also improve the potentials of AMWFA method for component identification. Then, determination of pure chromatographic profile ($\mathbf{c}_t$) of the target component has

been a key step. Some conventional reported methods such as residual bi-linearization (RBL) [36,37] and constrained background bi-linearization (CBBL) [38] proposed the strategies for quantification of target components. The present method is constructed on the main principles of RBL for quantitative analysis of multi-component of complex chromatographic mixtures.

If N components present in data set $\mathbf{X}$ (or $\mathbf{Y}$), it can be written as the following equation according to Lambert–Beer law:

$$\mathbf{X} = \mathbf{c}_t\mathbf{s}_t^T + \sum(\mathbf{c}_i\mathbf{s}_i^T) + \mathbf{E} = \mathbf{c}_t\mathbf{s}_t^T + \mathbf{R} + \mathbf{E} = \mathbf{X}_t + \mathbf{R} + \mathbf{E},$$
$$i = 1, 2, \ldots, t-1, t+1, \ldots, N \quad (1)$$

Here, $\mathbf{c}_t$ and $\mathbf{s}_t$ represent the pure chromatographic and spectral profiles of the target components. Denotations $\mathbf{X}$, $\mathbf{X}_t$, $\mathbf{R}$ and $\mathbf{E}$ mean the original data matrix, the target matrix only including the information of target component, interferential matrix excluding the information of $\mathbf{X}_t$, and noise matrix, respectively. The superscript T means transpose of vector or matrix. After acquiring the target spectrum ($\mathbf{s}_t$) by AMWFA method, only the target chromatographic profile ($\mathbf{c}_t$) and the interferential matrix $\mathbf{R}$ are unknown in the above equation besides the noise matrix $\mathbf{E}$. It is easy to understand matrix $\mathbf{E}$ can be combined with $\mathbf{R}$ mathematically. Then, the target in Eq. (1) ($\mathbf{c}_t$) can be purified step by step through iterative operations with matrix $\mathbf{R}$. That is to say, with an initial chromatographic profile of the target component ($\mathbf{c}_t^0$) at hand, a more accurate $\mathbf{c}_t$ will possibly be determined using the previously obtained $\mathbf{R}$ for computation, just like RBL method described above. The main working procedures of TICM are shown in Fig. 1.

Supposing the spectral profile of target component ($\mathbf{s}_t$) is acquired by AMWFA method, the working principles of quan-

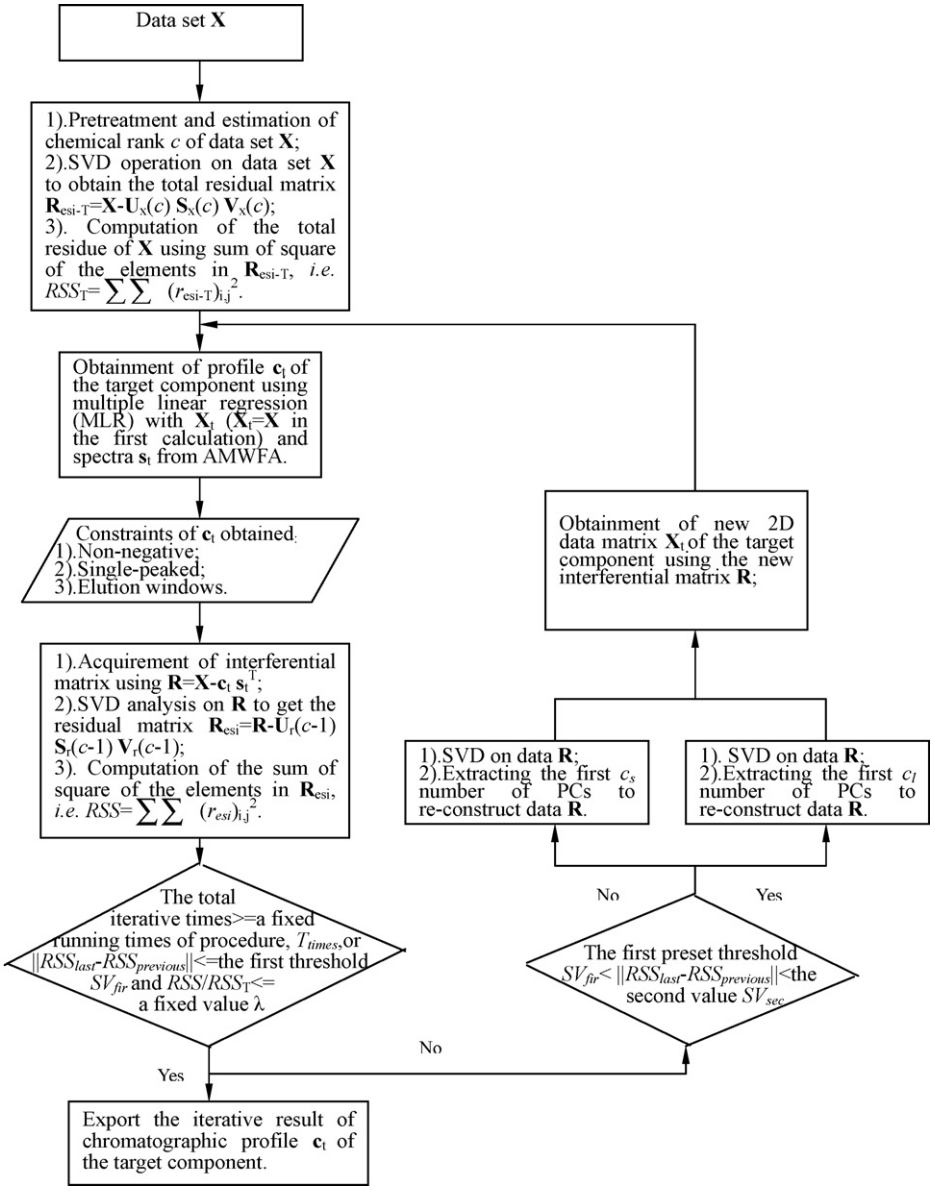

Fig. 1. Schematic illustration of the procedures of TICM method for quantification of target components in mixture systems.

tification of target components in mixture samples using TICM are described as follows:

(1) Data pretreatment like background deduction, signal smoothing, and estimation of chemical rank (c) in data set $\mathbf{X}$. This is a common step of most chemometric resolution methods. Next, SVD analysis is done on data set $\mathbf{X}$ (namely, $\mathbf{X} = \mathbf{U}_x\mathbf{S}_x\mathbf{V}_x^{\mathrm{T}}$) to obtain the total residual matrix with Eq. (2).

$$\mathbf{R}_{\text{esi-T}} = \mathbf{X} - \mathbf{U}_x(c)\mathbf{S}_x(c)\mathbf{V}_x(c) \tag{2}$$

Here, $\mathbf{U}_x$, $\mathbf{S}_x$ and $\mathbf{V}_x$ mean the three loadings, diagonal, and scores matrices from SVD operation of data $\mathbf{X}$ including singular vectors or values, and $\mathbf{U}_x(c)$, $\mathbf{S}_x(c)$ and $\mathbf{V}_x(c)$ mean the matrices constructed by the first c numbers of principal components (PCs) of $\mathbf{U}_x$, $\mathbf{S}_x$ and $\mathbf{V}_x$, respectively. The total residue of data $\mathbf{X}$ is assessed with the sum of square of all the elements in matrix $\mathbf{R}_{\text{esi-T}}$, i.e. $\mathrm{RSS_T} = \sum\sum(\mathrm{r_{esi-T}})_{i,j}^2$. Denotation $(\mathrm{r_{esi\text{-}T}})_{i,j}$ means the element of $\mathbf{R}_{\text{esi-T}}$ at the ith row and jth column.

(2) Acquirement of the chromatographic profile ($\mathbf{c}_\mathrm{t}$) using multiple linear regression (MLR) method. In the initial iterative operation with no prior matrix $\mathbf{R}$ at hand, the whole original matrix $\mathbf{X}$ is regarded as target matrix $\mathbf{X}_\mathrm{t}$ for computation and used to get the target chromatographic profile $\mathbf{c}_\mathrm{t}$ (let $\mathbf{c}_\mathrm{t}^0$ mean the target profile $\mathbf{c}_\mathrm{t}$ in the first computation).

(3) The constraint conditions such as non-negative and single-peaked properties of peaks, and zero-concentration outside of the chromatographic elution windows are employed to optimize the obtained profile ($\mathbf{c}_\mathrm{t}$).

(4) Computation of matrix $\mathbf{R}$ using equation $\mathbf{R} = \mathbf{X} - \mathbf{c}_\mathrm{t}\mathbf{s}_\mathrm{t}^{\mathrm{T}}$ and obtainment of new residue from matrix $\mathbf{R}$. First, SVD analysis on matrix $\mathbf{R}$ (namely, $\mathbf{R} = \mathbf{U}_\mathrm{r}\mathbf{S}_\mathrm{r}\mathbf{V}_\mathrm{r}^{\mathrm{T}}$) is done to get the total residual matrix using the following equation:

$$\mathbf{R}_{\text{esi}} = \mathbf{R} - \mathbf{U}_\mathrm{r}(c-1)\mathbf{S}_\mathrm{r}(c-1)\mathbf{V}_\mathrm{r}(c-1) \tag{3}$$

Here, $\mathbf{U}_\mathrm{r}$, $\mathbf{S}_\mathrm{r}$ and $\mathbf{V}_\mathrm{r}$ mean the three matrices from SVD analysis of matrix $\mathbf{R}$. $\mathbf{U}_\mathrm{r}\ (c-1)$, $\mathbf{S}_\mathrm{r}\ (c-1)$ and $\mathbf{V}_\mathrm{r}\ (c-1)$ mean the first $c-1$ numbers of PCs extracted from $\mathbf{U}_\mathrm{r}$, $\mathbf{S}_\mathrm{r}$ and $\mathbf{V}_\mathrm{r}$. That is to say, the first $c-1$ numbers of PCs are used to reconstruct the data matrix $\mathbf{R}$, excluding the target component from the total c components. Then, total residue of data $\mathbf{R}$ is assessed using the sum of square of the elements in $\mathbf{R}_{\text{esi}}$, i.e. $\mathrm{RSS} = \sum\sum(r_{\text{esi}})_{i,j}^2$. It is easy to see the entire remaining residue should be included in RSS. If the total iterative times is equal to a pre-setting number of running time (T_{times}, the default is 10^3), or the alteration between two neighboring values of RSS is equal to or less than a small pre-setting threshold ($\mathrm{SV_{fir}}$, the default is 10^{-6}), and $\mathrm{RSS/RSS}_T$ is also equal to or smaller than a pre-setting value (λ, the default is 3.0), the present $\mathbf{c}_\mathrm{t}$ can be extracted as the final result. The iterative operation can be stopped at the moment. Otherwise, if the alteration of RSS is larger than $\mathrm{SV_{fir}}$ but smaller than a large pre-setting threshold ($\mathrm{SV_{sec}}$, the default is 10^{-3}), matrix $\mathbf{R}$ is obtained according to the definition:

$$\mathbf{R} = \mathbf{U}_\mathrm{r}(c_\mathrm{l})\mathbf{S}_\mathrm{r}(c_\mathrm{l})\mathbf{V}_\mathrm{r}(c_\mathrm{l}) \tag{4}$$

Here, matrices $\mathbf{U}_\mathrm{r}(c_\mathrm{l})$, $\mathbf{S}_\mathrm{r}(c_\mathrm{l})$ and $\mathbf{V}_\mathrm{r}(c_\mathrm{l})$ are constructed with the first c_l numbers of PCs of matrix $\mathbf{R}$ after SVD analysis. If the alteration of RSS is larger than $\mathrm{SV_{sec}}$, a smaller threshold, c_s, will replace the number of c_l for iterative procedures. This is the adjustable strategy to extract the accurate result of the target chromatographic profile in TICM.

(5) New computation of target matrix $\mathbf{X}_\mathrm{t}$ using the obtained matrix $\mathbf{R}$ from Eq. (4). Next, the iterative procedure returns to step 2 until the acceptable results are acquired finally.

Compared with the conventional RBL method, there are two main differences of the proposed TICM method. The first one is the two-step iterative strategy, and another one is the effective constraints of the chromatographic profiles in iterative procedures. In TICM method, a relatively weak condition is employed to change the acquirement of matrix $\mathbf{R}$ through extracting least numbers of PCs (c_s), not using only one definitive termination condition like RBL method, as shown in Fig. 1. Next, more numbers of PCs (c_l) is used to get the accurate results when the second condition is attained. This strategy is just like the coarse and delicate adjustments in some daily cases. The conventional RBL method attempts to make full use of the information of target components in every iterative step, but reduce the efficiency in getting the results. In addition, not only the conventional constraints such as non-negative and single-peaked of chromatographic profiles, but also a novel property of zero-concentration outside of the elution window of the target component, are employed to further improve the method.

It should be pointed out that the setting of the parameters of TICM depends on the experimental data sets. The above-mentioned default values can only be used for reference. They are determined on the basis of the precision for quantification.

3. Simulated and experimental data sets

In this work, simulated LC–DAD data for validation of the proposed method were introduced in the previous study [33]. The real applications, including quantification of volatile components in ginseng collected from different planting conditions and medicinal parts, are used to deliver the strategies of AMWFA and TICM methods for analysis. Combination of the two methods are really helpful for us to determine the quality medicines from the fakes, and elucidate the mechanism of the same HMs having different pharmacological activities only because of different geographic places and/or curative parts, and others. Extraction of qualitative and quantitative information of components hidden in HMs is the first step of some other studies. The obtained results show strong advantages of chemometric resolution methods in solving these problems.

3.1. Investigation of volatile chemical components in ginseng collected from different planting places and different medicinal parts

The volatile chemical components existing in three kinds of ginseng, including cultivated, wildly cultivated and wild ginseng (abbreviate to G-ginseng, U-ginseng and W-ginseng, respectively), are studied in detail with TICM method. G-ginseng is a kind of artificially cultivated herb. U-ginseng is planted artificially but under the simulated wild growth conditions. W-ginseng is the orthodox wild growth ginseng. Also, different curative parts of ginseng including the rhizome, main root, and side and fibre root are compared in this investigation (called part A, B, C and D of ginseng, respectively). In Fig. 2(a), the total ion current (TIC) chromatograms of the whole part A of G-, U- and W-ginseng, and four different medicinal parts from A to D of W-ginseng are shown for comparison. From Fig. 2(b1) to (b3) and (c1) to (c4), two groups of chromatographic peak cluster are used as examples to deliver the strategies, which are extracted from part A of the three different kinds of ginseng, and from parts A to D of W-ginseng. The purpose of this study is to find the resemblance and difference of qualitative and quantitative information of volatile components among the related ginseng samples, even their variation rules. It is a crucial step for pharmacological research, as well as the study of absorption, distribution, metabolism, and toxicity (ADMETOX) of ginseng *in vivo*.

3.1.1. Extraction of volatile chemical components in ginseng

The ginseng samples were ground and crushed firstly. Then, hexane was added for ultrasonic extraction at room temperature for 1 h. After centrifugation, the supernatant was used for GC–MS analysis.

3.1.2. Instruments and experimental conditions

GC–MS analysis of the volatile constituents in ginseng was performed on Shimadzu QP-2010 GC–MS spectrometer (Tokyo, Japan). Separation was carried out on an Agilent DB-5MS capillary GC column (30 m × 0.25 mm, 0.25 μm). The column temperature was set at 100 °C initially, which was increased to 170 °C at a rate of 1.5 °C/min. Then, it was increased to 190 °C at a rate of 8.0 °C/min, and finally increased to 240 °C at a rate of 2.0 °C/min. The inlet temperature was kept at 270 °C. The carrier gas was set to a constant flow-rate of 1.3 ml/min. The split ratio was 2:1. To the experimental conditions of the mass spectrometer, the ratios of mass to charge (m/z) in full scan model were 1–380 with scan distant time of 0.5 s. The temperatures of EI-ionization source and interface were set at 200 °C and 250 °C, respectively.

3.2. Data analysis

All computer programs used in this study were coded in MATLAB 6.5 and all computations were performed on a Pentium

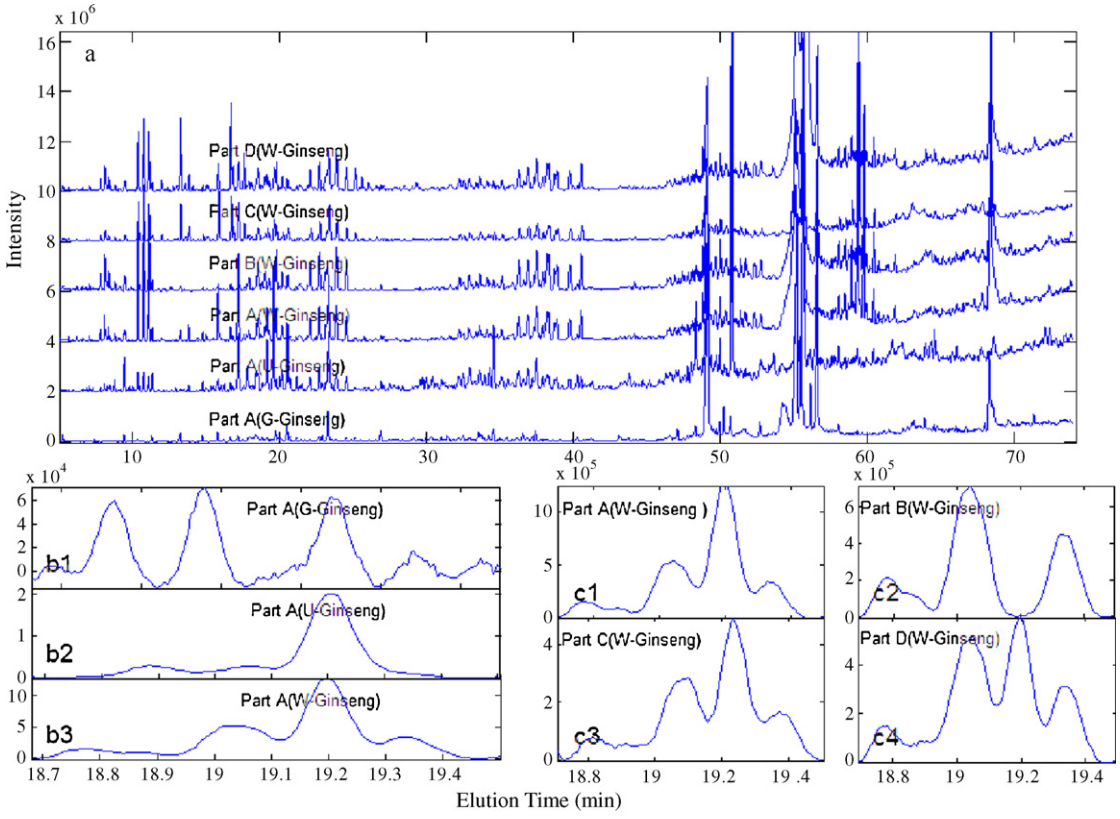

Fig. 2. Total ion current (TIC) chromatograms of ginseng. (a) TIC chromatograms of medicinal part A of G-, U- and W-ginseng, and from parts A to D of W-ginseng; (b1)–(b3) TIC chromatograms of part A of G-, U- and W-ginseng as example; (c1)–(c4) TIC chromatograms from parts A to D of W-ginseng as example.

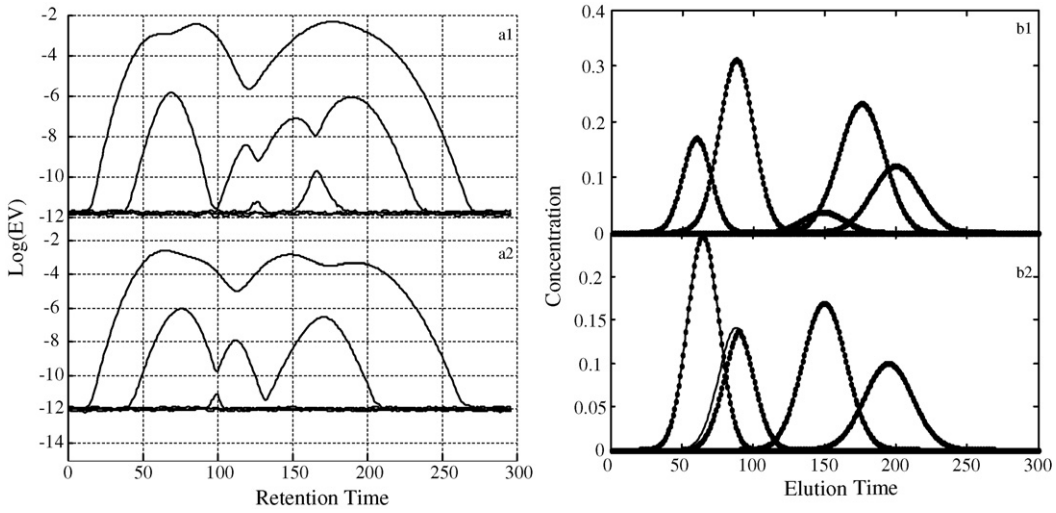

Fig. 3. Two simulated LC–UV systems (**X** and **Y**) and results from AMWFA and TICM for identification and quantification. (a1) and (a2) Results from FSMWEFA of data sets **X** and **Y**; (b1) and (b2) results of pure chromatographic profiles of components in data sets **X** and **Y** using the proposed method. The solid lines are original simulated profiles and the dotted lines are resolution results.

IV processor based IBM compatible personal computer with 256 MB RAM memories.

4. Results and discussion

4.1. Data set 1: simulated LC–DAD data

The simulated chromatograms and spectra of components in data sets **X** and **Y** are shown in Ref. [33]. In this investigation, FSMWEFA is also employed to determine the elution chromatographic pattern, namely, the starting and end points of components in the elution windows. Then, the zero-concentration regions of target components can be identified and used for iterative constraint operations in TICM analysis. In addition, SVD analysis is also utilized for the estimation of chemical ranks. To the two simulated data sets, the pure spectra of common components between data sets **X** and **Y** were obtained with AMWFA first [33]. As to the non-common components, the spectra were extracted with the widely used SFA method independently after resolution of the common components [14,15]. With the pure spectra information at hand, TICM method is further used for quantification of the target components one by one. According to the graphs shown in Fig. 3(a1) and (a2), the determined left and right elution time points (abbreviated to denotation *L* and *R* here) of every target component in data sets **X** and **Y** are listed in Table 1. When these points cannot be accurately defined in complex real applications, the approximate positions can also be used for analysis. But this will probably increase the running times during the iterative operations. Also, other parameters in the programs of TICM method are clearly shown in the same table. It should be pointed out the new target data for analysis will appear after obtainment of a certain target component. The new data can be used for further identification and quantification of the remaining target analytes included. This will improve the resolution efficiency because they are simpler in contrast to the original data set **X** or **Y**. In Fig. 3(b1) and (b2), the simulated chromatographic profiles (solid lines) and resolution results (dotted lines) from data sets **X** and **Y** are shown, respectively. The results are almost identical with the original simulated chromatograms. From the results, TICM method shows powerful abilities and good performance with two-step iterative strategy, even to the strongly overlapped or minor components. Especially, the programs can be run semi-automatically as AMWFA method. It is very useful to the users with no strong chemometric background and experience.

Table 1
Setting of the parameters of TICM method for quantification, including all the chemical components of the simulated LC–DAD mixture systems **X** and **Y**

Program parameters	Different mixture systems								
	Data set **X**					Data set **Y**			
	C-1	C-2	C-3	C-4	C-5	C-1	C-2	C-3	C-4
Number of principal components $c/c_s/c_l$	5/1/4	5/1/4	5/1/4	5/1/4	5/1/4	4/1/3	4/1/3	4/1/3	4/1/3
Left (starting) elution time point *L*	20	42	106	100	130	20	40	90	120
Right (end) elution time point *R*	100	136	192	116	270	100	140	220	270
Setting value of SV_{fir}/SV_{sec}	$10^{-7}/10^{-3}$	$10^{-7}/10^{-3}$	$10^{-7}/10^{-3}$	$10^{-7}/10^{-3}$	$10^{-7}/10^{-3}$	$10^{-7}/10^{-3}$	$10^{-7}/10^{-3}$	$10^{-7}/10^{-3}$	$10^{-7}/10^{-3}$

4.2. Data set 2: medicinal part A of ginseng from different planting conditions

As an example, TIC chromatograms of three peak clusters of part A extracted from G-, U- and W-ginseng are shown in Fig. 2(b1)–(b3). It is easy to know that the accurate qualitative and quantitative information of the components in them cannot be obtained only from these TIC plots. Obtainment of the pure components using AMWFA and TICM is introduced in detail below. First, SVD analysis is employed for the determination of chemical ranks of the three systems. Then, with the help of FSMWEFA and AMWFA methods, the spectra of components between U- and W-ginseng are determined. In order to shorten the length of the paper and improve the legibility of the present work, the detail information for identification of spectra by AMWFA is not discussed here. The main principles and procedures are identical as the descriptions in the previous report [33]. In Fig. 4(a), mass spectra (MS) of these components are shown. The left column is the standard MS extracting from the NIST standard mass spectral library corresponding to the obtained MS in the right one. Also, detail information of the five components is listed in Table 2. It can be found that the similarities between the standard and resolution MS are very high with less difference. Combining AMWFA and SFA methods, the spectra of common and non-common components in G-ginseng and the only one non-common component in U-ginseng are acquired, as shown in Fig. 4(b). The top two MS are non-common components from G-ginseng. Unfortunately, they cannot be matched well with the standard components of the NIST database. The bottom two MS are standard and resolution results of the non-common components in U-ginseng. It can be determined as 7-methyl-hexadecane ($C_{17}H_{36}$) with similarity of 0.9861. Next, TICM method can be further used to get the pure chromatographic profiles for quantification of these components with the above spectra information at hand. The chemical components in the mixture systems of U- and W-ginseng are very similar to each other. But the quantitative difference of components leads to different pharmacological efficacies. The adjustable parameters in TICM method, such as SV_{fir} and SV_{sec}, are identical as shown in Table 1. Determination of the starting and end points of the target components is attained using AMWFA method with the results from FSMWEFA. According to the procedures described in the theory section, the chromatographic profiles are semi-automatically obtained, as Fig. 4(c1)–(c3) shows. From these figures, the quantitative variation rules of these components can be used to elucidate the action mechanism of HMs on disease treatment. This is the main advantage of AMWFA and TICM in qualitative and quantitative analysis of complex systems through improving the potentials of AMWFA. In many cases, it will be very useful for the analysis of complicated systems with embedded overlapping components.

4.3. Data set 3: different medicinal parts (A–D) of W-ginseng

Four different medicinal parts of the same ginseng (A–D) also have different pharmacological efficacies. In this section, one chromatographic example extracted from W-ginseng is used to deliver the strategies of TICM. In Fig. 2(c1)–(c4), TIC chromatograms of the four different parts of W-ginseng are shown. The part A is the same peak cluster of W-ginseng described in the above. From these plots, it is also clear to see the components existing in these samples are very similar besides a little qualitative difference of the second curve. It seems at least one

Table 2
Identification of the common components between the rhizome (part A) of U- and W-ginseng

No.	Similarity	Information of the identified components		
		Molecular formula	Name	Structure
1	0.9187	$C_{13}H_{28}O$	Tridecanol	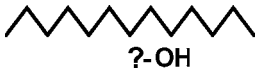
2	0.9200	$C_{14}H_{30}$	2,2,3,3,5,6,6-Pheptamethyl	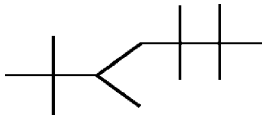
3	0.9573	$C_{17}H_{36}$	*n*-Heptadecane	
4	0.9369	$C_{15}H_{24}$	1-Ethyl-1-methyl-2-[1-methylethenyl]-4-[1-methylethylidene]-cyclohexane	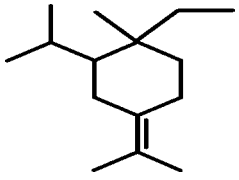
5	0.8877	$C_{15}H_{12}O$	3,7,11-Trimethyl-1-dodecanol	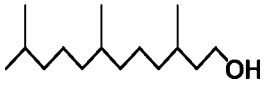

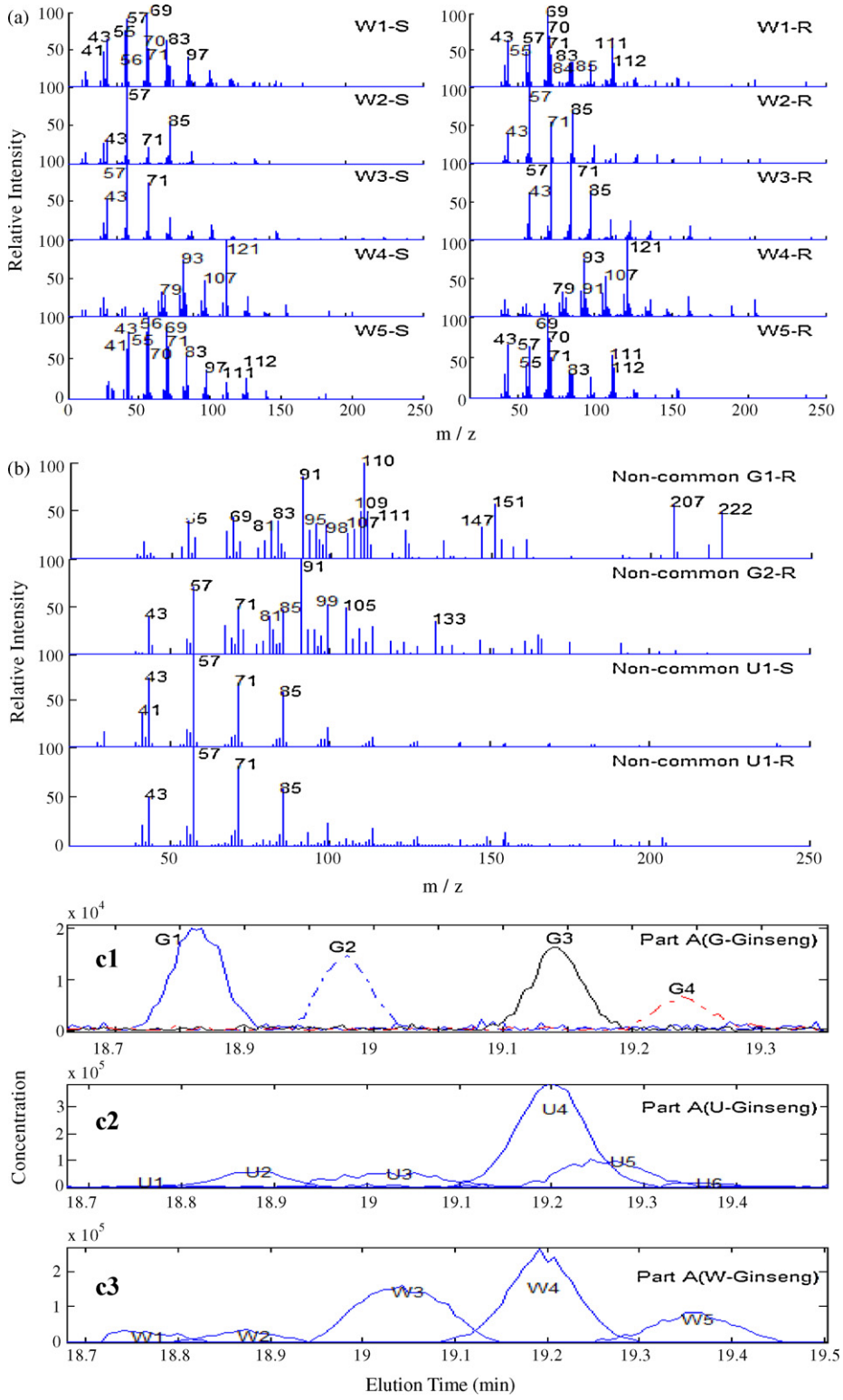

Fig. 4. Spectra of pure common and non-common chemical components among part A of G-, U- and W-ginseng (see Fig. 2(b1)–(b3)). The mass spectrum (MS) with a last letter "S" means standard spectra extracted from NIST database, or "R" means resolution results using AMWFA or SFA methods in the subplots. (a) Results of common components among different samples of ginseng; (b) Results of non-common components among different samples of ginseng; (c1)–(c3) results of chromatographic profiles of pure chemical components present in the example data of part A of G-, U- and W-ginseng using TICM methods (see the marks in the figures). The solid lines mean common components and the dotted lines mean non-common components.

component (at about retention time 19.2 min) present in parts A, C and D but absent in part B. Through comparison of the two mixture systems of medicinal parts A and B, C and D with AMWFA method, the spectra of common components are identical as Fig. 4(a) shows. Only the fourth components cannot be found in part B. So, TICM method can be easily used for quantitative analysis of these common and non-common components, according to the principles described above. In Fig. 5, pure chromatographic profiles of components of the four medicinal parts of W-ginseng are shown with different marked lines. The quantitative variation of volatile components in the four parts is very clear from this figure. In terms of the results obtained from these real applications, chemometric resolution methods show powerful ability in treating complex mixture samples like HMs. They can be very promising methods in the future studies.

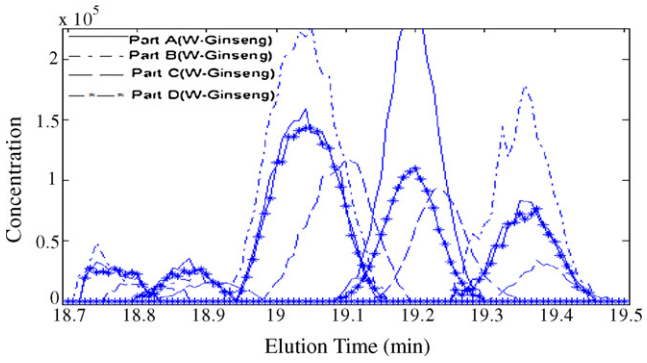

Fig. 5. Results of pure chromatographic profiles of chemical components existing in the example data set of parts A–D of W-ginseng using TICM (see the original data sets from Fig. 2(c1)–(c4)).

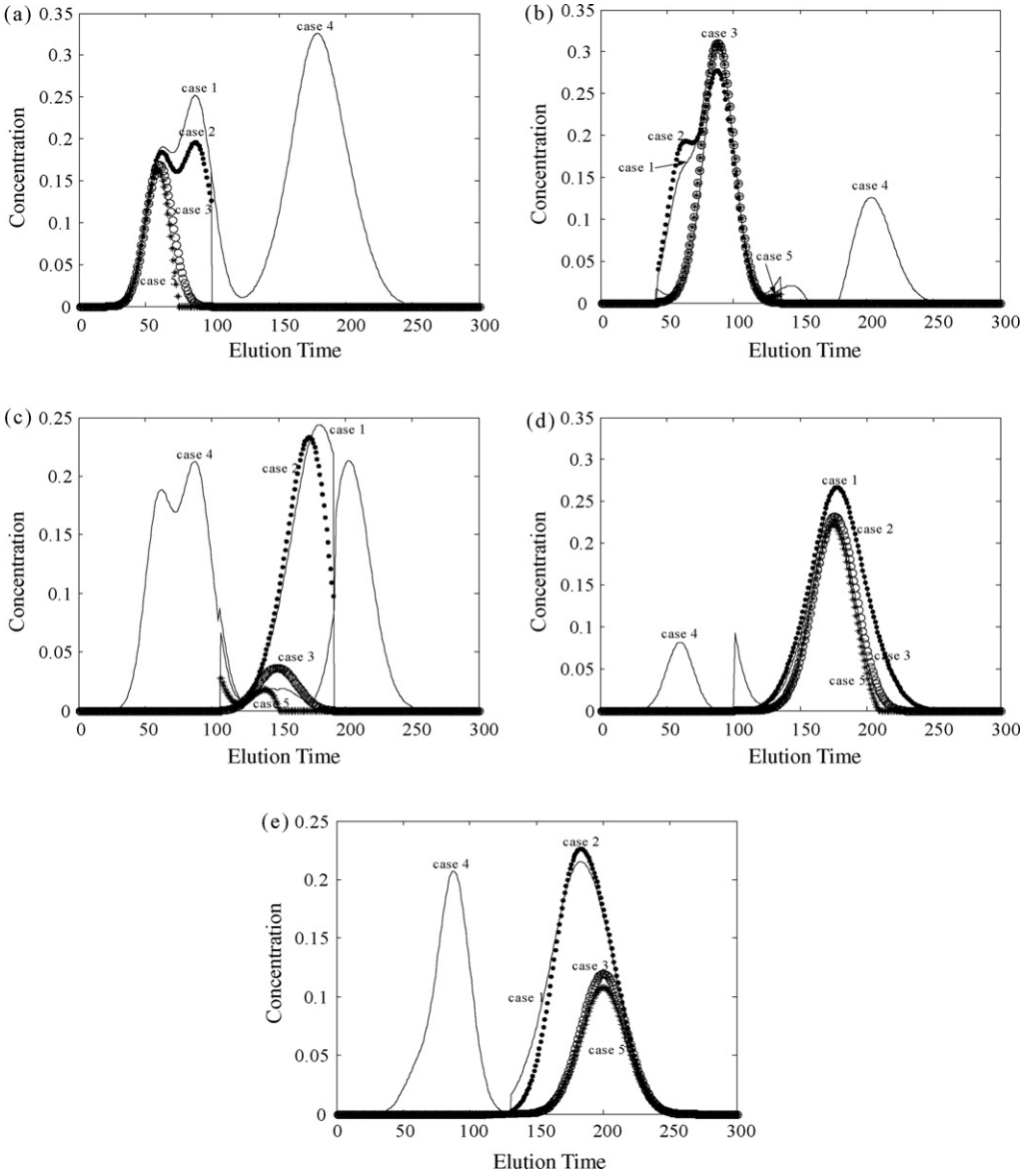

Fig. 6. Comparison results of chromatographic profiles of five components in the simulated data set **X** using AMWFA and TICM methods under different temporary parameters and conditions, as shown in Table 3. The third cases in the subplots from (a) to (e) are results with true conditions in TICM for resolution. Other four cases are used for comparison purpose.

Table 3
The effects of program parameters, as well as the iterative and constraint conditions used in TICM method on quantification analysis

Program parameters	Simulated data set **X**				
	C-1	C-2	C-3	C-4	C-5
Number of principal components c_s/c_l	0/0; 1/1; 1/4; 1/4; 4/4	0/0; 1/1; 1/4; 1/4; 4/4	0/0; 1/1; 1/4; 1/4;4/4	0/0; 1/1; 1/4; 1/4; 4/4	0/0; 1/1; 1/4; 1/4; 4/4
Chromatographic elution window constraints	Yes; yes; yes; no; yes	Yes; yes; yes; no; yes	Yes; yes; yes; no; yes	Yes; yes; yes; no; yes	Yes; yes; yes; no; yes
Two-step iterative procedure	No; no; yes; yes; no	No; no; yes; yes; no	No; no; yes; yes; no	No; no; yes; yes; no	No; no; yes; yes; no
Results	–; –; +;–; –	–; –; +; –; –	–; –; +; –; –	–; –; +; –; –	–; –; +; –; –

Denotations "yes" and "no" in this table mean the conditions in the left used or not for analysis; and "+" and "−" mean the acquired chromatographic profiles acceptable or not, respectively.

Combination of AMWFA and TICM shows powerful ability for quantification of target components in mixture samples. TICM also further extends the applications of AMWFA and improves the potentials. Through simultaneous qualitative and quantitative analysis of target components, the complicated systems can be simplified into several easily processed sub-system for analysis with the help of the two methods. The selective information of the strongly overlapped components can be then found for components identification and quantification. Therefore, the two methods are interactional and interdependent in practice. It is extremely useful for the study of mixture systems with high complexity.

4.4. The effects of parameters and iterative constraints in TICM method for quantification of components

In this section, the simulated data set **X** is used to study the possible effects of the parameters and constraint conditions used in the proposed method for quantitative analysis of complex mixtures. Mainly, four factors including the two different numbers c_s and c_l of PCs in the two iterative steps, constraints of chromatographic elution region and two-step iterative procedures are considered in analysis. In Table 3, four different cases of c_s/c_l are listed in detail. In fact, the first case 0/0 of c_s/c_l means the initial iterative step of chromatographic profile in TICM method. Other two cases 1/1 and 4/4 mean c_s and c_l with the same values. Then, the two-step iterative procedure of TICM method has been a one-step iterative operation as RBL method. In Table 3, there are five different cases to every target component for consideration. Obviously, only the case with two-step iterative procedures and chromatographic constraints of zero-concentration regions performs well under the pre-setting values of T_{times}, SV_{fir} and SV_{sec}. From Fig. 6(a) to (e), comparison results of every component in Table 3 with different parameters and operation conditions are shown. TICM provides a choice for quantification of target components buried in complex mixture systems.

5. Conclusions

Quantification of target chemical components hidden in complex mixture systems has been attained using a two-step iterative strategy and AMWFA method. With the spectrum of pure target analyte from AMWFA at hand, the chromatographic profile can be mined out through stepwise purification of contaminated mixture data set. The iterative procedures are stopped until the pre-setting conditions are achieved. The main advantageous principles of TICM method are the two-step iterative operation, as well as the constraints of chromatographic profiles to further improve the results. Combination of TICM and AMWFA methods can extend the ability on qualitative and quantitative analysis of chemical components embedded in mixture systems like HMs, metabolite profiling, metabonomics, and others. The proposed method will be a considerable choice in study of the above-mentioned scientific fields in the future.

Acknowledgements

This research work is financially supported by National Natural Science Foundation of China (Grant No. 20235020 and 20475066), the cultivation fund of the key Scientific and Technical Innovation Project, Ministry of Education of China (No. 704036) and University Grant Council (UGC) of Hong Kong SAR (Area of excellent project "Chinese Medicine Research and Further Development").

References

[1] M.T. Lohnes, R.D. Guy, P.D. Wentzell, Anal. Chim. Acta 389 (1999) 95.
[2] C. Vendeuvre, R.G. Rosario, F. Bertoncini, L. Duval, D. Thiébaut, M.C. Hennion, J. Chromatogr. A 1086 (2005) 21.
[3] N.V.S. Ramakrishna, K.N. Vishwottam, S. Wishu, M. Koteshwara, J. Chidambara, J. Chromatogr. B 823 (2005) 189.
[4] K. Kadokami, K. Tanada, K. Taneda, K. Nakagawa, J. Chromatogr. A 1089 (2005) 219.
[5] F. Hernández, Ó.J. Pozo, J.V. Sancho, F.J. López, J. Maún, M. Ibáñez, Trends Anal. Chem. 24 (2005) 596.
[6] Y. Hu, Y.Z. Liang, B.Y. Li, Z.D. Zeng, Acta Chim. Sin. 61 (2003) 1466.
[7] M. Maeder, Anal. Chem. 59 (1987) 527.
[8] M. Maeder, A. Zilian, Chemom. Intell. Lab. Syst. 3 (1988) 205.
[9] E.R. Malinowski, J. Chemom. 6 (1992) 29.
[10] E.R. Malinowski, J. Chemom. 10 (1996) 273.
[11] O.M. Kvalheim, Y.Z. Liang, Anal. Chem. 64 (1992) 936.
[12] Y.Z. Liang, O.M. Kvalheim, H.R. Keller, D.L. Massart, P. Kiechle, F. Erni, Anal. Chem. 64 (1992) 946.
[13] Y.Z. Liang, O.M. Kvalheim, A. Rahmani, R.G. Brereton, J. Chemom. 7 (1993) 15.
[14] R. Manne, H.L. Shen, Y.Z. Liang, Chemom. Intell. Lab. Syst. 45 (1999) 171.
[15] H.L. Shen, R. Manne, Q.S. Xu, D.Z. Chen, Y.Z. Liang, Chemom. Intell. Lab. Syst. 45 (1999) 323.

[16] F.C. Sánchez, S.C. Rutan, M.D.G. García, D.L. Massart, Chemom. Intell. Lab. Syst. 36 (1997) 153.
[17] W. Willem, G. Jean, Anal. Chem. 63 (1991) 1425.
[18] K.D. Braekeleer, D.L. Massart, Chemom. Intell. Lab. Syst. 39 (1997) 127.
[19] P.J. Martin, W.P. Alan, W. Willem, Anal. Chim. Acta 318 (1995) 43.
[20] M. Cocchi, C. Durante, M. Grandi, P. Lambertini, D. Manzini, A. Marchetti, Talanta 69 (2006) 1166.
[21] J.M. Jurado, O. Ballesteros, A. Alcazar, F. Pablos, M.J. Martin, J.L. Vilchez, A. Navalon, Talanta 72 (2007) 506.
[22] H.T. Gao, T.H. Li, K. Chen, W.G. Li, X. Bi, Talanta 66 (2005) 65.
[23] J.H. Jiang, Y. Ozaki, Appl. Spectrosc. Rev. 37 (2002) 321.
[24] L.Z. Yi, Y.Z. Liang, Z.D. Zeng, D.L. Yuan, P. Wang, Chem. J. Chin. Univ. 27 (2006) 2052.
[25] L.Z. Yi, Y.Z. Liang, Z.D. Zeng, P. Wang, D.L. Yuan, Chem. J. Chin. Univ. 27 (2006) 1626.
[26] X.R. Li, Y.Z. Liang, F.Q. Guo, X.N. Li, Z.D. Zeng, Chem. J. Chin. Univ. 35 (2007) 532.
[27] Y.L. Wang, Y.Z. Liang, Y. Hu, B.Y. Li, Z.D. Zeng, Y.K. He, Chemom. Intell. Lab. Syst. 82 (2006) 229.
[28] Y.L. Wang, Y.Z. Liang, Y. Hu, B.Y. Li, Z.D. Zeng, S.P. Xu, Chem. J. Chin. Univ. 27 (2006) 222.
[29] D.L. Giokas, A.G. Vlessidis, Talanta 71 (2007) 288.
[30] H. Li, J.R. Hou, K. Wang, F. Zhang, Talanta 70 (2006) 336.
[31] P.M. Kroonenberg, Three-mode Principal Component Analysis Theory and Application, DSWO Press, Leiden, 1989.
[32] R.A. Harshman, M.E. Lundy, The PARAFAC model for three-way factor analysis and multidimensional scaling, in: H.G. Law, C.W. Snyder, J.A. Hattie, R.P. McDonald (Eds.), Research Methods for Multimode Data Analysis, Praeger, New York, 1984.
[33] Z.D. Zeng, Y.Z. Liang, Y.L. Wang, X.R. Li, L.M. Liang, Q.S. Xu, C.X. Zhao, B.Y. Li, F.T. Chau, J. Chromatogr. A 1107 (2006) 273.
[34] M. Tatsuka, M. Maeda, T. Ota, Jpn. J. Cancer Res. 92 (2001) 1184.
[35] D.D. Kitts, A.N. Wijewickreme, C. Hu, Mol. Cell. Biochem. 203 (2000) 1.
[36] J. Öhman, P. Geladi, S. Wold, J. Chemom. 4 (1990) 79.
[37] J. Öhman, P. Geladi, S. Wold, J. Chemom. 4 (1990) 135.
[38] Y.Z. Liang, R. Manne, O.M. Kvalheim, Chemom. Intell. Lab. Syst. 14 (1992) 175.

Available online at www.sciencedirect.com
ScienceDirect
Talanta 74 (2008) 1154–1159
Talanta
www.elsevier.com/locate/talanta

Determination of folic acid by chemiluminescence based on peroxomonosulfate-cobalt(II) system

Bo-Tao Zhang, Lixia Zhao *, Jin-Ming Lin *

State Key Laboratory of Environmental Chemistry and Ecotoxicology, Research Center for Eco-Environmental Sciences, Chinese Academy of Sciences, P.O. Box 2871, 100085 Beijing, China

Received 18 July 2007; received in revised form 15 August 2007; accepted 19 August 2007
Available online 30 August 2007

Abstract

Based on the chemiluminescence (CL) phenomena of folic acid in peroxomonosulfate-cobalt(II) system, a rapid and sensitive CL method was developed for determination of folic acid in pharmaceutical preparations and its urinary metabolism processes. Under the optimum conditions, the relative CL intensity was linear over the concentration ranging from 10^{-9} to 8×10^{-7} mol L^{-1} ($R^2 = 0.9991$) with a detection limit as low as 6×10^{-10} mol L^{-1} (S/N = 3) and relative standard deviation was 2.63% for 2×10^{-8} mol L^{-1} folic acid ($n = 11$). This method has been successfully applied to the determination of folic acid in tablets and human urine. The blank CL emission was yielded owing to the formation of singlet oxygen molecular pair from the quenching experiment of 1,4-diazabicyclo[2.2.2]octane, and pterine-6-carboxylic acid might be the degradation intermediate in this system and it also acts an energy acceptor and sensitizes the chemiluminescence based on the studies of the CL and fluorescence spectra.
© 2007 Elsevier B.V. All rights reserved.

Keywords: Chemiluminescence; Peroxomonosulfate; Folic acid; Flow-injection analysis

1. Introduction

Folic acid, otherwise known as vitamin M or pteroylglutamic acid (PGA), is made up of a bicyclic pterine linked by a methylene bridge to *para*-aminobenzoic acid, which is joined by peptide linkage to a single molecule of L-glutamic acid. Folic acid is susceptible to cleavage under acidic conditions, light, and high temperature [1]. Folic acid can promote the formation of red blood cells and is identified as an anti-anemia and growth factor. It prevents neural tube defects like spina bifida, while its ability to lower homocysteine suggests it might have a positive influence on cardiovascular disease. The role of this vitamin in maintaining good health may extend beyond these clinical conditions to encompass other birth defects, several types of cancer, dementia, affective disorders, Down's syndrome, and serious conditions affecting pregnancy outcome [2,3].

Therefore, it is important to develop simple, sensitive and accurate methods for being able to detect folic acid. But analysis of folic acid is not easy due to its lower stability, presence in lower concentration in biological systems, and complex extraction and detection techniques. Methods of analysis for folic acid are grouped into microbiological, bio-specific procedures, chromatographic, and chemical methods [1]. Although microbiological assay is the most commonly used method, it is time consuming, needs great care and skill [4]. Chromatographic methods have the advantage of separating and quantifying different forms of folic acid and its derivations and minimum interference from enzymes but involve set up cost, a complex extraction, and purification procedure [5,6]. Enzyme protein binding assay is much cheaper, rapider, and easier but there exits considerable variation between different kits and self-life of kits is very short [7].

Chemiluminescence (CL) is a powerful analytical technique that has excellent sensitivity, wide linear dynamic range and requires relatively simple and inexpensive instrumentation [8,9]. To our knowledge, there were a few reports for the determination of folic acid based on CL analysis system [10–12]. But the proposed methods had their own shortages in the respectively

* Corresponding authors. Tel.: +86 10 62841953; fax: +86 10 62841953.
E-mail addresses: zlx@rcees.ac.cn (L. Zhao), jmlin@mail.rcees.ac.cn (J.-M. Lin).

0039-9140/$ – see front matter © 2007 Elsevier B.V. All rights reserved.
doi:10.1016/j.talanta.2007.08.027

CL system such as poor linearity, lack of selectivity or high limit of detection. Furthermore, they almost had been developed for the measurement of folic acid only in tablets.

In our research, we found that a strong CL signal was given out when a trace amount of folic acid was added to peroxomonosulfate(PMS)/Co(II) mixed solution and the CL intensity was strongly dependent on folic acid concentration. Based on this phenomenon, a new, rapid, simple, sensitive and inexpensive method is proposed to determine folic acid. Comparing with the other CL methods, it has more widely linear range and much lower detection limit. Furthermore, the method has been used for the determination of folic acid not only in real pharmaceutical preparations but also in human urine with satisfactory results.

2. Experimental

2.1. Reagents

All the reagents used in these experiments were of analytical grade or higher without further purification. Water was purified using a compact ultra pure water system (18.3 MΩ cm^{-1}, Barnstead, Iowa, USA). A 10^{-4} mol L^{-1} folic acid stock solution was prepared by dissolving 4.41 mg of folic acid (Sigma–Aldrich, St. Louis, USA) in 1 mL of 0.1 mol L^{-1} NaOH solution and diluting to 100 mL with water, then stored at 4 °C and protected from the light. Solutions of $KHSO_5$ available in the form of a triple salt ($2KHSO_5 \cdot KHSO_4 \cdot K_2SO_4$) as Oxone (Alfa Aesar-A Johnson Matthey Company, Ward Hill, USA) and cobalt(II) sulfate heptahydrate (Beijing Chemical Reagent Company, Beijing, China) were prepared daily. 1,4-Diazabicyclo[2.2.2]octane (DABCO) is the products of Acros Organics (New Jersey, USA). Cobalt(II) chloride hexahydrate, cobalt(II) acetate tetrahydrate and cobalt(II) nitrate hexahydrate were purchased from Beijing Chemical Reagent Company (Beijing, China).

2.2. Apparatus and procedure

Batch chemiluminescence experiments were carried in a BPCL luminescence analyzer (Institute of Biophysics, Chinese Academy of Sciences, Beijing, China). A flow CL analyzer (Lumiflow LF-800, Microtec NITI-ON, Funabashi, Japan) was used for flow-injection chemiluminescence experiments. UV–vis absorbance spectra were collected by a UV-2401 Spectrophotometer (Shimadzu, Japan) and the fluorescence spectra were measured by an F-2500 fluorescence spectrometer (Hitachi, Japan).

The flow-injection analysis (FIA) system is illustrated in Fig. 1. PTFE tubing (1.0 mm i.d.) was used as connection material in the flow system. Reagent solutions (R1-R3) were delivered by two peristaltic pumps (SJ-1211, Atto, Tokyo, Japan) through three flow lines. Folic acid standard solution or sample solution was injected into the carrier stream (water) with a 150 μL loop injector. The flow cell was a flat spiral-coiled colorless glass tube (1.0 mm i.d.; total diameter of the flow cell, 3 cm) and placed closed to the window of the photomultiplier tube (PMT, operated at −800 V). Before each measurement, the instruments were allowed to carry solutions for 10 min to achieve

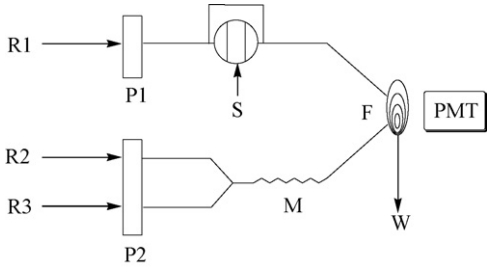

Fig. 1. Schematic diagram of the flow-injection system. R1, H_2O as carrier stream; R2, 0.01 mol L^{-1} HSO_5^-; R3, 0.01 mol L^{-1} Co^{2+}; P1 (4.0 mL min^{-1}), P2, P3 (0.5 mL min^{-1}), peristaltic pump; S, 150 μL sample injector; M, mixing tube; F, flow cell; W, waste; PMT, photomultiplier tube.

good mechanical and thermal stability. The concentration of folic acid was quantified via the peak height of the relative CL intensity obtained by subtracting the blank CL intensity which emitted when mixing PMS and Co(II) solutions.

2.3. Sample preparation

The tablets were purchased from Changzhou Pharmaceutical Factory (sample 1, Changzhou, China) and Tianjin Feiying Pharmaceutical Co. Ltd. (sample 2, Tianjin, China). Not less than 10 tablets were ground into fine power and mixed. A sample equivalent to one tablet were weighed accurately and dissolved in 1 mL of 0.1 mol L^{-1} NaOH solution and diluting to 100 mL with water. Then the solution was filtered and appropriately diluted when determined.

Urine samples were collected in dark glass bottle and diluted at 10^4 with distilled water before determination. Sometimes urine samples were supplemented with folic acid to test the recovery of the method. In view of the photo lability of folic acid, all the sample solutions should be protected from blazing light during the experiment.

3. Results and discussion

3.1. Batch chemiluminescence

The catalytic decomposition of peroxymonosulfate by cobaltous ion was first reported in 1956 [13], and cobalt was proved to be the best catalyst activator of this peroxide [14]. The dynamic profile of chemiluminescence of folic acid in PMS/Co(II) in batch experimental is shown in Fig. 2. From the chemiluminescence (CL) kinetic curve, a weak luminescence was yielded when the $CoSO_4$, $Co(NO_3)_2$ and $CoCl_2$ solution was added to PMS solution, which would be the blank of determination of PGA in this system. There was a strong CL when the cobalt acetate ($CoAc_2$) solution was added to PMS solution, whose blank would be too high to suit for CL analysis, because aliphatic monocarboxylic acids, such as acetic and butyric, were found to enhance the CL emission generation from the PMS/$CoSO_4$ reaction [15]. A very strong luminescence was given after the adding of the solution of 10^{-6} mol L^{-1} PGA to the mixing solution of PMS and Co(II) except PMS/$CoCl_2$ solution whose intensity as low as its blank. The latter phenomenon might due to the fact

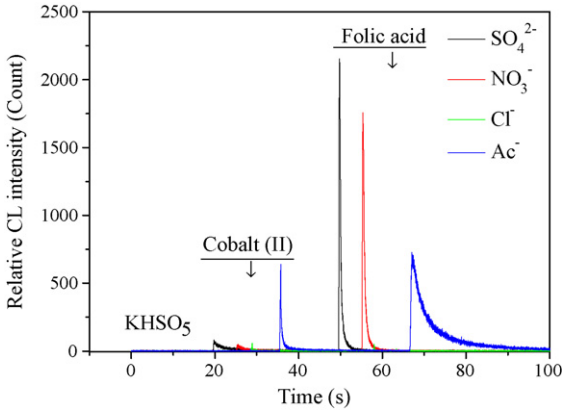

Fig. 2. Effect of counter ion of Co(II) on the chemiluminescence. The concentrations of folic acid, HSO_5^-, and Co^{2+} are 10^{-6}, 0.01 and 0.01 mol L^{-1}, respectively. The volume of each reagent is 50 μL. Different Co^{2+} solution is injected into system firstly (at time of 25–45 s in the graph), and then folic acid is injected into system after 30 s.

that the peroxymonosulfate ion can be consumed by oxidizing chloride ion through reactions (1) and (2) [16].

$$HSO_5^- + Cl^- \rightarrow SO_4^- + HOCl \quad (1)$$

$$HSO_5^- + 2Cl^- + H^+ \rightarrow SO_4^- + Cl_2 + H_2O \quad (2)$$

So the counter ion of cobalt greatly affected the CL signal greatly. For further experiments, $CoSO_4$ was employed since PMS itself contained sulfate and hydrogen sulfate anions. Based on the results of batch chemiluminescence, the flow-injection analysis (FIA) system was developed for determination of folic acid.

3.2. Determination of PGA by FIA-CL of PMS/Co(II) system

3.2.1. Optimization of flow-injection CL system

In order to determinate the optimum operating condition of the flow system, the CL intensity for 2×10^{-8} mol L^{-1} folic acid was measured with respect to the reaction variables.

The CL intensity decreased with the length of mixing tube according to Fig. 3A because of the catalytic decomposition of peroxymonosulfate, so it was no necessary to set up mixing tube and PMS and Co(II) was mixed at the input of the flow CL analyzer, which was a little different from our previous researches [17,18]. The CL intensity decreased slightly with the flow rates of the reagent solutions in the range of 0.5–2.5 mL min^{-1} from Fig. 3B, so the flow of 0.5 mL min^{-1} was select as an appropriate condition in the view of analytical precision and lower solution consumption. But the CL intensity increased almost linearly with the flow rates of carrier steam in the range of 0.5–5.0 mL min^{-1} because the higher flow rate of the carrier solution was, the more enough the reagent solutions mixed in the flow cell. A flow rate of 4.0 mL min^{-1} was selected considering the stability of peristaltic pump.

The concentration of PMS and Co(II) had a very important effect on the relative CL intensity for the determination of folic

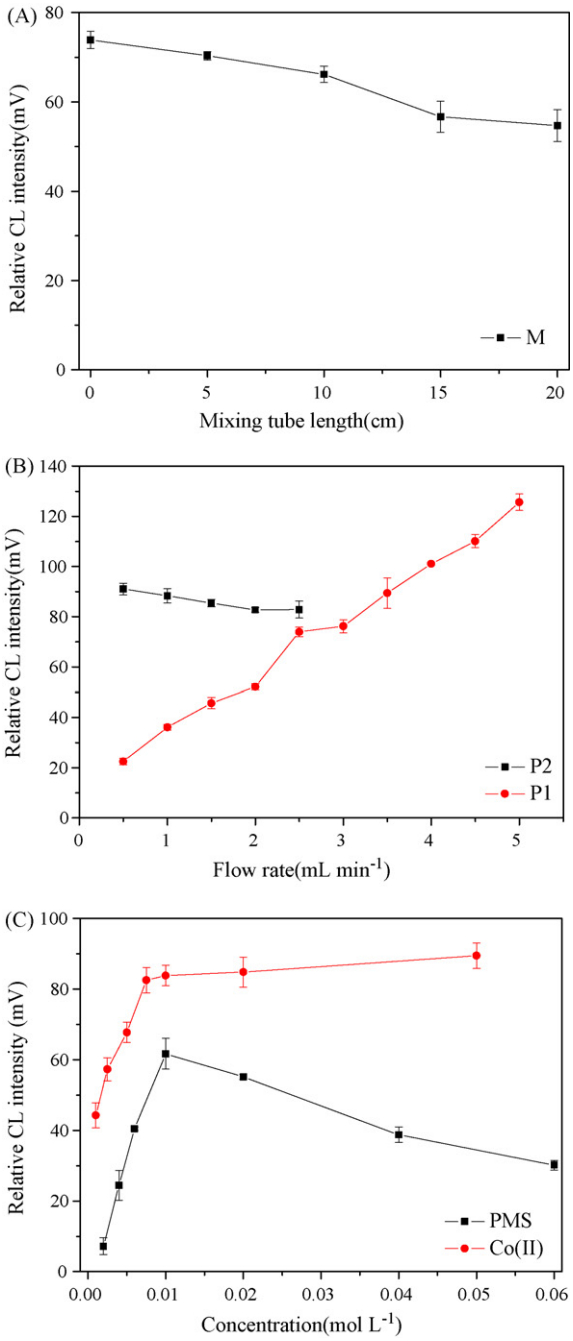

Fig. 3. Effect of mixing tube length (A), flow rate (B) and PMS or Co concentration (C) on relative chemiluminescence intensity in FIA system ($n = 5$).

acid, as is shown in Fig. 3C. The effect of PMS concentration on the CL signal was investigated in the 0.002–0.06 mol L^{-1} range. The relative CL intensity reached its peak at the concentration of 0.01 mol L^{-1} PMS, so it was operated as one of the FIA optimum condition. Although the CL signal increase with the concentration of $CoSO_4$ in the range of 0.001–0.05 mol L^{-1}, the relative CL intensity grew nearly stable when concentration was over 0.01 mol L^{-1}. So the concentration of 0.01 mol L^{-1} $CoSO_4$ was select in further experiments for lower cobalt consumption.

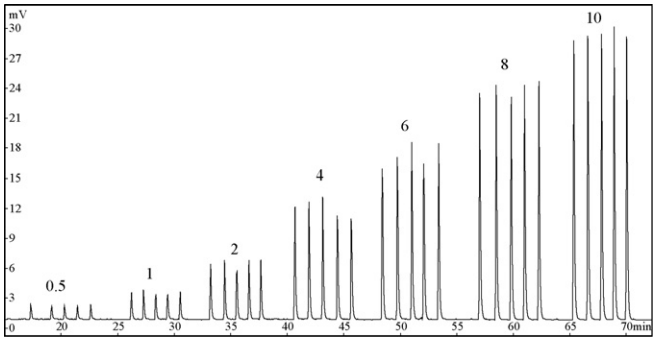

Fig. 4. Typical recorder response for the determination of standard folic acid solution (10^{-8} mol L^{-1}).

3.2.2. Analytical performance

Under the optimum experimental conditions as above, the calibration curve of relative CL intensity versus folic acid concentration over range 10^{-9} to 8×10^{-7} mol L^{-1} was obtained. Fig. 4 shows typical recorder response for the determination of standard folic acid solution. The relative CL intensity which has subtracted the blank from the maximum peak increased linearly with the increasing PGA concentration, as expressed by the equations $\Delta I = 3.095 C_{FA}(10^{-9}$ mol $L^{-1}) + 17.53$ ($R^2 = 0.9991$).

The determination limit was 6×10^{-10} mol L^{-1} (S/N = 3) of folic acid in the PMS/Co(II) system. The present method has a wider linear range and much lower detection limit than previously reported [10–12]. The relative standard deviation was found to be 2.63% by 11 replicate determination of 2×10^{-8} mol L^{-1} folic acid.

3.2.3. Interference studies

The effect of various interferences for determination folic acid was investigated. The tolerable concentration ratios with respect to 2.0×10^{-8} mol L^{-1} folic acid for interference at 5% level were examined. Thousand-fold excess lactose, glucose, fructose, dextrin, starch, magnesium stearate, albumin, Na^+, Al^{3+}, Mg^{2+}, Zn^{2+}, Ca^{2+}, NO_3^-, CO_3^{2-}, HPO_4^{2-}, NH_4^+, 500-fold urea, uric acid, Fe^{2+}, 100-fold ascorbic acid, Cl^-, 10-fold I^-, had almost no effect on the determination of PGA.

3.2.4. Determination of folic acid in pharmaceutical tablets

The excipients of starch, lactose and magnesium stearate in PGA tablets do almost not interfere in the determination, so the flow method proposed has adequate selectivity for the analysis of folic acid in pharmaceutical preparation analysis. The measured folic acid contents are listed in Table 1. The recoveries for PGA in spiked samples were found to be acceptable, between 98 and 104%. The results obtained agreed well with the PGA content that labeled on the bottle of pharmaceutical preparations.

3.2.5. Determination of folic acid in human urine

The proposed method was also applied to the determination of folic acid in human urine samples. Folic acid tablets (10 mg) were took orally in morning with empty stomach. From then on, urine samples were collected in dark glass bottle periodically. After urinary PGA was diluted, it could be determined by this FIA-CL method without any pre-treatment. The results of the

Table 1
Determination of folic acid in tablet samples of different companies

Sample	Sample 1		Sample 2	
	1	2	1	2
Measured (10^{-8} mol L^{-1})	1.14	2.41	1.13	2.42
R.S.D ($n = 5$, %)	3.62	0.77	4.14	5.64
Added (10^{-8} mol L^{-1})	1.00	2.00	1.00	2.00
Total (10^{-8} mol L^{-1})	2.18	4.43	2.11	4.46
Recovery (%)	1.04	1.01	0.98	1.02
Content (mg $tablet^{-1}$)	5.04	5.32	4.99	5.35
Label (mg $tablet^{-1}$)	5.00	5.00	5.00	5.00

Sample 1: Changzhou Pharmaceutical Factory, Sample 2: Tianjin Feiying Pharmaceutical Co. Ltd.

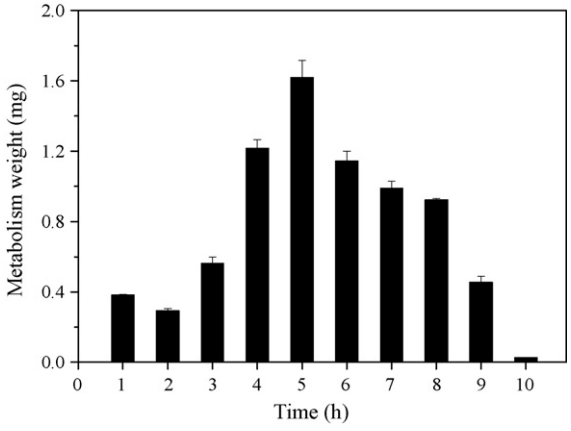

Fig. 5. Metabolism of folic acid in human urine ($n = 3$).

metabolic profile of PGA are shown in Fig. 5. The excretive folic acid reached a maximum in 5 h after taking the tablets, and the total PGA excreted through urine was 7.61 mg in total volume 1551 ml in 10 h.

3.3. The chemiluminescence mechanism of PGA in the PMS/Co(II) system

The transition metal ion-catalyzed decomposition of peroxymonosulfate has been reported by several studies. And cobalt, the best catalyst, activates the PMS through reactions (3)–(5) with the formation of several radical, such as $SO_5^{\bullet -}$, $SO_4^{\bullet -}$, $^{\bullet}OH$, which have been identified by optical pulse radiolysis [14,19–22].

$$HSO_5^- + Co^{2+} \rightarrow SO_4^{\bullet -} + Co^{3+} + OH^- \quad (3)$$

$$HSO_5^- + Co^{2+} \rightarrow SO_4^{2-} + Co^{3+} + {}^{\bullet}OH \quad (4)$$

$$HSO_5^- + Co^{3+} \rightarrow Co^{2+} + SO_5^{\bullet -} + H^+ \quad (5)$$

The evident blank CL emission was yielded from Fig. 2 owing to the formation of singlet oxygen molecular pair, $(^1O_2)_2{}^*$, which has higher energy than the ground state triplet oxygen. CL phenomena occur when the molecular pair lose excess energy and turn to the latter according to reactions (6)–(9) [19,20,23,24].

$$HSO_5^- + SO_4^{\bullet -} \rightarrow SO_5^{\bullet -} + HSO_4^- \quad (6)$$

Table 2
Effect of DABCO on the CL signal

Concentration (mol L^{-1})	Blank (Count)	Signal (Count)
0	64	2351
10^{-6}	52	1895
10^{-5}	45	1592
10^{-4}	32	1383
10^{-3}	11	1244
10^{-2}	Not detected	Not detected

The concentrations of folic acid, HSO_5^-, and Co^{2+} are 10^{-6}, 0.01 and 0.01 mol L^{-1}, respectively. The volume of each reagent is 50 μL.

$$HSO_5^- + {}^{\bullet}OH \rightarrow SO_5^{\bullet -} + H_2O \quad (7)$$

$$2SO_5^{\bullet -} + H_2O \rightarrow 2HSO_4^- + 1.5\,{}^1O_2 \quad (8)$$

$${}^1O_2 + {}^1O_2 \rightarrow ({}^1O_2)_2{}^* \rightarrow 2O_2 + h\nu \quad (9)$$

And the mechanism can be confirmed by the effect of the singlet oxygen quencher 1,4-diazabicyclo[2.2.2]octane (DABCO) [25], as shown in Table 2. The blank and the signal CL emission all decreased with the increasing of the DABCO concentration, and the CL cannot be detected when the DABCO concentration is above 0.01 mol L^{-1}. And it can also infer from the phenomena that the CL signal of the system was given out by energy transfer from higher energy state singlet oxygen.

Which compound acts the energy acceptor and sensitizes the CL emission is a little difficult to interpret. Folic acid might not be the acceptor, because its fluorescence intensity is very weak from Fig. 6. The maximum fluorescence wavelength of folic acid is 446 nm which is different from the maximum CL wavelength located at ca. 460 nm according to Fig. 7. The fluorescence intensity and the adsorption of PGA were decreased to blank very quickly under experimental concentration of PMS and Co(II) solutions, so it is difficult for us to find degradation intermediates that might be CL acceptor.

Interestingly, the fluorescence intensity increased dramatically and the maximum fluorescence wavelength shifted from 446 to 465 nm after folic acid solution was treated with ultraviolet (UV) irritation. High performance liquid chromatography methods have been used for the assay of folic acid and its photodegradation products [26]. The photolysis of folic acid showed that it degraded to pterine-6-carboxylic acid (PCA) and *p*-aminobenzoyl-glutamic acid, as are concluded in Scheme 1. The fluorescence spectrum of UV-irradiated folic acid was quite similar to that of pterine-6-carboxylic acid, which is a strong fluorescence molecule. But the pteridine moiety of folic acid shows very weak fluorescence, which is due to an intramolecular electron transfer from the *p*-aminobenzoyl-glutamic acid moiety to the pteridine moiety [27,28].

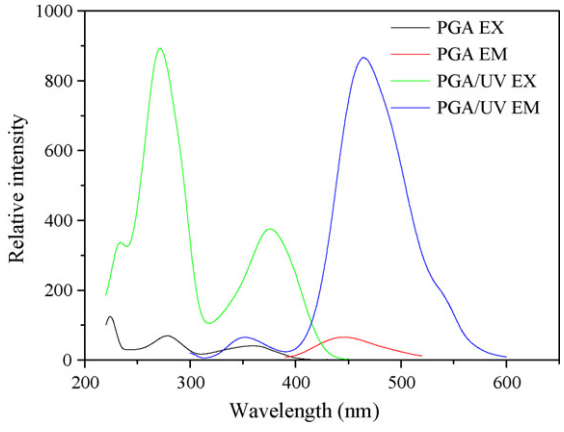

Fig. 6. Fluorescence spectra of folic acid and after irradiated with high pressure mercury lamp for 1 h. The concentration of folic acid was 10^{-5} mol L^{-1}.

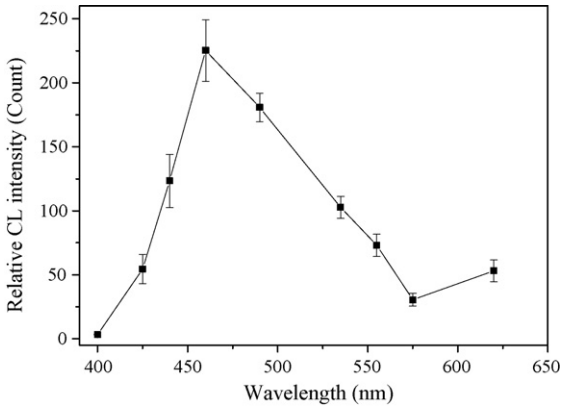

Fig. 7. CL spectra of the Co/PMS/PGA reaction. The concentrations of folic acid, HSO_5^-, and Co^{2+}, are 10^{-6}, 0.01 and 0.01 mol L^{-1} respectively. The volume of each reagent is 50 μL. Batch CL of each spectrum was repeated three times.

The maximum emission fluorescence wavelength of pterine-6-carboxylic acid is 465 nm, which is accordance with the CL spectrum of folic acid in PMS/Co(II) system. It can be inferred that PCA might be the degradation intermediate in PMS/Co(II) system and it also acts an energy acceptor and sensitizes the CL emission. PCA and other intermediates were oxidized to inorganic compound by the radicals, such as $SO_5^{\bullet -}$, $SO_4^{\bullet -}$, ${}^{\bullet}OH$, from the fact that the fluorescence intensity and the adsorption

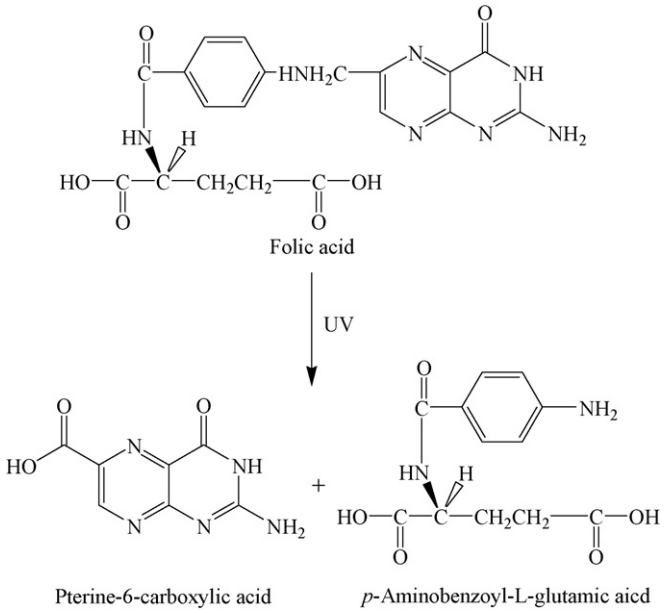

Scheme 1. The photodegration of folic acid.

of PGA were decreased to blank [29]. The chemiluminescence mechanism of PGA in the PMS/Co(II) system can be summarized as the following reactions:

$$\mathrm{PGA} \xrightarrow{\mathrm{PMS/Co(II)}} \mathrm{PCA} + \text{other intermediates} \quad (10)$$

$$^1\mathrm{O_2} + \mathrm{PCA} \rightarrow \mathrm{O_2} + \mathrm{PCA}^* \quad (11)$$

$$\mathrm{PCA}^* \rightarrow \mathrm{PCA} + h\nu\,(465\,\mathrm{nm}) \quad (12)$$

$$\mathrm{PCA} + \text{other intermediates} \xrightarrow{\mathrm{PMS/Co(II)}} \text{inorganic compound} \quad (13)$$

4. Conclusion

A flow-injection chemiluminescence method based on peroxomonosulfate-cobalt(II) system was proposed for determination of folic acid. The presented method had a good sensitivity, selectivity, precision and wider linear range, which allowed application in determination of PGA in pharmaceutical preparations and biological sample analysis. Additionally, the enhancing of the chemiluminescence emission by folic acid due to the energy transfer from $^1\mathrm{O_2}$ to its degradation intermediate pterine-6-carboxylic acid was confirmed.

Acknowledgements

This work was supported by National Natural Science Foundation of China (No. 20575073) and Major Research Program of Chinese Academy of Sciences (KZCX3-SW-432).

References

[1] J. Arcot, A. Shrestha, Trends Food Sci. Technol. 16 (2005) 253.
[2] M. Lucock, Mol. Genet. Metab. 71 (2000) 121.
[3] S. Zhao, H. Yuan, C. Xie, D. Xiao, J. Chromatogr. A 1107 (2006) 290.
[4] L.M. Wallock, T. Tamura, C.A. Mayr, K.E. Johnston, B.N. Ames, R.A. Jacob, Fertil. Steril. 75 (2001) 252.
[5] A. Leporati, D. Catellani, M. Suman, R. Andreoli, P. Manini, W.M.A. Niessen, Anal. Chim. Acta 531 (2005) 87.
[6] B.C. Nelson, K.E. Sharpless, L.C. Sander, J. Chromatogr. A 1135 (2006) 203.
[7] J. Arcot, A.K. Shrestha, U. Gusanov, Food Control 13 (2002) 245.
[8] J.-M. Lin, X. Shan, S. Hanaoka, M. Yamada, Anal. Chem. 73 (2001) 5043.
[9] M. Liu, L. Zhao, J.-M. Lin, J. Phys. Chem. A 110 (2006) 7509.
[10] A.A. Al-Warthan, Anal. Sci. 10 (1994) 919.
[11] F. Nie, Y. He, J. Lu, J. Microchem. 65 (2000) 319.
[12] Z. Song, X. Zhou, Spectrochim. Acta Part A 57 (2001) 2567.
[13] D.L. Ball, J.O. Edwards, J. Am. Chem. Soc. 78 (1956) 1125.
[14] G.P. Anipsitakis, D.D. Dionysiou, Environ. Sci. Technol. 38 (2004) 3705.
[15] M. Wang, L. Zhao, J.-M. Lin, Luminescence 22 (2007) 182.
[16] G.P. Anipsitakis, D.D. Dionysiou, M.A. Gonzalez, Environ. Sci. Technol. 40 (2006) 1000.
[17] S. Tsukada, H. Miki, J.-M. Lin, T. Suzuki, M. Yamada, Anal. Chim. Acta 371 (1998) 163.
[18] M. Wang, L. Zhao, M. Liu, J.-M. Lin, Spectrochim. Acta Part A 66 (2007) 1222.
[19] J.-M. Lin, M. Yamada, Anal. Chem. 72 (2000) 1148.
[20] P. Maruthamuthu, P. Neta, J. Phys. Chem. 81 (1977) 937.
[21] G.P. Anipsitakis, E. Stathatos, D.D. Dionysiou, J. Phys. Chem. B 109 (2005) 13052.
[22] J.G. Muller, P. Zheng, S.E. Rokita, C.J. Burrows, J. Am. Chem. Soc. 118 (1996) 2320.
[23] Z. Zhang, J.O. Edwards, Inorg. Chem. 31 (1992) 3514.
[24] J. Stauff, H. Schmidkunz, G. Hartmann, Nature 198 (1963) 281.
[25] C. Ouannes, T. Wilson, J. Am. Chem. Soc. 90 (1968) 6527.
[26] M.J. Akhtar, M.A. Khan, I. Ahmad, J. Pharm. Biomed. Anal. 19 (1999) 269.
[27] K. Hirakawa, H. Suzuki, S. Oikawa, S. Kawanishi, Arch. Biochem. Biophys. 410 (2003) 261.
[28] J.-C. Huang, D.-J. Li, J.-C. Diao, J. Hou, J.-L. Yuan, G.-L. Zou, Talanta 72 (2007) 1283.
[29] G.P. Anipsitakis, D.D. Dionysiou, Environ. Sci. Technol. 37 (2003) 4790.

Available online at www.sciencedirect.com
ScienceDirect
Talanta 74 (2008) 1400–1407
Talanta
www.elsevier.com/locate/talanta

Indirect fluorescent determination of selected nitro-aromatic and pharmaceutical compounds via UV-photolysis of 2-phenylbenzimidazole-5-sulfonate

Wei Zhang, Christopher R. Wilson, Neil D. Danielson *

Department of Chemistry and Biochemistry, Miami University, Oxford, OH 45056, United States

Received 28 January 2006; received in revised form 18 September 2007; accepted 19 September 2007
Available online 29 September 2007

Abstract

An indirect fluorescence (FL) detection method via the reactivity of UV-photolyzed 2-phenylbenzimidazole-5-sulfonate (PBSA) has been developed for non-fluorescent aromatic compounds. At high pH with UV photolysis, PBSA in the excited state is known to be quenched by reaction with oxygen species and analyte compounds that are reactive toward these oxygen species produced during photolysis can lessen the loss of PBSA FL. After off-line photolysis of PBSA in the presence of various nitro-aromatic test compounds, the increase in PBSA FL is clearly evident. A flow injection (FI) instrument using a PBSA mobile phase propelled through a Teflon coil wrapped around a Hg lamp is optimized and modified for use for liquid chromatography (LC). For the on-line FI determination of the non-fluorescent nitro-aromatic compounds such as 4-nitroaniline, 2-nitrophenol, 3-nitrophenol, 4-nitrophenol, and α-nitronaphthalene, a positive linear response for PBSA FL from about 0.5 to 15 μM and detection limits generally between 0.2 and 1 μM (4–20 pmol) are found. Linear responses and detection limits of selected pharmaceutical compounds such as the antibacterial nitrofurantoin, antihistamines chlorpheniramine and brompheniramine, and other compounds were similar. In general, detection limits using UV detection at about 214 nm were not as good in the 1–2 μM range but linearity extended up to 100 μM. The amino acid phenylalanine and small peptides containing this aromatic amino acid were also determined using this method. Application of this detection method for the liquid chromatography determination of 4-nitroaniline, 2-nitrophenol, nitrofurantoin, and salicylate is shown.
© 2007 Elsevier B.V. All rights reserved.

Keywords: Indirect fluorescence detection; 2-Phenylbenzimidazole-5-sulfonate; Nitro-aromatic compounds; Antihistamines; Amino acids

1. Introduction

For reproducibility and selectivity, aromatic compounds are often determined by flow injection (FI) or liquid chromatography (LC) with fluorescence (FL) detection. For those non-fluorescent or weakly fluorescent aromatic compounds, e.g. nitro or halogen functional group-substituted aromatics, chemical derivatization that introduces fluorophores to those molecules is generally required for FL detection [1–3]. Off-line derivatization procedures for nitro-aromatics accommodate reaction versatility, but sometimes extreme conditions, e.g. long reaction times and time-consuming sample purification and preconcentration procedures are required [4–6]. Therefore, some on-line derivatization techniques have been published for FL detection of non-fluorescent compounds such as aminoglycoside antibiotics [7] and polyamines [8] using a Cu^{2+}–tryptophan ligand displacement reaction. After LC separation, weakly fluorescent phenols were oxidized electrochemically on-line to dimers and higher oligomers before fluorescent detection [9]. Nitro-substituted polynuclear aromatic hydrocarbons can be determined by FL detection method via post-column reduction of the NO_2 group to NH_2 using either a catalyst column packed with alumina particles coated with Pt or Pd metal [10] or an electrochemical cell [11]. Lifetime and fouling of the column or electrode could be problematic.

Photochemical derivatization, applied to pharmaceuticals such as methotrexate [12], chloramphenicol [13], sulfamethazine [14], and efavirenz [15] as well as agricultural products such as pesticides [16,17], pyrethoids [18], and benzoylureas [19], can lead to the formation of strongly fluorescent photoproducts. The FL response of dansyl derivatives of chlorophenols can be enhanced by several orders of magnitude after photo-

* Corresponding author.
E-mail address: danielnd@muohio.edu (N.D. Danielson).

0039-9140/$ – see front matter © 2007 Elsevier B.V. All rights reserved.
doi:10.1016/j.talanta.2007.09.016

chemical reaction [20]. Because UV light is used instead of chemical reagents, on-line photochemical derivatization is simple and flexible as compared to on-line chemical derivatization approaches. However, application of photochemical derivatization is restricted to certain types of photoreactive compounds or drugs that can efficiently convert into fluorophores under UV irradiation. Nitro-aromatic compounds such as 2-nitrophenol can be degraded photolytically batch wise in suspensions of titanium dioxide [21] but analytical flow studies using on-line detection are uncommon [22].

2-Phenylbenzimidazole-5-sulfonate (PBSA) is a UV-B sunscreen agent with characteristic UV absorbance at 302 nm and strong fluorescence in both the UV and visible light regions [23]. PBSA is also a photoreactive compound that readily undergoes photodecomposition in alkaline solution under UV irradiation [24], resulting in a marked decrease in FL. It has been reported that PBSA acts as a sensitizer for photogeneration of singlet oxygen ($^1O_2$) and superoxide ($O_2^{\bullet -}$) that are capable of damaging DNA [25]. Those oxygen species could also be the cause for PBSA radical formation [26]. PBSA in an alkaline solution was shown to react with nitromethane or nitrobenzoic acid to give the corresponding nitro anion radicals [26]. Compounds that are reactive toward these oxygen species can protect PBSA in the excited state promoting the possibility of FL.

To the best of our knowledge, analytical consideration of this PBSA reaction for the indirect determination of particularly non-fluorescent organic compounds with FL detection has not been made. Nitro-aromatics including 4-nitroaniline, 2-nitrophenol, 3-nitrophenol, 4-nitrophenol, and α-nitronaphthalene were considered as representative non-fluorescent test compounds. Nitrophenols can be intermediates in the synthesis of many drugs, dyes, and various pesticides as well as major metabolic or photolytic degradation products [27], some widely present in the environment. Nitroaniline is widely produced as a dye or pesticide intermediate and is also used as a photoinitiator of polymerization processes [28]. Off-line photolysis of PBSA in the presence of these test compounds showed an increase in PBSA FL that was clearly evident indicating this approach was analytically viable. The optimization of experimental conditions for photolysis and FL detection was investigated with a FI instrument using PBSA propelled through a Teflon coil wrapped around an Hg lamp. Detectability by FI of selected pharmaceutical compounds such as the antibacterial nitrofurantoin, antihistamines chlorpheniramine and brompheniramine, and other compounds such as amino acids showed wide applicability of this PBSA FL method. Modification of this FI instrument for the LC determination of nitro-aromatic compounds was shown.

2. Experimental

2.1. Chemicals and solutions

2-Phenylbenzimidazole-5-sulfonic acid, 4-nitroaniline, 2-nitrophenol, 3-nitrophenol, 4-nitrophenol, 4-nitrobenzoic acid, α-nitronaphthalene, and *tert*-octylamine were purchased from Aldrich (Milwaukee, WI). Nitrofurantoin, chlorpheniramine, brompheniramine, sodium salicylate, gallic acid, atropine, and the selected amino acids were provided from Sigma (St. Louis, MO). *Trans*-cinnamic acid was purchased from Tokyo TCI (Tokyo, Japan). LC grade methanol (MeOH) and acetonitrile (MeCN) were obtained from Burdick & Jackson (Muskegon, MI) and Pharmaco (Brookfield, CT), respectively. All other chemicals used are at least of analytical reagent grade as well. Distilled, deionized water used for preparation of solutions was taken from the E-Pure deionization system (Barnstead, Dubuque, IA).

A 1 mM PBSA stock solution was prepared daily by dissolving 0.028 g of PBSA in 1 mL of 0.2 M NaOH solution and then diluting to 100 mL with water. PBSA solutions of 100 μM (pH 7 and 12) for off-line photolysis studies were prepared by a 10-fold dilution of PBSA stock solution with 0.1 M potassium phosphate monobasic buffer solution (pH 7) or a NaOH/KCl solution (pH 12). PBSA solutions of 1 μM for off-line studies were obtained from serial dilution of the PBSA stock solution with NaOH/KCl (pH 12). For the study of the pH effect on FL detection in HPLC, dibasic phosphate and NaOH/KCl solutions described in the literature [29] were used to prepare 2 μM PBSA solutions with the pH values in the range between 11.6 and 12.6. All PBSA solutions were stored in flasks or vials that were covered with aluminum foil to avoid light and kept in the dark when not in use.

Most of the 1 mM stock sample solutions used for FI or LC were prepared in aqueous solution except α-nitronaphthalene and gallic acid which were made in MeCN. Salicylate, *trans*-cinnamic acid, and nitrofurantoin stock solutions required dissolution of the solid in 2 mL of 0.2 M NaOH solution and then dilution with water to 100 mL. For LC analysis, a 1 mM nitrofurantoin stock solution was prepared in MeCN. For the LC–MS study, a 10 mM *tert*-octylamine stock solution was prepared by mixing an equimolar amount of 0.877 mL *tert*-octylamine (95%) and 0.287 mL acetic acid (100%) in 10 mL MeOH and then diluting to 500 mL with water. All flasks and vials containing light sensitive sample solutions were covered with aluminum foil and stored in a dark cabinet.

2.2. Apparatus

The instrumental setup for FI and LC determination of aromatic compounds with on-line FL detection via shielding of the photolysis of PBSA is given in Fig. 1. Ultra-plus micro LC pumps (pump #1 and pump #2) (Micro-Tech Scientific, Sunnyvale, CA) were used to transport the non-degassed sample carrier buffer in the FI system (Fig. 1A) or the mobile phase and PBSA solutions in the LC instrument (Fig. 1B). Samples of interest were injected using a Rheodyne model 7125 injection valve with a 20 μL loop. A MetaChem Polaris C18-A 3 μm HPLC column (50 mm × 4.6 mm i.d.) (ANSYS Technologies, Lake Forest, CA) was used to separate aromatic analytes in the sample mixture. Two tandem photoreactors were necessary for on-line UV photolysis of PBSA and analyte mixture solutions that were usually premixed before injection for FI or combined on-line using a low dead volume mixing tee for HPLC. Each one was made from 3048 mm (*l*) × 1.6 mm (o.d.) × 0.25 mm

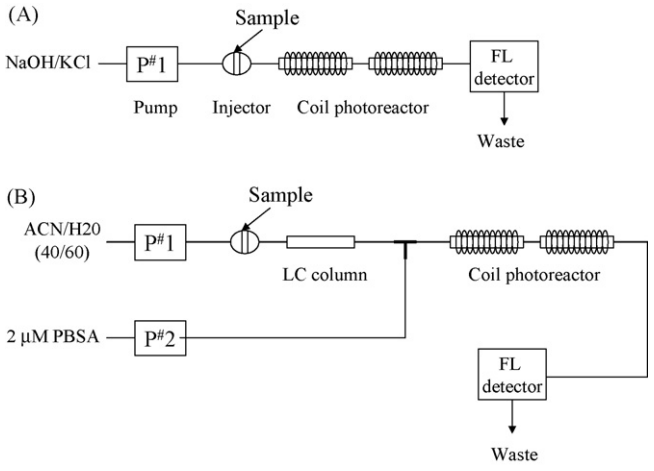

Fig. 1. Instrumental set-up for the indirect FL determination of aromatic compounds by (A) FI and (B) LC.

(i.d.) fluoroethylene polymer (FEP) tubing (Upchurch Scientific, Oak Harbor, WA) circling around a NIPPO GL4 Hg lamp. These lamps have strong emission at 254 nm. Oxygen permeability through such Teflon tubing is well known. The FL emission of photolyzed samples was measured at 350 nm using a Shimadzu RF-551 spectrofluorometric detector (Shimadzu, Columbia, MD) with an excitation wavelength set at 302 nm. FL signals were recorded as FI peak heights (mV or FL signal units) or LC peak areas (μV s) by a Shimadzu Chromatopac C-R6A integrator. Using the same instrument set-up, FI with UV detection at the specified wavelength was done using a Shimadzu Model SPD-6AV UV–vis LC detector.

The off-line photolysis experiments were carried out in a round 5 mL quartz cell placed against a NIPPO GL4 Hg lamp. FL spectra of photolyzed sample solutions were measured using a Perkin Elmer LS 55 luminescence spectrometer (Perkin Elmer, Boston, MA) with an excitation wavelength of 302 nm. Absorption spectra of PBSA and analyte samples were recorded using a Hewlett-Packard 8453 UV–vis spectrophotometer (Agilent, Palo Alto, CA). MS spectra of photolyzed PBSA samples were obtained using an Esquire electrospray ion trap mass spectrometer (Bruker Daltonics, Billerica, MA) interfaced to a Hewlett-Packard series 1100 LC equipped with a binary mobile phase delivery system and vacuum degasser, an autosampler, and a variable wavelength UV–vis detector. A MetaChem Polaris C18-A 3 μm HPLC column (50 mm × 4.6 mm i.d.) was used to separate PBSA and its associated photolyzed species from the sample matrix.

2.3. Procedures

2.3.1. Off-line photolysis of PBSA and PBSA with aromatic compounds

A 4 mL volume of 100 μM PBSA prepared in pH 7 and 12 solution were photolyzed for 0, 15, 45 min. A 100-fold dilution of the PBSA samples after photolysis was required before taking the FL spectra. UV absorption spectra were obtained directly from the photolyzed samples without further dilution.

PBSA aqueous solutions of 100 μM (pH 12) were photolyzed for 0, 30 and 60 min. A 250 μL volume of each photolyzed sample was diluted with 750 μL MeOH before a 20 μL injection into the LC–MS. The mobile phase for the separation of anionic PBSA and its associated species by LC–MS was 40/60 MeOH/H_2O (v/v) in the presence of 2.5 mM *tert*-octylamine (b.p. 137–143 °C) as an ion-pairing agent. The flow rate of the mobile phase was set at 320 μL/min and the negative ionization mode was chosen for ESI-MS. Nitrogen dry gas, temperature, and nebulizer pressure were set at 9 L/min, 365 °C, and 40 psi, respectively. The capillary high voltage was set at 3500 V. Total-ion current chromatograms and MS spectra of photolyzed PBSA samples were obtained and the number of spectra averaged was four.

Seven aqueous solutions containing 1 μM PBSA and 4-nitroaniline with concentrations from 0.1 to 15 μM were prepared in a pH 12 buffer solution. The 4 mL sample solution was photolyzed for 30 min before the FL spectrum was taken. To study the protecting effect of other aromatic compounds, 1 μM PBSA aqueous solutions each containing 5 μM 4-nitrobenzoate, sodium salicylate, 3-nitrophenol, 2-nitrophenol, 4-nitrophenol, and 4-nitroaniline were prepared with a pH 12 buffer solution. Their FL spectra were taken after 30 min UV photolysis of each 4 mL sample solution.

2.3.2. Flow injection and LC of aromatic compounds

After experimental factors, including PBSA concentration, flow rate, and solvent were investigated by FI, 10–12 standard solutions for each analyte containing 2 μM PBSA with concentrations from 0.1 to 100 μM were prepared by appropriate dilution of their stock solutions with pH 12 NaOH/KCl buffer solution. The non-degassed pH 12 NaOH/KCl solution was used as a FI mobile phase. With a flow rate of 175 μL/min, five injections for each standard solution generated a calibration curve for each aromatic compound. Sensitivity, detection limit, and linear range for this FI indirect FL detection method were compared to direct UV detection. Sensitivity was the slope of the calibration curve. Detection limits were calculated from the sum of the intercept + three times the standard deviation of five replicate FL measurements of a 2 μM PBSA solution divided by the sensitivity. FL linearity was determined for the maximum concentration range providing a minimum correlation coefficient of 0.995. The lower level was generally approximately the limit of quantitation value and/or the lowest measured concentration that did not show more than 20% R.S.D. ($n = 4$). The upper level limit for linearity was the analyte concentration that deviated not more than 5% from its linear theoretical value. UV linearity correlation coefficients were all 0.999 or better and the upper level limit for linearity was likely beyond the most concentrated measured value (generally 100 μM).

Concentration, flow rate, and pH of the PBSA solution delivered from pump #2 were optimized for indirect FL detection with LC by separation of a three-component standard mixture that contained 25 μM nitrofurantoin, 5 μM 4-nitrophenol, and 4-nitroaniline. Under flow conditions of 150 μL/min with a 40/60 MeCN/H_2O mobile phase from pump #1 and 125 μL/min for a non-degassed 2 μM PBSA solution (pH 12) from pump

#2, a five-component standard mixture that was made up of salicylate, nitrofurantoin, 4-nitroaniline, 4-nitrophenol, and 2-nitrophenol was separated by HPLC. Thirteen five-component standard solutions with concentrations from 1 to 100 μM for nitrofurantoin and concentrations from 0.1 to 40 μM for the other four components were injected four times for each standard mixture to generate the calibration curves for this LC method.

3. Results and discussion

3.1. Off-line photolysis of PBSA

Before the development of the on-line indirect FL detection method based on the protection by analytes on the photolysis of PBSA, experimental effects including pH, photolysis time, and reaction scope were studied by off-line photolysis of PBSA. Reverse phase ion-pair LC–MS was also used to study the photolyzed PBSA sample.

3.1.1. pH and photolysis time

FL spectra of the photolyzed PBSA standard are shown in Fig. 2A. Photolysis of the PBSA aqueous solutions proceeded slowly at pH 7 as compared to that at pH 12 consistent with previous work [26]. A decrease of FL intensity by approximately one third of the original value was observed after UV photolysis of 100 μM PBSA solution at pH 12 for 15 min (spectrum (e)). UV absorption spectra of a PBSA sample photolyzed at pH 7 and 12, which are shown in Fig. 2B, exhibited similar results to the florescence data with little change at pH 7 and a matched absorbance decrease at pH 12. The UV absorbance displayed a large change at 217, 247, and 302 nm before and after UV photolysis of PBSA at pH 12 for 45 min, which can be observed in the inserted diagram in Fig. 2B, similar to previous work [24]. The existence of different absorbance and florescence spectra for aqueous PBSA under neutral and alkaline pH is the result of the difference in the electronic distribution in the ground state and excited states because the singly charged PBSA anion ($pK_{a1} = 5.23$) and doubly charged PBSA anion ($pK_{a2} = 11.91$) are formed at pH 7 and 12, respectively. The reasons for a fast photodecomposition of PBSA in alkaline solution were not clear. Besides the excited states of PBSA, pH might affect the photogeneration of oxygen species such as singlet oxygen ($^1O_2$) and superoxide ($O_2^{\bullet -}$) that were believed to be involved in the self-oxidation of PBSA during the UV photolysis [26]. From our previous work on photooxidation of phenolic compounds, phenol, nitrophenols, and chlorophenol were reactive toward oxygen species generated from photolysis [30]. The reactivity order in that work was 4-nitrophenol > 2-nitrophenol > 3-nitrophenol, which is in accordance with sensitivity results from the current study (Fig. 3). The FL response of six PBSA photolyzed mixtures containing 4-nitroaniline from 0.1 to 10 μM increased systematically showing the analytical potential of this method (data not shown).

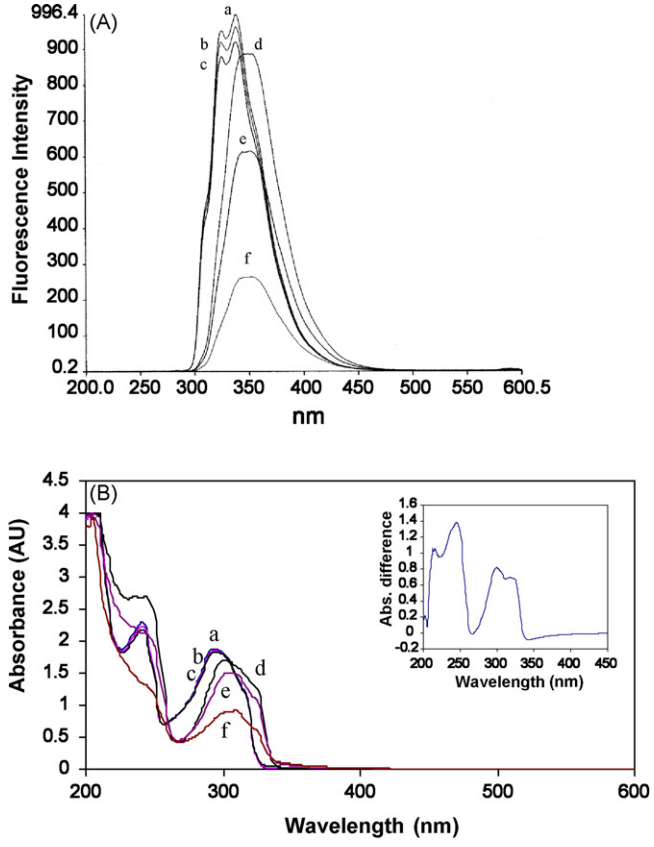

Fig. 2. Molecular spectra showing the effect of pH and photolysis time on the off-line photolysis of PBSA: (A) FL spectra obtained after a 100-fold dilution of the 100 μM PBSA solutions and (B) UV spectra obtained from 100 μM PBSA solutions with the inserted plot of UV absorbance difference before and after photolysis for 45 min vs. wavelength. Photolysis of 100 μM PBSA (pH 7): (a) 0 min; (b) 15 min; (c) 45 min. Photolysis of 100 μM PBSA (pH 12): (d) 0 min; (e) 15 min; (f) 45 min.

3.1.2. Study of photolyzed PBSA standards by reverse phase ion pair LC–MS

The total ion current (TIC) chromatograms consisted of two major peaks, the sample matrix peak eluted around

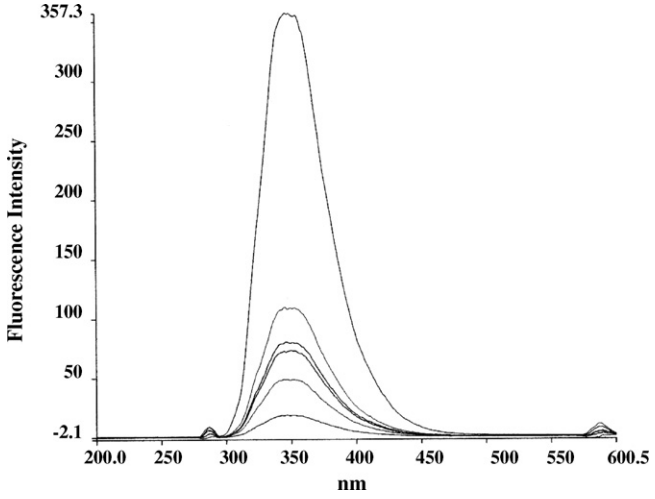

Fig. 3. Off-line photolysis of PBSA with various analytes. FL spectra of 1 μM PBSA solutions (pH 12) containing 5 μM of 4-nitrobenzoate, sodium salicylate, 3-nitrophenol, 2-nitrophenol, 4-nitrophenol, and 4-nitroaniline (in order of increasing peak height) after 30 min photolysis.

2 min, and the PBSA peak eluted around 7.5 min. Ions in the sample matrix peak due were mostly cluster ions that were made up of K^+, Na^+, Cl^-, and sulfonate (SO_3^-) ions. The MS spectra of photolyzed PBSA samples contained *m/z* 273.3 (deprotonated molecular ion $[M-H]^-$), 193.7 (desulfonated ion $[M–SO_3–H]^-$), 222.8 ($[(M–SO_3–H)+CHO]^-$), 315.3 ($[Ø(NHCOph)_2–H]^-$ or $[Ø(NHCOph)(NH_2)(COph)]^-$) generated from the oxidative breakage of the imidazole ring), 340.7 ($([Ø(NHCOph)(NHCOH)(SO_3Na)–H]^-$), 359.4 ($[Ø(NHCOph)_2(COOH)–H]^-$), 547.2 (PBSA dimer anion $[2M-H]^-$), 569.4 ($[2M-2H+Na]^-$), 585.0 ($[2M-2H+K]^-$), 821.0 ([PBSA trimer anion $[3M-2H]^-$), 842.9 ($[3M-3H+Na]^-$), and 858.9 ($[3M-3H+K]^-$). Photolysis had a great effect on the intensity and chemical composition of ions comprised in the PBSA sample peak as shown in the total ion current chromatograms. As compared to the ion intensity of PBSA and its associated species before photolysis, a decrease of ion intensity (all ratios less than 1) by a range of 31–79% for 30 min photolysis and 54–98% for 60 min photolysis was observed for ions with *m/z* values at 193.7, 222.8, 273.3, 547.2, and 821. However, a remarkable increase in ion intensity from the original values obtained with intact PBSA (all ratios greater than 1) by 35–65% for 30 min photolysis and 105–139% for 60 min photolysis was generated for ions with *m/z* values at 315.4, 340.7, and 359.3. The presence of those ions that had increased ion intensity with photolysis time indicated that the opening of the benzimidazole ring in the PBSA molecular structure could occur leading to the formation of products that exhibited weak or non-fluorescence. Photogenerated active oxygen species are considered the most possible agents to attack the benzimidazole ring but further study is needed of what we believe is a previously unreported ring opening reaction for PBSA.

3.2. Application of the indirect FL detection method for on-line determination of aromatic compounds by FI

The effects of experimental conditions such as PBSA concentration, flow rate, and organic solvent composition on the on-line photolysis of PBSA were optimized by measuring the FL intensity ratios of PBSA samples without and with UV photolysis. A large ratio of FL(UV-off)/FL(UV-on) (peak area/peak area) represented a high photolysis efficiency. Using FI, linearity and detection limits for selected aromatic compounds were compared between this on-line FL detection method and direct UV detection.

3.2.1. PBSA concentration

Fig. 4 shows the effect of PBSA concentration on the photodecomposition of PBSA. The FL intensity ratio increased rapidly with PBSA concentrations from 0.05 to 0.4 μM but just had a little change from 0.4 to 2 μM. A large decrease in the FL intensity ratios occurred when PBSA concentrations were increased in the range of 2–16 μM. Although the photolysis efficiencies for 0.4 and 2 μM PBSA samples were close to each other, FL signal intensity (peak height) for 2 μM PBSA samples with and without photolysis was 117.4 and 890.8, respectively, as compared to 22.8 and 180.6 for 0.4 μM PBSA. To make this detection method sensitive, 1 or 2 μM PBSA was used for the remaining FI work.

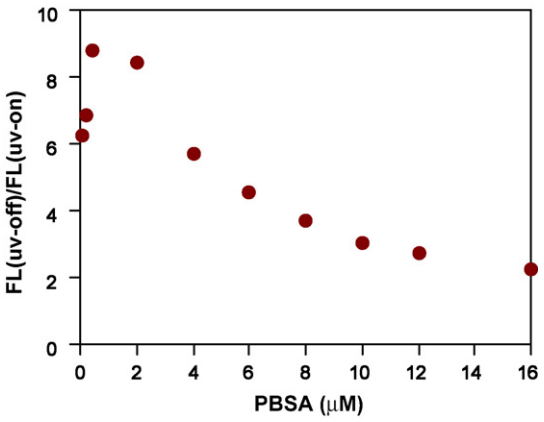

Fig. 4. Concentration effect on the on-line photolysis of PBSA as measured by the FL intensity ratio. A 20 μL volume of each PBSA sample (pH 12) with concentration in the range from 0.04 to 16 μM was injected into the FI system. Flow rate of sample carrier buffer (pH 12) was set at 200 μL/min. The ratio of FL intensity without and with UV photolysis was used to represent the photolysis efficiency. R.S.D. for these data ranged from 0.2 to 2.6% ($n=4$).

3.2.2. Flow rate

Flow rate controlled both the photolysis and analysis times. Using 2 μM PBSA, the FL intensity ratio increased from 2 to 16 as the flow rate decreased from 500 to 150 μL/min. Fig. 5 shows the effect of flow rate as measured by FL peak area on the photolysis of 2 μM PBSA using three aromatic amino acid test compounds. Low flow rate leaded to high photodecomposition yields. The optimum flow rate range was from 150 to 200 μL/min for all three compounds. On-line photolysis at the flow rate of 175 μL/min was considered to optimum to provide good sample throughput.

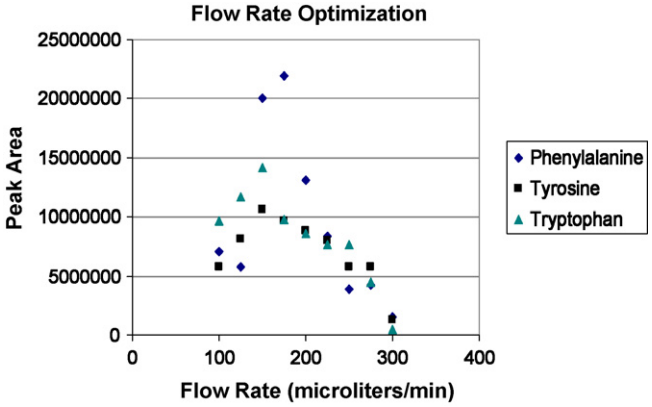

Fig. 5. Flow rate effect on the on-line photolysis of PBSA as measured by the FL peak area. Standard solutions of three amino acids (20 μM phenylalanine, 10 μM tyrosine, and 10 μM tryptophan) were injected into the FI system with 1 μM PBSA in the mobile phase at flow rates in the range between 100 and 300 μL/min.

Table 1
Quantitative study of nitro-aromatic compounds comparing the PBSA FI and UV FI methods

Compound	FL sensitivity, mV/μM	FL detection limit, μM (mg/L)	FL linear range, μM (n = #)	UV sensitivity Abs., μM	UV detection limit, μM	UV linear range[a], μM (n = #)
4-Nitrophenol	34.0	0.2 (0.03)	0.5–10 (7)	0.0016	1.9	3–100 (11)
2-Nitrophenol	29.6	0.2 (0.03)	0.5–10 (8)	0.0026	1.2	2–100 (10)
3-Nitrophenol	25.5	0.2 (0.03)	0.5–10 (6)	0.0024	1.3	2–100 (10)
4-Nitroaniline	28.9	0.2 (0.03)	0.5–5 (5)	0.0017	1.8	3–200 (10)
1-Nitro-naphthalene	12.5	1.0 (0.2)	1–15 (6)	0.0032	0.9	2–100 (10)
4-Nitrobenzoate	1.4	4.3 (0.7)	5–75 (9)	0.0016	1.9	3–100 (9)

[a] UV wavelength at 226 nm for nitrophenols and nitroaniline; other compounds at detected at 214 nm.

Table 2
Quantitative study of selected aromatic carboxylates and pharmaceutical compounds comparing PBSA FI and UV FI methods

Compound	FL sensitivity, mV/μM	FL detection limit, μM (mg/L)	FL linear range, μM (n = #)	UV sensitivity Abs., μM	UV detection limit, μM	UV linear range, μM (n = #)
Salicylate	20.5	0.3 (0.04)	0.5–10 (6)	0.0021	1.4	2–100 (9)
Trans-cinnamate	3.8	1.6 (0.2)	5–40 (4)	0.0015	2.0	3–100 (11)
Gallate	2.7	4.7 (0.8)	5–50 (7)	0.0011	2.7	5–100 (11)
Atropine	18.2	0.3 (0.09)	0.5–8 (6)	0.0022	1.4	2–100 (11)
Chlorpheniramine	9.1	0.7 (0.2)	1–15 (9)	0.0027	1.1	2–100 (12)
Brompheniramine	8.4	0.7 (0.2)	1–15 (9)	0.0026	1.1	2–100 (12)
Nitrofurantoin	5.0	1.2 (0.3)	5–50 (9)	0.0029	1.0	2–100 (10)

UV wavelength for all compounds at 214 nm except the pheniramines (209 nm).

3.2.3. Solvent

On-line photolysis of 2 μM PBSA samples prepared in MeCN–H_2O and MeOH–H_2O was about a factor of 3–4 less than in aqueous solution. The influence of increasing organic solvent content from 5 to 30% on photolysis showed a slightly downward trend for the FL intensity ratio. A considerable decrease of the FL intensity ratio occurred for increasing MeOH content in the range from 1.25 to 5%. The reason that photolysis of PBSA in MeCN–H_2O was a little more efficient than in MeOH–H_2O was not clear. The solvent polarity parameters P' for MeOH and MeCN are similar (5.1 and 5.8, respectively) but there could be some effect on the excited states of PBSA, which are important for the photogeneration of active oxygen species.

3.2.4. Flow injection determination of aromatic compounds

Tables 1 and 2 list FL and UV sensitivity, linearity, and detection limit data for the nitro-aromatic compounds and selected aromatic carboxylate, pharmaceutical compounds, respectively. Example FL calibration curves are shown in Fig. 6. The nitrophenols and salicylate showed higher FI sensitivities and better detection limits than 4-nitrobezoate. The phenolic group may likely be effective in protecting PBSA from reaction with oxygen species in the photochemical reaction. Atropine was also similar to the phenols in detectability possibly due to the hydroxymethyl group in the alpha position on the benzene ester structure. Calibration data for 4-nitroaniline indicated similar sensitivities and detection limits to the nitrophenols. Higher sensitivity and a better detection limit were noted for nitronaphthalene and the pheniramines as compared to nitrofurantoin, *trans*-cinnamic acid, and gallic acid. Gallic acid is quite unstable and oxidized rapidly in alkaline solution [31]. UV detection limits of 1–2 μM were generally not as good as FL with the exception of 4-nitrobenzoate and gallate. However, UV linearity consistently extended up to at least 100 μM.

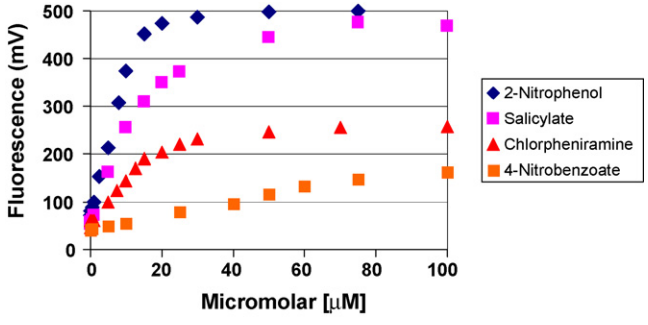

Fig. 6. Calibration curves for 2-nitrophenol, salicylate, chlorpheniramine, and salicylate. The FL relative standard deviation (R.S.D.) values for all the compounds in Tables 1 and 2 with a concentration of 5 μM are in the range of 0.7–3.4% (n = 5).

Primarily optical chemical sensor-based FL quenching detection techniques have been reported for the direct determination of nitro-aromatic compounds without prederivatization [32–35]. The sensor-based detection limits for 4-nitrophenol [32], 2-nitrophenol [33], nitrofurantoin [34], 2-nitroaniline [35] are 10, 80, 0.48, and 0.1 μM, respectively, but detection of 4-nitroaniline is not as sensitive as 2-nitroaniline. Atropine can also be detected at 4.3 μM by this optical sensor method [36]. As compared to our FL detection method, those sensor methods are about 12–380 times higher in terms of detection limit although sensor detection of nitrofurantoin is better. Furthermore, sensor response times from 10 s to min are generally required to get stable quenched FL signals and this response recovery time may prevent continuously monitoring of analytes in a flow stream,

such as FI and LC. The FL detection limits in Table 1 are comparable to a previous indirect on-line FL derivatization reaction for polyamines [8] involving displacement of Cu^{2+} from the tryptophan–Cu^{2+} complex freeing tryptophan.

Amino acids such as phenylalanine, tyrosine, and tryptophan have also been determined using this PBSA FI method. Detection limits for tyrosine and tryptophan were 1 μM (both 0.2 mg/L) while that for phenylalanine (Phe) was 2 μM (0.3 mg/L). Peptides such as Phe-glycyl-glycine, Phe-alanine, and the chemotactic compound *N*-formyl-methionine-leucine-Phe showed detection limits from 2 to 8 μM. Linearity data for Phe and the peptides were similar to that for chlorpheniramine in Fig. 6. Compared to direct fluorescence of Phe and tyrosine by FI using their respective optimum excitation and emission wavelengths, the PBSA FI method was about four times more sensitive for Phe but only two times more sensitive for tyrosine. Not too surprising, the direct fluorescence FI method for tryptophan was about 33 times better than the PBSA FI method. Amino acids such as histidine with some double bond structure and cysteine with the active SH group could also be detected using the PBSA FI method similar to Phe and the peptides.

3.3. Application of this FL detection method for on-line determination of aromatic compounds by LC

3.3.1. Characterization of LC conditions for FL detection

It has been previously shown that photolysis of PBSA in solutions containing an organic solvent is quite different from that in aqueous solutions because pH and solvent polarity affected the excited states of PBSA. A description of experimental conditions for FL detection, including concentration, flow rate, and pH of the PBSA solution that was on-line mixed with the eluent from the HPLC column as shown in Fig. 1B, is provided here.

The influence of PBSA concentration on FL detection (data not shown) indicated a definite increase when the PBSA concentration increased beyond 1 μM and FL detection of nitrofurantoin, 4-nitrophenol, and nitrophenol reached a plateau. A further increase in PBSA concentration above 2 μM generated a FL background too high to be subtracted. Therefore, 2 μM was considered the optimal PBSA concentration as shown previously for FI.

The flow rate effect on FL detection was optimized for LC (data not shown) and seemed to have little effect on the FL intensity of nitrofurantoin. FL detection of 4-nitrophenol was more intense as the flow rate decreased to 100 μL/min or below, but FL intensity of 4-nitroaniline was increased in the flow rate range of 50–150 μL/min. The PBSA flow rate of 125 μL/min was chosen as an optimal compromise for indirect FL detection with LC.

The influence of pH on FL detection using LC was slight in the alkaline region (data not shown). FL intensity of nitrofurantoin was affected very little by a pH change between 11.6 and 12.6, but FL intensity started to decline at pH > 12 for 4-nitrophenol and pH > 12.2 for 4-nitroaniline. The optimal pH for the PBSA solution remained the same at pH 12.

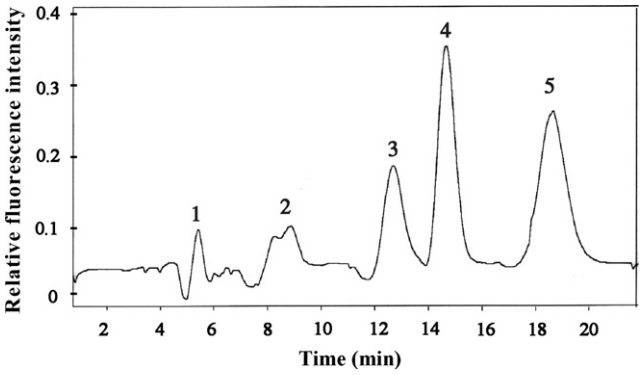

Fig. 7. Chromatogram of five aromatic compounds taken by LC with indirect FL detection via UV photolysis of PBSA. A 20 μL injection of standard mixture containing 7.5 μM salicylate (1), 30 μM nitrofurantoin (2), 7.5 μM 4-nitroaniline (3), 7.5 μM 4-nitrophenol (4), and 7.5 μM 2-nitrophenol (5). See Section 2 for chromatography conditions.

3.3.2. Analytical LC results

Under the optimal experimental conditions for FL detection, five aromatic compounds were separated by LC as shown in Fig. 7. All standard peaks were well resolved with the retention factor (k') of 1.3, 2.9, 4.7, 5.7, and 7.6 for salicylate, nitrofurantoin, 4-nitroaniline, 4-nitrophenol, and 2-nitrophenol, respectively. The nitrofurantoin peak is the smallest among the five standard peaks and also has a split top. Nitrofurantoin is definitely known for its instability [37].

All calibration data and detection limits (S/N = 3) of the nitro-aromatic compounds studied by indirect PBSA FL detection after LC are similar to those listed in Table 1 for FI because the higher column flow rate compensated for peak band broadening without a significant change in the FL signal due to the shorter reaction time. For example, the detection limits for the nitrophenols and nitroaniline are 0.3 μM. The LC detection limits for nitrofurantoin and salicylate were about 2.0 and 3.6 μM, respectively. It seems the presence of organic solvent in the mobile phase can lower the indirect PBSA FL for some analytes such as salicylate. The relative standard deviation (R.S.D.) ($n = 4$) values for the LC determination of 7.5 μM salicylate, 4-nitrophenol, 4-nitroaniline, 2-nitrophenol, salicylate as well as 30 μM nitrofurantoin in a sample mixture were 2.2%, 4.0%, 4.2%, 5.0%, and 13.3%, respectively.

4. Conclusions

An indirect fluorescence (FL) detection method via the reactivity of UV-photolyzed 2-phenylbenzimidazole-5-sulfonate (PBSA) has been developed for non-fluorescent aromatic compounds. At high pH with UV photolysis, PBSA in the excited state is likely quenched by reaction with oxygen species and analyte compounds that are reactive toward these oxygen species produced during photolysis can prevent at least partially the loss of PBSA FL. After off-line photolysis of PBSA in the presence of various nitro-aromatic test compounds, the increase in PBSA FL was clearly evident. A flow injection (FI) instrument using a PBSA mobile phase propelled through a Teflon

coil wrapped around a Hg lamp was optimized and modified for use for liquid chromatography (LC). FL detection limits below 1 μM were better than those found by direct UV detection. The potential advantage of this FL detection method is the on-line determination of a wide variety of non-fluorescent pharmaceuticals such as the non-aromatic compound erythromycin [38]. In addition, this FL detection method could be applied as a general detection method for capillary electrophoresis using a fluorocarbon polymer coated capillary and a FL detector equipped with a light emitting diode source at 280–300 nm [39,40].

References

[1] M. Wada, S. Kinoshita, Y. Itayama, N. Kuroda, K. Nakashima, J. Chromatogr. B 721 (1999) 179.
[2] C. Nistor, A. Oubina, M.-P. Marco, D. Barcelo, J. Emneus, Anal. Chim. Acta 426 (2001) 185.
[3] Y. Miyamoto, J. Chromatogr. Biomed. Appl. 420 (1987) 63.
[4] K. Arashidani, M. Yoshikawa, Y. Kodama, J. UOEH (Japan) 9 (1987) 19.
[5] D.J. Djozan, M.A. Faraj-Zadeh, Chromatographia 43 (1996) 25.
[6] M. Ciganek, J. Neca, M. Machala, J. Raszyk, Toxicol. Environ. Chem. 72 (1999) 183.
[7] M. Yang, S.A. Tomellini, J. Chromatogr. A 939 (2001) 59.
[8] M. Yang, S.A. Tomellini, J. Chromatogr. A 841 (1999) 9.
[9] J. Meyer, A. Liesence, S. Gotz, H. Hayen, U. Karst, Anal. Chem. 75 (2003) 922.
[10] S. Schlemitz, W. Pfannhauser, Food Addit. Contam. 13 (1996) 969.
[11] M. Murayama, P.K. Dasgupta, Anal. Chem. 68 (1996) 1226.
[12] J. Salamoun, M. Smrz, F. Kiss, A. Salamounorn, J. Chromatogr. 419 (1987) 213.
[13] V. David, R.M.M. Saez, J.V.G. Mateo, J.M. Calafayud, Analyst 125 (2000) 1313.
[14] Q. He, H. Chen, X. Cao, Microchem. J. 61 (1999) 125.
[15] C.Z. Matthews, E.J. Woolf, R.S. Mazenko, H. Haddix-Wiener, C.M. Chavez-Eng, M.L. Constanzer, G.A. Doss, B.K. Matuszewski, J. Pharm. Biomed. Anal. 28 (2002) 925.
[16] A. Coly, J.J. Aron, Analusis 24 (1996) 107.
[17] A. Coly, J.J. Aaron, Anal. Chim. Acta 360 (1998) 129.
[18] T. Lopez, M.D. Gil-Garcia, J.L. Martinez-Vidal, M. Martinez-Galera, Anal. Chim. Acta 447 (2001) 101.
[19] M. Martinez-Galera, T. Lopez, M.D. Gil-Garcia, J.L. Martinez-Vidal, J. Chromatogr. A 918 (2001) 79.
[20] C. DeRuiter, J.F. Bohle, G.J. DeJong, U.A.T. Brinkman, R.W. Frei, J. Chromatogr. 60 (1988) 666.
[21] K.-H. Wang, Y. Hsieh, M.-Y. Chou, C.-Y. Chang, Appl. Catal. B: Environ. 21 (1999) 1.
[22] B.A. Musial, N.D. Danielson, J. Liq. Chromatogr. Relat. Technol., submitted for publication.
[23] M.T. Vidal, A. Chisvert, A. Salvador, Talanta 59 (2003) 591.
[24] N. Serpone, A. Salinaro, A.V. Emeline, S. Horikoshi, H. Hikada, J. Zhao, Photochem. Photobiol. Sci. 1 (2002) 970.
[25] C. Stevenson, R.J.H. Davies, Chem. Res. Toxicol. 12 (1999) 38.
[26] J. Johnson Inbaraj, P. Bilski, C.F. Chignell, Photochem. Photobiol. 75 (2002) 107.
[27] T. Heberer, H.J. Stan, Anal. Chem. Acta 341 (1997) 21.
[28] A. Costela, I. Garcia-Moreno, J. Dabrio, R. Sastre, J. Photochem. Photobiol. A 109 (1997) 77.
[29] CRC Handbook of Chemistry and Physics, 64th ed., CRC Press, Boca Raton, FL, 1984–1984, D 150.
[30] W. Zhang, N.D. Danielson, Anal. Chim. Acta 493 (2003) 167.
[31] M. Strlic, T. Radovic, J. Kolar, B. Pihlar, J. Agric. Food Chem. 50 (2002) 6313.
[32] D. Patra, A.K. Mishra, Sens. Actuator B 80 (2001) 278.
[33] Y. Wang, K.-M. Wang, G.-L. Shen, R.-Q. Yu, Talanta 44 (1997) 1319.
[34] C.-G. Niu, X. Yang, W.-Q. Lin, G.-L. Shen, R.-Q. Yu, Analyst 127 (2002) 512.
[35] H.-M. Huang, K.-M. Wang, S.-S. Huang, L.-J. Zhou, D. Li, Anal. Chim. Acta 481 (2003) 109.
[36] P.J. Devine, N.A. Anis, J. Wright, S. Kim, A.T. Eldefrawi, M.E. Eldefrawi, Anal. Biochem. 227 (1995) 216.
[37] M.C. Mahedero, T.G. Diaz, S.G. Pascual, J. Pharm. Biomed. Anal. 29 (2002) 477.
[38] N.D. Danielson, C.R. Wilson, D.L. Kramer, W. Zhang, 36th Central Regional Meeting of the American Chemical Society, Indianapolis, IN, June 2–4, 2004 (abstract no. 435023).
[39] C. Sluszny, Y. He, E.S. Yeung, Electrophoresis 26 (2005) 4197.
[40] K. Davitt, Y.-S. Song, W.R. Patterson, A.V. Nurmikko, M. Gherasimova, J. Han, Y.-L. Pan, R.K. Chang, Opt. Express 13 (2005) 9548.

Available online at www.sciencedirect.com
ScienceDirect
Talanta 74 (2008) 1686–1691
Talanta
www.elsevier.com/locate/talanta

Short communication

The interaction mechanisms between *Saccharomyces cerevisiae* and menadione and its application in toxicology study

Jinsheng Zhao [a,*], Zhong Wang [b], Min Wang [b], Huaisheng Wang [a], Qingpeng He [a], He Zhang [a]

[a] *Department of Chemistry and Chemical Engineering, Liaocheng University, 252059 Liaocheng, PR China*
[b] *School of Medicine, Ehime University, 791-0295 Toon, Japan*

Received 2 July 2007; received in revised form 6 October 2007; accepted 12 October 2007
Available online 22 October 2007

Abstract

This study describes interaction mechanism between menadione and the yeast with the aid of the catabolite assay and the culture fluorescence method, with a view towards exploitting the potential of the mediator in toxicology study. Double mediator system containing menadione and the hydrophilic mediator, ferricyanide, was employed for evaluating the toxic effects of furfural on the yeast and the results showed the well consistence between the MICREDOX method and the conventional method.
© 2007 Elsevier B.V. All rights reserved.

Keywords: Double mediator system; Menadione; *Saccharomyces cerevisiae*; Toxicology

1. Introduction

The MICREDOX method, developed by Lincoln Technology, has shown great potential as a rapid biotoxicity assessment method. The ease to use, real time analysis and good correlation to reported EC_{50} (the concentration that gives 50% of the maximal response) values are particularly encouraging [1–3]. The method is characterized by high levels of biocatalyst (microorganisms) and mediator, facilitating the fast reaction. Mediators are fundamentally lipophilic chemical electron carriers that are able to pass through the cell walls of microorganisms, and thereby move between intracellular space and the extracellular environment. Once inside the microbial cell they are believed to interact with the metabolic process by participating in redox reactions with there bioelectrochemical counterparts such as NAD, NADP, flavoproteins, iron–sulfur proteins, quinones and cytochromes [1,4]. The microbially reduced mediator accumulates as a product registering the amount of bioconversion. Microbial catalyze the reduction of the mediator smoothly when they find themselves in an optimal environment. The reduction activity is a sensitive indicator of noxious toxicity to microorganisms because it is directly coupled to respiration via the electron transport chain, and thus reflects the metabolic status of the cell. If noxious substance are present, the reduction activity decreases. The higher the degree of toxicity, the less the amount of reduced mediator produced by the microbial [5,6].

The successful development of cell-based biosensors for biotoxicity assay requires the selection of a sensitive biocatalyst and a mediator capable of detecting the metabolic perturbations caused by the toxic substance [7,8]. To reveal the potential hazards of toxic chemicals to higher organisms such as human, the simplest eukaryotes (yeast) are often used instead. *Saccharomyces cerevisiae* is a relevant model to be used instead for studies of higher eukaryotes since the major metabolic pathways in yeast and humans are highly conserved. In this context, electrochemical studies of living yeast cells can substantially contribute to the understanding of the pathophysiological state of higher eukaryotic cells if the origin of the measured current in the presence of cells and electron mediators could be better understood [9]. Menadione has been traditionally considered to interact with the electron transport chain of eukaryotic cells, which forms the basis for menadione to act as a mediator in the MICREDOX biotoxicity assay method [10]. In most cases, not only the biotoxicity assessment but also the toxicology of toxic chemicals on biological materials are required to veritably

* Corresponding author. Tel.: +86 635 8537064; fax: +86 635 8239196.
E-mail address: zhaojinsheng@lcu.edu.cn (J. Zhao).

0039-9140/$ – see front matter © 2007 Elsevier B.V. All rights reserved.
doi:10.1016/j.talanta.2007.10.024

reflect the organism/ecosystem health in the contaminated environment [11]. Since the lack of an explicit understanding of the origin of the measured current in the presence of cells and electron transfer mediators, the MICREDOX biotoxicity assay method cannot be used in toxicology studies.

The aim of the present work was to elucidate the interaction mechanism between menadione and the yeast with the aid of the catabolite assay and the culture fluorescence method, with a view towards exploitting the potential of the mediator in toxicology study. For optimizing the measurement condition purpose, the double mediator system was employed, containing menadione and the hydrophilic mediator, ferricyanide, which was used as an extracellular electron acceptor and only for quantitative purpose [12]. Based on the understanding of the interaction mechanism between menadione and the yeast, the menadione/ferricyanide system was employed in evaluating the toxic effects of furfural on the yeast and, the results showed the well consistence between the MICREDOX method and the conventional method, and also showed the promising potential of the application of the MICREDOX method in toxicology study.

2. Experimental parts

2.1. Microorganisms and maintenance conditions

S. cerevisiae was obtained from the strain collection center of the Institute of Microbiology, Chinese Academy of Science. The yeast were maintained on agar slants containing ($g\,L^{-1}$): glucose, 30; yeast extracts, 3; peptone, 5; and agar, 15; pH 6.0, at 4 °C [13].

2.2. Solution preparations

Phosphate buffer (pH 6.0), containing 0.1 M KH_2PO_4 and 0.08 M Na_2HPO_4, was used for washing of cell pellets. Phosphate buffered saline (pH 6.0) prepared from 0.1 M KH_2PO_4, 0.08 M Na_2HPO_4 and 0.1 M KCl. Potassium ferricyanide solutions were prepared in phosphate buffered saline to give a concentration of 0.30 M. Glucose solution was prepared in phosphate buffered saline to give a concentration of 50 mM. Menadione was dissolved in 96% ethanol to give a 20 mM solution, filter-sterilized and stored in a light-proof container at 4 °C [14].

2.3. Cultivation of microorganisms

S. cerevisiae was prepared in the medium containing the following compounds ($g\,L^{-1}$): D-glucose, 25; yeast extracts, 1; peptone, 1; KH_2PO_4, 4; Na_2HPO_4, 4; pH 5.5. The media were sterilized by autoclaving at 120 °C for 15 min, and D-glucose was autoclaved separately at 110 °C for 10 min. After sterilization and cooling, solutions were mixed to form a complete medium prior to inoculation. A 250 mL Erlenmeyer flask containing 50 mL medium was inoculated from a fresh agar plant, and inoculated at 30 °C on a rotary shaker at 250 rpm. Growth proceeded overnight for 9 h to allow the yeast growth to its exponential phase, after which the broth was centrifuged at 10,000 rpm for 10 min the cell pellet was washed twice in phosphate buffer and suspended in phosphate buffered saline solution. The cells were adjusted to the desired optical density measured at 600 nm ($OD_{600} = 9.0$).

2.4. Incubation of cells with mediator(s) and substrates

A total volume of 20.0 mL incubation suspension was prepared for each trial. The standard incubation suspension comprised: 12 mL of cell suspension, 3.0 mL of ferricyanide solution, 100 μL of menadione solution, 3.0 mL of glucose solution, required amounts of furfural or not. Cell suspensions were adjusted to the desired pH with 2 M HCl or 2 M NaOH, the final volume of cell suspension was fulfilled with sterile distilled water to 20 mL. Incubation of cells with mediators and substrate was at 30 °C under anaerobic (oxygen-free nitrogen sparging) or aerobic condition and, on a rotary shaker at 250 rpm. After the completion of incubation, the cells were pelleted by centrifugation (10,000 rpm, 4 °C, 10 min) and the supernatants were taken for analysis [4].

2.5. Determination of optical density

A measured aliquot of the cell suspension was centrifuged at 10,000 rpm for 10 min. The supernatant was removed, and the pellet was reconstituted by the addition of 1.5 mL of distilled water. Sample dilution factors were chosen such that the measured optical density (600 nm) was between 0.1 and 0.6 au, using water as a reference.

2.6. The decrease in intracellular NAD(P)H levels by external ferricyanide reduction

The cell pellets after the incubation reactions at specific time intervals were washed twice with distilled water, and resuspended in phosphate buffered saline to give a concentration of $OD_{600} = 0.5$. The obtained cell suspensions were then subjected to culture fluorescence measurement.

2.7. The decrease in intracellular NAD(P)H levels by the presence of furfural

The exponential cell suspensions obtained at part 2.3 ($OD_{600} = 9.0$) were diluted to the concentration of $OD_{600} = 1.0$. A total volume of 20.0 mL incubation suspension was prepared for each experiment. The incubation suspension comprised: 10 mL of cell suspension, 3.0 mL of glucose solution, required amounts of furfural or not. Cell suspensions were adjusted to the pH 6.0 with 2 M HCl or 2 M NaOH, the final volume of cell suspension was fulfilled with sterile distilled water to 20 mL. The cultivation of the suspensions were conducted at 30 °C for 2.5 h, on a rotary shaker at 250 rpm.

2.8. Electroanalysis of the supernatant

Steady-state voltammetry was conducted using an electrochemical working station (CHI 900, USA) controlled by CHI

900 software. Steady-state voltammograms were obtained at a scan rate of 10 mV s^{-1} scanning from 500 to 100 mV versus saturated Ag/AgCl reference electrode. A 15 μm diameter Pt disk working electrode was used as the working electrode and a Pt gauze auxiliary electrode was used to complete the three-electrode electrochemical cell. The microelectrode was pretreated by polishing with 0.05 μm alumina/water slurry on a flocked twill polishing cloth. The steady-state current at 500 mV was measured and the mean current from three repeat voltammograms was calculated [15].

2.9. Glucose and ethanol analysis

Glucose concentration was measured by HPLC using a Hewlett–Packard 1050 equipped with a pulse amperometric detector. HPLC analyses were carried out using an AMINEX HPX-87P carbohydrate analysis column operating at 85 °C with deionized water mobile-phase at a flow of 1 mL/min. Ethanol was determined by gas chromatography using a Packard chromatograph equipped with a chromosorb 101 column.

2.10. Culture fluoromeasure measurement

Fluorescence spectra of yeast samples were obtained using a Hitachi F-4500 fluorescence spectrophotometer. Yeast samples (2 mL) were placed in a quartz cuvette. Fluorescence emission spectra (380.0–600.0 nm, resolution: 1 nm) were recorded with excitation wavelength set at 360 nm. The scan speed was 240 nm/min, the slit was (EX/EM) 5.0/2.5 nm, the PMT voltage was 700 V and, the response was auto. The shutter control was off [16].

3. Results and discussion

3.1. Intracellular redox activities detection by microelectrode voltammetric method

Voltammetric microelectrode provides a simple, reliable and rapid method for spelling the concentrations of electroactive species and, diffusion limiting currents can be established in second time scale with virtually zero destruction of analyte. The ferrocyanide accumulations arising from menadione mediated reduction of ferricyanide indicate the intracellular redox activity of yeast cells. Fig. 1 shows the steady-state voltammogram of ferrocyanide accumulations before or after a 2.5 h incubation of the yeast suspensions. The steady-state anodic plateau current measured at $E = 500$ mV was used as a relative measure of the amount of ferrocyanide produced. Before incubation, the mediator is fully in the oxidized form, and the steady-state anodic plateau current measured at $E = 500$ mV was about zero (Fig. 1, curve). The magnitude of the diffusion limiting currents for the responses in Fig. 1 can be quantitatively related to the concentration of microbially produced ferrocyanide via the relationship [14].

$$i_{\mathrm{Lim}} = 4nFDrC$$

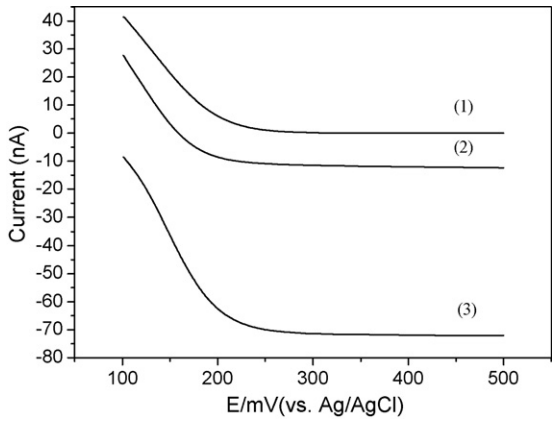

Fig. 1. Steady-state voltammograms of the supernatants. (1) Before incubation; (2) after a 2.5 h aerobic incubation; (3) after a 2.5 h anaerobic condition. Yeast absorbance (OD_{600}), 5.4; ferricyanide concentration, 45 mM; menadione concentration, 100 μM; glucose concentration, 7.5 mM; initial pH, 6.0; scan rate, 10 mV s^{-1}.

Where i_{Lim} is the experimentally measured diffusion limiting current, n the number of electrons, F the Faraday constant, D the diffusion coefficient (7.96×10^{-6} cm^2 s^{-1}), r the radius of microelectrode, and C is the concentration of the electroactive species.

3.2. Effects of oxygen on the electrochemical response in the double mediator system

The incubation experiments were conducted in two treatment groups: under anaerobic or under aerobic condition. After incubation for 2.5 h with the yeast cells, glucose and the dual mediator system, the electrochemical responses were 72.0 and 12.4 nA, respectively, under anaerobic condition and under aerobic condition. Therefore, the presence or absence of oxygen in the menadione/ferricyanide mediator system influenced the responses greatly, which might be related with the switchover in catabolic modes of *S. cerevisiae* when the inoculation conditions were changed from anaerobic to aerobic. In a recent work, we have shown that under anaerobic condition the menadione/ferricyanide system enabled the facultative yeast to switch to a nearly complete respiratory metabolism (anaerobic respiration), and then benefits the electrochemical response by enabling more complete oxidation of the substrate (glucose), and by generating a larger pool of reducing equivalents [8]. However, the origin of the electrochemical response under aerobic condition remained unknown. With respect to the much lower response under aerobic condition than that under anaerobic condition, we assumed that under aerobic condition the menadione/ferricyanide mediator system would interact with the fermentative pathway of the yeast. The above assumption was supported by the following glucose fermentation experiments, which showed that after incubation for 2.5 h, the ethanol yields were 0.45 g ethanol g^{-1} glucose (88.2% of theoretical maximum yield) and 0.09 g ethanol g^{-1} glucose (17.6% of theoretical maximum yield), respectively, under aerobic condition and under anaerobic condition. The more specific explanations concerning

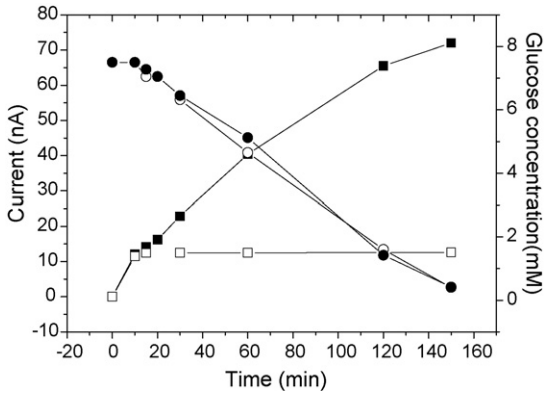

Fig. 2. The time course of the electrochemical response and the glucose consumption during the 2.5 h incubations of the dual mediator system and the yeast suspensions. Closed and open symbols represent the results from the experiments conducted under anaerobic and aerobic conditions, respectively. The other experimental conditions are as which stated in Fig. 1.

the interaction mechanism between the menadione/ferricyanide system and the yeast under both anaerobic and aerobic conditions will be discussed in the following sections.

3.3. The time course of the electrochemical response and glucose consumption

Fig. 2 shows the time course of the electrochemical response and glucose consumption during the mediated electrochemical reactions under anaerobic condition. The curve for the electrochemical response showed three distinct rate regions. Initially, the magnitude of the current increased rapidly, before reaching a lag period at around 10 min. This was followed by a slower, almost linear increase up to 120 min, after which the course levelled off. Different with the immediate increase in the electrochemical response, the glucose consumption started only after a lag phase of about 10 min, and then the glucose concentration decreased linearly along with the reactions proceeded. Previous report showed that NADH is the intracellular reductant for menadione reduction by the mitochondrial redox system of the yeast cells and, the addition of glucose enhanced the mediated reduction of ferricyanide by the presence of menadione greatly. Perhaps the endogenous NADH pool might be accounting for the abrupt increase in the response during the initial 10 min incubation since the exogenous glucose has remained untouched at the same time. After the initial 10 min incubation reactions, the related catabolic enzymes of the yeast were reactivated and, the increase in the response and the glucose consumption occurred simultaneously, which indicated that the catabolism of exogenous glucose rendered the NADH pool for the catalyzed reduction of ferricyanide by menadione.

As mentioned in the proceeding section, under anaerobic condition the menadione/ferricyanide mediator system enable the yeast to switch to a nearly complete anaerobic respiration. This initially involves Embden–Meyerhof pathway from glucose to pyruvate, which includes one NAD reduction. Pyruvate is then oxidized to acetyl-CoA by the pyruvate dehydrogenase complex with one more NAD reduction, after which the TCA cycle adds a further three NAD reductions and one FAD reduction. With 2 mol of pyruvate generated and two turns of the TCA cycle needed to completely oxidize a mole of glucose, 10 NADH and 2 $FADH_2$ are generated per mole of glucose by respiring yeast (Eq. (1)) [17]. As a quinone analogue, the primary role of menadione is as a electron acceptor approximately matched to the redox potential of coenzyme Q. Menadione thereby acts as surrogate for coenzyme Q and enables a switch to anaerobic respiration. In this case about 142 mM ferrocyanide should be expected during the respiration of 6.18 mM glucose (82.4% of the consumed 7.18 mM glucose). But the actually obtained ferrocyanide concentration was 35.9 mM, representing about 25.28% of the theoretical turnout. The majority of the reduced equivalents produced in the respiration of glucose might be reoxidized in biosynthetic reactions for the purpose of maintaining and restoring intracellular redox balance [18].

$$\text{Glucose} + 6H_2O + 10NAD^+ + 2FAD + 14ADP + 14Pi \rightarrow 6CO_2 + 10NADH + 2FADH_2 + 14ATP \quad (1)$$

$$\text{Glucose} + 2ADP + 2Pi + 2H^+ \rightarrow 2\text{ethanol} + 2CO_2 + 2ATP + 2H_2O \quad (2)$$

Fig. 2 also shows the time course of the electrochemical response and glucose consumption during the mediated electrochemical reactions under aerobic condition. The curve for the electrochemical response showed two distinct rate regions. Initially, the magnitude of the current increased abruptly, before levelling off at around 10 min, after which the electrochemical response did not experience any increase during the last 140 min. The time course of glucose consumption was similar with the corresponding one conducted under anaerobic condition. Normal yeast fermentation of glucose use NAD as the sole electron carrier, acting as a reducing coenzyme for glyceraldehyde-3-phosphate dehydrogenase (GAPDH) and as an oxidizing coenzyme for alcohol dehydrogenase (ADH) in balanced reactions. No net NADH was generated for each mole of glucose (Eq. (2)) [17]. Under aerobic condition, the catabolism of glucose made no contribution to the electrochemical response, which confirmed the above declaration that the addition of the dual mediator system under aerobic condition made the yeast remain in its original fermentation mode.

3.4. The decrease in intracellular NADH level by the mediated electrochemical reactions

Fig. 3 presents the fluorescence spectrum of the yeast, which was characterized by a maximum located at 413 nm. The intrinsic NADH fluorescence of the yeast was used to obtain insights into the interaction mechanism between menadione and the yeast. Fig. 3 also shows the time course of intracellular NADH level during the 2.5 h mediated reactions. A rapid decrease in the intracellular NADH level of the yeast was observed during the initial 10 min, but no further decrease was observed during

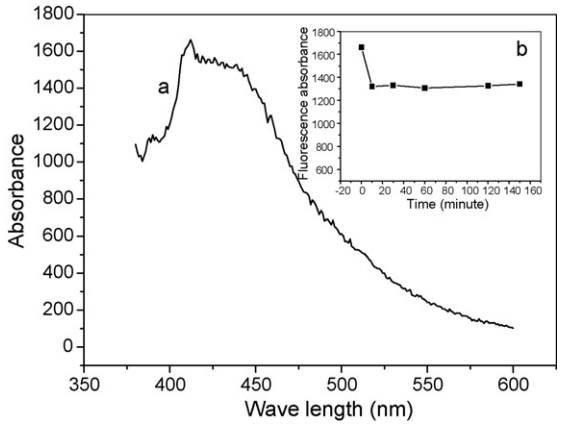

Fig. 3. The intracellular NADH intrinsic fluorescence spectra of the yeast suspensions (a), and (b, inset) the reduction in intracellular NADH levels of the yeast during the 2.5 h anaerobic incubation of the dual mediator system and the yeast suspensions. The experimental conditions are as which stated in the experimental part.

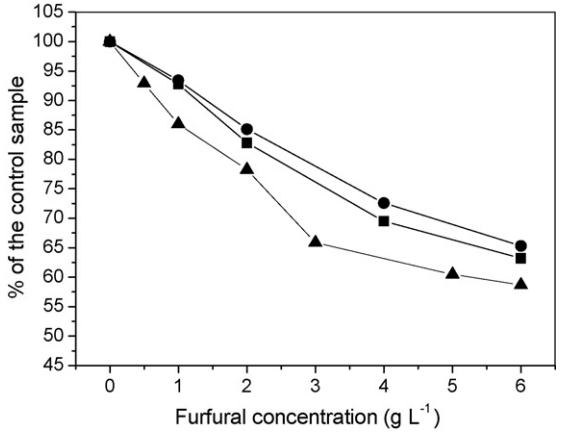

Fig. 4. The toxic effect of furfural on the yeast, and the toxic effects were measured by the initial 10 min aerobic response (●), the 2.5 h anaerobic response (■) and by the intracellular NADH intrinsic fluorescence of the yeast (▲), respectively. The experiments conditions are stated in the experimental part.

the following 140 min reactions. The magnitude of the decrease in intracellular NADH level represents the endogenous NADH level of the yeast. The endogenous NADH of the yeast was depleted in the initial 10 min incubation with the dual mediator system under both anaerobic and aerobic conditions, and the response from which was the function of the endogenous NADH pool and the activity of the NADH oxidizing enzymes (NOEs). As shown in Fig. 2, the respiration of glucose commence after a 10 min period of lag phase, which provided the exogenous NADH for the subsequent ferricyanide reduction mediated by menadione, and also prevent the further decrease in the intracellular NADH level (Fig. 3). The exogenous electrochemical response under anaerobic condition was the function of the enzymatic activity of the NOEs, the substrate and the activity of the enzymes involved in Embden–Meyerhof pathway and the TCA cycle.

3.5. Electrochemical measurement of the inhibitory effect of furfural on the yeast

As discussed above, the origin of the electrochemical response of the menadione/ferricyanide system in the presence of *S. cerevisiae* cells was more complicated than the one which has been ever considered, and the refurbished understanding should be helpful in understanding of the pathophysiological state of the yeast by the presence of toxic substance. The menadione/ferricyanide mediator system was employed in this section for electrochemical studies of the toxic effects of furfural on *S. cerevisiae*. The inhibitory effect of furfural on *S. cerevisiae* represent one of the major obstacles preventing the industrialization of the bioconversion of biomass to ethanol. Fig. 4 shows the dose–response curves for the initial 10-min aerobic incubation and the whole 150-min anaerobic incubation, respectively, by the presence of increasing concentrations of furfural. The data were plotted as the percent of control, which is the value of relative to that of furfural-free incubation. The electrochemical response of the initial 10-min aerobic incubation continuously decreased, and the reduction was 36.8% by the presence of 6 g L^{-1} furfural. As shown in the proceeding sections, the response of the initial 10-min incubation was related with the endogenous NADH level and the enzymatic activity of the NOEs. With respect to the specific yeast cells cultivated under determined conditions (including culture medium and incubation time, etc.), the endogenous NADH level of the yeast is a constant and, the magnitude of the endogenous response is related only to the enzymatic activity of the NOEs. In this case, the continuous decrease in the electrochemical response shows that the enzymatic activities of the NOEs were inhibited by the presence of increasing concentrations of furfural. To the best of our knowledge, it is for the first time to be reported *in vivo* that the enzymatic activities of the NOEs were inhibited by the presence of furfural.

The electrochemical response from the whole 150-min anaerobic incubation was slightly more sensitive to furfural than that from the initial 10-min aerobic incubation (Fig. 4), which indicates that some of the catabolic enzymes were inhibited by furfural according to the above findings that the exogenous electrochemical response under anaerobic condition was the function of the enzymatic activity of the NOEs, the substrate and the enzyme activities of the enzymes involved in the Embden–Meyerhof pathway and the TCA cycle. Fig. 4 also shows how the intracellular NADH levels of the yeast varied by the presence of increasing concentrations of furfural. The relative intracellular NADH levels of the yeast continuously decreased, and the reduction was 41.32% by the presence of 6 g L^{-1} furfural, which also indicates that the catabolic activity and then the enzymatic activities of some catabolic enzyme were inhibited by the presence of furfural. The inhibitory effects of furfural on the yeast cells have been extensively studied and, some studies based on in vitro enzymatic assay have reported that some glycolytic enzymes including hexokinase, triosephophate dehydrogenase and aldolase, etc., are sensitive to the inhibitory of furfural [19]. The results clearly showed the well consistence between the mediated electrochemical method and the conventional in vitro enzymatic assay method. The results of

this study showed the promising potential of the application of the MICREDOX method in toxicology study.

4. Conclusion

The results of this communication suggested that the response of the initial 10-min aerobic incubation with the menadione/ferricyanide system was related with the endogenous NADH level and the enzymatic activity of the NOEs catalyzing the reduction of menadione, and the exogenous electrochemical response under anaerobic condition was the function of the enzymatic activity of the NOEs, the substrate and the activity of the enzymes involved in the Embden–Meyerhof pathway and the TCA cycle. Double mediator system containing menadione and the hydrophilic mediator, ferricyanide, was employed for evaluating the toxic effects of furfural on the yeast and the results showed the well consistence between the MICREDOX method and the conventional method.

Acknowledgements

Financial support by the National Natural Science Foundation of China (20475024) is gratefully acknowledged.

References

[1] A. Tizzard, J. Webber, R. Gooneratne, R. John, J. Hay, N. Pasco, Anal. Chim. Acta 522 (2004) 197.
[2] N. Pasco, K. Baronian, C. Jeffries, J. Webber, J. Hay, Biosens. Bioelectron. 20 (2004) 524.
[3] K. Catterall, H. Zhao, N. Pasco, R. John, Anal. Chem. 75 (2003) 2584.
[4] K.H.R. Baronian, A.J. Downard, R.K. Lowen, N. Pasco, Appl. Microbiol. Biotechnol. 60 (2002) 108.
[5] J.S. Zhao, Z.Y. Yang, M. Wang, Y. Lu, Z.Y. Yang, J. Agric. Food Chem. 52 (2004) 7246.
[6] J.S. Zhao, M. Wang, Z.Y. Yang, Z.Y. Yang, Enzyme Microbiol. Technol. 37 (2005) 246.
[7] D.M. Rawson, A.J. Willmer, A.P.F. Turner, Biosens. Bioelectron. 4 (1989) 299.
[8] J.S. Zhao, M. Wang, Z.Y. Yang, Z. Wang, H. Wang, Anal. Chem. Acta 597 (2007) 67.
[9] A. Heiskanen, J. Yakovleva, C. Spégel, R. Taboryski, M. Koudelka-Hep, J. Emnéus, T. Ruzgas, Electrochem. Commun. 6 (2004) 219.
[10] P. Ertl, E. Robello, F. Battaglini, S.R. Mikkelsen, Anal. Chem. 72 (2000) 4957.
[11] B.S. Moraes, V.L. Loro, L. Glusczak, A. Pretto, C. Menezes, Chemosphere 68 (2007) 1597.
[12] H. Nakamura, K. Suzuki, H. Ishikuro, S. Kinoshita, R. Koizumi, S. Okuma, M. Gotoh, I. Karube, Talanta 72 (2007) 210.
[13] H.H. Nieuwoudt, I.S. Pretorius, F.F. Bauer, D.G. Nel, B.A. Prior, J. Microbiol. Method 67 (2006) 248.
[14] K. Catterall, K. Morris, C. Gladman, H. Zhao, N. Pasco, R. John, Talanta 55 (2001) 1187.
[15] Z.Y. Yang, J.S. Zhao, Y. Lu, Z.K. Du, Z.Y. Yang, Chem. Phys. 307 (2004) 71.
[16] L. Leblanc, É. Dufour, FEMS Microbiol. Lett. 211 (2002) 147.
[17] S. Wilkinson, J. Klar, S. Applegarth, Electroanalysis 18 (2006) (2001).
[18] J. Nicklin, K. Graeme-Cook, T. Paget, P. Killington, Instant Notes in Microbiology, Bios Scientific Publishing Limited, China, 2002, pp. 22–27.
[19] N. Banerjee, R. Bhatnagar, L. Viswanathan, Eur. J. Appl. Microbiol. Biotechnol. 11 (1981) 226.

Available online at www.sciencedirect.com
ScienceDirect
Talanta 74 (2008) 1414–1419
Talanta
www.elsevier.com/locate/talanta

Direct electrochemistry and electrocatalysis of hemoglobin immobilized in TiO_2 nanotube films

W. Zheng [a,b], Y.F. Zheng [a,*], K.W. Jin [c], N. Wang [c]

[a] *LTCS and Department of Advanced Materials and Nanotechnology, College of Engineering, Peking University, Beijing 100871, China*
[b] *Center for Biomedical Materials and Engineering, Harbin Engineering University, Harbin 150001, China*
[c] *Department of Physics, The Hong Kong University of Science and Technology, Hong Kong, China*

Received 1 June 2007; received in revised form 18 September 2007; accepted 20 September 2007
Available online 29 September 2007

Abstract

Titanium oxide nanotubes (TiO_2-NTs) synthesized by the hydrothermal method had been prepared as the co-immobilization matrix to incorporate hemoglobin (Hb) successfully. The nanostructures of TiO_2-NTs were investigated by X-ray diffraction and high-resolution electron microscopy. The Hb immobilized in TiO_2-NTs had a similar structure to the native of Hb and retained its near-native conformations as characterized by the UV–vis and FT-IR spectroscopy. A couple of quasi-reversible redox peaks with a formal potential of −0.34 V (vs. SCE) in 0.10 M pH 7.0 phosphate buffered saline (PBS) were observed. The amperometric response of the immobilized Hb linearly to H_2O_2 concentration ranged from 4 μM to 64 μM with a detection limit of 4.637×10^{-6} M and the high stability of the immobilized Hb in TiO_2-NTs constituted a promising platform for the development of biosensors.
© 2007 Elsevier B.V. All rights reserved.

Keywords: Titanium oxide nanotubes; Hemoglobin; Electrochemistry; Hydrogen peroxide; Biosensors

1. Introduction

The direct electrochemistry of redox proteins, particularly enzymes, has received increasing attention in view of its importance in elucidating the intrinsic thermodynamic and kinetic properties of proteins and its potential application in bioelectronic devices [1–3]. However, the proteins or enzymes exhibit a rather slow rate of heterogeneous electron-transfer at conventional electrodes, because of the deep burying of the electroactive prosthetic groups, the adsorptive denaturation of proteins onto electrodes and the unfavorable orientations at electrodes, although their electron-transfer is quite fast in biological systems [2]. Therefore, an understanding of the interactions between proteins and device/material surfaces is critically important in many fields of biomedical science, from biosensors to biocompatible materials.

Since the discovery of carbon nanotubes [4], much attention has been given to the study of preparation, structural characteristics, properties, and applications for their unique physical and mechanical properties [5,6]. One-dimensional nanomaterials usually exhibit special properties and potential applications, therefore, inorganic one-dimensional nanostructured materials have attracted considerable research attention in the recent 10 years [7–9]. The oxide-nanotubes became the research hot spot due to their superior performance and extensive applications in various research and industrial fields [10]. Many oxide one-dimensional nanomaterials have been successfully synthesized, such as TiO_2, ZnO, ZrO_2, Al_2O_3 and so on [11–14].

Titanium dioxide is a widely used, inorganic material, which occurs in various structural types and can be engineered into many different forms such as nanoparticles, sol–gels, nanofibers, and nanotubes [11,15,16]. It shows good biocompatibility, stability and environmental safety. One-dimensional TiO_2 nanotubes (TiO_2-NTs), owing to their large length–diameter ratio, have physical, electronic and chemical properties that are different from other forms. Since the first report claiming the hydrothermal synthesis of TiO_2-NTs [17], there have been many studies on the growth and structure of this kind of peculiar nanotubes. Recent studies have shown that the structures of TiO_2-NTs are diverse, the different synthesis parameters, such

* Corresponding author. Tel.: +86 10 6276 7411; fax: +86 10 6276 7411.
E-mail address: yfzheng@pku.edu.cn (Y.F. Zheng).

0039-9140/$ – see front matter © 2007 Elsevier B.V. All rights reserved.
doi:10.1016/j.talanta.2007.09.017

as temperature, pH and TiO_2 concentration, may result in TiO_2-NTs with different diameters, degrees of porosity and crystalline structures [18]. Different crystalline structures of the nanotube walls have been suggested, e.g., the shell structure models based on anatase, and protonic titanates [11,19–22]. Due to the unusual nanotubular structure and the interesting physicochemical properties, TiO_2-NTs are used in many applications such as gas sensor, dye-sensitised solar cells, batteries materials and optical biosensors [23–26].

In this paper, we studied the direct electron transfer and electrocatalysis of Hb in the TiO_2-NTs interfaces, which were synthesized by hydrothermal method. The Hb embedded in the TiO_2-NTs electrodes had high stability and displayed significant biological activities as characterized by the UV–vis and FT-IR spectroscopy. The amperometric response of the immobilized Hb linearly to H_2O_2 concentration constituted a promising platform for the future development of biosensors.

2. Experimental

2.1. Materials and chemicals

TiO_2-NTs used for the present study were synthesized by the hydrothermal method. Detailed experimental condition had been reported in the previous work [11]. Bovine hemoglobin (Hb, MW 67,000) purchased from Sigma Chemical Co. was used without further purification. Carboxymethyl cellulose (CMC) and hydrogen peroxide (30%, w/w) were bought from Beijing Chemical Company (Beijing, China). The dilute solution of H_2O_2 was prepared daily. Potassium dihydrogen orthophosphate (0.10 M) was used to prepare the supporting electrolyte and its pH value was adjusted to 7.0 using KOH. Aqueous solutions were prepared using doubly distilled water. All other chemicals were of analytical grade and used without further purification.

2.2. Preparation of the modified CMC–TiO_2-NTs electrodes

Glassy carbon (GC) electrodes (3 mm in diameter) were polished first using emery paper (# 2000) and then alumina slurries with particle sizes of 0.3 μm and 0.05 μm, respectively, on polishing cloths. The electrodes were cleaned by sonication for 10 min and finally rinsed with distilled water. For the preparation of the Hb/CMC–TiO_2-NTs/GC electrodes, TiO_2-NTs were dispersed into the aqueous solution of CMC (1 mg mL^{-1}), and the solution was sonicated for 1 h to obtain a white dispersion containing TiO_2-NTs (5 mg mL^{-1}). A 5 μL of the dispersion was dip-coated onto the GC electrodes. Subsequently, a small glass bottle was fitted over the electrode, followed by a period of standing in air until dry. CMC, as one of the hydrogel, could fix TiO_2-NTs on the GC electrodes. Then, CMC–TiO_2-NTs/GC electrodes were immersed into 0.10 M phosphate buffer containing 20 mg mL^{-1} Hb for 24 h. The electrodes were rinsed in distilled water prior to the electrochemical measurements.

2.3. Apparatus and electrochemical measurements

The electrochemical measurements were carried out using a computer-controlled electrochemical analyzer (CHI 650C, CHI, Austin, TX) with a two-compartment and three-electrode cell. The CMC–TiO_2-NTs/GC electrodes were used as the working electrode, a platinum spiral wire as the counter electrode, and a saturated calomel electrode (SCE) as the reference electrode. A 0.10 M phosphate buffer (pH 7.0) was used as the supporting electrolyte. For the experiments conducted under anaerobic conditions, the electrolyte was bubbled with pure N_2 gas for more than 30 min, and N_2 gas was kept flowing over the solution during the electrochemical measurements. All electrochemical measurements were performed at ambient temperature ($18 \pm 2\,^{\circ}C$).

The structure and morphology of TiO_2-NTs were characterized by a Philips X-ray diffractometer (X′-Pert Pro Instrument) with Cu Kα radiation ($\lambda = 0.15418$ nm) and a Philips transmission electron microscope (Tecnai G^2 S-TWIN) operating at 200 kV. The FT-IR spectra were obtained with a Perkin-Elmer Spectrometer 100 at room temperature. The UV–vis absorption spectroscopy study was carried out using a UV–vis 2550 Spectrophotometer (Shimadzu, Kyoto, Japan).

3. Results and discussion

3.1. Structural characteristic of TiO_2-NTs

Fig. 1 is a typical X-ray diffraction (XRD) data taken from the TiO_2 nanotube samples. The strong diffraction peak at 2θ angles of 25.0°, 27.4° and 48.5° may correspond to the *d*-spacings of (1 0 1), (1 0 2) and (2 0 0) of the anatase (tetragonal) phase. Because the nanotubes may form by rolling up the two-dimensional sheets of TiO_2 structure, some diffraction peaks of rutile phase TiO_2 may not appear in the XRD pattern. Fig. 2 illustrates that the as-prepared TiO_2-NTs have nearly uniform diameters of around 10 nm and nanotube walls of around 5 nm. All nanotubes are open at both ends, and their lengths range from several hundreds of nanometers to several micrometers.

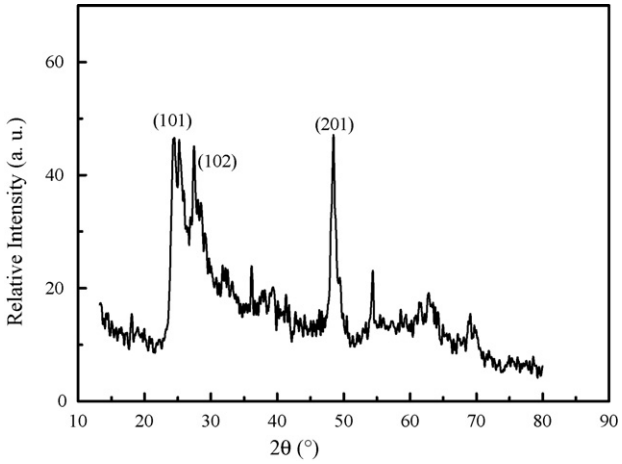

Fig. 1. X-ray diffraction patterns of TiO_2-NTs.

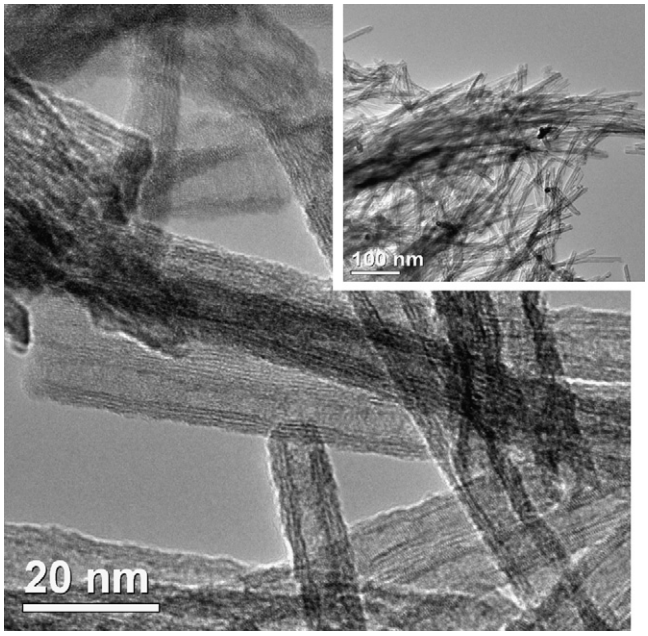

Fig. 2. TEM images of TiO_2-NTs. Scale bar: 20 nm.

3.2. Impedance characterization of Hb immobilized onto CMC–TiO_2-NTs films

Fig. 3A shows the cyclic voltammetric responses of the CMC–TiO_2-NTs film and the Hb/CMC–TiO_2-NTs film modified GC electrodes in the 5.0 mM $K_3[Fe(CN)_6]$ solution with 0.10 M KCl as the supporting electrolyte. A decrease of the peak current and an increase in the peak-to-peak separation between the cathodic and the anodic waves are clearly visible when the Hb is adsorbed on the CMC–TiO_2-NTs film. We further study the surface-modified electrodes by electrochemical impedance spectroscopy, which is a powerful tool for probing the features of surface-modified electrodes [27]. Fig. 3B shows the typical Nyquist plots ($-Z''$ vs. Z') for the pre- and post-adsorptions of Hb on the CMC–TiO_2-NTs film modified GC electrode using 5.0 mM $[Fe(CN)_6]^{4-/3-}$ as the marker ions at their formal potential in 0.10 M KCl solutions. There are significant differences between the two electrodes. The CMC–TiO_2-NTs film modified GC electrode exhibits almost a straight line, indicating a very low electron-transfer resistance on CMC–TiO_2-NTs film to the redox probe dissolved in the electrolyte solution. However, the result from the Hb/CMC–TiO_2-NTs film modified GC electrode shows a clear semicircle domain, indicating an increase of the electron-transfer resistance for the redox probe after the adsorption of Hb on the CMC–TiO_2-NTs film. The impedance change resulted by the electrode modification process implies that Hb can be easily adsorbed onto the CMC–TiO_2-NTs film.

3.3. Conformational studies of Hb

UV–vis absorption spectroscopy is a conventional means for characterizing the structure of protein. The Soret absorption band of heme prosthetic group may provide the information on the tertiary structure of heme proteins, especially that of conformational change around the heme region [28]. As can be seen from Fig. 4, Hb incorporated in the CMC–TiO_2-NTs film (curve b in Fig. 4) has a characteristic Soret absorption at 415 nm, shifting only 3 nm toward the red with the Soret band of 412 nm for native Hb film (curve a in Fig. 4). It is indicated that Hb entrapped in the CMC–TiO_2-NTs film has a similar structure to the native of Hb, and retains its near-native conformations. The UV–vis absorption spectra of CMC–TiO_2-NTs is also shown in Fig. 4 (curve c), from which no characteristic peak can be observed.

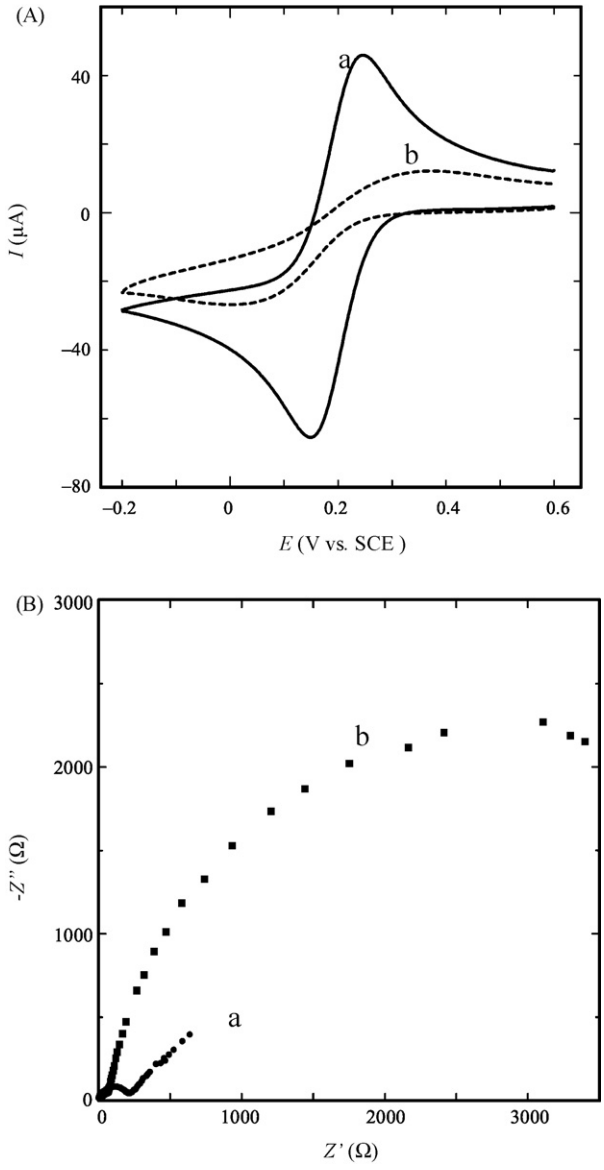

Fig. 3. CVs (A) and impedance spectroscopy (B) obtained at CMC–TiO_2-NTs (curve a) and Hb/CMC–TiO_2-NTs (curve b) modified GC electrodes in 0.10 M KCl containing 5 mM $K_3Fe(CN)_6$. Scan rate: 100 mV s^{-1}.

We have employed FT-IR spectroscopy to investigate the structural variations of Hb immobilized into the CMC–TiO_2-NTs composite films since this is an effective means to probe the secondary structure of proteins. The characteristic amide I and II bands of proteins provide detailed information on the secondary structure of polypeptide chain [29]. The amide I band (1700–1600 cm^{-1}) is caused by C=O stretching vibra-

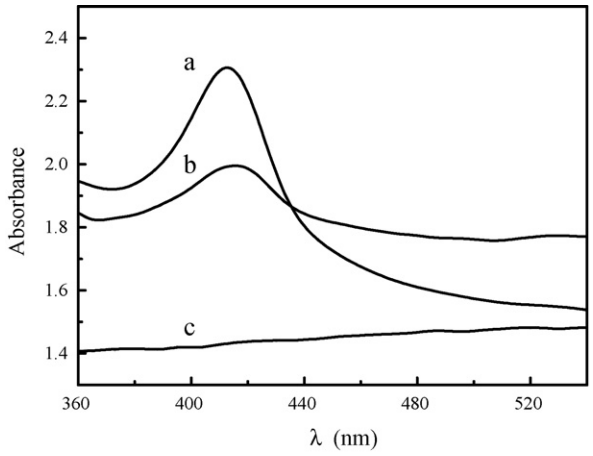

Fig. 4. UV–vis spectra of Hb (curve a), Hb/CMC–TiO_2-NTs (curve b) and CMC–TiO_2-NTs (curve c) films.

tions of peptide linkages in the backbone of the protein. The amide II band (1600–1500 cm^{-1}) results from the combination of N–H bending and C–N stretching of the peptide groups. Fig. 5 shows the FT-IR spectra taken from Hb, CMC–TiO_2-NTs and Hb/CMC–TiO_2-NTs composite films. As shown in Fig. 5, curves b and c, the spectra of amide I and II bands of the Hb/CMC–TiO_2-NTs composite film (1652 and 1544 cm^{-1}) are nearly the same as those obtained for the native Hb (1656 and 1546 cm^{-1}). The similarities of the two spectra suggest that Hb retains the essential features of its native secondary structure in the Hb/CMC–TiO_2-NTs composite film. Moreover, the characteristic absorption bands of the Hb are also observed in curve d, which is obtained by subtracting CMC–TiO_2-NTs spectra from Hb/CMC–TiO_2-NTs spectra. Thus, the CMC–TiO_2-NTs composite film may provide a promising matrix for the protein immobilization and biosensor fabrication because of its satisfying biocompatibility.

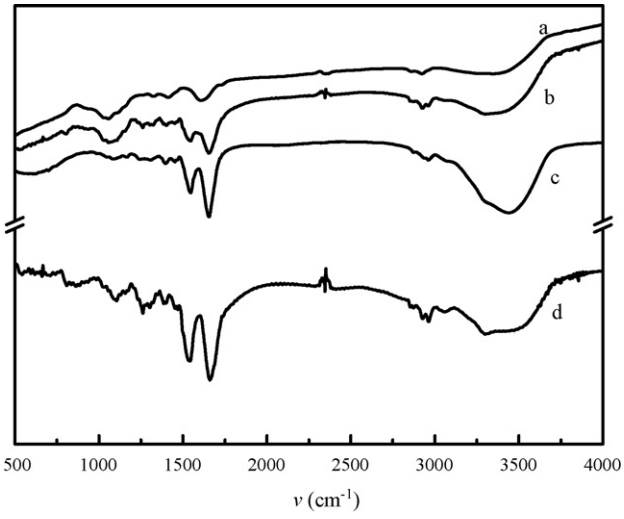

Fig. 5. FT-IR spectra of CMC–TiO_2-NTs (curve a), Hb/CMC–TiO_2-NTs (curve b) and Hb (curve c) films. The curve (d) is obtained by the spectra subtracting CMC–TiO_2-NTs from Hb/CMC–TiO_2-NTs.

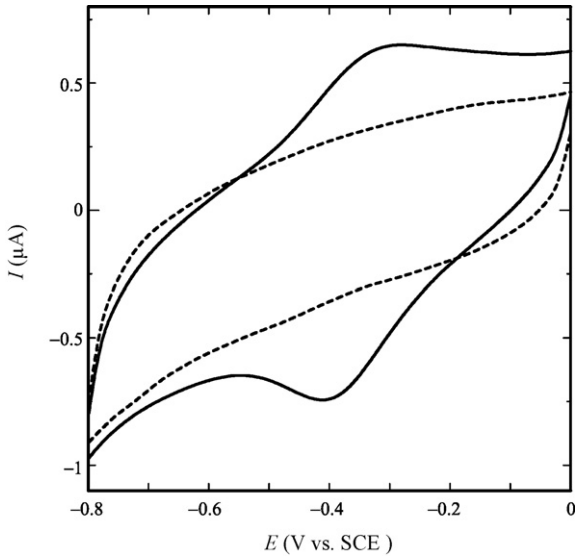

Fig. 6. CVs obtained at Hb/CMC–TiO_2-NTs/GC (solid line) and CMC–TiO_2-NTs/GC (dashed line) electrodes in 0.10 M N_2-saturated phosphate buffer. Scan rate: 100 mV s^{-1}.

3.4. *Electrochemistry and electrocatalysis of Hb in CMC–TiO_2-NTs film*

Fig. 6 depicts the typical cyclic voltammogram (CVs) of the CMC–TiO_2-NTs/GC and the Hb/CMC–TiO_2-NTs/GC electrodes in 0.10 M phosphate buffer of pH 7.0 at 100 mV s^{-1}, respectively. No redox peaks can be observed for the CMC–TiO_2-NTs/GC electrode (dashed curve in Fig. 6), but a pair of well-defined redox peaks are visible for the Hb/CMC–TiO_2-NTs/GC electrode (solid curve in Fig. 6). The formal potential $E^{0'}$ (defined as the average of anodic peak potential, E_{pa} and cathodic peak potential, E_{pc}) is −0.34 V (vs. SCE) with a peak-to-peak separation of ca. 100 mV, which is consistent with the reported values for the Fe(III)/Fe(II) redox center of the heme group in Hb [30–32]. This formal potential is more negative than that in our previous reports [33] due to the different interface components which may interact with the protein or affect the electrode double layer [30]. These results indicate that in CMC–TiO_2-NTs films, the direct electron transfer between Hb and GC electrodes is greatly enhanced. The CMC–TiO_2-NTs film can provide a favorable microenvironment for Hb to exchange electrons with the electrode and facilitate the rate of electron transportation.

The dependence of the peak currents on the scan rate is showed in Fig. 7A. It can be observed that the cathodic and anodic peak currents (I_p) of the Hb increase with the increase of the scan rate, at the same time, the cathodic and anodic peak potentials exhibit a small shift and the peak-to-peak separation also increases. As shown in Fig. 7B, the cathodic and anodic peak currents increase linearly with the scan rate from 100 to 900 mV s^{-1}. Thus, it is clear that the Hb adsorbed onto the surface undergoes a reversible and surface-confined electron transfer.

The detection of hydrogen peroxide (H_2O_2) is of great importance in environmental, industrial, chemical, food, phar-

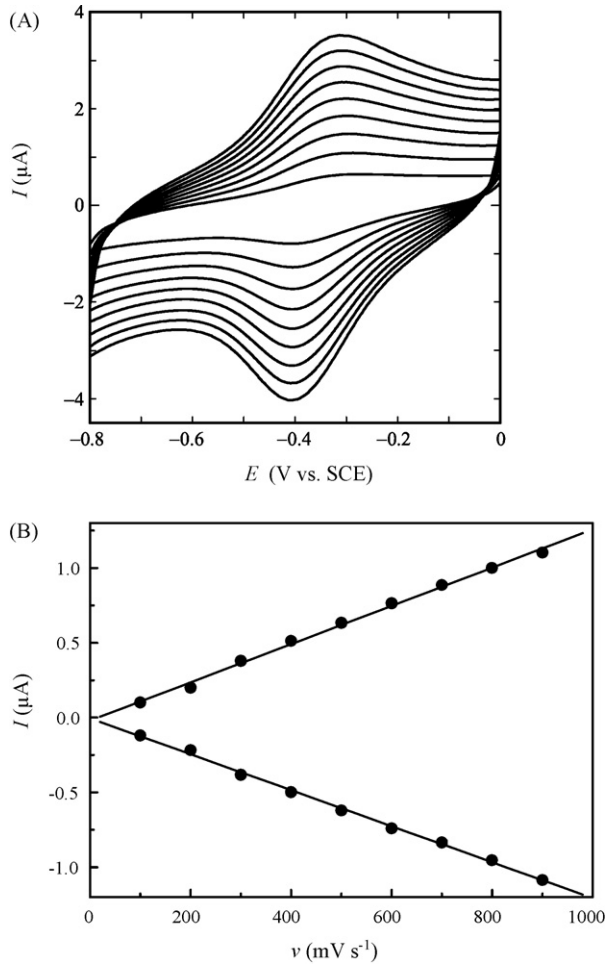

Fig. 7. (A) CVs obtained at the Hb/CMC–TiO_2-NTs/GC electrode in 0.10 M N_2-saturated phosphate buffer. Scan rate (from inner to outer): 100, 200, 300, 400, 500, 600, 700, 800 and 900 mV s^{-1}. (B) A plot of the cathodic and anodic peak currents against the potential scan rate.

maceutical and biological fields. The main methods traditionally used for determining H_2O_2 include titrimetry, spectrometry, chemiluminescence and electrochemical methods. The electrochemical technique for determination of H_2O_2 coupled with the intrinsic selectivity and sensitivity of enzymatic reactions is promising for the fabrication of simple and low-cost enzyme sensors [34,35]. Hb has close structural similarity to the peroxidase with an intrinsic catalytic activity toward peroxide compounds [36]. Fig. 8 shows catalytic reduction of H_2O_2 at the CMC–TiO_2-NTs modified GC electrode. It can be seen that, when H_2O_2 was added to the buffers, the reduction peak on the Hb/CMC–TiO_2-NTs film electrodes increased in height at approximately −0.43 V, accompanied by a decrease and disappearance of the oxidation peak. Moreover, the reduction peak current increased with an increase of H_2O_2 in PBS. The mechanisms can be expressed as the following [37]:

$$Hb(Fe^{3+}) + H_2O_2 \rightarrow \text{Compound I}\,(Fe^{4+}{=}O) + H_2O$$

$$\text{Compound I}\,(Fe^{4+}{=}O) + e + H^+ \rightarrow \text{Compound II}$$

$$\text{Compound II} + e + H^+ \rightarrow Hb(Fe^{3+}) + H_2O$$

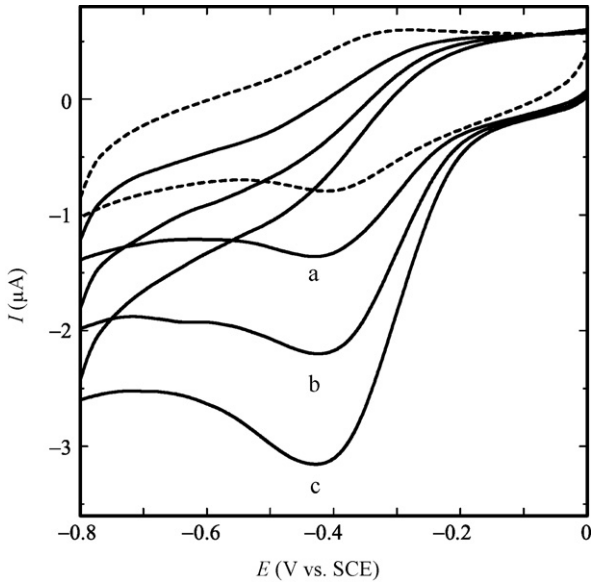

Fig. 8. CVs obtained at Hb/TiO_2-NTs/GC electrode in 0.10 M N_2-saturated phosphate buffer in the absence (dotted line) and presence of 10 μM H_2O_2 (solid line a), 20 μM H_2O_2 (solid line b) and 30 μM H_2O_2 (solid line c). Scan rate: 100 mV s^{-1}.

The amperometric responses of the Hb/CMC–TiO_2-NTs and CMC–TiO_2-NTs films modified GC electrode upon the successive additions of H_2O_2 to 0.10 M pH 7.0 PBS at an applied potential of −0.30 V are shown in Fig. 9. The CMC–TiO_2-NTs films modified GC electrode (curve a) show a much smaller response to H_2O_2 than that of the Hb/CMC–TiO_2-NTs modified GC electrode (curve b) at the same H_2O_2 concentration. This indicates that Hb has close structural similarity to the peroxidase with an intrinsic catalytic activity toward the peroxide compounds. Moreover, the electrocatalytic current of the Hb/CMC–TiO_2-NTs modified GC electrode increases clearly with each addition of H_2O_2 to the solution. The current reaches its maximum value within 10 s after each addition

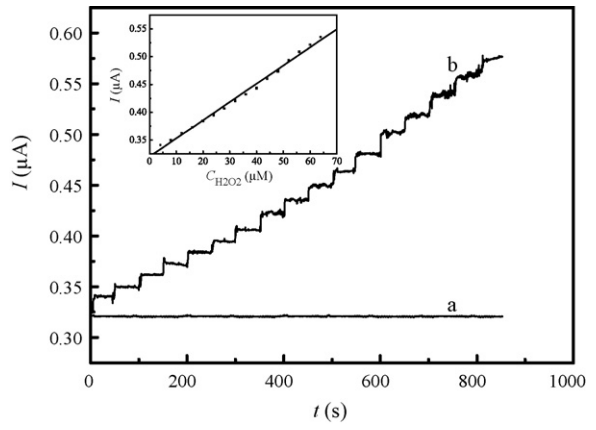

Fig. 9. Amperometric responses of CMC–TiO_2-NTs (curve a) and Hb/CMC–TiO_2-NTs (curve b) modified GC electrodes in stirred solutions to the successive additions of H_2O_2 (each increment, 4 μM). Applied potential, −0.30 V vs. SCE; supporting electrolyte, 0.10 M pH 7.0 PBS. The inset is the calibration curve of steady-state currents vs. concentrations of H_2O_2.

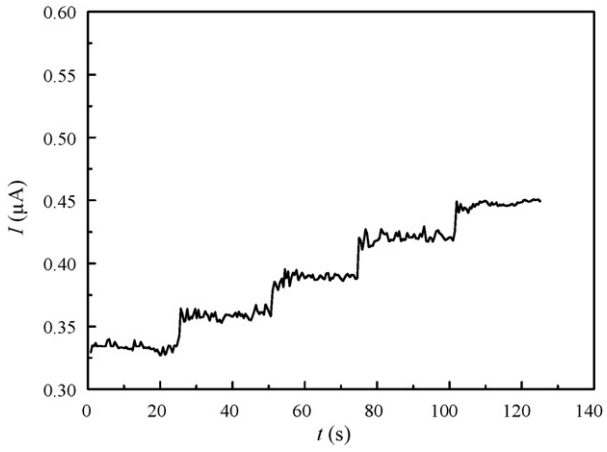

Fig. 10. Amperometric responses of Hb/CMC–TiO_2-NTs modified GC electrodes in stirred solutions to the successive additions of diluted real samples.

of H_2O_2, which suggests that the Hb/CMC–TiO_2-NTs modified GC electrode can respond rapidly to the change of the concentration of H_2O_2. Thus, the Hb/CMC–TiO_2-NTs modified GC electrode shows an excellent electrocatalytic response to the reduction of H_2O_2. The inset of Fig. 9 is the typical calibration curve of the steady-state current vs. H_2O_2 concentration. Obviously, the steady-state response current increases with increasing H_2O_2 concentration. The linear range of this biosensor to H_2O_2 concentration is 4–64 μM which can be described by a linear regression equation of $I(\mu A) = 0.3195 + 0.00328C$ (μM) ($R = 0.997$). The detection limit of the biosensor is 4.637×10^{-6} M at a signal-to-noise ratio of 3, which is similar to others' reports [38,39]. These results indicate that the Hb entrapped in the composite film possesses electrocatalytic activity to H_2O_2. The stability of the biosensor is further studied in the linear range of H_2O_2. When the H_2O_2 biosensor has been stored in a 0.10 M PBS for 3 weeks at 4 °C, the biosensor retains over 90% response of its initial sensitivity to the reduction of H_2O_2, demonstrating its good long-term stability.

In addition, we also investigated the concentration of H_2O_2 in eyedrop as real world example using the proposed method, as shown in Fig. 10. The sample was diluted with PBS (pH 7.0) before the detection, in order to make the concentration of H_2O_2 locating in the detection limit range. The concentration of H_2O_2 was calculated to be about 0.238 mM by linear equation and dilution ratio. This value obtained by the proposed method was consistent with that obtained by the conventional permanganate index method (0.241 mM), which indicated that this method might be reliable and effective in future applications.

4. Conclusions

We demonstrate that Hb immobilized in the CMC–TiO_2-NTs composite films retains its original conformation by UV–vis and FT-IR spectra, and the direct electron transfer between the redox proteins and the electrode are easily performed at the CMC–TiO_2-NTs interface. The biosensors based on the Hb/CMC–TiO_2-NTs are stable and response linearly to H_2O_2 concentrations in the range from 4 μM to 64 μM with a detection limit of 4.637×10^{-6} M. The properties of the immobilized Hb in the TiO_2-NTs composites provide a promising platform for the future development of biosensors.

References

[1] F.A. Armstrong, H.A.O. Hill, N.J. Walton, Acc. Chem. Res. 21 (1988) 407.
[2] A. Heller, Acc. Chem. Res. 23 (1990) 128.
[3] C. Legar, S.J. Elloitt, K.R. Hoke, L.J.C. Jeuken, A.K. Jones, F.A. Armstrong, Biochemistry 42 (2003) 8653.
[4] M. Monthioux, V.L. Kuznetsov, Carbon 44 (2006) 1621.
[5] S. Iijima, Nature 354 (1991) 56.
[6] P.M. Ajayan, Chem. Rev. 99 (1999) 1787.
[7] C.M. Lieber, Solid State Commun. 107 (1998) 607.
[8] G.R. Patzke, F. Krumeich, R. Nesper, Angew. Chem. Int. Ed. 41 (2002) 2446.
[9] Y. Xia, P. Yang, Y. Sun, Y. Wu, B. Mayers, B. Gates, Y. Yin, F. Kim, H. Yan, Adv. Mater. 15 (2003) 353.
[10] W. Tremel, Angew. Chem. Int. Ed. 38 (1999) 2175.
[11] B.D. Yao, Y.F. Chan, X.Y. Zhang, W.F. Zhang, Z.Y. Yang, N. Wang, Appl. Phys. Lett. 82 (2003) 281.
[12] J. Zhang, L. Sun, C. Liao, C. Yan, Chem. Commun. 3 (2002) 262.
[13] C.N.R. Rao, B.C. Satishkumar, A. Govindaraj, Chem. Commun. 16 (1997) 1581.
[14] L. Pu, X. Bao, J. Zou, D. Feng, Angew. Chem. Int. Ed. 40 (2001) 1490.
[15] G.F. Fu, P.S. Vary, C.T. Lin, J. Phys. Chem. B 19 (2005) 8889.
[16] Z.Y. Yuan, B.L. Su, Colloids Surf. A 241 (2004) 173.
[17] T. Kasuga, M. Hiramatsu, A. Hoson, T. Sekino, K. Niihara, Langmuir 14 (1998) 3160.
[18] D.V. Bavykin, V.N. Parmon, A.A. Lapkin, F.C. Walsh, J. Mater. Chem. 14 (2004) 3370.
[19] Q. Chen, G.H. Du, S. Zhang, L.M. Peng, Acta Crystallogr. B 58 (2002) 587.
[20] Y.Q. Wang, G.Q. Hu, X.F. Duan, H.L. Sun, Q.K. Xue, Chem. Phys. Lett. 365 (2002) 427.
[21] R. Ma, Y. Bando, T. Sasaki, Chem. Phys. Lett. 380 (2003) 577.
[22] G. Armstrong, A.R. Armstrong, J. Canales, P.G. Bruce, Chem. Commun. 19 (2005) 2454.
[23] K. Lobato, L.M. Peter, U. Wurfel, J. Phys. Chem. B 110 (2006) 16201.
[24] B. He, B. Dong, H. Li, Electrochem. Commun. 9 (2007) 425.
[25] O.K. Varghese, D. Gong, M. Paulose, K.O. Ong, E.C. Dickey, C.A. Grimes, Adv. Mater. 15 (2003) 624.
[26] H. Zhou, X. Gan, T. Liu, Q. Yang, G. Li, Bioelectrochemistry 69 (2006) 34.
[27] J. Bobacka, A. Lawenstam, A. Ivaska, J. Electroanal. Chem. 489 (2000) 17.
[28] H. Theorell, A. Ehrenberg, Acta Chem. Scand. 5 (1951) 823.
[29] J.K. Kauppinen, D.J. Moffate, H.H. Mantsch, D.G. Lameron, Appl. Spectrosc. 35 (1981) 271.
[30] A.F. Nassar, Z. Zhang, N. Hu, J.F. Rusling, T.F. Kumosinski, J. Phys. Chem. B 101 (1997) 2224.
[31] Z. Zhang, S. Chouchane, R.S. Magliozzo, J.F. Rusling, Anal. Chem. 74 (2002) 163.
[32] S. Chen, R. Yuan, Y. Chai, L. Zhang, N. Wang, X. Li, Biosens. Bioelectron. 22 (2007) 1268.
[33] W. Zheng, Q. Li, Y. Yan, L. Su, L. Mao, Indian J. Chem. Sec. A 44 (2005) 950.
[34] S.S. Razola, B.L. Ruiz, N.M. Diez, H.B. Mark, J.-M. Kauffmann, Biosens. Bioelectron. 17 (2002) 921.
[35] Q. Deng, S.J. Dong, J. Electroanal. Chem. 377 (1994) 191.
[36] S.A. Adediran, A.M. Lambeir, Eur. J. Biochem. 186 (1989) 571.
[37] H.Y. Xiao, H.X. Lu, H.Y. Chen, Anal. Biochem. 278 (2000) 22.
[38] G. Zhao, J.J. Feng, J.J. Xu, H.Y. Chen, Electrochem. Commun. 7 (2005) 724.
[39] F. Yin, H.K. Shin, Y.S. Kwon, Talanta 67 (2005) 221.

Available online at www.sciencedirect.com
ScienceDirect
Talanta 74 (2008) 1579–1585
Talanta
www.elsevier.com/locate/talanta

Quantitative analysis of hydrolysis of carbaryl in tap water and river by excitation–emission matrix fluorescence coupled with second-order calibration

Shao-Hua Zhu, Hai-Long Wu *, A-Lin Xia, Qing-Juan Han, Yan Zhang, Ru-Qin Yu

State Key Laboratory of Chemo/Biosensing and Chemometrics, College of Chemistry and Chemical Engineering, Hunan University, Changsha 410082, China

Received 23 June 2007; received in revised form 30 September 2007; accepted 1 October 2007
Available online 7 October 2007

Abstract

A novel method was proposed to determine simultaneously carbaryl and its degradation product 1-naphthol in river and tap water in this paper. The parallel factor analysis (PARAFAC) algorithm was adopted to analyze the excitation–emission matrix (EEM) fluorescence data. The second-order advantage of the PARAFAC-based second-order calibration algorithm was exploited, which make it possible that calibration can be performed even in the presence of unknown interferences. Good recoveries were obtained although the excitation and emission spectral profiles of the analytes were overlapped with background in the river water. It was also applied to investigate the hydrolysis kinetics of carbaryl in river water and tap water. The rate equation, the rate constant and the half life were calculated.
© 2007 Elsevier B.V. All rights reserved.

Keywords: Carbaryl; 1-Naphthol; Hydrolysis; Second-order calibration; PARAFAC

1. Introduction

Carbaryl (the chemical name 1-naphthol *N*-methylcarbamate) which is shown in Fig. 1, is the successful carbamate insecticide used due to its broad-spectrum efficacy to control over 100 species of insects. More over, it is used to treat human body louse infestation. The pesticide is used indiscriminately, so the toxicity has raised the public concern about the ecosystem and human health. Carbaryl is lethal to many non-target insects such as honeybee. Accumulation of the pesticide occurs in many aquatic organisms such as catfish and algae [1].

Simultaneous determination of carbaryl and its degradation product 1-naphthol, therefore, is useful and essential. Most of analytical methods employed for quantification of pesticides are based on a separation by chromatographic technique such as thin-layer chromatography (TLC) [2–4], gas chromatography (GC) [5–8] and high pressure liquid chromatography (HPLC) [9–12] with detectors of ultraviolet (UV), diode array detector (DAD) and mass spectrometry (MS). These methods mentioned above have many advantages such as high sensitivity and accuracy and some have been adopted by regulatory agencies. But some disadvantages obstruct their application in many cases. The costs of these methods are high. They usually use high volumes of toxic solvents and its separation procedure is time-consuming. Sometimes you have to develop an extremely complex gradient for the separation and develop specific preprocessing procedures for samples or sophisticated cleanup strategies because a satisfying separation is often a painful work to achieve.

Fluorescence spectroscopy can be used for determination of residue of carbamate pesticides. The method has been exploited in recent years because of its inherent sensitivity. Nevertheless, fluoremetric measurement only based on selection of excitation and/or emission wavelengths generally lack of selectivity. Fluorescence signal peak of matter is usually broad, so in complex mixtures the signal will be often overlap. A remarkable increase of selectivity can be obtained by the strategy of excitation–emission matrix fluorescence coupled with second-order calibration algorithms. The method makes the quantification possible even if the unknown interferences are

* Corresponding author. Tel.: +86 731 8821818; fax: +86 731 8821818.
E-mail addresses: hlwu@hnu.cn, hlwu529@gmail.com (H.-L. Wu).

0039-9140/$ – see front matter © 2007 Elsevier B.V. All rights reserved.
doi:10.1016/j.talanta.2007.10.002

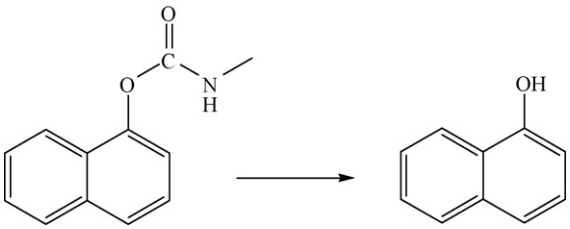

Fig. 1. The degradation of the carbaryl.

present in the sample. The property was called the second-order advantage. Several second-order calibration algorithms have been proposed for three-way data array, such as parallel factor analysis (PARAFAC) [13,14], multivariate curve resolution (MCR) [15,16], alternating trilinear decomposition (ATLD) [17], self-weighted alternating trilinear decomposition (SWATLD) [18] and alternating penalty trilinear decomposition (APTLD) [19]. And the second-order calibration algorithms have been used for quantification of pesticides [20–22].

The carbaryl is rather stable in acidic condition and in basic condition, however, hydrolysis readily in water. The major degradation product is 1-naphthol. Reaction monitoring is of increasing importance in chemistry where the aim is to follow the progress of a reaction within time. The user can obtain a variety of information from this, for example the kinetic model, the reaction rate constant, end-points, half life and so on. Conventional methods might require samples to be analyzed using chromatography or NMR. This technique is time-consuming and expensive in instrumentation [23]. The results may not be known for several hours or days, and there is often a limit to the frequency of sampling. The spectroscopy, such as UV, NIR and Raman, are used to monitor a reaction [24–26]. In a general way the multivariate calibration algorithms PLS, MLR and PCR were adopted to analyze the first-order data got by the probes [24–26]. So this requires that the matrix of the calibration samples should be uniform with the matrix in which the reaction runs. When the matrix in which the reaction runs contains an unknown interference which is not present in the calibration samples, the algorithms can not give a correct result. In Ref. [24] the glacial acetic acid were added into the calibration samples although the acid would catalyze the reaction. For this reason, the calibration samples will have to be made again when the reaction runs in a different matrix.

In this work the hydrolysis of carbaryl in tap water and river water would be studied. The EEM fluorescence spectroscopy with the aid of the second-order calibration algorithm PARAFAC is adapted to perform the task.

2. Theory

2.1. PARAFAC

In three-way data analysis there are two kinds of models, PARAFAC model and Tucker model. The PARAFAC model, which is also known as the name canonical decomposition, proposed by Harshman [13] and Carroll and Chang [14] has been accepted owing to its consistency with Beer's law in chemistry. The model can be expressed as following form:

$$x_{ijk} = \sum_{n=1}^{N} a_{in} b_{jn} c_{jn} + e_{ijk} \quad i = 1, 2, \ldots, I; \quad j = 1, 2, \ldots, J; \; k = 1, 2, \ldots, K \tag{1}$$

And the model can be also expressed in matrix form as [17].

An important and attractive feature of the PARAFAC model is the uniqueness of solution, so additional constraints, such as orthogonality or external information to solve rotational freedom need not. This feature is a great advantage. The true underlying spectra will be received if the data is indeed trilinear and the right number of components is used.

Along with the above model, Harshman [13] and Carroll and Chang [14] proposed an alternating least-squares approach to solve the above decomposition problem. ALS at first assumes the loading matrices in two modes and then estimates the unknown parameters of the third mode. This is advantageous because the algorithm is simple to implement, simple to incorporate constraints. For this superiority, the method has been accepted and used widely in chemistry.

In the PARAFAC algorithm the loss function to be minimized is the sum of squared residuals (SSR), which may be written as:

$$\mathrm{SSR} = \sum_{i=1}^{I}\sum_{j=1}^{J}\sum_{k=1}^{K} e_{ijk}^2 \tag{2}$$

The solution for PARAFAC model can be found based on the alternating least-squares principle.

The PARAFAC algorithm is preferable in practice for three-way data analysis and its favorable statistic merits, such as optimal unbiased estimations of the final results in least-square sense comparing to non-iterative methods. However, PARAFAC requires an accurate estimation of the number of underlying factor in the system studied. Either overestimation or underestimation of the number of factor will lead to wrong results. In this paper the core consistency diagnostic, which was proposed by Bro [27], was chosen to estimate the number of underlying factor. Bro defines a function as follows:

$$\text{core consistency} = 100\left[\frac{\sum_{i=1}^{F}\sum_{j=1}^{F}\sum_{k=1}^{F}(g_{ijk} - t_{ijk})^2}{\sum_{i=1}^{I}\sum_{j=1}^{J}\sum_{k=1}^{K} t_{ijk}^2}\right] \tag{3}$$

where g_{ijk} is the element of the core matrix calculated using the Tucker3 model (the core matrix which is got in Tucker3 model when the correct number of factor is chosen.), t_{ijk} is the element of three-way matrix whose elements in superdiagonal are ones and others elements are zeros. This function reflects how well the Tucker3 core fits to the assumptions of model. When the selected number is bigger than the correct number of factor, the core consistency is close to zero even negative. When the selected number is equal to or smaller than the correct number, the core consistency is close to one. Thus, the true factor number in the three-way data may be estimated.

3. Experiment

3.1. Apparatus

The measurement of fluorescence was performed with a HITACHI F-4500 Fluorescence spectrophotometer with 10 mm quartz cells. A PINGFAN TGL-16A centrifuge and a BOXUN YXQ-LS-30 SII autoclave was employed to handle the river water.

The spectra data were imported to computer and analyzed in the Matlab environment. The programs of the PARAFAC and linear regression algorithms were homemade. All programs were run on IBM compatible microcomputer.

3.2. Reagents

Carbaryl was purchased from FUTESI (Changsha, China). 1-naphthol was bought from DINGGUO (Changsha, China). NaH_2PO_4 (analytical grade), H_3PO_4 (analytical grade), Na_2HPO_4 (analytical grade) and methanol (HPLC-grade) were purchased from YUFENG (Changsha, China). The river water was collected from the Xiangjiang river, China.

Stock solutions of 145 μg/ml carbaryl were prepared by dissolving appropriate amount in methanol. Stock solutions of 103 μg/ml 1-naphthol were prepared by the same way. Working solutions were prepared by appropriate dilution. All the solutions were placed in the refrigerator at 4 °C.

Buffer solutions were obtained by mixing appropriate NaH_2PO_4, H_3PO_4 and Na_2HPO_4 in doubly distilled water.

3.3. Procedure

The river water was centrifuged to remove the particulate matter and then was sterilized in autoclave.

3.3.1. Simultaneous determination of carbaryl and 1-naphthol in river water and tap water

Simultaneous determination of carbaryl and 1-naphthol in river water was done by the proposed method. Seven calibration samples were built by adding appropriate stock solutions of the two analytes and 2 ml phosphate buffer (pH 5) into 10 ml volumetric flask and marking in doubly distilled water with carbaryl concentration from 0 to 0.363 μg/ml and 1-naphthol concentration from 0 to 0.515 μg/ml (in the concentration regions the fluorescence intensity was proportional to the concentrations of carbaryl and 1-naphthol). An eleven-sample set was built with the concentration of analytes within calibration range. The first three samples were built in the same way of confecting calibration samples as test samples to testify the calibration model constructed from the calibration sample. The samples 11, 12, 13 and 14 were built in the approach as follows. Appropriate stock solutions of carbaryl and 1-naphthol were mixed with the tap water. 4 ml of the mixture and 2 ml of phosphate buffer (pH 5) were added into 10 ml volumetric flask and marked in tap water. The samples 15, 16, 17 and 18 were prepared by mixing appropriate stock solutions of carbaryl and 1-naphthol with the river water. The concentration of carbaryl and 1-naphthol in all samples were shown in Table 1.

Table 1
The concentration of carbaryl and 1-naphthol in calibration and predication samples

	Added concentration (ng/ml)	
	Carbaryl	1-Naphthol
Calibration samples		
1	36	0
2	0	51
3	218	103
4	145	206
5	363	309
6	290	412
7	73	515
Test samples		
8	36	83
9	319	134
10	123	175
Prediction samples		
11[a]	73	155
12[a]	109	258
13[a]	181	361
14[a]	254	464
15[b]	73	134
16[b]	109	237
17[b]	181	340
18[b]	254	443

[a] Prepared using the tap water as matrix.
[b] Prepared using the river water as matrix.

The EEM spectra of the samples were measured and recorded at excitation wavelength from 244 to 308 nm at regular steps of 2 nm and emission wavelength from 311 to 491 nm at regular steps of 5 nm. The excitation and emission monochromator slit widths were 5 nm and the scanning rate was maintained at 1200 nm/min.

3.3.2. Application to investigation of carbaryl hydrolysis in river water

The pesticide is rather stable in acidic condition, in basic conditions, however, hydrolysis readily in water. So hydrolysis of carbaryl in basic solution was examined with various pH phosphate buffers at temperature 26 °C. There was no distinct degradation for carbaryl within 4 h when the pH value as 7 or 8. And when the pH value was 10 or 11, hydrolysis of carbaryl was too fast and almost reached the end with in 1 h. The pH value was set to 9 to make the degradation of carbaryl almost complete within 4 h. When pH value was less than 7, the carbaryl was stable. So the phosphate buffer with pH 5 was used to interrupt the hydrolysis reaction.

The experiment was initiated by adding 1.4 ml carbaryl stock solution to 44 ml river water and 15 ml phosphate buffer (pH 9). The temperature of the reaction vessel was preserved at 27 °C using water bath. The experiment was interrupted at a series of specific moment (1, 6, 11, 16,. . ., 191 min). 1 ml of reaction mixture was taken out from reaction vessel and mixed with 2 ml of phosphate buffer (pH 5). All the samples were measured in

the fluorescence spectrometer with the same parameters at the Section 3.3.1.

3.3.3. Application to investigation of carbaryl hydrolysis in tap water

The experiment was initiated by adding 1.4 ml carbaryl stock solution to 15 ml tap water and 5 ml phosphate buffer (pH 9). The temperature of the reaction vessel was preserved at 20 °C using water bath. The experiment was interrupted at a series of specific moment (0.5, 5.5, 10.5, 15.5, . . ., 165, 175, 185, 195,. . ., 285 min). 0.4 ml reaction mixture was taken out from reaction vessel and mixed with 2 ml of phosphate buffer (pH 5). All the samples were measured in the fluorescence spectrometer with the same parameters at the Section 3.3.1.

4. Result and discussion

4.1. Simultaneous determination of carbaryl and 1-naphthol in river water and tap water

Before researching the hydrolysis in the nature water, the carbaryl and 1-naphthol should be quantified accurately by second-order calibration algorithm. So the process of determining carbaryl and 1-naphthol in river water and tap water was performed.

The excitation and emission wavelengths were from 244 to 308 nm and from 311 to 491 nm, respectively. In this range the Rayleigh and Raman scatterings can be avoided. For each sample an EEM fluorescent array with sizes 37 × 33 (emission wavelength × excitation wavelength) were obtained. All the samples including calibration set and test set and predication set were measured and the recorded data were combined and constitute a 37 × 33 × 18 data array.

The second-order calibration algorithm based on PARAFAC, which is used widely in chemistry and has been accepted by the chemist for its performance, was adopted to resolve the overlapped spectroscopes and to give a satisfying result.

PARAFAC required the estimated factor numbers to analyze the data array. So the factor numbers should be designated in advance. In this paper, the core consistency diagnostic was chosen to find the correct factor numbers. The entire 37 × 33 × 14 data array including calibration samples, test samples and the river water samples were analyzed and the result obtained by the core consistency diagnostic was illustrated in Fig. 2. It indicated the correct factor numbers should be three for decomposition of the data using the PARAFAC. Chemically, three factors are a reasonable conclusion. The three factors represent the carbaryl, 1-naphthol and the background, respectively.

Fig. 3 shows the profiles of the three factors from the decomposing the data array by the PARAFAC with three factors. Fig. 3(A) shows loadings related to the excitation spectral profiles and the Fig. 3(B) shows loadings related to the emission spectral profiles. The resolved spectra (excitation and emission) by using PARAFAC algorithm are compared with the pure spectra to confirm the compounds in samples. The figure displayed that the spectra of interferes in river water spread all measured wavelength both excitation and emission and overlapped

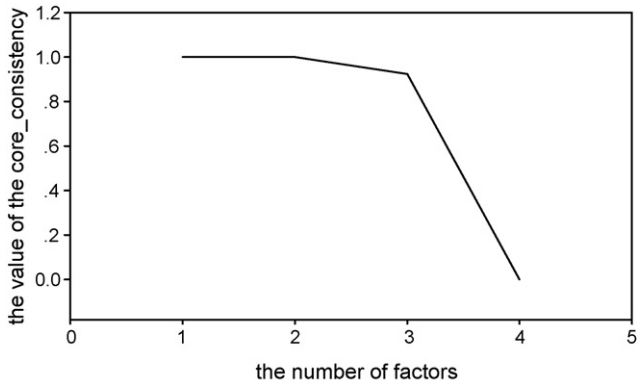

Fig. 2. The core consistency value about the river water samples.

with the two analytes. This implied the difficulty in directly determining the carbaryl and 1-naphthol without separation disposal.

In the same way, all the 37 × 33 × 14 data array include calibration samples, test samples and the tap water samples were analyzed by the core consistency diagnostic and it indicated the number of factors should be two. This means that there was almost no interference in the tap water. Fig. 4 shows the loadings

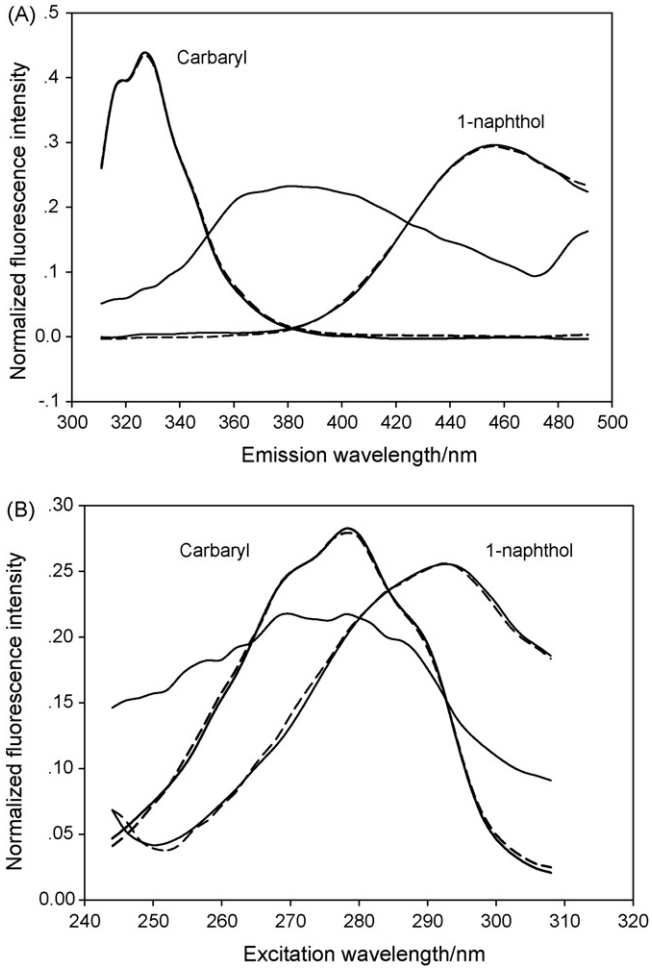

Fig. 3. Resolved (full line) and actual (broken line) profiles using the PARAFAC when the number of factors was chosen as three.

from the decomposing the data array by the PARAFAC with two factors. Fig. 4(A) shows loadings related to the excitation spectral profiles of the components and the Fig. 4(B) shows loadings related to the emission spectral profiles of the components. The resolved spectra (excitation and emission) by using PARAFAC algorithm are compared with the pure spectra.

With the PARAFAC algorithm the good results for the prediction samples including the river water samples and the tap water samples are obtained and were shown in Table 2. The table shows that the method is reliable to quantify the pesticides carbaryl and 1-naphthol. The SWATLD algorithm, which is based on the PARAFAC model, has the uniqueness property and the second-order advantage. If the three-way data is trilinear and there is no matrix effect, the proposed procedure will perform well when the interferences are different.

4.2. Application to investigation of carbaryl hydrolysis in river water

Using the above method, the concentrations of carbaryl and 1-naphthol in the running of reaction were obtained as follows. During the hydrolysis of the carbaryl 39 samples were collected at the 39 specific moments. According to the discussion above, the samples were measured at the range of excitation wavelength from 244 to 308 nm at regular steps of 2 nm and emission wavelength from 311 to 491 nm at regular steps of 5 nm. With the seven calibration samples a $37 \times 33 \times 46$ data array were obtained. The data array was decomposed by the PARAFAC algorithm with three factors and the overlapped spectral profiles were resolved. The loadings related to excitation spectral profiles and emission spectral profiles were similar with Fig. 3.

The concentrations of carbaryl and 1-naphthol during the hydrolysis were got by the calibration based on the PARAFAC and illustrated in Fig. 5(A). From Fig. 1, it is known that 1 mol carbaryl hydrolyzes to produce 1 mol 1-naphthol. Therefore, the sum of molarity of the compounds should be invariable in the process of the reaction. The average sum of molarity of the compounds during the reaction was calculated to be 1.56 nmol L^{-1} and the standard deviation was 0.055 nmol L^{-1}.

If the conversion of carbaryl to 1-naphthol accords with the first-order kinetic model, the concentration of carbaryl at

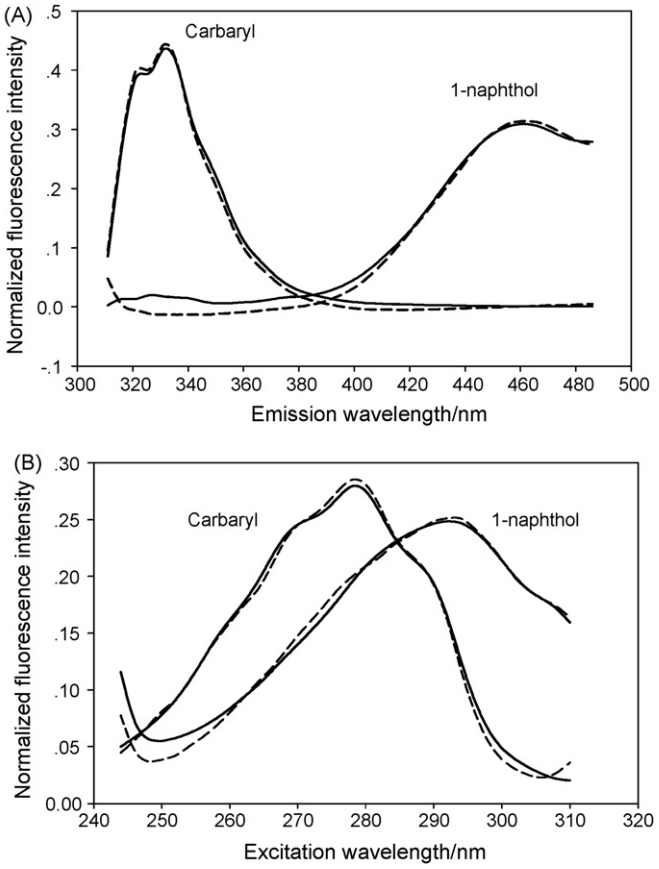

Fig. 4. Resolved (full line) and actual (broken line) profiles using the PARAFAC when the number of factors was chosen as two.

Table 2
The concentration obtained by the PARAFAC for the river water and the tap water

	Added concentration (ng/ml)		Founded (ng/ml)	
	Carbaryl	1-Naphthol	Carbaryl	1-Naphthol
Predication sample				
11[a]	72	155	70 (97.2%)	159 (102%)
12[a]	109	258	106 (97.2%)	266 (103%)
13[a]	181	361	179 (98.9%)	372 (103%)
14[a]	254	464	256 (101%)	457 (98.5%)
RMSEP (ng/ml)			2.29	7.90
15[b]	73	134	75 (103%)	128 (95.6%)
16[b]	109	237	111 (102%)	232 (98.0%)
17[b]	181	340	180 (99.2%)	356 (104%)
18[b]	254	443	256 (101%)	447 (101%)
RMSEP (ng/ml)			1.08	10.2

The root mean-square error of prediction (RMSEP) is determined as: RMSEP $= \left[\sum_{m=1}^{M}(c_i - \hat{c}_i)^2/M\right]^{1/2}$ where M is the number of samples, c_i and $\hat{c}_i$ are the actual and predicted concentrations, respectively.

[a] Prepared using the tap water as matrix; it is the recovery in bracket.

[b] Prepared using the river water as matrix; it is the recovery in bracket.

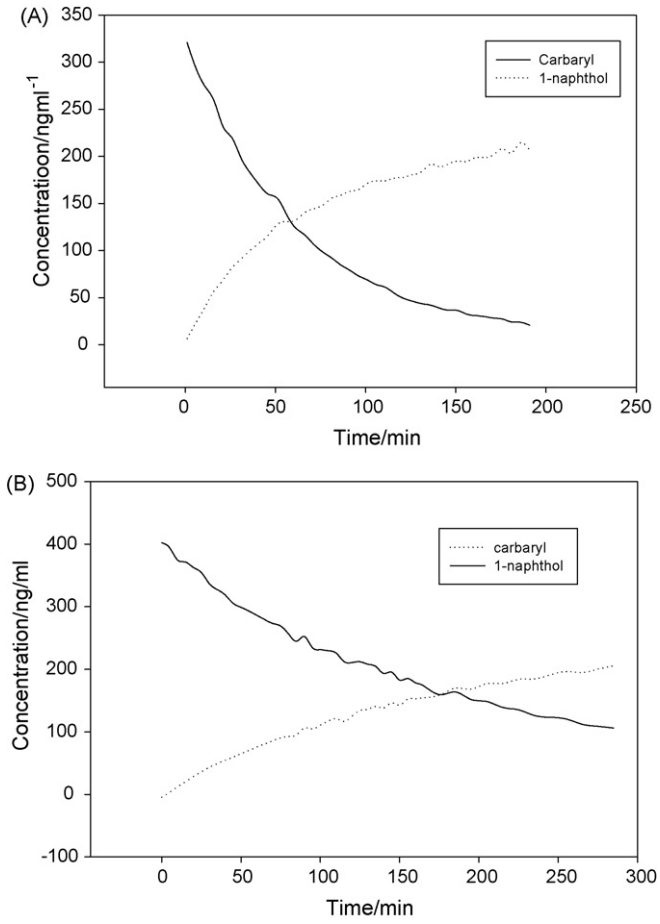

Fig. 5. The concentration profiles of the carbaryl and the 1-naphthol in the river water (A) and in the tap water (B).

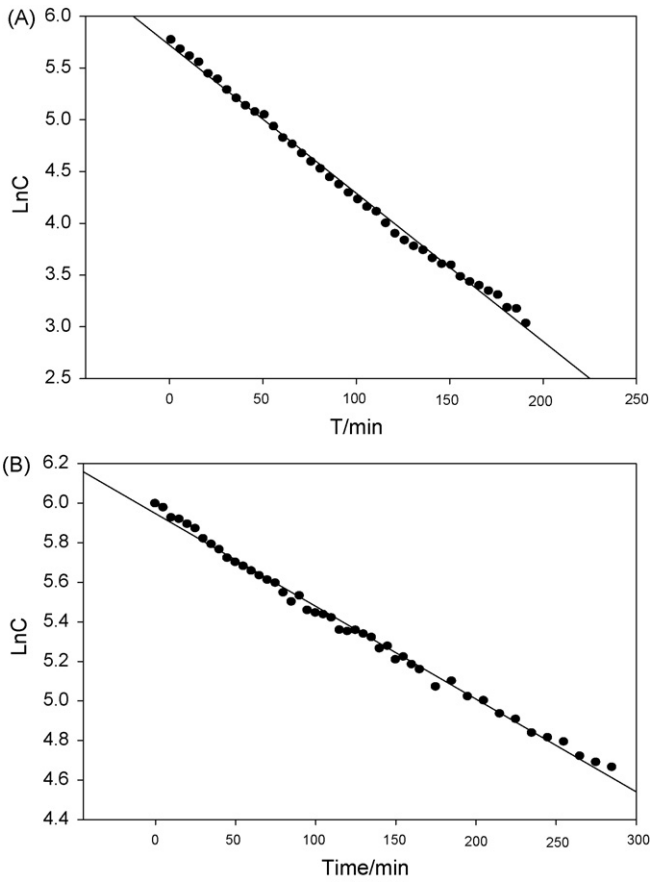

Fig. 6. Plot of the nature logarithm of carbaryl concentration vs. time t in river water (A) and in tap water (B).

t moment can be determined by the function:

$$-\frac{dC_{car}}{dt} = K \times C_{car} \quad (4)$$

According to the function one could get the function:

$$Ln(C_{car,t}) = Ln(C_{car,0}) - K \times t \quad (5)$$

where Ln(*) denoted the natural logarithm of *, $C_{car,0}$ is the initial concentration of reactant, $C_{car,t}$ represented the concentration of reactant at the monment t since the reaction started. K indicated the reaction rate constant (min^{-1}). Therefore, if the concentrations of reactant are known, the K could be get. Then the reaction rate equation can be determined too.

The natural logarithm of the carbaryl concentrations at the 39 specific moments versus time t was plotted in Fig. 6(A). It could be observed that all the points were almost in one line and the logarithmic concentrations linearly related to time. The regression equation and correlation coefficient of carbaryl were shown in Table 3. From the regression equation, the half life of carbaryl can be obtained. The half life of carbaryl is 48 min in this condition. The Fig. 6(A) implies that the half life is around 46 min which approximates the 48 min.

4.3. Application to investigation of carbaryl hydrolysis in tap water

The hydrolysis of carbaryl in tap water can be studied in the same way. The loadings related to excitation spectral profiles and emission spectral profiles were similar with Fig. 4.

The concentrations of carbaryl and 1-naphthol during the hydrolysis were obtained by the calibration with the PARAFAC and it was illustrated in Fig. 5(B). From the figure, it was obvious that the hydrolysis reaction is slower than that in river water. This was caused by the mild reaction condition that the reaction temperature was set at 20 °C. So the monitoring time was

Table 3
Regression equation, rate constant, correlation coefficient and the half life of degradation reactions of carbaryl

	Regression equation	Correlation coefficient	Rate constant (min^{-1})	Half life (min)
River water	$c = 5.72–0.0143t$	0.998	0.0143	48
Tap water	$c = 5.94–0.00466t$	0.995	0.00466	148

longer than the time in river water. The average sum of molarity of the compounds during the reaction was calculated to be 1.95 nmol L^{-1} and the standard deviation was 0.035 nmol L^{-1}.

The natural logarithm of the carbaryl concentrations versus time t was plotted in Fig. 6(B). The regression equation could be get and it was shown in Table 3. The half life was calculated and the value is 148 min. The figure implies that the half life is around 140 min which approximate 148 min.

5. Conclusion

In this paper excitation–emission matrix fluorescence coupled with second-order calibration was used to determine the carbaryl and 1-naphthol in river and tap water. The second-order calibration based on PARAFAC provides satisfactory concentration estimates with simple sample disposal and it shows PARAFAC is a powerful tool which can resolve heavily overlapped peaks into their pure spectral profiles and concentration profiles even in the presence of unknown interferences. Then the method was applied to the hydrolysis of carbaryl in river and tap water and provides the rate equation, rate constant and half life. The proposed procedure will perform well when the interferences are different in different samples, because the chemometric methodology selected exploits the second-order advantage of the three-way data arrays. The present paper provided not only a new approach to study the kinetics but also a promising tool for exploring the kinetic behaviors of complex system.

Acknowledgements

The authors wish to thank the National Nature Science Foundation of China (Grant Nos. 20475014, 20375012 and 20435010) and the National Basic Research Program of China (2007CB216404) Program for financial support.

References

[1] Carbaryl (EHC 153, 1994), http://www.inchem.org/documents/ehc/ehc/ehc153.htm.
[2] V.B. Patil, M.S. Shingare, J. Chromatogr. 653 (1993) 181.
[3] J. Bladek, A. Rostkowski, M. Miszczak, J. Chromatogr. A 754 (1996) 273.
[4] F. Tang, S. Ge, Y. Yue, R. Hua, R. Zhang, J. Planar Chromat.: Mod. TLC 18 (2005) 28.
[5] S.-L. Song, X.-D. Ma, C.-J. Li, Food Control 18 (2007) 448.
[6] Y.-S. Oh-Shin, M. Ko, H.-S. Shin, J. Chromatogr. A 769 (1997) 285.
[7] B.L.L. Tan, M.A. Mustafa, Talanta 61 (2003) 385.
[8] S.-S.E. Petropoulou, A. Tsarbopoulos, P.A. Siskos, Anal. Bioanal. Chem. 385 (2006) 1444.
[9] S. Totti, M. Fernández, S. Ghini, Y. Picó, F. Fini, J. Mañes, S. Girotti, Talanta 69 (2006) 724.
[10] H.-P. Li, J.-H. Li, G.-C. Li, J.-F. Jen, Talanta 63 (2004) 547.
[11] G.S. Nunes, M.L. Ribeiro, L. Polese, D. Barcelo, J Chromatogr. A 795 (1998) 43.
[12] J.S. Aulakha, A.K. Malikb, R.K. Mahajana, Talanta 66 (2005) 266.
[13] R.A. Harshman, UCLA Working Papers in Phonetics, 16 (1970) 1.
[14] J.D. Carroll, J.J. Chang, Psychometrika 35 (1970) 283.
[15] J. Saurina, S. Hemandez-Cassou, R. Tauler, Anal. Chem. 69 (1997) 2329.
[16] A. Juan, S.C. Rutan, R. Tauler, D.L. Massart, Chemometr. Intell. Lab.: Syst. 40 (1998) 19.
[17] H.-L. Wu, M. Shibukawa, K. Oguma, J. Chemometr. 12 (1998) 1.
[18] Z.-P. Chen, H.-L. Wu, R.-Q. Yu, J. Chemometr. 15 (2001) 439.
[19] A-L. Xia, H.-L. Wu, D.-M. Fang, Y.-J. Ding, L.-Q. Hu, R.-Q. Yu, J. Chemometr. 19 (2005) 65.
[20] M.J. Rodriguez-Cuesta, R. Boque, F.X. Rius, D.P. Zamora, M.M. Galera, A.G. Frenich, Anal. Chim. Acta 491 (2003) 47.
[21] R.D. JiJi, G.A. Cooper, K.S. Booksh, Anal. Chim. Acta 397 (1999) 61.
[22] J. Saurina, C. Leal, R. Compañó, M. Granados, R. Tauler, M.D. Prat, Anal. Chim. Acta 409 (2000) 237.
[23] T.J. Thurston, R.G. Brereton, Analyst 127 (2002) 659.
[24] A.R. de Carvalho, M. del Nogal Sánchez, J. Wattoom, R.G. Brereton, Talanta 68 (2006) 1190.
[25] O. Svensson, M. Josefson, F.W. Langkilde, Chemometr. Intell. Lab.: Syst. 49 (1999) 49.
[26] T. Rohe, W. Becker, S. Kölle, N. Eisenreich, P. Eyerer, Talanta 50 (1999) 283.
[27] R. Bro, H.A.L. Kiers, J. Chemometr. 17 (2003) 274.